WASH – 1400
(NUREG-75/014)

Reactor Safety Study

An Assessment of Accident Risks in U.S. Commercial Nuclear Power Plants

Appendices VII, VIII, IX and X

United States Nuclear Regulatory Commission

October 1975

DISCLAIMER

This report was prepared as an account of work sponsored by an agency of the United States Government. Neither the United States Government nor any agency Thereof, nor any of their employees, makes any warranty, express or implied, or assumes any legal liability or responsibility for the accuracy, completeness, or usefulness of any information, apparatus, product, or process disclosed, or represents that its use would not infringe privately owned rights. Reference herein to any specific commercial product, process, or service by trade name, trademark, manufacturer, or otherwise does not necessarily constitute or imply its endorsement, recommendation, or favoring by the United States Government or any agency thereof. The views and opinions of authors expressed herein do not necessarily state or reflect those of the United States Government or any agency thereof.

DISCLAIMER

Portions of this document may be illegible in electronic image products. Images are produced from the best available original document.

NOTICE

This report was prepared as an account of work sponsored by the United States Government. Neither the United States nor the United States Nuclear Regulatory Commission, nor any of their employees, nor any of their contractors, subcontractors, or their employees, makes any warranty, express or implied, nor assumes any legal liability or responsibility for the accuracy, completeness or usefulness of any information, apparatus, product or process disclosed, nor represents that its use would not infringe privately owned rights.

Available from
National Technical Information Service
Springfield, Virginia 22161
Price: Printed Copy $13.75; Microfiche $2.25

Second printing

WASH–1400
(NUREG 75/014)

RELEASE OF RADIOACTIVITY

in

REACTOR ACCIDENTS

APPENDIX VII

to

REACTOR SAFETY STUDY

by

R. L. Ritzman

E. F. Aber
C. Alexander
M. H. Fontana
D. K. Landstrom
D. L. Lessor
H. L. McMurry
D. L. Morrison
P. C. Owzarski
G. W. Parker
L. F. Parsly
M. Pobereskin
A. K. Postma
H. S. Rosenberg
W. A. Yuill

Contract W-7405-eng-92
Battelle Columbus Laboratories

U.S. NUCLEAR REGULATORY COMMISSION

OCTOBER 1975

MASTER

DISTRIBUTION OF THIS DOCUMENT IS UNLIMITED

Appendix VII

Table of Contents

Section			Page No.
INTRODUCTION			VII-1
1	FISSION PRODUCT RELEASE FROM REACTOR CORE MATERIAL		VII-3
	1.1	Gap Release Component	VII-3
		1.1.1 The Release Fraction	VII-4
		1.1.2 The Escape Fraction	VII-4
		1.1.2.1 Noble Gases	VII-4
		1.1.2.2 Halogens	VII-4
		1.1.2.3 Alkali Metals	VII-5
		1.1.2.4 Alkaline Earths	VII-5
		1.1.2.5 Tellurium	VII-6
		1.1.2.6 Other Species	VII-6
	1.2	Meltdown Release Component	VII-6
	1.3	Vaporization Release Component	VII-8
		1.3.1 Volatile Fission Products	VII-9
		1.3.2 Low Volatility Fission Products	VII-10
	1.4	Oxidation Release Component	VII-11
	1.5	Use of Release Component Values	VII-11
REFERENCES			VII-12
2	FISSION PRODUCT RELEASE FROM THE PRIMARY COOLANT SYSTEM		VII-17
	2.1	General Primary System Escape Fractions	VII-17
		2.1.1 Noble Gases	VII-17
		2.1.2 Iodine	VII-17
		2.1.3 Solid Fission Products	VII-17
	2.2	Special Cases of Primary System Retention of Fission Products	VII-18
		2.2.1 PWR Cold Leg Pipe Break	VII-18
		2.2.2 BWR Core Meltdown With ECC Injection	VII-18
		2.2.3 BWR Dry Vessel Meltdown	VII-19
	2.3	Summary of Primary System Escape Fractions	VII-19
		2.3.1 PWR Systems	VII-19
		2.3.2 BWR Systems	VII-19
REFERENCES			VII-20
3	FISSION PRODUCT LEAKAGE FROM THE CONTAINMENT SYSTEM		VII-23
	3.1	PWR Containment Models	VII-23
		3.1.1 Single Volume Containment Model	VII-23
		3.1.2 Multicompartment Containment Model	VII-24
		3.1.2.1 Natural Deposition	VII-26
		3.1.2.2 Spray Removal	VII-26

Table of Contents (Continued)

Section		Page No.
	3.1.2 Multicompartment Containment Model (Continued)	
	3.1.2.3 I_2 Equilibrium	VII-27
	3.1.2.4 Intercompartmental Flow Rates	VII-28
	3.1.2.5 Design of Corral for PWR Analyses	VII-28
3.2	BWR Multicompartment Model	VII-29
	3.2.1 Natural Deposition - Effect of Heat Transfer from BWR Vessel Walls	VII-29
	3.2.2 Pool Scrubbing	VII-30
	3.2.3 Standby Gas Treatment System - (SGTS)	VII-30
	3.2.4 Natural Deposition in the Drywell Annuar Airspace	VII-31
	3.2.5 The Computer Code CORRAL	VII-33
3.3	Estimation of Methyl Iodide Fraction Used in PWR and BWR Analyses With the Corral Code	VII-35
	3.3.1 Methyl Iodide Fraction For PWR Analyses	VII-35
	3.3.2 Methyl Iodide Fraction For BWR Analyses	VII-36
	3.3.3 Fission Product Decontamination During Leakages to the Atmosphere	VII-36
	3.3.4 Potential Groundwater Contamination in a Meltdown Accident	VII-37
	3.3.4.1 Problem Definition	VII-37
	3.3.4.2 The Hydraulic and Ion Transport Models	VII-38
	3.3.4.3 Results of the Depressurization Release Problem	VII-39
	3.3.4.4 Results of the Glass Leaching Release Problem	VII-40
	3.3.4.5 Exposure Reduction Processes and Contamination Control Measures	VII-40
REFERENCES		VII-42
APPENDIX A	CALCULATION OF FISSION PRODUCT RELEASE TO FUEL ROD GAS GAP	VII-55
APPENDIX B	RELEASE OF FISSION PRODUCTS FROM PWR AND BWR FUEL PINS	VII-69
APPENDIX C	CALCULATION OF GAP RELEASE OF RADIOACTIVE FISSION PRODUCTS	VII-87
APPENDIX D	SURVEY OF EXPERIMENTAL WORK ON FISSION PRODUCT RELEASE FROM MOLTEN UO_2	VII-107
APPENDIX E	AN EVALUATION OF FISSION PRODUCT AND FUEL CONSTITUENT RELEASE FROM REACTOR FUELS BASED ON A THERMODYNAMIC ANALYSIS OF THE COMPOUND SPECIES PRESENT IN THE FUEL	VII-121
APPENDIX F	SUMMARY OF DATA ON FISSION PRODUCT RELEASE FROM UO_2 DURING OXIDATION IN AIR	VII-133
APPENDIX G	ESTIMATIONS OF FISSION PRODUCT RELEASE FROM MELT DURING CONCRETE PENETRATION	VII-143
APPENDIX H	EXAMINATION OF SOLID FISSION PRODUCT PLATEOUT IN PRIMARY SYSTEMS	VII-151
APPENDIX I	IODINE DEPOSITION IN PWR AND BWR REACTOR VESSELS AND ASSOCIATED EQUIPMENT	VII-163

Table of Contents (Continued)

Section		Page No.
APPENDIX J	TRANSPORT AND DEPOSITION OF AIRBORNE FISSION PRODUCTS IN CONTAINMENT SYSTEMS OF WATER COOLED REACTORS FOLLOWING POSTULATED ACCIDENTS	VII-179
APPENDIX K	DIFFUSION OF RADIOACTIVE FLUID THROUGH SOIL SURROUNDING A LARGE POWER-REACTOR STATION AFTER A CORE MELTDOWN ACCIDENT	VII-259

List of Tables

Table		Page No.
VII 1-1	Fractions Released to Gap (Total Core)	VII-13
VII 1-2	Gap Release Component Values	VII-13
VII 1-3	Meltdown Release Component Values	VII-14
VII 1-4	Vaporization Release Component Values	VII-14
VII 1-5	Fission Product Releases During Steam Explosions	VII-15
VII 1-6	Fission Product Release Service Summary - Best Estimate Total Core Release Fractions	VII-15
VII 2-1	Estimated Average Temperatures of Upper Structural Material in a BWR Pressure Vessel During Dry Meltdown	VII-21
VII 3-1	Fission Product Removal Rate Constants Calculated for a Large PWR Containment Vessel	VII-44
VII 3-2	Equilibrium Data for I_2 With Boric Acid Sprays	VII-44
VII 3-3	Equilibrium Data for I_2 With Caustic Sprays	VII-45
VII 3-4	Input Data and Results for Filter Overbeating Criteria	VII-45
VII 3-5	DF vs Particle Size and Reynolds Number in Drywell Annular Gap	VII-45
VII 3-6	Hydraulics Model Parameters	VII-45
VII 3-7	Distribution Coefficients for Various Radionuclides in Groundwater	VII-46
VII 3-8	Core Inventory Depressurization Release Fractions	VII-46
VII 3-9	Comparison of Calculated Groundwater Effluent Concentrations to MPC Limits - Depressurization Release Case	VII-47
VII 3-10	Comparison of Calculated Groundwater Effluent Concentrations To MPC Limits - Glass Leaching Release Case	VII-47

List of Figures

Figure		Page No.
VII 3-1	Drop-Collection Efficiency as a Function of Liquid Volume Sprayed	VII-48
VII 3-2	Schematic of CORRAL-PWR	VII-48
VII 3-3	Schematic of CORRAL-BWR	VII-49
VII 3-4	Computer Code CORRAL Flow Diagrams	VII-49
VII 3-5	Idealized Flow System Used for Analysis	VII-50
VII 3-6	Radionuclide Elution Curves for Depressurization Release	VII-51
VII 3-7	Radionuclide Elution Curves for Glass Leaching Release	VII-52

Appendix VII

Release of Radioactivity in Reactor Accidents

Introduction

This report describes results of the Fission Product Source Term Task which has been conducted by Battelle's Columbus Laboratories as part of the U.S. Atomic Energy Commission's Reactor Safety Study. The objective of the Reactor Safety Study is the evaluation of postulated accidents in large water-cooled power reactors with respect to the probability of occurrence and the magnitude of resulting consequences. The primary purpose of the Fission Product Source Term Task has been to specify the size of the fission product source which would escape the containment boundary as a function of time for various accident conditions defined by the Reactor Safety Study. In doing this, specialists in the areas of fission product release, transport, and deposition met periodically with the Reactor Safety Study to guide the development of realistic source term estimates. In addition, key analyses on one or more portions of the total problem were performed at the different laboratories represented by each of the specialists. The group was composed of D. L. Morrison and R. L. Ritzman from Battelle-Columbus, W. A. Yuill from Aerojet Nuclear Company, A. K. Postma and P. C. Owzarski from Battelle-Northwest, and G. W. Parker and M. H. Fontana from Oak Ridge National Laboratory.

A dominant portion of the effort on the task concerned fission product behavior under reactor core meltdown conditions. Accordingly, considerable interaction occurred between this task and the Reactor Core Meltdown Task, which was also conducted at the Battelle-Columbus Laboratories. The Reactor Core Meltdown Task (Ref. 1) provided data on physical events and conditions that were essential in developing the definitions and procedures used to specify fission product movement within and loss from the containment boundary.

This report specifically presents the methodology that was evolved to enable the performance of calculations of fission product escape to the atmosphere for various accident sequences in a large PWR or BWR. The essentials of the methodology are described in the sections which follow. Supporting documentation or more detailed treatment of certain components can be found in the collection of papers that are appended at the rear of the report.



Section 1

Fission Product Release From Reactor Core Material

Fission product release from core material during accidents involving meltdown would probably occur more or less continuously until the system finally cools. During this period, release rates should vary over wide limits depending on fission product properties, system temperatures, and the surface to volume ratio of the molten material. However, it is possible to identify four conditions or times at which major driving forces for release exist. These periods of high rates should account for most of the total release. The four major release components are:

a. Gap release - fission product release which occurs when the claddings experience initial rupture. It consists mostly of activity that was released to void spaces within the fuel rods during normal reactor operation and rapid depressurization of contained gases provides the driving force for escape.

b. Meltdown release - fission product release which occurs from the fuel while it first heats to melting and becomes molten. High gas flows in the core during this period sweep the activity out of the core region.

c. Vaporization release - fission product release which occurs after large amounts of molten core material fall into the reactor cavity from the pressure vessel. Turbulence caused by internal convection and melt sparging by gaseous decomposition products of concrete produce the driving forces for escape.

d. Oxidation release - fission product release which occurs just after and is a result of a steam explosion event. Finely divided fuel material is scattered into an oxygen atmosphere and undergoes extensive oxidation which liberates specific fission products.

By concentrating on the processes and factors which will control these four components, it was decided that release terms for representative accident sequences could be developed. Each one pertains to a specific, identifiable time period in the core meltdown scenario of either water reactor type. Therefore, PWR and BWR analyses both can utilize the same set of release components but the particular number of components and the timing of the releases will depend on the reactor type and the particular accident sequence being examined. The subsections which follow describe each component in more detail and present the release values that were arrived at on the basis of the current interpretations of fission product behavior that are contained in appendices to this report. The relevant appendices are cited within the text.

1.1 GAP RELEASE COMPONENT

For the purposes of this work, gap release is defined as the fission product inventory that is free to escape in gaseous or vapor form from core fuel rods if the cladding ruptures. The number of core fuel rod claddings that will rupture depends on the effectiveness of the emergency core cooling systems. For highly effective emergency cooling no claddings may rupture, while for degraded cooling conditions, leading to fuel rod melting, essentially all claddings will rupture during the temperature rise to melting. Between these two extremes there exist a large series of core cooling temperature conditions which can lead to various percentages of cladding ruptures.

Cladding rupture temperatures depend upon several factors; rate of temperature rise, internal gas pressure, and cladding physical and mechanical properties. However, rupture temperatures are likely to range from about 1400 to 2000 F. Fission products which have migrated to the surface of the fuel pellets or to the interior surface of the cladding during normal reactor operation can potentially be released. The driving force for escape comes from the rapid release of inert gases (helium and fission gas) stored in the plenum and gas gap spaces of the fuel rods. Internal gas pressures ranging from a few hundred psia to 2000 psia can exist.

Only fission product material which exists in vapor form should escape during the rod depressurization. Therefore, if vaporization from condensed phases or reaction layers within the fuel rod is incomplete when depressuri-

zation takes place, the potential release would not be realized. After the depressurization, very little driving force exists to carry fission product vapors along the narrow annulus to the rupture location in the cladding. Consequently, in this work the gap release component will be confined to an estimate of the release that occurs at the time of cladding rupture only. For accident conditions which are less severe than core meltdown, the gap release component values developed here may be reduced according to the percentage of the fuel rod claddings that are expected to experience rupture.

Two fractions make up the gap release component: (1) the release fraction, and (2) the escape fraction. The release fraction defines the potential for release from UO_2 fuel and is the result obtained from most fission product release models. The escape fraction represents an estimate of the degree of volatility of the fission product at fuel rod cladding rupture. The processes and reactions that need to be considered in estimating the escape fraction include physical condensation and reactions with fuel material, cladding, other fission products and gaseous impurities in the rods.

1.1.1 THE RELEASE FRACTION

The three sets of gap release calculations which are reported in Appendices A, B, and C produced the release fraction estimates shown in Table VII 1-1. These results are based on PWR core properties but results for a BWR are so similar that Table VII 1-1 values will be used for both reactor types. The values in Table VII 1-1 also represent best estimate releases for the several species and these contain different uncertainties depending upon the release models used, variations in basic parameters, or differences in methods to compute temperature profiles in operating fuel. Inspection of results given in Appendices A, B, and C show that uncertainties range from factors of ± 2 for some species to factors ± 10 or more for others. As a rule, the magnitude of the uncertainty tends to decrease as the decay half-life increases.

The ultimate use of these release fractions in total accident release calculations demands that a single value be assigned for each chemical group; that is, isotopic dependent release behavior must be ignored. Consequently, in the last column of Table VII 1-1, average release values are listed which will be used for all isotopes of each of the applicable chemical elements. The average values in each case are the simple arithmetic means of the three calculated releases for the particular isotope. This isotope was selected on the basis that it represents the radiologically important one for the element. Note that no direct calculations of tellurium releases were made. Results of out-of-pile experiments (Ref. 2) indicate that its release should be similar to iodine and cesium, and on this basis the value of 0.10 for the principal isotope, Te-132, was selected. Since the isotopes that were selected to represent each chemical group have relatively long half lives, the uncertainties in the average release fractions should be nearer the lower end of the uncertainty range as noted above. This was the basis for the uncertainty factors that are specified in Table VII 1-1.

The data in Table VII 1-1 represent the best effort that can be made with current mathematical models in calculating fission product releases during reactor operation. Due to lack of basic information for some species or parameters, simplifying assumptions are often made which tend to overestimate rather than underestimate releases. Therefore, the results should be interpreted as current state-of-the-art and not as absolute values. Future experimental and theoretical study may indicate lower releases, and when this occurs the models and results used here can be modified.

1.1.2 THE ESCAPE FRACTION

The rationale used to select escape fraction values will be discussed on an element by element basis.

1.1.2.1 Noble Gases.

The noble gases are gaseous at room temperature and are known to be very unreactive chemically. At cladding rupture the only mechanism which could retard their escape would be flow restrictions along the gas gap to the hole or split in the cladding. Since this constitutes only a delay process, which depends on very specific details of fuel rod structure, no retention of released noble gases in the fuel rod gas space can be claimed.

1.1.2.2 Halogens.

Elemental iodine would be entirely gaseous at normal reactor fuel rod operating temperatures and particularly at the cladding rupture temperatures. However, iodine readily reacts with

metals to form iodides which have different volatilities. Possibilities include zirconium iodides (reaction with cladding), cesium iodine (reaction with fission-product cesium), and hydrogen iodide (reaction with trace hydrogen or water vapor).

Experimental work by Feuerstein (Ref. 3) has shown that a series of zirconium iodides can form when iodine in Zircaloy capsules is heated, and several minutes is required to volatilize appreciable fractions of the reaction product at a temperature of 800 C (1472 F). Indirect evidence of iodine reaction with Zircaloy in operating fuel rods has been obtained by Weidenbaum (Ref. 4). Collins, et al (Ref. 5) performed puncture tests with irradiated Zircaloy-2 clad UO_2 in steam at about 1000 C (1832 F) from which it was concluded that only 10 percent of the iodine that was expected to be free within the cans escaped through the puncture hole. Lorenz and Parker (Ref. 6) have conducted a pair of in-reactor fuel rod failure transient tests with pressurized Zircaloy-2 clad fuel rods. The fission product release data for the two experiments indicated 25 percent and 100 percent escape of the free iodine relative to free noble gases. These limited studies suggest that iodine retention by Zircaloy cladding could limit the escape of iodine from the gas spaces of fuel rods during rupture. The escape fraction value cannot be specified very accurately but would be expected to fall within the range 0.1 to 1.

Contrary to the cladding reaction mechanism, thermodynamic analyses of the fuel-cladding fission product system consistently predict that CsI would be the most stable chemical form for iodine at elevated temperatures (see Appendix E). Since the fission yield for cesium isotopes is more than ten times that for iodine isotopes, there is sufficient cesium for complete conversion of the iodine. If CsI is the dominant iodine species in fuel rods then iodine would exhibit a significantly lower volatility at cladding rupture temperature i.e., a vapor fraction in the range of 0.01 to 0.1 would be expected. As shown above, experimental escape data do not coincide with these low values. In addition there is limited evidence that cesium may undergo compound formation with UO_2 and thus prevent formation of CsI (Refs. 7,8). Thermodynamic analyses have not considered this reaction. Finally, there appears to be no experimental confirmation of the presence of CsI in irradiated fuel rods. Therefore, the possibility of CsI being a major chemical form is not sufficiently established to justify consideration in this work. However, additional experimental work in this area would be useful.

The formation of hydrogen iodide, which might be significant at high temperatures, also has not been verified by experimental work on irradiated fuel rods. The existence of HI as a major species would not alter iodine volatility at cladding rupture temperatures appreciably. Therefore HI will not be considered an important iodine form in this analysis.

In summary the escape fraction for iodine gap release should be based on available experimental evidence that indicates at least partial retention by Zircaloy cladding. On the basis of the range indicated a best estimate value of 1/3 with an uncertainty factor ± 3 is appropriate.

1.1.2.3 Alkali Metals.

The normal boiling point of cesium metal is about 960 K (1270 F) and, if the fission product exists in this elemental form, the gap release fraction could be completely vaporized at cladding rupture temperatures. On the other hand the thermal transient may be too rapid and incomplete vaporization would have occurred at this point. Also, compound formation with the fuel (noted above) or with the cladding (possibly with corrosion products) could result in significantly reduced volatility. There is almost no experimental data related to escape of fission product cesium under these conditions. The in-pile transient tests of Lorenz and Parker (Ref. 6) provide the only known experimental estimate. The results of two tests indicate an escape fraction value of about 2/3. Because of the approximate nature of these measurements, it was decided to use the same escape fraction for cesium that is used for iodine; i.e., 1/3 with an uncertainty factor of ± 3.

1.1.2.4 Alkaline Earths.

Depending upon the oxygen activity in the system, fission product strontium would predominately exist as either the metal or the monoxide. However, neither condensed phase has appreciable volatility at clad rupture temperatures. The metal which exhibits the higher vapor pressure should limit vapor fractions to less than 10^{-4} of the total strontium. The ANC fission product release model calculation for strontium, which considers thermodynamic equilibrium in the

fuel body; obtained a maximum release fraction of 4×10^{-6} (Appendix B). The in-pile transient test data of Lorenz and Parker (Ref. 6), while quite crude for strontium, indicate escape fractions ranging from about 10^{-2} to 10^{-6}. On the basis of this evidence, it appears that in conjunction with a release fraction of 0.01, a best estimate value for the escape fraction would be 10^{-4} with an uncertainty factor of ± 100.

1.1.2.5 Tellurium.

Thermodynamic calculations indicate that tellurium can exist as either the element or an oxide in the fuel. The stable vapor form at cladding rupture temperatures is probably Te_2, but several experimental studies indicate that tellurium will react with Zircaloy. Genco, et al. (Ref. 9) demonstrated extensive reaction of tellurium vapor with zirconium at temperatures above 400 C (752 F). The in-pile transient tests of Lorenz and Parker (Ref. 6) while very limited indicate an escape fraction for tellurium of between 10^{-1} and 10^{-5}. A complex kinetic situation involving competition among vaporization, reaction with cladding, and escape in the gaseous puff probably determines the escape fraction. Therefore, the value was set at 10^{-3} with an uncertainty factor of ± 100.

1.1.2.6 Other Species.

The volatilities of other fission product species, besides those which are chemical analogs of the elements discussed above, are expected to be so low that their escape at cladding rupture can be considered negligible. Therefore, the results of all the gap release component analysis can now be summarized. Table VII 1-2 presents such a summary showing the gap release fractions, the escape fractions, and the product of these two - the gap release component. The release and escape fractions listed here may be somewhat different from values obtained or recommended by the individual laboratories that contributed to the analyses. This is because current knowledge does not clearly show one analytical approach is superior to the others.

1.2 MELTDOWN RELEASE COMPONENT

The conditions pertaining to this release period begin with rapid boiloff of the water coolant which uncovers the reactor core. Steam, flowing up through the heating core, initiates Zr-H_2O reaction and this accelerates the rate of temperature rise. The cladding begins to melt within one minute and in a few more minutes fuel-melting temperatures are approached in the hotter regions. The process spreads throughout the core and within 30 minutes to 2 hours (Ref. 1) nearly the whole core is molten at temperatures ranging from roughly 2000 to 3000 C. During the later stages of this process molten core material can run through or melt through the grid plate and fall into the bottom of the pressure vessel. If a steam explosion does not occur when residual water is contacted in the lower portion of the pressure vessel, partial quenching and temporary solidification of portions of the molten mass can take place. However, the internal heat generation causes remelting and the inevitable downward migration continues until the pressure vessel fails, probably by meltthrough. Pressure vessel failure is expected to require about 1 hour after most of the core has melted (Ref. 1). Prior to this the high internal temperatures have caused melting of some of the pressure vessel steel and interior structural components. The molten iron is not miscible with the core material (oxide phase) although partial conversion to iron oxides could produce some dissolution in and dilution of the core material. Nevertheless some fission products (i.e., the noble metals) would tend to distribute to the metallic iron phase.

Initial fuel melting is expected to occur in only the center regions of the rods on almost a pellet by pellet scale. Thus the melting fuel will offer a relatively high surface area for release of fission products. As the melting front moves outward, the melting of the individual pellets may continue, but it is also conceivable that larger sections of fuel may collapse into the molten mass. If this fuel melts within the mass rather than at the edge, then fission product release could be inhibited by the time required for transport to a free surface. On the other hand, gaseous fission products, present as bubbles in the UO_2 could rise quickly to the surface of the molten mass and escape. It appears that most of the fission product release that does occur will take place early in the melting period at each core location. Then as the melted fuel mixes with the rest of the molten mass and the mass increases in size, fission product release rates will become much slower. The melting of structural steel in the pressure vessel during this later period is expected to produce a layer of molten iron above the molten core material which would offer a further barrier to

fission product release. Other factors which can inhibit release during meltdown in the pressure vessel include the possibility of crust formation at the melt surface and partial quenching when melt runs or falls into water that may be left in the bottom of the vessel.

The atmosphere in the core region and pressure vessel during meltdown is expected to be a steam-hydrogen mixture with small concentrations of fission product and core material vapors and aerosols. This may be classified a nonoxidizing atmosphere for most fission products, and it, of course, results from partial consumption of steam by metal-water reaction, yielding H_2 in the core region. Although the metal-water reaction that does occur is steam supply limited, some steam flow passes through cooler portions of the core region without complete reaction. It is estimated that during the meltdown phase only about half the Zircaloy is reacted and other metal-water reaction produces only about 50 percent more H_2. Thus total metal-water reaction is only the equivalent of 75 percent $Zr-H_2O$ reaction.

Thermal analyses of core meltdown provide only generalized data on core temperature profiles, geometry changes, and melt behavior versus time. This, combined with the uncertainties which exist in fission product properties at very high temperatures, argue against construction of a highly mechanistic model to calculate fission product release during the meltdown phase. Therefore, in this work, fission product release is treated as being simply proportional to the fraction of core melted.

Mathematically,

$$RCFx(t) = [RFx] \cdot [FCM(t)]$$

where RCFx(t) = Core release fraction for fission product x as a function of time (t):

RFx = Release fraction of fission product x from melted fuel

FCM(t) = Fraction of core melted as a function of time (t)

It is important to note that this approach assigns all release which is expected to occur during the time core material remains in the pressure vessel, to the early period of first melting. This is consistent with two key observations; (1) the highest steam flows and (2) the highest fuel surface areas are expected during the early period. Thus this should be the period of maximum driving force for fission product escape from the core region. The release fractions (RFx) for the various fission products were estimated by considering:

a. The limited data that are available from small-scale experiments with UO_2 (Appendix D), and

b. The predictions of limited thermodynamic analyses of fuel-cladding-fission product system at high temperature (Appendix E)

The results are summarized in Table VII 1-3 and a short description of the rationale connected with each value is given in the following paragraphs.

a. Noble Gases (Xe, Kr) - Experimental work shows that nearly total release of these essentially chemically inert gases would be expected during the meltdown period if the surface-to-volume ratio of melting material remains high. Although this seems likely and considerable release should occur even before the fuel melts, some gases could become trapped as the molten mass enlarges during the later stages of meltdown. Accordingly, a range of 50 to 100 percent release is considered reasonable but 90 percent should be assumed probable.

b. Halogens (I, Br) - Again nearly total release is expected due to the high volatility, but the rate of release could be limited by transport in the melt to an external surface. Therefore, the same range (50-100 percent release) should apply and 90 percent is considered the probable value.

c. Alkali Metals (Cs, Rb) - Nearly total release would be expected but experimental data on cesium release from molten UO_2 and thermodynamic studies show that the alkali metals are not so highly volatile as the noble gases or halogens. Therefore, the release rate could be somewhat affected by internal transport in the melt or by the possible tendency toward compound formation. Experimental evidence indicates a range of 40 to 90 percent with a probable value of 80 percent.

d. Tellurium - Simple thermodynamics indicate that Te should volatilize almost completely from melting core material in the elemental form. However, experimental data indicate

extensive reaction with unoxidized Zircaloy cladding would tend to hold tellurium in the melt, even though much of the cladding may oxidize during the meltdown period. The tellurium apparently migrates farther into the cladding to react with remaining free metal rather than diffuse out through the oxide layer. Release of the tellurium from a particular core region will occur when nearly all or all of the cladding has been oxidized. Since an average of 50 percent of the core cladding is expected to become oxidized during meltdown, this represents an upper limit for release. However, the oxidation is spread unevenly over the core and a smaller amount of cladding undergoes complete reaction. On this basis tellurium release is estimated to range from 5 to 25 percent.

e. Alkaline Earths (Sr, Ba) - The chemical form and the volatility of these two fission products are very sensitive to the oxygen partial pressure in the system. Strontium metal is more volatile than barium metal but barium oxide is more volatile than strontium oxide. Thermodynamic analyses produce conflicting estimates of volatility and chemical form due to variations in oxygen activities. Experimental data on release from molten fuel material indicate that the two elements would experience about the same release. Data obtained with zirconium clad UO_2 showed up to 20 percent release of strontium and barium over several minutes in a neutral atmosphere, while only a few percent loss was found for bare or stainless steel clad UO_2. The lower volatility of these elements and the probable existence of unoxidized cladding suggest that releases in the range of 2 to 20 percent would occur. Since incomplete cladding oxidation is expected, the probable release value should lie above the geometric mean for this range. Hence, 10 percent is used as the probable value.

f. Noble Metals (Ru, Rh, Pd, Mo, Tc) - Although these elements probably volatilize as the oxides, thermodynamic calculations suggest that the volatile oxide forms are not very stable at the high temperatures and the lower oxygen partial pressure that are expected to be associated with the core meltdown. The first three elements probably exist in the metallic form in the fuel, while the latter two are probably in the form of lower oxides. The metallic species could partially distribute to the molten iron phase and be retained. Experimental data on ruthenium release from molten UO_2 in an oxygen-deficient atmosphere indicate low release. Releases in the range of 1 to 10 percent are considered possible, and 3 percent (the approximate geometric mean) is used as the probable value.

g. Rare Earths (including Y and Np, Pu) - The rare earth elements will generally exist in the fuel as the sesquioxides (M_2O_3) while the actinides, neptunium and plutonium, should form the dioxides (MO_2). The oxides characteristically exhibit low volatility but an estimate of the release fraction is difficult to make. Experimental data for cerium release from small specimens of molten UO_2 indicate losses of several tenths of a percent over a few minutes, or about the same as the UO_2 vaporization loss. In Appendix H, estimates of fuel vaporization rates indicate losses in the range of 0.01 to 1 percent. This range can also be used for the rare earth species but the probable value, 0.3 percent, reflects caution in selecting a characteristic release when the estimate is so approximate.

h. Refractory Oxides (Zr, Nb) - The oxides of these elements are so stable and of such low volatility that they probably would experience less release than the rare earths. However, for simplicity the same release definitions are used here as for the rare earths.

1.3 VAPORIZATION RELEASE COMPONENT

When the molten core and iron penetrate the pressure vessel and fall (or run) into the reactor cavity, the material will be exposed to oxygen from the containment atmosphere, steam from contact with water or vaporized from concrete, and carbon dioxide from thermal decomposition of the limestone aggregate in the concrete. Passage of steam and carbon dioxide through the molten mass will produce a gas sparging effect. In addition these gases or their dissociation products will create highly oxidizing conditions. One can speculate that the iron phase would be (at least partially) converted to oxide which could then dissolve in the core melt. The melt should also contain products of the concrete decomposition; silica, calcium

silicates, or calcium oxide. The products would eventually reduce the density of the oxide phase and the then heavier iron phase might sink to the bottom of the mass (Ref. 10). Conversely, incomplete dissolution could leave a relatively pure UO_2 phase which would continue penetrating downwards (Ref. 11). Lower melting mixed oxide phases forming ahead of the UO_2 would tend to rise and cover the UO_2. Thus, development of several immiscible or partially miscible phases is conceivable. Internal convection would promote mixing within and exchange between phases. Depending upon their solute properties, fission product oxides could distribute to these phases thereby altering the heat source distribution and the temperature profile in the melt system (Ref. 10). Vaporization of fuel and structural materials from the upper surface of the molten mass should produce dense aerosol clouds (smokes) above the melt and buildup of condensation products on nearby surfaces. Agglomeration and growth of smoke particles is expected to cause some vaporized material to settle back. Thus much of the vaporized material should be retained in the reactor vessel cavity. Vaporized fission products, mixed with the much larger quantities of structural material vapors and smoke, should generally follow the distribution of the bulk material. Exceptions to this would be the high volatility species which could escape into the upper part of the containment.

Only highly simplified analyses of the physical situation just outlined have been performed (Refs. 10,11,12). There are many unknown details concerning most of the chemical, physical, thermal, mechanical, and metallurgical properties of the complex system. Analytical results are dependent on basic assumptions which differ among models. No large-scale experimental work on the relevant system has been performed to guide modeling. Concrete penetration rates cannot be estimated accurately because of uncertainties in heat transfer mechanism, melt interaction effects, and/or boundary limit definitions. Release calculations can and have been performed, but the assumptions and data extrapolations needed, lead to estimates that are usually upper limit values (Ref. 11) (See Appendices E and G). The release models are useful in identifying key release processes and species that have a high potential for release by one or more of these processes.

To a first approximation, the extent of release will depend upon species volatility and the rate of transport in the molten mass to an external surface. For the large molten masses that result from core meltdown, the latter process should control release for all except the very low volatility species. For example, estimates have shown that pure diffusion transport would require several hundred hours to achieve significant release fractions, regardless of volatility (Ref. 13). However, additional estimates indicated that thermally induced internal convection currents might increase mass transfer rates such that corresponding releases would occur within several hours (Ref. 13). Very recent approximations based on gas sparging assumptions suggest total release for volatile species in fractions of an hour (Appendix G). The release rates that would actually occur would probably be some mixture between the latter two processes. Also, gross vaporization of the melt could assist the release by creating a receding surface. The uncertainties of the problem require that a simple approach be used to specify fission product releases for this portion of the accident.

1.3.1 VOLATILE FISSION PRODUCTS

The very volatile fission products will escape the melt if they can reach an external surface. The gas sparging process offers a mechanism for inducing mixing and creating a large effective external surface area. The convective mass transfer process offers an alternative and usually slower rate for transport to surfaces where vaporization can occur. Both processes would result in an exponential decrease in the volatile fission product inventory with time. In each case the half-time for release might range from less than one hour to many hours, depending on the gas flow or mass transfer conditions.

Other work on the Reactor Safety Study has resulted in an estimated time for core penetration of the concrete base of about 18 hours (Ref. 1). The analyses also indicate that considerable spalling and decomposition of the concrete would occur within the first half-hour of contact. This would be a period of rapid gas (steam and carbon dioxide) generation during which the sparging process could be a dominant driving force for escape of volatile fission products. Subsequently, lower rates of release would be expected as gas flows decrease but sparging could still efficiently deplete the melt of volatile species (See Appendix G). Thermally induced internal convection and also surface evaporation might assist in the release.

The potential importance of gas sparging to the release of volatiles from the massive melt dictated that treatment of the vaporization release component should be based on this process. Accordingly, a pseudo-exponential rate expression was designed which required only a single input parameter, the characteristic release half-time. Mathematically,

$$VLF(t) = 1 - \exp[-0.693t/\tau]$$

where

VLF(t) = The vaporization loss fraction after time (t)

τ = The characteristic release half-time

In order to avoid excessive calculations during actual accident sequence analyses, a cut-off time for the expression, equivalent to four half-time intervals, was selected. In practice the rate expression was used exactly as written for the first three half-time intervals, but then complete escape of the remaining activity was compressed into the fourth interval. Since this last step involves only 12.5% of the total vaporization release, the approximation should produce only slight perturbations in results.

The value of the characteristic release half-time would be a function of the fission product volatility, the gas sparging rate, and other kinetic factors. In a rigorous sense, there would be a unique value for each fission product species which would vary continuously with the sparging conditions. This complexity is not warranted here and so the half-time value was assigned only to roughly match the period of high sparge gas flow. This period, as noted earlier, has been estimated to last on the order of one-half hour. Thus the best estimate half-time value is considered to be 30 minutes. Use of this uniform value for all fission products probably produces underestimates of the rate of release for the most volatile species and overestimates of the rate of release for species of lesser volatility. Also, the sparging process may not be fully effective in sweeping volatile fission products from the melt either because some sections of the melt are not exposed to sparge gas or because mass transfer limitations inhibit vapor saturation of sparge gas bubbles. Due to uncertainties such as these the 30 minute half-time value which is used in calculations should be considered uncertain by at least an order of magnitude.

The fission products that are sufficiently volatile to experience total loss during this vaporization phase are Xe, Kr, I, Br, Cs, Rb, Te, Se, and Sb. The meltdown release of the first six of these is expected to be quite large, because of their high volatilities, and so little will be left to contribute to the vaporization release component. This is not true for the tellurium group elements, whose meltdown release is considered inhibited by compound formation with Zircaloy cladding. However, by the time the vaporization release begins most of the free zirconium, which exists during core meltdown, should be oxidized (probably from reaction with UO_2). If not, then the oxidizing sparge gases (steam and CO_2) should quickly eliminate free zirconium so that tellurium and its chemical analogues, selenium and antimony, will become very volatile and also experience total release.

1.3.2 LOW VOLATILITY FISSION PRODUCTS

Essentially all the remaining important fission product species must be considered low volatility components. Thus total release of these species should not occur. With one exception this group of elements should be present as oxides in the oxide phase. The noble metals (Ru, Rh, Pd) and to a lesser extent Mo and Tc probably exist as the metals and would be expected to partition into the metallic iron phase of the molten system (Ref. 14). Low release (less than 1 percent) of these species is expected unless complete oxidation of the iron should occur (Appendix G). Although this is not considered likely, localized oxidation could lead to some release and a value of 5 percent is considered to be a realistic estimate. This is probably uncertain by a factor of $\pm$ 5. The other fission products (alkaline earth oxides and rare earth oxides) should be dissolved in the oxide phase of the melt (Ref. 14). Under the generally oxidizing conditions which persist over this period these species are less volatile than UO_2 (Appendix E). The vaporization of UO_2 and of other oxide materials in the melt is very difficult to estimate owing to uncertainties in composition and temperature. High vaporization rates (high temperatures and oxygen pressures) should produce dense aerosol clouds above the melt which would tend to settle out, carrying condensable fission products back down. Low vaporization rates (lower temperatures) would also indicate low losses for these fission products. Considering these limiting processes it is doubtful that more

than 1 percent of these fission product species could be distributed to the atmosphere in the containment over the course of the reactor melt-through period. This estimate is also probably uncertain by a factor of ±5.

The rate of release of the low volatility fission products, for lack of better definition, is assumed here to follow the same exponential function that is used to describe the release rate of the volatile species. On this basis the percentage release values given in Table VII 1-4 indicate the amount of each fission product, remaining in the core material after gap release and melt-down release have occurred, that will escape to the containment atmosphere during the vaporization period.

1.4 OXIDATION RELEASE COMPONENT

A steam explosion event will result in the scattering of finely divided UO_2 (containing fission products) into the atmosphere outside the containment or into the air-steam atmosphere inside containment. In either case, the UO_2 particles will cool and undergo reaction with oxygen to form U_3O_8 at temperatures below about 1500 C (Ref. 15). The reaction is exothermic and is accompanied by release of fission products that are volatile under these conditions. Oak Ridge work on measurement of fission product release during fuel oxidation by air at elevated temperatures is directly applicable (Ref. 16). These data summarized and discussed in Appendix F show large releases of rare gases, iodine, tellurium, and ruthenium during 10 to 15 minute exposures to air at temperatures of 1100 and 1200 C. Since the data indicate positive temperature coefficients for each species, comparable releases should occur in much shorter times at higher temperatures. On this basis the release percentage given in Table VII 1-5 may be treated as essentially instantaneous values. Note, however, that the releases apply only to the fraction of the UO_2 fuel that is expected to be dispersed into an air (oxygen)-containing atmosphere.

1.5 USE OF RELEASE COMPONENT VALUES

The four release components described above would occur more or less sequentially during a reactor meltdown accident. In all cases, the gap component would occur first, followed by the meltdown component, and then by the vaporization component. However, steam explosions could potentially occur any time after appreciable amounts of the core have melted. Thus, the oxidation component is somewhat randomly time oriented.

In using the release component values from Tables VII 1-2 through VII 1-5 to specify release source terms for a particular accident sequence, it should be obvious that proper inventory balances for each fission product must be maintained. For example, the fraction of the total inventory that experiences gap release is then not available for release by any of the other three processes. Consequently, care must be exercised in setting up release source terms. To illustrate this point, a basic release source summary is provided in Table VII 1-6. Here individual core release fractions are given for each component and fission product assuming that, except for the steam explosion fraction, the total core is involved in the release processes. That is, all fuel rod claddings rupture to give the gap release fraction, total core melting occurs, and all of the core melt contributes to the vaporization release fraction (unless preceded by a steam explosion). It is also implicitly assumed that a steam explosion will not precede total meltdown release.

It is emphasized that the single values listed in Table VII 1-6 are based on the best estimate values taken from Tables VII 1-2 through 1-5. Each of the values contains uncertainties as noted in those Tables and should, therefore, not be considered absolute release fractions.

References

1. Carbiener, W. A., et al "Physical Processes in Reactor Meltdown Accidents", WASH-1400, Appendix VIII, October, 1975.

2. Parker, G. W., et al., "Out-of-Pile Studies of Fission Product Release from Overheated Reactor Fuels at ORNL, 1955-1965", ORNL-3981, p 81 (July, 1967).

3. Feuerstein, H., "Behavior of Iodine in Zircaloy Capsules", ORNL-4543 (August, 1970).

4. Weidenbaum, B., et al., "Release of Fission Products from UO_2 Operating at High Power Rating", CONF-650407, Vol. 2, p 885-904, USAEC (1965).

5. Collins, R. D., et al., "Air Cleaning for Reactors with Vented Containments", CONF-660904, Vol. 1, p 419-452 (1967).

6. Lorenz, R. A., and G. W. Parker, "Final Report on the Second Fuel Rod Failure Transient Test of a Zircaloy-Clad Fuel Rod Cluster in TREAT", ORNL-4710 (January, 1972).

7. Chen, H., and P. E. Blackburn, "ANL Reactor Development Program Progress Report for September, 1969", ANL-7618, p 117 (October, 1969).

8. Crouthamel, C. E. and I. Johnson, "ANL Reactor Development Program Progress Report for July, 1971", ANL-7845, p 522 (August, 1971).

9. Genco, J. M., et al., "Fission-Product Deposition and Its Enhancement Under Reactor Accident Conditions: Deposition on Primary System Surfaces", BMI-1863, p 38 (March, 1969).

10. Jansen, G. and D. D. Stepnewski, "Fast Reactor Fuel Interactions with Floor Material After a Hypothetical Core Meltdown", Nucl. Tech. 17, 85-95 (1973).

11. Morrison, D. L., et al., "An Evaluation of the Applicability of Existing Data to the Analytical Description of a Nuclear Reactor Accident-Core Meltdown Evaluation", BMI-1910, Appendix B (July, 1971).

12. Ergen, W. K., et al., "Emergency Core Cooling: Report of Advisory Task Force on Power Reactor Emergency Cooling (USAEC).

13. Fontana, M. H., "An Estimate of the Enhancement of Fission Product Release from Molten Fuel by Thermally Induced Internal Circulation", Nucl Appl, 9, 364-375 (1970).

14. Fischer, J., J. D. Schilb, and M. G. Chasonov, "Investigation of the Distribution of Fission Products Among Molten Fuel and Reactor Phases. Part I - The Distribution of Fission Products Between Molten Iron and Molten Uranium Dioxide", ANL-7864 (October, 1971).

15. Parker, G. W., et al., "Out-of-Pile Studies of Fission Product Release from Overheated Reactor Fuels at ORNL, 1955-1965", ORNL-3981, p 4 (July, 1967).

16. Parker, G. W., et al., "Out-of-Pile Studies of Fission Product Release from Overheated Reactor Fuels at ORNL, 1955-1965", ORNL-3981, p 85 (July, 1967).

TABLE VII 1-1 FRACTIONS RELEASED TO GAP (TOTAL CORE)

Fission Product (decay half-life)	Calculated Fractions ANC[a]	BCL[b]	ORNL[c]	Chemical Groups	Average Release Fraction
Xe, Kr (long lived)	0.06	0.10	0.08		
Xe-133 (5.27 day)	0.04	0.02	0.02	Noble Gases	0.03[d]
Xe-135 (9.2 hour)	0.0002	0.004	0.004		
I, Br (long lived)	0.06	0.10	0.14		
I-131 (8.06 day)	0.06	0.03	0.05	Halogens	0.05[d]
I-132 (2.3 hour)	0.0007	0.005	0.006		
I-133 (20.8 hour)	0.007	0.01	0.02		
Cs, Rb (long lived)	0.20	0.05	0.21		0.15[e]
Cs-138 (32 minutes)	0.00001	0.0005	0.005	Alkali Metals	
Sr, Ba (long lived)	0.000004[f]	0.02	0.02		0.01[d]
Sr-89 (51 day)	-	0.01	0.015		
Sr-91 (9.7 hour)	-	0.002	0.01	Alkaline Earths	
Te-132 (78 hour)	(estimated value)			Tellurium	0.10[d]

(a) See Appendix B

(b) See Appendix A

(c) See Appendix C

(d) Values can be higher or lower by a factor of 4

(e) Value can be higher by a factor of 2 or lower by a factor of 4

(f) This value results from thermodynamic restrictions not considered in the other two models. See discussion of the escape fraction for this species.

TABLE VII 1-2 GAP RELEASE COMPONENT VALUES

Fission Product Species	Gap Release Fraction	Gap Escape Fraction	Total Gap Release Value
Xe, Kr	0.03[a]	1	0.03
I-Br	0.05[a]	1/3[c]	0.017
Cs, Rb	0.15[b]	1/3[c]	0.05
Sr, Ba	0.01[a]	10^{-4}[d]	0.000001
Te, Se, Sb	0.10[a]	10^{-3}[d]	0.0001
Others	-		Negligible[e]

(a) Values can be higher or lower by a factor of 4

(b) Value can be higher by a factor of 2 or lower by a factor of 4

(c) Values can be higher or lower by a factor of 3

(d) Values can be higher or lower by a factor of 100

(e) While no numerical value was developed for these various species, the number should not exceed that used for strontium-barium.

TABLE VII 1-3 MELTDOWN RELEASE COMPONENT VALUES

Elements	Release Range (percent)	Best Estimate (percent)
Xe, Kr	50-100	90
I, Br	50-100	90
Cs, Rb	40-90	80
Te[a]	5-25	15
Ba, Sr	2-20	10
Noble Metals[b]	1-10	3
Rare Earths[c]	.01-1	0.3
Zr, Nb	.01-1	0.3

(a) Includes Se, Sb
(b) Includes Ru, Rh, Pd, Mo, Tc
(c) Includes Y, La, Ce, Pr, Nd, Pm, Sm, Eu, Np, Pu

TABLE VII 1-4 VAPORIZATION RELEASE COMPONENT VALUES[a]

Fission Product	Release, Percent
Xe, Kr	100
I, Br	100
Cs, Rb	100
Te, Se, Sb	100
Ru, Rh, Pd, Mo, Tc	5[c]
Refractory Oxides[b]	1[c]

(a) Releases for the amount that remains after the gap and meltdown releases have occurred. The rate is approximated by an exponential function with a half-time of 30 min although this value is considered uncertain by an order of magnitude.

(b) Includes Sr, Ba, Y, La, Ce, Nd, Pr, Eu, Pm, Sm, Np, Pu.

(c) Values can be higher or lower by a factor of 5.

TABLE VII 1-5 FISSION PRODUCT RELEASES DURING STEAM EXPLOSIONS

Fission Product	Release From Oxidation, Percent	
	Range	Best Value
Xe, Kr	80-100	90
I, Br	80-100	90
Te, Se (Sb)	40-80	60
Ru (Mo, Tc, Pd, Rh)	80-100	90

TABLE VII 1-6 FISSION PRODUCT RELEASE SOURCE SUMMARY-BEST ESTIMATE TOTAL CORE RELEASE FRACTIONS

Fission Product	Gap Release Fraction	Meltdown Release Fraction	Vaporization Release Fraction[d]	Steam Explosion Fraction[e]
Xe, Kr	0.030	0.870	0.100	(X)(Y) 0.90
I, Br	0.017	0.883	0.100	(X)(Y) 0.90
Cs, Rb	0.050	0.760	0.190	--
Te[a]	0.0001	0.150	0.850	(X)(Y) (0.60)
Sr, Ba	0.000001	0.100	0.010	--
Ru[b]	--	0.030	0.050	(X)(Y) (0.90)
La[c]	--	0.003	0.010	--

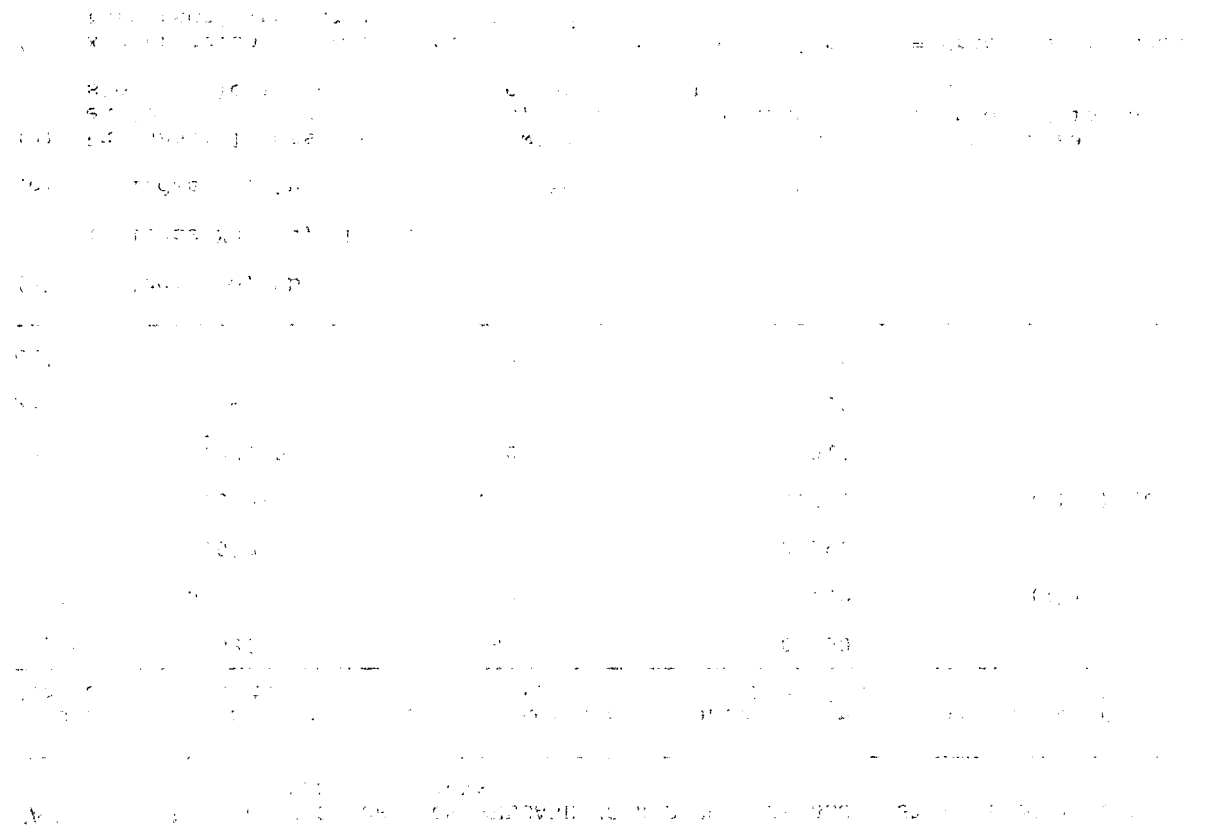
(a) Includes Se, Sb

(b) Includes Mo, Pd, Rh, Tc

(c) Includes Nd, Eu, Y, Ce, Pr, Pm, Sm, Np, Pu, Zr, Nb

(d) Exponential loss over 2 hours with halftime of 30 minutes. If a steam explosion occurs prior to this, only the core fraction not involved in the steam explosion can experience vaporization.

(e) X = Fraction of core involved in the steam explosion. Y = Fraction of inventory remaining for release by oxidation.



Section 2

Fission Product Release From The Primary Coolant System

Once fission products escape the core region, transport through portions of the primary coolant system is required to reach the containment atmosphere. Plateout or deposition on internal surfaces in the primary system could potentially limit the amount of activity that leaves the system. The retention of fission products would depend upon bulk gas flow rates (mass transfer rates), temperatures, materials properties (fission products and structural materials), and geometry, all of which vary with time and position in the system. Comprehensive analysis of this problem, if all the needed data were available, would require a complex mathematical model and would generate involved sets of fission product primary system release rates as a function of time. It was determined that such an approach was not feasible for this study. Instead, it was decided to use generalized bounding calculations of fission product behavior to develop simple retention factors for the primary system transport step. These factors are analogous to the gap escape fractions described earlier and can be termed primary system escape fractions.

General calculations relating to fission product retention in the primary system are described in Appendix I for iodine and in Appendix H for the solid fission products. These analyses concentrate on the upper region of the pressure vessel and on bulk steam flow conditions which would be characteristic of water boiloff during core meltdown. Therefore, the results are applicable to all PWR and some BWR accident sequences. Conclusions reached from the analyses regarding primary system escape fractions are summarized and discussed in the next subsection. This is then followed by an assessment of several special cases which can be encountered in some accident sequences where the analyses in Appendices H and I are not applicable.

2.1 GENERAL PRIMARY SYSTEM ESCAPE FRACTIONS

2.1.1 NOBLE GASES

Xenon and krypton are gases at room temperature and essentially inert chemically. These fission products would be carried directly out of the primary system by the bulk gas flow. Therefore, an escape fraction of unity should be used.

2.1.2 IODINE

The analysis presented in Appendix I utilizes experimental deposition data. It indicates that very limited deposition (at most a few percent) would occur in the upper region of either a PWR or a BWR pressure vessel, whether the iodine is assumed to be elemental or HI. This amount of retention is insignificant compared to that which would be carried out by the bulk gas flow so an escape fraction of unity should be used.

2.1.3 SOLID FISSION PRODUCTS

The bounding calculations described in Appendix H indicate that fission products, having normal boiling points below roughly 1500 F, should experience only temporary retention on internal pressure vessel surfaces during a reactor core meltdown. The slight time delay in transport out of the vessel is expected to have no appreciable effect on the subsequent fate of these species in the containment volume. The fission products that would generally exhibit this behavior include the alkali metals (cesium and rubidium) the tellurium group (tellurium, selenium, and probably antimony), and the alkaline earths (strontium and barium). Therefore, an escape fraction of one should be used for these species.

Conclusions formulated in Appendix H also indicate that an escape fraction of one should be used for the noble metals (ruthenium) and rare earth group (yttrium) because of the potential for particle formation. If ruthenium released from the core region should convert to the volatile oxide during transport in the pressure vessel, then an escape fraction of unity is even more certain.

It is important to note that the core meltdown release values given in Table VII-1-3 being used for the solid fission products are based to a large extent on experimental melting studies. The experimental data are usually indicative of releases from a high temperature region of the apparatus rather than from the peak (melting) temperature location. Since the pressure vessel should reach comparable temperatures during and fol-

lowing core meltdown, one would, by analogy, expect complete escape of the meltdown release fractions. The calculations pertaining to plateout in Appendix H tend to support this conclusion and offer some insight concerning the reasons and processes that could be involved.

2.2 SPECIAL CASES OF PRIMARY SYSTEM RETENTION OF FISSION PRODUCTS

Three special situations were identified in which the use of unit escape fractions for released fission products in the primary coolant system should perhaps be modified. Modifications were made in two of these cases but not in the third.

2.2.1 PWR COLD LEG PIPE BREAK

For a cold leg break in a PWR, steam or steam-hydrogen flow from the core region will pass through the upper plenum of the pressure vessel just as for a hot leg break. However, instead of exiting directly to the containment vessel, the gas and fission product vapors must then travel through the steam generator section in order to reach the containment. The large surface area of the steam generator tubes and the relatively low temperatures (initially about 500 F) would present favorable conditions for plateout of condensable species. No retention of the noble gases would occur and the analysis in Appendix I indicates that very limited deposition of fission product iodine would be expected. Therefore, an escape fraction of unity for these two species is still valid.

The solid fission products should experience high retention during the early phases of core meltdown. Exceptions could result from penetration of particulates containing low volatility fission products. Otherwise, plateout would be expected to occur at the head end of the steam generator tubes. The plateout area would heat-up due to heat transfer from the incoming bulk gas and absorption of decay energy from the condensed fission products. Fission product vaporization followed by re-condensation farther along the tubes could occur repetitively and smear the activity out. The eventual loss of bulk gas flow might leave this fission product material deposited in the steam generator. On the other hand, steam generator tube temperatures may rise sufficiently to cause significant fission product escape before loss of bulk gas flow.

This complex heat and mass transfer problem was not analyzed. Instead, it was decided to treat both types of pipe breaks identically with respect to primary system solid fission product retention; i.e., unit escape fractions were used regardless of break location. This represents worst conditions for release of radioactvity to the containment space, an assumption which appears valid for hot leg breaks but possibly overpessimistic for cold leg breaks.

2.2.2 BWR CORE MELTDOWN WITH ECC INJECTION

For a BWR loss of coolant accident resulting from a recirculation line break, it is conceivable that a situation develops in which abnormal conditions in the reactor core prevent effective cooling even though normally adequate emergency coolant pump flow is achieved. Thus, core melting and metal-water reaction occurs, but either the affected region is surrounded by ECC water (due to core spray and low pressure injection flow) or the opening in the pressure vessel is submerged under several feet of water (due to flooding to the top of the jet pumps). This presents a unique environment for the fission products that are liberated during fuel melting.

In either condition the released fission products, carried by the bulk steam-hydrogen mixture, must pass through several feet of water in order to escape from the pressure vessel. The steam should be condensed but the remaining hydrogen will provide the driving force for carrying fission product activity out to the primary containment. The amount of fission product activity which does escape will depend on the trapping capability of the water and the degree of deposition on upper vessel structures. Deposition may only delay the escape of activity as vessel temperatures eventually rise, and fission products trapped in the ECC water could circulate within the pressure vessel, sometimes encounter the melting core region, and undergo vaporization again. Consequently, the determination of a primary system retention factor is not as straight-forward as it would first appear.

Recognizing that the core meltdown fission product release fractions defined earlier contain an implied primary system plateout factor, the escape fraction for this flooded meltdown situation should consider only the retention effect of the ECC water. Limited work on fission product cleanup in steam suppression systems (Ref. 1) offers some basis for estimating this effect. The

data indicate decontamination factors (the reciprocal of escape fraction) ranging from about 10^1 to 10^3 for iodine and particle removal from steam-air mixtures passed through a water flute. While the geometry and temperature conditions are different than indicated for the present problem, the fundamental process in both cases is the removal of trace species from a condensable-noncondensable gas mixture during passage through a water column. Because of the more severe conditions, the possibility of ineffective removal must be considered.

Therefore, escape fractions extending from one (no retention) down to 0.001 (high retention) appear feasible. A value of 0.1 should be used for realistic accident calculations.[1]

2.2.3 BWR DRY VESSEL MELTDOWN

A second BWR accident situation that leads to unique conditions for escape of released fission products from the pressure vessel is a dry core heatup starting with the end-of-blowdown conditions. In this accident there is no water in the pressure vessel (no ECC delivery) and consequently no boiloff steam flow occurs to carry fission products out of the vessel. Therefore, the only gas flow driving fission products out of the vessel is due to simple gas expansion as internal temperatures increase from decay heating. (The fission product noble gas inventory, about 4.5 lb-moles, would not contribute significantly to the total gas content of the vessel.)

Thermal analyses (Ref. 2), for dry heatup in a typical BWR indicate steam flow velocities in the steam separators of less than a foot per minute. Thus, fission products escaping from the core should spend at least on the order of half an hour in the steam separator and dryer region of the pressure vessel. As the fission products plate out and decay, much of the fission product decay heat would be absorbed in the structural material above the core during this time period. Table VII 2-1 lists average temperatures of the structural material above the core for different accident times. These temperatures were calculated assuming that all of the decay heat lost from the core due to fission product release is absorbed in the material above the core. The weight of the material was 229,000 lb. The results indicate that the decay heat of the released fission product is insufficient to completely melt all the steel structure above the core at an accident time of one hour. However, since core meltdown has been estimated to require about two hours, it appears that pressure vessel temperatures of about 2800 F would be reached sometime during the latter half of the meltdown period.

Therefore, from the beginning to the end of core melting, the absolute temperature inside the pressure vessel should approximately triple, producing a corresponding expansion of the contained gases. Accordingly, when the meltdown period is completed about two-thirds of the original gas will have expanded out of the vessel. Ignoring retention on internal surfaces because of the high temperatures, this fraction can be used to approximate the escape of fission products released from the core during meltdown. Thus, at the end of core meltdown in accident sequences of this type, 2/3 of the fission product release term is assumed to have escaped the pressure vessel, and the other 1/3 is assumed to remain as vapors inside the vessel.

2.3 SUMMARY OF PRIMARY SYSTEM ESCAPE FRACTIONS

2.3.1 PWR SYSTEMS

An escape fraction of one for all fission products is used in all calculations of PWR accidents regardless of pipe break location.

2.3.2 BWR SYSTEMS

In BWR accident sequences where water boiloff after ECC interruption occurs, an escape fraction of one is used for all fission products.

In BWR accident sequences where ECC flow occurs but with core meltdown, an escape fraction of one is used for noble gas fission products but a value of 0.1 is used for all other fission products.

In BWR accident sequences where no ECC delivery ever occurs, it is assumed that at the end of core meltdown, 2/3 of all fission products that have been released will have escaped the pressure vessel.

---

[1] For noble gases a value of unity should be used.

References

1. Diffey, H. R., C. H. Rummary, M. J. S. Smith and R. A. Stinchcombe, "Iodine Cleanup in a Steam Suppression System", British Report AERE R-4882 (1965).

2. Carbiener, W. A., et al "Physical Processes in Reactor Meltdown Accidents", WASH-1400, Appendix VIII, October, 1975.

TABLE VII 2-1 ESTIMATED AVERAGE TEMPERATURES OF UPPER STRUCTURAL MATERIAL IN A BWR PRESSURE VESSEL DURING DRY MELTDOWN

Accident Time (minutes)	Average Temperature, F
0	550
20	800
40	1200
60	1680
80	2240
95	2750

Section 3

Fission Product Leakage From The Containment System

Analysis of fission product behavior in the reactor containment system is the final step in specifying the accident source term. The amount of radioactive material which escapes this barrier constitutes the source for dispersion in the natural environment. Fission products injected into the containment space by one of the four release processes will undergo removal from the internal atmosphere by a combination of mechanisms. The exact combination would vary among different plant types and accident-sequence conditions, but common to all is the removal that would occur as a result of natural transport and deposition processes. Various engineered safety systems can operate to remove fission products from containment atmospheres; i.e., aqueous spray systems and recirculating filter units in PWR plants, and suppression pool scrubbing and once-through filter units in BWR plants. The size of the fission product source which escapes to the environment critically depends upon how effectively the removal processes within containment compete with leakage from the containment. Analysis of this problem of competing rate processes required development of rate models.

3.1 PWR CONTAINMENT MODELS

Models developed for PWR accident sequence analyses were of two types; (1) a single-volume hand calculation model, and (2) a multicompartment computer coded model. The single volume model was used for preliminary hand calculations of PWR accident sequences using simplified constant rate coefficient values. The multicompartment model was developed and used for all detailed accident sequence calculations, incorporating variable rate coefficients, multivolume capabilities, and time variable fission product input and containment leakage quantities. The two models are described below.

3.1.1 SINGLE VOLUME CONTAINMENT MODEL

The single volume containment model assumes that the vapor phase consists of one well-mixed compartment. This assumption enables one to write the following single differential equation for each fission product species:

$$\frac{dC_i}{dt} = -\left(\sum_j \lambda_{ij}\right) C_i - \alpha_i C_i + R_i(t) \qquad \text{(VII 3-1)}$$

Initial Condition: $C_i = C_i(t')$ at $t = t'$

C_i = airborne moles of component i

λ_{ij} = removal rate constant via mechanism j

α_i = leak rate, fraction of the volume/time

$R_i(t)$ = source term (moles/time).

This equation is easily solved for constant λ_{ij}, α_i and R_i to get

$$C_i = \frac{R_i}{(\Sigma\lambda_{ij} + \alpha_i)} - \left[\frac{R_i}{(\Sigma\lambda_{ij} + \alpha_i)} - C_i(t')\right] \exp -(\Sigma\lambda_{ij} + \alpha_i)(t-t') \qquad \text{(VII 3-2)}$$

The escaped amount during the interval $t-t'$ is the integral

$$Q_i = \int_{t'}^{t} C_i V \alpha_i \, dt,$$

where V is the volume of the vessel. Thus

$$Q_i = \frac{R_i V \alpha_i}{(\Sigma\lambda_{ij} + \alpha_i)}(t-t') - \left[\frac{R_i}{(\Sigma\lambda_{ij} + \alpha_i)} - C_i(t')\right]\left(\frac{\alpha_i V}{\Sigma\lambda_{ij} + \alpha_i}\right) \times \left[1 - \exp\left[-(\Sigma\lambda_{ij} + \alpha_i)(t-t')\right]\right]. \qquad \text{(VII 3-3)}$$

The two equations for $C_i(t)$ and $Q_i(t-t')$ can be used to calculate airborne fractions and leakage fractions for various accident sequences by hand. The values of R_i to be used for various species are

described in earlier sections of this report. The only release of fission products encountered where R_i = constant for some time period is the melt release. This simplifies most of the computations to using an initial condition for a time period where the λ_{ij}'s and α_i's are considered to be constant. If the λ's or α's change at some time, t', a new t' should be considered as the beginning of a new time period of constant new λ's or α's. The bases for the various values of λ_{ij} are discussed in Appendix J and a list of these coefficients is given in Table VII 3-1. Values of α_i must be specified from analyses of containment response for the accident sequence being calculated.

3.1.2 MULTICOMPARTMENT CONTAINMENT MODEL

To better simulate containment geometry and time variable removal rates, a model was developed to analyze the atmospheric source from a set of compartments whose airborne contents are well mixed and are altered by intercompartmental flow in addition to deposition rates, leak rates, spray removal rates, etc. This system is described by a set of equations of the form

$$dC_i^{mr}/dt = \sum_j H_{ij}^{mr} C_j^{mr} \qquad \text{(VII 3-4)}$$

where

C_i^{mr} = airborne fraction of initial release of material m in release type r contained in compartment i

$$H_{ij}^{mr} = \left(\lambda_i^{mr} + \sum_j G_{ki}/V_k\right)\delta_{ij} + (G_{ji}/V_j)\left(1-E_{ji}^{mr}\right)$$

λ_i^{mr} = removal coefficient from compartment i by settling, leak, spray removal, and other processes not involving flow to or from another compartment

G_{ji} = volume flow rate from compartment j to compartment i

E_{ji}^{mr} = filter removal fraction for material m from release r

V_j = volume of compartment j

$\delta_{ij} = 1$ if $i = j$

$\delta_{ij} = 0$ if $i \neq j$

Note that the flow terms assume uniform mixing within each compartment.

For a given release type and material type, the equation set can be written in matrix notation

$$\frac{dC}{dt} = HC \qquad \text{(VII 3-5)}$$

Where C is the column vector of airborne release fractions in the respective compartments and H is the matrix of rate constants governing the evolution. The solution of this differential equation for the column vector C for constant coefficients in the H matrix is given exactly by

$$C(t) = e^{Ht} C(o) \qquad \text{(VII 3-6)}$$

or

$$C(t) = C(t_o) + (t-t_o) H \left(\frac{e^{(t-t_o)H}-1}{(t-t_o)H}\right) C(t_o). \qquad \text{(VII 3-7)}$$

Fast computer techniques for generating this solution have been developed by B. H. Duane (Ref. 1) and were utilized here. By calling the numerical integration subroutines developed by Duane at each time step after calculating the H matrix, the accuracy limit becomes that imposed by the assumption of constant H matrix elements within the time step. Numerical error in generating the solution to the coupled set of equations with constant coefficients can be made on the order of 10^{-6} percent.

To integrate the amount leaked within the time step, N additional fictitious compartments were defined whose function is to accumulate the leaked material from the N real compartments. The fractions C_{i+N}, i = 1, 2, ···N, are cumulative leaks obtained from the solution of

$$\frac{d}{dr}(C_{i+N}) = \alpha_i C_i$$

where α_i is one part of H_{ii}. The previously defined N x NH matrix was

augmented to form a 2N x 2N H matrix according to

$$H_{i+N,j} = \alpha_k \delta_{ij}$$

$$H_{i,j+N} = 0 \qquad \text{For } i = 1, 2, \cdots, N$$

$$H_{i+N,\ j+N} = 0 \qquad j = 1, 2, \cdots, N$$

If one takes the material quantity in the fictitious compartments to be zero at the start of a time step, the fraction of the initial release material leaked during the time step will be

$$\sum_{i=N}^{2N} C_i .$$

Computer code CORRAL[1] was written to solve the set of equations and at the same time compute each rate parameter as a function of time and/or as a function of vessel conditions (p, T, humidity). A more detailed description of the various models used to compute rate parameters follows.

Nine time dependent parameters are computed from input data at the time of solution of the differential equations. These are:

1. Compartment pressure, p(k), psig
2. Compartment temp, T(k), F
3. Compartment vapor mole fraction, VAP(k)
4. Compartment wall-bulk temperature difference, DELTA T(k), F
5.-6. Leak rates of molecular iodine and particulates from each compartment, ELI2(k), ELP(k), fractions/hr
7. Flow rates between compartments, G(j, k), ft^3/hr
8.-9. Filter decontamination efficiencies for flow between compartments, EFI2(J,K), EFP2 (j,k); dimensionless.

The first four parameters enable one to compute transport coefficients involved in depletion rate coefficient calculations.

The bulk gas viscosities of steam-air mixtures (μ_m) are computed according to the following equations (Ref. 2):

$$\mu_m = \frac{\mu_A}{1 + \frac{y_s}{y_a}\phi_{As}} + \frac{\mu_s}{1 + \frac{y_A}{y_s}\phi_{sA}}, \qquad \text{(VII 3-8)}$$

where

μ_m = viscosity of mixture

$$\mu_A = 0.0414 \left[\frac{T, R}{492}\right]^{0.768}, \text{ lb/ft/hr}$$

$$\mu_s = \frac{0.003339\ (T, R)^{1.5}}{(T_R + 1224.2)}$$

y_A = mole fraction of air

y_s = mole fraction of steam

$$\phi_{As} = \frac{\left[1 + \left(\frac{\mu_A}{\mu_s}\right)^{1/2}\left(\frac{\mu_s}{\mu_A}\right)^{1/4}\right]^2}{2\sqrt{2}\left[1 + \left(\frac{\mu_A}{\mu_s}\right)\right]^{1/2}}$$

ϕ_{sA} = above with subscripts reversed.

The diffusivity of I_2 in the steam-air mixtures was found using data and equations from Knudsen (Ref. 2).

$$D_{I_2} = \frac{1}{\frac{y_A}{D_A} + \frac{y_s}{D_s}}, \qquad \text{(VII 3-9)}$$

where

$$D_A = 2.03\ \text{E-05}\ (T, K)^{1.5}/(P, atm)/W_A, \ cm^2/sec$$

$$D_B = 3.24\ \text{E-05}\ (T, K)^{1.5}/(P, atm)/W_S$$

$$W_A = 0.7075 + 141.73/T, K$$

$$W_S = 0.7075 + 454.72/T, K.$$

The diffusivity of I_2 in water (spray drops) was computed using the standard Wilke-Chang relationship (Ref. 2), where

[1] Containment Of Radionuclides Released After LOCA.

$$D_\ell = \frac{(7.4 \times 10^{-8})(xM_\ell)^{1/2} T(K)}{\mu_L V^{0.6}}, \text{ cm}^2/\text{sec}, \quad \text{(VII 3-10)}$$

where

x = degree of solvent association = 2.6 for H_2O

M_ℓ = molecular weight of solvent

μ_L = solvent viscosity, cp

μ_L = 100/{2.1484 [(T, (K) - 281.6) + (8078.4 + (T,(K)-281.6)^2)$^{0.5}$] -120} for H_2O

V = molar volume of diffusing substance = 71.5 cm^3/gmole for I_2.

3.1.2.1 Natural Deposition.

The mechanism of natural deposition of I_2 is governed by diffusion with natural convection generated by temperature differences between bulk gas and the wall (DELTAT(k)). Knudsen and Hilliard (Ref. 3) claim that a mass transfer analogy can be made with correlations predicting natural convective heat transfer coefficients. In similar manner, the model uses expressions for Sherwood numbers for laminar and turbulent flow using a thermal Grasholf number,

$$Gr = \ell^3 \frac{(T_{wall} - T_{bulk})}{(\mu_M/\rho_m)^2 T_{bulk}} g.$$

Thus for laminar flow ($Gr < 10^9$), the Sherwood number is

$$N_{Sh} = \frac{k_c \ell}{D_{I_2}} = 0.59 (Gr\ Sc)^{1/4}, \quad \text{(VII 3-11)}$$

and for turbulent flow ($10^9 < Gr < 10^{12}$),

$$N_{Sh} = \frac{k_c \ell}{D_{I_2}} = 0.13 (Gr\ Sc)^{1/3}, \quad \text{(VII 3-12)}$$

where

Sc = Schmidt number = $\mu_M/\rho_M D_{I_2}$

ℓ = length of the wall

k_c = mass transfer coefficient.

A combination of the two Sherwood numbers is used to compute the actual Sherwood number. Since the turbulence in most cases occurs around 10 ft from the top of the wall, a weighted average was used.

$$N_{Sh}\ (\text{overall}) = \frac{\ell - 10}{\ell} N_{Sh}\ (\text{turbulent}) + \frac{10}{\ell} N_{Sh}\ (\text{laminar}).$$

To convert the mass transfer coefficient into a deposition lambda (λ_{ij}) is a simple step. Thus,

$$\lambda_{ij}(k) = k_c(k)\ A(k)/V(k)$$

where A(k) and V(k) are surface area and volume of compartment k, respectively.

Another natural deposition process of interest is the settling of particulates. This involves a calculation of terminal settling velocities, V_s assuming spherical, unit density particles.

$$d^2 (\rho_p - \rho_m)\ g/18\ \mu_m = V_s \quad \text{(VII 3-13)}$$

Particle diameters used were considered as functions of time. Hilliard and Coleman (Ref. 4) report that the settling velocities decrease with time after release. In CORRAL it was decided to use their data and assign an early particle diameter (15μ) and a late particle diameter (5μ) ("several hours" later = 4 hours) and linearly interpolate between them. After 4 hours the particle size was kept constant at the late value. To get the natural deposition lambda for particulates use

$$\lambda = V_s \frac{A\ (\text{floor area})}{V\ (\text{compartment volume})}$$

3.1.2.2 Spray Removal.

The spray removal model of I_2 by boric acid and caustic sprays used in CORRAL combines a gas phase mass transfer coefficient, a drop-gas interfacial equilibrium distribution coefficient and a stagnant liquid film mass transfer coef-

ficient. The expression for the spray lambda (s) is given by

$$\lambda = \frac{FH}{V}\left[1 - \exp - \left(6\frac{k_g\, t_e}{d(H + k_g/k_\ell)}\right)\right] \qquad \text{(VII 3-14)}$$

where

F = spray flow rate

H = equilibrium distribution coefficient ($C_g = C_\ell/H_j$ at equil.)

V = spray compartment volume

d = spray drop diameter

t_e = drop residence time - height of fall/terminal velocity

and the gas mass transfer coefficient, k_g, is given by Ranz and Marshall (Ref. 5) as

$$k_g = \frac{D_{I_2}}{d}\left\{2.0 + 0.60\ Re^{1/2}\ Sc^{1/3}\right\}$$

and

$$k_\ell = \frac{2\pi^2 D_\ell}{3d}$$

$D_\ell = I_2$ diffusivity in liquid.

The latter is the Griffiths model discussed by Postma (Ref. 6). Incorporating the latter is a more conservative approach when $k_g/k_\ell \geq 5$ H. The terminal velocities of the falling drops are found by matching the velocity independent dimensionless number

$$f_D\ Re^2 = 4\ \rho_M\ (\rho_L - \rho_M)\ d^3\ g/3\mu_M^2$$

with the appropriate range of Reynolds number (Re). For spray drops the range of Re is 10-700. For $10 < Re < 100$, $f_D Re^2 = 15.71\ Re^{1.417}$, and for $100 < Re < 700$, $f_D Re^2 = 6.477\ Re^{1.609}$ (Ref. 7).

Spray lambdas for removal of particles follow the equation (Ref. 8):

$$\lambda = \frac{3F\ Eh}{2\ V\ d}, \qquad \text{(VII 3-15)}$$

where

F = spray flow rate
h = spray fall height
d = spray diameter
V = compartment volume
E = Spray collection efficiency.

In CORRAL empirical results from CSE data are used to predict E. Apparently the efficiency is a function of a normalized liquid volume sprayed (total volume sprayed/total compartment volume - Ft/V). Figure VII 3-1 shows the CSE data, and the curve in this figure was used to compute drop collection efficiencies in CORRAL. The diffusiophoresis was subtracted from the efficiency and the following expressions were fit to the remaining curve. To make these relationships apply to a spray lambda

Ft/V	E
0 - 0.002	$E = -15.825\ (Ft/V) + .055$
.002 - .0193	$E = .04125 - [.08626 + 42.68\ (Ft/V)]^{1/2}/21.34$
.0193	$E = .0015$

with multiple sprays being used at various times, the quantity Ft/V is now the sum $\Sigma\ F_i\ t_i/V$ for any one release of particles. Each release of particles would have its own spray aging relationship, and at this time no simple means of tying sequential release together into one relationship seems possible. Only when particle size distributions are known throughout a spray aging process can sequential releases be tied together.

It should be noted that in CORRAL, no spray cutoff is used at $C(t)/C(0) = .02$; spray aging is used in its place.

3.1.2.3 I_2 Equilibrium.

When airborne molecular iodine is depleted by either sprays or natural deposition, the depletion rate becomes independent of the two above mechanisms when the concentration falls below about 1 percent of the initial value (a conservative estimate, i.e., a lower value is less conservative (Ref. 8). At concentrations below this level, an apparent equilibrium situation exists where the concentrations in liquid and gas phases are related by an equilibrium distribu-

tion constant, $H = C_\ell/C_g$. H is a function of time (probably due to slow liquid phase chemical reaction) and has been experimentally determined. In program CORRAL it has been possible to incorporate $H = H(t)$ when equilibrium conditions exist.

To get the equilibrium described quantitatively, an equivalent lambda for depletion of gas phase I_2 had to be developed, since the value of H increases with increasing time, the gas phase is being depleted as time goes on. To get this equivalent lambda, we can write a mass balance for I_2. If C_{go} is the initial airborne concentration, then

$$C_{go}\, V_g = C_\ell\, V_\ell + C_g\, V_g \qquad \text{(VII 3-16)}$$

or

$$\frac{C_g}{C_{go}} = \frac{C_g\, V_g}{C_\ell V_\ell + C_g V_g} = \frac{1}{\frac{C_\ell V_\ell}{C_g V_g} + 1} = \frac{1}{H\frac{V_\ell}{V_g} + 1}. \qquad \text{(VII 3-17)}$$

Then for $H = H(t)$, we can write the removal rate of I_2 by

$$d\,\frac{C_g/C_{go}}{dt} = -\frac{1}{\left(H\,\frac{V_\ell}{V_g} + 1\right)^2}\left(\frac{V_\ell}{V_g}\right)\frac{dH}{dt}$$

where the equivalent lambda is

$$\frac{dCg}{Cg} = -\left\{\left(\frac{1}{H\,\frac{V_\ell}{V_g} + 1}\right)\frac{V_\ell}{V_g}\,\frac{dH}{dt}\right\} dt = -\lambda dt. \qquad \text{(VII 3-18)}$$

Data show that $H\, V_\ell/V_g >> 1$ for boric acid and caustic solutions in equilibrium with I_2, so that

$$\lambda = \frac{1}{H}\,\frac{dH}{dt}. \qquad \text{(VII 3-19)}$$

Typical data for sprays are shown in Tables VII 3-2 and VII 3-3.

3.1.2.4 Intercompartmental Flow Rates.

In two cases intercompartmental flow rates can be calculated. If circulation fans move air throughout the containment vessel or if boil-off occurs with steam evolution into one compartment, one can use these flow rates to provide a basis for estimating intercompartmental flows. In addition, natural convection driven by wall-bulk gas temperature differences can be a major contributor to flow rates. These rates can be estimated but with a high degree of uncertainty. In this study, high flow rates have been used to eliminate mixing as a parameter. Numerically, the high flow rate selected was equivalent to 10 PWR containment volumes per hour.

3.1.2.5 Design of CORRAL for PWR Analyses.

A schematic diagram of the containment geometry used in CORRAL-PWR calculations is given in Fig. VII 3-2. Four internal compartments of a large PWR containment vessel are modeled.

a. The Primary Cubicle - The small internal compartment which houses the piping, steam generator, and pump of one of the primary coolant loops, specifically the loop which experiences the large pipe break.

b. The Main Volume - The large space above the reactor cavity inside the polar crane wall and including the high dome. This volume is sprayed.

c. The Outer Annulus - The annular volume between the polar crane wall and the containment vessel outer wall.

d. The Lower Volume - This corresponds to the basement or the lowest level inside the containment structure.

The gas flow path between the four compartments is indicated on the diagram. The interchange between compartments 1 and 2 (Q_O) is determined by the primary system steam generation rate, while the circulation flow between compartments 2, 3, and 4 (Q_F) is set at a high value (as noted in the previous section) to simulate efficient interchange between these volumes. The PWR contaminant is thus divided into four well-mixed regions having different rates of airborne fission product removal. The removal processes that are included for each compartment are listed below the diagram along with the fission product injection locations. Note that all external leakage from the containment is assumed to occur from the outer annulus. Due to the well-mixed condition that is used, this affects only the amount of deposition that is calculated to occur in this

compartment and not the total inventory that leaks. An exception to this leakage path definition occurs when accident sequence analysis specifies puff releases from containment (i.e., sudden failure by explosion or overpressure). In such cases the same volume percent of the airborne contents of all four compartments is included in the puff loss value.

3.2 BWR MULTICOMPARTMENT MODEL

The multicompartment feature of code CORRAL was essential to estimating atmospheric source calculations from a BWR. A BWR containment system is not a set of openly connected compartments like a PWR, where the whole containment system can be usually considered as "well mixed". The compartments of a BWR are usually closed to one another and flows between them occur in complex ways during postulated accidents.

As many as six compartments are used in some BWR accident sequences. The first five are:

a. The Drywell where natural deposition can occur.

b. The Wetwell where pool scrubbing and natural deposition can occur.

c. The Drywell annular gap where natural deposition can occur.

d. The Reactor Building where natural deposition can occur.

e. The Standby Gas Treatment System (a series of filters).

The sixth compartment used was a fictitious dumping ground for ground level atmospheric sources when elevated (stack) sources occurred simultaneously. The schematic diagram of CORRAL for BWR accidents is shown in Fig. VII 3-3.

Natural deposition is the most common removal mechanism for fission products, although it is not necessarily the most effective mechanism. Natural deposition of particulates occurs on horizontal surfaces in all large compartments just as in a PWR. Turbulent deposition of particulates and iodine in the drywell annular air gap are via different mechanisms to be discussed later. Natural deposition of iodine occurs on all surfaces with the rate controlled by natural convection as discussed for the PWR model. However, since the wall-bulk gas temperature difference that drives the natural convection is highly variable in a BWR, transient heat transfer analyses are made to estimate this temperature difference.

3.2.1 NATURAL DEPOSITION - EFFECT OF HEAT TRANSFER FROM BWR VESSEL WALLS

The mass transfer coefficient for I_2 removal (see Appendix J) is proportional to the temperature-difference,

$$T_{wall} - T_{bulk} = \Delta T_w$$

raised to the 1/4 or 1/3 power. For an order of magnitude range in ΔT_w, the mass transfer coefficient changes by only a factor of 2, a relatively insignificant change. However, during rapid cooling of the drywell (depressurization), ΔT_w can span more than an order of magnitude for short durations. During rapid heating, the condensing heat transfer coefficient is large (h = 150 Btu/hr ft^2 F) and a steady ΔT_w is rapidly reached. This is about 0.14 F in the drywell. In cooling, the heat transfer coefficient from the steel (approximately one inch thick) wall is low (2-5 Btu/hr ft F), and can lag behind the bulk gas temperature for some time. Neglecting any temperature gradient in the steel, for a sudden step change in bulk gas temperature, ΔT_s, the temperature-difference, ΔT_w, is given by

$$\Delta T_w = \Delta T_s \exp\left(-ht/\ell_\rho c_p\right) \qquad \text{(VII 3-20)}$$

where

h = heat transfer coefficient

t = time after ΔT_s

ℓ = wall thickness

ρ = wall mass density

C_p = wall heat capacity (per unit mass)

If the temperature change is gradual, i.e., linear with respect to time, the temperature-difference, ΔT_w, is now given by

$$\Delta T_w = (\beta\, \ell_\rho c_p/h)\left[\exp - (ht/\ell\rho c_p) - 1\right] \qquad \text{(VII 3-21)}$$

where β is the linear bulk-gas cooling rate, F/hr. Equations VII 3-20 and VII 3-21 are used to compute ΔT_w for various time intervals during cooling in the drywell and wetwell. Values of h depend on gas velocities in the above compartments as well as the drywell annular air gap.

Little information could be readily obtained to estimate ΔT_w's in the main reactor building. These would be highly dependent on positions in the building and the outside environment temperatures, as well as gas flow parameters from the reactor. To allow for some minimum natural deposition in the main building, $\Delta T_w = 0.1$ F was used. This would result in a natural deposition rate of $\lambda = 0.5\ hr^{-1}$ in the main reactor building for I_2. This λ is five times the gas displacement rate for the building under normal conditions (2,000 cfm through the Gas Treatment System).

3.2.2 POOL SCRUBBING

In a number of BWR accident sequences, gas flow occurs through the vent lines from the drywell to the wetwell water pool. The water pool occupies slightly over one-half the toroidal volume of the wetwell and is approximately 17-feet deep. Pool scrubbing is a major decontamination mechanism. Some data exists on pool scrubbing, but comprehensive experimental studies on pool scrubbing in a BWR wetwell pool that include investigations of all parameters (a wide range of particle sizes, steam quality, pool temperatures, flow rates, I_2 concentrations, downcomer L/D ratios, etc...) have not been reported. Applying such data, if available, would not have refined atmospheric source estimates greatly because the available data show that scrubbing is fairly effective on the fission products entering the pool. Also, trial calculations showed that often 30 percent or more of the available fission products in any sequence would escape the primary containment by other paths (such as through the drywell annular gap directly to the secondary containment system).

The best available data appear in a paper by Diffey, Rumary, et al. (Ref. 10), where I_2, methyl iodide, and .06 μ particles in a steam-air mixture were pool scrubbed. The typical decontamination factors were 100 for I_2, 2 for CH_3I, and 50-100 for the .06 μ particles with 90 percent steam-air mixtures (higher steam fractions give better decontamination). For CORRAL-BWR cases, the values used are 100 for both I_2 and particles, and 1.0 for CH_3I. A decontamination factor of 1.0 is also used for the noble gas fission products.

The frequent result of higher than 90 percent steam partially justifies the use of DF = 100 for particles. Even though the BWR accident particles are assumed to be 5-15 μ, or much more massive than those studied above, the scrubbing of particles is largely due to diffusiophoresis (condensing steam on the bubble wall carries particles), and therefore largely independent of particle size. However, larger particles would have more boundary layer penetration inertia in a rapidly circulating bubble and this should then further justify the choice of DF = 100 for particles, rather than the lower DF = 50.

3.2.3 STANDBY GAS TREATMENT SYSTEM - (SGTS)

The SGTS in a typical BWR is a set of two parallel filter trains upstream from three exhaust fans that releases filtered secondary containment building air at an elevated level via a stack. However, under accident conditions only one of the filter trains would normally be used; the other being held in reserve. The SGTS keeps the building at subatmospheric pressures to minimize ground level leaks.

Under normal conditions, the flow rate through the system is about 2,000 cfm but the exhaust fans are capable of 10,000 cfm. Sources in excess of this maximum would create positive building pressures and produce a ground level, unfiltered source. The filter trains, according to plant Technical Specifications, are routinely tested to insure the following removal efficiencies at all flow rates up to the 10,000 cfm maximum:

- 99% for particulates
- 99% for elemental iodine
- 99% for organic iodide

These specifications are derived essentially from in-place testing criteria published by the USAEC in Regulatory Guide 1.52. The criteria incorporate limits on bypass flow for the filter and adsorber sections. It is recognized that substantially better performance may be realized for the filter system during actual use. This is because the specifications implicitly anticipate some deterioration in system effectiveness between testing steps which may or may not occur. However, since filtered leakage will be a minor contributor to overall accident consequences for meltdown sequences in the BWR, the efficien-

cies given above were used in all CORRAL calculations. In addition, CORRAL is programmed to identify the filter and adsorber activity loadings to discover possible overheating conditions, at which time the filtration efficiencies would decrease significantly.

The overheating criteria for both the HEPA filters and for the charcoal beds were based upon typical thermal performance data obtained from Safety Analysis Reports and the design temperature limits for the components; 250 F at 2000 cfm for the HEPA filters and 640 F at 2000 cfm for the charcoal filters. The heating rate of the filters (Q_F) was assumed proportional to the temperature difference between the filter material and the flowing inlet air.

$$Q_F \alpha (T_{Filter} - T_{Air,\ inlet}) \qquad \text{(VII 3-22)}$$

For the maximum heating rate $T_{Filter} = T_{Design}$. The inlet air temperature, by definition, is

$$T_{Air,inlet} = \bar{T}_{Air} - \frac{\Delta T_{Air}}{2} . \qquad \text{(VII 3-23)}$$

The change in air temperature is given by a heat balance,

$$\Delta T_{Air} = \frac{Q_F}{\rho w C_p} \qquad \text{(VII 3-24)}$$

where

ρ = air density
w = air flow rate
C_p = air specific heat

Reference thermal performance data can be used to obtain an average air temperature from,

$$Q_F \alpha \left(T_{Filter} - \bar{T}_{Air}\right) . \qquad \text{(VII 3-25)}$$

Using Equations (VII 3-22) through (VII 3-25) and the reference data given in Table VII 3-4, the maximum heat loads for the HEPA and charcoal filters were obtained for an air flow rate of 2000 cfm. The results are also given in Table VII 3-4.

In CORRAL calculations the fraction of the core fission product inventory which is captured by the filter components (all particulate species on the HEPA filter and elemental and organic iodine on the charcoal filter) is continuously recorded. Data from inventory computations of fission product decay energy emission rates are used to convert the fractions to heat loads. If the calculated heat loads equal or exceed the design limits the filters are assumed to fail. At this point, the activity which has been sorbed by either filter type is assumed to remain fixed, but the filtering efficiency for any further activity which passes through the system is set equal to zero. This procedure is based on the conclusion that the filter media will experience a physical degradation due to the elevated temperature rather than chemical combustion. For HEPA's the degradation consists of deteriation of fiber binder materials and sealer materials such that structural damage to the filter media and bypass flow can occur. For the charcoal beds it is assumed that the water dousing system operates, so that combustion is prevented, but the waterlogged beds will develop channels resulting in bypass flow. The use of zero filter efficiencies under these conditions is probably overly pessimistic but conditions are too uncertain to estimate another value with reasonable confidence.

3.2.4 NATURAL DEPOSITION IN THE DRYWELL ANNULAR AIRSPACE

The drywell shell is surrounded by a two-inch air gap between the steel shell and the concrete shield containing the shell. Under normal leakage, isolation loss leakage, or under certain primary containment failure conditions, gas flow from the primary containment is assumed to pass through the space and exit at the operating floor of the reactor building. Therefore, any fission product transport and deposition which occurs in the region of secondary containment below the operating floor are approximated in CORRAL by behavior in this annular air space. For cases in which leakage occurs directly from the drywell shell, the wetwell torus, or the connecting vent pipes this provides an accurate description of the flow path to the operating floor level. For cases in which primary containment leakage occurs in one of the many subcompartments in the lower region of the secondary containment building, the model constitutes a simplified approximation of the geometry and flow paths between the various leakage locations and the operating floor level. However, the method

described below for calculating fission product transport and deposition in the annular region, is expected to produce overestimates rather than underestimates of fission product concentrations reaching the refueling building under this alternate leakage path condition. This is because the combination of longer residence time with deposition in the lower regions of secondary containment would usually be more effective than the decontamination factors predicted for the annulus. Only under high flow conditions should decontamination in the annulus predict concentrations lower than might be obtained for the other leak path.

The annular region cannot be modeled like the well-mixed compartments with deposition on the walls and/or floor. It is better described as plug flow along a cylindrical annulus with mass transfer to the walls. A simple first order differential equation defines a mass transfer coefficient, k, that can be estimated from known correlations for I_2 transfer. For particles, k can be estimated from particle deposition data from moving gas streams with more difficulty and uncertainty. The differential equation for transfer to the walls of an annular slit is:

$$\frac{dC}{(C-C_w)} = -\left(\frac{2k}{U\Delta r}\right)dx, \qquad \text{(VII 3-26)}$$

where

C = the concentration of the transferring substance

C_w = wall concentration

U = plug average annual velocity

Δr = annulus width

x = axial distance

k = mass transfer coefficient.

If $C_w = 0$, Equation (VII 3-26) integrates for $0 \leq x \leq \ell$ to

$$\frac{C}{C(x=0)} = \exp\left[-\left(\frac{2\ k}{\underline{U}\Delta r}\right)\ell\right], \qquad \text{(VII 3-27)}$$

assuming an average axial velocity, $\underline{U}$,

$$\underline{U} = \frac{Q}{A_{av}}$$

where

$A_{av} = \Delta r \int_0^{\ell} \pi\ r\ dx/\ell$, average annulus cross section, and

Q = volumetric flow rate

For the annular gap described earlier for a typical BWR, Equation (VII 3-27) becomes

$$\frac{C}{C(x=0)} = \exp(-1200\ k/\underline{U}) \qquad \text{(VII 3-28)}$$

The assumption that $C_w = 0$ for both particulates and I_2 is reasonable for most conditions in the BWR accident cases. Molecular I_2 has been experimentally verified to have a high affinity for steel and paint surfaces (Ref. 4,11). Normally the overall mass transfer coefficient for I_2 would be

$$k^{-1} = k_w^{-1} + K_g^{-1} \qquad \text{(VII 3-29)}$$

where k_g is the boundary layer coefficient and k_w is a first order rate constant for the surface reaction (Ref. 4). The value of k_w is difficult to predict for the annulus since it is a function of temperature, surface composition, surface roughness, I_2 concentration, and vapor pressure. Thus, for the drywell annulus the surface was assumed to be a "perfect sink" for I_2 with no desorption occurring.

The gas phase mass transfer coefficients for I_2 are estimated using the following analogies from heat transfer correlations (Ref. 5). For developed turbulent flow ($Re \leq 20{,}000$),

$$Sh = \frac{k\ 4Rh}{D_{I_2}} = 0.026\ Re^{0.8}\ Sc^{1/3}, \qquad \text{(VII 3-30)}$$

and for laminar isothermal flow ($Re < 2{,}100$),

$$Sh = 1.86\ (Re \cdot Sc \cdot 4Rh/\ell)^{1/3}. \qquad \text{(VII 3-31)}$$

where

Re = Reynolds number = $\frac{\rho \underline{U}(4Rh)}{\mu}$

Rh = Hydraulic radius

$$= \frac{\text{flow cross sectional area}}{\text{wetted parameter}}$$

$= \Delta r/2$ for the annulus.

The transition region, $2100<Re<20,000$, is not well understood and Equation (VII 3-30) could overestimate the mass transfer coefficient by a factor of 3-5 at Re = 2100. This error is offset by the non-smooth nature of the annular gap, which could also cause an underestimation of k for high Reynolds numbers. For BWR cases encountered, the Reynolds number ranges from the laminar region to about 30,000. The maximum DF's occur at Re = 0 and Re = 2101. A cutoff of DF = 100 maximum for I_2 is assumed in CORRAL-BWR calculations for the annular gap. This is done because of the possibility of desorption or saturation of the annular surface.

The behavior of particulates is more difficult to predict because deposition velocities from moving gas streams are a function of particle size as well as gas velocity. Sehmel (Ref. 12) has recently published experimental data that allow an estimation of particle deposition in the annular gap. The deposition velocity (or mass transfer coefficient) is highly affected by gravity. Most of Sehmel's data are for deposition on floors and ceilings, and the deposition in the drywell is on an essentially vertical wall. Wall deposition velocities are closest to floor deposition velocities, but are slightly lower for inertial particles (usually $\geq$ 0.1 μ). For these inertial particles, Brownian diffusion is nil, so $k = 0$ has been assigned a DF = 1 for Re < 2100 for all particles. Only the largest of the 5-15-μ particles have a significant turbulent deposition velocity.

An empirical fit of Sehmel's data is possible for $k = k(\bar{U}, d_p)$, but he has only two $\bar{U}$ values for vertical wall deposition. For this reason only a first order approximation can be made for k. This also eliminates major overhaul of CORRAL's matrix computations to incorporate a new set of variables. The ratio $k/\bar{U} = 1/300 \approx$ constant for all k and $\bar{U}$ for a particle size midway between 10-15μ. Table VII 3-5 shows the wide range of particle DF's versus Reynolds number.

To be conservative, an upper limit of DF = 100 seems more reasonable to assign to d_p = 15 μ (for $k/\bar{U} = 1/300$, DF = 27). With this upper limit, the following empirical equation fits the particle range:

$$DF = 1.0 + 0.1\left[\frac{d_p - 5}{5}\right]^{9.95} \qquad \text{(VII 3-32)}$$

for $10 \leq d_p < 15$ μ particles and DF = 1.0 for $d_p < 10$ μ. Integrating Equation VII 3-32 over the aging process of the particles as they settle out in 4 hours (see paragraph 3.1.2.2), produces DF (avg) - 10.0. Since the age of airborne particles undergoing natural deposition is important longer than the 4 hour time period (approximately two of these periods), the average DF = 5.5. This value was used in CORRAL-BWR calculations for all particles passing through the annular gap for $Re \geq 2100$. It is a conservative number because approximately 90 percent of the mass of particles released is >10 μ in the CSE data and also in the CORRAL calculations. The mass average particle is 13.5 μ which has a DF = 21. Thus picking DF = 5.5 over-estimates early atmospheric sources and under-estimates additional sources on a long time basis. Certainly on a mass average basis, DF = 5.5 is conservative.

3.2.5 THE COMPUTER CODE CORRAL

The multicompartment containment model was programmed with Fortran V for use on a Univac 1108. The program incorporates the models for fission product removal discussed in the previous section. Figure VII 3-4 shows the basic flow chart for CORRAL. A summary of each of the five flow chart sections follows.

a. Input Parameters

1. Constants

(a) Core fractions for gap, melt, steam explosion and vaporization releases.

(b) Numbers of compartments.

(c) Volumes, wall areas, floor areas, heights of each compartment.

(d) Spray parameters (flow rates, drop sizes, fall heights, equilibrium conditions for I_2 removal, I_2 distribution coefficients).

(e) Times of all events.

(f) Compartment filter decontamination rates.

(g) Fractions of compartments released during a puff release.

2. Variables (with time)

(a) Pressure, temperature, and water vapor content of each compartment. Temperature difference between bulk gas and walls.

(b) Flow rates between compartments.

(c) Decontamination factors between compartments.

(d) Particle sizes.

(e) Leak rates to atmosphere and leak DF's (decontamination factors).

b. Initial Conditions

1. All concentrations set equal to zero at t = 0 except gas release concentrations in first compartment.

2. Spray set to operate in main compartment (PWR).

3. All amounts released and DRF's (dose reduction factors) set equal to zero. A zero DRF means that nothing has been released.

c. Computation of Properties and Removal Rates

1. Pressure, temperature, and water vapor content and T(bulk)-T(wall) by parabolic interpolation.

2. Intercompartmental flow rates and decontamination factors and leak rates and respective DF's by parabolic interpolation.

3. Particle sizes by linear interpolation.

4. Gas phase viscosities and I_2 diffusivities and Schmidt numbers.

5. Mass transfer Grashof numbers and corresponding deposition rates.

6. Particles settling velocities and their natural deposition.

7. Spray lambdas for particle.

8. Terminal spray velocities, gas phase mass transfer coefficient, liquid phase mass transfer coefficient, and spray lambdas.

9. I_2 equilibrium equivalent lambdas (if needed).

10. Overall lambdas.

d. Solution of Differential Equations

The solution of the differential equations is discussed in the previous section. To properly age the continuous releases, it was necessary to divide these releases into discrete impulses releases. The melt release was divided into ten equally spaced and sized releases, each independent age wise from the other nine. The vaporization release (released at an exponentially decaying rate) was divided into 20 impulse releases, each successive release at an exponentially lower value than the first. The sum of the first ten releases equals 1/2 the total release, and the remaining ten equals the remaining 1/2. The duration of the period of the first ten is one half life. The duration of the second ten should be three half lives for a reasonable approximation of an exponential decay.

Thus the total number of differential equations solved (one each for particulates, organic iodides and I_2) for any time step is (N=number of compartments)

GAP RELEASE	3N equations
EXPLOSION RELEASE	3N
MELT RELEASE	30N
VAPORIZATION RELEASE	60N
	96N equations

The accuracy of the output depends on the rate of change of the rate coefficients, so short time steps would be desirable immediately after each discrete release (aging is rapid at first, especially if sprays are on). Long time steps are sufficient for old releases.

e. Output Variables

1. Airborne contained fractions relased at time, t.

   (a) For each release: I_2, organic iodides, particulates.

   (b) For each compartment for each release: I_2, organic iodides, particulates, at time, t.

2. Escaped fractions released (for each release: I_2, organic iodides, particulates, at time, t).

3. Escape fractions of the core for any desired isotope.

4. Dose reduction factor for each release (I_2 and particulates) at time, t.

5. Overall dose reduction factor (I_2 and particulates) at time, t.

6. Total fraction of core iodine escaped and core particulates escaped up to time, t.

3.3 ESTIMATION OF METHYL IODIDE FRACTION USED IN PWR AND BWR ANALYSES WITH THE CORRAL CODE

Considerable experimental evidence exists that some relatively small portion of the fission product iodine which is released from the reactor fuel will appear in the containment volume as organic iodide compounds. The dominant compound, methyl iodide, because of its chemical properties would tend to remain in the gas phase rather than deposit on surfaces, dissolve in water, or react with spray solutions. Trapping on charcoal filters is also less effective for organic iodides than for inorganic iodine species. Therefore, estimates of the amount of this difficult-to-remove form that could be produced in an accident are necessary. This task is hampered by uncertainties in the mechanism of formation and limited data, but conversion values have been obtained based on the information that is currently available. The approach used and the resulting values for each water reactor type are described in the two following subsections.

3.3.1 METHYL IODIDE FRACTION FOR PWR ANALYSES

The fraction of iodine airborne as methyl iodide following postulated accident cases has been estimated from the information summarized by Postma and Zavadoski (Ref. 13). The total percentage formation was obtained by adding that formed by radiolysis to that formed by nonradiolytic mechanisms.

For nonradiolytic formation, the least squares fit of experimental measurements indicates conversion of 0.056 percent of iodine. Upper and lower limits indicated by the measurements are 1 percent and 0.004 percent, respectively. These values were summarized as

Nonradiolytic Percent

$$\text{Conversion} = 0.1\% \quad {}^{+0.9\%}_{-0.1\%}$$

Radiolytic formation process lead to combination of elemental iodine and trace level organic materials in the gas phase. On the basis of available experimental data, the maximum percentage conversion for a DBA case is 2.1 percent. The minimum formation due to radiolysis is near zero. Therefore, for no removal, we estimate

Radiolytic Conversion For No Removal Case = $1.1\% \pm 1\%$.

The no-removal case can never be realized because natural processes will deplete an appreciable fraction of the airborne iodine, making it unavailable for radiolysis. For natural removal, the percentage conversion was reduced by a factor of 2. The result may be summarized as follows:

Radiolytic Conversion For Natural Removal Case = $0.6\% \pm 0.5\%$.

Sprays will remove iodine rapidly from the gas phase, further reducing the potential for organic iodide formation. The effect of spray removal was handled by reducing the conversion by an additional factor of 2. The result is summarized as follows:

Radiolytic Conversion For Spray Removal Case = $0.3\% \pm 0.2\%$.

Total formation of organic iodides will be the sum of that for radiolysis and that formed by nonradiolytic mechanisms. For the natural transport case the result is

Total Conversion For Natural Removal

$$\text{Case} = 0.7\% \quad {}^{+1.4\%}_{-0.6\%}$$

and for the spray case,

Total Conversion For Spray Removal

Case = $0.4\%^{+1.1\%}_{-0.3\%}$

It should be noted that this approach defines an instantaneous methyl iodide fraction existing near the beginning of the accident sequence when most of the core iodine has been released. A more sophisticated approach would account for nonradiolytic formation as above, but would account for gas phase radiolysis through use of a G value for formation. A continued formation of organic iodides, based on the instantaneous airborne iodine concentration, G value for formation, and radiation dose would be used in place of the fractional conversions listed for the two conditions. However, this was considered an unnecessary complication because overall accident consequences are only partly dependent on iodine releases to the environment.

3.3.2 METHYL IODIDE FRACTION FOR BWR ANALYSES

It appears there is not enough evidence that methyl iodide formation in a BWR should be significantly different than in a PWR. Although radiolytic formation rates are higher in a BWR due to higher dose, radiolytic destruction is higher too. The net rate is perhaps much the same in both reactor types. Natural deposition lambdas are nearly identical. The driving force for natural convection is the bulk gas - wall temperature difference (ΔT). For the condensing atmosphere of the accidental sequences

$$\Delta T\ (PWR) \triangleq 10\ \Delta T\ (BWR)$$

$$\lambda(BWR) = \lambda\left(\frac{\Delta T(BWR)}{\Delta T(PWR)}\right)^{1/3}\left(\frac{A(BWR)/V(BWR)}{A(PWR)/V(PWR)}\right)$$

If we compare the drywell A/V with the PWR, then $\{A(BWR)/V(BWR)\}/\{A(PWR)/V(PWR)\} \triangleq 10^{1/3}$, therefore

$$\lambda(BWR) \triangleq \lambda(PWR)\ .$$

Since the natural transport case is the only condition requiring consideration in BWR analyses, a total conversion value for organic iodides of

$$0.7\%^{+1.1\%}_{-0.6\%}$$

will be used.

3.3.3 FISSION PRODUCT DECONTAMINATION DURING LEAKAGES TO THE ATMOSPHERE

Several different types of leakage from reactor containment to the atmosphere can occur during accident sequences for either reactor system. These can be classified as follows: (1) low (design) leakage from one or a collection of small undefined paths, (2) isolation loss leakage from a single and relatively large open path, and (3) massive leakage (a puff) from a failed containment vessel. In PWR systems the key structure with respect to atmospheric leakage is the steel-lined concrete containment vessel, while in BWR systems the important structure is the concrete and metal panel reactor building, also known as the secondary containment. During leakage from these structures it is possible that some of the fission product vapors and aerosols, which are carried by the bulk gas flow, would deposit on surfaces along the leak passage. Leakage through a network of rough-walled cracks would favor deposition while little deposition should occur during flow through an orifice.

In analyses performed throughout this study no credit has been taken for fission product deposition along the leak path when the leak path leads directly to the atmosphere. For large leaks (classes (2) and (3) above) this approach is probably close to actual experience. However, it is also considered an acceptable, although conservative, approximation for small leaks because; (1) the generally undefined nature of small leak distributions inhibits the ability to predict accurate decontamination factors, and (2) the accident sequences which are analyzed include containment failure at some point in the accident scenario and fission-product leakages beyond these points overwhelm the earlier low leakage values. In calculations the assumption of no decontamination is represented by using DF = 1.

There is one containment leakage situation where the release of activity to the atmosphere is modified by using a DF value greater than one. This case occurs only in PWR analyses where melt-through of the concrete base mat is followed by a puff release of the contained gas until the internal pressure equalizes with the external pressure.[1] Any gases and airborne fission products

---

[1] Since the bottom steel containment liner is embedded and anchored in concrete all around the reactor cavity area, no significant gaseous release from the base of containment is expected until the mat is actually penetrated by the melt.

escaping in this manner would have to pass through many feet of ground material in order to reach the atmosphere. The base of large PWR containments typically extend 40 to 60 feet below grade and part of this height is usually saturated with subsurface groundwater. The ground material may be low or high permeability soils, but next to the containment wall (perhaps within a coffer dam) the material is likely to consist of layers of gravel, sand, and/or porous concrete backfill.

This combination of external media should act as an effective filter for water soluble and particulate contaminants in the permeating gas stream. Work reported in Appendix K indicates many minutes or hours will be required for active gas to penetrate to the ground surface; that is, containment pressure relief by a single huge puff is not expected. In the water saturated zone of this natural filter bed soluble vapor species such as elemental iodine should be absorbed. Even though partial channeling may occur along fissures caused by the pressure gradients, the interfaces between the several layers of different materials should act as crack arrestors to produce meandering transport paths. Aerosol particles should be efficiently removed during passage through the dry upper layers of the backfill material. Work on the effectiveness of sand filters for removing aerosols from air streams (Ref. 14,15) indicate that efficiencies in the range of 99 percent to 99.99 percent are typical for one to three foot deep beds depending upon gas flow velocity, particle size, and degree of bed packing. Equivalent or better efficiencies should be expected for the situation of interest here because dry bed depths of 10 to 20 feet are anticipated.

Based on the above rationale it was concluded that fission product escape to the atmosphere via pressure relief from the base of the containment would be characterized by a large DF value for most species. Preliminary calculations were performed which indicated that any DF greater than 1000 would produce at most a ten percent decrease in the total atmospheric source term for accident sequences involving containment meltthrough; that is for DF$\geq$1000 the leakage prior to meltthrough accounts for nearly all of the atmospheric release. Therefore, a conservative value of 1000 was used in all such calculations. This DF applies only to elemental iodine and the particulate fission products. A DF = 1 was always used for the fission product noble gases and the organic iodide fraction. It is also emphasized that this procedure is followed only in PWR accident sequence analyses. In BWR accident sequences containment failure by some other process always precedes the meltthrough pathway.

3.3.4 POTENTIAL GROUNDWATER CONTAMINATION IN A MELTDOWN ACCIDENT[1]

Most of the reactor meltdown accident sequences are considered to ultimately result in melthrough of the bottom of the containment structure. This event will bring the molten mass into contact with the natural soil system at estimated depths of 50 to 100 feet. Radioactive contamination of the local groundwater can occur by several processes during this event. In meltthrough accidents where sprays have operated, some portion of the spray liquid may be released to the soil-water system. In accidents where sprays have not operated, airborne activity in the containment may be carried into the groundwater during containment building depressurization. Finally, groundwater leaching of the core mass itself can provide a delayed but long-term contamination source. The radionuclides introduced by any of these processes can be transported along the groundwater route to locations of potential interaction with human usage. It is of interest to the present study to obtain an estimate of the magnitude of this potential contamination pathway.

3.3.4.1 Problem Definition.

The analysis assumes a 3200 MW(th) reactor, after operating for 550 days at full power, experiences an accident event which results in core meltdown followed by meltthrough of the concrete floor of the containment structure as described in Appendix I. It has been estimated that containment meltthrough would occur about one day after the accident-initiating event (Ref. 36). Therefore, contamination of groundwater is unlikely before this time. Two basic modes were defined for analysis; one to examine the implications of early radioactivity release and the other to examine the effect of delayed leaching of radioactivity from the solidified core mass.

---

[1]The discussion presented here is based on the analyses performed by A. E. Reisenaur and R. C. Routson of Battelle's Pacific Northwest Laboratories.

In the first mode, it is assumed that containment meltthrough at one day is followed by rapid depressurization, and the airborne radioactivity in containment is delivered to the underlying soil-water system. This condition is indicative of a meltthrough accident in which containment sprays have not operated. Since detailed accident sequence calculations were performed in the Reactor Safety Study for this type of accident, core activity release fraction data are available. The release fractions range from a fraction of a percent of the core inventory for the less volatile species up to several percent of the core inventory for the more volatile species. Exact values used will be defined later in this section. The above contamination source term for the groundwater system is probably excessive for those accident sequences in which contaminated spray solution might leak into the soil because an equivalent radioactivity release would require leakage of several thousand gallons of solution past the molten core material. It is more likely the solution would vaporize back into the containment atmosphere. Accordingly, the depressurization release should be considered a worst case assumption. The analysis further assumes the airborne activity which is so released dissolves rapidly and completely in the receiving groundwater. This is probably highly conservative because much of the radioactivity will be in the form of oxide aerosol particles which should experience a relatively slow dissolution rate. In addition, the particulate source may have to penetrate a "dried-out" soil zone around the molten mass in order to reach the groundwater system. These two effects should delay the appearance of contamination in the groundwater and lead to lower peak concentrations than will be obtained under the present groundrules.

The second mode considers the effect of long-term leaching of fission products from the core-soil mass after it has cooled and solidified in the ground underneath the containment floor. It is expected that, during penetration into the ground, the size of the melt will increase as soil material is melted. Additional oxide and silicate phases will probably form which should mix with or partially dissolve in the core material. Fission products would be expected to distribute among the several molten phases under the influence of convective transport and chemical reaction driving forces. During this time the molten material should be surrounded by a relatively dry soil zone so that direct contact with groundwater would be unlikely. Eventually the melt penetration would stop because of decreasing decay-heat generation and the diluting effect of the molten soil constituents. Then the melt should gradually cool forming a solidified glass-like mass (Ref. 16). It is expected the mass would fracture during the cooling process and subsequent return of groundwater to the surface could begin leaching out fission products. The dimensions of the core-soil mass and the time delay for leaching to begin are difficult to predict accurately. Bounding heat-transfer calculations have indicated melt sizes may increase to maximum radii of 30 to 50 feet in 1 or 2 years in dry soils (Ref. 18). The presence of groundwater would tend to lower the numbers but results of the overall analysis here are not highly sensitive to exact dimensions. Elementary heat balance calculations also indicate that at about 1 year the heat removal capacity of the anticipated water flow (without boiling) would balance the decay-heat generation rate of the mass. The above results provide some guidance for selecting source dimensions and the starting time for leaching.

In both modes the source is modeled as a cylinder 70 feet in diameter and extending over the assumed 60 feet depth of the groundwater system. Radioactivity released from this boundary enters the groundwater where it is transported by the groundwater flow to a nearby outlet water body such as a river, lake, or bay. Therefore the rate of appearance of radionuclides at the outlet will depend on: (1) the release rate, (2) the groundwater flow velocity, and (3) the distribution coefficients for sorption of the dissolved radionuclides on the soil material of the groundwater system. In other words the soil-water system acts as a large chromatographic column to selectively separate and delay the discharge of the individual radionuclides in aqueous solution.

3.3.4.2 The Hydraulic and Ion Transport Models.

The hydraulics model for the two modes defined above was formulated as follows. An analytic solution to a point source and point sink in a uniform flow field was expanded to include a fully penetrating cylindrical source of finite radius. A diagram of the flow system used is given in Fig. VIII 3-5. The data chosen for the slope of the groundwater system, distance to the outlet water body, and soil type were selected from examining several eastern United

States power reactor site reports and generally represent conditions which would cause the most rapid dispersion of the radionuclides. Table VII 3-6 shows the input values used in the hydraulics model calculations. The normal groundwater flow was assumed to be perpendicular to the outlet water body.

In performing calculations with the model, the presence of the cylindrical source was assumed to disturb the uniform flow system out to twice the source radius. Therefore, the cross section of the contaminated flow system was 140-feet wide by 60-feet deep. The volumetric rate of fluid flow in this rectangular channel was 11,200 ft^3/day, and the linear flow velocity was 7 feet/day. Accordingly, the travel time for water from the source to the outlet water body was 215 days or 0.59 year.

The radionuclide transport calculations were made using a model based on the theoretical cell concept in which equilibration between the liquid and solid phases is achieved before the fluid is convected into the next cell (Ref. 17). The equilibrium stage approach has traditionally been considered satisfactory for groundwater systems because of the speed of the chemical reactions in relation to the fluid flow rate.

Sorption coefficients (Kd) for each isotope of concern were determined in the following fashion

a. Kd's for Sr and Cs in a typical[1] groundwater system were determined from direct data.

b. The Kd's for all other components in the given solution were calculated by assuming that the ratio of Kd_x to Kd_{Cs} or Kd_{Sr} reported in other references is constant.

Using the best available data, a conservative distribution coefficient (Kd) was chosen for each specie of concern. These coefficients with appropriate references are listed in Table VII 3-7.

3.3.4.3 Results of the Depressurization Release Problem.

The radionuclides chosen for calculation in this mode were selected on the basis of their half-life, distribution coefficient, and inventory. The fraction of the reactor core inventory of each radioactive species released to the groundwater system was based on calculated depressurization release fractions for a core meltthrough accident. The values used are given in Table VII 3-8. In executing these calculations, the mixed cell transport model utilized 100 column segments, and the individual radionuclide inventories (corresponding to the release fractions in Table VII 3-8) were "injected" to the groundwater flow channel over a two segment interval. This translates to an injection period of about 4.3 days which may or may not correspond to actual periods. However, final results are not too sensitive to this factor, particularly for species which experience adsorption and delay during transport to the outlet water body.

Resulting activity release rates of selected radionuclides contained in the groundwater released to the water body have been plotted and the curves are shown in Fig. VII 3-6. The semi-log plots show the release rates in curies/day as a function of time. Note the analysis predicts breakthrough of the non-sorbed Ru-106 at about 0.35 year with the release rate peaking at 0.59 year (215 days). The indicated axial dispersion is an artifact of the mixed cell model and may overestimate actual conditions. However, less dispersion would lead to higher peak release rates because the activity balance of the radionuclide must be maintained. In contrast to the non-sorbed ruthenium-106, the sorbed ruthenium-106 ions break through only after about 7 years and the ions leached from the soil have a much lower and broader elution curve. Technicium 99, with a low distribution coefficient (Kd = 0.1) breaks through in significant concentrations in about 0.7 years and peaks before one year. Strontium-90 which has an intermediate distribution coefficient (Kd = 2) arrives in significant quantities in 3 to 4 years and peaks at about 6 years. The Antimony-125 and the Cesium-137 with their higher Kd values lag behind the other nuclides arriving approximately 22 and 30 years after release and reaching their peak concentrations at 35 and 51 years, respectively.

The other radionuclides investigated were significantly delayed allowing radioactive decay to reduce them to innocuous levels at the time of arrival in the water body. In order to place these results in perspective with respect to radiological impact, the peak effluent

---

[1] Groundwater having 28 ppt total salinity and having a composition of 0.38 M Na^+, 0.008 M K^+, 0.008 M Ca^{++} and 0.04 M Mg^+.

concentrations discharged from the groundwater system for each of the radionuclides calculated may be compared to the maximum permissible concentrations specified in 10CFR20 (Ref. 30) for waters discharged to uncontrolled areas. This comparison along with other information is given in Table VII 3-9. It may be noted that three of the radionuclide effluent concentrations (Ru-106, Sr-90, and Cs-137) are predicted to be much higher than their respective MPC values. However, it must be emphasized that these are likely to be overestimates and they do not include the effects of several processes which would act to limit human exposure to this contamination source. These processes will be discussed following presentation of the results for the glass leaching release mode.

3.3.4.4 Results of the Glass Leaching Release Problem.

In accordance with estimates given earlier, the inventory of radionuclides in the core mass one year after the initial event was used to specify the leaching source strength. The significant species and their inventories were determined from the fuel irradiation history and consideration of prior fission product releases from the molten core. All isotopes of the noble gases, halegens, alkali metals, and tellurium group elements were assumed absent from the core-soil mass.[1] From the remaining refractory elements the following key species were selected; Tc-99, Sr-90, Ce-141, Zr-95, Eu-155, Pm-147, Eu-153, Sm-151, U-235, U-238, Pu-241, Pu-239, Pu-240, and Pu-242. The relationship used to predict the rate of leaching for all components can be expressed as

$$y = -5.222 + 0.334_x$$

y = $\log_{10}$ (fraction leached from time ϕ to time T)

x = $\log_{10}$ (elapsed time from time ϕ to time T)

Time is in hours, ϕ is fixed at 1 year and T is variable.

The relationship was derived from data presented by Saidl and other (Ref. 31,32,33). The melt was conservatively assumed to be basalt glass since it is probably much more soluble than any other glass, and the characteristic components were Sr and Cs which are the most leachable of the components of interest.

The elution curves obtained for several of the more important nuclides are presented in Fig. VII 3-7. All the curves characteristically rise to a peak and then slowly decay. The peak efflux rates and concentrations of the radionuclides for this case are generally a factor of 100 to 1000 lower than for the corresponding nuclides in the depressurization release case. However, the elution continues for extended periods of time. Each of these features is a direct result of the very slow leaching process. In Table VII 3-10, the peak effluent concentrations discharged from the groundwater system for each of the radionuclides calculated are compared to the maximum permissible concentrations specified in 10CFR20 (Ref. 30) for waters discharged to uncontrolled areas. It is apparent that except for Sr-90 all the predicted peak effluent concentrations are well below the MPC limits.

3.3.4.5 Exposure Reduction Processes and Contamination Control Measures.

It should be emphasized that the hydraulic model parameters, the radionuclide distribution coefficients, and the radionuclide leaching rate used in these analyses were selected to produce overestimates for the rate of appearance of the radionuclide sources at the outlet water body. For example, the soil permeability coefficient is indicative of well-sorted sands with gravel and of fissured limestone formations (Ref. 34), the distribution coefficients are probably low by factors of 10 or 100 (Ref. 35), and the leaching expression assumes a relatively highly soluble glass containing fissures which increase the effective surface area by a factor of 100 or more (Ref. 32). In addition, calculations of human radiation dose from use of the receiving water body resource would have to include the dilution effect that would occur in the water body beyond the efflux point for the contaminated groundwater. Thus, the groundwater contamination problem at many reactor sites is expected to be less severe than indicated here.

Another important factor to consider in evaluating the above results is the significant times which are required for

---

[1] This assumption is consistent with the release fractions presented earlier in this report for the volatile fission products.

movement of radionuclides through a groundwater system. Several months and in many cases years should elapse before contamination would appear in water bodies used for the support of a significant population group. This delay would allow ample time for instituting monitoring operations and for setting up an effective warning network. More importantly, the time would most likely be used to execute procedures for controlling or even eliminating the spread of contamination beyond the reactor site. This would involve drilling wells for monitoring and pumping purposes to control the local groundwater flow gradient. The withdrawn water could be stored temporarily in surface tanks or in sealed holding ponds for subsequent treatment. After movement of the radionuclides is under control, it would seem feasible if it were to be considered necessary to form a vault-like barrier around the radioactive zone using a combination of excavation, drilling, and concrete injection operations.

Even without the above engineered mitigating actions, the basic conclusion of this analysis would not be changed. Specifically, the analysis has shown the hydrologic contamination problem occurs on a much longer time scale than does the atmospheric contamination problem for a core meltthrough accident. Therefore, warning actions alone should be sufficient to limit population radiation doses from the hydrologic source to low levels compared to the doses received as a result of the atmospheric source.

References

1. Reactor Physics Quarterly Report, April-June 1969, BNWL-1150, Battelle-Northwest, Richland, Wash., (B. H. Duane, p 2.5-2.7), (1969).

2. Knudsen, J. G., "Properties of Air-Steam Mixtures Containing Small Amounts of Iodine", BNWL-1326, Battelle-Northwest (1970).

3. Knudsen, J. G., and R. K. Hilliard, "Fission Product Transport by Natural Processes in Containment Vessels", BNWL-943, Battelle-Northwest, Richland, Washington (1969).

4. Hilliard, R. K. and L. F. Coleman, "Natural Transport Effects On Fission Product Behavior in the Containment Systems Experiment", BNWL-1457, Battelle-Northwest, Richland, Washington (1970).

5. Bird, R. B., Stewart, W. E., and E. N. Lightfoot, "Transport Phenomena", John Wiley and Sons, N. Y. (1960).

6. Postma, A. K. and W. F. Pasedag, "A Review of Mathematical Models for Predicting Spray Removal of Fission Products in Reactor Containment Vessels", BNWL-B-268, Battelle-Northwest, Richland, Washington (1973).

7. Postma, A. K. and R. K. Hilliard, "Absorption of Methyl Iodine by Sodium Thiosulfate Sprays", AND Trans. 12, p 898-899 (November, 1969).

8. Hilliard, R. K., Postma, A. K., et al., "Removal of Iodine and Particles by Sprays in the Containment System Experiment", Nuclear Technology, 10, p 499-519 (1971).

9. Postma, A. K., L. F. Coleman, and R. K. Hilliard, "Iodine Removal from Containment Atmospheres by Boric Acid Spray", Report No. BNP-100, Battelle-Northwest, Richland, Washington (197).

10. Diffey, H. R., Fumary, C. H., M. J. S. Smith and R. A. Stinchcombe (AERE, Harwell, England), "Iodine Cleanup in a Steam Suppression System," CONF-650407 (Vol. 2), Internation Symposium on Fission Product Release and Transport Under Accident Conditions, Oak Ridge, Tennessee, p 776-804 (April, 1965).

11. Rosenberg, H. S., Genco, J. M., and D. L. Morrison, "Fission-Product Deposition and Its Enhancement Under Reactor Accident Conditions: Deposition on Containment-System Surfaces", BMI-1865, Battelle-Columbus (May, 1969).

12. Sehmel, G. A.,"Particle Eddy Diffusivities and Deposiition Velocities For Isothermal Flow and Smooth Surfaces", Aerosol Science 4, p 125-139 (1973).

13. Postma, A. K., and R. W. Zavadoski, "Review of Organic Iodine Formation Under Accident Conditions in Water-Cooled Reactors", WASH-1233, (October, 1972).

14. Yoder, R. E., and Empson, "The Effectiveness of Land as a Filter Medium", Amer. Ind. Hyg. Assoc. J., 19, 107 (1958).

15. McFee, D. R., and Sedlet, J., "Plutonium-Uranium-Molybdenum Fume Characteristics and Land Filtration", J. Nucl. Energy, 22, 641 (1968).

16. Jansen, G. and D. D. Stepnewski, "Fast Reactor Fuel Interactions with Floor Material After a Hypothetical Core Meltdown,", Nucl Tech, 17, 85 (1973).

17. Routson, R. C. and R. J. Serne, "One-Dimensional Model of the Movement of Trace Radioactive Solute Through Soil Columns" The PERCOL Model", BNWL-1718 (1972).

18. Ergen, W. K., et al., "Emergency Core Cooling: Report of Advisory Task Force on Power Reactor Emergency Cooling (USAEC).

19. Schroeder, M. C., "Laboratory Studies of the Radioactive Contamination of Aquifers", AEC Document UCRL 13074 (1963).

20. Rhodes, D. W., "The Effect of pH on the Update of Radioactive Isotopes from Solution by a Soil", Soil Sci. Soc. Amer. Proc. 21:389-396 (1957).

21. Pillai, K. C. and T. R. Folson, "The Concentration of Lithium, Potassium, Rubidium and Cesium in some Western American Rivers", Geochim. and Cosmochim. Acta, 32:1229-1234 (1968).

22. Barrow, N. J., "Comparison of the Adsorption of Molybdate, Sulfate, and Phosphate by Soil", Soil Sci., 109:282-288 (1970).

23. Geering, H. R., E. E. Gary, L. H. P. Jones and W. H. Allaway, "Solubility and Redox Criteria for the Possible Forms of Selenium in Soil", Soil Sci. Soc. Amer. Proc., 32:35-40 (1968).

24. Pourboug, M., "Atlas of Electrochemical Equilibria in Aqueous Solution", Pergamon Press, New York (1966).

25. Touhill, C. J., B. W. Mercer and A. J. Schuckrow, "Treatment of Waste Solidification Condensates", AEC Document BNWL-723 (1968).

26. Raja, M. E. and K. L. Babcock, "On the Soil Chemistry of Radio-Iodine", Soil Sci., 91:1-5 (1961).

27. Price, K. R., Unpublished Data, Battelle-Northwest, Richland, Washington (1973).

28. Wildung, R. E., Unpublished Data, Battelle-Northwest, Richland, Washington (1973).

29. Routson, R. C., Unpublished Data, Battelle-Northwest, Richland, Washington (1973).

30. Code of Federal Regulations, Title 10, Part 20, "Standards for Protection Against Radiation". USAEC. Appendix B, Table II.

31. Ralkova, J. and J. Saidl, "Solidification of High Level Wastes: Part 3, Diffusion and Rates of Radionuclides Incorporated in Basalts", Kernergie, 10:161 (1967).

32. Mendell, J. E., "A Review of Leaching Test Methods and the Leachability of Various Solid Media Containing Radioactive Wastes", AEC Document BNWL-1765 (1973).

33. Saidl, J. and J. Ralkova, "Immobilization of Strontium and Cesium by Fixation of Radioactive Waste in Baslat", Collection, Czechoslov. Comun., 31, 871 (1966).

34. Fisher, H. L., "Prediction of the Dosage to Man From Fallout of Nuclear Devices - Transport of Nuclear Debris by Surface and Groundwater" UCRL-50163 Pt. 6 (January, 1972).

35. Higgins, G. H. "Evaluation of the Groundwater Contamination Hazard from Underground Nuclear Explosions", J. Geoph. Res, 64, 1509 (1959).

36. Carbiener, W. A., et al "Physical Processes in Reactor Meltdown Accidents", WASH-1400, Appendix VIII, October, 1975.

TABLE VII 3-1 FISSION PRODUCT REMOVAL RATE CONSTANTS CALCULATED FOR A LARGE PWR CONTAINMENT VESSEL

Spray System	Flow Rate gpm	Fraction Initial Release	λ, hr^{-1}
Molecular Iodine			
1 CSR, Boric Acid	3500	1.0 → .01	3.12
2 CSR[(a)], Boric Acid (pH = 5)	7000	1.0 → .01	6.24
Equilibrium Conditions — Boric Acid	--	$10^{-2} \rightarrow 1.8 \times 10^{-3}$	1.15
Equilibrium Conditions — Boric Acid	--	$1.8 \times 10^{-3} \rightarrow 3 \times 10^{-5}$	
Equilibrium Conditions — Boric Acid	--	$<3 \times 10^{-5}$	0
1 CSR, NaOH (pH 9.5)	3500	1.0 → .01	67
2 CSR, NaOh	7000	1.0 → .01	134
Equilibrium Conditions — NaOH	--	Next 2 hrs	0
Equilibrium Conditions — NaOH	--	$10^{-2} \rightarrow 3 \times 10^{-5}$	0.223
Equilibrium Conditions — NaOH	--	$3.8 \times 10^{-4} \rightarrow 3 \times 10^{-5}$	0.0422
Equilibrium Conditions — NaOH	--	$<3 \times 10^{-5}$	0
1 CSI[(a)], Boric Acid	3200	1.0 → 0.1	2.85
Boric Acid	--	<.01	Same as boric acid equilibrium
No spray (natural deposition)		1.0 → .01	1.38
No spray		<.01	0
Particulates			
1 CSR	3500	1.0 → .02	6.0
2 CSR	7000	1.0 → .02	12.0
2 CSR	7000	<.02	0.9
1 CSI	3200	1.0 → .02	12.6
1 CSI	3200	<.02	0.945
No spray (natural deposition)		1.0 → .02	0.13
No spray		<.02	0

(a) CSR = Recirculation spray. CSI = Injection spray.

TABLE VII 3-2 EQUILIBRIUM DATA FOR I_2 WITH BORIC ACID SPRAYS (Ref. 9)

Time, min	H	C_g/C_{go}
0	2676	.01
100	1.5×10^4	1.8×10^{-3}
500	4.0×10^4	6.75×10^{-4}
1000	7.0×10^4	3.86×10^{-4}
2000	1.5×10^5	1.8×10^{-4}
4000	5×10^5	5.4×10^{-5}
$\geq$7000	1×10^6	2.7×10^{-5}

TABLE VII 3-3 EQUILIBRIUM DATA FOR I_2 WITH CAUSTIC SPRAYS (Ref. 9)

Time, min	H	C_g/C_{go}
0-100	Constant H, λ=0	.01
100-1000	Variable H, λ=.095 hr^{-1}	.01
1000	7.0×10^4	3.86×10^{-4}
2000	1.5×10^5	1.8×10^{-4}
4000	5×10^5	5.4×10^{-5}
$\geq$7000	1×10^6	2.7×10^{-5}

TABLE VII 3-4 INPUT DATA AND RESULTS FOR FILTER OVERBEATING CRITERIA

Filter Type	Air Flow cfm	Filter Temperature F	Heat Load Watts
HEPA	2000	105	2.2×10^3
HEPA	2000	112	5.7×10^3
HEPA	2000	250(a)	5.4×10^4(a)
Charcoal	2000	110	1.3×10^3
Charcoal	2000	126	3.4×10^3
Charcoal	2000	640(a)	6.4×10^4(a)

(a) Design Limit

TABLE VII 3-5 DF vs PARTICLE SIZE AND REYNOLDS NUMBER IN DRYWELL ANNULAR GAP

d_p, μ	DF (Re $\leq$2100)	DF (Re = 2100)	DF (Re = 30,000)
5	1.0	1.0	1.0
10	1.0	1.1	1.1
15	1.0	4.4×10^5	2.2×10^4

TABLE VII 3-6 HYDRAULICS MODEL PARAMETERS

Length of Flow Field	1500 Feet
Slope of the Groundwater	1 Foot in 5000 Feet
Depth of the Groundwater System	60 Feet
Soil Permeability Coefficient	6666. Feet/Day
Radius of Source	35 Feet
Effective Porosity	0.19

TABLE VII 3-7 DISTRIBUTION COEFFICIENTS FOR VARIOUS RADIONUCLIDES IN GROUNDWATER

Radionuclide	Kd (ml/g)	Reference
I	0.1	25
Br	0.1	25
Cs	20	18
Rb	15	20
Te	20	23
Se	20	22
Sb	15	27
Ba	3	18,23
Sr	2	18
1/2 Ru	4	24
1/2 Ru	0	24
Mo	5	21
Pd	25	23
Rh	25	23
Tc	0.1	23,25
Y	200	19
Zr	200	19
Ce	50	28
Pr	60	28
Pm	60	28
Sm	60	28
Eu	60	28
U	100	26
Pu	200	19

TABLE VII 3-8 CORE INVENTORY DEPRESSURIZATION RELEASE FRACTIONS[(a)]

Group	Chemical Element	Release Fraction
1	I, Br	0.011
2	Cs, Rb	0.027
3	Te, Se, Sb	0.040
4	Ba, Sr	0.029
5	Ru, Mo, Pd, Rh, Tc	0.0028
6	Others	0.0005

(a) Obtained from CORRAL calculated output for PWR accident sequence ABε.

TABLE VII 3-9 COMPARISON OF CALCULATED GROUNDWATER EFFLUENT CONCENTRATIONS TO MPC LIMITS - DEPRESSURIZATION RELEASE CASE

Nuclide	Source Inventory, Curies	Time of Peak, years	Peak Effluent Concentration µCi/cc[a]	MPC µCi/cc
Ru-106[b]	2.6×10^{4}	0.59	5.1×10^{-1}	1×10^{-5}
Tc-99	2.1×10^{0}	0.85	1.4×10^{-4}	2×10^{-4}
Ba-140	4.5×10^{6}	3.3	7.2×10^{-43}	2×10^{-5}
Sr-89	3.1×10^{6}	4.7	7.4×10^{-10}	3×10^{-6}
Sr-90	1.5×10^{5}	5.6	7.0×10^{-1}	3×10^{-7}
Ru-103	2.7×10^{5}	6.5	1.1×10^{-23}	8×10^{-5}
Ru-106	2.6×10^{4}	10	5.5×10^{-5}	1×10^{-5}
Te-129	4.2×10^{5}	11	2.9×10^{-71}	8×10^{-4}
Te-127m	5.1×10^{4}	24	1.9×10^{-36}	5×10^{-5}
Sb-125	1.1×10^{4}	35	6.6×10^{-7}	1×10^{-4}
Cs-134	4.5×10^{4}	43	2.0×10^{-9}	9×10^{-6}
Cs-135	3.7×10^{-1}	51	2.2×10^{-7}	1×10^{-4}
Cs-137	1.5×10^{5}	51	2.8×10^{-2}	2×10^{-5}

(a) Taken at 1500 ft from the point of release
(b) Non-sorbed fraction

TABLE VII 3-10 COMPARISON OF CALCULATED GROUNDWATER EFFLUENT CONCENTRATIONS TO MPC LIMITS - GLASS LEACHING RELEASE CASE

Nuclide	Source Inventory, Curies	Time of[a] Peak, years	Peak Effluent Concentration µCi/cc[c]	MPC µCi/cc
Tc-99	7.5×10^{2}	0.9	3.6×10^{-6}	2×10^{-4}
Sr-90	5.1×10^{6}	5.9	7.1×10^{-4}	3×10^{-7}
Ce-141	7.6×10^{4}	13	(b)	9×10^{-5}
Zr-95	3.2×10^{6}	27	(b)	6×10^{-5}
Eu-155	6.9×10^{4}	103	(b)	2×10^{-4}
Pm-147	1.4×10^{7}	115	(b)	2×10^{-4}
Eu-154	5.6×10^{4}	148	1.3×10^{-8}	2×10^{-5}
Sm-151	5.8×10^{3}	158	2.3×10^{-7}	4×10^{-4}
U-235	2.3×10^{0}	267	2.5×10^{-10}	3×10^{-5}
U-238	3.2×10^{1}	267	3.5×10^{-9}	4×10^{-5}
Pu-241	3.8×10^{6}	418	(b)	2×10^{-4}
Pu-239	1.2×10^{4}	535	8.0×10^{-7}	5×10^{-6}
Pu-240	1.2×10^{4}	535	8.0×10^{-7}	5×10^{-6}
Pu-242	3.9×10^{1}	535	2.6×10^{-9}	5×10^{-6}

(a) Time started from beginning of leaching or 1 year after the incident.
(b) Peak concentration less than 1×10^{-10} µCi/cc.
(c) Taken at 1500 ft from the point of release.

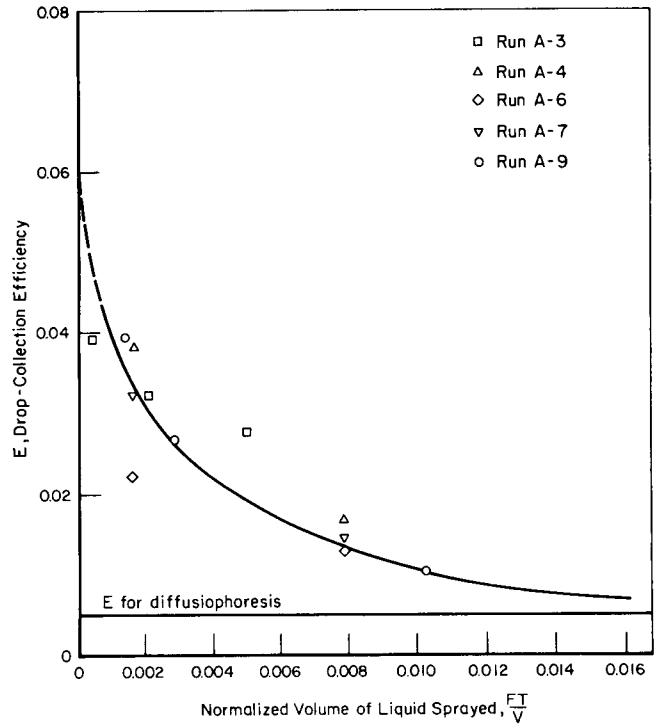
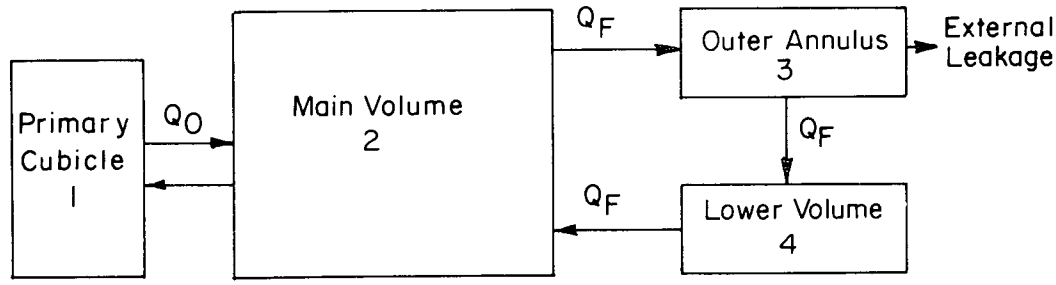


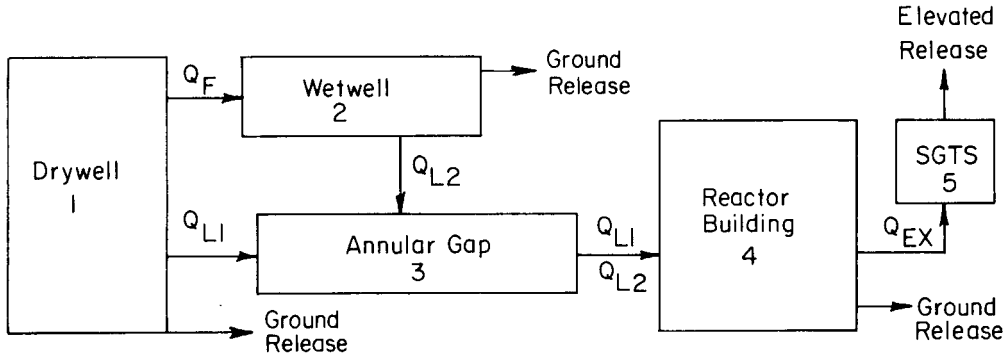
FIGURE VII 3-1 Drop-Collection Efficiency as a Function of Liquid Volume Sprayed

Points are plotted at mid-times of spray periods (fresh spray only)



Compartment	Removal Processes	Fission Product Sources
1	Natural deposition	Gap and melt releases
2	Natural deposition	Steam explosion releases
	Spray absorption	
	Recirculation filters	
3	Natural deposition	
	Leakage	
4	Natural deposition	Vaporization release

FIGURE VII 3-2 Schematic of CORRAL-PWR



Compartment	Removal Processes	Fission Product Sources
1	Natural deposition External leakage	Gap, melt, steam explosion, and vaporization releases
2	Pool scrubbing Natural deposition External leakage	
3	Natural deposition	
4	Natural deposition External leakage	
5	Once-through filtration	

FIGURE VII 3-3 Schematic of CORRAL-BWR

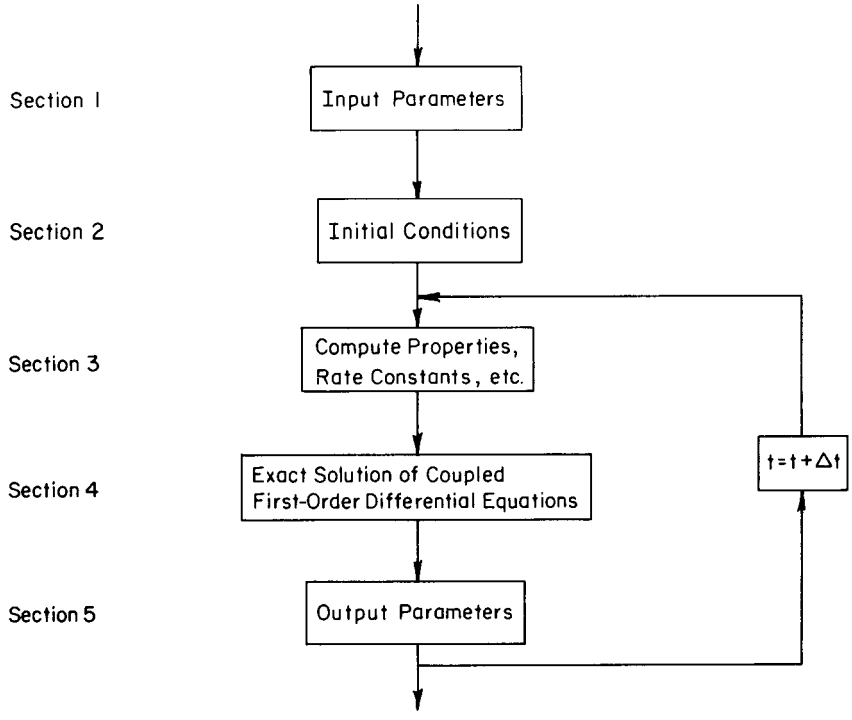


FIGURE VII 3-4 Computer Code CORRAL Flow Diagrams

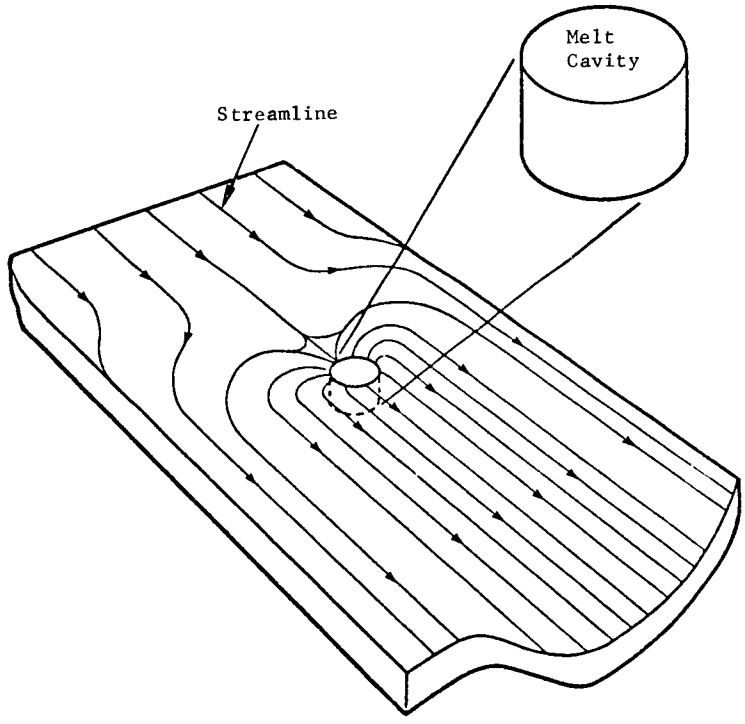


FIGURE VII 3-5 Idealized Flow System Used for Analysis

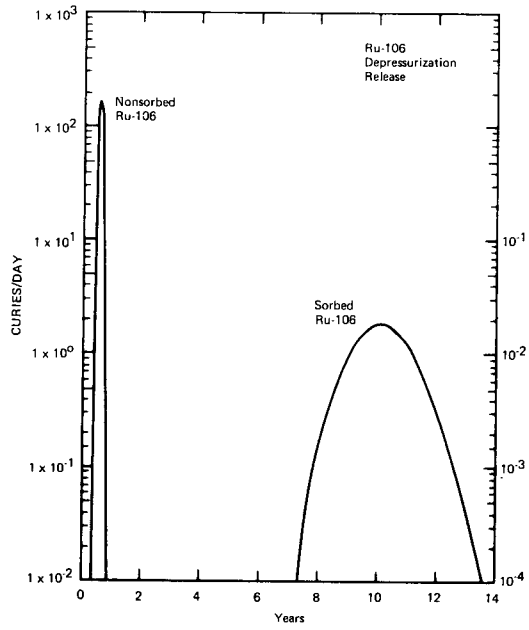
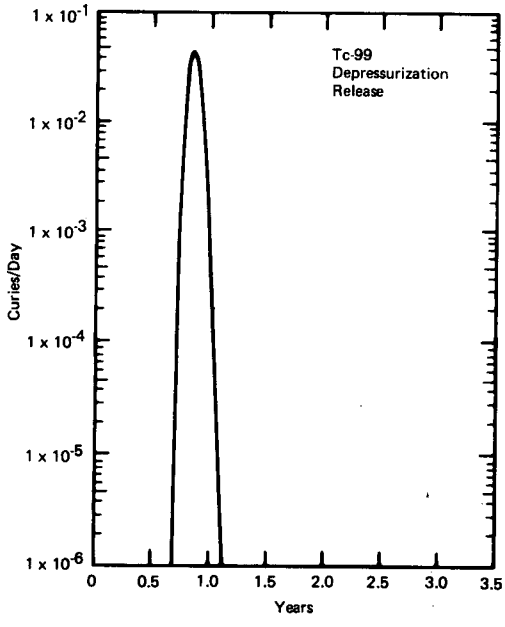


FIGURE VII 3-6 Radionuclide Elution Curves for Depressurization Release



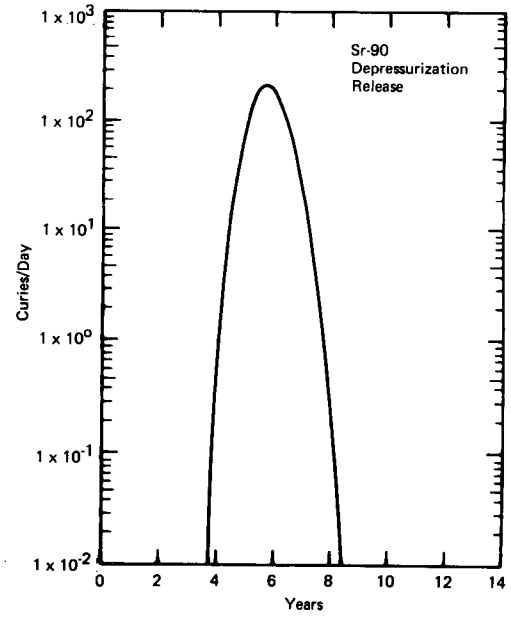


FIGURE VII 3-6 (Continued)

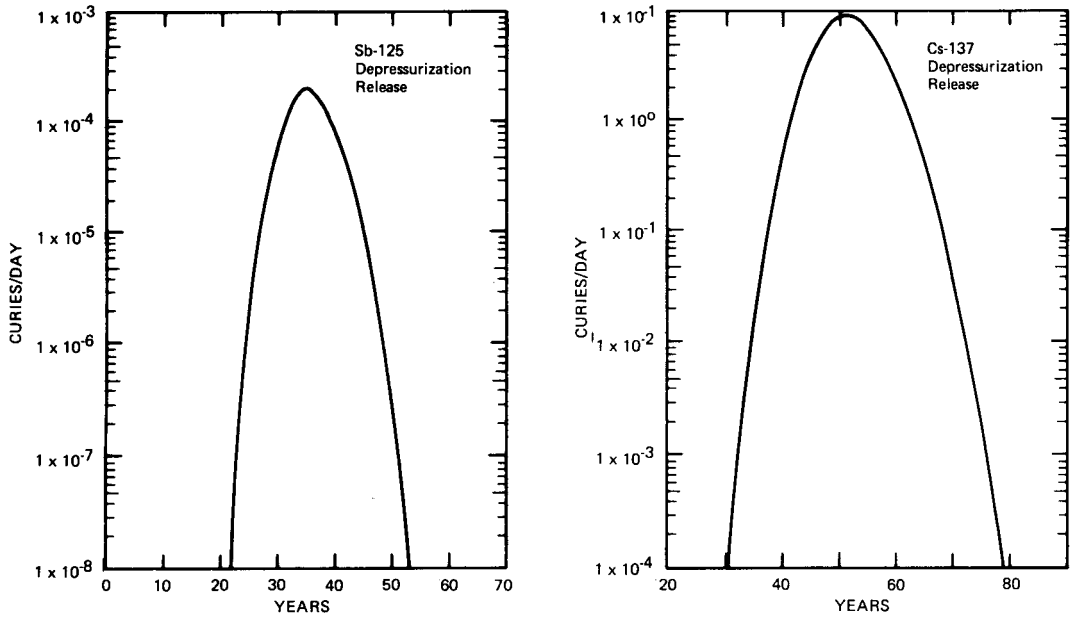


FIGURE VII 3-6 (Continued)

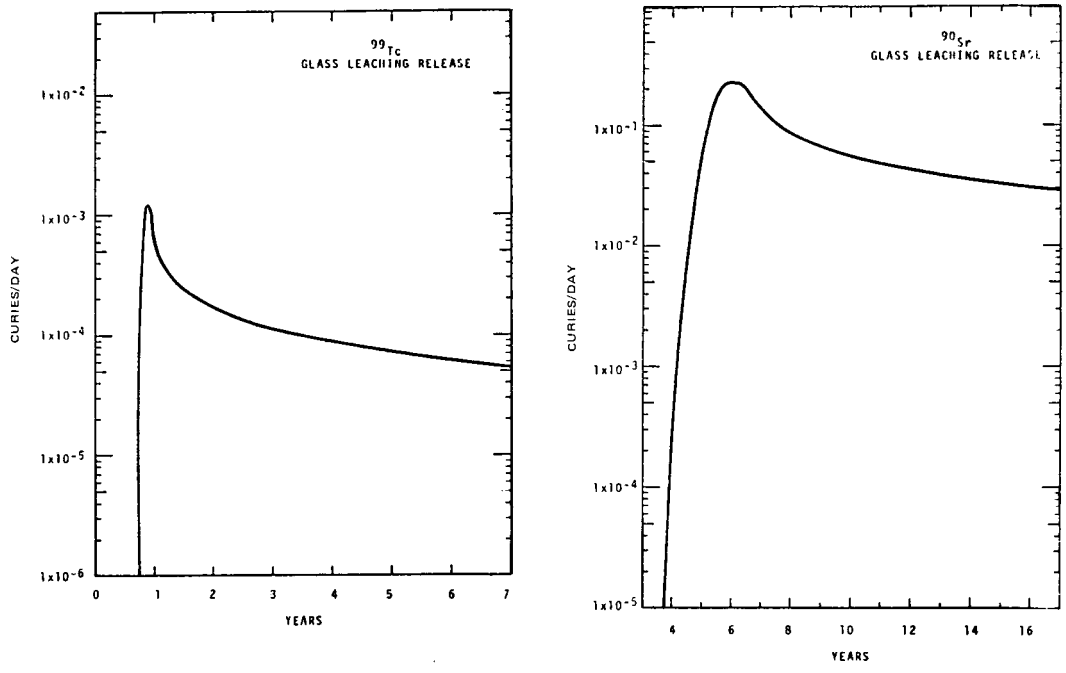
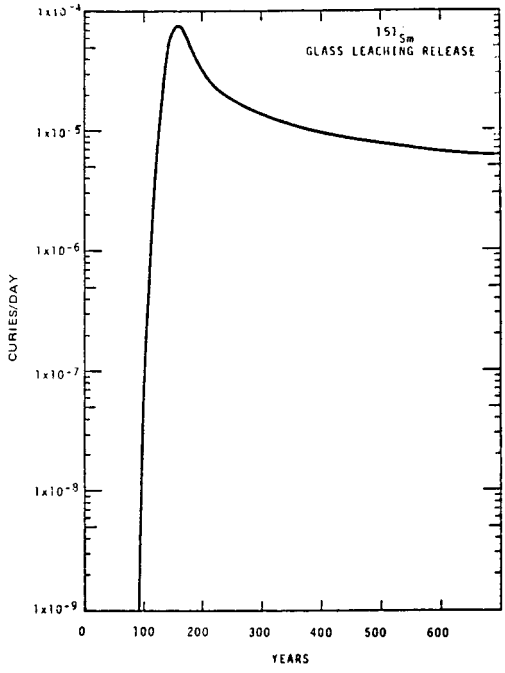


FIGURE VII 3-7 Radionuclide Elution Curves for Glass Leaching Release



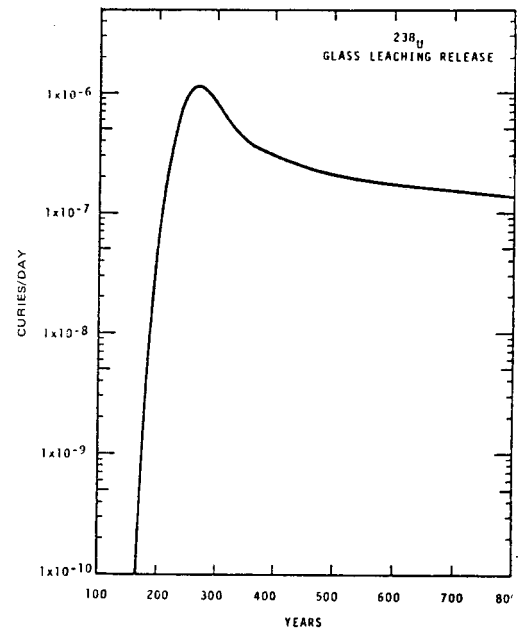


FIGURE VII 3-7 (Continued)

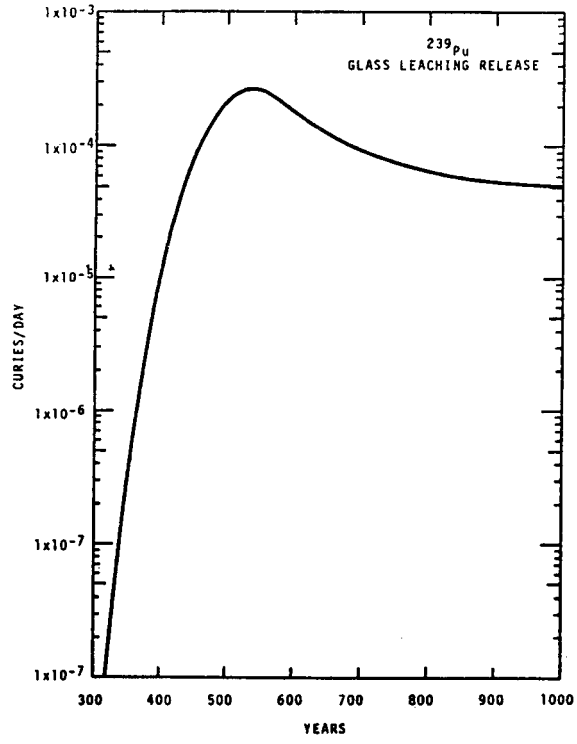


FIGURE VII 3-7 (Continued)

APPENDIX A

CALCULATION OF FISSION PRODUCT RELEASE TO FUEL ROD GAS GAP

by

R. L. Ritzman
Battelle's Columbus Laboratories

Appendix A

Table of Contents

Section		Page No.
A1.	THE REGAP METHOD	VII-59
A2.	RESULTS OF REGAP CALCUALTIONS	VII-61
	REFERENCES	VII-63

List of Tables

Table		Page No.
VII A-1	Specified Input Data for Fission Product Gap Release Calculations	VII-64
VII A-2	Regap Method Results for Best Estimate Conditions - Noble Gases	VII-65
VII A-3	Regap Method Results for Best Estimate Conditions - Halogens	VII-66
VII A-4	Regap Method Results for Best Estimate Conditions - Alkali Metals and Alkaline Earths	VII-66
VII A-5	Final Gap Release Estimates from the Regap Method	VII-67

Appendix A

Calculation of Fission Product Release to Fuel Rod Gas Gap

by

R. L. Ritzman

Battelle's Columbus Laboratories

One of the fission product release terms for a reactor loss-of-coolant accident is the rapid escape of gaseous activity that occurs when fuel claddings first rupture. The rapid depressurization of the ruptured rods carries out the fission products that have accumulated in the gas gap and the gas plenum during the normal operating period of the fuel rods. This release term is frequently referred to as the gap release component. Analytical techniques have been developed by different laboratories for estimating the magnitude of the release. These techniques rely on different mathematical models or different interpretations of experimental release data in making gap release estimates. One of these techniques is the REGAP computer code developed at Battelle-Columbus. This Appendix describes the results of applying the REGAP code to calculate the fractions of various fission products that would be released from the fuel in a reactor core under normal operating conditions. The results obtained by the other two laboratories involved in the exercise are given in Appendicies B and C.

All calculations were performed for a common group of fission product nuclides and a common set of reactor operation input specifications. Two typical end-of-life core conditions were used; one for a large PWR and the other for a large BWR. The specified data input are listed in Table VII A-1. With the input conditions fixed in this manner the release results obtained from the different calculation methods should depend only on variations in release models and/or the approach that each uses to generate fuel temperature profiles from the core power distribution data.

A1. THE REGAP METHOD

In this method calculations are performed assuming that the fission products migrate through the fuel by a diffusion process during reactor operation, and are released to the rod gap and plenum spaces by escape from external surfaces, surface-connected cracks, or surface-connected porosity. The equivalent sphere model originally proposed by Booth (Ref. 1)[1] and discussed by Lustman (Ref. 2) constitutes the basis for calculating release from the sintered UO_2 characteristic of water reactor fuels. The sintered fuel, although near theoretical density, contains some interconnected porosity which effectively increases the surface area for release of fission gases. In the equivalent sphere approach, the fuel body is considered to be composed of spherical particles of uniform size whose surface to volume ratio is equivalent to the actual surface area to fuel volume ratio of the sintered material. Solutions for the appropriate diffusion equations for a sphere in which production and decay of the fission product are taken into account have been obtained by Beck (Ref. 3) and these are used directly in the REGAP method.

The diffusion equation for the concentration in a sphere is:

$$\frac{\partial C}{\partial t} = \frac{D}{r} \frac{\partial^2 (rC)}{\partial r^2} + B - \lambda C \ , \qquad \text{(VII A-1)}$$

with boundary and initial conditions

$$C\ (a,t) = C\ (r,0) = 0 \ ,$$

where

C = concentration in the sphere, atoms per cm^3

D = diffusion coefficient, cm^2 per sec

[1] References are listed at end of this Appendix.

B = production rate, atoms/ (sec) (cm^3)

λ = decay constant, sec^{-1}

t = time, sec

r = radial coordinate in the sphere, cm

a = equivalent-sphere radius, cm.

The rate of release (R) is found from the concentration gradient at the outer surface and for a unit volume of the solid is given by

$$R = \frac{3D}{a}\left(\frac{\partial C}{\partial r}\right)_{r=a} . \qquad \text{(VII A-2)}$$

The accumulation of a fission product external to the solid can be calculated by considering the rate at which it is released and the rate at which it decays:

$$\frac{dN}{dt} = R - \lambda N , \qquad \text{(VII A-3)}$$

where N is the accumulation of undecayed release atoms from a unit volume of sphere (atoms per cm^3). Beck (Ref. 3) restated the problem in terms of dimensionless variables and obtained the following solution:

$$G = 3\left(\frac{1}{\sqrt{\mu}}\coth\sqrt{\mu} - \frac{1}{\mu}\right)[1 - \exp(-\mu\tau)]$$

$$- \frac{6\mu\exp(\mu\tau)}{\pi^2}\sum_{n=1}^{\infty}\frac{1 - \exp(-n^2\pi^2\tau)}{n^2(n^2\pi^2 + \mu)} , \qquad \text{(VII A-4)}$$

where

$G = \frac{N}{B/\lambda}$ = the ratio of non-decayed atoms outside the sphere at any time to the total non-decayed atoms in the system at equilibrium

$\mu = \frac{\lambda a^2}{D}$

$\tau = \frac{Dt}{a^2}$

$D = D_o \exp(-Q/RT)$

D_o = limiting diffusion coefficient, cm^2 per sec

Q = activation energy for diffusion, cal per g-mole

R = gas constant, cal/(deg) (g-mole)

T = absolute temperature, deg K.

For reactor operating times that are long with respect to the half-life of a radioactive fission product, G approaches the equilibrium value:

$$G_\infty = 3[(1/\sqrt{\mu})\coth\sqrt{\mu} - 1/\mu]. \qquad \text{(VII A-5)}$$

For stable fission-product species, the release is expressed in terms of the ratio of the amount released to the amount produced. Thus

$$G = F = \frac{N}{Bt} = 1 - \frac{1}{15\tau}$$

$$+ \frac{6}{\pi^4\tau}\sum_{1}^{\infty}\frac{\exp(-n^2\pi^2\tau)}{n^4} , \qquad \text{(VII A-6)}$$

The first five terms of the summation are usually sufficient to obtain an accurate value for G.

Equations (VII A-5) and (VII A-6) constitute the basis of the REGAP method. However, each requires some basic input data for the various parameters. The diffusion coefficients (D) are obtained from the Arrhenius expression as a function of temperature by specifying the limiting diffusion coefficient value (D_o) and the activation energy for diffusion (Q). Of course, these values are different for each fission product chemical element. Extensive experimental work has been done over the past two decades, heavily directed at the noble gas elements krypton and xenon, to determine the fundamental D_o and Q values for UO_2 fuel. Most of the work has involved post-irradiation laboratory heating experiments although some effort has been spent on extracting diffusion coefficients from results of inpile UO_2 irradiation studies. Many reviews or summaries of the field have appeared including ones by Lustman (Ref. 2), Childs (Ref. 4), Parker, et al. (Ref. 5), Morrison, et al (Ref. 6), and Carroll (Ref. 7). The basic diffusion parameter data used in the present calculations were obtained from fission product release results reported by Parker, et al. (Ref. 5) for trace irradiated UO_2.

The D_o and Q values used for each fission product are listed in Table 10 of Reference 6.

The fuel temperatures that are needed for the calculation of diffusion coefficients are generated within the computer code that incorporates the REGAP method. The radial temperature profile inside the fuel is approximated by first dividing the pellets into five radial segments of nearly equal volume. The temperature at each radius is computed starting from the outside surface using a constant UO_2 thermal conductivity and the appropriate operating surface heat flux value according to the equation:

$$T_r = T_s + \frac{Q\alpha}{2k}\left[1 - \left(\frac{r}{\alpha}\right)^2\right], \qquad \text{(VII A-7)}$$

where

T_r = temperature at radius r, F

T_s = temperature at fuel surface, F

Q = surface heat flux, Btu/(sec)(in.^{2})

k = fuel thermal conductivity, Btu/(sec)(in.)(F)

α = fuel-pellet outside radius, in.

The fuel surface temperature is calculated by computing the temperature rise across the rod gas gap and adding this to the cladding surface temperature. Mathematically,

$$T_s = T_c = Q/K \qquad \text{(VII A-8)}$$

where

T_c = cladding surface temperature, F

K = gas gap conductance, Btu/sec in^2,F.

Once the radial temperature profile is obtained a simple average temperature is assigned to each of the five radial zones. This process is carried out for all subregions of the reactor core (axial and radial) that are required. In the present cases, the cores of both reactor types were divided into 9 axial and 8 radial increments, so temperature profiles and fission product releases were calculated for 72 separate subregions.

The remaining parameter that is critical to the release calculation is the equivalent sphere radius value. This is related to the density of the UO_2 fuel as noted earlier, and is easily obtained from a knowledge of the percent theoretical density for the fuel pellets using Figure 9.18 and Equation 9.23 of Reference 2.

The mechanics of the REGAP method consist of first calculating the fuel pellet temperature profiles as outlined above. This step requires the following input data: The core average surface heat flux, the total power peaking factor for each subregion, the assumed value for fuel rod gap conductance, and a suitable fuel thermal conductivity value. As noted, five zone temperatures are calculated for each core subregion. These temperatures are then used in the Arrhenius equation to compute diffusion coefficient values for each fission product species. Finally the diffusion coefficient values are used along with the specified equivalent sphere radius and the appropriate radioactive decay constant in Equation (VII A-5) or (VII A-6) to compute the fractional release of each fission product specie from each zone of each core subregion. The release fractions for a particular specie are summed over the radial zones and then these values, weighted according to the core power distribution, are collected along the axial direction of each radial core region to generate a set of core fractional release values on a full length rod basis. Since the present cases use eight radial core regions, the set contains eight values. These may then be summed to produce a total core release fraction for each of the fission product species.

A2. RESULTS OF REGAP CALCULATIONS

A series of calculations was performed in which the values of various parameters were changed to examine the effect on release predictions. As indicated in Table VII A-1, two average gap conductance values were used, 500 and 1000 Btu/hr,ft^2,F. In addition the fuel thermal conductivity was varied from 1.2 to 1.5 Btu/hr,ft,F, the equivalent sphere radius was varied from 0.00613 to 0.0184 cm, and D_o values for each fission product specie were varied from 1 to 100 times the reference values. The ranges of these variations were considered to represent the approximate degree of uncertainty in the available input data although the variation in D_o

values could also be interpreted as an estimate of the possible effect of fuel burnup on the release rates. The best estimate values for this series of parameters are considered to be the following:

a. Gap Conductance = 1000 Btu/hr, ft^2, F

b. UO_2 Thermal Conductivity = 1.2 Btu/hr,ft,F

c. Equivalent Sphere Radius = 0.00613 cm

d. The D_o Parameter = the reference value for each fission product element.

The fission product release results obtained using the REGAP method for each of the reactor types (PWR and BWR) are listed in Tables VII A-2 to VII A-4.

The results for the stable fission product species are not of great interest except that they indicate the magnitude of release of radioactive species whose half-lives are long compared to the core lifetime of about 3 years (10^8 seconds). This includes species such as Kr-85, I-129, Cs-137, and Sr-90. The results for the much shorter lived species calculated here illustrate the square root of half-life dependence for release that the diffusion model contains. Comparing results for the two reactor types shows very little difference and so there is no need to separate the release values. The total core release results are the data of principal interest. The effect on these values of the parameter sensitivity examinations can be summarized as follows:

a. The total core release values for the shorter lived fission product species were affected to a greater degree than were the values for the stable (or very long lived) species.

b. A factor of two change in gap conductance produced a factor of 1.4 to 4 change in release values.

c. A twenty-five percent change in UO_2 thermal conductivity produced a factor of 1.4 to 6 change in release values.

d. A factor of three change in equivalent sphere radius produced a factor of 2 to 3 change in release values.

e. A factor of one hundred change in D_o values produced a factor of 2 to 10 change in release values.

Because of these variations and the semi-empirical nature of the REGAP method itself, it is possible to provide only a rough estimate of the gap release. A listing of the estimates that are indicated by this work are given in Table VII A-5. These total core release values are generally applicable to water-cooled power reactors and should be considered the "best estimate" that is currently possible. Nevertheless the sensitivity calculations suggest that each is uncertain by a factor of about five, either higher or lower. Finally it deserves mention that the data in Table VII A-5 indicates potential for release from the UO_2 fuel only, the volatility of released species in the fuel rod gas spaces has not been considered. Therefore, the occurrence of plateout on or of chemical reactions with the cladding could cause a reduction in the fraction of the gap release inventory that is available for rapid escape when the cladding perforates.

References

1. Booth, A. H., "A Method of Calculating Fission Gas Diffusion from UO_2 and Its Application to the X-2-f Loop Test", AECL Report CRDC-721 (Sept. 1957).

2. Lustman, B., "Irradiation Effects in Uranium Dioxide", Chapter 9 in Uranium Dioxide: Properties and Nuclear Applications, edited by J. Belle, USAEC, 1961.

3. Beck, S. D., "The Diffusion of Radioactive Fission Products from Porous Fuel Elements", BMI-1433 (April, 1960).

4. Childs, B. G., "Fission Product Effects in Uranium Dioxide:, J. Nucl. Mater, 9, 217 (1963).

5. Parker, G. W., et al., "Out-of-Pile Studies of Fission Product Release from Overheated Reactor Fuels at ORNL, 1955-1965", ORNL-3981 (July, 1967).

6. Morrison, D. L., et al., "An Evaluation of the Applicability of Existing Data to the Analytical Description of a Nuclear Reactor Accident", BMI-1779 (August, 1966).

7. Carroll, R. M., "Fission Gas Behavior in Fuel Materials", Nucl. Safety, 8, 345 (1967).

TABLE VII A-1 SPECIFIED INPUT DATA FOR FISSION PRODUCT GAP RELEASE CALCULATIONS

	PWR	BWR
Fuel Data		
Fuel pellet diameter, in.	0.367	0.488
Cladding O.D., in.	0.422	0.562
Cladding thickness, in.	0.024	0.032
Fuel density, % T.D.	94	94
Thermal Data		
Average heat flux, Btu/hr, ft^2	191,000	163,000
Peak heat flux, Btu/hr, ft^2	534,000	425,000
Maximum peaking factor	2.8	2.6
Average cladding surface temp., F	610	560
Average gap conductance, Btu/hr, ft^2, F	1000	1000
Average gap conductance, Btu/hr	500	500
Average thermal output, Kw/ft	6.2	6.2
Maximum thermal output, Kw/ft	17.3	18.3
Other Operational Data		
Core end-of-life burnup, MWD/MTU	30,000	30,000
Core end-of-life operating time, sec	10^8	10^8

Core Segmentation and Power Distributions

Axial - 9 equal length sections - same for both reactor types

Axial Section	Power Factor
1 (top)	0.48
2	0.80
3	1.12
4	1.30
5	1.48
6	1.32
7	1.15
8	0.82
9 (bottom)	0.53

Radial and Local - 8 unequal volume, full-length regions for each reactor but with different power factors as tabulated below. These regions really represent different groups of full length rods with the higher power regions of the core being segmented in greater detail.

Radial X Local Region	Fraction of Total Core Rods	Sum of Fractions	Radial X Local Power Factor	
			PWR	BWR
1	0.01	0.01	1.85	1.70
2	0.02	0.03	1.65	1.54
3	0.02	0.05	1.50	1.44
4	0.05	0.10	1.45	1.35
5	0.10	0.20	1.33	1.26
6	0.15	0.35	1.19	1.14
7	0.25	0.60	1.05	1.02
8	0.40	1.00	0.68	0.76

TABLE VII A-1 (CONTINUED)

Fission Product Species

Stable or Long-Lived

Xe, I, Cs, Sr

Radioactive	Half-Life
Xe-133	(5.27da)
Xe-135	(9.2hr)
I-131	(8.06da)
I-132	(2.3hr)
I-133	(20.8hr)
Cs-138	(32min)
Sr-89	(51da)
Sr-91	(9.7hr)

TABLE VII A-2 REGAP METHOD RESULTS FOR BEST ESTIMATE CONDITIONS - NOBLE GASES

Radial Region	Fraction of Core Volume	Total Core Release Percentages for Noble Gas Species					
		Stable Xe		Xe-133		Xe-135	
		BWR	PWR	BWR	PWR	BWR	PWR
1	0.01	0.56	0.66	0.15	0.18	0.05	0.05
2	0.02	0.83	0.90	0.17	0.18	0.05	0.05
3	0.02	0.63	0.65	0.11	0.10	0.03	0.03
4	0.05	1.37	1.54	0.21	0.23	0.06	0.07
5	0.10	1.91	1.98	0.25	0.26	0.07	0.07
6	0.15	1.96	1.89	0.24	0.23	0.07	0.06
7	0.25	1.97	1.76	0.24	0.20	0.06	0.06
8	0.40	0.40	1.29	0.04	0.01	0.01	0.004
Total Core	1.00	9.63	10.67	1.41	1.39	0.40	0.39

TABLE VII A-3 REGAP METHOD RESULTS FOR BEST ESTIMATE CONDITIONS - HALOGENS

Radial Region	Fraction of Core Volume	Total Core Release Percentages for Halogen Species							
		Stable I		I-131		I-132		I-133	
		BWR	PWR	BWR	PWR	BWR	PWR	BWR	PWR
1	0.01	0.67	0.78	0.33	0.40	0.071	0.086	0.17	0.21
2	0.02	1.01	1.11	0.44	0.46	0.071	0.073	0.19	0.20
3	0.02	0.80	0.83	0.28	0.28	0.039	0.038	0.11	0.11
4	0.05	1.74	1.95	0.60	0.69	0.077	0.088	0.22	0.26
5	0.10	2.64	2.75	0.64	0.63	0.077	0.074	0.23	0.22
6	0.15	2.65	2.58	0.61	0.53	0.072	0.061	0.21	0.18
7	0.25	2.44	2.07	0.54	0.39	0.063	0.045	0.19	0.13
8	0.40	0.18	0.02	0.02	0.003	0.003	-	0.01	0.001
Total Core	1.00	12.13	12.09	3.46	3.38	0.47	0.47	1.33	1.31

TABLE VII A-4 REGAP METHOD RESULTS FOR BEST ESTIMATE CONDITIONS - ALKALI METALS AND ALKALINE EARTHS

Radial Region	Fraction of Core Volume	Total Core Release Percentages for Alkali Metal and Alkaline Earth Species									
		Stable Cs		Cs-138		Stable Sr		Sr-89		Sr-90	
		BWR	PWR	BWR	PWR	BWR	PWR	BWR	PWR	BWR	PWR
1	0.01	0.43	0.51	0.012	0.015	0.34	0.39	0.24	0.28	0.065	0.078
2	0.02	0.59	0.63	0.010	0.011	0.42	0.46	0.26	0.28	0.042	0.043
3	0.02	0.42	0.41	0.005	0.005	0.28	0.24	0.15	0.12	0.018	0.013
4	0.05	0.81	0.91	0.008	0.009	0.41	0.44	0.18	0.20	0.019	0.020
5	0.10	0.97	0.96	0.008	0.008	0.43	0.38	0.15	0.14	0.015	0.013
6	0.15	0.75	0.66	0.006	0.005	0.15	0.13	0.05	0.04	0.004	0.003
7	0.25	0.55	0.42	0.004	0.003	0.01	0.008	0.004	0.003	-	-
8	0.40	0.30	0.005	-	-	-	-	-	-	-	-
Total Core	1.00	4.55	4.51	0.053	0.056	2.04	2.05	1.03	1.06	0.16	0.17

TABLE VII A-5 FINAL GAP RELEASE ESTIMATES FROM THE REGAP METHOD

Species	Total Core Release[a] (Percent)
Kr, Xe (stable-long lived)	10.0
I (stable-long lived)	10.0
Cs (stable-long lived)	5.0
Sr (stable-long lived)	2.0
Xe-133	2.0
Xe-135	0.4
I-131	3.0
I-132	0.5
I-133	1.0
Cs-138	0.05
Sr-89	1.0
Sr-91	0.2

(a) Values estimated uncertain by about a factor of ± 5.

APPENDIX B

RELEASE OF FISSION PRODUCTS FROM PWR AND BWR FUEL PINS

by

H. L. McMurry and E. F. Aber
Aerojet Nuclear Company

Appendix B

Table of Contents

Section		Page No.
B1.	METHODS	VII-73
B2.	APPLICATION TO RELEASE OF LONG-LIVED NOBLE GASES AND IODINES	VII-74
B3.	APPLICATION TO SHORT-LIVED NOBLE GASES AND IODES	VII-74
B4.	TREATMENT OF CESIUM	VII-75
B5.	EQUATIONS FOR THE POWER DISTRIBUTION	VII-75
	B5.1 Equation for the Time Dependent Average Concentration in a Pin	VII-76
	B5.2 The Release Fraction F_i from a Single Pin in Radial Segment i	VII-76
	B5.3 Release Fraction for the Entire Core	VII-77
	B5.4 Calculations of T_{bji} and $(DT/dr)_{bji}$	VII-77
B6.	EQUATIONS FOR STRONTIUM	VII-78
B7.	RESULTS	VII-80
REFERENCES		VII-81
ADDENDUM		VII-86

List of Tables

Table		Page No.
VII B-1	Specified Input Data for Fission Product Gap Release Calculations	VII-82
VII B-2	Long Lived Fission Product Species	VII-83
VII B-3	Short Lived Isotopes	VII-84
VII B-4	Release Percentages of Xe and I Isotopes At 10^8 Second	VII-84
VII B-5	Cesium Release Percentages at 10^8 Seconds	VII-85
VII B-6	Boundary Temperatures and Heat Ratings for the Hot Pin in the PWR	VII-85

Appendix B

Release of Fission Products from PWR and BWR Fuel Pins

by

H. L. McMurry and E. F. Aber
Aerojet Nuclear Company

This work is in support of the Reactor Safety Study which aims at realistic evaluations of the effects of reactor accidents. To determine the result of cracking of the cladding in fuel pins of operating reactors, it is important to know the amount of fission products which have migrated to the fuel-cladding interface during operation. This calculation gives the fractions of various fission products which have accumulated in the gap next to the inner surface of the cladding. The isotopes considered were the noble gases, their iodine precursors and cesium and strontium.

To give a common base for comparing calculations from different groups, two rather typical cases were considered. One reactor is a PWR while the other is a BWR. The operating conditions used are the same as those used by the other laboratories. These input conditions are given in Table VII B-1.

BI. METHODS

The methods used here are based on a balance equation for fission product diffusion which assumes that the driving force for diffusion of fission products is the gradient of the chemical potential of the diffusing particles (Ref. 1). W. Yuill has incorporated this idea into his models for calculating fission production diffusion (Ref. 2-5).

The balance equation in cylindrical coordinates is (Ref. 6)

$$\frac{dc}{dt} = P(r) - \lambda c(r,t) + \frac{1}{r}\frac{d}{dr}\, r\left[\frac{Dc}{RT}\frac{d\mu}{dr}\right] \qquad \text{(VII B-1)}$$

where

$c(r,t)$ = concentration at radial position r at time t of some particular fission product. (mols/cc)

$P(r)$ = Production of the fission product at r (mols/cc sec.)

λ = decay constant for the fission product (sec^{-1})

D = Fick's law diffusion constant for the product (cm^2/sec)

$\mu = \left(\frac{\partial G}{\partial c}\right)_T$ = chemical potential for the fission product. The G is the Gibbs free energy. [Cal/mol/cc]

The expression $(Dc/RT)\cdot(d\mu/dr)$ which appears in Equation (VII B-1) involves approximation. First it is assumed that it may be approximated by the ideal equation (Ref. 7).

$$\mu = \mu^{o}(T) + RT \ln c \,. \qquad \text{(VII B-2)}$$

The equation for the diffusion current is (Ref. 6).

$$J = -D'\frac{d\mu}{dr} = -D'\left[\left(\frac{\partial \mu}{\partial T}\right)_c \frac{dT}{dr} + \left(\frac{\partial \mu}{\partial c}\right)_T \frac{dc}{dr}\right].$$

If there were no temperature gradients this would reduce to Fick's law. Using $(\partial\mu/\partial c)_T$ from Equation (VII B-2) this yields

$$D' = \frac{Dc}{RT}\,.$$

This is how the Dc/RT appears in Equation (VII B-1).

To apply Equation (VII B-1) requires a knowledge of $(\partial\mu/\partial T)_c$, D and dT/dr throughout the pin. The temperature gradient dT/dr can be calculated from a knowledge of the heat generation within the pin and the heat conductivity $K_c(T)$ as a function of temperature. This is readily accomplished if it is assumed

that K_c depends only on temperature and is not seriously affected by such structural changes as may occur within the UO_2 pellet due to the marked temperature changes between the boundary and the interior. The methods used for calculating dT/dr will be discussed in connection with the calculation on Cs and Sr isotopes where explicit determination of dT/dr at the boundary has been made. For the noble gases and their iodine precursors the code used (Ref. 5) calculates the boundary temperature from an empirical relation involving the heat rating $\int K_c dT$ (see Addendum).

The diffusion coefficient D is assumed to have a temperature dependence given by

$$D = D_o e^{-Q/RT} \qquad \text{(VII B-3)}$$

Data on D_o and Q for noble gases are incorporated into the FPFM code (Ref. 5). Data for Cs and Sr are given in Reference 4. Data for $(\partial\mu/\partial T)_c$ are available only for Cs and Sr (Ref. 4). Because of this the releases of noble gases and their iodine precursors are calculated using a correlation which is partly based on Equation (VII B-1) and partly empirical.

B2. APPLICATION TO RELEASE OF LONG-LIVED NOBLE GASES AND IODINES

In calculating releases of long-lived noble gases and iodines Yuill, et al. (Ref. 4) developed equations based on the steady state form of Equation (VII B-1) with dc/dt = 0. For stable gases ($\lambda = 0$) they cast their equations into the form (Ref. 5).

$$\ln (1-F) = - \frac{e^{-Q/RT_b}}{b^2 T_b} e \; [A+BG+CG^2] \qquad \text{(VII B-4)}$$

where

F = release fraction

b = pellet radius (cm)

T_b = boundary temperature of pellet (°K)

Q = activation energy for Fickian diffusion as in Equation (VII B-3)

G = heat rating (see below) $= \int_{T_b}^{T_o} K_c dT = \frac{\bar{P}_z}{4\pi}$

$\bar{P}_z$ = watts/cm in pin

K_c = heat conductivity (watts/cm·C)

A, B, C are constants derived from analysis of capsule data.

The heat rating and the power per centimeter is used in several places. These are related through the heat conduction equation. Thus in cylindrical coordinates

$$\frac{\partial}{\partial r}\left(rK_c \frac{dT}{dr}\right) = - \frac{\bar{P}_z}{\pi b^2} \psi(r) \times r \; .$$

Where $\bar{P}_z$ is the average watts/cm and $\psi(r)$ is a function to take account of the variation in production rate with position r. In this work a flat production is used and $\psi(r) = 1$. The case $\psi(r) = 1.0$ is discussed in the Addendum to this Appendix. When $\psi(r) = 1.0$,

$$\int_{T_b}^{T_o} K_c \, dT = \frac{\bar{P}_z}{4\pi} = G. \qquad \text{(VII B-5)}$$

Also,

$$\left(\frac{dT}{dr}\right)_b = - \frac{2}{b}\left(\frac{P_z}{4\pi} \cdot \frac{1}{K_c}\right)_b \qquad \text{(VII B-6)}$$

To apply Equation (VII B-4) to an actual reactor, account must be taken of the power distribution. The FPFM code does this from the power distribution specifications. These have been provided for the PWR and BWR cases (see Table VII B-1).

B3. APPLICATION TO SHORT-LIVED NOBLE GASES AND IODINES

Yuill has shown that the release fractions for short-lived isotopes is proportional to $1/\lambda$. A detailed account of this is given in connection with the Cs and Sr calculations.

Following Yuill's suggestion, the assumption has been made in this work that the release of 8.05d I^{131} is the same as

for its stable Xe^{131} daughter. Then the releases of all other noble gases and iodines with half lives shorter than 8.05d are calculated from (see equation VII B-20)

$$F_m = F_{Xe^{131}} \frac{\lambda_{I^{131}}}{\lambda_m} = F_{Xe^{131}} \frac{t_m}{t_{I^{131}}} \cdot \qquad \text{(VII B-7)}$$

In Equation (VII B-7) $t_{I^{131}}$ and t_m refer to the half lives of I^{131} and the species m, respectively. The Equation is applied for noble gases or iodines for which $t_m < t_{I^{131}}$.

B4. TREATMENT OF CESIUM

The diffusion of Cs and Sr isotopes was calculated by means of special approximations to Equation (VII B-1). Since data were provided for $(\partial\mu/\partial T)_C$, a less empirical procedure is followed than that used for the noble gases. However, there are still many quesions such as the influence of local variation in structure on $(\partial\mu/\partial T)_C$. In the case of Sr, $(\partial\mu/\partial T)_C$ is negative and this means that the temperature gradient drives these isotopes into the interior. Special treatment of the outer boundary condition is given later to assess release of Sr by evaporation.

First the general equations for F are derived in forms suited to the present PWR and BWR reactors.

B5. EQUATIONS FOR THE POWER DISTRIBUTION

The core is assumed to be divided into axial levels (9 uniformly spaced increments in this problem) and radial segments (8 in this problem). The power in any pin in a given radial segment is assumed to be the average for that segment.

Let

- P = total power
- P_i = power in one pin in radial segment i
- g_i = fraction of the core pins which are in radial segment i
- N = total pins
- Z = core height.

Define

1. $f_i = \dfrac{P_i}{P/N}$

2. $h_j = \dfrac{\text{Power per cm at axial level j in one pin in radial segment i}}{[P_i/Z]}$

   (h_j is taken to be the same for all i)

3. $P_z = \dfrac{P}{ZN}$.

From 1,

$$f_i \frac{P}{N} = P_i$$

and also

$$\left(f_i \frac{P}{N}\right) \frac{1}{Z} = \frac{P_i}{Z} \; ;$$

and from 2,

$$\left(f_i \frac{P}{N}\right) \frac{1}{Z} h_j = P_{ji} = \text{power per cm in a pin at axial level j and in radial segment i.}$$

From 3,

$$P_Z f_i h_j = P_{ji} \cdot \qquad \text{(VII B-8)}$$

From Equation (VII B-5)

$$G_{ji} = \frac{P_{ji}}{4\pi} = \frac{P_Z f_i h_i}{4\pi} \quad \text{(heat rating in the i,j location)} \qquad \text{(VII B-9)}$$

These relations will be used in what follows.

B5.1 EQUATION FOR THE TIME DEPENDENT AVERAGE CONCENTRATION IN A PIN

If

$$\frac{du}{dr} = \left(\frac{\partial \mu}{\partial t}\right)_c \frac{dT}{dr} + \left(\frac{\partial \mu}{\partial c}\right)_T \frac{dc}{dr} \simeq \left(\frac{\partial \mu}{\partial T}\right)_c \frac{dT}{dr} + \frac{RT}{c}\frac{dc}{dr}$$

Then Equation (VII B-1) yields

$$\frac{d}{dt}\int_o^b Cr\,dr = \int_o^b Pr\,dr - \lambda \int_o^b Cr\,dr + b\left[DKc + D\frac{dc}{dr}\right]_b . \qquad \text{(VII B-10)}$$

Define

$$\bar{C}(t) = \frac{2}{b^2}\int_o^b C(r,t)rdr$$

$$\bar{P} = \frac{2}{b^2}\int_o^b P(r)rdr .$$

Then

$$\frac{d\bar{c}(t)}{dt} = \bar{P} - \lambda\bar{c} + \frac{2}{b}\left[DKc + \frac{Ddc}{dr}\right]_b . \qquad \text{(VII B-11)}$$

In Equations (VII B-10) and (VII B-11)

$$K = \left(\frac{\partial \mu}{\partial T}\right)_c \frac{1}{RT}\frac{dT}{dr} .$$

With the temperature gradients characteristic of these pellets Kc>> dc/dr and $(Ddc/dr)_b$ may be neglected in Equation (VII B-11).

The further simplification is now made that $C_b(t) \sim \bar{C}(t)$. Then Equation (VII B-11) yields

$$\bar{C}(t) \simeq \frac{\bar{P}}{\alpha-\lambda}(e^{(\alpha-\lambda)t}-1)$$

$$\alpha = \frac{2}{b} KD . \qquad \text{(VII B-12)}$$

B5.2 THE RELEASE FRACTION F_i FROM A SINGLE PIN IN RADIAL SEGMENT i

Let

N_{gji} = amount of the fission product in the gap at the j,i location (mols)

$c_{ji}(t)$ = average concentration of fission product in a pin in radial segment i at the jth axial level. (mols/cc)

$$\frac{dN_{gji}}{dt} = 2\pi\Delta hb[DK]_{bji}c_{ji} - \lambda N_{gji} \qquad \text{(VII B-13)}$$

Δh = length of a segment ($9\Delta h = Z$ in this problem)

$(DK)_{bji}$ = value of DK on the pellet boundary of a pin in radial segment i at the jth axial level.

The first term in Equation (VII B-13) is the leakage rate from the pellet, the second is the decay of the material. Integrating,

$$N_{gji}(t) = -\pi b^2\Delta h\alpha_{ji}e^{-\lambda t}\int_o^t c_{ji}(t)e^{\lambda t}dt$$

$$\alpha_{ji} = \frac{2}{b}(DK)_{bji} \qquad \text{(VII B-14)}$$

Using Equation (VII B-12) and writing the power density in the ji elements as

$$\frac{P_z h_i f_i}{\pi b^2}$$

yields

$$N_{gji}(t) = \Delta h P_z h_j f_i \frac{\alpha_{ji}}{\alpha_{ji}-\lambda}$$

$$\left\{ e^{-\lambda t}\frac{(e^{\alpha_{ji}t}-1)}{\alpha_{ji}} - \frac{1}{\lambda}(1-e^{-\lambda t}) \right\} .$$

(VII B-15)

The fractional release from a pin at radial segment i is given by

$$F_i \equiv \frac{\Sigma_j N_{gji}}{\Sigma_j [N_{pji} + N_{gji}]} . \qquad \text{(VII B-16)}$$

In Equation (VII B-16)

N_{pji} = fission products within a pin at radial segment i and axial level j. (mols).

$$N_{pji} = \pi b^2 \Delta h c_{ji}(t)$$

$$= \frac{\Delta h P_z h_j f_i}{[\alpha_{ji}-\lambda]} \left[e^{(\alpha_{ji}-\lambda)t}-1\right].$$

(VII B-17)

Using Equation (VII B-15), (VII B-17) in Equation (VII B-11) yields

$$F_i = \frac{1}{9}\left\{\sum_j \frac{h_j \lambda}{(\alpha_{ji}-\lambda)} \left[\frac{\alpha_{ji}}{\lambda} + \frac{e^{-\lambda t}}{1-e^{-\lambda t}}\left(1-e^{\alpha_{ji}t}\right)\right]\right\}$$

(VII B-18)

In obtaining Equation (VII B-18), use is made of the fact that in this problem $\Sigma_j h_j = 9$.

For long lived Cs isotopes

$\lambda t << 1$ and $\lambda/\alpha_{ji} < = 1$

then

$$F_i = 1 + \frac{1}{9t}\sum_j \frac{h_j}{\alpha_{ji}}\left(1-e^{\alpha_{ji}t}\right) .$$

(VII B-19)

Equation (VII B-19) was used to calculate release of Cs^{137}. It has the correct asymptotic form, namely

$F_i \to 0$ as $t \to 0$

$F_i \to 1$ as $t \to \infty$.

For short lived isotopes $\lambda t >> 1$ and $\alpha_{ji}/\lambda << 1$.

Then

$$F_i \simeq \frac{-1}{9\lambda}\Sigma_j h_j \alpha_{ji} . \qquad \text{(VII B-20)}$$

This displays the $1/\lambda$ dependence of F_i.

B5.3 RELEASE FRACTION FOR THE ENTIRE CORE

For the entire core

$$F = \frac{\Sigma_{ji} N_{g_{ji}} g_i}{\Sigma_{ji}\left[N_{P_{ji}} + N_{g_{ji}}\right] g_i} . \qquad \text{(VII B-21)}$$

g_i = fraction 1 total pins in radial segment 1.

Using Equations (VII B-15, 17) this leads to

$$F = \Sigma_i g_i f_i F_i . \qquad \text{(VII B-22)}$$

B5.4 CALCULATIONS OF $T_{b_{ji}}$ AND $(DT/dr)_{bji}$

The surface temperature T_{bji} and the temperature gradient $(dT/dr)_{bji}$ at the pellet boundary for a pin in radial segment i at axial level j are needed to calculate the α_{ji} which appear in Equations (VII B-14) through (VII B-20).

The $T_{b_{ji}}$ was calculated from

$$T_{b_{ji}} = T_w + \frac{2\alpha G}{b} G_{ji}$$

$G_{ji} = \frac{P_z h_j g_i}{4\pi}$ (see Equation (VII B-5))

(VII B-23)

The α in Equation (VII B-23) is a heat transfer coefficient calculated from the equation

$$\alpha = \frac{1}{h_b} + \frac{\Delta r}{K_C} + \frac{1}{h_g} \cdot \frac{r_b}{b} . \qquad \text{(VII B-24)}$$

h_b is a conductance for the water-clad boundary layer. It was estimated by using the temperature difference between the average water temperature and the average clad boundary temperature. Water temperatures for the typical reactors were used, to compute h_b for the PWR and BWR cases, respectively. The K_C is the clad conductivity and r is the clad thickness. The h_g is the gap conductance given in Table VII B-1 and r_b/b is the ratio of the clad radius to pellet radius. Equation (VII B-24) is written so that $T_b - T_w = \alpha \phi$ where ϕ is the heat flux.

This is given by

$$-\left(K \frac{dT}{cdr}\right)_{b_{ji}} = \left(\frac{P_z}{2\pi b}\right)_{ji} = \phi_{ji}$$

This leads to

$$T_{b_{ji}} = T_w + \frac{2}{b} G_{ji}\alpha \qquad \text{(VII B-25)}$$

$\frac{2}{b} G_{ji}$ = flux out of the j,i location.

The $(dT/dr)_{b_{ji}}$ is given [see Equation (VII B-6)] by

$$\left(\frac{dT}{dr}\right)_{b_{ji}} = -\frac{2}{b} \frac{G_{ji}}{K_{cb}} \qquad \text{(VII B-26)}$$

$K_{cb_{ji}}$ = conductivity on the boundary. This is temperature dependent and was computed using Lyon's equation (Ref. 8).

$$K_C = \frac{A}{B+T} + CT^3; \quad A = 28.24\ ^\circ K, \quad B = 129.4\ ^\circ K, \quad C = 4.79 \times 10^{-13}$$

B6. EQUATIONS FOR STRONTIUM

Equations (VI B-19,22) assume that the thermal gradient drives the fission products out of the pin. This is true for Cs because $(\partial\mu/\partial t)_c$ is positive (Ref. 4). For Sr $(\partial\mu/\partial t)_c$ is negative[1] and the thermal gradient alone will keep the fission products in the pin. However, there must be some release due to evaporative processes. This has been estimated as follows.

Consider an annular segment of thickness ℓ at the outer boundary of the pellet. At equilibrium the fission products produced within the segment per second equals the outflow. For the j,i location this may be written

$$2\pi b \Delta h \ell \frac{P_{ji}}{\pi b^2} = 2\pi b \Delta h [KDC + \phi]_{bji} \qquad \text{(VII B-27a)}$$

$$\frac{\ell \bar{P}_z h_i f_i}{\pi b^2} = [KDC + \phi]_{b_{ji}} . \qquad \text{(VII B-27b)}$$

In Equations (VII B-27a, 27b), P_{ji} is the average watts/cm in the pin at j,i.

Δh = length of the segment

ℓ = thickness of the annular region adjacent to the boundary (cm)

ϕ = flux of particle leaving the segment due to evaporative processes, moles/cm^2/sec. They go into the gap and are assumed not to return.

An equation for ϕ_b is needed. Let Q be the potential barrier which must be overcome for a particle to emerge into the gap. Assume, for simplicity, that the particles in the boundary layer have a Maxwellian distribution of energies defined by

$$\frac{C(E)}{C_b} = \frac{2\pi}{[\pi kT]^{3/2}} \sqrt{E}\, e^{-E/kT} = N \sqrt{E}\, e^{-E/kT}$$

---

[1] Values of D_o, Q, $(\partial\mu/\partial T)_c$ for Sr given in Table X of Reference 4 are $D_o = 5.14 \times 10^{-7}$ cm^2/sec, and $Q = 24{,}400$ cal/mol, $(\partial\mu/\partial T)_c = -4$ cal/mol deg. This leads to DK being positive when dT/dr is negative. The result is an inward driving force from the thermal gradient.

$C(E)dE$ = mols/cc of particles with energies in dE at E.

Assume that particles emerging into the gap have energies E-Q (E>Q) and particles with E<Q cannot get out. Then

$$v\,(E-Q) = \sqrt{\frac{2}{m}\,(E-Q)}$$

and

$$\phi = C_b \int_{E=Q}^{\infty} v(E-Q)P(E)d(E)$$

$$= NC_b\sqrt{\frac{2}{m}}\int_{Q}^{E}[E-Q]^{1/2}E^{1/2}e^{-E/kT}$$

(VII B-28)

This integral will be solved with some simplifying approximations. The assumption will be made that most of the integral is achieved before E gets far from Q. Then use

$E' = E-Q$

$$Q = NC_b\sqrt{\frac{2}{m}}\int_{o}^{\infty}\sqrt{E'+Q}\;\sqrt{E'}\;e^{-Q/kT}\;e^{-E'/kT}dE'$$

$$\simeq NC_b\sqrt{\frac{2}{m}}\;\sqrt{Q}\;e^{-Q/kT}\int_{o}^{\infty}\sqrt{E'}\;e^{-E'/kT}dE'$$

$$\sim C_b\sqrt{\frac{2}{m}}\;\sqrt{Q}\;e^{-Q/kT} = C_b\bar{v} \quad \text{(VII B-29)}$$

$$\bar{v} = \sqrt{\frac{2}{m}\,Q}\;e^{-Q/kT}\,. \quad \text{(VII B-30)}$$

Using Equation (VII B-29) in Equation (VII B-27b) yields

$$C_b = \frac{\ell}{\pi b^2}\,\frac{P_z h_j f_i}{\left[(DK)_{ji} + \bar{v}\right]} \quad \text{(VII B-31)}$$

$$\phi_{ji} = \frac{\ell}{\pi b^2}\,\frac{P_z h_j f_i}{\left[(DK)_{ji} + \bar{v}\right]}\;x\;\bar{v}\,. \quad \text{(VII B-32)}$$

The gap release is calculated from

$$\frac{dN_{g_{ji}}}{dt} = 2\pi b\Delta h\phi_{ji} - \lambda N_{g_{ji}}$$

$$N_{g_{ji}} = 2\pi b\Delta h\phi_{ji}\,\frac{[1-e^{-\lambda t}]}{\lambda}$$

$$N_{g_{ji}} = \frac{2\ell}{b}\,\Delta h\,\frac{P_z h_i f_i}{\left[(DK)_{ji} + \bar{v}\right]}\,\bar{v}\,\frac{[1-e^{-\lambda}]}{\lambda}\,.$$

For this situation most of the fission products must be inside the pin or

$$N_{P_{ji}} = \Delta h P_{ji}\,\frac{(1-e^{\lambda t})}{\lambda}$$

$$= \Delta h P_z h_j f_i\,\frac{(1-e^{-\lambda t})}{\lambda}\,.$$

This leads to

$$F_i = \frac{\Sigma_j N g_{ji}}{\Sigma_j\left[N_{P_{ji}} + N_{g_{ji}}\right]}$$

$$\simeq \frac{2\frac{\ell}{b}\,\bar{v}\,\frac{\Sigma h_j}{\left[(DK)_{ji} + \bar{v}\right]}}{9}\,. \quad \text{(VII B-33)}$$

To estimate $\bar{v}$ a value is needed for Q. This could be taken to be the heat of vaporization of strontium at the boundary temperature of the pellet. This is of the order of 30,000 cal/mol (value at 1657°K, Cf Handbook of Chemistry and Physics, 52nd Ed. p D-57). A more conservative estimate would be to use the value associated with diffusion in the lattice, i.e., the same as appears in D. This is 24,000 cal/mol.

The speed $\bar{v}$ may be estimated by writing

$$\bar{v} = \sqrt{\frac{2}{m}}\sqrt{kT}\left[\frac{Q}{kT}\right]^{1/2} e^{-Q/kT} .$$

$$= 2.2 \times 10^5 \left[\sqrt{\frac{\pi}{2}}\sqrt{\frac{1}{m}}\sqrt{\frac{T}{293}}\right]\sqrt{\frac{Q}{kT}}\, e^{-Q/kT}$$

(VII B-34)

In Equation (VII B-34) the 2.2×10^5 cm/sec is the speed of an atom of one atomic unit at 293°K. The next factor in brackets converts this to the speed which an atom of mass m would have at temperature T. The $[Q/kT]^{1/2}\ e^{-Q/kT}$ then appears as a factor which takes account of the barrier. The result is, using m = 88 for Sr,

$$\bar{v} = 2.1 \times 10^4 \sqrt{\frac{T}{293}}\sqrt{\frac{Q}{kT}}\, e^{-Q/kT} .$$

Using $T \sim 1000$, $Q/kT \sim 3$,

$$\bar{v} \sim 6 \times 10^4 e^{-Q/kT} \sim 1 \text{ m/sec}$$

if Q = 24,000 cal/mol.

This is to be compared with

$$DK \simeq D_o\, e^{-Q/kT}\, \frac{1}{RT}\, \frac{dT}{dr} \left(\frac{\partial \mu}{\partial t}\right)_c$$

$$\sim .5 \times 10^{-13} \text{ cm/sec.}$$

It is seen that $\bar{v} >> DK$.

Assuming $\bar{v} >> DK$

$$F_i = \frac{2\ell}{b} \qquad \text{(VII B-35)}$$

and

$$F = F_i . \qquad \text{(VII B-36)}$$

Equation (VII B-35) simply says that the entire production adjacent to the gap leaves by evaporation. The release depends on the depth from which Sr atoms can be expected to evaporate. This cannot be very large, 100 Å or 10^{-6} cm would seem large. This would lead to a fractional release of the order of 4×10^{-4} percent.

B7. RESULTS

The PWR and BWR operating conditions used in the calculations are contained in Table VII B-1.

Tables VII B-2 and VII B-3 give data on the long-lived and short-lived products, respectively.

Table VII B-4 gives releases in percent for xenon and iodine isotopes. Two values are given. The higher value is an upper bound to what might be expected. The lower value (1/3 of the higher) is a more probable or "realistic" value. The factor 1/3 was suggested by W. A. Yuill as being an appropriate scaling factor.

The high values were calculated directly from the FPFM code (Ref. 5) which was designed to give an upper bound to what would actually occur. The power distributions given in Table VII B-1 were used to compute the required heat fluxes at different core locations. Equation (VII B-1) was used to estimate releases of short-lived species relative to the Xe^{131} release. This is certainly conservative.

Table VII B-5 lists the releases for Cs^{137} (29y) and Cs^{138} (32 min). These were calculated using Equation (VII B-19) for the three long-lived isotopes Cs^{133} (stable), Cs^{135} (2.6×10^6 y) and Cs^{137} (29 y). Equation (VII B-20) was used for the short-lived Cs^{138} (32 min). The data on D_o, $(\partial\mu/\mu t)_c$, and Q are from Table X, Reference 4.

$$D_o = 8.53 \times 10^{-9} \text{ cm}^2/\text{sec}$$

$$\left(\frac{\partial \mu}{\partial T}\right)_c = 5 \text{ cal/mol deg.}$$

$$Q = 6100 \text{ cal/mol}$$

The methods used here based on Equation (VII B-35) indicate that the release for 28 y Sr^{90} is very small - less than 0.0004 percent. It would be completely negligible for the short lived isotopes.

Since the releases are strongly affected by the calculated boundary temperatures and temperature gradients, they are given in Table VII B-6 for the hot pin in the PWR. This is the most extreme case.

References

1. An excellent discussion of the ideas involved is given in "The Thermodynamics of the Steady State," by K. G. Denbigh, John Wiley, (1950). Yuill gives additional references to recent applications. A forthcoming report describes the derivation and gives a different result for Equation (VII B-1).

2. Baston, V. F., E. G. Good, W. A. Yuill, "Fission Product Release Analysis," IDO-17242, May 1969.

3. Yuill W. A., V. F. Baston, J. H. McFadden, "Release of Noble Gases from UO_2 Fuel Rods," IN-1346, November 1969.

4. Yuill, W. A., V. F. Baston, J. H. McFadden, "An Analytical Model Describing the Behavior of Fission Products in Operating Fuel Pins," IN-1467, June 1971.

5. Baston, V. F., J. H. McFadden and W. A. Yuill, "An Analytical Method for Calculating Steady-State Fission Gas Release...Fission Product Fuel Model (FPFM) Code," ANCR-1010, September 1971.

6. The derivation of Equation (VII B-1) is discussed in a forthcoming report (H. L. McMurry, "Theoretical Basis for Calculating Diffusion of Fission Products in Fuel Pins," CI-1253.) A variant of Equation (VII B-1) replaces

$$\frac{d\mu}{dr} \text{ by } \frac{Q^x}{T}\frac{dT}{dr} + \left(\frac{\partial \mu}{\partial c}\right)_T \frac{dc}{cr}$$

Here Q^x is the heat of transport. This is the form actually used in the calculations.

7. Denbigh, K. G., "The Principles of Chemical Equilibrium," Cambridge University Press 1964, Chapter 3.

8. Lyons, M. F., et al, "UO_2 Pellet Conductivity from Irradiations with Central Melting," GEAP=4724, July 1964.

TABLE VII B-1 SPECIFIED INPUT DATA FOR FISSION PRODUCT GAP RELEASE CALCULATIONS

	PWR	BWR
Fuel Data		
Fuel pellet diameter, in.	0.367	0.488
Cladding O.D., in.	0.422	0.562
Cladding thickness, in.	0.024	0.032
Fuel density, % T.D.	94	94
Thermal Data		
Average heat flux, Btu/hr, ft^2	191,000	163,000
Peak heat flux, Btu/hr, ft^2	534,000	425,000
Maximum peaking factor	2.8	2.6
Average cladding surface temp., F	610	560
Average gap conductance, Btu/hr, ft^2,F	1000	1000
Average gap conductance, Btu/hr	500	500
Average thermal output, Kw/ft	6.2	7.0
Maximum thermal output, Kw/ft	17.3	18.3
Other Operational Data		
Core end-of-life burnup, MWD/MTU	30,000	30,000
Core end-of-life operating time, sec	10^8	10^8

Core Segmentation and Power Distributions

Axial - 9 equal length sections - same for both reactor types

Axial Section	Power Factor
1 (top)	0.48
2	0.80
3	1.12
4	1.30
5	1.48
6	1.32
7	1.15
8	0.82
9 (bottom)	0.53

Radial and Local - 8 unequal volume, full-length regions for each reactor but with different power factors as tabulated below. These regions really represent different groups of full length rods with the higher power regions of the core being segmented in greater detail.

Radial X Local Region	Fraction of Total Core Rods	Sum of Fractions	Radial X Local Power Factor PWR	BWR
1	0.01	0.01	1.85	1.70
2	0.02	0.03	1.65	1.54
3	0.02	0.05	1.50	1.44
4	0.05	0.10	1.45	1.35
5	0.10	0.20	1.33	1.26
6	0.15	0.35	1.19	1.14
7	0.25	0.60	1.05	1.02
8	0.40	1.00	0.68	0.76

TABLE VII B-1 (CONTINUED)

Fission Product Species	Radioactive	Half-Life
Stable or Long-Lived	Xe-133	(5.27da)
	Xe-135	(9.2hr)
Xe, I, Cs, Sr	I-131	(8.06da)
	I-132	(2.3hr)
	I-133	(20.8hr)
	Cs-138	(32min)
	Sr-89	(51da)
	Sr-91	(9.7hr)

TABLE VII B-2 LONG LIVED FISSION PRODUCT SPECIES[a]

		Chain Yield (%)	σ_a(b), barns
$_{54}Xe^{131}$	Sn^{131}(3.4m)→Sb^{131}(23m)—.85→ Te^{131}(24m)→I^{131}(8.05d)—0.992→ Xe^{131}(stable)	2.9	Xe^{131} 85 I^{131} 0.7
$_{54}Xe^{132}$	Sn^{132}(2.2m)→Sb^{132}(2.1m)→Te^{132}(77h)→I^{132}(2.30h)→Xe^{132}(stable)	4.3	Se^{132} <5
$_{54}Xe^{134}$	Sb^{134}(0.8m)→Te^{134}(44m)→I^{134}(52.5m)→Xe^{134}(stable)	7.9	Xe^{134} <5
$_{54}Xe^{136}$	I^{136}(86s)→Xe^{136}(stable)	6.4	Xe^{136} 0.15
Total $_{34}Xe$		21.5	
$_{53}I^{127}$	Sn^{127}(1.9h)→Sb^{127}(91h)—0.78→Te^{127}(9.3h)→I^{127}(stable)	small	I^{127} 6.4
$_{53}I^{129}$	Sb^{129}(4.6h)—0.64→Te^{129}(72m)→I^{129}(1.7×10^7y)----Xe^{129}(stable)	0.9	I^{129} 28
Total $_{53}I$		0.9	
$_{55}Cs^{133}$	Sb^{133}(4.1m)$_{0.72}$→ Te^{133}(63m)→I^{133}(20.8h)$_{0.976}$→ Xe^{133}(5.27d)→Cs^{133}	6.5	X^{133} 190
$_{55}Cs^{135}$	Te^{135}(<0.5m)→I^{135}(6.7h)$_{0.70}$→Xe^{135}(9.2h)→Cs^{135}(2.6×10^6y)----Ba^{137}(stable)	6.3	Xe^{135} 2.7×10^6
$_{55}Cs^{137}$	I^{137}(24.0s)$_{0.92}$→ Xe^{137}(3.9m)→Cs^{137}(29y)→Ba^{137}(stable)	6.1	Cs^{137} 0.11 Ba^{137} 4
Total $_{55}Cs$		18.9	
$_{38}Sr^{88}$	Br^{88}(15.53)$_{0.96}$→ Kr^{88}(2.8h)→Rb^{88}(17.8m)→Sr^{88}(stable)	36	Rb^{88} 1.0 Sr^{88} 0.006
$_{38}Sr^{90}$	Kr^{90}(33s)→Rb^{90}(2.7m)→Sr^{90}(28y)→Y^{90}(64.3h)---Zr^{90}(stable)	5.8	Sr^{90} 1

(a) Chain data and yields are from "Reactor Physics Constants," ANL-5800, 2nd Edition, 1963. Chains are in Table 1-3, p. 4. Yields are in Table 1-6, p. 8.

(b) Thermal neutron absorption cross section data, where given, are from "Table of Isotopes," 6th Edition, C. M. Lederer, J. M. Hollander, Z. Perlman (Editors), John Wiley (1968).

TABLE VII B-3 SHORT LIVED ISOTOPES
(See Table VII B-2 for references)

Isotopes		Chain Yield, %	σ_a, barns
$_{54}Xe^{133}$(5.27d)	Sb^{133}(4.1m)$_{72}\rightarrow Te^{133}$(63m)$\rightarrow I^{133}$(20.8h)$\rightarrow Xe^{133}$(5.27d)	6.6	Xe^{133} 190
$_{53}I^{133}$(20.8h)			
$_{54}Xe^{135}$(9.2h)	Te^{135}(<0.5m)$\rightarrow I^{135}$(6.7h)$_{0.70}\rightarrow Xe^{135}$(9.2h)	6.1	Xe^{135} 2.7 x 10^6
$_{53}I^{135}$(6.7h)			
$_{53}I^{131}$(8.05d)	Sn^{131}(3.4m)$\rightarrow Sb^{131}$(23m)$_{0.85}\rightarrow Te^{131}$(24m)$\rightarrow^{131}$(8.05d)	3.1	I^{131} 0.7
$_{53}I^{132}$(2.3h)	Sn^{132}(2.2m)$\rightarrow Sb^{132}$(2.1m)$\rightarrow Te^{132}$(77h)$\rightarrow I^{132}$(2.3h)	4.3	
$_{55}Cs^{138}$(32m)	I^{138}(5.8s)$\rightarrow Xe^{138}$(17m)$\rightarrow Cs^{138}$(32.2m)	5.7	
$_{38}Sr^{89}$(51d)	Br^{89}(4.5s)$_{0.85}\rightarrow Kr^{89}$(3.2m)$\rightarrow Rb^{89}$(15.4m)$\rightarrow Sr^{89}$(51d)	4.8	
$_{38}Sr^{91}$(9.7h)	Kr^{91}(10s)$\rightarrow Rb^{91}(^{1.67m}_{14m})\rightarrow Sr^{91}$(9.7h)	5.8	

TABLE VII B-4 RELEASE PERCENTAGES OF Xe AND I ISOTOPES[a,b] AT 10^8 SECOND

Radial Region	$Xe^{131} = I^{131} = I^{129}$ and Xe^{132}, Xe^{134}, Xe^{136}		Xe^{133}(5.17d)		Xe^{135}(9.2h)[c]		I^{132}(2.3h)		I^{133}(20.8h)	
	PWR	BWR	PWR	BWR	PWR	BWR	PWR	BWR	PWR	BWR
1	41 14	27 9	27 9	18 6	.14 .05	.09 .03	.49 .16	.32 .11	4.4 1.5	2.9 1.0
2	37 12	25 8	24 8	16 5	.13 .04	.09 .03	.45 .15	.30 .10	4.0 1.3	2.7 0.9
3	34 11	23 8	22 7	15 5	.11 .04	.08 .03	.40 .13	.28 .09	3.6 1.2	2.5 0.8
4	32 11	22 7	21 7	14 5	.11 .04	.07 .02	.38 .13	.26 .09	3.5 1.2	2.3 0.8
5	28 9	20 7	18 6	13 4	.09 .03	.06 .02	.34 .11	.23 .08	3.0 1.0	2.1 0.7
6	23 8	16 5	15 5	10 3	.08 .03	.06 .02	.27 .09	.20 .07	2.5 0.8	1.8 0.6
7	17 6	13 4	11 4	8 3	.06 .02	.04 .01	.20 .07	.15 .05	1.8 0.6	1.4 0.5
8	4 1	5 2	3 1	3 1	.01 .003	.02 .007	.05 .02	.07 .02	1.4 0.5	0.6 0.2
Total Core	19 6	14 5	12 4	9 3	.06 .02	.04 .01	.22 .07	.16 .05	2.0 0.7	1.5 0.5

(a) I^{131}(8.05d) and I^{129} (stable) assumed equal to Xe^{131} for conservatism. Xe and I isotopes with half lives shorter than 8.05d calculated from Equation (VII B-7) which is based on Equation (VII B-20) which shows releases of short lived products is proportional to half life.

(b) The present model employs an algorithm which calculates the boundary temperature from the heat rating. The large value is an upper bound. The smaller value is a more likely or "realistic" estimate.

(c) An effective decay constant $(\lambda + \sigma(th)) = 3 \times 10^{-4} sec^{-1}$ was assumed.

TABLE VII B-5 CESIUM RELEASE PERCENTAGES AT 10^8 SECONDS

Radial Region	Cesium-137-135-133 Gap Conductance, Btu/hr-ft^2-F				Cesium-138 (32 min) Gap Conductance, Btu/hr-ft2-F			
	PWR		BWR		PWR		BWR	
	1000	500	1000	500	1000	500	1000	500
1	44	61	24	40	0.0040	0.0079	0.0017	0.0033
2	38	54	20	34	0.0031	0.0060	0.0014	0.0026
3	33	49	19	31	0.0025	0.0048	0.0012	0.0024
4	31	47	16	27	0.0023	0.0046	0.00096	0.0019
5	28	41	14	25	0.0020	0.0036	0.00087	0.0017
6	24	35	11	20	0.0016	0.0028	0.00067	0.0013
7	19	29	9	16	0.0012	0.0022	0.00056	0.00097
8	8	13	5	9	0.0005	0.0008	0.00030	0.00050
Total Core	20	31	10	17	0.0014	0.0026	0.00063	0.0012

$D = D_o e^{-Q/RT}$ with $D_o = 8.53 \times 10^{-9}$ cm^2/sec and $Q = 6100$ cal/mol $\cdot \left(\frac{\partial \mu}{\partial t}\right)_c$

$= 5$ cal/mol deg (see Ref. 4).

TABLE VII B-6 BOUNDARY TEMPERATURES AND HEAT RATINGS FOR THE HOT PIN IN THE PWR

Axial Region	G (watts/cm)	Gap Cond = 1000 Btu/hr ft^2 F		Gap Cond = 500 Btu/hr ft^2 F	
		T (°K)	(dT/dr (°C/cm)	T_b (°K)	(dT/dr (oc/cm)
1	14.4	726	-1370	835	-1540
2	24.0	827	-2550	1010	-3000
3	33.6	927	-3930	1180	-4780
4	38.9	984	-4790	1280	-5930
5	44.3	1040	-5720	1375	-7130
6	39.5	990	-4900	1290	-6050
7	34.4	937	-4070	1200	-4980
8	24.6	833	-2630	1020	-3090
9	15.9	742	-1540	862	-1750

T_b calculated from $T_{b_{ji}} = T_2 + \alpha\phi_{ji}$

$$\alpha = \frac{1}{h_{film}} + \frac{\Delta R_{clad}}{k_{clad}} + \frac{r_{clad}}{b} \cdot \frac{1}{h_{gap}}$$

For PWR h_{film} = 5788 Btu/hr-ft^2-F based on average bulk water T of 577 F and average cladding T of 560 F.

K_{clad} for Zircaloy - 4 = 8.89 Btu/hr-ft^2-F.

PWR

h_g = 1000 Btu/hr ft^{2}F

α = 2.39 C/w/cm^{2}C

h_g = 500

α = 4.16

BWR

Fh_g = 1000

α = 2.55

h_g = 500

α = 4.31

Addendum
to
Appendix B
of
Appendix VII

Relation of Heat Rating to Power Per Unit Length of Rod

Fission product releases are often expressed in terms of the heat rating

$$\int_{T_b}^{T_o} K_c dT \ , \qquad \text{(A2.1)}$$

where K_c is the conductivity and T_o and T_b are the temperatures at the centerline and outer boundary, respectively. The heat rating is related to the power per unit length, P_z, in the pin. The relation is particularly simple when the power density in the pin is flat.

Let P(r) be the heat production (power density) in cal/cc sec or watts/cc. Then if the P depends on r, but not on the radial angle Θ

$$2\pi \int_o^r P(r) r dr = -K_c \frac{dT}{dr} \cdot 2\pi r \ . \qquad \text{(A2.1)}$$

In this equation the left side gives the total heat production out to the radius r_o. Under steady state conditions this must all flow outward over the boundary at r by conduction. The right side of Equation (A2.1) expresses this conduction.

Integration of Equation (A2.1) yields

$$\int_o^b \frac{1}{r} \left[\int_o^r P(r') r' dr' \right] dr = \int_{T_b}^{T_o} K_c dT \ . \qquad \text{(A2.2)}$$

Assume

$$P(r) = \bar{P} \left\{ 1 + \sum_{n=o}^{\infty} a_n \left(\frac{r}{b} \right)^n \right\} . \qquad \text{(A2.3)}$$

In Equation (A2.3) the $\bar{P}$ is the average power density

$$\bar{P} = \frac{2}{b^2} \int_c^b P(r) r dr \ .$$

If Equation (A2.3) is used in Equation (A2.2) the result is

$$\int_o^b K_c dT = \frac{\bar{P} b^2}{4} \left\{ 1 + 4 \sum_{n=1}^{\infty} \frac{a_n}{(n+2)^2} \right\} . \qquad \text{(A2.4)}$$

The average power density, $\bar{P}(r)$, if related to the power per unit length in the rod, $\bar{P}_z$, by

$$\bar{P}_z = 2\pi \int_o^b \bar{P}(r) r dr$$

$$\bar{P} = \frac{\bar{P}_z}{\pi b^2} \qquad \text{(A2.5)}$$

Using Equation (A2.5) in Equation (A2.4) yields

$$\int_o^b K_c dT = \frac{\bar{P}_z}{4\pi} \left\{ 1 + 4 \sum_{n=0}^{\infty} \frac{a_n}{(n+2)^2} \right\} .$$

It is seen that the heat rating is simply related to $\bar{P}_z$ when $P = \bar{P}$, i.e., when the power distribution in the pin is uniform. This approximation is often assumed in release analyses.

APPENDIX C

CALCULATION OF GAP RELEASE OF RADIOACTIVE FISSION PRODUCTS

by

G. W. Parker
Oak Ridge National Laboratory

Appendix C

Table of Contents

Section		Page No.
C1.	BACKGROUND	VII-93
C2.	CALCULATION OF PWR AND BWR FUEL ROD GAP RELEASES	VII-94
	C2.1 Diffusion Coefficient Values	VII-94
	C2.2 Release Computation Procedure	VII-95
C3.	THERMAL ANALYSES OF THE REFERENCE CORES	VII-96
	C3.1 Thermal Analysis of the PWR Fuel (Nine Capsule Positions)	VII-96
	C3.2 Thermal Analysis of the PWR Fuel at the Peak and Average Heat Fluxes and With Gap Conductances of 1000 & 500 BTU/HR·Ft^2·F	VII-98
	C3.3 Thermal Analysis of the BWR Fuel (Nine Capsule Positions)	VII-98
	C3.4 Thermal Analysis of the BWR Fuel at the Peak and Average Heat Fluxes and With Gap conductances of 1000 and 500 BTU/HR·Ft^2·F	VII-98
REFERENCES		VII-99

List of Tables

Table		Page No.
VII C-1	Values for Constants in the Arrhenius Equation	VII-100
VII C-2	Initial Gap Release Results	VII-100
VII C-3	Final Estimate of Gap Release Values	VII-101
VII C-4	Results of the Nine Capsule Position Calculations at Peak Radial Power Position in PWR Core	VII-102
VII C-5	Results of the Nine Capsule Position Calculations at Peak Radial Power Position in BWR Core	VII-102

List of Figures

Figure		Page No.
VII C-1	Diffusion Parameter D' Derived from ORNL - Xenon Annealing Data with Comparison Data of OI and TAGAKI and AECL.....	VII-103
VII C-2	Computed D' Values for Fission Products.....	VII-103
VII C-3	Section of PWR Fuel Rod Showing Geometry and Thermal Data Used for Temperature Analysis.....	VII-104
VII C-4	Urania UO_2 Thermal Conductivity.....	VII-104
VII C-5	Section of BWR Fuel Rod Showing Geometry and Thermal Data Used for Temperature Analysis.....	VII-105

Appendix C

Calculation of Gap Release of Radioactive Fission Products

by

G. W. Parker
Oak Ridge National Laboratory

C1. BACKGROUND

Conventional methods for calculating fission gas release from UO_2 are based mainly on the Booth diffusion model concept; however, calculating the release of radioiodine is slightly more involved since the diffusion parameter, D', for iodine often is reported to exceed that for xenon by a factor of at least two. In fact, the results of experimental diffusion studies, the annealing type, show several fission products (Cs and Te) with higher diffusion coefficients. The effect of extended fuel irradiation (burnup) is also significant and may account for more than an order of magnitude in the equilibrium rate of release. Calculations based on conservative assumptions for radioiodine release to the clad gap were given in a recent paper (Ref. 1). An important conclusion is drawn from this paper in that at heat ratings below 10 kw/ft only a few percent of the iodine is released while doubling the power increases the release by a factor of ten.

In addition to the steady-state diffusion process, a second contribution of fission gases, radioiodine and perhaps cesium may come from the heating burst during the thermal transient phase of the accident. In exploratory analyses the release of iodine (i.e., the gap inventory) has been estimated to increase only 10 percent in highly rated fuel but up to 300 percent in fuel at normally low heat rating.

Actual release requires rupture of the sheathing and depends as well upon other inherent retention processes likely to be in effect in a fuel element (e.g., iodine and cesium interaction). Unfortunately, only token credit can be afforded the retention effect until some additional experimental work or experience is actually reported.

The assessment of the potential inventory of volatile fission products (rare gases and halogens) may be outlined by use of an accident sequence and core response process as follows:

a. Reactor vessel depressurization on rapid loss-of-coolant.

b. Core heatup from sensible heat and radioactive decay.

c. Rod rupture beginning at 1200-1400 F accompanied by prompt release of most of the gap inventory of rare gases, a fraction of the iodine, cesium, etc.

d. Continued core heatup prior to turn-around by emergency coolant. This is accompanied by an additional release consisting of a heating burst and a time dependent, slower, thermal transient diffusional release. The peak temperature achieved may be between 1800 and 2200 F.

e. Upon cooling of the core, some additional gaseous release is incurred by fuel pellet breakup.

f. Assuming that fuel rod fragmentation is prevented by the safeguard coolant, the remaining contribution may come only from aqueous leaching of the exposed or expelled fuel including any incurred by a UO_2-water reaction.

g. If the maximum clad temperature reached is conservatively taken as 2200 F (no cladding will melt); however, 100 percent of the rods will fail. The time elapse of the transient before turn-around could be 5 minutes.

Six critical points seem to be involved in the justification of this method of evaluation of the loss-of-coolant prompt release fission product source term:

a. The validity of the application of classical diffusion theory or the

Booth model (Ref. 2) which correlates the experimental release data with temperature, UO_2 density, length of irradiation time, etc. with the equilibrium fuel gap radionuclide inventory.

b. The validity of the higher release rate or diffusion parameter, for iodine compared to xenon from UO_2 to the fuel voids. We cite mainly two references 3,4 using 70 separate determinations of which 63 give D' ratios of iodine over xenon ranging from 1.5 to 12. The median ratio is 6.25 and the square root of the ratio (2.5) is approximately the increase in diffusion rate of iodine over xenon in reactor grade 94 percent dense UO_2.

c. The correlation of burnup with the rate of release of individual fission product elements. ORNL diffusion annealing data (Ref. 5) show a significant burnup effect; however, one cannot assign a quantitative relation from it. Therefore, use of BMI (Ref. 6) and UK (Ref. 7) analyses of the Westinghouse data (Ref. 8) has been proposed. These suggest an increase of one order of magnitude in D' for each 15,000 Mwd/T of accumulated burnup. This correction, however, may be over-conservative according to a recent study by Bailey, et al. (Ref. 9).

d. The significance and magnitude of the heating and cooling burst contribution. This effect is recognized by most experimenters as a departure from simple diffusion or grain growth. It is characterized by a rapid adjustment of fission product inventory remaining in the UO_2 for the transient temperature change, and may be about one-third of the equilibrium difference inventory between the two temperatures.

e. Since radioiodine may be retained in the ruptured rod, by fuel and cladding interaction, a release coefficient escape fraction must be assigned to each release process. At present, this value is mainly speculative; however, tentative values derived by Collins (Ref. 10) and Feuerstein (Ref. 11) may be used. These range from about 0.10 to 0.65 depending upon pressure, rupture temperature, etc.

C2. CALCULATION OF PWR AND BWR FUEL ROD GAP RELEASES

C2.1 DIFFUSION COEFFICIENT VALUES

In order to formulate a direct determination of gap releases of the various fission products, extensive use was made of both the experimentally determined relative diffusion rates for different elements from early ORNL work, as well as an empirically determined absolute relation between temperature and the diffusion parameter $D_i^!$ (D Prime, Empirical) by Lorenz at ORNL (Ref. 12) based on a series of Canadian capsule experiments in which only xenon and krypton were measured. The ORNL data, like most experimental data, are derived from so-called annealing type experiments which then must be critically evaluated for the initial burst contribution as was done for Fig. VII C-1 by Oi and Tagake (Ref. 13) and by Lorenz and Creek (Ref. 14).

Percent release vs temperature values were taken initially from Fig. 6.3 of ORNL Report 3981 (Ref. 3) and the release values were used to compute D' (D-prime) values according to the original method of Booth and Rymer (Ref. 2).

$$F = 1 - \frac{6}{\pi^2} \sum_{n=1}^{\infty} \frac{1}{n^2} e^{-\pi^2 n^2 D' t} \qquad \text{(VII C-1)}$$

where

F = fraction released

t = time in seconds at temperature

Reliable approximations of Equation (VII B-1) are possible.

1. When $F \geq 0.77$

$$F = 1 - \frac{6}{\pi^2} e^{-\pi^2 D' t}. \qquad \text{(VII C-2)}$$

2. When $F < 0.77$

$$F = 6(D't/\pi)^{1/2} - 3D't. \qquad \text{(VII C-3)}$$

The computed D' values were then plotted as log D' versus $10^4/T$ (see Fig. VII C-2) and least squares fitted to a straight line by the expression:

$$\ln D' = a + B(10^4/T) \qquad \text{(VII C-4)}$$

or

$$D' = Ae^{B\left(\frac{10^4}{T}\right)} \qquad \text{(VII C-5)}$$

where

T = absolute temperature and ln(A) = a .

The constants are listed in Table VII C-1.

With these constants, an expression for D-primes for each element can be obtained by the use of the relationship in Equation (VII C-5). For example for Xe & Kr,

$$D' = 232.3\ e^{-4.00534(10^4/T)}.$$

(VII C-6)

Using the data from Lorenz (Ref. 14) (Fig. VII C-1), the relationship used to compute D-primes would:

$$D' = 0.206\ e^{-3.08778(10^4/T)}.$$

(VII C-7)

The D' values obtained by using Equation (VII C-6), as expected, were inordinately high due to the fact that the "burst-effect" could not be evaluated from the data from which the equation was derived. The D-primes for the rare gases, based on the corrected data (Fig. VII C-1) and expressed by Equation (VII C-7) were assumed to be accurate, so that a correction factor, dividing Equation (VII C-7) by Equation (VII C-6), was used to adjust all the D-primes derived from Equation (VII C-6). The value of the correction factor obtained was

$$8.8793 \times 10^{-4}\ e^{0.91756(10^4/T)}.$$

(VII C-8)

Multiplying each D' expression by this factor then uniformly corrects all D-primes for the burst contribution as though each element responded in the same way. While this is probably acceptable for the semivolatile cesium and tellurium, it is most unlikely to be correct for strontium or ruthenium.

The diffusion parameters (D's) were also adjusted for burnup by a correction, K, as follows:

$$D' = D_o' \exp\left[2.303\left(\frac{MWD/T}{25000} - 1\right)\right] = D_o' K$$

(VII C-9)

where D_o' = D calculated from the reference experimental data,

(MWD/T)	K
5,000	0.158
15,000	0.398
25,000	1.000

The D's derived from the ORNL experimental data were empirically normalized to those for 25,000 MWD/T burnup, by comparison of the xenon-krypton data from numerous other measurements (Refs. 7, 8, 9) of the relation between gaseous release and burnup at constant temperature.

C2.2 RELEASE COMPUTATION PROCEDURE

During loading, for both types of reactors, the fuel rods are shifted annually in approximately the following manner: (1) fresh rods are loaded into the outer 1/3 of the reactor, (2) those rods, formerly in the outer 1/3, are shifted to the middle third of the reactor, and (3) those rods in the center third, are removed and the rods formerly in the middle third, are shifted to the center third of the reactor.

A simple computer code was written, called DIREL, which summarizes the fractional release of twenty principal nuclides using the thermal profile predicted by the thermal analysis code described later. In addition consideration is taken of the following approximations:

a. The maximum fission product inventory that a reactor may have should reoccur at the end of any equilibrium cycle. In a typical third-year fuel replacement scheme, the average time of irradiation would be two cycles or about 650 days. This value affects mainly the longlived or stable nuclides.

b. The average burnups for fuel in the outer, middle, and center thirds of a reactor core are assumed to be about 5000, 15,000 and 25,000 megawatt days/ton (MWD/T), respectively, at the end of an equilibrium cycle.

c. Diffusion coefficients for fission products increase by a factor of 10 for every 15,000 MWD/T burnup (Ref. 6).

d. Thermal conductance across the cladding gap is assumed to range between 500 and 1000 Btu/hr/ft^2. The outer one third and half of the center one-third are assumed to be unrestructured and to conform to the lower conductance.

e. Six reactor volume fractions were assigned to the 25,000-Mwd/T region, the 7th to the 15,000 Mwd/T region, and the 8th to the 5000-Mwd/T region and burnup corrections are made on the D's accordingly.

In the reference LWR reactor core, eight thermal zones are defined with zones 1 to 6 inclusive, being in the center one-third of the reactor; zone 7 is in the middle one-third and zone 9 is in the outer one-third.

For thermal analysis, a fuel rod is divided into nine equal lengths. Seven temperature values are given for seven points along the fuel radius of each length. In the gap release computer program: (1) a D-prime for each activity is calculated for each of the seven temperatures using Equation (VII C-5); (2) F (fraction release) values, at equilibrium, are computed using the D' values according to:

$$F = 3(WD'/\lambda)^{1/2}. \qquad \text{(VII C-10)}$$

When $T \leq 400$ C, F = 0 and W = correction factors. If λ is less than 2×10^{-8}, then the isotope is considered to be stable and F is computed according to

$$F = 4(WD't/\pi)^{1/2} \qquad \text{(VII C-11)}$$

where F = fraction released and t = time in seconds; (3) the seven values of "F" are averaged; (4) steps 1 and 2 are repeated for the remaining eight lengths of the fuel rod; (5) the nine "average F" values are averaged to produce the "fuel rod release"; and (6) the average release is computed for the eight regions specified and then

$$\text{Total release} = \sum_{i=1}^{8} \%\ \text{release}_i \times VF_i \times PF_i \qquad \text{(VII C-12)}$$

where VF = volume fraction and PF = power factor.

Initial results of the gap release calculation for the PWR and the BWR systems are tabulated in Table VII C-2 as a function of gap conductance (fuel temperature) and possible variation in computed D' values. From these results the final release estimates for each reactor type, including effects of the gap release coefficient escape fraction and the heating burst, were obtained as shown in Table VII C-3.

C3. THERMAL ANALYSES OF THE REFERENCE CORES

C3.1 THERMAL ANALYSIS OF THE PWR FUEL (NINE CAPSULE POSITIONS)

The "Little Mamu" (Ref. 15) program designed for the IBM 360-91 or 75 computer was used to calculate the temperature distribution within the fuel pin. This is a one dimensional (radial) heat transfer program used in many ORNL reactor experiments and furnished the fuel zone temperature needed for gap release gas and halogen inventory calculations. In this problem the 12 foot long fuel pin was divided into nine equal capsule positions of 16 inches. Capsule position 1 is at the bottom. The radial and axial power factors for a reference reactor were used and the peak heat flux (534,000 Btu/hr/ft^2) was used to calculate a volumetric heat generation in the fuel at the central capsule position No. 5. It is assumed that all the heat is generated in the fuel (none in the cladding, gap or coolant). A peak heat generation rate (capsule position 5) was calculated to be 2.796 watts/gram within the UO_2 fuel. The heat rates at the other capsule positions were calculated by proportion according to the given axial power factor distribution. For computer input the fuel pin was divided into eight regions at each of the nine capsule positions in the geometry shown in Fig. VII C-3. In Fig. VII C-3, Region 1 represents the Zircaloy-2 cladding which was given; (1) a density of zero (for no heat generation) and (2) a linear thermal conductivity versus temperature function of K = 6.7 + 0.004T. Region 2 represents the gap or a material whose density is zero (for no heat generation) and whose thermal conductivity (K) is equal to the product of the thermal conductance (1000 or 500 Btu/hr-ft^2-F) and the gap thickness (X + 0.0035 inch). Regions 3 through 8 represent six equal volumes of UO_2 fuel which were given a thermal conductivity initially according to CURVE C of Fig. VII C-4. The coolant was given; (1) an

inlet temperature of 543 F, (2) a density of zero (for no heat generation), (3) a specific heat, flow area, and flow rate. A thermal heat transfer coefficient was also calculated and input. No thermal expansion was considered. All heat is assumed to flow radially to the coolant by conduction. Given the above data, the computer program first calculates the heat generated in capsule position 1. Half of this heat is added to the coolant to increase its temperature from T_c inlet to T_{c1} at the midlength of capsule position 1 by the equation

$$T_{c1} - T_{c_{inlet}} = Q_{T1}/2WC_P$$

where

Q_{T1} = total heat in cap. pos. 1, Btu/hr
W = flow rate, lb/hr
C_p = specific heat coolant Btu/lb, F

The computer then calculates the outside cladding temperature, T_o, at the midlength of Capsule Position 1, Btu/hr

$$T_o - T_c = Q_{T1}/(HTC)A_s$$

where

HTC = heat transfer coefficient, Btu/hr, ft, F
A_s = area surface outside clad, ft^2

The thermal gradient across the Zircaloy cladding is then calculated by the equation

$$T_1 - T_o = Q_{T1}(\ln R0/R1)/2\pi LK,$$

where

R_o and R_1 are the outside and inside radii of the cladding

L is capsule length = 16 inches

K is thermal conductivity of the cladding at clad mean temp. (Obtained by an iterative process).

The thermal gradient across the gap is then calculated by the equation

$$T_2 - T_1 = Q_{T1} (\ln R1/R2)/2\pi LK$$

where

R1 and R2 are outside and inside gap radii

K is thermal conductivity of gap - C(R1 - R2), where C is the thermal conductance (1000 or 500 Btu/hr ft^2 F).

The thermal gradient in region 3 (the outside fuel region) is then calculated by the equation

$$T_3 - T_2 = (q''' (R2^2 - R3^2)/4K) - (q''' R3^2 (\ln R2/R3)/2K) + (Q_{4-8}(\ln R2/R3)/2\pi LK)$$

where

R2 and R3 are the outside and inside radii of region 3

K is the thermal conductivity at the mean temperature of region 3 according to Figure VII C-4, Curve C, Btu/hr-ft-F

q''' is volumetric heat generation in the fuel, Btu/hr/in^3

Q_{4-8} is the heat generated in regions 4 through 8, Btu/hr.

The thermal gradients in the remaining fuel regions 4 through 8 are calculated in the same manner as above.

The computer then calculates the coolant temperature at the midlength of capsule position 2. Half the total heat generated in capsule positions 1 and 2 is added to the coolant to increase its temperature to Tc_2 by the equation

$$Tc_2 - Tc_1 = (Q_{T1} + Q_{T2})/2\ WC_p$$

where

Q_{T2} is the total heat generated in capsule position 2, Btu/hr.

The temperature distribution at the various region boundaries at each of the succeeding capsule positions is calculated in a like manner. Initial computer runs were made and the coolant flow rate was adjusted to 5686 lb/hr to obtain an outlet coolant temp. of 608.3 F. Also the heat transfer coefficient was made HTC = 6586 Btu/hr - ft^2 - F to attain a peak outside cladding temperature of $T_{o(peak)}$ = 657 F(347.2 C) at

capsule position 5. Two final computer runs were made, one case with the gap conductance equal to 1000 Btu/hr, ft^2, F and the other case with the gap conductance equal to 500 Btu/hr, ft^2, F. Table VII C-4 lists the computer calculated temperature distribution for the two cases.

C3.2 THERMAL ANALYSIS OF THE PWR FUEL AT THE PEAK AND AVERAGE HEAT FLUXES AND WITH GAP CONDUCTANCES OF 1000 & 500 BTU/HR · FT² · F

Four computer runs were made in this analysis, one run or case each for the 1000 and 500 gap conductance for the peak and the average heat fluxes. Only one capsule position of unit length is used for these cases. The input was made such that the outside cladding temperature was 610 F (321.1 C) for the two cases of average heat flux and 657 F (347.2 C) for the two cases of peak heat flux. Heat generation rates in the fuel were calculated and input for each condition of heat flux. The geometry and data (as applicable) of Fig. VII C-3 were input and the calculations for the temperature distribution were made in the manner described for the PWR nine capsule position cases.

C3.3 THERMAL ANALYSIS OF THE BWR FUEL (NINE CAPSULE POSITIONS)

Two cases were run for the BWR fuel (9 capsule positions) - one each for gap conductances of 1000 and 500 Btu/hr,-ft^2,F.

The manner in which temperatures were attained is the same as that described for the PWR fuel except that UO_2 thermal conductivities were taken from CURVE B of Fig. VII C-4. Figure VII C-5 shows the geometry and heat transfer data used for the BWR fuel. The coolant flow rate and specific heat were made large so that the coolant temperature (Tc) would remain constant at each of the 9 capsule positions. The inlet coolant temperature was made 546.4 F which is the saturation temperature at the 1000 psig operating pressure. A coolant heat transfer coefficient was calculated at the average heat flux position from the equation

$$(Q/A)_{ave} = (HTC)\ t_f, \text{ where } (Q/A)_{ave}$$

$$= 163{,}000 \text{ Btu/hr - ft}^2$$

and

$$\Delta t_f = To_{ave} - Tc = 588 - 546.4$$

$$= 11.6 \text{ F.}$$

The HTC_{ave} equals 14,069 Btu/hr - ft^2 - F. From the relation

$$\Delta t_f ave/\ \Delta t_f peak = [(Q/A_{ave})/ (Q/A_{peak})]^{1/4},$$

a Δt_f peak was obtained to calculate a $(HTC)_{peak}$ = 28,912 Btu/hr,ft^2,F for computer input. Table VII C-5 lists the computer calculated temperature distribution for the two cases.

C3.4 THERMAL ANALYSIS OF THE BWR FUEL AT THE PEAK AND AVERAGE HEAT FLUXES AND WITH GAP CONDUCTANCES OF 1000 AND 500 BTU/HR · FT² · F

Same as PWR except BWR fuel and the outside cladding temperature was made 560 F (293.3 C) for the average heat flux conditions and 565.7 F (296.5 C) for the peak heat flux conditions. The geometry and data (as applicable) of Fig. VII C-5 were input for the four cases.

References

1. Parker, G. W., R. A. Lorenz, and G. E. Creek, "The Calculation of Fission Product Release from Core Coolant Safeguarded Reactors", ANS Trans. 12, No. 2, p. 902-3, San Francisco (Nov. 3, 1969).

2. Booth, A. H. and G. T. Rymer, "Determination of the Diffusion Constant of Fission Xenon in UO_2 Crystals and Sintered Compacts", CRDC-720, National Research Council of Canada (August, 1958).

3. Parker, G. W., G. E. Creek, W. J. Martin, C. J. Barton, and R. A. Lorenz, "Out-of-Pile Studies of Fission-Product Release from Overheated Reactor Fuels at ORNL, 1955-1965", ORNL-3981, Oak Ridge National Laboratory (July, 1967).

4. Davies, D., G. Long, and W. P. Stanaway, "The Emission of Volatile Fission Products from Uranium Dioxide", AERE-R-4342, Atomic Energy Research Estab. (June, 1963).

5. Parker, G. W., G. E. Creek, R. A. Lorenz, and W. J. Martin, "Parametric Studies of Fission Product Release from UO_2 Fuels", TID-7641, Third Conf. on Nuclear Reactor Chemistry, Gatlinburg, Tenn. (1962).

6. Morrison, D. L., W. Carbiener, and R. L. Ritzman, "An Evaluation of the Applicability of Existing Data to the Analytical Description of a Nuclear-Reactor Accident", BMI Report 1856 (January, 1969).

7. Evans, D. M. and A. W. Shilling, "Parameters for Estimating the Release of Fission Gases from UO_2 Fuel", TRG Report 1240 (w) (May, 1966).

8. Daniels, R. C., et al., "Effects of High Burnup on Zircaloy-Clad Bulk UO_2 Plate Fuel Samples", WAPD-263, Westinghouse Electric Corp. (September, 1962).

9. Baily, W. E., C. N. Spalaris, D. W. Sandusky, and E. L. Zebroski, "Effect of Temperature and Burnup on Fission Gas Release in Mixed Oxide Fuel", Paper presented at American Ceramic Society Meeting, to be published (May, 1969).

10. Collins, R. D., J. T. Hillary and J. C. Taylor, "Air Cleaning for Reactors with Vented Containment", UKAEA Report TRG 1318(w) (August, 1966).

11. Feuerstein, Horst, "Behavior of Iodine in Zircaloy Capsules", USAEC Report ORNL-4543 (August 1970).

12. Parker, G. W. and R. A. Lorenz, "Prompt Release of Fission Products from Zircaloy-Clad UO_2 Fuels", in Nuclear Safety Program Annual Progress Report for Period Ending December 31, 1967, ORNL-4228, Oak Ridge National Laboratory (April, 1968).

13. Oi, N., and J. Takagi, Zeit Naturf 20a, 673 (1965).

14. Lorenz, R. A., and G. E. Creek, unpublished work supplied by personal communication at ORNL (1973).

15. For a discussion of the basis for "Little Mamu" calculations, see: Olsen A. R., "Preirradiation Data for ORNL Series II and BNW Oxide Fuel Tests in EBR II", ORNL-TM-3446, p. 22, Nov. 1971.

TABLE VII C-1 VALUES FOR CONSTANTS IN THE ARRHENIUS EQUATION

Radioelement	Constant A	Constant B
Xenon-krypton	232.3	-4.00534
Iodine	2.936	-2.95177
Cesium	1.369	-2.62966
Strontium	3.37×10^{15}	-11.2368
Ruthenium	3.8495	-7.01379
Tellurium	53.27	-3.3510

TABLE VII C-2 INITIAL GAP RELEASE RESULTS

Reactor Gap Conductance Conditions	PWR 1000 (1)	PWR 1000 (2)	PWR 500 (1)	PWR 500 (2)	BWR 1000 (1)	BWR 1000 (2)	BWR 500 (1)	BWR 500 (2)
Xe-133	0.75	2.0	2.6	5.9	0.62	1.7	2.0	4.7
Xe-135	0.21	0.63	0.76	2.2	0.17	0.52	0.58	1.7
Kr-85	3.4	6.2	9.4	14.2	2.9	5.4	7.6	11.6
I-129	7.3	12.8	16.0	23.8	6.5	11.2	13.5	20.1
I-131	1.8	4.7	4.9	10.8	1.6	4.0	3.9	8.8
I-132	0.2	0.58	0.54	1.6	0.17	0.5	0.43	1.3
I-133	0.59	1.75	1.6	4.6	0.51	1.5	1.3	3.7
Cs-137	12.1	19.4	23.3	32.8	10.9	17.2	20.2	28.4
Cs-138	0.17	0.49	0.42	1.2	0.15	0.42	0.34	0.96
Sr-89	0.42	0.74	2.2	3.1	0.32	0.57	1.6	2.3
Sr-90	0.63	0.88	2.6	3.8	0.45	0.74	2.0	2.9
Sr-91	0.12	0.24	0.83	1.3	0.08	0.19	0.54	0.96

Conditions:

(1) Used one tenth (1/10) of computed D-primes.

(2) Used burn-up factors on computed D-primes.

TABLE VII C-3 FINAL ESTIMATE OF GAP RELEASE VALUES

	Percent in Gap	Gap Release Coefficient[b]	Percent[a] Released from Rods
		Summary of PWR Data	
Xe^{133}	2.3	1.0	3.1
Xe^{135}	0.7	1.0	1.0
Kr^{85}	7.8	1.0	10.5
I^{129}	14.4	0.5	9.6
I^{131}	4.8	0.5	3.2
I^{132}	0.6	0.5	0.4
I^{133}	1.7	0.5	1.2
Cs^{137}	21.3	0.5	11.0
Cs^{138}	0.5	0.5	0.25
Sr^{89}	1.5	10^{-4}	1.5×10^{-4}
Sr^{90}	1.7	10^{-4}	1.7×10^{-4}
Sr^{91}	1.0	10^{-4}	1.0×10^{-4}
		Summary of BWR Data	
Xe^{133}	1.9	1.0	2.5
Xe^{135}	0.6	1.0	0.8
Kr^{85}	6.5	1.0	8.7
I^{129}	12.4	0.5	8.3
I^{131}	4.0	0.5	2.7
I^{132}	0.5	0.5	0.4
I^{133}	1.4	0.5	0.9
Cs^{137}	17.1	0.5	8.6
Cs^{138}	0.4	0.5	0.2
Sr^{89}	1.1	10^{-4}	1.1×10^{-4}
Sr^{90}	1.4	10^{-4}	1.4×10^{-4}
Sr^{91}	0.4	10^{-4}	0.4×10^{-4}

(a) Noble gases and halogen releases have been increased by one-third for "burst effect" for the thermal transient following loss of coolant.

(b) Gap release coefficient corresponds to the escape fraction terminology used in the main text.

TABLE VII C-4 RESULTS OF THE NINE CAPSULE POSITION CALCULATIONS AT PEAK RADIAL POWER POSITION IN PWR CORE

Position	TC	TO	T1	T2	T3	T4	T5	T6	T7	T8
					Gap Conductance - 1000 Btu/hr, ft^2, F					
1	285.0	301.1	325.9	446.8	508.3	573.3	642.5	716.8	797.6	885.0
2	287.7	312.6	350.4	537.6	642.8	760.4	894.9	1037.9	1191.3	1357.9
3	291.6	326.6	378.8	641.2	810.5	1005.8	1220.9	1463.4	1725.1	1975.2
4	296.6	336.7	396.1	697.2	909.4	1146.3	1415.4	1713.3	1999.8	2254.1
5	302.3	347.3	413.1	750.8	998.7	1278.7	1601.6	1931.6	2223.5	2471.0
6	307.9	347.4	405.4	702.0	911.8	1145.2	1409.7	1702.5	1985.7	2237.9
7	312.7	346.8	396.9	652.5	819.1	1009.9	1219.5	1455.0	1709.0	1954.0
8	316.6	340.9	377.1	559.6	664.5	781.9	914.2	1054.9	1205.8	1369.5
9	319.2	333.8	355.7	465.2	521.7	581.1	644.1	711.2	783.6	862.1
					Gap Conductance = 500 Btu/hr, ft^2, F					
1	285.0	301.1	325.9	567.7	636.5	710.4	790.5	877.7	968.3	1062.9
2	287.7	312.6	350.4	724.7	854.3	994.6	1144.7	1307.1	1483.9	1669.7
3	291.6	326.6	378.8	903.6	1107.8	1335.0	1587.4	1847.6	2087.2	2301.8
4	296.6	336.7	396.1	998.4	1246.4	1530.5	1832.5	2107.1	2348.0	2553.9
5	302.2	347.3	413.1	1088.4	1383.0	1715.7	2035.2	2314.0	2547.9	2752.3
6	307.9	347.4	405.4	998.6	1242.6	1522.0	1820.4	2092.6	2332.6	2537.5
7	312.7	346.8	396.9	908.0	1107.1	1327.9	1573.0	1827.7	2063.6	2275.1
8	316.6	340.9	377.1	742.2	871.2	1009.1	1156.5	1315.8	1488.6	1669.9
9	319.2	333.8	355.7	574.8	637.3	704.0	775.7	854.0	935.0	1019.1

TC = temperature of coolant, C.
TO = temperature of outside surface of Region 1, C.
TX = temperature of inside surface of Region X, C.

TABLE VII C-5 RESULTS OF THE NINE CAPSULE POSITION CALCULATIONS AT PEAK RADIAL POWER POSITION IN BWR CORE

Position	TC	TO	T1	T2	T3	T4	T5	T6	T7	T8
					Gap Conductance = 1000 Btu/hr,ft^2, F					
1	285.8	289.6	316.2	412.5	476.1	542.2	611.2	683.5	759.5	840.0
2	285.8	291.7	332.5	481.5	585.4	696.7	817.3	950.2	1099.8	1267.8
3	285.8	294.1	350.8	559.8	715.6	890.6	1094.6	1334.6	1610.9	1918.7
4	285.8	295.3	360.2	600.1	785.7	1001.2	1263.6	1573.7	1925.5	2297.7
5	285.8	296.5	368.9	637.9	853.9	1114.5	1435.0	1814.7	2230.8	2634.3
6	285.8	295.2	359.1	595.3	777.3	987.7	1243.7	1546.2	1889.6	2255.7
7	285.8	293.9	349.2	552.7	703.5	872.0	1066.7	1295.8	1559.9	1855.0
8	285.8	291.5	331.4	476.8	577.7	685.6	802.2	930.0	1073.0	1234.0
9	285.8	289.3	313.4	400.6	457.7	516.8	578.1	641.9	708.6	778.5
					Gap Conductance - 500 Btu/hr,ft^2,F					
1	285.8	289.6	316.2	508.9	576.4	646.9	721.0	799.1	882.1	971.0
2	285.8	291.7	332.5	630.6	745.5	870.7	1009.8	1168.7	1344.2	1538.7
3	285.8	294.1	350.8	768.9	951.7	1168.4	1420.6	1707.8	2024.6	2349.6
4	285.8	295.3	360.2	840.0	1066.3	1339.9	1660.7	2021.7	2394.8	2747.1
5	285.8	296.5	268.9	906.9	1181.8	1518.1	1908.6	2326.1	2723.8	3099.0
6	285.8	295.2	359.1	831.6	1052.5	1319.1	1631.8	1983.9	2351.1	2700.5
7	285.8	293.9	349.2	756.3	932.2	1138.5	1378.6	1652.6	1955.7	2271.5
8	285.8	291.5	331.4	622.2	733.5	854.4	988.0	1139.3	1307.1	1493.6
9	285.8	289.3	313.4	487.8	548.0	610.6	675.9	744.2	816.0	892.0

TC = temperature of coolant, C.
TO = temperature of outside surface of Region 1, C.
TX = temperature of inside surface of Region X, C.

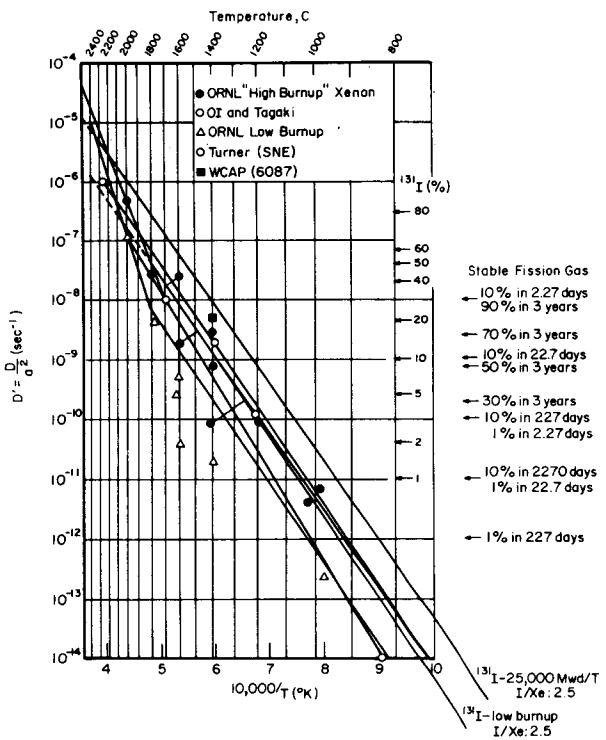


FIGURE VII C-1 Diffusion Parameter D' Derived from ORNL - Xenon Annealing Data with Comparison Data of OI and TAGAKI and AECL

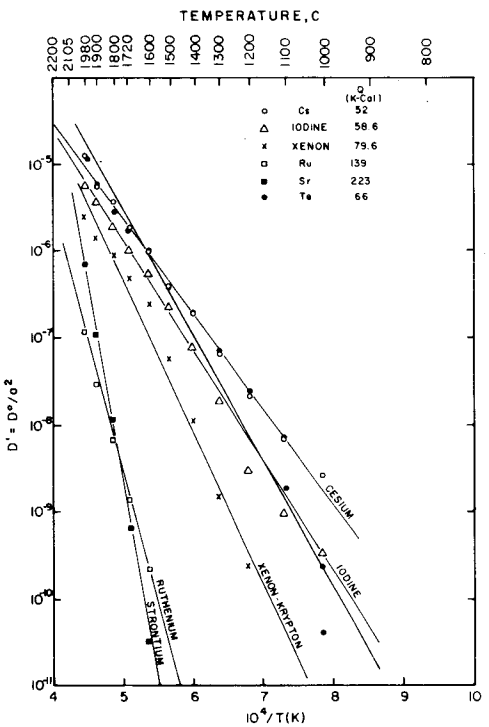


FIGURE VII C-2 Computed D' Values for Fission Products

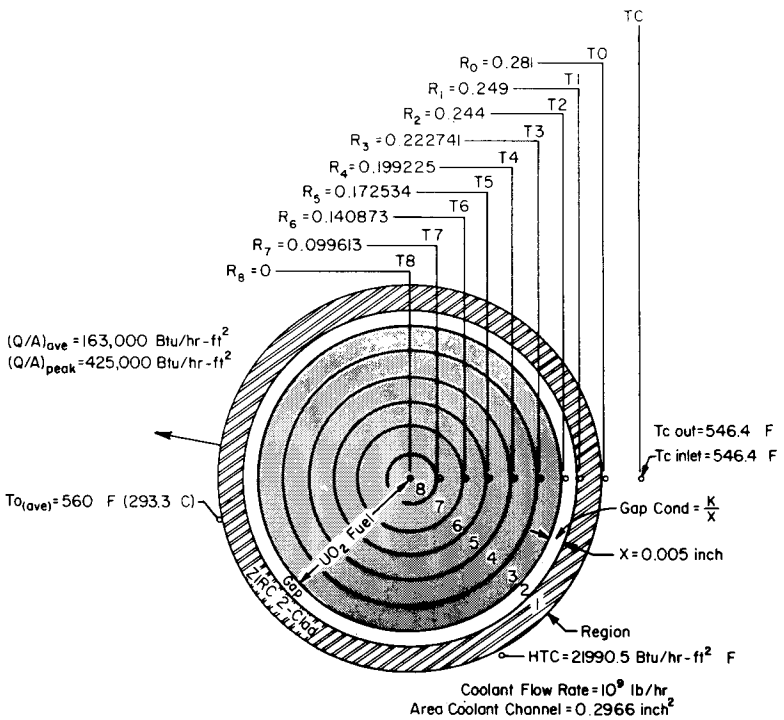


FIGURE VII C-3 Section of PWR Fuel Rod Showing Geometry and Thermal Data Used for Temperature Analysis

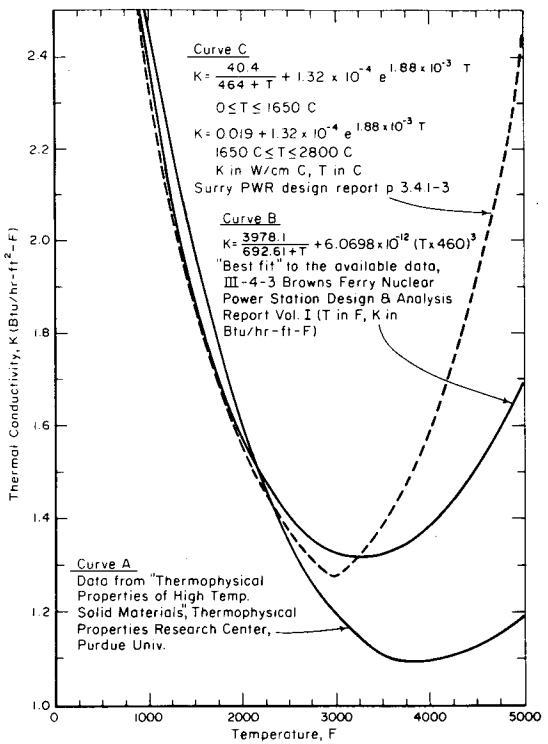


FIGURE VII C-4 Urania UO_2 Thermal Conductivity

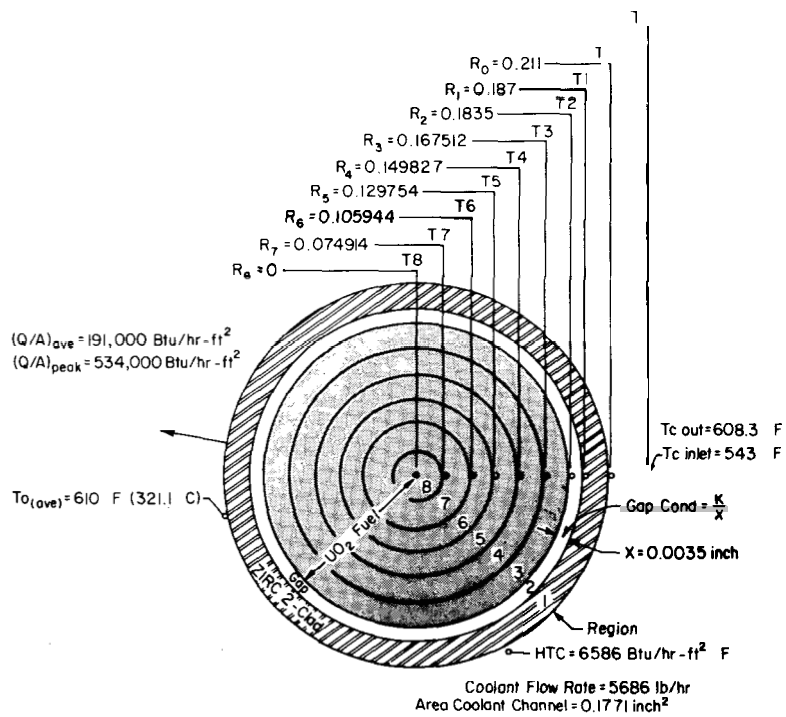


FIGURE VII C-5 Section of BWR Fuel Rod Showing Geometry and Thermal Data Used for Temperature Analysis

APPENDIX D

SURVEY OF EXPERIMENTAL WORK ON FISSION PRODUCT RELEASE FROM MOLTEN UO_2

by

R. L. Ritzman
Battelle, Columbus Laboratories

and

G. W. Parker
Oak Ridge National Laboratory

Appendix D

Table of Contents

Section		Page No.
D1.	OUT-OF-PILE MELTING STUDIES	VII-111
	D1.1 ARC-Image Furnace Experiments	VII-111
	D1.2 Tunsgten Crucible Melting Experiments	VII-112
	D1.3 Tungsten Resistor Melting Experiments	VII-112
	D1.4 Melting Experiments at the NSPP	VII-113
	D1.5 Melting Experiments at the CDE	VII-113
D2.	IN-PILE MELTING STUDIES	VII-114
D3.	SUMMARY AND CONCLUSIONS	VII-115
	REFERENCES	VII-116

List of Tables

Table		Page No.
VII D-1	Fission Product Release from UO_2 Melted in Impure Helium	VII-117
VII D-2	Fission Product Release from UO_2 Melted in Pure Helium by the Tungsten-Crucible Method	VII-117
VII D-3	Fission Product Release from Trace-Irradiated PWR-Type UO_2 Melted in a Single Element Tungsten-Resistor Furnace Filled with Helium	VII-118
VII D-4	Summary of Fission Product Releases Observed in NSPP UO_2 Melting Experiments	VII-118
VII D-5	Fission Product Release from Heated Zircaloy-Clad UO_2	VII-119
VII D-6	Results of ORNL Experiments on Fission-Product Release During In-Pile Melting of Stainless-Steel Clad UO_2	VII-120

Appendix D

Survey of Experimental Work on Fission Product Release From Molten UO_2

by

R. L. Ritzman
Battelle, Columbus Laboratories

and

G. W. Parker
Oak Ridge National Laboratory

Experimental work on the release of a number of important fission products during melting of UO_2 samples has been performed at several laboratories. Numerous factors which can affect release magnitudes or rates have been examined to various degrees, but an extensive data base for use in predicting release during a reactor core meltdown does not exist. This is mainly because no moderate or large amounts of irradiated UO_2 have been melted, particularly in a reactor core configuration. The studies that have been done with small fuel samples do, however, provide useful insights to the general release behavior of the more important fission products. The purpose of this survey is to summarize the more pertinent findings of these studies without developing a comprehensive review of all the work that has been done. Emphasis will be placed on the general conclusions that can be drawn from the data as a whole regarding release magnitudes and significant interactions which should affect the magnitudes.

D1. OUT-OF-PILE MELTING STUDIES

Most of the experimental work of this type has been performed at Oak Ridge National Laboratory (ORNL), but some additional useful data have been obtained at the Contamination-Decontamination Experiment (CDE). Much of the ORNL work consisted of melting small samples of irradiated UO_2 using different furnace heating techniques. The work has been described in a report by Parker, et al. (Ref. 1). Limited investigation of parameters which can affect fission product release was made including burnup, sample size, time molten, atmosphere composition, melting method, and type of cladding. Most of the melting experiments were performed in helium because of reactivity of container or heater materials with oxygen, but a few experiments were performed with CO_2 and air.

D1.1 ARC-IMAGE FURNACE EXPERIMENTS

The first melting experiments were conducted with small (0.2 to 0.6 gram) trace-irradiated and unclad UO_2 specimens held in a BeO support tube. The entire assembly was melted (sometimes incompletely) in an arc-image furnace for periods of 1-1/2 to 3 minutes. Following melting the release of rare gases, iodine, tellurium, cesium, ruthenium, strontium, barium, and rare earth elements was measured by radiochemical analysis. Release was defined as the percentage of each specie that escaped the UO_2-BeO assembly. The helium cover gas used in the experiment contained small amounts of air as an impurity. Table VII D-1 lists the results of the fission product release measurements for these experiments. The rare gas release values should be considered indicative of the degree of melting that was achieved. In general, the data from these small specimens indicate two ranges of release values; one set of high releases which includes rare gases, iodine, tellurium, cesium, and ruthenium, and another set of low releases which include strontium, barium, and rare earths. It is possible that the air impurity in the helium cover gas influenced some of the release values. Strontium, the rare earth elements, and to some extent barium, are known to form quite stable oxides with volatilities significantly less than the respective metals (Ref. 2 and 3). Such reactions may have contributed to the low releases observed for these fission products. On the other hand, ruthenium can form volatile oxides (Ref. 2), and this may have caused the observed high release values. The releases of the remaining fission products would not be expected to be particularly sensitive to the presence of air impurities, since at UO_2 melting temperatures both the oxides, if formed, and the elements exhibit high volatility.

Limited additional experiments of this type were performed in air and carbon dioxide and impure helium atmospheres using UO_2 having burnup levels up to 11,000 Mwd/T. All fission product release data were very similar to the results described above; i.e., either high or low release for the identical sets of fission products. A weak positive correlation of release with burnup level was suggested, but the effect also correlates with differences in sample sizes. No appreciable effect of the different cover gases used on the extent of release was indicated. This was probably because each of the atmospheres created an essentially oxidizing environment. Generally, the data indicate that burnup level should be considered no more than a secondary factor and that air and CO_2 have about the same effect on fission product release from molten UO_2.

D1.2 TUNGSTEN CRUCIBLE MELTING EXPERIMENTS

The next series of experiments consisted of trace-irradiated UO_2 specimens that were melted by induction in tungsten crucibles. The results of these experiments are more useful for two reasons: (1) the larger samples, about 29 grams, are comparable to actual reactor fuel pellet sizes, and (2) an essentially inert furnace atmosphere was maintained so that release data are indicative of non-oxidizing conditions. The data obtained from these experiments are given in Table VII D-2. Comparison with Table VII D-1 shows that, generally, the same release results were obtained by the two melting techniques except for the fission product ruthenium. As noted earlier, ruthenium is known to be quite oxygen sensitive and it is quite possible that its higher release on melting in the arc-image furnace can be attributed to traces of oxygen in the helium supply and the absence of the good oxygen getter (tungsten) that was available in the later experiments with larger samples. Note also in Table VII D-2 that the certain (rare earths) release values approximately correspond to the percent UO_2 that vaporized. This observation is consistent with the known refractory nature of the rare earth oxides. The time that the UO_2 remained molten in these experiments varied to some extent and a weak correlation may exist between release and time molten for the more volatile elements. Nevertheless, the data lead to the conclusion that the melting of bare UO_2 fuel pellets will cause rapid and high release of the more volatile fission products (rare gases, iodine, tellurium, and cesium). The release of ruthenium is very sensitive to the oxidizing nature of the system. Strontium and rare earth release rates should be low and comparable to UO_2 vaporization rates while barium release rates may be somewhat higher (probably due to the lesser stability or higher volatility of its oxide).

D1.3 TUNGSTEN RESISTOR MELTING EXPERIMENTS

The third and final type of laboratory scale out-of-pile melting experiment involved use of a tungsten rod resistor heating element which was passed through cored UO_2 pellets. Both clad and unclad elements were employed in these experiments, but they were limited to a helium atmosphere and complete melting of specimens could not be accomplished before the tungsten rods melted. Nevertheless, the results are quite useful because the high interior fuel temperature and cooler surface achieved with this heating method more nearly simulate nuclear heating than any other out-of-pile technique. The release data obtained from the melting of trace-irradiated UO_2 are given in Table VII D-3. The results from the unclad specimens, after adjusting for the fraction melted, are very similar to the results of the other melting methods with respect to rare gases, iodine, tellurium, cesium, and cerium (rare earths). The releases of strontium and barium are somewhat higher and the release of ruthenium is again low, which suggests that the oxygen activity in the system was even lower than in the tungsten crucible melting experiments. The release from the stainless-steel clad specimen was quite similar to that from unclad fuel.

However, it is evident that the zirconium clad specimens gave very different results for some fission products. The releases of strontium and barium were significantly higher while tellurium release experienced a sharp decrease. Post-melting examinations indicated that the molten zirconium had wet the UO_2 and spread over the surface. Since zirconium is known to have a high affinity for oxygen, this behavior probably caused the clad to serve as a very effective oxygen getter. This led to a very low oxygen activity in the system causing conversion of both strontium and barium to the more volatile metallic forms. The low tellurium release can apparently be explained on the basis of reaction with and retention by the molten zirconium. This conclusion is supported by independent results obtained by Genco, et al. (Ref. 4) which shows that tellurium vapor reacts extensively with zir-

conium metal at temperatures above about 400 C. Since tellurium belongs to the same periodic group as oxygen, it is not too surprising that stable zirconium tellurides could exist at high temperatures. The same considerations provide some insight regarding the lack of effect of stainless steel cladding on fission product releases. Iron, the major component of stainless steel, has a much lower affinity for oxygen (less negative free energy of formation) (Ref. 5) than does zirconium. Consequently, it should not have a strong effect on the oxygen activity in the system (which can influence strontium, barium, and perhaps ruthenium volatility), and by analogy should not tend to form thermally stable tellurides either.

D1.4 MELTING EXPERIMENTS AT THE NSPP

A different series of UO_2 melting experiments were performed at ORNL as part of the Nuclear Safety Pilot Plant (NSPP) program (Refs. 6-9). Samples of clad UO_2 were passed under a plasma torch in different atmospheres to generate an aerosol source for the study of containment behavior processes in an adjacent model containment vessel. The experiments were characterized by many differing conditions and material balances were poor in some instances but the results provide some useful general observations. The release data for these experiments are summarized in Table VII D-4. Two sets of release percentages for various fission products are listed; one for release from the immediate fuel region and another for release from the steel transfer line to the model containment vessel. Looking at the first five experiments (stainless-steel cladding) the data in general indicate high releases from molten fuel for iodine, tellurium, and cesium with much lower releases for the other species. Ruthenium behavior was erratic and probably indicative of the oxygen level in the furnace. None of the release results appear to depend on changes in furnace atmosphere except ruthenium. The latter two experiments with Zircaloy clad high burnup UO_2 are more difficult to interpret. The difference in degree of melting probably masks most atmosphere effects except for ruthenium. Consistent with other data the ruthenium release was relatively high in an air atmosphere. The low ruthenium release in steam could be attributed to a more reducing environment resulting from hydrogen produced by the zirconium-water reaction that would take place between cladding and steam. Also consistent with the out-of-pile melting work described earlier, iodine and cesium releases remain high and apparently independent of atmosphere. The barium release in Experiment 14 and strontium, barium, and cerium releases in Experiment 15 appear somewhat anomalous. The oxygen gettering ability of Zircaloy leading to volatilization of strontium and barium metal could possibly explain the high releases in Experiment 15, but cerium should not be strongly affected and the ruthenium release is not consistent with this hypothesis. The explanation is unknown and much more information about exact conditions in the furnace during melting would be needed in order to analyze the data further. The second set of release numbers in Table VII D-4 provides an indication of the effectiveness with which fission products released from the fuel region were transported to the MCV. Even though temperatures in the transfer line were low (probably several hundred degrees) the transit time was short. In general, plateout factors for all species during this transfer were about the same and ranged from factors of about 2 to factors of about 10. Thus, plateout in the transfer line did not cause a major change in the character of the fission product source that was transported to the model containment vessel.

D1.5 MELTING EXPERIMENTS AT THE CDE

Another short series of out-of-pile experiments in which fission product release from molten UO_2 was measured was conducted at the CDE by Freeby, et al. (Ref. 10). These consisted of five runs in which Zircaloy clad UO_2 pellets were melted by induction in steam atmospheres. The fuel weight ranged from 70 to 80 grams and molten times of about 30 minutes were achieved in each case. Fuel burnups among the five samples ranged from about 500 to 2000 Mwd/T. Some difficulties in achieving material balances were encountered, particularly for iodine and tellurium. However, these experiments are specifically relevant to the conditions that would exist during reactor core melting. The combined results of the five experiments are given in Table VII D-5 along with other pertinent data that investigators obtained from reports of related work. The CDE results generally agree with other out-of-pile release data in that high volatility is indicated for the noble gases, iodine, tellurium, and cesium, and relatively low volatility for strontium, barium, and ruthenium. However, contrary to the ORNL results, the release data do not indicate a dominant effect of the Zircaloy cladding on tellurium or strontium and barium release.

This may be due to the steam atmosphere in the CDE experiments which caused extensive oxidation of the Zircaloy cladding (possibly liberating some retained tellurium) and perhaps producing a high enough oxygen activity in the system to hold strontium and barium as their oxides. The data listed in the table under CMF were the result of a single melting experiment under a steam-air atmosphere in that facility at ORNL. The data continue to support the earlier observations at ORNL concerning the effect of zirconium cladding on tellurium and strontium release. Therefore, the release behavior of tellurium and strontium and barium during melting of Zircaloy clad UO_2 is somewhat uncertain. A comparison of the data obtained in the different experiments identified in Table VII D-5 shows a possible trend toward increase in iodine release with increasing fuel burnup. However, differences in specimen temperatures or melting periods probably influence the results such that the indicated burnup effect is quite indefinite.

In the CDE experiments efforts were made to record the plateout of released fission products that occurred within a short stainless steel transfer line to a containment vessel. The temperature of the line was maintained at about 800 F and transit times ranged from about one to two seconds. In general, it was found that less than 1/3 of the entering fission products deposited in the line except for cerium which was nearly all deposited. The results roughly agree with experience at the NSPP and indicate that longer residence times or higher surface areas would be needed to promote efficient plateout. Another significant observation was recorded during the CDE melting experiments. Even though the small fuel pins were kept molten for 30 minutes or so, most of the fission product release took place within a one- to two-minute period relatively early in the experiments. This rapid release coincided with melt-through of the Zircaloy cladding (pin lying on its side in UO_2 powder). Subsequently large quantities of particulates (cladding and fuel) were released creating a white smoke in the furnace. A continuous slow release of fission products occurred during the period the fuel was maintained in the molten state. Although unconfirmed, it seems probable that the early rapid release was due to escape of the highly volatile fission products while the slower continuous release was due to the low volatility species. The appearance of a dense aerosol in the furnace is indicative of the ease with which released vapors will condense and agglomerate to form a particulate source.

D2. IN-PILE MELTING STUDIES

In addition to the out-of-pile melting experiments, a series of in-pile fuel melting experiments were conducted at ORNL (Ref. 15). These experiments consisted of melting miniature stainless-steel-clad UO_2 fuel elements (~30 grams UO_2) in various atmospheres in the Oak Ridge Research Reactor and measuring the fission products released. Fission and gamma heat in the reactor raised the temperature of the miniature fuel elements sufficiently high to melt the UO_2 without the use of external heat. Data were obtained for fission product release from the fuel zone (fuel element and thoria holder) and from the high temperature zone (thoria and zirconia insulation) which had a minimum temperature of 1000 C. Although over twenty experiments were run most of the major results are contained in the summary of seven runs that are given in Table VII D-6. The first set of values (release from the fuel zone) show extensive release of iodine, tellurium, and cesium regardless of the type of atmosphere. The other fission products and the UO_2 fuel also experienced relatively large releases which were reduced somewhat in high steam concentration atmospheres. The second set of values in the table (release from the high temperature zone) are more useful to reactor accident analysis because they give a better indication of escape from a core region which is not entirely molten. These data are also more comparable with out-of-pile studies which often achieve incomplete melting and have steep thermal gradients in the sample region of the furnaces. The release data in Table VII D-6 can, in general, be divided into two groups, a group having high values and another group having low values. Iodine, tellurium, and cesium belong to the high group while ruthenium, strontium-barium, and zirconium - cerium belong to the low group. In Experiments 13 and 18 ruthenium release was exceptionally high which was probably due to the highly oxidizing nature of the atmosphere in the system. These observations are generally consistent with the results that have been obtained from the various out-of-pile melting studies. The in-pile experiments resulted in a number of other conclusions (Ref. 17) which are pertinent to reactor core meltdown analysis.

a. Stainless steel appears to retain ruthenium and, under oxidizing conditions, to lower the melting

point of the UO_2. However, retention of the ruthenium by oxidized stainless steel was not observed.

b. Fission product release showed only a weak, if any, correlation with a factor of 1,000 increase in fuel burnup.

c. Electron photomicrographs of particles collected on filters in the in-pile apparatus indicated the source consisted of sub-micron sized particles which were generally spherical in shape.

D3. SUMMARY AND CONCLUSIONS

The experimental work that has been done regarding fission product release from UO_2 during melting can be generally summarized as follows:

a. Nearly total release of the noble gases, iodine, cesium, tellurium should be expected within a few minutes from standard pellet-size masses of UO_2. The release of these species seems largely independent of whether oxidizing or reducing conditions exist during melting. Release of the four elements is unaffected by stainless steel cladding and only tellurium is influenced by Zircaloy cladding. Considerable retention of tellurium, probably through compound formation with zirconium, can occur but complete oxidation of the Zircaloy would be expected to liberate such reacted tellurium.

b. The release behavior of ruthenium can be quite complex because it forms volatile oxides. The degree of oxide formation appears quite sensitive to the oxygen activity in the system. The oxygen activity depends on both the gaseous atmosphere that exists and the other oxygen reactive materials that are present. Air, carbon dioxide, and also steam represent oxidizing atmospheres for ruthenium. However, zirconium (and Zircaloy) is a very effective oxygen getter. Consequently, the release of ruthenium from Zircaloy clad UO_2 in the above atmospheres should be expected to depend on the degree of cladding oxidation. If the cladding is completely oxidized, then excess air, CO_2, or steam would be available and fission product ruthenium should experience large release. If the Zircaloy is only partly oxidized, the oxygen activity would be low, ruthenium should remain in the metallic state and be expected to experience only small release. Since stainless steel is less reactive with oxygen, it should have less effect on oxygen activities than Zircaloy. However, evidence indicates that metallic ruthenium will partition into stainless steel from UO_2 and considerable oxidation of the stainless-steel may be necessary to cause release of the dissolved ruthenium.

c. The release behavior of strontium and barium should also depend on the oxygen activity in the system but not to the degree nor in the manner of ruthenium. Metallic strontium and barium are not very volatile and their oxides are even less volatile. Therefore, the higher releases of these fission products should occur under conditions of low oxygen activity, or, for clad UO_2, in situations where incomplete oxidation of the Zircaloy has left some free zirconium. The limited experimental data tend to confirm this behavior and indicate that even under very reducing conditions, the release of these elements will not reach high values. The data also show that stainless-steel has essentially no effect on strontium or barium release from UO_2. Thus, stainless steel is apparently not effective in reducing the oxygen activity far enough to cause conversion of the alkaline earth oxides to the respective metals. If these fission products exist as oxides then low release from molten UO_2 is to be expected.

The release of cerium (a rare earth) and fission product zirconium were found to be quite low in essentially all the melting experiments. These elements form very stable nonvolatile oxides and their release from UO_2 should be nearly insensitive to external atmosphere and chemical effects of cladding materials. The experimental results almost entirely support this conclusion.

References

1. Parker, G. W., et al., "Out-of-Pile Studies of Fission-Product Release from Overheated Reactor Fuels at ORNL, 1955-1965", ORNL-3981 (July, 1967), p. 92-102.

2. Bedford, R. G., and Jackson, D. D., "Volatilities of the Fission Product and Uranium Oxides", UCRL-12314 (January, 1965).

3. Gabelnick, S. D., and Chasanov, M. G., "A Calculational Approach to the Estimation of Fuel and Fission-Product Vapor Pressure and Oxidation States to 6000 K", ANL-7867 (October, 1972).

4. Genco, J. M., et al., "Fission-Product Deposition and Its Enhancement Under Reactor Accident Conditions: Deposition on Primary System Surfaces", BMI-1863 (March, 1969) p. 38-42.

5. Coughlin, J. P., "Contributions to the Data on Theoretical Metallurgy. XII Heats and Free Energies of Formation of Inorganic Oxides", U.S. Bureau of Mines Bulletin 542 (1954).

6. Parsly, L. F. and Row, T. H., "Study of Fission Products Released from Trace-Irradiated UO_2 into Steam-Air Atmospheres (Nuclear Safety Pilot Plant Runs 8 and 9)", ORNL-TM-1588 (May, 1966).

7. Parsly, L. F. and Row, T. H., "Behavior of Fission Products Released From Synthetic High Burnup UO_2 in Steam Atmospheres (Nuclear Safety Pilot Plant Runs 10-12)", ORNL-TM-1698 (February, 1967).

8. Parsly, L. F. and Row, T. H., "Behavior of Fission Products Released into a Steam-Air Atmosphere From Overheated UO_2 Previously Irradiated to 20,000 Mwd/T (Nuclear Safety Pilot Plant Run No. 14, Part I), ORNL-TM-1908 (September, 1967).

9. Parsly, L. F., et al., "Release and Transport of Fission Products Released From Fuel Pins Irradiated to 20,000 Mwd/T: Summary Report of NSPP Run 15", ORNL-TM-3533 (February, 1972).

10. Freeby, W. A., Lakey, L. T., and Black, D. E., "Fission Product Behavior Under Simulated Loss-of-Coolant Conditions in the Contamination-Decontamination Experiment", IN-1172 (January, 1969).

11. Collins, R. D., and Hillary, J. J., "Some Experiments Related to the Behavior or Gas-Borne Iodine", TRG-933 (W) (1967), p. 5.

12. Collins, R. D., Hillary, J. J., and Taylor, J. C., "Air Cleaning for Reactors With Vented Containment", TRG-1318 (W) (August, 1966), p. 18.

13. Cottrell, WM., B (prog. dir.), "Nuclear Safety Program Annual Progress Report for Period Ending December 31, 1966", ORNL-4071 (March, 1967), p. 76.

14. Browning, W. E., Jr., et al, "Release of Fission Products During In-Pile Melting of UO_2", Nucl. Sci. and Eng., 18, 151-162 (1964).

15. Cottrell, Wm. B. (prog. dir.), "Nuclear Safety Program Semiannual Progress Report for Period Ending June 30, 1964", ORNL-3691 (November, 1964), p. 32.

16. Cottrell, Wm. B. (prog. dir.), "Nuclear Safety Program Semiannual Progress Report for Period Ending December 31, 1964", ORNL-3776 (March, 1965) p. 113.

17. Cottrell, Wm. B. (prog. dir.) "Nuclear Safety Program Semiannual Progress Report for Period Ending June 30, 1965", ORNL-3843 (September, 1965), p. 37.

18. Fischer, J., Schilb, J. D., and Chasanov, M.G., Investigation of the Distribution of Fission Products Among Molten Fuel and Reactor Phases. (Part I - The Distribution of Fission Products Between Molten Iron and Molten Uranium Dioxide)", ANL-7864 (October, 1971).

TABLE VII D-1 FISSION PRODUCT RELEASE FROM UO_2[a] MELTED IN IMPURE HELIUM[b]

Run No.	Sample Weight (g)	Time at Temp. (sec)	Percentage of Individual Fission Product Released							
			Rare Gases	I	Te	Cs	Ru	Sr	Ba	TRE[c]
1	0.57	120	64	71	60	59	28	0.18		
2	0.34	120	91	70	72	25	60	0.07	0.8	0.2
3	0.56	120	93	84	86	34	32	0.16	0.9	1.1
4	0.56	180	56	67	63	24	75	0.11	1.3	0.7
5	0.58	180	63	46	54	12	36	0.11	2.6	0.5
6	0.37	120	69	51	43	7.1	20	0.26	0.5	0.3
7	0.18	120	99.4	84	86	90	72	0.20	2.0	0.7
8	0.25	90	99.6	95	96	93	76	3.9	7.3	3.8

(a) Trace-irradiated pellet melted simultaneously with BeO support tube in arc-image furnace.

(b) Helium flow rate, 100 cc/min.

(c) Total rare earths.

TABLE VII D-2 FISSION PRODUCT RELEASE FROM UO_2[a] MELTED IN PURE HELIUM[b] BY THE TUNGSTEN-CRUCIBLE METHOD

Molten Time (min.)	Percent UO_2 Vaporized	Percentage of Individual Fission Product Released							
		Xe-Kr	I	Te	Cs	Ru	Sr	Ba	Ce
1.0	0.10	93	77	90	63	0.45	0.33	4.8	0.05
1.5	0.16	98	98	98	66	0.05	0.47	2.6	0.07
2.0	0.16	99	99	99	60	0.32	0.41	3.0	0.17
2.5	0.25	99	95	99	72	0.33	0.53	2.4	0.13
1.5[c]		99	88	92	80	0.20	0.26	2.6	0.40
2.5[c]		99	93	96	89	0.70	0.50	3.6	0.10

(a) Sample: 29g; PWR UO_2; irradiated at tracer level and preheated in helium for 4.5 to 5.0 min.
(b) Atmosphere: purified helium flowing at a rate of 700 cc/min.
(c) UO_2 sample had a slightly higher density than the first four samples.

TABLE VII D-3 FISSION PRODUCT RELEASE[(a)] FROM TRACE-IRRADIATED PWR-TYPE UO_2 MELTED IN A SINGLE ELEMENT TUNGSTEN-RESISTOR FURNACE FILLED WITH HELIUM[(b)]

Element	Heat Duration (min.)	UO_2 Vaporized (%)	Percentage of Individual Fission Product Released							
			Xe-Kr	I	Te	Cs	Ru	Sr	Ba	Ce/RE
UO_2	5.0	0.8	63	47	56	44	1.6	1.6	5.3	0.6
UO_2	4.0	0.2	50	30	42	41	0.4	0.8	2.9	0.5
UO_2	4.4	0.3	34	25	33	40	0.05	1.2	4.3	0.5
UO_2 (SS clad)	4.7	0.2	56	52	31	46	0.5	1.0	4.2	0.3
UO_2 (Zr clad)	7.0	0.1	52	24	1.1	28	0.1	10.1	10.6	0.5
UO_2 (Zr clad)	6.7	0.04	41	50	0.6	32	0.2	10.0	7.5	0.5

(a) Results are not corrected for the fraction of the sample melted which is approximately equal to the percent rare gas release. Release is from fuel and cladding.

(b) Helium flow rate, 400 cc/min.

TABLE VII D-4 SUMMARY OF FISSION PRODUCT RELEASES OBSERVED IN NSPP UO_2 MELTING EXPERIMENTS

Expt. No.	Furnace Atmos.	Clad Mater.	Degree Melted	Percent Release From Fuel Mass								
				I	Te	Cs	Sr	Ba	Ru	Ce	Zr	U
8[(a)]	He-steam	SS	5%	9	2	6	0.1	1.0	0.3	0.1	0.01	0.1
9[(a)]	He-steam	SS	80%	61	30	29	0.1	0.3	16.0	0.7	0.1	1.0
10[(b)]	A-H_2	SS	70-80%	26	--	20	0.07	--	2.0	0.2	--	0.3
11[(b)]	Air	SS	70-80%	96	--	44	0.05	--	27.0	0.2	--	1.0
12[(b)]	A-H_2	SS	50%	74	32	85	--	2.0	0.9	0.5	--	2.0
14[(c)]	Steam	Zry-2	limited	10	--	6	0.9	64.0	0.4	0.3	--	--
15[(c)]	He-air	Zry-2	high	70	--	56	41.0	32.0	29.0	10.0	--	--
				Percent Transferred to MCV								
8	He-steam	SS	5%	2	0.3	0.1	0.02	0.2	0.02	0.02	--	0.01
9	He-steam	SS	80%	35	8.0	10.0	0.08	0.06	2.0	0.2	0.03	0.3
10	A-H_2	SS	70-80%	24	--	19.0	0.03	--	1.0	0.2	--	0.2
11	Air	SS	70-80%	84	--	26.0	0.02	--	12.0	0.008	--	0.6
12	A-H_2	SS	50%	9	3.0	4.0	--	0.02	0.09	0.05	--	0.02
14	Steam	Zry-2	limited	2	--	0.7	0.2	2.0	0.1	0.2	--	--
15	He-Air	Zry-2	high	27	--	42.0	14.0	12.0	0.4	1.0	--	--

(a) Clad UO_2 trace irradiated.
(b) Simulated high burnup UO_2-premixed.
(c) Irradiated to 20,000 Mwd/T.

TABLE VII D-5 FISSION PRODUCT RELEASE FROM HEATED ZIRCALOY-CLAD UO_2

Experiment	CDE	CMF[b]
Fuel Burnup (Mwd/T)	460-2000	7000
Fission Product Releases - Percent of Fuel Inventory		
Xe, Kr	86-90	
I[a]	15-44	91.0
Te	7-22	2.0
Cs	3-21	30.0
Sr	0.01-0.05	0.2
Ba	0.04-0.20	-
Mo	2-8	-
Ru	0.003-0.7	0.2
Zr-Nb	0.0001-0.1	

(a) Some British work at low burnup has been performed:

Reference	Burnup	Iodine Release,%
11	1-2	14-15
12	100	8-35

(b) See Reference 13.

TABLE VII D-6 RESULTS OF ORNL EXPERIMENTS ON FISSION-PRODUCT RELEASE DURING IN-PILE MELTING OF STAINLESS-STEEL CLAD UO_2

Expt. No.	Sweep Gas	UO_2 Melted, %	I	Te	Cs	Ru	Sr-Ba	Zr-Ce	UO_2
				Material Released from the Fuel Zone[b] - %					
4,5,9	Dry He	100	99+	99	99	78	77	65	48
13,18	Moist air[a]	100	98	97	95	38	33	28	27
16	87% steam	100	90	96	96	13	16	9	7
	13% air								
17	87% steam	100	95	90	89	21	19	5	3
	12% He								
	1% H_2								
				Material Released from the High Temperature Zone[c] - %					
4,5,9	Dry He	100	86	86	71	4	1.4	0.4	0.09
13,18	Moist air[a]	100	95	89	83	16	1.4	0.6	0.90
16	87% steam	100	67	92	42	0.8	0.8	0.1	0.2
	13% air								
17	86% steam	100	73	87	30	1.2	3.6	0.5	1.3
	12% He								
	1% H_2								

(a) The steam concentration in this atmosphere was low, corresponding to air saturated with water vapor at 23 C.

(b) Molten times lasted about 5 minutes.

(c) Minimum temperature, 1000 C.

APPENDIX E

AN EVALUATION OF FISSION PRODUCT AND FUEL CONSTITUENT RELEASE FROM REACTOR FUELS BASED ON A THERMODYNAMIC ANALYSIS OF THE COMPOUND SPECIES PRESENT IN THE FUEL

by

M. Pobereskin, C. Alexander and R. Ritzman
Battelle's Columbus Laboratories

Appendix E

Table of Contents

Section		Page No.
E1.	INTRODUCTION	VII-125
E2.	ANALYSIS FOR TEMPERATURES BELOW FUEL MELTING	VII-126
E3.	ANALYSIS FOR MOLTEN FUEL	VII-127
E4.	CONCLUSIONS	VII-127
	REFERENCES	VII-128

List of Tables

Table		Page No.
VII E-1	Results of Thermodynamic Analysis at T = 800 K	VII-129
VII E-2	Results of Thermodynamic Analysis at T = 1300 K	VII-129
VII E-3	Results of Thermodynamic Analysis at T = 1900 K	VII-130
VII E-4	Results of Thermodynamic Analysis at T = 2500 K	VII-130
VII E-5	Vapor Species and Maximum Volatilization Rate Estimates, T = 3100K	VII-131

Appendix E

An Evaluation of Fission Product and Fuel Constituent Release From Reactor Fuels Based on a Thermodynamic Analysis of the Compound Species Present in the Fuel

by

M. Pobereskin, C. Alexander and R. Ritzman
Battelle's Columbus Laboratories

E1. INTRODUCTION

Considerable research has been performed aimed at establishing the nature and amount of fission products released from the core of a light water nuclear reactor in event of a loss-of-coolant. Experimental and analytical approaches have both been attempted (Ref. 1). Generally speaking, the experiments have been on a laboratory scale, and require extensive interpretation to reflect real life conditions. Similarly, the analytical approaches have been predicted on existence of chemical species presumed from general knowledge of the chemistry of the element.

In this study, the evaluation of fission product behavior is based upon a thermodynamic analysis of the fission product and fuel species present in the fuel under pertinent conditions. This is made possible through the application of the EQUICA computer program to the analysis of the nature, amount, and state of the species at thermodynamic equilibrium.

EQUICA rapidly computes the composition of a given set of reaction species. It is especially versatile in its ability to accept input data which can incorporate thermal and entropy effects other than those of the tabulated values given in handbooks and the JANAF Tables.

EQUICA consists of a basis which may contain 20 species in which all elements present in the computation are present in either elemental or some combined form. An additional 40 species may be included in the computation. There are no other stipulations applied to the basis other than it can contain no more than 20 different elements. As a matter of fact, the program has provision for shifting the basis so that the species richest in a certain element would form the basis for that element in all species in which it appeared, and all equilibrium constants would be based on its equilibrium value in that particular composition. For instance, in a computation at very high temperature gaseous carbon may form the basis for carbon, under pyrolysis conditions elemental carbon may form the basis, and under combustion conditions carbon in carbon dioxide may form the basis for carbon. This ability to shift basis greatly improves the convergence for complex systems when the final composition differs markedly from the initial estimate. Unlike most thermochemical programs there is no limit on the number of solids in either the basis or nonbasis sets, and one can have the same chemical substance present as both a gas or vapor and a condensed phase or as a component in a solution. Under these conditions EQUICA will correctly determine the saturation vapor pressure of the vapor species. EQUICA will also allow for the vanishing of a condensed phase if it is established thermodynamically that the phase should not exist. This is in keeping with the phase rule and ensures that the proper degrees of freedom are maintained.

The program utilizes a composition matrix made up of N molecular species comprised of S chemical elements. A composition matrix relates the species to the elements. If one considers then that the composition N_i of the I^{th} species be changed by $\Delta\xi$, then to preserve stoichiometry the following changes in the composition of the basis are needed:

$$N_i^1 = N_i + \Delta\xi.$$

It is possible that for some minor species N_i^1 could go negative, and since N_i enters the program for the form of ($\ln N_i$), then this relation becomes undefined as $N_i \to 0$. For this reason a subroutine FUDGE has been written and

incorporated to determine if the current $\Delta\xi$ produces non-positive N_i values. If it is found that negative compositions exist then the subroutine computes a new $\Delta\xi$ value which allows all N_i's to remain constant. The input data include initial estimates of composition and Gibbs free energies of all species at the desired temperature and pressure. The output consists of the following:

a. The equilibrium compositions of all species.

b. The equilibrium constants of all species. (Although equilibrium constants for the basis species are not defined, the program sets their value to one. Thus a one in the equilibrium constant column indicates that this species currently is a basis species.)

c. A defined by $A = \frac{P}{\sum_{i}^{n} \gamma_i N_i}$

This A value is then related to the volume the gaseous products would occupy at pressure P and temperature T.

d. The convergence vector, C, which defines the extent of convergence of all major and minor species.

e. Partial pressure for each species.

f. Total pressure (sum of partial pressures).

E2. ANALYSIS FOR TEMPERATURES BELOW FUEL MELTING

In the present analysis, it was necessary, of course, to include uranium, oxygen, zirconium, hydrogen, and helium among the element inputs to the program. This left room in the program for fifteen elements to be selected from the major fission products. It was found that selecting these elements was not as limiting as was the condition that only 60 compound species could be considered. In addition to the elements listed above, Cs, Ba, La, Sm, Mo, Ru, Te, I, Br, and Sr were included in the analysis. This choice of elements was based not only on abundance in fission yield and representation of the major chemical groups, but also on uniqueness of thermochemical properties. For example, the lanthanum oxide would satisfactorily represent the sesquioxides except that elemental samarium was considered to be sufficiently volatile that in the first analysis samarium needed to be considered apart from the other rare earths.

Two computer runs were made based on approximate preaccident and postaccident conditions. The initial run was designed to provide some prediction of the chemical species that could exist in fuel rods just before the accident, and to indicate fission product volatility as a function of temperature for periods after this. The effect of several parameters was examined.

a. Fuel burnup - 1 and 4 percent were used to produce variations in fission product concentration.

b. Temperature - equilibrium calculations were made for 800, 1300, 1900, and 2500K, corresponding roughly to temperature regions in operating fuel rods and to accident temperatures for an overheating reactor core.

c. Pressure - 1000 and 2000 psia were used to simulate internal rod pressures.

d. Steam concentration - 30 ppm water in the fuel and unlimited steam supply were used to simulate normal conditions and more oxidizing conditions for the fuel-fission product-cladding system.

Elemental compositions were predicted on a nominal fuel rod containing 10 pounds of UO_2 and 2 pounds of zirconium. Solution effects of oxides in the parent fuel were not included because, for the most part, the oxides have very limited solid solubility in UO_2.

The results of the parametric analysis to 2500K are summarized in Tables VII E-1 through VII E-4, which for each temperature give the predicted dominant condensed phase and vapor phase forms and the approximate mole ratio of material in the vapor phase to material in the condensed phase. This ratio indicates the volatility of the fission product species. Several conclusions were drawn from the data.

a. The degree of burnup and the total pressure had negligible effects on the results.

b. The volatility of some species (generally Ba, La, Sm, Zr, and Sr) is depressed by excess steam (more oxidizing conditions) with the effect more evident at lower temperatures.

c. The volatility of some species is enhanced by excess steam - Ru and U at higher temperatures and Te, I, Br, and Cs at lower temperatures.

d. The most volatile fission product species are Cs, Te, and CsI. At higher temperatures, particularly under more reducing conditions, Ba and Sr begin to approach the above three in volatility.

Generally speaking, the results confirmed what one might have predicted from a general knowledge of the chemistry of the involved elements. An exception was the indication that iodine and bromine react with the excess cesium in the fuel. In the subsequent runs, with HI as a species in the matrix, the CsI was still the indicated major iodine carrying species, even at temperatures to 3100K. Furthermore, CsI will not oxidize in air to Cs_2O and I_2 nor in water vapor to $Cs_2O + 2HI$. Therefore, based on these calculations it appears that CsI may be present in the released fission product vapors. It should be noted though that no experimental confirmation of this prediction is available, and other reactions that cesium might undergo could alter the conclusion.

E3. ANALYSIS FOR MOLTEN FUEL

In this computer run, several new species were introduced; e.g., stainless steel constituents Fe, Cr, Ni (and their oxides), and Zr(g), Mo(g), Ru(g), and HI(g). To make room for these species a number of the nonreactive species from the first run were dropped from the matrix. Conditions were fixed at 3100K, 1000 psia, 1 percent burnup, and unlimited water. For this run the free energies were adjusted and the oxides were considered to form an ideal solution.

The results of the run showed that the Fe, Cr, Ni compound species did not affect the reaction patterns established in the systems at temperatures to 2500K. The overall situation with excess water present was quite oxidizing in that the partial pressure of UO_3 was more than two orders of magnitude greater than UO_2 in all cases.

The data were used to calculate volatilization rates utilizing the Knudsen-Mayer equation:

$$Z = 44\ P\sqrt{M/T} \qquad \text{(VII E-1)}$$

where Z is the volatilization rate in grams per second per square centimeter, P is the vapor pressure in atmospheres, M the molecular weight, and T is the temperature in degrees Kelvin. Although this relationship holds for molecular flow in vacuum, Fonda (Ref. 2) has indicated that in the presence of an inert cover gas, the same relationship applies but the rate is effectively reduced by a factor of 1/80 to 1/100. For practical purposes, at temperatures near 3000K, one may utilize the relation:

$$Z \sim 0.01\ P\sqrt{M}\ \text{g/sec/cm}^2 \qquad \text{(VII E-2)}$$

as long as the rate-controlling step of diffusion through a boundary layer film Equation (VII E-2) is expected to be applicable. Under conditions tending to be more static, the evolution rate would be even lower. Thus Equation (VII E-2) may be considered as an upper limit for vaporization loss. Equation (VII E-2) appears to be only a slowly changing function of pressure at atmospheric pressure or greater. Thus at pressures as high as 50 psia Equation (VII E-2) should closely approximate actual release conditions.

The vapor species expected to be released and the maximum-volatilization rates obtained for the molten fuel case are given in Table VII E-5.

It is assumed that convective forces are operative in the gas phase which will lift the volatiles along with the gaseous currents and these species will be entrained in the gas at least until the species are contacted by a surface where they may condense. They could be carried as aerosol particles however.

These results indicate that uranium is about as volatile as anything else and its volatilization should assist the loss of volatile fission products from the receding surface. Care must be used in attempting to extrapolate the volatilization rates to any real core meltdown situation. The values given in Table VII E-5 should be considered only indicative of the relative volatility of the different species under the precise conditions selected for the calculation; i.e., excess water and 3100K. In this context the data show the potential volatile nature of species in molten UO_2--even some species which are normally considered refractory.

E4. CONCLUSIONS

In order to provide a basis for evaluating the dynamics of release, an analysis

was made of the degree of volatilization of the fission product species as a function of temperature. These data are summarized in Tables VII E-1 to VII E-4. Assuming cladding rupture at 800 K, three major phases in the release process are recognized. These are identified below and estimates of release magnitudes are provided.

a. Release at Time of Rupture

Cs - Several percent of inventory

Te - Less than 1 percent of inventory

I_2 - Less than 1 percent of inventory

b. Release During Heat-up to Melting

Cs - remainder, mostly as Cs vapor (early in period)

Te - remainder as Te vapor (early in period)

I - remainder, as CsI vapor (later in period)

Ba - a large percent as Ba or BaO vapor

Sr - a few percent as Sr vapor

c. Release from Molten Fuel

Ru - potential for rapid release as RuO_3

Sr - potential for rapid release as Sr

Mo - potential for rapid release as MoO_3

La - potential for slow release as LaO

Zr - potential for very slow release as ZrO_2

U - potential for rapid vaporization as UO_3

Certainly, the release characteristics of the fission products indicated above are restricted to the thermodynamic systems, components, and conditions that were analyzed. Kinetic limitations and an exhaustive treatment of all potential compound species could not be included. Nevertheless the predictions in many cases tend to agree with other methods used to estimate fission product releases. Exceptions appear to be tellurium and iodine release during fuel heatup to melting, but here possible tellurium reaction with the cladding was not included and cesium iodide stability was considered only with respect to formation of cesium oxide or formation of hydrogen iodide. The results indicated for molten fuel are based on a rather extreme condition; i.e., pure molten fuel in equilibrium with excess water. In fact fuel will probably be diluted with lower melting oxides of structural materials, the mass is likely to be non-isothermal, and the availability of water should be limited. Consequently, the releases from molten fuel have only a potential for occurring and acutally represent upper limit predictions at this time. Considerable experimental work is needed in the area of core meltdown and materials interactions before much improved projections of fission product escape can be made. Thermodynamic analyses such as these are very useful in revealing the important problems which require investigation.

References

1. Morrison, D. L., et al., "An Evaluation of the Applicability of Existing Data to the Analytical Description of a Nuclear Reactor Accident", BMI-1779 (August, 1966).

2. Fonda, G. R., "Evaporation of Tungsten Under Various Pressures of Argon", Phys. Rev., 31, 260 (1928).

TABLE VII E-1 RESULTS OF THERMODYNAMIC ANALYSIS AT T = 800 K

Fission Product	Dominant Condensed Form	Dominant Vapor Form	Approximate Composition Ratio Vapor/Condensed
	Limited Steam		
Cs	Cs	Cs	2×10^{-2}
Ba	Ba	Ba	2×10^{-9}
La	La_2O_3	LaO	1×10^{-25}
Sm	Sm_2O_3	Sm	1×10^{-14}
Zr	Zr	N.C.	-
Mo	MoO_2	N.C.	-
Ru	Ru	N.C.	-
Te	Te	Te	7×10^{-4}
I	CsI	I_2	1×10^{-3}
Br	CsBr	Br_2	1×10^{-3}
Sr	SrO	Sr	4×10^{-8}
U	UO_2	N.C.	-
	Unlimited Steam		
Cs	Cs	Cs	5×10^{-1}
Ba	BaO	BaO	1×10^{-20}
La	La_2O_3	N.C.	-
Sm	Sm_2O_3	N.C.	-
Zr	ZrO_2	N.C.	-
Mo	N.C.	N.C.	-
Ru	Ru	N.C.	-
Te	Te	Te	1×10^{-2}
I	CsI	CsI	1×10^{-3}
Br	CsBr	CsBr	5×10^{-3}
Sr	SrO	Sr	3×10^{-23}
U	UO_2	N.C.	-

N.C. = Not certain because convergence not achieved in the iteration limit.

TABLE VII E-2 RESULTS OF THERMODYNAMIC ANALYSIS AT T = 1300 K

Fission Product	Dominant Condensed Form	Dominant Vapor Form	Approximate Composition Ratio Vapor/Condensed
	Limited Steam		
Cs	Cs_2O	Cs	1×10^{5}
Ba	Ba	Ba	2×10^{-5}
La	La_2O_3	LaO	2×10^{-13}
Sm	Sm_2O_3	Sm	2×10^{-7}
Zr	Zr	ZrO	1×10^{-18}
Mo	MoO_2	N.C.	-
Ru	Ru	N.C.	-
Te	Te	Te	4×10^{0}
I	CsI	CsI	3×10^{-2}
Br	CsBr	CsBr	2×10^{-1}
Sr	SrO	Sr	5×10^{-5}
U	UO_2	UO	5×10^{-17}
	Unlimited Steam		
Cs	CS_2O	Cs	1×10^{5}
Ba	BaO	BaO	1×10^{-9}
La	La_2O_3	LaO	1×10^{-16}
Sm	Sm_2O_3	Sm	2×10^{-19}
Zr	ZrO_2	ZrO_2	1×10^{-23}
Mo	N.C.	N.C.	-
Ru	Ru	RuO_3	1×10^{-27}
Te	TeO_2	Te	3×10^{4}
I	CsI	CsI	7×10^{-1}
Br	CsBr	CsBr	4×10^{3}
Sr	SrO	Sr	1×10^{-11}
U	UO_2	UO_2	1×10^{-17}

N.C. = Not certain because convergence not achieved in the iteration limit.

TABLE VII E-3 RESULTS OF THERMODYNAMIC ANALYSIS AT T = 1900 K

Fission Product	Dominant Condensed Form	Dominant Vapor Form	Approximate Composition Ratio Vapor/Condensed
	Limited Steam		
Cs	None	Cs	$>1 \times 10^{8}$
Ba	Ba	Ba	2×10^{-3}
La	La_2O_3	LaO	2×10^{-7}
Sm	Sm_2O_3	Sm	7×10^{-4}
Zr	Zr	ZrO	4×10^{-11}
Mo	N.C.	N.C.	-
Ru	Ru	RuO_3	2×10^{-33}
Te	TeO_2	Te	3×10^{4}
I	CsI	CsI	$>8 \times 10^{3}$
Br	CsBr	CsBr	$>4 \times 10^{3}$
Sr	SrO	Sr	7×10^{-2}
U	UO_2	UO	1×10^{-10}
	Unlimited Steam		
Cs	None	Cs	$>1 \times 10^{8}$
Ba	BaO	BaO	2×10^{-4}
La	La_2O_3	LaO	7×10^{-9}
Sm	Sm_2O_3	Sm	2×10^{-9}
Zr	ZrO_2	ZrO_2	1×10^{-13}
Mo	N.C.	N.C.	-
Ru	Ru	RuO_3	1×10^{-16}
Te	None	Te	$>2 \times 10^{7}$
I	CsI	CsI	$>8 \times 10^{3}$
Br	CsBr	CsBr	$>4 \times 10^{3}$
Sr	SrO	Sr	5×10^{-6}
U	UO_2	UO_3	2×10^{-9}

N.C. = Not c' tain because convergence not achieved in the iteration limit.

TABLE VII E-4 RESULTS OF THERMODYNAMIC ANALYSIS AT T = 2500 K

Fission Product	Dominant Condensed Form	Dominant Vapor Form	Approximate Composition Ratio Vapor/Condensed
	Limited Steam		
Cs	None	Cs	$>1 \times 10^{8}$
Ba	Ba	Ba	3×10^{-2}
La	La_2O_3	LaO	3×10^{-4}
Sm	Sm_2O_3	Sm	3×10^{-3}
Zr	Zr	ZrO	3×10^{-7}
Mo	N.C.	N.C.	-
Ru	Ru	RuO_3	2×10^{-23}
Te	None	Te	$>2 \times 10^{7}$
I	CsI	CsI	$>8 \times 10^{3}$
Br	CsBr	CsBr	$>4 \times 10^{3}$
Sr	SrO	Sr	3×10^{4}
U	UO_2	UO	2×10^{-7}
	Unlimited Steam		
Cs	None	Cs	$>1 \times 10^{8}$
Ba	BaO	BaO	8×10^{-2}
La	La_2O_3	LaO	1×10^{-4}
Sm	Sm_2O_3	Sm	7×10^{-7}
Zr	ZrO_2	ZrO_2	1×10^{-8}
Mo	N.C.	N.C.	-
Ru	Ru	RuO_3	6×10^{-13}
Te	None	Te	$>2 \times 10^{7}$
I	CsI	CsI	7×10^{3}
Br	CsBr	CsBr	3×10^{3}
Sr	SrO	Sr	1×10^{-2}
U	UO_2	UO_2	1×10^{-6}

N.C. = Not certain because convergence not achieved in the iteration limit.

TABLE VII E-5 VAPOR SPECIES AND MAXIMUM VOLATILIZATION RATE ESTIMATES, T = 3100K

Species	Equilibrium Vapor Fraction	Equilibrium Partial Pressure, atm	Limiting Volatilization Rate, $g/cm^2/sec$
Cs	1.0	-	(a)
BaO	1.0	-	(a)
Te, TeO	1.0	-	(a)
CsI	1.0	-	(a)
RuO_3	0.47	1×10^{-2}	1×10^{-3}
Sr	0.034	8×10^{-4}	8×10^{-5}
MoO_3	0.024	1×10^{-3}	1×10^{-4}
LaO	0.017	8×10^{-5}	1×10^{-5}
ZrO_2	0.009	2×10^{-6}	1×10^{-7}
UO_3	0.51	7	2×10^{-1}

(a) These are too highly volatile to estimate rates. No condensed phase exists at 3100 K.

APPENDIX F

SUMMARY OF DATA ON FISSION PRODUCT RELEASE FROM UO_2 DURING OXIDATION IN AIR

by
R. L. Ritzman
Battelle's Columbus Laboratories
and
G. W. Parker
Oak Ridge National Laboratory

Appendix F

Table of Contents

Section		Page No.
	SUMMARY OF DATA ON FISSION PRODUCT RELEASE FROM UO_2 DURING OXIDATION IN AIR	VII-137
	REFERENCES	VII-138

List of Tables

Table		Page No.
VII F-1	Fission Product Release from UO_2 Oxidized in Air Sample:	VII-139
VII F-2	Fission-Product Relase from PWR-Type UO_2 - Irradiated to 4000 Mwd/T	VII-140
VII F-3	Fission-Product Release from PWR-Type UO_2 - Irradiated to 7000 Mwd/T	VII-140

List of Figures

Figure		Page No.
VII F-1	Fission Product Release by the Oxidation of UO_2 to U_3O_8 in Air, Showing Discontinuity between 600 and 900 C	VII-141
VII F-2	Effect of Burnup on Fission-Product Release by Oxidation at 1000 and 1200 C	VII-141

Appendix F

Summary of Data on Fission Product Release From UO_2 During Oxidation in Air

by

R. L. Ritzman

Battelle's Columbus Laboratories

and

G. W. Parker

Oak Ridge National Laboratory

When uranium dioxide is heated in air at temperatures below about 1550 C, the UO_2 is oxidized to U_3O_8 with an accompanying expansion of the solid lattice (Ref. 1). The U_3O_8 surface layer cracks upon accumulation of sufficient stress and exposes the underlying UO_2 to continued oxidation (Ref. 2). The oxidation reaction is exothermic and ignition or burning of UO_2 has been observed (Ref. 3). These conditions--increased surface area, phase change with lattice expansion, and elevated temperatures--are conductive to fission product release during the oxidation process. Parker et al.(Ref. 2) first studied release from trace-irradiated PWR-type UO_2 pellets of 94 percent theoretical density and later (Ref. 4) from the same type of fuel irradiated to different levels of burnup to a maximum of 7000 Mwd/T. Approximately one-gram samples were heated for different periods in air flowing at 100 cc/minute at temperatures ranging from 500 C to 1400 C.

The pertinent fission product release data that were obtained in these series of experiments at ORNL are summarized in Fig. VII F-1 and in Tables VII F-1, VII F-2, and VII F-3. Release values determined with specimens irradiated at trace level ($\sim$1 Mwd/T) are plotted in Fig. VII F-1. Results show that release is not a simple function of temperature, but above 900 C releases tend to increase with temperature.

The effect of varying the heating time at different temperatures is shown in Tables VII F-2 and VII F-3. Specimens employed to obtain these data were PWR-type material with a density of 93 to 94 percent of theoretical, irradiated to a burnup of 1000 Mwd/T and 4000 Mwd/T, respectively. Increasing exposure time in air in the range investigated seemed to have no significant effct on fission-product release below 800 C, but at this temperature and above, increasing release of some isotopes with increasing exposure was observed.

The effect of burnup on oxidation release of the more volatile fission products is shown graphically in Fig. VII F-2 for two temperatures. The largest effect in the case of iodine and ruthenium came in the first 1000 Mwd/T of burnup and this was also true of the rare gases at 1200 C. The release of tellurium appeared to increase more or less regularly with increasing burnup in the range tested. The release of cesium, even at 1200 C, was too low to establish an unequivocal correlation but the results obtained indicate a slight increase in release with increasing burnup.

The outstanding feature of these results, particularly at the higher temperatures, is the high release of rare gases, iodine, ruthenium, and tellurium. Tellurium release is not quite as large as the other three but still much greater than cesium, strontium, or barium. Ruthenium release is probably largely due to formation of a volatile oxide. Tellurium oxide is also reasonably volatile at the higher temperatures. The very low releases of cesium, strontium, and barium are indicative of the lower volatility of their oxides. In general, the results also indicate that only a few minutes exposure to air at temperatures of 1200 C or above would be necessary to cause large releases of rare gas, iodine, ruthenium, and tellurium fission products.

References

1. Belle, J., Editor, Uranium Dioxide: Properties and Nuclear Applications, USAEC, 1961, Chapter 8.

2. Parker, G. W., G. E. Creek, and W. J. Martin in "Chemistry Division Annual Progress Report for Period Ending June 30, 1961", ORNL-3176 (Sept 1961), p 68.

3. Leitnaker, J. M., M. L. Smith, and C. M. Fitzpatrick, "Conversion of Uranium Nitrate to Ceramic Grade Oxide for the Light Water Breeder Reactor: Process Development", ORNL-4755 (April 1972).

4. Parker, G. W., et al., in "Nuclear Safety Program Semiannual Progress Report for Period Ending June 30, 1962", ORNL-3319 (Aug 1962), p 11.

TABLE VII F-1 FISSION PRODUCT RELEASE FROM UO_2 OXIDIZED IN AIR
Sample: Intermediate density PWR UO_2 (93-94%)
Irradiation: 1000 Mwd/ton
Air flow: 100 cc/min

Temp (C)	Time at Temperature (min) He	Air	Percentage of Individual Fission Products Released: Rare Gases	I	Te	Cs	Ru	Sr	Ba	U
500		9	4.4	4.6	<0.014	0.02	0.013	<0.001	<0.0009	
	15.0	13	4.0	2.5	<0.003	<0.0008	<0.014	<0.004	<0.001	
	15.0	90	4.0	4.7	0.008	<0.002	0.36	<0.004	<0.0008	
600		11	6.6	3.4	0.003	0.004	0.33	0.003		
	15.0	13	6.0	5.6	<0.003	<0.0007	<0.23	<0.001	0.0009	
	12.0	90	5.5	6.0	0.005	0.003	0.9	<0.0009	<0.0009	
700		12	8.5	9.4	0.01	0.001	0.63	0.001		
	15.0	12	7.2	10.1	<0.003	<0.003	1.25	<0.0009	<0.001	
	13.0	90	8.3	10.0	<0.003	0.02	3.8	<0.0008	<0.0007	
800		15	10.5	9.1	0.05	0.016	5.2	0.0006		
	13.0	14	8.56	11.2	0.033	0.038	6.6	0.008	0.0006	
	13.5	90	15.1	14.1	0.08	<0.007	35.3	<0.001	0.002	
900		15	11.2	15.2	<0.4	0.005	18.9	<0.001		
	10.0	14	11.9	14.4	<0.85	0.03	11.5	<0.002	<0.01	
	12.5	90	13.7	26.9	0.41	<0.002	30.3	<0.001	<0.0015	
1000		26	30.3	55.2	<7.7	0.07	81.5	<0.001	<0.007	
	10.0	18	22.2	42.2	<0.6	~0.03	69.8	<0.001	0.002	0.007
	12.0	90	30.5	73.3	31.3	0.02	97.9	0.002	0.005	<0.0012
1100	8.0	10	60.0	70.4	75.3	2.8	85.7	<0.001	<0.002	0.002
	12.5	11	49.9	64.1	28.0	<0.01	95.5	0.001	<0.016	
	12.5	90	52.7	71.2	58.0	<0.4	99.9	<0.2	<0.2	0.19
1200	17.0	15	79.6	86.6	59.4	<0.1	97.8	<0.03	0.1	
	14.5	90	77.0	83.4	75.9	4.5	99.7	0.14	0.14	0.142

TABLE VII F-2 FISSION-PRODUCT RELEASE FROM PWR-TYPE UO_2 [a] Irradiated to 4000 Mwd/T and Heated in Air [b]

Temp (c)	Time at Temperature (min.) He	Time at Temperature (min.) Air	Percentage of Individual Fission Products Released: Rare Gases	I	Te	Cs	Ru	Sr	Ba	U
500	16.0	23.0	1.5	3.6	<0.007	<0.0004	<0.005	<0.0004		
	18.0	90.0	2.9	3.2	<0.01	<0.0007	<0.01	<0.0004	<0.0008	
600	14.0	18.0	4.4	10.0	<0.006	0.002	0.08	<0.001		
	15.0	90.0	4.5	8.0	8.4	<0.001	1.8	<0.001	<0.004	
700	14.0	12.0	9.3	9.6	0.01	0.001	1.7	<0.0002	<0.0004	
	13.5	15.0	7.0	10.0	0.004	<0.001	0.4	<0.0003	<0.0006	
	14.0	90.0	6.8	6.5	<0.05	<0.0005	2.3	<0.0004	<0.002	
800	13.0	15.0	14.0	7.1	0.007	0.015	1.0	<0.0004	<0.0007	
	14.0	90.0	14.0	16.0	<0.06	<0.01	12.0	<0.0004	<0.001	
900	14.0	19.0	21.0	49.0	0.4	0.001	17.0	<0.001	0.01	
	15.0	90.0	22.0	47.0	6.0	0.015	53.0	<0.0008	<0.004	
1000	16.0	15.0	40.0	84.0	12.0	0.09	72.0	<0.003	<0.02	
	13.5	90.0	44.0	75.0	32.0	0.37	92.0	0.1	0.08	0.06
1100	14.0	14.0	66.0	79.0	16.0	<0.02	91.0	<0.05	<0.003	
	14.0	90.0	73.0	84.0	39.0	0.2	99.0	0.006	0.01	<0.003
1200	14.0	16.5	71.0	82.0	37.0	0.8	99.0	<0.01	<0.001	
	13.0	90.0	80.0	95.0	66.0	6.4	99.6	0.007	0.7	<0.003

(a) Sample approximately 1g of intermediate density (93 to 94 percent) material in porous alundum cups.

(b) Air flow, 100 cc/min.

TABLE VII F-3 FISSION-PRODUCT RELEASE FROM PWR-TYPE UO_2 [a] Irradiated to 7000 Mwd/T and Heated in Air [b] for 90 Minutes

Temp (C)	Percent of Individual Fission Products Released: Rare Gases	I	Te	Cs	Ru	Sr	Ba
500	3.1	4.1	<0.5	0.0006	0.1	<0.0007	<0.0004
600	4.2	3.1	<0.1	<0.002	0.7	<0.0004	<0.009
700	6.1	15.0	<0.08	<0.005	0.1	<0.0005	<0.007
800	9.4	9.0	<0.3	0.002	9.8	<0.0005	0.03
850	15.0	34.0	1.4	0.02	35.0	<0.005	<0.08
900	34.0	29.0	80.0	<0.01	78.0	<0.03	<0.08
1000	86.0	78.0	37.0	<0.03	93.0	<0.04	<0.3

(a) Samples 0.5 to 0.9 g of 96 percent density material in porous alundum cups, preheated for 13 to 16 minutes in helium.

(b) Air flow, 100 cc/min.

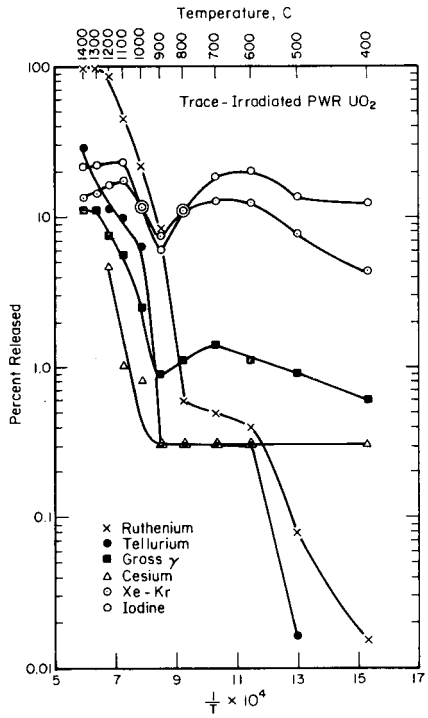


FIGURE VII F-1 Fission Product Release by the Oxidation of UO_2 to U_3O_8 in Air, Showing Discontinuity between 600 and 900 C

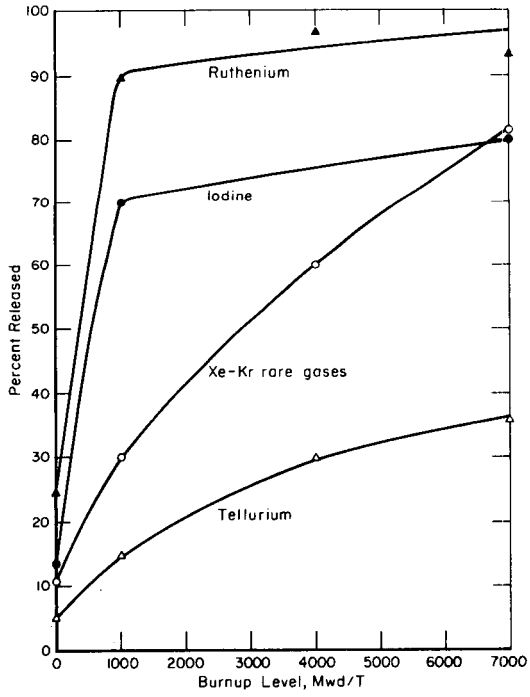


FIGURE VII F-2 Effect of Burnup on Fission-Product Release by Oxidation at 100 and 1200 C

APPENDIX G

ESTIMATIONS OF FISSION PRODUCT RELEASE FROM MELT DURING CONCRETE PENETRATION

by

L. F. Parsly, Jr., and M. H. Fontana
Oak Ridge National Laboratory

Appendix G

Table of Contents

Section	Page No.
ESTIMATIONS OF FISSION PRODUCT RELEASE FROM MELT DURING CONCRETE PENETRATION	VII-147
Release During Gas Sparging	VII-147
REFERENCES	VII-148

List of Tables

Table		Page No.
VII G-1	Removal of Fission Products from Melt by Sparging with CO_2 from Concrete Decomposition	VII-149

Appendix G

Estimations of Fission Product Release From Melt During Concrete Penetration

by

L. F. Parsly, Jr., and M. H. Fontana
Oak Ridge National Laboratory

Conditions are created which could promote fission product release from the molten core material during its penetration of the containment concrete base. Carbon dioxide generated from decomposition of limestone aggregate, and steam liberated from solid hydrates or included water, may pass through the melt producing a gas sparging effect. Analyses performed in the core meltdown task indicate that high-gas generation rates would occur during the first half-hour after the molten core contacts the concrete base. Subsequently, the gas generation rates should decrease as concrete penetration slows, but the cumulative gas generation during this period would exceed that of the early period. In order to obtain an estimate of the effectiveness of this process in promoting fission product release, simple volatilization calculations were performed.

RELEASE DURING GAS SPARGING

The assumption was made that concrete would be decomposed and that a significant decomposition product would be CO_2. The CO_2 at 3000 K and 1 atm pressure was assumed to bubble through the molten core, and it was assumed that equilibrium distribution of fission products between the melt and the gas bubbles would be established. Distribution coefficients for the fission products between the melt and the CO_2 were calculated from the data given in Gabelnick and Chassnov (Ref. 1) for 3000 K, 5 percent burnup and 5 g/cc smear density. These were assumed to be independent of concentration. Based on the assumed equilibrium, a differential material balance can be written. From this we find that:

$$C = C_o \exp\left(-\frac{H\,V_G}{V_L}\right), \qquad \text{(VII G-1)}$$

where

C = final concentration

C_o = initial concentration

H = distribution coefficient = concentration in gas/concentration in liquid

V_G = volume of gas which has bubbled through the melt

V_L = volume of melt.

Thus, the fraction retained is

$$\frac{C}{C_o} = \exp\left(-\frac{H\,V_G}{V_L}\right) \qquad \text{(VII G-2)}$$

and the fraction removed is

$$\frac{C_o - C}{C_o} = 1 - \exp\left(-\frac{H\,V_G}{V_L}\right) \qquad \text{(VII G-3)}$$

The calculated distribution coefficients and the fraction removed values obtained from Equation (VII G-3) are given in Table VII G-1. The results are based on a melt volume (V_L) of 932 ft^3 and a total CO_2 volume (V_G) of 1.25×10^6 ft^3. This volume of CO_2 corresponds to decomposition of approximately 5.8×10^4 lb of concrete (Ref. 2). Complete decomposition of this mass may not occur and/or the generated CO_2 may partially bypass the melt. Thus, two columns of fraction removed values are given in Table VII G-1; one assuming only 20 percent of the total CO_2 volume sparges the melt and another which assumes 100 percent. The V_G/V_L values in Equation (VII G-3) applying to these two conditions are respectively 268 and 1340.

The results of these calculations indicate that the fission products can be grouped into four classes as follows:

a. Highly volatile - essentially completely removed by even limited sparging. These include Ag, Cd, Cs, In, I, Rb, Sb, Se, Sn, and Te.

b. Refractory - almost completely retained after sparging. These include Ce, Nb, Rh, and Zr.

c. Moderately volatile - extent of removal depends on amount of sparging. These include Eu, La, Mo, Nd, and Pd.

d. Uncertain - has one volatile and one non-volatile form. These include Ba, Gd, Pm, Pr, Ru, Sm, Sr, Tc, and Y. However, as noted in the table, the volatile form of each of these fission products is the minor species in the thermodynamic system analyzed. The sparging process would create highly oxidizing conditions. On this basis, Ba, Gd, Pm, Pr, Sm, Sr, and Y should exist as oxides and can legitimately be considered refractory. Under the same conditions Ru and Tc should form the volatile oxides but the presence of metallic iron in the real melt system would interfere. Therefore, only the volatility classification for these two fission products remains questionable.

It must be cautioned that the volatilization fractions listed in Table VII G-1 were obtained using a simple rate expression based on convenient assumptions regarding chemical and physical equilibrium. While very useful in developing the qualitative conclusions just presented, the data should not be considered a quantitative prediction of actual releases in a containment melt-through situation.

References

1. Gabelnick, S. D. and Chasanov, M. G., "A Calculational Approach to the Estimation of Fuel and Fission Product Vapor Pressures and Oxidation States to 6000 K", ANL-7867 (October, 1972).

2. Reimers, R. A., and Seidenfeld, A., "Investigation of the Consequences of a Nuclear Reactor Core Melt-through Accident, ORNL-MIT-62 (October, 1968).

TABLE VII G-1 REMOVAL OF FISSION PRODUCTS FROM MELT BY SPARGING WITH CO_2 FROM CONCRETE DECOMPOSITION

Fission Product	Distribution Coefficient[b]	Percent Sparge Gas Volume	
		20	100
		Fraction Removed from Melt	
Ag	3.26×10^{-2}	>0.999	>0.999
Ag_2O	1.62×10^{-1}	>0.999	>0.999
Ba[a]	9.35×10^{-2}	>0.999	>0.999
BaO	4.09×10^{-5}	0.01	0.045
Cd	4.93	>0.999	>0.999
CdO	3.45×10^{-2}	>0.999	>0.999
Ce	4.14×10^{-5}	0.01	0.045
Ce_2O_3	1.25×10^{-5}	<0.01	0.017
Cs	6.51×10^{-1}	>0.999	>0.999
Cs_2O	1.53	>0.999	>0.999
Eu	2.73×10^{-1}	>0.999	>0.999
Eu_2O_3	2.43×10^{-3}	0.48	0.96
Gd[a]	3.33×10^{-3}	0.59	>0.999
Gd_2O_3	5.68×10^{-6}	<0.01	<0.01
I		>0.999	>0.999
In	4.78×10^{-2}	>0.999	>0.999
In_2O_3	406.0	>0.999	>0.999
La[a]	2.00×10^{-4}	0.05	0.23
La_2O_3	3.67×10^{-5}	0.01	0.051
Mo	3.35×10^{-7}	<0.001	<0.001
MoO_2	1.21×10^{-4}	0.03	0.15
Nb	2.47×10^{-8}	<0.001	<0.001
NbO_2	2.92×10^{-6}	<0.001	<0.001
Nd[a]	9.65×10^{-4}	0.23	0.73
Nd_2O_3	1.27×10^{-4}	0.03	0.16
Pd	6.12×10^{-4}	0.15	0.56
PdO	3.80×10^{-4}	0.10	0.40
Pm[a]	8.84×10^{-3}	0.91	>0.999
Pm_2O_3	3.25×10^{-6}	<0.001	0.001
Pr[a]	1.03×10^{-3}	0.24	0.75
Pr_2O_3	1.38×10^{-5}	<0.01	0.02
Rb	7.53×10^{-1}	>0.999	>0.999
Rb_2O	4.08×10^{-1}	>0.999	>0.999
Rh	2.06×10^{-5}	<0.01	0.03
Rh_2O	7.93×10^{-6}	<0.01	0.01
Ru	1.11×10^{-5}	<0.01	0.02
RuO_2[a]	6.12×10^{-1}	>0.999	>0.999
Sb	4.40×10^{-2}	>0.999	>0.999
Sb_2O_3	8.80	>0.999	>0.999

TABLE VII G-1 (Continued)

Fission Product	Distribution Coefficient[b]	Percent Sparge Gas Volume	
		20	100
		Fraction Removed from Melt	
Se	4.49×10^{-1}	>0.999	>0.999
SeO_2	4.10	>0.999	>0.999
Sm[a]	3.24×10^{-1}	>0.999	>0.999
Sm_2O_3	5.45×10^{-5}	0.01	0.07
Sn	4.02×10^{-3}	0.66	0.995
SnO	3.62×10^{-2}	>0.999	>0.999
Sr[a]	2.45×10^{-1}	>0.999	>0.999
SrO	8.18×10^{-7}	<0.001	0.001
Tc	3.69×10^{-7}	<0.001	<0.001
TcO_2[a]	1.57×10^{-3}	0.34	0.88
Te	0.62×10^{-1}	>0.999	>0.999
TeO_2	3.40×10^{-1}	>0.999	>0.999
Y[a]	3.45×10^{-4}	0.056	0.384
Y_2O_3	1.77×10^{-5}	0.01	0.02
Zr	5.2×10^{-7}	<0.001	<0.001
ZrO_2	1.59×10^{-8}	<0.001	<0.001
UO_2	4.71×10^{-6}	0.001	0.006
PuO_2	2.64×10^{-7}	<0.001	<0.001

(a) Minor species

(b) Distribution coefficient = $\frac{\text{Concentration in gas}}{\text{Concentration in liquid}}$

APPENDIX H

EXAMINATION OF SOLID FISSION PRODUCT PLATEOUT IN PRIMARY SYSTEMS

by

R. L. Ritzman
Battelle's Columbus Laboratories

Appendix H

Table of Contents

Section		Page No.
H1.	ESTIMATED VAPOR CONCENTRATIONS OF FISSION PRODUCTS AND CONDENSATION CONDITIONS	VII-155
H2.	ESTIMATION OF THE THERMAL HISTORY OF UPPER PRESSURE VESSEL INTERNALS	VII-156
H3.	ESTIMATED VAPORIZATION OF CORE STRUCTURALS AND BEHAVIOR IN UPPER PLENUM	VII-157
H4.	CONCLUSIONS	VII-158
REFERENCES		VII-159

List of Tables

Table		Page No.
VII H-1	Estimated Solid Fission Product Partial Pressures as a Function of Gas Temperature after Leaving Core Region	VII-160
VII H-2	Approximate Supersaturation Ratio for the Solid Fission Products as a Function of Gas Temperature	VII-160
VII H-3	Average Exit Gas Temperatures from Core Heatup Analyses	VII-160
VII H-4	Upper Plenum Structural Temperatures Versus Time for Heating by Steam Only	VII-161
VII H-5	Materials Data and Potential Vaporization Loss Rates	VII-161
VII H-6	Saturation Vaporization Rates and Concentrations	VII-161

Appendix H

Examination of Solid Fission Product Plateout in Primary Systems

by
R. L. Ritzman
Battelle's Columbus Laboratories

Fission products that are released from the reactor fuel before and during core melting must travel through the rest of the primary system in order to escape into the containment atmosphere. The first and principal component of the system is the pressure vessel, and it is possible that some of the released fission products could be retained on internal structures inside this vessel. Specifically fission product vapors that are swept out of the core region will encounter cooler temperatures in the upper plenum. The vapors may condense on the cooler structural surfaces in this region thus preventing their escape into the containment. However, it is also conceivable that the vapors might undergo gas phase condensation with other vaporized materials, forming an aerosol which would be swept out of the vessel. The following sections of this document present the results of several calculations that were performed to provide some insight into the fate of solid fission products in the reactor vessel. Examination of iodine deposition in the primary system is covered in another document.

H1. ESTIMATED VAPOR CONCENTRATIONS OF FISSION PRODUCTS AND CONDENSATION CONDITIONS

In order to obtain an estimate of the potential for solid fission product plateout in the upper plenum region of the pressure vessel, a series of volatility calculations were performed. Fission product vapor concentrations in the bulk gas flowing through the upper plenum were estimated using the meltdown release rates and bulk steam-hydrogen flow rates that would be characteristic of the meltdown period.

The estimated length of the meltdown period for a PWR or BWR varies somewhat (Ref. 1) but 45 minutes is a reasonable value. In this analysis it is assumed that the solid fission product meltdown component releases are released at a constant rate over the 45 minute period. Combining the fraction released values with calculated core fission product inventory data, an estimate of the individual mass release rates can be made. Then knowing the bulk gas flow rate from the core region one can calculate the fission product gas phase partial pressures. The bulk gas (steam-hydrogen) flow originates from water boiloff inside the pressure vessel and the rate is estimated to range from about 5000 to 10,000 cfm (Ref. 1). The smaller rate will be used to maximize the estimated partial pressures. The results of performing this exercise for a series of gas temperatures are summarized in Table VII H-1. Note that the partial pressures are calculated without regard to vapor saturation restrictions. The result of considering saturation conditions for each of the fission product elements is presented in Table VII H-2. Here the ratio of the calculated partial pressures given in Table VII H-1 to the respective saturation pressures (Ref. 2) for each fission product element and temperature are tabulated. This ratio indicates the degree of supersaturation that would occur in each case if the hot gas mixture leaving the core region were suddenly cooled to the given temperatures. Values greater than one indicate that condensation of the fission product would be favored under such conditions while values less than one tend to preclude any condensation.

Although the supersaturation ratios in Table VII H-2 are only approximations, several useful observations can be made. For example, at gas or system temperatures above about 1000 F, no stable condensed cesium or tellurium phase should exist. Above about 1500 F the same is expected for strontium. However, at all temperatures considered here, condensation of ruthenium and yttrium is strongly favored, and at the lowest temperature (530 F) strontium, tellurium, and probably cesium should also condense. These results indicate the importance that thermal conditions will have on the behavior of solid fission products in primary systems.

H2. ESTIMATION OF THE THERMAL HISTORY OF UPPER PRESSURE VESSEL INTERNALS

The upper plenum of a PWR pressure vessel (above the upper core plate) contains a collection of support columns and control rod guide tubes. When the reactor core begins to heat up, after the LOCA, the temperatures in this region would be about 500 to 600 F. During the core meltdown period, hot steam and hydrogen flowing from the core would heat the internal masses. This heatup process would also be assisted by decay heat from fission products that are carried into the upper plenum.

From thermal analysis of core heatup (Ref. 3) a typical water boiloff rate for the meltdown period is 0.01 lb/min per channel or about 400 lb/min for the entire core. Also from core thermal analyses the average temperature of this steam as it entered the upper plenum can be obtained. These data, listed in Table VII H-3, indicate average gas temperatures of 2000 to 3000 F during the first half of core meltdown and increasing temperatures afterwards. The point of interest here pertains to the first half of core meltdown; specifically how rapidly the steam would heat the structural internals of the upper plenum to temperatures in the range of 1000 to 1500 F. Therefore, a simple model was formulated to solve the heat transfer problem.

The plenum was considered to be a well mixed chamber with steam entering at F lb/hr and at constant temperature T_i and leaving at the same rate but at a lower temperature T_S. Inside the chamber the structural masses are at temperature T_{MO} initially and heat to increasing temperatures denoted by T_M as a function of time. On this basis the following equations can be written:

$$M_M C_M \frac{dT_M}{dt} = hA\,(T_S - T_M)$$

$$V\rho_S C_S \frac{dT_S}{dt} = FC_S\,(T_i - T_S) - HA\,(T_S - T_M)$$

or

$$\frac{dT_M}{dt} = \lambda_1 T_S - \lambda_1 T_M$$

$$\frac{dT_S}{dt} = \lambda_2 T_i - \lambda_3 T_S + \lambda_4 T_M$$

where

$$\lambda_1 = \frac{hA}{M_M C_M} \qquad \lambda_2 = \frac{F}{V\rho_S} \qquad \lambda_4 = \frac{hA}{V\rho_S C_S}$$

$$\lambda_3 = \frac{F}{V\rho_S} + \frac{hA}{V\rho_S C_S} = \lambda_2 + \lambda_4.$$

Here,

M_M = mass of structural masses, lb

C_M = heat capacity of the solid, Btu/lb, F

ρ_S = steam density, lb/ft^3

C_S = heat capacity of steam, Btu/lb, F

V = volume of chamber, ft^3

F = steam delivery rate, lb/hr

A = surface area of masses, ft^2

h = heat transfer coefficient, Btu/hr, ft^2, F.

The solution for T_M as a function of time for this problem is:

$$T_M = T_i + \left[\frac{T_{MO}(\lambda_3 - a_2)}{a_1 - a_2} - \frac{\lambda_1 T_i (\lambda_2 - a_2)}{a_2 (a_1 - a_2)} \right] \exp(-a_2 t) + \left[\frac{T_{MO}(\lambda_3 - a_1)}{a_2 - a_1} - \frac{\lambda_1 T_i (\lambda_2 - a_1)}{a_1 (a_2 - a_1)} \right] \exp(-a_1 t)$$

where

$$a_1 = \frac{(\lambda_1 + \lambda_3)}{2} + \sqrt{\frac{(\lambda_1 + \lambda_3)^2}{4} - \lambda_1 \lambda_2}$$

$$a_2 = \frac{(\lambda_1 + \lambda_3)}{2} - \sqrt{\frac{(\lambda_1 + \lambda_3)^2}{4} - \lambda_1 \lambda_2}.$$

The heat transfer coefficient, h, was estimated from a dimensionless equation (Ref. 4) for gases flowing normal to banks of staggered tubes for D_oG_{max}/μ_f from 2000 to 32,000. Thus,

$$\frac{hD_o}{k_f} = 0.33 \left[\frac{C_p\mu}{k}\right] 0.33 \left[\frac{D_oG_{max}}{\mu_f}\right]^{0.6}.$$

The value obtained for h at a steam delivery rate of 400 lb/min or 24,000 lb/hr was 26.8 Btu/hr, ft^2, F. Values of T_M as a function of time (t) were calculated for the case; T_{MO} = 500 F at time zero and an inlet steam temperature T_i = 2000 F. The results are given in Table VII H-4 along with the values used for the various parameters. It can be seen that upper plenum structural temperatures are predicted to exceed 1000 F within 15 min and 1500 F within 45 min. Considering these results in conjunction with the data shown in Table VII H-3, it appears that structural surfaces in the upper plenum would be well above 1000 F and probably exceed 1500 F before half the core has melted. This is because average steam temperatures continue to rise as melting occurs and heating prior to the onset of melting would raise the materials temperatures above the 500 F value used in the heat-transfer calculation.

H3. ESTIMATED VAPORIZATION OF CORE STRUCTURALS AND BEHAVIOR IN UPPER PLENUM

The structural components in and near the molten core region will vaporize during the meltdown period. In fact these vapors may comprise most of the total mass which is carried by steam flow into the upper region of the pressure vessel. Cooling of the hot vapor-steam mixture as it mixes with steam that has passed through unmelted sections of the core will create supersaturated vapor conditions. Assuming this causes particles to form it is necessary to estimate the particulate concentrations that could occur and to determine how the resulting particulate surface area compares with the upper plenum system surface area.

The first step in the analysis requires an estimate of the core vaporization rates for important components. This was made by using the Knudsen-Mayer equation modified for the presence of an external atmosphere (Ref. 5). Thus,

$$Z \cong 0.44\, P\sqrt{M/T},$$

where

Z = vaporization rate in $g/cm^2/sec$
P = vapor pressure in atmospheres
M = molecular weight in grams
T = temperature in degrees Kelvin.

Two vaporization temperatures (T) were selected; 2800 C (the approximate melting point of UO_2 and also close to the boiling point of iron) and 2300 C. The latter temperature takes into account melting point depression of the fuel through possible eutectic reactions and it is also well into the liquid region for molten iron (melting point about 1550 C). In order to obtain a core vaporization rate the above equation must be multiplied by an effective surface area. A value of 4×10^5 cm^2 was used since this is about 1 percent of the total fuel rods surface area in a large reactor core and it is also only a few times larger than the cross sectional area of the reactor pressure vessel. On this basis the potential vaporization loss rates and other pertinent data for important materials were obtained as shown in Table VII H-5. It can be seen that under the assumed conditions, nearly all the vaporized material will be made up of tin and iron at both temperatures. Fuel vaporization contributes minor amounts and zirconium loss is insignificant. Therefore, zirconium vaporization may be ignored during the rest of the analysis.

The potential vaporization loss rates in Table VII H-5 would not be realized if insufficient gas flow is available to carry away vapors from the vaporizing surfaces. Therefore, the rates must be modified to take into account gas phase saturation limitations. This requires specification of the gas flow rate in the core, and since boiloff calculations indicate steam flows in the range of 5000 to 10,000 cfm (Ref. 1), the higher value was used to correspond with the high core temperatures that were selected. Assuming ideal gas behavior, the potential vaporization rates from Table VII H-5 would exceed saturation concentrations at this bulk gas flow rate; that is, the 10,000 cfm steam flow is too low to achieve the potential vaporization rates. The rates that could be achieved at each temperature are tabulated in Table VII H-6 along with the gas phase vapor saturation concentration these represent. It can be seen that tin still exhibits the highest mass release rate, with iron a close second, and then UO_2 somewhat less. However, there is insufficient tin in a large reactor core (about 2.6×10^5g) to sustain these rates for the entire meltdown

period (about 45 minutes). Since iron and fuel vaporization are not so limited, the remainder of this analysis is based only on these two materials.

The vapor concentration values in Table VII H-6 can now be used to arrive at estimates of particle concentrations in the upper plenum of a pressure vessel during meltdown. However, one further factor must be considered in developing this estimate. In the early stages of core meltdown only a fraction of the total steam flow will pass through the region of the core that is melting. Therefore, only a fraction of the vapor concentrations given in Table VII H-6 will occur in the upper plenum as this steam mixes with the remaining steam that has passed through cooler core regions. On this basis a rather wide range of vapor concentrations is possible for the upper plenum which practically could extend from about 2 x 10^{-4} g/l up to about 2 x 10^{-1} g/l. This range was used to estimate particle concentrations, the lower value being indicative of very early core meltdown and the higher one indicative of very late core meltdown.

According to experimental studies, the mean size of particles formed when both clad and unclad UO_2 are melted in gas streams ranges from about 0.02 to 0.1 μm (Ref. 6). Assuming all the vaporized material condenses in the gas phase forming 0.1 μm diameter particles, using a particle density of 5 g/cc, and considering the effect of reduced temperature in the plenum region on specific volume (roughly a factor of two), the vapor mass concentration range given above indicates a concentration range of 0.1 μm particles from 1.5 x 10^{11} particles/l to 1.5 x 10^{14} particles/l. These concentrations can now be used to estimate particulate surface areas for the upper plenum volume even though agglomeration would be expected to occur. This is because in forming agglomerates, the surface area represented by the primary particles is probably only slightly reduced (less than a factor of two). Electron photomicrographs of particle agglomerates usually show a very loose, open structure in which most of the primary particle surface area is exposed to the gas (Ref. 7). Therefore, assuming spherical particles, the specific particulate surface areas corresponding to the above concentrations could range from about 4.5 x 10^{1} cm^2/l up to 4.5 x 10^{4} cm^2/l. These values translate into a total particulate surface area for the upper plenum volume (about 1850 ft^3) of from 2600 sq ft up to 2.6 x 10^{6} sq ft. Since the structural surface area of the plenum region is estimated at about 3000 sq ft, the calculations indicate a particulate surface area roughly equivalent to the structural surface area at the beginning of core meltdown and tens or hundreds times greater during following parts of the meltdown period.

The above analysis of course assumes that all the material vaporized in the core region condenses to form particles as the hot gas mixture cools in the upper plenum rather than condensing on the cooler surfaces. This probably is not the case but the process of cooling the hot gas-vapor mixture through mixing with cooler gases will rapidly produce highly supersaturated vapor conditions directly in the gas phase. Such conditions are favorable for particle nucleation and it can be shown from collision theory that collision frequencies between species in the gas phase will exceed collision frequencies with solid surfaces. Therefore, it seems that particulate aerosols would be present and the surface area of the aerosol could exceed the surface area of structural components in the upper plenum region during much of the meltdown period. During the late stages of meltdown, this condition is less probable because of the predicted high gas temperatures (see Table VII H-3). However, the steel structurals might very well have melted by this time.

H4. CONCLUSIONS

The three sets of analyses that have been presented lead to several expectations regarding solid fission product behavior in primary systems during core meltdown. For example, it is doubtful that either cesium or tellurium would, through condensation, become associated with the particulate aerosol. By the time appreciable aerosol concentrations occur the expected gas temperatures, and hence particle temperatures, are too high (over 1000 F) to allow cesium or tellurium condensation. However, in the early stages of core meltdown cesium and tellurium vapors would probably plateout on the relatively cool (below 1000 F) structure in the upper plenum. Then within a few minutes, as the structure heats above 1000 F, this condensed material would vaporize and be swept out to the containment atmosphere. Hence plateout in the primary system is expected to offer only a temporary delaying effect in the escape of released cesium and tellurium to the containment volume.

The behavior of strontium should be similar to that of cesium and tellurium with escape to containment delayed somewhat longer by the need for higher upper plenum temperatures to vaporize the portion that would experience early plateout. Some of the early condensation of strontium vapor could occur on aerosol particles however. This material would then be carried directly to the containment without significant delay.

Materials like ruthenium (noble metals) or yttrium (rare earths) have sufficiently low volatilities that condensation should be expected in the plenum region throughout most of the core meltdown period. Competition may occur between condensation on structural surfaces and condensation on or with the particulate aerosol. The gas phase is expected to be so highly supersaturated that co-condensation with structural vapors from the core should be very competitive. In fact, these materials may enter the plenum region not as vapors but as very small particulates and act there as condensation nuclei for the structural vapors. In either case, it seems inappropriate to assume significant retention of the meltdown release fractions for these species in the primary vessel.

References

1. Carbiener, W. A., et al., "Investigations of Reactor Meltdown in Light Water Reactors" Report on the Reactor Safety Study (Nov. 1973).

2. Nesmeyanov, A. N., "Vapor Pressure of the Elements", Translated and Edited by J. I. Corasso, Academic Press, New York (1963).

3. Carbiener, W. A., et al., "Investigation of Reactor Meltdown in Light Water Reactors", Report on the Reactor Safety Study, Appendix A (Nov. 1973).

4. Colburn, A. P., Trans Am Inst. Chem. Engnrs., 29, 174-210 (1933).

5. Fonda, G. R., "Evaporation of Tungsten Under Various Pressures of Argon", Phys Rev, 31, 260 (1928).

6. Morrison, D. L., et al., "An Evaluation of the Applicability of Existing Data to the Analytical Description of a Nuclear Reactor Accident", BMI-1779, p. 147-150 (Aug. 12, 1966).

7. Baurmash, L., C. T. Nelson and R. L. Koontz, "The Characterization of Aerosols by Aerodynamic Parameters" in Treatment of Airborne Radioactive Wastes, IAEA, Vienna, p. 63-75 (1968).

TABLE VII H-1 ESTIMATED SOLID FISSION PRODUCT PARTIAL PRESSURES AS A FUNCTION OF GAS TEMPERATURE AFTER LEAVING CORE REGION

Species	Meltdown Release Fraction	Estimated Release Rate lb/min	Molecular Weight lb/lb-mole	Estimated Partial Pressure(f) (atm) for Indicated Gas Temperatures 530F	980F	1520F	2060F
Cs(a)	0.81	6.0	133	6.5×10^{-3}	9.5×10^{-3}	1.3×10^{-2}	1.7×10^{-2}
Te(b)	0.15	0.2	345	8.4×10^{-5}	1.2×10^{-4}	1.7×10^{-5}	2.1×10^{-4}
Sr(c)	0.10	0.3	88	4.9×10^{-4}	7.2×10^{-4}	9.9×10^{-4}	1.3×10^{-3}
Ru(d)	0.03	0.15	103	2.1×10^{-4}	3.0×10^{-4}	4.2×10^{-4}	5.3×10^{-4}
Y(e)	0.003	0.005	89	8.1×10^{-6}	1.2×10^{-5}	1.6×10^{-5}	2.1×10^{-5}

(a) Indicator species for alkali metals
(b) Indicator species for Te, Se, Sb
(c) Indicator species for alkaline earths
(d) Indicator species for noble metal group
(e) Indicator species for lanthanides and actinides
(f) Estimated from ideal gas equation ignoring saturation restrictions.

TABLE VII H-2 APPROXIMATE SUPERSATURATION RATIO FOR THE SOLID FISSION PRODUCTS AS A FUNCTION OF GAS TEMPERATURE

$$\text{Supersaturation Ratio} = \frac{\text{Partial Pressure In Gas At Assumed Release Rate}}{\text{Saturation Pressure of the Element}}$$

Species	530 F	980 F	1520 F	2060 F
Cs	3.8	0.049	<0.013	<0.017
Te_2	1380.0	0.065	0.00085	<0.0002
Sr	2.6×10^6	65.0	0.16	0.0075
Ru	$>2.1 \times 10^7$	$>3.0 \times 10^7$	$>4.2 \times 10^7$	$>5.3 \times 10^7$
Y	$>8.1 \times 10^5$	$>1.2 \times 10^6$	1.5×10^6	310

TABLE VII H-3 AVERAGE EXIT GAS TEMPERATURES FROM CORE HEATUP ANALYSES(a)

Accident Time (Min)	Approximate T (gas) (°F)	Approximate Percent Core Melt
30	1400	0
40	2000	5
50	2600	25
60	3300-3600	50-60
70	4200-4700	60-90
80	4600-5000	70-100

(a) Range of values for higher core melt fractions due to differences in core heatup model assumptions regarding steam flow through melted regions.

TABLE VII H-4 UPPER PLENUM STRUCTURAL TEMPERATURES VERSUS TIME FOR HEATING BY STEAM ONLY

Time (min)	Tm (°F)
0	500
6	732
15	1011
30	1349
45	1569
60	1714

M_M = 35, 130 lb
C_M = 0.17 Btu/lb, F
ρ_S = 0.0433 lb/ft^3
C_S = 0.5 Btu/lb, F
V = 1850 ft^3
F = 24000 lb/hr
A = 2186 ft^2
h = 26.8 Btu/hr, ft^2, F

TABLE VII H-5 MATERIALS DATA AND POTENTIAL VAPORIZATION LOSS RATES

Material	Molecular Weight	Vapor Pressure, atm		Potential Vaporization Loss Rate, g/sec	
		2300 C	2800 C	2300 C	2800 C
UO_2	270	4×10^{-4}	6×10^{-2}	23	3100
Iron	56	8.5×10^{-2}	>1	2200	>24000
Zirconium	91	5×10^{-6}	4×10^{-4}	0.17	12
Tin	119	1.7×10^{-1}	>1	6400	>35000

TABLE VII H-6 SATURATION VAPORIZATION RATES AND CONCENTRATIONS

Material	Vaporization Rate, g/sec		Vapor Concentrations, g/l	
	2300 C	2800 C	2300 C	2800 C
UO_2	2.3	300	5×10^{-4}	6.4×10^{-2}
Iron	110	>1000	2.3×10^{-2}	$>2.2 \times 10^{-1}$
Tin	460	>2100	9.6×10^{-2}	$>4.7 \times 10^{-1}$

APPENDIX I

IODINE DEPOSITION IN PWR AND BWR REACTOR VESSELS AND ASSOCIATED EQUIPMENT

by

H. S. Rosenberg and D. K. Landstrom
Battelle's Columbus Laboratories

Appendix I

Table of Contents

Section		Page No.
I1.	CONSTANT RELEASE VERSUS PUFF RELEASE	VII-167
I1.1	Constant Release Rate	VII-167
I1.2	Puff Release	VII-167
I2.	DETERMINATION OF THE OVERALL DEPOSIITION COEFFICIENT, K_t, AND CALCULATION OF DEPOSITION FRACTIONS	VII-168
I2.1	PWR Reactor, Upper Internals	VII-168
I2.2	PWR Reactor, Steam Generator	VII-169
I2.3	BWR Reactor, Steam Separators	VII-169
I2.4	BWR Reactor Steam Dryers	VII-170
I3.	SUMMARY OF RESULTS	VII-170
REFERENCES		VII-170

List of Tables

Table		Page No.
VII I-1	Values of K_g, K_w, K_t, M_d and f_d for Various Conditions of Iodine Deposition PWR Upper Internals	VII-171
VII I-2	Values of K_g, K_w, K_t, M_d, f_d, M_d (Total) and f_d for Various Conditions of Iodine Deposition PWR Steam Generators	VII-171
VII I-3	Values of K_g, K_w, K_t, M_d and f_d for Various Conditions of Iodine Deposition BWR, Steam Separators	VII-172
VII I-4	Values of K_g, K_w, K_t, M_d, f_d, M_d (Total) and f_d Total for Various Conditions of Iodine Deposition	VII-172
VII I-5	Definition of Terms and Units Used to Calculate Iodine Deposition	VII-173
VII I-6	Summary of Typical PWR Surface Areas	VII-174
VII I-7	Summary of Typical BWR Surafce Areas	VII-176

Appendix I

Iodine Deposition in PWR and BWR Reactor Vessels and Associated Equipment

H. S. Rosenberg and D. K. Landstrom
Battelle's Columbus Laboratories

A model to predict the deposition of fission-product iodine on the internals and associated equipment of PWR and BWR reactors was developed and calculations were made as a function of temperature, concentration, gas flow rate, gas composition, and puff versus constant release rate. It can be shown that the amount of iodine deposited is independent of the release model and depends only on the steam boil-off rate (Q), the surface area available for deposition (A), and the overall deposition coefficient, (K_t). Further, it can be shown that the deposition of iodine is controlled by the wall deposition velocity (K_w), and for all cases of interest $K_t \cong K_w$.

I1. CONSTANT RELEASE VERSUS PUFF RELEASE[1]

I1.1 CONSTANT RELEASE RATE

For a constant release over a time period, the concentration of iodine is given by the following equation:

$$C_g = \frac{W}{Q}\left[1 - e^{-(Q/V)t}\right] \qquad \text{(VII I-1)}$$

where, C_g = concentration of I_2 in gas, W = mass release rate of I_2, Q = volumetric flow rate, V = volume of chamber, and t = time period.

The amount of iodine deposited is given by:

$$M_d = \int_o^t C_g K_t A dt \qquad \text{(VII I-2)}$$

where, K_t = overall deposition coefficient, A = deposition area and C_g is as defined in Equation (VII I-1).

Inserting and integrating gives:

$$M_d = \frac{WK_tA}{Q}\left[t + \frac{V}{Q}\left(e^{-(Q/V)t} - 1\right)\right]. \qquad \text{(VII I-3)}$$

Now, by definition

$$W = M_o/t \qquad \text{(VII I-4)}$$

where M_o = the total mass of I_2, and since the product of Q and t is large compared to V, Equation (VII I-3) reduces to

$$M_d = M_o K_t A/Q \qquad \text{(VII I-5)}$$

I1.2 PUFF RELEASE

For the case of a puff release of a mass (M_o) of iodine into a chamber of volume V, the concentration is given by:

$$C_o = M_o/V \qquad \text{(VII I-6)}$$

Steam being produced at a rate (Q) removes iodine at a rate $C_g'Q$.

Therefore:

$$V\frac{dC_g'}{dt} = -C_g'Q \qquad \text{(VII I-7)}$$

and

$$\frac{dC_g'}{dt} = -QC_g'/V. \qquad \text{(VII I-8)}$$

Therefore:

$$C_g' = C_o e^{-Qt/V} \qquad \text{(VII I-9)}$$

where t is the deposition time.

The amount of iodine deposited is therefore:

---

[1] See Table VII I-5 for units and definitions of terms.

$$M_d = \int_o^t C_g' K_t A dt \qquad \text{(VII I-10)}$$

$$M_d = K_t A C_o \int_o^t e^{-Qt/V} dt \qquad \text{(VII I-11)}$$

$$M_d = \frac{-K_t A C_o V}{Q} \left[e^{-Qt/V} - 1 \right] \qquad \text{(VII I-12)}$$

Since the product of Q and t is large with respect to V, this equation will reduce to:

$$M_d = K_t A C_o V/Q. \qquad \text{(VII I-13)}$$

Since from Equation (VII I-6) $C_o = M_o/V$, Equation (VII I-13) further reduces to

$$M_d = M_o K_t A/Q. \qquad \text{(VII I-14)}$$

Equation (VII I-14) is the same as Equation (VII I-5) for the constant release case so that M_d is independent of the release model and depends only on the steam boil-off rate (Q), the surface area available for deposition (A), and the overall deposition coefficient, K_t.

I2. DETERMINATION OF THE OVERALL DEPOSITION COEFFICIENT, K_t, AND CALCULATION OF DEPOSITION FRACTIONS

As will be described later, it was determined for both the PWR and BWR reactors that the deposition of iodine is essentially controlled by the wall deposition velocity, K_w, since the calculated value of the mass-transport coefficient, K_g is large with respect to K_w. The following relationship exists between the coefficients:

$$\frac{1}{K_t} = \frac{1}{K_g} + \frac{1}{K_w} . \qquad \text{(VII I-15)}$$

If K_g is large with respect to K_w, Equation (VII I-13) will reduce to a simple equivalent between K_t and K_w, i.e.:

$$K_t = K_w \qquad \text{(VII I-16)}$$

If the above is true then Equations (VII I-3) and (VII I-12) can be written as follows:

$$M_d = M_o K_w A/Q . \qquad \text{(VII I-17)}$$

I2.1 PWR REACTOR, UPPER INTERNALS

In order to prove the validity of using Equation (VII I-16) it was necessary to calculate values of K_g and compare them to previously determined values of K_w (Ref. 1). For the PWR reactor upper internals this was done by using the Chilton-Colburn analogy between heat and mass transfer to determine K_g, since an empirical equation is available to calculate the heat transfer coefficient, h_m, for fluid flowing normal to banks of staggered tubes. The heat transfer coefficient equation is (Ref. 2)

$$\frac{h_m D_o}{k_f} = 0.33 \left[\frac{C_p \mu}{k_f} \right]^{1/3} \left[\frac{D_o G_{max}}{\mu} \right]^{0.6} . \qquad \text{(VII I-18)}$$

where D_o = outside diameter of tubes, C_p = fluid heat capacity, μ = viscosity of fluid, k_f = thermal conductivity of fluid, G_{max} = mass velocity of fluid through minimum cross section.

Using the definitions of Chilton and Colburn (Ref. 3) for j_H and J_D:

$$j_H = \frac{h_m}{C_p \rho U_{ave}} \left[\frac{C_p \mu}{k_f} \right]^{2/3} \qquad \text{(VII I-19)}$$

$$j_D = \frac{K_g' P_{Bm}}{G_{max}} \left[\frac{\mu}{\rho D_v} \right]^{2/3} \qquad \text{(VII I-20)}$$

where h_m, C_p, μ, k_f, G_{max} are previously defined, K_g' = gas film coefficient P_{Bm} = logarithmic mean of the partial pressure, ρ = density, D_v = diffusivity of iodine in fluid, U_{ave} = mean fluid velocity.

Assuming $j_H = j_D$, adjusting the units of K_g' such that

$$Kg = \frac{K_g' U_{ave} P_{Bm}}{G_{max}} ,$$

defining

$$\frac{C_p \mu}{k_f} = \text{Prandtl Number} = N_{pr} \text{ and } \frac{\mu}{\rho D_v}$$

$$= \text{Schmidt Number} = N_{sc}, \text{ then}$$

$$\frac{h_m}{C_p \rho}\left[N_{pr}\right]^{2/3} = K_g \left[N_{sc}\right]^{2/3} \qquad \text{(VII I-21)}$$

Thus

$$K_g = \frac{h_m}{C_p \rho}\left[N_{pr}\right]^{2/3}\left[N_{sc}\right]^{-2/3} \qquad \text{(VII I-22)}$$

h_m is obtained from Equation (VII I-16) and the diffusivity term, D_v, in the Schmidt number is evaluated using the following equation (Ref. 4)

$$D_{12} = \frac{1.858 \times 10^{-3}\, T^{3/2}\left[\frac{m_1 + m_2}{m_1 m_2}\right]^{1/2}}{P\, G_{12}^{2}\, \Omega_D} \qquad \text{(VII I-23)}$$

where T = temperature (K), m_1 and m_2 are the molecular weights of the two components, G_{12} = Lennard-Jones force constant, and Ω_D = Collision integral for diffusion.

Values of G_{12} and Ω_D can be obtained from tables listed in Reference 4. Solving Equation (VII I-22) for K_g at various conditions produce the values listed in Table VII I-1, which also shows the values of K_w taken from Reference 1. Table VII I-1 also shows the amount of iodine deposited (M_d) from Equation (VII I-17) and the fraction deposited $f_d = M_d/M_o$ for various conditions. All calculations assume an iodine mass release of 22 lbs (10kg), deposition surfaces of pre-filmed 304 stainless steel, the atmosphere in the pressure vessel is well-mixed, and steam boil-off rates of 12 lbs/sec (3×10^6 cc/sec) and 1.2 lbs/sec (3×10^5 cc/sec). The area available for deposition was estimated from scale drawings and is approximately 3000 sq ft. for PWR upper internals (see Table VII I-6). Calculations were performed for temperatures of 250 F, 500 F, 1000 F, and 2000 F. At the two higher temperatures, two iodine species, elemental iodine and hydrogen iodide, were considered along with different fluid compositions because iodine could conceivably react with hydrogen in the core region to form HI.

I2.2 PWR REACTOR, STEAM GENERATOR

For the deposition of iodine in the steam generator, Gilliland's Equation (VII I-7) which represents mass transfer inside wetted-wall columns was used to obtain j_D as follows:

$$j_D = 0.023\ (Re)^{-0.17}\ (N_{sc})^{0.11}, \qquad \text{(VII I-24)}$$

where

$$Re = \text{Reynolds Number} = \frac{4R_H G_{max}}{\mu},$$

where

R_H = hydraulic radius

and N_{sc} is the Schmidt number as previously defined. Therefore combining Equations (VII I-20) and (VII I-21)

$$K_g' = \frac{0.023\ G_{max}}{P_{Bm}}(Re)^{-0.17}(N_{sc})^{-0.56}. \qquad \text{(VII I-25)}$$

By adjusting units to obtain K_g in ft/hr. we have:

$$K_g = \frac{0.023\ G_{max}}{\rho}(Re)^{-0.17}(N_{sc})^{-0.56}. \qquad \text{(VII I-26)}$$

Solving Equation (VII I-26) for K_g at various conditions produces the values listed in Table I-2. K_w is taken from Reference 1 and M_d was calculated using Equation (VII I-17). All calculations assume the same conditions used for the upper internal calculations except that the deposition area is approximately 51,500 sq. ft. Table VII I-2 also lists the M_d (total) and f_d (total) by summing the deposition from the reactor upper internals and the steam generators.

I2.3 BWR REACTOR, STEAM SEPARATORS

A procedure identical to that used to calculate deposition in a PWR steam generator was used to calculate the iodine deposition in the steam separators of a BWR. Gilliland's Equation (Ref. 5) was used with a suitable

modification of the Reynolds Number to the steam separator geometry. The same steam generation conditions as noted previously were used with a deposition area of approximately 9,850 sq. ft. Since the results were expected to be similar to the previous cases only the depositions at 500 and 1000 F were calculated. Table VII I-3 lists the values of K_g, K_w, K_t, M_d, and f_d for these conditions.

I2.4 BWR REACTOR STEAM DRYERS

A procedure similar to that used to calculate deposition in the BWR steam separators was used to calculate the iodine deposition in the steam dryers of a BWR. Gilliland's Equation (Ref. 5) was again used with a modification of the Reynolds Number to the steam dryer geometry. The same steam generating conditions as noted previously were used with a deposition area of 32,400 sq. ft. Again, deposition was calculated only at 500 and 1000 F. Table VII I-4 lists the values of K_g, K_w, K_t, M_d, F_d (total), and f_d (total) for these conditions.

I3. SUMMARY OF RESULTS

In all the cases examined for both the PWR and BWR primary systems, comparison of K_g and K_w values show that iodine deposition would be surface rate controlled even at relatively low bulk gas flows. The results in Table VII I-2 also show that minimal deposition of elemental iodine should be expected in the PWR primary system under LOCA conditions; that is, at temperatures above 500 F and at bulk steam generation rates in the range of 5 to 10 lb per second. In addition, considerably less than half the HI (if it should form) would be expected to deposit under these conditions either.

Deposition predictions for iodine in the upper regions of a BWR vessel (Tables VII I-3 and VII I-4) show results that are very similar to those obtained for the PWR cases. Therefore, primary system deposition should not cause significant retention of iodine during its transport to the containment region in either reactor system.

References

1. Genco, J. M., W. E. Berry, H. S. Rosenberg, D. L. Morrison, "Fission-Product Deposition and its Enhancement under Reactor Accident Conditions: Deposition on Primary-System Surfaces", BMI Report No. 1863 (March, 1969).

2. McAdams, W. H., Heat Transmission, McGraw Hill Book Co., pg. 272 (1954).

3. Sherwood, T. K., R. L. Pigford, "Absorption and Extraction", McGraw-Hill Book Co., Inc., pg. 61 (1952).

4. Reid, R. C., T. K. Sherwood, "The Properties of Gases and Liquids", McGraw Hill Book Co., Incl, pg 523 (1966).

5. Sherwood and Pigford, op. cit., p 78.

TABLE VII I-1 VALUES OF K_g, K_w, K_t, M_d AND f_d FOR VARIOUS CONDITIONS OF IODINE DEPOSITION

PWR UPPER INTERNALS[a]

Temperature F	Iodine Species	Fluid Composition	Steam Boil-off Rate lbs/sec	K_g ft/hr	K_w[b] ft/hr	K_t ft/hr	M_d lbs.	f_d
250	I_2	100% H_2O	12.0	339.0	0.354	0.354	6.13×10^{-2}	2.79×10^{-3}
250	I_2	100% H_2O	1.2	85.2	0.354	0.352	6.10×10^{-1}	2.77×10^{-2}
500	I_2	100% H_2O	12.0	233.7	0.0236	0.0236	4.09×10^{-3}	1.86×10^{-4}
500	I_2	100% H_2O	1.2	58.7	0.0236	0.0236	4.09×10^{-2}	1.86×10^{-3}
1000	I_2	100% H_2O	12.0	421.8	1.53×10^{-3}	1.53×10^{-3}	2.65×10^{-4}	1.20×10^{-5}
1000	I_2	100% H_2O	1.2	106.0	1.53×10^{-3}	1.53×10^{-3}	2.65×10^{-3}	1.20×10^{-4}
1000	HI	50% H_2O 50% H_2	12.0	906.7	0.590	0.590	0.102	4.64×10^{-3}
1000	HI	50% H_2	1.2	227.7	0.590	0.588	1.02	0.0463
2000	I_2	100% H_2O	12.0	844.8	2.01×10^{-4}	2.01×10^{-4}	3.48×10^{-5}	1.58×10^{-6}
2000	I_2	100% H_2O	1.2	212.1	2.01×10^{-4}	2.01×10^{-4}	3.48×10^{-4}	1.58×10^{-5}
2000	HI	50% H_2O 50% H_2	12.0	1807.7	0.354	0.354	6.13×10^{-2}	2.79×10^{-3}
2000	HI	50% H_2O 50% H_2	1.2	454.1	0.354	0.354	6.13×10^{-1}	2.79×10^{-2}

(a) Based on Deposition area of approximately 3000 sq. ft. - See Table VII I-6.
(b) Values obtained from Reference 1.

TABLE VII I-2 VALUES OF K_g, K_w, K_t, M_d, f_d, M_d (TOTAL) AND f_d FOR VARIOUS CONDITIONS OF IODINE DEPOSITION

PWR STEAM GENERATORS[a]

Temperature F	Iodine Species	Steam Boil-off Rate lbs/sec	K_g ft/hr	K_w[d] ft/hr	K_t ft/hr	M_d lbs	f_d	M_d Total lbs	f_d Total
250[b]	I_2	12.0	520.0	0.354	0.354	1.05	4.78×10^{-2}	1.11	0.051
250[b]	I_2	1.2	76.9	0.354	0.354	10.52	4.78×10^{-1}	1.09	0.51
500[b]	I_2	12.0	327.0	0.0236	0.0236	7.02×10^{-2}	3.19×10^{-3}	7.28×10^{-3}	3.38×10^{-3}
500[b]	I_2	1.2	48.4	0.0236	0.0236	7.02×10^{-1}	3.19×10^{-2}	0.0729	0.0338
1000[b]	I_2	12.0	545.0	1.53×10^{-3}	1.53×10^{-3}	4.55×10^{-3}	2.07×10^{-3}	4.82×10^{-3}	2.08×10^{-3}
1000[b]	I_2	1.2	80.6	1.53×10^{-3}	1.53×10^{-3}	4.55×10^{-2}	2.07×0.0^{-2}	0.023	0.021
1000[c]	HI	12.0	1142.0	0.590	0.590	1.754	7.97×10^{-2}	1.855	0.0843
1000[c]	HI	1.2	169.0	0.590	0.590	17.54	7.97×10^{-1}	18.55	0.844
2000[b]	I_2	12.0	972.0	2.01×10^{-4}	2.01×10^{-4}	5.98×10^{-4}	2.72×10^{-5}	6.33×10^{-4}	2.88×10^{-5}
2000[b]	I_2	1.2	143.0	2.01×10^{-4}	2.01×10^{-4}	5.98×10^{-3}	2.72×10^{-4}	6.33×10^{-3}	2.88×10^{-4}
2000[c]	HI	12.0	2057.0	0.354	0.354	1.05	4.77×10^{-2}	1.11	0.051
2000[c]	HI	1.2	304.0	0.354	0.354	10.52	4.77×10^{-1}	11.1	0.506

(a) Based on deposition area of approximately 51,500 sq. ft. - See Table VII I-6.
(b) Fluid composition, 100% H_2O.
(c) Fluid composition, 50% H_2O - 50% H_2.
(d) Values obtained from Reference 1.

TABLE VII I-3 VALUES OF K_g, K_w, K_t, M_d AND f_d FOR VARIOUS CONDITIONS OF IODINE DEPOSITION

BWR, STEAM SEPARATORS[a]

Temperature F	Iodine Species	Fluid Composition	Steam Boil-off Rate lbs/sec	K_g ft/hr	K_w[b] ft/hr	K_t ft/hr	M_d lbs.	f_d
500	I_2	100% H_2O	12.0	8.98	0.0236	0.0235	0.0134	6.90×10^{-4}
500	I_2	100% H_2O	1.2	1.33	0.0236	0.0232	0.133	6.02×10^{-3}
1000	I_2	100% H_2O	12.0	14.34	1.53×10^{-3}	1.53×10^{-3}	8.7×10^{-4}	3.96×10^{-5}
1000	I_2	100% H_2O	1.2	2.12	1.53×10^{-3}	1.53×10^{-3}	8.7×10^{-3}	3.96×10^{-4}

(a) Based on deposition area of approximately 9,850 sq. ft. - See Table VII I-7.
(b) Values obtained from Reference 1.

TABLE VII I-4 VALUES OF K_g, K_w, K_t, M_d, f_d, M_d (TOTAL) AND f_d TOTAL FOR VARIOUS CONDITIONS OF IODINE DEPOSITION

BWR, STEAM DRYERS[a]

Temperature F	Iodine Species	Steam Boil-off Rate lbs/sec	K_g ft/hr	K_w[c] ft/hr	K_t ft/hr	M_d lbs	f_d	M_d Total lbs	f_d Total
500[b]	I_2	12.0	2.131	0.0236	0.0233	0.043	1.95×0.0^{-3}	0.0564	2.56×10^{-3}
500[b]	I_2	1.2	0.3156	0.0236	0.0220	0.412	0.019	0.545	0.025
1000[b]	I_2	12.0	4.088	1.53×10^{-3}	1.53×10^{-3}	2.86×10^{-3}	1.3×10^{-4}	3.73×10^{-3}	1.69×10^{-4}
1000[b]	I_2	1.2	0.504	1.53×10^{-3}	1.52×10^{-3}	0.0286	1.3×10^{-3}	0.0373	1.69×10^{-3}

(a) Based on deposition area of approximately 32,400 sq. ft. - See Table VII I-7.
(b) Fluid Composition, 100% H_2O.
(c) Values obtained from Reference 1.

TABLE VII I-5 DEFINITION OF TERMS AND UNITS USED TO CALCULATE IODINE DEPOSITION

A	=	Deposition Area, ft^2
C_g	=	Concentration of iodine in gas (constant release), lbs/ft^3
C'_g	=	Iodine concentration (puff release), lbs/ft^3
C_o	=	Initial concentration of iodine in gas (puff release), lbs/ft^3
C_p	=	Fluid heat capacity, Btu/(lb) (°F)
D_o	=	Outside diameter of tubes, ft.
D_{12}	=	Diffusion coefficient (diffusivity of species 1 through a mixture of 1 and 2) $cm^2/sec.$
D_v	=	Molecular diffusivity of iodine in fluid, ft^2/hr
f_d	=	Fraction of iodine deposited, dimensionless
G_{max}	=	Mass velocity of fluid through minimum cross section, lbs/(hr) (ft^2)
G_{12}	=	Lennard-Jones force constant
h_m	=	heat transfer coefficient, Btu/(hr) (ft^2) (F)
k_f	=	thermal conductivity of fluid, Btu/(hr) (ft) (F)
k_g	=	mass transport coefficient, ft/hr
K'_g	=	Individual or gas-film coefficient, lb-moles/(hr) (ft^2) (atm)
K_t	=	Overall deposition coefficient, ft/hr
K_w	=	Wall deposition velocity, ft/hr
M_d	=	Amount of iodine deposited, lbs
M_o	=	Initial mass of iodine, lbs
m_1	=	Molecular weight of species 1
m_2	=	Molecular weight of species 2
N_{pr}	=	Prandtl Number, dimensionless
N_{sc}	=	Schmidt Number, dimensionless
P	=	Pressure, atm
P_{Bm}	=	Logarithmic means of the partial pressure, atm.
Q	=	Volumetric flow rate (steam boil off rate) ft^3/hr
Re	=	Reynolds Number, dimensionless
R_H	=	Hydraulic radius, ft
T	=	Temperature, (°K)
t	=	time period, hr.
U_{ave}	=	Mean fluid velocity (volumetric flow rate, Q divided by cross section), ft/hr
V	=	Volume, ft^3
Ω_D	=	Collision integral for diffusion
ρ	=	fluid density, lbs/ft^3
μ	=	fluid viscosity, lbs/(ft) (hr)

TABLE VII I-6 SUMMARY OF TYPICAL PWR SURFACE AREAS

Thermal Shield

Surface Area (Inside) = 7.75×10^4 in^2 = 538.2 ft^2

Surface Area (Outside) = 8.0×10^4 in^2 = 555.8 ft^2

Core Barrel (Lower)

Surface Area (Inside) = 6.99×10^4 in^2 = 485.5 ft^2

Surface Area (Outside) = 7.20×10^4 in^2 = 500.0 ft^2

Core Barrel (Upper)

Surface Area (Inside) = 4.1×10^4 in^2 = 284.8 ft^2

Surface Area (Outside) = 4.2×10^4 in^2 = 294.1 ft^2

Coolant opening area (3764 in^2 = 26 ft^2) subtracted from above.

Top Support Plate

Under Surface Area = 17,066 in^2 = 118.5 ft^2 (hole area subtracted)

Volume (minus holes) = 54,612 in^3 = 31.6 ft^3

Mass = 15,834 lbs (for 304 SS)

Upper Structural Support Columns

External Surface area (per column) = 15 ft^2

For 14 Support Columns = 210 ft^2

For 25 Support Columns = 375 ft^2

Volume of each Support Column = 4951 in^3 = 2.87 ft^3

For 14 Columns = 40.1 ft^3

For 25 Columns = 71.6 ft^3

Mass of each Support Column = 1438 lbs

For 14 Columns = 20,130 lbs

For 25 Columns = 35,950 lbs

Control Rod Guide Tubes

Surface Area (per tube) = 37.3 ft^2

53 Control rods = 1,976 ft^2

Mass (per tube) = 283 lbs

53 Tubes = 15,000 lbs (total)

Pressure Vessel

Inside Surface Area (Upper Core Plate to Upper Support plate) = 364 ft^2

Areas of water inlets and outlets subtracted

Bottom Support Casting

Assuming approximately 50% open area

Volume = 43 ft^3

Mass = 21,650 lbs

Instrument Guide Tubes

Information not available to estimate total number of tubes.

Estimated weight for each tube = 144.7 lbs.

TABLE VII I-6 (Continued)

Steam Generator (Heat Exchanger U tubes) Single Unit

Internal Surface Area	=	51,500 ft^2 (3338 U tubes)
I.D. of tubes	=	0.775 in
Length of single tube	=	914 in = 76 feet
Surface Area/tube	=	2222 in^2 = 15.4 ft^2/tube

Reactor Coolant Pumps

Internal Surface Area (approx.) = 61.5 ft^2 per pump (3 total)

Piping (Single Loop)

Approx. total length of piping	=	81 ft
Approx. total Internal Surface Area	=	600 ft^2
Approx. length Reactor to Steam Generator	=	25 ft (29" I.D.)
Approx. length Steam Generator to Pump	=	22 ft (31" I.D.)
Approx. length Pump to Reactor	=	34 ft (27.5" I.D.)

TABLE VII I-7 SUMMARY OF TYPICAL BWR SURFACE AREAS

Steam Dome		
Volume	=	1,560 ft^3
Surface Area	=	515 ft^2
Core		
Empty Volume (without bypass)	=	2,420 ft^3
Bypass Volume	=	267 ft^3
Fuel Rod Volume	=	221 ft^3
Fuel Assembly Volume	=	99.1 ft^3
Net Core Volume	=	2,100 ft^3
Cladding Surface Area	=	59,100 ft^2
Channel Surface Area	=	29,800 ft^2
Core Shroud		
Inside and Outside Surface Area	=	2,160 ft^2
Mass	=	84,122 lb
Lower Plenum and Control Rod Drives		
Empty Volume	=	2,910 ft^3
Control Rod Guide Tube Displaced Volume	=	426 ft^3
Net Volume	=	2,482 ft^3
Guide Tube Outside Surface Area	=	3,410 ft^2
Total Surface Area	=	4,439 ft^2
Downcomer and Jet Pumps		
Empty Volume	=	1,510 ft^3
Jet Pump Volume	=	182 ft^3
Net Volume	=	1,328 ft^3
Jet Pump Outside Surface Area	=	874 ft^2
Total Surface Area	=	3,244 ft^2
Jet Pumps Total Mass (20 Pumps)	=	20,000 lb
Steam Separators		
Empty Volume	=	4,300 ft^3
Separator Displaced Volume	=	2,500 ft^3
Separator Volume	=	224 ft^3
Net Volume	=	1,800 ft^3
Separator Outside Surface Area	=	8,900 ft^2
Total Surface Area	=	9,850 ft^2

TABLE VII I-7 (Continued)

Steam Driers		
Empty Volume	=	2,970 ft^3
Drier Volume	=	132 ft^3
Net Volume	=	2,838 ft^3
Drier Surface Area	=	31,700 ft^2
Total Surface Area (approx.)	=	32,400 ft^2
Recirculation Piping		
Length (approx.)	=	80 ft
Inside Volume	=	64 ft^3
Inside Surface Area	=	254 ft^2
Inlets (approx. length)	=	15 ft
Inlets (volume)	=	75 ft^3
Inlets (inside surface area)	=	375 ft^2
Suction Lines and Pumps Approx. Length	=	100 ft each (2 total)
Suction Lines and Pumps Inside Volume	=	340 ft^3
Suction Lines and Pumps Inside Surface Area	=	920 ft^2

APPENDIX J

TRANSPORT AND DEPOSITION OF AIRBORNE FISSION PRODUCTS IN CONTAINMENT SYSTEMS OF WATER COOLED REACTORS FOLLOWING POSTULATED ACCIDENTS

by

A. K. Postma, P. C. Owzarski,
and D. L. Lessor
Battelle Pacific Northwest Laboratories

Appendix J

Table of Contents

Section		Page No.
J1.	MECHANISMS WHICH CONTROL THE REMOVAL OF AIRBORNE FISSION PRODUCTS FROM CONTAINMENT ATMOSPHERES	VII-185
J1.1	Physical and Chemical Forms of Airborne Fission Products	VII-185
J1.2	Mechansims Expected to Control Depletion from the Gas Phase	VII-185
J1.2.1	Noble Gases	VII-185
J1.2.2	Methyl Iodide	VII-185
J1.2.3	Elemental Iodine	VII-186
J1.2.4	Aerosol Particles	VII-186
J2.	NUMERICAL EVALUATION OF REMOVAL RATES	VII-187
J2.1	Noble Gases	VII-187
J2.2	Methyl Iodide	VII-187
J2.3	Elemental Iodine	VII-188
J2.4	Aerosol Particles	VII-190
J3.	CONTAINMENT MODELS	VII-190
J3.1	Single Volume Containment Model	VII-190
J3.2	Multicompartment Containment Model - PWR	VII-191
J3.2.1	Natural Deposition	VII-193
J3.2.2	Spray Removal	VII-194
J3.2.3	I_2 Equilibrium	VII-195
J3.2.4	Intercompartmental Flow Rates	VII-195
J3.3	Multicompartment Containment Model - BWR	VII-196
J3.3.1	Natural Deposition - Effect of Heat Transfer from BWR Vessel Walls	VII-197
J3.3.2	Pool Scrubbing	VII-197
J3.3.3	Standby Gas Treatment System - (SGTS)	VII-198
J3.3.4	Natural Deposition in the Drywell Annular Airspace	VII-198
J3.4	Computer Code Corral	VII-200
REFERENCES		VII-202
ADDENDUM		VII-209

List of Tables

Table		Page No.
VII J-1	Fission Product Removal Rate Constants Calculated for a Large PWR Containment Vessel	VII-203
VII J-2	Equilibrium Data for I_2 with Boric Acid Sprays	VII-203
VII J-3	Equilibrium Data for I_2 with Caustic Sprays	VII-204
VII J-4	DF Versus Particle Size and Reynolds Number in Drywell Annular Gap	VII-204
VII J-5	Fission Product Releases	VII-204

List of Figures

Figure		Page No.
VII J-1	Partitioning of Elemental Iodine by Recirculated Sprays	VII-205
VII J-2	Schematic of Quantity of Airborne-Contained Fission Products Versus Time	VII-205
VII J-3	Schematic of Quantity of Fission Products Released to Atmospheres Versus Time	VII-206
VII J-4	Drop-Collection Efficiency as a Function of Liquid Volume Sprayed	VII-206
VII J-5	Gas Flow for PWR Cases	VII-207
VII J-6	Flow Schematic for a BWR - (Possible Atmospheric Source)	VII-207
VII J-7	Computer Code CORRAL Flow Diagram	VII-208
VII J-8	Typical Sequence of Spike Fission Product Releases for Postulated Accidents	VII-208

Appendix J

Transport and Deposition of Airborne Fission Products in Containment Systems Of Water Cooled Reactors Following Postulated Accidents

by

A. K. Postma, P. C. Owzarski,
and D. L. Lessor
Battelle Pacific Northwest Laboratories

In this report, fission product transport and deposition in containment systems of water cooled reactors is analyzed. The scope of the work involves prediction of fission product behavior from the point of release from the primary coolant system to the entry to the earth's atmosphere.

This study is one element in the Fission Product Source Term Task of the USAEC Reactor Safety Study. The goal of the Reactor Safety Study is to realistically evaluate the risk to the public of postulated catastrophic accidents in water cooled nuclear reactors.

This report contains a description of removal mechanisms which will deplete fission products airborne in containment systems, a listing of the calculational methods used to predict removal rates, and a description of a computer code for calculating atmospheric release of airborne substances from a multicompartmented containment system.

J1. MECHANISMS WHICH CONTROL THE REMOVAL OF AIRBORNE FISSION PRODUCTS FROM CONTAINMENT ATMOSPHERES

J1.1 PHYSICAL AND CHEMICAL FORMS OF AIRBORNE FISSION PRODUCTS

The mechanisms which control depletion of a specific fission product specie depend on its physical and chemical form. For example, gaseous fission product forms such as noble gases, organic iodides and elemental iodine are removed at widely different rates because of great differences in equilibrium solubility in water. Except for the noble gases and halogens, fission products will be present as solid particles.

Fission product forms considered in the present study include the following:

- elemental iodine
- methyl iodide
- noble gases
- aerosol particles.

These categories are expected to be sufficiently broad to include all fission products of importance.

J1.2 MECHANSIMS EXPECTED TO CONTROL DEPLETION FROM THE GAS PHASE [1]

J1.2.1 NOBLE GASES

For the accident cases considered, no removal mechanisms of importance were present. Therefore, removal of noble gases from the gas phase was considered to be negligible. It is recognized that several means for collecting noble gases have been proposed. These include clathrate compound formation, trapping by surface active agents such as refrigerated charcoal, separation by selective membranes, and absorption by fluorocarbon solvents. If any of these processes were considered operable following postulated accidents, a removal term would be added to the present formulations.

J1.2.2 METHYL IODIDE

Methyl iodide and other alkyl halides are relatively unreactive and are only slightly soluble in water. Organic iodides are removed by hydrolysis in water, by adsorption on special reactive paints, by solution reaction with reactive spray additives such as sodium thiosulfate, and by activated charcoal filters.

---

[1] The discussion here is oriented mainly toward PWR systems but portions apply also to BWR systems. These plus additional BWR processes are described later in the report.

For accident cases where engineered safety systems do not function, removal will be governed by hydrolysis in water and by adsorption on paint. The removal rate due to both of these mechanisms is slow, being equivalent to a removal half-time of many hours. Thus methyl iodide removal may be neglected for these accident cases.

Removal of methyl iodide by both caustic and boric acid spray is primarily by hydrolysis of methyl iodide in the spray solution. This hydrolysis rate is slow, and, like the case for no spray, the removal rate is usually negligible.

Addition of 1 percent by weight of sodium thiosulfate to the spray solution markedly increases the methyl iodide removal rate compared to that for boric acid or caustic spray. For the thiosulfate spray, methyl iodide removal is the result of adsorption with simultaneous chemical reaction into wall films and into falling spray drops.

Activated charcoal filters such as those used in a recirculating air cleaning system remove methyl iodide at appreciable efficiencies. For the saturated air-steam atmospheres encountered under accident conditions in PWR's, removal efficiencies in the neighborhood of 70 percent are anticipated. Thus the removal rate will depend primarily on the air flow rate through the filters.

J1.2.3 ELEMENTAL IODINE

Elemental iodine is reactive in aqueous solution and may be rapidly absorbed by sprays. The absorption rate for boric acid is limited by the gas-liquid equilibrium partition coefficient. For caustic sprays the absorption rate is controlled more by gas phase mass transfer resistance than by equilibrium. Liquid phase mass transfer resistance is negligible for sprays containing 1 percent by weight of sodium thiosulfate.

Activated charcoal filters are quite efficient for removal of elemental iodine. A removal efficiency of 99 percent could be expected for a charcoal filter installed in a recirculating filter loop. The removal rate would be controlled primarily by the air flow rates.

Elemental iodine is also removed by natural processes if engineered safety systems do not work. The removal rate may be estimated from models in which iodine mass transfer is limited by diffusion through a gas boundary layer which flows along the walls of the containment vessel. Mass transfer coefficients for the natural convection boundary layer are relatively small, so the removal rate by natural deposition is small compared to that which can be achieved by reactive sprays.

J1.2.4 AEROSOL PARTICLES

All non-gaseous fission products which become airborne will be present in the form of aerosol particles. Due to the relatively high mass concentration of airborne particles, the particles will consist of numerous primary nuclei agglomerated into larger particles. The agglomerate particles would be expected to contain primary particles of the many fission product nuclides present. Thus it is expected that the transport characteristics of all solid fission products would follow the behavior of the aerosol particles.

Particles may be removed by sprays, by filters, by deposition onto surfaces, and by gravitational settling.

Mechanisms which cause collection of particles by spray drops include inertial impaction, interception, diffusiophoresis, and diffusion. Prediction of the collection rate requires knowledge of the single drop collection efficiency. In the present study, the single drop collection efficiency was calculated from large scale spray experiments in which particle removal was measured under simulated accident conditions. This means for estimating the collection efficiency is expected to result in an under-prediction, because in the postulated accidents higher aerosol concentrations favor formation of larger, easier-to-remove particles.

Particulate filters used in recirculating filter systems are highly efficient in removing airborne particles of all sizes. Therefore, recirculating filters systems, if included in a containment system design, could be relied on to remove more than 99 percent of airborne particles per pass.

Under natural transport conditions, gravity settling of particles on horizontal surfaces, and turbulent deposition on vertical surfaces represent the primary removal mechanisms. Experiments have demonstrated that gravity settling will dominate in the post accident containment atmosphere. In the present study, the particle gravity settling velocity, and hence the aerodynamic diameter, were obtained from experimental data obtained in large scale containment vessels.

J2. NUMERICAL EVALUATION OF REMOVAL RATES

J2.1 NOBLE GASES

For the accident cases which have been studied to date, no specific means have been included to remove noble gases. Since these gases would not be removed to a significant extent by sprays, filters, or natural deposition, the removal rate from the total system has been set equal to zero. Removal from a specific compartment of the containment vessel may occur by convective flow of gas, but this output term would represent an input term to the connected compartment.

J2.2 METHYL IODIDE

Methyl iodide is removed only very slowly under conditions of natural deposition or where sprays of boric acid or caustic are used. Removal half-times are many hours for these three cases, hence methyl iodide removal may be neglected without excessive error.

Appreciable removal of methyl iodide would occur if a recirculating charcoal filter system were incorporated in the containment system. Results obtained in the Containment Systems Experiment (Ref. 1) have demonstrated that a removal efficiency of approximately 80 percent is achieved for methyl iodide when saturated steam-air atmospheres pass through charcoal filters impregnated with 5 percent iodine. The removal rate constant for such a filter system may be expressed as

$$\left(\frac{dc}{dt}\right)_f = \lambda_f C = \frac{FE}{V} C \qquad \text{(VII J-1)}$$

where

$\left(\frac{dC}{dt}\right)_f$ = removal rate due to filter system,

λ_f = removal rate constant for filter system,

F = gas flow rate through filter,

E = fractional removal efficiency,

C = airborne concentration of removed species.

Based on the CSE tests, E should be chosen as 0.8 for methyl iodide, and equal to 1.0 for both elemental iodine and aerosol particles.

Methyl iodide is removed at an appreciable rate by sprays containing sodium thiosulfate at a level of one weight percent. The removal rate constant for reactive drops may be predicted (Ref. 2) by

$$\lambda_{drops} = \frac{FH\ (1+kt_e)}{V} \qquad \text{(VII J-2)}$$

where

λ_{drops} = methyl iodide removal by spray drops,

F = spray flow rate,

V = volume of contained gas phase,

H = equilibrium partition coefficient,

k = first order solution reaction rate,

t_e = drop exposure time.

This equation applies for a well mixed drop model, and is expected to realistically represent the situation prevailing for containment sprays.

In addition to removal by spray drops, methyl iodide will also be removed by spray liquid which has wet the wall of the containment vessel. If the wall film is assumed to be stagnant, the methyl iodide absorption rate is given by

$$\lambda_{(wall)} = \frac{AH\ \sqrt{kD}\ \tanh\ [\sqrt{(k/D)}\,\delta]}{V} \qquad \text{(VII J-3)}$$

where

$\lambda_{(wall)}$ = removal rate constant for wall film,

A = surface area wet by wall film,

H = equilibrium partition coefficient,

D = diffusivity of methyl iodide in spray liquid,

δ = wall film thickness,

V = volume of contained gases.

The net removal rate will be the sum of that for wall film and spray drops:

$$\lambda = \frac{FH\ (1+kt_e)}{V} + \frac{AH\ \sqrt{kD}\ \tanh\ [\sqrt{(k/D)}\,\delta]}{V} \ . \qquad \text{(VII J-4)}$$

Predictions based on equation (VII J-4) are in good agreement with large scale experiments (Ref. 2).

J2.3 ELEMENTAL IODINE

Elemental iodine is removed by natural deposition at a rate which is controlled by mass transfer through the gas boundary layer at the walls of the containment vessel. The natural deposition removal rate constant is simply

$$\lambda_{(NT)} = \frac{k_g\ A}{V} \qquad \text{(VII J-5)}$$

where

$\lambda_{(NT)}$ = removal rate constant for natural deposition,

A = surface area for mass transfer,

V = volume of contained gases.

Knudsen and Hilliard (Ref. 3) have discussed methods for calculating k_g for containment vessels. The value of k_g is governed primarily by the Grashov number for natural convection. For laminar flow, the mass transfer coefficient is given by

$$\frac{k_c \ell}{D_v} = 0.59\ (Gr\ Sc)^{1/4} \qquad \text{(VII J-6)}$$

where

k_c = mass transfer coefficient,

ℓ = length along surface,

D_v = diffusivity of iodine in gas phase,

Gr = Grashov no. for wall boundary layer,

Sc = Schmidt no. for iodine in steam.

For turbulent flow

$$\frac{k_c \ell}{D_v} = 0.13\ (Gr\ Sc)^{1/3} \ . \qquad \text{(VII J-7)}$$

Laminar flow persists until the Grashof number exceeds a transition value. According to an analysis presented by Hales (Ref. 4) transition from laminar to turbulent flow occurs for lengths which correspond to Grashof numbers between 1.5 and 10^{-8} and 1.5 x 10^{10}. For containment atmospheres, this transition would occur at distances 5 to 10 ft down the vertical wall. (Ref. 5) Thus Equation (VII J-6) would apply for the first 10 ft, and Equation (VII J-7) would apply for the remainder of the distance.

Hilliard and Coleman (Ref. 5) have provided estimates of iodine removal by natural deposition based on use of Equations (VII J-6) and (VII J-7). The airborne concentration is predicted to be

$$\frac{C_g}{C_{go}} = 0.96e^{-1.42t} + 0.04e^{-0.0143t} \qquad \text{(VII J-8)}$$

where

C_g = airborne concentration,

C_{go} = airborne concentration at time zero,

t = time in hours.

The first term in Equation (VII J-8) represents removal by mass transfer through the wall boundary layer. The second term accounts for an approach to pseudo-equilibrium between the gas and liquid phases. The initial removal half life for a large vessel as predicted by Equation (VII J-8) is approximately 30 minutes.

For spray removal of elemental iodine, the removal rate may be predicted from a model in which the spray is considered to be an assemblage of noninteracting single drops. The overall drop absorption process includes the following steps:

- mass transfer across the gas film
- equilibrium dissolution at the gas-liquid interface
- diffusion into the drop
- reaction within the liquid phase.

A conservative model for spray absorption may be formulated under the assumption that the drop consists of an outer stagnant film and a well-mixed interior. For this model, the absorption efficiency (defined as fractional saturation achieved by a drop falling through the containment vessel) is given by

$$E = 1 - \exp\left[-\frac{6k_g t_e}{d\left(H+\frac{k_g}{k_L}\right)}\right] \qquad \text{(VII J-9)}$$

where

E = drop absorption efficiency,

$k_g = \frac{D_v}{d}(2 + 0.6\ Re^{0.5}\ Sc^{0.33})$

= gas phase mass transfer coef.,

$k_L = \frac{2\pi^2 D_L}{3d}$ = liquid phase mass transfer coefficient,

t_e = drop exposure time,

H = equilibrium partition coefficient.

The basis and assumptions involved in formulating Equation (VII J-9) are discussed in detail by Postma and Pasedag (Ref. 6).

The spray removal rate constant may be related to the spray flow rate and drop absorption efficiency by

$$\lambda_s = \frac{F\ H\ E}{V} \qquad \text{(VII J-10)}$$

where

λ_s = spray removal rate constant,

H = equilibrium partition coefficient,

E = drop absorption efficiency,

V = volume of contained gas.

The partition coefficient appearing in Equations (VII J-9) and (VII J-10) is the value attained in a few seconds. This time specification is necessary because iodine dissolution is greatly influenced by chemical reactions. Only those reactions which are fast enough to convert elemental iodine to non-volatile forms within a time period shorter than the drop exposure time will aid spray absorption.

On the basis of available information, Postma and Pasedag (Ref. 6) have concluded that applicable H values are as follows:

- for caustic, pH 9.5, H = 5000
- for boric acid, pH = 5, H = 200
- for basic sodium thiosulfate, H = 100,000.

The first order removal rate predicted by Equation (VII J-10) will not continue to apply for an indefinite time because of equilibrium between the gas and liquid phase. For the first two hours following spray initiation, equilibrium may be accounted for by limiting spray removal to 1 percent of the release concentration (Ref. 6). Beyond the time needed to remove 99 percent of airborne iodine, the concentration should be assumed to remain constant at 1 percent of the release concentration.

For times longer than two hours, the gas concentration may be allowed to decrease further as a result of chemical reactions in the liquid phase. For equilibrium conditions, which would be attained for times longer than a few hours, the airborne iodine concentration is given by

$$\frac{C_g}{C_{go}} = \frac{1}{1 + H\frac{V_L}{V_g}} \qquad \text{(VII J-11)}$$

where

C_g = equilibrium airborne concentration

C_{go} = initial airborne concentration for puff release,

H = equilibrium partition coefficient,

V_L = volume liquid phase,

V_g = volume of gas phase.

The partition coefficient, H, in Equation (VII J-11) increases with time due to kinetically slow liquid phase reac-

tions. In this study, the variation of H with time was taken from experimental results reported by Postma, et al. (Ref. 7). Experimental results for caustic and boric acid solutions are shown in Fig. VII J-1. The data presented in Fig. VII J-1 were used to conjunction with Equation (VII J-11) to predict long term behavior of elemental iodine in caustic and boric acid spray.

For spray containing 1 percent sodium thiosulfate, partition coefficients will be large. As discussed by Postma and Pasedag, (Ref. 6) the cutoff concentration for sodium thiosulfate sprays may be taken as 0.1 percent of the release concentration.

J2.4 AEROSOL PARTICLES

Particles are removed by natural transport primarily by gravitational settling (Ref. 5). The removal rate constant is related to the particle settling velocity by

$$\lambda = \frac{U_t A_{cs}}{V} \qquad \text{(VII J-12)}$$

where

λ = removal constant for settling,

A_{cs} = cross sectional area of vessel,

V = volume of contained gases,

U_t = terminal settling velocity of particles.

Results from CSE experiments (Ref. 5) indicate that soon after fission product release, particle diameter was 15 microns. A few hours later, average particle size decreased to about 5 microns.

The CSE results indicate that aerosol particles will be removed slowly by natural processes. Because of higher aerosol mass concentrations in postulated core meltdown accidents, the CSE results will tend to underpredict removal for the meltdown accidents. We have not attempted to account for this difference in the present study.

For recirculating filter systems, particle removal would be described by Equation (VII J-1) with an efficiency fraction of unity.

Spray removal of aerosol particles may be predicted from a model in which the spray is considered to be an assemblage of non-interacting single drops. The overall removal rate is the sum of removal rates for individual drops. For a well-mixed gas space, the removal rate constant is expressible as

$$\lambda = \frac{3\ h\ F\ E}{2\ d\ V} \qquad \text{(VII J-13)}$$

where

λ = spray removal rate constant for particles,

h = drop fall height,

F = spray flow rate,

E = drop collection efficiency,

d = mean drop size,

V = volume of gas phase.

The magnitude of the drop collection efficiency, E, depends on a number of factors as discussed earlier. Particle size of the aerosol is the most important single parameter, and size was estimated from CSE spray experiments.

In applicable CSE tests (Ref. 8) the effective particle collection efficiency varied from a maximum value (E = 0.06) achieved early to a minimum value (E = 0.0015) reached after most of the aerosol was removed. In single volume, hand calculation models an average value of 0.02 may be used. After the airborne concentration reduces to 2 percent of the release concentration, the drop collection efficiency used in the calculation should be lowered to 0.0015. In multicompartment containment models, E should be allowed to vary with the degree of removal as was observed in the CSE experiments.

Examples of removal rates calculated for a large PWR containment vessel are shown in Table VII J-1. These values were used in preliminary hand calculations with a single volume containment model.

J3. CONTAINMENT MODELS

J3.1 SINGLE VOLUME CONTAINMENT MODEL

The single volume containment model assumes that the vapor phase consists of one well-mixed compartment. This assumption enables one to write the following single differential equation for each species:

$$d\frac{C_i}{dt} = -\left(\sum_j \lambda_{ij}\right) C_i - \alpha_i C_i + R_i(t)$$

(VII J-14)

Initial Condition: $C_i = C_i(t')$ at $t = t'$

C_i = Airborne moles of component i

λ_{ij} = Removal rate constant via mechanism j

α_i = leak rate, fraction of the volume/time

$R_i(t)$ = source term (moles/time)

This equation is easily solved for constant λ_{ij}, α_i and R_i to get

$$C_i = \frac{R_i}{(\Sigma\lambda_{ij} + \alpha_i)} - \left[\frac{R_i}{(\Sigma\lambda_{ij} + \alpha_i)} - C_i(t')\right] \exp - (\Sigma\lambda_{ij} + \alpha_i)(t-t')$$

(VII J-15)

The escaped amount during the interval t-t' is the integral

$$Q_i = \int_{t'}^{t} C_i V \alpha_i \, dt ,$$

where V is the volume of the vessel. Thus

$$Q_i = \frac{R_i V\alpha_i}{(\Sigma\lambda_{ij} + \alpha_i)} (t-t') - \left[\frac{R_i}{(\Sigma\lambda_{ij} + \alpha_i)} - C_i(t')\right] \left(\frac{\alpha_i V}{\Sigma\lambda_{ij} + \alpha_i}\right) \times 1-\exp\left[-(\Sigma\lambda_{ij} + \alpha_i)(t-t')\right]$$

(VII J-16)

The two equations for $C_i(t)$ and $Q_i(t-t')$ can be used to calculate airborne fractions and leakage fractions for various accident sequences by hand. The values of λ_{ij}, used for various species are discussed earlier in this report and summarized in Table VII J-1. Typical curves describing the moles airborne and escaped are shown in Fig. VII J-2 and VII J-3.

The only release of fission products encountered where R_i = constant for some time period is the melt release. This simplifies most of the computations to using an initial condition for a time period where the λ_{ij}'s and α_i's are considered to be constant. If the λ's or α's changed at some time, t', a new t' can be considered as the beginning of a new time period of constant new λ's or α's.

J3.2 MULTICOMPARTMENT CONTAINMENT MODEL - PWR

To better simulate containment geometry and time variable removal rates, a model was developed to analyze the atmospheric source from a set of compartments whose airborn contents are well mixed and are altered by intercompartmental flow in addition to deposition rates, leak rates, spray removal rates, etc. This system is described by a set of equations of the form

$$dC_i^{mr}/dt = \sum_j H_{ij}^{mr} C_j^{mr} \qquad \text{(VII J-17)}$$

where

C_i^{mr} = air borne fraction of initial release of material m in release type r contained in compartment i

$$H_{ij}^{mr} = \left(\lambda_i^{mr} + \sum_k G_{ki}/V_k\right)\delta_{ij} + \left(G_{ji}/V_j\right)\left(1-E_{ji}^{mr}\right)$$

λ_i^{mr} = removal coefficient from compartment i by settling, leak, spray removal, and other processes not involving flow to or from another compartment

G_{ji} = volume flow rate from compartment/compartment j to compartment i

E_{ji}^{mr} = filter removal fraction for material m from release r

V_j = volume of compartment j

δ_{ij} = 1 if i = j, δ_{ij} = 0 if i ≠ j

Note that the flow terms assume uniform mixing within each compartment.

For a given release type and material type, the equation set can be written in matrix notation

$$\frac{dC}{dt} = HC \qquad \text{(VII J-18)}$$

Where C is the column vector of airborn release fractions in the respective compartments and H is the matrix of rate constants governing the evolution. The solution of this differential equation for the column vector C for constant coefficients in the H matrix is given exactly by

$$C(t) = e^{Ht}\, C(o) \qquad \text{(VII J-19)}$$

or

$$C(t) = C(t_o) + (t-t_o)H\left(\frac{e^{(t-t_o)H} - 1}{(t-t_o)H}\right) C(t_o). \qquad \text{(VII J-20)}$$

Fast computer techniques for generating this solution have been developed by B. H. Duane (Ref. 9) and were utilized here. By calling the numerical integration subroutines developed by Duane at each time step after calculating the H matrix, the accuracy limit becomes that imposed by the assumption of constant H matrix elements within the time step. Numerical error in generating the solution to the coupled set of equations with constant coefficients can be made on the order of 10^{-6} percent.

To integrate the amount leaked within the time step, N additional fictitious compartments were defined whose function is to accumulate the leaked material from the N real compartments. The fractions C_{i+N}, i = 1, 2, ···N, are cumulative leaks obtained from the solution of

$$\frac{d}{dt}\,(C_{i+N}) = \alpha_i C_i$$

where α_i is the leak rate coefficient from compartment i. Note $-\alpha_i$ is one part of H_{ii}. The previously defined N x N H matrix was augmented to form a 2N x 2N H matrix according to

$$H_{i+N,j} = \alpha_i \delta_{ij}$$

$$H_{i,\,j+N} = 0$$

$$H_{i+N,\,j+N} = 0$$

For i = 1, 2, ···, N

j = 1, 2, ···, N

If one takes the material quantity in the fictitous compartments to be zero at the start of a time step, the fraction of the initial release material leaked during the time step will be

$$\sum_{i=N}^{2N} C_i$$

Computer code CORRAL[1] was written to solve the set of equations and at the same time compute each rate parameter as a function of time and/or as a function of vessel conditions (p, T, humidity). A more detailed description of the various models used to compute rate parameters follows.

Nine time dependent parameters are computed from input data at the time of solution of the differential equations. These are:

1. Compartment pressure, p(k), psig
2. Compartment temp, T(k), F
3. Compartment vapor mole fraction, VAP(k)
4. Compartment wall-bulk temperature difference, DELTA T(k), F

5.-6. Leak rates of molecular iodine and particulates from each compartment, ELI2(k), ELP(k), fractions/hr.

7. Flow rates between compartments, G(j, k), ft^3/hr.

8.-9. Filter decontamination efficiencies for flow between compartments, EFI2(J,KO, EFP (j, k), dimensionless.

The first four parameters enable one to compute transport coefficients involved in depletion rate coefficient calculations.

---

[1]Containment Of Radionuclides Released After LOCA.

The bulk gas viscosities of steam-air mixtures (μ_m) are computed according to the following equations (Ref. 10):

$$\mu_m = \frac{\mu_A}{1 + \frac{Y_s}{Y_a}\phi_{As}} + \frac{\mu_s}{1 + \frac{Y_A}{Y_s}\phi_{sA}} \qquad \text{(VII J-21)}$$

where

μ_m = viscosity of mixture

$\mu_A = 0.0414 \left[\frac{T,R}{492}\right]^{0.768}$, lb/ft/hr

$\mu_s = \frac{0.003339\ (T,\ R)^{1.5}}{(T_R + 1224.2)}$,

y_A = mole fraction of air

y_s = mole fraction of steam

$$\phi_{As} = \frac{\left[1 + \left(\frac{\mu_A}{\mu_s}\right)^{1/2}\left(\frac{\mu_s}{\mu_A}\right)^{1/4}\right]^2}{2\sqrt{2}\left[1 + \left(\frac{\mu_A}{\mu_s}\right)\right]^{1/2}}$$

ϕ_{sA} = above with subscripts reversed.

The diffusivity of I_2 in the steam-air mixtures were found using data and equations from Knudsen (Ref. 10).

$$D_{I_2} = \frac{1}{\frac{Y_A}{D_A} + \frac{Y_s}{D_s}} \qquad \text{(VII J-22)}$$

where

$D_A = 2.03 \times 10^{-5}\ (T,K)^{1.5}/P,\ atm)W_A$, cm^2/sec

$D_B = 3.24 \times 10^{-5}\ (T,\ K)^{1.5}/(P,\ atm)/W_S$

$W_A = 0.7075 + 141.73/T,\ K$

$W_S = 0.7075 + 454.72/T,\ K$

The diffusivity of I_2 in water (spray drops) was computed using the standard Wilke-Chang relationship (Ref. 10), where

$$D_\ell = \frac{(7.4 \times 10^{-8})(xM_\ell)^{1/2}\ T(K)}{\mu_L\ V^{0.6}},\ cm^2/sec \qquad \text{(VII J-23)}$$

where

x = degree of solvent association = 2.6 for H_2O

M_ℓ = molecular weight of solvent

μL = solvent viscosity, cp

$\mu L = 100/\{2.1484\ [(T,(K)-281.6) + (8078.4 + (T,(k)-281.6)^2)^{0.5}] - 120\}$ for H_2O

V = molar volume of diffusing substance = 71.5 cm^3/gmole for I_2.

J3.2.1 NATURAL DEPOSITION

The mechanism of natural deposition of I_2 is governed by diffusion with natural convection generated by temperature differences between bulk gas and the wall (DELTAT(k)). Knudsen and Hilliard (Ref. 3) claim that a mass transfer analogy can be made with correlations predicting natural convective heat transfer coefficients. In similar manner, the model uses expressions for Sherwood numbers for laminar and turbulent flow using a thermal Grashof number,

$$Gr = \ell^3 \frac{(T_{wall} - T_{bulk})}{(\mu_m/\rho_m)^2\ T\ bulk}\ g$$

Thus for laminar flow ($Gr < 10^9$), the Sherwood number is

$$Sh = \frac{k_c \ell}{D_{I_2}} = 0.59\ (Gr\ Sc)^{1/4} \qquad \text{(VII J-24)}$$

and for turbulent flow ($10^9 < Gr < 10^{12}$)

$$Sh = \frac{k_c \ell}{D_{I_2}} = 0.13\ (Gr\ Sc)^{1/3} \qquad \text{(VII J-25)}$$

where Sc = Schmidt number = $\mu_M/\rho_M\ D_{I_2}$

and

ℓ = length of the wall

k_c = mass transfer coefficient.

A combination of the two Sherwood numbers is used to compute the actual Sherwood number. Since the turbulence in most cases occurs around 10 ft from the top of the wall, a weighted average was used.

$$Sh(\text{overall}) = \frac{\ell-10}{\ell} Sh(\text{turbulent}) + \frac{10}{\ell} Sh(\text{laminar}).$$

To convert the mass transfer coefficient into a deposition lambda (λ_{ij}) is a simple step. Thus,

$$\lambda_{ij}(k) = k_c(k)\ A(k)/V(k)$$

where A(k) and V(k) are suface area and volume of compartment k, respectively.

Another natural deposition process of interest is the settling of particulates. This involves a calculation of terminal settling velocities, V_s, assuming spherical, unit density particles.

$$d^2\ (\rho_p - \rho_m)\ g/18\ \mu_m = V_s$$

(VII J-26)

Particle diameters used were considered as functions of time. Hilliard and Coleman (Ref. 5) report that the settling velocities decrease with time after release. In CORRAL it was decided to use their data and assign an early particle diameter (15μ) and a late particle diameter (5μ) ("several hours" later = 4 hrs) and linearly interpolate between them. After 4 hrs., the particle size was kept constant at the late value. To get the natural deposition lambda for particulates use

$$\lambda = V_s \frac{A(\text{floor area})}{\bar{V}(\text{compartment volume})}$$

J3.2.2 SPRAY REMOVAL

The spray removal model of I_2 by boric acid and caustic sprays used in CORRAL combines a gas phase mass transfer coefficient, a drop-gas interfacial equilibrium distribution coefficient and a stagnant liquid film mass transfer coefficiet. The expression for the spray lambda is given by

$$\lambda = \frac{FH}{V}\left[1 - \exp - \left(6\ \frac{k_g t_e}{d(H + k_g/k_\ell)}\right)\right]$$

/H at equilibrium

(VII J-27)

where

F = spray flow rate

H = equilibrium distribution coefficient

($C_g = C_\ell/H_j$ at equil.)

V = spray compartment volume

d = spray drop diameter

t_e = drop residence time - height of fall/terminal velocity

and the gas mass transfer coefficient, k_g, is given by Ranz and Marshall (Ref. 11) as

$$k_g = \frac{D_{I_2}}{d}\left\{2.0 + 0.60\ Re^{1/2}\ Sc^{1/3}\right\}$$

and

$$k_\ell = \frac{2\pi^2 D_\ell}{3d},\ D_\ell = I_2 \text{ diffusivity in liquid.}$$

The latter is the Griffiths model discussed by Postma (Ref. 6). Incorporating the latter is a more conservative approach when $k_g/k_\ell \geq 5H$. The terminal velocities of the falling drops are found by matching the velocity independent dimensionless number

$$f_D\ Re^2 = 4\ \rho_M\ (\rho_L - \rho_M)\ \ d^3 g/3\mu_M^2$$

with the appropriate range of Reynolds number Re. For spray drops the range of Re is 10-700. For $10<Re<100$, $f_D Re^2 = 15.71\ Re^{1.417}$, and for $100<Re<700$, $f_D Re^2 = 6.477\ Re^{1.609}$ (Ref. 2).

Spray lambdas for removal of particles follow the equation (Ref. 8):

$$\lambda = \frac{3F\ Eh}{2\ V\ d}$$

(VII J-28)

where

F = spray flow rate
h = spray fall height
d = spray diameter
V = compartment volume
E = spray collection efficiency.

In CORRAL empirical results from CSE data are used to predict E. Apparently the efficiency is a function of a normalized liquid volume sprayed (total volume sprayed/total compartment volume - Ft/V). Figure VII J-4 shows the CSE data, and the curve in this figure was used to compute drop collection efficiencies in CORRAL. The diffusiophoresis was subtracted from the efficiency and the following expressions were fit to the remaining curve. To make these relationships apply to a spray lambda

Ft/V	E
0 - 0.002	$E = -15.825\ (Ft/V) + 0.055$
0.002 - 0.0193	$E = 0.04125 - [0.08626 + 42.68\ (Ft/V)]^{1/2}/21.34$
0.0193	$E = 0.0015$

with multiple sprays being used at various times, the quantity ft/V is now the sum $\Sigma\ F_i\ t_i/V$ for any one release of particles. Each release of particles would have its own spray aging relationship, and at this time no simple means of typing sequential release together into one relationship seems possible. Only when particle size distributions are known throughout a spray aging process will sequential releases be able to be tied together.

It should be noted that in CORRAL, no spray cutoff is used at C(t)/C(0) = 0.02; spray aging is used in its place.

J3.2.3 I_2 EQUILIBRIUM

When airborn molecular iodine is depleted by either sprays or natural deposition, the depletion rate becomes independent of the two above mechanisms when the concentration falls below about 1 percent of the initial value (a conservative estimate, i.e., a lower value is less conservative (Ref. 8). At concentrations below this level, an apparent equilibrium situation exists where the concentrations in liquid and gas phases are related by an equilibrium distribution constant, $H = C_\ell/C_g$. H is a function of time (probably due to slow liquid phase chemical reaction) and has been experimentally determined. In program CORRAL it has been possible to incorporate H = H(t) when equilibrium conditions exist.

To get the equilibrium described quantitatively, an equivalent lambda for depletion of gas phase I_2 had to be developed. Since the value of H increases with increasing time, the gas phase is being depleted as time goes on. To get this equivalent lambda, we can write a mass balance for I_2. If C_{go} is the initial airborn concentration, then

$$C_{go}\ V_g = C_\ell V_\ell + C_g V_g\ . \qquad \text{(VII J-29)}$$

or

$$\frac{C_g}{C_{go}} = \frac{C_g V_g}{C_\ell V_\ell + C_g V_g} = \frac{1}{\frac{C_\ell V_\ell}{C_g V_g} + 1} = \frac{1}{H\frac{V_\ell}{V_g} + 1}\ . \qquad \text{(VII J-30)}$$

Then for H = H(t), we can write the removal rate of I_2 by

$$d\,\frac{C_g/C_{go}}{dt} = -\frac{1}{\left(H\frac{V_\ell}{V_g} + 1\right)^{-2}}\left(\frac{V_\ell}{V_g}\right)\frac{dH}{dt}$$

where the equivalent lambda is

$$d\,\frac{C_g}{dt} = -\left\{\left(\frac{1}{H\frac{V_\ell}{V_g} + 1}\right)\frac{V_\ell}{V_g}\frac{dH}{dt}\right\}dt = -\lambda dt \qquad \text{(VII J-31)}$$

Data shows that $H\ V_\ell/V_g >> 1$ for boric acid and caustic solutions in equilibrium with I_2, so that

$$\lambda = \frac{1}{H}\frac{dH}{dt}\ . \qquad \text{(VII J-32)}$$

Typical data for sprays are shown in Tables VII J-2 and VII J-3.

J3.2.4 INTERCOMPARTMENTAL FLOW RATES

In two cases intercompartmental flow rates can be calculated. If circulation fans move air throughout the containment vessel or if boil-off occurs with steam evolution into one compartment, one can use these flow rates to provide a basis for estimating intercompartmental flows.

In addition, natural convection driven by wall-bulk gas temperature differences can be a major contributor to flow rates. These rates can be estimated but with a high degree of uncertainty.

In this study, high flow rates have been used to eliminate mixing as a parameter. The flows for PWR cases follow the schematic in Fig. VII J-5. Flow rates used were Q_1 = blow down steam rate and Q_2 = 10 PWR containment volumes per hour.

J3.3 MULTICOMPARTMENT CONTAINMENT MODEL - BWR

The multicompartment feature of code CORRAL was essential to estimating atmospheric source calculations from a BWR. A BWR containment system is not a set of openly connected compartments like a PWR, where the whole containment system can be usually considered as "well mixed". The compartments of a BWR are usually closed to one-another and flows between them occur in complex ways during postulated accidents.

As many as six compartments are used in some BWR accident sequences. The first five are:

a. The Drywell where natural deposition can occur.

b. The Wetwell where pool scrubbing and natural deposition can occur.

c. The Drywell annular gap where natural deposition can occur.

d. The Reactor Building where natural deposition can occur.

e. The Standby Gas Treatment System (a series of filters).

The sixth compartment used was a fictitious dumping ground for ground level atmospheric sources when elevated (stack) sources occurred simultaneously. The schematic flow diagram for BWR accidents is shown in Fig. VII J-6.

Although the BWR containment model is rather specific, it still must be considered an approximate treatment of actual conditions. For example, pool scrubbing of vapor-phase fission products in the wetwell is modeled using a simple decontamination factor rather than a rigorous solution of the dynamic transport and absorption problem. In addition, the drywell annular air gap is used to simulate the entire lower region of the secondary containment building. For situations in which leakage from the primary containment boundary occurs directly from the drywell or wetwell steel shells, this provides an accurate description of the geometry and flow path to the refueling floor level of the secondary containment. For cases in which the leakage site is in one of the several sublevels of secondary containment (e.g., isolation valve failure), the model represents an approximation of the geometries and flow paths between these various leakage locations and the refueling floor level. However, the method described later for calculating fission product transport and deposition in the annular region is expected to overestimate rather than underestimate fission product concentrations that would reach the refueling building under such conditions. This is because the combination of longer residence time and deposition in the lower regions of secondary containment would usually be more effective than the decontamination factors predicted for the annulus.

Note in Fig. VII J-6 that potential releases of fission products directly to the atmosphere are indicated for all compartments. Release from the standby gas treatment system is the normal mode, and this would be an elevated release via the plant stack. All other potential releases would be at ground level. Direct releases from the main reactor (refueling) building could occur because of failure to isolate the building or because gas flow into the building during a particular accident might exceed the exhaust capacity of the standby gas treatment system blowers. Direct releases from the annulus (and/or lower secondary containment) could occur if high volume gas flow, caused by isolation failure of a large penetration in primary containment, would result in structural failure of the reactor building wall panels. This could also result from rupture of primary containment, provided the event does not cause failure of an outside wall in the sublevels of secondary containment. The alternative (i.e., structural failure of outside walls) could produce the direct release from either the drywell or wetwell compartments. In calculating such direct release cases, internal fission product removal is considered only for compartments up to and including the one from which the direct release occurs.

Natural deposition is the most common removal mechanism for fission products, although it is not necessarily the most effective mechanism. Natural deposition of particulates occurs on horizontal surfaces in all large compartments just as in a PWR. Turbulent deposition of particulates and iodine in the drywell annular air gap occur by different mech-

anisms to be discussed later. Natural deposition of iodine occurs on all surfaces with the rate controlled by natural convection discussed in paragraph J3.2.1. However, since the wall-bulk gas temperature-difference that drives the natural convection is highly variable in a BWR, transient heat transfer analyses are made to estimate this temperature-difference.

J3.3.1 NATURAL DEPOSITION - EFFECT OF HEAT TRANSFER FROM BWR VESSEL WALLS

The mass transfer coefficient for I_2 removal (see Equations VII J-6 and VII J-7), is proportional to the temperature-difference,

$$T_{wall} - T_{bulk} = \Delta T_w \qquad \text{(VII J-33)}$$

raised to the 1/4 or 1/3 power. For an order of magnitude range in ΔT_w, the mass transfer coefficient changes by only a factor of 2, a relatively insignificant change. However, during rapid cooling of the drywell (depressurization), ΔT_w can span more than an order of magnitude for short durations. During rapid heating, the condensing heat transfer coefficient is large (H $\doteq$ 150 Btu/hr,ft^2,F) and a steady ΔT_w is rapidly reached. This is about 0.14F in the drywell. In cooling, the heat transfer coefficient from the steel (approximately one-inch thick) wall is low (2-5 Btu/hr, ft, F), and can lag behind the bulk gas temperature for some time. Neglecting any temperature gradient in the steel, for a sudden step change in bulk gas temperature, ΔT_s, the temperature-difference, ΔT_w, is given by

$$\Delta T_w = \Delta T_s \exp(-ht/\ell\rho c_p) \qquad \text{(VII J-34)}$$

where

h = heat transfer coefficient

t = time after ΔT_s

ℓ = wall thickness

ρ = wall mass density

c_p = wall heat capacity (per unit mass).

If the temperature change is gradual, i.e., linear with respect to time. The temperature-difference, ΔT_w, is now given by

$$\Delta T_w = (\beta\, \ell\rho c_p/h)[\exp - (ht/\ell\rho c_p) - 1] \qquad \text{(VII J-35)}$$

where β is the linear bulk-gas cooling rate, F/hr. Equations (VII J-34) and (VII J-35) are used to compute ΔT_w for various time intervals during cooling in the drywell and wetwell. Values of h depend on gas velocities in the above compartments as well as the drywell annular air gap.

Little information could be readily obtained to estimate ΔT_w's in the main reactor building. These would be highly dependent on positions in the building and the outside environment temperatures, as well as gas flow parameters from the reactor. To allow for some minimum natural deposition in the main building, ΔT_w = 0.1 F was used. This would result in a natural deposition rate of $\lambda \doteq 0.5$ hr^{-1} in the main reactor building for I_2. This λ is five times the gas displacement rate for the building under normal conditions (2,000 cfm through the Gas Treatment System).

J3.3.2 POOL SCRUBBING

In a number of BWR accident sequences gas flow occurs through the vent lines from the drywell to the wetwell water pool. The water pool occupies slightly over one-half the toroidal volume of the wetwell and is approximately 17-feet deep. Pool scrubbing is a major decontamination mechanism. Some data exists on pool scrubbing, but comprehensive experimental studies on pool scrubbing in a BWR wetwell pool that include investigations of all parameters (a wide range of particle sizes, steam quality, pool temperatures, flow rates, I_2 concentrations, downcomer L/D ratios, etc...) have not been reported. Applying such data, if available, would not have refined atmospheric source estimates greatly, because the available data show that scrubbing is fairly effective on the fission products entering the pool. Also, trial calculations showed that often 30 percent or more of the available fission products in any sequence would escape the primary containment by other paths (such as through the drywell annular gap directly to the secondary containment system).

The best available data appears in a paper by Diffey, Rumary, et al., (Ref. 12) where I_2, methyl iodide, and .06 μ particles in a steam-air mixture were pool scrubbed. The typical decontamination factors were 100 for I_2, 2 for CH_3I, and 50-100 for the 0.06 μ particles with 90 percent steam-air mixtures (higher steam fractions give better decontamination). For CORRAL-BWR cases, the values used are 100 for both I_2 and particles, provided the bulk gas is mostly steam and condensation is expected in the pool. A

decontamination factor of 1.0 is always used for methyl iodide and the noble gases.

Even though the BWR accident particles are assumed to be 5-15 μ, or much more massive than those studied above, the scrubbing of particles is largely due to diffusiophoresis (condensing steam on the bubble wall carries particles), and therefore largely independent of particle size. However, larger particles would have more boundary layer penetration inertia in a rapidly circulating bubble and this should then further justify the choice of DF=100 for particles, rather than the lower DF of 50.

J3.3.3 STANDBY GAS TREATMENT SYSTEM - (SGTS)

The SGTS in a typical BWR is a set of two parallel filter trains upstream from three exhaust fans that releases filtered secondary containment building air at an elevated level via a stack. However, under accident conditions only one of the filter trains would normally be used, the other being held in reserve. The SGTS keeps the building at subatmospheric pressures to minimize ground level leaks. Under normal conditions, the flow rate through the system is about 2,000 cfm but the exhaust fans are capable of 10,000 cfm. Sources in excess of this maximum would create positive building pressures and produce a ground level, unfiltered source. The filter trains, according to plant Technical Specifications, are routinely tested to ensure the following removal efficiencies at all flow rates up to 10,000 cfm maximum:

- 99% for particulates
- 99% for elemental iodine
- 99% for organic iodide

These specifications are derived essentially from in-place testing criteria published by the USAEC in Regulatory Guide 1.52. The criteria incorporate limits on bypass flow for the filter and adsorber sections. It is recognized that substantially better performance may be realized for the filter system during actual use. This is because the specifications implicitly anticipate some deterioration in system effectiveness between testing steps which may or may not occur. However, since filtered leakage will be a minor contributor to overall accident consequences for meltdown sequences in the BWR, the efficiencies given above were used in all CORRAL calculations. In addition, CORRAL is programmed to identify the filter and adsorber activity loadings to discover possible overheating conditions, at which time the filtration efficiencies would decrease significantly.

J3.3.4 NATURAL DEPOSITION IN THE DRYWELL ANNULAR AIRSPACE

The drywell shell is surrounded by a two-inch air gap between the steel shell and the concrete shield containing the shell. Normal leakage across the shell or rupture of the shell can result in transport through the air gap with an exit into the secondary containment. For analysis purposes, the drywell leakage point is considered to occur near the base, in the vicinity of the eight vent lines leading to the wetwell. The exit point is at the top flange assembly. The flow path of gases from the shell rupture is thus around the spherical part of the shell, longitudinally through the cylindrical upper annulus and out the flange.

The annular region cannot be modeled like the well mixed compartments with deposition on the walls and/or floor. It is better described as plug flow along a cylindrical annulus with mass transfer to the walls. A simple first order differential equation defines a mass transfer coefficient, k, that can be estimated from known correlations for I_2 transfer. For particles, k can be estimated from particle deposition data from moving gas streams with more difficulty and uncertainty. The differential equation for transfer to the walls of an annular slit is:

$$\frac{dC}{(C-C_w)} = -\left(\frac{2k}{U\Delta r}\right)dx \qquad \text{(VII J-36)}$$

where

C = the concentration of the transferring substance

C_w = wall concentration

U = axial plug flow velocity

Δr = annulus width

x = axial distance

k = mass transfer coefficient.

If $C_w = 0$, Equation (VII J-36) integrates for $0 \leq x \leq \ell$ to

$$\frac{C}{C(x=0)} = \exp\left[-\left(\frac{2\,k}{U\Delta r}\right)\ell\right] \qquad \text{(VII J-37)}$$

assuming an average axial velocity, $\underline{U}$,

$$\underline{U} = \frac{Q}{A_{av}}$$

where

$A_{av} = \Delta r \int_0^{\ell} \pi r \, dx/\ell$, average annulus cross section, and

Q = volumetric flow rate.

For the annular gap described earlier for a typical BWR, Equation (VII J-37) above becomes

$$\frac{C}{C(x=0)} = \exp(-1200\ k/\underline{U}). \quad \text{(VII J-38)}$$

The assumption that $C_w = 0$ for both particulates and I_2 is reasonable for most conditions in the BWR accident cases. Molecular I_2 has been experimentally verified to have a high affinity for steel and paint surfaces (Refs. 5,13). Normally the overall mass transfer coefficient for I_2 would be

$$k^{-1} = k_w^{-1} + k_g^{-1} \quad \text{(VII J-39)}$$

where k_g is the boundary layer coefficient and k_w is a first order rate constant for the surface reaction (Ref. 13). The value of k_w is difficult to predict for the annulus since it is a function of temperature, surface composition, surface roughness, I_2 concentration, and vapor pressure. Thus, for the drywell annulus the surface was assumed to be a "perfect sink" for I_2 with no desorption occurring.

The gas phase mass transfer coefficients for I_2 are estimated using the following analogies from heat transfer correlations (Ref. 11). For well developed turbulent flow (Re > 20,000)

$$Sh = \frac{k\ 4Rh}{D_{I_2}} = 0.026\ Re^{0.8}\ Sc^{1/3} \quad \text{(VII J-40)}$$

and for laminar isothermal flow (Re < 2,100)

$$Sh = 1.86\ (Re \cdot Sc \cdot 4Rh/\ell)^{1/3} \quad \text{(VII J-41)}$$

where

Re = Reynolds number = $\frac{\rho \underline{U}(4Rh)}{\mu}$

Rh = hydraulic radius

$$= \frac{\text{flow cross sectional area}}{\text{wetted parameter}}$$

$= \Delta r/2$ for the annulus

The transition region, 2100<Re<20,000, is not well understood and Equation (VII J-40) could overestimate the mass transfer coefficient by a factor of 3-5 at Re=2100. This error is offset by the non-smooth nature of the annular gap, which could also cause an underestimation of k for high Reynolds numbers. For BWR cases encountered, the Reynolds number ranges from the laminar region to about 30,000. The maximum DF's occur at Re=0 and Re=2101. A cutoff of DF = 100 maximum for I_2 is assumed in CORRAL-BWR calculations for the annular gap. This is done because of the possibility of desorption or saturation of the annular surface.

The behavior of particulates is more difficult to predict because deposition velocities from moving gas streams are a function of particle size as well as gas velocity. Sehmel (Ref. 14) has recently published experimental data that allows an estimation of particle deposition in the annular gap. The deposition velocity (or mass transfer coefficient) is highly affected by gravity. Most of Sehmel's data is for deposition on floor and ceilings, and the deposition in the drywell is on an essentially vertical wall. Wall deposition velocities are closest to floor deposition velocities, but are slightly lower for inertial particles (usually $\geq$ 0.1 μ). For these inertial particles, Brownian diffusion is nil, so k = o has been assigned. (DF = 1 for Re < 2100 for all particles). Only the largest of the 5-15 μ particles have a significant turbulent deposition velocity.

An emperical fit of Sehmel's data is possible for $k = k(\underline{U}, d_p)$, but he has only two $\underline{U}$ values for vertical wall deposition. For this reason, only a first order approximation can be made for k. This also eliminates major overhaul of CORRAL's matrix computations to incorporate a new set of variables. The ratio $k/\underline{U}$ = 1/300 = constant for all k and $\underline{U}$ for a particle size midway between 10 and 15 μ. Table VII J-4 shows the wide range of particle DF's versus Reynolds number.

To be conservative, an upper limit of DF = 100 seems more reasonable to assign to d_p = 15 μ (for $k/\underline{U}$ = 1/300, DF = 27). With this upper limit, the following

emperical equation fits the particle range:

$$DF = 1.0 + 0.1 \left\{ \frac{d_p - 5}{5} \right\}^{9.95}$$

(VII J-42)

for $10 < d_p \leq 15$ μ particles and DF = 1.0 for $d_p < 10$ μ. Integrating Equation (VII J-42) above over the aging process of the particles as they settle out in 4 hours (see paragraph J3.2.2) produces DF (avg) = 10.0 Since the age of airborne particles undergoing natural deposition is important longer than the 4 hours time period (approximately two of these periods), the average DF = 5.5. This value was used in CORRAL-BWR calculations for all particles passing through the annular gap for $Re \geq 2100$. It is a conservative number because approximately 90 percent of the mass of particles released is >10 μ in the CSE data and also in the CORRAL calculations. The mass average particle is 13.5 μ which has a DF - 21. Thus picking DF = 5.5 over-estimates early atmospheric sources and under-estimates additional sources on a long time basis. Certainly on a mass average basis, DF = 5.5 is conservative.

J3.4 COMPUTER CODE CORRAL

The multicompartment containment model was programmed with Fortran V for use on a Univac 1108. The program incorporates the models for fission product removal discussed in the previous section. Figure VII J-7 shows the basic flow chart for CORRAL. A summary of each of the five flow chart sections follows:

a. Input Parameters

1. Constants

(a) Core fractions for gap, melt, steam explosion and vaporization releases.

(b) Numbers of compartments.

(c) Volumes, wall areas, floor areas, heights of each compartment.

(d) Spray parameters (flow rates, drop sizes, fall heights, equilibrium conditions for I_2 removal, I_2 distribution coefficient).

(e) Times of all events.

(f) Compartment filter decontamination rates.

(g) Fractions of compartments released during a puff release.

2. Variables (with time)

(a) Pressure, temperature, and water vapor content of each compartment. Temperature difference between bulk gas and walls.

(b) Flow rates between compartments.

(c) Decontamination factors between compartments.

(d) Particle sizes.

(e) Leak rates to atmosphere and leak DF's (decontamination factors).

b. Initial Conditions

1. All concentrations set equal to zero at T=0 except gap release concentrations in first compartment.

2. Spray set to operate in main compartment (PWR).

3. All amounts released and DRF's (dose reduction factors) set equal to zero. A zero DRF means that nothing has been released.

c. Computation of Properties and Removal Rates

1. Pressure, temperature, and water vapor content and T(bulk)-T(wall) by parabolic interpolation.

2. Intercompartment flow rates and decontamination factors and leak rates and respective DF's by parabolic interpolation.

3. Particle sizes by linear interpolation.

4. Gas phase viscosities and I_2 diffusivities and Schmidt numbers.

5. Mass transfer Grashof number's and corresponding depositing rates.

6. Particles settling velocities and their natural deposition.

7. Spray lambdas for particles.

8. Terminal spray velocities, gas phase mass transfer coefficient, liquid phase mass transfer coefficient, and spray lambdas.

9. I_2 equilibrium equivalent lambdas (if needed).

10. Overall lambdas.

d. Solution of Differential Equations

The solution of the differential equations is discussed in the previous section. To properly age the continuous releases, it was necessary to divide these releases into discrete impulse releases. The melt release was divided into ten equally spaced and sized releases, each independent age wise from the other nine. The vaporization release (released at an exponentially decaying rate) was divided into 20 impulse releases, each successive release at an exponentially lower value than the first. The sum of the first ten releases equals 1/2 the total release, and the remaining ten equals the remaining 1/2. The duration of the period of the first ten is one half-life. The duration of the second ten should be three half-lives for a reasonable approximation of an exponential decay.

Thus the total number of differential equations solved (one each for particulates, organic iodides, and I_2) for any time step is (N = number of compartments).

GAP RELEASE	3N	equations
EXPLOSION RELEASE	3N	
MELT RELEASE	30N	
VAPORIZATION RELEASE	60N	
	96N	equations

The accuracy of the output depends on the rate of change of the rate coefficients, so short time steps would be desirable immediately after each discrete release (aging is rapid at first, especially if sprays are on). Long time steps are sufficient for old releases.

e. Output Variables

1. Airborne contained fractions released at time, t.

   (a) For each release: I_2, organic iodides, particulates.

   (b) For each compartment for each release: I_2, organic iodides, particulates, at time, t.

2. Escaped fractions released (for each release: I_2, organic iodides, particulates, at time, t).

3. Escape fractions of the core for any desired iosotope.

4. Dose reduction factor for each release (I_2 and particulates) at time, t.

5. Overall dose reduction factor (I_2 and particulates) at time, t.

6. Total fraction of core iodine escaped and core particulates escaped up to time, t.

For more complete details on actual operation of the CORRAL code refer to the Addendum to this Appendix which provides a user's guide for the code.

References

1. McCormack, J. D., R. K. Hilliard, and A. K. Postma, "Removal of Airborne Fission Products by Recirculating Filter Systems in the Containment Systems Experiment", BNWL-1587, Battelle-Northwest, Richland, Washington (June 1971).

2. Postma, A., and R. K. Hilliard, "Absorption of Methyl Iodide by Sodium Thiosulfate Sprays", ANS Trans. 12, p 898-899 (November 1969).

3. Knudsen, J. G., and R. K. Hilliard, "Fission Product Transport by Natural Processes in Containment Vessels", BNWL-943, Battelle-Northwest, Richland, Washington (1969).

4. Hales, J. M., T. W. Horst, and L. C. Schwendiman, "Aerosol Transport In a Condensing-Steam Boundary Layer", BNWL-1125, Battelle-Northwest, Richland, Washington (1970).

5. Hilliard, R., and L. F. Coleman, "Natural Transport Effects on Fission Product Behavior in the Containment Systems Experiment", BNWL-1457, Battelle-Northwest, Richland, Washington (1970).

6. Postma, A. K., and W. F. Pasedag, "A Review of Mathematical Models for Predicting Spray Removal of Fission Products in Reactor Containment Vessels", BNWL-B-268, Battelle-Northwest, Richland, Washington (1973).

7. Postma, A. K., L. F. Coleman, and R. K. Hilliard, "Iodine Removal from Containment Atmospheres by Boric Acid Spray", Report No. BNP-100, Battelle-Northwest, Richland, Washington (1970).

8. Hilliard, R. K., A. K. Postma, et al., "Removal of Iodine and Particles by Sprays in the Containment System Experiment", Nuclear Technology, 10, pp 499-519 (1971).

9. Reactor Physics Quarterly Report, April-June 1969, BNWL-1150, Battelle-Northwest, Richland, Washington (1969) (B. H. Duane, pp 2.5-2.7).

10. Knudsen, J. G., "Properties of Air-Steam Mixtures Containing Small Amounts of Iodine", BNWL-1326, Battelle-Northwest (1970).

11. Bird, R. B., W. E. Stewart, and E. N. Lightfoot, "Transport Phenomena", John Wiley and Sons, N. Y. (1960).

12. Diffey, H. R., C. H. Rumary, M. J. S. Smith and R. A. Stinchcombe (AERE, Harwell, England), "Iodine Cleanup in a Steam Suppression System", CONF-650407 (Vol 2), International Symposium on Fission Product Release and Transport under Accident Conditions, Oak Ridge, Tenn, pp 776-804 (April 1965).

13. Rosenberg, H. S., J. M. Genco, and D. L. Morrison, "Fission-Product Deposition and its Enhancement under Reactor Accident Conditions: Deposition on Containment-System Surfaces", BMI-1865, Battelle-Columbus (May 1969).

14. Sehmel, G. A., "Particle Eddy Diffusivities and Deposition Velocities for Isothermal Flow and Smooth Surfaces", Aerosol Science 4, pp 125-139 (1973).

TABLE VII J-1 FISSION PRODUCT REMOVAL RATE CONSTANTS CALCULATED FOR A LARGE PWR CONTAINMENT VESSEL

Spray System	Flow Rate gpm	Fraction Initial Release	λ, hr^{-1}
Molecular Iodine			
1 CSR, Boric Acid	3500	1.0 → .01	3.12
2 CSR[(a)], Boric Acid (pH = 5)	7000	1.0 → .01	6.24
Equilibrium Conditions: Boric Acid	--	$10^{-2} \rightarrow 1.8 \times 10^{-3}$	1.15
Equilibrium Conditions: Boric Acid	--	$1.8 \times 10^{-3} \rightarrow 3 \times 10^{-5}$	
Equilibrium Conditions: Boric Acid	--	$<3 \times 10^{-5}$	0
1 CSR, NaOH (pH 9.5)	3500	1.0 → .01	67
2 CSR, NaOh	7000	1.0 → .01	134
Equilibrium Conditions: NaOH	--	Next 2 hrs	0
Equilibrium Conditions: NaOH	--	$10^{-2} \rightarrow 3 \times 10^{-5}$	0.223
Equilibrium Conditions: NaOH	--	$3.8 \times 10^{-4} \rightarrow 3 \times 10^{-5}$	0.0422
Equilibrium Conditions: NaOH	--	$<3 \times 10^{-5}$	0
1 CSI[(a)], Boric Acid	3200	1.0 → 0.1	2.85
Boric Acid	--	<.01	Same as boric acid equilibrium
No spray (natural deposition)		1.0 → .01	1.38
No spray		<.01	0
Particulates			
1 CSR	3500	1.0 → .02	6.0
2 CSR	7000	1.0 → .02	12.0
2 CSR	7000	<.02	0.9
1 CSI	3200	1.0 → .02	12.6
1 CSI	3200	<.02	0.945
No spray (natural deposition)		1.0 → .02	0.13
No spray		<.02	0

(a) CSR = Recirculation spray. CSI = Injection spray.

TABLE VII J-2 EQUILIBRIUM DATA FOR I_2 WITH BORIC ACID SPRAYS[(a)]

Time, min	H	C_g/C_{go}
0	2676	0.01
100	1.5×10^4	1.8×10^{-3}
500	4.0×10^4	6.75×10^{-4}
1000	7.0×10^4	3.86×10^{-4}
2000	$1.5 \times 10^{+5}$	1.8×10^{-4}
4000	$5 \times 10^{+5}$	5.4×10^{-5}
≥7000	1×10^6	2.7×10^{-5}

(a) See Reference 7

TABLE VII J-3 EQUILIBRIUM DATA FOR I_2 WITH CAUSTIC SPRAYS[(a)]

Time, min	H	C_g/C_{go}
0-100	Constant H, λ=0	0.01
100-1000	Variable H, λ=.095 hr^{-1}	
1000	7.0×10^4	3.86×10^{-4}
2000	1.5×10^5	1.8×10^{-4}
4000	5×10^5	5.4×10^{-5}
7000	1×10^6	2.7×10^{-5}

(a) See Reference 7

TABLE VII J-4 DF VERSUS PARTICLE SIZE AND REYNOLDS NUMBER IN DRYWELL ANNULAR GAP

d_p, μ	DF(Re $\leq$ 2100)	DF(Re = 2100)	DF(Fe = 30,000)
5	1.0	1.0	1.0
10	1.0	1.1	1.1
15	1.0	4.4×10^5	2.2×10^4

TABLE VII J-5 FISSION PRODUCT RELEASES

Release Name	Fraction in Compartment J At Time Index L (Internal and Output Variable)	Time of Beginning and End of Release (Hrs)	Remarks	Compartment of Release (PWR)
Gap	CGI2(J,L) (molecular iodine) CGØI(J,L) (organic iodide) CGP(J,L) (particles)	0.0	Single puff event at beginning of CORRAL calculations	2 (primary cubicle)
Melt	CMI2(J,K,L) CMØI(J,K,L) CMP (J,K,L)	TMR TMF	Continuous release simulated by ten equally spaced spike events in CORRAL (K=1,10).	2
Steam Explosion	CSI2(J,L) CSØI(J,L) CSP(J,L)	TEX1	Single spike release. If containment is breached simultaneously, enter TPUFF (time of puff) and XPUFF (fraction gas remaining)	1 (Main Room)
Vaporization (first half)	CAI2(J,K,L) CAØT(J,K,L) CAP(J,K,L)	TVR1 TVR2	Continuous but exponentially decreasing over ten equally spaced spike releases.	1
Vaporization (second half)	CBI2(J,K,L) CBØI(J,K,L) CAP(J,K,L)	TVR2 TVRE	Same as above except spacing is three times larger between individual puffs.	1

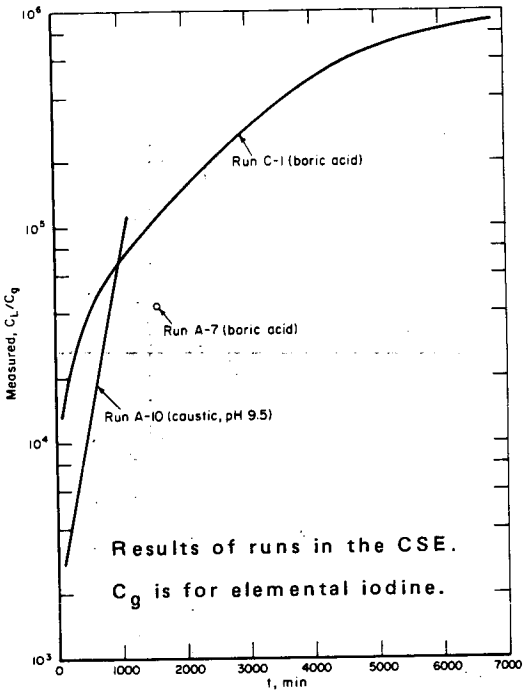


FIGURE VII J-1 Partitioning of Elemental Iodine by Recirculated Sprays

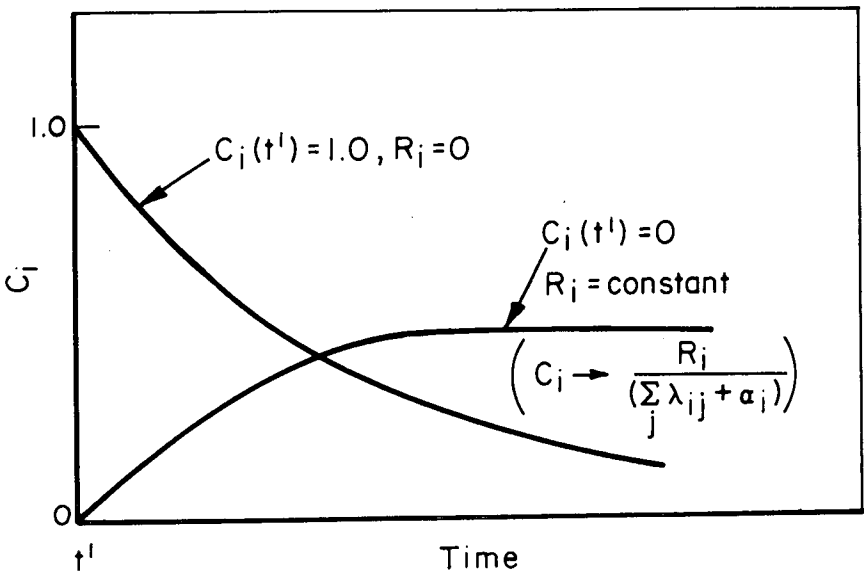


FIGURE VII J-2 Schematic of Quantity of Airborne-Contained Fission Products Versus Time

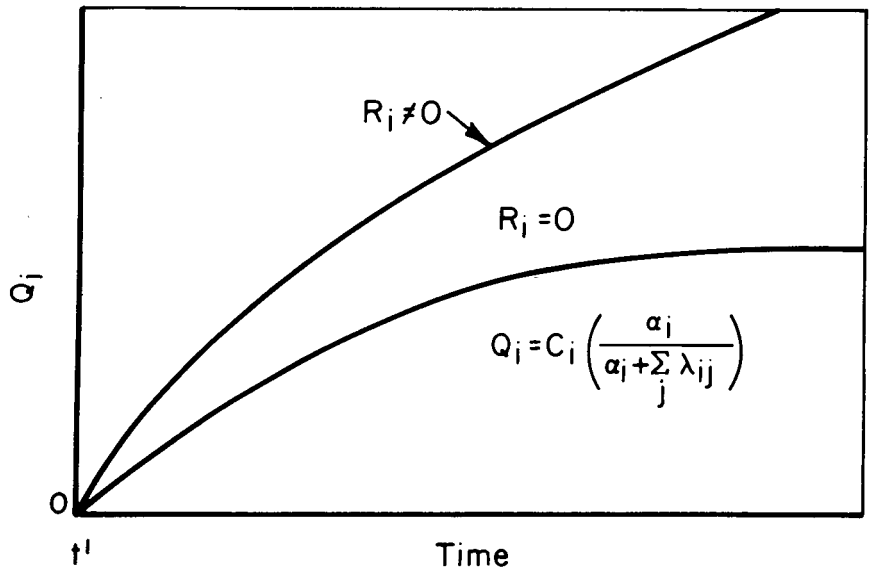


FIGURE VII J-3 Schematic of Quantity of Fission Products Released to Atmospheres Versus Time

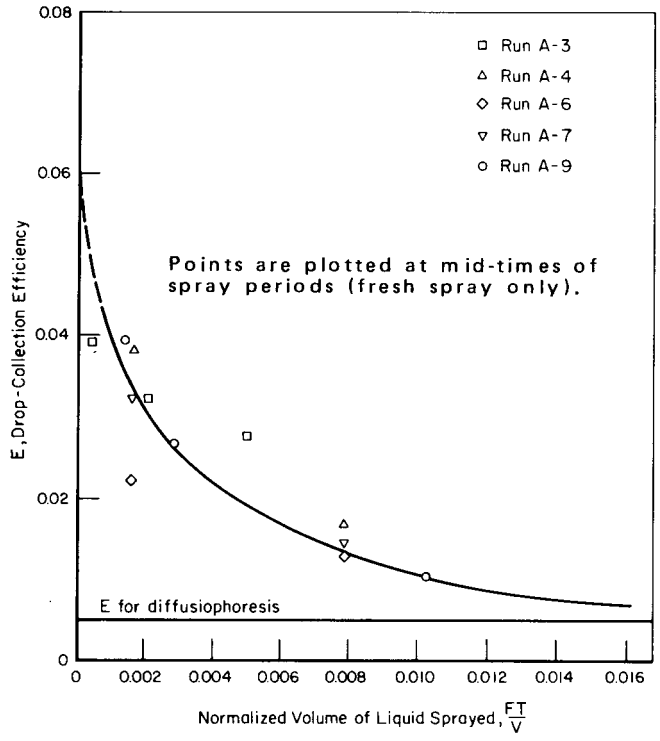


FIGURE VII J-4 Drop-Collection Efficiency as a Function of Liquid Volume Sprayed

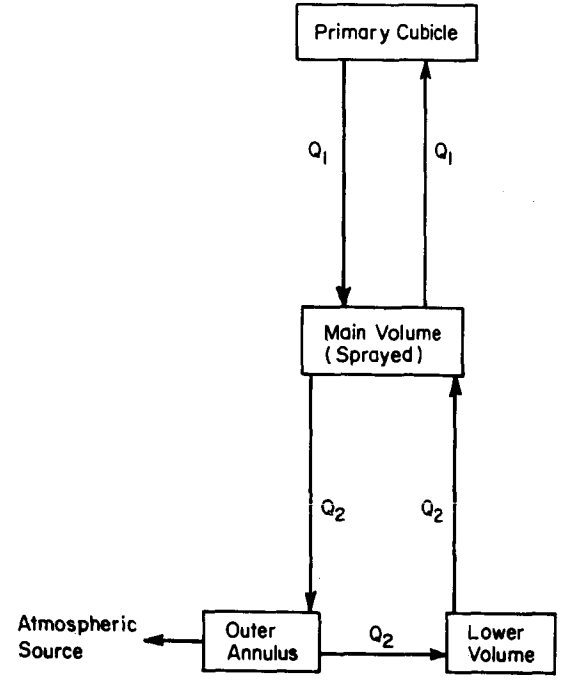


FIGURE VII J-5 Gas Flow for PWR Cases

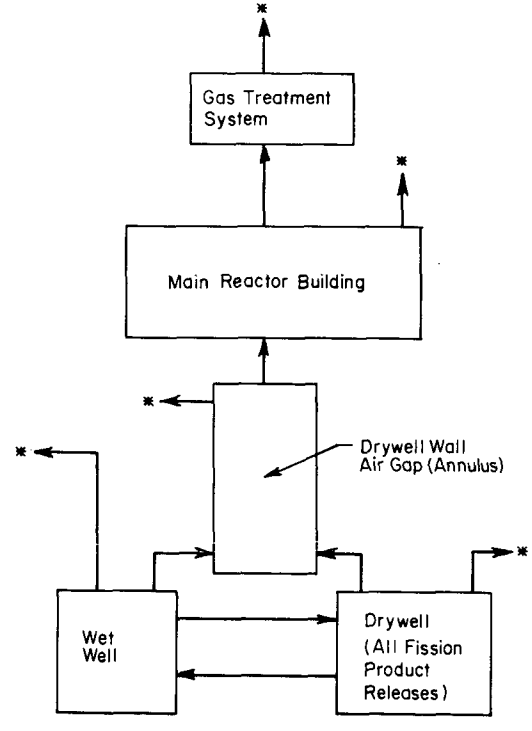


FIGURE VII J-6 Flow Schematic for a BWR - (*Possible Atmospheric Source)

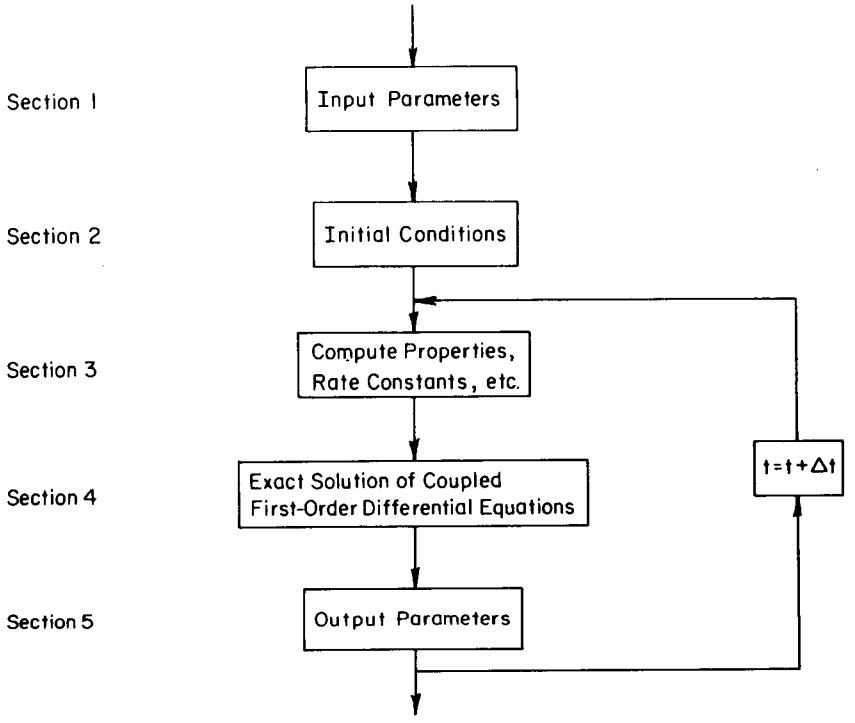


FIGURE VII J-7 Computer Code CORRAL Flow Diagram

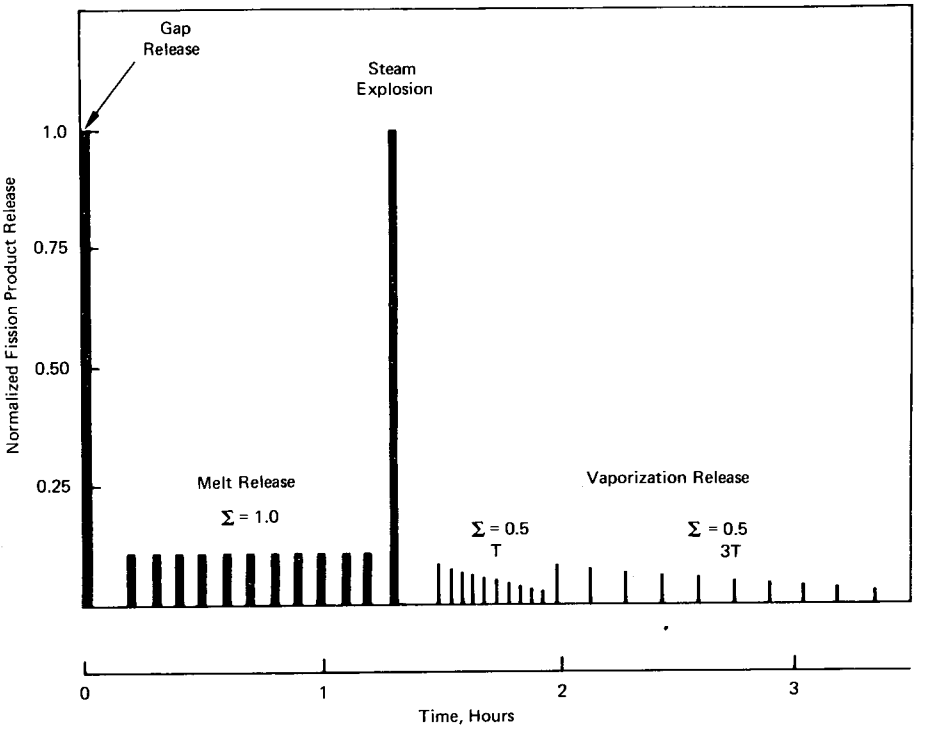


FIGURE VII J-8 Typical Sequence of Spike Fission Product Releases for Postulated Accidents

ADDENDUM TO APPENDIX J

CORRAL CODE USER'S GUIDE

by

P. C. Ouzarski and A. K. Postma
Battelle Pacific Northwest Laboratories

Addendum to Appendix J

Table of Contents

Section		Page No.
J1.	INTRODUCTION	VII-213
J2.	INPUT DATA	VII-213
	J2.1 Fission Product Release Data	VII-213
	J2.2 Multicompartment Input Data	VII-214
	J2.3 Spray Input Data	VII-214
	J2.4 Other Input Data	VII-215
J3.	OUTPUT DESCRIPTION	VII-215
J4.	EXAMPLE PWR CASE	VII-215
J5.	EXAMPLE BWR CASE	VII-217
J6.	COMPUTER CODE CORRAL LISTING FOR BWR ACCIDENT SEQUENCES	VII-223
J7.	COMPUTER CODE CORRAL LISTING FOR PWR ACCIDENT SEQUENCES	VII-238
J8.	SUBROUTINES IN CORRAL	VII-253

Addendum to Appendix J
of Appendix VII

CORRAL Code User's Guide

by

P. C. Owzarski and A. K. Postma
Battelle
Pacific Northwest Laboratories

J1. INTRODUCTION

This addendum to Appendix J is intended to provide a workable tool to anyone desiring to do further containment analyses of particulates, molecular iodine and noble gases. When the realization that a multicompartment containment model was needed to analyze the complex accident sequences, we hoped that a fairly generalized computer code could be developed. We think that with the two versions of CORRAL (PWR and BWR) described herein are quite versatile.

CORRAL was always under constant revision. The final version of CORRAL includes revisions required to handle the many accident sequences and core releases that were defined. Built into the two versions are four types of fission product releases, capability of spraying in one compartment with boric acid or caustic solutions, and natural deposition in as many as nine compartments. These rooms can be connected in any way with filtration within or between them.

The user of CORRAL must input the containment thermodynamics (pressure, temperature, vapor composition) the intercompartmental flow rates and leak rates as a function of time. CORRAL interpolates between input data and computes all natural deposition rates and spray removal rates. It solves a large array of simultaneous differential equations, and keeps an inventory on the airborne fission products. CORRAL outputs the cumulative amount leaked of the various core radionuclides based on the input data of the core fraction airborne with each release. CORRAL can compute the losses for one explosive event per sequence where the containment pressure is rapidly reduced to atmospheric by flow through a large hole.

This users manual in conjunction with the rest of Appendix J describes the code input requirements and output. A simple PWR example is shown followed by an elaborate BWR accident sequence example. Both versions of CORRAL are listed along with subroutines.

J2. INPUT DATA

CORRAL was coded to use the very informal NAMELIST method of input. Depending on the type of computer, the use of NAMELIST permits input simply by naming the variable, followed by an equal sign, the value, and then a comma. For CORRAL on the Univac 1108, the procedure is to enter beginning in column 2 on the first data card $BREAK N=5, NDATA=12, etc. for all input variables. The last datum is followed by $. Two complete lists of input data are shown in section J4 of this addendum.

J2.1 FISSION PRODUCT RELEASE DATA

Both PWR and BWR accident sequences types of releases are discussed elsewhere in this study. The first release is the Gap Release that is at t=0. This is a single spike release occurring in the PWR primary cubical (Compartment 2). The other releases occur at later times. Figure VII J-8 shows a typical sequence of events. Table VII J-5 lists the other releases and pertinent variables as programmed into CORRAL. All releases in BWR accidents occur in the drywell (Compartment 1). All times designated as a variable name in Table VII J-5 must be entered in the NAMELIST.

The continuous Melt and Vaporization Releases were programmed as discreet spikes so each release could be "aged" properly. Aging is necessary for settling particles as well as sprayed particles. Molecular iodine equilibrium is also time dependent. The aging of nonsprayed particles is controlled by three input constants:

DPE = 15. (micron, initial average diameter)

DPL = 5. (micron, final average size)

TD = 4. (hrs, time to go from DPE to DPL).

These are discussed in paragraph J3.2.2.

Since the total of each of the four releases is normalized to 1.0, to get the amount of each isotope escaped to the atmosphere, an appropriate isotope core fraction per release must be entered in the input data. Eight basic groups of isotopes were identified as having similar "release" behavior. The eight can be grouped into three classes according to their airborne character: molecular iodine (I_2-Br group), inert gas (organic iodides and Xe-Kr) and particulates (C_s-R_b, Te, Ba-Sr, Ru, La groups). The input array in fractions of core airborne per release is CFR(I,J):

J =

1 Xe-Kr

2 Org-I

3 I_2-Br

4 C_s-R_b

5 Te

6 Ba-Sr

7 Ru

8 La

I =

1, GAP REL.

2, MELT REL.

3, STEAM EXPL.

4, VAP. REL.

CORRAL computes a cumulative leak amount for each isotope, e.g.,

$$I_2 \text{ leaked} = \sum_{I=1}^{4} \text{CFR}(I,3) \times \text{Fraction of release } I_2 \text{ leaked}) .$$

It does not correct for radioactive decay loss.

J2.2 MULTICOMPARTMENT INPUT DATA

Basic input data is the number of containment system compartments, N, the volume of each V(I), ft^3, floor area, AF(I), ft^2, and wall area, AW(I), ft^2, and ceiling height HT(I), ft. The maximum N is 9 as dimensioned in the program.

For each accident sequence, the user of CORRAL has a choice of up to 20 sequential event changes. For our analyses these were matched primarily to changes in leak rates from the containment system. However, changes in other parameter can be programmed into the accident. The time input variable is TI(I), I=1, NDATA (NDATA=1-20). The time dependent variables are:

TMY(J,I), J + 1-N, I = 1-NDATA	Compartment temperature, °F
PI(J,I)	Compartment pressure, psig
VAPI(J,I)	Compartment water vapor mole fraction
DELTTI(J,I)	Compartment wall-bulk gas temperature difference, °F. (para. J3.2.1 and J3.4.1 of Appendix J)
GI(J,K,I)	Intercompartmental gas flow rate (J to K), ACFH.
EP(J,K,I)	Corresponding particulate decontamination for J to K flow. (fraction removed)[1]
EI2(J,K,Z)	Same for molecular iodine.[1]
ELKP(J,I) ELK12(J,I) ELKØI(J,I)	Fractional loss per hour of compartment J particulates, iodine or organic iodide leaked from containment to environment. Normally these would be identical at any time J.
FDP(I)	Removal rate of particulates within compartment by filters, ice condenser, etc. Fractions of vol I/Hr.
FDI2(I)	Same for molecular iodine.

J2.3 SPRAY INPUT DATA

Sprays to remove particulates and iodine are important in the postulated PWR accident sequences. Two types of sprays, the containment system injection spray (CSI), and the recirculation sprays

[1] (e.g., refer to para. J3.4.2 for pool scrubbing EP(1,2,K)=0.99 for a decontamination factor of 100)

(CSR) could be operating in the main PWR volume (Compartment 1). The input variables for these are:

HCSI, height of CSI spray above the floor, ft

HCSR, height of CSR spray above the floor, ft

DCSI, CSI droplet diameter, cm

DCSR, CSR droplet diameter, cm

CSI, flow rate, ft^3/hr.

CSR1, flow rate for first set of CSR sprays, ft^3/hr

CSR2, flow rate for second set of CSR sprays

HØ, equilibrium partition coefficient for I_2

HØ = 5000 for caustic spray
= 200 for HBO_3 spray

CUTØV, fraction of an I_2 release below which airborne concentrations are in equilibrium with the spray liquid. CUTØV = 0.01 for the caustic and HBO_3 sprays.

TCSI, beginning time of CSI sprays, hrs.

TCSIE, ending time of CSI sprays, hrs.

TCSR1, TCSR1E, TCSR2, TCSR2E } same for CSR sprays

The I_2 equilibrium calculations in CORRAL are carried out for the sprayed volume only (Compartment 1). A subroutine ELAM must be compiled along with CORRAL for the type of spray used. Three versions of ELAM exist:

ELAM, for HBO_3 sprays

ELAM/CAUS, for caustic sprays

ELAM/NONE, for sequences not having any spraying

The first two versions use the data in Tables VII J-2 and VII J-3 and Equation VII J-32 to calculate an equivalent removal λ for iodine when the concentration falls below CUTØV = 0.01. ELAM/NONE puts λ=0. See last section for listings of these subroutines.

J2.4 OTHER INPUT DATA

If the containment vessel is breached with rapid loss of containment atmosphere, such as in a steam explosion or floor meltthrough, then the variables necessary are: TPUFF, in hours, when the puff occurs. XPUFF, the fraction of containment atmospheric still contained, and DFPP, DFPØI and DFPI2, the respective particulate, organic iodide and iodine decontamination factors. A puff release takes an equal fraction (1.-XPUFF) from each PWR compartment and adds it to the total atmospheric source term. Since N=4 was the BWR SGTS Charcoal Filter compartment, CORRAL-BWR avoids dumping (1.-XPUFF) of compartment 4 into the source term. Even if there is no puff in the accident sequence, a number greater than zero must be entered for DFPP, DFPØI, DFPI2 and XPUFF. Also, enter TPUFF > TEND to avoid a puff. (See below). This is also true for avoiding TEX1, TMR, and TVR1 and TVR2.

The last of the input data necessary for the execution of CORRAL are the time input controls. The first is DT, in hours, the time between computations. DT must be entered for each case if multiple cases are being run, since it gets altered in the execution. The value of DT will control the spacing of output between the gap and the next release, and will control the spacing after the last release is completed until TJUMP1 which triggers the new spacing level DT2, both in hours. The calculations progress until TJUMP2 which triggers a jump to TEND where the last set of calculations in the execution is completed.

CORRAL-BWR has two additional input integers. These are MCOMP and MANN. If MANN is any integer other than 1, gas flow can proceed through the drywell annulus from compartment number MCOMP (1 or 2). Some accident sequences had flow from the drywell (compartment 1) to wetwell (compartment 2) and then back through the annulus.

J3. OUTPUT DESCRIPTION

The first output is the input data with labeled descriptions. The same units are in this output as in the input. See the example cases for a comparison.

The calculational output follows. For each time value TT = TT+DT, CORRAL writes:

a. The inventory of airborne particles, iodine and organic iodides (or noble gases) in each compartment for each release. The values are expressed in fractions of the normalized release (1.0).

b. The inventory summed over the N compartments.

c. The cumulative fraction of particles, iodine and organic iodides of each release escaped to the outside atmosphere.

d. The dose reduction factor of particles and iodine for each release. This number is the cumulative amount of isotope leaked divided into the cumulative amount leaked if there were no deposition or washout in the containment system. This was done simply by dividing the cumulative fractions leaked into the cumulative fraction of organic iodides leaked, since no credit was given for washout of organic iodides.

e. The cumulative fractions of core leaked for each of the eight isotope groups described earlier.

The last item constituted the bulk of the data used for determining population doses.

J4. EXAMPLE PWR CASE

The case selected to represent PWR input/output data was a typical Design Base Accident (Case A) where only a gap release occurred after the large pipe break. This accident sequence is very simple and illustrates how CORRAL can be used to study one of many parameters that have some influence on the fission product loss to the environment. For example, the flow rate between the outer annulus, the main sprayed compartment, and the lower volume was slowed down by a factor of 10 in this run compared to Case A examined in the Reactor Safety Study. This slowdown lowered the fission product losses in the first few minutes after the gap release, but had no long term effect. Figure VII J-5 is the schematic of the gas flow. Discharge to the atmosphere was from Compartment 3, the outer annulus. The sprayed main volume is Compartment 1, the primary cubicle is Compartment 2, and the lower volume is Compartment 4. In all PWR cases with the 10 containment volumes/hour circulating from Compartment 1 to 3 to 4 to 1 again the containment was essentially "well-mixed." There was rapid interchange between compartments 1 and 2.

INPUT CARDS

```
PWR SAMPLE CASE - DESIGN BASE ACCIDENT WITH LOW INTERNAL CIRCULATION

 $BREAK N=4, NDATA=6,   V(1)=.94+6, .6+5, 4.5+5, 1.6+5,
 TI(1)=0.,.15,.151,.316,.317,.483,
 GI(1,1,1)=1620*0.,
 GI(1,2, 1)=1.2+06, GI(4,2, 1)=0., GI(2,1, 1)=1.2+06,
 GI(1,2, 2)=1.2+06, GI(4,2, 2)=0., GI(2,1, 2)=1.2+06,
 GI(1,2, 3)=1.2+06, GI(4,2, 3)=0., GI(2,1, 3)=1.2+06,
 GI(1,2, 4)=1.2+06, GI(4,2, 4)=0., GI(2,1, 4)=1.2+06,
 GI(1,2, 5)=1.2+06, GI(4,2, 5)=0., GI(2,1, 5)=1.2+06,
 GI(1,2, 6)=1.2+06, GI(4,2, 6)=0., GI(2,1, 6)=1.2+06,
 GI(1,3, 1)=1.61+6, GI(3,4, 1)=1.61+6, GI(4,1, 1)=1.61+6,                LO FLO
 GI(1,3, 2)=1.61+6, GI(3,4, 2)=1.61+6, GI(4,1, 2)=1.61+6,
 GI(1,3, 3)=1.61+6, GI(3,4, 3)=1.61+6, GI(4,1, 3)=1.61+6,
 GI(1,3, 4)=1.61+6, GI(3,4, 4)=1.61+6, GI(4,1, 4)=1.61+6,
 GI(1,3, 5)=1.61+6, GI(3,4, 5)=1.61+6, GI(4,1, 5)=1.61+6,
 GI(1,3, 6)=1.61+6, GI(3,4, 6)=1.61+6, GI(4,1, 6)=1.61+6,
 EP(1,1,1)=1620*0., EDP(1)=4*0., EDI2(1)=4*0., HO=5000., HCSI=100.,
 HCSR=47.,  DELTTT(1,1)=180*1.4,
 TMY(1,1)=4*264., PI(1,1)=4*35., VAPI(1,1)=4*.75,
 TMY(1,2)=4*210., PI(1,2)=4*12., VAPI(1,2)=4*.55,
 TMY(1,3)=4*210., PI(1,3)=4*12., VAPI(1,3)=4*.55,
 TMY(1,4)=4*167., PI(1,4)=4*2.3, VAPI(1,4)=4*.34,
 TMY(1,5)=4*167., PI(1,5)=4*2.3, VAPI(1,5)=4*.34,
 TMY(1,6)=4*150., PI(1,6)=4*0.0, VAPI(1,6)=4*.26,
 ELKI2(3,1)=1.503-3, ELKP(3,1)=1.503-3, ELKOI(3,1)=1.503-3,
 ELKI2(3,2)=1.503-3, ELKP(3,2)=1.503-3, ELKOI(3,2)=1.503-3,
 ELKI2(3,3)=1.217-3, ELKP(3,3)=1.217-3, ELKOI(3,3)=1.217-3,
 ELKI2(3,4)=1.217-3, ELKP(3,4)=1.217-3, ELKOI(3,4)=1.217-3,
 ELKI2(3,5)=2.147-4, ELKP(3,5)=2.147-4, ELKOI(3,5)=2.147-4,
 ELKI2(3,6)=2.147-4, ELKP(3,6)=2.147-4, ELKOI(3,6)=2.147-4,
 EI2(1,1,1)=1620*0., EP(1,1,1)=1620*0.,
 HT(1)=110., 49., 120., 22.,
 AW(1)=4.06+4, 7.289+3, 8.75+4, 1.662+4,
 AF(1)=8.825+3, 1.224+3, 3.75+3, 7.36+3,
 GSI=2.5668+04, GSR1=2.8075+04, GSR2=2.8075+04,
 DPF=15., DPL=5., DCSI=.1, DCSR=.11,
 TD=4., TMR=1.65, TMF=2.483, TEX1=2.484, TCSI=0., TCSIF=.767,
 TCSR1F=10000., TCSR2F=10000., TVR1=3.483, TVR2=3.983, TVRF=5.483,
 TCSR1=.0383, TCSR2=.0383, TJUMP1=.317, TJUMP2=.4,DT2=.0384,
 CFR(1,1)=40*0.,
 CFR(1,1)=.03,CFR(1,2)=6.8-5,CFR(1,3)=.017,CFR(1,4)=.05,CFR(1,5)=1.-4,
 CFR(1,6)=1.-6,
 TEND=.483, TPUFF=100., CUTOV=.01,  DT=.0001,
```

PWR CASE A - SAMPLE FISSION PRODUCT OUTPUT DATA

TIME= 5.00000E+04 SEC

COMPARTMENT AIRBORNE FRACTIONS CONTAINED

C O M	GAP RELEASE PARTICLES	GAP RELEASE I2	GAP RELEASE OI	MELT RELEASE PARTICLES	MELT RELEASE I2	MELT RELEASE OI	EXPLOSION RELEASE PARTICLES	EXPLOSION RELEASE I2	EXPLOSION RELEASE OI	VAPOR RELEASE PARTICLES	VAPOR RELEASE I2	VAPOR RELEASE OI
1	9.7545-03	9.8998-03	9.8427-0	0.0000	0.0000	0.0000	0.0000	0.0000	0.0000	0.0000	0.0000	0.0000
2	9.6915-01	9.8078-01	9.7035-01	0.0000	0.0000	0.0000	0.0000	0.0000	0.0000	0.0000	0.0000	0.0000
3	4.2085-06	4.2467-06	4.2630-0	0.0000	0.0000	0.0000	0.0000	0.0000	0.0000	0.0000	0.0000	0.0000
4	2.9159-09	2.9578-09	2.9416-09	0.0000	0.0000	0.0000	0.0000	0.0000	0.0000	0.0000	0.0000	0.0000

TOTAL AIRBORNE FRACTIONS CONTAINED

GAP RELEASE PARTICLES	GAP RELEASE I2	GAP RELEASE OI	MELT RELEASE PARTICLES	MELT RELEASE I2	MELT RELEASE OI	EXPLOSION RELEASE PARTICLES	EXPLOSION RELEASE I2	EXPLOSION RELEASE OI	VAPOR RELEASE PARTICLES	VAPOR RELEASE I2	VAPOR RELEASE OI
9.9891-01	9.9902-01	1.0000+00	0.0000	0.0000	0.0000	0.0000	0.0000	0.0000	0.0000	0.0000	0.0000

ESCAPE FRACTIONS OF EACH RELEASE

GAP RELEASE PARTICLES	GAP RELEASE I2	GAP RELEASE OI	MELT RELEASE PARTICLES	MELT RELEASE I2	MELT RELEASE OI	EXPLOSION RELEASE PARTICLES	EXPLOSION RELEASE I2	EXPLOSION RELEASE OI	VAPOR RELEASE PARTICLES	VAPOR RELEASE I2	VAPOR RELEASE OI
1.0589-12	1.0875-12	1.0691-12	0.0000	0.0000	0.0000	0.0000	0.0000	0.0000	0.0000	0.0000	0.0000

DOSE REDUCTION FACTORS OF EACH RELEASE

GAP RELEASE PARTICLES	GAP RELEASE I2	GAP RELEASE OI	MELT RELEASE PARTICLES	MELT RELEASE I2	MELT RELEASE OI	EXPLOSION RELEASE PARTICLES	EXPLOSION RELEASE I2	EXPLOSION RELEASE OI	VAPOR RELEASE PARTICLES	VAPOR RELEASE I2	VAPOR RELEASE OI
1.0097+00	1.0015+00		0.0000	0.0000		0.0000	0.0000		0.0000	0.0000	

FRACTIONS OF CORE INVENTORY LEAKED

KR-XE	OI	I2-BR	CS-RB	TE	BA-SR	RU	LA
3.2072-14	7.2696-17	1.8147-14	5.2940-14	1.0588-16	1.0588-18	0.0000	0.0000

J5. EXAMPLE BWR CASE

In contrast to the simple PWR example, one of the most complex BWR sequences is presented as an example. Sequence AGJ-δ had a number of features that made it difficult to fit into CORRAL's usual capabilities. CORRAL normally calculates one lumped atmospheric source. This sequence had:

a. An elevated stack source through the Gas Treatment System (SGTS, Compartment 4).

b. A ground level source.

c. Charcoal filter beds whose trapping capacity for I_2 and organic iodide could fail if too much I_2 collected on them.

d. Flow from the drywell (Compartment 1) to the wetwell (Compartment 2) with pool scrubbing.

e. Return flow to the drywell.

f. Flow from the drywell through the drywell annulus to the Main Reactor Building (Compartment 5).

A Compartment 3 was used as an artificial dumping ground for the drywell annulus. To segregate the ground level source from the elevated source, another artificial Compartment 6 was created. Flow to it was considered as the ground source and core fractions in it had to be hand calculated from the sets CFR(I,J) and CGØI(6,2) etc.

The elevated source from filtered air was easy to handle as a simple low level leak rate from Compartment 5 for particulates and I_2 only. This meant that for normal filter operation, the total flow of particulates from Compartment 5 was 1.001 times larger than it should have been. The flow of I_2 was 1.001 times too high. This was negligible. The normal organic iodide leak rate was 150 times larger than the I_2 leak rate creating a 1.15 overdepletion rate. To avoid this, no organic iodide leaked from Compartment 5, but rather was allowed to build up on the filter (Compartment 4) and 15 percent of it was hand calculated to add to the total atmospheric source.

The SGTS overheat problem was easily handled by checking on the I_2 buildup. When the charcoal beds did overheat, it was necessary to hand calculate all the I_2 and organic iodide as a difference between the buildup of new I_2 and organic iodide in Compartment 4 and the buildup level at the time of overheat.

No real problems arose but the Univac 1108 chugged 1512 seconds for the 24-hour accident sequence. This is largely due to the use of N=6 compartments. The time for matrix solution of the differential equations increases dramatically as N increases.

```
BWR EXAMPLE INPUT DATA FOR ACCIDENT SEQUENCE AGJ-DELTA

 $BREAK N=6, NDATA=20, MCOMP=1, MANN=2,
 TI(1)=0.,.116,.117,1.5,1.51,4.15,4.151,4.483,5.483,5.65,5.651,6.15,
 6.151,6.483,6.484,10.15,10.151,13.15,13.151,24.,
 HT(1)=100.,29.9,.1,.1,56.,
 AF(1)=3526.,10832.,0.,0.,1.96+4,
 AW(1)=14810.,16300.,0.,0.,3.14+4,
 V(1)=1.59+5,1.19+5,27.8,27.8,1.1+6,
 GI(1,1,1)=1620*0.,EP(1,1,1)=1620*0.,EI2(1,1,1)=1620*0.,
 TMY(1,1)=180*75.,PI(1,1)=180*0.,VAPI(1,1)=180*.03,DELTTI(1,1)=180*.1,
 ELKP(1,1)=180*0.,ELKOI(1,1)=180*0.,ELKI2(1,1)=180*0.,
 TMY(1,1 )=272., PI(1,1 )=28.3, VAPI(1,1 )=.99, DELTTI(1,1 )=1.0,
 TMY(1,2 )=180., PI(1,2 )=7.30, VAPI(1,2 )=.99, DELTTI(1,2 )=50.,
 TMY(1,3 )=180., PI(1,3 )=7.30, VAPI(1,3 )=.99, DELTTI(1,3 )=50.,
 TMY(1,4 )=180., PI(1,4 )=4.00, VAPI(1,4 )=.99, DELTTI(1,4 )=3.3,
 TMY(1,5 )=180., PI(1,5 )=4.00, VAPI(1,5 )=.99, DELTTI(1,5 )=3.3,
 TMY(1,6 )=190., PI(1,6 )=.300, VAPI(1,6 )=.99, DELTTI(1,6 )=.14,
 TMY(1,7 )=190., PI(1,7 )=.300, VAPI(1,7 )=.99, DELTTI(1,7 )=.14,
 TMY(1,8 )=158., PI(1,8 )=19.3, VAPI(1,8 )=.99, DELTTI(1,8 )=.14,
 TMY(1,9 )=308., PI(1,9 )=61.3, VAPI(1,9 )=.99, DELTTI(1,9 )=.14,
 TMY(1,10)=329., PI(1,10)=87.3, VAPI(1,10)=.99, DELTTI(1,10)=.14,
 TMY(1,11)=329., PI(1,11)=87.3, VAPI(1,11)=.99, DELTTI(1,11)=1.0,
 TMY(1,12)=297., PI(1,12)=49.3, VAPI(1,12)=.90, DELTTI(1,12)=4.8,
 TMY(1,13)=297., PI(1,13)=49.3, VAPI(1,13)=.90, DELTTI(1,13)=.14,
 TMY(1,14)=322., PI(1,14)=77.3, VAPI(1,14)=.90, DELTTI(1,14)=.14,
 TMY(1,15)=322., PI(1,15)=77.3, VAPI(1,15)=.90, DELTTI(1,15)=.14,
 TMY(1,16)=328., PI(1,16)=85.3, VAPI(1,16)=.90, DELTTI(1,16)=.14,
 TMY(1,17)=328., PI(1,17)=85.3, VAPI(1,17)=.90, DELTTI(1,17)=.62,
 TMY(1,18)=216., PI(1,18)=1.30, VAPI(1,18)=.90, DELTTI(1,18)=.62,
 TMY(1,19)=216., PI(1,19)=1.30, VAPI(1,19)=.90, DELTTI(1,19)=.14,
 TMY(1,20)=216., PI(1,20)=1.30, VAPI(1,20)=.90, DELTTI(1,20)=.10,
 AF(2)=0.,AW(2)=0.,AF(6)=0.,AW(6)=0.,V(6)=1000.,
 GI(1,2,7 )=1.94+6, EP(1,2,7 )=.99, EI2(1,2,7 )=.99,
 GI(1,2,8 )=9.66+5, EP(1,2,8 )=.99, EI2(1,2,8 )=.99,
 GI(1,2,9 )=6.24+5, EP(1,2,9 )=.99, EI2(1,2,9 )=.99,
 GI(1,2,10)=6.24+5, EP(1,2,10)=.99, EI2(1,2,10)=.99,
 GI(1,2,13)=4.81+5, EP(1,2,13)=.99, EI2(1,2,13)=.99,
 GI(1,2,14)=4.81+5, EP(1,2,14)=.99, EI2(1,2,14)=.99,
 GI(1,2,15)=3.55+4, EP(1,2,15)=.99, EI2(1,2,15)=.99,
 GI(1,2,16)=3.55+4, EP(1,2,16)=.99, EI2(1,2,16)=.99,

                                                    } FLOW TO WETWALL WITH POOL SCRUBBING

 GI(2,1,11)=8.87+4,
 GI(2,1,12)=8.87+4,
 GI(2,1,17)=3.32+4,
 GI(2,1,18)=3.32+4,
                    } RETURN FLOW FROM WETWELL

 GI(1,3,1 )=2.31+5, GI(3,5,1 )=2.31+5, GI(5,4,1 )=2.52+5,
 GI(1,3,2 )=2.31+5, GI(3,5,2 )=2.31+5, GI(5,4,2 )=2.52+5,
 GI(1,3,3 )=2.31+5, GI(3,5,3 )=2.31+5, GI(5,4,3 )=2.52+5,
 GI(1,3,4 )=2.31+5, GI(3,5,4 )=2.31+5, GI(5,4,4 )=2.52+5,
 GI(1,3,5 )=1.17+5, GI(3,5,5 )=1.17+5, GI(5,4,5 )=1.20+5,
 GI(1,3,6 )=1.17+5, GI(3,5,6 )=1.17+5, GI(5,4,6 )=1.20+5,
 GI(1,3,7 )=6.48+5, GI(3,5,7 )=6.48+5, GI(5,4,7 )=6.00+5,
 GI(1,3,8 )=3.22+5, GI(3,5,8 )=3.22+5, GI(5,4,8 )=6.00+5,
 GI(1,3,9 )=2.08+5, GI(3,5,9 )=2.08+5, GI(5,4,9 )=6.00+5,
 GI(1,3,10)=2.08+5, GI(3,5,10)=2.08+5, GI(5,4,10)=6.00+5,
 GI(1,3,11)=1.64+5, GI(3,5,11)=1.64+5, GI(5,4,11)=6.00+5,
 GI(1,3,12)=1.64+5, GI(3,5,12)=1.64+5, GI(5,4,12)=6.00+5,
 GI(1,3,13)=1.69+5, GI(3,5,13)=1.69+5, GI(5,4,13)=6.00+5,
 GI(1,3,14)=1.69+5, GI(3,5,14)=1.69+5, GI(5,4,14)=6.00+5,
 GI(1,3,15)=2.18+5, GI(3,5,15)=2.18+5, GI(5,4,15)=6.00+5,
 GI(1,3,16)=2.18+5, GI(3,5,16)=2.18+5, GI(5,4,16)=6.00+5,
 GI(1,3,17)=1.34+5, GI(3,5,17)=1.34+5, GI(5,4,17)=5.10+5,
 GI(1,3,18)=1.34+5, GI(3,5,18)=1.34+5, GI(5,4,18)=5.10+5,
 GI(1,3,19)=1.87+5, GI(3,5,19)=1.87+5, GI(5,4,19)=2.70+5,
 GI(1,3,20)=1.87+5, GI(3,5,20)=1.87+5, GI(5,4,20)=2.70+5,

                                                    } 1ST COLUMN IS FLOW THROUGH DRYWELL ANNULUS
                                                    2ND COLUMN IS FLOW INTO MAIN REACTOR BUILDING
                                                    3RD COLUMN IS FLOW INTO THE FILTER

 GI(5,6,7 )=2.58+5,
 GI(5,6,8 )=2.58+5,
 GI(5,6,9 )=2.58+5,
 GI(5,6,10)=2.58+5,
 GI(5,6,15)=3.60+5,
 GI(5,6,16)=3.60+5,
                    } FLOW AS A GROUND LEVEL SOURCE

 ELKP(5,1 )=2.29-5, ELKI2(5,1 )=2.29-4,
 ELKP(5,2 )=2.29-5, ELKI2(5,2 )=2.29-4,
 ELKP(5,3 )=2.29-5, ELKI2(5,3 )=2.29-4,
 ELKP(5,4 )=2.29-5, ELKI2(5,4 )=2.29-4,
 ELKP(5,5 )=1.10-5, ELKI2(5,5 )=1.10-4,
 ELKP(5,6 )=1.10-5, ELKI2(5,6 )=1.10-4,
 ELKP(5,7 )=9.45-5, ELKI2(5,7 )=9.45-4,
 ELKP(5,8 )=9.45-5, ELKI2(5,8 )=9.45-4,
 ELKP(5,9 )=9.45-5, ELKI2(5,9 )=9.45-4,
 ELKP(5,10)=9.45-5, ELKI2(5,10)=9.45-4,
 ELKP(5,11)=9.45-5, ELKI2(5,11)=9.45-4,
```

```
FLKP(5,12)=5.45-5, FLKI2(5,12)=5.45-4,
FLKP(5,13)=5.45-5, FLKI2(5,13)=5.45-4,
FLKP(5,14)=5.45-5, FLKI2(5,14)=5.45-4,
FLKP(5,15)=5.45-5, FLKI2(5,15)=5.45-4,
FLKP(5,16)=5.45-5, FLKI2(5,16)=5.45-4,
FLKP(5,17)=4.64-5, FLKI2(5,17)=4.64-4,
FLKP(5,18)=4.64-5, FLKI2(5,18)=4.64-4,
FLKP(5,19)=2.45-5, FLKI2(5,19)=2.45-4,
FLKP(5,20)=2.45-5, FLKI2(5,20)=2.45-4,
CFR(1,1)=.03,.87,0.,.1,
CFR(1,2)=0.,.007,0.,0.,
CFR(1,3)=.0017,.883,0.,.1,
CFR(1,4)=.005,.76,0.,.19,
CFR(1,5)=1.-5,.15,0.,.85,
CFR(1,6)=1.-7,.1,0.,.01,
CFR(1,7)=0.,.03,0.,.05,
CFR(1,8)=0.,.003,0.,.01,
TD=4.,DPE=15.,DPL=5.,
CSI=1.,CSR1=1.,CSR2=1.,DCSI=1.,DCSR=1.,VCL=1.,FCCI=1.,                    DUMMY
TCSR1=1.+4,TCSR2=1.+4,  TCSI=1.+4,TCSIF=1.+4,TCSR1F=1.+4,TCSR2F=1.+4,
HCSR=1.,HO=1.,HCSI=1.,CUTOV=.01,
TEX1=1.+4,TPUFF=1.+4,XPUFF=1.,DFPP=1.,DFPOI=1.,DFPI2=1.,
TMR=4.483,TMF=5.483,TVR1=6.15,TVR2=6.65,TVRF=8.15,
DT=.4483,DT2=.5,TJUMP1=8.2,TJUMP2=13.2,TEND=24.,
$
```

OUTPUT - BWR SEQUENCE AGI-6
FISSION PRODUCT RELEASE AND CLEANUP

DATA AND ASSUMPTIONS
NO. OF COMPARTMENTS N= 6

COMPARTMENT PRESSURES
((PI(I,J),I=1, 6),J=1,20)=

2.830000+01	0.000000	0.000000	0.000000	0.000000	0.000000
7.300000+00	0.000000	0.000000	0.000000	0.000000	0.000000
7.300000+00	0.000000	0.000000	0.000000	0.000000	0.000000
4.000000+00	0.000000	0.000000	0.000000	0.000000	0.000000
4.000000+00	0.000000	0.000000	0.000000	0.000000	0.000000
3.000000-01	0.000000	0.000000	0.000000	0.000000	0.000000
3.000000-01	0.000000	0.000000	0.000000	0.000000	0.000000
1.930000+01	0.000000	0.000000	0.000000	0.000000	0.000000
6.130000+01	0.000000	0.000000	0.000000	0.000000	0.000000
8.730000+01	0.000000	0.000000	0.000000	0.000000	0.000000
8.730000+01	0.000000	0.000000	0.000000	0.000000	0.000000
4.930000+01	0.000000	0.000000	0.000000	0.000000	0.000000
4.930000+01	0.000000	0.000000	0.000000	0.000000	0.000000
7.730000+01	0.000000	0.000000	0.000000	0.000000	0.000000
7.730000+01	0.000000	0.000000	0.000000	0.000000	0.000000
8.530000+01	0.000000	0.000000	0.000000	0.000000	0.000000
8.530000+01	0.000000	0.000000	0.000000	0.000000	0.000000
1.300000+00	0.000000	0.000000	0.000000	0.000000	0.000000
1.300000+00	0.000000	0.000000	0.000000	0.000000	0.000000
1.300000+00	0.000000	0.000000	0.000000	0.000000	0.000000

COMPARTMENT TEMPERATURES
((TMY(I,J),I=1, 6),J=1,20)=

2.720000+02	7.500000+01	7.500000+01	7.500000+01	7.500000+01	7.500000+01
1.800000+02	7.500000+01	7.500000+01	7.500000+01	7.500000+01	7.500000+01
1.800000+02	7.500000+01	7.500000+01	7.500000+01	7.500000+01	7.500000+01
1.800000+02	7.500000+01	7.500000+01	7.500000+01	7.500000+01	7.500000+01
1.800000+02	7.500000+01	7.500000+01	7.500000+01	7.500000+01	7.500000+01
1.900000+02	7.500000+01	7.500000+01	7.500000+01	7.500000+01	7.500000+01
1.900000+02	7.500000+01	7.500000+01	7.500000+01	7.500000+01	7.500000+01
1.580000+02	7.500000+01	7.500000+01	7.500000+01	7.500000+01	7.500000+01
3.080000+02	7.500000+01	7.500000+01	7.500000+01	7.500000+01	7.500000+01
3.290000+02	7.500000+01	7.500000+01	7.500000+01	7.500000+01	7.500000+01
3.290000+02	7.500000+01	7.500000+01	7.500000+01	7.500000+01	7.500000+01
2.970000+02	7.500000+01	7.500000+01	7.500000+01	7.500000+01	7.500000+01
2.970000+02	7.500000+01	7.500000+01	7.500000+01	7.500000+01	7.500000+01
3.220000+02	7.500000+01	7.500000+01	7.500000+01	7.500000+01	7.500000+01
3.220000+02	7.500000+01	7.500000+01	7.500000+01	7.500000+01	7.500000+01
3.280000+02	7.500000+01	7.500000+01	7.500000+01	7.500000+01	7.500000+01
3.280000+02	7.500000+01	7.500000+01	7.500000+01	7.500000+01	7.500000+01
2.160000+02	7.500000+01	7.500000+01	7.500000+01	7.500000+01	7.500000+01
2.160000+02	7.500000+01	7.500000+01	7.500000+01	7.500000+01	7.500000+01
2.160000+02	7.500000+01	7.500000+01	7.500000+01	7.500000+01	7.500000+01

TEMPERATURE DIFFERENCES TBULK-TWALL
((DELTTI(I,J),I=1, 6),J=1,29)=

1.000000+00	1.000000-01	1.000000-01	1.000000-01	1.000000-01	1.000000-01
5.000000+01	1.000000-01	1.000000-01	1.000000-01	1.000000-01	1.000000-01
5.000000+01	1.000000-01	1.000000-01	1.000000-01	1.000000-01	1.000000-01
3.300000+00	1.000000-01	1.000000-01	1.000000-01	1.000000-01	1.000000-01
3.300000+00	1.000000-01	1.000000-01	1.000000-01	1.000000-01	1.000000-01
1.400000-01	1.000000-01	1.000000-01	1.000000-01	1.000000-01	1.000000-01
1.400000-01	1.000000-01	1.000000-01	1.000000-01	1.000000-01	1.000000-01
1.400000-01	1.000000-01	1.000000-01	1.000000-01	1.000000-01	1.000000-01
1.400000-01	1.000000-01	1.000000-01	1.000000-01	1.000000-01	1.000000-01
1.400000-01	1.000000-01	1.000000-01	1.000000-01	1.000000-01	1.000000-01
1.000000+00	1.000000-01	1.000000-01	1.000000-01	1.000000-01	1.000000-01
4.800000+00	1.000000-01	1.000000-01	1.000000-01	1.000000-01	1.000000-01

```
   1.400000-01   1.000000-01   1.000000-01   1.000000-01   1.000000-01   1.000000-01
   1.400000-01   1.000000-01   1.000000-01   1.000000-01   1.000000-01   1.000000-01
   1.400000-01   1.000000-01   1.000000-01   1.000000-01   1.000000-01   1.000000-01
   1.400000-01   1.000000-01   1.000000-01   1.000000-01   1.000000-01   1.000000-01
   6.200000-01   1.000000-01   1.000000-01   1.000000-01   1.000000-01   1.000000-01
   6.200000-01   1.000000-01   1.000000-01   1.000000-01   1.000000-01   1.000000-01
   1.400000-01   1.000000-01   1.000000-01   1.000000-01   1.000000-01   1.000000-01
   1.000000-01   1.000000-01   1.000000-01   1.000000-01   1.000000-01   1.000000-01

 WATER VAPOR MOLE FRACTIONS
((VAPI(I,J),I=1, 6),J=1,20)=
   9.900000-01   3.000000-02   3.000000-02   3.000000-02   3.000000-02   3.000000-02
   9.900000-01   3.000000-02   3.000000-02   3.000000-02   3.000000-02   3.000000-02
   9.900000-01   3.000000-02   3.000000-02   3.000000-02   3.000000-02   3.000000-02
   9.900000-01   3.000000-02   3.000000-02   3.000000-02   3.000000-02   3.000000-02
   9.900000-01   3.000000-02   3.000000-02   3.000000-02   3.000000-02   3.000000-02
   9.900000-01   3.000000-02   3.000000-02   3.000000-02   3.000000-02   3.000000-02
   9.900000-01   3.000000-02   3.000000-02   3.000000-02   3.000000-02   3.000000-02
   9.900000-01   3.000000-02   3.000000-02   3.000000-02   3.000000-02   3.000000-02
   9.900000-01   3.000000-02   3.000000-02   3.000000-02   3.000000-02   3.000000-02
   9.900000-01   3.000000-02   3.000000-02   3.000000-02   3.000000-02   3.000000-02
   9.900000-01   3.000000-02   3.000000-02   3.000000-02   3.000000-02   3.000000-02
   9.900000-01   3.000000-02   3.000000-02   3.000000-02   3.000000-02   3.000000-02
   9.900000-01   3.000000-02   3.000000-02   3.000000-02   3.000000-02   3.000000-02
   9.900000-01   3.000000-02   3.000000-02   3.000000-02   3.000000-02   3.000000-02
   9.900000-01   3.000000-02   3.000000-02   3.000000-02   3.000000-02   3.000000-02
   9.900000-01   3.000000-02   3.000000-02   3.000000-02   3.000000-02   3.000000-02
   9.900000-01   3.000000-02   3.000000-02   3.000000-02   3.000000-02   3.000000-02
   9.900000-01   3.000000-02   3.000000-02   3.000000-02   3.000000-02   3.000000-02
   9.900000-01   3.000000-02   3.000000-02   3.000000-02   3.000000-02   3.000000-02
   9.900000-01   3.000000-02   3.000000-02   3.000000-02   3.000000-02   3.000000-02
   9.900000-01   3.000000-02   3.000000-02   3.000000-02   3.000000-02   3.000000-02
   9.900000-01   3.000000-02   3.000000-02   3.000000-02   3.000000-02   3.000000-02

 FRACTION OF I2 LEAKED PER HOUR
((ELKI2(I,J),I=1, 6),J=1,20)=
   0.000000      0.000000      0.000000      0.000000      2.290000-04   0.000000
   0.000000      0.000000      0.000000      0.000000      2.290000-04   0.000000
   0.000000      0.000000      0.000000      0.000000      2.290000-04   0.000000
   0.000000      0.000000      0.000000      0.000000      2.290000-04   0.000000
   0.000000      0.000000      0.000000      0.000000      1.100000-04   0.000000
   0.000000      0.000000      0.000000      0.000000      1.100000-04   0.000000
   0.000000      0.000000      0.000000      0.000000      5.450000-04   0.000000
   0.000000      0.000000      0.000000      0.000000      5.450000-04   0.000000
   0.000000      0.000000      0.000000      0.000000      5.450000-04   0.000000
   0.000000      0.000000      0.000000      0.000000      5.450000-04   0.000000
   0.000000      0.000000      0.000000      0.000000      5.450000-04   0.000000
   0.000000      0.000000      0.000000      0.000000      5.450000-04   0.000000
   0.000000      0.000000      0.000000      0.000000      5.450000-04   0.000000
   0.000000      0.000000      0.000000      0.000000      5.450000-04   0.000000
   0.000000      0.000000      0.000000      0.000000      5.450000-04   0.000000
   0.000000      0.000000      0.000000      0.000000      4.640000-04   0.000000
   0.000000      0.000000      0.000000      0.000000      4.640000-04   0.000000
   0.000000      0.000000      0.000000      0.000000      2.450000-04   0.000000
   0.000000      0.000000      0.000000      0.000000      2.450000-04   0.000000

 FRACTION OF PARTICULATES LEAKED PER HOUR
((ELKP(I,J),I=1, 6),J=1,20)=
   0.000000      0.000000      0.000000      0.000000      2.290000-05   0.000000
   0.000000      0.000000      0.000000      0.000000      2.290000-05   0.000000
   0.000000      0.000000      0.000000      0.000000      2.290000-05   0.000000
   0.000000      0.000000      0.000000      0.000000      2.290000-05   0.000000
   0.000000      0.000000      0.000000      0.000000      1.100000-05   0.000000
   0.000000      0.000000      0.000000      0.000000      1.100000-05   0.000000
   0.000000      0.000000      0.000000      0.000000      5.450000-05   0.000000
   0.000000      0.000000      0.000000      0.000000      5.450000-05   0.000000
   0.000000      0.000000      0.000000      0.000000      5.450000-05   0.000000
   0.000000      0.000000      0.000000      0.000000      5.450000-05   0.000000
   0.000000      0.000000      0.000000      0.000000      5.450000-05   0.000000
   0.000000      0.000000      0.000000      0.000000      5.450000-05   0.000000
   0.000000      0.000000      0.000000      0.000000      5.450000-05   0.000000
   0.000000      0.000000      0.000000      0.000000      5.450000-05   0.000000
   0.000000      0.000000      0.000000      0.000000      5.450000-05   0.000000
   0.000000      0.000000      0.000000      0.000000      4.640000-05   0.000000
   0.000000      0.000000      0.000000      0.000000      4.640000-05   0.000000
   0.000000      0.000000      0.000000      0.000000      2.450000-05   0.000000
   0.000000      0.000000      0.000000      0.000000      2.450000-05   0.000000

 FRACTION OF ORGANIC IODIDE$ LEAKED PER HOUR FROM COMPARTMENT I

((ELKOI(I,J),I=1, 6),J=1,20)=
   0.000000      0.000000      0.000000      0.000000      0.000000      0.000000
   0.000000      0.000000      0.000000      0.000000      0.000000      0.000000
   0.000000      0.000000      0.000000      0.000000      0.000000      0.000000
   0.000000      0.000000      0.000000      0.000000      0.000000      0.000000
   0.000000      0.000000      0.000000      0.000000      0.000000      0.000000
   0.000000      0.000000      0.000000      0.000000      0.000000      0.000000
   0.000000      0.000000      0.000000      0.000000      0.000000      0.000000
   0.000000      0.000000      0.000000      0.000000      0.000000      0.000000
   0.000000      0.000000      0.000000      0.000000      0.000000      0.000000
   0.000000      0.000000      0.000000      0.000000      0.000000      0.000000
   0.000000      0.000000      0.000000      0.000000      0.000000      0.000000
   0.000000      0.000000      0.000000      0.000000      0.000000      0.000000
   0.000000      0.000000      0.000000      0.000000      0.000000      0.000000
   0.000000      0.000000      0.000000      0.000000      0.000000      0.000000
   0.000000      0.000000      0.000000      0.000000      0.000000      0.000000
   0.000000      0.000000      0.000000      0.000000      0.000000      0.000000
   0.000000      0.000000      0.000000      0.000000      0.000000      0.000000
   0.000000      0.000000      0.000000      0.000000      0.000000      0.000000
   0.000000      0.000000      0.000000      0.000000      0.000000      0.000000
   0.000000      0.000000      0.000000      0.000000      0.000000      0.000000
```

```
   0.000000       0.000000       0.000000       0.000000       0.000000       0.000000
   0.000000       0.000000       0.000000       0.000000       0.000000       0.000000
   0.000000       0.000000       0.000000       0.000000       0.000000       0.000000
   0.000000       0.000000       0.000000       0.000000       0.000000       0.000000
   0.000000       0.000000       0.000000       0.000000       0.000000       0.000000
   0.000000       0.000000       0.000000       0.000000       0.000000       0.000000
   0.000000       0.000000       0.000000       0.000000       0.000000       0.000000
 PRECEDING DOUBLY INDEXED EXPRESSIONS WERE INDEXED ON COMPARTMENT (I) AND TIME (J). THE INPUT TIME ARRAY IS TI.
(TI(J),J=1,20)=
   0.000000       1.160000-01    1.170000-01    1.500000+00    1.510000+00    4.150000+00    4.151000+00    4.483000+00
   5.483000+00    5.650000+00    5.651000+00    6.150000+00    6.151000+00    6.483000+00    6.484000+00    1.015000+01
   1.015100+01    1.315000+01    1.315100+01    2.400000+01

 TIMES TCHANG SIGNAL REINTERPOLATION OF FLOW RATES AND THERMODYNAMIC DATA
TCHANG=
   0.000000       0.000000       0.000000       0.000000       0.000000       0.000000       0.000000       0.000000
   0.000000       0.000000       0.000000       0.000000       0.000000       0.000000       0.000000       0.000000
   0.000000       0.000000       0.000000       0.000000

 FRACTION OF PARTICULATES REMOVED PER HOUR BY INTERIOR FILTER IN COMPARTMENT I
(FDP(I),I=1, 6)=
   0.000000       0.000000       0.000000       0.000000       0.000000       0.000000

 FRACTION OF IODINE (I2) REMOVED PER HOUR BY INTERIOR FILTER IN COMPARTMENT I
(FDI2(I),I=1, 6)=
   0.000000       0.000000       0.000000       0.000000       0.000000       0.000000

INTER-COMPARTMENTAL TRANSFER COEFFICIENTS

 CUBIC FEET OF FLOW PER HOUR FROM COMPARTMENT I TO COMPARTMENT K AT DATA TIME ENTRY J
 (GI( 1,K, 1),K=1, 6)=
   0.000000       0.000000       2.310000+05    0.000000       0.000000       0.000000
 (GI( 2,K, 1),K=1, 6)=
```

14 OUTPUT PAGES OMITTED HERE TO SHORTEN REPORT

```
   0.000000       0.000000       0.000000       0.000000       0.000000       0.000000
(EP( 2,K,18),K=1, 6)=
   0.000000       0.000000       0.000000       0.000000       0.000000       0.000000
(EP( 3,K,18),K=1, 6)=
   0.000000       0.000000       0.000000       0.000000       0.000000       0.000000
(EP( 4,K,18),K=1, 6)=
   0.000000       0.000000       0.000000       0.000000       0.000000       0.000000
(EP( 5,K,18),K=1, 6)=
   0.000000       0.000000       0.000000       0.000000       0.000000       0.000000
(EP( 6,K,18),K=1, 6)=
   0.000000       0.000000       0.000000       0.000000       0.000000       0.000000
(EP( 1,K,19),K=1, 6)=
   0.000000       0.000000       0.000000       0.000000       0.000000       0.000000
(EP( 2,K,19),K=1, 6)=
   0.000000       0.000000       0.000000       0.000000       0.000000       0.000000
(EP( 3,K,19),K=1, 6)=
   0.000000       0.000000       0.000000       0.000000       0.000000       0.000000
(EP( 4,K,19),K=1, 6)=
   0.000000       0.000000       0.000000       0.000000       0.000000       0.000000
(EP( 5,K,19),K=1, 6)=
   0.000000       0.000000       0.000000       0.000000       0.000000       0.000000
(EP( 6,K,19),K=1, 6)=
   0.000000       0.000000       0.000000       0.000000       0.000000       0.000000
(EP( 1,K,20),K=1, 6)=
   0.000000       0.000000       0.000000       0.000000       0.000000       0.000000
(EP( 2,K,20),K=1, 6)=
   0.000000       0.000000       0.000000       0.000000       0.000000       0.000000
(EP( 3,K,20),K=1, 6)=
   0.000000       0.000000       0.000000       0.000000       0.000000       0.000000
(EP( 4,K,20),K=1, 6)=
   0.000000       0.000000       0.000000       0.000000       0.000000       0.000000
(EP( 5,K,20),K=1, 6)=
   0.000000       0.000000       0.000000       0.000000       0.000000       0.000000
(EP( 6,K,20),K=1, 6)=
   0.000000       0.000000       0.000000       0.000000       0.000000       0.000000

 INPUT TIME VARIABLES

TD=TIME INTERVAL OVER WHICH EFFECTIVE PARTICLE DIAMETER CHANGES LINEARLY FROM DPE (DIAMETER PARTICLES EARLY)
TO DPL (DIAMETER PARTICLES LATE).
DT,DT2=TIME STEP(HRS) BEFORE MELT AND AFTER TJUMP1
TVR1=TIME OF FIRST VAPORIZATION RELEASE
TVR2=TIME OF VAPORIZATION RELEASE 2.
TVRE=TIME OF VAPORIZATION RELEASE END
TMR=TIME OF MELT RELEASE
TMF=TIME OF MELT RELEASE FINISH
TCSI=TIME CONTAINMENT SYSTEM INJECTION SPRAY PUMP STARTS
TCSIE=TIME CONTAINMENT SYSTEM INJECTION SPRAY ENDS
TECCI=TIME OF EMERGENCY CORE COOLANT INJECTION
```

```
TCSR1=TIME CONTAINMENT SYSTEM RECIRCULATING SPRAY STARTS
TCSR1E=TIME CONTAINMENT SYSTEM RECIRCULATING SPRAY ENDS
TEX1=TIME OF EXPLOSION NO. 1
TPUFF=TIME OF PUFF RELEASE
TJUMP1=TIME TO SWITCH TO TIME STEP DT2
TJUMP2=TIME TO STEP TO END

 TO= 4.00000+00   DT= 4.48300-01   TVR1= 6.15000+00  TVR2= 6.65000+00  TVRE= 8.15000000+00   TMR= 4.48300000+00
TMF= 5.48300000+00   TCSI= 1.00000000+04   TCSIE= 1.00000000+04   TECCI= 0.00000000      TCSR1= 1.00000000+04
TCSR1E= 1.00000000+04   TCSR2= 1.00000000+04   TCSR2E= 1.00000000+04   TEX1= 1.00000000+04   TPUFF= 1.00000000+04
DT2= 5.00000000-01   TJUMP1= 8.19999990+00   TJUMP2= 1.31999999+01   TEND= 2.40000000+01

 REACTOR COMPARTMENT DATA

 COMPARTMENT WALL AREA
(AW(I),I=1, 6)=
   1.481000+04   0.000000      0.000000      0.000000      3.140000+04   0.000000
 COMPARTMENT FLOOR AREA
(AF(I),I=1, 6)=
   3.526000+03   0.000000      0.000000      0.000000      1.960000+04   0.000000
 COMPARTMENT HEIGHT
(HT(I),I=1, 6)=
   1.000000+02   2.990000+01   1.000000-01   1.000000-01   5.600000+01   0.000000
 COMPARTMENT VOLUME (CUBIC FEET)
(V(I),I=1, 6)=
   1.590000+05   1.190000+05   2.780000+01   2.780000+01   1.100000+06   1.000000+03

 CONTAINMENT AND CLEANUP SPECIFICATIONS

CSI=CONTAINMENT SYSTEM INJECTION FLOW IN CUBIC FEET/HR.
CSR1=CONTAINMENT SYSTEM NO.1 RECIRCULATING FLOW IN CUBIC FEET/HR.
HCSI,HCSR=HEIGHT THROUGH WHICH CONTAINMENT SYSTEM SPRAYS FALL
DCSI,DCSR=DIAMETER OF CONTAINMENT SYSTEM SPRAY DROPLETS
CUTOV=CONCENTRATION OF I2 BELOW WHICH SPRAY REMOVAL IS INEFFECTIVE
VCL=VOLUME OF COOLANT LIQUID
HO=RATIO OF IODINE IN SOLUTION IN WATER TO THAT IN VAPOR AT EQUILIBRIUM
ECCI=EMERGENCY CORE COOLANT FLOW RATE
DFPP,DFPOI,DFPI2=PUFF RELEASE DECONTAMINATION FACTORS
XPUFF=FRACTION OF AIRBORNE MATERIAL RETAINED AFTER PUFF RELEASE
DPE,DPL=EFFECTIVE DIAMETER OF PARTICLES IN MICRONS AT EARLY AND LATE TIMES

 CSI= 1.00000000+00   CSR1= 1.00000000+00   HCSI= 1.00000000+00   HCSR= 1.00000000+00   DCSI= 1.00000000+00
DCSR= 1.00000000+00   CUTOV= 9.99999990-03   VCL= 1.00000000+00   HO= 1.00000000+00   ECCI= 1.00000000+00
DFPP= 1.0000000+00   DFPOI= 1.0000000+00   DFPI2= 1.0000000+00   CSR2= 1.0000000+00   XPUFF= 1.0000000+00
 DPE= 1.5000000+01   DPL= 5.0000000+00

 CORE FRACTIONS RELEASED BY METHOD J IN ISOTOPE GROUP I CFR(J,I)

      GAP RELEASE    MELT RELEASE    STEAM EXPLOSION VAPORIZATION


KR-XE  3.00000-02      8.70000-01      0.00000         1.00000-01
OI     0.00000         7.00000-03      0.00000         0.00000
I2-BR  1.70000-03      8.83000-01      0.00000         1.00000-01
CS-RB  5.00000-03      7.60000-01      0.00000         1.90000-01
TE     1.00000-05      1.50000-01      0.00000         8.50000-01
BA-SR  1.00000-07      1.00000-01      0.00000         1.00000-02
RU     0.00000         3.00000-02      0.00000         5.00000-02
LA     0.00000         3.00000-03      0.00000         1.00000-02
```

SAMPLE OF FISSION PRODUCT OUTPUT DATA

```
 TIME= 5.48130+00   HRS

  COMPARTMENT AIRBORNE FRACTIONS CONTAINED
```

C O M	GAP RELEASE PARTICLES	GAP RELEASE I2	GAP RELEASE OI	MELT RELEASE PARTICLES	MELT RELEASE I2	MELT RELEASE OI	EXPLOSION RELEASE PARTICLES	EXPLOSION RELEASE I2	EXPLOSION RELEASE OI	VAPOR RELEASE PARTICLES	VAPOR RELEASE I2	VAPOR RELEASE OI
1	6.2212-09	2.2949-08	9.2327-07	8.8233-02	1.2575-01	1.3296-01	0.0000	0.0000	0.0000	0.0000	0.0000	0.0000
2	1.4220-06	3.6499-06	1.4684-02	5.0654-03	6.2838-03	6.5028-01	0.0000	0.0000	0.0000	0.0000	0.0000	0.0000
3	1.0885-12	2.9706-12	1.6154-10	1.5442-05	1.6279-05	2.3264-05	0.0000	0.0000	0.0000	0.0000	0.0000	0.0000
4	1.5332-02	2.4462-02	6.5264-01	1.2950-02	2.0502-02	4.4345-02	0.0000	0.0000	0.0000	0.0000	0.0000	0.0000
5	1.7361-03	5.0880-03	2.0437-01	5.8998-02	8.5738-02	1.5332-01	0.0000	0.0000	0.0000	0.0000	0.0000	0.0000
6	1.2534-03	3.3853-03	1.2831-01	5.5686-03	8.8158-03	1.9068-02	0.0000	0.0000	0.0000	0.0000	0.0000	0.0000

  TOTAL AIRBORNE FRACTIONS CONTAINED

GAP RELEASE PARTICLES	GAP RELEASE I2	GAP RELEASE OI	MELT RELEASE PARTICLES	MELT RELEASE I2	MELT RELEASE OI	EXPLOSION RELEASE PARTICLES	EXPLOSION RELEASE I2	EXPLOSION RELEASE OI	VAPOR RELEASE PARTICLES	VAPOR RELEASE I2	VAPOR RELEASE OI
1.8323-02	5.2939-02	1.0000+00	1.7083-01	2.4711-01	1.0000+00	0.0000	0.0000	0.0000	0.0000	0.0000	0.0000


```
```

ESCAPE FRACTIONS OF EACH RELEASE

GAP RELEASE PARTICLES	GAP RELEASE I2	GAP RELEASE OI	MELT RELEASE PARTICLES	MELT RELEASE I2	MELT RELEASE OI	EXPLOSION RELEASE PARTICLES	EXPLOSION RELEASE I2	EXPLOSION RELEASE OI	VAPOR RELEASE PARTICLES	VAPOR RELEASE I2	VAPOR RELEASE OI
1.5554-06	2.4514-05	0.0000	1.2939-06	2.0485-05	0.0000	0.0000	0.0000	0.0000	0.0000	0.0000	0.0000

DOSE REDUCTION FACTORS OF EACH RELEASE

GAP RELEASE PARTICLES	GAP RELEASE I2	GAP RELEASE OI	MELT RELEASE PARTICLES	MELT RELEASE I2	MELT RELEASE OI	EXPLOSION RELEASE PARTICLES	EXPLOSION RELEASE I2	EXPLOSION RELEASE OI	VAPOR RELEASE PARTICLES	VAPOR RELEASE I2	VAPOR RELEASE OI
0.0000	0.0000		0.0000	0.0000		0.0000	0.0000		0.0000	0.0000	

FRACTIONS OF CORE INVENTORY LEAKED

KR-XE	OI	I2-BR	CS-RB	TE	BA-SR	RU	LA
0.0000	0.0000	1.8130-05	9.9108-07	1.9411-07	1.2940-07	3.8818-08	3.8818-09

J6. COMPUTER CODE CORRAL LISTING FOR BWR ACCIDENT SEQUENCES

```
 1*   C
 2*   C     THIS VERSION OF CORRAL IS FOR BWR ACCIDENT SEQUENCES
 3*   C
 4*         DIMENSION PI(9,20),TI(20),GI(9,9,20),VAPI(9,20),V(9),
 5*        1VAP(9),P(9),TMP(9),DELTTI(9,20),DELTAT(9),ELKP(9,20),ELKI(9,9,20),
 6*        1EP(9,9,20),EFI2(9,9),HT(9),ELI2(9),ELPI(9),G(9,9),CMP(9,10,2),
 7*        1ELKI2(9,20),CKG(9),OKM(10),OKA(10),OKB(10),
 8*        1CAOI(9,10,2),
 9*        1CBOI(9,10,2),
10*        1CBI2(9,10,2),
11*        1CAI2(9,10,2),
12*        1EFP(9,9)
13*         DIMENSION CGP(9,2),
14*        1CSP(9,2),
15*        1CGI2(9,2),
16*        1CMI2(9,10,2),
17*        1CSI2(9,2),
18*        1CGOI(9,2),
19*        1CMOI(9,10,2),
20*        1CSOI(9,2),
21*        1CMTP(9),
22*        1CMTI2(9),
23*        1CMTOI(9),
24*        1TM1(10),
25*        1TM3(10),
26*        1TM4(10),
27*        1OKICM(10)
28*         DIMENSION BETAPG(9),
29*        1BETAPM(9,10),
30*        1BETAPS(9),
31*        1AW(9),AF(9),
32*        1SKGG(9),
33*        1SKG(9,10),
34*        1FDP(9),
35*        1FDI2(9),
36*        1BTAI2S(9),
37*        1BTAI2M(9,10),
38*        1BTAI2G(9),
39*        1CVTOI(9),CVTI2(9),
40*        1OKNCM(9,10),
41*        1OKNCG(9),
42*        1OKNCS(9)
43*         DIMENSION
44*        1OKICA(10),
45*        1OKICB(10),
46*        1OKNCA(9,10),
47*        1BTAI2A(9,10),
48*        1BTAI2B(9,10),
49*        1AMDAMP(10),
50*        1AMDAIM(10),
51*        1AMDAIA(10),
52*        1AMDAIB(10),
53*        1ELOI(9),ELKOI(9,20),
54*        1OKNCB(9,10),
55*        1CATOI(9)
56*         DIMENSION CBTOI(9),
57*        1TA1(10),
58*        1TB1(10),
59*        1TA3(10),
60*        1TB3(10),
61*        1TB4(10),
62*        *TA4(10)
63*         DIMENSION
64*        1DNST(9),
65*        1VAIR(9),
```

```
     1VST(9),
     1PAS(9),
     1PSA(9),
     1VM(9),
     1WA(9),
     1WS(9),
     1DS(9),
     1DA(9),
     1DI2(9),
     1SC(9)
      DIMENSION AMDAPA(10),AMDAPB(10),BTAPVA(9,10),BTAPVB(9,10),CAP(9,
     110,2),CBP(9,10,2),CATP(9),CBTP(9),CVTP(9),DVA(10),DVB(10),EFA(10)
     2,EFB(10),SKGA(9,10),SKGB(9,10),TVA(10),TVB(10)
      DIMENSION GR(9),
     1SKG1(9),
     1COM(10),
     1COB(10),
     1COA(10),
     1 ELAMM(10),
     1ELAMA(10),
     1ELAMB(10),
     1EFM(10),
     1DM(9),
     1TMY(9,20),TCHANG(20)
C     CFR(JREL,ISOT)=CORE FRACTION RELEASED FOR MATERIAL ISOT BY
C     METHOD JREL.
      DIMENSION CFR(4,10),NAMES(10),CORLEK(10)
      EQUIVALENCE(TA4(1),TVA(1)),(TB4(1),TVB(1))
C     THE ISOTOPE GROUPS WILL BE TAKEN AS XR=XE AND OI (ORGANIC IODIDE
C     LIKE),I2=BR(I2 LIKE),AND CS=RB,TE,BA=SR,RU,PU(PARTICULATE LIKE)
      DATA NAMES(1)/6HKR-XE /,NAMES(2)/6HOI    /,NAMES(3)/6HI2-BR /,
     1NAMES(4)/6HCS-RB /,NAMES(5)/6HTE    /,NAMES(6)/6HBA-SR /,
     2NAMES(7)/6HRU    /,NAMES(8)/6HLA    /
      DATA NOI/2/,NI2/1/,NPAR/5/
      LOGICAL SWITCH
      COMMON//A(50),ABSMAX,ABSRMS,B(50),F(50),FABZ(50,50),FT(50,50)
     1,H(50,50),II,IND,INF,L,LL,LOST,MAPS,MARK,NTT,NA,NB,NEXT,NT
     2,PLOT(5,2,100),Q(50,50),RELMAX,RELRMS,RUN(10),T(50),TAG(50),TYPE
     3,UNITF,UNITT,W(50),Z(50,50),ZN(50,50),ZNII(50)
      NAMELIST/BREAK/N,NDATA,TI,DELTTI,DT,DT2,TJUMP1,TJUMP2,
     1PI,GI,EP,EI2,AW,AF,ELKI2,ELKP,HT,TCHANG,TEND,TVR1
     2,TVR2,TVRE,GK,DPE,DPL,VAPI,V,FDP,FDI2,TCSI,ELKOI,TMR,TMF,TCSR2F,
     3CSR2,TCSR2,HCSI,TD,TEX1,TCSIE,CSI,WO,TCSP1E,CSR1,
     4DCSR,HCSR,CUTOV,DCSI,TECCI,VCL,TMY,TCSP1,ECCI,DF
     5,TPUFF,DFPP,DFPOI,DFPI2,CFR,XPUFF,MCOMP,MANN
C     MCOMP= COMP FLOW FROM MCOMP THRU ANNULUS
C     MANN=1, BYPASS ANNULUS
      NAMELIST/TRIVIA/DI2,GR,SC,CKG,P,TMP,DNST,VM,BTAI2G,ORNGG,ELI2
      NAMELIST/MIX/P,TMP,DNST,VAIR,VST,PAS,PSA,VM
      DATA ABSMAX/1.E-8  /,ABSRMS/1.E-8  /,RELMAX/1.E-8  /,RELRMS/1.E-8/
    1 CONTINUE
      READ(5,BREAK,END=999)
      WRITE(6,2001)N
 2001 FORMAT(1H1,///,32X,35HFISSION PRODUCT RELEASE AND CLEANUP,//,
     15X,20HDATA AND ASSUMPTIONS,/,6X,22HNO. OF COMPARTMENTS N= ,I2)
      WRITE(6,2002)N,NDATA
 2002 FORMAT(1H0,6X,21HCOMPARTMENT PRESSURES,/,6X,
     114H((PI(I,J),I=1,,I2,6H),J=1,,I2,2H)=)
      DO 1500 J=1,NDATA
      WRITE(6,2003)(PI(I,J),I=1,N)
 1500 CONTINUE
 2003 FORMAT(6X,1P8E14.6)
      WRITE(6,2004)N,NDATA
 2004 FORMAT(1H0,6X,24HCOMPARTMENT TEMPERATURES,/,6X,15H((TMY(I,J),I=1,,
     1I2,6H),J=1,,I2,2H)=)
      DO 1505 J=1,NDATA
      WRITE(6,2003)(TMY(I,J),I=1,N)
 1505 CONTINUE
      WRITE(6,2006)N,NDATA
 2006 FORMAT(1H0,6X,35HTEMPERATURE DIFFERENCES TBULK-TWALL,/,6X,
     118H((DELTTI(I,J),I=1,,I2,6H),J=1,,I2,2H)=)
      DO 1510 J=1,NDATA
      WRITE(6,2003)(DELTTI(I,J),I=1,N)
 1510 CONTINUE
      WRITE(6,2008)N,NDATA
 2008 FORMAT(1H0,6X,26HWATER VAPOR MOLE FRACTIONS ,/,6X,
     116H((VAPI(I,J),I=1,,I2,6H),J=1,,I2,2H)=)
      DO 1520 J=1,NDATA
      WRITE(6,2003)(VAPI(I,J),I=1,N)
 1520 CONTINUE
      WRITE(6,2010)N,NDATA
 2010 FORMAT(1H0,6X,30HFRACTION OF I2 LEAKED PER HOUR,/,6X,
     117H((ELKI2(I,J),I=1,,I2,6H),J=1,,I2,2H)=)
      DO 1525 J=1,NDATA
      WRITE(6,2003)(ELKI2(I,J),I=1,N)
 1525 CONTINUE
      WRITE(6,2012)N,NDATA
 2012 FORMAT(1H0,6X,40HFRACTION OF PARTICULATES LEAKED PER HOUR ,/,6X,
     116H((ELKP(I,J),I=1,,I2,6H),J=1,,I2,2H)=)
      DO 1530 J=1,NDATA
      WRITE(6,2003)(ELKP(I,J),I=1,N)
 1530 CONTINUE
      WRITE(6,2016)N,NDATA
```

```
 2016 FORMAT(1H0,6X,62HFRACTION OF ORGANIC IODIDES LEAKED PER HOUR FROM
     1COMPARTMENT I ,/,6X,17H((ELKOI(I,J),I=1,,I2,6H),J=1,,I2,2H)=)
      DO 11530 J=1,NDATA
11530 WRITE(6,2003)(ELKOI(I,J),I=1,N)
      WRITE(6,2014)NDATA,(TI(J),J=1,NDATA)
 2014 FORMAT(1H ,6X,110HPRECEDING DOUBLY INDEXED EXPRESSIONS WERE INDEXE
     1D ON COMPARTMENT (I) AND TIME (J). THE INPUT TIME ARRAY IS TI.
     2,/,6X,11H(TI(J),J=1,,I2,2H)=,/,(6X,1P8E14.6))
      WRITE(6,22015)TCHANG
22015 FORMAT(1H0,6X,72HTIMES TCHANG SIGNAL REINTERPOLATION OF FLOW RATES
     * AND THERMODYNAMIC DATA ,/,6X,7HTCHANG=,/,(6X,1P8E14.6))
      WRITE(6,2018)N
 2018 FORMAT(1H0,6X,77HFRACTION OF PARTICULATES REMOVED PER HOUR BY INTE
     1RIOR FILTER IN COMPARTMENT I ,/,6X,12H(FDP(I),I=1,,I2,2H)=)
      WRITE(6,2003)(FDP(I),I=1,N)
      WRITE(6,2020)N
 2020 FORMAT(1H0,6X,76HFRACTION OF IODINE (I2) REMOVED PER HOUR BY INTER
     1IOR FILTER IN COMPARTMENT I  ,/,6X,13H(FDI2(I),I=1,,I2,2H)=)
      WRITE(6,2003)(FDI2(I),I=1,N)
      WRITE(6,2021)
 2021 FORMAT(1H0,/,6X,41HINTER-COMPARTMENTAL TRANSFER COEFFICIENTS  ,/)
      WRITE(6,2022)
 2022 FORMAT(1H0,6X,84HCUBIC FEET OF FLOW PER HOUR FROM COMPARTMENT I TO
     1 COMPARTMENT K AT DATA TIME ENTRY J  )
      DO 1540 J=1,NDATA
      DO 1540 I=1,N
      WRITE(6,2024)I,J,N
      WRITE(6,2003)(GI(I,K,J),K=1,N)
 1540 CONTINUE
 2024 FORMAT(1H ,6X,4H(GI(,I2,3H,K,,I2,6H),K=1,,I2,2H)=)
      WRITE(6,2026)
 2026 FORMAT(1H0,6X,107HFRACTION OF IODINE (I2)  REMOVED BY FILTER IN FL
     1OW FROM COMPARTMENT I TO COMPARTMENT K AT DATA TIME ENTRY J  )
      DO 1545 J=1,NDATA
      DO 1545 I=1,N
      WRITE(6,2028)I,J,N
      WRITE(6,2003)(EI2(I,K,J),K=1,N)
 1545 CONTINUE
 2028 FORMAT(1H ,6X,5H(EI2(,I2,3H,K,,I2,6H),K=1,,I2,2H)=)
      WRITE(6,2030)
      DO 1550 J=1,NDATA
 2030 FORMAT(1H0,6X,107HFRACTION OF PARTICULATES REMOVED BY FILTER IN FL
     1OW FROM COMPARTMENT I TO COMPARTMENT K AT DATA TIME ENTRY J  )
      DO 1550 I=1,N
      WRITE(6,2032)I,J,N
      WRITE(6,2003)(EP(I,K,J),K=1,N)
 1550 CONTINUE
 2032 FORMAT(1H ,6X,4H(EP(,I2,3H,K,,I2,6H),K=1,,I2,2H)=)
      WRITE(6,2034)
 2034 FORMAT(1H0,6X,20HINPUT TIME VARIABLES ,//,6X,108HTD=TIME INTERVAL
     1OVER WHICH EFFECTIVE PARTICLE DIAMETER CHANGES LINEARLY FROM DPE (
     2DIAMETER PARTICLES EARLY) ,/,6X,33HTO DPL (DIAMETER PARTICLES LATE
     3).  ,/,6X,51HDT,DT2=TIME STEP(HRS) BEFORE MELT AND AFTER TJUMP1  ,
     A/,6X,39HTVR1=TIME OF FIRST VAPORIZATION RELEASE ,
     4/,6X,36HTVR2=TIME OF VAPORIZATION RELEASE 2. ,/,
     56X,37HTVRE=TIME OF VAPORIZATION RELEASE END ,/,
     66X,24HTMR=TIME OF MELT RELEASE ,/,
     76X,31HTMF=TIME OF MELT RELEASE FINISH ,/,
     86X,56HTCSI=TIME CONTAINMENT SYSTEM INJECTION SPRAY PUMP STARTS,/,
     86X,50HTCSIE=TIME CONTAINMENT SYSTEM INJECTION SPRAY ENDS ,/,
     96X,46HTECCI=TIME OF EMERGENCY CORE COOLANT INJECTION ,/,
     06X,56HTCSR1=TIME CONTAINMENT SYSTEM RECIRCULATING SPRAY STARTS ,/,
     16X,55HTCSR1E=TIME CONTAINMENT SYSTEM RECIRCULATING SPRAY ENDS ,/,
     26X,28HTEX1=TIME OF EXPLOSION NO. 1 ,/,
     36X,26HTPUFF=TIME OF PUFF RELEASE     ,/,
     46X,38HTJUMP1=TIME TO SWITCH TO TIME STEP DT2  ,/,
     56X,26HTJUMP2=TIME TO STEP TO END  ,/)
      WRITE(6,2036)TD,DT,TVR1,TVR2,TVRE,TMR,TMF,TCSI,TCSIE,TECCI,TCSR1,
     *TCSR1E,TCSR2,TCSR2E,TEX1,TPUFF,DT2,TJUMP1,TJUMP2,TEND
 2036 FORMAT(1H ,6X,3HTD=,1PE12.5,3X,3HDT=,1PE12.5,3X,5HTVR1=,1PE12.5,2X
     A,5HTVR2=,1PE12.5,2X
     1,5HTVRE=,1PE14.8,3X,4HTMR=,1PE14.8,/,6X,4HTMF=,1PE14.8,3X,5HTCSI=,
     11PE14.8,3X,6HTCSIE=,1PE14.8,3X,6HTECCI=,1PE14.8,3X,6HTCSR1=,1PE14
     1.8,/,6X,7HTCSR1E=1PE14.8,3X,6HTCSR2=,1PE14.8,3X,7HTCSR2E=,1PE14.8,
     13X,5HTEX1=,1PE14.8,3X,6HTPUFF=,1PE14.8,/,
     16X,4HDT2=,1PE14.8,3X,7HTJUMP1=,1PE14.8,3X,7HTJUMP2=,1PE14.8,3X,
     15HTEND=,1PE14.8)
      WRITE(6,2038)
 2038 FORMAT(1H0,6X,24HREACTOR COMPARTMENT DATA ,/)
      WRITE(6,2040)N
 2040 FORMAT(1H ,6X,21HCOMPARTMENT WALL AREA,/,6X,11H(AW(I),I=1,,I2,
     12H)=)
      WRITE(6,2003)(AW(I),I=1,N)
      WRITE(6,2042)N
 2042 FORMAT(1H ,6X,22HCOMPARTMENT FLOOR AREA,/,6X,11H(AF(I),I=1,,I2,
     12H)=)
      WRITE(6,2003)(AF(I),I=1,N)
      WRITE(6,2044)N
 2044 FORMAT(1H ,6X,18HCOMPARTMENT HEIGHT,/,6X,11H(HT(I),I=1,,I2,2H)=)
      WRITE(6,2003)(HT(I),I=1,N)
      WRITE(6,2046)N
 2046 FORMAT(1H ,6X,31HCOMPARTMENT VOLUME (CUBIC FEET),/,6X,
     110H(V(I),I=1,,I2,2H)=)
```

```
      WRITE(6,2003)(V(I),I=1,N)
      WRITE(6,2048)
 2048 FORMAT(1H0,6X,36HCONTAINMENT AND CLEANUP SPECIFICATIONS,//,6X,55
     1HCSI=CONTAINMENT SYSTEM INJECTION FLOW IN CUBIC FEET/HR.,/,6X,65
     1HCSR1=CONTAINMENT SYSTEM NO.1 RECIRCULATING FLOW IN CUBIC FEET/HR,
     1,/,6X,61HHCSI,HCSR=HEIGHT THROUGH WHICH CONTAINMENT SYSTEM SPRAYS
     1FALL ,/,6X,59HDCSI,DCSR=DIAMETER OF CONTAINMENT SYSTEM SPRAY DROPL
     2ETS ,/,6X,66HCUTOV=CONCENTRATION OF I2 BELOW WHICH SPRAY REMOVAL I
     3S INEFFECTIVE ,/,6X,28HVCL=VOLUME OF COOLANT LIQUID ,/,
     16X,71HH0=RATIO OF IODINE IN SOLUTION IN WATER TO THAT IN VAPOR AT
     1EQUILIBRIUM,/,6X,37HECCI=EMERGENCY CORE COOLANT FLOW RATE,/,6X,
     153HDFPP,DFPOI,DFPI2=PUFF RELEASE DECONTAMINATION FACTORS,/,6X,
     163HXPUFF=FRACTION OF AIRBORNE MATERIAL RETAINED AFTER PUFF RELEASE
     1    ,/,6X,74HDPE,DPL=EFFECTIVE DIAMETER OF PARTICLES IN MICRONS AT
     1 EARLY AND LATE TIMES    )
      WRITE(6,2050)CSI,CSR1,HCSI,HCSR,DCSI,DCSR,CUTOV,VCL,H0,ECCI,
     1DFPP,DFPOI,DFPI2,CSR2,XPUFF,DPE,DPL
 2050 FORMAT(1H0,6X,4HCSI=,1PE14.8,3X,5HCSR1=,1PE14.8,3X,5HHCSI=,1PE14.8
     1,3X,5HHCSR=,1PE14.8,3X,5HDCSI=,1PE14.8//,6X,5HDCSR=,1PE14.8,3X,
     16HCUTOV=,1PE14.8,3X,4HVCL=,1PE14.8,3X,3HH0=,1PE14.8,3X,5HECCI=,
     11PE14.8,3X,/,6X,5HDFPP=,1PE13.7,3X,6HDFPOI=,1PE13.7,3X,
     16HDFPI2=,1PE13.7,3X,5HCSR2=,1PE13.7,3X,6HXPUFF=,1PE13.7,/,
     17X,4HDPE=,1PE13.7,3X,4HDPL=,1PE13.7  )
      WRITE(6,2052)
      NISO=NOI+NI2+NPAR
      WRITE(6,2054)((NAMES(J),(CFR(I,J),I=1,4)),J=1,NISO)
 2052 FORMAT(1H0,6X,63HCORE FRACTIONS RELEASED BY METHOD J IN ISOTOPE GR
     1OUP I CFR(J,I)//,12X,11HGAP RELEASE,4X,12HMELT RELEASE,4X,
     215HSTEAM EXPLOSION,1X,12HVAPORIZATION )
 2054 FORMAT(6X,A6,1X,1PE10.5,6X,1PE10.5,6X,1PE10.5,6X,1PE10.5)
C     INITIAL CONDITIONS OF COMPUTED VARIABLES
      VTOT=0.
C     VTOT=TOTAL CONTAINMENT VOLUME,FT3
      DO 8  I=1,N
      CGOI(I, 1)= 0.
      CGPI(I, 1)= 0.
      CSPI(I, 1)= 0.
      CSOI(I, 1)= 0.
      CGOI(I, 2)= 0.
      CGPI(I, 2)= 0.
      CSPI(I, 2)= 0.
      CSOI(I, 2)= 0.
      CMTP(I)=0.
      CMTI2(I)=0.
      CMTOI(I)=0.
      CMTI2(I)=0.
      CVTI2(I)=0.
      CATOI(I)=0.
      CBTOI(I)=0.
      CATP(I)=0.
      CBTP(I)=0.
      CGI2(I, 1)= 0.
      CSI2(I, 1)= 0.
      CGI2(I, 2)= 0.
      CSI2(I, 2)= 0.
      VTOT=VTOT+V(I)
      DO 8 J=1,10
C     SET I2 CONCENTRATIONS NON-ZERO FOR CUTOV TEST ONLY
      CMI2(I,J,1)=1.
      CAI2(I,J,1)=1.
      CBI2(I,J,1)=1.
      CAOI(I, J, 1)= 0.
      CBOI(I, J, 1)= 0.
      CBPI(I, J, 1)= 0.
      CAPI(I, J, 1)= 0.
      CMPI(I, J, 1)= 0.
      CMOI(I, J, 1)= 0.
      CAOI(I, J, 2)= 0.
      CBOI(I, J, 2)= 0.
      CBPI(I, J, 2)= 0.
      CAPI(I, J, 2)= 0.
      CMPI(I, J, 2)= 0.
      CMOI(I, J, 2)= 0.
      CAI2(I, J, 2)= 0.
      CBI2(I, J, 2)= 0.
      CMI2(I, J, 2)= 0.
    8 CONTINUE
      TEX=TEX1
      TX=0.
      DO 10 J=1,10
      TM3(J)=0.
      TM4(J)=TMR+FLOAT(J-1)*(TME-TMR)/10.
      TM1(J)= 0.
      TA1(J)= 0.
      TB1(J)= 0.
      TA3(J)=0.
      TB3(J)=0.
      TA4(J)=TVR1+FLOAT(J-1)*(TVR2-TVR1)/10.
      TB4(J)=TVR2+FLOAT(J-1)*(TVRE-TVR2)/10.
   10 CONTINUE
      TA= 0.
      TSA= 0.
      CMLKP=0.
```

```
      CSLKP=0.
      CGLKP=0.
      CMLKI2=0.
      CVLKP=0.
      CSLKI2=0.
      CGLKI2=0.
      CVLKI2=0.
      CMLKOI=0.
      CSLKOI=0.
      CGLKOI=0.
      CVLKOI=0.
      QKEQG1=0.
      TG1=0.
      QKEQG2=0.
      TG2=0.
      QKEQS1=0.
      TS1=0.
      QKEQS2=0.
      TS2=0.
      POOF=1.
C     BEGIN CALCULATIONS
      M=1
      TT=0.
C     SAVE DT
      DT1=DT
      NCHANG=1
    6 CONTINUE
      IF(TT.LT.TMR)DT=AMIN1(DT1,TMR)
      IF(TT.GE.TMR)DT=.05*(TMF-TMR)
      IF(TT.GE.TVR1)DT=.05*(TVR2-TVR1)
      IF(TT.GE.TVR1.AND.TT.LT.TMF)DT=.05*AMIN1(TMF-TMR,TVR2-TVR1)
      IF(TT.GE.TVR2)DT=.1*(TVRF-TVR2)
      IF(TT.GE.TVRF)DT=DT1
      IF(TT.GT.TJUMP1)DT=DT2
      IF(TT.LT.TPUFF.AND.TT+DT.GT.TPUFF)DT=TPUFF-TT+1.E-8
      IF(TT.LT.TCSI.AND.TT+DT.GT.TCSI)DT=TCSI-TT+1.E-8
      IF(TT.LT.TCSR1.AND.TT+DT.GT.TCSR1)DT=TCSR1-TT+1.E-8
      IF(TT.LT.TCSR2.AND.TT+DT.GT.TCSR2)DT=TCSR2-TT+1.E-8
      IF(TT.GT.TJUMP2)DT=TEND-TT
      TT=TT+DT
C     BYPASS PARAMETER RECOMPUTATION IF THERMODYNAMICS IS UNCHANGED.
C     CHANGES OCCUR AT TIMES TCHANG
      SWITCH=.FALSE.
C     IF(M.GT.1.AND.TT.LT.TCHANG(NCHANG))GO TO 1333
      NCHANG=NCHANG+1
      SWITCH=.TRUE.
C     COMPUTE P(N),T(N),DELTAT(N),VAP(J),ELI2(J),ELP(J) FOR THE PARTICU-
C     LAR TIME TT.
      NN=1
      DO 11 J=2,NDATA
      IF(ABS(TI(J)-TT).LT.ABS(TI(NN)-TT))NN=J
   11 CONTINUE
      NN=MAX0(2,MIN0(NN,NDATA-1))
      A1=TI(NN-1)
      A2=TI(NN)
      A3=TI(NN+1)
      DO 13 K=1,N
      P(K)=QINT(A1,A2,A3,TT,PI(K,NN-1),PI(K,NN),PI(K,NN+1))
      TMP(K)=QINT(A1,A2,A3,TT,TMY(K,NN-1),TMY(K,NN),TMY(K,NN+1))
      DELTAT(K)=QINT(A1,A2,A3,TT,DELTTI(K,NN-1),DELTTI(K,NN),DELTTI(K,
     1NN+1))
      VAP(K)=QINT(A1,A2,A3,TT,VAPI(K,NN-1),VAPI(K,NN),VAPI(K,NN+1))
      ELI2(K)=QINT(A1,A2,A3,TT,ELKI2(K,NN-1),ELKI2(K,NN),ELKI2(K,NN+1))
      ELP(K)=QINT(A1,A2,A3,TT,ELKP(K,NN-1),ELKP(K,NN),ELKP(K,NN+1))
      ELOI(K)=QINT(A1,A2,A3,TT,ELKOI(K,NN-1),ELKOI(K,NN),ELKOI(K,NN+1))
C     COMPUTE G(I,J),EFI2(I,J),EFI2(I,J) FOR ANY TIME TT
      DO 13 L=1,N
      G(K,L)=QINT(A1,A2,A3,TT,GI(K,L,NN-1),GI(K,L,NN),GI(K,L,NN+1))
      EFI2(K,L)=QINT(A1,A2,A3,TT,EI2(K,L,NN-1),EI2(K,L,NN),EI2(K,L,NN+1
     1))
      EFP(K,L)=QINT(A1,A2,A3,TT,EP(K,L,NN-1),EP(K,L,NN),EP(K,L,NN+1))
   13 CONTINUE
C1333 CONTINUE
C
C     COMPUTE GAS PARAMETERS,TRANSPORT COEFFICIENTS, DIMENSIONLESS NO.S
C
      DO 14 K=1,N
      CALL ERR(3,18HFRACAS DO 14
      IF(.NOT.SWITCH)GO TO 1102
      P(K)=P(K)+14.7
      TR=TMP(K)+460.                                                RANKINE
      DNST(K)=P(K)/(10.73*TR)
      DNST(K)=DNST(K)*VAP(K)*18.+(1.-VAP(K))*DNST(K)*29.
C     ABOVE IN  LBS/FT3
      TRIPS=TR*SQRT(TR)
      VST(K)=.003339*TRIPS/(TR+1224.2)
      VAIR(K)=.0414*(TR/492.)**.768
      IF(VAP(K).EQ.1.)GO TO 7
      IF(VAP(K).EQ.0.)GO TO 773
      PAS(K)=(1.+SQRT((VAIR(K)/VST(K))*SQRT(18./29.)))**2/4.5704
      PSA(K)=(1.+SQRT((VST(K)/VAIR(K))*SQRT(29./18.)))**2/3.6008
      RMOL=VAP(K)/(1.-VAP(K))
      VM(K)=VAIR(K)/(1.+PMOL*PAS(K))+VST(K)/(1.+PSA(K)/RMOL)
```

```
438*          GO TO 778
439*        7 VM(K)=VAIR(K)
440*          GO TO 778
441*      773 VM(K)=VST(K)
442*      778 CONTINUE
443*  C       ABOVE IN  LB/FT/HR
444*          WA(K)=0.7075+141.73/(TR/1.8)
445*          WS(K)=0.7075+454.72/(TR/1.8)
446*  C       DA(K)=.0020435*(TR/1.8)**1.5*.1961/((P(K)/14.7)*4.436**2*WA(K))
447*          DA(K)=.8432578E-5*TR1P5/(P(K)/14.7*WA(K))
448*  C       DS(K)=.0020201*((T(K)+460.)/1.8)**1.5*.2438/((P(K)/14.7)*3.901**2
449*  C      1*WS(K))
450*          DS(K)=.13401269E-4*TR1P5/( P(K)/14.7*WS(K))
451*  C       ABOVE DIFFUSIVITIES IN CM2/SEC
452*          DI2(K)=1./(VAP(K)/DS(K)+(1.-VAP(K))/DA(K))
453*          DI2(K)=DI2(K)*3.875
454*  C       DI2(K) IN FT2/HR
455*  C       SCHMIDT NO= VISCOSITY/(DENSITY*DIFFUS.)=SC(K)
456*          SC(K)=VM(K)/(DNST(K)*DI2(K))
457*  C       GRASHOF NO. FOR NATURAL CONVECTION,CKG=MT COEFF IN FT/HR
458*          GR(K)=4.17312E+8*HT(K)**3*DNST(K)**2*DELTAT(K)/(TR*VM(K)**2)
459*          GRSC=GR(K)*SC(K)
460*          IF(GRSC.LE.1.+9) CKG(K)=.59*SQRT(SQRT(GRSC))*DI2(K)/HT(K)
461*          IF(GRSC.GT.1.+9) CKG(K)=.13*CBRT(GRSC)*DI2(K)/HT(K)
462*   1102 CONTINUE
463*  C       COMPUTE SETTLING VELOCITIES FOR PARTICLES
464*  C       HAVE PARTICES FROM 13 SOURCES *GAP RELEASE,10 TIME INTERVALS OF
465*  C       THE MELT RELEASE + 2 EXPLOSIONS + 20 VAPORIZATION RELEASES
466*  C       DG,DM(10),DEX1,DEX2,DVA(10),DVB(10)
467*          DG=AMAX1(DPE+(DPL-DPE)*(TT/TD),DPL)
468*          DEX1=AMAX1(DPE+(DPL-DPE)*(TT-TEX1)/TD,DPL)
469*          IF(TT.LT.TEX1)  DEX1=0.
470*          SPRAY=0.
471*          IF(((TT.GT.TCSI.AND.TT.LT.TCSIE).OR.(TT.GT.TCSR1.AND.TT.LT.
472*         1TCSR1E).OR.(TT.GT.TCSR2.AND.TT.LT.TCSR2E)).AND.K.EQ.1)SPRAY=1.
473*          IF(TT.LT.TMR)GO TO 1555
474*          DO 15  ID=1,10
475*          DM(ID)=AMAX1(DPL,DPE+(DPL-DPE)*(TT-TM4(ID))/TD)
476*          IF(TT.LT.TM4(ID))DM(ID)=0.
477*  C       PARTICLE DIAMETERS ARE IN MICRONS
478*          SKG(K,ID)=(1.-SPRAY)*(.01557*DM(ID)**2/VM(K))*AF(K)/V(K)
479*       15 CONTINUE
480*     1555 CONTINUE
481*          SKGG(K)=(1.-SPRAY)*(.01557*DG**2/VM(K))*AF(K)/V(K)
482*          SKG1(K)=(1.-SPRAY)*(.01557*DEX1**2/VM(K))*AF(K)/V(K)
483*          IF(TT.LT.TMF)GO TO 3016
484*          DO 2015 ID = 1,10
485*          DVA(ID)=AMAX1(DPL,DPE+(DPL-DPE)*(TT-TVA(ID))/TD)
486*          IF(TT.LT.TVA(ID))DVA(ID)=0.
487*          DVB(ID)=AMAX1(DPL,DPE+(DPL-DPE)*(TT-TVB(ID))/TD)
488*          IF(TT.LT.TVB(ID))DVB(ID)=0.
489*          SKGA(K,ID)=(1.-SPRAY)*(.01557*DVA(ID)**2/VM(K))*AF(K)/V(K)
490*          SKGB(K,ID)=(1.-SPRAY)*(.01557*DVB(ID)**2/VM(K))*AF(K)/V(K)
491*   2015 CONTINUE
492*   3016 CONTINUE
493*  C       SKG=NATURAL DEPOSITION LAMBDA IN HR-1
494*
495*       14 CONTINUE
496*          IF(MANN.EQ.1) GO TO 8004
497*          IF(G(2,3).GT..01) MCOMP=2
498*          IF(G(1,3).GT..01) MCOMP=1
499*          IF(G(2,3).LE..01.AND.G(1,3).LE..01) GO TO 8004
500*          VEL=G(MCOMP,3)/23.7
501*  C       DRY WELL ANNULUS REYNOLDS NO.= REANN
502*          REANN=0.333*DNST(1)*VEL/VM(1)
503*          IF(REANN.LE.2100.) GO TO 8005
504*          IF(REANN.GT.2100.) GO TO 8002
505*   8005 EFP(MCOMP,3)=0.
506*          EFI2(MCOMP,3)=1.-EXP(-11160.*DI2(1)*(REANN*SC(1)*.0033)**.33/VEL)
507*          GO TO 8003
508*   8002 EFP(MCOMP,3)=.82
509*          EFI2(MCOMP,3)=1.-EXP(-156.*DI2(1)*REANN**.8*SC(1)**.33/VEL)
510*   8003 IF(EFI2(MCOMP,3).GT..99) EFI2(MCOMP,3)=.99
511*   8004 CONTINUE
```

DEPOSITION IN DRYWELL ANNULUS

```
512*  C       CARDS FOLLOWING TO 35420 TEST CHARCOAL FILTERS FOR OVERLOADING
513*  C       OF RADIOIODINE
514*          C4I2=CMTI2(4)*CFR(2,3)+CVTI2(4)*CFR(4,3)+CGI2(4,1)*CFR(1,3)
515*          FILCAP=.000007*G(5,4)*POOF/60.
516*          XSI2=C4I2-FILCAP
517*          IF(G(5,4).NE.0..AND.XSI2.GT.1.E-8) GO TO 35421
518*          GO TO 35420
519*   35421 POOF=0.
520*          WRITE(6,35422)
521*   35422 FORMAT(18H FILTER OVERHEATED)
522*   35420 CONTINUE
523*  C
524*  C
525*  C
526*  C       SPRAY LAMBDAS NEED TO BE COMPUTED NOW
527*  C
528*  C       PARTICULATE SPRAY LAMBDA IN COMPARTMENT 1
529*  C
530*  C       FIRST ESTABLISH SUM(FT/V(1)) AND IMPACT EFFICIENCY
```

CHARCOAL BED OVERHEAT CHECK + I2 and ORGANIC IODIDE LEAK ADJUST

```
531*          FI=AMAX1(0.,AMIN1(TT-TCSI-AMIN1(DT/2.,(TT-TCSI)/2.),TCSIE-TCSI))
532*         1*CSI
533*          FR1=AMAX1(0.,AMIN1(TT-TCSR1-AMIN1(DT/2.,(TT-TCSR1)/2.),TCSR1E-
534*         1TCSR1))*CSR1
535*          FR2=AMAX1(0.,AMIN1(TT-TCSR2-AMIN1(DT/2.,(TT-TCSR2)/2.),TCSR2E-
536*         1TCSR2))*CSR2
537*          FA=(FR1+FR2+FI)/V(1)
538*          IF(FA.GE.0..AND.FA.LT.0.002)E=-15.825*FA+.06
539*          IF(FA.GE.0.002.AND.FA.LT.0.193)E=.04625-SQRT(.08626+42.68*FA)/21.3
540*         14
541*          IF(FA.GT..0193)E=.0015
542*    C     THESE EFFICIENCIES ARE FOR GAP RELEASE ONLY
543*    C     IN THE EVENT THAT THE SPRAYS ARE WORKING AFTER ANY EXPLOSION AND
544*    C     SOURCE RELEASE S,THE EFFICIENCY OF REMOVAL MUST BE RECALCULATED
545*    C     FOR REMOVING S.THE REMOVAL EFFICIENCY IS EEX
546*    C
547*          FI=AMAX1(0.,AMIN1(TT-TEX1-AMIN1(DT/2.,(TT-TEX1)/2.),TCSIE-
548*         1TEX1))*CSI
549*          FI=AMAX1(0.,AMIN1(TT-TEX1-AMIN1(DT/2.,(TT-TEX1)/2.),TCSR1E-
550*         1TEX1))*CSR1
551*          F2=AMAX1(0.,AMIN1(TT-TEX1-AMIN1(DT/2.,(TT-TEX1)/2.),TCSR2E-
552*         1TEX1))*CSR2
553*          ES=F1+F2+FI
554*          ES=ES/V(1)
555*          IF(ES.GE.0..AND.ES.LT.0.002) EEX=-15.825*ES+.06
556*          IF(ES.GE..002.AND.ES.LT.0.0193) EEX=.04625-(.08626+42.68*ES)**.5/2
557*         11.34
558*          IF(ES.GT..0193)EEX=.0015
559*    C     CALCULATE EFF. FOR PARTICULATES FROM MELT RELEASE FOR EACH OF THE
560*    C     10 DIVISIONS, CALL IT EFM(J)
561*          IF(TT.LT.TMR)GO TO 1777
562*          DO 17  J=1,10
563*          AMDAMP(J)=0.
564*          IF(TT.LT.TM4(J))GO TO 17
565*          FMI=AMAX1(0.,AMIN1(TT-TM4(J)-AMIN1(DT/2.,(TT-TM4(J))/2.),
566*         1TCSIE-TM4(J)))*CSI
567*          FM1=AMAX1(0.,AMIN1(TT-TM4(J)-AMIN1(DT/2.,(TT-TM4(J))/2.),
568*         1TCSR1E-TM4(J)))*CSR1
569*          FM2=AMAX1(0.,AMIN1(TT-TM4(J)-AMIN1(DT/2.,(TT-TM4(J))/2.),
570*         1TCSR2E-TM4(J)))*CSR2
571*          ET=    FMI+FM1+FM2
572*          ET=ET/V(1)
573*          IF(ET.GE.0..AND.ET.LT.0.002)EFM(J)=-15.825*ET+.06
574*          IF(ET.GE..002.AND.ET.LT.0.0193) EFM(J)=.04625-(.08626+42.68*ET)**.
575*         15/21.34
576*          IF(ET.GT..0193) EFM(J)=.0015
577*    C     COMPUTE
578*          IF(TT.GT.TCSI.AND.TT.LT.TCSIE) AMDAMP(J)=AMDAMP(J)+1.5*HCSI*CSI*EF
579*         1M(J)/(DCSI*V(1)/30.48)
580*          IF(TT.GT.TCSR1.AND.TT.LT.TCSR1E) AMDAMP(J)=AMDAMP(J)+1.5*HCSR*CSR1
581*         1*EFM(J)/(DCSR*V(1)/30.48)
582*          IF(TT.GT.TCSR2.AND.TT.LT.TCSR2E) AMDAMP(J)=AMDAMP(J)+1.5*HCSR*CSR2
583*         1*EFM(J)/(DCSR*V(1)/30.48)
584*       17 CONTINUE
585*     1777 CONTINUE
586*    C     MELT RELEASE PARTICULATE LAMDAS ARE COMPLETE
587*    C     COMPUTE OTHER PARTICULATE LAMDAS NOW
588*          AMDAPG=0.
589*          AMDAPS=0.
590*          IF(TT.GT.TCSI.AND.TT.LT.TCSIE) AMDAPG=AMDAPG+1.5*HCSI*CSI*E/(DCSI*
591*         1V(1)/30.48)
592*          IF(TT.GT.TCSI.AND.TT.LT.TCSIE)AMDAPS=AMDAPS+1.5*HCSI*CSI*EEX/(DCS
593*         1I*V(1)/30.48)
594*          IF(TT.GT.TCSR1.AND.TT.LT.TCSR1E) AMDAPG=AMDAPG+1.5*HCSR*CSR1*E/(DC
595*         1SR*V(1)/30.48)
596*          IF(TT.GT.TCSR1.AND.TT.LT.TCSR1E) AMDAPS=AMDAPS+1.5*HCSR*CSR1*EEX/(
597*         1DCSR*V(1)/30.48)
598*          IF(TT.GT.TCSR2.AND.TT.LT.TCSR2E) AMDAPS=AMDAPS+1.5*HCSR*CSR2*EEX/(
599*         1DCSR*V(1)/30.48)
600*          IF(TT.GT.TCSR2.AND.TT.LT.TCSR2E) AMDAPG=AMDAPG+1.5*HCSR*CSR2*E/(DC
601*         1SR*V(1)/30.48)
602*    C     COMPUTE VAPORIZATION PARTICULATE REMOVAL BY SPRAYS
603*          DO 217 J=1,10
604*          AMDAPA(J)=0.
605*          AMDAPB(J)=0.
606*          IF(TT.LT.AMIN1(TCSI,TCSR1,TCSR2).OR.TT.GT.AMAX1(TCSIE,TCSR1E,
607*         1TCSR2E))GO TO 217
608*          IF(TT.LT.TA4(J))GO TO 217
609*          FAI=AMAX1(0.,AMIN1(TT-TA4(J)-AMIN1(DT/2.,(TT-TA4(J))/2.),
610*         1TCSIE -TA4(J)))*CSI
611*          FA1=AMAX1(0.,AMIN1(TT-TA4(J)-AMIN1(DT/2.,(TT-TA4(J))/2.),
612*         1TCSR1E-TA4(J)))*CSR1
613*          FA2=AMAX1(0.,AMIN1(TT-TA4(J)-AMIN1(DT/2.,(TT-TA4(J))/2.),
614*         1TCSR2E-TA4(J)))*CSR2
615*          FBI=AMAX1(0.,AMIN1(TT-TB4(J)-AMIN1(DT/2.,(TT-TB4(J))/2.),
616*         1TCSIE -TB4(J)))*CSI
617*          FB1=AMAX1(0.,AMIN1(TT-TB4(J)-AMIN1(DT/2.,(TT-TB4(J))/2.),
618*         1TCSR1E-TB4(J)))*CSR1
619*          FB2=AMAX1(0.,AMIN1(TT-TB4(J)-AMIN1(DT/2.,(TT-TB4(J))/2.),
620*         1TCSR2E-TB4(J)))*CSR2
621*          EA=(FAI+FA1+FA2)/V(1)
622*          EB=(FBI+FB1+FB2)/V(1)
623*          IF(EA.LT..0193)GO TO 4750
```

```
624*          EFA(J)=.0015
625*          GO TO 4850
626*     4750 IF (EA.LT..002)GO TO 4760
627*          EFA(J)=.04625-SQRT(.08626+42.68*EA)/21.34
628*          GO TO 4850
629*     4760 EFA(J)=-15.825*EA+.06
630*     4850 CONTINUE
631*          IF(EB.LT..0103)GO TO 5750
632*          EFB(J)=.0015
633*          GO TO 5850
634*     5750 IF (EB.LT..002)GO TO 5760
635*          EFB(J)=.04625-SQRT(.08626+42.68*EB)/21.34
636*          GO TO 5850
637*     5760 EFB(J)=-15.825*EB+.06
638*     5850 CONTINUE
639*          IF(TT.LT.TCSI.OR.TT.GT.TCSIE)GO TO 5854
640*          AMDAPA(J)=1.5*HCSI*CSI*EFA(J)/(DCSI*V(1)/30.48)
641*          AMDAPB(J)=1.5*HCSI*CSI*EFB(J)/(DCSI*V(1)/30.48)
642*     5854 IF(TT.LT.TCSR1.OR.TT.GT.TCSR1E)GO TO 5856
643*          AMDAPA(J)=AMDAPA(J)+1.5*HCSR*CSR1*EFA(J)/(DCSR*V(1)/30.48)
644*          AMDAPB(J)=AMDAPB(J)+1.5*HCSR*CSR1*EFB(J)/(DCSR*V(1)/30.48)
645*     5856 IF(TT.LT.TCSR2.OR.TT.GT.TCSR2E)GO TO 217
646*          AMDAPA(J)=AMDAPA(J)+1.5*HCSR*CSR2*EFA(J)/(DCSR*V(1)/30.48)
647*          AMDAPB(J)=AMDAPB(J)+1.5*HCSR*CSR2*EFB(J)/(DCSR*V(1)/30.48)
648*      217 CONTINUE
649*     C    ALL PARTICULATE SPRAY LAMDAS COMPLETE
650*     C
651*     C    IODINE-I2- REMOVAL BY SPRAY CALCULATED NOW
652*     C
653*     C    SPRAY LAMBDAS, COMPUTED NOW FOR I2(AMDAIG+AMDAIS+AMDAIM(K))
654*     C
655*     C    COMPUTE TERMINAL VELOCITY OF SPRAY DROPS
656*     C
657*          FDREI=(4./3.)*62.4*DNST(1)*(DCSI/30.48)**3*.17312000./VM(1)**2
658*          FDRER=FDREI*(DCSR/DCSI)**3
659*          IF(FDREI.LT.10700.) REI=(FDREI/15.71)**.7027
660*          IF(FDREI.GE.10700.) REI=(FDREI/6.477)**.6215
661*          IF(FDRER.LT.10700.) RER=(FDRER/15.71)**.7027
662*          IF(FDRER.GE.10700.) RER=(FDRER/6.477)**.6215
663*          UTI=REI*VM(1)/(DNST(1)*DCSI/30.48)
664*          UTR=RER*VM(1)/(DNST(1)*DCSR/30.48)
665*     C    UTI,UTR IN FT/HR
666*     C    MASS XFR COEFF TO THESE DROPS COMPUTED BELOW (GGI,GGR) IN FT/HR
667*          GGI=DI2(1)*(2.+.6*REI**.5*SC(1)**.33)/(DCSI/30.48)
668*          GGR=DI2(1)*(2.+.6*RER**.5*SC(1)**.33)/(DCSR/30.48)
669*     C    GAS PHASE COMPLETE,NOW COMPUTE LIQUID PHASE MASS XFR COEFF.GLI,GLR
670*     C    UL=LIQUID VISCOSITY,CP, DL=DIFFUSIVITY OF I2 IN H2O,FT2/HR
671*          T1=(TMP(1)+460.)/1.8
672*          UL=100./(2.1482*((T1-281.6)+(8078.4+(T1-281.6)**2)**.5)-120.)
673*          DL=1.5137E-07*(T1/UL)
674*          GLI=6.58*DL/(DCSI/30.48)
675*          GLR=6.58*DL/(DCSR/30.48)
676*     C    STAGNANT DROP MODEL USED,EFFICIENCY=1-EXP(-6.*KGOT/S(H+KG/KL))
677*          ECSI=1.-EXP(-6.*GGI*(HCSI/UTI)/((DCSI/30.48)*(HO+GGI/GLI)))
678*          ECSR=1.-EXP(-6.*GGR*(HCSR/UTR)/((DCSR/30.48)*(HO+GGR/GLR)))
679*     C    SPRAY LAMBDAS=F*HO*E/V,IF C/V(1).GT.C(EMITTED)/(SUM V(I))*CUTOFF
680*     C    EQUILIBRIUM LAMBDAS USED AT LOWER CONC.
681*     C    INSERT A SPECIAL DECK TO HANDLE EQUILIBRIUM CALCULATIONS  FOR EACH
682*     C    TYPE OF SPRAY
683*          COG=CGI2(1,1)*VTOT/V(1)
684*          COS=CSI2(1,1)*VTOT/V(1)
685*          DO 16 J=1,10
686*          COM(J)=CMI2(1,J,1)*VTOT/V(1)/.1
687*          COB(J)=CBI2(1,J,1)*VTOT/V(1)/(.07528*EXP(-.1*FLOAT(J-1)))
688*          COA(J)=CAI2(1,J,1)*VTOT/V(1)/(.07528*EXP(-.1*FLOAT(J-1)))
689*       16 CONTINUE
690*          OKG=0.
691*          OKS=0.
692*          IF(COG.GT.CUTOV      ) OKG=1.
693*          IF(COS.GT.CUTOV      ) OKS=1.
694*          DO 19 J=1,10
695*          OKM(J)=0.
696*          OKA(J)=0.
697*          OKB(J)=0.
698*          IF(COM(J).GT.CUTOV)OKM(J)=1.
699*          IF(COA(J).GT.CUTOV)OKA(J)=1.
700*          IF(COB(J).GT.CUTOV)OKB(J)=1.
701*       19 CONTINUE
702*          IF(TT.LT.TCSIE.AND.TT.GE.TCSI) OKCSI=1.
703*          IF(TT.GE.TCSIE.OR.TT.LT.TCSI)  OKCSI=0.
704*          IF(TT.LT.TCSR1E.AND.TT.GE.TCSR1) OKCSR1=1.
705*          IF(TT.GE.TCSR1E.OR.TT.LT.TCSR1) OKCSR1=0.
706*          IF(TT.LT.TCSR2E.AND.TT.GE.TCSR2) OKCSR2=1.
707*          IF(TT.GE.TCSR2E.OR.TT.LT.TCSR2) OKCSR2=0.
708*          AMDAIG=CSI*HO*ECSI*OKG*OKCSI/V(1)+CSR1*HO*ECSR*OKG*OKCSR1/V(1)+HO*
709*         1CSR2*ECSR*OKG*OKCSR2/V(1)
710*          AMDAIS=(HO*OKS/V(1))*(CSI*ECSI*OKCSI+CSR1*ECSR*OKCSR1+CSR2*ECSR*OK
711*         1CSR2)
712*          DO 20 J=1,10
713*          AMDAIM(J)=(HO*OKM(J)/V(1))*(CSI*ECSI*OKCSI+CSR1*ECSR*OKCSR1+CSR2*
714*         1ECSR*OKCSR2)
715*          AMDAIA(J)=(HO*OKA(J)/V(1))*(CSI*ECSI*OKCSI+CSR1*ECSR*OKCSR1+CSR2*
716*         1ECSR*OKCSR2)
```

```
717*          AMDAIB(J)=(HO*OKB(J)/V(1))*(CSI*ECSI*OKCSI+CSR1*ECSR*OKCSR1+CSR2*
718*         1ECSR*OKCSR2)
719*       20 CONTINUE
720*    C     SUMP LIQUID VOL. AND I2 CONC. IN THE LIQ.CONTROL EQUILIBRIUM*VSUMP
721*    C     EQ  ECCI+VCL+CSI*(TT-TCSI)
722*          IF(TT.GE.TECCI) OKECCI=1.
723*          IF(TT.LT.TECCI) OKECCI=0.
724*          IF(TT.GT.TCSIE) OKCSIE=1.
725*          IF(TT.LE.TCSIE) OKCSIE=0.
726*          VSUMP=VCL+ECCI*OKECCI+(TCSIE-TCSI)*CSI*OKCSIE+(TT-TCSI)*CSI*OKCSI
727*    C     VSUMP=TOTAL SUMP LIQUID*FT3
728*    C     CALCULATION OF LAMDAS FOR EQUILIBRIUM PROCEED BELOW. THESE ARE
729*    C     ELAMG*ELAMS*ELAMM(I).EACH SPRAY TYPE REQUIRES A SPECIAL DECK TO
730*    C     COMPUTE THESE. FOR THE CASE OF NO SPRAY, USE HB03 DECK.
731*    C
732*    C     BORIC ACID*HB03 DECK FOR COMPUTING EQUILIBRIUM CONCENTRATIONS
733*    C     DESIGNATE TG1 AND TG2 AS  TIME POINTS WHEN CGI2(1*K) EXCEEDS AND
734*    C     IS LT THE  EQUIL. CUTOFF*CUTOV=.01 FOR ALL SPRAYS EXCEPT THIOSULFA
735*    C     TE*
736*          IF(COG.GT.CUTOV)GO TO 6542
737*          IF(.NOT.((TT.GE.TCSI.AND.TT.LE.TCSIE).OR.(TT.GE.TCSR1.AND.TT.LE.
738*         2TCSR1E).OR.(TT.GE.TCSR2.AND.TT.LE.TCSR2E))) GO TO 6542
739*          TA=TA+DT
740*          ELAMG=ELAM(TA)
741*          GO TO 6545
742*     6542 CONTINUE
743*          ELAMG=0.
744*          TA=0.
745*     6545 CONTINUE
746*    C     ELAMG IN  1/HR
747*          IF(COS.GT.CUTOV.OR.TT.LT.TEXI)GO TO 6583
748*          IF(.NOT.((TT.GE.TCSI.AND.TT.LE.TCSIE).OR.(TT.GE.TCSR1.AND.TT.LE.
749*         2TCSR1E).OR.(TT.GE.TCSR2.AND.TT.LE.TCSR2E))) GO TO 6583
750*          TSA=TSA+DT
751*          ELAMS=ELAM(TSA)
752*          GO TO 6585
753*     6583 CONTINUE
754*          ELAMS=0.
755*          TSA=0.
756*     6585 CONTINUE
757*    C     ELAMS IN HR-1
758*          IF(TT.LT.TMR)GO TO 8001
759*          DO 8000 J=1*10
760*          IF(COM(J).GT.CUTOV.OR.TT.LT.TM4(J))GO TO 7123
761*          IF(.NOT.((TT.GE.TCSI.AND.TT.LE.TCSIE).OR.(TT.GE.TCSR1.AND.TT.LE.
762*         2TCSR1E).OR.(TT.GE.TCSR2.AND.TT.LE.TCSR2E))) GO TO 7123
763*          TM1(J)=TM1(J)+DT
764*          ELAMM(J)=ELAM(TM1(J))
765*          GO TO 8000
766*     7123 CONTINUE
767*          ELAMM(J)=0.
768*          TM1(J)=0.
769*     8000 CONTINUE
770*     8001 CONTINUE
771*          IF(TT.LT.TVR1)GO TO 9001
772*          DO 9000 J=1*10
773*          IF(COA(J).GT.CUTOV.OR.TT.LT.TA4(J))GO TO 3644
774*          IF(.NOT.((TT.GE.TCSI.AND.TT.LE.TCSIE).OR.(TT.GE.TCSR1.AND.TT.LE.
775*         2TCSR1E).OR.(TT.GE.TCSR2.AND.TT.LE.TCSR2E))) GO TO 3644
776*          TA1(J)=TA1(J)+DT
777*          ELAMA(J)=ELAM(TA1(J))
778*          GO TO 9000
779*     3644 CONTINUE
780*          ELAMA(J)=0.
781*          TA1(J)=0.
782*     9000 CONTINUE
783*     9001 CONTINUE
784*          IF(TT.LT.TVR2)GO TO 5001
785*          DO 5000 J=1*10
786*          IF(COB(J).GT.CUTOV.OR.TT.LT.TB4(J))GO TO 4821
787*          IF(.NOT.((TT.GE.TCSI.AND.TT.LE.TCSIE).OR.(TT.GE.TCSR1.AND.TT.LE.
788*         2TCSR1E).OR.(TT.GE.TCSR2.AND.TT.LE.TCSR2E))) GO TO 4821
789*          TB1(J)=TB1(J)+DT
790*          ELAMB(J)=ELAM(TB1(J))
791*          GO TO 5000
792*     4821 CONTINUE
793*          ELAMB(J)=0.
794*          TB1(J)=0.
795*     5000 CONTINUE
796*     5001 CONTINUE
797*    C     ELAMM(J) IN HR**-1
798*    C     AT THIS POINT EQUILIBRIUM LAMBDAS ARE COMPLETE
799*    C
800*    C     DIFFERENTIAL EQNS (AS DIFFERENCE EQNS) ARE TO BE SOLVED NOW
801*    C
802*    C     ESTABLISH RELEASE INPUTS AS INITIAL CONCENTRATIONS FOR EXPLOSION
803*    C     RELEASE AND MELT RELEASE.FOR GAP RELEASE, ICS ARE ESTABLISHED
804*    C     INCLUDE VAPOR RELEASES
805*    C     EXPLOSION RELEASE
806*          IF(TT.GE.TEXI.AND.TX.EQ.0.)TX=TT
807*          IF(TX.EQ.TT) OKICS=1.
808*          IF(TX.NE.TT) OKICS=0.
809*    C     MELT RELEASE
```

```
      DO 23 J=1,10
      IF(TT.GE.TM4(J).AND.TM3(J).EQ.0.) TM3(J)=TT
      IF(TM3(J).EQ.TT) OKICM(J)=.1
      IF(TM3(J).NE.TT) OKICM(J)=0.
      IF(TT.GE.TA4(J).AND.TA3(J).EQ.0.) TA3(J)=TT
      IF(TT.GE.TB4(J).AND.TB3(J).EQ.0.) TB3(J)=TT
      IF( TA3(J).EQ.TT) OKICA(J)=.0752*EXP(-.1*FLOAT(J-1))
      IF( TB3(J).EQ.TT) OKICB(J)=.2045*EXP(-.1*FLOAT(J+9))
      IF( TA3(J).NE.TT) OKICA(J)=0.
      IF( TB3(J).NE.TT) OKICB(J)=0.
   23 CONTINUE
C
C     WRITE DIFFERENCE EQNS FOR GAP P  CONC.  IN COMPARTMENT 1 TO N
      CALL ERR(3,13HCORRAL S.N. 23     )
      DO 190 IMAT=1,3
C     SET ALCEMY FIXED INPUT VARIABLES
      NT=1
      II=2*N
      LL=0
      GO TO(30,60,120),IMAT
   30 CONTINUE
C     SET OFF DIAGONAL MATRIX ELEMENTS FOR P BRANCH
      DO 24 ICOM=1,N
      H(ICOM+N,ICOM)=ELP(ICOM)
      DO 24 JCOM=1,N
   24 H(JCOM,ICOM)=G(ICOM,JCOM)*(1.-EFP(ICOM,JCOM))/V(ICOM)
      DO 50 IREL=1,5
      GO TO (31,41,51,1061,1071),IREL
C     PRECEDING BRANCH IS TO GAP RELEASE,MELT RELEASE,STEAM EXPLOSION,
C     VAPORIZATION RELEASE  PHASE A, VAPORIZATION RELEASE PHASE B
   31 CONTINUE
C     RELEASE IN PARTICULATES BRANCH

      T(1)=DT
      DO 37 ICOM=1,N
      H(ICOM,ICOM)=0.
      BETAPG(ICOM)=SKGG(ICOM)+ELP(ICOM)+FDP(ICOM)
      IF(ICOM.EQ.1)BETAPG(ICOM)=BETAPG(ICOM)+AMDAPG
      F(ICOM)=CGP(ICOM,1)
      F(ICOM+N)=0.
      IF(M.EQ.1.AND.ICOM.EQ.1) F(ICOM)=1.
      DO 39 JCOM=1,N
   39 H(ICOM,ICOM)=H(ICOM,ICOM)-G(ICOM,JCOM)/V(ICOM)
   37 H(ICOM,ICOM)=H(ICOM,ICOM)-BETAPG(ICOM)
      CALL ALCEMY
      DO 38 ICOM=1,N
      CGLKP=CGLKP+FT(ICOM+N,1)
   38 CGP(ICOM,2)=FT(ICOM,1)
C     GAP RELEASE PARTICULATES COMPLETE FOR PRESENT TIME STEP.
      GO TO 50
   41 CONTINUE
C     IF MELT RELEASE HAS NOT STARTED, BYPASS
      IF(TT.LT.TMR)GO TO 50
      DO 45 JREL=1,10
      IF(TT.LT.TM4(JREL))GO TO 45
      T(1)=AMIN1(DT,TT-TM4(JREL))
      DO 47 ICOM=1,N
      F(ICOM)=CMP(ICOM,JREL,1)
      IF(ICOM.EQ.1.AND.OKICM(JREL).NE.0.) F(ICOM)=OKICM(JREL)
      F(ICOM+N)=0.
      H(ICOM,ICOM)=0.
      BETAPM(ICOM,JREL)=SKG(ICOM,JREL)+ELP(ICOM)+FDP(ICOM)
      IF(ICOM.EQ.1)BETAPM(ICOM,JREL)=BETAPM(ICOM,JREL)+AMDAMP(JREL)
      DO 49 JCOM=1,N
   49 H(ICOM,ICOM)=H(ICOM,ICOM)-G(ICOM,JCOM)/V(ICOM)
   47 H(ICOM,ICOM)=H(ICOM,ICOM)-BETAPM(ICOM,JREL)
      CALL ALCEMY
      DO 48 ICOM=1,N
      CMLKP=CMLKP+FT(ICOM+N,1)
   48 CMP(ICOM,JREL,2)=FT(ICOM,1)
   45 CONTINUE
C     MELT RELEASE PARTICULATES COMPLETE FOR PRESENT TIME STEP
      GO TO 50
   51 CONTINUE                                                    STEAM EX
C      IF STEAM EXPLOSION HAS NOT OCCURRED,BYPASS
      IF(TT.LT.TEX1)GO TO 50
      T(1)=AMIN1(DT,TT-TEX1)
      DO 57 ICOM=1,N
      H(ICOM,ICOM)=0.
      F(ICOM)=CSP(ICOM,1)
      F(ICOM+N)=0.
      IF(ICOM.EQ.1.AND.OKICS.NE.0.)F(ICOM)=OKICS
      BETAPS(ICOM)=SKG1(ICOM)+ELP(ICOM)+FDP(ICOM)
      IF(ICOM.EQ.1)BETAPS(ICOM)=BETAPS(ICOM)+AMDAPS
      DO 59 JCOM=1,N
   59 H(ICOM,ICOM)=H(ICOM,ICOM)-G(ICOM,JCOM)/V(ICOM)
   57 H(ICOM,ICOM)=H(ICOM,ICOM)-BETAPS(ICOM)
      CALL ALCEMY
      IF(MOD(M-1,10).NE.0)GO TO 5086
 5086 CONTINUE
C     END OF AD HOC WRITE
      DO 58 ICOM=1,N
      CSLKP=CSLKP+FT(ICOM+N,1)
```

```
      58 CSP(ICOM,2)=FT(ICOM,1)
C     STEAM EXPLOSION PARTICULATES COMPLETE FOR PRESENT TIME STEP
      GO TO 50
 1061 CONTINUE                                                        VAPREL A
C     IF VAPORIZATION HAS NOT STARTED, BYPASS.
      IF(TT.LT.TVR1)GO TO 50
      DO 1065 JREL=1,10
      IF(TT.LT.TVA(JREL))GO TO 1065
      T(1)=AMIN1(DT,TT-TVA(JREL))
      DO 1067 ICOM=1,N
      F(ICOM)=CAP(ICOM,JREL,1)
      IF(ICOM.EQ.1.AND.OKICA(JREL).NE.0.)F(ICOM)=OKICA(JREL)
      F(ICOM+N)=0.
      H(ICOM,ICOM)=0.
      BTAPVA(ICOM,JREL)=SKGA(ICOM,JREL)+ELP(ICOM)+FDP(ICOM)
      IF(ICOM.EQ.1)BTAPVA(ICOM,JREL)=BTAPVA(ICOM,JREL)+AMDAP(JREL)
      DO 1069 JCOM=1,N
 1069 H(ICOM,ICOM)=H(ICOM,ICOM)-G(ICOM,JCOM)/V(ICOM)
 1067 H(ICOM,ICOM)=H(ICOM,ICOM)-BTAPVA(ICOM,JREL)
      CALL ALCEMY
      DO 1068 ICOM=1,N
      CVLKP=CVLKP+FT(ICOM+N,1)
 1068 CAP(ICOM,JREL,2)=FT(ICOM,1)
 1065 CONTINUE
C     PHASE A VAPORIZATION RELEASE PARTICULATES COMPLETE FOR THIS TIME STEP
      GO TO 50
 1071 CONTINUE                                                        VAPREL B
C     IF VAPORIZATION RELEASE PHASE B HAS NOT STARTED, BYPASS
      IF(TT.LT.TVR2)GO TO 50
      DO 1075 JREL=1,10
      IF(TT.LT.TVB(JREL))GO TO 1075
      T(1)=AMIN1(DT,TT-TVB(JREL))
      DO 1077 ICOM=1,N
      F(ICOM)=CBP(ICOM,JREL,1)
      IF(ICOM.EQ.1.AND.OKICB(JREL).NE.0.)F(ICOM)=OKICB(JREL)
      F(ICOM+N)=0.
      H(ICOM,ICOM)=0.
      BTAPVB(ICOM,JREL)=SKGB(ICOM,JREL)+ELP(ICOM)+FDP(ICOM)
      IF(ICOM.EQ.1)BTAPVB(ICOM,JREL)=BTAPVB(ICOM,JREL)+AMDAP(JREL)
      DO 1079 JCOM=1,N
 1079 H(ICOM,ICOM)=H(ICOM,ICOM)-G(ICOM,JCOM)/V(ICOM)
 1077 H(ICOM,ICOM)=H(ICOM,ICOM)-BTAPVB(ICOM,JREL)
      CALL ALCEMY
      DO 1078 ICOM=1,N
      CVLKP=CVLKP+FT(ICOM+N,1)
 1078 CBP(ICOM,JREL,2)=FT(ICOM,1)
 1075 CONTINUE
C     PHASE B VAPORIZATION RELEASE COMPLETED FOR THIS TIME STEP.
   50 CONTINUE
      GO TO 190
   60 CONTINUE                                                        ORGANICI
C     SET OFF DIAGONAL MATRIX ELEMENTS FOR ORGANIC IODIDE BRANCH
      DO 600 ICOM=1,N
      H(ICOM+N,ICOM)=ELOI(ICOM)
      DO 600 JCOM=1,N
  600 H(JCOM,ICOM)=G(ICOM,JCOM)/V(ICOM)
      GO 80 IREL=1,5
      GO TO(61,71,81,91,101),IREL
C     FIVE WAY BRANCH IS TO EXPLOSION, GAP, MELT, PHASE A VAPORIZATION,
C     AND PHASE B VAPORIZATION
   61 CONTINUE                                                        EXPLODE
C      IF STEAM EXPLOSION HAS NOT OCCURRED, BYPASS
      IF(TT.LT.TEX1)GO TO 80
      T(1)=AMIN1(DT,TT-TEX1)
      DO 67 ICOM=1,N
      H(ICOM,ICOM)=0.
      F(ICOM)=CSOI(ICOM,1)
      F(ICOM+N)=0.
      IF(ICOM.EQ.1.AND.OKICS.NE.0.)F(ICOM)=OKICS
      DO 69 JCOM=1,N
   69 H(ICOM,ICOM)=H(ICOM,ICOM)-G(ICOM,JCOM)/V(ICOM)
   67 H(ICOM,ICOM)=H(ICOM,ICOM)-ELOI(ICOM)
      CALL ALCEMY
      DO 68 ICOM=1,N
      CSLKOI=CSLKOI+FT(ICOM+N,1)
   68 CSOI(ICOM,2)=FT(ICOM,1)
C     ORGANIC IODIDE EXPLOSION RELEASE COMPLETED FOR THIS TIME STEP
      GO TO 80
   71 CONTINUE                                                        GAP REL
      T(1)=DT
      DO 77 ICOM=1,N
      H(ICOM,ICOM)=0.
      F(ICOM)=CGOI(ICOM,1)
      F(ICOM+N)=0.
      IF(ICOM.EQ.1.AND.M.EQ.1) F(ICOM)=1.
      DO 79 JCOM=1,N
   79 H(ICOM,ICOM)=H(ICOM,ICOM)-G(ICOM,JCOM)/V(ICOM)
   77 H(ICOM,ICOM)=H(ICOM,ICOM)-ELOI(ICOM)
      CALL ALCEMY
      DO 78 ICOM=1,N
      CGLKOI=CGLKOI+FT(ICOM+N,1)
   78 CGOI(ICOM,2)=FT(ICOM,1)
C     ORGANIC IODIDE RELEASE DONE FOR THIS TIME STEP
```

```
      GO TO 80
   81 CONTINUE                                                    MELT REL
C      IF MELT RELEASE HAS NOT STARTED, BYPASS
      IF(TT.LT.TMP)GO TO 80
      DO 85 JREL=1,10
      IF(TT.LT.TM4(JREL))GO TO 85
      T(1)=AMIN1(DT,TT-TM4(JREL))
      DO 87 ICOM=1,N
      H(ICOM,ICOM)=0.
      F(ICOM)=CMOI(ICOM,JREL,1)
      F(ICOM+N)=0.
      IF(ICOM.EQ.1.AND.OKICM(JREL).NE.0.) F(ICOM)=OKICM(JREL)
      DO 89 JCOM=1,N
   89 H(ICOM,ICOM)=H(ICOM,ICOM)-G(ICOM,JCOM)/V(ICOM)
   87 H(ICOM,ICOM)=H(ICOM,ICOM)-ELOI(ICOM)
      CALL ALCEMY
      DO 88 ICOM=1,N
      CMLKOI=CMLKOI+FT(ICOM+N,1)
   88 CMOI(ICOM,JREL,2)=FT(ICOM,1)
   85 CONTINUE
C     ORGANIC IODIDE MELT RELEASE COMPLETED FOR THIS TIME STEP
      GO TO 80
   91 CONTINUE                                                    VAPREL A
C      IF VAPOR RELEASE HAS NOT STARTED, BYPASS
      IF(TT.LT.TVR1)GO TO 80
      DO 95 JREL=1,10
      IF(TT.LT.TA4(JREL))GO TO 95
      T(1)=AMIN1(DT,TT-TA4(JREL))
      DO 97 ICOM=1,N
      H(ICOM,ICOM)=0.
      F(ICOM)=CAOI(ICOM,JREL,1)
      F(ICOM+N)=0.
      IF(ICOM.EQ.1.AND.OKICA(JREL).NE.0.)F(ICOM)=OKICA(JREL)
      DO 99 JCOM=1,N
   99 H(ICOM,ICOM)=H(ICOM,ICOM)-G(ICOM,JCOM)/V(ICOM)
   97 H(ICOM,ICOM)=H(ICOM,ICOM)-ELOI(ICOM)
      CALL ALCEMY
      DO 98 ICOM=1,N
      CVLKOI=CVLKOI+FT(ICOM+N,1)
   98 CAOI(ICOM,JREL,2)=FT(ICOM,1)
   95 CONTINUE
C     ORGANIC IODIDE VAPOR RELEASE PHASE A COMPLETED FOR THIS TIME STEP
      GO TO 80
  101 CONTINUE                                                    VAPREL B
C     IF PHASE B VAPOR RELEASE HAS NOT STARTED, BYPASS
      IF(TT.LT.TVR2)GO TO 80
      DO 105 JREL=1,10
      IF(TT.LT.TB4(JREL))GO TO 105
      T(1)=AMIN1(DT,TT-TB4(JREL))
      DO 107 ICOM=1,N
      H(ICOM,ICOM)=0.
      F(ICOM)=CBOI(ICOM,JREL,1)
      F(ICOM+N)=0.
      IF(ICOM.EQ.1.AND.OKICB(JREL).NE.0.)F(ICOM)=OKICB(JREL)
      DO 109 JCOM=1,N
  109 H(ICOM,ICOM)=H(ICOM,ICOM)-G(ICOM,JCOM)/V(ICOM)
  107 H(ICOM,ICOM)=H(ICOM,ICOM)-ELOI(ICOM)
      CALL ALCEMY
      DO 108 ICOM=1,N
      CVLKOI=CVLKOI+FT(ICOM+N,1)
  108 CBOI(ICOM,JREL,2)=FT(ICOM,1)
  105 CONTINUE
C     ORGANIC IODIDE VAPOR RELEASE PHASE B COMPLETED FOR THIS TIME STEP.
   80 CONTINUE
      GO TO 190
  120 CONTINUE                                                    I2BRANCH
C          NATURAL CONVECTION LAMBDA WILL BE ASSUMED ZERO IN ANY COMPART-
C          MENT WHERE  CI2/V.LT.CUTOV/VTOT.
      DO 1037 I=1,N
      KSPRAY=0
      IF(I.EQ.1.AND.((TT.GT.TCSR1.AND.TT.LT.TCSR1E).OR.(TT.GT.TCSR2.AND
     *.TT.LT.TCSR2E).OR.(TT.GT.TCS1.AND.TT.LT.TCS1E)))KSPRAY=1
      OKNCG(I)=FLOAT(1-KSPRAY)
      OKNCS(I)=FLOAT(1-KSPRAY)
      IF(CSI2(I,1)/V(I).LT.CUTOV/VTOT)OKNCS(I)=0.
      IF(CGI2(I,1)/V(I).LT.CUTOV/VTOT)OKNCG(I)=0.
      DO 1037 J=1,10
      SCALE=.07528*EXP(-.1*FLOAT(J-1))
      OKNCA(I,J)=FLOAT(1-KSPRAY)
      OKNCB(I,J)=FLOAT(1-KSPRAY)
      OKNCM(I,J)=FLOAT(1-KSPRAY)
      IF(CAI2(I,J,1)/V(I)/SCALE.LT.CUTOV/VTOT)OKNCA(I,J)=0.
      IF(CBI2(I,J,1)/V(I)/SCALE.LT.CUTOV/VTOT)OKNCB(I,J)=0.
      IF(CMI2(I,J,1)/V(I)/.1.LT.CUTOV/VTOT)OKNCM(I,J)=0.
 1037 CONTINUE
C     SET OFF DIAGONAL MATRIX ELEMENTS FOR I2 BRANCH
      DO 1200 ICOM=1,N
      H(ICOM+N,ICOM)=ELI2(ICOM)
      DO 1200 JCOM=1,N
 1200 H(JCOM,ICOM)=G(ICOM,JCOM)*(1.-EFI2(ICOM,JCOM))/V(ICOM)
      DO 170 IREL=1,5
      GO TO(121,131,141,151,161),IREL
C     FIVE WAY BRANCH IS TO GAP RELEASE,STEAM EXPLOSION,MELT RELEASE,
```

```
C     VAPORIZATION PHASE A, AND VAPORIZATION PHASE B.
  121 CONTINUE                                                          GAP REL
      T(1)=DT
      DO 127 ICOM=1,N
      H(ICOM,ICOM)=0.
      F(ICOM)=CGI2(ICOM,1)
      F(ICOM+N)=0.
      IF(M.EQ.1) F(ICOM)=DKRON(ICOM,1)
      BTAI2G(ICOM)=ELI2(ICOM)+FDI2(ICOM)+DKNCG(ICOM)*CKG(ICOM)*(AW(ICOM
     *)+AF(ICOM))/V(ICOM)

      IF(ICOM.EQ.1)BTAI2G(ICOM)=BTAI2G(ICOM)+AMDAIG+ELAMG
      DO 129 JCOM=1,N
  129 H(ICOM,ICOM)=H(ICOM,ICOM)-G(ICOM,JCOM)/V(ICOM)
  127 H(ICOM,ICOM)=H(ICOM,ICOM)-BTAI2G(ICOM)
      CALL ALGEMY
      DO 128 ICOM=1,N
      CGLKI2=CGLKI2+FT(ICOM+N,1)
  128 CGI2(ICOM,2)=FT(ICOM,1)
C     I2 GAP RELEASE COMPLETED FOR THIS TIME STEP
      GO TO 170
  131 CONTINUE                                                          ST EXPLO
C     IF STEAM EXPLOSION HAS NOT OCCURRED,BYPASS
      IF(TT.LT.TEX1)GO TO 170
      T(1)=AMIN1(DT,TT-TEX1)
      DO 137 ICOM=1,N
      H(ICOM,ICOM)=0.
      F(ICOM)=CSI2(ICOM,1)
      F(ICOM+N)=0.
      IF(DKICS.GT.0.)F(ICOM)=DKRON(ICOM,1)
      BTAI2S(ICOM)=ELI2(ICOM)+FDI2(ICOM)
      IF(DKNCS(ICOM).NE.0.)BTAI2S(ICOM)=BTAI2S(ICOM)+CKG(ICOM)
     1*(AW(ICOM)+AF(ICOM))/V(ICOM)
      IF(ICOM.EQ.1)BTAI2S(ICOM)=BTAI2S(ICOM)+AMDAIS+ELAMS
      DO 139 JCOM=1,N
  139 H(ICOM,ICOM)=H(ICOM,ICOM)-G(ICOM,JCOM)/V(ICOM)
  137 H(ICOM,ICOM)=H(ICOM,ICOM)-BTAI2S(ICOM)
      CALL ALGEMY
      DO 138 ICOM=1,N
      CSLKI2=CSLKI2+FT(ICOM+N,1)
  138 CSI2(ICOM,2)=FT(ICOM,1)
C     I2 STEAM EXPLOSION COMPLETED FOR THIS TIME STEP
      GO TO 170
  141 CONTINUE                                                          MELT REL
C     IF MELT RELEASE HAS NOT STARTED,BYPASS
      IF(TT.LT.TMR)GO TO 170
      DO 145 JREL=1,10
      IF(TT.LT.TM4(JREL))GO TO 145
      T(1)=AMIN1(DT,TT-TM4(JREL))
      DO 147 ICOM=1,N
      H(ICOM,ICOM)=0.
      F(ICOM)=CMI2(ICOM,JREL,1)
      F(ICOM+N)=0.
      IF(DKICM(JREL).GT.0.) F(ICOM )= DKRON(ICOM,1)*DKICM(JREL)
      BTAI2M(ICOM,JREL)=ELI2(ICOM)+FDI2(ICOM)+DKNCM(ICOM,JREL)*
     1(CKG(ICOM)*(AW(ICOM)+AF(ICOM))/V(ICOM))
      IF(ICOM.EQ.1)BTAI2M(ICOM,JREL)=BTAI2M(ICOM,JREL)+AMDAIM(JREL)+
     *ELAMM(JREL)
      DO 149 JCOM=1,N
  149 H(ICOM,ICOM)=H(ICOM,ICOM)-G(ICOM,JCOM)/V(ICOM)
  147 H(ICOM,ICOM)=H(ICOM,ICOM)-BTAI2M(ICOM,JREL)
      CALL ALGEMY
      DO 148 ICOM=1,N
      CMLKI2=CMLKI2+FT(ICOM+N,1)
  148 CMI2(ICOM,JREL,2)=FT(ICOM,1)
  145 CONTINUE
C     I2 MELT RELEASE COMPLETED FOR THIS TIME STEP
      GO TO 170
  151 CONTINUE                                                          VAP REL
C     IF VAPOR RELEASE HAS NOT STARTED,BYPASS
      IF(TT.LT.TVR1)GO TO 170
      DO 155 JREL=1,10
      IF(TT.LT.TA4(JREL))GO TO 155
      T(1)=AMIN1(DT,TT-TA4(JREL))
      DO 157 ICOM=1,N
      H(ICOM,ICOM)=0.
      F(ICOM)=CAI2(ICOM,JREL,1)
      F(ICOM+N)=0.
      IF(DKICA(JREL).GT.0.)F(ICOM)=DKRON(ICOM,1)*DKICA(JREL)
      BTAI2A(ICOM,JREL)=ELI2(ICOM)+FDI2(ICOM)+DKNCA(ICOM,JREL)*
     1(CKG(ICOM)*(AW(ICOM)+AF(ICOM))/V(ICOM))
      IF(ICOM.EQ.1)BTAI2A(ICOM,JREL)=BTAI2A(ICOM,JREL)+AMDAIM(JREL)
     1+ELAMA(JREL)
      DO 159 JCOM=1,N
  159 H(ICOM,ICOM)=H(ICOM,ICOM)-G(ICOM,JCOM)/V(ICOM)
  157 H(ICOM,ICOM)=H(ICOM,ICOM)-BTAI2A(ICOM,JREL)
      CALL ALGEMY
      DO 158 ICOM=1,N
      CVLKI2=CVLKI2+FT(ICOM+N,1)
  158 CAI2(ICOM,JREL,2)=FT(ICOM,1)
  155 CONTINUE
C     I2 VAPORIZATION RELEASE PHASE A COMPLETED FOR THIS TIME STEP
      GO TO 170
  161 CONTINUE                                                          VAPREL B
```

```
C     IF PHASE B VAPOR RELEASE HAS NOT STARTED, BYPASS
      IF(TT.LT.TVR2)GO TO 170
      DO 165 JREL=1,10
      IF(TT.LT.TR4(JREL))GO TO 165
      T(1)=AMIN1(DT,TT-TR4(JREL))
      DO 167 ICOM=1,N
      H(ICOM,ICOM)=0.
      F(ICOM)=CBI2(ICOM,JREL,1)
      F(ICOM+N)=0.
      IF(QKICB(JREL).GT.0.)F(ICOM)=QKRCN(ICOM,1)*QKICB(JREL)
      BTAI2B(ICOM,JREL)=FLI2(ICOM)+FDI2(ICOM)+QKNC8(ICOM,JREL)*
     *CKG(ICOM)*(AJ(ICOM)+AF(ICOM))/V(ICOM)
      IF(ICOM.EQ.1)BTAI2B(ICOM,JREL)=BTAI2B(ICOM,JREL)+
     *AMDAIR(JREL)+ELAMB(JREL)
      DO 169 JCOM=1,N
  169 H(ICOM,ICOM)=H(ICOM,ICOM)-G(ICOM,JCOM)/V(ICOM)
  167 F(ICOM,ICOM)=H(ICOM,ICOM)-BTAI2B(ICOM,JREL)
      CALL ALCEMY
      DO 168 ICOM=1,N
      CVLKI2=CVLKI2+FT(ICOM+N,1)
  168 CBI2(ICOM,JREL,2)=FT(ICOM,1)
  165 CONTINUE
C     I2 VAPORIZATION RELEASE PHASE B COMPLETED FOR THIS TIME STEP
  170 CONTINUE
  190 CONTINUE
      IF(ABS(TT-TPUFF).GT.3.E-8)GO TO 20000
C     MULTIPLY ALL AIRBORNE FRACTIONS EXCEPT THOSE FROM STEAM EXPLOSIONS BY
C     XPUFF. INCREASE LEAKED FRACTION FOR THESE BY (1.-XPUFF)*AIRBORNE
C     FRACTION PRESENT PRIOR TO PUFF.
      XPC=1.-XPUFF
      XPCS=XPC/XPUFF
      DO 21001 ICOM=1,N
      IF(ICOM.EQ.4) GO TO 21001
      CGLKP=CGLKP+XPC*CGP(ICOM,2)/DFPP
      CGP(ICOM,2)=XPUFF*CGP(ICOM,2)
      CSLKP=CSLKP+XPCS*CSP(ICOM,2)/DFPP
      CGLKOI=CGLKOI+XPC*CGOI(ICOM,2)/DFPOI
      CGOI(ICOM,2)=XPUFF*CGOI(ICOM,2)
      CSLKOI=CSLKOI+XPCS*CSOI(ICOM,2)/DFPOI
      CGLKI2=CGLKI2+XPC*CGI2(ICOM,2)/DFPI2
      CGI2(ICOM,2)=XPUFF*CGI2(ICOM,2)
      CSLKI2=CSLKI2+XPCS*CSI2(ICOM,2)/DFPI2
      DO 21000 JREL=1,10
      CMLKP=CMLKP+XPC*CMP(ICOM,JREL,2)/DFPP
      CMP(ICOM,JREL,2)=XPUFF*CMP(ICOM,JREL,2)
      CVLKP=CVLKP+XPC*(CAP(ICOM,JREL,2)+CBP(ICOM,JREL,2))/DFPP
      CAP(ICOM,JREL,2)=XPUFF*CAP(ICOM,JREL,2)
      CBP(ICOM,JREL,2)=XPUFF*CBP(ICOM,JREL,2)
      CMLKOI=CMLKOI+XPC*CMOI(ICOM,JREL,2)/DFPOI
      CMOI(ICOM,JREL,2)=XPUFF*CMOI(ICOM,JREL,2)
      CVLKOI=CVLKOI+XPC*(CAOI(ICOM,JREL,2)+CBOI(ICOM,JREL,2))/DFPOI
      CAOI(ICOM,JREL,2)=XPUFF*CAOI(ICOM,JREL,2)
      CBOI(ICOM,JREL,2)=XPUFF*CBOI(ICOM,JREL,2)
      CMLKI2=CMLKI2+XPC*CMI2(ICOM,JREL,2)/DFPI2
      CMI2(ICOM,JREL,2)=XPUFF*CMI2(ICOM,JREL,2)
      CVLKI2=CVLKI2+XPC*(CAI2(ICOM,JREL,2)+CBI2(ICOM,JREL,2))/DFPI2
      CAI2(ICOM,JREL,2)=XPUFF*CAI2(ICOM,JREL,2)
      CBI2(ICOM,JREL,2)=XPUFF*CBI2(ICOM,JREL,2)
21000 CONTINUE
21001 CONTINUE
20000 CONTINUE
C     TOTAL  VAPORIZATION AND MELT RELEASE COMPONENTS  PER COMPARTMENT
      DO 450 I=1,N
      SUMA=0.
      SUMB=0.
      SUMC=0.
      SUMD=0.
      SUME=0.
      SUMH=0.
      DO 44 J=1,10
      SUMA=SUMA+CMP(I,J,2)
      SUMB=SUMB+CMI2(I,J,2)
      SUMC=SUMC+CMOI(I,J,2)
      SUMD=SUMD+CAI2(I,J,2)+CBI2(I,J,2)
      SUME=SUME+CAOI(I,J,2)+CBOI(I,J,2)
      SUMH=SUMH+CAP(I,J,2)+CBP(I,J,2)
   44 CONTINUE
      CMTP(I)=SUMA
      CMTI2(I)=SUMB
      CMTOI(I)=SUMC
      CVTOI(I)=SUME
      CVTI2(I)=SUMD
      CVTP(I)=SUMH
  450 CONTINUE
      CTMPP=0.
      CTSPP=0.
      CTGPP=0.
      CTMI2=0.
      CTSI2=0.
      CTGI2=0.
      CTVI2=0.
      CTVOI=0.
      CTSOI=0.
```

```
      CTGROI=0.
      CTVROI=0.
      CTVRP=0.
      DO  46 I=1,N
      CTMRP=CTMRP+CMTP(I)
      CTSRP=CTSRP+CSP(I,2)
      CTGRP=CTGRP+CGP(I,2)
      CTSROI=CTSROI+CSOI(I,2)
      CTGROI=CTGROI+CGOI(I,2)
      CTMROI=CTMROI+CMTOI(I)
      CTVROI=CTVROI+CVTOI(I)
      CTVRI2=CTVRI2+CVTI2(I)
      CTSRI2=CTSRI2+CSI2(I,2)
      CTGRI2=CTGRI2+CGI2(I,2)
      CTMRI2=CTMRI2+CMTI2(I)
      CTVRP=CTVRP+CVTP(I)
   46 CONTINUE
C     AIRBORNE FRACTIONS (TOTAL) COMPUTED ABOVE
C     COMPUTE AMOUNTS LEAKED
C     COMPUTE DOSE REDUCTION FACTORS
      DRFMI2=0.
      DRFSI2=0.
      DRFMP=0.
      DRFVI2=0.
      DRFSI2=0.
      DRFGP=0.
      DRFSP=0.
      IF(CMLKP.GT.0.) DRFMP=CMLKOI/CMLKP
      IF(CSLKP.GT.0.) DRFSP=CSLKOI/CSLKP
      IF(CGLKP.GT.0.) DRFGP=CGLKOI/CGLKP
      IF(CMLKI2.GT.0.) DRFMI2=CMLKOI/CMLKI2
      IF(CSLKI2.GT.0.) DRFSI2=CSLKOI/CSLKI2
      IF(CGLKI2.GT.0.) DRFGI2=CGLKOI/CGLKI2
      IF(CVLKI2.GT.0.) DRFVI2=CVLKOI/CVLKI2
      IF(CVLKP.GT.0.)DRFVP=CVLKOI/CVLKP
      N=N+1
C     IF YOU WANT TO BYPASS WRITING, PUT A GO TO 998 HERE.
      WRITE(6,3000)TT
 3000 FORMAT(1H1,/,5X,5HTIME=,1PE11.5,3X,3HHRS)
      WRITE(6,3001)
      WRITE(6,3002)
 3001 FORMAT(1H0,5X,40HCOMPARTMENT AIRBORNE FRACTIONS CONTAINED ,/)
 3002 FORMAT(1X,1HC,11H    GAP    ,11H    GAP    ,11H    GAP    ,
     111H    MELT   ,11H    MELT   ,11H    MELT   ,11H EXPLOSION ,
     211H EXPLOSION ,11H EXPLOSION ,11H   VAPOR   ,10H  VAPOR   ,10H  VA
     3POR   ,/,1X,1H0,11H  RELEASE  ,11H  RELEASE  ,11H  RELEASE  ,11H  RELEASE  ,
     411H  RELEASE  ,11H  RELEASE  ,11H  RELEASE  ,11H  RELEASE  ,
     511H  RELEASE  ,11H  RELEASE  ,11H  RELEASE  ,10H RELEASE  ,
     610H RELEASE  ,/,1X,1HM,11H PARTICLES ,11H     I2     ,
     711H     OI     ,
     711H PARTICLES ,11H     I2     ,11H     OI     ,11H PARTICLES ,
     811H     I2     ,11H     OI     ,11H PARTICLES ,10H     I2     ,
     910H     OI     ,/)
      WRITE(6,3003)((I,CGP(I,2),CGI2(I,2),CGOI(I,2),CMTP(I),CMTI2(I),
     1CMTOI(I),CSP(I,2),CSI2(I,2),CSOI(I,2),CVTP(I),CVTI2(I),CVTOI(I)),
     2I=1,N)
 3003 FORMAT(I2,1PE10.4,1P10E11.4,1PE10.4)
      WRITE(6,3004)
 3004 FORMAT(1H0,//,5X,34HTOTAL AIRBORNE FRACTIONS CONTAINED  ,/)
      WRITE(6,3007)
      WRITE(6,3006)CTGRP,CTGRI2,CTGROI,CTMRP,CTMRI2,CTMROI,CTSRP,
     1CTSRI2,CTSROI,CTVRP,CTVRI2,CTVROI
      WRITE(6,3005)
 3005 FORMAT(1H0,/,5X,32HESCAPE FRACTIONS OF EACH RELEASE   ,/)
      WRITE(6,3007)
      WRITE(6,3006)CGLKP,CGLKI2,CGLKOI,CMLKP,CMLKI2,CMLKOI,CSLKP,
     1CSLKI2,CSLKOI,CVLKP,CVLKI2,CVLKOI
 3006 FORMAT(2X,1PE10.4,1P10E11.4,1PE10.4)
 3007 FORMAT(1X,1H ,11H    GAP    ,11H    GAP    ,11H    GAP    ,
     111H    MELT   ,11H    MELT   ,11H    MELT   ,11H EXPLOSION ,
     211H EXPLOSION ,11H EXPLOSION ,11H   VAPOR   ,10H  VAPOR   ,
     310H  VAPOR   ,/,1X,1H ,11H  RELEASE  ,11H  RELEASE
     411H  RELEASE  ,
     411H  RELEASE  ,11H  RELEASE  ,11H  RELEASE  ,11H  RELEASE  ,
     511H  RELEASE  ,11H  RELEASE  ,11H  RELEASE  ,10H RELEASE  ,10H REL
     6EASE  ,/,1X,1H ,11H PARTICLES ,11H     I2     ,11H     OI     ,
     711H PARTICLES ,11H     I2     ,11H     OI     ,11H PARTICLES ,
     811H     I2     ,11H     OI     ,11H PARTICLES ,10H     I2
     9,10H     OI     ,/)
      WRITE(6,3010)
 3010 FORMAT(1H0,/,5X,38HDOSE REDUCTION FACTORS OF EACH RELEASE  ,/)
      WRITE(6,3007)
      WRITE(6,3015)DRFGP,DRFGI2,DRFMP,DRFMI2,DRFSP,DRFSI2,DRFVP,DRFVI2
 3015 FORMAT(2X,1PE10.4,1PE11.4,11X,1P2E11.4,11X,1P2E11.4,11X,
     1PE11.4,1PE10.4)
C     AD HOC WRITE TO SEE IF COEFFICIENTS ARE BEING CALCULATED CORRECTLY.
C     PUT NEW VALUES INTO NO. 1 BUCKETS.
      DO 9780 J=1,N
      CGP(J,1)=CGP(J,2)
      CGI2(J,1)=CGI2(J,2)
      CGOI(J,1)=CGOI(J,2)
      IF(TT.LT.TEX1)GO TO 9775
      CSP(J,1)=CSP(J,2)
```

```
      CSI2(J,1)=CSI2(J,2)
      CSOI(J,1)=CSOI(J,2)
 9775 CONTINUE
      DO 9780 K=1,10
      IF(TT.LT.TM4(K))GO TO 9778
      CMP(J,K,1)=CSP(J,K,2)
      CMI2(J,K,1)=CMI2(J,K,2)
      CMOI(J,K,1)=CMOI(J,K,2)
 9778 IF(TT.LT.TA4(K))GO TO 9780
      CAP(J,K,1)=CAP(J,K,2)
      CAI2(J,K,1)=CAI2(J,K,2)
      CAOI(J,K,1)=CAOI(J,K,2)
      IF(TT.LT.TB4(K))GO TO 9780
      CBP(J,K,1)=CBP(J,K,2)
      CBI2(J,K,1)=CBI2(J,K,2)
      CBOI(J,K,1)=CBOI(J,K,2)
 9780 CONTINUE
C     DEFINE 3 TYPES OF RADIONUCLIDE DEPOSITION AND TRANSPORT TYPES,
C     ORGANIC IODIDE LIKE, IODINE LIKE, AND PARTICULATE LIKE
      DO 6601 I=1,NOI
 6601 CORLEK(I)=CGLKOI*CFR(1,I)+CMLKOI*CFR(2,I)+CSLKOI*CFR(3,I)*XPUFF
     1+CVLKOI*CFR(4,I)
      NOIP1=NOI+1
      NI2END=NOI+NI2
      DO 6602 I=NOIP1,NI2END
 6602 CORLEK(I)=CGLKI2*CFR(1,I)+CMLKI2*CFR(2,I)+CSLKI2*CFR(3,I)*XPUFF
     1+CVLKI2*CFR(4,I)
      NSTART=NI2END+1
      NISO=NOI+NI2+NPAR
      DO 6603 I=NSTART,NISO
 6603 CORLEK(I)=CGLKP*CFR(1,I)+CMLKP*CFR(2,I)+CSLKP*CFR(3,I)*XPUFF
     1+CVLKP*CFR(4,I)
      WRITE(6,3032)(NAMES(I),I=1,NISO)
 3032 FORMAT(1H0,6X,34HFRACTIONS OF CORE INVENTORY LEAKED,//,9X,10(A6,5X
     1))
      WRITE(6,3034)(CORLEK(I),I=1,NISO)
 3034 FORMAT(1H ,5X,10(1PE10.4,1X))
      IF(TT.LT.TEND-1.-8)GO TO 6
      CALL ERR(3,1HCORRAL S.N. 3034
      GO TO 1
  999 CONTINUE
      STOP
      END
```

J7. COMPUTER CODE CORRAL LISTING FOR PWR ACCIDENT SEQUENCES

```
      DIMENSION PI(9,20),TI(20),GI(9,9,20),VAPI(9,20),V(9),
     1VAP(9),P(9),TMP(9),DELTTI(9,20),DELTAT(9),ELKP(9,20),EI2(9,9,20),
     1EP(9,9,20),EFI2(9,9),HT(9),ELI2(9),ELP(9),G(9,9),CMP(9,10,2),
     1ELKI2(9,20),CKG(9),OKM(10),OKA(10),OKB(10),
     1CAOI(9,10,2),
     1CBOI(9,10,2),
     1CBI2(9,10,2),
     1CAI2(9,10,2),
     1EFP(9,9)
      DIMENSION CGP(9,2),
     1CSP(9,2),
     1CGI2(9,2),
     1CMI2(9,10,2),
     1CSI2(9,2),
     1CGOI(9,2),
     1CMOI(9,10,2),
     1CSOI(9,2),
     1CMTP(9),
     1CMTI2(9),
     1CMTOI(9),
     1TM1(10),
     1TM3(10),
     1TM4(10),
     1OKICM(10)
      DIMENSION BETAPG(9),
     1BETAPM(9,10),
     1BETAPS(9),
     1AW(9),AF(9),
     1SKGG(9),
     1SKG(9,10),
     1FOP(9),
     1FDI2(9),
     1BTAI2S(9),
     1BTAI2M(9,10),
     1BTAI2G(9),
     1CVTOI(9),CVTI2(9),
     1OKNCM(9,10),
     1OKNCG(9),
     1OKNCS(9)
      DIMENSION
     1OKICA(10),
     1OKICB(10),
     1OKNCA(9,10),
     1BTAI2A(9,10),
     1BTAI2B(9,10),
     1AMDAMP(10),
     1AMDAIM(10),
     1AMDAIA(10),
     1AMDAIB(10),
```

```
     1ELOI(9),ELKOI(9,20),
     10KNCB(9,10),
     1CATOI(9)
      DIMENSION CBTOI(9),
     1TA1(10),
     1TB1(10),
     1TA3(10),
     1TB3(10),
     1TB4(10),
     *TA4(10)
      DIMENSION
     1DNST(9),
     1VAIR(9),
     1VST(9),
     1PAS(9),
     1PSA(9),
     1VM(9),
     1WA(9),
     1WS(9),
     1DS(9),
     1DA(9),
     1DI2(9),
     1SC(9)
      DIMENSION AMDAPA(10),AMDAPB(10),BTAPVA(9,10),BTAPVB(9,10),CAP(9,
     110,2),CBP(9,10,2),CATP(9),CBTP(9),CVTP(9),DVA(10),DVB(10),EFA(10)
     2,EFB(10),SKGA(9,10),SKGB(9,10),TVA(10),TVB(10)
      DIMENSION GR(9),
     1SKG1(9),
     1COM(10),
     1COB(10),
     1COA(10),
     1 ELAMM(10),
     1ELAMA(10),
     1ELAMB(10),
     1EFM(10),
     1DM(9),
     1TMY(9,20),TCHANG(20)
C     CFR(JREL,ISOT)=CORE FRACTION RELEASED FOR MATERIAL ISOT BY
C     METHOD JREL.
      DIMENSION CFR(4,10),NAMES(10),CORLEK(10)
      EQUIVALENCE(TA4(1),TVA(1)),(TB4(1),TVB(1))
C     THE ISOTOPE GROUPS WILL BE TAKEN AS KR-XE AND OI (ORGANIC IODIDE
C     LIKE),I2-BR(I2 LIKE),AND CS-RB,TE,BA-SR,RU,PU(PARTICULATE LIKE)
      DATA NAMES(1)/6HKR-XE /,NAMES(2)/6HOI    /,NAMES(3)/6HI2-BR /,
     1NAMES(4)/6HCS-RB /,NAMES(5)/6HTE    /,NAMES(6)/6HBA-SR /,
     2NAMES(7)/6HRU    /,NAMES(8)/6HLA    /
      DATA NOI/2/,NI2/1/,NPAR/5/
      LOGICAL SWITCH
      COMMON//A(50),ABSMAX,ABSRMS,B(50),F(50),FABZ(50,50),FT(50,50)
     1,H(50,50),II,IND,INF,L,LL,LOST,MAPS,MARK,NTT,NA,NB,NEXT,NT
     2,PLOT(5,2,100),Q(50,50),RELMAX,RELRMS,RUN(10),T(50),TAG(50),TYPE
     3,UNITF,UNITT,W(50),Z(50,50),ZN(50,50),ZNII(50)
      NAMELIST/BREAK/N,NDATA,TI,DELTTI,DT,DT2,TJUMP1,TJUMP2,
     1PI,GI,EP,EI2,AW,AF,ELKI2,ELKP,HT,TCHANG,TEND,TVR1
     2,TVR2,TVRE,GK,DPE,DPL,VAPI,V,FDP,FDI2,TCSI,ELKOI,TMR,TMF,TCSR2E,
     3CSR2,TCSR2,HCSI,TD,TEX1,TCSIE,CSI,HO,TCSR1E,CSR1,
     4DCSR,HCSR,CUTOV,DCSI,TECCI,VCL,TMY,TCSR1,ECCI,DF
     5,TPUFF,DFPP,DFPOI,DFPI2,CFR,XPUFF
      NAMELIST/TRIVIA/DI2,GR,SC,CKG,P,TMP,DNST,VM,BTAI2G,OKNCG,EL12
      NAMELIST/MIX/P,TMP,DNST,VAIR,VST,PAS,PSA,VM
      DATA ABSMAX/1.E-8  /,ABSRMS/1.E-8  /,RELMAX/1.E-8  /,RELRMS/1.E-8/
    1 CONTINUE                    CONTINUE TO NEXT CASE
      READ(5,BREAK,END=999)       READ INPUT DATA
      WRITE(6,2001)N
 2001 FORMAT(1H1,///,32X,35HFISSION PRODUCT RELEASE AND CLEANUP,//,
     15X,20HDATA AND ASSUMPTIONS,/,6X,22HNO. OF COMPARTMENTS N= ,I2)
      WRITE(6,2002)N,NDATA
 2002 FORMAT(1H0,6X,21HCOMPARTMENT PRESSURES,/,6X,
     114H((PI(I,J),I=1,,I2,6H),J=1,,I2,2H)=)
      DO 1500 J=1,NDATA
      WRITE(6,2003)(PI(I,J),I=1,N)
 1500 CONTINUE
 2003 FORMAT(6X,1P8E14.6)
      WRITE(6,2004)N,NDATA
 2004 FORMAT(1H0,6X,24HCOMPARTMENT TEMPERATURES,/,6X,15H((TMY(I,J),I=1,,
     1I2,6H),J=1,,I2,2H)=)
      DO 1505 J=1,NDATA
      WRITE(6,2003)(TMY(I,J),I=1,N)
 1505 CONTINUE
      WRITE(6,2006)N,NDATA
 2006 FORMAT(1H0,6X,35HTEMPERATURE DIFFERENCES TBULK-TWALL,/,6X,
     118H((DELTTI(I,J),I=1,,I2,6H),J=1,,I2,2H)=)
      DO 1510 J=1,NDATA
      WRITE(6,2003)(DELTTI(I,J),I=1,N)
 1510 CONTINUE
      WRITE(6,2008)N,NDATA
 2008 FORMAT(1H0,6X,26HWATER VAPOR MOLE FRACTIONS ,/,6X,
     116H((VAPI(I,J),I=1,,I2,6H),J=1,,I2,2H)=)
      DO 1520 J=1,NDATA
      WRITE(6,2003)(VAPI(I,J),I=1,N)
 1520 CONTINUE
      WRITE(6,2010)N,NDATA
 2010 FORMAT(1H0,6X,30HFRACTION OF I2 LEAKED PER HOUR,/,6X,
```

```
     117H((ELKI2(I,J),I=1,,I2,6H),J=1,,I2,2H)=)
      DO 1525 J=1,NDATA
      WRITE(6,2003)(ELKI2(I,J),I=1,N)
 1525 CONTINUE
      WRITE(6,2012)N,NDATA
 2012 FORMAT(1H0,6X,40HFRACTION OF PARTICULATES LEAKED PER HOUR ,/,6X,
     110H((ELKP(I,J),I=1,,I2,6H),J=1,,I2,2H)=)
      DO 1530 J=1,NDATA
      WRITE(6,2003)(ELKP(I,J),I=1,N)
 1530 CONTINUE
      WRITE(6,2016)N,NDATA
 2016 FORMAT(1H0,6X,62HFRACTION OF ORGANIC IODIDES LEAKED PER HOUR FROM
     1COMPARTMENT I ,/,6X,17H((ELKOI(I,J),I=1,,I2,6H),J=1,,I2,2H)=)
      DO 11530 J=1,NDATA
11530 WRITE(6,2003)(ELKOI(I,J),I=1,N)
      WRITE(6,2014)NDATA,(TI(J),J=1,NDATA)
 2014 FORMAT(1H ,6X,110HPRECEDING DOUBLY INDEXED EXPRESSIONS WERE INDEXE
     1D ON COMPARTMENT (I) AND TIME (J). THE INPUT TIME ARRAY IS TI.

      WRITE(6,22015)TCHANG
22015 FORMAT(1H0,6X,72HTIMES TCHANG SIGNAL REINTERPOLATION OF FLOW RATES
     * AND THERMODYNAMIC DATA ,/,6X,7HTCHANG=,/,(6X,1P8E14.6))
      WRITE(6,2018)N
 2018 FORMAT(1H0,6X,77HFRACTION OF PARTICULATES REMOVED PER HOUR BY INTE
     1RIOR FILTER IN COMPARTMENT I ,/,6X,12H(FDP(I),I=1,,I2,2H)=)
      WRITE(6,2003)(FDP(I),I=1,N)
      WRITE(6,2020)N
 2020 FORMAT(1H0,6X,76HFRACTION OF IODINE (I2) REMOVED PER HOUR BY INTER
     1IOR FILTER IN COMPARTMENT I  ,/,6X,13H(FDI2(I),I=1,,I2,2H)=)
      WRITE(6,2003)(FDI2(I),I=1,N)
      WRITE(6,2021)
 2021 FORMAT(1H0,/,6X,41HINTER-COMPARTMENTAL TRANSFER COEFFICIENTS  ,/)
      WRITE(6,2022)
 2022 FORMAT(1H0,6X,84HCUBIC FEET OF FLOW PER HOUR FROM COMPARTMENT I TO
     1 COMPARTMENT K AT DATA TIME ENTRY J  )
      DO 1540 J=1,NDATA
      DO 1540 I=1,N
      WRITE(6,2024)I,J,N
      WRITE(6,2003)(GI(I,K,J),K=1,N)
 1540 CONTINUE
 2024 FORMAT(1H ,6X,4H(GI(,I2,3H,K,,I2,6H),K=1,,I2,2H)=)
      WRITE(6,2026)
 2026 FORMAT(1H0,6X,107HFRACTION OF IODINE (I2)  REMOVED BY FILTER IN FL

     1OW FROM COMPARTMENT I TO COMPARTMENT K AT DATA TIME ENTRY J  )
      DO 1545 J=1,NDATA
      DO 1545 I=1,N
      WRITE(6,2028)I,J,N
      WRITE(6,2003)(EI2(I,K,J),K=1,N)
 1545 CONTINUE
 2028 FORMAT(1H ,6X,5H(EI2(,I2,3H,K,,I2,6H),K=1,,I2,2H)=)
      WRITE(6,2030)
      DO 1550 J=1,NDATA
 2030 FORMAT(1H0,6X,107HFRACTION OF PARTICULATES REMOVED BY FILTER IN FL
     1OW FROM COMPARTMENT I TO COMPARTMENT K AT DATA TIME ENTRY J  )
      DO 1550 I=1,N
      WRITE(6,2032)I,J,N
      WRITE(6,2003)(EP(I,K,J),K=1,N)
 1550 CONTINUE
 2032 FORMAT(1H ,6X,4H(EP(,I2,3H,K,,I2,6H),K=1,,I2,2H)=)
      WRITE(6,2034)
 2034 FORMAT(1H0,6X,20HINPUT TIME VARIABLES ,//,6X,108HTD=TIME INTERVAL
     1OVER WHICH EFFECTIVE PARTICLE DIAMETER CHANGES LINEARLY FROM DPE (
     2DIAMETER PARTICLES EARLY) ,/,6X,33HTO DPL (DIAMETER PARTICLES LATE
     3).  ,/,6X,51HDT,DT2=TIME STEP(HRS) BEFORE MELT AND AFTER TJUMP1  ,
     A/,6X,39HTVR1=TIME OF FIRST VAPORIZATION RELEASE ,
     4/,6X,36HTVR2=TIME OF VAPORIZATION RELEASE 2. ,/,
     56X,37HTVRE=TIME OF VAPORIZATION RELEASE END ,/,
     66X,24HTMR=TIME OF MELT RELEASE ,/,
     76X,31HTMF=TIME OF MELT RELEASE FINISH ,/,
     86X,56HTCSI=TIME CONTAINMENT SYSTEM INJECTION SPRAY PUMP STARTS,/,
     96X,50HTCSIE=TIME CONTAINMENT SYSTEM INJECTION SPRAY ENDS ,/,
     96X,46HTECCI=TIME OF EMERGENCY CORE COOLANT INJECTION ,/,
     06X,56HTCSR1=TIME CONTAINMENT SYSTEM RECIRCULATING SPRAY STARTS ,/,
     16X,55HTCSR1E=TIME CONTAINMENT SYSTEM RECIRCULATING SPRAY ENDS ,/,
     26X,28HTEX1=TIME OF EXPLOSION NO. 1 ,/,
     36X,26HTPUFF=TIME OF PUFF RELEASE     ,/,
     46X,38HTJUMP1=TIME TO SWITCH TO TIME STEP DT2  ,/,
     56X,26HTJUMP2=TIME TO STEP TO END  ,/)
      WRITE(6,2036)TD,DT,TVR1,TVR2,TVRE,TMR,TMF,TCSI,TCSIE,TECCI,TCSR1,
     *TCSR1E,TCSR2,TCSR2E,TEX1,TPUFF,DT2,TJUMP1,TJUMP2,TEND
 2036 FORMAT(1H ,6X,3HTD=,1PE12.5,3X,3HDT=,1PE12.5,3X,5HTVR1=,1PE12.5,2X
     A,5HTVR2=,1PE12.5,2X
     1,5HTVRE=,1PE14.8,3X,4HTMR=,1PE14.8,/,6X,4HTMF=,1PE14.8,3X,5HTCSI=,
     11PE14.8,3X,6HTCSIE=,1PE14.8,3X,6HTECCI=,1PE14.8,3X,6HTCSR1=,1PE14
     1.8,/,6X,7HTCSR1E=1PE14.8,3X,6HTCSR2=,1PE14.8,3X,7HTCSR2E=,1PE14.8,
     13X,5HTEX1=,1PE14.8,3X,6HTPUFF=,1PE14.8,/,
     16X,4HDT2=,1PE14.8,3X,7HTJUMP1=,1PE14.8,3X,7HTJUMP2=,1PE14.8,3X,
     15HTEND=,1PE14.8)
      WRITE(6,2038)
 2038 FORMAT(1H0,6X,24HREACTOR COMPARTMENT DATA ,/)
      WRITE(6,2040)N
 2040 FORMAT(1H ,6X,21HCOMPARTMENT WALL AREA,/,6X,11H(AW(I),I=1,,I2,
```

```
235*          12H)=)
236*           WRITE(6,2003)(AW(I),I=1,N)
237*           WRITE(6,2042)N
238*     2042 FORMAT(1H ,6X,22HCOMPARTMENT FLOOR AREA,/,6X,11H(AF(I),I=1,,I2,
239*          12H)=)
240*            WRITE(6,2003)(AF(I),I=1,N)
241*           WRITE(6,2044)N
242*     2044 FORMAT(1H ,6X,18HCOMPARTMENT HEIGHT,/,6X,11H(HT(I),I=1,,I2,2H)=)
243*           WRITE(6,2003)(HT(I),I=1,N)
244*           WRITE(6,2046)N
245*     2046 FORMAT(1H ,6X,31HCOMPARTMENT VOLUME (CUBIC FEET),/,6X,
246*          110H(V(I),I=1,,I2,2H)=)
247*           WRITE(6,2003)(V(I),I=1,N)
248*           WRITE(6,2048)
249*     2048 FORMAT(1H0,6X,38HCONTAINMENT AND CLEANUP SPECIFICATIONS,//,6X,55
250*          1HCSI=CONTAINMENT SYSTEM INJECTION FLOW IN CUBIC FEET/HR.,/,6X,65
251*          1HCSR1=CONTAINMENT SYSTEM NO.1 RECIRCULATING FLOW IN CUBIC FEET/HR.
252*          1,/,6X,61HHCSI,HCSR=HEIGHT THROUGH WHICH CONTAINMENT SYSTEM SPRAYS
253*          1FALL ,/,6X,55HDCSI,DCSR=DIAMETER OF CONTAINMENT SYSTEM SPRAY DROPL
254*          2ETS ,/,6X,66HCUTOV=CONCENTRATION OF I2 BELOW WHICH SPRAY REMOVAL I
255*          3S INEFFECTIVE ,/,6X,28HVCL=VOLUME OF COOLANT LIQUID ,/,
256*          16X,71HH0=RATIO OF IODINE IN SOLUTION IN WATER TO THAT IN VAPOR AT
257*          1EQUILIBRIUM,/,6X,37HECCI=EMERGENCY CORE COOLANT FLOW RATE,/,6X,
258*          153HDFPP,DFPOI,DFPI2=PUFF RELEASE DECONTAMINATION FACTORS,/,6X,
259*          163HXPUFF=FRACTION OF AIRBORNE MATERIAL RETAINED AFTER PUFF RELEASE
260*          1    ,/,6X,74HDPE,DPL=EFFECTIVE DIAMETER OF PARTICLES IN MICRONS AT
261*          1 EARLY AND LATE TIMES    )
262*           WRITE(6,2050)CSI,CSR1,HCSI,HCSR,DCSI,DCSR,CUTOV,VCL,H0,ECCI,
263*          1DFPP,DFPOI,DFPI2,CSR2,XPUFF,DPE,DPL
264*     2050 FORMAT(1H0,6X,4HCSI=,1PE14.8,3X,5HCSR1=,1PE14.8,3X,5HHCSI=,1PE14.8
265*          1,3X,5HHCSR=,1PE14.8,3X,5HDCSI=,1PE14.8,/,6X,5HDCSR=,1PE14.8,3X,
266*          16HCUTOV=,1PE14.8,3X,4HVCL=,1PE14.8,3X,3HH0=,1PE14.8,3X,5HECCI=,
267*          11PE14.8,3X,/,6X,5HDFPP=,1PE13.7,3X,6HDFPOI=,1PE13.7,3X,
268*          16HDFPI2=,1PE13.7,3X,5HCSR2=,1PE13.7,3X,6HXPUFF=,1PE13.7,/,
269*          17X,4HDPE=,1PE13.7,3X,4HDPL=,1PE13.7  )
270*           WRITE(6,2052)
271*           NISO=N0I+NI2+NPAR
272*           WRITE(6,2054)((NAMES(J),(CFR(I,J),I=1,4)),J=1,NISO)
273*     2052 FORMAT(1H0,6X,63HCORE FRACTIONS RELEASED BY METHOD J IN ISOTOPE GR
274*          1OUP I CFR(J,I),//,12X,11HGAP RELEASE,4X,12HMELT RELEASE,4X,
275*          215HSTEAM EXPLOSION,1X,12HVAPORIZATION )
276*     2054 FORMAT(6X,A6,1X,1PE10.5,6X,1PE10.5,6X,1PE10.5,6X,1PE10.5)
277*     C     INITIAL CONDITIONS OF COMPUTED VARIABLES
278*           VTOT=0.
279*     C     VTOT=TOTAL CONTAINMENT VOLUME,FT3
280*           DO 8  I=1,N
281*           CGOI(I, 1)= 0.
282*           CGP(1, 1)= 0.
283*           CSP(I, 1)= 0.
284*           CSOI(I, 1)= 0.
285*           CGOI(I, 2)= 0.
286*           CGP(I, 2)= 0.
287*           CSP(I, 2)= 0.
288*           CSOI(I, 2)= 0.
289*           CMTP(I)=0.
290*           CMTI2(I)=0.
291*           CMTOI(I)=0.
292*           CMTI2(I)=0.
293*           CVTI2(I)=0.
294*           CATOI(I)=0.
295*           CBTOI(I)=0.
296*           CATP(I)=0.
297*           CBTP(I)=0.
298*           CGI2(I, 1)= 0.
299*           CSI2(I, 1)= 0.
300*           CGI2(I, 2)= 0.
301*           CSI2(I, 2)= 0.
302*           VTOT=VTOT+V(I)
303*           DO 8 J=1,10
304*     C     SET I2 CONCENTRATIONS NON-ZERO FOR CUTOV TEST ONLY
305*           CMI2(I,J,1)=1.
306*           CAI2(I,J,1)=1.
307*           CBI2(I,J,1)=1.
308*           CAOI(I, J, 1)= 0.
309*           CBOI(I, J, 1)= 0.
310*           CBP(I, J, 1)= 0.
311*           CAP(I, J, 1)= 0.
312*           CMP(I, J, 1)= 0.
313*           CMOI(I, J, 1)= 0.
314*           CAOI(I, J, 2)= 0.
315*           CBOI(I, J, 2)= 0.
316*           CBP(I, J, 2)= 0.
317*           CAP(I, J, 2)= 0.
318*           CMP(I, J, 2)= 0.
319*           CMOI(I, J, 2)= 0.
320*           CAI2(I, J, 2)= 0.
321*           CBI2(I, J, 2)= 0.
322*           CMI2(I, J, 2)= 0.
323*         8 CONTINUE
324*           TEX=TEX1
325*           TX=0.
326*           DO 10 J=1,10
327*           TM3(J)=0.
```

```
328*          TM4(J)=TMR+FLOAT(J-1)*(TMF-TMR)/10.
329*          TM1(J)= 0.
330*          TA1(J)= 0.
331*          TB1(J)= 0.
332*          TA3(J)=0.
333*          TB3(J)=0.
334*          TA4(J)=TVR1+FLOAT(J-1)*(TVR2-TVR1)/10.
335*          TB4(J)=TVR2+FLOAT(J-1)*(TVRE-TVR2)/10.
336*       10 CONTINUE
337*          TA= 0.
338*          TSA= 0.
339*          CMLKP=0.
340*          CSLKP=0.
341*          CGLKP=0.
342*          CMLKI2=0.
343*          CVLKP=0.
344*          CSLK12=0.
345*          CGLKI2=0.
346*          CVLKI2=0.
347*          CMLKOI=0.
348*          CSLKOI=0.
349*          CGLKOI=0.
350*          CVLKOI=0.
351*          OKEQG1=0.
352*          TG1=0.
353*          OKEQG2=0.
354*          TG2=0.
355*          OKEQS1=0.
356*          TS1=0.
357*          OKEQS2=0.
358*          TS2=0.
359*    C     BEGIN CALCULATIONS
360*          M=1
361*          TT=0.
362*    C     SAVE DT
363*          DT1=DT
364*          NCHANG=1
365*       6 CONTINUE                                   CONTINUE TO NEXT TIME STOP
366*          IF(TT.LT.TMR)DT=AMIN1(DT1,TMR)
367*          IF(TT.GE.TMR)DT=.05*(TMF-TMR)
368*          IF(TT.GE.TVR1)DT=.05*(TVR2-TVR1)
369*          IF(TT.GE.TVR1.AND.TT.LT.TMF)DT=.05*AMIN1(TMF-TMR,TVR2-TVR1)
370*          IF(TT.GE.TVR2)DT=.1*(TVRE-TVR2)
371*          IF(TT.GE.TVRE)DT=DT1
372*          IF(TT.GT.TJUMP1)DT=DT2
373*          IF(TT.LT.TPUFF.AND.TT+DT.GT.TPUFF)DT=TPUFF-TT+1.E-8
374*          IF(TT.LT.TCSI.AND.TT+DT.GT.TCSI)DT=TCSI-TT+1.E-8
375*          IF(TT.LT.TCSR1.AND.TT+DT.GT.TCSR1)DT=TCSR1-TT+1.E-8
376*          IF(TT.LT.TCSR2.AND.TT+DT.GT.TCSR2)DT=TCSR2-TT+1.E-8
377*          IF(TT.GT.TJUMP2)DT=TEND-TT
378*          TT=TT+DT                                 NEW TIME TT, HRS
379*    C     BYPASS PARAMETER RECOMPUTATION IF THERMODYNAMICS IS UNCHANGED.
380*    C     CHANGES OCCUR AT TIMES TCHANG
381*          SWITCH=.FALSE.
382*    C     IF(M.GT.1.AND.TT.LT.TCHANG(NCHANG))GO TO 1333   THIS TEST CAN BE USED TO
383*          NCHANG=NCHANG+1                                BYPASS TO 1333 IF NO CHANGES OCCUR
384*          SWITCH=.TRUE.
385*    C     COMPUTE P(N),T(N),DELTAT(N),VAP(J),ELI2(J),ELP(J) FOR THE PARTICU-
386*    C     LAR TIME TT.
387*          NN=1
388*          DO 11 J=2,NDATA
389*          IF(ABS(TI(J)-TT).LT.ABS(TI(NN)-TT))NN=J
390*       11 CONTINUE
391*          NN=MAX0(2,MIN0(NN,NDATA-1))
392*          A1=TI(NN-1)
393*          A2=TI(NN)
394*          A3=TI(NN+1)
395*          DO 13 K=1,N
396*          P(K)=QINT(A1,A2,A3,TT,PI(K,NN-1),PI(K,NN),PI(K,NN+1))
397*          TMP(K)=QINT(A1,A2,A3,TT,TMY(K,NN-1),TMY(K,NN),TMY(K,NN+1))
398*          DELTAT(K)=QINT(A1,A2,A3,TT,DELTTI(K,NN-1),DELTTI(K,NN),DELTTI(K,
399*         1NN+1))
400*          VAP(K)=QINT(A1,A2,A3,TT,VAPI(K,NN-1),VAPI(K,NN),VAPI(K,NN+1))
401*          ELI2(K)=QINT(A1,A2,A3,TT,ELKI2(K,NN-1),ELKI2(K,NN),ELKI2(K,NN+1))
402*          ELP(K)=QINT(A1,A2,A3,TT,ELKP(K,NN-1),ELKP(K,NN),ELKP(K,NN+1))
403*          ELOI(K)=QINT(A1,A2,A3,TT,ELKOI(K,NN-1),ELKOI(K,NN),ELKOI(K,NN+1))
404*    C     COMPUTE G(I,J),EFI2(I,J),EFI2(I,J) FOR ANY TIME TT
405*          DO 13 L=1,N
406*          G(K,L)=QINT(A1,A2,A3,TT,GI(K,L,NN-1),GI(K,L,NN),GI(K,L,NN+1))
407*          EFI2(K,L)=QINT(A1,A2,A3,TT,EI2(K,L,NN-1),EI2(K,L,NN),EI2(K,L,NN+1
408*         1))
409*          EFP(K,L)=QINT(A1,A2,A3,TT,EP(K,L,NN-1),EP(K,L,NN),EP(K,L,NN+1))
410*       13 CONTINUE
411*    C1333 CONTINUE
412*    C
413*    C     COMPUTE GAS PARAMETERS,TRANSPORT COEFFICIENTS, DIMENSIONLESS NO.S
414*    C
415*          DO 14 K=1,N
416*          CALL ERR(3,18HFRACAS DO 14
417*          IF(.NOT.SWITCH)GO TO 1102
418*          P(K)=P(K)+14.7                                  PSIA
419*          TR=TMP(K)+460.                                  RANKINE
420*          DNST(K)=P(K)/(10.73*TR)
```

INTERPOLATION OF INPUT DATA TO GET VALUE AT TT.

ADJUST DT TO PROPER SIZE

```
421*          DNST(K)=DNST(K)*VAP(K)*18.+(1.-VAP(K))*DNST(K)*29.          DENSITY
422*    C     ABOVE IN  LBS/FT3
423*          TR1P5=TR*SQRT(TR)
424*          VST(K)=.003339*TR1P5/(TR+1224.2)                    VISCOSITIES WATER VAPOR
425*          VAIR(K)=.0414*(TR/492.)**.768                       AIR
426*          IF(VAP(K).EQ.1.)GO TO 7
427*          IF(VAP(K).EQ.0.)GO TO 773
428*          PAS(K)=(1.+SQRT((VAIR(K)/VST(K))*SQRT(18./29.)))**2/4.5704
429*          PSA(K)=(1.+SQRT((VST(K)/VAIR(K))*SQRT(29./18.)))**2/3.6008
430*          RMOL=VAP(K)/(1.-VAP(K))
431*          VM(K)=VAIR(K)/(1.+RMOL*PAS(K))+VST(K)/(1.+PSA(K)/RMOL)     EQUATION (VII J-21)
432*          GO TO 778
433*        7 VM(K)=VAIR(K)
434*          GO TO 778
435*      773 VM(K)=VST(K)
436*      778 CONTINUE
437*    C     ABOVE IN  LB/FT/HR
438*          WA(K)=0.7075+141.73/(TR/1.8)
439*          WS(K)=0.7075+454.72/(TR/1.8)                                          ] I2 DIFFUSIVITY
440*    C     DA(K)=.0020435*(TR/1.8)**1.5*.1961/((P(K)/14.7)*4.436**2*WA(K))       ] (EQUATION VII J-22)
441*          DA(K)=.843257E-5*TR1P5/(P(K)/14.7*WA(K))                              ]
442*    C     DS(K)=.0020201*((T(K)+460.)/1.8)**1.5*.2438/((P(K)/14.7)*3.901**2     ]
443*    C    1*WS(K))                                                               ]
444*          DS(K)=.134012E9E-4*TR1P5/( P(K)/14.7*WS(K))                           ]
445*    C     ABOVE DIFFUSIVITIES IN CM2/SEC                                        ]
446*          DI2(K)=1./(VAP(K)/DS(K)+(1.-VAP(K))/DA(K))                            ]
447*          DI2(K)=DI2(K)*3.875                                                   ]
448*    C     DI2(K) IN FT2/HR                                                      ]
449*    C     SCHMIDT NO= VISCOSITY/(DENSITY*DIFFUS.)=SC(K)
450*          SC(K)=VM(K)/(DNST(K)*DI2(K))
451*    C     GRASHOF NO. FOR NATURAL CONVECTION,CKG=MT COEFF IN FT/HR
452*          GR(K)=4.17312E+8*HT(K)**3*DNST(K)**2*DELTAT(K)/(TR*VM(K)**2)          MASS TRANSFER
453*          IF(HT(K).LE.10.)CKG(K)=.59*DI2(K)*SQRT(SQRT(GR(K)*SC(K)))/HT(K)       ] COEFF, EQNs
454*          IF(HT(K).GT.10.)CKG(K)=DI2(K)*(5.9*SQRT(SQRT(GR(K)*SC(K)))/HT(K)      ] VII J-24, J-25
455*         1+.13*(HT(K)-10.)*CBRT(GR(K)*SC(K))/HT(K))/HT(K)
456*     1102 CONTINUE
457*    C     COMPUTE SETTLING VELOCITIES FOR PARTICLES
458*    C     HAVE PARTICES FROM 13 SOURCES ,GAP RELEASE,10 TIME INTERVALS OF
459*    C     THE MELT RELEASE + 2 EXPLOSIONS + 20 VAPORIZATION RELEASES
460*    C     DG,DM(10),DEX1,DEX2,DVA(10),DVB(10)
461*          DG=AMAX1(DPE+(DPL-DPE)*(TT/TD),DPL)
462*          DEX1=AMAX1(DPE+(DPL-DPE)*(TT-TEX1)/TD,DPL)
463*          IF(TT.LT.TEX1)  DEXI=0.
464*          SPRAY=0.
465*          IF(((TT.GT.TCSI.AND.TT.LT.TCSIE).OR.(TT.GT.TCSR1.AND.TT.LT.
466*         1TCSR1E).OR.(TT.GT.TCSR2.AND.TT.LT.TCSR2E)).AND.K.EQ.1)SPRAY=1.
467*          IF(TT.LT.TMR)GO TO 1555
468*          DO 15  ID=1,10
469*          DM(ID)=AMAX1(DPL,DPE+(DPL-DPE)*(TT-TM4(ID))/TD)
470*          IF(TT.LT.TM4(ID))DM(ID)=0.
471*    C     PARTICLE DIAMETERS ARE IN MICRONS
472*          SKG(K,ID)=(1.-SPRAY)*(.01557*DM(ID)**2/VM(K))*AF(K)/V(K)
473*       15 CONTINUE
474*     1555 CONTINUE
475*          SKGG(K)=(1.-SPRAY)*(.01557*DG**2/VM(K))*AF(K)/V(K)
476*          SKG1(K)=(1.-SPRAY)*(.01557*DEX1**2/VM(K))*AF(K)/V(K)
477*          IF(TT.LT.TMF)GO TO 3016
478*          DO 2015 ID = 1,10
479*          DVA(ID)=AMAX1(DPL,DPE+(DPL-DPE)*(TT-TVA(ID))/TD)
480*          IF(TT.LT.TVA(ID))DVA(ID)=0.
481*          DVB(ID)=AMAX1(DPL,DPE+(DPL-DPE)*(TT-TVB(ID))/TD)
482*          IF(TT.LT.TVB(ID))DVB(ID)=0.
483*          SKGA(K,ID)=(1.-SPRAY)*(.01557*DVA(ID)**2/VM(K))*AF(K)/V(K)
484*          SKGB(K,ID)=(1.-SPRAY)*(.01557*DVB(ID)**2/VM(K))*AF(K)/V(K)
485*     2015 CONTINUE
486*     3016 CONTINUE
487*    C     SKG=NATURAL DEPOSITION LAMBDA IN HR-1  (PARTICULATES)
488*
489*       14 CONTINUE
490*    C     REMOVAL COEFF FOR I2 AWD +PARTICULATES COMPLETE  (W/O SPRAYS)
491*    C     SPRAY LAMBDAS NEED TO BE COMPUTED NOW
492*    C
493*    C     PARTICULATE SPRAY LAMBDA IN COMPARTMENT 1
494*    C
495*    C     FIRST ESTABLISH SUM(FT/V(1)) AND IMPACT EFFICIENCY                    ] EQN VII J-28 and
496*          FI=AMAX1(0.,AMIN1(TT-TCSI-AMIN1(DT/2.,(TT-TCSI)/2.),TCSIE-TCSI))      ] FIGURE VII J-4
497*         1*CSI                                                                  ]
498*          FR1=AMAX1(0.,AMIN1(TT-TCSR1-AMIN1(DT/2.,(TT-TCSR1)/2.),TCSR1E-        ]
499*         1TCSR1))*CSR1                                                          ]
500*          FR2=AMAX1(0.,AMIN1(TT-TCSR2-AMIN1(DT/2.,(TT-TCSR2)/2.),TCSR2E-        ]
501*         1TCSR2))*CSR2                                                          ]
502*          FA=(FR1+FR2+FI)/V(1)                                                  ]
503*          IF(FA.GE.0..AND.FA.LT.0.002)E=-15.825*FA+.06                          ]
504*          IF(FA.GE.0.002.AND.FA.LT.0.193)E=.04625-SQRT(.08626+42.68*FA)/21.3    ]
505*         14                                                                     ]
506*          IF(FA.GT..0193)E=.0015                                                ]
507*    C     THESE EFFICIENCIES ARE FOR GAP RELEASE ONLY                           ]
508*    C     IN THE EVENT THAT THE SPRAYS ARE WORKING AFTER ANY EXPLOSION AND      ]
509*    C     SOURCE RELEASE S,THE EFFICIENCY OF REMOVAL MUST BE RECALCULATED       ]
510*    C     FOR REMOVING S.THE REMOVAL EFFICIENCY IS EEX                          ]
511*    C                                                                           ]
512*          FI=AMAX1(0.,AMIN1(TT-TEX1-AMIN1(DT/2.,(TT-TEX1)/2.),TCSIE-            ]
513*         1TEX1))*CSI                                                            ]
```

```
514*          F1=AMAX1(0.,AMIN1(TT-TEX1-AMIN1(DT/2.,(TT-TEX1)/2.),TCSR1E-
515*         1TEX1))*CSR1
516*          F2=AMAX1(0.,AMIN1(TT-TEX1-AMIN1(DT/2.,(TT-TEX1)/2.),TCSR2E-
517*         1TEX1))*CSR2
518*          ES=F1+F2+FI
519*          ES=ES/V(1)
520*          IF(ES.GE.0..AND.ES.LT.0.002) EEX=-15.825*ES+.06
521*          IF(ES.GE..002.AND.ES.LT.0.0193) EEX=.04625-(.08626+42.68*ES)**.5/2
522*         11.34
523*          IF(ES.GT..0193)EEX=.0015
524*    C     CALCULATE EFF. FOR PARTICULATES FROM MELT RELEASE FOR EACH OF THE
525*    C     10 DIVISIONS, CALL IT EFM(J)
526*          IF(TT.LT.TMR)GO TO 1777
527*          DO 17  J=1,10
528*          AMDAMP(J)=0.
529*          IF(TT.LT.TM4(J))GO TO 17
530*          FMI=AMAX1(0.,AMIN1(TT-TM4(J)-AMIN1(DT/2.,(TT-TM4(J))/2.),
531*         1TCSIE-TM4(J)))*CSI
532*          FM1=AMAX1(0.,AMIN1(TT-TM4(J)-AMIN1(DT/2.,(TT-TM4(J))/2.),
533*         1TCSR1E-TM4(J)))*CSR1
534*          FM2=AMAX1(0.,AMIN1(TT-TM4(J)-AMIN1(DT/2.,(TT-TM4(J))/2.),
535*         1TCSR2E-TM4(J)))*CSR2
536*          ET=    FMI+FM1+FM2
537*          ET=ET/V(1)
538*          IF(ET.GE.0..AND.ET.LT.0.002)EFM(J)=-15.825*ET+.06
539*          IF(ET.GE..002.AND.ET.LT.0.0193) EFM(J)=.04625-(.08626+42.68*ET)**.
540*         15/21.34
541*          IF(ET.GT..0193) EFM(J)=.0015
542*    C     COMPUTE
543*          IF(TT.GT.TCSI.AND.TT.LT.TCSIE) AMDAMP(J)=AMDAMP(J)+1.5*HCSI*CSI*EF
544*         1M(J)/(DCSI*V(1)/30.48)
545*          IF(TT.GT.TCSR1.AND.TT.LT.TCSR1E) AMDAMP(J)=AMDAMP(J)+1.5*HCSR*CSR1
546*         1*EFM(J)/(DCSR*V(1)/30.48)
547*          IF(TT.GT.TCSR2.AND.TT.LT.TCSR2E) AMDAMP(J)=AMDAMP(J)+1.5*HCSR*CSR2
548*         1*EFM(J)/(DCSR*V(1)/30.48)
549*       17 CONTINUE
550*     1777 CONTINUE
551*    C     MELT RELEASE PARTICULATE LAMDAS ARE COMPLETE
552*    C     COMPUTE OTHER PARTICULATE LAMDAS NOW
553*          AMDAPG=0.
554*          AMDAPS=0.
555*          IF(TT.GT.TCSI.AND.TT.LT.TCSIE) AMDAPG=AMDAPG+1.5*HCSI*CSI*E/(DCSI*
556*         1V(1)/30.48)
557*          IF(TT.GT.TCSI.AND.TT.LT.TCSIE)AMDAPS=AMDAPS+1.5*HCSI*CSI*EEX/(DCS
558*         1I*V(1)/30.48)
559*          IF(TT.GT.TCSR1.AND.TT.LT.TCSR1E) AMDAPG=AMDAPG+1.5*HCSR*CSR1*E/(DC
560*         1SR*V(1)/30.48)
561*          IF(TT.GT.TCSR1.AND.TT.LT.TCSR1E) AMDAPS=AMDAPS+1.5*HCSR*CSR1*EEX/(
562*         1DCSR*V(1)/30.48)
563*          IF(TT.GT.TCSR2.AND.TT.LT.TCSR2E) AMDAPS=AMDAPS+1.5*HCSR*CSR2*EEX/(
564*         1DCSR*V(1)/30.48)
565*          IF(TT.GT.TCSR2.AND.TT.LT.TCSR2E) AMDAPG=AMDAPG+1.5*HCSR*CSR2*E/(DC
566*         1SR*V(1)/30.48)
567*    C     COMPUTE VAPORIZATION PARTICULATE REMOVAL BY SPRAYS
568*          DO 217 J=1,10
569*          AMDAPA(J)=0.
570*          AMDAPB(J)=0.
571*          IF(TT.LT.AMIN1(TCSI,TCSR1,TCSR2).OR.TT.GT.AMAX1(TCSIE,TCSR1E,
572*         1TCSR2E))GO TO 217
573*          IF(TT.LT.TA4(J))GO TO 217
574*          FAI=AMAX1(0.,AMIN1(TT-TA4(J)-AMIN1(DT/2.,(TT-TA4(J))/2.),
575*         1TCSIE -TA4(J)))*CSI
576*          FA1=AMAX1(0.,AMIN1(TT-TA4(J)-AMIN1(DT/2.,(TT-TA4(J))/2.),
577*         1TCSR1E-TA4(JT))*CSR1
578*          FA2=AMAX1(0.,AMIN1(TT-TA4(J)-AMIN1(DT/2.,(TT-TA4(J))/2.),
579*         1TCSR2E-TA4(J)))*CSR2
580*          FBI=AMAX1(0.,AMIN1(TT-TB4(J)-AMIN1(DT/2.,(TT-TB4(J))/2.),
581*         1TCSIE -TB4(J)))*CSI
582*          FB1=AMAX1(0.,AMIN1(TT-TB4(J)-AMIN1(DT/2.,(TT-TB4(J))/2.),
583*         1TCSR1E-TB4(J)))*CSR1
584*          FB2=AMAX1(0.,AMIN1(TT-TB4(J)-AMIN1(DT/2.,(TT-TB4(J))/2.),
585*         1TCSR2E-TB4(J)))*CSR2
586*          EA=(FAI+FA1+FA2)/V(1)
587*          EB=(FBI+FB1+FB2)/V(1)
588*          IF(EA.LT..0193)GO TO 4750
589*          EFA(J)=.0015
590*          GO TO 4850
591*     4750 IF (EA.LT..002)GO TO 4760
592*          EFA(J)=.04625-SQRT(.08626+42.68*EA)/21.34
593*          GO TO 4850
594*     4760 EFA(J)=-15.825*EA+.06
595*     4850 CONTINUE
596*          IF(EB.LT..0193)GO TO 5750
597*          EFB(J)=.0015
598*          GO TO 5850
599*     5750 IF (EB.LT..002)GO TO 5760
600*          EFB(J)=.04625-SQRT(.08626+42.68*EB)/21.34
601*          GO TO 5850
602*     5760 EFB(J)=-15.825*EB+.06
603*     5850 CONTINUE
604*          IF(TT.LT.TCSI.OR.TT.GT.TCSIE)GO TO 5854
605*          AMDAPA(J)=1.5*HCSI*CSI*EFA(J)/(DCSI*V(1)/30.48)
606*          AMDAPB(J)=1.5*HCSI*CSI*EFB(J)/(DCSI*V(1)/30.48)
```

PARTICULATE SPRAY γ's IN COMPARTMENT 1

```
607*    5654 IF(TT.LT.TCSR1.OR.TT.GT.TCSR1E)GO TO 5656
608*         AMDAPA(J)=AMDAPA(J)+1.5*HCSR*CSR1*EFA(J)/(DCSR*V(1)/30.48)
609*         AMDAPB(J)=AMDAPB(J)+1.5*HCSR*CSR1*EFB(J)/(DCSR*V(1)/30.48)
610*    5656 IF(TT.LT.TCSR2.OR.TT.GT.TCSR2E)GO TO 217
611*         AMDAPA(J)=AMDAPA(J)+1.5*HCSR*CSR2*EFA(J)/(DCSR*V(1)/30.48)
612*         AMDAPB(J)=AMDAPB(J)+1.5*HCSR*CSR2*EFB(J)/(DCSR*V(1)/30.48)
613*     217 CONTINUE
614*   C     ALL PARTICULATE SPRAY LAMDAS COMPLETE
615*   C
616*   C     IODINE,I2, REMOVAL BY SPRAY CALCULATED NOW
617*   C
618*   C     SPRAY LAMBDAS COMPUTED NOW FOR I2(AMDAIG,AMDAIS,AMDAIM(K))
619*   C
620*   C     COMPUTE TERMINAL VELOCITY OF SPRAY DROPS
621*   C
622*         FDREI=(4./3.)*62.4*DNST(1)*(DCSI/30.48)**3*417312000./VM(1)**2
623*         FDRER=FDREI*(DCSP/DCSI)**3
624*         IF(FDREI.LT.10700.) REI=(FDREI/15.71)**.7027
625*         IF(FDREI.GE.10700.) REI=(FDREI/6.477)**.6215
626*         IF(FDRER.LT.10700.) RER=(FDRER/15.71)**.7027
627*         IF(FDRER.GE.10700.) RER=(FDRER/6.477)**.6215
628*         UTI=REI*VM(1)/(DNST(1)*DCSI/30.48)
629*         UTR=RER*VM(1)/(DNST(1)*DCSR/30.48)
630*   C     UTI,UTR IN FT/HR
631*   C     MASS XFR COEFF TO THESE DROPS COMPUTED BELOW (GGI,GGR) IN FT/HR
632*         GGI=DI2(1)*(2.+.6*REI**.5*SC(1)**.33)/(DCSI/30.48)
633*         GGR=DI2(1)*(2.+.6*RER**.5*SC(1)**.33)/(DCSR/30.48)
634*   C     GAS PHASE COMPLETE,NOW COMPUTE LIQUID PHASE MASS XFR COEFF.GLI,GLR
635*   C     UL=LIQUID VISCOSITY,CP, DL=DIFFUSIVITY OF I2 IN H2O,FT2/HR
636*         T1=(TMP(1)+460.)/1.8
637*         UL=100./(2.1482*((T1-281.6)+(8078.4+(T1-281.6)**2)**.5)-120.)
638*         DL=1.5137E-07*(T1/UL)
639*         GLI=6.58*DL/(DCSI/30.48)
640*         GLR=6.58*DL/(DCSR/30.48)
641*   C     STAGNANT DROP MODEL USED,EFFICIENCY=1-EXP(-6.KGOT/S(H+KG/KL))
642*         ECSI=1.-EXP(-6.*GGI*(HCSI/UTI)/((DCSI/30.48)*(HO+GGI/GLI)))
643*         ECSR=1.-EXP(-6.*GGR*(HCSR/UTR)/((DCSR/30.48)*(HO+GGR/GLR)))
644*   C     SPRAY LAMBDAS=F*HO*E/V,IF C/V(1).GJ.C(EMITTED)/(SUM V(I))*CUTOFF
645*   C     EQUILIBRIUM LAMBDAS USED AT LOWER CONC.
646*   C     COMPILE PROPER ELAM ( )
647*   C     SUBROUTINE
648*         COG=CGI2(1,1)*VTOT/V(1)
649*         COS=CSI2(1,1)*VTOT/V(1)
650*         DO 18 J=1,10
651*         COM(J)=CMI2(1,J,1)*VTOT/V(1)/.1
652*         COB(J)=CBI2(1,J,1)*VTOT/V(1)/(.07528*EXP(-.1*FLOAT(J-1)))
653*         COA(J)=CAI2(1,J,1)*VTOT/V(1)/(.07528*EXP(-.1*FLOAT(J-1)))
654*      18 CONTINUE
655*         OKG=0.                              G= GAP RELEASE
656*         OKS=0.                              S= STEAM EXPLOSION
657*         IF(COG.GT.CUTOV      ) OKG=1.
658*         IF(COS.GT.CUTOV      ) OKS=1.
659*         DO 19 J=1,10
660*         OKM(J)=0.                           M= MELT RELEASE
661*         OKA(J)=0.                           A= 1st HALF OF VAPORIZATION RELEASE
662*         OKB(J)=0.                           B= 2nd HALF OF VAPORIZATION RELEASE
663*         IF(COM(J).GT.CUTOV)OKM(J)=1.
664*         IF(COA(J).GT.CUTOV)OKA(J)=1.
665*         IF(COB(J).GT.CUTOV)OKB(J)=1.
666*      19 CONTINUE
667*         IF(TT.LT.TCSIE.AND.TT.GE.TCSI) OKCSI=1.
668*         IF(TT.GE.TCSIE.OR.TT.LT.TCSI)  OKCSI=0.
669*         IF(TT.LT.TCSR1E.AND.TT.GE.TCSR1) OKCSR1=1.
670*         IF(TT.GE.TCSR1E.OR.TT.LT.TCSR1) OKCSR1=0.
671*         IF(TT.LT.TCSR2E.AND.TT.GE.TCSR2) OKCSR2=1.
672*         IF(TT.GE.TCSR2E.OR.TT.LT.TCSR2) OKCSR2=0.
673*         AMDAIG=CSI*HO*ECSI*OKG*OKCSI/V(1)+CSR1*HO*ECSR*OKG*OKCSR1/V(1)+HO*
674*        1CSR2*ECSR*OKG*OKCSR2/V(1)
675*         AMDAIS=(HO*OKS/V(1))*(CSI*ECSI*OKCSI+CSR1*ECSR*OKCSR1+CSR2*ECSR*OK
676*        1CSR2)
677*         DO 20 J=1,10
678*         AMDAIM(J)=(HO*OKM(J)/V(1))*(CSI*ECSI*OKCSI+CSR1*ECSR*OKCSR1+CSR2*
679*        1ECSR*OKCSR2)
680*         AMDAIA(J)=(HO*OKA(J)/V(1))*(CSI*ECSI*OKCSI+CSR1*ECSR*OKCSR1+CSR2*
681*        1ECSR*OKCSR2)
682*         AMDAIB(J)=(HO*OKB(J)/V(1))*(CSI*ECSI*OKCSI+CSR1*ECSR*OKCSR1+CSR2*
683*        1ECSR*OKCSR2)
684*      20 CONTINUE
685*   C     SUMP LIQUID VOL. AND I2 CONC. IN THE LIQ.CONTROL EQUILIBRIUM,VSUMP
686*   C     EQ  ECCI+VCL+CSI*(TT-TCSI)
687*         IF(TT.GE.TECCI) OKECCI=1.
688*         IF(TT.LT.TECCI) OKECCI=0.
689*         IF(TT.GT.TCSIE) OKCSIE=1.
690*         IF(TT.LE.TCSIE) OKCSIE=0.
691*         VSUMP=VCL+ECCI*OKECCI+(TCSIE-TCSI)*CSI*OKCSIE+(TT-TCSI)*CSI*OKCSI
692*   C     VSUMP=TOTAL SUMP LIQUID,FT3
693*   C     CALCULATION OF LAMDAS FOR EQUILIBRIUM PROCEED BELOW. THESE ARE
694*   C     ELAMG,ELAMS,ELAMM(I).EACH SPRAY TYPE REQUIRES A SPECIAL DECK TO
695*   C     COMPUTE THESE. FOR THE CASE OF NO SPRAY, USE HB03 DECK.
696*   C
697*   C     BORIC ACID,HB03 DECK FOR COMPUTING EQUILIBRIUM CONCENTRATIONS
698*   C     DESIGNATE TG1 AND TG2 AS  TIME POINTS WHEN CGI2(1,K) EXCEEDS AND
699*   C     IS LT THE  EQUIL. CUTOFF,CUTOV=.01 FOR ALL SPRAYS EXCEPT THIOSULFA
```

EQN VII J-27 AND FOLLOWING ON PARA. J3.2.2

EQUILIBRIUM CALCULATIONS FOR COMPARTMENT 1 ONLY BASED ON EQNS VII J-30, VII J-32 AND TABLES VII J-2 and VII J-3. EACH ELAM ( ) BASED ON TYPE OF SPRAY (NaOH, HB03, NONE). EACH RELEASE (GAP, MELT, VAPORIZATION, STEAM EXPLOSION) IS TREATED AS AN ISOLATED CASE.

```
700*   C      TE.
701*          IF(COG.GT.CUTOV)GO TO 6542
702*          IF(.NOT.((TT.GE.TCSI.AND.TT.LE.TCSIE).OR.(TT.GE.TCSR1.AND.TT.LE.
703*         2TCSR1E).OR.(TT.GE.TCSR2.AND.TT.LE.TCSR2E))) GO TO 6542
704*          TA=TA+DT
705*          ELAMG=ELAM(TA)
706*          GO TO 6545
707*     6542 CONTINUE
708*          ELAMG=0.
709*          TA=0.
710*     6545 CONTINUE
711*   C      ELAMG IN  1/HR
712*          IF(COS.GT.CUTOV.OR.TT.LT.TEX1)GO TO 6583
713*          IF(.NOT.((TT.GE.TCSI.AND.TT.LE.TCSIE).OR.(TT.GE.TCSR1.AND.TT.LE.
714*         2TCSR1E).OR.(TT.GE.TCSR2.AND.TT.LE.TCSR2E))) GO TO 6583
715*          TSA=TSA+DT
716*          ELAMS=ELAM(TSA)
717*          GO TO 6585
718*     6583 CONTINUE
719*          ELAMS=0.
720*          TSA=0.
721*     6585 CONTINUE
722*   C      ELAMS IN HR-1
723*          IF(TT.LT.TMR)GO TO 8001
724*          DO 8000 J=1,10
725*          IF(COM(J).GT.CUTOV.OR.TT.LT.TM4(J))GO TO 7123
726*          IF(.NOT.((TT.GE.TCSI.AND.TT.LE.TCSIE).OR.(TT.GE.TCSR1.AND.TT.LE.
727*         2TCSR1E).OR.(TT.GE.TCSR2.AND.TT.LE.TCSR2E))) GO TO 7123
728*          TM1(J)=TM1(J)+DT
729*          ELAMM(J)=ELAM(TM1(J))
730*          GO TO 8000
731*     7123 CONTINUE
732*          ELAMM(J)=0.
733*          TM1(J)=0.
734*     8000 CONTINUE
735*     8001 CONTINUE
736*          IF(TT.LT.TVR1)GO TO 9001
737*          DO 9000 J=1,10
738*          IF(COA(J).GT.CUTOV.OR.TT.LT.TA4(J))GO TO 3644
739*          IF(.NOT.((TT.GE.TCSI.AND.TT.LE.TCSIE).OR.(TT.GE.TCSR1.AND.TT.LE.
740*         2TCSR1E).OR.(TT.GE.TCSR2.AND.TT.LE.TCSR2E))) GO TO 3644
741*          TA1(J)=TA1(J)+DT
742*          ELAMA(J)=ELAM(TA1(J))
743*          GO TO 9000
744*     3644 CONTINUE
745*          ELAMA(J)=0.
746*          TA1(J)=0.
747*     9000 CONTINUE
748*     9001 CONTINUE
749*          IF(TT.LT.TVR2)GO TO 5001
750*          DO 5000 J=1,10
751*          IF(COB(J).GT.CUTOV.OR.TT.LT.TB4(J))GO TO 4821
752*          IF(.NOT.((TT.GE.TCSI.AND.TT.LE.TCSIE).OR.(TT.GE.TCSR1.AND.TT.LE.
753*         2TCSR1E).OR.(TT.GE.TCSR2.AND.TT.LE.TCSR2E))) GO TO 4821
754*          TB1(J)=TB1(J)+DT
755*          ELAMB(J)=ELAM(TB1(J))
756*          GO TO 5000
757*     4821 CONTINUE
758*          ELAMB(J)=0.
759*          TB1(J)=0.
760*     5000 CONTINUE
761*     5001 CONTINUE
762*   C      ELAMM(J) IN HR**-1
763*   C      AT THIS POINT EQUILIBRIUM LAMBDAS ARE COMPLETE
764*   C
765*   C      DIFFERENTIAL EQNS                          ARE TO BE SOLVED NOW
766*   C
767*   C      ESTABLISH RELEASE INPUTS AS INITIAL CONCENTRATIONS FOR EXPLOSION
768*   C      RELEASE AND MELT RELEASE.FOR GAP RELEASE, ICS ARE ESTABLISHED
769*   C      INCLUDE VAPOR RELEASES
770*   C      EXPLOSION RELEASE
771*          IF(TT.GE.TEX1.AND.TX.EQ.0.)TX=TT
772*          IF(TX.EQ.TT) OKICS=1.
773*          IF(TX.NE.TT) OKICS=0.
774*   C      MELT RELEASE
775*          DO 23 J=1,10
776*          IF(TT.GE.TM4(J).AND.TM3(J).EQ.0.) TM3(J)=TT
777*          IF(TM3(J).EQ.TT) OKICM(J)=.1
778*          IF(TM3(J).NE.TT) OKICM(J)=0.
779*          IF(TT.GE.TA4(J).AND.TA3(J).EQ.0.) TA3(J)=TT
780*          IF(TT.GE.TB4(J).AND.TB3(J).EQ.0.) TB3(J)=TT
781*          IF( TA3(J).EQ.TT) OKICA(J)=.07528*EXP(-.1*FLOAT(J-1))
782*          IF( TB3(J).EQ.TT) OKICB(J)=.2045*EXP(-.1*FLOAT(J+9))
783*          IF( TA3(J).NE.TT) OKICA(J)=0.
784*          IF( TB3(J).NE.TT) OKICB(J)=0.
785*       23 CONTINUE
786*   C
787*   C      SOLVE MULTICOMPARTMENT DIFFENTIAL EQUATIONS
788*          CALL ERR(3,18HCORRAL S.N. 23     )
789*          DO 190 IMAT=1,3
790*   C      SET ALCEMY FIXED INPUT VARIABLES
791*          NT=1
792*          II=2*N
```

(EQN VII J-17) BY SUBROUTINE ALCEMY (SEE PARA. J3-2)

```
      LL=0
      GO TO(30,60,120),IMAT
   30 CONTINUE
C     SET OFF DIAGONAL MATRIX ELEMENTS FOR P BRANCH
      DO 24 ICOM=1,N
      H(ICOM+N,ICOM)=ELP(ICOM)
      DO 24 JCOM=1,N
   24 H(JCOM,ICOM)=G(ICOM,JCOM)*(1.-EFP(ICOM,JCOM))/V(ICOM)
      DO 50 IREL=1,5
      GO TO (31,41,51,1061,1071),IREL
C     PRECEDING BRANCH IS TO GAP RELEASE,MELT RELEASE,STEAM EXPLOSION,
C     VAPORIZATION RELEASE  PHASE A, VAPORIZATION RELEASE PHASE B
   31 CONTINUE
C     RELEASE IN PARTICULATES BRANCH
C
      T(1)=DT
      DO 37 ICOM=1,N
      H(ICOM,ICOM)=0.
      BETAPG(ICOM)=SKGG(ICOM)+ELP(ICOM)+FDP(ICOM)
      IF(ICOM.EQ.1)BETAPG(ICOM)=BETAPG(ICOM)+AMDAPG
      F(ICOM)=CGP(ICOM,1)
      F(ICOM+N)=0.
      IF(M.EQ.1.AND.ICOM.EQ.2)F(ICOM)=1.
      DO 39 JCOM=1,N
   39 H(ICOM,ICOM)=H(ICOM,ICOM)-G(ICOM,JCOM)/V(ICOM)
   37 H(ICOM,ICOM)=H(ICOM,ICOM)-BETAPG(ICOM)
      CALL ALCEMY
      DO 38 ICOM=1,N
      CGLKP=CGLKP+FT(ICOM+N,1)
   38 CGP(ICOM,2)=FT(ICOM,1)
C     GAP RELEASE PARTICULATES COMPLETE FOR PRESENT TIME STEP.
      GO TO 50
   41 CONTINUE                                                        MELT R
C     IF MELT RELEASE HAS NOT STARTED, BYPASS
      IF(TT.LT.TMR)GO TO 50
      DO 45 JREL=1,10
      IF(TT.LT.TM4(JREL))GO TO 45
      T(1)=AMIN1(DT,TT-TM4(JREL))
      DO 47 ICOM=1,N
      F(ICOM)=CMP(ICOM,JREL,1)
      IF(ICOM.EQ.2.AND.OKICM(JREL).NE.0.)F(ICOM)=OKICM(JREL)
      F(ICOM+N)=0.
      H(ICOM,ICOM)=0.
      BETAPM(ICOM,JREL)=SKG(ICOM,JREL)+ELP(ICOM)+FDP(ICOM)
      IF(ICOM.EQ.1)BETAPM(ICOM,JREL)=BETAPM(ICOM,JREL)+AMDAMP(JREL)
      DO 49 JCOM=1,N
   49 H(ICOM,ICOM)=H(ICOM,ICOM)-G(ICOM,JCOM)/V(ICOM)
   47 H(ICOM,ICOM)=H(ICOM,ICOM)-BETAPM(ICOM,JREL)
      CALL ALCEMY
      DO 48 ICOM=1,N
      CMLKP=CMLKP+FT(ICOM+N,1)
   48 CMP(ICOM,JREL,2)=FT(ICOM,1)
   45 CONTINUE
C     MELT RELEASE PARTICULATES COMPLETE FOR PRESENT TIME STEP
      GO TO 50
   51 CONTINUE                                                        STEAM EX
C      IF STEAM EXPLOSION HAS NOT OCCURRED,BYPASS
      IF(TT.LT.TEX1)GO TO 50
      T(1)=AMIN1(DT,TT-TEX1)
      DO 57 ICOM=1,N
      H(ICOM,ICOM)=0.
      F(ICOM)=CSP(ICOM,1)
      F(ICOM+N)=0.
      IF(ICOM.EQ.1.AND.OKICS.NE.0.)F(ICOM)=OKICS
      BETAPS(ICOM)=SKG1(ICOM)+ELP(ICOM)+FDP(ICOM)
      IF(ICOM.EQ.1)BETAPS(ICOM)=BETAPS(ICOM)+AMDAPS
      DO 59 JCOM=1,N
   59 H(ICOM,ICOM)=H(ICOM,ICOM)-G(ICOM,JCOM)/V(ICOM)
   57 H(ICOM,ICOM)=H(ICOM,ICOM)-BETAPS(ICOM)
      CALL ALCEMY
      IF(MOD(M-1,10).NE.0)GO TO 5086
 5036 CONTINUE
C     END OF AD HOC WRITE
      DO 58 ICOM=1,N
      CSLKP=CSLKP+FT(ICOM+N,1)
   58 CSP(ICOM,2)=FT(ICOM,1)
C     STEAM EXPLOSION PARTICULATES COMPLETE FOR PRESENT TIME STEP
      GO TO 50
 1061 CONTINUE                                                        VAPREL A
C     IF VAPORIZATION HAS NOT STARTED, BYPASS,
      IF(TT.LT.TVR1)GO TO 50
      DO 1065 JREL=1,10
      IF(TT.LT.TVA(JREL))GO TO 1065
      T(1)=AMIN1(DT,TT-TVA(JREL))
      DO 1067 ICOM=1,N
      F(ICOM)=CAP(ICOM,JREL,1)
      IF(ICOM.EQ.1.AND.OKICA(JREL).NE.0.)F(ICOM)=OKICA(JREL)
      F(ICOM+N)=0.
      H(ICOM,ICOM)=0.
      BTAPVA(ICOM,JREL)=SKGA(ICOM,JREL)+ELP(ICOM)+FDP(ICOM)
      IF(ICOM.EQ.1)BTAPVA(ICOM,JREL)=BTAPVA(ICOM,JREL)+AMDAPA(JREL)
      DO 1069 JCOM=1,N
 1069 H(ICOM,ICOM)=H(ICOM,ICOM)-G(ICOM,JCOM)/V(ICOM)
```

```
866*    1067 H(ICOM,ICOM)=H(ICOM,ICOM)-BTAPVA(ICOM,JREL)
867*         CALL ALCEMY
868*         DO 1068 ICOM=1,N
869*         CVLKP=CVLKP+FT(ICOM+N,1)
870*    1068 CAP(ICOM,JREL,2)=FT(ICOM,1)
871*    1065 CONTINUE
872*    C    PHASE A VAPORIZATION RELEASE PARTICULATES COMPLETE FOR THIS TIME STEP
873*         GO TO 50
874*    1071 CONTINUE                                                    VAPREL B
875*    C    IF VAPORIZATION RELEASE PHASE B HAS NOT STARTED, BYPASS
876*         IF(TT.LT.TVR2)GO TO 50
877*         DO 1075 JREL=1,10
878*         IF(TT.LT.TVB(JREL))GO TO 1075
879*         T(1)=AMIN1(DT,TT-TVB(JREL))
880*         DO 1077 ICOM=1,N
881*         F(ICOM)=CBP(ICOM,JREL,1)
882*         IF(ICOM.EQ.1.AND.OKICB(JREL).NE.0.)F(ICOM)=OKICB(JREL)
883*         F(ICOM+N)=0.
884*         H(ICOM,ICOM)=0.
885*         BTAPVB(ICOM,JREL)=SKGB(ICOM,JREL)+ELP(ICOM)+FDP(ICOM)
886*         IF(ICOM.EQ.1)BTAPVB(ICOM,JREL)=BTAPVB(ICOM,JREL)+AMDAPB(JREL)
887*         DO 1079 JCOM=1,N
888*    1079 H(ICOM,ICOM)=H(ICOM,ICOM)-G(ICOM,JCOM)/V(ICOM)
889*    1077 H(ICOM,ICOM)=H(ICOM,ICOM)-BTAPVB(ICOM,JREL)
890*         CALL ALCEMY
891*         DO 1078 ICOM=1,N
892*         CVLKP=CVLKP+FT(ICOM+N,1)
893*    1078 CBP(ICOM,JREL,2)=FT(ICOM,1)
894*    1075 CONTINUE
895*    C    PHASE B VAPORIZATION RELEASE COMPLETED FOR THIS TIME STEP.
896*      50 CONTINUE
897*         GO TO 190
898*      60 CONTINUE                                                    ORGANICI
899*    C    SET OFF DIAGONAL MATRIX ELEMENTS FOR ORGANIC IODIDE BRANCH
900*         DO 600 ICOM=1,N
901*         H(ICOM+N,ICOM)=ELOI(ICOM)
902*         DO 600 JCOM=1,N
903*    600  H(JCOM,ICOM)=G(ICOM,JCOM)/V(ICOM)
904*         DO 80 IREL=1,5
905*         GO TO(61,71,81,91,101),IREL
906*    C    FIVE WAY BRANCH IS TO EXPLOSION, GAP, MELT, PHASE A VAPORIZATION,
907*    C    AND PHASE B VAPORIZATION
908*      61 CONTINUE                                                    EXPLODE
909*    C     IF STEAM EXPLOSION HAS NOT OCCURRED, BYPASS
910*         IF(TT.LT.TEX1)GO TO 80
911*         T(1)=AMIN1(DT,TT-TEX1)
912*         DO 67 ICOM=1,N
913*         H(ICOM,ICOM)=0.
914*         F(ICOM)=CSOI(ICOM,1)
915*         F(ICOM+N)=0.
916*         IF(ICOM.EQ.1.AND.OKICS.NE.0.)F(ICOM)=OKICS
917*         DO 69 JCOM=1,N
918*      69 H(ICOM,ICOM)=H(ICOM,ICOM)-G(ICOM,JCOM)/V(ICOM)
919*      67 H(ICOM,ICOM)=H(ICOM,ICOM)-ELOI(ICOM)
920*         CALL ALCEMY
921*         DO 68 ICOM=1,N
922*         CSLKOI=CSLKOI+FT(ICOM+N,1)
923*      68 CSOI(ICOM,2)=FT(ICOM,1)
924*    C    ORGANIC IODIDE EXPLOSION RELEASE COMPLETED FOR THIS TIME STEP
925*         GO TO 80
926*      71 CONTINUE                                                    GAP REL
927*         T(1)=DT
928*         DO 77 ICOM=1,N
929*         H(ICOM,ICOM)=0.
930*         F(ICOM)=CGOI(ICOM,1)
931*         F(ICOM+N)=0.
932*         IF(ICOM.EQ.2.AND.M.EQ.1)F(ICOM)=1.
933*         DO 79 JCOM=1,N
934*      79 H(ICOM,ICOM)=H(ICOM,ICOM)-G(ICOM,JCOM)/V(ICOM)
935*      77 H(ICOM,ICOM)=H(ICOM,ICOM)-ELOI(ICOM)
936*         CALL ALCEMY
937*         DO 78 ICOM=1,N
938*         CGLKOI=CGLKOI+FT(ICOM+N,1)
939*      78 CGOI(ICOM,2)=FT(ICOM,1)
940*    C    ORGANIC IODIDE RELEASE DONE FOR THIS TIME STEP
941*         GO TO 80
942*      81 CONTINUE                                                    MELT REL
943*    C     IF MELT RELEASE HAS NOT STARTED, BYPASS
944*         IF(TT.LT.TMR)GO TO 80
945*         DO 85 JREL=1,10
946*         IF(TT.LT.TM4(JREL))GO TO 85
947*         T(1)=AMIN1(DT,TT-TM4(JREL))
948*         DO 87 ICOM=1,N
949*         H(ICOM,ICOM)=0.
950*         F(ICOM)=CMOI(ICOM,JREL,1)
951*         F(ICOM+N)=0.
952*         IF(ICOM.EQ.2.AND.OKICM(JREL).NE.0.)F(ICOM)=OKICM(JREL)
953*         DO 89 JCOM=1,N
954*      89 H(ICOM,ICOM)=H(ICOM,ICOM)-G(ICOM,JCOM)/V(ICOM)
955*      87 H(ICOM,ICOM)=H(ICOM,ICOM)-ELOI(ICOM)
956*         CALL ALCEMY
957*         DO 88 ICOM=1,N
958*         CMLKOI=CMLKOI+FT(ICOM+N,1)
959*      88 CMOI(ICOM,JREL,2)=FT(ICOM,1)
```

```
 900*      85 CONTINUE
 901*   C     ORGANIC IODIDE MELT RELEASE COMPLETED FOR THIS TIME STEP
 902*         GO TO 80
 903*      91 CONTINUE                                                    VAPREL A
 904*   C      IF VAPOR RELEASE HAS NOT STARTED, BYPASS
 905*         IF(TT.LT.TVR1)GO TO 80
 906*         DO 95 JREL=1,10
 907*         IF(TT.LT.TA4(JREL))GO TO 95
 908*         T(1)=AMIN1(DT,TT-TA4(JREL))
 909*         DO 97 ICOM=1,N
 910*         H(ICOM,ICOM)=0.
 911*         F(ICOM)=CAOI(ICOM,JREL,1)
 912*         F(ICOM+N)=0.
 913*         IF(ICOM.EQ.1.AND.OKICA(JREL).NE.0.)F(ICOM)=OKICA(JREL)
 914*         DO 99 JCOM=1,N
 915*      99 H(ICOM,ICOM)=H(ICOM,ICOM)-G(ICOM,JCOM)/V(ICOM)
 916*      97 H(ICOM,ICOM)=H(ICOM,ICOM)-ELOI(ICOM)
 917*         CALL ALCEMY
 918*         DO 98 ICOM=1,N
 919*         CVLKOI=CVLKOI+FT(ICOM+N,1)
 920*      98 CAOI(ICOM,JREL,2)=FT(ICOM,1)
 921*      95 CONTINUE
 922*   C     ORGANIC IODIDE VAPOR RELEASE PHASE A COMPLETED FOR THIS TIME STEP
 923*         GO TO 80
 924*     101 CONTINUE                                                    VAPREL B
 925*   C     IF PHASE B VAPOR RELEASE HAS NOT STARTED, BYPASS
 926*         IF(TT.LT.TVR2)GO TO 80
 927*         DO 105 JREL=1,10
 928*         IF(TT.LT.TB4(JREL))GO TO 105
 929*         T(1)=AMIN1(DT,TT-TB4(JREL))
 930*         DO 107 ICOM=1,N
 931*         H(ICOM,ICOM)=0.
 932*         F(ICOM)=CBOI(ICOM,JREL,1)
 933*         F(ICOM+N)=0.
 934*         IF(ICOM.EQ.1.AND.OKICB(JREL).NE.0.)F(ICOM)=OKICB(JREL)
 935*         DO 109 JCOM=1,N
 936*     109 H(ICOM,ICOM)=H(ICOM,ICOM)-G(ICOM,JCOM)/V(ICOM)
 937*     107 H(ICOM,ICOM)=H(ICOM,ICOM)-ELOI(ICOM)
 938*         CALL ALCEMY
 939*         DO 103 ICOM=1,N
 940*         CVLKOI=CVLKOI+FT(ICOM+N,1)
 941*     108 CBOI(ICOM,JREL,2)=FT(ICOM,1)
 942*     105 CONTINUE
 943*   C     ORGANIC IODIDE VAPOR RELEASE PHASE B COMPLETED FOR THIS TIME STEP.
 944*      80 CONTINUE
 945*         GO TO 190
 946*     120 CONTINUE                                                    I2BRANCH
 947*   C          NATURAL CONVECTION LAMBDA WILL BE ASSUMED ZERO IN ANY COMPART-
 948*   C          MENT WHERE  CI2/V.LT.CUTOV/VTOT.
 949*         DO 1037 I=1,N
 950*         KSPRAY=0
 951*         IF(I.EQ.1.AND.((TT.GT.TCSR1.AND.TT.LT.TCSR1E).OR.(TT.GT.TCSR2.AND
 952*        *.TT.LT.TCSR2E).OR.(TT.GT.TCSI.AND.TT.LT.TCSIE)))KSPRAY=1
 953*         OKNCG(I)=FLOAT(1-KSPRAY)
 954*         OKNCS(I)=FLOAT(1-KSPRAY)
 955*         IF(CSI2(I,1)/V(I).LT.CUTOV/VTOT)OKNCS(I)=0.
 956*         IF(CGI2(I,1)/V(I).LT.CUTOV/VTOT)OKNCG(I)=0.
 957*         DO 1037 J=1,10
 958*         SCALE=.07528*EXP(-.1*FLOAT(J-1))
 959*         OKNCA(I,J)=FLOAT(1-KSPRAY)
 960*         OKNCB(I,J)=FLOAT(1-KSPRAY)
 961*         OKNCM(I,J)=FLOAT(1-KSPRAY)
 962*         IF(CAI2(I,J,1)/V(I)/SCALE.LT.CUTOV/VTOT)OKNCA(I,J)=0.
 963*         IF(CBI2(I,J,1)/V(I)/SCALE.LT.CUTOV/VTOT)OKNCB(I,J)=0.
 964*         IF(CMI2(I,J,1)/V(I)/.1.LT.CUTOV/VTOT)OKNCM(I,J)=0.
 965*    1037 CONTINUE
 966*   C     SET OFF DIAGONAL MATRIX ELEMENTS FOR I2 BRANCH
 967*         DO 1200 ICOM=1,N
 968*         H(ICOM+N,ICOM)=ELI2(ICOM)
 969*         DO 1200 JCOM=1,N
 970*    1200 H(JCOM,ICOM)=G(ICOM,JCOM)*(1.-EFI2(ICOM,JCOM))/V(ICOM)
 971*         DO 170 IREL=1,5
 972*         GO TO(121,131,141,151,161),IREL
 973*   C     FIVE WAY BRANCH IS TO GAP RELEASE,STEAM EXPLOSION,MELT RELEASE,
 974*   C     VAPORIZATION PHASE A, AND VAPORIZATION PHASE B.
 975*     121 CONTINUE                                                    GAP REL
 976*         T(1)=DT
 977*         DO 127 ICOM=1,N
 978*         H(ICOM,ICOM)=0.
 979*         F(ICOM)=CGI2(ICOM,1)
 980*         F(ICOM+N)=0.
 981*         IF(M.EQ.1)F(ICOM)=DKRON(ICOM,2)
 982*         BTAI2G(ICOM)=ELI2(ICOM)+FDI2(ICOM)+OKNCG(ICOM)*CKG(ICOM)*(AW(ICOM
 983*        *)+AF(ICOM))/V(ICOM)
 984*
 985*         IF(ICOM.EQ.1)BTAI2G(ICOM)=BTAI2G(ICOM)+AMDAIG+ELAMG
 986*         DO 129 JCOM=1,N
 987*     129 H(ICOM,ICOM)=H(ICOM,ICOM)-G(ICOM,JCOM)/V(ICOM)
 988*     127 H(ICOM,ICOM)=H(ICOM,ICOM)-BTAI2G(ICOM)
 989*         CALL ALCEMY
 990*         DO 128 ICOM=1,N
 991*         CGLKI2=CGLKI2+FT(ICOM+N,1)
 992*     128 CGI2(ICOM,2)=FT(ICOM,1)
```

```
1073*   C      I2 GAP RELEASE COMPLETED FOR THIS TIME STEP
1074*          GO TO 170
1075*     151  CONTINUE                                                    ST EXPLO
1076*   C      IF STEAM EXPLOSION HAS NOT OCCURRED,BYPASS
1077*          IF(TT.LT.TEX1)GO TO 170
1078*          T(1)=AMIN1(DT,TT-TEX1)
1079*          DO 137 ICOM=1,N
1080*          H(ICOM,ICOM)=0.
1081*          F(ICOM)=CSI2(ICOM,1)
1082*          F(ICOM+N)=0.
1083*          IF(OKICS.GT.0.)F(ICOM)=DKRON(ICOM,1)
1084*          BTAI2S(ICOM)=ELI2(ICOM)+FDI2(ICOM)
1085*          IF(OKNCS(ICOM).NE.0.)BTAI2S(ICOM)=BTAI2S(ICOM)+CKG(ICOM)
1086*         1*(AW(ICOM)+AF(ICOM))/V(ICOM)
1087*          IF(ICOM.EQ.1)BTAI2S(ICOM)=BTAI2S(ICOM)+AMDAIS+ELAMS
1088*          DO 139 JCOM=1,N
1089*     139  H(ICOM,ICOM)=H(ICOM,ICOM)-G(ICOM,JCOM)/V(ICOM)
1090*     137  H(ICOM,ICOM)=H(ICOM,ICOM)-BTAI2S(ICOM)
1091*          CALL ALCEMY
1092*          DO 138 ICOM=1,N
1093*          CSLKI2=CSLKI2+FT(ICOM+N,1)
1094*     138  CSI2(ICOM,2)=FT(ICOM,1)
1095*   C      I2 STEAM EXPLOSION COMPLETED FOR THIS TIME STEP
1096*          GO TO 170
1097*     141  CONTINUE                                                    MELT REL
1098*   C      IF MELT RELEASE HAS NOT STARTED,BYPASS
1099*          IF(TT.LT.TMR)GO TO 170
1100*          DO 145 JREL=1,10
1101*          IF(TT.LT.TM4(JREL))GO TO 145
1102*          T(1)=AMIN1(DT,TT-TM4(JREL))
1103*          DO 147 ICOM=1,N
1104*          H(ICOM,ICOM)=0.
1105*          F(ICOM)=CMI2(ICOM,JREL,1)
1106*          F(ICOM+N)=0.
1107*          IF(OKICM(JREL).GT.0.)F(ICOM)=DKRON(ICOM,2)*OKICM(JREL)
1108*          BTAI2M(ICOM,JREL)=ELI2(ICOM)+FDI2(ICOM)+OKNCM(ICOM,JREL)*
1109*         1(CKG(ICOM)*(AW(ICOM)+AF(ICOM))/V(ICOM))
1110*          IF(ICOM.EQ.1)BTAI2M(ICOM,JREL)=BTAI2M(ICOM,JREL)+AMDAIM(JREL)+
1111*         *ELAMM(JREL)
1112*          DO 149 JCOM=1,N
1113*     149  H(ICOM,ICOM)=H(ICOM,ICOM)-G(ICOM,JCOM)/V(ICOM)
1114*     147  H(ICOM,ICOM)=H(ICOM,ICOM)-BTAI2M(ICOM,JREL)
1115*          CALL ALCEMY
1116*          DO 148 ICOM=1,N
1117*          CMLKI2=CMLKI2+FT(ICOM+N,1)
1118*     148  CMI2(ICOM,JREL,2)=FT(ICOM,1)
1119*     145  CONTINUE
1120*   C      I2 MELT RELEASE COMPLETED FOR THIS TIME STEP
1121*          GO TO 170
1122*     151  CONTINUE                                                    VAP REL
1123*   C      IF VAPOR RELEASE HAS NOT STARTED,BYPASS
1124*          IF(TT.LT.TVR1)GO TO 170
1125*          DO 155 JREL=1,10
1126*          IF(TT.LT.TA4(JREL))GO TO 155
1127*          T(1)=AMIN1(DT,TT-TA4(JREL))
1128*          DO 157 ICOM=1,N
1129*          H(ICOM,ICOM)=0.
1130*          F(ICOM)=CAI2(ICOM,JREL,1)
1131*          F(ICOM+N)=0.
1132*          IF(OKICA(JREL).GT.0.)F(ICOM)=DKRON(ICOM,1)*OKICA(JREL)
1133*          BTAI2A(ICOM,JREL)=ELI2(ICOM)+FDI2(ICOM)+OKNCA(ICOM,JREL)*
1134*         1(CKG(ICOM)*(AW(ICOM)+AF(ICOM))/V(ICOM))
1135*          IF(ICOM.EQ.1)BTAI2A(ICOM,JREL)=BTAI2A(ICOM,JREL)+AMDAIA(JREL)
1136*         1+ELAMA(JREL)
1137*          DO 159 JCOM=1,N
1138*     159  H(ICOM,ICOM)=H(ICOM,ICOM)-G(ICOM,JCOM)/V(ICOM)
1139*     157  H(ICOM,ICOM)=H(ICOM,ICOM)-BTAI2A(ICOM,JREL)
1140*          CALL ALCEMY
1141*          DO 158 ICOM=1,N
1142*          CVLKI2=CVLKI2+FT(ICOM+N,1)
1143*     158  CAI2(ICOM,JREL,2)=FT(ICOM,1)
1144*     155  CONTINUE
1145*   C      I2 VAPORIZATION RELEASE PHASE A COMPLETED FOR THIS TIME STEP
1146*          GO TO 170
1147*     161  CONTINUE                                                    VAPREL B
1148*   C      IF PHASE B VAPOR RELEASE HAS NOT STARTED, BYPASS
1149*          IF(TT.LT.TVR2)GO TO 170
1150*          DO 165 JREL=1,10
1151*          IF(TT.LT.TB4(JREL))GO TO 165
1152*          T(1)=AMIN1(DT,TT-TB4(JREL))
1153*          DO 167 ICOM=1,N
1154*          H(ICOM,ICOM)=0.
1155*          F(ICOM)=CBI2(ICOM,JREL,1)
1156*          F(ICOM+N)=0.
1157*          IF(OKICB(JREL).GT.0.)F(ICOM)=DKRON(ICOM,1)*OKICB(JREL)
1158*          BTAI2B(ICOM,JREL)=ELI2(ICOM)+FDI2(ICOM)+OKNCB(ICOM,JREL)*
1159*         *CKG(ICOM)*(AW(ICOM)+AF(ICOM))/V(ICOM)
1160*          IF(ICOM.EQ.1)BTAI2B(ICOM,JREL)=BTAI2B(ICOM,JREL)+
1161*         *AMDAIB(JREL)+ELAMB(JREL)
1162*          DO 169 JCOM=1,N
1163*     169  H(ICOM,ICOM)=H(ICOM,ICOM)-G(ICOM,JCOM)/V(ICOM)
1164*     167  H(ICOM,ICOM)=H(ICOM,ICOM)-BTAI2B(ICOM,JREL)
1165*          CALL ALCEMY
```

```
1166*          DO 165 ICOM=1,N
1167*          CVLKI2=CVLKI2+FT(ICOM+N,1)
1168*      165 CGI2(ICOM,JREL,2)=FT(ICOM,1)
1169*      165 CONTINUE
1170*    C     I2 VAPORIZATION RELEASE PHASE 3 COMPLETED FOR THIS TIME STEP
1171*      170 CONTINUE
1172*      190 CONTINUE
1173*          IF(ABS(TT-TPUFF).GT.3.E-8)GO TO 20000
1174*    C     MULTIPLY ALL AIRBORNE FRACTIONS EXCEPT THOSE FROM STEAM EXPLOSIONS BY
1175*    C     XPUFF. INCREASE LEAKED FRACTION FOR THESE BY (1.-XPUFF)*AIRBORNE
1176*    C     FRACTION PRESENT PRIOR TO PUFF.
1177*          XPC=1.-XPUFF
1178*          XPCS=XPC/XPUFF
1179*          DO 21000 ICOM=1,N
1180*          CGLKP=CGLKP+XPC*CGP(ICOM,2)/DFPP
1181*          CGP(ICOM,2)=XPUFF*CGP(ICOM,2)
1182*          CSLKP=CSLKP+XPCS*CSP(ICOM,2)/DFPP
1183*          CGLKOI=CGLKOI+XPC*CGOI(ICOM,2)/DFPOI
1184*          CGOI(ICOM,2)=XPUFF*CGOI(ICOM,2)
1185*          CSLKOI=CSLKOI+XPCS*CSOI(ICOM,2)/DFPOI
1186*          CGLKI2=CGLKI2+XPC*CGI2(ICOM,2)/DFPI2
1187*          CGI2(ICOM,2)=XPUFF*CGI2(ICOM,2)
1188*          CSLKI2=CSLKI2+XPCS*CSI2(ICOM,2)/DFPI2
1189*          DO 21000 JREL=1,10
1190*          CMLKP=CMLKP+XPC*CMP(ICOM,JREL,2)/DFPP
1191*          CMP(ICOM,JREL,2)=XPUFF*CMP(ICOM,JREL,2)
1192*          CVLKP=CVLKP+XPC*(CAP(ICOM,JREL,2)+CBP(ICOM,JREL,2))/DFPP
1193*          CAP(ICOM,JREL,2)=XPUFF*CAP(ICOM,JREL,2)
1194*          CBP(ICOM,JREL,2)=XPUFF*CBP(ICOM,JREL,2)
1195*          CMLKOI=CMLKOI+XPC*CMOI(ICOM,JREL,2)/DFPOI
1196*          CMOI(ICOM,JREL,2)=XPUFF*CMOI(ICOM,JREL,2)
1197*          CVLKOI=CVLKOI+XPC*(CAOI(ICOM,JREL,2)+CBOI(ICOM,JREL,2))/DFPOI
1198*          CAOI(ICOM,JREL,2)=XPUFF*CAOI(ICOM,JREL,2)
1199*          CBOI(ICOM,JREL,2)=XPUFF*CBOI(ICOM,JREL,2)
1200*          CMLKI2=CMLKI2+XPC*CMI2(ICOM,JREL,2)/DFPI2
1201*          CMI2(ICOM,JREL,2)=XPUFF*CMI2(ICOM,JREL,2)
1202*          CVLKI2=CVLKI2+XPC*(CAI2(ICOM,JREL,2)+CBI2(ICOM,JREL,2))/DFPI2
1203*          CAI2(ICOM,JREL,2)=XPUFF*CAI2(ICOM,JREL,2)
1204*          CBI2(ICOM,JREL,2)=XPUFF*CBI2(ICOM,JREL,2)
1205*    21000 CONTINUE
1206*    20000 CONTINUE
1207*    C     TOTAL  VAPORIZATION AND MELT RELEASE COMPONENTS  PER COMPARTMENT
1208*          DO 450 I=1,N
1209*          SUMA=0.
1210*          SUMB=0.
1211*          SUMC=0.
1212*          SUMD=0.
1213*          SUME=0.
1214*          SUMH=0.

1215*          DO 44 J=1,10
1216*          SUMA=SUMA+CMP(I,J,2)
1217*          SUMB=SUMB+CMI2(I,J,2)
1218*          SUMC=SUMC+CMOI(I,J,2)
1219*          SUMD=SUMD+CAI2(I,J,2)+CBI2(I,J,2)
1220*          SUME=SUME+CAOI(I,J,2)+CBOI(I,J,2)
1221*          SUMH=SUMH+CAP(I,J,2)+CBP(I,J,2)
1222*       44 CONTINUE
1223*          CMTP(I)=SUMA
1224*          CMTI2(I)=SUMB
1225*          CMTOI(I)=SUMC
1226*          CVTOI(I)=SUME
1227*          CVTI2(I)=SUMD
1228*          CVTP(I)=SUMH
1229*      450 CONTINUE
1230*          CTMRP=0.
1231*          CTSRP=0.
1232*          CTGRP=0.
1233*          CTMRI2=0.
1234*          CTSRI2=0.
1235*          CTGRI2=0.
1236*          CTVRI2=0.
1237*          CTMROI=0.
1238*          CTSROI=0.
1239*          CTGROI=0.
1240*          CTVROI=0.
1241*          CTVRP=0.
1242*          DO  46 I=1,N
1243*          CTMRP=CTMRP+CMTP(I)
1244*          CTSRP=CTSRP+CSP(I,2)
1245*          CTGRP=CTGRP+CGP(I,2)
1246*          CTSROI=CTSROI+CSOI(I,2)
1247*          CTGROI=CTGROI+CGOI(I,2)
1248*          CTMROI=CTMROI+CMTOI(I)
1249*          CTVROI=CTVROI+CVTOI(I)
1250*          CTVRI2=CTVRI2+CVTI2(I)
1251*          CTSRI2=CTSRI2+CSI2(I,2)
1252*          CTGRI2=CTGRI2+CGI2(I,2)
1253*          CTMRI2=CTMRI2+CMTI2(I)
1254*          CTVRP=CTVRP+CVTP(I)
1255*       46 CONTINUE
1256*    C     AIRBORNE FRACTIONS (TOTAL) COMPUTED ABOVE
1257*    C     COMPUTE AMOUNTS LEAKED
1258*    C     COMPUTE DOSE REDUCTION FACTORS
```

```
1259*          DRFMI2=0.
1260*          DRFSI2=0.
1261*          DRFMP=0.
1262*          DRFVI2=0.
1263*          DRFGI2=0.

1264*          DRFGP=0.
1265*          DRFSP=0.
1266*          IF(CMLKP.GT.0.) DRFMP=CMLKOI/CMLKP
1267*          IF(CSLKP.GT.0.) DRFSP=CSLKOI/CSLKP
1268*          IF(CGLKP.GT.0.) DRFGP=CGLKOI/CGLKP
1269*          IF(CMLKI2.GT.0.) DRFMI2=CMLKOI/CMLKI2
1270*          IF(CSLKI2.GT.0.) DRFSI2=CSLKOI/CSLKI2
1271*          IF(CGLKI2.GT.0.) DRFGI2=CGLKOI/CGLKI2
1272*          IF(CVLKI2.GT.0.) DRFVI2=CVLKOI/CVLKI2
1273*          IF(CVLKP.GT.0.)DRFVP=CVLKOI/CVLKP
1274*          M=M+1
1275*    C     IF YOU WANT TO BYPASS WRITING, PUT A GO TO 998 HERE.
1276*          WRITE(6,3000)TT
1277*     3000 FORMAT(1H1,/,5X,5HTIME=,1PE11.5,3X,3HHRS)
1278*          WRITE(6,3001)
1279*          WRITE(6,3002)
1280*     3001 FORMAT(1H0,5X,40HCOMPARTMENT AIRBORNE FRACTIONS CONTAINED ,/)
1281*     3002 FORMAT(1X,1HC,11H    GAP    ,11H    GAP    ,11H    GAP    ,
1282*         111H    MELT   ,11H    MELT   ,11H    MELT   ,11H EXPLOSION ,
1283*         211H EXPLOSION ,11H EXPLOSION ,11H   VAPOR   ,10H  VAPOR   ,10H  VA
1284*         3POR   ,/,1X,1H0,11H  RELEASE  ,11H  RELEASE  ,11H  RELEASE  ,
1285*         411H  RELEASE  ,11H  RELEASE  ,11H  RELEASE  ,11H  RELEASE  ,
1286*         511H  RELEASE  ,11H  RELEASE  ,11H  RELEASE  ,10H RELEASE  ,
1287*         610H RELEASE  ,/,1X,1HM,11H PARTICLES ,11H     I2    ,
1288*         711H     OI    ,
1289*         711H PARTICLES ,11H     I2    ,11H     OI    ,11H PARTICLES ,
1290*         811H     I2    ,11H     OI    ,11H PARTICLES ,10H    I2    ,
1291*         910H    OI    ,/)
1292*          WRITE(6,3003)(I,CGP(I,2),CGI2(I,2),CGOI(I,2),CMTP(I),CMTI2(I),
1293*         1CMTOI(I),CSP(I,2),CSI2(I,2),CSOI(I,2),CVTP(I),CVTI2(I),CVTOI(I)),
1294*         2I=1,N)
1295*     3003 FORMAT(I2,1PE10.4,1P10E11.4,1PE10.4)
1296*          WRITE(6,3004)
1297*     3004 FORMAT(1H0,//,5X,34HTOTAL AIRBORNE FRACTIONS CONTAINED  ,/)
1298*          WRITE(6,3007)
1299*          WRITE(6,3006)CTGRP,CTGRI2,CTGROI,CTMRP,CTMRI2,CTMROI,CTSRP,
1300*         1CTSRI2,CTSROI,CTVRP,CTVRI2,CTVROI
1301*          WRITE(6,3005)
1302*     3005 FORMAT(1H0,/,5X,32HESCAPE FRACTIONS OF EACH RELEASE   ,/)
1303*          WRITE(6,3007)
1304*          WRITE(6,3006)CGLKP,CGLKI2,CGLKOI,CMLKP,CMLKI2,CMLKOI,CSLKP,
1305*         1CSLKI2,CSLKOI,CVLKP,CVLKI2,CVLKOI
1306*     3006 FORMAT(2X,1PE10.4,1P10E11.4,1PE10.4)
1307*     3007 FORMAT(1X,1H ,11H    GAP    ,11H    GAP    ,11H    GAP    ,
1308*         111H    MELT   ,11H    MELT   ,11H    MELT   ,11H EXPLOSION ,
1309*         211H EXPLOSION ,11H EXPLOSION ,11H   VAPOR   ,10H  VAPOR   ,
1310*         310H  VAPOR   ,/,1X,1H ,11H  RELEASE  ,11H  RELEASE  ,
1311*         411H  RELEASE   ,
1312*         411H  RELEASE  ,11H  RELEASE  ,11H  RELEASE  ,11H  RELEASE  ,
1313*         511H  RELEASE  ,11H  RELEASE  ,11H  RELEASE  ,10H RELEASE  ,10H REL
1314*         6EASE  ,/,1X,1H ,11H PARTICLES ,11H     I2     ,11H    OI     ,
1315*         711H PARTICLES ,11H     I2     ,11H     OI     ,11H PARTICLES ,
1316*         811H    I2     ,11H    OI     ,11H PARTICLES ,10H    I2
1317*         9,10H    OI    ,/)
1318*          WRITE(6,3010)
1319*     3010 FORMAT(1H0,/,5X,38HDOSE REDUCTION FACTORS OF EACH RELEASE  ,/)
1320*          WRITE(6,3007)
1321*          WRITE(6,3015)DRFGP,DRFGI2,DRFMP,DRFMI2,DRFSP,DRFSI2,DRFVP,DRFVI2
1322*     3015 FORMAT(2X,1PE10.4,1PE11.4,11X,1P2E11.4,11X,1P2E11.4,11X,
1323*         11PE11.4,1PE10.4)
1324*    C
1325*    C     PUT NEW VALUES INTO NO. 1 BUCKETS.
1326*          DO 9780 J=1,N
1327*          CGP(J,1)=CGP(J,2)
1328*          CGI2(J,1)=CGI2(J,2)
1329*          CGOI(J,1)=CGOI(J,2)
1330*          IF(TT.LT.TEX1)GO TO 9775
1331*          CSP(J,1)=CSP(J,2)
1332*          CSI2(J,1)=CSI2(J,2)
1333*          CSOI(J,1)=CSOI(J,2)
1334*     9775 CONTINUE
1335*          DO 9780 K=1,10
1336*          IF(TT.LT.TM4(K))GO TO 9778
1337*          CMP(J,K,1)=CMP(J,K,2)
1338*          CMI2(J,K,1)=CMI2(J,K,2)
1339*          CMOI(J,K,1)=CMOI(J,K,2)
1340*     9778 IF(TT.LT.TA4(K))GO TO 9780
1341*          CAP(J,K,1)=CAP(J,K,2)
1342*          CAI2(J,K,1)=CAI2(J,K,2)
1343*          CAOI(J,K,1)=CAOI(J,K,2)
1344*          IF(TT.LT.TB4(K))GO TO 9780
1345*          CBP(J,K,1)=CBP(J,K,2)
1346*          CBI2(J,K,1)=CBI2(J,K,2)
1347*          CBOI(J,K,1)=CBOI(J,K,2)
1348*     9780 CONTINUE
1349*    C     DEFINE 3 TYPES OF RADIONUCLIDE DEPOSITION AND TRANSPORT TYPES,
1350*    C     ORGANIC IODIDE LIKE, IODINE LIKE, AND PARTICULATE LIKE
1351*          DO 6601 I=1,NOI
```

```
1352*    6601 CORLEK(I)=CGLKOI*CFR(1,I)+CMLKOI*CFR(2,I)+CSLKOI*CFR(3,I)*XPUFF
1353*        1+CVLKOI*CFR(4,I)
1354*         NOIP1=NOI+1
1355*         NI2END=NOI+NI2
1356*         DO 6602 I=NOIP1,NI2END
1357*    6602 CORLEK(I)=CGLKI2*CFR(1,I)+CMLKI2*CFR(2,I)+CSLKI2*CFR(3,I)*XPUFF
1358*        1+CVLKI2*CFR(4,I)
1359*         NSTART=NI2END+1
1360*         NISO=NOI+NI2+NPAR
1361*         DO 6603 I=NSTART,NISO
1362*    6603 CORLEK(I)=CGLKP*CFR(1,I)+CMLKP*CFR(2,I)+CSLKP*CFR(3,I)*XPUFF
1363*        1+CVLKP*CFR(4,1)
1364*         WRITE(6,3032)(NAMES(I),I=1,NISO)
1365*    3032 FORMAT(1HO,6X,34HFRACTIONS OF CORE INVENTORY LEAKED,//,9X,10(A6,5X
1366*        1))
1367*         WRITE(6,3034)(CORLEK(I),I=1,NISO)
1368*    3034 FORMAT(1H ,5X,10(1PE10.4,1X))
1369*         IF((TT+1.E-8).LT.TEND)GO TO 6                                    *NEW
1370*         CALL ERR(3,18HCORRAL S.N. 3034                                   **-1
1371*         GO TO 1
1372*     999 CONTINUE
1373*         STOP
1374*         END
```

J8. SUBROUTINES IN CORRAL

The following listings are subroutines used in CORRAL or in the subroutines. These were programmed for the UNIVAC 1108, and might not be universally adaptable to other machines.

```
*DECK     ERR      (CHECK FOR DIVISION BY ZERO OR OVERFLOW)
      SUBROUTINE ERR(MANY,LIST)
C       PCE CREATION DATE =  7 JUN 73, TIME 13.17.21
      DIMENSION LIST(MANY)
      DATA WORD1/6H SPILL/,WORD2/6H  /0  /
C     CALL OVEREL (MUCH)                                                UNIVAC
      MUCH= 2                                                           SET GOOD
C     CALL DVCHK (NULL)                                                 UNIVAC
      NULL= 2                                                           SET GOOD
      IF((MUCH.NE.1).AND.(NULL.NE.1))GO TO 100
      IF(MUCH.EQ.1)WRITE(6,2000)WORD1,LIST
      IF(NULL.EQ.1)WRITE(6,2000)WORD2,LIST
  100 CONTINUE
 2000 FORMAT(1H ,7H*****  ,5A6)
      RETURN
      END
*DECK     ERROR    (CHECK FOR DIVISION BY ZERO OR OVERFLOW)
      SUBROUTINE ERROR
C     IF SPILL, DIVIDE/0, OR DIVERGENCE, SET RUN BAD, DIAGNOSE TROUBLE
C       PCE CREATION DATE =  7 JUN 73, TIME 13.17.24
      COMMON // A(50),ABSMAX,ABSRMS,B(50),E(50),EABZ(50,50),ET(50,50)
     1,H(50,50),IT,IND,INF,L,LL,LOST,MAPS,MAPK,NTT,NA,NB,NEXT,NT
     2,PLOT(5,2,100),Q(50,50),RELMAX,RELRMS,RUN(10),T(50),TAG(50),TYPE
     3,UNITE,UNITT,W(50),Z(50,50),ZN(50,50),ZNI1(50)
      LOGICAL TYPE
      COMMON /GRAPHS/ BUFFER(2048),END(2),INK,NX,NY,XY(2,102)
      DIMENSION YESNO(2)
      DATA LIMIT/13/,YESNO/6H(YES) ,6H(NO)  /

C     CALL OVEREL (MUCH)                                          UNIVAC 1YESNO2
      MUCH= 2
C     CALL DVCHK (NULL)                                           UNIVAC 1YESNO2
      NULL= 2
      LOSS=2                                                              1YESNO2
      IF(IND.GT.INF) LOSS=1                                             DIVERGED
      IF(MUCH+NULL+LOSS.EQ.6) GO TO 200                                   GOOD

      LOST=MAXO(LOST,LOST+1)                                            NO ERASE
      IND=0
      IF(LOST.GT.LIMIT) GO TO 200                                         TOO BAD
      WRITE(6,100)YESNO(MUCH),YESNO(NULL),YESNO(LOSS),NTT,L,INK
  100 FORMAT(7H  SPILLA6,8HDIVIDE/0A6,7HDIVERGEA6,6H TIME(I2,10H) LAPLAC 72 COL
     1E(I3,6H) MAP(I3,1H))
C SPILL(YES) DIVIDE/0(YES) DIVERGE(YES)  TIME(001) LAPLACE(000) MAP(000) MESSAGE
C       (NO)         (NO)         (NO)        050         050       100
C     IF(TYPE)PUNCH 100,YESNO(MUCH),YESNO(NULL),YESNO(LOSS),N,L,INK       TELETYPE

  200 RETURN
      END
*DECK FABZM/CP      (GENERATES Z-1(eZ-I) WHERE Z IS A SQUARE MATRIX)
      SUBROUTINE FABZM
C     MATRIX HYPERGEOMETRIC FUNCTION F(A(50),B(50),Z(50,50))        (CHOP)
C       PCE CREATION DATE =  7 JUN 73, TIME 13.17.25
      COMMON // A(50),ABSMAX,ABSRMS,B(50),E(50),EABZ(50,50),ET(50,50)
     1,H(50,50),IT,IND,INF,L,LL,LOST,MAPS,MAPK,NTT,NA,NB,NEXT,NT
     2,PLOT(5,2,100),Q(50,50),RELMAX,RELRMS,RUN(10),T(50),TAG(50),TYPE
     3,UNITE,UNITT,W(50),Z(50,50),ZN(50,50),ZNI1(50)
      INF= 1000
```

```
C      MAGNUS-OBERHETTINGER FORM, WITH FACTORIAL(N) GENERATED BY B(NB)=1.
C INPUT ABSMAX RELMAX ABSRMS RELRMS NA NB II INF A(N),N=1,NA B(N),N=1,NB
C INPUT (Z(I2,I1),I2=1,II),I1=1,II
C      OUTPUT  F(A,B,Z)=(FABZ(I2,I1),I2=1,II),I1=1,II  IND=SERIES INDEX

       EII=II
       NA=MAXO(NA,NB)
       IND=0
C      HYPERGEOMETRIC MATRIX POWER SERIES LOOP
   10  DN=IND
       IND=IND+1
C      NON-CONVERGED EXIT  INDEX IND GREATER THAN INFINITY INF
       IF(IND-INF) 20,20,200

C      SET UP RECURSORS AN, BN, CN
   20  CN=1.
       DO 60 M=1,NAB
       IF(M-NA) 30,30,40
   30  CN=CN*(DN+A(M))
   40  IF(M-NB) 50,50,60
   50  CN=CN/(DN+B(M))
   60  CONTINUE

       IF(DN) 70,70,100
C      FIRST PASS   SET UP SERIES TERM ZN AND SERIES SUM FABZ
   70  DO 90 I1=1,II
       DO 80 I2=1,II

       ZN(I2,I1)=CN*Z(I2,I1)
   80  FABZ(I2,I1)=ZN(I2,I1)
   90  FABZ(I1,I1)=1.+FABZ(I1,I1)
       GO TO 10

C      SET UP ERROR MEASURE
  100  DE=0.
       DLE=0.
       DES=0.
       DLES=0.
C      FORM NEXT TERM, SUM SERIES, MEASURE ERROR
       DO 140 I1=1,II
       DO 110 I2=1,II
       ZN1(I2)=0.
       DO 110 I3=1,II
  110  ZN1(I2)=ZN1(I2)+ZN(I3,I1)*Z(I2,I3)
       DO 140 I2=1,II
       ZN(I2,I1)=CN*ZN1(I2)
       FABZ(I2,I1)=FABZ(I2,I1)+ZN(I2,I1)
       IF(FABZ(I2,I1)) 120,130,120
  120  DN=ABS(ZN(I2,I1)/FABZ(I2,I1))
       DLE=AMAX1(DLE,DN)
       DLES=DLES+DN*DN
  130  DN=ABS(ZN(I2,I1))
       DE=AMAX1(DE,DN)
  140  DES=DES+DN*DN
       DES=SQRT(DES)/EII
       DLES=SQRT(DLES)/EII

C      CONVERGENCE DECISION
       IF(AMIN1(ABSMAX-DE,RELMAX-DLE,ABSRMS-DES,RELRMS-DLES)) 10,200,200

C IND IS POWER SERIES INDEX   IF(IND-INF) CONVERGED, CONVERGED, DIVERGED
C      AUTOMATIC SPILL TRAP   CHECK FOR SPILL AND DIVISION BY ZERO
  200  RETURN
       END
```

```
*DECK ALCEMY/CP      (SOLVES SET OF SIMULTANEOUS 1ST ORDER DIFFERENTIAL EQUATIONS)
       SUBROUTINE ALCEMY
C      TIME-VARIANT ISOTOPIC TRANSMUTATION  BNW PROGRAM ALCHEMY-II (CHOP)
C        PCE CREATION DATE =  7 JUN 73, TIME 13.17.28
       COMMON // A(50),ABSMAX,ABSRMS,B(50),F(50),FABZ(50,50),FT(50,50)
      1,H(50,50),II,IND,INF,L,LL,LOST,MAPS,MARK,NTT,NA,NB,NEXT,NT
      2,PLOT(5,2,100),Q(50,50),RELMAX,RELRMS,RUN(10),T(50),TAG(50),TYPE
      3,UNITE,UNITT,W(50),Z(50,50),ZN(50,50),ZN1(50)
       DOUBLE PRECISION DEXP
C      DATA POWER2/037740000000000/,TOP/88.0296919/                    UNIVAC
       DATA POWER2 /3776400000000000000008/, TOP /741.66748327

C  SET MATRIX HYPERGEOMETRIC FUNCTION TO EXPONENTIAL INTEGRAL (E**Z-1)/Z
       NA=0
       NB=1
       B(1)=2.
C      ENTER TIME LOOP, STORE TIME INDEX NTT IN COMMON
       DO 230 N1=1,NT
       NTT=N1

C      LOGIC          F(T) = F(0) + F(0)*H*((E**T*H-1)/(T*H))*T
C           + (Q(L)*((E**T*(H-W(L))-1)/(T*(H-W(L))))*T*E**T*W(L),L=1,LL)

C      SET UP BUFFERED FIELD ACCRUAL IN A
       DO 10 I2=1,II
       FT(I2,N1)=F(I2)
       A(I2)=0.
       DO 10 I1=1,II
   10  A(I2)=A(I2)+F(I1)*H(I2,I1)
       WL=-0.
C      ENTER LAPLACE TRANSFORM LOOP   STORE LAPLACE INDEX L IN COMMON
```

```
      LLL=LL+1
      DO 220 L1=1,LLL
      I=IABS(L1-1)

C ASSEMBLE T*(H-W) IN Z WITH SUM OF SQUARES OF ELEMENTS SCALED UNDER ONE
      R=0.
      DO 30 I1=1,II
      DO 20 I2=1,II
   20 Z(I2,I1)=H(I2,I1)
      Z(I1,I1)=WL+Z(I1,I1)
      DO 30 I2=1,II
   30 R=R+Z(I2,I1)**2
C     SCALE BY POWERS OF TWO, FOR FAST UNSCALING
      TN=T(N1)
      R=ABS(TN*SQRT(R))
      IF(1.-R) 40,50,50
   40 R=AND(R,POWER2)
      R=R+R
      TN=TN/R
   50 DO 60 I1=1,II
      DO 60 I2=1,II
   60 Z(I2,I1)=TN*Z(I2,I1)

C     SUM MATRIX HYPERGEOMETRIC SERIES (E**Z-1)/Z IN FABZ
      CALL FABZM

C ASSEMBLE EXPONENTIALLY-SCALED SOURCE FIELD Q*(E**Z-1)/Z IN ZN11 BUFFER
      DO 70 I2=1,II
      ZN11(I2)=0.
      DO 70 I1=1,II
   70 ZN11(I2)=ZN11(I2)+A(I1)*FABZ(I2,I1)
C IF SCALED, ASSEMBLE UNSCALE GENERATOR MATRIX E**Z=1+Z*(E**Z-1)/Z IN ZN
      IF(1.-R) 80,160,160
   80 DO 100 I1=1,II
      DO 90 I2=1,II
      ZN(I2,I1)=0.
      DO 90 I3=1,II
   90 ZN(I2,I1)=ZN(I2,I1)+FABZ(I3,I1)*Z(I2,I3)
  100 ZN(I1,I1)=1.+ZN(I1,I1)

C   UNSCALE LOOP Q*((E**Z-1)/Z)*((E**Z+1)/2)*...*((E**Z*(2**(R-1))+1)/2)
  110 DO 120 I2=1,II
      A(I2)=0.
      DO 120 I1=1,II
      A(I2)=A(I2)+ZN1(I1)*ZN(I2,I1)
C     SET UP NEXT PASS
  120 Z(I2,I1)=ZN(I2,I1)
C     MODIFY AND TRANSFER BUFFERED SUM
      DO 130 I2=1,II
  130 ZN11(I2)=.5*(A(I2)+ZN11(I2))

      R=.5*R
C     UNSCALE LOOP EXIT
      IF(1.5-R) 140,160,160

C     SQUARE UNSCALING GENERATOR MATRIX
  140 DO 150 I1=1,II
      DO 150 I2=1,II
      ZN(I2,I1)=0.
      DO 150 I3=1,II
  150 ZN(I2,I1)=ZN(I2,I1)+Z(I3,I1)*Z(I2,I3)
C     CONTINUE UNSCALING
      GO TO 110

C     ASSEMBLE T*E**T*W(L)
  160 ETW=-WL*T(N1)
      ETW=SIGN(SNGL(DEXP(DBLE(AMIN1(ETW,TOP)))),TOP-ETW)                    OLD EXP
C     FABZM RETURNS SERIES INDEX AS CONVERGENCE-STATUS INDICATOR
      IF(INF-IND) 180,190,190
  170 ETW=-ETW
      IND=MAXO(IND,INF+1)                                                   DIVERGED
C     IF SPILL, DIVIDE/0, OR DIVERGENCE, SET RUN BAD, DIAGNOSE TROUBLE
  180 CALL ERROR                                                            DIVERGED
C     OLD EXP RETURNS MINUS SIGN AS ERROR INDICATOR
  190 IF(ETW) 170,200,200
  200 ETW=ETW*T(N1)

C     ASSEMBLE AND ACCRUE SOURCE FIELD Q(L)*(E**T*H-E**T*W(L))/(H-W(L))
      DO 210 I2=1,II
      ET(I2,N1)=ET(I2,N1)+ETW*ZN11(I2)
C     SET UP NEXT PASS
  210 A(I2)=Q(I2,L1)
      WL=-W(L1)
C     IF SPILL, DIVIDE/0, OR DIVERGENCE, SET RUN BAD, DIAGNOSE TROUBLE
      CALL ERROR
  220 CONTINUE
C     END LAPLACE TRANSFORM LOOP
  230 CONTINUE
C     END TIME LOOP

C     OUTPUT  TIME-VARIANT VECTOR FIELD IN (ET(I,N),I=1,II),N=1,NT
C     OUTPUT  STATUS INDICATOR IN LOST    LOST=(0, NON-ZERO)=(GOOD, BAD)
      RETURN
      END
```

```
*DECK     QINT   (QUADRATIC OR LINEAR INTERPOLATION SCHEME)
      FUNCTION QINT(X1,X2,X3,X4,Y1,Y2,Y3)
C       PCF CREATION DATE - 24 JUL 73, TIME 21.50.35
      DIMENSION X(4),Y(3)
C     FUNCTION QINT RETURNS QUADRATICALLY INTERPOLATED VALUE Y4
C     CORRESPONDING TO X4, GIVEN INDEPENDENT VARIABLE VALUES X1,X2,X3,
C     AND CORRESPONDING DEPENDENT VARIABLE VALUES Y1,Y2,Y3.
      Y(1)=X1
      X(2)=X2
      Y(3)=X3
      Y(4)=X4
      Y(1)=Y1
      Y(2)=Y2
      Y(3)=Y3
      YMAX=AMAX1(ABS(Y1),ABS(Y2),ABS(Y3))
      XMAX=AMAX1(ABS(X1),ABS(X2),ABS(X3))
      IF(YMAX.EQ.0.)GO TO 25
      DO 100 I=1,3
      X(I)=X(I)/XMAX
  100 Y(I)=Y(I)/YMAX
      X(4)=X(4)/XMAX
C     AD HOC BYPASS OF QUADRATIC IN FAVOR OF LINEAR INTERPOLATION
      IF(YMAX.GT.0.)GO TO 8000
      D=X(2)*X(2)*X(3)-X(3)*X(3)*X(2)+X(3)*X(3)*X(1)-X(1)*X(1)*X(3)+X(1)
     1*X(1)*X(2)-X(2)*X(2)*X(1)
      IF(D.EQ.0.) GO TO 1
      A=(Y(2)*X(3)-Y(3)*X(2)+Y(3)*X(1)-Y(1)*X(3)+Y(1)*X(2)-Y(2)*X(1))/D
     . B=(X(2)*X(2)*Y(3)-X(3)*X(3)*Y(2)+X(3)*X(3)*Y(1)-X(1)*X(1)*Y(3)+X(1
     1)*X(1)*Y(2)-X(2)*X(2)*Y(1))/D
      C=(Y(1)*X(2)*X(3)*(X(2)-X(3))+Y(2)*X(3)*X(1)*(X(3)-X(1))+Y(3)*X(1)
     1*X(2)*(X(1)-X(2)))/D
      QINT=(A*X(4)*X(4)+B*X(4)+C)*YMAX
      GO TO 30
    1 WRITE(6,3000)X,Y

 3000 FORMAT(1H ,'QUADRATIC INTERPOLATION FAILURE-X,Y=',7E10.4,//,2X,
     1'RESORT TO LINEAR INTERPOLATION')
 8000 CONTINUE
      J=1
      IF(ABS(SIGN(1.,(X(4)-X(2)))-SIGN(1.,(X(3)-X(2)))).LT..5)J=3
      DENOM = X(J) - X(2)
      IF (DENOM.EQ.0.0) GO TO 22
      QINT = Y(J) + (X(4) - X(J))/DENOM * (Y(J) - Y(2))
      QINT=QINT*YMAX
      GO TO 30
   22 QINT=Y(J)*YMAX
      GO TO 30
   25 QINT=0.
   30 CONTINUE
      CALL ERR(1,6HQINT  )
      RETURN
      END
*DECK     DKRON      (GENERATES KRONECKER DELTA)
      FUNCTION DKRON(I,J)
C       PCF CREATION DATE -  3 AUG 73, TIME 13.25.39
C     KRONECKER DELTA FUNCTION
      DKRON=0.
      IF(I.EQ.J)DKRON=1.
      RETURN
      END
*DECK ELAM/NONE      (EQUILIBRIUM LAMBDA, NO SPRAY)
      FUNCTION ELAM(TA)
C       PCF CREATION DATE - 31 JUL 73, TIME  6.29.18
      ELAM=0.
      RETURN
      END
*DECK     ELAM       (EQUILIBRIUM LAMBDA, HB03, SPRAY)
      FUNCTION ELAM(TA)
C       PCF CREATION DATE - 27 JUN 73, TIME  5.26.45
      IF(TA.GT.100./60.)GO TO 10
      DHSDT=(1.5E+04-2676.)*60./100.
      HS=2676.+TA*DHSDT
      GO TO 100
   10 IF(TA.GT.500./60.)GO TO 20
      DHSDT=2.5E+04*60./400.
      HS=1.5E+04+(TA-100./60.)*DHSDT
      GO TO 100
   20 IF(TA.GT.1000./60.)GO TO 30
      DHSDT=3.E+04*60./500.
      HS=4.E+04+DHSDT*(TA-500./60.)
      GO TO 100
   30 IF(TA.GT.2000./60.)GO TO 40
      DHSDT=8.E+04*60./1000.
      HS=7.E+04+(TA-1000./60.)*DHSDT
      GO TO 100
   40 IF(TA.GT.4000./60.)GO TO 50
      DHSDT=3.5E+05*60./2000.
      HS=1.5E+05*(TA-2000./60.)*DHSDT
      GO TO 100
   50 IF(TA.GT.7000./60.)GO TO 60
      DHSDT=1.E+04
      HS=5.E+05+(TA-4000./60.)*DHSDT
      GO TO 100
   60 DHSDT=0.
```

```
      HS=1.E+06
  100 FLAM=DHSDT/HS
      RETURN
      END
*DECK FLAM/CAUS          (EQUILIBRIUM LAMBDA, NaOH SPRAY)
      FUNCTION FLAM(TA)
C       PCF CREATION DATE - 11 AUG 73, TIME *8.*0.*4
C     FUNCTION FLAM TO RETURN EQUILIBRIUM RATE CONSTANTS FOR CAUSTIC
C     SPRAY
      IF(TA.GT.100./60.)GO TO 10
      DHSDT=0.
      HS=1.
      GO TO 100
   10 IF(TA.GT.1000./60.)GO TO 20
      DHSDT=.095
      HS=1.
      GO TO 100
   20 IF(TA.GT.2000./60.)GO TO 30
      DHSDT=8.E+04*60./1000.
      HS=7.E+04*DHSDT*(TA-1000./60.)
      GO TO 100
   30 IF(TA.GT.4000./60.)GO TO 40
      DHSDT=3.5E+05*60./2000.
      HS=1.5E+05+DHSDT*(TA-2000./60.)
      GO TO 100
   40 IF(TA.GT.7000./60.)GO TO 50
      DHSDT=1.E+04
      HS=5.E+05+DHSDT*(TA-4000./60.)
      GO TO 100
   50 DHSDT=0.
      HS=1.E+06
  100 FLAM=DHSDT/HS
      RETURN
      END
*00
*17
*
```

APPENDIX K

DIFFUSION OF RADIOACTIVE FLUID THROUGH SOIL SURROUNDING A LARGE POWER-REACTOR STATION AFTER A CORE MELTDOWN ACCIDENT

by

J. H. Pitts, B. R. Bowman, R. W. Martin, and J. P. McKay
Lawrence Livermore Laboratory

Appendix K

Table of Contents

Section		Page No.
K1.	INTRODUCTION	VII-265
K2.	METHOD OF ANALYSIS	VII-266
	K2.1 One-Dimensional Ideal Gas	VII-266
	K2.2 One-Dimensional Multiphase Flow	VII-267
	K2.3 Two-Dimensional Ideal Gas	VII-268
	K2.4 Heat Transfer	VII-268
K3.	RESULTS	VII-269
	K3.1 One-Dimensional Ideal Gas	VII-269
	K3.2 One-Dimensional Multiphase Flow	VII-270
	K3.3 Two-Dimensional Ideal Gas	VII-271
	K3.4 Steam Generation by Molten Pool	VII-271
K4.	ADDITIONAL CONSIDERATIONS	VII-272
K5.	CONCLUSIONS	VII-272
ACKNOWLEDGMENT		VII-273
REFERENCES		VII-273

List of Figures

Figure		Page No.
VII K-1	Schematic of Two Possible Configurations After a Core Meltdown Accident in a Large Power-Reactor Station	VII-274
VII K-2	Configuration for the Two-Dimensional, Single-Phase Calculation in Cylindrical Coordinates	VII-275
VII K-3	Schematic of the Element Mesh for the Steam Generation Calculation	VII-275
VII K-4	The Effect of Time and Pressure on the Normalized Active Mass Efflux Calculated in Cartesian Coordinates for an Ideal Gas and for a Value p_o of 14.7 psia	VII-275
VII K-5	Normalized Time at which the Active Containment-Shell Gas is Released at Radius R_o; Calculated in Cylindrical Coordinates for an Ideal Gas and a Value of p_o of 14.7 psia	VII-275
VII K-6	Normalized Time at which Active Containment-Shell Gas is Released at Radius R_o for Varying Radius Ratios	VII-276
VII K-7	Containment-Shell-Pressure Decay and Active Mass Efflux for Core Meltdown Analysis	VII-276

List of Figures (Continued)

Figure		Page No.
VII K-8	Water Saturation, Normalized Pressure, and Temperature Distribution for p_1 = 100 psia	VII-277
VII K-9	Water Saturation, Normalized Pressure, and Temperature Distribution for p_1 = 50 psia	VII-277
VII K-10	Water Saturation, Normalized Pressure, and Temperature Distribution for p_1 = 25 psia	VII-277
VII K-11	Part (A) Shows Water Saturation, Normalized Pressure, and Normalized Temperature Distribution for Pressure Decay for p_1 = 1 p_1 = 100 psia. Part (B) Shows Containment-Shell Pressure as a Function of Time at p_1 = 100 PSIA	VII-277
VII K-12	Pressure Profile of a Two-Dimensional Calculation at t = 2.9 H	VII-278
VII K-13	Pressure Profile of a Two-Dimensional Calculation at t = 6.2 H	VII-278
VII K-14	Pressure Profile of a Two-Dimensional Calculation at t = 14.7 H	VII-278
VII K-15	Steam Generation for Core Melt in Contact with Wet Soil for a Core After-Heat of 3.5×10^{-7} BTU/H and a Containment-Shell Volume of 2×10^6 Ft^3	VII-278

Appendix K

Diffusion of Radioactive Fluid Through Soil Surrounding a Large Power-Reactor Station After a Core Meltdown Accident

by

J. H. Pitts, B. R. Bowman, R. W. Martin, and J. P. McKay
Lawrence Livermore Laboratory

The flow of fluids through the soil surrounding a large power-reactor station after a core meltdown accident was analyzed. Fracture of, or penetration through, a portion of the containment floor was assumed so that radioactive gases would be driven through the soil by pressure within the containment shell.

Results for both one-dimensional ideal gas and multiphase flow were obtained using dimensionless variables so that results are applicable for all soil conditions. Two-dimensional results are included for a specific case where permeability of the soil varies spatially. These calculations show that the time required for radioactive gases to permeate to the ground surface are years for silty-type clays and about 10 h for sand-type soil.

Heat transfer calculations that estimate the amount of steam generated should the core melt penetrate the containment floor and contact wet soil show that cooling systems must be in operation within four or five days in order to prevent overpressurization of the containment shell. Fluid motion existing in the region immediately around the containment shell and also caused by fissure propagation is mentioned.

K1. INTRODUCTION

A reactor accident which causes core meltdown will probably never occur in a large power-reactor station. However, because the effects of such an unlikely accident could be serious, a study of conditions following core meltdown should be included as part of any safety analysis report. Such studies are useful in the design of future power stations. Also they help to minimize or eliminate adverse effects should an accident occur in an existing power plant.

We examined one means by which radioactive matter could reach the ground surface and be released into the atmosphere following a core meltdown accident. Consider that the melted core interacts with the containment floor so that either the molten pool penetrates the floor, or the floor is fractured to such an extent that it no longer can be considered as a containment barrier. Radioactive fluids would then be released into the soil beneath the containment shell and permeate in all directions through the soil (see Fig. VII K-1). From a calculational standpoint, the analysis is approximately the same for both cases since active material is released by essentially the same point source. The driving pressure is that present in the containment shell. Changes in the concentration of radioactive matter due to filtering interaction with the soil or adsorption are not included.

We have completed a four-part analytical study that predicts the extent of penetration of radioactive fluid into the soil and possible release into the atmosphere using methods similar to those developed by Morrison (Ref. 1,2). The problem was first bounded using our one-dimensional programs with a noncondensible gas. Geometries included applicable cases in Cartesian, cylindrical, and spherical coordinates.

In the first study, we considered a Cartesian model of a constant-area column with a length equal to the distance from the expected source through the soil to the ground surface. Soil properties (e.g., permeability and porosity) were assumed constant. The results of this calculation are used as a bound on the time for release of active gas to the atmosphere and for comparison with condensible fluid calculations described later. Use of dimensionless parameters permits application of the results to numerous cases with different gases and having different soil properties. A model using cylindrical coordinates simulates possible radial flow of noncondensible gases in a single layer of soil. For example, consider the earth around the reactor to consist of a horizontal layer of sand with clay above and below. The permeability in the sand region would be probably several orders

of magnitude above that of the clay. Should gases reach this relatively high permeability region, vertical flow could be neglected in comparison to radial flow. Spherical coordinates may be used to determine the extent of flow below the containment floor shown in Fig. VII K-1. This model is accurate until a pressure response is felt at the outer radius of the cofferdam. Beyond this time, gases would be able to permeate both vertically toward the ground surface and radially outward in a two-dimensional fashion. If the outer radius of the one-dimensional spherical coordinate problem is taken equal to the sum of the distance from the source to the outer cofferdam radius and the vertical distance to the ground surface, the predicted time of arrival would be shorter than that actually occurring.

A second set of calculations using our one-dimensional, Cartesian coordinate, multiphase flow model was completed so that effects of steam condensing within the pores of the soil could be included. In all calculations, a mass balance was maintained so that the pressure within the containment shell decreased as flow into the soil occurred. We found that this pressure decay due to flow out of the containment shell was small for most cases. (A more rapid decay would occur if the permeability was high or if the gas source volume was reduced in size.) As a result, we also studied effects at a constant containment-shell pressure since this permitted further generalization of results and the use of similarity solutions.

The third part of the study utilized Bowman's (Ref. 3) two-dimensional extension of the noncondensible program. This permitted us to closely model the geometry of the containment shell shown in Fig. VII K-1, and to include various layers of soil, each with appropriate properties. The extent of radioactive gas penetration with time for condensible flow may be estimated by comparison of changes found for a noncondensible gas on a one-dimensional basis.

The fourth and last series of calculations was aimed at bounding the extent of heat dissipation from the outer wall of the containment shell and the steam generation caused by contact of the core melt with surrounding ground water should the molten pool penetrate the containment floor. These results were used to justify the use of a constant pressure (25, 50, or 100 psia) inside the containment shell. The last two values correspond to what might be the design pressure and rupture pressure of the containment shell.

K2. METHOD OF ANALYSIS

K2.1 ONE-DIMENSIONAL IDEAL GAS

In the first part of the study we considered one-dimensional, isothermal flow of an ideal gas. The restriction of isothermal flow is reasonable since the heat capacity of the soil is much larger than the energy present in the gas flowing through the pores of the soil. The continuity equation for compressible flow through porous media with constant porosity may be written as

$$\nabla \cdot (\rho \vec{u}) + \varepsilon \frac{\partial \rho}{\partial t} = 0 , \qquad \text{(VII K-1)}$$

where ρ is the fluid density, ε is the porosity, t is time, and $\vec{u}$ is an apparent velocity equal to the volume flow rate per unit area normal to the flow.

Conservation of momentum is satisfied using Darcy's law (Ref. 4)

$$\vec{u} = - \frac{k}{\mu} \nabla p , \qquad \text{(VII K-2)}$$

which is a constitutive equation for low-Reynolds-number flow through porous media. Here p is the pressure in the fluid, μ is the fluid viscosity, and k is the permeability of the solid. Using an ideal gas equation of state

$$p = \rho R T , \qquad \text{(VII K-3)}$$

where R is the gas constant and T is the fluid temperature which we take to be constant, the governing equation becomes

$$r^{1-n} \frac{\partial}{\partial r} \left(r^{n-1} p \frac{\partial p}{\partial r} \right) = \frac{\varepsilon \mu}{k} \frac{\partial p}{\partial t} , \qquad \text{(VII K-4)}$$

where r is the spatial variable and n is set equal to 1 for Cartesian coordinates, 2 for cylindrical coordinates, and 3 for spherical coordinates.

Equation (VII K-4) is placed in dimensionless form by defining

$$X = \frac{r}{R_o} , \qquad \text{(VII K-5)}$$

where R_o is the outer radius of the porous medium,

$$P = \frac{p - p_1}{p_1 - p_o} , \qquad \text{(VII K-6)}$$

where p_o is the initial fluid pressure in the pores of the solid and p_1 is the initial driving pressure and

$$\tau = \frac{k(p_1 - p_o)}{\varepsilon \mu R_o^2} t , \qquad \text{(VII K-7)}$$

where τ is dimensionless time and

$$N = p_1/p_o . \qquad \text{(VII K-8)}$$

In terms of these dimensionless quantities, Equation (VII K-4) becomes

$$\frac{\partial^2}{\partial X^2}\left(P^2 + \frac{2P}{N-1}\right) + \frac{n-1}{X}\frac{\partial}{\partial X}\left(P^2 + \frac{2P}{N-1}\right) = 2\frac{\partial P}{\partial \tau} . \qquad \text{(VII K-9)}$$

Boundary conditions used are:

$P = 0$ at $\tau = 0$

$P = 0$ at $X = 1$ for all τ

$P = 1$ at $X = X_o$ at $\tau > 0$.

The value X_o is the ratio of inner to outer radius and is set equal to zero if Cartesian coordinates are used. A time-dependent driving pressure at $X = X_o$, instead of a constant value, may be incorporated if desired. The time dependency of pressure decay may be calculated to correspond to the mass flow rate into the porous media or any other mathematical relationship.

If we define a dimensionless mass

$$M = \frac{m}{m_o} , \qquad \text{(VII K-10)}$$

where m is the total mass that has left the outer radius of the solid, and m_o is the mass of gas originally in the pores of the solid, we may write the continuity relation where A is the flow area as

$$\frac{dM}{dt} = \frac{d(m/m_o)}{dt} = \frac{\rho \vec{u} A}{m_o} . \qquad \text{(VII K-11)}$$

When combined with Darcy's law and the definitions of dimensionless parameters, this becomes

$$\frac{dM}{d\tau} = -\frac{n}{(1 - X_o)^n}\frac{N-1}{2} \times \frac{d}{dX}\left(P^2 + \frac{2P}{N-1}\right)\Big|_{X=1} \qquad \text{(VII K-12)}$$

The total mass having left the porous solid is

$$M = -\frac{n}{(1 - X_o)^n}\frac{N-1}{2} \times \int_o^\tau \frac{d}{dX}\left(P^2 + \frac{2P}{N-1}\right)\Big|_{X=1} d\tau . \qquad \text{(VII K-13)}$$

When M equals unity, the mass having left the solid will just equal the original mass of gas in the pores. Gas originally in the containment shell would start to be released at this time.

Equation (VII K-9) is solved using a finite difference technique with Equations (VII K-12) and (VII K-13) used to determine the rate and amount of mass that has left the solid. Use of dimensionless parameters is very advantageous since it makes the results applicable for all values of permeability, porosity, and gas viscosity.

K2.2 ONE-DIMENSIONAL MULTIPHASE FLOW

In the second series of calculations we considered one-dimensional flow of steam and air in a Cartesian-coordinate system. Even though pure steam was considered to be injected into the soil, air or other noncondensible gases are present under ambient conditions in the pores of the solid so that the solution must consider two species as well as two phases. For each species we write a continuity equation of the form

$$\frac{\partial}{\partial x}(\rho u) + \varepsilon \frac{\partial}{\partial t}(\rho S) = 0 , \qquad \text{(VII K-14)}$$

where S is the saturation of the species or the fraction of the pore volume accessible to the component species. If ℓ represents liquid water, m the mixture of air and water vapor, a the noncondensible air alone, and v the water vapor alone; we may write the two necessary continuity equations as

$$\frac{\partial}{\partial x}(\rho_a u_m) + \varepsilon \frac{\partial}{\partial t}(\rho_a S_m) = 0 \text{ (air)} \qquad \text{(VII K-15)}$$

and

$$\frac{\partial}{\partial x}(\rho_\ell u_\ell + \rho_v u_m) + \varepsilon \frac{\partial}{\partial t}(\rho_\ell S_\ell + \rho_v S_m) = 0 \ (H_2O \text{ liquid and vapor}). \qquad \text{(VII K-16)}$$

All species in gaseous phase are assumed to move at the velocity of the gaseous mixture. Each phase obeys Darcy's law with a relative permeability included to account for the interaction of the two phases;

$$u_\ell = - \frac{k}{\mu_\ell} k_{r\ell} \frac{\partial p}{\partial x} , \qquad \text{(VII K-17)}$$

$$u_m = - \frac{k}{\mu_m} k_{rm} \frac{\partial p}{\partial x} . \qquad \text{(VII K-18)}$$

The relative permeabilities, $k_{r\ell}$ and k_{rm}, are taken to be functions of water saturation in the pores of the solid and are the ratio of effective permeability of a phase to the absolute permeability of the solid.

For an elemental volume of the column the energy equation is written as

$$\frac{\partial}{\partial x} (\rho_\ell u_\ell h_\ell + \rho_v u_m h_v + \rho_a u_m h_a)$$

$$+ \varepsilon \frac{\partial}{\partial t} (\rho_\ell S_\ell e_\ell + \rho_v S_m e_v + \rho_a S_m e_a)$$

$$+ (1 - \varepsilon) \rho_s \frac{\partial e_s}{\partial t} = 0 , \qquad \text{(VII K-19)}$$

where h is enthalpy and e is internal energy. Equations (VII K-15) through (VII K-19) are combined using dimensionless variables as shown in Reference 2 with equations of state for steam, water, vapor, and air, and then solved using finite difference techniques. By neglecting gravitational effects and axial heat conduction, and considering a semi-infinite medium, a similarity solution exists where water saturation, pressure, and temperature may be determined as a function of the similarity variable, θ, where

$$\theta = \frac{x}{2} \sqrt{\frac{\varepsilon \mu_a}{k p_1 t}} \qquad \text{(VII K-20)}$$

K2.3 TWO-DIMENSIONAL IDEAL GAS

A third set of calculations modeled the geometry of a typical, large, power reactor in a two-dimensional ideal gas calculation (see Fig. VII K-2). We used the equations of the one-dimensional ideal gas calculation and extended them to two dimensions. That is, the transient flow is governed by Equations (VII K-1) through (VII K-3) except that now the permeability takes on the form of a tensor. The equations are solved for the pressure in cylindrical coordinates using an explicit, finite-difference approximation with a constant temperature.

Variations of soil permeability between layers of sand and clay are permitted as shown in Fig. VII K-2. The permeability is assumed to be isotropic within each soil layer and does not vary with time. Porosity values are typical for the gas-filled porosity in alluvial clays and sand (Ref. 5). This porosity represents the fraction of interconnected void volume available for flow of gas in the porous media. It is assumed that the only effect of liquid in the pores is to reduce the porosity.

Pressure within the containment shell is assumed to decay with time as a result of mass flow from the shell into the surrounding soil; however, this decay was again found to be small except for cases of reduced gas source volume or high soil permeability. The containment shell is assumed to be impermeable except for a 10.3-ft-radius cylinder representing the volume occupied by the mass of the molten core.

K2.4 HEAT TRANSFER

We estimated the dissipation of heat generated after core meltdown by considering conduction through the containment-shell wall. If the core does not penetrate the containment floor and all cooling systems are inoperative, a simple heat balance may be used to estimate the inside surface temperature of the containment shell. Taking an average heat generation rate of 3.5×10^7 Btu/h over the first 30 h after core meltdown, the temperature drop through a 2.5-ft-thick concrete containment shell exceeds 3000 F. This temperature is in excess of what concrete will withstand. Without an operative cooling system or the addition of material whose heat capacity is very large, failure of the containment shell would be certain.

Should the core melt penetrate the containment floor, the energy generated would vaporize the water present in the pores of the soil adjacent to the molten pool. We examined the problem of heat conduction in an infinite, homogeneous medium capable of undergoing phase change in order to determine the amount of steam which could be generated by the core under these conditions. The internal boundary was a sphere of 10.3-ft radius with a constant internal heat generation rate of 3.5×10^7 Btu/h (see Fig. VII K-3).

The solution followed the finite element method of Wilson and Nickell (Ref. 6).

The molten pool was assumed to be stationary and the thermal properties of the soil during phase change were taken to be an average of the saturated and dry conditions. Steam was assumed to flow from the soil into the containment shell with negligible pressure loss since any substantial buildup of pressure would fracture the soil.

The basic solution technique uses the matrix equations

$$[K](\theta) = (Q) \qquad \text{(VII K-21)}$$

with

$$[K] = [\kappa] + [C] \qquad \text{(VII K-22)}$$

where κ and C are matrices which include the thermal conductivity and heat capacity, θ is the temperature difference vector, and Q is a thermal force vector which includes heat flux across the element surface and internal heat generation. The solution begins at time zero with given initial conditions, and proceeds until the average temperature of the first spherical shell of soil equals the saturation temperature specified. When saturation temperature is attained, the thermal properties of the soil in that shell are changed to those representing the average moisture condition during phase change and the appropriate thermal matrices are reevaluated. When the added energy is equal to that required to transform the water to steam, the phase change is complete. Soil properties are then modified again to reflect the dry condition of the soil.

K3. RESULTS

K3.1 ONE-DIMENSIONAL IDEAL GAS

Results for the one-dimensional, ideal-gas calculations are shown in Figs. VII K-4 to VII K-7 using dimensionless variables. In Fig. VII K-4, the normalized active mass efflux[1], M_o, is defined as the amount of active mass released to the atmosphere divided by the amount of inactive gas initially contained within the pores of the earth in the column. In conjunction with the dimensionless time, τ, defined previously in Equation (VII K-7), the results are universally applicable for any area or length of the column and any porosity, permeability, or gas viscosity. Three values of containment shell pressures are shown, which should bracket expected values for most foreseeable accidents.

In order to explain the use of dimensionless parameters, we shall consider the following example of axial flow in the annular space between the outer surface of the containment shell and the cofferdam (see Fig. VII K-1). Since the flow is axial, we use the Cartesian coordinate results in Fig. VII K-4.

Length = 40 ft

Area = $\pi/4 \times (150^2 - 135^2) = 3360\ ft^2$

Porosity = 0.1

Pore volume = $0.1 \times (40 \times 3360)$

$= 13{,}400\ ft^3$

$p_1 - p_o = (50 - 14.7) = 35.3\ lb/in.^2$

Density at ambient conditions

$= 0.075\ lb/ft^3$

Gas viscosity = $5.0 \times 10^{-7}\ \frac{lb \cdot s}{ft^2}$

Permeability = 0.1 Darcy

$$t = \frac{\varepsilon\ \mu\ R_o^2}{k\ (p_1 - p_o)}\ \tau$$

$$= [0.1 \times 5.0 \times 10^{-7}\ (lb \cdot s/ft^2) \times 40^2\ ft^2 \times \tau]/[0.1\ Darcy \times 1.06 \times 10^{-11}\ (ft^2/Darcy) \times 35.3\ (lb/in.^2) \times 144\ (in^2/ft^2)]$$

$= 14{,}800\ \tau$ (t in seconds)

$= 4.12\ \tau$ (t in hours)

The initial mass of gas in the pores of the solid, calculated from the density at ambient conditions, is

$$m_i = 0.075\ \frac{lb}{ft^3} \times 13{,}400\ ft^3 = 1{,}000\ lb$$

$m = 1{,}000 \times M_o$ (m in lb).

[1] Active mass is defined as the mass of material initially contained in the containment shell.

We conclude for this example that no active gas is released until $\tau = 0.70$ (from Fig. VII K-4) or t = 2.88 h. At $\tau = 1.0$, or t = 4.12 h, the amount of active gas released would be $M_o = 0.65$ or m = 650 lb. The average flow rate over this time period is 524 lb/h.

Results for cylindrical coordinates where the dimensionless time for initial release of active gas to the atmosphere is plotted against the ratio of inner to outer radius are presented in Fig. VII K-5. The radius ratio is a parameter which must be included in cylindrical and spherical coordinates since the flow area is a function of radius. As in the case of Cartesian coordinates, there is a period of time when no active gas is released into the atmosphere. During this delay time, active gas is permeating through the solid and displacing the gas initially in the pores. The flow rate increases gradually from zero; however, by the time active gas starts to be released the flow rate is normally substantial. Use of results from the cylindrical coordinate case would be appropriate, for example, if active gas was released into a sand layer just beyond the radius of the cofferdam (see Fig. VII K-1). Since the clay above and below the sand layer would prevent appreciable vertical flow, gas would permeate radially outward to a place where it could be released such as a river channel.

The spherical coordinate results of Fig. VII K-6 may be applied to the analysis of the flow of pressurized gas after penetration of the containment floor. From a calculational standpoint both cases shown in Fig. VII K-1 are nearly identical.

In Fig. VII K-4 to VII K-6, results are presented for a constant driving pressure. Figure VII K-7 shows a specific case in spherical coordinates when the mass leaving the containment shell and permeating into the soil was calculated. The driving pressure in the containment shell would then decay as mass was lost to the soil. At the time active gas starts to be released from the outer boundary ($\tau = 1.0$) the driving pressure has decayed by only 5%. This pressure decay would have been less if cylindrical or Cartesian coordinates were used. We felt that the use of a constant pressure, in lieu of the more accurate pressure decay, is justified since the effect of mass loss is usually small and other factors such as operation of the emergency containment cooling system are probably more dominant.

K3.2 ONE-DIMENSIONAL MULTIPHASE FLOW

Two phase flow with condensation was studied and the results are presented in Figs. VII K-8 through K-11. Containment shell gas is taken to be pure saturated steam at the indicated pressure. If the containment shell pressure is held constant for example at 100 psia, the pressure, temperature, and water saturation distributions may be found for any position and time using the similarity variable θ (see Fig. VII K-8). This similarity variable gives spatial variation for a given time where a small value of θ corresponds to positions close to the pressure source. It also gives temporal variation for a given spatial position with time increasing from right to left in the direction of decreasing θ.

If we consider a given time, the interface between the soil and the cavity filled with steam is at $\theta = 0$. Here, the temperature and pressure are equal to the containment shell conditions so that the normalized values are unity. Also the steam quality is 100% yielding a water saturation that is zero. As we focus on increasing values of X (or θ), the pressure decreases as a result of momentum loss in the pores of the solid. In this region, $0 < \theta < 0.04$, the soil has been heated to the saturation temperature of the steam. The slightly negative slope corresponds to a decrease in saturation temperature with decreasing pressure. Steam had previously condensed to water in raising the temperature of the soil, but no further condensation is taking place in this region. Some of this water remains in the pores resulting in an increase in water saturation.

As θ increases just beyond 0.04, a point is reached where the soil has not yet reached the steam saturation temperature. Condensation here results in an abrupt increase in water saturation. This region is very narrow and the temperature decreases abruptly to ambient temperature.

Beyond $\theta = 0.04$, the water saturation remains higher for some distance because the previously condensed water has been pushed ahead of the condensation region. Water and gas flow are nearly incompressible in this region and the pressure gradient is almost linear. For $\theta > 0.2$, flow is essentially that of the gas phase alone.

The active fluid front is determined by integrating the velocity of the gaseous phase with time. For all three values

of pressure examined, this interface occurred at a value of $\theta = 0.05$.

In comparing the ideal gas calculation to the two-phase, condensible flow calculation in order to determine the extent of radioactive penetration, we must consider that while the total porosity of the soil is probably close to 30%, the liquid fills most of the void space. If we choose the initial saturation of 70%, then we should compare an ideal gas calculation with porosity of about 10% to the two-phase calculation of total porosity equal to 30%. Comparing results of Figs. VII K-4 and VII K-9 for 50 psia, we have an interface time τ and similarity variable θ of 0.07 and 0.05, respectively. Converting to a dimensional time for the ideal gas and two-phase flow cases, we have

$$t_i = \frac{\varepsilon_i \mu R_o^2}{k(p_1 - p_o)} \tau \quad \text{(ideal gas)} \qquad \text{(VII K-23)}$$

$$t_t = \frac{X^2 \varepsilon_t \mu R_o^2}{4 k p_1 \theta^2} \quad \text{(two-phase flow)} \qquad \text{(VII K-24)}$$

where as before $X = x/R_o$. We are interested in the downstream face of the column where $X = 1$, so that

$$\frac{t_t}{t_i} = \frac{\varepsilon_t (p_1 - p_o)}{4 \varepsilon_i p_1 \theta^2 \tau}$$

$$= \frac{0.3 \times (50 - 14.7) \text{ psia}}{4 \times 0.1 \times 50 \text{ psia} \times 0.05^2 \times 0.70}$$

$$= 303 . \qquad \text{(VII K-25)}$$

In other words, the estimated time for release of active material in the two-phase, flow calculation is about 300 times longer than in the ideal gas approximation. These two sets of results (containment-shell gas consisting of 100% steam or ideal gas) are bounds for release of radioactive material. Cases where mixtures of steam and ideal gas are forced through the soil would give results in between these limits.

Figures VII K-9 and VII K-10 show similar results for containment-shell pressures of 50 and 25 psia. Figure VII K-11 shows containment-shell pressure decay as fluid is lost into the soil. The initial containment-shell pressure does not change appreciably for this case so that results are similar to those of Fig. VII K-8. The pressure curve is normalized using the cavity pressure in all cases, but in Fig. VII K-11 this pressure is a function of time. Temperature curves are normalized in a similar fashion.

K3.3 TWO-DIMENSIONAL IDEAL GAS

We performed a two-dimensional calculation with the specific geometry shown in Fig. VII K-2 to show effects of spatial variation in soil permeability and a specific power-station geometry. These calculations were found to be time consuming. Results in Figs. VII K-12 to VII K-14 show the pressure distribution and the location of the active gas front at three different times. At the later times, a deviation from the one-dimensional spherical case occurs which delays the propagation of the active gas front. An initial value of containment shell pressure equal to 100 psia was chosen and allowed to decay as mass diffused into the soil. The change in driving pressure was negligible for this case.

Note that the permeability of 0.1 Darcy, which corresponds to that expected for sand, was chosen for the lower region. Had a lower value of permeability been used, results would have been similar except that propagation of the front would have taken a longer time.

K3.4 STEAM GENERATION BY MOLTEN POOL

If the core melt has penetrated the containment floor (second case in Fig. VII K-1), the after-heat from the reactor would vaporize the water present in the pores of the adjacent soil. This steam generation is described in Fig. VII K-15 along with values of the quantity of steam required to pressurize a 2×10^6-ft^3 containment shell to 50 and 100 psia. Although the heat generation rate was held constant at 3.5×10^7 Btu/h in the molten pool, the steam generation rate decreases with time since heat must penetrate more and more soil before reaching an area where water saturation is still significant. Some steam is lost by flow into the soil. This loss of steam is normally an insignificant percentage of the steam generated and only becomes important if release of radioactive gases occurs within a few hours after the accident.

Heat dissipation through the containment shell into the atmosphere was found to be negligible. Some cooling system must be functioning to keep the pressure within the containment shell below its

selected design or burst pressure of 50 or 100 psia, respectively.

K4. ADDITIONAL CONSIDERATIONS

No study would be complete without mentioning peripheral areas of interest. Although we studied permeation of fluids through soils, some attention should be given to the annular region between the cofferdam and the containment shell as a possible area from which some radioactive material might be released to the atmosphere. Our experience indicates adequate containment can be achieved with proper attention to the materials used in filling this region. It may be desirable to experimentally obtain an effective permeability through regions considered to be nearly gas tight seals. Results presented in this and future studies could be used to estimate the severity of any leakage and to specify any corrective action needed.

Another subject which requires special attention is the propagation of fissures through the soil outside the cofferdam. These fissures (Ref. 7) may open should pressures below the containment shell reach values near the hydrostatic overburden pressure exerted by the soil. The overburden pressure is of the order of 1 psi per ft of depth which generally exceeds the design pressure of the containment shell. From a standpoint of fissure propagation, the most susceptible soils are those with low permeability. One would desire a high permeability to eliminate fissure propagation and a low permeability to prevent release of radioactive debris by diffusion through the soil. Backfill can be selected to achieve optimum conditions.

K5. CONCLUSIONS

a. Results for constant driving pressures of 100, 50, or 25 psia show that the time required for ideal radioactive gases to reach the surface of the ground are of the order of years if soil permeabilities are near those anticipated for silty type clays (0.0001 Darcy). These release times are shortened to about 10 h if permeabilities expected for sand type materials (0.1 Darcy) exist.

b. Decay of the driving pressure in a typical containment shell due to leakage of gas into the soil is insignificant for most cases because of the large volume of the shell. Incorporation of a pressure decay is important for small gas source volumes or if the soil permeability is large. Other factors such as operation of various cooling systems are probably more dominant in affecting the driving pressure.

c. An estimate of the release time for multiphase flow (injection of all steam from the containment shell) indicates that it may be over two orders of magnitude longer than that predicted with injection of ideal gas. Cases where mixtures of steam and ideal gas are forced through the soil would give results falling between these bounds.

d. Steam generation, which results from core melt penetrating the containment floor, is large enough that some cooling systems must be in operation within 4 or 5 days after the accident in order to prevent overpressurization of the containment shell. Heat dissipation through the containment shell to the atmosphere is negligible.

e. Examination of the permeability between a typical cofferdam and containment shell is suggested since this annular region is an area from which some radioactive material might possibly be released to the atmosphere. Results depend upon detailed knowledge of material properties and exact construction details.

f. This analysis and future studies may be used to specify materials at reactor sites yet to be built. Backfill near the reactor may be specified for optimum conditions and materials adjacent to the containment shell may be chosen to assure adequate confinement of radioactive materials.

Acknowledgments

A study such as this is most efficient if several people combine their different talents. Calculations of flow through the soil were performed by B. R. Bowman and J. H. Pitts. J. P. McKay calculated dissipation of heat through the containment shell wall to the atmosphere, organized most of the input numbers used in the calculations, and performed some of the computer work. R. W. Martin performed the steam generation calculation. J. E. Mellor helped with a portion of the computer work.

V. N. Karpenko, C. E. Walter, and D. M. Norris offered suggestions for the study and reviewed the writing of the report. H. Lentzner edited this report and made numerous improvements to the writing.

R. Ritzman of Battelle Memorial Institute was responsible for the instigation of this study, formulation of the problem, and determination of the basic input parameters. He also guided our work as we progressed so that results would be of general applicability to safety analysis problems.

References

1. F. A. Morrison, Jr., Transient Gas Flow in a Porous Column, Lawrence Livermore Laboratory, Rept. UCRL-52929 (1971).

2. F. A. Morrison, Jr., Transient Multiphase Multicomponent Flow in Porous Media, Lawrence Livermore Laboratory, Rept. UCRL-74327, Rev. 1 (1972).

3. B. R. Bowman, TWIG, A Computer Code for the Calculation of Two-Dimensional Ideal Gas Flow in Porous Media, Lawrence Livermore Laboratory, Rept. UCID-16320 (1972).

4. R. J. M. Dewiest, Flow Through Porous Media (Academic Press, 1969) pp. 1-6.

5. Ibid, pp. 78-82.

6. E. L. Wilson and R. E. Nickell, "Application of the Finite Element Method to Heat Conduction Analysis," Nuclear Engineering and Design 4, 276 (1966).

7. J. H. Pitts, Gas Initiated Crack Propagation in a Porous Solid - A Progress Report, Lawrence Livermore Laboratory, Rept. UCID-16236 (1973). a40 a40

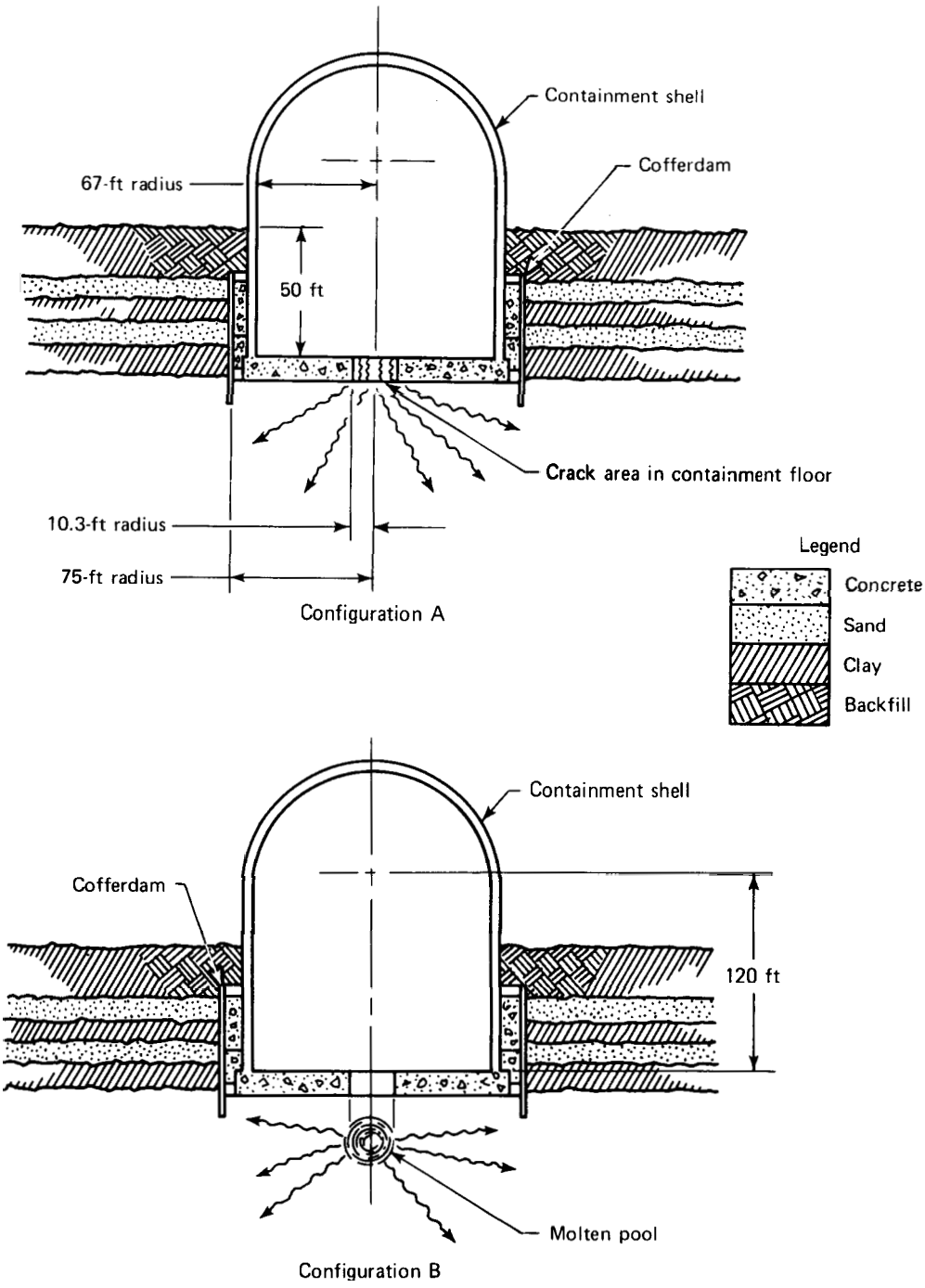
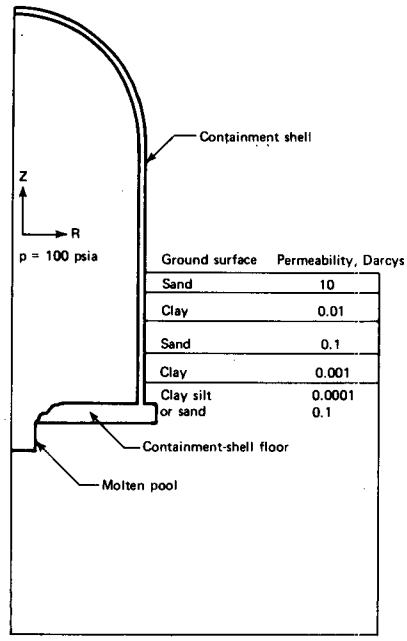
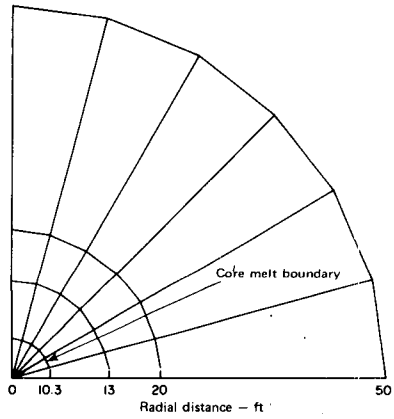


FIGURE VII K-1 Schematic of Two Possible Configurations After a Core Meltdown Accident in a Large Power-Reactor Station



Ground surface	Permeability, Darcys
Sand	10
Clay	0.01
Sand	0.1
Clay	0.001
Clay silt or sand	0.0001 0.1

FIGURE VII K-2 Configuration for the Two-Dimensional, Single-Phase Calculation in Cylindrical Coordinates



	Conditions			
	Core melt	Soil		
		Wet	Average	Dry
κ, Btu/ft·h·°R	10.0	1.0	0.75	0.5
C, Btu/lb·°R	1.12	0.44	0.35	0.26
ρ, lb/ft^3	270	125	118	112

No. of divisions in each region

Range, ft	No. of radial divisions
0.0 to 10.3	8
10.3 to 13.0	10
13.0 to 20.0	14
20.0 to 50.0	30

FIGURE VII K-3 Schematic of the Element Mesh for the Steam Generation Calculation

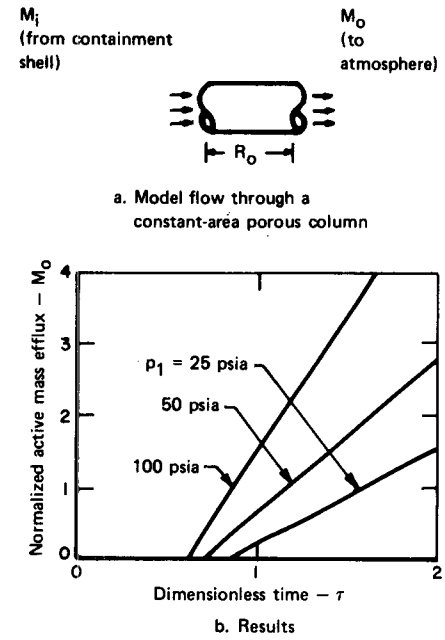


FIGURE VII K-4 The Effect of Time and Pressure on the Normalized Active Mass Efflux Calculated in Cartesian Coordinates for an Ideal Gas and for a Value p_o of 14.7 PSIA

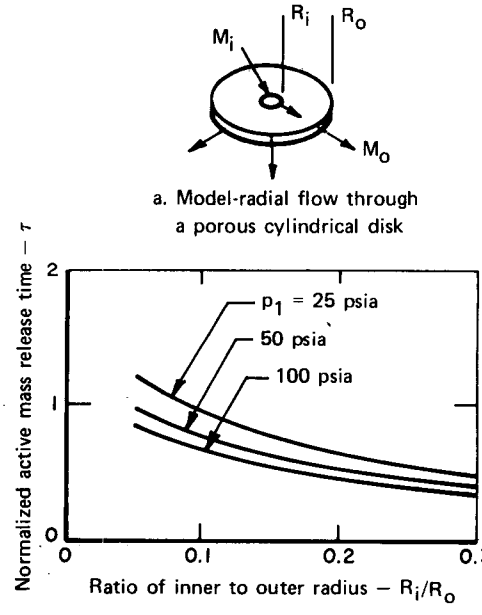


FIGURE VII K-5 Normalized Time at which the Active Containment-Shell Gas is Released at Radius R_o; Calculated in Cylindrical Coordinates for an Ideal Gas and a Value of p_o of 14.7 PSIA

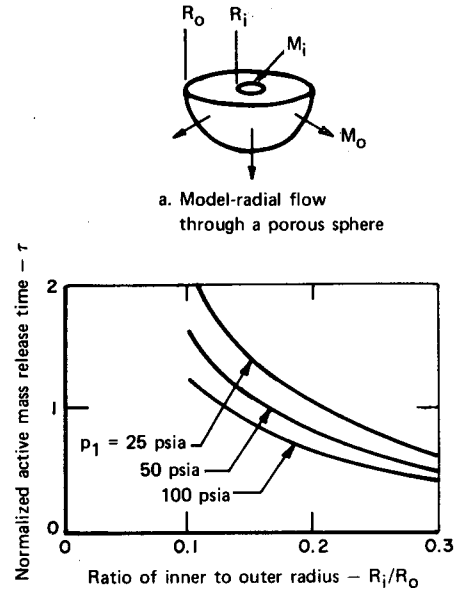


FIGURE VII K-6 Normalized Time at which Active Containment-Shell Gas is Released at Radius R_o for Varying Radius Ratios: Calculated for a p_o Value of 14.7 PSIA

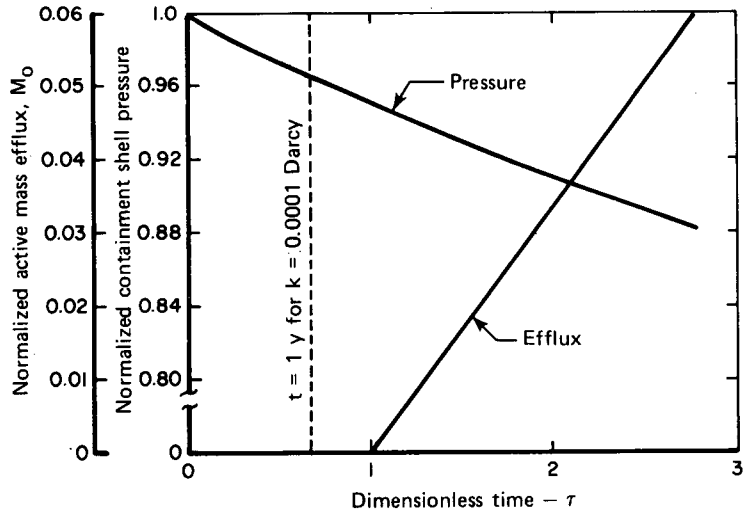


FIGURE VII K-7 Containment-Shell-Pressure Decay and Active Mass Efflux for Core Meltdown Analysis: Calculated in Spherical Coordinates for an Ideal Gas and the Following Parameters: p_1 = 100 PSIA, ε = 0.08, R_i = 15 Ft, R_o = 120 Ft, $\mu = 5 \times 10^{-7}$ Lb • S/Ft^2, and t = 1.3 τ/K, where t is the Time in Hours

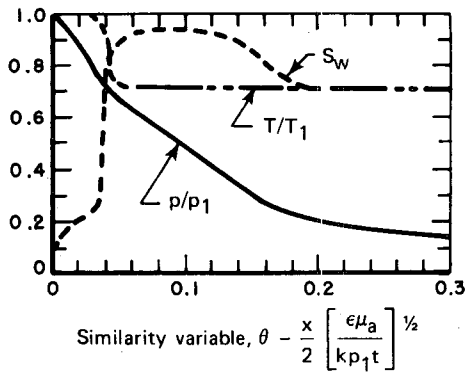


FIGURE VII K-8 Water Saturation, Normalized Pressure, and Temperature Distribution for p_1 = 100 PSIA

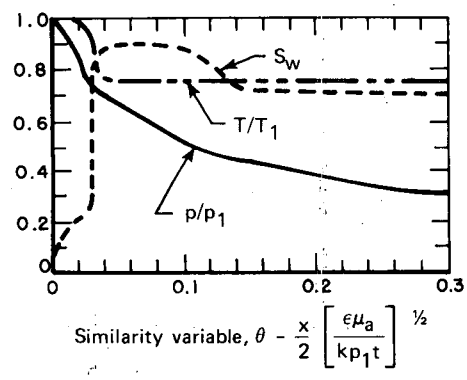


FIGURE VII K-9 Water Saturation, Normalized Pressure, and Temperature Distribution for p_1 = 50 PSIA

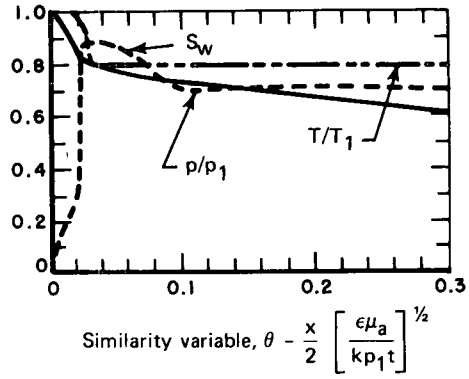


FIGURE VII K-10 Water Saturation, Normalized Pressure, and Temperature Distribution for p_1 = 25 PSIA

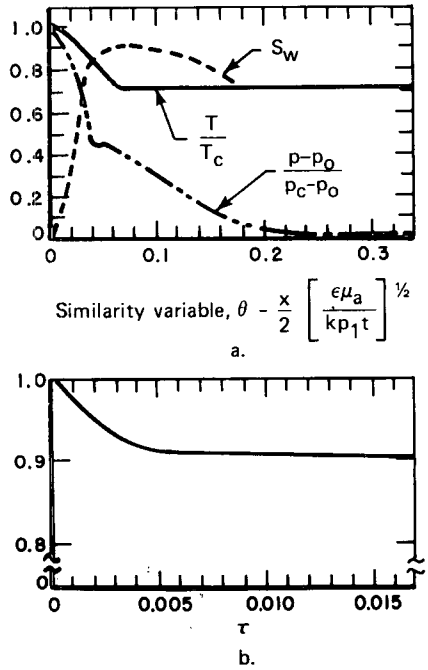


FIGURE VII K-11 Part (A) Shows Water Saturation, Normalized Pressure, and Normalized Temperature Distribution for Pressure Decay for p_1 = 1 p_1 = 100 PSIA. Part (B) Shows Containment-Shell Pressure as a Function of Time at p_1 = 100 PSIA

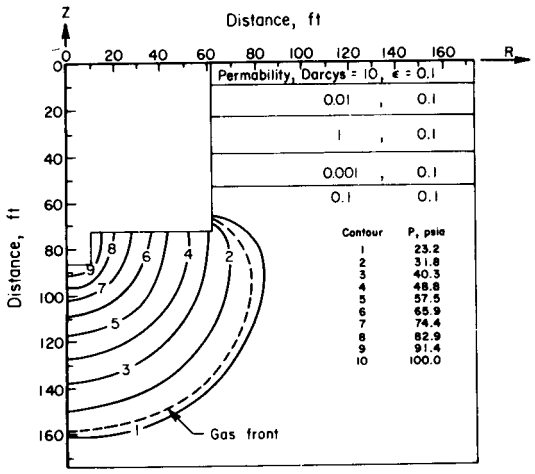


FIGURE VII K-12 Pressure Profile of a Two-Dimensional Calculation at t = 2.9 H

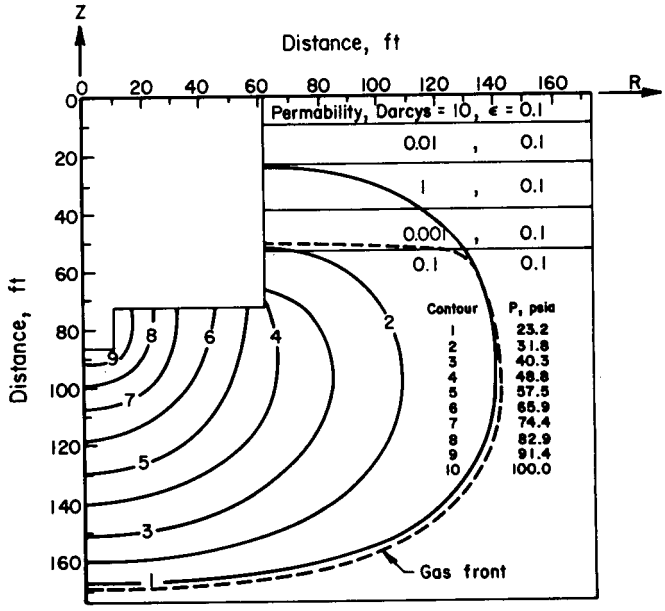


FIGURE VII K-14 Pressure Profile of a Two-Dimensional Calculation at t = 14.7 H

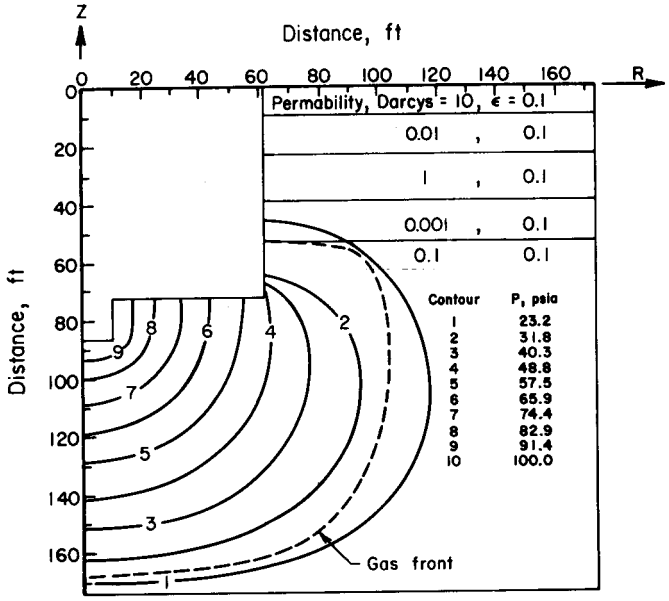


FIGURE VII K-13 Pressure Profile of a Two-Dimensional Calculation at t = 6.2 H

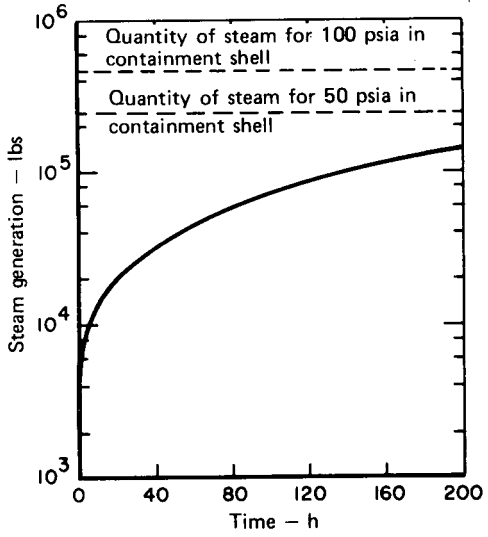


FIGURE VII K-15 Steam Generation for Core Melt in Contact with Wet Soil for a Core After-Heat of 3.5×10^{-7} BTU/H and a Containment-Shell Volume of 2×10^{6} Ft^3

WASH–1400
(NUREG 75/014)

PHYSICAL PROCESSES

in

REACTOR MELTDOWN ACCIDENTS

APPENDIX VIII

to

REACTOR SAFETY STUDY

by

W. A. Carbiener
P. Cybulskis
R. S. Denning
J. M. Genco
N. E. Miller
R. L. Ritzman
R. Simon
R. O. Wooton

Contract W-7405-eng-92
Battelle Columbus Laboratories

U.S. NUCLEAR REGULATORY COMMISSION

OCTOBER 1975

Appendix VIII

Table of Contents

Section			Page No.
1.	INTRODUCTION		VIII-1
	1.1	Objectives	VIII-1
	1.2	Interactions	VIII-1
	1.3	Approach	VIII-2
	1.4	Limitations	VIII-2
	1.5	Definitions	VIII-2
		1.5.1 Sequence	VIII-2
		1.5.2 Subsequence	VIII-2
2.	PWR ANALYSES		VIII-9
	2.1	Accident Sequences Resulting in Core Meltdown	VIII-9
	2.2	Analysis of Degraded Accident Behavior	VIII-10
		2.2.1 Basic Assumptions	VIII-10
		2.2.2 Accident Time Scale	VIII-11
		2.2.3 Core Meltdown	VIII-11
		2.2.4 Primary Vessel Meltthrough	VIII-12
		2.2.5 Containment Vessel Penetration	VIII-12
		2.2.6 Steam Explosions	VIII-13
		2.2.7 Hydrogen Combustion	VIII-14
		2.2.8 Containment Response	VIII-14
		2.2.9 Leak Rate from Containment	VIII-16
	2.3	Subsequent Probabilities	VIII-16
		2.3.1 Definitions	VIII-17
		2.3.2 Containment Failure Resulting from a Steam Explosion	VIII-17
		2.3.3 Containment Meltthrough with Containment Isolation Failure	VIII-19
		2.3.4 Hydrogen Combustion	VIII-19
		2.3.5 Containment Overpressurization	VIII-19
		2.3.6 Containment Meltthrough	VIII-20
3.	BWR ANALYSES		VIII-27
	3.1	Accident Sequence Resulting in Core Meltdown	VIII-27
		3.1.1 Electric Power System (EPS)	VIII-27
		3.1.2 Vapor Suppression System (VSS)	VIII-27
		3.1.3 Containment Leakage (CL)	VIII-27
		3.1.4 Emergency Cooling Injection (ECI)	VIII-27
		3.1.5 Emergency Cooling Function (ECF)	VIII-27
		3.1.6 Scram	VIII-27
		3.1.7 Long-Term Cooling (LTC)	VIII-28
	3.2	Analysis of Degraded Accident Behavior	VIII-28
		3.2.1 Basic Assumptions	VIII-28
		3.2.2 Accident Time Scale	VIII-28
		3.2.3 Core Meltdown	VIII-28
		3.2.4 Pressure Vessel Meltthrough	VIII-29
		3.2.5 Steam Explosions	VIII-29
		3.2.6 Containment Vessel Penetration	VIII-30
		3.2.7 Hydrogen Combustion	VIII-30
		3.2.8 Containment Response	VIII-30

Table of Contents (Continued)

Section		Page No.
3.2.9	Containment Isolation Failures	VIII-32
3.2.10	Secondary Containment	VIII-32
3.3	Subsequence Probabilities	VIII-33
APPENDIX A	THERMAL ANALYSES	VIII-41
APPENDIX B	PHYSICAL EXPLOSIONS RESULTING FROM CONTACT OF MOLTEN MATERIALS AND WATER	VIII-73
APPDNDIX C	MODEL STUDY OF PHYSICAL EXPLOSIONS	VIII-89
APPENDIX D	NONCONDENSABLE GASES	VIII-113
APPENDIX E	CONTAINMENT FAILURE MODES EVALUATION	VIII-129

Appendix VIII

List of Tables

Table		Page No.
VIII 1-1	PWR Data	VIII-4
VIII 1-2	BWR Data	VIII-7

List of Figures

Figure		Page No.
VIII 2-1	Time Required for 80 Percent Core Melting from the Onset of Melting	VIII-21
VIII 2-2	PWR Containment Pressure Response During the Design Basis Accident and with the Assumed Failure of the Low Pressure Recirculation System	VIII-21
VIII 2-3	PWR Containment Pressure Response with Assumed Failures of the Containment Spray Injection System and Low Pressure Recirculation System	VIII-22
VIII 2-4	PWR Containment Pressure Response with Assumed Failures of the Containment Spray Recirculation System and Low Pressure Recirculation System	VIII-22
VIII 2-5	PWR Containment Pressure Response with Assumed Failures of Containment Heat Removal System and Low Pressure Recirculation System	VIII-23
VIII 2-6	PWR Containment Pressure Response with Assumed Failures of Containment Spray Injection System, Containment Spray Recirculation System, and Low Pressure Recirculation System	VIII-23
VIII 2-7	PWR Containment Pressure Response with Assumed Failure of the Electric Power System and the Attendant Loss of All Engineered Safeguards	VIII-24
VIII 2-8	PWR Containment Pressure Response with Assumed Failures of Safety Injection System, Containment Spray Injection System, and Containment Spray Recirculation System	VIII-24
VIII 2-9	PWR Containment Pressure Response with Assumed Failures of Safety Injection System, Containment Spray Recirculation System, and Containment Heat Removal System	VIII-25
VIII 2-10	PWR Containment Pressure as a Function of Leak Rate for an Assumed LOCA with No Containment Safeguards	VIII-25
VIII 2-11	PWR Containment Event Tree	VIII-26
VIII 3-1	PWR Containment Pressure as a Function of Composition and Temperature	VIII-37

List of Figures (Continued)

Figure		Page No.
VIII 3-2	BWR Containment Pressure Response with Assumed Failure of Emergency Core Cooling System Function.....	VIII-37
VIII 3-3	BWR Containment Pressure Response with Assumed Failure of Emergency Core Cooling System Operation.....	VIII-38
VIII 3-4	BWR Containment Pressure Response as a Function of Leak Rate with Assumed Loss of Long-Term Cooling and All the Noncondensables in the Suppression Chamber.....	VIII-38
VIII 3-5	BWR Containment Pressure as a Function of Leak Rate with Assumed Loss of Long-Term Cooling and Noncondensables Equalized Between the Drywell and Suppression Chamber.....	VIII-39
VIII 3-6	BWR Containment Event Tree.....	VIII-39

Section 1
Introduction

This report describes the results of the Reactor Meltdown Task conducted at Battelle's Columbus Laboratories as a part of a larger effort being undertaken by the U. S. Atomic Energy Commission to evaluate the probabilities and consequences of postulated accidents in large light water power reactors. The details of the investigations performed under this task are presented in the appendices to this report. The body of the report gives the results and conclusions that are required as input to the other tasks of the overall study.

1.1 OBJECTIVES

The objective of this study has been to describe the course of events that would be expected to occur during various hypothetical reactor meltdown accidents. The key parameters and physical processes considered included:

a. Times for the initiation and completion of core melting

b. Steam generation rates during core meltdown

c. Rate and extent of reaction between Zircaloy cladding and water (steam)

d. Likelihood and potential consequences of hydrogen burning or exploding in the containment building

e. Probability and magnitude of steam explosions in the reactor vessel due to the interaction of the molten core with water; probability of containment failure as a result of such steam explosions

f. Time at which the molten core penetrates the reactor vessel

g. Potential for steam explosions as the molten core drops to the floor of the reactor cavity and the probability of containment failure due to such explosions

h. Pressure-time histories within the containment building, including the potential and timing of containment failure due to internal over-pressurization

i. Interaction of the molten core with the concrete foundation mat of the containment, including the possibility and timing of containment melt-through.

In the cases analyzed, core degradation was a result of a loss-of-coolant accident (LOCA) accompanied by the assumed failure of various combinations of engineered safety features.[1] For the pressurized water reactors (PWR) the initiating event was a complete severance of a large cold-leg or hot-leg pipe in the primary system. For the boiling water reactors (BWR) severance of a recirculation line was assumed. It is expected that the consequences of these large pipe-break accidents will bound the consequences of other potential accidents in which the principal difference is an extension of the time scale.

1.2 INTERACTIONS

As one facet of the AEC's investigation of reactor accidents, this Task interacted closely with other areas of AEC's overall study. The combinations of engineered safety features which are assumed to fail in the various LOCA sequences leading to core meltdown were furnished to Battelle by the Reactor Safety Study located at the AEC. The event trees and fault trees that define the various accident sequences and failures of engineered safety features involved were developed by the AEC. Further, the Reactor Meltdown Task has been closely associated with the Fission Product Source Term Task, also performed at Battelle's Columbus Laboratories,[2] which involved the definition of the size of the fis-

---

[1] Subsequent analyses have been performed for small-break and transient accidents based upon the methods described in this Appendix. These sequences are discussed in Appendices V and XI. The results of these analyses are included in Appendix V.

[2] With assistance from Battelle Northwest Laboratory, Oak Ridge National Laboratory, and Aerojet Nuclear Company.

sion product source term that would escape the containment boundary as a function of time for the various accident sequences delineated by the AEC Reactor Safety Study. The results of the Reactor Meltdown Task are a necessary input for the evaluation of the release of radioactivity from the containment.

1.3 APPROACH

The Reactor Meltdown Task was undertaken in the realization that it may not be possible to describe with certainty some of the complex physical phenomena that may occur during a meltdown accident. In those instances where data or understanding of a particular aspect were incomplete, bounding calculations were performed to establish the limits of uncertainty. Typically, the accident sequence was divided into a few discrete time intervals and the events in each interval were modeled to the extent possible. Basic assumptions of, and inputs into the models were then varied to establish the bounds of uncertainty for the course and consequences of the events of interest.

1.4 LIMITATIONS

The PWR design utilized is a three-loop plant with subatmospheric containment; the BWR design assumed a steel drywell and toroidal suppression pool containment.[1] Since reactor design clearly affects the probabilities and consequences of accidents, it may not be appropriate to generalize the conclusions drawn from these studies to all PWR's and BWR's. Although the specific cases analyzed were based on design basis pipe breaks, it is expected that the results can be used to approximate or bound the consequences of other accidents, such as smaller pipe breaks, involving the same failures of engineered safety features. However, care must be exercised in extending these results to other accidents to ensure that the same physical phenomena occur at the same relative time in the meltdown accident as those that have been evaluated. The methods discussed in this report should be applicable to meltdown accidents resulting from initiating events other than those specifically assumed here.

As noted above, the Reactor Meltdown Task is one portion of a larger study. The output of this task has been directed at supplying the needs of the overall program and a concerted effort has been made to keep the assumptions in this task consistent with those of the broader study. Therefore care should be exercised in excerpting results or in drawing conclusions from the results presented in this report divorced from the greater context. In particular, the seriousness of the consequences of reactor accidents cannot be evaluated separately from the probabilities of their occurrence.

In reporting times for events, magnitudes of various effects, and probabilities of the occurrence of particular events, a best estimate for the value is accompanied by an error band. The error or uncertainty bands have been derived from sensitivity studies and physical constraints on the system and should encompass the actual value of any given parameter. Thus the best-estimate values reported here should be considered together with the associated uncertainty bands.

1.5 DEFINITIONS

The use of event trees to describe the combinations of events that might occur in a reactor accident has been extremely helpful in studying the accidents and in providing a common basis for the exchange of information between the different tasks. However, since the event trees were subject to change during the investigation, it was felt that the results of this report should not be related to the format of a specific tree. In the realization that the results of the report will be employed in conjunction with event trees the following definition are used to distinguish between branches which represent failure of engineered safety features and the branches which represent alternative paths to containment failure in a meltdown accident.

1.5.1 SEQUENCE

An accident sequence involves a specified combination of failures of engineered safety features accompanying a LOCA. If A, B, and C represent engineered safety features in an event tree, then Sequence ABC represents the accident which involves the combined failure of the three safety features. The probability of the occurrence of ABC is determined by fault tree analysis.

1.5.2 SUBSEQUENCE

A subsequence is defined as a path to containment failure within a meltdown

[1] Basic data for the PWR and BWR investigated are presented in Tables VIII 1-1 and VIII 1-2, respectively.

accident. Thus for Sequence ABC possible subsequences might involve melt-through of the containment floor, overpressurization failure of the containment, or breaching of the containment by missiles developed in a steam explosion.

In the terminology of Appendix I "Event Trees" of the Reactor Safety Study report, a sequence is a branch of an accident event tree and a subsequence is a branch of a containment event tree.

Since engineered safety systems are generally composed of diverse and redundant components, the inoperability of a safety system implies multiple failures. When safety features do operate it is necessary to establish the level or capacity at which they perform. Since safety systems are overdesigned to assure a margin of safety in their performance, partial operation of systems is often adequate to provide the required function. Therefore, a set of minimum safeguards has been determined to set clearly defined limits for functioning or nonfunctioning of systems. In the analysis of meltdown accidents, minimum safeguards are assumed for those cases in which safety system performance is indicated. The times at which systems begin to operate and/or fail to operate will also have a bearing on the consequences of a given accident sequence. For the present analyses it is assumed a system failure, if it occurs, will take place at the earliest time that the particular system is required to function.

TABLE VIII 1-1 PWR DATA

Nominal power	2,441 Mwt
	8,331 x 10^6 Btu/hr
Internal energy of water	246.9 x 10^6 Btu
Sensible heat in the core	16.35 x 10^6 Btu
Total water in the system	423,200 lb
Aug. temperature (Excl. pres.)	571.8 F
Pressure	2280 psig
Reactor coolant system volume	8,387 ft^3
Pressurizer volume, total	1,336 ft^3
water	816
steam	520
Three accumulators, total volume	4,350 ft^3
water volume	2,775 ft^3
pressure	675 psig
temperature	120 F
Containment recirculation spray 2 systems, flow each	3,500 gpm
Containment free volume	1.8 x 10^6 ft^3
Initial temperature	105 F
Initial pressure	10 psia
Dew point	80 F
Primary system hot metal	1,686,285 lb
Temperature	572 F

Containment Heat Sinks

	Thickness, ft	Area, ft^2
Walls inside containment	1.0	3,320
Walls inside containment	2.0	27,600
Walls inside containment	3.0	19,400
Walls inside containment	4.0	5,000
Walls inside containment	6.5	2,100
Containment wall	4.5	46,747
Dome	2.5	25,000
Floor above foundation mat	2.0	11,250
Foundation mat	10.0	11,250
Containment liner		
Walls	0.38 in.	46,747
Dome	0.50 in.	25,000
Floor	0.25	11,250
Miscellaneous metal - 1,200,000 lb		

Core

Equivalent diameter	119.7 in.
Active height	144.0 in.
L/D	1.202
Total cross sectional area	78.3 ft^2

TABLE VIII 1-1 (Continued)

Core (Continued)		
No. of fuel assemblies		157
Rods per assembly		204
Pitch		0.563 in.
Assembly dimensions		8.426 in. square
Fuel rod diameter		0.422 in.
Clad (Zr-4) thickness		0.0243 in.
Total number of fuel rods		32,028
Core weight		226,200 lb
UO_2		175,600
Zircaloy		36,300
Misc.		14,300
Fuel pellet diameter,	Region 1	0.3669 in.
	2 and 3	0.3659 in.
Fuel pellet length		0.6 in.
Diametral gap,	Region 1	0.0065 in.
	2 and 3	0.0075 in.
Fuel density,	Region 1	94%
	2	92
	3	91
Fuel enrichment,	Region 1	1.85 w/o
	2	2.55
	3	3.10
No. of grid spacers		7
Neutron adsorber		Ag-In-Cd
Clad		304 ss
Clad thickness		0.024 in.
No. of control assemblies		53
Full length		48
Part length		5
Rods per assembly		20
Burnable poison rods		816
No. per assembly		12
No. of assemblies		68
Material		Borosilicate glass
O.D.		0.4395 in.
I.D.		0.2365 in.
Clad		304 ss
Boron (natural) loading		0.0429 g/cm
Reactor vessel		
I.D. of shell		157 in.
Belt line thickness (w/o clad)		7.875 in.
Head thickness		5.0 in.
Clad thickness		0.125 in.
Overall height		40 ft-5 in.

TABLE VIII 1-1 (Continued)

Reactor vessel (Continued)	
Inlet nozzles	27.5 in. tapered to 35.4 in.
Outlet nozzles	29 in.
Water volume with core and internals in place	3,718 ft^3
Core barrel I.D.	133.9 in.
O.D.	137.9 in.
Thermal shield I.D.	142.6 in.
O.D.	148.0 in.
Safety Injection Charging Pumps	
Number	3
Design pressure, discharge	2750 psig
Design pressure, suction	250 psig
Design temperature	250 F
Design flow	150 gpm
Maximum flow	600 gpm
Design head	5800 ft
Low Head Safety Injection Pumps	
Number	2
Design pressure, discharge	300 psig
Design temperature	300 F
Design flow	3000 gpm
Design head	225 ft
Maximum flow	4000 gpm
Containment Spray Pumps	
Number	2
Design flow	3,200 gpm
Design head	225 ft
Design pressure	250 psig
Recirculation Spray Pumps Inside Containment	
Number	2
Design flow	3,500 gpm
Design head	230 gpm
Recirculation Spray Pumps Outside Containment	
Number	2
Design flow	3,500 gpm
Design head	249 ft
Recirculation Spray Coolers	
Number	4
Design duty, each	55,534,520 Btu/hr
Refueling Water Storage Tank	
Volume	350,000 gal
Boron concentration	2,500 ppm
Design pressure	Hydraulic head
Design temperature	150 F
Water temperature	45 F

TABLE VIII 1-2 BWR DATA

Rated power	3,293 Mwt
	1.12456×10^{10} Btu/hr
Steam flow rate	13.381×10^{6} lb/hr
Core coolant flow	102.5×10^{6} lb/hr
Feedwater flow	13.3×10^{6} lb/hr
Feedwater temperature	376.1 F
Steam pressure in dome	1020 psig
Coolant enthalpy at inlet	521.2 Btu/lb
Core Avg. quality	13.2% steam
Recirculation pump flow	45,200 gpm
Normal primary system operating temperature	547 F
Primary System Coolant Inventory During Operation	
Reactor Vessel	
Subcooled liquid	7,847.4 ft^3
Saturated liquid	4,004.7 ft^3
Steam	8,813.5 ft^3
Piping	
Recirculation	1,227.7 ft^3
Feedwater	815.9 ft^3
Steam	3,125.6 ft^3
Volume in Reactor Vessel up to Jet Pump Inlet	
Control rods fully in	4,100 ft^3
Control rods fully out	4,000 ft^3
Reactor Vessel	
Inside diameter	251 in.
Inside height	72 ft-11-1/8 in.
Design pressure	1250 psig
Design temperature	575 F
Thickness (with clad)	6-5/16 in.
Vessel Weights	
Bottom head	207,500 lb
Vessel shell	842,300
Vessel flange	105,800
Support skirt	28,200
Other components	65,000
Top head	252,200
Total vessel	1,501,000 lb
Vessel Internals	
Core shroud	116,900 lb
Shroud head-steam separator	139,600
Core support	20,500
Top guide	15,200
Fuel support pieces	11,300
Control rod guide tubes	46,350
Jet pumps	22,700
Steam dryers	90,000
Core spray sparger	4,317
Total Weight of Internals (excluding fuel, control rods, feedwater spargers, vessel head cooling nozzles, in-core guide tubes, start-up sources, temporary control contains)	462,000 lb

TABLE VIII I-2 (Continued)

Primary System Weights	
Recirculation pipes	124,612 lb
Recirculation pumps and motors	140,000
Recirculation valves	50,800
Steam lines	164,000
Steam valves	52,000
Safety relief valves	13,000
Feedwater pipe	94,000
Feedwater valves	25,000
Concrete Heat Sinks	
2 ft thick	1,361,000 lb
3 ft thick	585,300
6 ft thick	622,050
12 ft thick	2,669,250
Miscellaneous metal in drywell	8×10^6 lb
Drywell	
Spherical section, diameter	67 ft
Spherical section, height	58 ft-4-3/8 in.
Spherical section, wall	3/4 - 1-1/4 in.
Knuckle section, diameter	Varies
Knuckle section, height	5 ft - 10-3/8 in.
Knuckle section, wall	2-7/8 in.
Cylindrical section, diameter	38 ft - 6 in.
Cylindrical section, height	34 ft - 2-1/4 in.
Cylindrical section, wall	3/4 - 1-1/2 in.
Top head (2:1 ell.), diameter	32 ft - 4 in.
height	15 ft - 1-1/2 in.
wall	1-1/2 in.
Vent Pipes	
Number	8
Internal diameter	6 ft - 9 in.
Downcomer Pipes	
Number	96
Internal diameter	2 ft
Submergence, nominal	4 ft
Pressure Suppression Chamber	
Chamber inner diameter	31 ft
Torus major diameter	111 ft - 6 in.
Drywell Free Volume	159,000 ft^3
Pressure Suppression Chamber Free Volume	119,000 ft^3
Drywell steel	1,550,980 lb
NPSH Requirements	
RHR pumps	35 ft at 11,900 gpm
	25 10,000
HPCI	18 4,000
Core Spray	28 3,850
	27 3,200

Section 2

PWR Analyses

2.1 ACCIDENT SEQUENCES RESULTING IN CORE MELTDOWN

Failures of the following engineered safety features have been considered in various combinations as they might affect the course of reactor meltdown following a LOCA: electric power, containment leakage, containment spray injection, containment heat removal, emergency core cooling injection and emergency core cooling recirculation. Definitions of the failures of these systems and their effect on the accident sequences are given below.

ELECTRIC POWER SYSTEM (EPS)

Insufficient a-c or d-c power available to the emergency buses to operate minimum design basis engineered safety feature equipment. Since the accumulators are a passive system, they are assumed to discharge in the loss-of-power case and deliver at least part of their water inventory to the reactor vessel. The accumulators by themselves are not, however, adequate to prevent reactor meltdown.

CONTAINMENT LEAKAGE (CL)

Inability to close one or more of the penetrations that serve as potential leak paths from the containment atmosphere in the event of a loss-of-coolant accident. Inability to isolate the containment will not in itself lead to reactor meltdown. Loss of isolation in the event of a reactor meltdown will, however, provide a path for fission product release and may affect the pressure transient in the containment.

CONTAINMENT SPRAY INJECTION SYSTEM (CSIS)

Delivery of borated water to the containment atmosphere through spray nozzles less than the equivalent of the capacity of one containment spray pump. The operation of the CSIS in a reactor meltdown accident affects both the pressure transient in containment and the scrubbing of fission products from the containment atmosphere.

CONTAINMENT SPRAY RECIRCULATION SYSTEM (CSRS)

Delivery of recirculation spray water through spray nozzles less than the equivalent of the output of two recirculation spray pumps for the first 24 hours or less than the equivalent of the output of one recirculation spray pump thereafter. In addition to containment pressure reduction and fission product scrubbing, the CSRS provides circulation to the hot side of the CSHX; thus, failure of the CSRS implies failure of CHRS.

SODIUM HYDROXIDE ADDITION SYSTEM (SHA)

NaOH injection less than a rate proportional to the total rate of depletion of the refueling water storage tank. NaOH that does not go directly to the CSIS is assumed to go into Emergency Coolant Injection System (ECI) water and then to the CSRS due to ECI overflow. Thus successful operation of CSIS is not a prerequisite for successful NaOH injection. The primary role of the NaOH is the removal of radioactive iodine from the containment atmosphere.

CONTAINMENT HEAT REMOVAL SYSTEM (CHRS)

Delivery of service water to the shell side of at least two of four containment heat exchangers corresponding to operating CSRS loops. Failure of CSHX constitutes loss of heat sink for the overall system and will lead to eventual core melting and containment failure even if the other safeguards are operating.

EMERGENCY COOLANT INJECTION (ECI)

Failure is defined as (1) delivery of less borated water than the equivalent to that contained in two accumulators (ACC) to the primary system cold leg immediately following a large pipe break, and (2) delivery of borated water at a rate less than the equivalent to the design output of one Low Pressure Injection System (LPIS) pump to the reactor system cold leg starting at about 30

seconds and continuing until the refueling water storage tank is effectively emptied. Operation of the High Pressure Injection System (HPIS) is not required for control of large pipe break accidents.

EMERGENCY COOLANT RECIRCULATION (ECR)

Delivery of water to the reactor coolant system cold legs from the containment sump at a rate less than the equivalent discharge from one LPIS pump. This mode of operation is designed to start at the end of ECI and requires the manual realignment of the pump suction from the refueling water storage tank to the containment sump.

2.2 ANALYSIS OF DEGRADED ACCIDENT BEHAVIOR

2.2.1 BASIC ASSUMPTIONS

The initiating event for the assessment of consequences has been assumed to be a double-ended cold-leg break, taking place instantaneously while the reactor is operating at full power with a core containing an equilibrium concentration of fission products. This type of accident has been found to result in the most rapid depressurization of the primary coolant system and leads to the most demanding requirements on the performance of the Emergency Core Cooling System (ECCS). The assumption of a double-ended cold-leg break implies that ECCS in the broken loop will not be able to perform their function and any emergency coolant supplied to that loop will spill out the break. If the primary system rupture were assumed in a hot leg of the system, then, since ECC injection is into the cold-leg piping, there would be a significantly higher probability that all of the emergency core coolant would perform its intended function.

A complete spectrum of accident conditions can be conjectured which involve the failure or partial performance of each of the redundant components of the engineered safety features. In performing detailed analyses of accident sequences, it is necessary to restrict the combinations of system performance to be evaluated to a finite tractable number. The results of the cases studied are then considered to be representative of a broader range of accidents that differ only slightly in detail. For the purposes of analysis, therefore, the failure and success of systems were assigned definitions which imply a precise level of performance rather than the range of performance that could occur in an accident. In the analysis of the accident consequences the potential availability and function of only the minimum design basis engineered safeguards were considered; i.e., if a component and/or system were assumed to function, only the minimum required capacity or capability was considered. For example, for a system consisting of two components with 100 percent redundancy, functioning would be taken as the operability of one of the two components at full capacity, although conceptually the same effect could be achieved by the operation of both components at some combination of reduced capacities.

For the PWR studied the minimum engineered safeguards would be:

- Two of three accumulators
- One of three high-pressure injection pumps
- One of two low-pressure injection pumps
- One of two containment spray injection pumps
- Two of four containment spray recirculation pumps
- Two of four containment heat exchangers.

For the purposes of these analyses, the emergency core cooling systems, if operable for any given accident sequence, are assumed to refill the reactor vessel and keep it filled to the level of the primary piping connections; excess capacity of the systems is assumed to spill to the containment sump. The LPIS, HPIS, and CSIS pumps, if initially operating, are assumed to function as long as a supply of water is available to each. Low Pressure Recirculation System (LPRS), if operable, starts as soon as ECI stops and continues to function as long as there is water in the containment sump, barring pump cavitation due to sudden containment depressurization. The CSRS pumps, if assumed to operate, start on demand and continue to function as long as there is water in the containment sump, again barring cavitation. The CHRS, if assumed operating, begin to function at the same time as the CSRS pumps and operate at their design capacity as long as the CSRS operates. For those accident sequences in which ECI was assumed to be inoperative, potential operation of ECR was not considered.

Since the accumulators comprise essentially a passive system, they were assumed to discharge in all cases and deliver at least part of their water inventory to the reactor vessel. This assumption tacitly implies that the probability of no emergency core cooling water being delivered to the vessel is significantly less than the probability of the delivery of some water by either the active or passive systems. Core meltdown sequences in which water is present in the vessel following blowdown entail significant metal-water reactions and the potential for steam explosions when the molten core comes into contact with the residual water in the bottom of the reactor vessel. If the accumulators were to fail to deliver any water to the reactor vessel at the same time that the pumped ECI failed, core melting would take place without significant metal-water reaction and there would be no possibility of steam explosions in the reactor vessel. The sequences of ECI failure which include accumulator failure are therefore expected to be of significantly lower probability and to have lower potential consequences than the cases which have been investigated. If the accumulators fail but the pump injection operates, the consequences of the meltdown that may ensue would not be expected to be significantly different from those considered.

2.2.2 ACCIDENT TIME SCALE

For an instantaneous double-ended cold-leg break, primary system depressurization would be essentially complete in 10-11 seconds. The accumulator discharge pressure of 650 lb/in.^{2} would be reached in 6-7 seconds after the break, and accumulator discharge would be completed at about 30 seconds into the accident. The safety injection charging pumps and the low-head safety injection pumps will be activated by any of a number of signals such as low pressurizer pressure and water level, high containment pressure. The time at which these systems can be considered to be operable will depend on the availability of off-site power. With off-site power the pumped injection can be activated extremely rapidly; in the absence of off-site power the pumped injection will be powered by the emergency diesels and will require on the order of half a minute to start. For the purposes of this evaluation, both the pumped injection and CSIS are assumed to start 30 seconds after the break. Given the assumption that pumped injection and/or CSIS operate, uncertainty of a few minutes as to their exact starting time is of little consequence since these systems will operate for time periods of the order of an hour.

Both the pumped injection and CSIS systems take their suction from the refueling water storage tank whose total capacity is 350,000 gal; 50,000 gal of this capacity is reserved for the exclusive use of the ECI. With both ECI and CSIS systems operating at their minimum design levels, i.e., one safety injection charging pump at 150 gpm, one low-head safety injection pump at 3000 gpm, and one containment spray injection pump at 3200 gpm, the containment spray injection will end at 47 minutes and core injection will last until 63 minutes. These times are based on utilizing the entire capacity of the refueling water storage tank. For those cases where the CSIS is assumed to fail, ECI will last until 111 minutes; if the ECI is assumed to fail, CSIS will last until 94 minutes. In the latter case 50,000 gal will remain in the refueling water storage tank. The operation of more than the minimum safeguards or at effective pump capacities other than the minimum values assumed would, of course, alter the time intervals.

The CSRS system is slated for activation in sequence, with half the capacity being available as early as 90 seconds and the other half starting as late as 5 minutes into the accident. For the purposes of the containment pressure analyses, operation of only two of the four containment recirculation spray pumps of 3500 gpm each was assumed, with a starting time of 200 seconds. Here again, since the total accident times of interest are much longer than the possible uncertainty in CSRS starting time, small variations in starting time would be of no consequence to the overall results. The ECCS is designed to be switched manually from the injection (ECI) to the recirculation (ECR) mode of operation upon the receipt of a low water level signal from the refueling water storage tank. For the present analyses the LPRS, if operating, was assumed to start at the end of ECI as determined above and, barring pump cavitation due to sudden containment depressurization, continue as long as there is water in the containment sump.

2.2.3 CORE MELTDOWN

Core meltdown in a LOCA is assumed to be the result of failure of ECI, ECR, CSRS, CHRS, or EPS. In each case the expected course of reactor meltdown is quite similar, varying primarily in time scale. Although containment pressure would be

expected to have some effect on the boiloff of water from the core, this effect is small and within the bounds of uncertainties on the progress of boiloff and meltdown. The time at which the flow of emergency cooling water stops and boiloff begins is therefore the controlling parameter that influences the time scale of meltdown for the different accident sequences. Since the decay heat decreases with time from the LOCA event, the later the time at which boiloff begins, the more extended the meltdown time scale. Although the boiloff which occurs for ECI failure begins with only a partially flooded core rather than fully covered, the remainder of the boiloff and meltdown follow the same course as for the other accident sequences.

In Appendix A, the computer code which was used to investigate core meltdown and the results obtained with various meltdown models are described. Due to the many uncertainties associated with the phenomena of the movement of molten UO_2 and its interactions with other materials it was necessary to utilize approximate models to describe the processes involved. Bounding calculations were performed to evaluate the important parameters in the meltdown process; among these are: fraction of zirconium reacted, time at which melting begins, rate at which melting proceeds, and the time at which the molten core leaves the normal confines of the fuel region. By varying the assumptions and inputs in the models a reasonable picture of the meltdown process is believed to have been developed.

As discussed in Appendix A, it is believed that during the period in which core melting is occurring, the fuel does not drop to the core support plate or the lower plenum of the vessel. Rather a molten pool is formed and is supported by a frozen crust which proceeds outward and downward with time as more of the core becomes molten.

The analyses described in the appendix indicate that when a major fraction of the core is molten, ~80 percent, it will no longer be possible to retain the core in the normal fuel region. Melting of the core support plate or failure of the upper core barrel will permit the molten fuel to move down and contact water in the lower plenum. The accident will then enter a new phase with the molten core proceeding into the reactor vessel bottom head where either a steam explosion or vessel meltthrough would occur.

The time at which melting begins can be obtained from the curve marked 0% melting in Fig. VIII A-6. In Fig. VIII 2-1 the additional time required to go from 0% to 80% melting of the core is plotted versus time after the LOCA at which boiloff is initiated. The estimated values and uncertainty bands were derived from the results of computations presented in Appendix A. Although the remaining 20 percent of the core will eventually melt, the melting may be extended over an appreciable time because of the low peaking factor in these regions. Since this fraction of the core contains a small fraction of the fission-product inventory, it is reasonable to assume that the principal period of fission-product release due to initial core melting is from the time of melting initiation to 80 percent molten. The hydrogen generated in the meltdown accident is estimated to be the equivalent of 75 $\pm$ 25 percent of the zirconium in the core reacted. This band provides for potential hydrogen sources from other reactions such as iron-water and UO_2-steam during the time period of core meltdown and primary vessel meltthrough. Total hydrogen release is relatively insensitive to the time scale of the meltdown accident.

2.2.4 PRIMARY VESSEL MELTTHROUGH

Appendix A describes the models used to analyze the time required to penetrate the lower head of the pressure vessel. The principal effect of the time required to melt through the pressure vessel is to delay contact of the molten core with the floor of the containment building. Since the estimated time for primary vessel meltthrough is much less than the band of uncertainty involved in containment meltthrough, the uncertainty in the time for vessel meltthrough is not considered particularly significant. If the molten core enters the lower plenum in 1-2 hours, the time required to penetrate the vessel is 60 (+40, -20) minutes. For accident sequences in which loss of containment heat removal capability is the cause of reactor meltdown the time of reactor meltdown is delayed a number of hours. In these cases containment failure precedes meltdown and the time of pressure vessel meltthrough is not particularly significant.

2.2.5 CONTAINMENT VESSEL PENETRATION

When the molten core (mixed with molten zirconium, zirconium oxide, steel, and iron oxides) falls on the concrete floor, the vaporization of free water below the surface of the concrete will

cause spalling of the concrete and a very rapid penetration rate of the melt into the concrete. As the products of concrete decomposition are dissolved in the melt, the melt temperature will decrease until the mixture becomes viscous or the constituents of the mixture begin to precipitate. From this point onward in time, the progress of the melt through the concrete is controlled by the rate of decay heat generation. While there are some sequences in which meltdown is delayed for many hours, they usually involve containment failure preceding meltdown and the time required to melt through the concrete pad does not affect the atmospheric consequences. For the subsequences in which the melt-through failure mode provides the major atmospheric release, the molten fuel contacts the concrete at approximately 2-3 hours after the LOCA. For these cases, containment meltthrough is estimated to require an additional 18 (+10, -5) hours. Although the molten core penetrates the steel liner shortly after falling on the containment floor, substantial pressure relief is not expected until a significant fraction of the reinforced concrete foundation mat has been penetrated. As discussed in Appendix A, the molten region is expected to proceed an additonal 10-50 ft into the earth before arresting.

For cases in which ECI or ECR failure is combined with CSRS or CHRS failure, a race can occur between overpressure failure of the containment and meltthrough. During the process of decomposition of the concrete, carbon dioxide and water vapor are generated and add to containment pressure. At the time of containment meltthrough, the CO_2 would typically contribute about 13 psi to the containment pressure. The effect of these components on containment pressure is included in Figs. VIII 2-2 through VIII 2-6.

Release of radioactive gases through the ground to the atmosphere and the interaction of the molten core with groundwater following containment meltthrough is discussed in Appendix VII.

2.2.6 STEAM EXPLOSIONS

During the time in which the core is melting down, it is possible for small or moderate amounts of molten UO_2 to interact with water with resultant pressure generation. Unless the amount of UO_2 is approximately 20 percent of the core or more, however, the analysis described in Appendix C indicates that containment integrity would not be threatened. If, during meltdown the molten material remains in a pool within the normal confines of the core until a major fraction of the fuel has melted (as has been indicated in the present evaluation), then, at the time the lower grid plate fails, large quantities of molten fuel and water can interact. Thus when a large fraction of the core has melted, the potential for a steam explosion in the primary vessel leading to containment failure must be considered. The consequences of a steam explosion which results in containment failure are serious not only because containment is breached at an early time in the accident but also because dispersal of the core into the containment atmosphere will result in oxidation of the UO_2 and an enhanced fission-product release.

There is the possibility that missiles generated in a steam explosion in the reactor vessel could damage the containment spray systems. In the design considered, the CSIS consists of two redundant full-capacity subsystems and the CSRS consists of four redundant half-capacity subsystems. Since damage of all the redundant subsystems is unlikely and since a small margin is believed to exist between explosions with the capacity to damage the containment sprays and those that will breach containment, this mode of spray failure was not included in the present evaluation.

A potential for steam explosions can also occur at other times in the meltdown sequence, e.g., when the core melts through the lower head of the primary vessel. Steam explosions in the reactor cavity are not expected to threaten containment integrity since the resulting pressures within the containment free volume are predicted to be small compared to the design levels and because internal structures and equipment provide effective shielding for the containment shell for any missiles originating from such steam explosions. Since the occurrence of steam explosions is considered to have low probability, the potential effect on fission-product release of steam explosions which do not result in containment failure is ignored. Dispersal of the core within containment in a steam explosion could also result in a core configuration that can be cooled and contained. It is unlikely, however, that the entire core could be dispersed into such a configuration. The posssibility of being able to contain part or all of the molten but dispersed core is recognized but is considered relatively unlikely.

Localized interactions can also occur at the surface of the melt when it comes in contact with concrete or when it contacts water-laden gravel after penetrating the floor of the containment building. These interactions do not have the potential for the rapid dispersal of a large quantity of molten material into water or a resulting large energy release. The consequences of these reactions will therefore be limited to the vicinity of the melt.

2.2.7 HYDROGEN COMBUSTION

The hydrogen generated in the meltdown accident is estimated to be the equivalent of 75 ± 25 percent of the zirconium in the core reacted. As discussed in Appendix D, the hydrogen concentration resulting from the reaction of 75 percent of the zirconium with water would be outside the detonation limits for the resulting hydrogen-air-steam mixture. With 100 percent of the zirconium reacted (the upper limit of the estimated extent of reaction), the mixture could be within the detonation range if the containment temperature is sufficiently low. In Appendix D it is shown that the impulse achieved in the shock wave from hydrogen detonation is not sufficient to fail the containment.

The effects on containment of a rapid self-propagating hydrogen deflagration have also been considered. For initial pressures higher than 32 psia, the steam concentration in containment is above that at which a self-propagating reaction will occur. At lower initial pressures, the incremental pressure from the reaction will not be sufficient to rupture containment.

The distribution of the energy source of hydrogen burning as it is evolved into the containment, in combination with high steam pressures, can be sufficient to increase the containment pressure at the end of the meltdown period to a point at which containment is threatened. This effect is included in the evaluation of the containment pressure response.

2.2.8 CONTAINMENT RESPONSE

Figures VIII 2-2 through VIII 2-9 illustrate the containment pressure responses for various assumed combinations of failures of engineered safety features; a typical design basis accident pressure-time history is included for comparison. The assumptions and methodology utilized in determining the containment pressure responses are discussed in Appendix A; the salient features of the results are discussed below.

During a design basis accident the containment is pressurized rapidly to a peak of 54 psia as a result of primary system blowdown. The CSIS and CSRS systems reduce the pressure to subatmospheric in approximately 30 minutes. After the delivery of chilled spray water by the CSIS stops, there is a slight increase in containment pressure to a level of about 14 psia where it is maintained by the combined action of the CSRS and CHRS.

With the failure of ECR and the other safeguards operating at their minimum design levels, the initial portion of the containment pressure transient will not be changed from the design basis accident case. The generation of hydrogen by the zirconium-water reaction will lead to a containment pressure of about 16 psia at the end of core meltdown. After the core melts through the bottom head of the reactor vessel, CO_2 and steam will be generated from the decomposition of the concrete by the molten core. The steam will be condensed by the containment sprays, but the CO_2 will raise the pressure to about 25 psia by the time of containment meltthrough. With the operation of the containment sprays the burning of hydrogen will have no appreciable effect on the pressure transient. This case is illustrated in Fig. VIII 2-2 together with the design basis accident.

The failure of CSIS alone would not, of course, lead to core melting; it would affect the rate of containment depressurization following primary system blowdown. In conjunction with the failure of ECR, the inoperability of CSIS would extend the time for which ECI is operable and thus delay core melting, although the overall effect would not be expected to be significant. Again, in the presence of containment sprays, hydrogen burning would not have a significant effect on the transient. The containment pressure responses for these two cases are given in Fig. VIII 2-3.

The containment pressure responses with assumed failures of CSRS and ECR are illustrated in Fig. VIII 2-4. With the initial failure of CSRS and the attendant failure of the CHRS, but with the ECR operating, the containment pressure will be decreased to about 25 psia by the CSIS system. After the CSIS stops, the pressure will increase continuously, due to the generation of

steam by the core decay heat until containment failure by overpressurization. At the time of containment failure the LPRS pumps would be expected to cavitate and core melting would follow. If the LPRS fails independently of CSRS, core melting would take place with the containment intact. The pressure in the containment will rise due to the steam generated by the boiloff in the reactor vessel. This pressure rise will stop when all the water in the reactor vessel has been vaporized. During pressure vessel meltthrough the containment pressure will decline due to steam condensation on cold surfaces. After the core melts through the pressure vessel a peak containment pressure of about 80 psia would be reached as a result of the evaporation of the water in the reactor cavity and the initial decomposition of the concrete. The magnitude of this pressure is limited by the quantity of water expected in the reactor cavity. As the molten core progresses through the containment foundation, the pressure would be expected to decrease since the rate of CO_2 and steam generation would be counteracted by steam condensation on the various surfaces within containment. If, in the case of LPRS failure independent of CSRS, the hydrogen from the zirconium-water reaction is assumed to burn as it is generated, higher pressures will result and containment failure by overpressurization can be expected after pressure vessel meltthrough.

In the event of CHRS failure, the pressure resulting from primary system depressurization will be quenched, largely by the chilled CSIS water. With continued steam generation from core decay heat, the water inventory within containment will heat and the pressure will increase until the containment fails due to overpressurization. Containment failure will be accompanied by LPRS pump cavitation and subsequent core melting. If LPRS fails independently of CHRS, core melting will take place with the containment intact; with the contribution of the hydrogen generated during core melting the containment pressure at the completion of core meltdown would be about 16 psia. When the molten core penetrates the reactor vessel bottom head it will come into contact with the water in the reactor cavity and the CSRS water. Vaporization of the water will lead to a continuous increase in containment pressure; at the same time the molten core will be attacking the containment foundation mat. As shown in Fig. VIII 2-5, in this case containment failure by overpressurization or meltthrough is predicted to occur at about the same time. Hydrogen burning, if it takes place as hydrogen is generated, would not have an appreciable effect on the pressure-time history.

Containment pressure response in the absence of containment sprays is shown in Fig. VIII 2-6. With both CSIS and CSRS failed but LPRS operating, the pressure would increase continuously due to steam generation from the decay heat until containment failure by overpressurization. Containment failure would be accompanied by LPRS pump cavitation and subsequent core meltdown. If the LPRS fails independently of the containment sprays, core melting would start while the containment is still intact; by the end of core meltdown, however, boiloff of the water in the reactor vessel would have raised the pressure sufficiently to fail containment. Should the containment be intact at the end of core meltdown, the pressure would decline somewhat due to steam condensation during pressure vessel meltthrough; it would probably fail after reactor vessel meltthrough with the pressure increase from the initial rapid decompositon of concrete. If, in the absence of containment sprays, LPRS failure is accompanied by hydrogen burning, the containment failure pressure would be exceeded even before the end of core meltdown.

Figure VIII 2-7 illustrates the containment pressure response with an assumed loss of electric power and the attendant loss of all active engineered safeguards. As would be expected, there is no reduction in the post-blowdown pressure, and the boiloff of the water injected from the accumulators raises the pressure to a peak of about 75 psia. The peak pressure is limited by the amount of water available for vaporization. As the core melts through the bottom of the reactor vessel there is a decrease in containment pressure due to condensation of steam by the various structures within containment. After the molten core falls to the bottom of the reactor cavity, pressure increases due to the initial rapid rate of concrete decomposition. Subsequently the pressure would be expected to decline as the melt works its way through the concrete foundation mat. Upon containment meltthrough, the pressure would be controlled by the static head of the ground water. If (in the absence of all active safeguards) core melting is accompanied by hydrogen burning, the containment pressure would reach about 100 psia at the end of core meltdown. At that level containment failure could be expected.

The effects of ECI failure in combination with various containment safeguard failures on containment pressure response are illustrated in Figs. VIII 2-8 and VIII 2-9. If ECI is the only failure, the containment sprays would reduce the pressure as in the design basis accident. Hydrogen generation during the meltdown in combination with the noncondensables initially present would limit the minimum pressure attainable to about 16 psia. The generation of CO_2 from the concrete after pressure vessel meltthrough would raise the pressure to about 25 psia; after containment meltthrough the pressure would be controlled by the external hydrostatic head. If, in the case of ECI failure, the hydrogen were to burn, the energy release would be accommodated by the sprays and the net result would be a minimum pressure of about 13 psia. With CSIS as well as ECI failing, the steam released by the primary system blowdown would be condensed by the CSRS acting in conjunction with CHRS, although the pressure would be at an elevated level longer than for the previous case. The pressure prior to containment meltthrough would again be controlled by the noncondensables. The containment pressure response with ECI, CSIS, and CSRS failure would be identical to that for complete loss of electric power which was discussed previously.

If the LOCA is accompanied by the failure of ECI and CHRS, the containment pressure will be reduced rapidly by the operation of CSIS and CSRS to a level of about 16 psia at the end of core meltdown. After the CSIS stops and the molten core has penetrated the bottom of the reactor vessel, the water inventory within containment will be heated to saturation and partially vaporized, leading to a rise in pressure. As the molten core is boiling off water, it is also attacking the concrete foundation mat; containment failure by the two competing mechanisms is predicted to occur at about the same time. The burning of hydrogen as it is generated would not have a significant effect on this pressure transient since the energy released would be spread over a substantial water inventory. In the event of the failure of the CSRS in conjunction with ECI, the blowdown pressure would be effectively suppressed by the CSIS, though not as quickly as in the previous case. After the CSIS stops and the molten core drops to the floor of the reactor cavity, the pressure would again increase due to the evaporation of water and the decomposition of concrete. In this case the quantity of water in the reactor cavity would be relatively small and the pressure resulting from its vaporization would not be sufficient to fail containment. Thus the expected failure mechanism would be containment meltthrough. Hydrogen burning, since it would be expected to take place while the CSIS is operating, would again have little effect on the overall pressure transient.

Figure VIII 2-10 illustrates the effect of leak rate on containment pressure-time response in the absence of any containment sprays. It can be seen that leak rates of about 200 v/o per day and greater will preclude containment failure by overpressurization. A leak rate of 200 v/o per day would require a hole 3.6 inches in diameter or its equivalent. Within this context the design basis leakage of 0.1 v/o per day can be considered negligible.

2.2.9 LEAK RATE FROM CONTAINMENT

The release of fission products to the environment is controlled by the leak rate from the containment. In the period of time preceding containment failure, the leakage is determined by the internal pressure of the containment and the hole sizes associated with either containment isolation success or containment isolation failure. At the time of containment failure by steam explosion, overpressurization, or meltthrough, the fraction of the contents of the containment that are released depends upon the containment pressure. After containment failure has occurred by one of these mechanisms, the leak rate from the containment will be determined by the generation rate of noncondensing gases. If sprays are operating with subcooled water, steam generated within containment will be condensed and the generation of hydrogen and CO_2 will provide the driving force for leakage. When sprays are not functioning, the steam generated within containment will also result in leakage. The assumptions used in calculating leak rate from containment for the PWR subsequences are described in Appendix A.

2.3 SUBSEQUENCE PROBABILITIES

The event tree shown in Fig. VIII 2-11 illustrates the five paths to containment failure that are postulated for a meltdown accident in a PWR: steam explosion in primary vessel, containment isolation failure, overpressurization of the containment resulting from hydrogen burning, overpressurization of contain-

ment from steam generation and carbon dioxide production, and containment floor meltthrough. It is expected that containment floor meltthrough would accompany each of the other containment failure events. However, meltthrough would not significantly add to the atmospheric fission-product source term in the cases where other containment failure modes have preceded it. It is assumed that the different paths to containment failure are exclusive. For example, if a steam explosion introduces a large hole in containment, it is not necessary to consider containment overpressurization.

For a given sequence some of these paths to containment failure may not be credible. These subsequences are assigned a probability of zero for that sequence. In the following paragraphs the method of obtaining the probabilities of the five subsequences (P_α, P_β, P_γ, P_δ, P_ε) for the different accident sequences are described.

For the purposes of estimating and combining uncertainties in the predicted values of the various parameters, four types of statistical distributions are considered: normal, log normal, skewed, and skewed log. The normal distribution is characterized by a mean value and a standard deviation which can be used to evaluate the probability of exceeding any given value by means of normal distribution tables. The log normal distribution is distinguished by a mean value and a standard deviation expressed as powers to the base ten. The skewed distributions are characterized by a mean value and two standard deviations, one representing the distribution for values greater than the mean and the other for values less than the mean.

2.3.1 DEFINITIONS

$P_\alpha, P_\beta, P_\gamma, P_\delta, P_\varepsilon$ = relative probabilities of each of the containment failure mechanisms

P_1, P_2, P_3, P_4 = probability of failure at each decision point in the containment failure event tree

P_{fw} = probability of a large mass of molten UO_2 (>20 percent core) contacting a similar mass of water during the meltdown process

α_{sxs} = probability of a dispersal event occurring when molten UO_2 falls into water (effective particle size <4000)

α_{cf} = fraction of steam explosions leading to containment failure

P_{hf} = probability of containment failure shortly after meltdown assuming hydrogen combustion has occurred

P_{hb} = probability of hydrogen combustion

P_{op} = probability of failure of containment at the peak pressure without hydrogen combustion

P_{oph} = probability of failure of containment at the peak pressure with hydrogen combustion

P_{om} = probability of containment overpressure preceding meltthrough

2.3.2 CONTAINMENT FAILURE RESULTING FROM A STEAM EXPLOSION

A broad band of uncertainty must be associated with a quantitative evaluation of the likelihood of failure of the containment as the result of a steam explosion in the primary vessel. The sequence of events which is postulated to lead to containment failure involves: the holdup of a large mass of molten UO_2 above the grid plate during core meltdown; dropping of the melt into water in the lower plenum; occurrence of a dispersal event which presents a large molten UO_2-water interface for rapid heat transfer; and acceleration of a fuel-water piston which impacts the upper head of the vessel, the control-rod shield, and the containment ceiling. The physical phenomena in each stage of the sequence are extremely complex and it is not possible at present to predict with accuracy the course of events. The time at which molten fuel and water interact, the masses of fuel and water involved, the character of the dispersal event, and the reaction that occurs between the fuel remaining above the grid plate and the expanding water column are all subject to uncertainty. To assess the probability of containment failure, this probability has artificially been divided into three independent terms. The definition of each term was given above.

$$P_l = P_{fw}\alpha_{sxs}\alpha_{cf}. \qquad \text{(VIII 2-1)}$$

Calculations discussed in Appendix A indicate that molten fuel cannot travel far through cooler regions of the core without refreezing. The accumulation of a large pool of molten fuel is therefore quite likely. The uncertainties in P_{fw} include potential for extensive vaporization of the fuel and the possibility of no water in the lower plenum at the time when the molten fuel and water would interact. The latter two factors are expected to be small for the PWR accidents considered. For these reasons the probability of P_{fw} is estimated to be near unity with a small uncertainty.

$$P_{fw} = 10^{-0.05\ (\pm 0.05)} .$$

Experience with explosive interactions between molten materials and water is described in Appendix A. Insufficient data exist for molten UO_2 in water to predict under any given conditions whether or not an explosive interaction will occur. From the observed behavior of other molten materials and water, particularly with regard to the significance of subcooling to known dispersal mechanisms, it is felt that the likelihood of steam explosions occurring under the given conditions in the primary vessel is small. Because of the lack of understanding of the UO_2-water interaction, however, the possibility of an explosion event must be recognized. The range of probability which has been assigned to α_{sxs} is intended to represent the probability of a dispersal event which is expected to be small but could be moderate. The numerical value assigned to this probability is largely a matter of judgment based on the history of physical explosions and discussions with researchers in this and related areas.

$$\alpha_{sxs} = 10^{-1\ (+0.5,\ -1)} .$$

Appendix C describes a series of calculations performed to determine the conditions under which containment failure would result from a steam explosion. Key parameters considered are effective surface area produced by the dispersal mechanism, time required to introduce the molten core into the water, and magnitude of heat-transfer coefficients. The results of these studies indicate that if the dispersal mechanism results in effective particle sizes less than 4000 μ, containment will be breached for insertion rates of fuel into the water of 200 percent core mass per second or greater. The minimum quantity of UO_2 that must be involved in the interaction to lead to containment failure is about 20 percent of the core. Although it would be unlikely to observe dropping rates of UO_2 into water of the magnitude of 200 percent per second, two phenomena enhance the likelihood of obtaining such effective insertion rates. Delay times are often observed in steam explosions between the time at which the hot fluid is introduced and the time of the explosion. During the period of the delay a large mass of hot fluid can be introduced into the water. Also, as the first amount of UO_2 interacts with the water in the lower plenum, the water surface will swell rapidly engulfing the remainder of the molten fuel. This fuel may then be able to participate in the explosion event.

Other uncertainties in the probability of failing containment in an explosion event involve the effective quantity of water with which the molten fuel interacts and the manner in which the rapidly expanding mixture interacts with the upper head. The estimated value for α_{cf} reflects results which indicate that the conditions required to rupture containment are difficult to achieve but might be expected with a moderately low probability. The numerical value of this probability is derived on the basis of the calculational results discussed in Appendix C.

$$\alpha_{cf} = 10^{-1\ (+0.5,\ -1)} .$$

The combined and rounded probability of this path to containment failure is

$$P_\alpha \approx 10^{-2\ (+1,\ -2)} .$$

Although small differences would exist in the consequences of a steam explosion with and without containment isolation, for the purposes of this analysis steam explosion consequences are considered to be independent of the condition of containment isolation.

$$P_\alpha = P_1 . \qquad \text{(VIII 2-2)}$$

2.3.3 CONTAINMENT MELTTHROUGH WITH CONTAINMENT ISOLATION FAILURE

As illustrated in Fig. VIII 2-10, leak rates of 200 v/o per day (3.6-in.-diam hole) and greater would preclude containment failure by overpressurization even in the absence of any containment sprays. This value was therefore taken as a convenient dividing point between leak rates considered as containment isolation success and containment isolation failure. The design leak rate for the type of containment considered is 0.1 v/o per day, with temporary increases up to 1 v/o per day considered permissible. Considering all possible leak rates up to 200 v/o per day, the probability of a leak greater than the normal operating range would be expected to be much less than the probability of a leak within the operating range. Thus a representative leak size for this region should be within the operating range. The upper limit on the normal operating range of leakage, or ~1 v/o per day, was, therefore, chosen to characterize containment isolation success.

For hole sizes greater than the 3.6-in. equivalent diameter, the average size is in the range 8-10 in., corresponding to a leak rate of about 1000 v/o per day. For leak rates of this magnitude, the exact size of the hole in containment has little effect on the consequences of a meltdown accident. The driving force for fission-product leakage from containment consists of the steam and noncondensables that are generated during the course of the accident. Except for short time periods, the production rate of gases and vapors available for leakage is less than the choked flow rate through a 8-10-in. diam hole. Thus the leak rate is effectively determined by the net production of gases and vapors and is independent of the exact hole size. Accident sequences involving containment isolation failure have accordingly been represented by a leak rate of 1000 v/o per day.

The probability of containment isolation failure will then be given by

$$P_2 = \sum_i \pi_i \text{ for } L_i > 3.6 \text{ in.}, \quad \text{(VIII 2-3)}$$

where

π_i = probability of leak size L_i.

The probability that loss of isolation will be the principal mode of containment failure will be

$$P_\beta = (1 - P_1)\, P_2. \quad \text{(VIII 2-4)}$$

2.3.4 HYDROGEN COMBUSTION

The containment pressure at the end of meltdown is calculated including the burning of hydrogen to evaluate the potential for overpressure failure. The contribution of hydrogen from 75 percent equivalent zirconium-water reaction is shown in Figs. VIII 2-4, VIII 2-6, and VIII 2-7. The probability of failure, P_{hf}, is assessed assuming a normal distribution of failure pressures with a standard deviation of 15 psi around the estimated failure pressure of 100 psia. For the pressure transients in which more than one peak is predicted, the maximum value of the pressure is used.

The likelihood of hydrogen burning as it is evolved from the primary vessel, P_{hb}, must also be considered. The location of the break (hot leg or cold leg) will affect the temperature at which the hydrogen leaves the vessel. For a cold-leg break, the hydrogen will pass through the unbroken loops and be cooled to the temperature of the steam generators before entering the containment atmosphere. Combustion will require the availability of oxygen as well as ignition source. In a hot-leg break, the hydrogen will probably enter the containment at a temperature above the autoignition temperature. Whether the hydrogen burns or not will then depend upon the availability of oxygen at the break. If the hydrogen is transported a significant distance before encountering oxygen, its temperature will decrease and an ignition source may again be required for combustion to take place. Another possibility is a condition of only partial burning. An overall value of $P_{hb} = 0.25$ (± 0.25) has been employed.

$$P_3 = P_{hf} P_{hb}, \quad \text{(VIII 2-5)}$$

$$P_\gamma = P_3 (1 - P_2)(1 - P_1). \quad \text{(VIII 2-6)}$$

2.3.5 CONTAINMENT OVERPRESSURIZATION

In some cases the rise in containment pressure is not water-limited and the

internal pressure would reach extremely high levels if the containment were to remain intact. In other cases the internal pressure literally runs out of steam at a point near the band of failure pressure. In the former sequences, the failure of containment is considered a certainty. In the latter sequences, the probability of failure, P_{op}, is assessed assuming a normal distribution of failure pressure. Again a standard deviation of 15 psi and a failure pressure of 100 psia are used. The calculated peak pressure includes that from the CO_2 and the steam generated from interaction of the molten fuel with the concrete floor.

Since overpressure of the containment and containment meltthrough can occur at approximately the same time, it is necessary to consider the competition between the two events. Since the uncertainty in containment meltthrough time is great, this time has been treated as having a skewed distribution about the estimated time, 18 (+10, -5 hours). The probability of containment overpressurization occurring prior to the time at which containment meltthrough can relieve pressure, P_{om}, is determined by using normal distribution tables.

$$P_4 = P_{op}P_{om} \qquad \text{(VIII 2-7)}$$

$$P_\delta = P_4\ (1 - P_3)(1 - P_2)(1 - P_1). \qquad \text{(VIII 2-8)}$$

2.3.6 CONTAINMENT MELTTHROUGH

If the other modes of containment failure are avoided, containment meltthrough is treated as a certainty.

$$P_\varepsilon = (1 - P_4)(1 - P_3)(1 - P_2)(1 - P_1). \qquad \text{(VIII 2-9)}$$

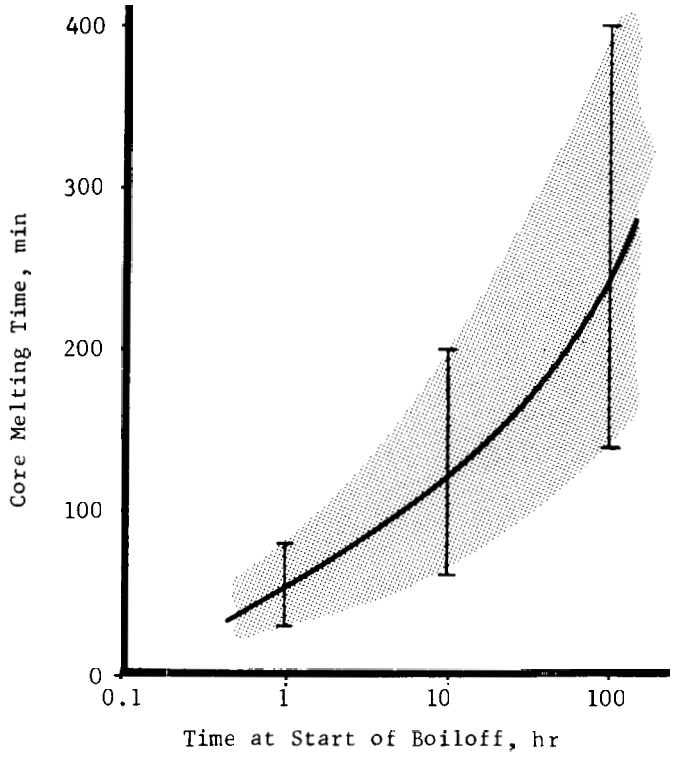


FIGURE VIII 2-1 Time Required for 80 Percent Core Melting from the Onset of Melting

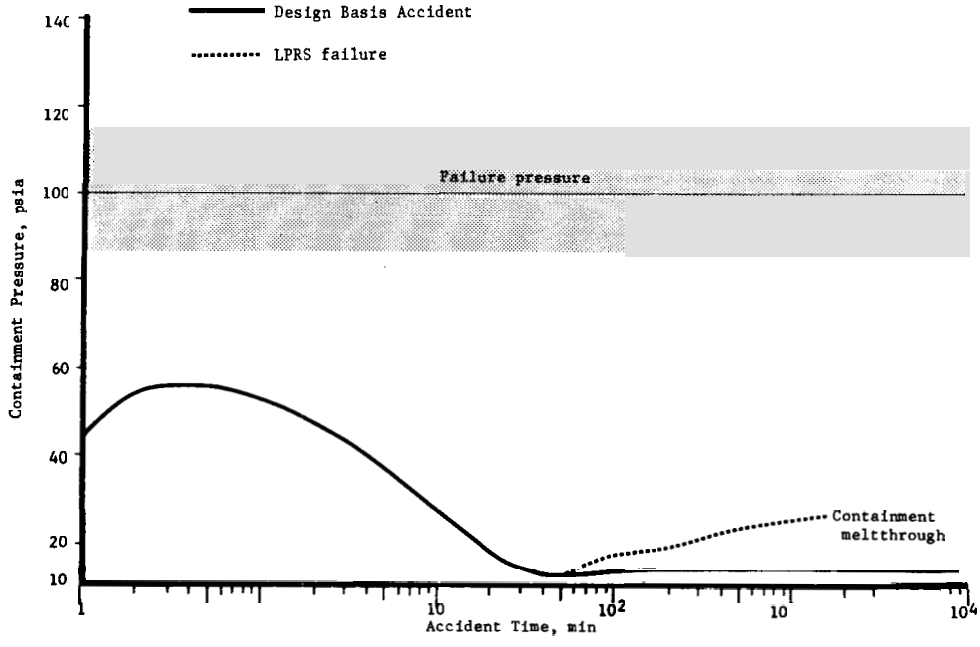


FIGURE VIII 2-2 PWR Containment Pressure Response During the Design Basis Accident and with the Assumed Failure of the Low Pressure Recirculation System

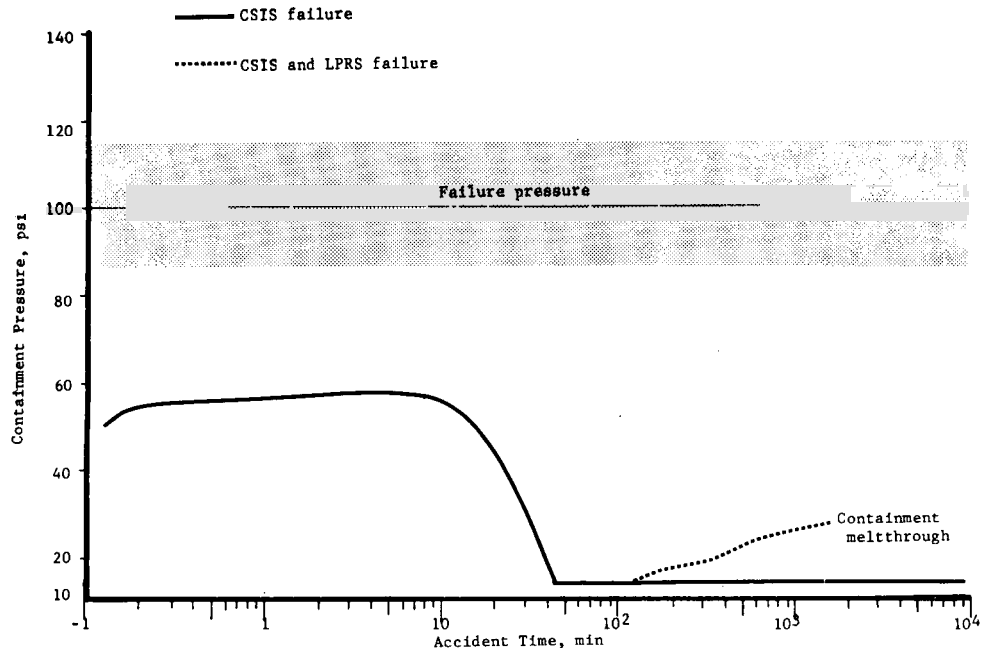


FIGURE VIII 2-3 PWR Containment Pressure Response with Assumed Failures of the Containment Spray Injection System and Low Pressure Recirculation System

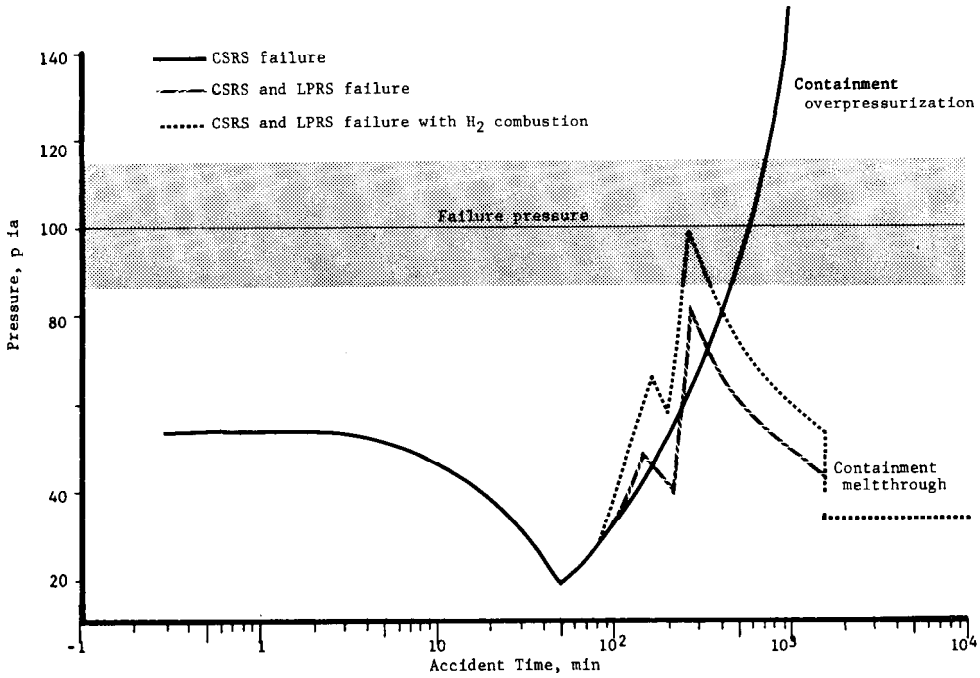


FIGURE VIII 2-4 PWR Containment Pressure Response with Assumed Failures of the Containment Spray Recirculation System and Low Pressure Recirculation System

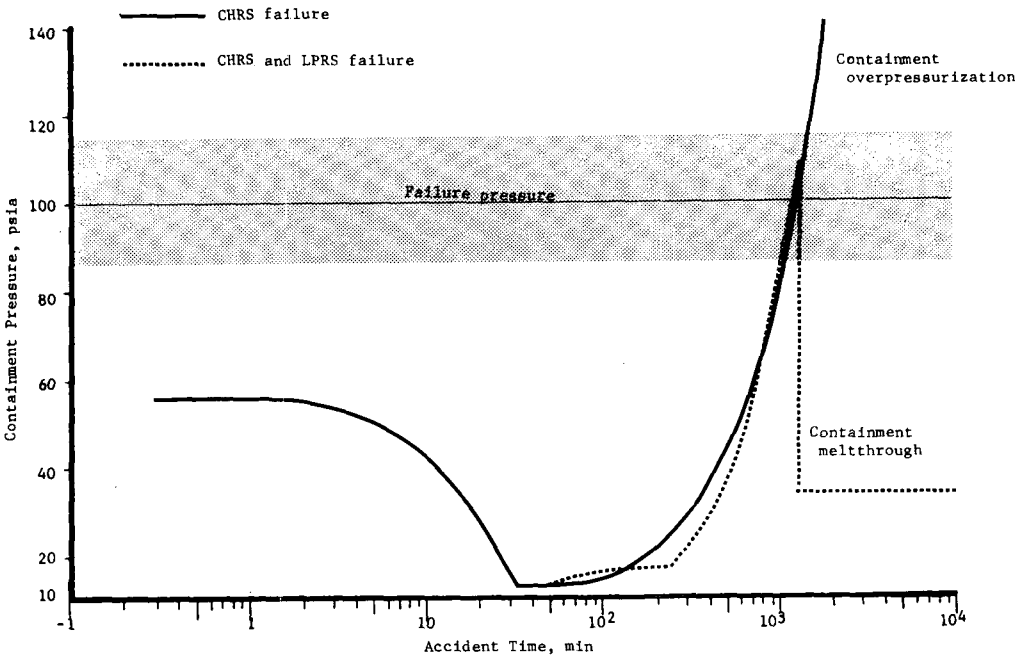


FIGURE VIII 2-5 PWR Containment Pressure Response with Assumed Failures of Containment Heat Removal System and Low Pressure Recirculation System

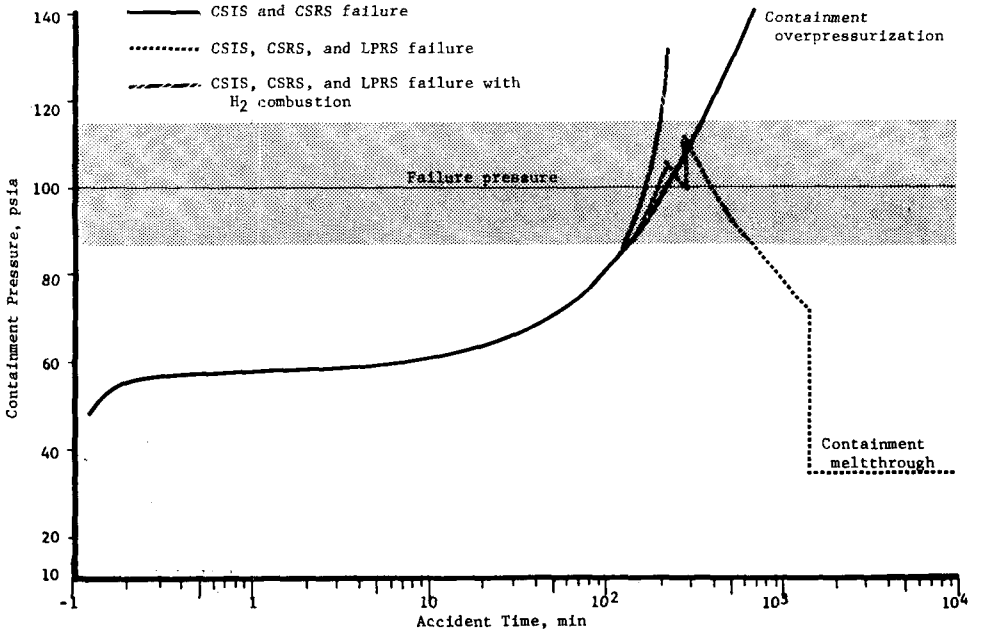


FIGURE VIII 2-6 PWR Containment Pressure Response with Assumed Failures of Containment Spray Injection System, Containment Spray Recirculation System, and Low Pressure Recirculation System

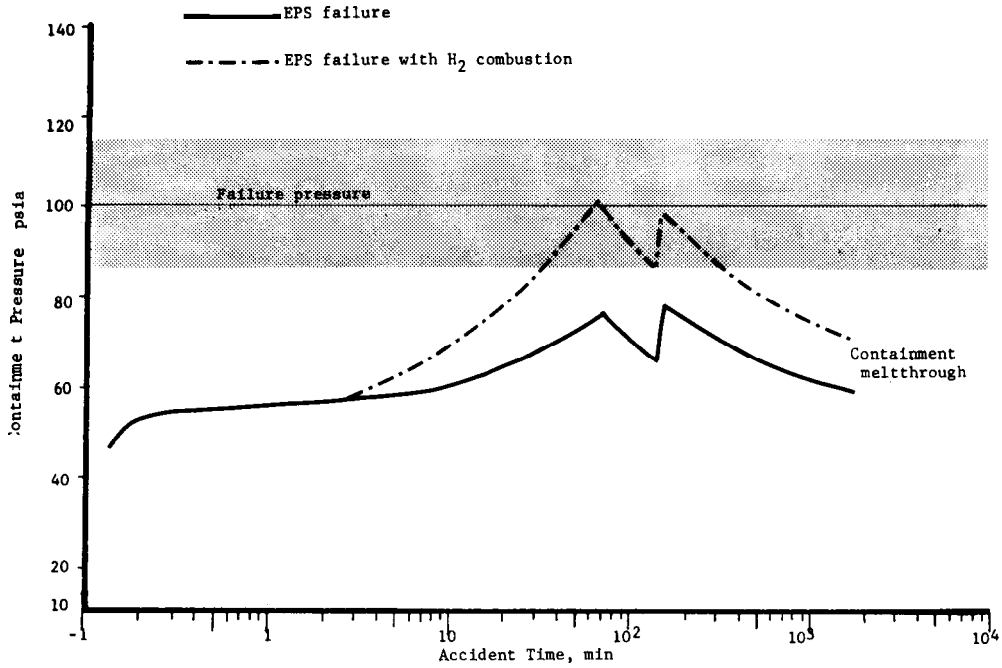


FIGURE VIII 2-7 PWR Containment Pressure Response with Assumed Failure of the Electric Power System and the Attendant Loss of All Engineered Safeguards

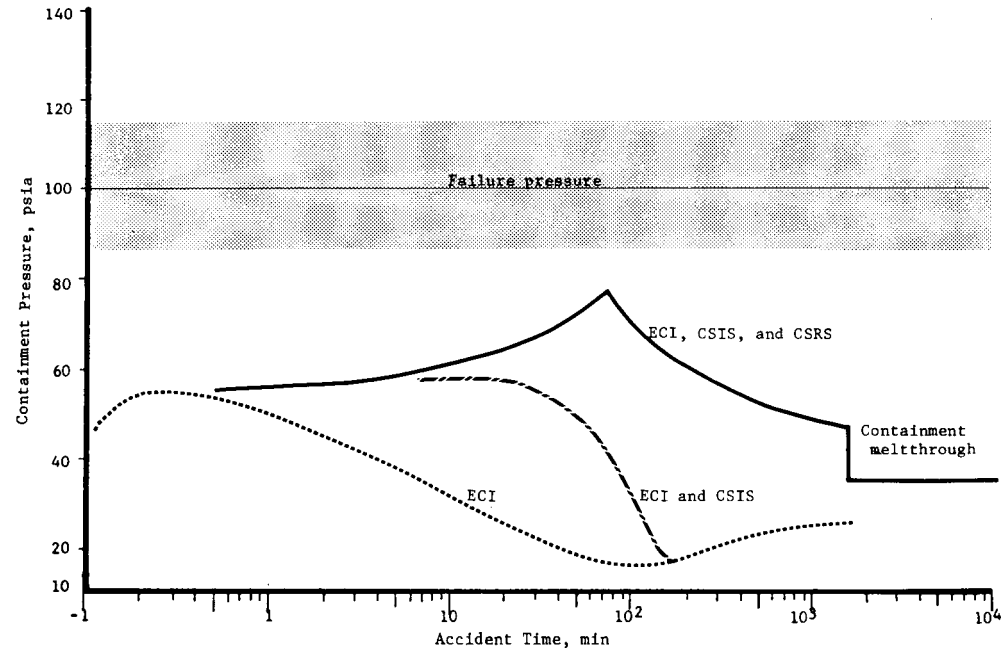


FIGURE VIII 2-8 PWR Containment Pressure Response with Assumed Failures of Safety Injection System, Containment Spray Injection System, and Containment Spray Recirculation System

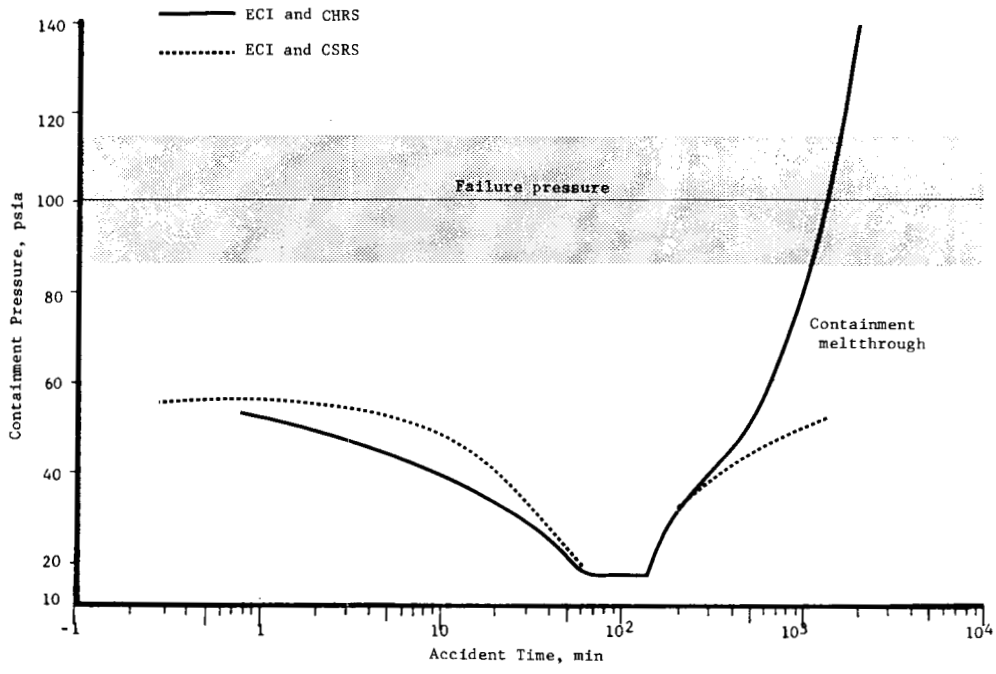


FIGURE VIII 2-9 PWR Containment Pressure Response with Assumed Failures of Safety Injection System, Containment Spray Recirculation System, and Containment Heat Removal System

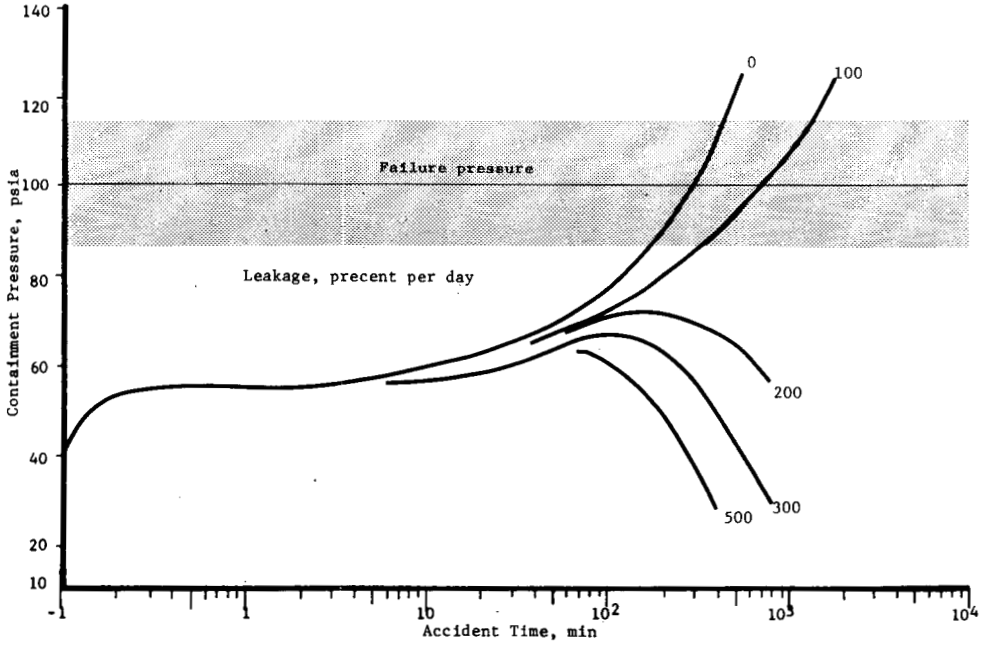
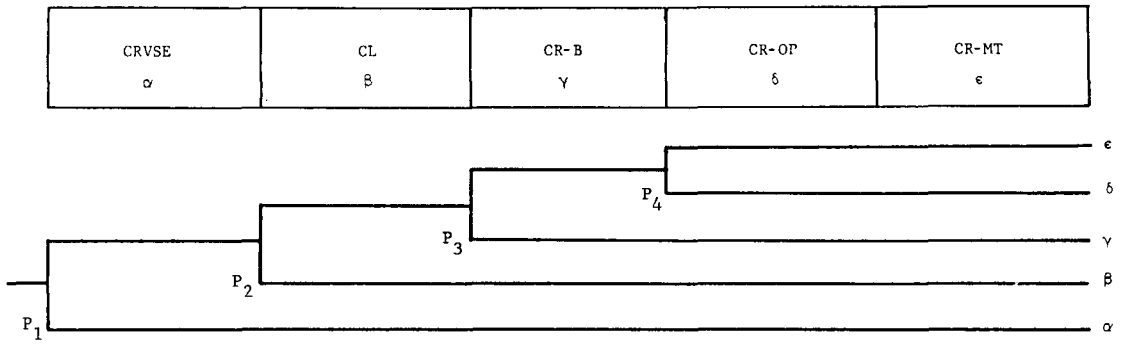


FIGURE VIII 2-10 PWR Containment Pressure as a Function of Leak Rate for an Assumed LOCA with No Containment Safeguards



$$P_\alpha = P_1$$

$$P_\beta = (1 - P_1)P_2$$

$$P_\gamma = (1 - P_1)(1 - P_2)P_3$$

$$P_\delta = (1 - P_1)(1 - P_2)(1 - P_3)P_4$$

$$P_\epsilon = (1 - P_1)(1 - P_2)(1 - P_3)(1 - P_4)$$

FIGURE VIII 2-11 PWR Containment Event Tree

Section 3

BWR Analyses

3.1 ACCIDENT SEQUENCE RESULTING IN CORE MELTDOWN

Failures of the following engineered safety features have been considered in various combinations as they might affect the development of degraded core conditions in the event of a recirculation line break in a BWR: electric power, loss of vapor suppression, loss of containment isolation, emergency core cooling system operation, emergency core cooling system function, scram, and long-term cooling. The definitions of the failures of these systems and their influence on the course of the accident are given below.

ELECTRIC POWER SYSTEM (EPS)

Failure to provide a-c and d-c power for the operation of the engineered safety features required to mitigate the initiating event.

VAPOR SUPPRESSION SYSTEM (VSS)

Failure of the vapor suppression system to condense an adequate quantity of steam discharged from the drywell to the wetwell to prevent an overpressurization of the primary containment sufficient to result in its rupture. Loss of vapor suppression with the attendant failure of containment may not of itself lead to core meltdown since the other safeguards could still be operable, assuming failure does not lead to the loss of water from the torus.

CONTAINMENT LEAKAGE (CL)

Three cases of containment isolations failures are considered:

a. Minor failures of Primary Containment System (PCS) isolation which result in leakage to the Secondary Containment System (SCS) of less than 100 v/o per day; this is equivalent to approximately a 1-in.-diam hole.

b. Failures of the PCS which result in leakage to the SCS in excess of 100 v/o per day but less than 3600 v/o per day. With these leak rates and the loss of long-term cooling of the ECCS pumps will fail due to the loss of the required Net Positive Suction Head (NPSH); however, these leakages are sufficiently high to prevent primary containment failure by overpressurization.

c. Leakage greater than 3600 v/o per day (approximately a 6-in.-diam opening). This will result in secondary containment failure during the blowdown phase of the accident.

EMERGENCY COOLING INJECTION (ECI)

Two definitions for emergency core cooling operational failures have been developed:

a. Failure of (a) any Core Spray Injection System (CSIS) pump with no Low Pressure Coolant Injection System (LPCIS) operational or (b) more than two CSIS pumps and one LPCI pump; as well as their associated controls, piping, etc.

b. Failure of (a) two CSIS pumps with no LPCIS operational or (b) three LPCI pumps with no core spray operational or (c) more than three LPCI pumps and more than three core spray pumps; as well as their associated controls, piping, etc.

For success, the minimum design ECCS (Emergency Core Cooling System) must operate until the core is reflooded at which time one ECCS pump is sufficient to maintain the water level in the vessel.

EMERGENCY COOLING FUNCTION (ECF)

Failure to provide the required quantity of water to the reactor core to prevent core melt, due to structural failures such as: core shroud failure, jet pump failure, or other damage which may result from initial blowdown.

SCRAM

The failure to insert control rods prior to reflooding the core with ECCS in order to ensure subcriticality of the reactor.

LONG-TERM COOLING (LTC)

Failure to provide core cooling through at least one Residual Heat Removal (RHR) loop consisting of one pump, one heat exchanger, one high-pressure service water pump, one emergency service water pump and the associated controls, valves, piping, etc., or by use of one core spray pump in conjunction with the above. Loss of long-term cooling will lead to overheating of the suppression pool water, overpressurization of the containment, failure of the ECCS, and core meltdown. The particular sequence of events may vary if failures of other safeguards accompany loss of long-term cooling.

3.2 ANALYSIS OF DEGRADED ACCIDENT BEHAVIOR

3.2.1 BASIC ASSUMPTIONS

The governing accident case for BWR safety evaluations is generally taken to be a double-ended rupture of a primary coolant recirculation line. This is the situation selected as the starting point for the present degraded accident consequence assessment. The design of BWR systems normally provides a diversity and redundancy of standby core cooling systems as protection against the entire spectrum of potential LOCA's. For the purpose of this study, however, the operability of only the minimum design basis safeguards has been assumed. Specifically, for the double-ended recirculation line break, the minimum required safeguards were assumed to consist of two Low Pressure Coolant Injection (LPCI) pumps, one Core Spray Loop which contains two Core Spray Injection (CSI) pumps, and one Residual Heat Removal (RHR) loop. No High Pressure Coolant Injection System (HPCIS) or Containment Spray operability were considered. It is recognized that several other combinations of the total available safeguards could provide the desired level of protection.

For purposes of degraded accident evaluation the ECCS, if operable, are assumed to refill the reactor vessel and keep it filled to the level of the jet pumps; excess capacity is assumed to spill to the floor of the drywell and flow back to the suppression pool. Failure of emergency core cooling operation is interpreted as no water injected into the reactor vessel. Loss of emergency core cooling function is taken as delivery of the requisite quantity of water to the reactor vessel but failure to provide the desired cooling due to some type of structural failure. LTC, if available, is assumed to be manually activated at 600 seconds into the accident.

3.2.2 ACCIDENT TIME SCALE

For the above accident and safeguards operation, the expected sequence of events would be as follows:

Event	Time, sec
Double-ended recirculation line break with attendant loss of normal auxiliary power	0.0
Reactor vessel low water level initiates main steam isolation valves closure	0.5
Reactor scram signal from high drywell pressure	1.0
Diesel generators signaled to start. Primary containment isolated. Core spray and low pressure coolant injection systems signaled to start	3.0
Primary system depressurization complete. Core spray system operating	30.0
Low-pressure coolant injection system operating	43.0
Signal for emergency service water pumps to start	55.0
Emergency service water pumps at rated speed	60.0
Core effectively reflooded	95.0
Manual activation of residual heat removal system	600.0
Maximum suppression pool temperature reached	4.6×10^4

The above sequence of events should be representative of most large BWR systems.

3.2.3 CORE MELTDOWN

Accident sequences involving the failure of the ECCS to operate or the loss of electric power lead to dry meltdowns in which the core heats essentially adiabatically. Since essentially all the primary system water is lost during the blowdown, there is no significant quantity of steam for the zirconium-water

reaction in these cases. There is also little driving force to remove fission products that have been released to the primary vessel. As in the PWR cases, the core is expected to remain above the grid plate until a large fraction of the core has melted. From Fig. VIII A-7 the time after the LOCA has occurred to that at which a large fraction of the molten core would be expected to move down into the lower head is estimated to be 150 ± 30 minutes.

Core degradation due to loss of emergency core cooling function is particularly difficult to evaluate and would be expected to depend on the particular nature and extent of damage encountered. The present analyses indicate that core melting in the presence of emergency coolant whose heat-removal effectiveness has been impaired would take place in two phases. In the hottest portions of the core, decreased cooling effectiveness would result in heat generation due to the zirconium-water reaction and thus accelerate the heatup and melting of those regions. The cooler portions of the core would take some time to reach temperatures where zirconium-water reactions would be significant and thus would reach melting at significantly later times. The time after LOCA for the hotter half of the core to melt is estimated to be 20 ± 10 minutes and for the cooler half it is 150 ± 30 minutes.

The cases in which LTC failure is the cause of reactor meltdown are similar to the PWR accidents analyzed. The core has been quenched and is partially flooded at the time the emergency cooling pumps fail. The water then boils off and the core melts. The time required to achieve 80 percent core melting is quite similar for the BWR and PWR boiloff meltdown cases. This time can therefore be estimated from Fig. VII A-6 as a function of time at which boiloff begins. For the BWR wet meltdowns the fraction of zirconium reacted is estimated to be 50 ± 15 percent of the core inventory.

3.2.4 PRESSURE VESSEL MELTTHROUGH

The lower plenum of the BWR is partially filled with control rod guide tubes and the lower head contains a number of control rod drive penetrations. When the molten core leaves the fuel region it may partially refreeze on control rod guide tubes or penetrate these tubes prior to failure of the bottom head. If the time required to heat the entire vessel to 2400 F with the decay heat is considered an upper bound to the time required to penetrate the primary vessel, then penetration must occur in less than 72 minutes. The best estimate for the meltthrough time after the core drops into the lower plenum is 30 ± 20 minutes for the dry meltdown cases. For the wet meltdown cases, an additional 30 minutes will be required for vaporization of the water in the bottom head and, for later onset of core melting, the meltthrough time will be further extended due to the decrease in decay heating.

3.2.5 STEAM EXPLOSIONS

If during the course of a meltdown accident large quantities of molten core materials can come into contact with water, the possibility of steam explosions must be considered. The analyses described in Appendix C indicate that if 20 or more percent of the core when molten comes in contact with water, steam explosions in the pressure vessel with the potential to fail containment could result. For meltdowns which are a consequence of loss of electric power or failure of the ECCS to operate there would be little or no water in the reactor vessel and hence little likelihood of steam explosions within the reactor vessel. If, however, meltdown were to result from failure of the ECCS to function effectively, failure of the reactor to scram, or emergency coolant pump cavitation, there would be the possibility of steam explosions as the molten core comes in contact with the water in the reactor vessel. If core meltdown takes place with the containment already failed, as would be the case with the loss of vapor suppression or loss of LTC, the occurrence of a steam explosion would not be expected to have a major effect on the accident consequences.

There is also the possibility of steam explosions upon the meltthrough of the reactor vessel bottom head as the mass of molten material falls into the water on the drywell floor. The configuration of the drywell to wetwell vents would permit approximately a 2-foot depth of water to remain on the drywell floor; the temperature of this water could range from subcooled to saturated, depending on the particular accident sequence and point in time of interest. If the molten materials were to fall into the water in relatively small quantities and over a period of time, they would simply be quenched and the steam generated in the process would be condensed in the suppression pool. If, on the other hand, a significant fraction of the core were to fall into the water coherently, there would be the potential

for a violent interaction. Such violent interactions are of concern if they have the potential to fail containment and if they occur while the containment is still intact.

3.2.6 CONTAINMENT VESSEL PENETRATION

When the molten core together with some of the reactor internals and part of the vessel bottom head fall to the floor of the drywell, vaporization of the water there as well as decomposition of the concrete will ensue. Any water on the drywell floor will be vaporized by the melt and in the absence of drywell failure will be forced into the suppression pool and condensed. The penetration of the concrete proceeds in a manner similar to that previously described for the PWR's. Initially the vaporization of free water below the surface of the concrete will cause spalling and a rapid rate of penetration of the concrete by the melt. As the products of concrete decomposition are dissolved in the melt, the melt temperature will decrease to the point where some of the constituents of the mixture begin to precipitate. From this point onward in time the progress of the melt through the concrete is controlled by the rate of decay heat generation. The initial rapid spalling is estimated to penetrate a 1.5-ft depth of concrete in about 20 minutes, the subsequent meltthrough proceeds at a rate of about 0.5 ft per hour. The CO_2 and water vapor generated by the decomposition of concrete will be forced into the suppression pool where the latter will condense. The CO_2 together with the other noncondensables will collect in the suppression chamber gas space and lead to containment failure by overpressurization. Figure VIII 3-1 gives the partial contributions as well as combined pressures of the various constituents within the containment. The CO_2 pressure contribution is based on the decomposition of approximately a 20-ft-diam x 8-ft-high cylinder of concrete below the reactor vessel within the drywell vessel. The quantity of CO_2 together with the other noncondensables when confined in the suppression pool gas space will result in a pressure more than sufficient to rupture the containment. If the melt progresses radially outward as well as down, as might be expected, a larger quantity of CO_2 would be generated prior to the time that the melt reaches the steel vessel. Further, since the bottom of the drywell vessel is embedded in concrete, meltthrough of the steel vessel would not necessarily imply a breach of containment. Thus, with less than about 100 percent per day leakage, containment would fail by overpressure rather than meltthrough of the concrete foundation.

Interaction of the molten core with groundwater following containment meltthrough is discussed in Appendix VII.

3.2.7 HYDROGEN COMBUSTION

BWR containment atmospheres are inerted by purging with nitrogen until the oxygen content is below 5 percent. The oxygen is maintained at or below this level during normal operation. At this oxygen concentration the containment atmosphere is outside hydrogen flammability limits, regardless of the quantity of hydrogen in the atmosphere. Radiolytic decomposition of water during the course of the accident would add oxygen as well as hydrogen to the atmosphere. During the accident times of interest here, i.e., of the order of a day or less, radiolytic decomposition of water would not result in a flammable mixture. For longer time periods, the containment would have failed by other mechanisms and hydrogen combustion would not be of concern. If the hydrogen generated by the zirconium-water reaction is included in the consideration, the atmosphere will be outside the flammability range even if oxygen in the containment approaches the equilibrium value achievable by radiolysis.

Thus it is concluded that hydrogen combustion can be eliminated as a mechanism of containment failure in the BWR degraded accident sequences. Some of the bases for this conclusion are further discussed in Appendix D.

3.2.8 CONTAINMENT RESPONSE

Functioning of the vapor suppression containment as designed leads to relatively low accident pressures within the containment except for the early portions of the blowdown. If, however, condensation of the steam generated by primary system depressurization does not take place, for whatever reason, pressures significantly in excess of design levels would result. Assuming that steam condensation does not take place and that the entire free volume of the containment is available, primary system depressurization would result in a pressure of about 250 psia within the reactor containment design assumed for this study. As this is well above the 175 $\pm$ 25 psia failure pressure determined in Appendix E, primary containment rupture would be expected. If this failure did not lead to loss of suppression pool water, but only in venting of the steam from the containment, it may still be

possible for the standby core cooling systems to operate and thus prevent core melting.

The failure of long-term cooling with all the other safeguards systems working would lead to a gradual increase in the suppression pool water temperature and attendant gradual containment pressure increase. With a design basis containment leak rate, the loss of LTC will lead to containment failure by overpressurization in about 25 hour. With larger leak rates the time to failure could be extended; in such cases, however, loss of standby core cooling system pumps due to cavitation must be considered. This aspect is discussed in a later section of the report.

The minimum safeguards for the purpose of this evaluation were assumed to be two LPCI pumps, two CSI pumps, and one RHR loop. This combination is sufficient to effectively reflood the core and more than sufficient to maintain the core water inventory. With the combination of bottom flooding and core spray, decay heat would be accommodated with little or no net steam generation. Under degraded ECCS operation, there may be continued generation of steam from the core; this could lead to the drywell pressure remaining about 3 psi higher than that in the suppression chamber with no equalization of the noncondensables. Under such conditions the containment would remain at an elevated pressure for an extended time.

The location of the noncondensable gases will have a significant effect on the overall BWR containment pressures following an accident. Figure VIII 3-1 gives the partial as well as combined pressures of the various constituents of the containment atmosphere as a function of containment temperature and disposition of the noncondensables. The pressure contribution due to hydrogen is based on the reaction with water of 50 percent of the zirconium in the core (equivalent of 83 percent of the fuel cladding); the carbon dioxide contribution assumes the decomposition of a 20-ft-diam by 8-ft cylinder of concrete at the bottom of the drywell. It may be noted that with minimum design basis safeguards operating, the containment temperature range of interest is 130 - 190 F.

Figure VIII 3-2 gives the expected containment pressure response for an accident sequence involving failure of emergency core cooling function. The initial rapid pressure decrease is associated with the condensation of steam by the suppression pool and the equilibration of the noncondensables. As the core overheats and melts, the containment pressure increases due to the generation of hydrogen by the zirconium-water reaction. The reaction of the cladding with water has been assumed to have run its course by the end of core meltdown, i.e., 150 minutes; thus there is little pressure change during the time of pressure vessel melt-through. Assuming no damaging steam explosion as the molten mass falls to the drywell floor, pressure vessel melt-through will be followed by vaporization of the water at the bottom of the drywell and the rapid attack of the concrete floor. During this period, the pressure within the system will increase rapidly and lead to large flow rates of steam and noncondensables from the drywell to the suppression pool, where the former will be condensed. The rapid pressure increase occurring between 210-230 minutes in Fig. VIII 3-2 is associated with the transport of all the noncondensables to the suppression chamber gas space. After 230 minutes the pressure will continue to increase but at a significantly lower rate due to the continued evolution of CO_2 from the decomposition of concrete. This will continue until the containment fails.

Containment pressure response for failure of emergency core cooling operation is shown in Fig. VIII 3-3. In this case there would not be enough water available in the reactor vessel for an appreciable extent of zirconium-water reaction and the containment pressure would remain at a low level during the core melting and pressure vessel meltthrough phases of the accident. When the molten mass falls to the drywell floor it will come into contact with water, and the reaction of the molten zirconium with water can be expected. However, since the geometry in this case will not be as favorable for the reaction as during the initial core meltdown, the extent of reaction is estimated to be 25 percent of the total zirconium in the core. Again barring a damaging steam explosion, pressure vessel meltthrough will be followed by a rapid pressure increase and the flow of steam and noncondensables into the suppression pool. The rapid pressure increase from 180-210 minutes in Fig. VIII 3-3 reflects the transport of the noncondensables to the suppression chamber. The slower pressure increase after that is due to the continued evolution of CO_2 from concrete decomposition; this continues until containment failure.

3.2.9 CONTAINMENT ISOLATION FAILURES

The LPCI and CSI pumps take their suction from the suppression pool and have NPSH requirements of 25 to 28 ft. They are not always designed to operate in the absence of positive pressure in the containment. Thus the possibility of pump cavitation must be considered in the evaluation of the various accident sequences, particularly those involving loss of containment isolation. The heat-removal capacity of a single RHR loop, the minimum design basis, is less than the decay power early in the accident. This imbalance is accommodated by an increase in the suppression pool water temperature until about 4.6×10^4 seconds; after that time the heat-removal capacity exceeds the decay heat generation and the pool temperature decreases gradually with time. With more than the minimum design basis LTC available there would not be this temporary imbalance between heat generation and heat removal. If containment integrity is maintained, i.e., leakage from the containment does not exceed the design leak rate, pump cavitation will not occur regardless of pool water temperature. In the event of loss of LTC the pool temperature will increase continuously and the containment will fail from overpressure. Containment failure will then be followed by pump cavitation.

Failure of containment isolation, i.e., excessive leakage rather than the total loss of containment integrity, would lead to the loss of noncondensables from the containment. This would not result in pump cavitation if the RHR system were functioning. With loss of containment isolation and failure of the RHR system, cavitation of the standby core cooling system pumps would be expected. Figures VIII 3-4 and VIII 3-5 illustrate containment pressure-time histories with loss of RHR and several containment leak rates with the noncondensables in the suppression chamber and equalized, respectively. It is seen that for leak rates in excess of 100 percent per day, pump cavitation will occur before containment overpressurization. Based on critical flow of steam with a discharge coefficient of 0.6, a leak rate equal to 100 percent of the free volume of the containment corresponds to an orifice size of 1 inch; a 1000 percent per day leak corresponds to a 3.2-in.-diam hole, etc. With the containment at atmospheric pressure, pump cavitation would be expected to occur when the suppression pool water temperature reaches 190 F, or about 1.5×10^4 seconds into the accident.

If the containment fails due to the failure of vapor suppression but without loss of water from the suppression pool, the standby core cooling systems could still operate. If loss of vapor suppression is accompanied by the loss of residual heat removal capability, pump cavitation would take place at about 2.4×10^4 seconds. In this situation, the pool water would not have absorbed the energy of the flashing primary coolant and thus would require longer to attain the temperature at which cavitation would occur.

The location as well as the size of containment isolation failures can have a bearing on the overall accident consequences. If the containment isolation failure takes place in the drywell, fission products released from the core may leak directly to the secondary containment. In the event of secondary containment failure this may result in a large release of radioactivity to the environment, even if gross failure of the primary containment is avoided. For isolation failures in the suppression chamber gas space, on the other hand, the leakage of fission products will be through the pool and then out to the secondary containment. The water in the pool would be expected to retain most of the particulates and a large fraction of the iodine. Thus even in the event of secondary containment failure there would be a significant reduction in the fission-product release for these cases.

3.2.10 SECONDARY CONTAINMENT

The secondary containment building for BWR's houses reactor auxiliary systems, radwaste equipment, refueling operations, etc. It is a controlled leakage structure which is normally maintained at a slightly subatmospheric pressure by ventilation fans which exhaust through the stack. In the event of an accident, the normal ventilation system is isolated and the building atmosphere is passed through the Standby Gas Treatment System (SBGTS) before being released through the stack. Thus the consequences of any activity release from the primary containment could be greatly reduced by the presence of the secondary containment. For the degraded accident analyses considered here, however, the possibility of secondary containment failure must also be considered.

The secondary containment assumed in this evaluation has a free volume of 2.5×10^6 ft^3 and is designed for an internal pressure of 0.25 psig. The design leak rate is 100 v/o per day at a differential pressure of 0.25 in. of water.

Due to the low pressure capability of the secondary containment, any catastrophic failure of the primary containment is expected to fail the secondary also. Thus steam explosions which fail the drywell would at the same time breach the secondary containment building; similarly, overpressurization failure of primary containment will fail the secondary. In addition to the above, loss of primary containment isolation could result in leakage to the secondary containment greater than the capacity of the SBGTS and the leakage out.

By considering the flow into the secondary containment through the containment isolation leak, flow to the SBGTS and building leakage as a function pressure, it is possible to determine the size of isolation failure at which the secondary containment building pressure will exceed 0.25 psig following blowdown into the drywell. It has been determined that loss of containment isolation equivalent to about 5 to 6-in.-diam hole would lead to the failure of the secondary containment in the event of a large LOCA.

The nature and location of secondary containment failure can in itself have an influence on the accident consequences. A steam explosion in the reactor vessel which fails the primary containment would be expected to breach the secondary containment above the reactor refueling floor. Thus any ensuing activity release would be directly to the environment. An overpressure failure, on the other hand, could take place anywhere along the primary containment envelope. If a failure of the latter type were to occur in the lower portions of the structure, the activity could be released into the various portions of the secondary containment where considerable holdup and decontamination could take place before the release reaches the environment. There are parts of the secondary containment structures whose failure would lead to a direct release of activity to the environment. In general, however, it would be expected that the activity released as a consequence of an overpressure failure of the primary containment would undergo some holdup and decontamination in passing through the secondary containment, even though the latter is also failed.

3.3 SUBSEQUENCE PROBABILITIES

Figure VIII 3-6 illustrates the various paths to containment failure that are postulated following meltdown accidents in BWR's: reactor vessel steam explosion, containment steam explosion, overpressurization, containment leakage from the drywell, containment leakage from the wetwell, secondary containment failure, and standby gas treatment system failure. It is expected that containment floor meltthrough would accompany each of the other containment failure modes. However, since meltthrough is not the primary mode of containment failure in any of the cases and since it would not add appreciably to the atmospheric fission-product source term, it has been omitted from the core melt event tree. The violent modes of containment failure, i.e., steam explosions and overpressurization, are treated as exclusive, e.g., if a steam explosion results in gross containment failure there is no need to consider the potential overpressurization. Also, violent primary containment failures as well as large containment isolation failures will be accompanied by failure of the secondary containment.

For a given accident sequence, i.e., LOCA in combination with various engineered safeguards failures, some of the paths to containment failure may not be relevant or credible. In such cases these paths are assigned a probability of zero for that particular accident sequence. The method of determining the various probabilities of containment failure for the accident sequences of interest are described below.

In Fig. VIII 3-6 the numerically subscripted factors, P_1, P_2, etc., represent the probability of failure at each decision point in the containment event tree. They are defined as follows:

- P_1 - probability of primary containment failure due to a reactor vessel steam explosion
- P_2 - probability of primary containment failure due to a containment steam explosion
- P_3 - probability of primary containment failure due to overpressure
- P_4 - probability of a containment leak in the wetwell
- P_5 - probability that a leak in the drywell is greater than 2400 percent per day
- P_6 - probability that a leak in the wetwell is greater than 2400 percent per day

P_7 - probability of secondary containment failure

P_8 - probability of standby gas treatment system failure.

The probabilities of containment leakage, P_4, P_5, and P_6, probability of secondary containment failure with primary containment intact, P_7, and independent probability of SBGTS filter failure, P_8, are not dependent on the core melting sequence. The numerical values of these probabilities have to be determined from other studies such as fault tree analyses of the particular systems. They are included in the present analysis since they can affect the course and consequences of the overall accident sequence. The other probabilities are dependent on the particular accident sequence in question, and their evaluation has been a significant part of the present study.

The relative probabilities of each of the branches of the BWR containment event tree for any given accident sequence can then be determined as follows.

$$P_\alpha = P_1$$

$$P_\beta = (1 - P_1)P_2$$

$$P_\gamma = (1 - P_1)(1 - P_2)P_3$$

$$P_{\varepsilon\zeta} = (1 - P_1)(1 - P_2)(1 - P_3)P_4P_6$$

$$P_{\varepsilon\eta} = (1 - P_1)(1 - P_2)(1 - P_3)P_4 (1 - P_6)P_7$$

$$P_{\varepsilon\theta} = (1 - P_1)(1 - P_2)(1 - P_3)P_4 (1 - P_6)(1 - P_7)P_8$$

$$P_\varepsilon = (1 - P_1)(1 - P_2)(1 - P_3)P_4 (1 - P_6)(1 - P_7)(1 - P_8)$$

$$P_{\delta\zeta} = (1 - P_1)(1 - P_2)(1 - P_3) (1 - P_4)P_5$$

$$P_{\delta\eta} = (1 - P_1)(1 - P_2)(1 - P_3) (1 - P_4)(1 - P_5)P_7$$

$$P_{\delta\theta} = (1 - P_1)(1 - P_2)(1 - P_3)(1 - P_4) (1 - P_5)(1 - P_7)P_8$$

$$P_\delta = (1 - P_1)(1 - P_2)(1 - P_3)(1 - P_4) (1 - P_5)(1 - P_7)(1 - P_8)$$

This latter set of probabilities takes into account the exclusive as well as dependent nature of the various failure modes for each accident sequence.

3.3.1 CONTAINMENT FAILURES RESULTING FROM A STEAM EXPLOSION

As discussed previously, the only cases in which primary vessel steam explosions are a concern are those in which meltdown takes place with water in the primary vessel and the containment intact. These would include sequences entailing failure of emergency core cooling function, loss of long-term cooling, and failure to scram. The probability of containment failure due to a steam explosion is given by

$$P_1 = P_{fw}\alpha_{sxs}\alpha_{cf}. \qquad \text{(VIII 3-1)}$$

The terms in this equation have been previously defined. The probability that a significant fraction of the core would accumulate in the molten state and be available to interact with the water, P_{fw}, is believed to be high. The bases for this conclusion are discussed in Appendix A. The numerical value assigned to this factor is the same as estimated for the PWR cases,

$$P_{fw} = 10^{-0.05\ (\pm 0.05)}.$$

The probability that a mass of molten core material upon contact with water will disperse finely enough for a violent interaction, α_{sxs}, is believed to be depending on the temperature of the water. If the water is subcooled, the probability of dispersal is significantly higher than if the water is at or near saturation conditions, as is discussed in Appendix B. For those degraded accident sequences in which the water in the reactor vessel can be expected to be at or near saturation, e.g., loss of LTC, the probability of a dispersal event is estimated to be the same as that for the PWR cases considered previously:

$$\alpha_{sxs} = 10^{-1\ (+0.5,\ -1)}.$$

In those cases where the water in the bottom of the reactor vessel may be subcooled, e.g., failure of emergency core cooling function, a higher probability of dispersal is utilized,

$$\alpha_{sxs} = 10^{-0.3\ (+0.25,\ -1)}.$$

Appendix C describes calculations performed to determine the conditions under which drywell failure might result from a steam explosion in the pressure vessel. These results indicate that the potential for containment failure from steam explosions in the reactor vessel in BWR's is comparable to that in PWR's. While the PWR containment shell is protected by a control rod drive shield and by some distance, the internal equipment in the upper portion of the BWR pressure vessel is effective in absorbing some of the energy of the expanding mixture of hot (molten) core materials and steam. Thus the probability of a reactor vessel steam explosion failing containment is estimated on the basis of these calculations to be

$$\alpha_{cf} = 10^{-1\ (+0.5,\ -1)}.$$

Combining the individual factors assuming a skewed log-normal distribution, the probability of a reactor vessel steam explosion leading to containment failure with saturated water is

$$P_1 \simeq 10^{-2\ (+1,\ -2)}$$

and with subcooled water it is

$$P_1 \simeq 10^{-1.35\ (+0.8,\ -2)}.$$

Steam explosions are also possible upon pressure vessel meltthrough as the mass of molten materials falls into the water on the drywell floor. As is the case with reactor vessel steam explosions, a significant quantity of molten material must interact coherently with water to produce a damaging explosion. Here again the probability that a large quantity of molten material would be available to interact with the water, P_{cfw}, is believed to be large. Accordingly,

$$P_{cfw} = 10^{-0.05\ (\pm 0.05)}.$$

The probability that the molten material is finely dispersed upon interaction with the water is taken to be identical to that for reactor vessel steam explosions, being $10^{-1(+0.5,\ -1)}$ and $10^{-3(+0.25,-1)}$ for saturated and subcooled water, respectively.

The containment steam explosion would taken place within the 20-ft-ID reactor vessel support cylinder which is steel-lined, reinforced concrete approximately 3 ft thick. The explosive vaporization of a significant fraction of the approximately 2 ft of water at the bottom of this cylinder will produce pressures well above the strength of the cylinder, the latter being a few hundred psi. Although there is an opening in the side of this cylinder for an access door and the space between the reactor vessel and the sacrificial shield provides partial opening at the top, the time scale of a steam explosion would be too short to permit significant pressure relief through these vent areas. The rise time of the steam explosion would be on the order of 30 msec, much larger than the sonic transit time through the concrete wall which is calculated to be about 0.3 msec. Thus spalling of the concrete would not be expected, and failure of the support cylinder will take place by an essentially static overpressurization.

The steam will then be released to the drywell. If the pressure rise within the drywell is sufficiently rapid, the drywell-to-wetwell vents may not be able to clear in time to avert overpressurization of the drywell. The time required to clear the vents for a pressure rise of the type considered here has been calculated to be 0.1 sec; an additional 0.1 sec would be required to flow 10 percent of the steam into the suppression pool. Thus, if a major fraction of the heat transfer between the molten core and water takes place in 0.2 sec or less, venting of the steam to the suppression pool will not be possible. The effective particle diameter associated with this heat transfer time is about 600 microns, based on the analyses in Appendix C. This particle size is well within the range of sizes observed in steam explosions.

If the water within the reactor vessel support structure were vaporized faster than it could be transported to the suppression pool, the incremental increase in the static pressure in the drywell would be 112 psi. The resulting potential for drywell failure from overpressure would depend upon the preexisting pressure in the drywell at the time of the event. Thus the potential for failure due to a containment steam explosion will have to be considered separately for each accident sequence in question. If drywell failure does not occur, the steam will subsequently flow into the suppression pool and condense.

In addition to the quasiequilibrium pressure of steam, missile generation could be a potential mechanism of failure in the event of a containment steam explosion. As discussed above, the rise time of steam explosions is not expected to be rapid enough to produce spalling on the outside of the reinforced concrete cylinder. The overpressure failure may produce concrete fragments, but these would not be expected to have a high velocity. After pressure relief, the reinforcing steel together with other supporting structures would still be expected to provide adequate support to the shell of the pressure vessel. The sheet metal door could be a potential missile, but one that is unlikely to penetrate the drywell. Further, after a 2-in. air gap, the drywell vessel is backed up by concrete; thus the steel shell could deform locally and transfer the missile loading to the concrete. Thus it is concluded that failure due to missiles in this case has a significantly lower probability than failure due to overpressure.

3.3.2 CONTAINMENT OVERPRESSURIZATION

For meltdown accidents resulting from loss of LTC or failure of vapor suppression, containment failure due to overpressurization precedes core meltdown and is accompanied by failure of the secondary containment. Thus, alternate paths to containment failure need not be considered for these cases. In cases involving failure of emergency core cooling operation or function, if the containment is still intact after initiation of meltthrough of the drywell floor, failure due to overpressurization is considered a certainty. As noted previously, the CO_2 generated by the decomposition of concrete together with the other noncondensables will raise the containment pressure above its failure level before the melt reaches the drywell vessel.

Small containment isolation failures, i.e., equivalent to 1-in.-diam holes or less, will not prelude containment failure by overpressurization.

3.3.3 SECONDARY CONTAINMENT FAILURE

As noted previously, violent failures of the primary containment would be expected to result in failure of the secondary containment. If large containment isolation failures existed during the blowdown, secondary containment would be expected to fail. Small containment isolation failures would not result in secondary containment failure directly, although the latter would occur when the primary containment fails due to overpressure or other mechanisms. Thus effectively the only degraded accident sequences which benefit from the secondary containment are those in which intermediate containment isolation failures are present. These failures are large enough to prevent overpressurization of the containment but not so large as to overpressurize the secondary containment building.

3.3.4 UNFILTERED ELEVATED RELEASE

The SBGTS, consisting of demisters, high-efficiency particulate filters, and activated-charcoal filters, is designed to clean the secondary containment atmosphere and exhaust through the stack. Thus the consequences of any radioactivity release from the primary containment could be greatly reduced by the SBGTS operation. The degraded accident analyses have also considered the possibility of failure of the SBGTS. The latter can occur in several ways:

a. Failure of the secondary containment, discussed above

b. Failure of the components of the treatment train, e.g., leakage through or around the filters, improper installation. (This probability requires separate studies on the reliability of gas treatment systems.)

c. Failure of some or all of the components of the train due to overloading when subjected to off-design conditions, as may be the case in many of the accidents considered here. (This possibility is being evaluated in the Fission Product Source Term Task.)

The SBGTS can mitigate the consequences of radioactivity release even with some of its components failed by leading to an elevated rather than a ground level release.

3.3.5 HYDROGEN COMBUSTION

Due to inerting of the containment atmosphere, the potential for hydrogen combustion in BWR's is small and its influence on the consequences of meltdown accidents would not be very significant. Accordingly this possibility has not been included in the containment failure evaluation.

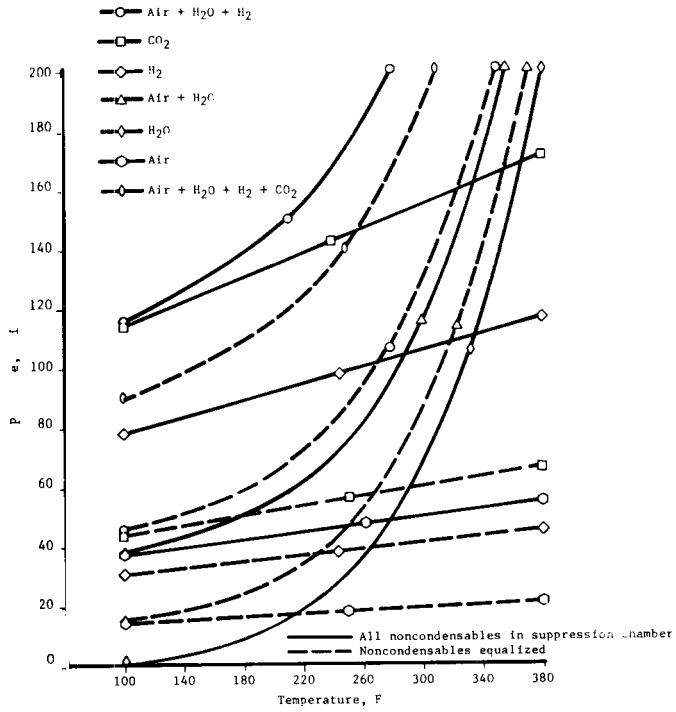


FIGURE VIII 3-1 PWR Containment Pressure as a Function of Composition and Temperature

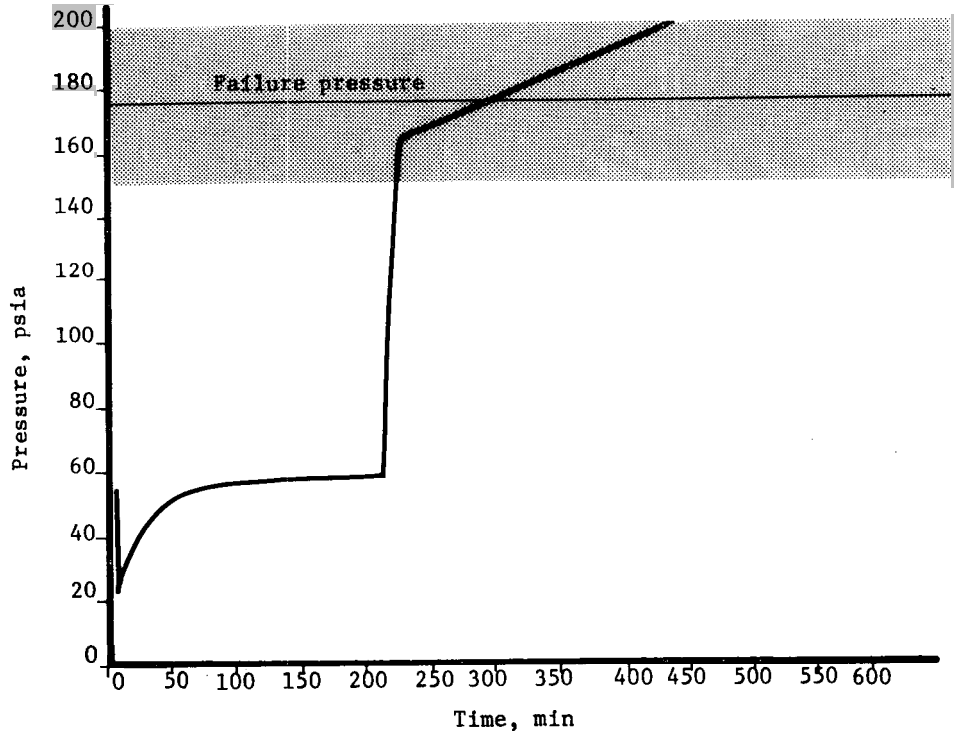


FIGURE VIII 3-2 BWR Containment Pressure Response with Assumed Failure of Emergency Core Cooling System Function

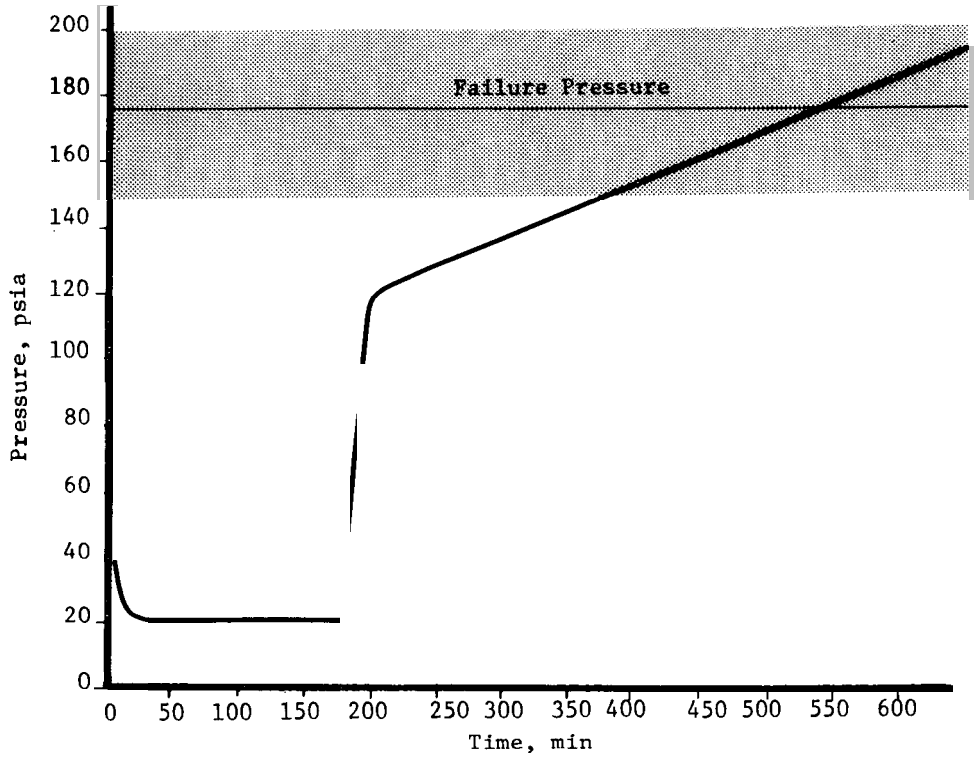


FIGURE VIII 3-3 BWR Containment Pressure Response with Assumed Failure of Emergency Core Cooling System Operation

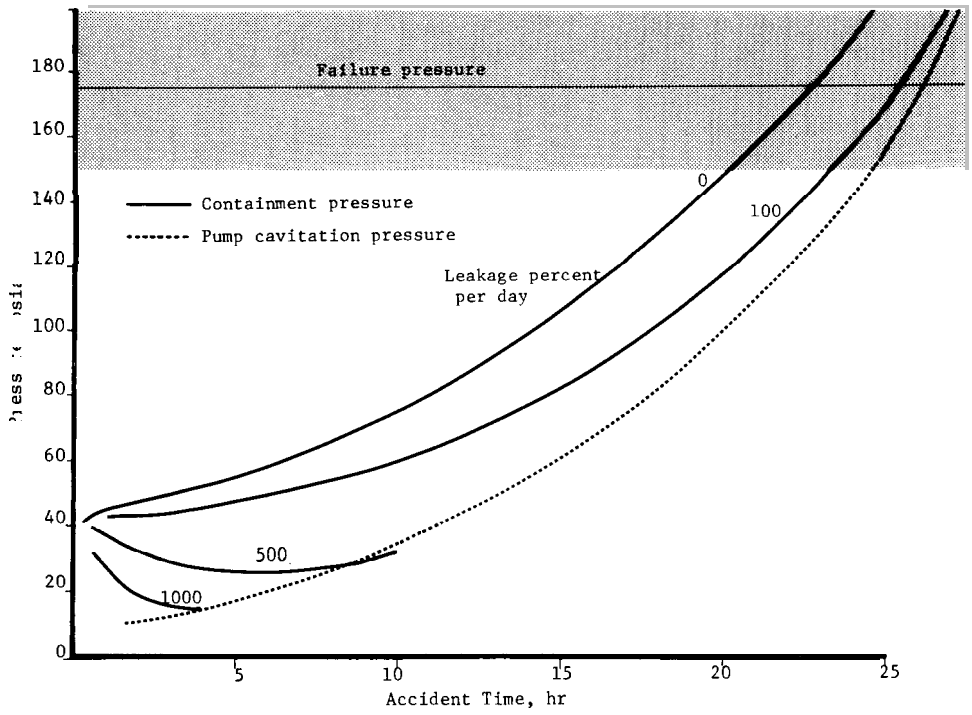


FIGURE VIII 3-4 BWR Containment Pressure Response as a Function of Leak Rate with Assumed Loss of Long-Term Cooling and All the Noncondensables in the Suppression Chamber

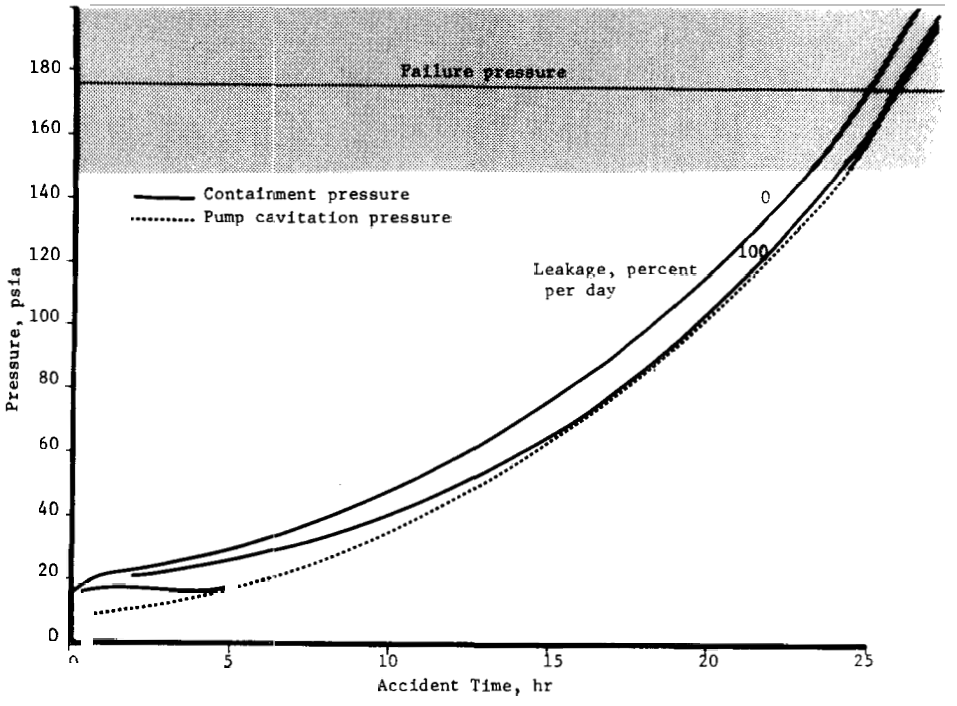


FIGURE VIII 3-5 BWR Containment Pressure as a Function of Leak Rate with Assumed Loss of Long-Term Cooling and Noncondensables Equalized Between the Drywell and Suppression Chamber

Core Melt	VSE	CSF	OP	DW vs WW Leak	LCL	SCF	SGTS	Sequence
	α	β	γ	δ/ε	ζ	η	θ	

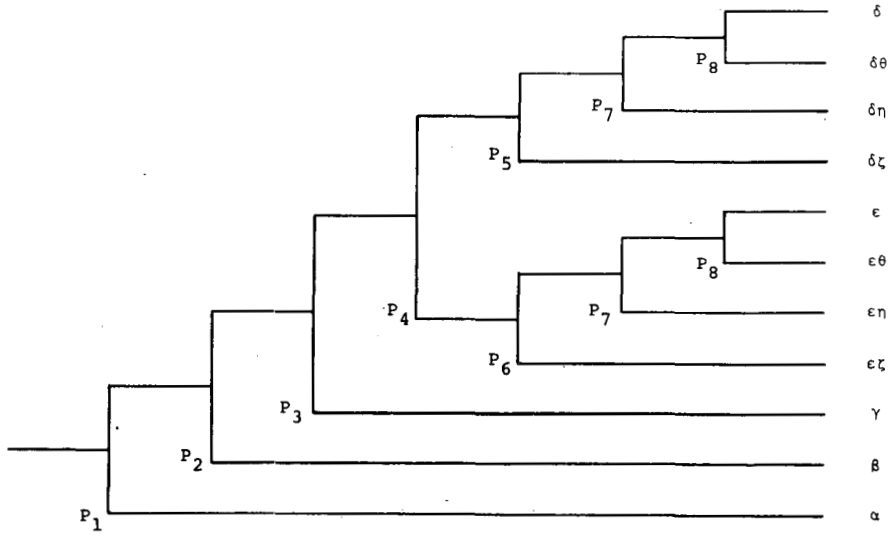


FIGURE VIII 3-6 BWR Containment Event Tree

APPENDIX A

THERMAL ANALYSIS

Appendix A

Table of Contents

Section		Page No.
A1.	CALCULATIONS	VIII-45
A1.1	Core Heatup Calculations	VIII-45
A1.1.1	Computer Program BOIL	VIII-45
A1.1.2	BOIL Calculations	VIII-45
A1.1.2.1	Heat Transfer	VIII-45
A1.1.2.2	Water Boiloff	VIII-45
A1.1.2.3	Core Meltdown	VIII-46
A1.2	Results of BOIL Calculations	VIII-55
A1.2.1	PWR Results	VIII-55
A1.2.2	BWR Results	VIII-57
A1.2.3	Bottom-Flooding	VIII-58
A2.	CONTAINMENT HEAT TRANSFER	VIII-58
A2.1	PWR Analyses	VIII-58
A2.1.1	Energy Sources	VIII-58
A2.1.2	Containment Heat Sinks	VIII-58
A2.1.3	Containment Atmosphere	VIII-59
A2.1.4	Containment Pressure-Time Evaluation	VIII-59
A2.1.5	Containment Leakage	VIII-59
A2.2	BWR Analyses	VIII-60
A2.2.1	Energy Sources	VIII-60
A2.2.2	Containment Heat Sinks	VIII-60
A2.2.3	Containment Response	VIII-61
A3.	PRESSURE VESSEL MELTTHROUGH	VIII-61
A3.1	PWR Analyses	VIII-61
A3.1.1	Realistic Failure Time	VIII-62
A3.1.2	Maximum Failure Time	VIII-63
A3.1.3	Minimum Failure Time	VIII-63
A3.2	BWR Analyses	VIII-63
A4.	CONTAINMENT VESSEL MELTTHROUGH	VIII-63
A4.1	PWR Analyses	VIII-63
A4.2	BWR Analyses	VIII-65
REFERENCES		VIII-67

List of Figures

Figure		Page No.
VIII A-1	Characteristics Curves For Release of Volatile Fission Products From Overheated Fuel.....	VIII-68
VIII A-2	Mixture Void Fraction and the Locations of the Mixture Level and Molten Fuel Regions in a PWR for Meltdown Models A and B as a Function of Time for Boiloff Starting at 1.0 Hr.....	VIII-68
VIII A-3	Steam Generation Rate During a Boiloff Accident Starting at 1.0 Hr in a PWR as a Function of Time for Meltdown Models A and B.....	VIII-69
VIII A-4	Fuel Rod Temperatures in the Central (Maximum Power) Core Zone of a PWR as a Function of Time for Boiloff Starting at 1.0 Hr for Meltdown Model A.....	VIII-69
VIII A-5	Effect of Meltdown Model on the Percent of a PWR Core Melted as Function of Time for Boiloff Starting at 1.0 Hr.....	VIII-70
VIII A-6	Effect of Meltdown Model on the Percent of the Cladding Reacted in a PWR Core as a Function of Time for a Boiloff Accident Starting at 1.0 Hr.....	VIII-70
VIII A-7	Effect of the Time When a Boiloff Accident Starts (Decay Time) on the Core Meltdown Sequences in a PWR for Meltdown Model A.....	VIII-71
VIII A-8	Percent of a BWR Core Melted as a Function of Time for (1) a Dry Core Heatup Starting with End-of-Blowdown Conditions at 25 Sec and (2) a Boiloff Accident Starting at 100 Hours with the Core Flooded to the 8 Foot Level.....	VIII-71

Appendix A

Thermal Analyses

A1. CALCULATIONS

The primary purpose of the calculations described in this appendix is to provide, as quantitatively as possible, a description of the physical conditions existing during the course of the accident and the time of occurrence of steam explosions, hydrogen explosions, containment meltthrough, the size of the fission-product source, and the size of the heat load on the containment. That is, the calculations in this appendix define the time spectrum during which conditions exist which may eventually lead to breach of the containment. For example, the core heatup calculations define the amounts of molten UO_2 and water available for a steam explosion as a function of time. These calculations also predict the quantity of Zircaloy cladding that has reacted with steam to produce hydrogen, which may possibly explode or burn to breach the containment.

A1.1 CORE HEATUP CALCULATIONS

This section describes core heatup calculations performed for several degraded core cooling situations. The calculations were performed for two specific reactors, representative of a large PWR and BWR, respectively. The models in the computer program and many of the results have general applicability to the accidents studied, although some of the results apply only to the specific designs considered. The computer program BOIL written for this evaluation is described and the results of the calculations are presented. Some of the calculated results appear elsewhere throughout the report, and are not always repeated or given further documentation in this appendix.

The situation of principal concern in this discussion is the "boiloff" accident. In the "boiloff" accident, as the term is used here, circulation of water through the core is assumed to stop. Because the core continues to generate decay heat and no further water is being added, the water in the core begins to boil off, and the water level decreases. The uncovered portions of the core heat up and eventually melt. The computer program BOIL was written to describe this sequence. The program may also be used in some cases to calculate: (1) core heatup for (very) low bottom-flooding rates which lead to core melting and (2) dry heatup of the core in the complete absence of water.

In the work that follows, the computer program BOIL is discussed, and the results of calculations with BOIL are presented.

A1.1.1 COMPUTER PROGRAM BOIL

The computer program BOIL was written to calculate core heatup in an accident where the fission-product-decay heat boils the water out of the pressure vessel and uncovers the core. The approach used is to divide the core into small volumes or nodes and (1) calculate the heat produced in each node and perform heat balances between the fuel and coolant nodes, (2) calculate the water-steam mixture level in the core and the steam-boiloff rate, and (3) perform a meltdown calculation when the temperature of a node exceeds the melting point of UO_2. The models in each of the three parts of the program are discussed below.

A1.1.2 BOIL CALCULATIONS

A1.1.2.1 Heat Transfer.

This section of BOIL (1) calculates the fission-product-decay heat as a function of time, (2) accounts for the reduction in the heat source due to fission-product volatilization, (3) calculates the heat produced by the zirconium-steam reaction in the cladding, (4) calculates convection heat transfer between the fuel rods and the steam or water coolant, (5) calculates radiation heat-transfer losses from the ends of the core, and (6) performs heat balances on the fuel and coolant.

A1.1.2.1.1 Core Nodalization. In the BOIL calculations, the core is divided into a maximum of 10 radial zones composed of fuel rods and their associated flow channels. The radial zones are sectioned into a maximum of 50 axial nodes. Most of the calculations have been performed for 5 radial and 24 axial nodes. The sizes of the radial zones are arbitrary, and are normally chosen in a manner which conveniently describes the radial power distribution of the core. In the heat-transfer calculations

the only coupling between radial zones before core melting occurs is by a uniform steam flow rate (lb/hr ft^2) at the inlet to the steam-covered region. At the channel exit, the steam concentration depends on the amount of metal-water reaction in that particular channel. There is normally no coupling of radial zones by conduction, convection, or radiation heat transfer. After core melting occurs, radial zones may (program option) be coupled by steam cross flow and mixing within the pool of molten fuel in the core. The axial fuel-rod nodes within a given radial zone are normally coupled in the heat-transfer calculations only through their connection to a common steam channel. During core meltdown, the axial nodes are assumed to be coupled within the molten region by convective mixing. The axial nodes are not coupled by conduction heat transfer. The axial nodes in the flow channel are connected by the axial flow of steam.

A1.1.2.1.2 Decay Heat. The fission product decay heat is calculated from the Proposed ANS Standard for infinite irradiation time:

$$P/P_o = 0.0766\ t^{-0.181},\quad 10 < t < 150 \text{ sec}, \qquad \text{(VIII A-1a)}$$

$$P/P_o = 0.130\ t^{-0.283},\quad 150 < t < 4 \times 10^6 \text{ sec}, \qquad \text{(VIII A-1b)}$$

where P/P_o is the fraction of operating power and t is the decay time in seconds (Ref. 1). For most of the time period of interest, the Proposed ANS Standard is estimated to give decay heats between 10 percent too low and 20 percent too high. The decay heat of a given core node as a function of time is obtained using Equation (VII A-1) with axial and radial power-peaking factors applied to the average core power density.

A1.1.2.1.3 Fission-Product Release. For fuel-rod temperatures below 1500 F, the heat-transfer calculations assume that no fission products are lost. For rod temperatures between 1500 F and 2000 F, the fission-product loss is primarily composed of a puff release (RP), which depends only on the operating power history of the fuel node. Above 2000 F, the total release depends on both the rod power and the current temperature of the fuel node. The fission-product-release fraction programmed in BOIL for temperatures between 1500 F and 2000 F is

$$RP = 0.13(F - 1.35), \qquad \text{(VIII A-2)}$$

where F is the local power-peaking factor. For local peaking factors less than 1.35, RP is taken to be zero. For temperatures above 2000 F the release fraction is

$$RT = 0.471\ (1 - F/3.65)(TR/3000 - 0.67), \qquad \text{(VIII A-3)}$$

where TR is the temperature (F) of the fuel-rod node. In the BOIL calculations, the fission-product-decay heat of a fuel node is reduced by the fraction RP or RT to account for loss of fission products. The maximum fractional reduction permitted in the program is 0.30. It is assumed the fission products are lost from the core and are not redeposited elsewhere in the core.

The above expressions for fission product release were derived from the curves shown in Fig. VIII A-1. These curves were constructed on the basis of calculations of fission-gas release presented in BMI-1885 (Ref. 2). The calculations were performed for the case of a loss-of-coolant accident with no emergency core cooling. The preaccident diffusion release of fission gas to the fuel rod gas gap was found to vary with the power peaking factor as shown by the initial (1500 F) values of the curves in Fig. VIII A-1. The preaccident gap contents were assumed to be available for release immediately upon rod rupture. The rod rupture temperature was taken as 1500 F, though it recognized that fuel rod failures could occur over a range of temperatures; the release values would not be sensitive to this parameter at the high core heatup rates associated with meltdown accidents. The release curves at temperatures above 1500 F given in Fig. VIII A-1 were developed from the postaccident fission gas release values in Table 1 of BMI-1885 and the core heatup rate data from Fig. 1 of BMI-1885. To accomplish this, an approximate relationship between fission gas release and fuel temperature was constructed. This approximate relationship is given by the bottom curve in Fig. VIII A-1, and it represents the thermally activated release of fission gas remaining in the UO_2 itself. The appropriate fractional releases from the UO_2 are added to the preaccident gap releases to generate the total release

curves for the various power peaking factors shown in Fig. VIII A-1. All the curves were extrapolated to 100 percent release at a temperature of 5000 F.

The release versus temperature curves, while specifically derived using noble gas diffusion coefficient values, were assumed to also apply to the other highly volatile fission products, namely iodine, cesium, and tellurium. While there is some experimental data that generally supports this assumption, it is clearly an approximation. The four groups of fission products classified here as volatile contribute about 30 percent of the total fission product decay energy at shutdown times of about an hour.

A1.1.2.1.4 Cladding - Water Reaction. The zirconium-steam reaction rate in the Zircaloy cladding is calculated from the minimum predicted by (1) Baker's rate law or (2) a gas phase diffusion model (Ref. 3). The model is the same as that used in NURLOC (Ref. 3, Eqs. 75-82), and the equations are not repeated here. The reaction is stopped at a node if all of the steam in a flow channel has been consumed or if all of the cladding has been consumed. The cladding-steam reaction is also stopped after a fuel-rod node is completely melted, on the assumption that steam will not penetrate a molten node. When core melting occurs, the user of the program may select various options which scope the effects of channel blockage on the metal-water reaction in the unmelted core zones. The program user may (1) let the steam flow continue through a channel as if no blockage occurs, (2) assume the channel plugs and stop the metal-water reaction in a given channel above the lowest melted node, (3) let the steam flow bypass melted (plugged) channels and, therefore, increase the steam flow rate in unplugged channels. Options (2) and (3) can significantly reduce the fraction of the cladding in the core which reacts with steam. In general, it is believed that Option (1) overestimates the amount of cladding reacted, particularly in BWR's with shrouded fuel elements. Options (2) and (3) probably underestimate the metal-water reaction in both open-lattice and shrouded elements.

A1.1.2.1.5 Thermal Radiation. Radiation heat transfer from the uncovered part of the core to (1) the internal structure above the core and (2) the water inside or below the core is evaluated in the BOIL calculations. The heat transferred by radiation from a node with emitting area A_R is

$$Q_{rad} = 0.173\ F\ A_R\ [(T_R/100)^4 - (T_o/100)^4], \qquad \text{(VIII A-4)}$$

where

Q_{rad} = radiation heat transfer, Btu/hr

A_R = radiating area, ft^2

T_R = temperature of radiating node, R

T_o = temperature of receiver node, R

F = radiation interchange factor.

The interchange factor is calculated assuming the radiating and receiving surfaces are parallel planes; thus,

$$F = \left(\frac{1}{\varepsilon_R} + \frac{1}{\varepsilon_o} - 1\right)^{-1}, \qquad \text{(VIII A-5)}$$

where

ε_R = emissivity of radiating node
ε_o = emissivity of receiver node.

The area, A_R, is computed in a plane perpendicular to the axis of the core. The total heat radiated is calculated by summing the Q_{rad} over the total cross section of the core. For radiation heat transfer from the core to the water, the T_R are evaluated in the plane of the first uncovered node above the water. For heat transfer to the internal structure above the core, the T_R are evaluated for nodes in a plane at the top of the core. It is assumed in the calculations that the maximum amount of heat that can be radiated from a (solid or unmelted) node is the decay heat of the node. This restriction is placed on the radiation heat transfer because the mechanisms for transfer of heat (by conduction and radiation) in the axial direction are normally limited. Since the core was divided into 24 axial nodes, the maximum amount of heat lost from the (unmelted) core by radiation is 2/24 of the decay heat. When the top of the core is melted, the radiation heat loss from the top of the core is limited (in meltdown Model B) to the total decay heat in the molten pool. The mechanism for moving this heat to the surface of the molten pool is internal natural convection.

The heat fluxes calculated from Equation (VIII A-4) are used to calculate the temperature of the structure above the core. In these calculations, the structure is divided into pieces of known mass and heat capacity. If one of the pieces melts, it is assumed to fall away and expose another piece to the radiation heat flux.

The radiation heat flux to the water contributes to the boiloff of the water and is included in the water mass balance equations. The boiloff rate from radiation heat transfer is generally small in comparison with the other mechanisms, unless the core is nearly uncovered.

A1.1.2.1.6 Convection Heat Transfer. The core is divided into two convection heat-transfer regions, a steam-covered region and a region covered with a water-steam mixture. In the region above the mixture, the rod-steam heat-transfer coefficient, h, is calculated from a simplified Dittus-Boelter correlation (Ref. 4),

$$h = 0.0144\ C_p G^{0.8}/D^{0.2}, \quad \text{(VIII A-6)}$$

where

C_p = specific heat of steam, Btu/lb F

G = steam flow rate, lb/hr ft^2

D = equivalent diameter of channel, ft.

Steam properties are used in the calculations, and the properties are not changed to account for changes in the steam-hydrogen mixture ratio due to metal-water reaction. For the steam flow rates obtained in the boiloff calculations, the convection heat loss from a fuel-rod node is generally a small fraction of the decay heat. That is, the heatup rates are nearly adiabatic at temperatures below 2200 F where the cladding-steam reaction is small, and the gas temperatures closely follow the rod temperatures. In view of its small effect, a more detailed treatment of convective heat transfer to steam and/or hydrogen does not appear warranted.

In the water- or mixture-covered regions of the core, the rod temperatures are assumed to be in a steady-state equilibrium with boiling water. The temperature of a fuel-rod node in the mixture-covered region is

$$T_R = T_W + Q_{D,R}/Ah_B, \quad \text{(VIII A-7)}$$

where

T_W = saturated water temperature = 300 F

$Q_{D,R}$ = decay heat of node, Btu/hr

A = node heat-transfer area, ft^2

h_B = boiling heat-transfer coefficient

= 350 Btu/hr ft^2 F.

According to Equation (VIII A-7), all of the decay heat produced in a water-covered fuel-rod node goes into boiling water. The fuel-rod temperatures given by Equation (VIII A-7) are generally less than 10 - 20 F greater than the water temperature. Thus a more sophisticated treatment, taking into account time-dependent changes in saturation temperature, heat transfer coefficient, etc., is not necessary. At the end of a time-step in the BOIL calculations it is possible that a fuel-node temperature in the mixture-covered region may be greater than that given by Equation (VIII A-7). This occurs in two situations: (1) when the mixture level increases during a time-step due to bottom flooding and covers a fuel node which was previously dry, and (2) when molten fuel drops into the mixture-covered region. When this occurs, the fuel node is assumed to be quenched (in one time-step) to the node temperature given by Equation (VIII A-7). The assumption of quenching in one time-step is justified by transient-conduction analysis. These calculations indicate that for a (typical) 1-minute time step, a fuel rod will lose about 90 percent of its stored heat.

A1.1.2.1.7 Node Heat Balances. Using the nodalization treatment, heat sources, and heat-loss mechanisms described above, BOIL performs heat balances and calculates the fuel-rod and flow-channel node temperatures. In the BOIL nodalization treatment, a fuel rod has only one radial node. Thus, the conduction heat-transfer problem is not solved, and the heat balances involve only changes in stored heat and the heat sources and losses. The use of only one radial node for a rod is a satisfactory treatment for the low, nearly adiabatic heatup rates (few hundred F/minute) encountered in the boiloff situations; at decay power levels the temperature dif-

ference between the fuel center and surface would be only the order of 100 F.

In the mixture-covered region, the fuel-to-water heat balance is

$$Q_{D,R} = h_B A\ (T_R - T_W) = \dot{m}_R h_{fg},$$

(VIII A-8)

where

$\dot{m}_R$ = boiloff rate per node, lb/min
h_{fg} = heat of vaporization, Btu/lb.

and the other notation is the same as in Equation (VIII A-7). Note that the rod temperature T_R changes very slowly (with the decay heat) in the water-covered region. The total contribution of the decay heat to the boiloff rate is obtained by summing the $\dot{m}_R$ for each mixture-covered fuel-rod node. If at the end of a time step the temperature of a fuel-rod node in the mixture-covered region is greater than that obtained from Equation (VIII A-7) (because the node was not water-covered during the previous time step), the node is quenched according to the relation,

$$Q_{melt} = \rho C V_R\ (T_R - T_R') = \dot{m}_{R,Q} \Delta t\ h_{fg},$$

(VIII A-9)

where

ρ = density of fuel rod, lb/ft^3

C = heat capacity of rod, Btu/lb F

V_R = volume or node, ft^3

Δt = time step in BOIL calculation, hr

$\dot{m}_{R,Q}$ = boiloff rate from quenching, lb/hr

T_R = Equation (VIII A-7)

T_R' = node temperature before quenching, F.

For a fuel-rod node in the steam-covered region, the node temperature increases because the steam flow is insufficient to carry off the decay heat. The generalized fuel-rod-node heat balance is

$$\rho C V_R \frac{\partial T_R}{\partial t} + F_{melt}\ \lambda \rho V_R = Q_{D,R} + Q_{MW} + Q_{melt} - Q_{rad} - hA\ (T_R - T_G),$$

(VIII A-10)

where

Q_{MW} = heat from metal-water reaction, Btu/hr

Q_{melt} = heat added to node from slumping during meltdown, Btu/hr

Q_{rad} = radiation heat-transfer losses, Btu/hr

F_{melt} = fraction of node melted

λ = heat of fusion of node, Btu/lb

h = Equation (VIII A-6)

T_G = gas or steam node temperature, F.

The increase in the steam temperature along the length of the channel is given by

$$\dot{m}\ C_p \frac{\partial T_G}{\partial Z} = h\ p(T_R - T_G), \quad \text{(VIII A-11)}$$

where

$\dot{m}$ = total steam flow rate, lb/hr

Z = distance measured up the channel, ft

p = fuel rod circumference, ft

and the other notation was given previously. In Equation (VIII A-10), Q_{melt} is calculated assuming the molten pool mixes and has a uniform temperature. During node melting, the node temperature is constant. (That is, $\partial T_R/\partial t = 0$ when $0 < F_{melt} < 1$). Q_{rad} is zero except for the node at the top of the core and immediately above the mixture level. Q_{MW} is always zero when $F_{melt} = 1$, and may also be zero (optional) if the node is above a molten region.

Equations (VIII A-10) and (VIII A-11) are programmed in finite-difference form for solution in BOIL. The finite-difference forms of the equations are

$$T_R\ (t + \Delta t) = T_R(t) + q\Delta t/\rho CV_R$$

(VIII A-10a)

$$T_G(z + \Delta z) = T_R(t + \Delta t) - (T_R(t + \Delta t) - T_G(z))e^{-\left(\frac{hp\Delta z}{\dot{m}C_p}\right)},$$

(VIII A-11a)

where q is the sum of all the heat losses and gains in Equation (VIII A-10). In most of the calculations, a time-step size of Δt = 1.0 minute and a node length of Δz = 6.0 inches was used. The calculation is numerically stable for all mesh sizes; however, accuracy appears to suffer if the temperature change is much greater than a few hundred degrees (F) per time step. Experience indicates that the primary effect of too large a time step is to overestimate the metal-water reaction rate and, consequently, the core heatup rate.

A1.1.2.1.8 Dry Heatup. BOIL permits any initial water level in the pressure vessel, including zero. Consequently, BOIL may also be used to calculate dry heatup of the core in the absence of any water.

An item of interest to the determination of fission-product release during dry heatup is the efflux of steam from the pressure vessel due to simple gas expansion. Since there is no steam boiloff to carry out fission products, gas expansion provides the principal driving force for fission-product transport. BOIL includes a simple gas-expansion model for calculating efflux during dry heatup. The model assumes the core is in volume V_1, and the remaining part of the pressure vessel is represented by volume V_2. The gas in volume V_1 follows the core temperature, expands, and flows into volume V_2. Volume V_2 contains a leak which vents to the containment. Heat transfer is permitted in volume V_2. The two volumes are assumed to be at approximately the same pressure with negligible flow resistance through the leak paths. The steam flow from V_1 into V_2 is

$$\dot{m} = -V_1 \frac{d\rho_1}{dt}, \qquad \text{(VIII A-12)}$$

and the flow out the break in V_2 is

$$\dot{m}_2 = \dot{m}_1 - V_2 \frac{d\rho_2}{dt}. \qquad \text{(VIII A-13)}$$

A heat balance on volume V_2 gives

$$\rho_2 V_2 C_p \frac{dT_2}{dt} = \dot{m}_1 C_p T_1 - \dot{m}_2 C_p T_2 - h_{PV}A_{PV}(T_2 - T_{PV}),$$

(VIII A-14)

where

ρ = steam density, lb/ft^3

T = gas temperature, F

h_{PV} = heat-transfer coefficient from V_2 to structures in V_2, Btu/hr ft^2 F

A_{PV} = heat-transfer area of structures in V_2, ft^2

T_{PV} = temperature of A_{PV}, F.

These equations, along with the perfect-gas law (P_o = constant = ρRT), are programmed in BOIL to obtain the steam flow ($\dot{m}_2$) out the break in V_2. The parameters A_{PV} and T_{PV} are input constants, and $h_{PV} = 0.2\ \Delta T^{1/3}$ is used to estimate the convection heat-transfer losses (Ref. 3) from V_2.

A1.1.2.2 Water Boiloff.

In this section of BOIL, the boiloff of the water in the pressure vessel is calculated. The components of the boiloff calculation discussed below include calculations of (1) the heat input to the mixture region, (2) the steam-generation rate, (3) the water mass, (4) the mixture level, and (5) limitations on the use of the model to calculate bottom flooding.

A1.1.2.2.1 Heat Input to Water. The heat input to the water includes (1) all of the decay heat in the fuel-rod nodes covered by the swollen mixture of water and steam, (2) radiation heat transfer from the first steam-covered node immediately above the mixture level, and (3) the stored heat from the quenching of fuel nodes which were dry during the previous time step. These components of

the heat input to the water are given in Equations (VIII A-8), (VIII A-5), and (VIII A-9). When molten fuel drops into the water, the decay heat and the stored heat are included in the heat input to the water, but metal-water reaction is neglected. It is also implicitly assumed that steam explosions do not occur, and the only effect of molten fuel is to boil water.

A1.1.2.2.2 Steam Flow Rate. It is assumed that the water in the pressure vessel is at the saturation temperature. The steam generation rate is

$$\dot{m} = Q_{total}/h_{fg}, \qquad \text{(VIII A-15)}$$

where Q_{total} is the sum of all the heat inputs to the water as discussed above. All of this steam is assumed to flow into the steam-covered part of the core; that is, bypass flow is neglected. When core melting occurs, steam flow may (optional) be diverted around channels assumed to be plugged.

A1.1.2.2.3 Water Mass. The water mass is calculated by adding the changes in the water mass to the value in the previous time step. The mass balance is

$$M(t + \Delta t) = M(t) - \dot{m}\Delta t + \rho_L A_C V_F \Delta t, \qquad \text{(VIII A-16)}$$

where

- M = water mass, lb
- ρ_L = density of saturated water, lb/ft^3
- A_C = flow area of core, ft^2
- V_F = "bottom flooding" rate, ft/hr
- $\dot{m}$ = Equation (VIII A-15).

A1.1.2.2.4 Mixture Level. The water in the pressure vessel is actually a mixture of water and steam. The volume of the mixture is larger than the equivalent mass of water; and, likewise, the swollen mixture level is greater than that of water. It is assumed in the BOIL calculations that core nodes covered by the mixture are cooled. Consequently, a given mass of water will cool more of the core if level swell is considered. However, level swell also increases the steam-generation rate and decreases the water mass more quickly. The net effect of level swell is to retard or delay core heatup by several minutes. A simple level-swell model which assumes a linear variation of the void fraction with height inside the core is incorporated in BOIL. For a mixture level, Y, the water mass is

$$M = \int_o^Y (1 - \alpha)\rho_L A_{tot} dZ$$

$$= A_{tot} Y \rho_L \left[1 - \left(\frac{\alpha_T}{2}\right)\right], \qquad \text{(VIII A-17)}$$

where

- A_{tot} = total cross-sectional area in pressure vessel occupied by mixture, ft^2
- Y = mixture level above bottom of core, ft
- α_T = void fraction at the top of the mixture, and
- α = $\alpha_T Z/Y$ and is used to evaluate the integral.

The void fraction at the top of the mixture is related to the boiloff rate according to the relation

$$Q_{DK} = \dot{m}\, h_{fg} = \rho_s U_T \alpha_T A_{tot} h_{fg}, \qquad \text{(VIII A-18)}$$

where

- Q_{DK} = total decay heat in the mixture-covered fuel nodes, Btu/hr
- ρ_s = density of saturated steam, lb/ft^3
- U_T = steam separation velocity at the top of the mixture, ft/hr.

The possible contributions of heat inputs from radiation heat transfer and the quenching of molten fuel are neglected in the evaluation of the mixture void fraction. In the level-swell calculations, Equation (VIII A-18) is first used to calculate α_T, and the Equation (VIII A-17) is used to calculate a new value of the mixture level Y. The void fraction in the water above and below

the core is assumed to be zero. If Y is greater than the core height, the total mixture height is

$$Y = H_o(M/\rho_L A_{tot} H_o + \alpha_T/2),$$

(VIII A-19)

where H_o = active fuel length, ft. If Y is at a level under the core, α_T = 0 in Equation (VIII A-19); and negative values of Y are calculated in BOIL. The level-swell model in BOIL is similar in concept to those used in RELAP (Ref. 5) and by General Electric (Ref. 6). However, RELAP assumes a linear variation of the mixture density, G. E. assumes a linear variation of the mixture quality, and BOIL assumes a linear variation of the void-fraction. RELAP and BOIL require the program user to specify (input constant) values of the steam separation velocity U_T. G. E. calculates values of U_T based on the data of Wilson (Ref. 7). Wilson's experiments did not mock up the axial variation of the steam void fraction. G. E. assumes that Wilson's constant or uniform void fraction is equivalent to the average void fraction in the volume. RELAP required use of a constant separation velc ity of U_T = 3.0 ft/sec to reproduce experimental blowdown in a one-volume vessel (Ref. 4). G. E. obtained experimental confirmation of its level-swell model in a 12-in.-diameter x 14-ft-high pressure vessel using (Wilson's) values of U_T between 1.0 and about 6 ft/sec. (G. E. assumes in the calculations the minimum value of U_T is 1.0 ft/sec.) Wilson's correlation at a saturation temperature of 300 F gives (assuming $\alpha_{ave} = 1/2\ \alpha_T$)

$$U_T = 3.47 \left(\frac{D}{0.67}\right)^{0.244} (\alpha_T)^{1.283} \text{ ft/sec},$$

(VIII A-20)

where D is the hydraulic diameter of the region in inches (Ref. 6). It is not clear, however, how D should be interpreted for a core composed of tube bundles. Wallis (Ref. 8, p. 287) indicates that D should be the bundle-housing diameter rather than the flow-channel equivalent diameter. In a typical BWR core the maximum value of U_T from Equation (VIII A-20) is 3.47 ft/sec if D is the equivalent diameter, and the maximum U_T is about 5.9 ft/sec if D is the housing diameter. In the BOIL calculations a constant value of U_T = 4.5 ft/sec was used. Use of this separation velocity in Equation (VIII A-18) results in a maximum value of the void fraction (all core nodes covered) of α_T = 0.75 for a decay time of 1.0 hr in a typical core. For decay time less than about 25 min, Equation (VIII A-17) predicts maximum values of α_T greater than 1.0; and BOIL reduces α_T to 1.0 in that case.

The BOIL calculations do not include an "entrainment" model. "Entrainment" is caused by steam being produced so rapidly in a channel that it "entrains" or suspends water droplets due to drag forces, and carries the water droplets up through the channel. This phenomenon is observed, for example; in the FLECHT bottom-flooding experiments. It is not believed, however, that the entrainment phenomenon occurs in the boiloff accident studied here. Entrainment is believed to require (1) large forced coolant-injection rates and (2) initially hot (~1600 F) rods. Neither factor is present in the boiloff calculations.

A1.1.2.2.5 Bottom Flooding. BOIL may be used, in some limited cases, for the study of core heatup with degraded "bottom flooding". It is assumed in the BOIL calculations that coolant is added at a very low rate to the water inventory at the bottom of the pressure vessel. BOIL calculates the response of the core to this bottom-flooding rate using exactly the same model assumptions (with regard to level swell, fuel-node quenching, steam generation, etc.) as are used in the other boiloff calculations. The limitations on the use of BOIL to calculate bottom flooding include (1) saturated water is injected, (2) the water is added to the inventory at the bottom of the pressure vessel, (3) the flooding rate should not result in covering more than about one rod node per minute. The latter restriction is primarily a consequence of the assumption in BOIL that a previously dry fuel-rod node can be quenched in one time step. Since the time constant ($\rho c r^2/k$) of a fuel rod is approximately 1 minute, the quenching assumption is questionable if more than one previously dry node per minute is covered. For the nodes considered in the BOIL calculations, a practical upper limit on the bottom-flooding rate is about 0.2 in./sec. It is also expected that for large flooding rates, liquid entrainment will become significant, particularly when the fuel rods are at initially high temperatures. A flooding rate of 0.2 in./sec of saturated water is just marginally able to remove the total core-decay heat at the end of blowdown assuming complete coolant vaporization. Flooding rates of this order will not prevent core heatup if

the fuel rods are initially at elevated temperatures and liquid entrainment is encountered.

A1.1.2.3 Core Meltdown.

To scope the effects of core meltdown on core heatup, three core meltdown models were developed for incorporation in BOIL. The models are not phenomenological in the sense that slumping is not based on calculations of stress levels, creep rates, or flow rates of molten materials. Fuel slumping is triggered when a fuel node reaches the melting point of UO_2 and absorbs additional energy equal to the latent heat of fusion. Two of the meltdown models (Models A and B) assume the molten fuel is retained in the core as a continuous region, and one model (Model C) assumes the molten fuel to fall out of the core as it melts. Calculations indicate that the different model assumptions can significantly affect the course of core heatup, primarily because of the influence of the core meltdown on the boiloff rate and the cladding-water reaction. This section of Appendix A, thus, contains a discussion of the core meltdown and a description of the meltdown models developed for BOIL.

A1.1.2.3.1 Core-Meltdown Behavior. The behavior of a core during a meltdown accident is uncertain. No cores have been melted. Experiments involving more than a cupful of molten UO_2 are still in the planning stages. Some properties of molten UO_2 are known: melting point, boiling point, and heat of fusion. However, little is known about the viscosity, internal thermal convection, surface tension, or the metallurgical effects of various diluents. Nevertheless, considerable insight has been developed by people working in the field about the possible course of core meltdown.

Because the core power tends to peak (about 2.5 times average) at the center of the core and because the cladding-steam reaction increases the heatup rate of the hotter regions, core melting starts at the center of the core. Because of the power peaking and the presence of water in the bottom of the core, the core temperatures a foot away from the melted region are frequently calculated to be more than 1000 F below the melting point of the fuel. In these relatively cool regions, the UO_2 would remain solid although the cladding could be melted. Because the fuel rods in the core are relatively closely packed, there is not room for solid fuel pellets to fall out of the core nor for gross distortion of the solid portions of the core. In this situation, it is believed a region of solid rubble would form under the molten fuel, and the molten fuel would tend to be retained in the core. However, since the rubble continues to generate heat, it will eventually melt, and the increasingly larger molten region will move downward. If the pool moves downward fast enough, it will intercept the water that is boiling out of the bottom of the core. When this happens either (1) steam explosions will occur or (2) the boiloff rate and, therefore, the cladding-steam reaction rate will increase. When the molten region grows to include 50 to 80 percent of the core, it becomes questionable whether or not the molten region can be retained inside the core. At this time, the molten pool will be 3 to 4 ft thick, and will presumably be held up by a layer of rubble. When large fractions of the core are molten, the core-support plates and shrouds are also exposed to high thermal loadings. Failure of these major structural members would release the molten pool and either (1) the rest of the water boils out of the pressure vessel or (2) a steam explosion results.

It is assumed in the development of meltdown models A and B that a large pool of molten UO_2 can be retained in the core. It should be noted that a consequence of this assumption is that damaging steam explosions become more probable. For a holdup mechanism to exist, at least two prerequisites are necessary: (1) there must be a mechanism for removing the decay heat from the molten pool of fuel and (2) there must be a solid crust or rubble layer at the bottom of the pool to retain the liquid UO_2.

The possible existence of a crust which supports or tends to restrain the motion of the molten pool of UO_2 has been investigated analytically. Attempts were made to show (by calculation) that (1) a hot liquid film of UO_2 flowing down a cold, solid, fuel rod or (2) a droplet of molten UO_2 falling in air through a cold array of rods would quickly resolidify. However, the calculations were inconclusive because of the difficulty of justifying the model assumptions and finding experimental data on the viscosity and surface tension of liquid UO_2. Neglecting surface-tension effects, these calculations indicate that small droplets and films ($\sim$50 mil) will resolidify. However, films and droplets as large as the rod-to-rod spacing may not resolidify before dropping out of the core. Another calculation including the effects of surface tension indicates

that droplets may have to weigh more than 5 grams before they will start to fall. It is concluded that the existence of a holdup mechanism for molten UO_2 is largely based on experience with other materials and, to some extent, intuition; based on present knowledge, the calculational evidence is inconclusive.

The work of Hesson indicates that internal natural convection will be adequate in most cases to remove the decay heat from the interior of a pool of molten UO_2 retained within the core (Ref. 9). Hesson's experiments were performed using internally heated saltwater solutions, and the data were correlated in terms of the usual dimensionless heat-transfer parameters. With thermophysical property data appropriate to molten UO_2, the correlations are used to estimate the maximum heat fluxes obtainable from the surfaces of a molten pool of UO_2 without boiling off the UO_2. In these correlations boiling inside the pool is assumed, but there is no net loss of UO_2 from the pool by vaporization. The boiling inside the pool drives the natural circulation, and the vapor is condensed inside the pool. Values obtained for the maximum downward (q_D) and horizontal (q_H) heat fluxes are

$$q_D = 133{,}000 \text{ Btu/hr ft}^2, \qquad \text{(VIII A-21a)}$$

and

$$q_H = 382{,}000 \text{ Btu/hr ft}^2. \qquad \text{(VIII A-21b)}$$

Hesson does not give a value for the upward heat flux. Since the natural convection heat transfer coefficients for horizontal and vertical plates are approximately equal (Ref. 4), it is assumed that the upward heat flux (q_T) equals the horizontal flux. Assuming the pool is a cylinder and using these heat fluxes, the total heat lost from the pool by convection can be calculated and compared with the decay heat. The results of the calculations indicate that natural convection will transport the decay heat from a completely melted core to the outside surface if the meltdown occurs after about 6 minutes in the BWR and after 17 minutes in the PWR. Since complete core meltdown is not likely to occur this early in the accident, it is concluded that a pool of molten UO_2 will not boil away during the core-meltdown process.

Although UO_2 boiloff is not expected to be a significant heat loss mechanism, some UO_2 vaporization may occur. A dense smoke, which is apparently UO_2 vapor, has been observed experimentally above molten samples of UO_2. This smoke could affect some core heat-transfer processes by inhibiting thermal-radiation heat transfer. In the BOIL calculations the heatup of the support structures above the core is controlled by radiation heat transfer. Thus, the existence of the UO_2 smoke could reduce the heatup rate of these structures as determined by radiation; this would be compensated by the heatup due to the condensation of the UO_2 smoke on the same surfaces. The UO_2 smoke would not significantly affect the core heatup rate, however.

A1.1.2.3.2 Meltdown Model A. In meltdown Model A, it is assumed that the heat in the molten pool is transferred downward. There is no convection of heat to the top and sides of the pool. This model maximizes the downward movement of the molten pool. According to the model assumptions in BOIL, if the molten region moved downward any faster, it would resolidify. Hesson's work indicates that the convection heat fluxes from a molten pool are in the ratio $q_D:q_H:q_T = 1:2.9:2.9$. Thus, the downward heat flux in Model A exceeds Hesson's pure convection value. For Model A to be physically consistent, it is necessary for the molten region to actually penetrate the solid regions below the molten pool. Thus, Model A is physically consistent with a meltdown situation in which the molten region tends to cover and mix (downward) with the solid region at such a rate that the homogenized molten region remains just at the melting temperature. It is assumed that no solid core material falls into the molten pool from above. Such an occurrence would tend to keep the temperature of the solid-liquid mixture at or below the melting point.

A1.1.2.3.3 Meltdown Model B. In meltdown Model B, it is assumed that the heat in the molten pool is transferred upward, and none is transferred down. Within the molten region, heat may be transferred radially if the average temperature of a radial power region exceeds the melting temperature. The heat transferred upward is used in the BOIL calculations to melt solid core material, which is assumed to fall into the molten pool. The amount of solid material falling into the molten pool is sufficient to keep the homogenized temperature of the molten pool at the melt-

ing point of UO_2. When the top nodes in the core are melted, it is assumed this heat may be radiated to the support structures above the core. Model B is physically more consistent than Model A with the pure convection heat fluxes given by Hesson's work, where the downward heat flux was comparatively small. Model A, on the other hand, considers the downward motion of the molten fuel. Whether Model A or Model B is a better description of an actual core meltdown cannot be stated definitely. The two models yield very similar results for core-meltdown fractions of up to about 50 percent. However, for larger meltdown fractions, Model A results in faster core heatup. In Model A, the more rapid downward progression of the molten region results in increased metal-water reaction when the molten region intercepts the water level. If it is assumed that at any time during the meltdown, as predicted by Model B, a small part of the molten core ($\sim$1 percent per time step) falls into the water, the results in the two models are similar.

A1.1.2.3.4 Meltdown Model C. In Model C it is assumed that when a fuel node melts, it immediately falls to the bottom of the pressure vessel. The fuel node is quenched in one time step, and the decay heat of the node is added to the water. The large boiloff rates obtained under these assumptions result in very high heatup rates, due to the cladding-steam reaction, between the times when core melting first starts and all of the water in the pressure vessel is boiled off. Model C is not believed to give a realistic picture of core meltdown. It was developed to illustrate the effect of molten fuel dropping out of the core rather than being retained in a molten zone within the core region.

A1.2 RESULTS OF BOIL CALCULATIONS

The results of calculations are presented in this section of the report. Although the details of the results depend on the particular reactor being studied, many of the conclusions and trends seen in the BOIL results have some general applicability. The most important variables in the calculations appear to be the time after shutdown that the boiloff sequence starts and the initial pressure-vessel water inventory. These variables control the core-decay heat, the water boiloff rate, and the subsequent core heatup rate. After core melting starts, the meltdown or slumping model used in the calculations can also significantly influence the core heatup.

In the calculations described in this appendix, the time when the boiloff part of the accident starts and the sequence of events preceding it are assumed to be known. These sequences and their probability are discussed elsewhere.

A1.2.1 PWR RESULTS

For most of the BOIL calculations on the PWR, the initial water inventory in the pressure vessel was equivalent to an unswollen water level at the top of the core. For these cases, the swollen-mixture level is actually above the core. This is representative of situations in which the emergency core cooling system has functioned in the injection mode. Many of the results in this section are plotted as a function of accident time, measured from some predetermined initial condition in the BOIL calculations. As used in this section of the report, the "time when the boiloff calculations starts" is not the time when the LOCA accident starts. It is the time when the water inventory in the pressure vessel decreases to a known unswollen level, usually the top of the core. The time when the boiloff calculation starts is discussed elsewhere; it depends on the particular accident sequence being considered, e.g., the time when the emergency core cooling recirculation system fails. In addition to results that illustrate the expected behavior of the reactor, the section includes results that illustrate effects of model assumptions in the BOIL program.

Figure VIII A-2 shows how the swollen-mixture level and void fraction at the top of the core decrease for a boiloff accident starting at 1.0 hr decay time. The initial unswollen water level was at the top of the core (12 ft from the bottom of the core). Note that after 30 min the average mixture void fraction ($\alpha_T/2$) is less than 7 percent, and the effect of level swell is not significant. The most important effect of level swell is to keep the core completely covered (and cooled) for almost the first 10 minutes after boiloff begins. Thus, the level swell retards the initial core heatup by about 10 minutes for this accident. Figure VIII A-1 also illustrates the growth of the molten-fuel zone in the core. The axial location of the melted fuel nodes in the highest (radial) power zone are shown. (The core is divided into 5 radial and 24 axial regions or nodes.) Note that significant melting occurs while there is still water in the bottom of the core. In meltdown Model A, the mixture level decreases rapidly after about 55

minutes as molten fuel intercepts the mixture level, and the core-meltdown rate increases due to increased metal-water reaction. In Model B the molten zone remains above the mixture for considerably longer, assuming no fuel falls out of the molten zone. In the Model A meltdown, the molten zone reaches the bottom of the core in about 60 minutes.

Figure VIII A-3 shows the water-boiloff or steam-production rates for the same situation considered in Fig. VIII A-2. The boiloff rate remains approximately constant, at a comparatively high value, for the first 10 minutes because the core is completely covered due to level swell. The boiloff rate decreases as the mixture level goes down and less of the core-decay heat is absorbed in the water. At 60 minutes in meltdown Model A, the boiloff rate increases rapidly from quenching molten fuel entering the water.

Figure VIII A-4 illustrates typical temperature transients for fuel-rod nodes (in the hottest radial zone) at the top, bottom, and midplane of the core. The accident sequence is the same as considered in Fig. VIII A-2. The top of the core uncovers first, and initially heats up at a rate dependent on the fuel-rod-decay heat. The midplane uncovers later, but heats up faster due to its larger decay heat. When the nodes reach temperatures above 2500 F, they show typical heatup rates produced by the zirconium-steam reaction. The rapid heatup of the bottom of the core after 55 minutes is primarily due to the molten fuel slumping in meltdown Model A.

Figure VIII A-5 shows, for the same accident considered in Fig. VIII A-1, the fraction of the core melted as a function of time for the three meltdown models discussed previously. Models A and B both predict that 50 percent core melting is reached in about 60 min. However, at about this time Model A predicts that molten fuel contacts the water, and the increased zirconium-steam reaction rate causes the results to diverge for larger meltdown fractions. A calculation is also shown, labeled Model B', which is the same as Model B except that, after 60 minutes, it assumes 1.0 percent per minute of the molten core falls into the water. The resulting increased steam flow and metal-water reaction produces a result similar to that obtained in Model A. Thus, if a small part of the molten region falls into the water, the Model A and B results are similar. Since this seems likely to occur, it is concluded that meltdown Model A probably gives a more realistic picture of core meltdown than Model B, particularly for very large (∿80 percent) fractions of the core melted.

In the calculations above, it is assumed that core melting does not prevent steam flow and stop the metal-water reaction in the core regions above the molten-fuel zone. If it is assumed that core melting (channel plugging) stops the metal-water reaction in a given channel above the melted zone, the result (labeled Model A') looks similar to that obtained for Model B. Channel plugging is probably more likely in a BWR core with shrouded fuel elements than in an open-lattice PWR core.

Acronyms (labeled OZM, MZAB, UCBM, UCPM) indicate situations where massive structural failure of the core is possible. These situations are noted but the BOIL calculation is continued as if the failure did not occur. If damaging steam explosions occur, they are likely to follow these massive structural failures. When the molten region reaches the outside of the core (OZM), the core barrel may be exposed to molten fuel. Since the core barrel supports the core, the core could drop into the bottom of the pressure vessel at this time. In meltdown Model B there is a large thermal radiation loading on the upper core plate and core barrel (after the upper core plate melts) above the core. The upper core barrel is predicted to melt (UCBM) at 110 minutes in Model B. In Model A, the molten zone reaches the bottom of the core (MZAB) in about 61 minutes, and the core would presumably fall to the bottom of the pressure vessel shortly after. The metal-water reaction with the molten iron is not considered in the BOIL calculation.

Model C shows a very rapid heatup after core melting starts due to the large steam flow rates and metal-water reaction. However, after about 40 minutes, all of the water in the pressure vessel is boiled off and the metal-water reaction stops. The results of the calculations indicate that all of the core nodes hot enough (over 2500 F) to have a large metal-water reaction rate quickly melted, and the nodes that were below 2000 F remained relatively cool. Thus, the calculated core condition shows about half of the core in the bottom of the pressure vessel at an average temperature of about 4000 F. The original core has a hole melted out of it, but the remaining fuel is relatively cool (∿1500 F). This core-meltdown model is not believed to be realistic; however,

it illustrates the significance of the metal-water reaction in the core heatup.

Figure VIII A-6 shows the fraction of the cladding reacted for the same accident shown in Fig. VIII A-2. For the reasons discussed above (Fig. VIII A-5), the results are sensitive to the meltdown-model and channel-plugging assumptions when more than about 30 percent of the cladding is reacted. The results of these calculations indicate it is highly likely that more than 30 percent of the cladding will react, and that much higher fractions are possible.

Figure VIII A-7 shows how the results in Figs. VIII A-2 to VIII A-6 can be generalized in terms of the time when the boiloff part of the accident starts. These results indicate that core meltdown in a boiloff accident can be expected in a few hours even for accidents starting several days after core shutdown, assuming no further preventative action is taken. A calculation is also shown in Fig. VIII A-7 for an accident starting at 60 sec with an initial pressure vessel water inventory equivalent to an unswollen water level of 6 ft (core midplane).

A1.2.2 BWR RESULTS

For a boiloff accident starting at the same decay time, the BWR and PWR results are quite similar. Differences in the boiloff calculations are primarily attributable to differences in the core power density, pressure-vessel water inventory at the start of the accident, and the fuel-element design (open lattice versus shrouded). At the start of the BWR boiloff calculations, the initial mixture level inside the core shroud is 8 ft above the bottom of the core. The presence of the fuel-bundle shroud has two effects: (1) the Zircaloy in the shroud adds to the potential for metal water reaction, and (2) shroud probably makes channel blockages more likely and steam bypass of the plugged channels less likely. Thus, there are compensating effects on the amount of zirconium reacted. A third consideration is that the BOIL programming does not perform a specific calculation of the shroud temperature. The shroud is treated approximately by including it in the fuel-rod cladding.

In addition to the boiloff calculations, BOIL calculations were also performed for a dry heatup (with no steam flow) and for a degraded bottom-flooding situation starting with the end-of-blowdown conditions.

Figure VIII A-8 shows the core-meltdown fraction as a function of time for two BWR accident situations: (1) a dry heatup starting with end-of-blowdown conditions, and (2) a boiloff accident starting at 100 hr decay time with the core covered to the jet pump nozzle (8 ft from the bottom of the core). The core temperatures at the end-of-blowdown were given by the relation (Ref. 10)

$$T_R = 923\ (F - 0.332) + 540 \qquad \text{(VIII A-22)}$$

where F is the local power-peaking factor (Ref. 10). This relation gives an average core temperature of 1157 F and a peak temperature (F = 2.1) of 2172 F at the end of blowdown. In the boiloff calculation it was assumed that the spray system was operative until the boiloff accident started at 100 hr. Thus, the whole core was assumed to be initially cooled even though the mixture level was only at an elevation of 8 ft.

For the dry heatup case in Fig. VIII A-8, meltdown Models A and B predict the same curve of fraction core melted versus time. However, the molten zone migrates to different axial positions in the two models. At 60 min in Model A, the molten zone has reached the bottom of the core. In Model B, the molten zone is still 2.5 ft from the bottom of the core at an accident time of 60 min. After about 80 min in Model B, the top of the core is melted, and the radiation heat transfer from the surface of the molten pool begins to melt the steel structure above the core.

For the boiloff accident starting at 100 hr, the core-meltdown behavior is similar to that obtained for the PWR. For boiloff starting at 100 hr, both Fig. VIII A-7 for the PWR and Fig. VIII A-8 for the BWR predict 80 percent core melting with the molten zone at the bottom of the core (Model A) in about 225 min. (Note that the boiloff in the two reactors starts with different water elevations in the core.) The above calculations assume there is steam flowing to unmelted core zones above the water. If it is assumed that melting causes channel blockage so that no Zircaloy cladding reacts above a melted fuel-rod node, then the meltdown results for Model A look approximately the same as those for Model B.

For the boiloff accident shown in Fig. VIII A-8, about 25 percent of the core Zircaloy (cladding plus shrouds) has

reacted at the time when 50 percent of the core is melted. This may increase to 35 to 60 percent Zircaloy reacted, depending on the meltdown model selected, when 80 percent of the core is melted.

A1.2.3 BOTTOM-FLOODING

BOIL calculations were performed for several degraded bottom-flooding rates. It was assumed that the core temperatures and decay heat were given by the end-of-blowdown conditions at 25 sec. The water level in the pressure vessel was assumed to be at the bottom of the core, and saturated water was added to the vessel inventory at rates equivalent to bottom-flooding rates between 0.02 and 0.2 in./sec. In these calculations, metal-water reaction with the fuel-bundle shroud was neglected. The results indicate that the worst flooding rate, in terms of producing the largest amount of zirconium-steam reaction, is about 0.1 in./sec. For higher or lower flooding rates, the metal-water reaction is reduced. For a flooding rate of 0.1 in./sec, the amount of cladding reacted is between 20 and 70 percent, depending on the assumptions made relative to channel blockage caused by fuel melting. For flooding rates less than 0.2 in./sec, the BOIL calculations predict more than 20 percent core melting. For meltdown Model A and a flooding rate of 0.02 in./sec, the molten zone is predicted to be at the bottom of the core at an accident time of 230 min.

A2. CONTAINMENT HEAT TRANSFER

A2.1 PWR ANALYSES

A2.1.1 ENERGY SOURCES

The reactor was assumed to be operating at full power at the time of the accident. The integrated power generation for the first 10 sec after the break was determined from a typical power shutdown curve for large breaks. From 10 sec on, power generation was determined by the proposed ANS standard (Ref. 1) for decay heat assuming infinite irradiation time. The assumption of infinite irradiation time, on the one hand, will overestimate decay heat generation; on the other hand, it should compensate for potentially nonconservative uncertainties in shutdown heating.

The sensible stored heat of the reactor vessel and internals was assumed to be given up to the cold injection water. It was found that the stored heat was approximately equal to that required to raise the injection water in the reflooded vessel to saturation. The heat stored in the primary piping as well as in secondary coolant in the steam generators was given up to the steam generated by core-decay heat. The rate of heat transfer was found to be limited by the heat capacity of the steam.

The energy generated by the zirconium-water reaction was not input into the containment pressure calculations directly, but was assumed to go into core heating. It is recognized that the gases (i.e., steam and hydrogen) leaving the core which is undergoing significant metal-water reaction will be at very high temperatures; the influence of this high-temperature gas on the containment pressure behavior is problematical, however. For a cold-leg break, the hot gases will have to pass through the primary-system piping as well as the steam generators to reach the containment atmosphere; in such situations the gases will be cooled to the temperature of the piping and steam generators. For a hot-leg break the heated gases will have a direct path to the containment; but, at extremely high temperatures, the hydrogen would be expected to ignite upon exposure to the containment atmosphere. The energy generated by hydrogen burning would far exceed the sensible heat of the gas stream. Energy releases due to hydrogen burning, where applicable, were included in containment energy balances.

A2.1.2 CONTAINMENT HEAT SINKS

The available passive heat sinks within containment consist of the containment liner, miscellaneous metal, and concrete structures. The quantities and geometrical parameters of each were taken or inferred from the FSAR. A steam-condensing coefficient of 150 Btu/hr-ft^2-F was assumed for all "cold" surfaces within containment: this value is consistent with the results obtained in the CVTR containment experiments (Ref. 13). The rate of heat absorption by the various sinks was evaluated by means of transient-conduction nomograms, as given by McAdams (Ref. 4) and others. With the above condensing coefficient, the containment liner would be heated to the temperature of the steam in the atmosphere in less than an hour. Since the specific dimensions and quantities of miscellaneous metal in the containment were not available, the latter was assumed to heat up at the same rate as the containment liner. The concrete walls within containment were heated on both sides; the external walls and foundation, on one side only. Heat

absorption by the concrete was found to be governed by conduction within the concrete itself and largely insensitive to the condensing coefficient utilized.

A2.1.3 CONTAINMENT ATMOSPHERE

The temperatures and pressures in the containment atmosphere are assumed to be homogeneous. The containment spray water, if available, is heated to the condensing temperature of the steam in its passage through the atmosphere. The energy due to hydrogen burning, if applicable, is distributed uniformly over the contents of the containment atmosphere.

A2.1.4 CONTAINMENT PRESSURE-TIME EVALUATION

The evaluation of the containment pressure-time history, taking into account the above described considerations, is carried out as follows. At any point in time, an energy balance in the containment atmosphere is calculated by summing the energy in the steam present at the previous time, the energy added by the steam from the core, the water added by the sprays, the heat removed by the heat exchangers, losses by condensation on the containment heat sinks, and leakage from the containment. This gives the total mass and average enthalpy of the water in the containment atmosphere. Using this enthalpy and an assumed pressure (which is based on the pressure at the previous iteration) a quality, and hence the amount of steam in the containment atmosphere, is determined. From this quantity of steam and the known volume of the containment building a resulting partial pressure of steam is determined. If the sum of this partial pressure of steam and the partial pressure of the noncondensables does not agree with the pressure assumed for the computation of the quality, the calculation is repeated with an adjusted pressure until a consistent solution is reached. The steam and water properties utilized are adjusted in accord with the predicted temperatures and pressures. The steam that condenses and the spray water are returned to the containment sump and mixed with the water there. Mass and energy balances are computed for the sump water at each point in time.

After the conditions in the containment atmosphere and in the sump have been evaluated, time is advanced and the procedure is repeated as many times as required to cover the accident sequence in question. As time is advanced, appropriate adjustments are made to the decay power level, safeguards operation, rates of heat loss, etc. The results of the containment pressure-time evaluation for the various accident sequences are given in the body of this report.

A2.1.5 CONTAINMENT LEAKAGE

The release of fission products to the environment is controlled by the leak rate from the containment. Prior to gross containment failure, the leakage is determined by the operational leak rate or by the characteristic hole size for containment-isolation failure and the containment pressure. If the internal pressure exceeds about 25 psia, the leakage flow through an assumed orifice will be choked and the leak rate will be 4.2×10^{-2} v/o/hr with the containment isolated and 42 v/o/hr with containment-isolation failure. The leak rate is assumed to vary linearly from zero to the choked flow rate in the pressure range 15-25 psia. If the containment pressure is subatmospheric, as would be the case with all safeguards functioning, the leakage is considered to be zero.

In the event of a containment-isolation failure, the pressure would approach one atmosphere rapidly after the blowdown. Leakage will then depend upon the availability of a driving force. With the containment sprays and containment heat exchangers operating, any steam generated will be condensed and the only contributors to leakage will be the hydrogen from the zirconium-water reaction and the carbon dioxide from the decomposition of concrete during meltthrough. In sequences where the containment sprays are not operating, steam generation could be the principal driving force for leakage. Similarly, if the sprays are working but the containment heat exchanger has failed, condensation will not take place after the spray water has reached saturation. If the effective generation rate of gases and vapors is less than 42 v/o/hr with containment-isolation failed, the leak rate is equal to the generation rate. If the generation rate exceeds 42 v/o/hr, the leak rate is held at this level and the pressure is allowed to rise as required to maintain consistency between production and loss of gases and vapors.

Containment failure by steam explosion, overpressure, or meltthrough is accompanied by a puff release of a fraction of the containment atmosphere; the magnitude of the puff release will depend on the containment pressure at the time of

the failure and the location of the failure. Failures due to steam explosions and overpressure are assumed to occur above ground and vent to the atmosphere. Meltthrough failures vent to the atmosphere against the static head of the groundwater; in some cases the latter may exceed the pressure within containment.

After containment failure due to a steam explosion or overpressure, the breach in containment is assumed to be too large to limit flow and the leak rates are taken equal to the net generation rates of gases and vapors. For sequences in which sprays are operating and a steam explosion fails containment, the sprays are assumed to continue operating, even though there is a significant probability that the steam explosion may fail the sprays also. For over-pressure failure the spray pumps would cavitate if they were operating at the time. If the primary mode of containment failure is meltthrough, the subsequent pressure within the building will be controlled by the static head of groundwater surrounding the building foundation. Any steam generation would be condensed as it flows through the breach in the foundation mat. Noncondensables will leak out through the ground as well as through normal leakage paths.

During the period of core melting the steam generation rate is approximately equal to the available decay heat, i.e., total decay heat reduced by the escape of the volatile fission products. All the hydrogen production is assumed to take place during initial core meltdown. After the molten core drops to the lower plenum, the water there is evaporated in 15 minutes by partial quenching of the core. During the remainder of pressure vessel meltthrough there is no further gas or vapor generation. After the melt drops into the vessel cavity it will start to vaporize any water there as well as attack the concrete. If neither the ECI or CSI operates, there will be little or no water in the vessel cavity. With both ECI and CSI operating, 1.83×10^5 lb of water will be available to produce steam. If the CSR is operating, a continuing supply of water will be available for steam generation in the cavity, although the steam may be condensed subsequently. Meltthrough of the concrete generates 0.2 lb of steam and 0.264 lb of CO_2 per lb of concrete decomposed.

The uncertainties in the calculated leak rates are believed to be relatively large. Many of the assumptions, particularly those associated with steam explosions and containment meltthrough, are intended to be representative of the phenomena that could exist, rather than attempts at an exact delineation of events. The range of possible leak rates is estimated to be within a factor of two of the calculated values. It is believed that in many sequences the consequences of fission product release will be dominated by the puff release and thus will be relatively insensitive to the uncertainties in the time-dependent leak rates.

A2.2 BWR ANALYSES

A2.2.1 ENERGY SOURCES

The reactor was assumed to be operating at full power at the time of the accident. Reactor scram, though not necessary for shutdown, was assumed to take place early in the accident. Decay power was determined from the proposed ANS standard for decay heat assuming an infinite irradiation time (Ref. 1). In the absence of a control-rod scram, the reactor would be shut down by core voids and the integrated power during shutdown would not differ appreciably from that of the scram case. The absence of scram or control rod run-in, however, could lead to recriticality and subsequent power generation on core reflooding by the emergency core-cooling system. As before, the assumption of an infinite irradiation time will overestimate decay-heat generation which could compensate for other, nonconservative uncertainties.

The sensible stored heat of the reactor vessel, internals, and primary piping inside the dry well were considered to be given up to the cold core-cooling water. The energy generated by the zirconium-water reaction was assumed to go into core heating.

A2.2.2 CONTAINMENT HEAT SINKS

The available passive heat sinks within containment in addition to the suppression pool water are the dry-well vessel, miscellaneous metal within the dry well, and the concrete in the dry well. Since the dry well is separated from its surrounding structures by a 2-in. air gap, the only heat-transfer path out of the dry well is by conduction through the concrete base. The dry-well vessel and the concrete base were assumed to be heated on one side, the concrete walls within the dry well were assumed to be heated on both sides. The rate of heat absorption by these sinks was evaluated by means of transient-conduction nomo-

grams, such as given by McAdams (Ref. 4) and others. A steam condensing coefficient of 150 Btu/hr-ft^2-F was assumed for "cold" surfaces within the dry well. Within the above guidelines the dry-well vessel was found to be heated to the temperature of the steam in less than an hour. Heat absorption by the concrete was found to be governed by conduction within the concrete and insensitive to the condensing coefficient utilized. The temperatures of the suppression-chamber components were assumed to be at the temperature of the water.

A2.2.3 CONTAINMENT RESPONSE

Primary-system depressurization leads to a rapid rise in dry-well pressure, which in turn leads to the flow of the released steam and water into the suppression pool where the steam is condensed. During the blowdown process, essentially all the air initially present in the dry well will be transported to the gas space in the suppression chamber. At the end of the blowdown, with both core-spray and core-flooding systems operating, the pressure in the dry well decreases as the relatively small quantity of steam remaining there begins to condense; the pressure in the suppression chamber, being largely controlled by the noncondensables, stays relatively constant. When the pressure in the dry well drops below that in the suppression chamber, vacuum breakers open and allow the noncondensables in the suppression chamber gas space to flow back into the dry well. This results in a decrease in the pressure level within containment as the noncondensables equilibrate between the dry well and wet well and the steam in the dry well continues to condense and move toward equilibrium with the pool. Under design conditions, the pressures in the two portions of containment remain equilized indefinitely.

Under design-basis accident conditions there is little or no net steam generation from the core during reflooding. As a consequence, what steam is generated will be condensed by the suppression pool, and the noncondensables will be equalized between the dry-well and wet-well gas spaces. With degraded performance of the standby core-cooling system, significant steam generation by the core may continue during the reflooding phases of the accident; this would result in the dry-well pressure remaining about 3 psi higher than that in the suppression chamber with no equalization of the noncondensables. Under such conditions the containment would remain at an elevated pressure for an extended time.

Functioning of the vapor-suppression containment as designed leads to relatively low accident pressures within the containment except for the early portions of the blowdown. If, however, condensation of the steam generated by primary-system depressurization does not take place, for whatever reason, pressures significantly in excess of design levels would result. Assuming that steam condensation does not take place and that the entire free volume of the containment is available, primary-system depressurization would result in a pressure of about 250 psia within the reactor-containment design assumed for this study.

The failure of long-term cooling with all the other safeguards functioning would lead to a gradual increase in the suppression-pool water temperature and a corresponding gradual increase in pressure. With a design-basis containment-leak rate the loss of long-term cooling will eventually lead to containment failure by overpressurization. For containment-leak rates in excess of about 100 percent per day, overpressurization failures would not be expected.

The containment pressure-time histories for the specific accident sequences considered are given in the body of this report.

A3. PRESSURE VESSEL MELTTHROUGH

A3.1 PWR ANALYSES

It is assumed that, as the core temperature rises, most of the core remains above the grid plate until a major fraction is molten (∿80 percent). At this time the molten fuel drops rapidly to the bottom of the vessel where it is partially quenched as it boils away the water in the lower plenum. The time required for the core to break through the pressure vessel serves as a delay period before the melt can begin to work on the containment floor. The time at which the molten fuel enters the lower plenum in the following analyses is ∿2 hours.

Using J. C. Hesson's model (Ref. 11), the heat convected downward from the molten pool through a solid layer of UO_2 into the steel head is

$$Q_t = \sqrt{2k\ (T_2 - T_1)\ q + Q^2},$$

(VIII A-23)

where

Q_t = heat flux into steel

k = thermal conductivity in solid UO_2

T_2 = melting point of UO_2

T_1 = melting point of steel

q = volumetric heat generation in core

Q = heat flux from liquid to solid UO_2.

Q is evaluated from

$$Q = C\frac{k}{L}\left(\frac{gS\rho^2L^3}{\mu^2}\right)^m\left(\frac{\mu C_p}{k}\right)^n \Delta t,$$

(VIII A-24)

where C, m, and n are constants

S = vapor fraction at different levels

L = pool depth

Δt = temperature difference in pool above the boiling point of UO_2.

Hesson found Q independent of L, $m \simeq 1/3$, and n between 0 and 1/3 in experiments with internally heated salt-water baths. Allowing S = 1 for maximum convection and using Cp = 0.124 cal/g-C, μ = 0.46 poise, ρ = 8.7 g/cm^3, and k = 0.005 cal/sec-cm-C values of Q of 8.52 cal/sec-cm^2 for n = 0, 10.43 for n = 1/4, and 10.22 for n = 1/3 determined.

Using the value 10.22 cal/sec-cm^2 C (136,000 Btu/ft^{2}hr F) and solving for the heat flux into the steel, we find that $Q_t = 1.39 \times 10^5$ Btu/ft^2-hr F for our case.

Since this total heat flux is only slightly greater than the convection component, the internal heating component in the solid layer is small and therefore the solid UO_2 layer is thin. Thus the quenched core will absorb heat until nearly the entire core remelts, or, ignoring this thin solid layer, heat equal to that removed by the evaporating water during quenching will be absorbed to remelt the core. In addition, the model assumes the temperature gradient in the melt to vary from its melting point to its boiling point which supplies the driving force for convection. The core will therefore absorb additional heat as its temperature is increased to an average between melting and boiling points, ~5475 F.

As the stress in the bottom head from the weight of the core is relatively low (< 1000 psi), failure of the head is not expected until it becomes quite weak at higher temperatures. By extrapolating lower temperature data, the tensile strength of vessel steel decreased to 1000 psi at about 2400 F. From this, an average steel temperature of 2400 F is assumed to be the failure point.

A3.1.1 REALISTIC FAILURE TIME

The time from the core falling into the bottom of the vessel until the bottom head fails is the time for the decay heat to heat the core to its equilibrium temperature, plus the time to heat the bottom head tc its failure temperature at the above heat flux Q_t.

$$t_1 = \frac{\Delta Q \text{ water} + (MC_p\ \Delta T) \text{ core}}{Q_{decay}}$$

(VIII A-25)

where ΔQ is the heat to evaporate the water; $MC_p\Delta T$ is the mass, specific heat, and temperature difference in the molten core; and Q_{decay} is the decay heat.

$$t_1 = \frac{3.13 \times 10^7 + 0.62 \times 10^7}{6.00 \times 10^7} = 0.625 \text{ hr},$$

(VIII A-26)

$$t_2 = \frac{(MC_p\Delta T) \text{ steel}}{Q_t} = \frac{224^* \times 0.12 \times 2100}{1.39 \times 10^5}$$

$$= 0.406 \text{ hr},$$

(VIII A-27)

and

$$t_1 + t_2 = 0.625 + 0.406$$

$$= 1.03 \text{ hr} = 62 \text{ min.}$$

(VIII A-28)

---

*Mass is expressed in lb/ft^2 of the steel head.

It is unrealistic to assume that these events occur consecutively. However, when bounding estimates are made on the time to failure, more detailed calculations do not appear to be warranted.

A3.1.2 MAXIMUM FAILURE TIME

If it is assumed that only the longer lived ($t_{1/2}$ > 3 min) noncondensable fission gases are lost from the vessel so that 80 percent of the decay heat remains in the vessel, the time required to heat the whole vessel and internals to 2400 F is

$$t = \frac{\Delta Q \text{ water} + (MC_p \Delta T) \text{ steel}}{Q_{decay}}$$

$$= 3.13 \times 10^7 + (6.855 \times 10^5 \times 0.113 \times 2.100 \times 10^3)/6.86 \times 10^7$$

$$= 2.67 \text{ hr} = 160 \text{ min.} \qquad \text{(VIII A-29)}$$

A3.1.3 MINIMUM FAILURE TIME

Some of Hesson's experiments showed horizontal heat flow approaching 4×10^5 Btu/ft^2-hr F. If it is assumed this heat flux is directed into the steel near the surface of the molten core

$$t = \frac{5.65 \times 10^4}{4.0 \times 10^5} + 0.625 = 0.766 \text{ hr}$$

$$= 46 \text{ min.} \qquad \text{(VIII A-30)}$$

A3.2 BWR ANALYSES

The lower head of a BWR pressure vessel is partially filled with control-rod guide tubes and contains a number of control-rod-drive penetrations. When the molten core drops into the bottom head, the drive penetrations may permit some of the molten material to escape prior to the failure of the bottom head as a whole. In other respects, analyses of BWR vessel meltthrough follows the same reasoning as given above for PWRs. If the time required to heat the entire vessel to 2400 F with decay heat is considered an upper bound to the time required for penetration, then penetration of the bottom head in the absence of water will occur in about 72 min. An additional 30 min will be required if there is water in the bottom head. The best estimate for the meltthrough time after the core drops into the lower plenum is 30 $\pm$ 20 min for the dry meltdown case and 60 $\pm$ 30 min if there is water in the bottom head. These results are based on core meltdowns taking place early in the accident; for the later onset of core melting, the meltthrough time will be extended due to the decrease in decay heating.

A4. CONTAINMENT VESSEL MELTTHROUGH

A4.1 PWR ANALYSES

The processes by which the molten core interacts with the concrete floor of the containment building are very complex and not fully understood. In the absence of definitive experimental information it is only possible to estimate approximately the time required for penetration of the containment floor by the molten core. When the molten fuel (together with molten zirconium, zirconium oxide, steel, iron oxide, etc.) falls onto the concrete, vaporization of free water below the surface will cause spalling of the concrete and result in a very rapid penetration rate of the melt into the concrete. Based on the vaporization of the free water, initial spalling rates are calculated to be 15-30 ft/hr. As the concrete heats up it will give up its water of hydration at about 900 F; then at 1400-1600 F the limestone will decompose into CO_2 and CaO. It is expected that the water vapor and carbon dioxide would escape from the melt and be released to the containment atmosphere, but the calcium and silicon oxides would stay with the melt. As the products of concrete decomposition are absorbed and/or dissolved by the melt, the melt temperature will decrease until constituents of the mixture begin to precipitate. It is estimated that by the time the melt has penetrated through 1-1/2 feet of concrete, UO_2 would begin to precipitate from the multicomponent mixture. From this point on the progress of the melt through the concrete is controlled by the rate of decay-heat generation, i.e., the quantity of concrete penetrated is directly proportional to the energy available to decompose the concrete and raise the temperature of the products to the temperature of the melt.

The temperature required to maintain the multicomponent mixture in a fluid state is not known. The principal components of the melt and their approximate

melting points are: UO_2 (5200 F), ZrO_2 (4900 F), Zr (3350 F), stainless steel (2550 F), Fe (2790 F), FeO (2590 F), Fe_2O_3 (2850 F), CaO (4680 F) and SiO_2 (3100 F). The melting point of $CaO \cdot SiO_2$ is 2750 F; however, in ordinary concrete there is almost twice as much calcia as silica. A melt temperature of 4000 F has been assumed for the present analysis.

After the initial rapid penetration of concrete by spalling, the melt is expected to remain relatively viscous, decomposing and dissolving concrete at a rate compatible with decay-heat generation. Because the silica and calcia that are introduced at the lower surface are less dense than the body of the melt, convection currents that should be established will prevent the center of the melt from reaching very high temperatures. Also, the carbon dioxide and water vapor released by the concrete, and/or their further decomposition products, will provide additional agitation as they rise through the melt.

The upper surface of the melt is likely to be covered with a solid crust and to be radiating heat to the remains of the pressure vessel and to the walls of the reactor cavity. If there is water in the cavity it will be vaporized by the melt, but even the continued addition of water would not avert containment meltthrough since the geometry of the molten mass is not favorable for effective cooling. If the structures above the melt reach elevated temperatures, they could fall into the melt.

That at least part of the mass of fuel, structural, and other material remain molten is required by heat-transfer considerations. If this mass should solidify at some point during the accident, then the only mechanism for dissipating decay heat would be conduction. For conduction to transfer the decay heat out of the largely low conductivity mass of material involved, temperatures at the center of the mass would have to exceed boiling points of some and melting points of all the constituents. Hence the conclusion that at least some of the mass will remain in a fluid state for considerable time, with convection within the melt tending to maintain the melt temperature near the effective melting point of the mixture. It is recognized that as the size of the melt increases and the heat-generation rate per unit volume decreases due to dilution, solidification must eventually occur. Solidification is not, however, expected to take place prior to the penetration of the containment foundation mat.

In estimating the time required to penetrate the 10-ft-thick foundation mat three different configurations were considered for the quantity of concrete decomposed by the molten core: (1) a 15-ft-diameter, 10-ft-high cylinder, (2) a 10-ft-radius hemisphere, and (3) a 32-ft-diameter, 10-ft-high cylinder. The first case assumed that the melt progressed downward through the concrete faster than it did horizontally; the second case assumed equal rates of progress of the melt downward and horizontally. The third case assumed that the molten core materials spread within the confines of the reactor cavity and then attacked the concrete at equal rates in the downward and horizontal directions. Because the carbon dioxide and water vapor produced by the decomposition of concrete would tend to sparge the melt of fission products, the decay heat utilized for this analysis corresponded to 60 percent of that at the time of LOCA. This implies complete loss of the volatile fission products and fractional removal of some of the less volatile species from the melt. Assuming all the decay heat goes into the concrete, the times required to penetrate the concrete and bring the entire melt to 4000 F will be 7, 9, and 36 hours for the three cases considered. These times are based on contact of the concrete by the molten core at 2-3 hr after the start of the accident. Making an allowance for heat losses from the upper surface of the melt, the best estimate for the time required to penetrate the containment foundation mat is 18 hours.

More rapid meltthrough of the concrete than calculated could occur if the spalled pieces of concrete were floated to the surface of the melt without undergoing dissolution and being elevated to the temperature of the melt. In choosing the distribution for the time of containment meltthrough as 18 (+10, -5) hours from within the broad range of uncertainty, attention was paid to the potential competition between containment meltthrough and containment overpressurization as failure modes. Whereas the consequences of meltthrough are relatively small and insensitive to meltthrough time, it was considered essential not to underpredict the meltthrough time in such a manner as to preclude the possibility of failure by overpressurization if it would have occurred at a later time in the absence of meltthrough. The distribution for containment meltthrough time overlaps the expected time of containment over-

pressurization in such a manner as to give a high probability of overpressurization failure in those accidents in which it is a potential failure mode.

The effect of the steel liner and rebar steel have not been included in the above analyses; the effect would not be expected to be large, the rebar being of the order of 5 percent of the concrete by volume.

An evaluation of the penetration of a molten core through basaltic concrete has been performed by Jansen and Stepnewski (Ref. 12). Their analysis assumed a basaltic concrete composition with the water removed; the melting point of the basalt was taken to be ∿2000 F; 80 percent of fission products were assumed to stay with the melt. This material is considerably different from the ordinary concrete utilized in the present analysis. Their results for a 3000-Mwt reactor indicate penetration of 10 ft of concrete in approximately 5 hours. The assumptions made in this analysis would tend to under-predict meltthrough time for the present study.

In calculating the response of the containment pressure to the release of gases during the time the core is melting through the concrete, the rate of carbon dioxide generation has been calculated for a typical concrete composition. It should be recognized that not all concretes contain carbonates that would result in carbon dioxide evolution. The water released from the concrete has been assumed to escape without interacting with constituents of the melt to produce hydrogen. Since a large amount of molten steel could accompany the molten core, hydrogen production would be expected to occur if the steam were to bubble up evenly through the melt rather than to bypass it. If a mass of steel equal to the lower head of the pressure vessel were reacted, enough hydrogen would be produced to increase the containment pressure by ∿ 15-20 psi for accidents in which containment sprays operate. The pressure at the time of meltthrough would still be well below the predicted failure pressure, however. For accidents in which containment sprays or containment heat removal are inoperative in the meltthrough period, water vapor and hydrogen would have equivalent effects on containment pressure. The pressure transient would therefore be essentially unaffected by whether or not the reaction occurred.

A4.2 BWR ANALYSES

The phenomena associated with the penetration of the concrete foundation by the molten core in a BWR would be the same as described above for the PWR. However, because of differences in containment configuration and volume, the consequences of containment meltthrough in a BWR are expected to be quite different than in a PWR.

When the molten core together with some of the reactor internals and part of the vessel bottom head fall to the floor of the dry well, vaporization of the water there as well as decomposition of the concrete will ensue. The CO_2 and water vapor will be forced into the suppression pool where the latter will condense. The CO_2 together with the other noncondensables will collect in the suppression-chamber gas space and, in the absence of pressure relief, lead to failure by overpressurization. Figure VIII 3-2 in the body of this report shows the partial contributions as well as combined pressures of the various constituents of the containment atmosphere. The partial pressure of CO_2 was based on the decomposition of approximately a 20-ft-diameter by 8-ft-high cylinder of concrete below the reactor vessel, implying that the lateral spread of the melt was fixed by the reactor-vessel-support cylinder and the progress of the melt was straight down. The quantity of CO_2 released from the above mass of concrete together with the other noncondensables when confined to the suppression-pool gas space will result in a pressure more than sufficient to rupture containment. If the melt progresses radially outward as well as down, as might be expected, a larger quantity of CO_2 would be generated prior to the time that the melt reaches the dry-well vessel. The time of the overpressure failure will depend on the particular accident sequence of interest. The melt is estimated to penetrate the dry-well shell in about 12 hours after the core falls on the concrete.

If some of the water produced by decomposition of the concrete were to react with molten steel to produce hydrogen rather than to bypass the melt, the time of overpressure failure of the drywell could be reduced. The uncertainty in failure time associated with the rate at which concrete is decomposed is much greater than the uncertainty associated with the potential for reaction between the iron and water, however.

Since the bottom of the dry-well vessel is embedded in concrete, initial melt-

through of the steel shell would not necessarily mean gross failure of containment. If a large hole were melted through the bottom of the shell without it having failed previously, the ultimate strength of the dry-well vessel could be reduced significantly.

After the melt has penetrated the dry-well shell, it will continue to progress through the concrete foundation underneath the containment. An additional 18 hours are estimated to be required for complete meltthrough.

After the molten material has penetrated the concrete floor, the melt front will proceed into the underlying gravel and possibly into the earth. The ultimate extent to which the molten zone can grow depends upon the heat removal processes at the upper and lower surfaces and the chemical and physical processes within the melt. Estimates have been made of the ultimate extent of the growth of this region. Assuming that heat removal at the surface is limited to conduction, the maximum radius of molten sphere has been calculated to be 30 ft and 50 ft for growth into media of limestone and dry sand, respectively (Ref. 14). The analyses of Jansen and Stepnewski (Ref. 12) for basaltic concrete indicated a maximum radius of 38 ft for a molten hemisphere. Since the ground underneath containment is well below the level of the water table, conduction heat transfer at the surface of the melt should be augmented by steam generation and convection. It is therefore likely that the melt will not proceed more than 10-50 ft below the bottom of the containment building. Greater depths could only be achieved if the core material were able to melt through the underlying material without mixing and being diluted by the products of decomposition. Although it has been predicted that small pellets of solid UO_2 could travel some distance before being dissolved into the molten products of the medium being penetrated (Ref. 14), good mixing should occur between molten UO_2 and the products of decomposition of concrete or soil in the configurations expected in the meltdown accident.

References

1. "Proposed ANS Standard, Decay Energy Release Rates Following Shutdown of Uranium-Fueled Thermal Reactors", Subcommittee ANS-5, ANS Standards Committee (October, 1971).

2. Carbiener, W. A., and Ritzman, R. L., "An Evaluation of the Applicability of Existing Data to the Analytical Description of a Nuclear Reactor Accient, Quarterly Report for April through June, 1970", BMI-1885 (July, 1970).

3. Walters, C. T., and Genco, J. M., "NURLOC-1.0, A Digital Computer Program for Thermal Analysis of a Nuclear-Reactor Loss-of-Coolant Accident", BMI-1807 (July 6, 1967).

4. McAdams, W. H., Heat Transmission, 3rd Ed., McGraw-Hill Book Co. (1954).

5. Rettig, W. H., et al., "RELAP-3, A Computer Program for Reactor Blowdown Analysis", IN-1321 (June, 1970).

6. Slifer, B. C., and Hench, J. E., "Loss-of-Coolant Accident and Emergency Core Cooling Models for General Electric Boiling Water Reactor", NEDO-10329 (April, 1971).

7. Wilson, J. F., et al., "The Velocity of Rising Steam in a Bubbling Two Phase Mixture", ANS Transactions, 5, (1), p. 151 (June, 1962).

8. Wallis, G. B., One-Dimensional Two-Phase Flow, McGraw-Hill Book Co., p. 287 (1969).

9. Baker, L., Jr., and Hesson, J. C., "Heat-Transfer Model for Internal Heat Generation in Pools", ANL-RDP-7, p. 9.25 (July, 1972).

10. Morrison, D. L., et al., "An Evaluation of the Applicability of Existing Data to the Analytical Description of a Nuclear-Reactor Accident, Core Meltdown Evaluation", BMI-1910, p. A-1 (July, 1971).

11. Hesson, J. C., ANL-RDP-2, p. 8.37.

12. Jansen, G., and Stepnewski, D. O., "Fast Reactor Fuel Interactions with Floor Material After a Hypothetical Core Meltdown", Nuclear Technology, 17 (1), 85-95 (January, 1973).

13. Schmitt, R. C., Bingham, G. E., and Norberg, J. A., "Simulated Design Basis Accident Tests of the Carolinas Virginia Tube Reactor Containment - Final Report", IN-1403 (December, 1970).

14. Ergen, W. K., et al., "Emergency Core Cooling, Report of Advisory Task Force on Power Reactor Emergency Cooling", U.S. Atomic Energy Commission.

15. Private communication with G. Jansen, Battelle's Northwest Laboratories.

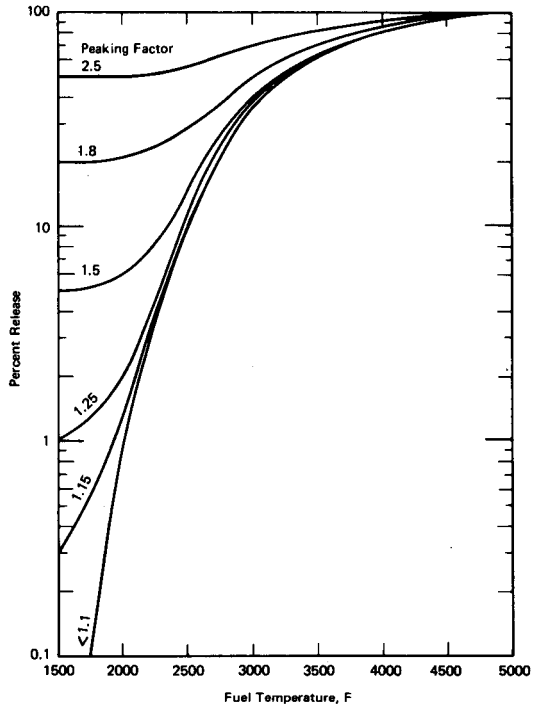


FIGURE VIII A-1 Characteristics Curves For Release of Volatile Fission Products From Overheated Fuel

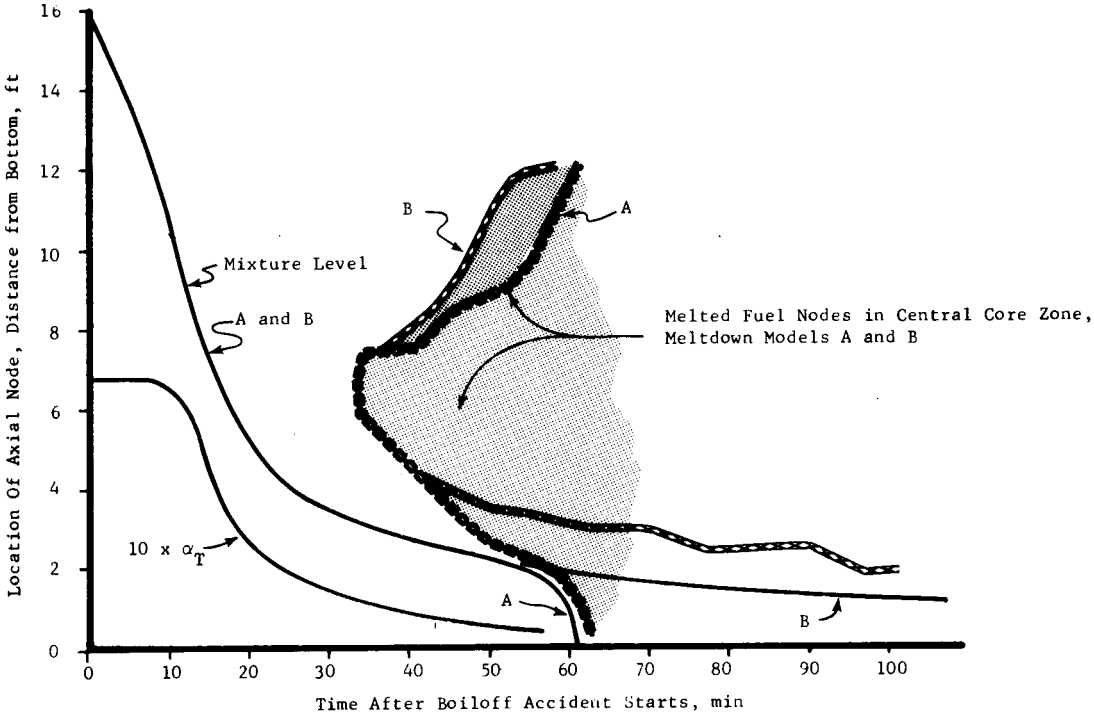


FIGURE VIII A-2 Mixture Void Fraction and the Locations of the Mixture Level and Molten Fuel Regions in a PWR for Meltdown Models A and B as a Function of Time for Boiloff Starting at 1.0 Hr

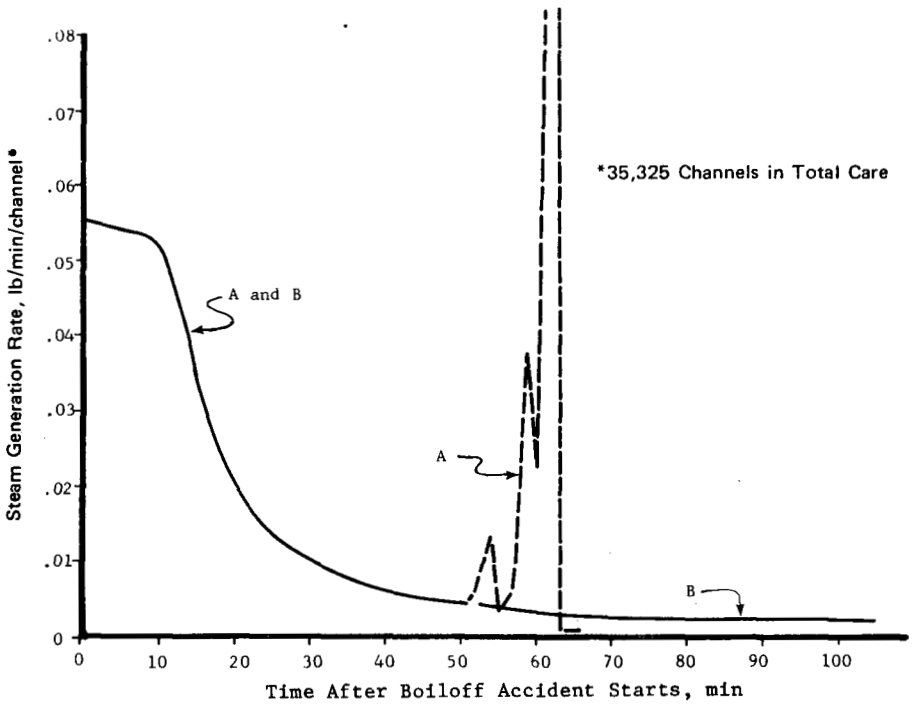


FIGURE VIII A-3 Steam Generation Rate During a Boiloff Accident Starting at 1.0 Hr in a PWR as a Function of Time for Meltdown Models A and B

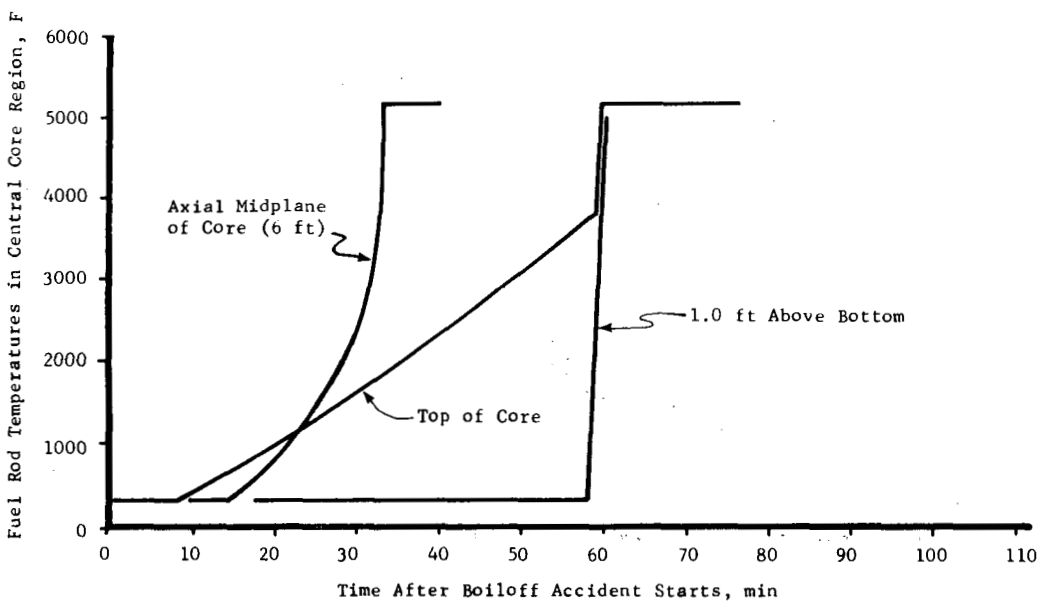


FIGURE VIII A-4 Fuel Rod Temperatures in the Central (Maximum Power) Core Zone of a PWR as a Function of Time for Boiloff Starting at 1.0 Hr for Meltdown Model A

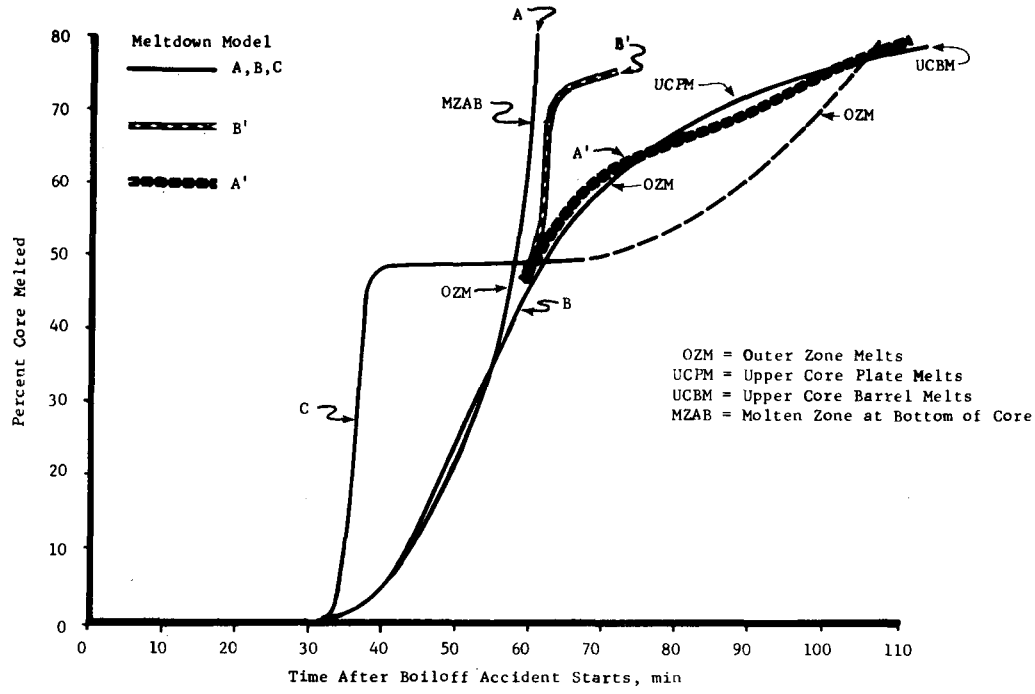


FIGURE VIII A-5 Effect of Meltdown Model on the Percent of a PWR Core Melted as Function of Time for Boiloff Starting at 1.0 Hr

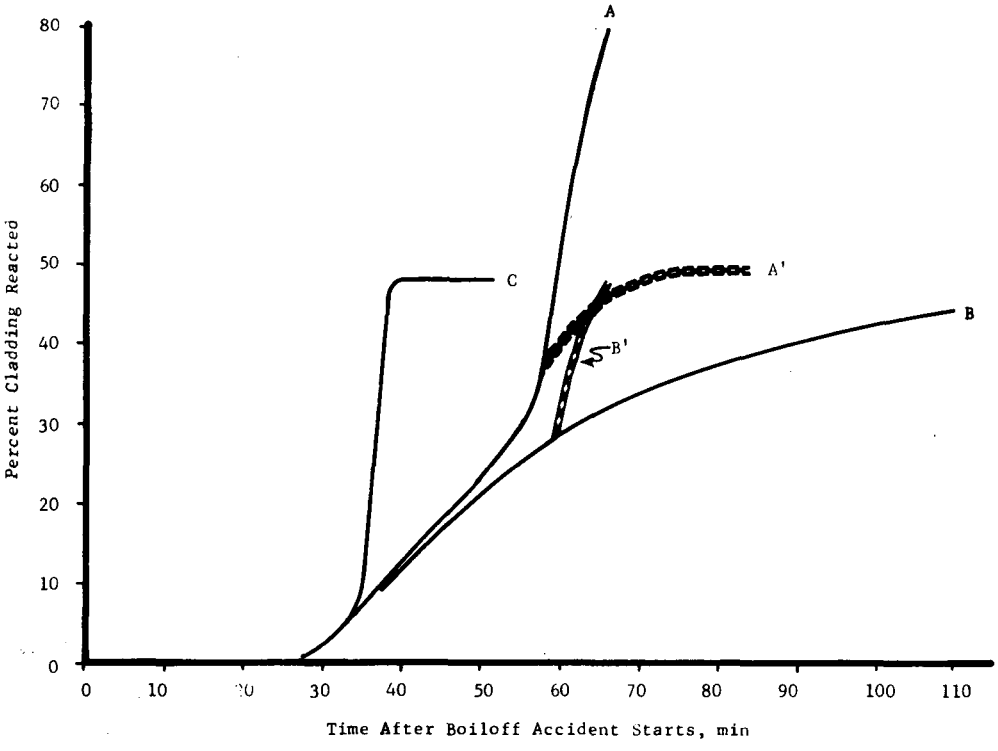


FIGURE VIII A-6 Effect of Meltdown Model on the Percent of the Cladding Reacted in a PWR Core as a Function of Time for a Boiloff Accident Starting at 1.0 Hr

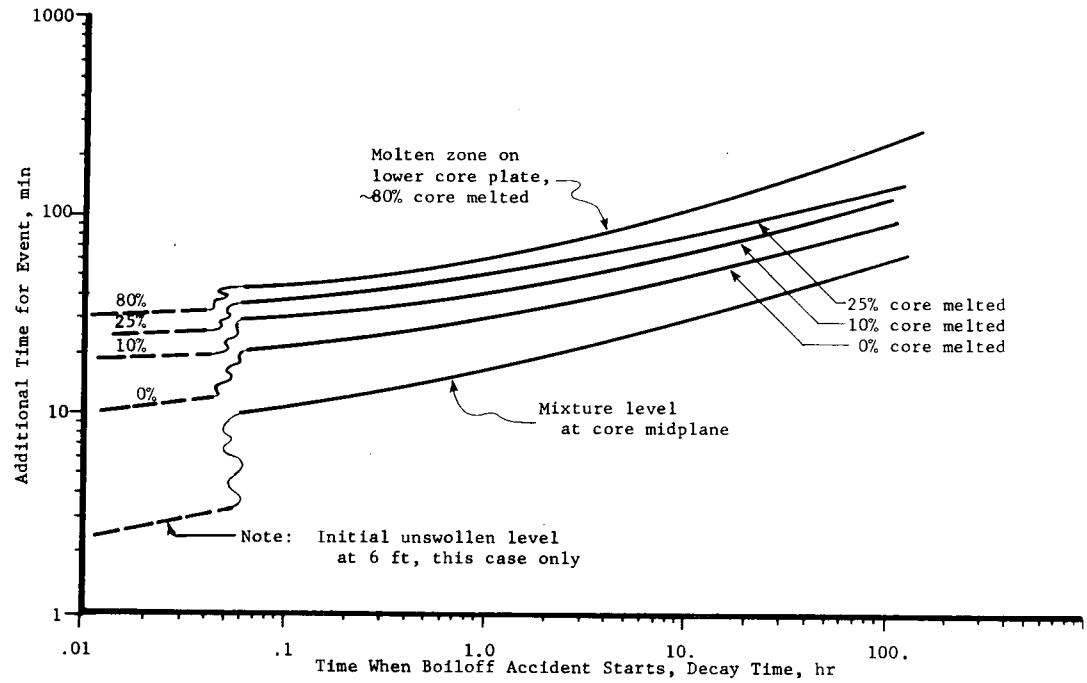


FIGURE VIII A-7 Effect of the Time When a Boiloff Accident Starts (Decay Time) on the Core Meltdown Sequences in a PWR for Meltdown Model A

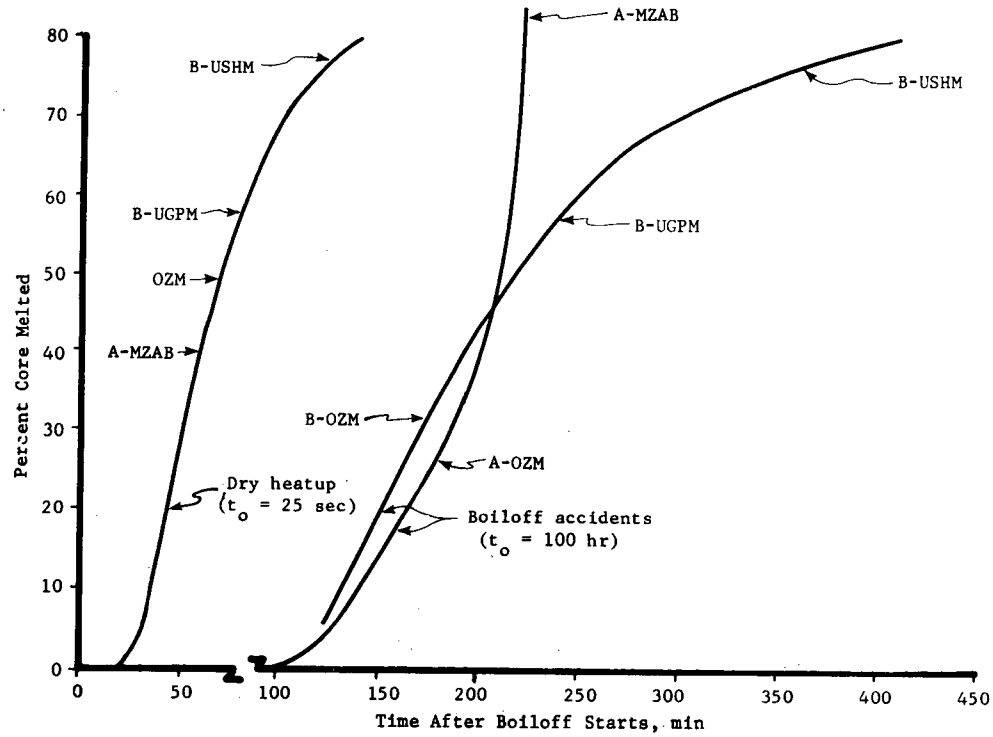


FIGURE VIII A-8 Percent of a BWR Core Melted as a Function of Time for (1) a Dry Core Heatup Starting with End-of-Blowdown Conditions at 25 Sec and (2) a Boiloff Accident Starting at 100 Hours with the Core Flooded to the 8 Foot Level

APPENDIX B

PHYSICAL EXPLOSIONS RESULTING FROM CONTACT OF MOLTEN MATERIALS AND WATER

Appendix B

Table of Contents

Section		Page No.
B1.	REVIEW OF LITERATURE	VIII-77
B1.1	Introduction	VIII-77
B1.2	Representative Incidents Involving Steam Explosions	VIII-77
B1.2.1	Metal Industry	VIII-77
B1.2.1.1	Mallory-Sharon Incident (Ref. 35)	VIII-77
B1.2.1.2	Reynolds Aluminum Incident (Ref. 35)	VIII-77
B1.2.1.3	Quebec Foundry Incident (Ref. 4)	VIII-78
B1.2.1.4	Western Foundries Incident (Ref. 36)	VIII-78
B1.2.1.5	Armco Steel Incident (Refs. 37,38)	VIII-78
B1.2.1.6	East German Slag Incident (Ref. 2)	VIII-78
B1.2.1.7	British Slag Incident (Ref. 3)	VIII-78
B1.2.2	Paper Industry	VIII-78
B1.2.3	Nuclear Reactor Industry	VIII-78
B1.2.3.1	Canadian NRX Reactor (Ref. 35)	VIII-78
B1.2.3.2	Borax I Reactor (Ref. 35)	VIII-79
B1.2.3.3	SPERT 1-D Reactor	VIII-79
B1.2.3.4	SL-1 Reactor	VIII-79
B1.3	Metal Fragmentation and the Initiation of Physical Explosions	VIII-79
B1.4	Interaction of UO_2 with Water	VIII-81
B1.5	Experiments with Metals in Water	VIII-82
B2.	CONCLUSIONS	VIII-83
REFERENCES		VIII-84

List of Tables

Table		Page No.
VIII B-1	Methods Leading to Metal Fragmentation and the Initiation of Physical Explosions.....	VIII-87
VIII B-2	Results of Molten UO_2 Being Dropped Into Water at Various Temperatures (Ref. 25).....	VIII-87

List of Figures

Figure		Page No.
VIII B-1	Particle Size Distribution of Quenched UO_2 Samples.....	VIII-88

Appendix B

Physical Explosions Resulting from Contact of Molten Materials and Water

B1. REVIEW OF LITERATURE

B1.1 INTRODUCTION

When molten metal comes into contact with a quenching fluid, a violent explosion can occur. This so-called "vapor or physical explosion" is a well-known, but little understood, phenomenon. A vapor explosion is usually characterized by an initiating event that leads to fragmentation and by the sudden conversion of thermal energy to mechanical energy due to very rapid heat transfer accompanied by a subsequent pressure wave. The violence, or magnitude, of such an explosion depends upon the quantity and rate of energy release. Numerous incidents have been reported in the literature (Refs. 1-12). Such explosions have occurred in the steel (Refs. 1-4), aluminum (Refs. 5,6), copper smelting (Ref. 5), paper (Refs. 7,8), and nuclear industries (Refs. 9,10).

The mechanism that triggers or initiates the explosion is not known; however, two basic facts have been established. First, the causative mechanism is not due to chemical reaction (Ref. 13), and second, fragmentation of the sample material is usually involved. Both experimental results and analyses (Ref. 14) have shown that the heat-transfer rates required to release the observed energy from a smooth metal sample are several orders of magnitude higher than the maximum rates that can be obtained in laboratory studies. Thus it has been concluded by numerous investigators that fragmentation of the metal to generate large surface areas is required to obtain the observed explosion violence.

Several review articles have considered the potential problem of steam explosions with reference to the safety of nuclear reactors (Refs. 12,15). The articles by Brauer, et al. (Ref. 16), Ergen (Ref. 17), Witte, et al. (Ref. 12), and Flory, et al. (Ref. 18) describe the various factors thought to be involved in steam explosions, while Pearlman (Ref. 19) reviewed chemical reactions which occur between water and certain metals at elevated temperature. Epstein summarized many of the early developments regarding both physical and chemical metal-water explosions (Ref. 15). A variety of materials have been examined including molten aluminum in water (Refs. 5,6,20), copper mat in water (Refs. 21,22), iron in water (Refs. 23,24), smelt in water (Refs. 7,8), and, more recently, molten UO_2 in water (Refs. 25,26) and UO_2 in sodium (Refs. 26,27,28,29). An intensive investigation into the fundamental causes of physical explosions is being pursued at the University of Houston (Refs. 11,30-34).

B1.2 REPRESENTATIVE INCIDENTS INVOLVING STEAM EXPLOSIONS

Explosive incidents periodically occurring in the paper and metal industries have been reported. Several such incidents have been summarized (Ref. 11) and are cited to demonstrate the magnitude of the destructive forces present and the physical circumstances leading to the incidents.

B1.2.1 METAL INDUSTRY

Explosive accidents are infrequent in the metal industry but when they do occur, the destruction is severe.

B1.2.1.1 Mallory-Sharon Incident (Ref. 35).

In 1954, a titanium arc-melting furnace, which was water-cooled, exploded at a plant in Ohio. Nine injuries included four fatalities and property damage was $30,000. The explosion was believed to result from water entering the melting crucible.

B1.2.1.2 Reynolds Aluminum Incident (Ref. 35).

In 1958, an aluminum-water explosion occurred in Illinois involving some 46 injuries, 6 fatalities and approximately $1,000,000 in property damage. The explosion "rocked a 25 mile" area. Wet scrap metal was being loaded into a furnace when the explosion was triggered.

B1.2.1.3 Quebec Foundry Incident (Ref. 4).

The accident occurred in a foundry building approximately 18 million cubic-foot volume. One hundred pounds of molten steel fell into a shallow trough containing about 78 gallons of water. The resulting explosion injured mill personnel (one fatally) and caused $150,000 damage to the foundry building including cracking a 20-inch concrete floor, breaking 6000 panes of glass, and structural damage to the walls and ceilings. Damage was also incurred by another structure separated some 75 yards from the foundry building. This accident is one of the better documented incidents.

B1.2.1.4 Western Foundries Incident (Ref. 36).

In 1966, while 3000 pounds of molten steel was being poured from an electric furnace into a tile-lined ladle, a cable broke and the hot steel dropped into a water filled pit. The result was a violent explosion that injured three workers and tore a 600-square-foot hole in the roof of a building of some 12,000-square-foot floor area. The explosion was heard some 3 miles from the foundry.

B1.2.1.5 Armco Steel Incident (Refs. 37,38).

In 1967, an explosion occurred when molten steel fell on "damp" ground. A ladle containing some 30 tons of molten steel had been elevated some 40 feet when the ladle fell. Injuries sustained by some 30 workers included 6 fatalities. Evidently, sufficient moisture was present in the porous ground to trigger small-scale explosions that showered molten steel over a wide area. Although the injuries were attributed primarily to burns, an explosion accompanied the incident.

B1.2.1.6 East German Slag Incident (Ref. 2).

Appearing in 1959, an East German article discusses a number of slag-water explosions that have occurred in German open-hearth steel mills. Two accidents were discussed in which explosions resulted from spraying water on molten slag in open slag pits. One of the explosions resulted in a fatality and a number of other injuries. Severe structural damage was also noted. The second explosion was less severe. Both explosions were attributed to excess water on the slag passing down into the cracks to the hot molten material below. A third instance resulting in an explosion occurred when a slag pot was placed on a slag bed that had been previously sprayed with water. An explosion occurred, killing one man. The explosion was attributed to the heavy slag pot causing cracks in the surface of the hot slag bed and excess water on the surface getting into these cracks. Other explosions briefly described include rainwater leaking through an unsealed roof over a slag bed, resulting in an explosion, and two instances of explosions resulting when molten slag was poured into dump cars that had small amounts of water in the bottom.

B1.2.1.7 British Slag Incident (Ref. 3).

In 1964, an explosion occurred in a British steel mill when a ladle being used to tap a blast furnace was sprayed with lime water and returned to service. When it was next used, the ladle exploded when it was about three-fourths full of slag (12 to 14 tons). Damage to the structure and injuries to personnel were reported.

B1.2.2 PAPER INDUSTRY

The paper industry experiences explosions similar to those in the metal industry more frequently but they are less destructive. Explosions occur when paper smelt (mostly fused sodium carbonate with a few percent of sodium sulfide, sodium chloride, and minor ingredients) is quenched in large containers of "green liquor" (Refs. 7,8). Also, explosions frequently occur when boiler tubes in waste-heat boilers fueled by "black liquor" fail, and water is injected into hot molten smelt and black liquor. These explosions occur with considerable destruction to the furnace and plant facilities.

B1.2.3 NUCLEAR REACTOR INDUSTRY

Explosive vapor formation when hot, molten core materials have come in contact with water have also been observed in nuclear reactors.

B1.2.3.1 Canadian NRX Reactor (Ref. 35).

In 1952, at Chalk River, Ontario, during a low-power experiment, a nuclear excursion was experienced. Although the duration of the incident was less than 62 seconds, the damage was sufficient to result in contamination of the facility. The reaction between uranium and steam (or water) was the principal cause of damage.

B1.2.3.2 Borax I Reactor (Ref. 35).

In 1954, at the National Reactor Testing station in Idaho, the Borax I reactor was deliberately subjected to a potentially damaging power excursion in reactor safety studies. A power excursion lasting approximately 30 milliseconds produced a peak power of 19,000 megawatts with a total energy release of 135 megawatt-seconds. The power excursion melted most of the fuel elements. The reactor tank (1/2-inch steel) was ruptured by the pressure (probably in excess of 10,000 psi) resulting from the reaction between the molten metal and the water. The sound of the explosion at the control station (1/2 mile away) was comparable to that from 1-2 pounds of 40 percent dynamite.

B1.2.3.3 SPERT 1-D Reactor.

During the final test of the destructive test program with the SPERT 1-D core, damaging pressure generation was observed. Pressure transducers recorded the generation of a pressure pulse larger than 3000 psi which caused the destruction of the core. The pressure pulse occurred some 15 milliseconds after initiation of the power excursion. The power excursion rapidly overheated the fuel plates; the increased temperature melted the metal and the cladding of the fuel plates. After the transient, much of the fuel that had been molten was found dispersed in the coolant.

B1.2.3.4 SL-1 Reactor.

In January, 1961, a nuclear excursion occurred in the SL-1 reactor in Idaho. The total energy released in the excursion was approximately 130 Mw-sec (Ref. 51). Of this, 50 Mw-sec was produced in the outer fuel elements in the core. This portion of the energy was slowly transferred to the water coolant over 2 sec period, and no melting (uranium-aluminum alloy) of the outer fuel elements occurred. About 50-60 Mw-sec of the total energy release was promptly released by 12 heavily damaged inner fuel elements to the water coolant in less than 30 msec. This prompt energy release resulted in rapid steam formation in the core which accelerated the water above the core and produced a water hammer that hit the pressure vessel lid. The vessel, weighing about 30,000 lbs with its internals, sheared its connecting piping and was lifted approximately 9 feet into the air by the momentum transferred from the water hammer. Calculations of the mechanical deformation of the vessel indicate that about 12 percent of the prompt energy release or 4.7 percent of the total nuclear release was converted into mechanical energy (Ref. 52).

In each instance, under differing circumstances, a hot molten material fell, dropped, or spewed into a mass of cooler liquid and destructive pressure generation resulted. The complex mechanisms triggering this type of reaction are not completely understood.

It may be noted that all of the above reactor tests and incidents involved plate-type fuel elements consisting of uranium-aluminum alloy fuel clad in aluminum. These are substantially different from the uranium oxide fuel, Zircaloy-clad rods used in power reactors.

B1.3 METAL FRAGMENTATION AND THE INITIATION OF PHYSICAL EXPLOSIONS

The nature of the initiating phenomena for physical explosions is not clearly understood. However, fragmentation or particle dispersion is thought to be a requirement for such events. As indicated by Witte, Cox, and Bouvier (Refs. 11,12), there appear to be several possible mechanisms for initiating physical explosions (Table VIII B-1). All initiation mechanisms result in the spontaneous subdivision of the molten metal in intimate contact with water. After exhaustive experimentation with aluminum-water explosions, Long postulated that trapping or encapsulation of cold water at a solid surface under molten metal can lead to its rapid subdivision (Refs. 27,28). By his theory, the trapped water is rapidly vaporized and overcomes the surface tension forces of the metal with the result that the metal becomes finely divided.

Sallack (Ref. 7) and Nelson and Kennedy (Ref. 8) have proposed a surface cracking mechanism to explain explosions that occur within the bulk of the liquid. It has also been applied by Tetzner to explosions occurring at a solid interface (Ref. 2). The hypothesis is that as an unshattered ball of molten material (for example, salt or slag) begins to freeze in an environment of cold water, surface cracking occurs due to thermal stress, some water enters the bulk of the molten material and is trapped within fissures and pores, and the ball of semimolten material shatters as the water is converted to steam in the interior of the material.

Another mechanism, termed violent boiling, is predicated upon the fact that when a mass of molten metal is introduced into a liquid, a quenching process occurs (Refs. 39,40,53). In the transition region between film and nucleate, the boiling process can become very violent hydrodynamically with the result that large mixing forces are generated. Under such conditions the steam-metal interface is ruptured with the rocket-like acceleration of volumes of liquid water and molten material into the steam interface between the two phases. This dispersion can be compared to the Leidenfrost phenomena when water contacts a hot surface or to water droplets in hot oil. Swift and Baker (Ref. 53) suggest that fragmentation may only occur when the materials pass through the range of temperature from the boiling point to critical point of the fluid (in which violent boiling can occur) prior to freezing of the melt. This restriction would not permit fragmentation in UO_2-H_2O systems.

The shell or encapsulation theory has been proposed by researchers at the University of Kansas (Refs. 16,18). These researchers performed a series of experiments using high-speed photography to study the fragmentation of molten metals in water. Experiments were performed by dropping a number of hot metals (Pb, Sn, Bi, Zn, Cu, Al, Hg and Wood's metal) into water and photographically recording the ensuing reaction. Brauer suggests that molten globules are blown apart by an internally generated pressure (Ref. 16). This theory hypothesizes that somehow liquid is trapped inside the molten-metal globules, the liquid rapidly vaporizes, and the resulting pressure increase fragments the metal. Brauer's hypothesis coincides to a great extent with the surface cracking hypothesis.

Molten-metal fragmentation may also result when inertial forces acting on the molten metal (as it is passing through the liquid) exceed the surface tension forces of the metal (Ref. 41). Such an initiation mechanism has been proposed by Witte and co-workers (Ref. 11). The ratio of the inertial forces to the surface-tension forces of a molten-metal globule is expressed as the Weber number, $N_W = prU^2/\gamma$. If the Weber number exceeds a critical value, about 5-10 for molten-metal drop tests with Hg, Pb, Bi, and Sn, the inertia of the particle overcomes the surface-tension energy and the globule fragments into smaller, more stable sizes.

Forced initiation refers to any event brought about by an external driving force which leads to the rapid dispersal of molten metal in water. Occurrences of this type have been observed in foundry practice. Also, Higgins brought about physical explosions by using blasting caps and spray injection techniques to disperse various molten metals (Zr, Zircaloy-2, Al, U, NaK, and stainless steel) in water (Refs. 42,43). The spray-injection experiments (performed in an explosion dynamometer) permitted measurement of explosive power, reaction time, reaction efficiency and the effects of temperature and droplet size (Ref. 43). Peak overpressures were of the order of 20 to 200 psig and pressure-rise rates were approximately 5000 to 120,000 psig/sec. Explosion periods or times required for the pressure rise were of the order of milliseconds.

The superheat theory used by Katz and others to explain the occurrence of vapor explosions in the LNG industry (Refs. 44,45,46) it has been extended by Fauske (Ref. 29) to explain the mechanism of UO_2-Na vapor explosions. Contact between LNG and water at first results in the establishment of film boiling of the LNG. The most volatile component of the LNG, methane, is preferentially depleted in time, and an increase in the boiling point of the LNG results. The stable vapor blanket becomes thinner, is eventually eliminated, and liquid-liquid wetting contact between the LNG and the water is substituted. Unlike that in solid-liquid contact, unstable nucleate boiling cannot commence because nucleation sites are lacking. A thin layer of LNG along this contact surface explodes because the instantaneous contact temperature is above the limit of superheat temperature of the enriched LNG, for which homogenous nucleation occurs. This exploding layer presumably fragments and disperses some or all of the remaining LNG into the water, thereby triggering the main explosion.

For UO_2 and Na, on the other hand, Fauske points out that the development of film boiling along the liquid-liquid interface would require a UO_2 temperature much higher than the melting point of UO_2, hence wetting contact occurs immediately. However, the instantaneous wetting contact temperature is well below the superheat limit for Na, and the type of triggering event described above for LNG does not occur. Instead, any globule of liquid Na that might become entrained in the UO_2 would heat up relatively slowly, depending upon its

size, until a substantial portion or all of the globule became superheated, in the absence of induced nucleation sites. When the interface temperature finally does reach the limit of superheat, the entire superheated portion of the globule would explode violently. There is no need for a prior fragmentation and dispersion mechanism, although whatever fragmentation and dispersion this explosion could produce in the rest of the mixture would contribute to the intensity of the explosion. In the actual reactor situation, the probability of the occurrence of such an explosion would depend upon the density of nucleation sites such as fission fragments and gas bubbles that could initiate prior boiling of the liquid Na.

The collapsing-vapor-bubble theory recently advanced by researchers at the University of Houston is based on study of the way in which the vapor film surrounding a heated silver sphere was destabilized, i.e., the sequence of events that causes the boiling behavior to become transitional between the film and nucleate regimes. Two distinctive mechanisms for destabilization were identified: one, a precipitous collapse and the other, progressive instability. The precipitous collapse occurs very rapidly, on the order of 0.250 millisecond, while the progressive instability requires from 50 to 100 milliseconds for completion. The progressive instability was triggered by small bubble-like irregularities that move on the liquid-vapor interface and it occurs only in saturated (or nearly-saturated) water. Precipitous collapse occurs in subcooled water. There appeared to be a direct relationship between the two types of vapor film collapse and observed fragmentation behavior for molten materials being rapidly quenched. Extensive fragmentation generally occurs only in subcooled systems; here, the vapor film collapse is very rapid and energetic. Little fragmentation occurs in saturated systems; here, the collapse is relatively slow and nonenergetic.

The superheat-limit theory has been combined with the collapsing-vapor-bubble theory to formulate a jet-action theory for triggering the usual type of vapor explosion - one that requires rapid fragmentation and dispersion of one liquid into the other (Ref. 47). In the jet-action theory, the exploding thin film degenerates into a multiplicity of vapor bubbles or globules as it expands. The expansion is greater toward the less dense liquid. When these globules collapse, the rectilinear motion toward the less dense liquid accelerates, as is necessary to conserve linear momentum. Shape instabilities, developing as the globules collapse, eventually result in the formation of jets of the more dense liquid that project through the globules into the less dense liquid (Ref. 48). Experimental evidence has been presented on the role played by collapsing cavities and the accompanying formation of microjets in initiating detonations in slow-burning liquid films (Ref. 49).

Violent high-frequency oscillations of the vapor film have been observed under some conditions following pulsed-laser-beam transient heating of a metal film immersed in water (Ref. 50). The resultant periodic liquid-liquid contact results in a greatly increased heat flux over that ordinarily obtained in the film-boiling regime. The authors postulate that the pressure pulses developed during the collapse phases of the oscillations may be important in the dispersal of the hot molten material in vapor explosions. This dispersion could also be augmented by the formation of jets, as previously described, during the collapse phases of the oscillations.

B1.4 INTERACTION OF UO_2 WITH WATER

Virtually no data could be found which were directly applicable to the light-water-reactor meltdown situations considered in this program, i.e., large amounts of molten UO_2 falling into saturated or near-saturated water (93 C for the cases considered). However, two experimental studies directed at investigating the reaction of molten UO_2 with water are applicable to some extent (Refs. 25,26).

At Battelle's Northwest Laboratory, the reaction of molten UO_2 with water was investigated in a high-pressure furnace by allowing melted UO_2 samples (1 to 10 grams) to fall into water heated to various temperatures (see Table VIII B-2). The tested UO_2 samples were analyzed for the degree of oxidation by coulimetric titration. Oxygen-to-metal ratios increased from an average initial value of 2.002 to values between 2.06 to 2.16, depending on the initial water temperature (30 to 250 C). Water temperatures were arbitrarily selected to determine the effects of water temperature on the final results and encompass the temperature range expected in the case of a major accident. The oxygen-to-metal ratio values correspond to a maximum hydrogen generation of 12 ml (STP)/g UO_2. The oxidation product, as deter-

mined from Guinier X-ray powder patterns, was U_4O_9.

Attempts to measure pressure transients, produced by evaporation and/or boiling of water in contact with the molten UO_2, were generally unsuccessful. Such measurements, if successful, would have been directly applicable to possible physical explosions of UO_2 in water. Of significance, however, was the fact that rapid injection of molten UO_2 into water did not produce a powdered end product. Rather, the quenched UO_2 was very friable and could be readily reduced to a coarse powder. Tyler screen analyses on three different powdered samples gave essentially identical average particle diameters of 620 microns (0.062 cm) (see Fig. VIII B-1).

In two experiments, Amblard, et al. dropped approximately 1 gram each of molten UO_2 at 3000 and 3100 C, respectively, into 10 grams each of water at 20 C and atmospheric pressure (Ref. 26). In both experiments, long hollow tubes of UO_2 that formed, imprisoned the coolant. In the first experiment (3000 C), the particles were about 10 to 12 mm long and 3 to 6 mm wide. In the second experiment (3100 C), the particle lengths ranged from about 6 to 27 mm and width from about 1.5 to 2.5 mm. In a third experiment, a cylindrical sample of UO_2 about 5.7 mm in diameter by 55 mm long (i.e., about 15 grams) clad in stainless steel was melted in a pressure vessel capable of withstanding a pressure of 850 bars (12,325 psi). The stainless steel cladding was cooled by hot water adjacent to the clad under pressure from a cover gas. Upon heating, the clad was pierced by the molten UO_2 and the fuel was able to disperse in the water which was at 230 C (446 F). The clad fusion and UO_2-water contact were photographed. Some pulverization of the UO_2 did occur, but was much less than experienced in similar experiments performed with UO_2 in liquid sodium. The pressure in the vessel was recorded as a function of time. This trace did not indicate appreciable dynamic overpressure but rather a slow pressure increase of 15 bars (218 psi), i.e., from 150 bars (2175 psi) absolute to 165 bars (2393 psi) absolute in approximately 10 seconds. The static pressure increase of water and cover gas was thought to correspond to an enthalpy increase resulting from 50 percent of the UO_2 in the sample being molten.

B1.5 EXPERIMENTS WITH METALS IN WATER

Numerous experiments have been conducted involving the potential for explosions when molten metals come into contact with water (Refs. 6,16,18).

Long conducted some of the initial experiments on explosive vapor formation by means of aluminum (m.p. = 1200 F) drop tests (Ref. 5). More than 880 experiments were conducted under conditions that simulated sudden accidental pouring of molten aluminum into a pool of water. Fifty pounds of commercially pure aluminum in the molten state was suspended in a crucible above a container partially filled with water. When the molten metal had obtained the desired temperature, a remote-controlled plug was removed from the crucible and the molten metal flowed through a tap hole into the water. Long investigated about ten variables and noted that the molten aluminum when at 1382 F falling into the water tank did not produce an explosion if the water temperature was at least 140 F or above,[1] provided the water was not highly ionic. Under highly ionic conditions (e.g., addition of NaCl to produce a 15 percent salt solution) explosions could be obtained at temperatures up to 172 F but not in saturated water.

Brauer, Green, and Mesler conducted a study in which aluminum (MP = 1220 F) and lead (MP = 621 F) were heated to temperatures well above the melting point and dropped into liquid water with the objective of obtaining fragmentation of the metal (Ref. 16). A high-speed motion picture camera recorded macroscopic observations. In general, it was noted that fragmentation did not occur for metal temperatures just slightly above the metal's melting point (i.e., the higher the metal temperature above its melting point the greater the fragmentation) or for cooling-water temperatures greater than 60 C (140 F). For a given metal, fragmentation if it occurred, was more violent for the lower water temperatures.

Flory, Paoli, and Mesler (Ref. 18) carried out numerous experiments at Kansas University. Heating was accomplished by an induction coil and the hot molten metal was dropped into a Plexiglas tank containing water. Pressure disturbances were monitored and the interactions were photographed with a high-speed camera. Tests included a wide range of metal and

[1] Actually, Long's data indicate that he observed explosions up to 122 F (see Table 7 of Reference 5).

bath temperatures. Metals studied included lead (MP = 621 F), tin (MP = 449 F), bismuth (MP = 520 F), zinc (MP = 787.1 F), copper (MP = 1981 F), aluminum (MP = 1220 F), mercury (MP = 37 F), Wood's metal, and Cerro Bend. Numerous experimental observations were made concerning fragmentation mechanisms. The temperature of the quench water was varied from ∿8 C to 100 C (17.6 F to 212 F). "Near the freezing point of water the violence of fragmentation is not a function of bath temperature, while above 25 C (77 F) the violence and extent of fragmentation decreased rapidly to zero at 90 to 100 C (194 to 212 F). Tests with several metals dropped into liquid nitrogen at its boiling point gave no fragmentation whatever, giving supporting evidence to the results of the water experiments, namely that metals will not fragment in a saturated liquid."

B2. CONCLUSIONS

The single most-pertinent question that must be resolved is whether molten UO_2 can be fragmented to give the high surface areas required to initiate a physical explosion when contacted with water. Although pertinent, the above described experiments with UO_2 and water are by no means definitive, and, in fact, no completely definitive experiments could be found in the literature.

It is questionable whether the experimental observations with regard to dropping modest amounts of "relatively low temperature" molten metals into water should be extrapolated to the case of large amounts of molten UO_2. The melting point of the UO_2 is so much higher than that of the other materials investigated that entirely different phenomena could govern the process. The quantity of molten material that could interact with water in a meltdown accident is orders of magnitude greater than has been investigated in any controlled experiments; such an extrapolation in size would be fraught with uncertainties even if the phenomenology were understood. The experiments with the various molten metals indicate that the probability of obtaining a high degree of fragmentation decreases as the temperature of the water approaches saturation.

Taking into account the history of steam explosion in industry observed under a wide variety of conditions, the modest amount of work available with UO_2-water interactions, and the considerable experimental work on various metals in water, it is concluded that the probability of initiating UO_2-water explosions that require a high degree of fragmentation is very low. Such would be the most violent types of explosions which require effective average particle diameters of less than about 2000 microns, as described in Appendix C. For the less violent explosions, also capable of causing containment failure, the average particle diameter can be between about 2000 to 5000 microns (2 to 5 mm) and the probability must be considered somewhat greater.

The overall probability of occurrence of an event in a PWR or BWR reactor vessel that would produce an effective surface area equivalent to 2- to 5-mm diameter particles of UO_2 and disperse them through a significant part of the volume of water is considered to be low.

References

1. Anonymous, "A Method for Handling Steelmaking Slag", Iron & Steel Eng., 28 (10), 85-89 (October, 1951).

2. Tetzner, Herman, "Slag Explosions in Open-Hearth Steelworks", Neue Hutte, 6 (4), 352-359 (June, 1959).

3. Anonymous, "Water was Energy Source in Ladle Explosion", Steel Times, pp. 56-57 (January, 1964).

4. Lipsett, S. B., "Explosions from Molten Material and Water", Fire Technology, 2 (2), 118-126 (May, 1966).

5. Long, G., Stroup, P. T., and Ennor, W. T., "Explosions of Aluminum and Water", Report No. 2-50-33 (NP-5471), Process Metallurgy Division, Aluminum Research Laboratories, Aluminum Company of America (1950); Long, G., "Explosions of Aluminum and Water - Cause and Prevention." Metal Progr., pp. 107-112 (May, 1957).

6. Rengstorff, G. W. P., Lemmon, A. W., Jr., and Hoffman, A. O., "Review of Knowledge on Explosions Between Molten Aluminum and Water to the Aluminum Association", Battelle's Columbus Laboratories, p. 53 (April, 1969).

7. Sallack, J. A., "An Investigation of Explosions in the Soda Smelt Dissolving Operation", Pulp and Paper Mag. (Canada), 56 (9), 114-118 (1955).

8. Nelson, W., and Kennedy, E. H., "What Causes Kraft Dissolving Tank Explosions - I. Laboratory Experiments", Paper Trade J., 140 (7), 50-56 (July, 1956).

9. Ivins, R. O., and Baker, L., "Chemical Engineering Division Semiannual Report, January-June, 1964", ANL-6900, pp. 270-280 (August, 1964).

10. Mally, C. T., et al., "Kinetic Studies of Heterogenous Water Reactors. Annual Summary Report, 1964", STL-372-12 (December 30, 1964).

11. Bouvier, J. E., Witte, L. C., and Cox, J. E., "The Vapor Explosion - Heat Transfer and Fragmentation. I. Introduction to Explosive Vapor Formation", Technical Report No. ORO-3936-1, Department of Mechanical Engineering, University of Houston, 21 pp. (November, 1969).

12. Witte, L. C., Cox, J. E., and Bouvier, J. E., "The Vapor Explosion", Journal of Metals, 22 (2) 39-44 (February, 1970).

13. Epstein, L. F., "Analytical Formulation for the Reaction Rate", Metal Water Reactions, 6 37-39 (September, 1959).

14. Higgins, H. M., "The Reaction of Molten Uranium and Zirconium Alloys With Water", Aerojet General Report No. AGC-AE-7, p. 18 (April, 1965).

15. Epstein, L. F., "Recent Development in the Study of Metal-Water Reactions", Progr. Nucl. Energy, Ser. IV, 4, 461-483 (1961).

16. Brauer, S. D., Green, N. W., and Masler, R. B., "Metal/Water Explosions", Nucl. Sci. Eng., 31 (3), 551-554 (1968).

17. Ergen, W. K., et al., "Emergency Core Cooling - Report of Advisory Task Force on Power Reactor Emergency Cooling", TID-24226 (1966).

18. Flory, K., Paoli, R., and Mesler, R., "Molten Metal-Water Explosions", Chemical Engineering Progress, 65 (12), 50-54 (December, 1969).

19. Pearlman, H., "Chemical Reactions Between Water and Certain Metals at Elevated Temperatures", U.S. Atomic Energy Commission, NAA-SR-Memo-858, p. 22 (1954).

20. Hess, P. D., and Brondyke, K. J., "Causes of Molten Aluminum-Water Explosions and Their Prevention", Metal Prog., (4), pp. 93-199 (April, 1969). (Presented at the Metals Congress, Detroit, October, 1968.)

21. Azuma, Kiyoshi, Goto, Sakichi, Kametani, Hiroshi, "The Explosion of Mat by Water. I. Nature of the Explosion", Nippon Kogyo Kaishi, 73, 295-300 (1957).

22. Azuma, Kiyoshi, Goto, Sakichi, Kametani, Hiroshi, "The Explosion of Mat by Water. II. Chemical Reaction Between the Molten Copper Mat and Steam", Nippon Kogyo Kaishi 73, 449-452 (1957).

23. Murty, G. V. L. N., Subba Rao, D., and Ramaswami, T. R., "Highly Water-Reactive Forms of Transitional Elements of the Iron Groups", Current Sci. (India) 25, 197-188 (1956).

24. Gasik, M. I., and Khitrik, S. I., "Interaction of Liquid Iron with a Steam-Hydrogen Mixture", Met. i Koksokhim., Mezhvedonstv. Resp. Nauchn.-Tekhn. Sb. 3, 5-16 (1965).

25. Gilby, R. L., "Reaction of Molten UO_2 With Water", BNWL-362 (1967).

26. Amblard, M., Semeria, R., Vernier, P., Gouzy, A., and Najuc, M., "Contact Effect Between Molten UO_2 and Sodium and Molten UO_2 and Water", EURFNR-811 (March 3, 1970).

27. Anderson, R. P., and Armstrong, D. R., "Laboratory Tests of Molten-Fuel-Coolant Interactions", Trans. Amer. Nucl. Soc., 15 (1), 313 (June, 1972).

28. Armstrong, D. R., Testa, F. J., and Raridon, D., Jr., "Interaction of Sodium With Molten UO_2 and Stainless Steel Using a Dropping Mode of Contact", ANL-7890 (December, 1971).

29. Fauske, Hans K., "On the Mechanism of UO_2-Na Vapor Explosions", Nuclear Science Engineering, 51, 95-101 (1973).

30. Stevens, J. W., Bullock, R. L., Witte, L. C., and Cox, J. E., "Transition Boiling From Spheres to Water", AEC Report ORO-3936-3 (April, 1970).

31. Hsico, K. H., Cox, J. E., Hedgecox, P. G., and Witte, L. C., "Pressurization of a Solidifying Sphere", AEC Report ORO 3936-4 (April, 1970).

32. Witte, L. C., et al., "Rapid Quenching of Molten Metal", AEC Report ORO-3936-6 (August, 1971).

33. Bradley, R. H., et al., "Investigation of the Vapor Explosion Phenomenon Using a Molten-Metal Jet Injected into Distilled Water", AEC Report ORO-3936-7 (October, 1971).

34. Witte, L. C., et al., "Transition Film and Transition Boiling from a Sphere", AEC Report ORO-3936-9 (September, 1972).

35. Epstein, L. F., "Reactor Safety Aspects of Metal-Water Reactions", Metal-Water Reactions VII, GEAP 3335, p. 2 (January 31, 1960).

36. Thomas, P., "Three Hurt in Foundry Blast", The Denver Post (February 14, 1966).

37. Anonymous, "Hot Metal Spilled at Plant", Houston Chronicle, 67 (66), Section 1, p. 1 (December 18, 1967).

38. Anonymous, "6th Worker Dies in Armco Tragedy", The Houston Post, No. 30, 211, Section 1, p. 10 (December 21, 1967).

39. Vogel, et al., "Reactor Development Program Progress Report for February 1969", ANL-7553 p. 118 (March 25, 1969); "Reactor Development Program Progress Report", ANL-7478, p. 128 (July, 1968).

40. Firstenberg, A. F., et al., "Kinetic Studies of Heterogenous Water Reactors. AEC Research and Development Report Annual Summary Report 1966", STL-372-50 (December, 1966).

41. Duffield, R. B., and Lawroski, S., Argonne National Laboratory, Reactor Development Progress Report, ANL-7399, pp. 162-167 (November, 1968).

42. Higgins, H. M., "A Study of the Reactions of Metals and Water - Interim Report", USAEC Report AECD-3664 (April, 1955).

43. Higgins, H. M., and Schultz, R. D., "The Reaction of Metals with Water and Oxidizing Gases at High Temperatures", USAEC Report IDO-28000, Aerojet-General Corp. (April 30, 1957).

44. Nakanishi, E., and Reid, R. C., "Liquid Natural Gas-Water Reactions", Chem. Eng. Prog., 67 (12), 36 (1971).

45. Katz, D. L., and Sliepcevich, C. M., "LNG/Water Explosions: Cause and Effect", Hydrocarbon Processing (November, 1971).

46. Enger, T., and Hartman, D. E., "Explosive Boiling of Liquified Gases on Water", paper presented at the National Research Council Conference on LNG Importation and Terminal Safety, Boston, Mass. (June 13, 1972).

47. Simon, R., "Computer Model Study of the Smelt-Water Physical Explosion", paper to be presented at the Atlanta Heat Transfer Conference, A.I.Ch.E. (August, 1973).

48. Chincholle, L., "Bubbles and the Rocket Effect", J. Appl. Phys., 41, 4532 (1970).

49. Bowden, F. P., and Chaudri, M. M., "Initiation of Explosion of AgN_3 and βPbN_6 Single Crystals by a Collapsing Bubble", Nature, 220, 690 (1968).

50. Board, S. J., Clare, A. J., Duffey, R. B., Hall, R. S., and Poole, D. H., "An Experimental Study of Energy Transfer Processes Relevant to Thermal Explosions", Int. J. Heat Mass Transfer, 14, 1631 (1971).

51. USAEC Idaho Operations Office, "IDO Report on the Nuclear Incident at the SL-1 Reactor, January 3, 1961, at the Nation Reactor Testing Station", IDO-19302 (1962).

52. Proctor, J. F., "Adequacy of Explosion-Response Data in Estimating Reactor-Vessel Damage", Nuclear Safety, 8 (6), 565 (November, 1967).

53. D. L. Swift and L. Baker, "Experimental Studies of the High-Temperature Interaction of Fuel and Cladding Materials with Liquid Sodium", ANL-7120, pp 839-847 (1965).

TABLE VIII B-1 METHODS LEADING TO METAL FRAGMENTATION AND THE INITIATION OF PHYSICAL EXPLOSIONS

Initiation Method	Reference
Trapping Water	27, 28
Fissures, Surface Cracking	2, 7, 8
Violent Boiling	39, 40, 53
Shell Theory	16, 18
Inertial Forces (Weber Number Effects)	11, 41
Forced Initiation	42, 43
Superheat Theory	29, 44, 45, 46
Collapsing Vapor Bubble	34
Jet Formation	47
Oscillating Vapor Blanket	50

TABLE VIII B-2 RESULTS OF MOLTEN UO_2 BEING DROPPED INTO WATER AT VARIOUS TEMPERATURES (Ref. 25)

Melted UO_2 Weight, g	Water Temperature, C	T, C	Ratio Oxygen/Uranium		Calculated H_2 Generation, ml (STP)/g UO_2
			Before	After	
0.756	27	5	2.002	2.058	4.5
9.37	28	73	2.005	2.080	6.2
0.571	100	5	2.002	2.077	6.2
1.126	105	15	2.004	2.082	6.5
7.705	110	61	2.012(a)	2.128	9.6
9.25	100	80	2.002	2.087	7.1
8.49	210	70	2.012(a)	2.155	11.9
11.381	255	49	2.029(a)	2.146	9.7
9.13	260	40	2.006	2.142	11.3

(a) Oxidation resulting from leakage of water into furnace chamber from water vessel.

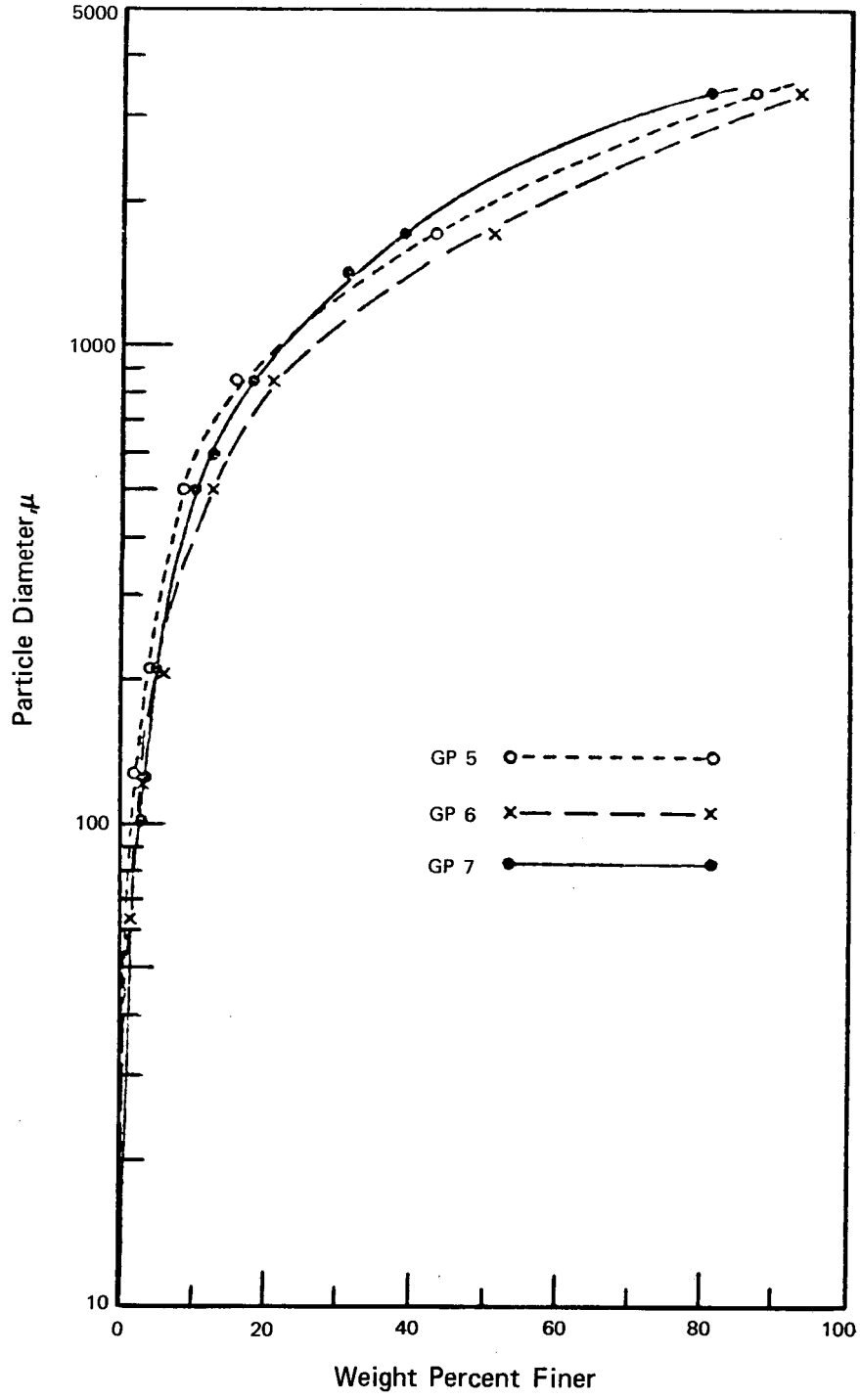


FIGURE VIII B-1 Particle Size Distribution of Quenched UO_2 Samples

APPENDIX C

MODEL STUDY OF PHYSICAL EXPLOSIONS

Appendix C

Table of Contents

Section		Page No.
C1.	MODEL GEOMETRY	VIII-93
C2.	EXPLODING MIXTURE	VIII-94
C3.	BASIC MODEL RELATIONSHIP	VIII-95
	C3.1 Mathematical Equations	VIII-95
	C3.2 Heat-Transfer Rate	VIII-95
	C3.3 Additional Assumptions	VIII-96
	C3.4 Chemical Reactions	VIII-97
	C3.5 Vessel - Wall Stresses	VIII-97
C4.	RESULTS OF COMPUTATIONS	VIII-98
C5.	MATHEMATICS OF THE MODEL	VIII-100
	C5.1 Basic Model Equations	VIII-100
	C5.1.1 Conservation of Energy	VIII-100
	C5.1.2 Conservation of Momentum	VIII-101
	C5.1.3 Conservation of Mass	VIII-102
	C5.1.4 Equations of State	VIII-102
	C5.2 Mechanical Response Time	VIII-102
	C5.3 Dynamic Stresses in Vessels Walls	VIII-103
C6.	HEAT-TRANSFER-RATE CONSIDERATIONS	VIII-103
	C6.1 Heat-Transfer Coefficient	VIII-103
	C6.1.1 Radiactive Heat Transfer	VIII-104
	C6.1.2 Conductive Heat Transfer	VIII-104
	C6.2 Convective Heat Transfer	VIII-104
	C6.3 Temperature Gradient in Melt Particles	VIII-105
REFERENCES		VIII-107

List of Tables

Table		Page No.
VIII C-1	Values of Parameters Used For Massive Grid-Plate Failure, Steam-Explosion Computations.....	VIII-109

List of Figures

Figure		Page No.
VIII C-1	Basic Computational Model Geometry.....	VIII-110
VIII C-2	Typical Computer Results.....	VIII-110
VIII C-3	PWR Results.....	VIII-111
VIII C-4	BWR Results.....	VIII-111
VIII C-5	Dimensionless Presentation of Calculational Results.....	VIII-112

Appendix C

Model Study of Physical Explosions

This appendix describes the analytical model used to provide information regarding both the probability and damage potential of rapid energy exchanges between large quantities of molten materials and water. These exchanges, termed "physical" or "steam explosions" in this description, are pertinent to the overall study as they could occur following a significant core meltdown during a postulated accident. For the purposes of this discussion the term "explosion" is broadly defined as any heat-transfer event during which sufficient mechanical energy could be developed in forms that could result in appreciable damage or deformation to surrounding structures.

The phenomenological model, though necessarily simplified, includes treatment of the basic physical phenomena. Using this model in parametric and sensitivity studies permitted the development of region mappings which provided guidance as to the probability and damage potential of the various events in addition to the identification of the more significant variables. The model proved to be adequate for the purposes intended and a more sophisticated treatment was not considered warranted. It should be reiterated that for the purposes of this evaluation the meltdown event was assumed to occur; only the potential ensuing events are addressed here.

It should be recognized that the simple model that has been used in this study probably yields an overestimate of the conversion of thermal energy to mechanical energy than would occur in an explosive event. The results of the model indicate conversion efficiencies of 10 percent or greater. Conversion efficiencies observed in experiments or accidents are typically lower.

This appendix presents the various aspects of the model along with the results, detailed mathematical and heat transfer aspects, and pertinent references.

C1. MODEL GEOMETRY

Figure VIII C-1 shows the geometry of the primary reactor vessel assumed in the model after all or a portion of the molten core has dropped into the water below it, at some time after the beginning of a meltdown accident. This geometry consists basically of a steel cylinder, closed on both ends with flat steel plates, and with the mixture initially occupying the lower portion of the cylinder and expanding upwards as the explosion proceeds.

The hemispherical top head of the actual vessel is replaced in the model with a cylindrical end cap of equal volume. The bottom plate of the model represents the top of the grid plate for the computations involving dropping of the molten portion of the core of the PWR into the water remaining above the grid plate. For the computations involving massive grid-plate failure, in which all of the core and the molten grid plate drop into the water reservoir below the grid plate, the hemispherical bottom head is also replaced by a cylindrical end cap of equivalent volume.

As shown in Fig. VIII C-1, the model also provides for orifices of a given total area located at a given distance above the bottom plate. The steam and hydrogen above the mixture leak out of these orifices, at a rate given by the standard orifice formula, as long as the top of the mixture is below the orifice level. When the mixture rises above the orifice level, it leaks out instead.

The actual geometry of the vessel, of course, could be simulated more closely by the model. The actual shapes of the end caps and changes in effective cross section as a function of vertical position in the vessel could be taken into account, including the effects of various structures within the vessel. Such refinements would add to the complexity of the computations, but would not be expected to have any major effect on the final results for the PWR. However, for the BWR calculations the effects of major internal structures above the reactor core cannot be neglected. How these effects are taken into account is described later.

The model provides for the possible existence of a reservoir of a given volume above the top of a vessel in order to simulate steam explosions that may occur at the bottom of the reactor cavity if the bottom head should melt through.

C2. EXPLODING MIXTURE

The "exploding" mixture consists of the volume of water, steam, and hydrogen gas below the melted-down portion of the reactor core plus the molten and solidified portion of the core that has dropped into this volume. The core materials dropping into the water are assumed to become uniformly dispersed throughout the volume.

Transfer of heat from the hot core components to the colder water-steam-gas components of the exploding mixture causes the mixture to expand, primarily due to the generation of steam. Expansion is essentially confined to the upward direction by the vessel walls and is impeded initially by the self-inertia of the exploding mixture and later by the compression of the steam and hydrogen gas above the top of this mixture. The pressure developed in the mixture by the inertial impedance to free expansion may become great enough to rupture the sides and bottom of the reactor vessel. It may also propel upward a substantial portion of the exploding mixture with sufficient kinetic energy to rupture the top head of the vessel, due to a combination of rapid compression of the gas and vapor above the mixture and impact of the mixture on the top head. It may thereafter impart considerable kinetic energy in the form of upward motion to the top head and to any shielding or other structures above it. The resultant "projectile" may reach the dome of the containment building and cause failure. The direct effect of pressure potentially rupturing the vessel walls as well as the later effect of the development of the "projectile" phenomenon are considered in the computational model.

As discussed in the introduction, the term "explosion" is broadly defined as any heat-transfer event in which sufficient mechanical energy is developed in forms that can result in an appreciable level of deformation or damage to surrounding structures. These forms may consist of potential energy (pressure) and/or kinetic energy (directed motion of mass). This broad definition of explosion also encompasses the ordinary definition of the rapid development of a high-pressure pulse that leads to the generation and propagation of a shock wave in a medium.

The exact procedure for computing the dynamic response of the exploding mixture, i.e., the pressure buildup and motion of the mixture as a function of vertical position, is to divide the mixture, or medium, into a number of horizontal layer pairs. Each layer pair consists of a lower layer that incorporates the expansion and compliant properties of the medium at the vertical location of the layer pair and an upper layer that incorporates its inertial properties. The resultant equations and their stepwise numerical integration in time, beginning with the initial conditions, simulate the solution of the nonlinear acoustic wave equation for the medium, with pressure generating sources distributed throughout the medium.

The simplified model shown in Fig. VIII C-1 consists on only one such layer pair. The use of a single layer pair results in simplification of the computations; the model then essentially solves a set of simultaneous ordinary differential equations rather than a set of partial differential equations with mixed boundary conditions. This simplification permitted the application of a previously developed computer code for smelt-water explosions (Ref. 1) to the reactor vessel case, an adaptation which involved conversion from spherical to rectilinear geometry and several other modifications.

If the upward motion of the top surface of the exploding mixture can be assumed to result from a uniform expansion of the mixture, the single layer pair is best approximated by considering the upper layer to be a "piston" containing half the mass of the mixture. Uniform expansion of a homogeneous medium with the bottom end fixed in position entails an acceleration, velocity, displacement, and negative of the pressure gradient that vary linearly from zero at the bottom to maximum values at the top surface. The pressure itself would vary quadratically from a maximum value at the bottom to a value corresponding to the pressure in the gas and vapor above the mixture at the top.

For acoustic wave propagation effects, the uniform expansion approximation is good for wavelengths greater than about 6 times the depth of the medium. The time scales of the pressure events obtained from the results of the computations show this wavelength condition

to be met under most circumstances of interest. However, it does break down under one important circumstance: when the gas above the top surface of the medium becomes rapidly compressed as this surface approaches the top head of the vessel, a compression wave also propagates downward into the medium. The Taylor-type of instabilities (Ref. 2) that can develop in the shape of this surface when its upward motion is rapidly decelerated may also contribute to the inaccuracy of the uniform-expansion assumption at this stage. Another factor that tends to question the uniform-expansion assumption to some extent is the pressure difference that develops between the bottom and the top of the medium. This precludes the uniformity of generation and expansion of steam throughout the medium which is inherent in the assumption of uniform expansion.

C3. BASIC MODEL RELATIONSHIP

C3.1 MATHEMATICAL EQUATIONS

The mathematical equations of the model, which are presented and discussed in detail in the Mathematics Section, are based on four fundamental laws.

a. Conservation of energy: The rate of heat input to the colder portion of the exploding mixture equals the sum of the rates of change in internal energy of the liquid water, steam, and gas, the rates of work done in their expansion, and the latent heat of vaporization of water multiplied by the mass rate of change of liquid water to steam. At the same time this must equal the rate of sensible heat loss from the various components of the melt plus the sum of the products of heats of fusion times mass rate of conversion from liquid to solid for the various melt components.

b. Conservation of momentum: The net force on the inertial layer equals the rate of change of its momentum (which includes effects of changes in its mass).

c. Conservation of mass: For each component, the sum of the products of volume and density for its two phases equals the original mass of the component less the loss of mass by flow through the orifices and by chemical reactions.

d. Equations of state: The density of each phase is a unique function of temperature and pressure.

C3.2 HEAT-TRANSFER RATE

The rate at which heat is transferred from the hot melt to the colder components of the exploding mixture is of primary importance in the model relationships. Heat-transfer considerations are discussed in detail in a later section. In brief, the rate of heat transfer is given by the product of a heat-transfer coefficient, the total surface area of the melt exposed to the colder components, and the temperature difference between the two.

The heat-transfer coefficient was computed by assuming that some fraction of the assumed spherical melt particles is surrounded by an essentially infinite body of steam, while the remainder is surrounded by a blanket of steam, as in stable film boiling, beyond which lies an essentially infinite body of liquid water. This fraction is equal to the volume fraction of the water that is in the form of steam. For the former, heat transfer is essentially by conduction into the steam. For the latter, heat transfer is essentially that required to replenish the steam film against loss by natural convection, as given by Bronley's equation (Ref. 3). Forced-convection heat transfer due to turbulent relative velocities between the melt particles and the water-steam-gas is neglected, since these velocities are not known. The average value of the relative velocity is zero, in accordance with one of the special assumptions discussed later. The radiative heat-transfer coefficient, which is significant at the tempeature of the melt in question (initial value, 2850 C - just above the melting point of UO_2), is added to the conductive and/or convective coefficients.

The surface area in the heat-transfer-rate equation is computed on the basis of the assumed average particle diameter for the dispersed melt. The surface temperature of the melt was initially taken to be the same as the average temperature of the melt particle (isothermal melt assumption). This is a good assumption for melt particles of 100 microns and smaller, but not for the larger particles. An approximate analysis developed to take into account the finite rate of heat transfer within the melt particles is described in the mathematics section.

The rate of transfer of heat from the melt to the water-steam per unit mass of water depends also on the speed that the melt drops into the water. The model assumes that the melt drops into the water at a uniform rate over a finite time interval, which is specified in the input information, and the heat-transfer mathematics takes this finite drop rate into account. Its effects on the results are discussed later.

C3.3 ADDITIONAL ASSUMPTIONS

Certain assumptions are needed in addition to the basic equations and the heat transfer rate equations in order to obtain definitive solutions with the model analyses. These are:

a. The liquid water, steam, and gas in the exploding mixture are at all times at the same uniform temperature throughout the mixture (except for the steep temperature gradient in the region adjacent to the surface of a melt particle). The existence of turbulent convective mixing would be necessary for this assumption to be valid, since the thermal diffusivities of liquid water and steam are both much too small for heat conduction to maintain temperature equilibrium and homogeneity over the time and distance scales involved. As long as some water exists in the liquid phase, a relationship between the temperature and the pressure is needed in order to be able to solve the problem. The most convenient and often used one is the vapor pressure-temperature relationship along the vapor-liquid equilibrium curve.

b. The exploding mixture is at a uniform pressure equal to that at the bottom of the mixture. This assumption is necessitated by the use of a single layer pair to represent the mechanical properties of the medium. The expansion and compliant properties of the medium are functions of both pressure and temperature as well as composition; they are evaluated at the single assumed uniform pressure and single uniform temperature. The entire pressure differential between the top and bottom of the mixture is assumed to appear across the upper inertial layer. Because of the parabolic variation in pressure which results from the uniform expansion assumption, the pressure of most of the medium is actually closer to that at its bottom than that at its top; the mean pressure is 2/3 of that at the bottom.

c. The melt is at a uniform temperature at all times, i.e., there is a more rapid interchange of heat between the various portions of the melt than between the melt and the water. Clearly, this assumption is not realistic for separated melt particles of different sizes, since the smaller ones would cool down faster than the larger ones and there is no opportunity for direct interchange of heat among the various particles. Furthermore, for melt dropped into the water over a finite period of time, the later additions would be at the original melt temperature whereas the particles dropped earlier would have cooled. There is also the difference between the average and surface temperature of a particle that depends upon its size, as previously mentioned. Despite the questionability of the details of the assumption of melt temperature homogeneity, this assumption should yield an average rate of heat exchange throughout the medium that is approximately correct.

d. As soon as any core material falls into the medium it becomes fragmented into the given average particle size and becomes uniformly dispersed throughout the medium. Furthermore, this particle size value and uniformity of dispersion remain unchanged as the mixture generates steam and expands. This assumption entails a very high relative velocity between the melt particles and the medium for a very short time, until their dispersion in the medium is completed. Thereafter the average relative velocity is zero, but the average square of the relative velocity is not zero, because of turbulence. If dispersion of the melt by one or another of the possible explosion-triggering mechanisms is delayed until some time after the melt had started to drop into the medium, the resultant explosion would be more severe, since this situation would correspond approximately to an instantaneous drop and dispersion of that portion of the core which had already reached the medium when the triggering event occurred. If the incoming melt were dispersed over only a portion of the medium when the explosion was triggered, the result may be more severe local deformation and damage of the vessel but less energy expended in acceleration of the mixture.

C3.4 CHEMICAL REACTIONS

Only one chemical reaction, that between the zirconium and the water, is incorporated in the model. This is considered to be the principal reaction for the conditions of interest (Ref. 4). The diffusion-limited parabolic reaction law as given by Baker was employed in the model (Ref. 5). The surface area of zirconium in contact with the water was taken to be the same as if the mass of zirconium were broken up into particles of the same average diameter as that specified for the entire melt.

The parabolic reaction law yields an infinite reaction rate at zero time. The computational difficulties with an infinite rate were avoided by assuming that the zirconium already had a thin film of oxide on its surface when the melt was dispersed in the water. The amount of hydrogen assumed to exist initially in the mixture was taken to result from the oxidation of this initial film. Although the initial rate of reaction is sensitive to the thickness of this initial oxide film, later values of the amount reacted and of the heat generated as functions of time are little affected by this assumption.

The liquid water and the steam were presumed to participate equally in the chemical reaction; that is, in proportion to their mass fractions. The heat generated by the chemical reaction turned out to be 1 percent or less of the heat transferred from the melt to the water in the short time interval involved in most cases of interest. The amount of hydrogen gas generated was also small, of the order of 10^{-5} that of the mass of the water. The chemical reaction could have been safely ignored in this phase of the computations.

C3.5 VESSEL—WALL STRESSES

Proper computation of the vessel-wall stresses and comparison of these stresses with the strength properties of the material are important considerations since the main consequences of a steam explosion depend upon whether or not the integrity of the vessel is preserved.

The distribution of stress in an engineering structure such as a reactor vessel is very complex. The vessel is subjected to many different types of loadings, some of which are alleviated and others intensified under the conditions of a melt-down accident. The main concern in the model computations is in the magnitude of the gross circumferential and longitudinal stresses in the vessel walls developed by the transient internal-pressure excursion resulting from the steam explosion. The onset of deformation and rupture should depend upon the combination of the new and the preexisting stresses. However, the latter are ignored in the model since they are expected to be small in comparison with the former.

An excess of pressure inside the vessel over that outside at the same vertical location produces a circumferential (hoop) tensile stress in the vessel wall equal to the excess pressure times the ratio of radius to wall thickness. If the vessel is closed on both ends there is also a longitudinal tensile stress equal to half the hoop stress. The hemispherical heads are subjected to membrane tensile stresses (equal in all directions) given by the same formula as for the longitudinal stress (Ref. 6). Superimposed upon these are bending stresses due to restraints to radial expansion at supports and flanges, pressure gradients in the mixture itself, and stress concentrations at tube entrances, at abrupt changes in shape or cross section, and at points of attachment of internal and external support structures. Failures of certain portions of the vessel structure might thus occur for exploding mixture pressures of 1/2 to 1/4 of those necessary for producing gross longitudinal ruptures from excessive hoop stress. To identify the possibility of such occurrences, a longitudinal "flaw" (of given length at a given distance from the bottom of the vessel with a stress-concentration factor of 4) was introduced into the computer program.

The simple direct proportionality between excess internal pressure and wall stress applies strictly only to static or slowly changing internal pressures. For pressures that change significantly in a time comparable to the natural period of radial vibrations of the cylinder, inertial effects prevent the wall stresses from following pressure changes instantaneously, since stresses are accompanied by strains and, hence, radial displacements of the walls. For pressure pulses that are extremely short compared to the radial vibration period, the maximum wall stress will be developed after the pulse is over and will be proportional to the pressure impulse, the integral of the pressure pulse over time, rather than to the maximum pressure value itself.

For some of the preliminary computations with the PWR, a differential equation was incorporated in the computer program for determining the dynamic hoop stresses from the computed pressure variations in the exploding mixture. With suitable damping incorporated into the equation to avoid "ringing" effects, the dynamic stress was found to follow the static stress variations rather faithfully except for a time delay of about 1/4 of the natural period for radial vibrations of 3 milliseconds. This is because the pressure changes for these computations occurred on a scale of tens of milliseconds for the assumed particle size (400 microns). As they had been shown to be unimportant to the situations of interest, computations of the dynamic stresses were then eliminated from the computer program.

In the computer program it is assumed that the wall would rupture wherever and whenever the hoop stress exceeds the tensile strength of the steel, or 1/4th of this value at the assumed flaw location. These cracks could not open fast enough to have any significant effect on the course of the remainder of the explosion. Computations were continued until the top head was assumed to rupture due to excessive longitudinal stress just below the flange. Cracks should also begin to form in the hemispherical shell of the top head at about this time, but only the development of a very large opening could relieve the internal pressure buildup fast enough for the cases involving high rates of heat transfer.

In the above considerations the response of the material to the applied stress is greatly simplified. Failure is assumed to take place when the vessel-wall stress exceeds the tensile strength of the material. The energy that could be absorbed by plastic deformation is not considered. For the more energetic interactions this is a good approximation since the kinetic energy of the moving mass by far exceeds the energy required to fail the vessel. In less-energetic interactions, where failure of the vessel is marginal, this approach is overly conservative.

C4. RESULTS OF COMPUTATIONS

A number of cases were computed for which it was assumed that the molten portion of the core at a given time following the initiation of a meltdown accident dropped suddenly into the water remaining above the grid plate at that time. PWR reactor specifications were used and the cases ranged from 3.9 percent of the core dropping into 37,400 pounds of water to 88.3 percent dropping into 4500 pounds of water. The average particle diameter of the dispersed melt was assumed to be 400 microns, in accordance with the findings of Higgins and Schultz (Ref. 7). In all cases the top head of the reactor vessel was ruptured and, except for the 3.9 percent case, sufficient energy remained after inelastic collision with the concrete shield above the vessel to breach the dome of the containment building.

It is considered unlikely that a partially molten core would drop down into the water above the grid plate; rather it would tend to resolidify as it progressed down the cooler core structure below it. Consequently, all subsequent computations were limited to the case of massive grid-plate failure, for which all of the molten core and the molten grid plate would drop into the bottom-head water reservoir.

Figure VIII C-2 shows the plotted results of a typical computer output for a dispersal of 400-micron-diameter melt particles. The various dependent variables shown as functions of time are:

P - Pressure in exploding mixture, psi/100

Q - Pressure in gas and steam above exploding mixture, psi/100

T - Temperature of steam-water, deg C/10

U - Temperature of melt, deg C/100

X - Position of the top of exploding mixture, ft

S - Mass fraction of steam, percent

H - Heat input to steam-water, cal/g/10

E - Conversion efficiency, heat to kinetic energy, percent.

The maximum pressure developed is not enough to rupture the bottom of the vessel for this particular case. (The vessel does rupture at its bottom for an average particle diameter of 320 microns). The pressure above the top of the mixture is seen to increase very rapidly as the model "piston" approaches the top head. Rupture of the top head occurs because of this pressure buildup in combination with a hammer effect as some of the exploding mixture penetrates the gas pocket above it to impact the top head. (The Taylor instability developed at the top of the mixture as

it rapidly decelerates explains the penetration.)

As discussed in Appendix B, it is not known whether there would be any operative mechanism to disperse molten core materials dropped into saturated water. In view of the possibility that fine fragmentation and dispersion would not occur with any great likelihood, a series of computations were made with larger average particle diameters, ranging up to 100,000 microns (10 cm). Melt-drop times were taken to vary from 0.001 second to 3.2 seconds. The values for the various input parameters used for these calculations are listed in Table VIII C-1.

The results of these computations are shown in Fig. VIII C-3 for PWR reactors. Computations were made for all combinations of values of APD, the average particle diameter, and TAU, the melt-drop time, for which a capital letter designator appears on the log-log grid. The number to the side of each letter, except for E, is the height in feet to which the top head and control-rod shield would rise against gravity if unimpeded by other forces or constraints. The significance of the letter designates is as follows:

A - The vessel wall ruptures near the bottom and also later at the assumed flaw position running from 6 to 8 feet above the bottom with a stress-concentration factor of 4. The top head also subsequently ruptures, hits the control-rod shield block, and the combined projectile penetrates the dome of the containment building, 95 feet above the shield block.

B - Same as A except that the vessel does not rupture near the bottom.

C - Same as A except that neither the bottom nor the assumed flaw location ruptures.

D - Same as C except that the projectile assembly does not have enough energy to reach the dome of the containment building.

E - No rupture of the vessel occurs.

The lines drawn on Fig. VIII C-3 delineate the approximate boundaries between the areas on the grid characterized by the above-lettered combination of events. The second line from the right is particularly significant since it is the dividing line between the set of conditions for which no containment failure is predicted to occur and those for which the containment might fail.

Figure VIII C-4 shows the results of similar computations for a BWR, for the values of the parameters listed in Table VIII C-1. The BWR reactor vessel contains a considerable amount of internal structure above the shroud head that covers the reactor core. The moving mass (the hypothetical piston that forms the top layer of the exploding mixture) is presumed to collide inelastically with the shroud head and to tear it loose from its mountings. Energy losses are suffered in flowing past the internal structures in the vessel both in the form of viscous drag resistance to flow and inelastic collisions when the shroud head is torn loose and as it is plastically deformed. The entire moving assembly then collides inelastically with the top head and ruptures it if it has enough energy to do so. The assembled mass then continues on upward toward the roof of the containment building. The BWR has no shield block above the vessel.

Despite the differences between the PWR and the BWR and the differences in initial and boundary conditions, the use of improved functions for the properties of liquid water near the critical point for the latter, and a first-order correction for the differences between the average and surface temperatures of melt particles of various sizes for the latter, the sets of curves for the PWR and the BWR are quite similar.

The ordinate scales of Figs. VIII C-3 and VIII C-4 can also be plotted on a time-scale basis, like the abscissa scales, by using the thermal relaxation time, TRT, rather than the average particle diameter. The thermal relaxation time is the time required for the heat content of the melt to decrease to 1/e of its initial value. In order to compute the heat content of the melt it is first necessary to find the final equilibrium temperature of the mixture, assuming a slow, constant pressure heat transfer and hence no dynamic effects. The equilibrium temperature turns out to be 1710 C for the PWR and 1150 C for the BWR (smaller melt to water ratio). The heat content for the former is thus 217 cal/g and for the latter 300 cal/g. The value of TRT is simply the heat content divided by the initial rate of heat transfer per gram of melt. The computer prints out the value of this initial rate of heat transfer. However, it is readily computable from the mass of melt, the total surface of the melt,

the initial temperature difference, and the sum of the radiative and film-boiling convective heat-transfer coefficients. For the purpose of this computation the average melt temperature is used as its surface temperature.

The TRT and the TAU scales can both be rendered dimensionless in a significant way by dividing them by TMR, the mechanical response time for the system. TMR is a measure of the time required for the piston mass equivalent of the inertia of the system to respond appreciably to changes in forces imposed on it. A formula for TMR is derived in the Mathematics Section. This formula is the same as that for about 1/6 of the natural period of oscillation of a mass equal to the piston mass supported on an air spring with the same cross-sectional area and initial depth as that of the exploding mixture, with the air spring pressurized above ambient pressure just sufficiently to support the weight of the piston against gravity. The values of TMR, the mechanical repsonse time, turn out to be nearly the same for the PWR and the BWR, 0.31 second for the former and 0.32 second for the latter.

The dimensionless plots of TRT/TMR versus TAU/TMR are given in Fig. VIII C-5 for the PWR and BWR. The curves differ slightly in shape and in where they intersect the coordinate axes. However, the similarities between the two sets of curves are more striking than the differences. They would not be expected to be exactly alike since there are many other dimensionless parameters involved in the behaviors of the two systems. However, TRT/TMR and TAU/TMR appear to be the primary parameters. Also significant is the fact that the change in system behavior from a nonexplosive one to a very explosive one is characterized by a dividing line corresponding to the value of unity for the vector sum (square root of sum of squares) for these two parameters. This dividing line is approximately that between Regions B and C of Fig. VIII C-5. No vessel ruptures occur for values of TRT/TMR of about 10 to 12 or greater or for values of TAU/TMR of 4 to 6 or greater, regardless of the value of the other parameter.

Maximum efficiency of conversion of heat energy to mechanical energy occurs when the heat-exchange rate is so great that essentially no expansion can take place until all of the water has been converted to very high pressure steam (constant volume boiling). The system would then become insensitive to heat-exchange rate, i.e., greater values of heat-exchange rate would be of no consequence. This condition would correspond to both of the parameters TRT/TMR and TAU/TMR being much less than 0.1, which would require average particle diameters of less than 100 microns and melt drop times of less than a millisecond.

The question of the likelihood of occurrence of a steam explosion of given severity in a reactor vessel seems to reduce itself to the question of the likelihood of occurrences of the various combinations of TRT/TMR and TAU/TMR along one of the actual curves or along an interpolated curve of Fig. VIII C-5. It is seen that if TAU is much less than TRT, the phenomenon depends only on the single parameter TRT/TMR. On the other hand, if TAU is much greater than TRT, the rate of heat exchange depends primarily on the rate at which melt drops into the water and not on how rapidly heat is exchanged between the water and an individual particle of the melt. Hence the value of TAU/TMR becomes the significant quantity.

C5. MATHEMATICS OF THE MODEL

C5.1 BASIC MODEL EQUATIONS

C5.1.1 CONSERVATION OF ENERGY

$$\dot{Q} = M_w\dot{q}_w + M_s\dot{q}_s + M_g\dot{q}_g + L_{vw}\dot{M}_{ws}, \qquad \text{(VIII C-1)}$$

where

$\dot{Q}$ = The rate of heat input to the colder components of the mixture from the melt,

M_w, M_s, M_g = Instantaneous values of the masses of the liquid water, steam, and gas, respectively,

$\dot{q}_w, \dot{q}_s, \dot{q}_g$ = Rates of heat input per unit mass to the water, steam, and gas, respectively, and

$L_{vw}\dot{M}_{ws}$ = Latent heat of vaporization times mass rate of conversion of water to steam.

In accordance with the first law of thermodynamics,

$$dQ = dH - VdP = C_{ps}\,dT - T\,(\partial V/\partial T)_p\,dP.$$

Hence, for the steam, for example,

$$\dot{q}_s = C_{ps}\,\dot{T} - T\,(\partial V_s/\partial T)_p\,\dot{P}_s, \quad \text{(VIII C-2)}$$

where

C_{ps} = Constant pressure specific heat as a function of P_s and T,

V_s = Volume per unit mass of steam as a function of P_s and T,

P_s = Partial pressure of the steam, and

T = Absolute temperature.

Equations analogous to Equation (VIII C-2) are also set up for the water and for the gas (hydrogen). Since the hydrogen is assumed to be a perfect gas, $T\,(\partial V_g/\partial T)_p = V_g$.

For the melt,

$$\dot{Q} = -\sum_{i=1}^{4} (C_{\ell i}M_{\ell i} + C_{si}M_{si})\,\dot{T}_m + \sum_{i=1}^{4} C_{\ell i}W_{\ell i}(T_{mo} - T_m)/\tau \quad \text{(VIII C-3a)}$$

or

$$\dot{Q} = -L_j\dot{M}_{sj} + \sum_{i=1}^{4} C_{\ell i}W_{\ell i}\,(T_{mo} - T_{mj})/\tau. \quad \text{(VIII C-3b)}$$

Equation (VIII C-3a) applies while the instantaneous melt temperature T_m is not at any of the melting points of the four components, UO_2, ZrO_2, Zr, and Fe. $\dot{Q}$ is the same quantity as on the left side of Equation (VIII C-1). $C_{\ell i}$ and $M_{\ell i}$ are the specific heat and instantaneous mass within the exploding mixture, respectively, of the liquid phase of Component i, and C_{si} and respective M_{si} are the same respective quantities for its solid phase.

Whenever the melt temperature reaches the melting point T_{mj} of the j-th component, Equation (VIII C-3b) begins to apply, wherein L_j is the latent heat of fusion of Component j and M_{sj} is the mass rate of increase of its solid phase. Equation (VIII C-3b) continues to apply until all of the liquid phase of Component j has been converted to solid, then control reverts to Equation (VIII C-3a). The various components of the melt are thus assumed to be in separate phases at thermal equilibrium: the possibility of formation of liquid or solid solutions is not considered.

The additive term on the right of both equations represents the rate at which thermal energy is added to the melt within the exploding mixture by the continual dropping into the mixture of additional melt from the core at its original temperature T_{mo} over a time period τ. Here $W_{\ell i}$ is the total mass of liquid over this time period. This second term is deleted from the two equations upon completion of the dropping process; i.e., when the time begins to exceed τ.

C5.1.2 CONSERVATION OF MOMENTUM

$$A(P - P_x) - W_g = W\ddot{x} + (W_m/\tau)\,\dot{x}, \quad \text{(VIII C-4)}$$

where

x = Position of the top of the exploding mixture,

W = Effective mass (half of instantaneous mass of melt plus water),

A = Cross-section area,

P = Pressure at the bottom of the mixture,

P_x = Pressure in the space above the mixture (filled with steam and hydrogen),

g = Acceleration of gravity, and

W_m = Total mass of the melt.

Since τ is the melt drop time, W_m/τ represents the rate of increase of melt in the mixture.

P_x is computed as a function of time by applying an equation similar to that of (VIII C-1) to the steam and hydrogen in the upper part of the vessel with $\dot{Q} = 0$. The steam in this part of the vessel is not quite saturated initially and becomes even less so as it is compressed adiabatically.

C5.1.3 CONSERVATION OF MASS

$$xA - V_m = w_t (1 - \alpha w_g)$$

$$W_w [FV_s + (1 - F) V_w].$$

(VIII C-5)

Equation (VIII C-5) states that the volume of the exploding mixture at any time, less the volume occupied by the melt components, equals the volume occupied by the steam plus the volume occupied by the water. W_w is the original mass of water; F is the mass fraction in the form of steam, and V_s is the volume per unit mass of steam; V_w is the volume per unit mass of water; w_t is the mass fraction of the mixture remaining after the escape of some through the orifice; and $1 - \alpha w_\lambda$ is the mass fraction of water remaining after chemical generation of a mass of hydrogen equal to $w_g W_w$, where α is the ratio of molecular weights of water to hydrogen. The standard orifice equations yields $\dot{w}_t$, from which w_t is obtained by numerical integration. Likewise, $\dot{w}_g$ comes from the chemical reaction rate equation.

Since the hydrogen gas occupies the same volume as the steam, we have, furthermore,

$$(1 - \alpha w_g) FV_s = w_g V_g. \qquad \text{(VIII C-6)}$$

The time derivatives of Equations (VIII C-5) and (VIII C-6) furnish needed relationships for the analysis. The value of $\dot{M}_{ws}$ in Equation (VIII C-1) can then be expressed in terms of $\dot{F}$ and the other parameters.

C5.1.4 EQUATIONS OF STATE

For steam, the analytic expression quoted by Justi for $V_s(P_s,T)$ was employed (Ref. 8). Tabulated density values for both saturated and super-heated steam could be reproduced to within an accuracy of 1 percent by using this expression, except in the neighborhood of the critical point. The needed pressure and temperature partial derivatives of V_s were also obtained from this expression.

The density of saturated liquid water as a function of temperature was obtained from a mathematical expression quoted by Dorsey (Ref. 9). This expression was modified to apply to subcooled water by adding a term proportional to the excess pressure over the saturation value, with the coefficient of proportionality a function of temperature, so as to approximate the tabulated values quoted by Dorsey (Ref. 10).

The specific heat at constant pressure for the steam as a function of P_s and T was obtained from an expression for the entropy, S, of steam as quoted by Justi (Ref. 8), using the thermodynamic relationship $C_{ps} = T(\partial S/\partial T)_p$. The specific heat of saturated water was obtained by matching a polynomial to published data (Ref. 11). In addition, analytic expressions were used for the vapor pressure of water as a function of temperature (Ref. 12) and for the latent heat of vaporization of water as a function of temperature (Ref. 13).

The ideal gas law was used for the equation of state and the specific heat of the hydrogen gas. This was deemed satisfactory because the hydrogen is a minor component with a low partial pressure.

The densities, specific heats, heats of fusion, and melting point temperatures of the various components of the melt were considered to be constants at average values over the temperature range of interest (Ref. 14). The effects of the variations in the density of the melt with temperature and pressure were neglected.

C5.2 MECHANICAL RESPONSE TIME

Equation (VIII C-4) may be rendered dimensionless by dividing through by AP_o, where P_o is the initial pressure at the bottom of the mixture, obtaining

$$\frac{Wx_o}{AP_o} \frac{d^2(x/x_o)}{dt^2} = \left(\frac{P}{P_o} - \frac{P_x}{P_o}\right) - \frac{W_g}{AP_o} - \frac{W_m x_o}{AP_o \tau} \frac{d(x/x_o)}{dt},$$

(VIII C-7)

wherein x_o is the initial depth of the exploding mixture.

The coefficient of the term on the left has the dimensions of time squared. Its square root, given by

$$t_{mr} = \sqrt{WX_o/AP_o}, \qquad \text{(VIII C-8)}$$

is precisely the factor needed to make the time scale of the equation dimensionless throughout; e.g., the left side becomes $d^2(x/x_o)/d(t/t_{mr})^2$. Since $P_o = P_a + P_g$, the ambient pressure plus the additional pressure at the bottom of the mixture due to gravity, equals $(W/A)/g$, Equation (VIII C-8) can also be expressed in the form

$$t_{mt} = \sqrt{(x_o/g)/(1 + P_a/P_g)}. \qquad \text{(VIII C-9)}$$

Equation (VIII C-9) for t_{mr} is the same as the equation for $1/2\pi$ times the period of a pendulum of length $x_o/(1 + P_a/P_g)$.

Equation (VIII C-8) is the same as that $1/2\pi$ times the period of small (isothermal) oscillations of a mass W mounted on an air spring of cross-section area A, length x_o, and filled to a pressure P_o, just enough above ambient pressure to support W. The differential equation for a small displacement, x, of W mounted on the air spring would be

$$W \frac{d^2x}{dt^2} = - \left(\frac{x}{x_o}\right) P_o A, \qquad \text{(VIII C-10)}$$

since $-(x/x_o P_o)$ is the isothermal pressure change produced by the displacement x (from Boyle's law). This equation integrates to simple harmonic motion with a period of

$$2\pi\sqrt{Wx_o/AP_o}.$$

C5.3 DYNAMIC STRESSES IN VESSEL WALLS

The static circumferential (hoop) tensile stress in a cylinder of radius R and wall thickness $t_w << R$ (thin-wall case), is given by

$$\sigma_{st} = (R/t_w)\ \Delta P \qquad \text{(VIII C-11)}$$

where ΔP is the excess of internal over external pressure (Ref. 6). If ΔP is a function of time, consideration of the force balance and inertial reaction on a slice of the cylinder between two radii leads to the following differential equation for the dynamic hoop stress, $\ddot{\sigma}$

$$\ddot{\sigma} = w^2 (\sigma_{st} - \sigma) - D_f w \dot{\sigma}, \qquad \text{(VIII C-12)}$$

where $w = \sqrt{E/\rho}/R$. E is Young's modulus and ρ is the density of the wall material (steel). Since $c = \sqrt{E/\rho}$ is the bar velocity of sound, w is the angular resonance frequency for radial vibrations of the cylinder, as given by the condition that the circumference ($2\pi R$) is equal to one wavelength ($2\pi c/w$).

A damping term $-D_f w\dot{\sigma}$ is added to the right side of Equation (VIII C-12), where D_f, the dissipation factor, $= 1/Q_r$ for the resonant system. Without this term, higher stresses would be predicted than expected in practice because of the "ringing" phenomenon. For example, with no damping added, the response to a pressure-step function (a sudden application of internal pressure) would be an overshoot in stress by a factor of 2 followed by an oscillation of indefinite duration with stresses varying from zero to double the static value. In practice, such oscillations would not occur because of dissipation of vibratory energy through the vessel supports and mountings; contacts with internal and external structures; and viscous losses for vibrations transmitted into internal fluids. In the absence of any ready means for estimating the magnitudes of such losses, D_f was given the value of 2, which represents just-critical damping.

C6. HEAT-TRANSFER-RATE CONSIDERATIONS

C6.1 HEAT-TRANSFER COEFFICIENT

The rate of heat transfer from the hot melt to the colder components of the exploding mixture is given by

$$\dot{Q} = H_{tc} \cdot S \cdot (T_{ms} - T), \qquad \text{(VIII C-13)}$$

where S is the total surface area of the melt particles; T_{ms} is the surface temperature of the melt; and T is the average temperature of the colder components (liquid water, steam, and gas). H_{tc} is the heat-transfer coefficient, the suitable representation of which is a primary consideration in the analysis. The effects of the high-temperature gradient in the colder components in the immediate vicinity of the hot melt surface are included in H_{tc}. The possible differences between T_{ms} and the average temperature of the melt, T_m, are discussed later.

H_{tc} consists of contributions from each of the three classical types of heat transfer: radiation, conduction, and convection.

C6.1.1 RADIATIVE HEAT TRANSFER

Radiative heat transfer is a major contribution at the melt temperature of interest. The net rate of radiation of heat per unit surface area away from a surface of emissivity ε_{ms} and temperature T_{ms} toward a surface of emissivity ε and temperature T is given by

$$\dot{q} = \frac{\sigma\left(T_{ms}^4 - T^4\right)}{\left(\frac{1}{\varepsilon_{ms}} + \frac{1}{\varepsilon} - 1\right)}, \qquad \text{(VIII C-14)}$$

where σ is the Stefan-Boltzmann constant (Ref. 15). If the melt particles are far enough apart and of such shape that one portion of a melt particle surface cannot receive radiation directly from another portion, and if the value of ε for the water-steam-gas is effectively unity (perfect absorber and radiator), then Equation (VIII C-14) becomes

$$\dot{q} = \varepsilon_{ms}\left(T_{ms}^4 - T^4\right). \qquad \text{(VIII C-15)}$$

Each melt particle is considered in the model to consist of the same mixture of the two oxides and the two metals. In practice, the proportions of these may vary greatly from one particle to another. However, the possibility that any metallic component, with a low emissivity, can form an appreciable fraction of the melt surface is ruled out, since a thin film of oxide would form almost immediately upon contact with steam or liquid water. The available information on the emissivities of UO_2 and ZrO_2 at temperatures in the neighborhood of 2800 C indicate that 0.8 would be an appropriate value for ε_{ms} (Ref. 14). Hence the contribution of radiation to the heat transfer coefficient is given by

$$H_{rad} = 0.80\ (T_{ms} + T)\left(T_{ms}^2 + T_{ms}\,T + T^2\right), \qquad \text{(VIII C-16)}$$

where T_{ms} and T are in degrees absolute.

C6.1.2 CONDUCTIVE HEAT TRANSFER

If a hot sphere of surface temperature T_{ms} and diameter D is immersed in a homogeneous medium of ambient temperature T and thermal conductivity K, the steady-state solution of the heat-conduction equation in spherical coordinates yields the value of the temperature gradient in the medium at the surface of the sphere and hence the rate of heat flow into the medium from the sphere. From this heat-flow rate the heat-transfer coefficient for conduction becomes

$$H_{cond} = 2K/D, \qquad \text{(VIII C-17)}$$

which corresponds to a value of 2 for the Nusselt number, HD/K.

Equation (VIII C-17) is employed in the model for the conductivity contribution to the heat-transfer coefficient when the fluid is all steam. If V_{ol} is the volume fraction of steam before all of the liquid has vaporized, then the expression incorporated in the model is

$$H_{co} = (1 - V_{ol})H_{br} + V_{ol} \cdot H_{cond}, \qquad \text{(VIII C-18)}$$

where H_{br} is the Bromley heat transfer coefficient applicable to stable film boiling, discussed later. Equation (VIII C-18) is tantamount to assuming that a V_{ol} fraction of the melt particles is surrounded primarily by steam and the remainder is surrounded by a film of steam only, beyond which is liquid water.

It is recognized that Equation (VIII C-17) represents an approximate evaluation of the contribution of heat conduction to the heat-transfer coefficient. Since conduction to steam would be expected to be a lesser contributor to overall heat transfer than natural convection and radiation to liquid water, this approximation is deemed reasonable.

C6.2 CONVECTIVE HEAT TRANSFER

No account was taken in the model of the contribution to the heat-transfer coefficient of a melt particle in steam due to either natural or forced convection, although the latter could be significant. Much turbulence no doubt would exist in practice, but the value of the Reynold's number, needed to compute the contribution due to forced convection, is unknown. As previously pointed out, the average relative velocity between the melt particles and the steam is presumed to be zero. The contribution to the heat transferred during the time that the melt particles are being rapidly dispersed throughout the medium is

neglected, by assuming this time to be relatively very small.

An important consideration is the rate of heat transfer in the initial stages of the explosion when the cold portion of the exploding mixture is almost entirely liquid water. The theory of heat transfer in the stable film boiling regime was developed by Bromley (Ref. 3). He assumed that the vapor blanket around a hot, horizontal, stationary tube rose continuously under the action of buoyant forces, at a rate limited by viscous drag on the tube. The heat transferred is that needed to replenish the vapor blanket by vaporization of the surrounding liquid. This heat is transported through the film primarily by conduction and radiation. The resultant contribution to the heat transfer coefficient is

$$H_{br} = 0.62 \left(\frac{K_v^3 \rho_v (\rho_\ell - \rho_v) g E_n}{D \eta_v (T_{ms} - \bar{T})} \right)^{1/4}, \qquad \text{(VIII C-19)}$$

where K_v, ρ_v and η_v are the thermal conductivity, density, and viscosity of the vapor, respectively; ρ_ℓ is the density of the liquid; and E_n is the difference in enthalpy between the vapor blanket at its mean temperature and the liquid.

Analytic expressions were used for the viscosity (Ref. 16) and the enthalpy (Ref. 8) of steam as functions of temperature and pressure in Equation (VIII C-19). The thermal conductivity was obtained from the viscosity and the constant-pressure specific heat (previously described) by using a Prandtl number value of 1/1.15 (Ref. 11). The analytic expressions for the liquid and vapor densities have been discussed.

A considerable amount of theoretical and experimental work has been reported on heat transfer to liquids from moving spheres, the case of forced convection (Refs. 17, 18). Heat-transfer rates of about one order of magnitude greater than those characteristic of natural convection can thus be attained. Forced convection effects are neglected in the model since the relative velocity between the melt particles and the water due to turbulence is not known. As pointed out previously, the average velocity difference is assumed to be zero and the heat transfer during dispersion is neglected.

Radiative heat transfer and natural convection (Bromley's correlation) make about equal contributions to the initial magnitude of the heat-transfer coefficient for 100-micron-size particles. However, as the particle size increases, the radiation contribution become predominant. Thus the overall heat-transfer rate predicted is not overly sensitive to the particular/film-boiling correlation utilized. These results of the present model computations are in accord with the meager amount of difficult-to-obtain experimental data on heat transfer at such high temperatures. In experiments on film boiling with an electrically heated carbon rod in water, Oki and Nabemoto measured heat-transfer coefficients for rod temperatures ranging from somewhat under 1500 C to somewhat over 3000 C above the saturated water temperature (Ref. 19). They claim their experimental results to be in agreement with radiative heat transfer and Bromley's equation. Attempts to obtain the individual magnitudes of the two terms from pairs of points along their curve proved to be futile for temperatures above 2000 C. The curve drawn through their data points agrees well with the assumption of only radiative heat exchange above this temperature, for an emissivity value close to unity.

C6.3 TEMPERATURE GRADIENT IN MELT PARTICLES

In all preliminary computations it was assumed that the surface temperature of each melt particle was the same as its average temperature. This assumption can be justified only for particles of about 60 microns or less in diameter on the time scale of events of interest, if thermal conduction is the only mechanism of internal heat transfer in the particle. (The thermal-diffusivity value for molten UO_2 is about 3.8×10^{-3} cm^2/sec.) Other mechanisms such as internal convection would have to be invoked to justity the isothermal assumption for the larger particles. However, since the assumed initial temperature of the melt is just above the melting point of UO_2, a solidification front would begin to progress from the surface inward as soon as the melt is dispersed throughout the water. The solid crystallites of UO_2 and ZrO_2 might form as a porous matrix that would hinder the convection of the lower-melting-point liquid metals.

An approximate procedure was devised to correct for the fact that the melt particle may not be isothermal. The temperature distribution within the melt particle is assumed to be parabolic, with a maximum temperature at the center of the assumed spherical particle and a maximum (negative) temperature gradient

at its surface. The value of this gradient is determined simply from the rate of heat transfer in the medium adjacent to the particle surface and the thermal conductivity of the particle (weighted average over the four components). Since the average temperature is known, the assumed parabolic distribution enables the surface temperature to be determined. The result is the following formula for the surface temperature of the melt:

$$T_{ms} = \frac{T_m + \frac{1}{10}\left(\frac{H_{tc}D}{K_m}\right)T}{1 + \frac{1}{10}\left(\frac{H_{tc}D}{K_m}\right)}, \qquad \text{(VIII C-20)}$$

where H_{tc} is the heat transfer coefficient for the medium adjacent to the surface and K_m is the thermal conductivity of the melt particle. The quantity T_m is the average temperature of the melt particle and T is the average water temperature away from the particle surface.

In applying Equation (VIII C-20) to determine the value of T_{ms} by computer, the value of T_{ms} is first assumed to be the same as T_m. This enables the value of H_{tc} to be computed in accordance with the formulas previously presented in this Appendix. Equation (VIII C-20) is then applied to obtain an improved value of T_{ms}, and H_{tc} is recomputed. The process is repeated until successive values of T_{ms} are in good agreement.

A solution exists for the transient-heat-transfer equation for the case of the cooling of an initially isothermal sphere immersed in a medium characterized by a fixed value of H_{tc} at the surface of the sphere (Ref. 20). Although this solution applies only to the assumption of a constant ambient temperature for the surrounding medium, it is instructive to compare it with the approximate one proposed above. The temperature gradient at the surface of the sphere for this case is initially much greater than that which would be given by a parabolic-temperature-distribution law. This is to be expected, since the sphere is assumed initially isothermal. However, an approximately parabolic distribution is attained after only a few percent of the total time it takes for the sphere to lose about 98 percent of its original temperature difference from the medium. Toward the end of the cooling process the parabolic distribution begins to give too high a value for the (negative) gradient at the surface. (The parabolic distribution is the exact steady-state solution for a sphere in a cooling medium with heat sources uniformly distributed throughout its volume (Ref. 21).

The computed initial differences between T_m and T_{ms} ranged from only a few degrees for a particle size of 100 microns to about 600 C for a particle size of 10,000 microns. The uniform-particle-temperature assumption would thus appear to be quite reasonable for all but the largest particle sizes considered.

References

1. Simon, R., "Computer Model Study of the Smelt-Water Physical Explosion", Presented at the Atlanta Heat Transfer Conference, A.I.Ch.E. (August, 1973).

2. Taylor, G. I., "The Instability of Liquid Surfaces When Accelerated in a Direction Perpendicular to Their Planes", Proc. Roy. Soc. London, A201, p. 290 (1950).

3. Bromley, L. A., "Heat Transfer in Stable Film Boiling", Chem. Eng. Progress, 46, p. 221 (1950).

4. Morrison, D. C., Ritzman, R. L., Wooton, R. O., Genco, J. M., Barnes, R. H., Fackelmann, J. M., and Carbiener, W. A., "An Evaluation of the Applicability of Existing Data to the Analytical Description of a Nuclear-Reactor Accident - Core Meltdown Evaluation", BMI-1910, Topical Report, Task 18, Battelle-Columbus Laboratories to AEC, p. C-7 (July, 1971).

5. Baker, W. L., and Ivins, R. O., "Analyzing the Effects of a Zirconium-Water Reaction", Nucleonics, 23, pp. 70-74 (July, 1965).

6. Jensen, A., Applied Strength of Materials, McGraw Hill, New York (1957), pp. 58-59.

7. Higgins, H. M., and Schultz, R. H., "The Reaction of Metals with Water and Oxidizing Gases at High Temperatures", Report No. IDO-28000 from Aerojet General Corporation to AEC (April 30, 1957).

8. Justi, E., Spezifische Warme, Enthalpie, Entropie and Dissoziation Technischer Case, Springer Verlag, Berlin (1938), p. 30.

9. Dorsey, E. N., Properties of Ordinary Water-Substance, Reinhold Publishing Corp., New York (1940), p. 584.

10. Dorsey, E. N., Ibid., p. 240.

11. Meyer, C. A., McClintock, R. B., Silvestri, G. J., and Spencer, R. C., Jr., Thermodynamic and Transport Properties of Steam, ASME Publication (1967).

12. Dorsey, E. N., Ibid., p. 574.

13. Dorsey, E. N., Ibid., p. 613.

14. Brassfield, H. C., White J. F., Sjodahl, L., and Bittel, J. T., "Recommended Property and Reaction Kinetics Data for Use in Evaluating a Light-Water-Cooled Reactor Loss-of-Coolant Incident Involving Zircalloy-4 or 304-SS-Clad UO_2", Report GEMP-482, General Electric Co., (April, 1968).

15. McAdmas, W. H., Heat Transmission, Third Edition, McGraw-hill, New York, (1954), p. 63.

16. Dorsey, N. E., Ibid, p. 64.

17. Stevens, J. W., Witte, L. C., and Cox, J. E., "The Vapor Explosion - Heat Transfer and Fragmentation. VI. Transient Film Boiling and Transition Boiling from a Sphere", Technical Report ORO-3936-9, University of Houston to AEC (September, 1972).

18. Vliet, G. C., and Leppert, G., "Forced Convection Heat Transfer from an Isothermal Sphere to Water", J. Heat Transfer, ASME Transactions, p. 163 (May, 1961).

19. Oki, H., and Nabemoto, A., "Film Boiling at a High Temperature of about 3000 C", Report presented at Int. Symposium of Japanese Society of Mechanical Engineers, September 1967, - Abstract #13 in Heat Transfer Newsletter No. 2, Committee of Reactor Safety Technology, European Nuclear Energy Agency, CREST-NL-2 (December, 1967).

20. Carslaw, H. S., and Jaeger, J. C., Conduction of Heat in Solids, Second Edition, Clarendon Press, Oxford (1959), p. 234.

21. Carslaw, H. S., and Jaeger, J. C., Ibid., p. 242.

TABLE VIII C-1 VALUES OF PARAMETERS USED FOR MASSIVE GRID-PLATE FAILURE, STEAM-EXPLOSION COMPUTATIONS

	PWR	BWR
Masses, lb		
UO_2	175,600	369,800
ZrO_2	30,000	105,200
Zr	6,300	22,100
H_2O	37,400	149,500
H_2	0.374	1.495
Top head, flange, and control-rod shield, PWR	323,500	358,000
Shroud head and internal structure	0	299,500
Initial Conditions		
Pressure, psia	13.2	14.7
Melt temperature, C	2,850	2,850
Water temperature, C	90	93
Vessel Parameters		
Radius, internal, ft	7.18	10.46
Height, internal, ft	34.60	65.95
Wall thickness, in.	7.875	6.313
Wall tensile strength, psi[(a)]	130,000	130,000
Flaw position, ft from bottom	6 to 8	12 to 16
Flaw strength, psi	32,500	32,500

(a) More representative values would be 70,000-80,000 psi. The energy imparted to the pressure vessel head is quite insensitive to the assumed tensile strength.

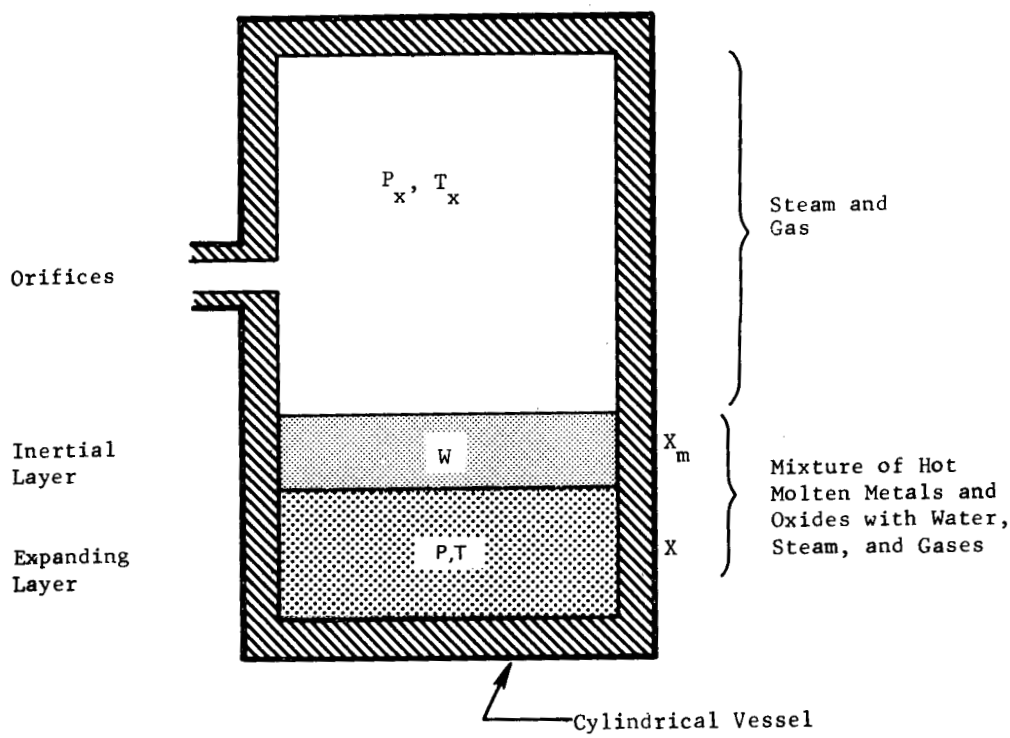


FIGURE VIII C-1 Basic Computational Model Geometry

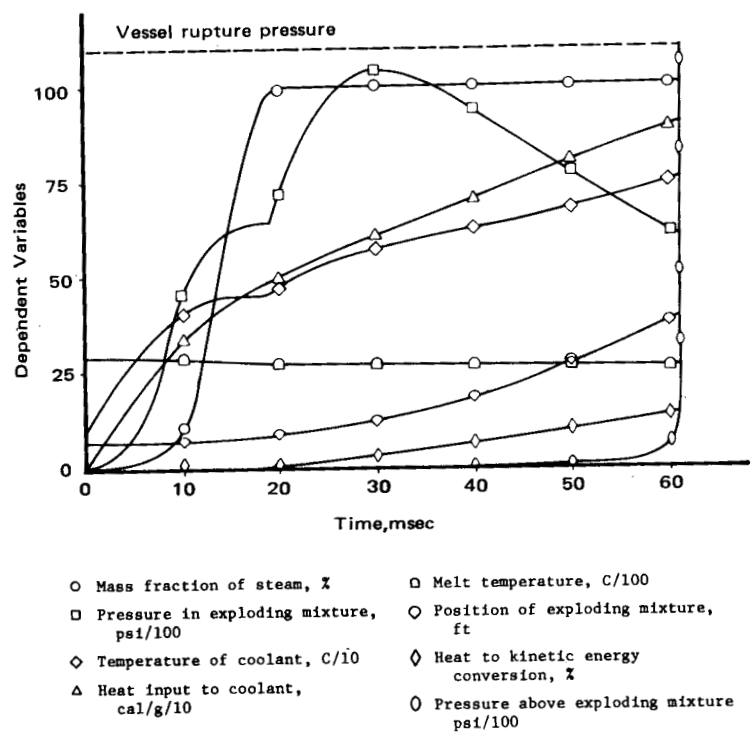


FIGURE VIII C-2 Typical Computer Results

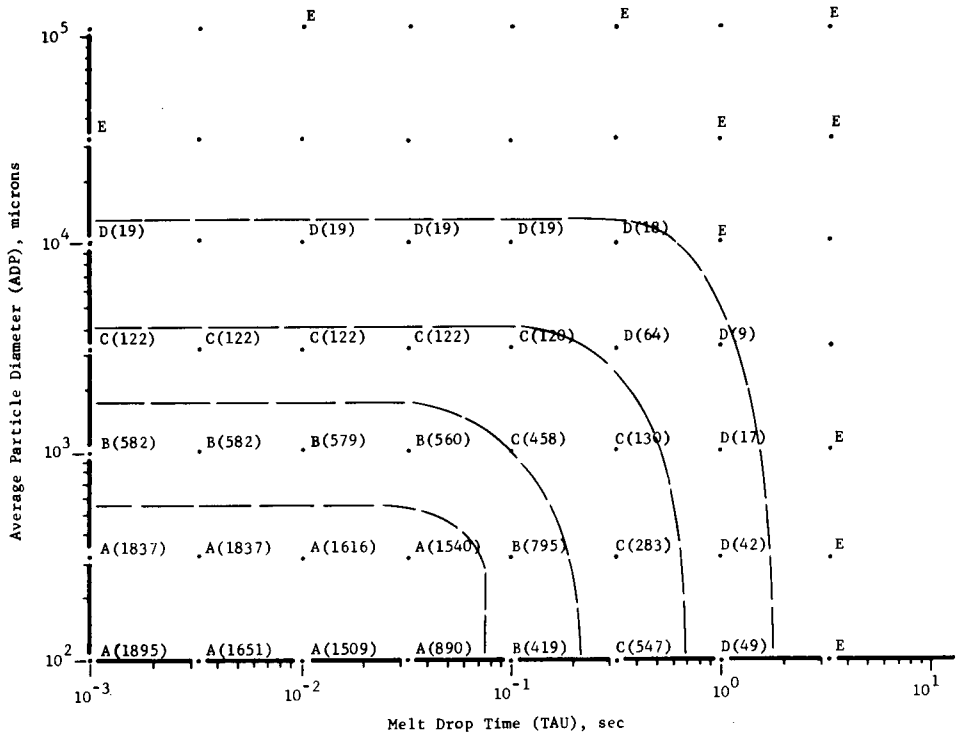


FIGURE VIII C-3 PWR Results

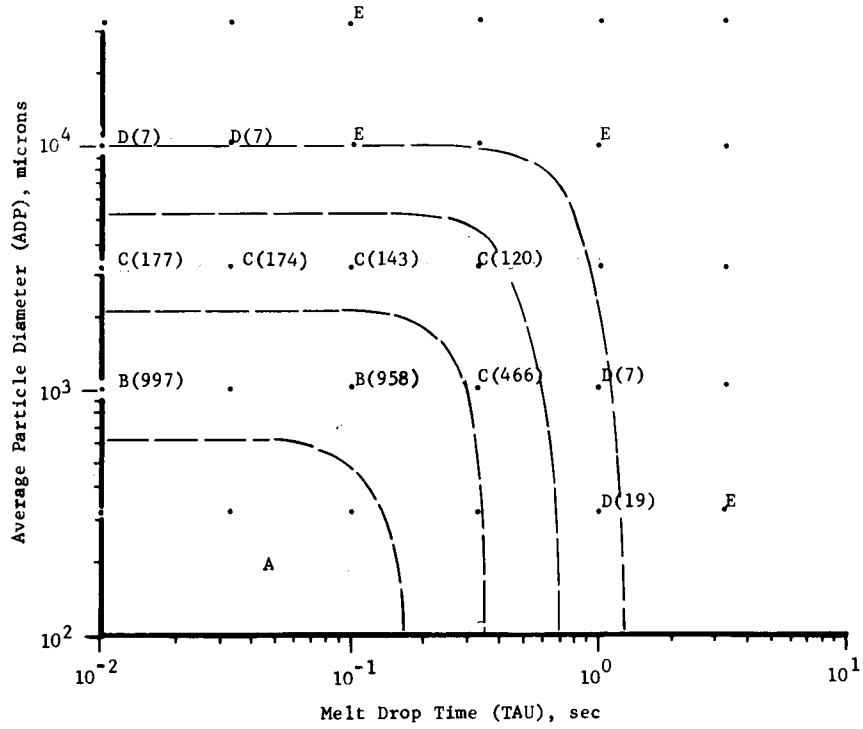


FIGURE VIII C-4 BWR Results

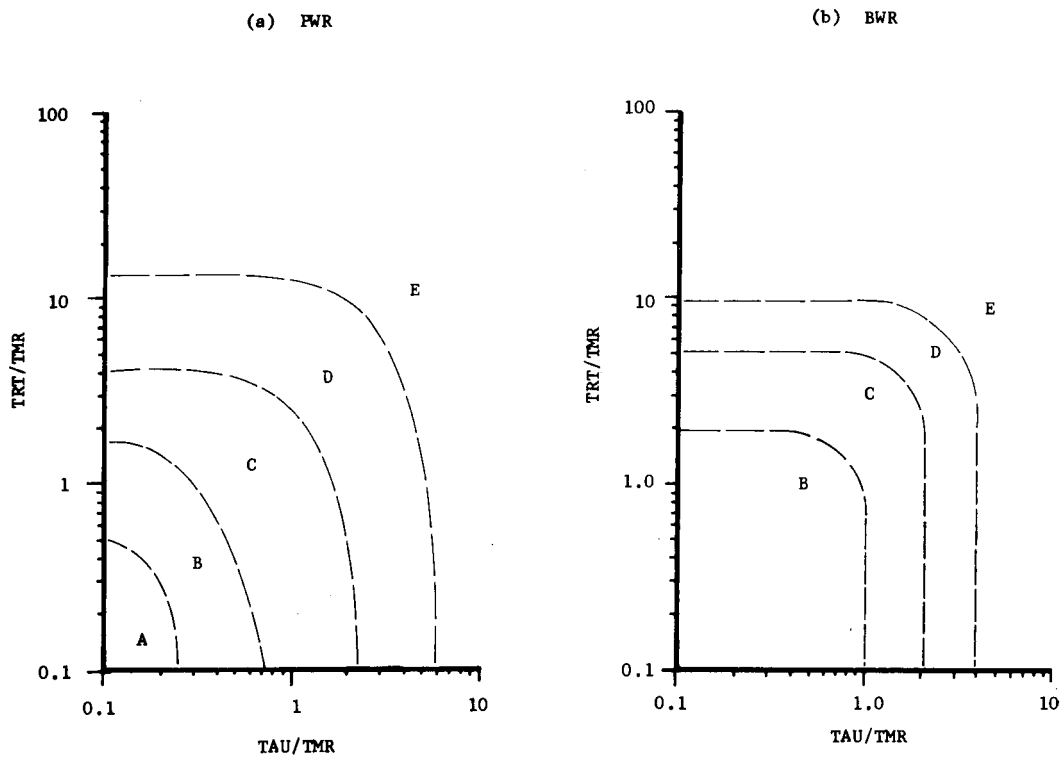


FIGURE VIII C-5 Dimensionless Presentation of Calculational Results

APPENDIX D

NONCONDENSABLE GASES

Appendix D

Table of Contents

Section		Page No.
D1.	HYDROGEN IN A PWR	VIII-117
D1.1	Production	VIII-117
D1.2	Transport to Containment	VIII-117
D1.3	Events in the Containment Atmosphere	VIII-117
D1.3.1	Flammability Limits	VIII-117
D1.3.2	Detonation Limits	VIII-118
D1.3.3	Combustion of Hydrogen at Entry to Containment	VIII-118
D2.	EXAMINATION OF DETONATION EVENTS	VIII-119
D2.1	The Mechanism of Detonation	VIII-119
D2.2	Calculations of Detonation Parameters	VIII-120
D2.3	Duration of the Shock Waves	VIII-121
D2.3.1	Application to a Large Vessel	VIII-122
D2.3.2	Hydrogen in a BWR	VIII-123
D2.4	Carbon Dioxide Generation in PWR and BWR	VIII-124
REFERENCES		VIII-125

List of Tables

Table		Page No.
VIII D-1	PWR Hydrogen Sources	VIII-126
VIII D-2	Calculated Detonation Parameters for Limiting Compositions	VIII-126

List of Figures

Figure		Page No.
VIII D-1	Flammability Limits of Hydrogen-Air-Steam Mixtures (Ref. 1)	VIII-127
VIII D-2	Composition Isotherms for Containment Atmosphere at Saturated Steam Conditions	VIII-128

Appendix D

Noncondensable Gases

There are two major sources of noncondensable-gas generation in a reactor accident in which core meltdown occurs. Metal-water reactions in the pressure vessel will produce hydrogen gas (H_2) shortly before and during the meltdown process. Later in the accident, carbon dioxide (CO_2) will be generated as the molten core material causes thermal decomposition of limestone aggregate in the concrete base mat of the containment structure. The production of these gases presents two potential threats to containment integrity. Both gases will cause a buildup in internal gas pressure in the system. Hydrogen generation can also lead to combustible mixtures with the oxygen already present in the containment atmosphere. Ignition of the hydrogen-oxygen mixtures can produce an exothermic chemical reaction which, depending upon conditions, might develop into a detonation. The introduction of additional thermal energy into the containment atmosphere will cause a rise in pressure, perhaps coupled with a shock-wave loading on the containment walls if the detonation occurs. The important question in all of these situations is whether, or under what conditions, would they likely result in containment failure by overpressurization. The hydrogen-generation problem is examined first for each type of water-reactor system; an analysis of the carbon dioxide generation problem follows.

D1. HYDROGEN IN A PWR

D1.1 PRODUCTION

Several sources of hydrogen exist for a PWR system during the course of a core-meltdown accident. The principal sources are identified in Table VIII D-1 along with an estimate of the rate of hydrogen production and the potential yield for each over a selected time period. It is apparent that the metal-water reaction is the most important source of hydrogen, both in amount and rate of generation. While the other sources could become significant at sufficiently long times, the metal-water reaction generated hydrogen will dominate during the important first several hours after the accident. The best estimate of the amount of hydrogen generated by this source is 600 lb-moles which corresponds to 75 percent zirconium reaction in the reactor-core region during the period of core meltdown. The value is based on parametric heat-transfer analyses of the meltdown process which takes into account steam-availability and core-slumping effects. More or less metal-water reaction can be predicted depending on assumed conditions, but it is shown that the final effects are not to sensitive to these uncertainties.

D1.2 TRANSPORT TO CONTAINMENT

The hydrogen-steam mixture will exit from the core at high temperatures, probably 2000 F or higher, and the paths from this location to the containment depends upon the type of pipe break. For a hot-leg break the gas mixture will exit from the primary system directly from the upper-plenum region of the pressure vessel without much cooling. For a cold-leg break the gas mixture must travel from the upper plenum through the steam-generator tubes before exiting to the containment. This will result in cooling of the gas mixture to temperatures of 500-600 F. Shapiro and Moffette have noted that the spontaneous-ignition temperatures of hydrogen-steam mixtures can range from about 1000 to 1500 F depending upon exit velocity, steam concentration, and geometry of the systems (Ref. 1). Thus the temperature of the steam-hydrogen mixture that exits from the broken pipe into the containment should be above the spontaneous ignition temperature in a hot-leg break but not for a cold-leg break.

D1.3 EVENTS IN THE CONTAINMENT ATMOSPHERE

D1.3.1 FLAMMABILITY LIMITS

Shapiro and Moffette reviewed this subject about 15 years ago and developed the limit composition curves shown in Fig. VIII D-1 (Ref. 1). In spite of the considerable amount of work on hydrogen-oxygen combustion since then there has been no adequate additional study of the effect of water vapor (steam) on the limits. However, the limit lines given in Fig. VIII D-1 probably represent the minimum compositions for flame propagation, i.e., the flammability region may

actually be smaller than indicated. Several factors may cause this reduction, such as downward rather than upward flame propagation and combustion in smaller vessels which would result in energy losses to the vessel walls. Note on the figure that increased temperature or pressure have a relatively small effect on the flammability limits. Therefore, the flammability region defined in the figure for a temperature of 300 F and a pressure of 100 psig is used as the basis for determining hydrogen-combustion conditions in this study.

D1.3.2 DETONATION LIMITS

Shapiro and Moffette state that in hydrogen-air mixtures (no steam) as the hydrogen concentration increases beyond 9 v/o, not only does the flame propagate in all directions but the rate of propagation increases rapidly (Ref. 1). Then when the hydrogen in air reaches 19 v/o, the mixture detonates. This condition persists until the hydrogen in air exceeds 57 v/o. The detonation occurs in a shock wave which may travel at velocities of several thousand meters per second. Very small ignition sources such as sparks can trigger detonations by initiating local combustion. The combustion advances quickly and produces turbulence and shock waves in and ahead of the flame front which rapidly transform the deflagration into a detonation. The detonation shock wave is sustained by the energy of the chemical reaction which is itself initiated by the temperature and pressure of the wave.

The detonation compositions noted above for hydrogen-air mixtures constitute the lower and upper limits of the assumed detonation limit boundary in Fig. VIII D-1. In constructing the boundary it appears that Shapiro and Moffette simply assumed parallel behavior (to the low temperature and pressure flammability limit boundary) at increasing steam concentrations. Thus, the assumed detonation limits must be considered quite uncertain, particularly in view of the very irregular detonation limits that have been observed in other three-component systems (Ref. 2). For the purposes of this study, as it is shown that results of hydrogen generation will not be sensitive to detonation-limit predictions, no effort was made to obtain better estimates.

D1.3.3 COMBUSTION OF HYDROGEN AT ENTRY TO CONTAINMENT

The hydrogen-steam mixture from the reactor primary system will enter the large containment volume via the relatively small room which contains the broken primary coolant loop. These rooms are typically only a few percent of the total containment free volume, so for expected hydrogen-steam flows in the range of 5000-10,000 cfm the residence time of hydrogen in the room would be only a few minutes. It is doubtful that any significant hydrogen burning would occur in this room for several reasons. First, the reactor-coolant blowdown would be expected to drive nearly all the original air out of the room, thus eliminating the source of oxygen for the reaction. In some accident sequences continued steam flow from water boiloff in the core would prevent return of air except by back diffusion. This would require many hours. In other accident sequences, containment spray water falling through upper gratings in the room could bring entrained air back more rapidly. The sprays would also reduce the steam partial pressure to the range where theoretically flammable hydrogen-air-steam concentrations could develop. Although some combustion might begin for the hot-leg break where the hydrogen-steam mixture could enter the room above the spontaneous ignition temperature, the oxygen supply probably could not be maintained and the reaction would soon cease. On this basis it is concluded that hydrogen combustion in the small-loop compartment can be ignored.

The next point at which the hydrogen-steam mixture might ignite and burn is at the floor grating to the large upper containment space (i.e., as the gas flows up out of the small-loop compartment). To maintain continued combustion would require a large ignition source and a continuous supply of air (oxygen). These conditions could not be met for a cold-leg break, but for a hot-leg break it is possible that the hydrogen-steam mixture would come through the grating at or above the spontaneous-ignition temperature. Once the combustion started, the heat liberated would favor continued reaction provided oxygen could be supplied at the necessary rate. Complete combustion of 600 lb-moles of H_2 (Table VIII D-1) would require 300 lb-moles of O_2 or about one-half the containment air supply. Assuming the hydrogen is generated at a uniform rate over 3/4 hour this fraction of the containment atmosphere would have to circulate to the combustion site within this time period. The required rate of circulation would steadily increase as oxygen was consumed by the reaction. Under these conditions it is doubtful how long the burning period would last.

However, if complete combustion of the hydrogen is assumed, the rate of thermal-energy addition to the containment atmosphere can be estimated. Since the heat of combustion of the hydrogen-oxygen reaction is 1.04×10^5 Btu per lb-mole H_2 consumed, the rate of energy addition (assuming uniform H_2 production) would be 8.3×10^7 Btu/hr for the 3/4 hour period. In some accident sequences this rate may be significant in terms of the internal pressure rise that would result.

If the hydrogen does not burn at the floor grating in the large upper containment space then it will tend to rise and accumulate in the upper regions of this space. Internal convection currents in the containment atmosphere will gradually mix the hydrogen throughout the volume, but after appreciable hydrogen has been generated, explosive mixtures can develop. For a typical PWR containment, 75 percent zirconium-water reaction will lead to the following hydrogen concentrations in the containment building assuming complete mixing and steam saturated conditions:

Temp, F	H_2, v/o
230	7
130	14

If only the upper containment space is considered, the hydrogen concentrations would be about twice these values. In Fig. VIII D-2 it can be seen that regardless of the hydrogen concentration in a steam-saturated atmosphere at temperatures above about 230 F, the composition will lie outside the flammability region. Therefore, a propagating combustion wave cannot occur. In accident sequences where containment sprays are not operable, the atmosphere must cool to 230 F or below before any explosive H_2-O_2 reaction is possible. However, in sequences where sprays operate, the atmosphere is cooled to 230 F in a matter of minutes and then down to the range of 130 F within an hour. The buildup of hydrogen under these conditions creates gas mixtures well within the flammability limits. The appearance of a small spark in such mixtures is often considered to present relatively high potential for initiating a detonation event. A detonation will produce two coupled effects on the containment structure. First the detonation shock wave will deliver an impulse loading to the containment wall. This dynamic loading will quickly decay to a somewhat more sustained pressure pulse from the expanding gas that has undergone adiabatic heating. Heat transfer from the gas to the wall and to internal structures will cause decay of this secondary pressure pulse. Because of the importance of these loadings to containment integrity, the detonation problem was analyzed in more detail. The results of this analysis are given in the next section.

D2. EXAMINATION OF DETONATION EVENTS

D2.1 THE MECHANISM OF DETONATION

A gaseous detonation may be initiated by a shock of sufficient intensity, or it may develop more slowly from a laminar flame. In the latter case the combustion will produce an increase in pressure which will start weak pressure waves propagating into the unburned gas. Such small disturbances, especially as they interact with the walls, promote the formation of turbulence in the flame front. Stronger shock waves are generated as a result of turbulent burning, especially as little pockets of gas explode in the flame front. These shock waves are propagated into the unburned gas, accompanied by local compression and temperature rise. When the shock wave is strong enough, the chemical reaction begins in advance of the flame front. The velocity of sound is greater at higher temperatures. Therefore successive shock waves overtake one another until a detonation results. The detonation is characterized by an exothermic reaction which is initiated by the shock wave and which in turn drives the shock wave. The velocity of the detonation is determined by the velocity of sound in the burned gas, and is usually several times the velocity of sound in the original unburned mixture.

By writing down equations expressing the conservation of mass, of momentum, and of energy in the gas as a shock wave passes through, one can describe the relationship between the pressure, p, and the specific volume, v, for any gas. This relationship is known as the Hugoniot curve. When no chemical reaction is involved, the original pressure and volume, p_1 and v_1, will be transformed into a pressure and volume in the shock wave, p_s and v_s, which depend on the intensity of the shock.

Such a shock wave will die out as it passes through an unreacting gas, the velocity will decay until it becomes equal to the velocity of sound. For a chemical reaction that proceeds to completion, the energy generated in the re-

action maintains the velocity constant. This additional constraint on the systems allows for the calculation of a unique detonation velocity, together with a specific volume and a temperature depending only on the composition of the gas and the original conditions of pressure, volume, and temperature. This calculable condition after complete reaction, is known as the Chapman-Jouquet state. This is not yet the final state of the gas; pressure equilibration has not yet taken place, and no heat has been exchanged with the surroundings.

According to this greatly simplified picture, the events transpiring as the detonation wave passes are approximately as follows: a shock wave, traveling at several times the velocity of sound, causes a very brief and very sharp increase in pressure, density, and temperature. It is caused by the net forward movement of molecules in the shock front. This net movement of molecules results in an impulse greater than that represented by the very considerable pressure spike. Immediately behind the shock front is a region of hot gas undergoing a prereaction "induction" period. During this period the concentration of reaction-causing free radicals is building up, but little energy is being released. At the end of the induction period the reaction rate increases rapidly and proceeds toward the condition of chemical equilibrium. Finally, the wave passes and the reaction products assume a final equilibrium state that marks the beginning of heat exchange with the vessel.

The simple theory sketched out above is now known to be entirely inadequate as an explanation of what happens in the detonation process. The detonation wave is not a simple plane discontinuity. It is, in fact, highly turbulent and is associated with transverse waves, the structure of which depends on the shape and size of the vessel. Nevertheless the older theory has been successful in predicting detonation velocities and other paramters of the system. It is used here to give at least a reliable order-of-magnitude estimate of the effect of a detonation under assumed conditions.

D2.2 CALCULATIONS OF DETONATION PARAMETERS

The first step in the calculation, as outlined, for example, by Lewis and von Elbe (Ref. 3), is the determination of the conditions at the Chapman-Jouquet plane. In addition to the specification of the starting conditions of composition, pressure, specific volume and temperature, this step requires that the following be known: the average specific heat of the final gas through the temperature range, the ratio of specific heats (specific heat at constant pressure divided by the specific heat at constant volume) of the final gas at the final temperature, and the heat of reaction. All of these, but especially the last, depend on the final composition, taking note of the fact that at elevated temperatures the partial pressures of H, O, and OH will not be zero. An iterative process is required; here only a few iterations are needed since temperatures were not extreme and high accuracy was not required. There is some question whether the time available is sufficient to fully excite the vibrational modes. It was assumed that sufficient time is available. The specific heats were therefore taken as the standard values without modification (Ref. 4).

Having determined the velocity of the detonation, it is possible to calculate the conditions in the initial shock plane, as outlined, for example, by Kistiakowsky and Kydd (Ref. 5). These calculations require the knowledge of the ratio of specific heats of the unreacted gas averaged over the temperature range. Again the question of the excitation of energy levels arises. The time is too short for vibrational modes to be excited. It was assumed, however, that rotational levels are excited. Therefore, the specific-heat ratio was taken as 1.4 for the diatomic molecules, and 1.33 for H_2O. The final value for the impulse must take into account the net forward motion of molecules in the shock wave. The momentum of these molecules passing unit area in unit time is w^2/v_s, where w is the net forward velocity (particle velocity) and v_s is the specific volume in the shock front. According to hydrodynamic theory, w^2 is calculated by

$$w^2 = (v_1 - v_s)\,(p_s - p_1), \quad \text{(VIII D-1)}$$

from the specific volume and pressure of the original and the shock-front gas. Therefore the pressure equivalent, that is, the rate of momentum transfer, is

$$\frac{w^2}{v_s} = \frac{v_1}{v_s}\,(p_s - p_1) - (p_s - p_1). \quad \text{(VIII D-2)}$$

If this is added to the pressure increase, $p_s - p_1$, the total impulse becomes

$$i = \frac{v_1}{v_s}(p_s - p_1). \qquad \text{(VIII D-3)}$$

From this value, the effect of the initial shock can be estimated.

Finally the gas reaches a state of equilibrium, which for an adiabatic process, is found from the heat of reaction, the average specific heat at constant volume, and the gas laws. In this calculation the equilibrium decomposition of water was neglected.

The results of these calculations for three assumed compositions are shown in Table VIII D-2. The starting compositions were selected by adding to air at 10 psia enough water vapor to saturate at 130 F and enough H_2 to approximate Shapiro and Moffette's assumed lean detonation limit (Case I), the stoichiometric composition (Case II), and Shapiro and Moffette's assumed rich detonation limit (Case III). The results are computed for idealized limiting circumstances which do not necessarily correspond to the conditions expected during an accident. Turbulence and transverse shock waves will result in many variations in temperature, pressure, and density. Obstructions in the vessel will cause perturbations. If a low-speed flame were to persist for some time before the transition to detonation, a considerable pressure increase could occur in the unburned gas before detonation, thus leading to a more severe shock (Ref. 6). The full calculated impulse is delivered to the wall only if the direction of propagation is normal to the wall.

The core-meltdown analyses described in Appendix A predict the extent of zirconium-water reaction to be 75 $\pm$ 25 percent of Zircaloy in the PWR cladding. Case I corresponds to approximately 100 percent Zircaloy reacted, or the upper limit of the Appendix A calculations. Case II, the stoichiometric composition, would require the equivalent of a 150 percent Zircaloy-water reaction. While this may be physically realizable from the reaction of all the cladding in combination with contributions from iron-water, UO_2-water, and other reactions, it is considered quite unlikely. Further, the reaction of the hydrogen generated in Case II would require the consumption of all the oxygen initially present in the containment building. Case III, the assumed rich detonation limit, is not believed attainable under the reactor-accident conditions of interest here.

The quasiequilibrium pressure resulting from the detonation or rapid self-propagating combustion of the hydrogen from an equivalent 75 percent cladding reaction would produce peak pressures of 71-77 psia within the PWR containment building. At these levels, containment failure would not be expected. The effect of the initial impulse of the shock wave is more difficult to assess. It will depend on the duration as well as the magnitude of the impulse. In the next section the time scale is examined.

D2.3 DURATION OF THE SHOCK WAVES

An examination of the literature on hydrogen-oxygen detonations shows that an enormous research effort has been expended on various aspects of this process. Almost all of it has been done in long narrow tubes at reduced pressure, diluted, if at all, with inert gas. It has not been possible to find specific information on the time required for the detonation process under conditions similar to those of the present study. Since detonation velocities are of the order of thousands of meters per second, the resolution of measuring instruments must be of the highest order. It is for this reason that low pressures and high dilutions have been so widely used. Nevertheless, with some judgment and some extrapolation, reasonable estimates can be made at least of the order of magnitude of the time scale.

Bradley reports some determinations of the thickness of shock fronts leading to an estimate of about $6L_o$, where L_o is the mean free path in the undisturbed gas (Ref. 7). The thickness of the shock front would then be about 4×10^{-7} m for Case I, and the duration of the initial shock, about 3×10^{-10} sec. The average molecule would remain in the front somewhat longer than that because it is swept forward with the shock front. One estimates, for this case then, that the average molecule would undergo approximately 100 collisions as the shock front passes by. This length of time is of the same order of magnitude as that required for rotational excitation, but is too short for the vibrational levels. This seems more reasonable than the 2 or 3 mean free paths calculated by Thomas (Ref.

8). Experimental evidence on weak shocks in N_2 at higher pressures also indicated thinner fronts, although not so thin as indicated by the Thomas calculation (Ref. 9).

It is concluded that a reasonable value for the duration of the original shock would be 3×10^{-10} sec.

The detonation wave is being driven forward by the formation of hot gas in the reaction immediately following. The pressure in the shock front decays not to the original ambient pressure, but to the pressure corresponding to the burned gas, that is, to the Chapman-Jouquet condition. The time duration of this period, during which the reaction goes to completion, was estimated from the measurements of the reaction rates in the hydrogen-oxygen system.

The reaction normally proceeds by way of an initiation step in which the free radicals, H and OH, are formed, followed by a chain-branching step in which the number of these radicals is multiplied. In this part of the reaction, known as the induction period, little H_2O is formed and little heat is produced. When sufficient chain carriers are formed, they begin to react to form H_2O, thus raising the temperature and accelerating the reaction. Throughout the induction period and the main reaction period chain-stopping reactions involving third bodies such as N_2 or H_2O serve to slow the process. The chain-stopping step involves the formation of a metastable radical, HO_2. At high temperatures, the induction period is probably negligible since the H_2O originally present will decompose and form H and OH and since the chain-stopping HO_2 becomes entirely unstable. Near the combustion limits and under marginal conditions, however, the length of the induction period may determine whether or not the detonation is propagated.

The induction period has been studied in shock tubes at relatively low pressures, and with inert gas, but not H_2O, as a diluent. The results are usually shown in straight-line plots of log $[O_2]\ \tau_i$ vs T^{-1}, where $[O_2]$ is oxygen concentration, τ_i is the induction time and T is the temperature. Using Case I as an example, these results indicate 0.8 to 1.6-μsec induction times (Refs. 7,10,11). These values are determined by a considerable extrapolation, however, since the work was done at low pressures, where τ_i was considerably greater.

Kistiakowsky and Kydd (Ref. 5) measured the density changes during the detonation reaction and interpreted these in terms of the time for 0.50 or 0.75 of the reaction to be completed. They found no evidence of an induction period. Their work was also done at low pressures. Extrapolating their results to atmospheric pressure gives 0.26 μsec for a stoichiometric mixture, 1.7 μsec for a mixture containing 14 percent H_2 and 30 percent O_2. Dove and Tribbeck devised a computational method for studying the duration of the reaction (Ref. 12). They give reaction times, for the undiluted mixture at 1 atm of 0.6 μsec for 16 percent H_2, 0.02 μsec for a stoichiometric mixture, and 0.2 μsec for 92 percent H_2. They report that experimental reaction times at lower pressures are 5-10 times longer.

In summary, reaction times in the range 0.1 to 10 μsec seem reasonable. In terms of its effect on the reaction time, water will probably act only as a diluent (Ref. 5). Because of the likelihood of compositions somewhat removed from stoichiometric, together with the presence of N_2 and H_2O diluents, the times are likely to be closer to the upper end of this range.

D2.3.1 APPLICATION TO A LARGE VESSEL

Most of the experimental work which underlies the discussion above was done in shock tubes. Pressures were generally of the order of 0.1 atm or less, and the diluents, if any, were N_2, Ar, or He. Since the present case differs in several respects, some attention may be given to each aspect of the difference.

Detonation in a tube represents, at first glance, a one-dimension process. The process is too rapid for any appreciable heat-transfer to the walls. It is now known, however, that the structure of transverse waves which accompany the longitudinal wave is dependent on the tube walls. This complex system of shock waves probably plays an important part in the course of the chemical reaction, especially near the detonation limits. In a freely expanding detonation, the transverse-wave structure will be considerably different. Struck and Reichenbach observed no turbulence behind the combustion zone, no cellular structure in the wave front, and no transition from deflagration to detonation except by interaction with the wall (Ref. 13). Soloukhin and Ragland observed more evidence of structure, but also noted the difficulty of establishing the detonation in a freely expanding shock wave (Ref. 14).

It has been necessary to use data obtained at subatmospheric pressure often with no inert ingredients (scarcely any in the presence of added water vapor) to evaluate detonations at pressures above atmospheric, with N_2 and H_2O present. With respect to the properties of the detonation wave, its velocity, pressure, and duration, these extrapolations are reasonably reliable. The theory on which calculations were based has not proved adequate in a descriptive sense, but it has been successful in predicting detonation parameters. More uncertainty is involved with respect to the limits of detonation. The presence of water vapor may serve to quench the incipient reaction by providing an efficient chain-stopping mechanism. Neither theory nor experimental evidence is adequate to establish the detonation limits very precisely under the free-expansion conditions that exist in the containment vessel. Furthermore, the conditions necessary for initiating a detonation under these circumstances is not well known. It seems likely that there is a considerable composition range in which detonation is possible, but detonation is highly unlikely because of the severity of the conditions needed for its initiation.

Nevertheless, if it is assumed that the initiation occurs and the detonation proceeds, the effect on the containment structure can be estimated as follows using the data in Table VIII D-2 and the estimated shock-duration times. The natural period of vibration of typical containment structures is much greater than the duration of a detonation shock wave, so the loadings can be approximated by an impulse loading. Newmark has developed a convenient empirical formula for such use which gives answers to $\pm$ 5 percent accuracy (Ref. 15). For a brittle material (the reinforced concrete wall) the formula is,

$$pt = 0.32\ RT, \qquad \text{(VIII D-4)}$$

where p is the maximum pressure in the impulse, t is the time of the detonation, R is the loading that produces the maximum elastic deflection for the structure, and T is the natural period of vibration. Letting R = 120 psia (i.e., twice the design pressure for a typical PWR (containment vessel) and T = 0.02 second, the estimated natural period for a typical reinforced concrete PWR containment vessel (Ref. 16), the right side of the above equation equals 0.77. Therefore, if the product, pt, is less than this value the structure will not fail under the impulse loading of the detonation shock wave. Using the pressure impulse values given for the three composition cases in Table VIII D-2 along with the estimated upper limit value of 10 μsec for the duration of the impulse, the following pt values are obtained:

Case	p, psia	t, sec	pt
I	1200	10^{-5}	0.012
II	1331	10^{-5}	0.013
III	1727	10^{-5}	0.017

The pt values are well below the allowable limit of 0.77 so failure of the containment due to the detonation shock wave is not expected.

The above shock-wave analyses were performed for the same idealized limiting compositions as considered previously for the evaluation of the quasiequilibrium pressures. For the actual quantity of hydrogen predicted to be available, the possibility of containment failure would be even less.

Since neither the shock wave nor the ensuing quasiequilibrium pressure of the detonated gas mixture approach the levels required for failure, the probability that a hydrogen detonation will result in PWR containment failure can be considered negligible.

D2.3.2 HYDROGEN IN A BWR

The influence of hydrogen production in accident sequences involving core meltdown in a large BWR is quite different from that in a large PWR. In sequences where the ECC systems do not operate, the primary coolant blowdown leaves the pressure vessel essentially dry so no appreciable metal-water reaction hydrogen will be produced during initial core meltdown. As the core melts through the pressure vessel and falls to the containment floor, it will come into contact with water and appreciable hydrogen generation may result. For sequences where the core meltdown occurs with water in the vessel, hydrogen production will be similar to PWR cases. If the containment fails prior to core melting, the subsequent generation of hydrogen will not be of concern.

BWR containment atmospheres are inerted by purging with nitrogen until the oxygen content is below 5 percent. The oxygen is maintained at or below this level during normal operation. At this oxygen concentration, the containment

atmosphere is outside hydrogen flammability limits, regardless of the quantity of hydrogen in the atmosphere (Ref. 18). Under these circumstances, the primary significance of hydrogen is as a noncondensable medium for containment pressurization. Since the free volume of BWR containment is much smaller than that of PWR's, the relative significance of hydrogen as a pressure source is much greater in BWR's.

Radiolytic decomposition of water during the course of the accident would add oxygen as well as hydrogen to the atmosphere. Maximum accident times of interest here are of the order of a day or less. Using an integrated fission product decay energy over one day or 14×10^{30} ev, an energy absorption factor of 0.1 in the core region, and the upper limit $G(H_2)$ value of 0.44, the maximum yield of hydrogen at the end of this period would be about 8100 SCF or 23 lb-moles. The radiolytic oxygen yield would be a factor of two lower. Neglecting any hydrogen from the zirconium-water reaction, the above would result in hydrogen and oxygen concentrations of 2.8 and 6.5 percent, respectively. This composition is outside the flammability range. If the hydrogen generated by the zirconium-water reaction is included, the atmosphere will be hydrogen rich and outside the flammable range.

Thus it is concluded that hydrogen combustion can be eliminated as a mechanism of containment failure in BWR degraded accident sequences.

D2.4 CARBON DIOXIDE GENERATION IN PWR AND BWR

Carbon dioxide can be generated in a reactor-meltdown accident through thermal decomposition of concrete containing limestone aggregate according to the reaction,

$$CaCO_3 + \text{heat} \rightarrow CaO + CO_2\uparrow. \quad \text{(VIII D-5)}$$

Standard texts indicate that the decomposition of $CaCO_3$ becomes rapid at a temperature of about 800 C (1470 F). Therefore, this represents a later source of gas in the accident when the molten core material penetrates the pressure vessel and falls onto the concrete floor and base mat of the containment structure. The CO_2 generation by itself probably would not be sufficient to cause overpressurization of either a PWR or a BWR containment, since other failure mechanisms are effective competitors. However, as CO_2 can contribute to overpressure failure under certain conditions, the generation cannot be ignored. The containment response analysis takes all the processes into account; thus, only the basic information needed to consider the CO_2 generation mechanism is provided here.

Reimer and Seidenfeld have presented a useful documentation of the problem and the pertinent basic data given below is taken from their work (Ref. 17). The composition of the concrete that has been used in this study is presented below. Although this characterization does not represent a typical concrete, it provides an upper bound to the quantities of gases (H_2O and CO_2) that might be released during the decomposition of concrete.

Material	Weight Percent
$CaCO_3$	60
H_2O	20
SiO_2	20

Concrete apparently will begin to rapidly disintegrate and spall at about 900 F as the free water expands, ruptures the surface, and escapes. The yield of CO_2 when the $CaCO_3$ decomposes can be given in various units as follows based on a concrete density of 150 lb/cu ft.

CO_2 Yield per Unit Amount of Concrete

325 ft^3 CO_2 (STP) per ft^3 concrete
0.905 lb-mole CO_2 per ft^3 concrete
0.264 lb CO_2 per lb concrete

The energy needed to decompose calcium carbonate is given as 42,500 cal/g-mole $CaCO_3$. This converts to a value of 460 Btu/lb concrete. Other energy requirements to heat the concrete materials to the decomposition temperature and above

can be determined with the following list of heat capacities.

Material	Heat Capacity
CO_2	0.26 Btu/lb/F
H_2O	0.58 Btu/lb/F
$CaO + SiO_2$	0.22 Btu/lb/F

Continued energy input after the calcium carbonate is decomposed can result in melting of first SiO_2 (MP = 3100 F) and then CaO (MP = 4400 F). The heat of fusion of these two materials is given as:

Material	Heat of Fusion
SiO_2	64.5 Btu/lb
CaO	578 Btu/lb

These physical parameters can be used to evaluate the gas yield and the thermal energy requirements of the concrete-decomposition problem.

References

1. Shapiro, Z. M., and Moffette, T. R., "Hydrogen Flammability Data and Application to PWR Loss-of-Coolant Accident", WAPD-SC-545 (September, 1957).
2. Miles, J. E. P., Munday, G., and Ubbelohde, A. R., "Effects of Additives on Marginal Detonation in Gases", Proc. Roy. Soc., 269, 165-179 (1962).
3. Lewis, Bernard, and Van Elbe, Guenther, "Combustion, Flames and Explosions of Gases", Second Edition, Academic Press, p. 524 (1961).
4. JANAF Thermochemical Tables, Second Edition, NSRDS-NBS 37 (1971).
5. Kistiakowsky, G. B., and Kydd, P. H., J. Chem. Phys., 25, 824-835 (1956).
6. Brinkley, S. R., Jr., and Lewis, B., Symp. Combust, p. 807 (1958).
7. Bradley, John, N., "Shock Waves in Chemistry and Physics", John Wiley & Sons (1962), Chapter VII.
8. Thomas, L. H., J. Chem. Phys., 12, 449 (1944).
9. Cowman, George R., and Harnig, Donald F., J. Chem. Phys., 18, 1008-1018 (1950).
10. Schott, G. L., and Kinsey, J. L., J. Chem. Phys., 29, 1177 (1958).
11. Mullaney, G. J., Kw, Peh S., and Botch, W. D., AIAA Inl., 3, 873 (1965).
12. Dove, J. E., and Tribbeck, T. D., Astronautica Acta, 15, 387-397 (1970).
13. Struck, W. G., and Reichenback, H. W., Symp. Combust., II, 677-82 (1966).
14. Soloukhin, R. I., and Ragland, K. W., Comb. and Flame, 13, 295-302 (1969).
15. Newmark, N. M., "An Engineering Approach to Blast Resistant Design", Proc ASCE Separate No. 306, Oct. 1953.
16. Morrison, D. L., et al., "An Evaluation of the Applicability of Existing Data to the Analytical Description of a Nuclear Reactor Accident - Core Meltdown Evaluation", BMI-1910, p. C-19, Table C-5 (July, 1971).
17. Reimer, R. A., and Seidenfeld, A., "Investigation of the Consequences of a Nuclear Reactor Core Melt-Through Accident", ORNL-MIT-62 (October, 1968).
18. Coward, H. F., and Jones, G. W., "Limits of Flammability of Gases and Vapors", Bulletin 503, U. S. Bureau of Mines (1952).

TABLE VIII D-1 PWR HYDROGEN SOURCES

Hydrogen Source	Estimate of H_2 Generation Rate, lb-moles/hr	Period of Generation, hr	Estimated Yield in Period, lb-moles
Core-metal/ water reaction (a)	800	0.75	600
Radiolysis of water (b)	1.9	24	46
Corrosion of metals by spray solutions (c)	0.15	48	7

(a) Based on core zirconium content and thermal analysis of meltdown period.

(b) Simple average based on decay integrated over one day, 20 percent absorbed, and $G(H_2) = 0.44$. The rate decreases with time.

(c) Based on corrosion of aluminum paint by alkaline spray. Rate will decrease by more than ten for longer times.

TABLE VIII D-2 CALCULATED DETONATION PARAMETERS FOR LIMITING COMPOSITIONS

Case		Composition, volume percent					Pressure		Impulse		Temperature		Specific Volume,	Energy of Combustion,	Detonation Velocity
		H_2O	H_2	O_2	N_2	OH	N/m^2	psia	N/m^2	psia	K	F	m^3/kg	J/kg	m/sec
I	(a)	15.0	18.0	14.1	52.9		1.029×10^5	14.9			327.6	130	1.182		
	(b)						1.906×10^6	276	8.30×10^6	1200	1360.0	1990	0.269		
	(c)	36.1		5.5	58.2	0.31	1.072×10^6	156			2175.0	3454	0.684	1.9325×10^6	1650
	(d)	36.2		5.6	58.2		6.30×10^5	91			2008.0	3156	1.182		
II	(a)	13.4	25.6	12.8	48.2		1.130×10^5	16.4			327.6	130	1.024		
	(b)						2.050×10^6	297	9.19×10^6	1331	1398.0	2930	0.216		
	(c)	44.4	0.1		55.3	0.32	1.469×10^6	213			2784.0	4550	0.583	2.998×10^6	1797
	(d)	44.7			55.3		9.06×10^5	131			2625.0	4275	1.024		
III	(a)	11.0	40.0	10.3	38.7		1.407×10^5	20.4			327.6	130	1.026		
	(b)						2.690×10^6	390	1.190×10^7	1727	1340.0	1952	0.219		
	(c)	35.1	21.6		43.2	0.10	1.670×10^6	242			2497.0	4035	0.590	2.926×10^6	1925
	(d)	35.2	21.6		43.2		9.75×10^5	142			2269.0	3625	1.026		

(a) Original gas
(b) Shock front
(c) C-J plane
(d) Final gas

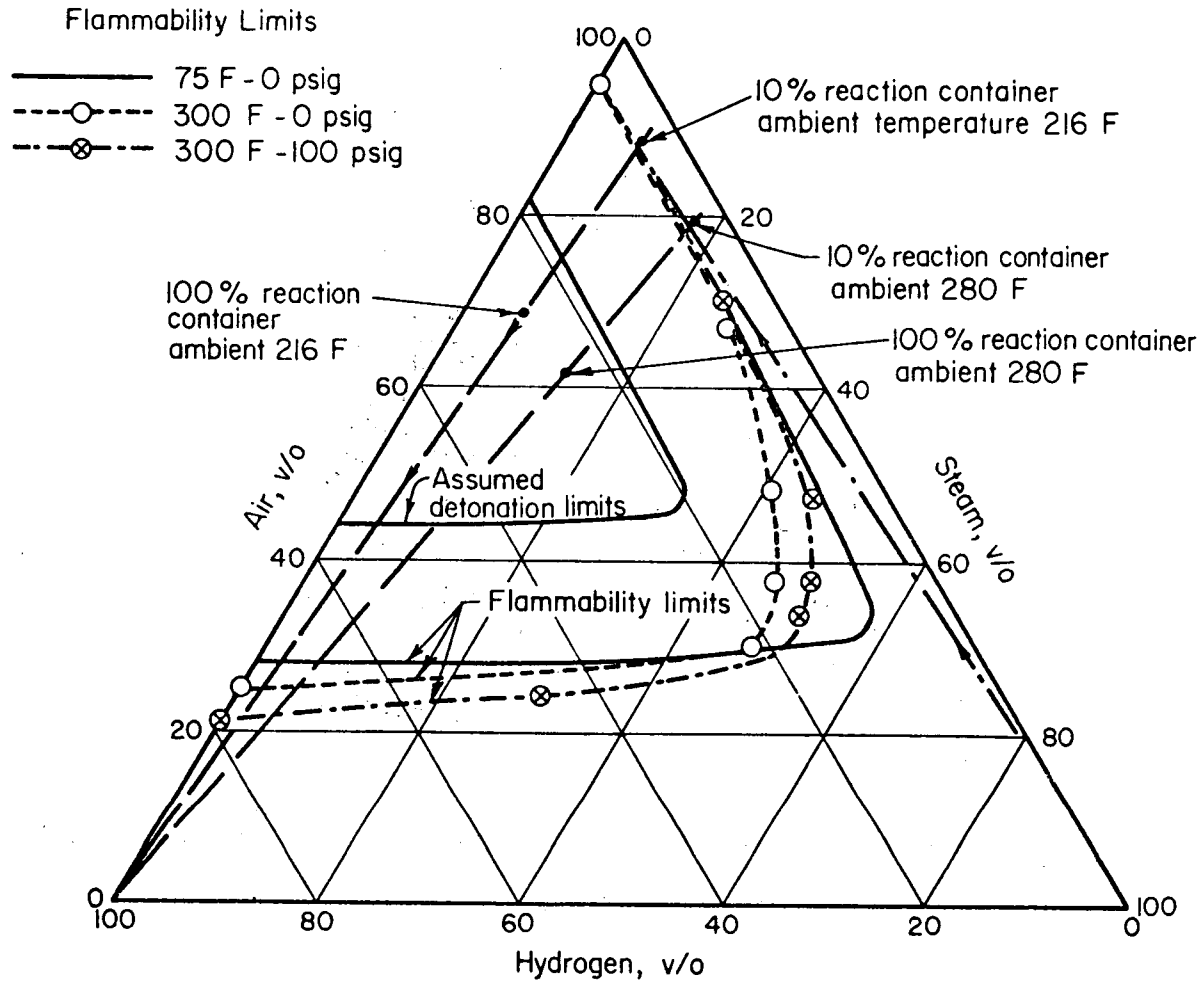


FIGURE VIII D-1 Flammability Limits of Hydrogen-Air-Steam Mixtures (Ref. 1)

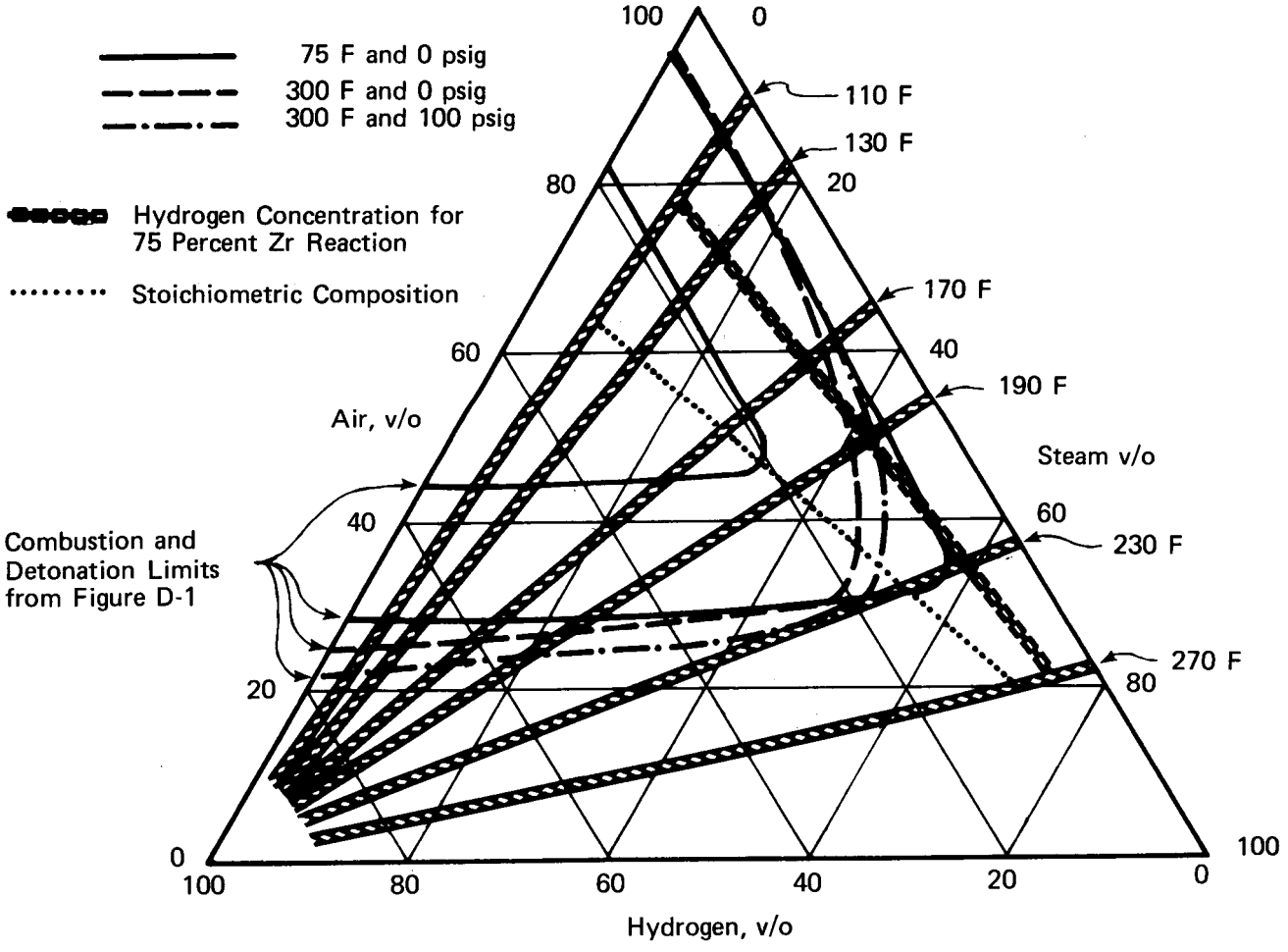


FIGURE VIII D-2 Composition Isotherms for Containment Atmosphere at Saturated Steam Conditions

APPENDIX E

CONTAINMENT FAILURE MODES EVALUATION

Appendix E
Table of Contents

Section		Page No.
E1.	SUMMARY AND CONCLUSIONS	VIII-133
E2.	DISCUSSION: PWR CONTAINMENT	VIII-133
E3.	DISCUSSION: BWR CONTAINMENT	VIII-136
Part I		VIII-139
1.	GENERAL	VIII-141
	1.1 Loading Conditions at Accident	VIII-141
	1.2 Design Basis	VIII-141
2.	EFFECT OF INCREASING INTERNAL PRESSURE	VIII-141
	2.1 General	VIII-141
	2.2 Conditions at the Yield Point of Reinforcement	VIII-142
	2.2.1 Summary for Conditions when Reinforcement at Yield	VIII-143
	2.3 Conditions at the Ultimate Strength of the Reinforcement	VIII-143
	2.4 Ultimate Strength of the Concrete in Shear	VIII-145
	2.5 Ultimate Strength of the Liner	VIII-147
3.	EFFECT OF RISE IN INTERNAL TEMPERATURE	VIII-148
4.	CONCLUSION	VIII-148
LIST OF REFERENCES		VIII-150
LIST OF FIGURES		VIII-150
Part II		VIII-153
1.	DESCRIPTION OF CONTAINMENT FAILURE ANALYSES	VIII-156
	1.1 Reinforced-Concrete Containment Structure	VIII-156
	1.2 Steel Containment Structure	VIII-157
	1.2.1 Computer Calculation for Axisymmetric Pressure Vesses	VIII-157
	1.2.2 Burst Pressure Calculations for Individual Components	VIII-158
2.	DISCUSSION AND RECOMMENDATIONS	VIII-158
	2.1 Reinforced-Concrete Containment Structure	VIII-158
	2.2 Steel Containment Structure	VIII-159
REFERENCES		VIII-160

List of Tables

Table		Page No.
VIII E-1	Estimated Containment-Building Failure Pressures.....	VIII-161
VIII E-2	Distortion Energy Failure Estimates.....	VIII-161
VIII E-3	Summary of Calculated Stresses in Typical Vapor-Suppression Containment for Boiling-Water Reactors.....	VIII-161
VIII E-4	Summary of Estimated Burst Pressures for Components of a Typical Vapor-Suppression Containment for Boiling-Water Reactors.....	VIII-162
VIII E-5	Summary of Computer Analysis Used for Vapor-Suppression Containment for Boiling-Water Reactors.....	VIII-162

List of Figures

Figure		Page No.
VIII E-1	Axisymmetric Model for Steel Shell Computer Analysis.....	VIII-163

Appendix E

Containment Failure Modes Evaluation

E.1 SUMMARY AND CONCLUSION

The objective of this subtask was to determine the thresholds and modes of failure for reactor containment buildings when subjected to internal pressures and temperature greater than the design values. Containment structures representative of boiling as well as pressurized water reactors were considered with the intent of determining the conditions at which failure would occur, identifying the probable failure locations, and defining the nature and size of the most likely failures.

Subatmospheric containment of reinforced-concrete construction was considered for the PWR, and the light bulb and torus vapor-suppression arrangement was taken to be representative of BWR containments. A specific containment structure of each type was selected for use in this study in order to have a meaningful basis for evaluation. To the extent possible, the extension of the results to other containments of similar design has been indicated.

Of necessity, the extent and depth of this evaluation were limited, with emphasis on the principal features, design criteria, and materials utilized. Nevertheless, a significant number of aspects were considered for each of the two containment concepts in arriving at the conclusions presented here. To refine the conclusions, consideration would have to be given to the as-built details of specific containment structures as well as to the results of tests and nondestructive examinations. Several consultants, both at BCL as well as external, were utilized to guide this evaluation; their reports are presented in Parts I and II of this Appendix. The conclusions presented here are based on the recommendations of the consultants as well as consideration of other factors and substantial additional analyses.

Subject to the limitations and conditions discussed below, the conclusions of this study are as follows:

a. A reinforced-concrete containment building designed for an internal pressure of 60 psia (45 psid) when subjected to slow overpressurization by steam would be expected to fail at a pressure of 100 ± 15 psia. The failure would be initiated by yielding of the reinforcing steel and/or crumbling of the concrete, and lead to a gross failure of the structure. Such a falure would take place in those parts of the structure without any radial reinforcement of the concrete, e.g., upper portions of the cylindrical shell and/or the hemispherical dome.

b. Vapor-suppression containment of the steel drywell and torus arrangement designed for an internal pressure of 71 psia (56 psid) when subjected to overpressurization would be expected to fail at a pressure of 175 ± 25 psia. Typically, the weakest portion in such a structure would be in the upper part of the toroidal suppression chamber; other highly stressed locations are the toroidal knuckle between the spherical and cylindrical parts of the drywell, the thinner cylindrical parts of the drywell, the thin part of the sphere, and the expansion joints on the drywell-wetwell vents. The failure would be expected to start at a weld or a discontinuity such as the attachment of a structural support, penetration, or embedment.

   As applied in this study the failure pressure is not a single discrete value, but a continuous variable with a normal distribution about the nominal value. This approach recognizes that the probability of structural failure is small at loads slightly above design, but increases with increasing loading. By definition, the probability of failure at the nominal failure pressure is 0.5; it approaches unity as the loading approaches the ultimate strength of the structure.

E.2 DISCUSSION: PWR CONTAINMENT

Subatmospheric containment of reinforced-concrete construction was assumed to be representative of pressurized water reactor practice. Typically, such a structure has a flat base mat, a vertical cylindrical shell, and a hemi-

spherical dome; a thin steel liner on the inside provides a leaktight barrier. The design was assumed to be in accordance with the ACI code for reinforced-concrete structures; the materials utilized are representative of current practice. In the prediction of failure thresholds the materials properties utilized are expected values rather than the minima specified by the various codes.

The determination of the failure threshold for reinforced concrete reactor containment buildings requires considering the complex interaction among the liner, concrete, and the reinforcing steel. The strength of the liner is low, but its integrity must be maintained if the structure as a whole is to function. Should the liner lose its integrity, the reinforced concrete, though structurally intact, will not be able to maintain internal pressures due to porosity and cracking of the concrete. The concrete, though it may be cracked, serves to transmit the internal pressure loads to the reinforcing steel. Deterioration of the concrete will defeat the function of the reinforcing steel and lead to failure of the structure. The reinforcing steel is the main load-bearing element in the structure and its failure is synonymous with the failure of the structure as a whole. The determination of the failure threshold of a reinforced-concrete containment building requires the definition of the conditions at which the three main elements of the structure cease to function as a whole.

The steel liner serves as the leak-tight barrier for the containment. It has a relatively low strength in comparison with that of the reinforced concrete and depends on the latter for support. No allowance is given to the strength of the liner in the design of the structure. The liner material is typically much more ductile than the reinforcing steel; thus in a gross sense the concrete behind the liner would have to fail first. Careful attention, however, must be paid to the details of the liner installation and anchoring, particularly at discontinuities (such as the building wall-to-foundation joint and penetrations) to ensure that the liner can deform without failure under all design loadings. In the designs considered, this objective appears to have been achieved.

The ideal ultimate strength of the containment structure considered is about 140 psia, based on the tensile strength of the reinforcing steel and liner. At this loading, failure of the structure would be a certainty. It is recognized, however, that the achievement of the ultimate strength in all parts of the structure may not be possible. Accordingly, the possibility of failure at less than the ultimate loading must be considered.

The design of reinforced-concrete containment structures is based on a safety factor of 1.5 on the yield strength of the reinforcing steel with an additional 10 percent reduction in working stresses to allow for nonuniformity in materials and workmanship. This results in a nominal safety factor of 1.67 on the yield strength of the reinforcing steel at the design loading. No allowance is given to the strength of the steel liner in determining the quantity of reinforcing, although the latter should be included in the evaluation of the ultimate strength of a structure. In Part I, Mast suggests that the ultimate strength of reinforced-concrete containment will be reached when the reinforcing steel is at its yield point. The large strains associated with stresses beyond yield will result in the separation of the steel from the concrete and loss of any strength from aggregate interlock as a result of cracks in the concrete. The failure would be expected to take place in those regions which lack radial reinforcement - typically the upper portions of the cylindrical shell as well as the hemispherical dome. For a structure designed for 45 psid this criterion leads to an ultimate strength of 75 psid. Adding to this the yield strength of the liner yields a maximum loading of 92 psid. Based on the criterion suggested by Mast, failure of the structure could thus be expected at an internal pressure of 107 psia.

The evaluation given in Part II argues that due to the overreinforced character of typical reactor containment structures the concrete will fail while the steel is at relatively low stress levels. That is, the differences in stress levels between the inner and outer layers of reinforcing due to the thermal effects and geometrical constraints will be greater than can be accommodated by the concrete as the loading exceeds design levels. If the concrete cannot effectively distribute the internal pressure loads among the various layers of reinforcing, most of the load will be taken up by the innermost layers of reinforcing and the containment liner. Using this line of argument and assuming that failure will take place approximately halfway between the yield and ultimate strength of the load-bearing

liner-reinforcing steel combination, a failure load of 75 psid corresponding to an internal pressure of 90 psia is estimated.

The value of 90 psia for the failure pressure must be considered conservative since it accounts for only part of the reinforcing provided. The 107 psia failure pressure should be more realistic. Both these values are considerably below the ideal ultimate strength of the structure noted above. In view of the physical bases for these two values, the nominal failure loading is taken as the approximate mean of the two.

In addition to the strength of the structure as a whole, the effects of discontinuities, penetrations, and other factors have been considered. Small penetrations are normally placed so as not to interfere with the pattern of reinforcing steel and thus require a minimum of effort to achieve a sound design. The evaluation of the failure potential of all the various small penetrations would require a detailed look at each and is beyond the scope of this study. Major penetrations such as personnel- and equipment-access hatches represent significant perturbations that could result in potentially weak points in the system. Their net effect is highly dependent on design details. Substantial additional reinforcing steel is provided to compensate for reinforcement interrupted by these large openings; the resultant structure, in theory, is at least as strong as the unperturbed structure. Such additional reinforcing steel, however, makes it extremely difficult to achieve sound concrete pours and good bond strength between the steel and concrete. In the absence of a sound concrete matrix the strength of the steel reinforcing cannot be effectively developed, and weakening of the structure will result. Such considerations are difficult to quantify, at best, and cannot be evaluated in the absence of specific details on design, quality of workmanship, and results of nondestructuve examinations. Other factors bearing on the failure potential of major penetrations include the manner in which they are anchored to the concrete and the reinforcing steel, the reinforcing of the liner around such penetrations, and the attachment of the liner to the penetrations. The significance of these factors will obviously vary with the details of each design.

A potential low-threshold-failure location exists in some reinforced-concrete containments near the apex of the hemispherical dome where the reinforcing bars end in a cylindrical ring. In such designs the final closure is achieved by bolting a flat plate across the opening and utilizing a gasket seal. While the thickness of the containment liner will typically be increased near such an opening, neither the flat plate nor the liner are necessarily backed by concrete or other rigid structures. Thus at pressures and temperatures appreciably above nominal design levels the gasketed surfaces may distort and lead to leakage past the gasket. Also, the gasket material could deteriorate at temperatures and pressures above design levels. Such factors could possibly lead to substantial leakage at pressures lower than those required for gross structural damage. Again, the potential failure threshold will be highly design dependent.

As noted above, the design of reinforced concrete containments incorporates a nominal safety factor of 1.67 on the yield strength of reinforcing steel. However, reductions of 10 percent in the strength of individual components, e.g., rebar splices are commonly permitted. Further, the large amount of reinforcing included in these structures often leads to difficulties in obtaining sound concrete pours. Thus it is possible that locally the strength of the structure can be lower than would be predicted on the basis of nominal design parameters. It can be expected, however, that highly localized weaknesses, should they occur, can be accommodated by local yielding and/or deformation without affecting the overall integrity of the structure.

As is typical practice with reactor containments, this structure has been strength and leak tested at loadings somewhat in excess of design levels. Successful performance during such testing indicates that the design objectives have been met in practice.

On the basis of the evaluations discussed above as well as the input of the consultants whose reports are given in Parts I and II of this Appendix, it is concluded that a typical reinforced-concrete containment building designed for an internal pressure of 60 psia can be expected to fail at 100 $\pm$ 15 psia. The error band should encompass uncertainties as to the mechanism and threshold of failure as well as expected variations in materials, properties, and workmanship. Structural failure would be expected in the upper portion of the cylindrical shell or hemispherical dome as a result of yielding of the reinforcing steel and/or shear failure of the

concrete matrix. The eventual size of the failure is difficult to evaluate, but it would be expected to be large enough to defeat the primary function of the containment, i.e., retention of the pressurized contents of the containment atmosphere. Major penetrations and discontinuities in the structure can be potential weak points; with careful attention to design detail they can be eliminated.

E.3 DISCUSSION: BWR CONTAINMENT

Boiling water reactor containment was assumed to be typified by a steel drywell and torus vapor-suppression arrangement. The nominal design pressure was taken to be 56 psid and the design assumed in accordance with Section III of the ASME Pressure Vessel Code. Materials selected are representative of industry practice; materials properties utilized in failure evaluation are expected values rather than code-specified minima.

A computer stress analysis on a typical drywell vessel was performed at BCL and the results compared with typical results presented in reactor-safety-analysis reports. This analysis indicated the primary stress distribution in the structure as a whole as well as pinpointed locations of high secondary stresses. The results of this analysis and comparison are discussed in Part II. The computer stress analysis did not include consideration of the suppression-chamber torus, the drywell top head and its closure, or the expansion joints on the drywell to wetwell vent pipes. Accordingly, additional detailed evaluations were performed on these components and other selected details of the BWR containment structure to provide a consistent basis for the prediction of a failure threshold.

The above combination of analyses indicated the most highly stressed region to be the inside upper part of the suppression-chamber torus. This is a consequence of the typically reduced wall thickness in this area combined with the geometrical configuration. Other highly stressed areas are the toroidal knuckle between the spherical and cylindrical parts of the drywell and the upper part of the drywell sphere. In addition to the above areas having high primary stresses, substantial bending stresses are predicted for the following locations: the attachment of the drywell to its support skirt, the embedment of the drywell in the concrete foundation, and the conical transition between cylinders of different diameters.

A number of factors have been considered in developing a failure criterion for BWR containment of the type considered in this study. These include the materials of construction, expected quality control, type of loading, and constraints on the system. The materials of construction are generally medium-carbon steels which are quite ductile and thus can undergo substantial plastic deformation before failure. These structures are designed and fabricated in accordance with Section III of the ASME Pressure Vessel Code, thus implying a high degree of quality control in materials and workmanship. The numerous penetrations through the structure, by the above code requirements, will be reinforced so as not to detract from the ultimate strength of the structure as a whole. These considerations support the selection of the ultimate strength of the base material as the failure criterion; this is the criterion selected in the evaluation of Part II to this Appendix. However, the conclusion that the structure can maintain its integrity until the ultimate strength of the base material is reached implies that all the welds have a strength and ductility equal to those of the base material. It further assumes that the structure can everywhere deform as required to accommodate secondary stresses such as local bending. It does not seem prudent to assume that the large number of field welds required in the fabrication of the drywell and wetwell structures can be accomplished without any flaws or imperfections. Also, at internal pressures above the design levels the drywell vessel will contact the concrete shielding and other structures surrounding it. On the one hand, the concrete may tend to support the steel vessel; on the other, it will impede free expansion and thus may lead to additional stresses and/or stress concentrations. Further, a number of internal structural supports are attached to the walls of the drywell; these will impede the free expansion and may act as stress raisers. It should also be noted that the varying metal thicknesses and changes in geometry and overall dimensions will result in non-uniform deformations in various parts of the structure; this in turn will lead to varying degrees of interaction with the surrounding concrete and possibly produce buckling-type loads on parts of the structure.

If the ultimate strength of the structure can be developed, the failure pressure would be 250 psia as indicated in

Part II of this Appendix. As discussed above, however, the potential for failure at lesser loadings must be recognized.

It is concluded that a reasonable failure criterion for the containment structure in the present study is a stress level in the base material halfway between the yield and ultimate strength of the metal. Thus the best estimate for the failure pressure for a typical drywell and torus vapor suppression containment, designed for 56 psid, is 175 ± 25 psia, with the failure taking place in the top half of the toroidal suppression chamber. Such a rupture would not be expected to lead to structural failure of the containment as a whole, but would be expected to be sufficiently large to rapidly depressurize the system. The mechanical properties utilized in this evaluation have been the expected properties of the materials rather than the minima specified in the applicable codes. Where appropriate, account has been taken of the expected changes in materials properties with changes in temperature.

Potential weak points in the type of containment considered here are the expansion joints on the vent pipes from drywell to suppression pool, unless specific measures are taken to ensure their integrity at pressures significantly in excess of design values. Such measures would consist of limiting the total axial motion of the joint and confining the flexible elements in such a way as to maintain their prescribed geometry. With such precautions, a common practice in the design of reactor containment, the ultimate strength of the expansion joints should be comparable to that of the rest of the structure. In their absence, the expansion joints could fail at about twice the design pressure, or at an internal pressure of about 125 psia within the context of the present discussion.

The top closure of the drywell is effected by a bolted head with sealing gaskets. Conceptually the head, flanges, and gaskets could be weak points in the system. The head, since it is not backed by concrete, is made extra strong so as to be able to resist localized jet forces. The bolted flanges are of necessity made quite rigid, and the cylindrical portion immediatey below the flange is typically heavier than other parts of the structure. Thus internal pressure stresses near the gasketed top closure are generally substantially lower than in other parts of the system. It is thus concluded that the top head or its seal do not generally constitute a structural weak link in the system. At temperatures and pressures above design levels, leakage past the gaskets however, may be possible before failure of the structure.

A steel drywell and torus vapor suppression containment structure designed for 56 psid could be expected to fail at an internal pressure of 175 ± 25 psia. The error band should encompass uncertainties as to the failure threshold as well as expected variations in materials, properties, and quality of workmanship. The most likely location for the failure is in the inner top half of the suppression chamber torus; additional highly stressed areas are the toroidal knuckle between the spherical and cylindrical parts of the drywell and the upper part of the drywell sphere.

APPENDIX E

PART I

ULTIMATE STRENGTH OF CONTAINMENT STRUCTURE

by

PAUL E. MAST

Paul E. Mast
Consulting Engineering

ENGINEERING BUILDING, SUITE 1819
205 WEST WACKER DRIVE
CHICAGO, ILLINOIS 60606

BUS.: (312) 641-3675
RES.: (312) 251-0450

June 25, 1973

ULTIMATE STRENGTH OF CONTAINMENT STRUCTURE

1. GENERAL

1.1 LOADING CONDITIONS AT ACCIDENT

It is assumed that after the hypothetical accident the temperature and the pressure will rise to 340° and to 120 PSI, respectively, both within approximately 1000 minutes or 17 hours. The purpose of this study is to predict the point of failure within this period and to describe the failure mode.

1.2 DESIGN BASIS

The structure has been designed for a design pressure of 45 PSI associated with an internal temperature of 150°. For these loading conditions, common reinforced concrete ultimate strength design principles were applied. According to the latter, the various components and materials of the structure at design level are stressed to approximately 60 per cent of their yield strength.

2. EFFECT OF INCREASING INTERNAL PRESSURE

2.1 GENERAL

Disregarding discontinuities, the structure is essentially a shell in a membrane state of stress. Therefore, increasing the internal pressure means increasing the membrane stresses, except the membrane shear stress. However, there will be an increase in radial shear stresses at discontinuities, commensurate with the increase of all other stresses.

2.2 CONDITIONS AT THE YIELD POINT OF REINFORCEMENT

The stress in the reinforcing steel at design pressure (45 PSI) is approximately

$$\frac{0.9}{1.5} \times 50 = 30 \text{ KSI.}$$

Therefore, with a yield stress of the main reinforcement of 50 KSI, the internal pressure at yield amounts to

$$P_1 = 45 \quad \frac{50}{30} = 75 \text{ PSI.}$$

The elastic strain in the reinforcement at this point is

$$\varepsilon = \frac{50}{30{,}000} = 0.0017.$$

The corresponding tension stress in the concrete surrounding the reinforcing steel at this point is way beyond its tensile strength, so that the concrete must be assumed cracked. To estimate the crack width at that stage, one can use the data obtained from the pressure test (Reference #2) which revealed cracks at about 18 inches on center. If one multiplies the strain in the reinforcing bars with the crack spacing, one arrives at a crack width of

$$d = 18 \times 0.0017 = 0.03 \text{ inches.}$$

This is the crack width for which concrete shear capacity due to aggregate interlock (surface roughness) was tested at MIT and Cornell University (Reference #1). Unfortunately, the tests were performed only for membrane shear strength but not for radial shear strength. The difference lies in the behavior of the reinforcement acting as dowels. Concerning membrane shear, practically all reinforcement perpendicular to the crack is engaged in full dowel action.

Concerning radial shear, dowel action of reinforcement near the faces of the concrete walls is nil, because the reinforcing bars will cause the thin concrete cover to spall (see Figure #1).

2.2.1 SUMMARY FOR CONDITIONS WHEN REINFORCEMENT AT YIELD

The knowledge about reinforced concrete at the yield point of conventional reinforcing steel is well founded. The mechanics of the failure mechanism are the basis for the Ultimate Strength Design Method on which all modern Concrete Building Codes are based. The crack width in the tension zone is in the neighborhood of the above described 0.03 inches, which assures conventional radial shear capacity due to aggregate interlock. Concerning in-plane (membrane) shear capacity, conditions are significently better because of the dowel action of the reinforcement. Only reinforcement near the center of a section (see Figure #2) can be considered effective to develop some radial shear capacity by dowel action.

In view of the above, it is concluded that the subject structure can withstand an internal pressure of 75 PSI with a uniform safety factor of 1.0 throughout. Based on the assumption that all components of the structure were equally designed by conventional ultimate strength principles, there should be no "weak link" up to this point.

2.3 CONDITIONS AT THE ULTIMATE STRENGTH OF THE REINFORCEMENT

The reinforcement consists of ASTM A615-50 steel which has a yield strength of 50 KSI and an ultimate strength of 80 KSI.

It would be wrong to assume from the above figures that the vessel can withstand an ultimate internal pressure of

$$P_u = 75 \times \frac{80}{50} = 120 \text{ PSI},$$

although it was stated before that at a pressure of 75 PSI the reinforcement would just reach its yield point (50 KSI).

The reason why the above correlation is not true lies in the strains associates with steel stresses above the yield point. For the reinforcing steel specified, it may be assumed that the following strains prevail:

1. At the beginning of strain hardening: = 0.015
2. At the end of strain hardening: = 0.030
3. At ultimate strength (fu = 80 KSI): = 0.15
4. At fracture: = 0.20

Looking at the above strains, one realizes that at the end of strain hardening, the strains in the reinforcing and, thereby, the cracks in the concrete are roughly 18 times bigger than at yield, but that the stress in the steel and thereby the resistance of the reinforcing cage have really not increased. In other words, there is a state of transition after the reinforcement has reached its yield point at which there is no increase in membrane tensile capacity, but at which the concrete undergoes extensive cracking. The above established crack width of o.o3inches at the end of strain hardening could easily reach

$$d = 0.03 \times 18 = 1/2 \text{ inch } \pm.$$

Needless to say that no shear capacity due to aggregate interlock can be developed across a crack width. Therefore, to assure the integrety of the structure, and the applicability of reinforced concrete design principles, one has to depend entirely on the radial shear capacity of the reinforcement, be it diagonal shear reinforcement, if any, or be it dowel action from bars perpendicular to the crack and positioned near the center of a section.

In other words, at this stage of progressive cracking, the formation of weak links will be in areas of high radial shears with insufficient reinforcement to absorb these shear forces. It was stated before that membrane shear in this investigation is no problem because of the radial symmetry of the loading conditions, and because of the diagonal earthquake-shear reinforcement, and because of the ability of all orthogonal reinforcement to provide shear resistance by dowel action. However, concerning radial shear, the magnitude of the latter will increase in direct proportion to the internal pressure applied.

Furthermore, only the region near the base has radial diagonal shear reinforcement, and the dowel shear capacity of the main reinforcement is neglible, because it is placed close to the faces of the concrete walls.

Reference #1 (page 32) shows that the slip resistance decreases with increasing crack width. In other words, the horizontal slip due to a shear force applied to a precracked specimen increased by 40 per cent when the pre-set crack width was increased from 0.02 in. to 0.03 in. It appears justified to extrapolate this result to the anticipated crack width of 1/2 inch at the end of strain hardening, and to evaluate the formation of weak links on the basis of large cracks, associated by large relative horizontal slip-type displacements of concrete chunks. The structure, in this stage, can be visualized as a cage of reinforcing bars bulging in regions of high radial shear, such as the vicinity of large penetrations (equipment hatch: 14.5 feet diameter).

Concerning public safety, it will be the liner integrety which becomes critical in these areas at this stage, before the structural integrety is jeopardized. Lateral liner deflections under design loads are usually limited to 0.01 inches. The strain imposed on a liner at wide cracks in the concrete, together with the bending stresses due to relative transverse slip of the back-up concrete, most likely will cause the liner to tear. This, in all probability, will be the ultimate failure mode of the structure. The design documents (Reference No. 1) described the liner to be of ASTM A-442, Grade 60 material, modified to A-300, with a yield strength of 32 KSI. No information concerning ductility or ultimate strain at rupture was included, which would waive the possibility of the above described failure mode.

2.4 ULTIMATE STRENGTH OF THE CONCRETE IN SHEAR

In case the liner material should be capable of enduring the above described longitudinal and transverse (slip-type) strains, another possibility of the formation of a weak link lies in the structural failure of the concrete in radial shear, per se.

Radial shear prevails at shell discontinuities, such as the boundaries at the top and at the bottom of the cylinder. Furthermore, radial shear prevails at the larger penetrations. While the latter increases in direct proportion to the internal pressure applied, radial shears at the other discontinuities (top and bottom of cylinder), are relieved by the overall yielding of the structure.

Some radial shear reinforcement was provided at the top and bottom boundaries of the cylinder. Therefore, and because of the aforementioned self-relieving behavior, radial shear failure around the large penetration appears to be more imminent than at the other boundaries.

One should not be mislead by the fact that no cracks appeared around the penetrations during the loadtest. The observed behavior was under conditions well below the yield strength, and thereby irrelevant to the anticipated behavior after extensive cracking of the concrete occurs. If the design provided reinforcement around the penetrations such that it would not yield before any other part of the structure breaks down, only then could one assume the penetrations to be no potential hazard concerning failure in radial shear.

It has become common practice in the design of concrete containment structures and concrete pressure vessels to provide the penetration sleeves with shear lugs. This was considered adequate to prevent a blow-out. In general, no welding to the reinforcing cage appeared necessary. With the internal pressure acting on the penetration, the shear lugs will bear on the surrounding concrete and they will prevent the sleeves from horizontal slip. The lugs, however, are ineffective in preventing the surrounding concrete from cracking under high strains and thereby from failing in radial shear and being blown out together with the penetration.

To really appreciate the condition under yielding reinforcing steel, the surrounding concrete at this stage of failure must be considered to consist of individual chunks held by a grid of reinforcing bars. The steel strain of the reinforcing bars times the

assumed crack spacing would result in ultimate crack widths of

$$d_u = 0.15 \times 18 = 2.7 \text{ inches.}$$

At these strains, bond between reinforcing bars and concrete has ceased to exist, so that the concrete is held by the reinforcing bars just like coarse gravel in a sieve. The ineffectiveness of shear lugs on the penetration sleeves in that stage of ultimate strain becomes obvious. One could avoid this potential weak link by a positive connection between the penetration sleeve and the surrounding reinforcing cage, such as welded straps or hooked anchors.

2.5 ULTIMATE STRENGTH OF THE LINER

It has been pointed out before that a high-ductile liner material may prevent the liner to tear before structural failure occurs.

Beneficial in this respect is the rise in internal temperature during the accident. The liner expansion due to a temperature rise of about 270° is equivalent to a strain of only $\varepsilon = 0.0017$. This is by far not enough to compensate for the large strains imposed on the liner by the yielding reinforcing bars. The increased ductility of the liner under high temperatures, however, may suffice to prevent its over-all failure. Therefore, the ductility of the liner under high temperature should be specified by the manufacturer and be evaluated by the designer, to check whether the liner will hold until structural failure of the vessel occurs.

The point of greatest weakness of the liner is its anchorage to the rigid base (see Figure 15.5.1.8-1 and Figure 15.5.1.1-1 of Reference No. 2). The 4'-6" long vertical anchors rigidly tie the liner to the base, at a point where large deformations must be anticipated under the hypothetical accident. The curved transition at the base joint is beneficial. Whether it will suffice to allow the liner to follow rotations and translations under gross deformations, can only be evaluated by a limit-design type failure mechanism analysis.

3. EFFECT OF RISE IN INTERNAL TEMPERATURE

The maximum temperature associated with the hypothetical accident is 340°. It is assumed that this temperature prevails over the entire 17 hours after the accident, until the structural failure occurs.

The structure is built of 3000 PSI concrete. Such concrete is expected to withstand temperatures up to 250° for an indefinite period of time without significent strength reduction. To provide a safety factor, most codes on concrete containment vessels specify a maximum operational temperature of 150 degree (Reference No. 3, paragraph 2.5.1.(a)). Over a short period of time, such as this hypothetical accident, an exposure to 340° may be considered to have no consequences because the other potential failure modes, as described above, are more serious and likely to occur sooner. Under short-duration accident conditions, exposure of the interior surface of the concrete shell to less than 350 deg. would even be permissible under common design practices (Reference No. 3, paragraph 2.5.1.(b)).

Exposure of the containment to 340° from the inside will result in an average temperature of the concrete walls of less than 150 degree. This is assurance enough that the very important shear capacity of the concrete will not be impaired (Reference No. 4). If the hypothetical accident would be associated with temperatures of over 350 degree, for this low-strength concrete a certain loss in shear strength would have to be taken into account. The corresponding loss in modulus of elasticity, in compression strength, and in tension strength would be of no significance for this investigation

4. CONCLUSION

4.1. It is predicted that the vessel will fail at an internal pressure of 80 PSI.

At that stage, the yielding reinforcement has undergone strain hardening and the concrete will show 1/2 inch wide cracks. The liner will tear at these cracks, and fission material will be released.

4.2. If the liner should be ductile enough to absorb huge longitudinal and transverse strains, the containment at this point will fail structurally in radial shear where no radial (diagonal) shear reinforcement is provided to absorb the latter. Especially in view of the low-strength concrete (3000 PSI), the concrete surrounding large penetrations is susceptible to such shear failure. This will cause a blow-out of the penetration, unless the penetration sleeve is welded or otherwise anchored to the reinforcing cage (Figure No. 3).

4.3. Should the penetration be designed to prevent the reinforcement in that area from yielding, and thereby prevent the concrete from cracking, under any over-pressure, the next weak link will be the junction of the cylindrical shell with the rigid base.

The bending stresses at this point are very high, even under design pressure. Yielding under an applied overpressure will cause the formation of a partial hinge and, thereby, partially relieve these stresses. However, the strains encountered in the reinforcing steel beyond the strain hardening area (ϵ = 0.03) are so big that one has to disregard the capacity of the concrete completely, both in shear, flexure and in compression.

Therefore, since the base is not designed as a true hinge, it will fail by horizontal translation (see Figure #4). However, if the liner should be capable to absorb these translations, the point of failure may be close to the ultimate strength of the reinforcing bars, i.e., close to an internal pressure of

$$P_{ult.} = 57 \times \frac{80}{50} = 120 \text{ PSI}$$

as derived before. At that stage, one may visualize the structure to act like a gas-filled balloon, with the reinforcing cage in pure membrane tension to provide the only system of resistance.

LIST OF REFERENCES

1. "Behavior of Pre-Cracked Concrete, Subjected to Reversing Shearing Stresses", by M. J. Holley (MIT) and R. H. White (Cornell University), published by Stone & Webster, Boston, 1969

2. Summary Description of Containment Structure furnished to Battelle by client.

3. "Criteria for Reinforced Concrete Nuclear Power Containment Structures", by ACI Committee 349, published Journal of the American Concrete Institute, January 1972, Detroit.

4. Effects of High Temperature Exposure on Concrete", by H. S. Davis, Proceedings, Meeting American Nuclear Society, June 20 - 24, 1965.

LIST OF FIGURES

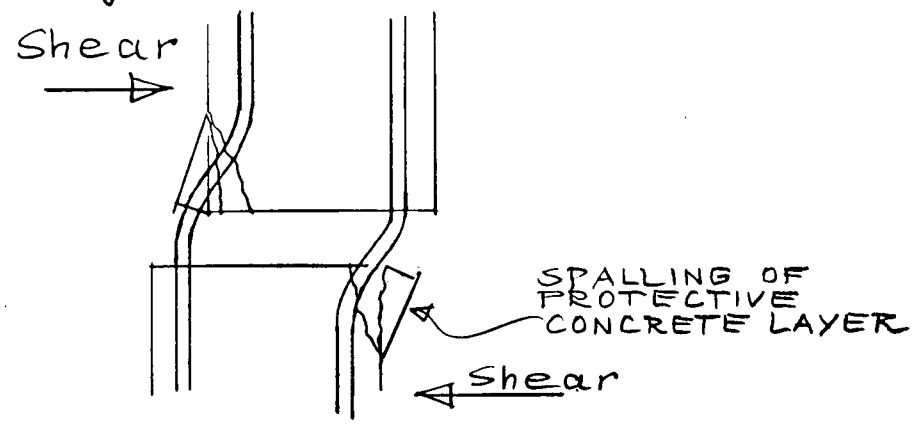
Fig. #1: Dowel Action of Reinforcing Bars near the Face

Fig. #2: Dowel Action of Reinforcing Bars at the Center

Fig. #3: Radial Shear Failure near Penetration

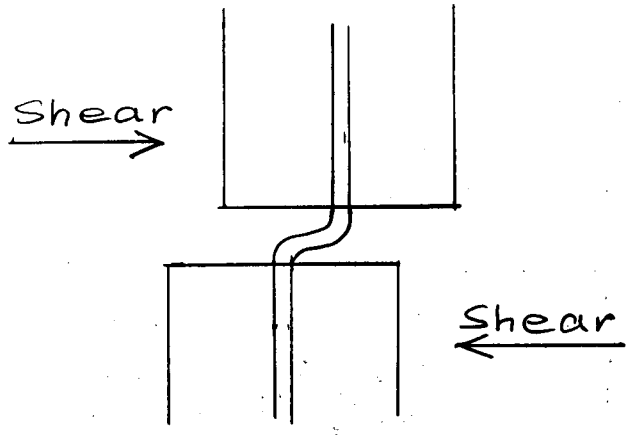
Fig. #4: Formation of Hinge at the Base

Fig. #1



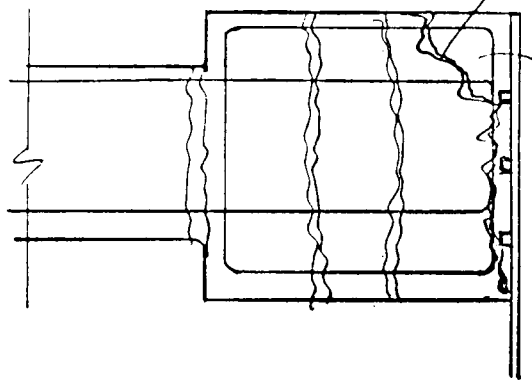
INEFFECTIVENESS OF
REINFORCING BARS
AS RADIAL SHEAR
DOWELS, IF PLACED
CLOSE TO THE SURFACE

Fig. #2



REINFORCING BARS PLACED
CLOSE TO THE CENTER OF
A SECTION ARE EFFECTIVE
AS DOWELS FOR RADIAL SHEAR

Fig. #3



PENETRATION FAILURE

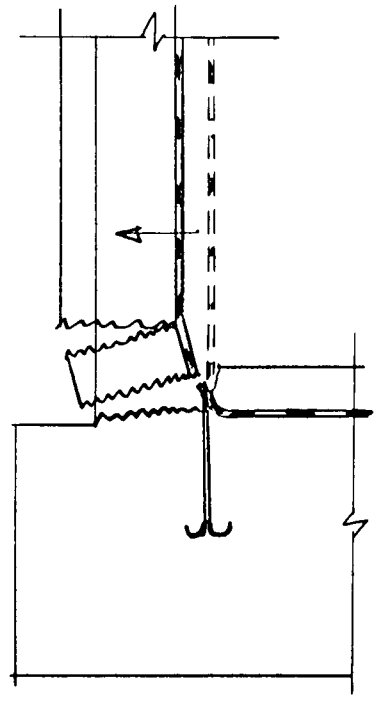


Fig. #4

COMBINED SHEAR & FLEXURAL FAILURE AT BASE.

APPENDIX E

PART II

CONTAINMENT FAILURE MODES STUDY

by

S. G. Sampath and M. F. Kanninen and P. E. Korda

PART II

CONTAINMENT FAILURE MODES STUDY

by

S. G. Sampath and M. F. Kanninen[1] and P. E. Korda[2]

This study was premised upon an accident in which the pressure within a given containment building increases steadily, but relatively slowly, without limit. The objective was to determine both the pressure level at which the structure fails and the most probable mode of failure. The results for the two containment buildings considered in this study are given in Table VIII E-1.

The analysis of the steel structure (BWR) was much the simpler of the two containment types considered. The calculations were performed by the authors after consultation with Mr. E. C. Rodabaugh[3], a recognized expert in the stress analysis of pressure vessels. The reinforced-concrete structure, however, represented a more formidable undertaking. Here, separate analyses were performed by the authors and by Mr. Paul Mast[4], an authority on reinforced concrete design. Interestingly, the two independent approaches predict failure pressures that are close enough that the single entry in Table VIII E-1 suffices.

The failure mode for the reinforced-concrete structure is believed to arise in the following manner. First, as the pressure rises above the design value, the concrete between the two layers of reinforcing bars will fail in shear. This will lead to a complete separation at the planes of reinforcing where the concrete is weakest. The structure will still retain its integrity, however, because the inner layer of reinforcing bars and the liner will remain intact. The point at which the latter section will fail is not certain, but it can be bounded. The lower bound, which corresponds to the pressure at which the liner and the reinforcing bars are just at yield, is 63.6 psig. The upper bound corresponds to the pressure at which they are stressed to their ultimate strength. This is 87.5 psig. The entry in Table VIII E-1 is approximately the average of the two bounds; it represents the best estimate presently obtainable in the absence of details of construction and workmanship.

The analysis of the reinforced-concrete structure performed by Paul Mast is fully described in Part I. He considers that an increase in pressure will give a proportional increase in the membrane stresses in the structure. Because under design conditions the stress in the steel reinforcing bars is 60 percent of the yield stress, the pressure at yield can be determined to be 75 psig. The bulk of his analysis consists of showing that failure must inevitably follow when this condition is reached. In essence, Mast's argument is that the strain associated with yielding in steel will cause cracks in the concrete that are wide enough to tear the liner whereupon fission material will be released at a catastrophic rate.

The analysis of the steel structure proceeded in two stages. The first was a computer stress-analysis computation designed to investigate the effect of stress concentrations at junction points in the complete structure. The second stage involved calculations of the burst pressure of individual components. The result was the finding that one sec-

---

[1]Applied Mathematics and Mechanics Section, Battelle's Columbus Laboratories.

[2]Korda and Associated, Ltd., Columbus, Ohio.

[3]Applied Solid Mechanics Section, Battelle's Columbus Laboratories.

[4]Consulting Engineer, Chicago, Illinois.

tion - the toroidal knuckle - can be singled out as the region in which a failure is most likely to occur. The burst pressure, as given in Table VIII E-1, is estimated as 250 psig.

It should be emphasized that the conclusions reported here must be considered as tentative. The reason is that, due to severe constraints on both time and the lack of details, many areas received only a cursory examination or were not pursued at all. Several of these aspects were suggested by the literature references contained in the Bibliography, others from the experience of the consultants. Some of the more serious areas of concern are given in the Discussion and Recommendation section.

EII–1. DESCRIPTION OF CONTAINMENT FAILURE ANALYSES

As noted above, the analyses of the two containment types considered were performed independently. Accordingly, these are described separately as follows. Note that the following does not include the analysis of Paul Mast. His work, performed in the capacity of a consultant, is described in Part I of this Appendix.

EII–1.1 REINFORCED–CONCRETE CONTAINMENT STRUCTURE

A number of different failure mechanisms were considered and, so far as possible, quantitative estimates made for each. The accuracy associated with the estimated failure pressures was limited by the lack of specific design details. It is felt that the uncertainty in the predicted results could be reduced with a more detailed examination. Specific areas that may warrant additional attention are noted in the concluding section of Part II.

A qualitative description of the most likely failure mode is as follows. As the pressure increases beyond the ordinary working levels, the stress in the outer layer of reinforcing bars will become significantly less than that in the inner layer. The reason is that the combined shear and tension imposed on the concrete by the hoop stress and the strain difference between the two layers quickly exceeds the strength of the concrete. This is in accord with the effects on the concrete of the thermal environment. As stated in a typical design evaluation:

"The thermal operating load in the containment concrete wall combined with incident condition loadings produces a stress difference of approximately 6,000 psi between the reinforcing steel adjacent to the inside face of the wall and the reinforcing steel adjacent to the outside face of the wall. This difference exists in both the longitudinal steel and the hoop reinforcing steel."

This conclusion was obtained from a calculation based on the assumption that the concrete will constrain the reinforcement to deform in accordance with the "plane sections remain plane" hypothesis. If this is the case, the thermal operating load alone would cause a shear stress equal to almost 4.5 ksi. This is approximately 40 times the ultimate capacity of the concrete. Obviously, strain compatibility will cease long before the theoretical stress pattern indicated by the computer analysis could develop.

With increasing internal pressure, the first major area of distress, then, will be a massive shear failure in the concrete. There will probably be complete separation at the planes of the reinforcing where the concrete is initially weakened. Concrete will crumble and crack away from the reinforcing bars. The outer layer of reinforcing will be effective for a time due to the physical restraint exercised over the enclosed volume. Eventually, chunks of concrete will spall off the outside. The outer layer of reinforcing will then be virtually relieved of all load-bearing capacity.

The liner and the reinforcing near the inside face are only inches apart. This circumstance probably required very careful workmanship during construction to achieve proper consolidation of the concrete and its integrity is somewhat suspect. However, assuming that this section is properly constructed, the continuous liner on the inside and the approximately 4 inches of concrete cover on the outside will probably result in sufficient confinement that the liner and the inner reinforcing will work together through the critical phases. It is this steel whose load-carrying capacity will determine the pressure at failure.

The reinforcing rods will yield at 50 ksi while the steel liner will yield at 32 ksi. The large strains accompanying yielding will accelerate the crumbling and pulverizing of the concrete, both outside the inner layer of reinforcing

and, eventually, between it and the liner. At some point, strain hardening will commence to accommodate further increase in the internal pressure. It is not possible to predict the precise extent to which this will happen prior to ultimate failure. But, while the stress level in the steel is between the yield and the ultimate strength, local deformations will cause the concrete failure to extend all the way to the liner. When this happens over a large enough area, the combined tension and bending will cause a blowout with the possibility of the crack propagating several feet before the sudden release of the internal pressure will cause it to stop. Because a catastrophic amount of containment will be released by this process, this is deemed a failure mode.

In the state described above, the hoop stress is twice the longitudinal stress, and the circumferential reinforcing available is twice that available in the longitudinal direction. Hence, the governing condition can be taken to be in the direction of the hoop stress. The reinforcing bars are in uniaxial tension with a minimum guaranteed yield strength of 50 ksi and a minimum tensile strength of 70 ksi. The steel liner is essentially in a state of biaxial tension with the hoop stress approximately equal to twice the longitudinal stress. Under these conditions, the maximum distortion energy failure criterion results in an increase by a factor of $2/\sqrt{3} = 1.155$. The guaranteed minimum yield strength is 32 ksi and the minimum tensile strength, 60 ksi. Estimates of unit stress and hoop force are shown in Table VIII E-2. The inside radius of the containment structure being 63 ft, these correspond to a lower bound pressure of 63.6 psig and an upper bound of 87.5 psig.

In summary, therefore, failure will occur no sooner than when the steel liner and the inner layer of reinforcing are stressed to yield and no later than when they are subjected to their ultimate tensile strength. This gives rise to an upper and lower bound for the failure pressure. One would most certainly anticipate a significant pressure increment to failure beyond the lower bound (the extent will primarily be a function of the uniformity of workmanship both in welding steel and in placing concrete). A good estimate of a likely single value would be somewhere near the middle of the range. This gives the value of 75 psig quoted in Table VII E-1.

EII—1.2 STEEL CONTAINMENT STRUCTURE

The analysis of the steel containment structure consisted of two phases: a computer analysis of the entire structure as an axisymmetric pressure vessel and failure calculations based on the stress concentrations existing in the individual components. Local stress concentrations arising from accesses, pipes and the like, of course, are ignored in an axisymmetric analysis. Hence, the computer calculation is intended to evaluate only the potential for failure at positions with discontinuities, e.g., changes of thickness. In turn, these effects are ignored in the evaluation of local stress concentrations which follow, it being reasonable to assume that the interaction between those effects can be neglected.

EII-1.2.1 COMPUTER CALCULATION FOR AXISYMMETRIC PRESSURE VESSEL

A Battelle computer program (MONSAS) was used to calculate the stresses in the primary containment shell under the design basis accident conditions. In essence, the program performs a nonlinear (large deformation) analysis of elastic shells of revolution using a multisegment, direct-integration technique coupled with a Newtonian-type iterative scheme. The shell geometry was modeled as shown in Fig. VIII E-1. Because tuberances, accesses, piping and vents in the shell were not taken into account so that the problem could be treated as axisymmetric. The profile of the shell consisted of five parts, as shown in Fig. VIII E-1. Because precise details of the structure were not available, the wall thickness had to be estimated. The assumed thickness distribution used in the computation is given in Table VIII E-3. Note that between any two points within a single part, the program assumes a linearly varying thickness.

At the concrete embedment at elevation 119'11", a fully clamped condition was assumed for the shell. The model was terminated at the flange connection at elevation 210'4", with a simple support and no inplane constraint. However, a statically equivalent in-plane load (6000 lb/in.) was prescribed at this point to account for the longitudinal stress that arises from the internal pressure. A value of 62 psig for the pressure was utilized with an assumed uniform temperature of 281 F. The elastic constants for the material of the shell were those specified for ASTM-

A516, Grade 70, Fire Box Quality, USS Steel.

The calculated principal stresses at various locations are given in Table VIII E-3. For comparison, the design values for a typical configuration are also given. The overall agreement between the two results appears fair; the variation in the thickness distribution assumed in the two cases probably accounts in large part for the specific differences. The discontinuity in the stress at elevation 119'11" due to bending can be expected to disappear if account is taken of the sand bed provided between elevation 117'1-5/8" and elevation 119'11". A high value for stress was also obtained at the junction between the conical section and the cylindrical part (see Fig. VIII E-1, elevation 202'). A large bending stress can also be expected at the flange connection at elevation 210'4". However, due to a lack of available detail of the joint and sealing arrangement, the present analysis did not take this into account.

Other factors which need to be considered for a detailed study of the failure mode of the shell are discussed in the concluding section.

EII-1.2.2 BURST-PRESSURE CALCULATIONS FOR INDIVIDUAL COMPONENTS

As mentioned above, the complexities introduced by the fittings and other nonaxisymmetric features of the containment structure precluded an exact analysis. Instead, guidance from design experience as incorporated into the ASME Nuclear Pressure Vessel Code was used to estimate the burst pressure for each part of the containment structure treated individually. These calculations were carried out under the following restrictions:

a. A single application of the load need be considered.

b. All welds are of uniformly high quality and are completely ductile.

c. The stiffness and strength contributed by the girders to the toroidal suppression chamber is neglected.

d. No large defects are present in the vessel which would cause catastrophic fracture by unstable crack propagation.

e. Flanged joints are adequately sealed to prevent leakage prior to bursting of vessel.

f. Reinforcements at nozzle openings are equivalent to at least 100 percent area replacement (as required by the ASME Code).

Given the above conditions, burst pressures for each of the major parts of the containment vessel can be calculated by the simple strength of materials relationships. The results are shown in Table VIII E-4.

Having determined from the computer analysis that the overall design of the containment structure is basically correct, it is expected that failure would occur at a local stress concentration within an individual part. Hence, from the results given in Table VIII E-4, it is concluded that failure would occur in the toroidal knuckle section of the typical configuration. The calculated value for this possibility given in Table VIII E-4 corresponds to the entry given in Table VIII E-1 of this report.

EII—2. DISCUSSION AND RECOMMENDATIONS

In this section, the principal areas of uncertainty in the analyses performed are discussed. The results given in the preceding section should be interpreted in the context of these uncertainties.

EII—2.1 REINFORCED—CONCRETE CONTAINMENT STRUCTURE

The primary uncertainties in the analysis of the reinforced-concrete containment vessel are deemed to be as follows.

a. The structure has an excess of steel (in the neighborhood of 5 percent whereas it is usual to find 1-2 percent steel in typical well-designed concrete structures). Proper compaction of concrete under such conditions would be difficult to achieve.

b. The currently accepted ACI Code 318-71 is more demanding than the 318-63 Code under which the structure was designed with regard to adequate developmental requirement for deformed bars. This is based on recent theoretical research and on field experiences. A calculation of the development length for Number 18 reinforcing bars indicates that a length of about 100 inches is required. This is greatly in excess of the lengths available in the design in local areas.

c. Seismic loads are assumed to appear nonconcurrent with an accident condition. No account of the seismic load has been taken into any of our discussions.

d. In the personnel- and access-hatch designs, the steel ring could carry the shearing forces as hoop tension. In this case, shear cracking of concrete and the consequent loss of lamination between the outer-inner reinforcement is not credible except as exists in the overall structure.

e. The liner is in a biaxial state of stress so that its yield stress is underestimated by uniaxial data. While some account was taken of this fact, the actual failure pressure may be sensitive to the exact value.

EII–2.2 STEEL CONTAINMENT STRUCTURE

In essence, the primary uncertainty in the analysis of the steel containment structure stems from a lack of some specific design details. To put the current effort into perspective, the computer analysis performed here is summarized in Table VIII E-5. It can be seen from this and the discussion in the preceding sections that many details of the design have not been considered. If a more precise prediction of failure pressure were desired, analyses should be performed to account for details of the reinforcing around pipe penetration and access holes.

A reactor building encloses the primary containment and also serves the additional purpose of limiting deflections of the steel shell under the action of concentrated forces to prevent failure. Although permanent deformations of the primary containment and the suppression chamber are not considered as failure per se, possible reactive pressures (arising due to the concrete shield wall as a result of the overall deflections of the primary chamber exceeding the gap provided between the two walls) warrants consideration.

The elastic computer analysis was performed with the pressure load assumed as 62 psig. The results gave shell deflections normal to the surface of about 1 inch. It is to be expected that reactive pressures would arise on the shell surface long before the hypothesized burst pressures (calculated without taking this point into consideration) were reached. The contour and the stiffness of the concrete shield not being known, it appears that unequal constraints will tend to alter the stress distribution calculated along the steel-shell contour under incipient burst conditions. Intuitively, the knuckle portion of the drywell and the double-gasketed flange, due to bending and subsequent leaking appear more vulnerable than had been stated earlier. An inclusive analysis should be worthwhile.

References

1. Merkle, J. G., "The Strength of Steel Containment Shells", Nuclear Safety, 7 (3), 346-353 (1966).

2. Doyle, J.M., and Chu, S.L., "Some Structural Considerations in the Design of Nuclear Containment Liners", Nuclear Engineering and Design, 16, 294-300 (1971).

3. Browne, R. D., and Blundell, R., "The Behavior of Concrete in Prestressed Concrete Pressure Vessels", Nuclear Engineering and Design, 20, 429-475 (1972).

4. Tan, Chen Pang, "A Review of the Technology of Prestressed Concrete Reactor Pressure Vessels", Nuclear Safety, 11 (1), 25-33 (1970).

5. Costantino, C. J., "The Strength of Thin-Walled Cylinders Subjected to Dynamic Internal Pressures", Trans. ASME, Jour. Appl. Mech., 32, 104-106 (1965).

6. Haydl, H. M., and Sherbourne, A. N., "Effect of Transverse Shear on Limit Load of Cylindrical Shells", Nuclear Engineering & Design, 22, 290-295 (1972).

7. Rashid, Y. R., "Ultimate Strength Analysis of Prestressed Concrete Pressure Vessels", Nuclear Engineering & Design, 7, 334-344 (1968).

8. Halligan, D. W., "Structural Design Criteria for Secondary Containment Structures", Nuclear Engineering and Design, 8, 427-434 (1968).

9. Whitman, G. D., "Technology of Steel Pressure Vessels for Water-Cooled Nuclear Reactors", Nuclear Safety, 8 (5), 429-442 (1967).

10. Denkins, F. R., and Northrup, T. E., "Concrete Containment Structures", Nuclear Safety, 6 (2), 194-211 (1964-65).

11. Langer, B. F., "Rupture of Cylindrical Shells", PVRC Interpretative Report of Pressure Vessel Research, Welding Research Council, 95 (August, 1964). Section I -Design Consideration.

TABLE VIII E-1 ESTIMATED CONTAINMENT-BUILDING FAILURE PRESSURES

Building Classification	Wall Structure	Failure Pressure, psig
Sub-atmospheric containment for pressurized water reactors	Reinforced concrete	75
Vapor suppression containment for boiling water reactors	Steel	250

TABLE VIII E-2 DISTORTION ENERGY FAILURE ESTIMATES

	Area, in.^{2}/ lin. ft	Unit Stress, ksi		Hoop Force, kip/lin. ft	
		Lower Bound	Upper Bound	Lower Bound	Upper Bound
2 Number 18 bars on 12-in. centers	8.00	50	70.0	400	560
3/8-in. steel liner	4.50	39	51.9	176	234
				576	794

TABLE VIII E-3 SUMMARY OF CALCULATED STRESSES IN TYPICAL VAPOR-SUPPRESSION CONTAINMENT FOR BOILING-WATER REACTORS

Elevation	Assumed Wall Thickness, inch	Principal Stresses at Design Basis Accident Conditions[a], psi		Calculated Deflections, inch
		Calculated (MONSAS)	Design	
119'11"	1.25	(b)	11,802	0.00
126'	1.25	10,400	10,679	1.04
132'8$\frac{1}{2}$"	1.25	9,977	10,147	1.06
137'7$\frac{1}{8}$"	1.25	9,975	16,327	1.08
154'9"	1.07	11,650	15,900	1.14
170'3$\frac{25}{32}$"	1.93	12,500	15,592	1.21
171'2$\frac{1}{8}$"	2.8125	16,895	14,200	1.26
172'8$\frac{1}{16}$"	2.8125	19,700	16,712	1.18
175'9$\frac{1}{2}$"	2.8125	11,284	9,714	0.65
178'5"	0.75	14,299	--	0.66
179'3"	0.78	18,178	--	0.69
183'8"	0.985	15,728	--	0.68
200'3"	1.25	15,747	--	0.65
202'	1.25	55,278[c]	--	0.44
204'11.6"	1.39	12,179	--	1.56
207'4"	1.5	33,481	--	1.70
210'4"	1.5	4,000	--	0.00

(a) Pressure = 62 psig, temperature - 281 F.
(b) Discontinuity stress, clamped boundary condition.
(c) High bending stress.

TABLE VIII E–4 SUMMARY OF ESTIMATED BURST PRESSURES FOR COMPONENTS OF A TYPICAL VAPOR-SUPPRESSION CONTAINMENT FOR BOILING-WATER REACTORS

Part	Model	Lower Elevation	Upper Elevation	Calculated Burst Pressure, psig
1	Spheroidal	119'11"	171'2$\frac{1}{8}$"	300
2	Toroidal knuckle	171'2$\frac{1}{8}$"	175'9$\frac{1}{2}$"	250
3	Cylinder	175'9$\frac{1}{2}$"	202'	260
4	Conical	202'	207'4"	375
5	Cylinder	207'4"	210'4"	620

TABLE VIII E-5 SUMMARY OF COMPUTER ANALYSIS USED FOR VAPOR-SUPPRESSION CONTAINMENT FOR BOILING-WATER REACTORS

		Accounted for or Assumed in Analysis	Not Accounted for in Analysis
1.	Program Code Used	MONSAS: Thin-shell analysis	---
2.	Analysis	Linear elastic, large deformations	Plasticity
3.	Geometry	Shell of revolution; axisymmetric (see Fig. VIII E-1)	Effect of protrusions, vents, accesses, sundry piping
		Modeled from elevation 119'11" and terminated at flange at elevation 210'4"	Ellipsoidal head above 210'4"; discontinuity flange (details of flange connection not available yet)
4.	Thickness	Variable thickness was assumed (see Table VIII E-1). The program assumes a linear distribution between prescribed points.	Detailed thickness distribution unavailable from drawing
5.	Load	Internal pressure = 62 psig and uniform temperature = 281 F	Dead load of structure, seismic loads (vertical and horizontal) hydrostatic load from flooded condition
6.	Boundary Condition	At elevation 119'11", the edge was assumed clamped; i.e., normal displacement w, meridional displacement u, and rotation was set = 0	Air gap between elevation 117'$\frac{5}{8}$" and elevation 119'11"
		At elevation 210'4", the edge was free with an axial tensile force being applied to account for the longitudinal stress due to pressure. This force was calculated from statics; i.e., force/unit circumference = $\frac{pR}{2}$.	Discontinuity and bending stresses at flange and the effect of the ellipsoidal head. This would cause compressive stresses.
7.	Mechanical Properties	$E = 29 \times 10^6$ psi, $\mu = 0.27$, $\alpha = 8.4 \times 10^{-6}$ in./in./F	σ_y, σ_{ult}

Part No.	Part Name	a, inches	b, inches
1	Spheroidal	402.0	---
2	Toroidal	303.0	72.0
3	Cylindrical	231.0	314.5
4	Conical	231.0	74.0
5	Cylindrical	194.0	35.914

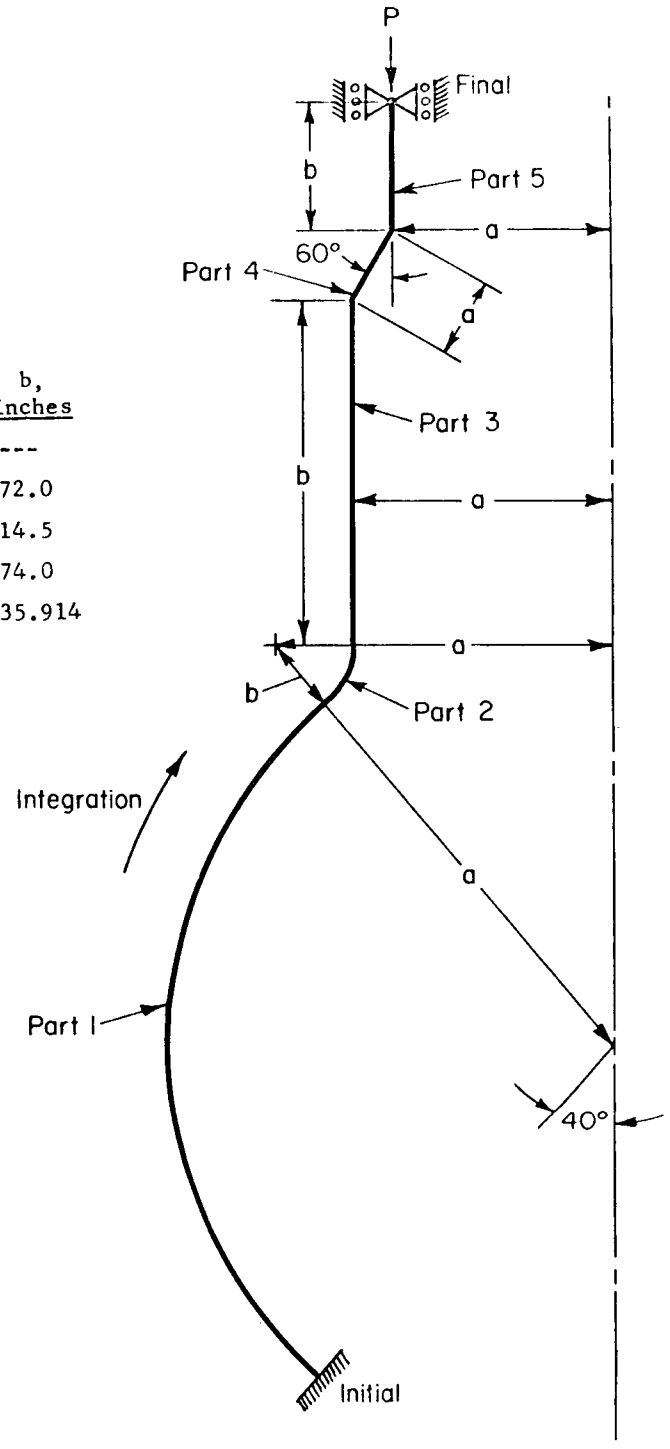


FIGURE VIII E-1 Axisymmetric Model for Steel Shell Computer Analysis

WASH—1400
(NUREG 75/014)

SAFETY DESIGN RATIONALE

for

NUCLEAR POWER PLANTS

APPENDIX IX

to

REACTOR SAFETY STUDY

U.S. NUCLEAR REGULATORY COMMISSION

OCTOBER 1975

APPENDIX IX
Table of Contents

Section		Page No.
1.	INTRODUCTION AND SUMMARY	IX-1
2.	PRIMARY BARRIERS TO RELEASE OF RADIOACTIVE MATERIAL	IX-5
	2.1 Fuel Rods	IX-5
	2.2 Reactor Coolant System and Containment	IX-5
3.	GENERAL BASIS FOR SAFETY DESIGN	IX-11
	3.1 Normal Operation at Power	IX-11
	3.1.1 Confinement of Radioactivity	IX-11
	3.1.2 Cooling of Fuel Rods	IX-11
	3.2 Anticipated Transients and Accidents	IX-12
4.	PROTECTION AGAINST OVERPOWER	IX-15
	4.1 Reduction in Temperature of Reactor Coolant	IX-15
	4.1.1 Temperature and Flow of Feedwater	IX-15
	4.1.2 Increase in Steam Demand	IX-16
	4.1.3 Rupture of a Main Steam Line in a PWR	IX-16
	4.2 Increase in Flow of Coolant to Reactor Core	IX-18
	4.3 Increase in Pressure in a BWR	IX-19
	4.4 Uncontrolled Movement of Control Absorber	IX-19
	4.4.1 Withdrawal of Control Assembly by Drive Mechanisms	IX-19
	4.4.2 Dilution of Boron in PWR Coolant	IX-20
	4.4.3 Insertion of a Control Assembly	IX-20
	4.4.4 Ejection of a Control Assembly	IX-21
5.	PROTECTION AGAINST A REDUCTION IN CORE COOLING	IX-23
	5.1 Reduction in Reactor Coolant Flow	IX-23
	5.2 Mismatch Between Feedwater and Steam Flows	IX-23
	5.3 Reduction in Steam Demand	IX-24
	5.4 Reduction in Pressure in Reactor Coolant System	IX-25
6.	PROTECTION AGAINST LOSS OF REACTOR COOLANT	IX-27
	6.1 Cooling of Fuel Rods	IX-27
	6.1.1 Small-Break Accidents	IX-27
	6.1.2 Large-Break Accidents	IX-28
	6.1.3 Breaks of Intermediate Size	IX-29
	6.2 Containment of Radioactivity During Accident	IX-30
	6.3 Post-Accident Heat Removal and Confinement of Fission Products	IX-31
	6.3.1 Cooling of Fuel Rods	IX-31
	6.3.2 Cooling of Containment and Retention of Fission Products	IX-31
	6.3.3 Control of Hydrogen Concentration in Containment	IX-31
	6.4 Special Containment Situations	IX-32

Table of Contents (Continued)

Section		Page No.
7.	MEASURES TO ENSURE PERFORMANCE OF SAFETY FUNCTIONS.....	IX-35
	7.1 Quality Assurance.....	IX-35
	7.2 Protection Against Effects of Severe Natural Phenomena.....	IX-35
	7.3 Reliable Power Supply.....	IX-36
	7.4 Redundancy in Safety Systems.....	IX-36
	7.5 Testability of Safety Systems.....	IX-37
8.	CONCLUSION.....	IX-39

List of Figures

Figure		Page No.
IX 2-1	Typical Reactor Core Fuel Rod.....	IX-7
IX 2-2	Typical PWR Reactor Coolant System.....	IX-8
IX 2-3	Typical BWR Reactor Coolant System.....	IX-9
IX 3-1	Heat Production of Decay Fission Products.....	IX-13
IX 6-1	Typical PWR Containment.....	IX-33
IX 6-2	Typical BWR Containment.....	IX-34

Section 1
Introduction and Summary

As indicated elsewhere in the Reactor Safety Study, the AEC's regulatory bodies have put into use a well developed set of safety design requirements for pressurized-water (PWR) and boiling-water (BWR) nuclear power plants. The primary purpose of this appendix is to describe, for the benefit of those not well-schooled in reactor safety, the basic logic for most of these safety requirements, unimpeded by the stylized language of regulations, licensing applications, and technical codes and standards. To avoid interfering with the logical development, a minimum of descriptive material is presented. The reader is presumed to have some understanding of the fission process and the operation of nuclear power reactors. For those without this understanding, many references are available.[1]

Another purpose of this appendix is to provide a bridge between the traditional "qualitative" approach to reactor safety and the "quantitative" approach taken in the Reactor Safety Study. This appendix, in essence, describes the conventional approach to reactor safety as currently used by the AEC's regulatory bodies and the industry. In the Study, this approach to safety is analyzed quantitatively and on a more realistic basis than is usually employed to predict the probabilities and consequences of reactor accidents. Although the Study is not limited to consideration of those accidents defined in the conventional approach, it has started with them and then expanded the scope of the safety investigation to include many other accidents of risk significance.

Nuclear power plants, like fossil-fueled plants, use heat produced by reaction of a fuel to generate steam to drive a turbine-generator to produce electricity. Both types of plants must be designed to protect against the hazards of handling large volumes of water and steam in large equipment and piping at high temperature and pressure. In the nuclear plant, however, the radioactive fission products that are the byproduct of the heat-producing fission reaction in the uranium fuel constitute an additional hazard. A plant generating electricity at a rate of 1 thousand megawatts (1000 MWe) contains about 10 billion curies of radioactivity.[1] Much of this radioactivity persists for long times after the fission reaction has been turned off. If it were possible to disperse the radioactive products from a large plant, people might receive severe radiation exposures and use of land could be restricted over many square miles in the vicinity of the plant.

The real business of reactor safety is prevention of the release of radioactivity from the reactor fuel. Although the fission process creates large amounts of radioactivity in the fuel rods, the ceramic pellets of uranium dioxide fuel retain more than 98% of this radioactivity. About 2% of the radioactivity, chiefly the gaseous krypton, xenon, and iodine, diffuses into the gas plenum between the fuel pellets and the sealed Zircaloy cladding.

Small amounts of radioactive gas may leak through the cladding in normal operation (the core of a large reactor contains roughly 40,000 fuel rods and some will surely leak), but this is of minor consequence. The leakage is confined by two additional barriers to the release of radioactivity to the environment - the piping and vessels of the reactor coolant system and the containment. Waste treatment systems are provided to dispose of this radioactivity, and, although the leakage slightly complicates the operation of the plant, it is not a hazard to the public.

If the fuel rod cladding is heated to a temperature several hundred degrees above the normal operating temperature, it can fail and release the radioactivity in the gas space plus a small quantity of volatile solid fission products

---

[1] Nuclear reactors and the fission process are described briefly and simply in the booklets entitled "Nuclear Power Plants" (IB-505) and "Nuclear Reactors" (IB-507) of the "Understanding the Atom" series, prepared by the U.S. Atomic Energy Commission, Office of Information Services.

[1] This excludes very rapidly decaying isotopes.

located at the surface of the ceramic pellets. This small fraction of the total radioactivity is easily confined by the reactor coolant system and/or the containment. The only way that a large fraction of the radioactivity can be released is to severely overheat or, in essence, melt the uranium dioxide pellets. If uranium dioxide remains molten, about 15% of the radioactivity is volatilized in a few minutes and about 25% is released in a few hours.

Melting of the fuel in a reactor core would also lead to failure of the other barriers as they are now designed. These facts have been known for many years. Consequently, in the design, engineering, construction, and operation of nuclear power plants, much effort has been expended on preventing damage to the cladding and melting of the fuel.

In principle, there is only one way for the fuel to melt: it must generate more heat than is being removed from it. When the reactor is operating, the fuel is cooled by water flowing at high velocity over the surfaces of the fuel rods. When the reactor is shut down, cooling must be continued, but at a significantly lower rate, to remove the heat due to radioactive decay of the fission products. Three kinds of events can cause the heat generation in the fuel to exceed the cooling capability of the water: the heat generation can rise, the cooling capability can decrease, or the coolant can be lost from the reactor core. Such events might be caused by equipment failures in the plant due to faulty design, construction, or operation. External forces exerted on the plant by earthquakes and other severe natural phenomena and by airplane crashes are also potential causes.

Measures are taken to ensure high quality in design, construction, and operation of the plant so that the number and severity of events caused by internal failures will be minimal. Abundant cooling is provided to remove heat from the fuel and allow flexibility in operation and margin for accommodating upsets. Control systems keep the reactor power and coolant conditions within prescribed limits when the plant is operating. The plant is designed to operate or be shut down and maintained in a safe condition in the event of an earthquake, flood, tornado, or hurricane of a magnitude not expected to occur during the lifetime of the plant.

In spite of these measures, it is assumed that operational upsets and accidents will occur, and measures are provided to cope with them. A reactor protection system is provided to shut down the plant and maintain it in a safe condition when limits on operating conditions are reached. Engineered safety features are incorporated to cool the fuel and augment confinement of the radioactivity by the containment under abnormal and accident conditions. These systems are designed to terminate anticipated transients - events that are likely to occur during the lifetime of the plant - without damage to the fuel rods or the coolant system. Severe accidents that have a lower probability of occurrence are also postulated and examined. Some damage to the fuel rods is considered acceptable in these events, but the safety features must prevent the rods from melting or radioactive materials from escaping from the plant in sufficient quantity to cause serious exposures to the public.

An unintended rise in power in the reactor core could be produced by:

a. A reduction in temperature of the coolant to the core. Such a reduction would increase the density of the coolant, increasing its ability to slow neutrons. This would lead to an increase in neutrons available for fissioning with a resultant increase in power. An increase in flow or decrease in temperature of the feedwater being returned to the reactor coolant system or, in a PWR, an increase in steam demand or rupture of a steam line will lower the coolant temperature.

b. An increase in flow of coolant to the core. Start-up of an inactive reactor coolant recirculation loop, or abnormal operation of the reactor coolant flow controller in a BWR, can increase the flow and in some instances lower the temperature of the coolant.

c. Uncontrolled removal of control absorber from the core. Uncontrolled withdrawal of control assemblies by the drive mechanisms, ejection of a control assembly by rupture of a control rod housing in a PWR or by gravity forces in a BWR, and dilution of the boron in the coolant of a PWR remove control absorber from the core.

d. An increase in pressure in a BWR. Abnormal operation of the pressure controller or rapid closing of valves in the main steam lines, as

in a turbine trip, increase the pressure in the core.

e. Insertion of a control assembly. If other control assemblies are withdrawn to maintain the total core power, the power will rise in some regions of the core to compensate for the reduction in the vicinity of the inserted assembly.

A reduction in cooling capability would result from:

a. A reduction in reactor coolant flow. Stoppage of one or more of the reactor coolant pumps or abnormal operation of the reactor coolant flow controller in a BWR will reduce the coolant flow.

b. A reduction in pressure of the coolant in a PWR. Release of steam from the pressurizer or an increase in steam demand can reduce the pressure.

c. A reduction in the inventory of water in the steam generators of a PWR or the reactor vessel of a BWR. A mismatch between the feedwater flow and the steam flow caused by abnormal operation of pumps and valves or breaks in pipes will lead to a reduction in inventory and in capacity to cool the core in the event of loss of feedwater flow.

d. A reduction in steam demand. Closing of valves in the main steam lines stops the flow of steam and the removal of heat from the reactor coolant.

Loss of reactor coolant would result from the opening of a valve or a break in a pipe that allowed water or steam to be discharged from the reactor coolant system in an uncontrolled manner. The opening can range in size from a small crack to a hole produced by severance of the largest pipe in the reactor coolant system.

Because of these considerations, the plants are designed so that fuel rods are likely to be slightly damaged only in the more severe accidents. Normal conditions are restored by the control systems without shutting down the reactor, or the protective system shuts down the power to prevent the fuel from overheating in most of the potential power-rise and reduction-in-cooling incidents. Auxiliary feedwater systems and high pressure coolant injection systems provide water for the steam generators and the reactor coolant system, and steam relief systems provide a means for dissipating the decay heat. The reactor protection system is designed to prevent the start-up of an inactive loop in a PWR under conditions that could cause fuel damage. Only the most severe control-assembly-ejection accidents are likely to damage fuel rods. Such accidents have a low probability of occurrence and the damage would be limited to perforation of the cladding of a small fraction of the rods.

Loss-of-coolant accidents fall into two general categories - small-break and large-break accidents. High pressure coolant injection systems are provided to maintain sufficient water in the core to keep the fuel rods from being damaged during the time required to depressurize and cool the reactor system in small-break accidents. In large-break accidents water and steam are discharged from the reactor coolant system so rapidly that no means has been found to prevent the core from being voided of liquid during the depressurization. Systems are provided to inject water into the reactor vessel at intermediate and low pressure to cool and reflood the core rapidly. Because a large-break loss-of-coolant accident is an event of low probability, the possibility of some damage to fuel rods is acceptable. The cooling systems are designed to ensure that the cladding will not melt or be seriously oxidized and embrittled during the temperature transient.

Depressurization of the reactor coolant system in the larger loss-of-coolant accidents results in the discharge of a large amount of water and steam into the containment and a consequent rise in temperature and pressure in the containment. Sprays are provided in most PWR containments to condense the steam and cool the containment and to remove iodine and other radioactive particles from the containment atmosphere. The pressure suppression system serves to condense steam in the BWR containment. Water recirculation systems are provided for removing the fission product decay heat from the reactor core and the containment for a long time after an accident. Recombiners in the PWR containment and a nitrogen atmosphere in the BWR containment prevent the hydrogen, produced chiefly from radiolysis of the water, from reaching a flammable concentration.

High quality of design, construction, and operation and redundancy and testability of equipment and systems are important factors in ensuring that the

safety features will function when called upon. If the containment and safety features perform as the designers expect, few, if any, of the fuel rods would be damaged, little radioactivity would be released, and little hazard to the public would result from any of the accidents.

Section 2
Primary Barriers to Release of Radioactive Material

The large power reactors now operating or under construction in the U.S. are pressurized water and boiling water reactors (PWR and BWR) that use water for cooling the uranium fuel. Although these reactors differ in some important features, the design approach to radiological safety for both is to provide a defense in depth against the release of radioactivity from the plant under all circumstances considered credible. This defense in depth consists of physical barriers augmented by the auxiliary systems, engineered safety features, procedures, and administrative controls necessary to make the barriers highly reliable and to maintain their effectiveness.

2.1 FUEL RODS

The first and most important physical barrier is the fuel rod. The fuel is uranium dioxide powder that has been formed into small cylinders and fired at high temperature to produce ceramic pellets. Groups of pellets are inserted in metal tubes made of a zirconium alloy, Zircaloy, and the ends of the tubes are sealed by welding to form fuel rods, as shown in Fig. IX 2-1, for use in the reactor core.

Most of the heat produced in the reactor is generated by fissioning of uranium and plutonium in the pellets of the fuel rods. Most of the radioactive materials produced - those of greatest health and safety concern - are the fission products left in the fuel pellets by the fission reaction. Some of the fission products are gasses which will diffuse from the pellets into the space around them. The principal gaseous products are krypton, xenon, and iodine. Typically, the fuel rods in a 1000-MWe reactor contain about 110 million curies of krypton, 250 million curies of xenon, and 700 million curies of iodine. Of these amounts, 0.4 million curies of krypton, 3.6 million curies of xenon, and 9.5 million curies of iodine are estimated to be present in the gas space. About 98% of the gaseous fission products and essentially all the solid fission products remain in the ceramic pellets.

At normal operating temperatures the fuel pellets are well below the melting temperature, the cladding is strong and ductile, and the fuel rod is an effective barrier to the release of fission products. However, abnormal or accident situations can be envisioned in which the temperature of the cladding would rise several hundred degrees, and the cladding would fail and release the fission products contained in the gas space.

If the temperature were to rise above about 4800°F, the uranium dioxide pellets would melt. All the krypton and xenon and about 90% of the iodine would be released quickly from the fuel, and some of the solid fission products would be dispersed as an aerosol. Release of this radioactivity from the plant could have serious, widespread effects.

2.2 REACTOR COOLANT SYSTEM AND CONTAINMENT

Two physical barriers beyond the fuel rod provide protection against the release of fission products during normal operation and in accident situations. The first of these is the reactor coolant system (Figs. IX 2-2 and IX 2-3). The fuel rods, grouped into fuel elements and installed in the reactor vessel, form the reactor core, which is cooled by the water circulating in the reactor coolant system. Fission products released by the fuel rods are confined by the piping and vessels of the reactor coolant system as long as they remain intact. The structure that houses the reactor coolant system - the containment (see Figs. IX 6-1 and IX 6-2) - is designed to confine radioactive materials that escape from the coolant system.

Preferably each barrier - fuel rod, reactor coolant system, and containment - should be independent and self sufficient. That is, failure of one of two barriers should not affect the integrity of the remaining barrier(s). Failures of the containment that are considered credible would not affect the integrity of the reactor coolant system or the fuel rods. The components and piping of the reactor coolant system are designed and supported and missile shields are provided so that failures of the reactor coolant system would not directly affect

the integrity of the containment. However, in the absence of special safety features, some failures of the reactor coolant system would lead to extensive melting of the fuel rods. Extensive melting, whatever the cause, would be followed by breaching of the reactor vessel and containment and the release of a large amount of fission products from the plant. Consequently, the foremost safety requirement in the design of a nuclear power plant is to provide reliable cooling for the fuel rods to prevent them from melting.

Typical Fuel Data

	PWR	BWR
Overall length, in.	149.7	∿164
Outside diam., in.	0.422	0.563
Metal wall thickness, in.	0.0243	0.037
Pellet diam., in.	0.366	0.477
Pellet length, in.	0.600	0.5
Pellet stack height, in.	144	144
Plenum length, in.	4.3	16
Fuel rods in fuel assembly	204	49
Fuel rod pitch, in.	0.563	0.738
Fuel assemblies in core	193	764

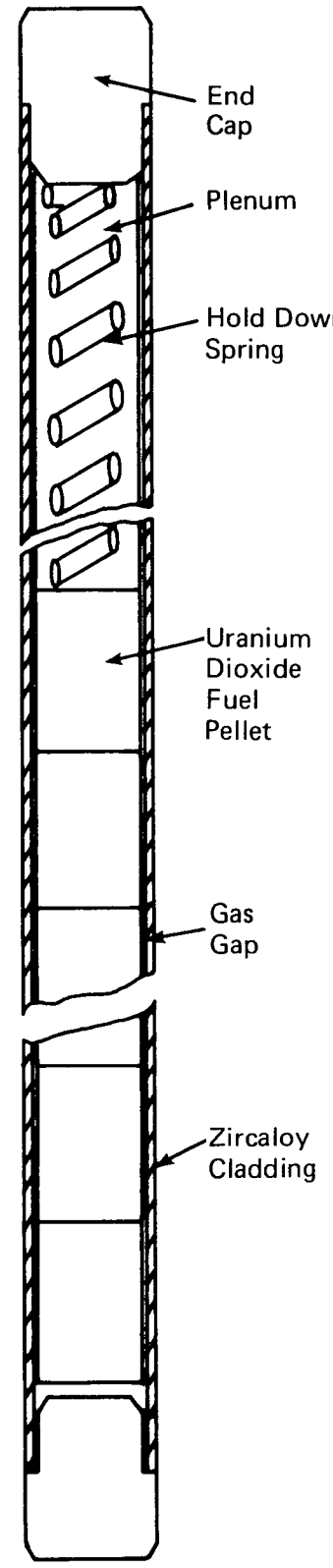


FIGURE IX 2-1 Typical Reactor Core Fuel Rod

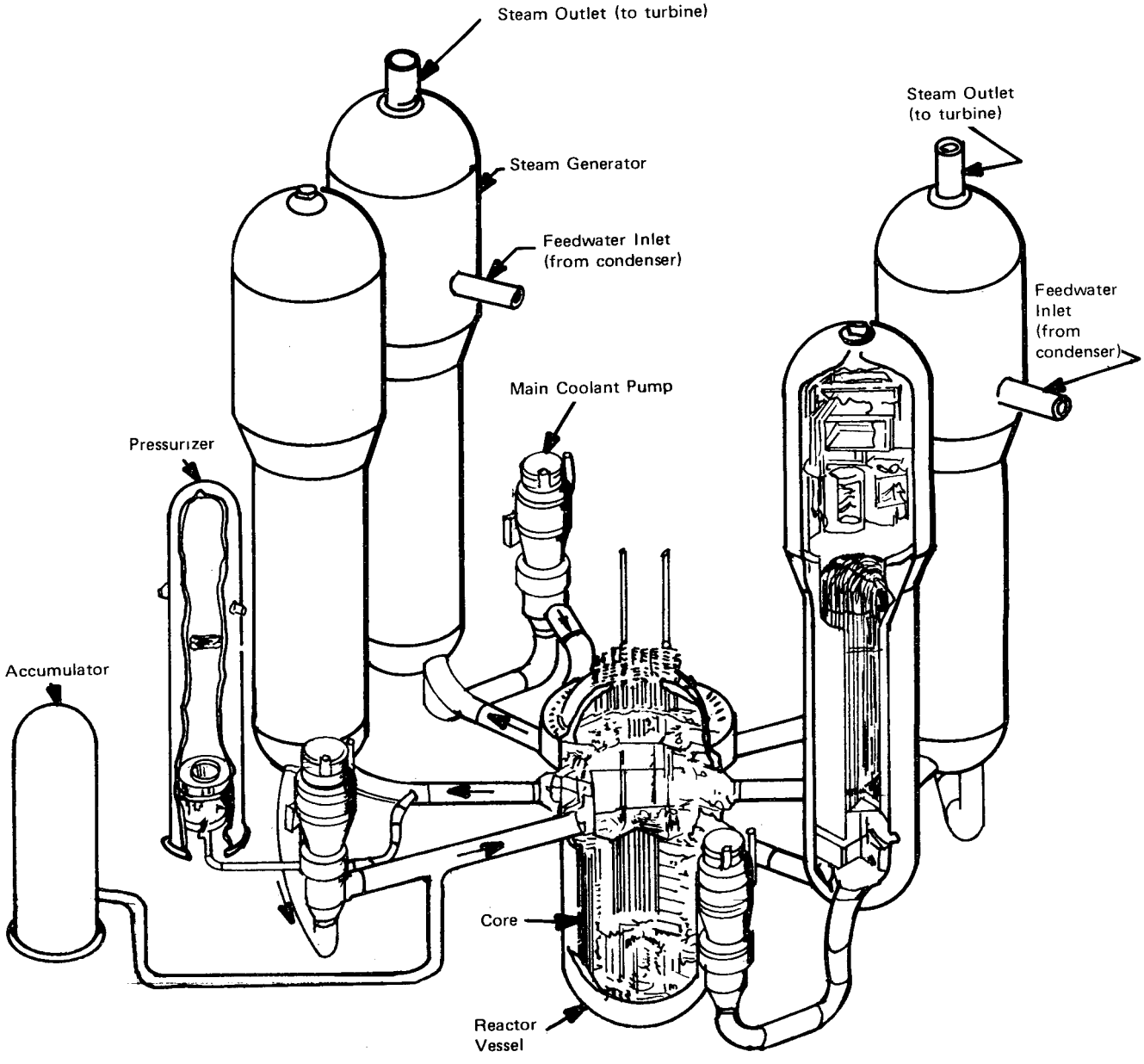


FIGURE IX 2-2 Typical PWR Reactor Coolant System

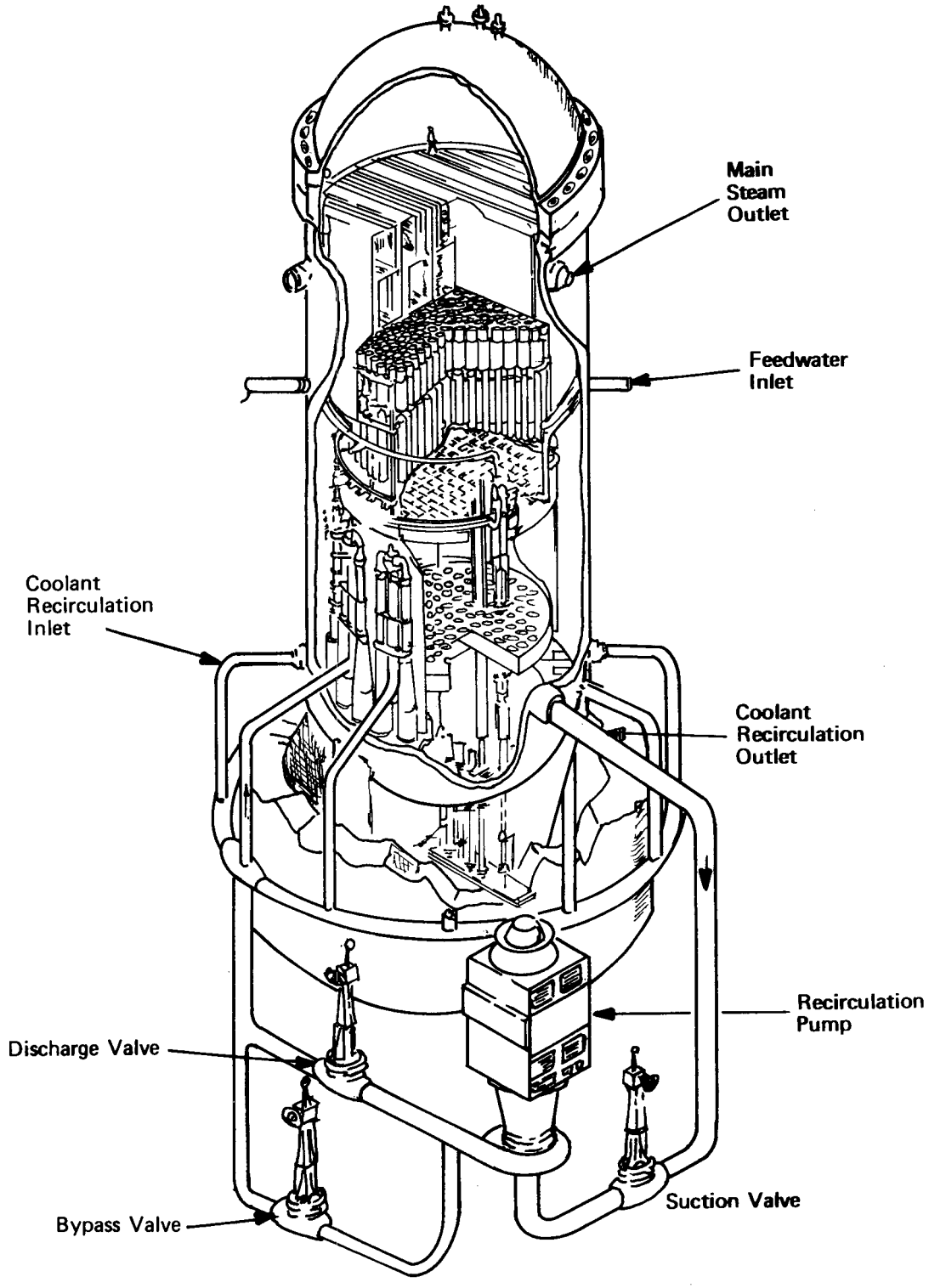


FIGURE IX 2-3 Typical BWR Reactor Coolant System

Section 3
General Basis for Safety Design

3.1 NORMAL OPERATION AT POWER

3.1.1 CONFINEMENT OF RADIOACTIVITY

Successful operation of the plant requires that almost all the fission products remain in the fuel rods. Should, for instance, the cladding of too many fuel rods contain imperfections that release products from the gas space, the level of radioactivity in the plant would be high enough to interfere seriously with operation and maintenance. Furthermore, it would be difficult to keep the radioactivity in routine effluents at the low level prescribed to protect the health of the public. Thus, as a part of normal plant operation, care is required to keep small the amounts of fission products and other long-lived radioactive materials in the cooling water.

This entails, first, the manufacture of fuel pellets and cladding of very high quality so that the number of imperfections will be small. However, a reactor core contains almost 40,000 fuel rods, and some do leak. Water from the reactor primary system is processed continuously by evaporation and ion exchange for several purposes, including the removal of radioactive fission products and corrosion products. Waste liquids, gases, and solids from this processing are stored until their radioactivity decays to a level safe enough for release to the surroundings; alternatively the wastes are packaged and shipped to a disposal facility.

Excessive leakage of water from the reactor coolant system into the containment would make operation and maintenance difficult, so the coolant system must be of highest quality. The reactor coolant system operates at about 1050 psi in a BWR and 2250 psi in a PWR, and a small amount of radioactive gas and water passes through seals on valves, pumps, and other equipment into the containment. The air in the containment and the liquid collected in sumps at the bottom of the containment are processed to remove and confine their radioactivity.

3.1.2 COOLING OF FUEL RODS

In addition to the requirement for fuel rods of high integrity for normal operation, the fuel must be prevented from reaching temperatures that could melt the uranium oxide pellets (>4800°F) or the cladding (3300°F). Because Zircaloy reacts exothermally with steam, the cladding is surrounded by water, causing clad oxidation and embrittlement, it is desirable to keep the cladding below 1800°F, the temperature at which this reaction begins to be significant. For this reason, the perturbations that could cause excessive fuel or cladding temperatures are examined and means are provided to control them.

All the processes that could cause the temperatures to become excessive depend on the same fundamental physical condition. The fuel is a source of heat and the heat must be removed at about the same rate that it is generated or the fuel pellets and the cladding will overheat. This is important not only when the reactor is operating but also after the fission reaction has been stopped. At full power the uranium oxide in the fuel rods is at a much higher temperature than the cladding - above 4000°F in the center of some pellets. The stored energy in the pellets is equivalent to about 4 sec of full power operation in regions of maximum heat generation, and the cladding must be kept at an acceptable temperature until the excess heat has been conducted to the coolant. Removal of this stored energy takes a few seconds, and thereafter only the heat produced by radioactive decay of the fission products establishes the cooling requirement. The heat production rate from this fission product source is about 7% of full power at the instant of shutdown and decreases as shown in Fig. IX 3-1. Fuel from a 1000-MWe reactor would still produce 6000 kilowatts of heat 30 days after shutdown.

Heat is removed from the fuel in normal operation by circulating water over the cladding at high velocity. A certain mass flow rate of water at the design temperature and pressure is required to cool the core adequately at it's design power; substantially more than the required flow is provided. The heat production is not uniform throughout the core, and this must be taken into consideration. The maximum heat generation rate in the fuel and the heat flux from

the cladding to the coolant in normal operation are 1.5 to 2 times the average for all the fuel in the core. A value well above 2 is assumed for design purposes to allow flexibility in operation of the reactor. On the basis of this higher value the coolant flow, temperature, and pressure are specified so that the critical heat flux[1] is greater by a factor of 1.8 or more than the local heat flux anywhere in the core. This does not mean that the reactor power could be increased by a factor of 1.8 without damage to the fuel rods. It does, however, provide considerable margin to bring upsets under control before the fuel rods are damaged.

3.2 ANTICIPATED TRANSIENTS AND ACCIDENTS

If the power level were increased beyond the capacity of the water flow to remove the heat; if the water flow, temperature, or pressure were changed in such a way as to reduce the effectiveness of the coolant; or if the water were lost from the reactor core, the fuel rods would overheat. Various events have the potential for producing such effects. Some involve changes in operating conditions, failure of equipment within the plant, or errors by the operators. Others involve external forces, such as earthquakes and other severe natural phenomena that can affect the plant equipment. Several levels of safety are provided in the plant to protect against and mitigate the effects of such events.

[1]The heat flux at which steam begins to blanket the surface and the cladding temperature begins to rise rapidly to damaging levels because the steam impedes transfer of the heat from the fuel to the bulk of the coolant.

The plants are designed conservatively and built, tested, operated, and maintained in accordance with high quality standards to reduce equipment faults and operating errors to a minimum. Special requirements are imposed on the design and operation to prevent external forces from causing failures. Instrumentation and control systems are provided to keep the plant operating steadily within prescribed limits.

In spite of these measures, some operational upsets must be expected to occur during the service life of the plant. The design of the plant is examined in light of the incidents believed most likely to occur and measures are provided to cope with them. One of the important measures is a reactor protection system that sounds alarms and holds or reduces the reactor power when operating limits are approached and then trips the reactor (stops the fission reaction) and establishes safe shutdown conditions if these limits are reached. A design requirement is that the safety features should terminate these anticipated transients without damage to the fuel rods or the reactor coolant systems.

Finally, additional systems and margins are included in the design to protect the public in the event that certain highly unlikely but very severe accidents occur. Major failures of plant components and systems are assumed and engineered safety systems are designed to control the accidents that would ensue. Fuel rods may be damaged and radioactivity may be released from them in these design-basis accidents, but the design of the plant and its engineered safety features must provide assurance that the fuel rods will not melt and that radioactive materials will not escape from the plant in sufficient quantity to cause serious exposures to the public.

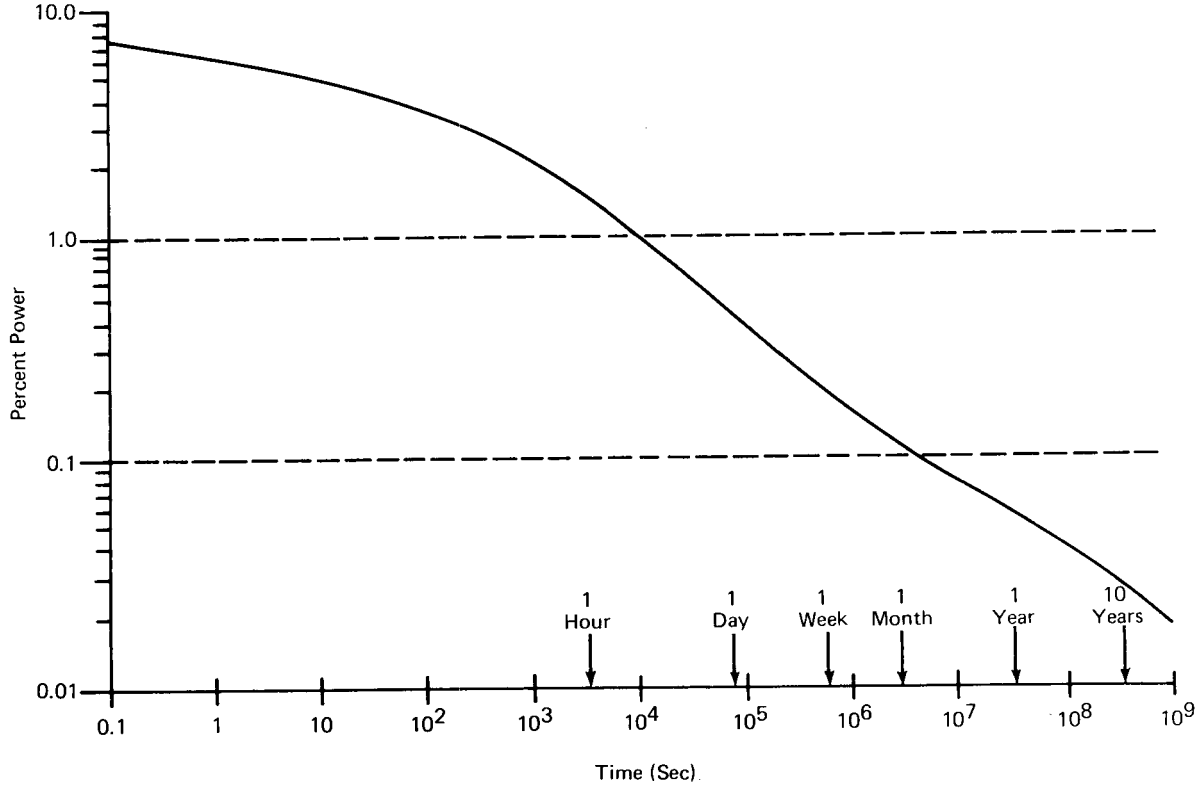


FIGURE IX 3-1 Heat Production of Decay of Fission Products

Section 4
Protection Against Overpower

Several types of events can cause the power generated in a reactor core to rise so that the control or protection system must act to prevent the fuel rods from overheating. A reduction in temperature or a rise in flow of coolant causes the average temperature of both fuel and coolant in the core of a PWR to begin to fall, and the nuclear characteristics of the core cause the power to rise in an effort to hold the average temperature near its initial value. A reduction in temperature or an increase in flow of coolant or in system pressure causes the volume of steam in the core of a BWR to begin to decrease and the power rises in an effort to maintain the steam volume fraction. The fission reaction is controlled by assemblies of neutron absorbing material which are moved in and out of channels in the reactor core. Uncontrolled withdrawal of control assemblies would cause a power transient and increases in fuel and coolant temperatures in the core of a PWR, or in fuel temperature and steam volume fraction in the core of a BWR. PWR's also use boron dissolved in the coolant for control purposes. Diluting the boron has an effect similar to the withdrawal of control rods.

Power reactors are designed to produce heat to satisfy the demand for steam by the turbine generator. The core power is permitted to vary with demand, and the control systems function to keep the coolant conditions within limits related to the power. Because an excess of cooling is provided, the core can be permitted to exceed design full power by 10 to 20% before being tripped by the protection system. Neutron detectors that measure the fission power directly and nearly instantaneously from radiation emitted by the core are the primary sensors for initiating protective action against overpower. The rise in temperature of the water on passing through the core is used as a backup indicator of reactor power to initiate protective action in a PWR.

4.1 REDUCTION IN TEMPERATURE OF REACTOR COOLANT

The temperature of the water entering the core of a PWR depends on the amount that the water was cooled in passing through the steam generators in the coolant loops outside the reactor vessel. Reducing the temperature or increasing the flow of feedwater to the steam generators or increasing the rate at which steam is withdrawn from them lowers the temperature of the water entering the reactor core. In a BWR the reactor core is the steam generator. The feedwater is mixed with the coolant as it recirculates to the core, and the temperature of the coolant is influenced directly by the feedwater temperature and flow.

4.1.1 TEMPERATURE AND FLOW OF FEEDWATER

Steam that is generated in the steam generators of a PWR and in the core of a BWR is passed through a turbine where about one-third of the energy is used in turning a generator to produce electricity. The remaining energy is removed in condensing the steam in a condenser at the outlet of the turbine. This condensate is then recycled as feedwater to the steam generators of the PWR and the reactor vessel of the BWR. The thermal efficiency of the steam cycle is optimized by withdrawing part of the steam from several points in the turbine and using that steam to preheat the feedwater as it is being returned to the reactor system. The temperature of the feedwater delivered to the reactor system can be lowered below its normal temperature by reducing the flow of steam to the feedwater heaters or by bypassing some of them. The characteristics of the feedwater systems are such that changes in feedwater temperature from these causes would occur slowly or would be small. The greatest effect is expected when the reactor is at full power. Analyses indicate that the power would rise and stabilize below the overpower trip level in most feedwater cooling incidents.

The rate of feedwater flow to a BWR reactor coolant system is controlled by several control valves and/or feedwater pumps operating in parallel. Malfunction of feedwater controllers could cause the flow to increase rapidly. With the reactor at full power, the amount of flow increase in many cases would not be sufficient to raise the power to the overpower limit. If, however, the flow were increased to the full output of the feedwater pumps, an overpower trip would ensue.

A rapid rise in feedwater flow to a rate well below full flow with the reactor at very low power would result in a power transient with a peak that could be several times the full power level. In such an incident a reactor trip would be initiated as the power passed through 10 to 25% of full power (the range of trip settings when the reactor is at low power). The reactivity of the uranium oxide fuel decreases with increasing temperature, and the rapid heating of the fuel would stop the rise in power and cause it to fall back rapidly. Insertion of the control assemblies in a second or two would end the incident. The amount that the feedwater flow could reasonably increase is limited by the system design. Within those limits the total energy released during a transient would not be enough to damage the fuel rods.

A BWR has systems other than the feedwater system that supply cold water to the reactor vessel in normal or emergency situations. They include a high pressure coolant injection system and shutdown cooling systems. Addition of water from any of these sources would cause the reactor vessel water level controllers to compensate by reducing the feedwater flow. The effect would be to lower the temperature of the net flow of water to the vessel, and the resulting transient would be less severe than one produced by interrupting the flow of steam to the feedwater heaters.

4.1.2 INCREASE IN STEAM DEMAND

The demand for steam from the reactor system can be increased by opening more fully the turbine control valves, by opening valves that release steam from the main steam lines, or by rupture of a steam line. If any of these events were to occur in a PWR at full power, the reactor core power would rise above design full power, but this could also happen with the plant initially at lower power. In bringing the plant from low power to full power the reactor core must provide the heat for warming the water and equipment in the plant systems as well as for generating the steam for the turbine. If the load were increased too rapidly, the reactor core power would rise above the design full power in satisfying the total demand.

The immediate response to a sudden release of steam in a BWR is a decrease in power. The steam pressure falls, the steam in the reactor core expands, which increases the steam volume fraction and decreases the reactivity, and the power falls. The control system responds by increasing the coolant flow to the core to maintain the water level within the operating range and raises the power level, which restores the pressure.

The PWR and BWR plants are designed to accommodate, without a reactor trip, rates of increase in demand over the range from low power to full power that are well above those normally imposed by the electrical transmission system. The turbines are equipped with load-limiting and/or speed-control devices to prevent the demand for steam from exceeding full rated flow by more than a few percent. Any malfunction or misoperation that caused the steam demand and reactor power to rise excessively would result in a reactor trip.

The steam systems contain turbine bypass valves that discharge steam from the main steam lines directly to the turbine condenser, power-operated relief valves, and code safety valves. These valves release steam under particular conditions to cool the reactor, control the reactor coolant system pressure in a BWR, and protect the steam system from excessive pressure in a PWR. Misoperation or malfunction of one or more of these valves would increase the demand for steam from the reactor coolant system. Numerous valves are used in these systems and they operate separately. Opening of one or two valves usually can be accommodated by the reactor control system without a reactor trip. The protection system would trip the reactor if the steam demand raised the power excessively.

4.1.3 RUPTURE OF A MAIN STEAM LINE IN A PWR

Rupture of a main steam line would cause the largest and most rapid increase in flow of steam of any of the increase-in-steam-demand incidents. This is one of the low probability accidents for which measures are taken in the design to protect the fuel rods from melting and the public from serious exposure to radiation from radioactivity in the steam. It is an overpower incident in a PWR plant. It is a loss-of-coolant accident, and is discussed later as such, in a BWR.

A steam line in a PWR might rupture when the reactor is operating at any power up to full power, or when the control assemblies are fully inserted and the reactor is shut down but near operating temperature. With the reactor operating, the power would rise very rapidly and the reactor would be tripped by the

protection system on indication of overpower by the nuclear power sensors. Shutdown would occur quickly enough to avoid damage to the fuel rods.

Simply inserting the control assemblies into the core would not be sufficient to keep the reactor shutdown under all circumstances. The control assemblies in a PWR are designed to stop the fission reaction quickly and to keep the reactor shut down at the operating temperature. Boron must be added to the water if the reactor is to remain shut down when the coolant temperature is lowered. Continued generation of steam in the steam generators would lower the reactor coolant temperature rapidly, and hence the possibility and consequence of starting the fission reaction again must be considered.

Several measures are taken to limit the cooling and to bring the reactor to a securely shutdown condition.

a. Block valves in each main steam line just outside the containment close automatically on indication of a break in a steam line. If the break were outside the containment closing the valves would in most instances stop the steam flow. If a block valve failed to close, however, connections between lines would allow steam to be discharged to the atmosphere until all the water had boiled out of one steam generator. If the break were inside the containment, the affected steam generator would discharge its steam inside the containment until dry. In any event the release would be limited to one steam generator.

b. The flow of feedwater to the steam generators is stopped until the accident is brought under control.

c. A concentrated boric acid solution is injected into the reactor coolant by high pressure pumps to minimize the rise in fission reaction.

The maximum rate, magnitude, and duration of cooling would occur if the reactor were at hot shut down with the control rods fully inserted and a steam pipe were to rupture at a steam generator. Safety analyses for a typical plant indicate that the cooling would allow the fission reaction to begin within 15 sec after a steam line rupture. The nuclear power would rise rapidly and stabilize at about 30% of full power. Concentrated boron solution would begin to enter the reactor coolant loops in about 90 seconds, about the time that the steam generator would boil dry, and the reactor would be shut down a few seconds later.

In the steam-pipe-rupture incident the power reached by the reactor on cooling would be well below full power. However, if the control assembly of greatest worth were to stick in the fully withdrawn position during the initial shutdown, the power distribution in the subsequent transient with all but one control assembly in the core would be severely peaked. The maximum heat generation rate in the fuel near the position of the withdrawn assembly at the lower power might exceed the maximum at full power allowed for in the design. In studies of this situation, it has been found that there is no danger of the fuel rods overheating even with the reactor coolant pumps stopped and the water circulating by thermal convection.

With the reactor shut down at operating temperature, the sticking open of a pressure-relief valve or a turbine bypass valve would cause a cooling incident similar to the steam line rupture incident. Although the fuel rods would not be damaged, it is not desirable to have the reactor resume operation in such events involving a large blowdown which are likely to happen more frequently than main steam line breaks. By use of a large number of small valves, the rate of cooling caused by the sticking open of one valve is reduced and the effect can be compensated by the boron injection system.

Steam would be discharged into the containment in some of these steam-release incidents and to the atmosphere in all of them.[1] If, during normal operation, reactor cooling water leaks into the steam system through flaws in the tubing or tube sheets of the steam generators, the steam discharged in an incident would contain some radioactivity. When the break is inside the containment, limiting the blowdown to the contents of one steam generator ensures that the peak pressure in the containment would be below the design pressure and the radioactivity would be confined, as in the loss-of-coolant accidents described in section 6. When the break is outside the containment, all the steam released would pass into the atmosphere. The

[1] Steam is released to the atmosphere to cool the reactor in cases where the steam line block valves close.

potential radiation doses to the public are small because the concentration of radioactivity in the reactor coolant, the rate of leakage of reactor coolant into the steam system, and the amount of radioactivity in the steam system are required to be at low levels.

4.2 INCREASE IN FLOW OF COOLANT TO REACTOR CORE

The reactor coolant pumps in a PWR run at a fixed speed and the coolant loops have no flow control valves; hence the flow cannot be increased in normal operation. However, PWR's have multiple coolant loops and 3 or 4 coolant pumps and are permitted to operate at reduced power with one pump out of service. Since uncontrolled startup of an inactive loop could, in some circumstances, cause a substantial rise in reactor power level, protection against such an event is included in the design. The BWR makes use of a variable speed pump in each of two loops to control the rate of recirculation of coolant through the core and, thereby, the reactor power. Increasing the flow lowers the steam volume fraction in the core and the power rises to restore it. A malfunction of the pump speed controls that increased the flow or startup of an inactive loop would produce a power transient.

Two types of startup of an inactive loop in a PWR must be considered - one in which a pump has been idle but the loop has no isolation valves or the valves have been left open, and the other in which the loop has been isolated by closing valves in the inlet and outlet lines. The latter is of greatest concern because it presents the possibility of adding rapidly, to the bulk of the coolant, water that is cool and low in boron content.

With the pump stopped but the loop open to the remainder of the reactor coolant system, water flows in the reverse direction through the inactive loop and the water in the steam generator tubes is cooled to a temperature below that of water being delivered to the reactor core by the operating loops. To bring an inactive loop into operation without tripping the reactor, operating procedures require that the plant be brought to low power in order to equalize the temperatures before starting the pump. Without this precaution, the rise in reactivity of the core caused first by the increase in flow and then by the decrease in coolant inlet temperature would be too rapid to be compensated by the control system. The nuclear power would rise to the trip point in less than a second and the protective system would trip the reactor. The peak power would be well above full design power, but the heat flux from the cladding to the coolant would not reach the full-power heat flux during the transient and the fuel rods would not be damaged.

In the instance of the isolated loop, simply opening the isolation valves and starting the pump could, under the most adverse conditions, cause a very large rise in core power and possibly damage the fuel. Therefore administrative controls require the power to be reduced to zero and the temperature and the boron concentration of the water in the isolated loop to be near those in the active loops before the isolation valves are opened. Because these administrative controls are judged to give insufficient protection, interlocks are also provided in the reactor protection system to ensure a low probability of startup of an isolated loop containing water at low temperature and boron concentration. These interlocks prevent the valve in the line from the discharge of the isolated coolant pump to the reactor vessel from being opened unless the water in the isolated loop has been recirculated and mixed slowly, through a relief line, with the water in the remainder of the reactor coolant system.

Because of the protective interlocks, the most drastic misoperation likely to occur would be to begin the startup in violation of administrative controls with the isolated loop containing water at low temperature and boron concentration. The flow through the relief line is limited by the line's size, and thus water from the isolated loop would mix slowly with the bulk of the reactor coolant. If the water in the isolated loop contained no boron, several minutes would be required before the shutdown margin of the control assemblies would be surpassed and the fission reaction would begin. The reduction in shutdown margin would be indicated as it occurred by the neutron flux monitors in the control room. The operators would have ample time to take corrective action which would include injection of concentrated boric acid to regain the shutdown margin.

In the BWR, a malfunction of equipment that controls the pump speed to increase the speed at the maximum rate has a greater effect than does startup of an idle loop. In either case, the most severe transient is found to occur when the initial power is ∿70% of full power

and the flow is ∿50% of full flow. In the case of malfunction of speed controls, the reactor would be tripped on indication of overpower by the neutron sensors. The thermal neutron flux would peak at a value above 200% of full power but the transient would be so short that the heat flux from the cladding to the coolant would at no time exceed the full-power heat flux. In the case of startup of an idle loop, the characteristics of the recirculation pump and power supply and of the jet pumps that it drives combine to make the incident a minor one. The reactor core power would rise briefly to only a few percent above the full-power value before settling at a new steady-state condition and the reactor would not be tripped.

4.3 INCREASE IN PRESSURE IN A BWR

An increase in reactor system pressure compresses the steam in the core of a BWR and the power rises rapidly in an effort to restore the steam volume fraction. The reactor is equipped with a pressure regulating system, but this system cannot reasonably be provided with the capacity and extra features needed to prevent the pressure from rising when the turbine control valves close rapidly, or the turbine block valves or the isolation valves in the main steam lines close. The turbine control valves close rapidly on rejection of a large percentage of the load by the electrical transmission system. The turbine block valves close on any signal that calls for a turbine or reactor trip. The main steam line isolation valves close to prevent steam from being discharged to the atmosphere on indication of certain potentially unsafe situations in the reactor, the containment, or the steam system. Misoperation or malfunctions can also cause the valves to close.

Rapid closing of the turbine control valves or stop valves interrupts the steam flow in a fraction of a second. A reactor trip is initiated when these valves close, and normally the pressure control system opens turbine bypass valves to release steam to the turbine condenser. The pressure rises sufficiently in a few seconds to cause relief valves to open briefly to limit the presure rise, but the control assemblies insert neutron absorbing material rapidly enough to keep small, any increase in power beyond rated full power.

The incident is more severe if the turbine bypass valves cannot open due to the condenser being out of service. Relief valves open as the pressure rises from the nominal operating pressure of 1050 psi to a peak just above 1200 psi. The core neutron level rises briefly to about double that at full power but the heat flux rises only a few percent before the power transient is terminated.

Closing the main steam line isolation valves produces a transient similar to that produced when the turbine block valves close and the turbine bypass system is inoperative. The transient is less severe, however, because the isolation valves close less rapidly. The pressure in a transient produced by the closing of one turbine block valve or steam line isolation valve is controlled by the turbine bypass valves alone, but the power increases enough to cause the reactor to trip from overpower.

4.4 UNCONTROLLED MOVEMENT OF CONTROL ABSORBER

Although the control systems are designed to prevent the heat flux in the reactor core from rising to excessive levels, malfunctions or accidents involving the control systems can cause such a rise. Three types of situation are considered in the reactor design: (1) uncontrolled withdrawal of neutron absorber by the control systems, (2) insertion of a control assembly into the core with the reactor at power, and (3) ejection of a control assembly from the core under pressure or gravity forces. The first and third result in increases in power, the second in a change in the power distribution and an increase in the local heat flux in the core. The consequences of these incidents are limited by limiting the worth of each control assembly and/or the rate of movement and using a large number of assemblies to satisfy the total neutron control requirements of the reactor.

4.4.1 WITHDRAWAL OF CONTROL ASSEMBLY BY DRIVE MECHANISMS

The uncontrolled withdrawal of a control assembly might occur with the reactor shut down or at power. Several provisions of the design, limit the rate at which the reactivity of the core can be increased in such an incident. The speed of the drive mechanism is limited by the design, and the number of assemblies that can be moved at one time is limited by interlocks in the control system and by the sequencing of power to the drives.

With the reactor initially at zero power, continuous withdrawal of a control assembly could cause the core power to rise very rapidly. The incident would be terminated automatically by reactor trips initiated at low, intermediate, and high power by signals from the neutron sensors. Under the most adverse conditions of the highest worth control assembly being withdrawn and time delays in the transmission of signals and operation of trip mechanisms, the neutron level might rise to almost 10 times the full design power, but only for a fraction of a second. The power rise would be stopped and the power would be momentarily reduced by the inherent negative reactivity effect from heating of the fuel. Insertion of the control assemblies, which takes 1 to 2 sec, would shut down the reactor. Because of the short duration of the transient, the temperatures of the fuel and cladding and the maximum heat flux from the cladding to the water would not reach the full-power values.

The effects of uncontrolled withdrawal of a control assembly have been studied over the full range of power for a wide range of withdrawal rates and assembly worths. Under most circumstances the incident is minor and the fuel rods are protected by a reactor trip on indication of overpower by the neutron sensors. This overpower trip does not, however, provide the desired degree of protection in a PWR when the reactivity is increased slowly. The steam control valves to the turbine limit the rate of generation of steam by the steam generators and thereby the cooling of the water in the reactor primary system. The water temperature rises as the power increases and the critical heat flux decreases with rising water temperature. A trip based on coolant temperature and reactor power is included in the reactor protection circuits for this situation. A reactor trip is initiated when the temperature rise of the reactor coolant in passing through the core (a measure of the reactor power) exceeds the temperature rise allowable for the prevailing coolant temperature in the reactor.

4.4.2 DILUTION OF BORON IN PWR COOLANT

During operation of a PWR, water is recycled at a small rate but continuously from the reactor coolant system, which is at high pressure, to a chemical and volume control system, which operates at low pressure. The boron concentration in the reactor coolant can be reduced, and the reactivity of the core thus increased, by returning unborated water to the reactor coolant system.

Boron dilution is a manual operation that is conducted under administrative controls. Valves must be opened and pumps started by the operator in order to add unborated water to the reactor coolant system. The chemical and volume control system is designed to limit the maximum rate of dilution to a value that, after indication through alarms and instrumentation, provides the operator with several minutes to correct the situation before the reactor is tripped by the protection system.

After a trip, the operators have many minutes to stop the dilution before the reduction in boron concentration causes the fission reaction to begin again with the control assemblies fully inserted. The procedures made erroneous dilution unlikely, numerous alarms and indications alert the operators to the condition, ample time is available to correct the situation, and therefore no other protection against a dilution incident is provided.

Dilution during startup is similar to the uncontrolled withdrawal of control assemblies, except that reactivity is added more slowly. The reactor operators would be alerted to the changing boron concentration by a gradually increasing count rate on the nuclear instruments in ample time to take corrective action.

4.4.3 INSERTION OF A CONTROL ASSEMBLY

Driving (or, in a PWR, dropping) one or more control assemblies into the core with the reactor at power, or leaving one in when the reactor is brought to power, reduces the heat generation rate in the fuel in the vicinity of the inserted assembly. The heat generation rates in other parts of the core must increase in order to hold the total power constant and thus the heat generation rate increases in these other regions. The same effect is obtained if the control assemblies are not kept properly positioned relative to each other during operation.

During operation, control assemblies are moved in a preselected sequence to maintain proper alignment. The positions are shown by indicators and lights. Alarms sound when assemblies deviate from prescribed positions by more than a few percent. In some designs, movement of control assemblies is inhibited when alignment limits are reached. Accidental insertion of a control assembly would shut down the reactor or would be indicated (1) by a sudden drop in power,

(2) by an asymmetric power distribution sensed by the neutron power detectors (also by thermocouples in the water leaving the core in a PWR), and (3) by the various position indicators and alarms.

The effect of control assembly misalignment is a factor considered in establishing the value for the maximum heat flux allowed by the reactor design. If a reactor were operated at full power with one control assembly fully inserted and the others aligned within the limits, the maximum heat flux from the cladding to the coolant would still be well below the critical heat flux. Since studies indicate that serious situations are not likely to arise from control-assembly-insertion incidents, the operator is largely depended on to take any corrective measures that might be needed.

4.4.4 EJECTION OF A CONTROL ASSEMBLY

The drive mechanisms for the control assemblies are mounted on the top head of the reactor vessel in a PWR and are supported from the bottom head in a BWR. If a drive mechanism housing were to rupture, the pressure inside the reactor vessel would tend to expel the drive shaft from the vessel. The attached control assembly would be ejected from the core very rapidly, with consequences to the fuel rods and reactor coolant system that would depend on the reactivity worth of the assembly.

Use of boron in the reactor coolant for part of the neutron control and use of many control assemblies makes the full worth of an individual assembly small in a PWR. The housings are manufactured to high standards of quality so that the probability of a drastic failure sufficient to eject a control assembly is small. Furthermore, the results of a rod ejection accident in the PWR is predicted to result in limited or negligible fuel rod damage. Because of these considerations, no mechanical features are provided in the design of a PWR to prevent rupture of a housing from causing a control assembly to be ejected from the core.

Although many control assemblies are used in a BWR the full worth of individual assemblies is greater than in a PWR. Structural members are thus incorporated in the BWR design to prevent the drive shaft from moving more than a short distance in the event of a housing rupture. Several types of failure could, however, occur in a drive mechanism that would permit a control assembly to drop out of the core. The control assembly incorporates a device that limits the velocity of fall in order to reduce the consequences of such an accident.

In most instances, a control assembly ejection incident would not produce a serious power transient. When the reactor is at power, the control assemblies are partly to fully withdrawn. In many instances, the power would not rise to the overpower trip level, in others the protective system would trip the reactor on indication of overpower and the transient would be terminated with the fuel rods undamaged. When the reactor is shut down with the control assemblies fully inserted, ejection of one would not produce a rise in power.

Under some circumstances, ejection of a control assembly could result in a damaging transient. Because the probability of such an accident is very low, the risk of limited damage to some fuel rods is accepted provided that only a small percentage of the fuel rods would be likely to fail and the failures would not cause a damaging pressure surge in the reactor coolant system.

By subjecting fuel rods to rapid power transients in test reactors, it has been shown that the damage sustained by a fuel rod can be related to the total energy generated in the fuel pellets during a transient. These data are used in assessing the consequences of control assembly ejection accidents in a PWR and control assembly drop accidents in a BWR. Analyses of plants of acceptable design show that less than 10% of the fuel rods would be perforated during the most severe accidents. The pressure in the coolant system would rise moderately but would not impose appreciable additional loads on the coolant system.

In the case of rupture of a control rod housing, reactor coolant would be discharged into the containment and the accident would also be a small-break loss-of-coolant accident. Measures taken to prevent the fuel rods from being damaged further and to protect the public from radioactivity in such accidents are discussed in section 6. In the case of a control rod drop accident in a BWR, no coolant would be lost and the fission products would be confined initially to the reactor coolant system and the steam system. Isolation valves in the main steam lines would close in a few seconds on indication of a high level of radioactivity in the steam and

thus limit the amount of radioactivity in the steam system. The steam system also would be isolated by closing valves to ensure that only a small fraction of the radioactive kryton, xenon, and iodine could escape to the surroundings.

Section 5

Protection Against a Reduction in Core Cooling

The cooling effectiveness of the reactor cooling water is reduced by changes in cooling conditions that lower the critical heat flux. A reduction in flow, a rise in temperature, or a reduction in pressure of the coolant are such changes. The cooling capacity, particularly in some types of abnormal occurrence, depends on the inventory of water in the steam generators of a PWR and in the reactor vessel of a BWR. Changes in operation that reduce the inventory and thus the cooling capacity include reduction in flow of feedwater to or increase in flow of steam from the steam generators in a PWR or the reactor vessel in a BWR.

The design approach to protecting against reductions in cooling effectiveness and capacity is to:

a. Design the plant so that such events will be infrequent and the magnitude and rate of reduction of cooling capability will be within limits.

b. Provide control and protection systems that will, on indication of a reduction in cooling effectiveness or capacity, reduce the power or trip the reactor, depending on the magnitude of the upset.

c. Ensure that the cooling capacity after a reactor trip will be sufficient to dissipate the energy stored in the fuel at high temperature and the fission-product decay heat.

5.1 REDUCTION IN REACTOR COOLANT FLOW

Loss of power to one or more of the reactor coolant recirculation pump motors, seizure of a pump rotor, or shaft breakage would cause the flow of coolant to the reactor core to decrease. The reduction in flow results in a reduction in the critical heat flux and the core power must be reduced to prevent the fuel rods from overheating. The pumps of a PWR are equipped with flywheels to increase the inertia of the rotary elements so that the pumps coast down slowly and the flow decreases gradually over many seconds. The combined inertia of the pumps and the motor generator sets used to control the pump speed serves the same purpose in a BWR. Seizure of a pump rotor or shaft breakage would decrease the flow in one coolant loop abruptly, but, because of the number of loops in a PWR and the characteristics of the jet pumps in the BWR, the flow through the core would not fall below about 60% of full flow.

In a PWR, as the flow decreased the core temperature would begin to rise and the power to fall. Until the average temperature and temperature rise of the coolant in passing through the core reached the operating limits, the reactor control system would withdraw control rods to hold the power constant. This would aggravate the situation, so the protective system is arranged to trip the reactor on indication of loss of power to one or more pumps or low flow in one or more coolant loops.

In a BWR, as the flow decreased the volume fraction of steam in the core would begin to rise and the power and the rate of steam production would begin to fall. The pressure regulating system, in order to hold the pressure steady, would gradually restrict the flow of steam to the turbine, the reactor would not be tripped, and the power would stabilize at a level appropriate to the reduced flow. The density difference resulting from the production of steam in the reactor core induces a substantial circulation of coolant when the pumps are stopped.

Stoppage of all the recirculation pumps would cause the greatest reduction in flow, but the initial rapid reduction while the reactor is still at full power makes seizure of a pump rotor or shaft breakage the most severe reduction-in-coolant-flow incident. Seizure of a pump rotor and shaft breakage are events with such low probabilities of occurrence that damage to a small percentage of the fuel rods could be tolerated. However, analyses show that the critical heat flux in decreasing with the decreasing flow would approach but still exceed the maximum heat flux in the core and thus the fuel rods are not likely to be damaged.

5.2 MISMATCH BETWEEN FEEDWATER AND STEAM FLOWS

A reduction in feedwater flow to the steam generators of a PWR, or to the

reactor vessel in a BWR that is not compensated by a reduction in flow of steam to the turbine, results in a decrease in the inventory of water in the respective steam generators and reactor vessel. An increase in steam flow uncompensated by an increase in feedwater flow has the same effect. Conversion to steam of inventory in the PWR steam generators and in the BWR reactor vessel provides the cooling for the reactor until water can be supplied from other sources when the normal flow of feedwater has been interrupted for any reason. A reduction in inventory represents a reduction in cooling capacity.

Events that can cause a reduction in feedwater flow include malfunctions of feedwater pumps, valves, and controllers, interruption of power to the pump, and breaks in feedwater lines. Malfunctions of valves and controllers and breaks in lines can cause the steam flow to increase. Signals to the reactor protection system that indicate, directly or indirectly, excessive steam flow or excessive steam flow relative to feedwater flow and low water level in the steam generators or reactor vessel are taken as indicators of reduction of the water inventory toward the minimum acceptable volume. The protective system trips the reactor and the turbine to reduce the steam flow and heat generation rate. The main feedwater pumps may continue to function and supply water to the reactor systems, but an auxiliary feedwater system in a PWR and a high pressure coolant injection system in the BWR are provided to supply water automatically when necessary.

Some potential incidents are not terminated quickly by these actions and additional measures are required to bring them under control. A break in a feedwater line inside the containment or in a steam line inside or outside the containment could result, in the case of a PWR, in the release of all the water and steam in one steam generator. The other steam generators contain enough water to cool the reactor, and other aspects of such an incident were discussed in section 4.1.3.

In a BWR, a break in a feedwater line or a steam line inside the containment gives rise to a loss-of-coolant accident that is discussed in section 6. If the break occurs outside the containment, valves in the feedwater lines and isolation valves in the main steam lines close in a few seconds to stop the flow of water and steam. Some of the radioactivity in the fluids is released in the turbine building and thence to the atmosphere. The potential doses to the public are limited by using valves that close rapidly and limiting the amount of radioactivity in the reactor coolant.

5.3 REDUCTION IN STEAM DEMAND

When a reactor is operating, the fuel rods are cooled, directly in a BWR and indirectly in a PWR, by release of steam to the turbine. Throttling the flow by the turbine control valves to satisfy a reduction in demand for electricity, or closing the turbine control valves, turbine block valves, or steam line isolation valves, for whatever cause, reduces the flow of steam and the cooling available to the core. If the reduction in demand for steam is partial and slow, the reactor control system can simply reduce the fission rate to compensate. At times, however, the steam demand must be reduced more rapidly than the control system can reduce the fission rate without tripping the reactor. Also, the energy stored in the fuel and fission products and reactor systems at high-power tends to sustain the high heat generation rate when the fission rate is reduced. Therefore, a system is provided to maintain sufficient steam flow to cool the fuel and keep the pressure in the steam and reactor systems from rising excessively while new steady-state conditions are being established. This is necessary whether the power is reduced partially or the reactor is tripped.

The steam relief system consists of turbine-bypass valves, power-operated relief valves, and ASME code safety valves on each main steam line. In the event of a rapid reduction in steam demand, the bypass valves are opened by the controllers and release steam to the turbine condenser at the rate required to hold the steam pressure in a BWR and the steam pressure and reactor coolant temperature in a PWR within the operating limits while the reactor power is reduced to match the demand of the turbine. The bypass valves have a capacity of 25 to 50% of full steam flow so that the plant can reduce load, without a reactor trip, at rates well above those normally required to satisfy the demands of the electrical transmission system.

A reactor trip is initiated automatically by a turbine trip from any power level above the design capacity of the bypass system, and a turbine trip is initiated by any reactor trip. After a trip, the turbine bypass system usually relieves the steam necessary to cool the

reactor to the shutdown condition. When the pressure in the turbine condenser is too high or the steam line isolation valves are closed, the bypass system cannot be used, and in some transients the bypass valves do not have enough capacity to hold the pressure within the design limit. Under these conditions, the power-operated relief valves and code safety valves discharge steam to the atmosphere in a PWR and the suppression pool or containment in a BWR to limit the pressure rise. Discharge to the atmosphere is acceptable in the case of the PWR, because the steam is not generated from the reactor coolant and contains much less radioactivity. When steam is discharged through the relief and safety valves, feedwater is drawn from a large supply of stored condensate. In the BWR, water can also be supplied from the suppression pool.

The steam pressure control and relief system acts directly to prevent the pressure from becoming excessive in the reactor coolant system of a BWR. However, it affects the pressure in the reactor coolant system of a PWR only indirectly, through its effects on the coolant temperature. Provisions are required in a PWR to protect the coolant system from being overpressured by expansion of the water as its temperature rises in the more severe transients that can follow a turbine trip. Sprays in the pressurizer condense steam from the vapor space to hold the pressure near the normal level. If the pressure rises above the set points of the power-operated relief valves and code safety valves, they discharge vapor from the pressurizer to reduce the pressure. Reactor trips on high-pressurizer pressure and high-pressurizer level are included in the protective system as backup to the automatic reactor trip on a turbine trip. They also ensure that the reactor coolant system pressure will not be excessive and that there will be ample free volume in the pressurizer at the time of a turbine trip.

5.4 REDUCTION IN PRESSURE IN REACTOR COOLANT SYSTEM

A reduction in pressure in the reactor coolant system reduces the effectiveness of the coolant by lowering the critical heat flux and also portends a reduction in inventory and cooling capacity. In a PWR, pressure reductions are associated with faults in the pressurizer such as breaks in pipes connected to the vapor space or the sticking open of pressurizer relief valves. In such an event, the fuel rods are protected initially by a reactor trip on indication of a lower-than-allowable pressure. If caused by a pipe break or an unclosable relief valve the incident evolves into a loss-of-coolant accident requiring the additional actions described in section 6. In a BWR, pressure reductions are ordinarily associated with breaks in steam lines or with malfunctions of the pressure control system or steam bypass and relief valves, all in the direction of increasing steam flow. This type of incident was discussed in section 5.2.

Section 6

Protection Against Loss of Reactor Coolant

Loss of reactor coolant can be a serious event. It could result from misoperation, malfunction, or failure of equipment, such as a break in a reactor coolant pipe, that allowed uncontrolled discharge of water or steam from the reactor coolant system. It constitutes a failure of a primary barrier to the escape of radioactivity from the plant. The escaping fluid must be confined. More important, loss of all coolant from the reactor core for minutes could lead to melting of fuel rods followed by destruction of the reactor vessel and penetration of the containment. Because of this, many provisions are included in the design to prevent loss-of-coolant incidents and to mitigate the consequences of any that do occur.

Measures taken include the following:

a. High standards are specified for the design, construction and operation of the reactor so that the number of misoperations, malfunctions, and failures of equipment in the reactor coolant system will be minimal.

b. Means are provided for detecting small rates of leakage from the reactor coolant system so that in most instances the plant can be shut down to repair the equipment before the leakage becomes serious.

c. The reactor coolant system, its auxiliaries and associated engineered safeguards are designed so that the fuel rods are not likely to be damaged in the most probable loss-of-coolant incidents and would be cooled acceptably in the most serious postulated accidents.

d. Features incorporated in the reactor coolant system and the containment and its related engineered safety features are designed to ensure confinement of all but a small amount of radioactivity in all types of loss-of-coolant accidents.

As suggested by (c) and (d) above, there are two general areas of concern in the initial phase of a loss-of-coolant accident. The fuel rods must be cooled sufficiently to prevent them from melting and also to prevent the cladding from becoming so embrittled by the reaction of Zircaloy with steam that it might shatter on cooling and permit the fuel pellets to fall into an uncoolable mass. The water, steam, and radioactivity discharged from the reactor coolant system must be confined. After the initial phase, the fuel rods and the containment must be cooled to remove the heat generated by the radioactive decay of the fission products and measures must be taken to ensure continued confinement of the fission products.

6.1 COOLING OF FUEL RODS

6.1.1 SMALL-BREAK ACCIDENTS

Loss-of-coolant accidents are classified according to the size of opening through which the fluid is discharged. In a small-break accident the water and steam would be expelled from the reactor coolant system relatively slowly and the system would remain at a pressure of several hundred psi until almost empty. The fuel rods would be uncovered and the cladding would melt before water could be added at low pressure, so a high pressure coolant injection system is provided to maintain sufficient inventory in the reactor vessel to cool the fuel rods until the system is depressurized and at low temperature.

The high pressure coolant injection system is designed to ensure that the fuel rods will be covered by water, or by water and the froth produced by boiling, when the water in the reactor vessel reaches its lowest level during the incident. Small-break incidents are more severe when the break is in a water line, because a larger rate of coolant loss occurs. A high pressure pumping system of reasonable capacity can maintain the normal water level when the opening is smaller than the equivalent of a hole about 3/4 in. in diameter and can maintain the required coverage of the fuel rods for breaks up to about 6 in. in diameter. The duration of the accident - the time during which the system depressurizes and, in the larger breaks where the water level must be returned to above the top of the core - may vary from about 15 min. for a 4-in. break to several hours for a very small break. Since the fuel rods are well cooled, they are expected to survive a small-break accident undamaged.

In some PWR's the high pressure coolant injection system makes use of the normal charging pumps operated up to full capacity to inject borated water into the reactor coolant system. In others, separate pumping systems are provided. If the break is quite small, ($\leq$ 3/4 in. in diameter) the pumps can maintain the operating level in the pressurizer and the operators can shut the reactor down and cool it by normal procedures. For larger breaks, the reactor trips on indication of low pressure and low level in the pressurizer, and the cooling is conducted in accordance with emergency procedures. In either event, steam is generated in the steam generators and released through the turbine bypass valves or the relief valves to cool the reactor coolant until the temperature and pressure are reduced to the level at which the reactor shutdown cooling system can function. Feedwater is supplied to the steam generators by the main feedwater system initially and then by the auxiliary feedwater system. The refueling water storage tank provides a large reserve of borated water for injection into the reactor coolant system.

Measures taken in the BWR are similar. If the break is small enough that the reactor core isolation cooling system can maintain the water level in the reactor vessel, the plant is shut down and depressurized by normal procedures. For larger breaks or those requiring the main steam line isolation valves to be closed, the high pressure coolant injection system automatically supplies water. Depending on the circumstances, steam is released through the turbine bypass valves or the relief valves at the rate required to cool the fuel rods. Water added to the vessel is drawn from a large supply of condensate or from the containment.

6.1.2 LARGE-BREAK ACCIDENTS

In a large-break accident, all the water and steam in the reactor coolant system would be discharged into the containment in a time from a few seconds to about 2 min. No way of preventing the core from being voided of liquid has been devised; so systems are provided to restore cooling before the fuel rods are damaged excessively. One of these is a low pressure coolant injection system that pumps water into the reactor coolant system at a high rate. It is not practical to provide a pumping system with the capacity to refill the reactor vessel and reflood the core in the time allowed under some postulated accident conditions, so additional measures are taken.

PWR's are equipped with an accumulator system consisting of several tanks partly filled with cool borated water, pressurized with nitrogen, and connected by separate lines to the reactor coolant system. Water from the accumulators passes into the coolant system through check valves when the pressure falls to the range of 600 to 300 psi, depending on the particular design, and the accumulators discharge until empty. The quantity of water is sufficient to refill the reactor vessel to a level at least high enough in the core so that the fuel rods will be cooled adequately by the low pressure coolant injection system as it completes the reflooding. In BWR's a core spray system sprays a large volume of water onto the top of the fuel elements to cool the fuel rods until the core is reflooded by the low pressure coolant injection system.

Large breaks range in size between the equivalent of about a 6 in. diameter opening and the two openings produced by severance of the largest pipe (about 30 in. diam) in the reactor coolant system. The instantaneous severance of a large pipe in the reactor coolant system - generally referred to as the design basis loss-of-coolant accident - is the most serious accident for which protection is provided in a nuclear power plant. Rupture of the reactor vessel would be more serious but extra measures are taken in design, manufacture, and testing to produce vessels of highest quality and in operation to ensure that the vessels will be operated well within the design specifications. These measures make the probability of rupture of a reactor vessel so small that protection against such an event is deemed unnecessary.

The severance of a large pipe is also a highly improbable event but by design of the safety features to protect against such a drastic event, the pipes are provided with considerable margin over the capacity required to cope with the more probable smaller breaks. To be certain of this, the performance of the safety features is analyzed for a wide range of possible break sizes and locations in water and steam lines.

The most severe accident is that resulting from a large break in the pipe between the discharge of a reactor coolant recirculation pump and the inlet to the reactor vessel. The sequence of events in such an accident in a PWR is described below with reference to Fig. IX 2-2. Figure IX 2-2 shows the configuration of a PWR reactor coolant system and

containment and the location of the break.

In a fraction of a second following severance of the pipe, the rush of water through the break and into the containment causes the pressure and level in the pressurizer to fall to the set points. This initiates a reactor trip and actuates the coolant injection systems. Actually, the pressure decreases so rapidly that boiling begins in the reactor core in less than a second. The negative reactivity effect of liquid being displaced by vapor in the core stops the fission reaction, and insertion of the control rods augments this effect.

During depressurization, or blowdown, of the reactor coolant system, water and steam flow from the reactor vessel to the break through inlet and outlet lines. The direction and rate of flow through the core vary with time, and the cladding temperature is calculated to rise and fall as the flow rate and quality of the coolant change in the core. The critical heat flux falls below the maximum heat flux generated early in the transient, so the temperature of the fuel rod cladding rises well above normal operating temperature. Since the fission reaction has been stopped, the major concern is that the cooling be sufficient to remove the heat stored in the fuel pellets and the fission product decay heat without the cladding exceeding a safe temperature.

Analyses indicate that in less than about 20 sec after the break all but a small amount of water is discharged from the reactor coolant system into the containment so that the pressure in the containment and that inside the coolant system are about equal. The accumulators begin to discharge into the coolant system at about 10 sec, but it is assumed that the accumulator water also leaves through the break until the end of the blowdown.

Following the blowdown phase there is a refill period of about 15 sec during which the liquid from the accumulators fills the reactor vessel to the level of the bottom of the fuel rods. Assuming loss of off-site power and delays in bringing the emergency supply into operation, the low pressure coolant injection pumps begin to deliver borated water from the refueling water storage tank to the reactor coolant system somewhat later in the refill period. The fuel rods are essentially uncooled during this period and the temperature rises about adiabatically.

Reflooding of the core begins when the water reaches the bottom of the fuel elements. As it rises into the core, it is heated by the lower ends of the fuel rods and begins to boil. When the water level is about 1 ft above the bottom of the core, the boiling becomes vigorous enough to entrain droplets of water in the steam. As the water level rises, the mixture of droplets and steam provides increasingly effective cooling of the fuel rod surfaces above the water level. The accumulators are empty at about somewhat less than one minute, and at about the same time the cooling at the hot spot becomes sufficient to terminate the temperature rise. The pumps continue to inject water, the peak cladding temperature falls gradually, and the water level rises to the top of the core completing flooding within a few minutes after the break. The reactor system continues to fill until water flows out the break in the pipe. Provisions for long-term cooling are brought into operation after most of the water in the refueling water storage tank has been pumped into the reactor coolant system and the containment.

The scenario for a design basis accident in a BWR is similar. Because of differences in design, the coolant flow is upward through the core throughout blowdown and depressurization takes about one minute. The water level drops below the bottom of the core in less than about 30 sec. The core sprays and the low pressure coolant injection systems begin to add water from the suppression pool at about 30 sec. The core is reflooded and the temperature rise terminated within a few minutes after the break.

Because the probability of a large-break loss-of-coolant accident is low, some damage to the fuel rods is acceptable. The cooling is designed to prevent the cladding from melting or being seriously embrittled during the transient. The fuel rods and the piping and equipment are designed so that movement produced by the blowdown forces cannot impede operation of the safety systems; thus the fuel rods should remain in a coolable configuration throughout the accident. Analyses indicate that only a small fraction of the fuel rods would reach a temperature at which the cladding would swell, rupture, and release the fission products from the gas space.

6.1.3 BREAKS OF INTERMEDIATE SIZE

Protection must also be provided against breaks of intermediate size. In the PWR the pressure at which the accumulators

begin to discharge is selected so that the high pressure coolant injection system and the accumulators combine to keep water in the core. In the BWR an automatic depressurization system operates the relief valves on the steam lines to reduce the pressure in the reactor coolant system rapidly if the high pressure coolant injection system is unable to maintain the water level above the core in the reactor vessel. This provides a backup to the high pressure injection system for breaks of small and intermediate size. With the reactor depressurized, the core spray and low pressure coolant injection systems cool the core.

6.2 CONTAINMENT OF RADIOACTIVITY DURING ACCIDENT

A large-break loss-of-coolant accident presents the greatest challenge to the reactor containment. Practically all the water and steam in the reactor coolant system is expelled into the containment in less than a minute, and the stored energy in the fluids and heat released by the fuel flash part of the water into a large volume of steam. The containment must be sealed tightly to prevent the escape of radioactivity. It must be capable of withstanding a moderate pressure and must have a large volume or the capacity to condense much of the steam as it is released.

Two general types of containment have evolved; one characteristic of PWRs, the other of BWRs and they are shown in Figs. IX 6-1 and IX 6-2. The typical PWR containment is a cylindrical building with a domed roof, all constructed of heavily reinforced concrete. Concrete is difficult to keep gas tight so the containment has a welded steel liner attached to the inside face of the concrete. Entrance to the containment when fuel is in the reactor is through an airlock. Electrical wiring and piping pass through special sleeves embedded in the concrete and welded to the liner.

The thick concrete structure provides strength to withstand the pressure produced by the flashing of reactor coolant into steam and it shields persons outside from radiation emitted by fission products that are dispersed in the containment atmosphere. In a typical containment the internal pressure in a large break accident would rise to about 40 psig. The containment is designed to withstand about 45 psig and is tested above 50 psig.

The BWR containment consists of a smaller structure, called a drywell, around the reactor coolant system that is coupled by vent pipes to a pressure suppression chamber. The fluids are expelled from the reactor coolant system into the dry well in a loss-of-coolant accident and the rise in presssure in the dry well causes the steam to flow through the vent pipes into the pressure suppression chamber. The pressure suppression chamber contains about one million gallons of water; the vent pipes terminate several feet below the water level; the steam disperses in bubbles and condenses as it rises through the water. The large volume of water also serves as one of the sinks for heat after the blowdown in a loss-of-coolant accident. Steam is discharged directly into the containment by the safety valves and into the suppression pool by the relief valves in incidents such as overpower and reduction-in-cooling discussed previously.

Typically, the dry well and the pressure suppression chamber, the latter a torus, have been constructed as steel tanks inside a reinforced concrete structure. The pressure in the dry well and that above the water level in the pressure suppression chamber are estimated to rise to less than 45 and 30 psig, respectively, in a design basis loss-of-coolant accident. The containment is designed for a pressure above 50 psig and is tested above 60 psig.

The BWR containment is inside a reactor building that provides an additional barrier to the escape of radioactivity in an accident. A standby gas treatment system is put into operation on indication of radioactivity in the building. Air from the building is passed through filters to remove radioactive particles and iodine before it is discharged up a stack to the atmosphere.

Many steam lines, water lines, and other pipes penetrate the containment and provide a multitude of potential paths for radioactive gases and liquids to pass outside. The lines are equipped with isolation valves. Valves in lines that have no safety function in an accident close automatically on signals that call certain of the safety systems into operation.

Making a large containment with its many penetrations completely gas tight is very difficult, if not impossible. Proving that one is gas tight might be equally difficult, so a reasonably attainable and demonstrable limit is placed on the leakage. Generally, the leakage at full design pressure must be less than 0.1 to 0.5% per day of the containment volume, depending on the

effectiveness of other provisions for confining the radioactivity. Conformance with this requirement must be demonstrated prior to operation and periodically during the life of the plant.

6.3 POST-ACCIDENT HEAT REMOVAL AND CONFINEMENT OF FISSION PRODUCTS

The loss-of-coolant accident is stabilized and under control when the fuel rods are reflooded and cooled below about 300°F and the reactor coolant system and the containment are at about the same low pressure. Cooling of the fuel rods must be continued after the accident to remove the fission product decay heat at the rates indicated in Fig. IX 3-1. Although the containments are designed to withstand the accident pressure for long times, good sense dictates that the potential hazard should be reduced by lowering the pressure and thus reducing the mobility and leakage of the radioactive iodine, one of the principal health hazards.

6.3.1 COOLING OF FUEL RODS

During the accident and early in the post-accident period, the fuel rods are cooled by water injected by the accumulator, core spray, and low pressure coolant injection systems. In the PWR the principal source of water is the refueling water storage tank, which contains about 300,000 gallons of cool borated water. In the BWR the water is drawn largely from the pressure suppression pool.

After the injection phase, systems for long-term cooling are put into operation. Basically, these systems recirculate water from the containment - the sumps in the PWR and the pressure suppression pool in the BWR - through heat exchangers and back to the containment. Part of the cooled water is pumped into the reactor coolant system and returns to the containment through the break. A reliable supply of cooling water from the heat exchangers is provided by the plant service water and high pressure service water systems. The residual heat removal system, which cools the fuel during normal shutdown operation, and other pumping systems are combined to provide a reliable post-accident heat removal system. The way in which this is accomplished differs considerably between plants.

6.3.2 COOLING OF CONTAINMENT AND RETENTION OF FISSION PRODUCTS

Spray systems are provided in the PWR containments to condense the steam, absorb radioactive iodine, and wash radioactive particles from the containment atmosphere. When the containment pressure reaches the range of 10 to 25 psig, these systems go into operation automatically and rain droplets down through the containment atmosphere from nozzles in the dome. Initially, the water is supplied from the refueling water storage tank. As it leaves the tank, sodium hydroxide or alkaline sodium thiosulphate is added to react with iodine and hold it in solution. Later, part of the water recycled by the post-accident heat removal system returns to the containment through the spray systems.

In some designs the spray system alone is depended on to cool the containment, condense the steam, and lower the pressure. In others the air circulation and cooling system that conditions the air in the containment during normal operation is designed to provide part of the capacity. This system may also contain charcoal filters for absorbing iodine. The containment spray and air circulation systems do not have enough capacity, nor can they go into operation rapidly enough if only emergency power is available, to affect the initial pressure rise in a large pipe break accident. They function to return the pressure to near the normal operating pressure and terminate or greatly reduce any leakage of radioactive gases in an hour or less.

Sprays are installed in BWR containments to cool the gases in the drywell and in the space over the pool in the pressure suppression chamber. Because transfer of heat to the large surface of water in the pressure suppression chamber and in the drywell after an accident is expected to provide adequate cooling, use of the sprays is optional. Water is supplied to the sprays from the pressure suppression pool. It contains no additives to immobilize iodine, since the large volume of water is somewhat effective in holding the iodine. Gases that leak from the containment pass into the reactor building and can be processed (filtered) to remove iodine before being released from the plant.

6.3.3 CONTROL OF HYDROGEN CONCENTRATION IN CONTAINMENT

During the temperature transient in a

loss-of-coolant accident, steam is expected to react with some of the Zircaloy cladding of the fuel rods to produce zirconium dioxide and hydrogen. In the PWR, the alkaline spray solution will react with aluminum in the containment to produce aluminum oxides, hydroxides, and hydrogen. Radiation emitted by the fission products will decompose water in the core and containment regions producing hydrogen and oxygen. If the hydrogen were permitted to accumulate in air in the containment, it could ignite after the concentration reached above 4 vol %. Recombiners are provided in PWR containments to prevent the hydrogen concentration from rising to the flammable limit. The BWR containment has a nitrogen atmosphere when the reactor is operating so a flammable mixture cannot be produced immediately following an accident.

6.4 SPECIAL CONTAINMENT SITUATIONS

The containment and its engineered safety features are designed to hold the water, steam, and radioactivity that would be released in a break, large or small, inside the containment in any water line, reactor coolant line, steam line, or piece of equipment except a major break of the reactor vessel. The number of safety features that must operate in an accident depends on the size of the break, the magnitude of the rise in containment pressure, and the need for emergency cooling. The role of the steam line block valves in limiting the escape of radioactivity in the event of water-line and steam-line breaks outside the containment has been mentioned previously. Incidents associated with rupture of a tube in a PWR steam generator, damage to a fuel element in handling during refueling or storage, and rupture of storage tanks containing waste liquids or gases must also be considered in the design.

Leakage of reactor coolant through cracks developing in steam generator tubes during operation has occurred frequently in PWR plants. In most instances the rate of leakage was small and the plant could continue to operate safely; the leaking tubes were plugged during a scheduled maintenance period. The probability of complete tube rupture is very small, but rupture of one tube in one steam generator is considered in the design of the plant. This is a small-break accident and the reactor coolant is discharged into the steam system, also a high pressure system. Many signals indicate the beginning of the accident, trip the reactor and the turbine, and bring the safety systems into operation. Among these is indication of a high radiation level in the noncondensable gases drawn from the turbine condenser by its vacuum system and in the normal liquid blowdown from the steam generators. The gaseous discharge can be diverted to the containment in some PWR designs and the liquid blowdown is interrupted by block valves. This limits the amount of radioactive gases released.

The next step is to cool the reactor coolant system and bring its pressure down to the level of the pressure of the steam system in order to stop the transfer of liquid. Normally, this is done by releasing steam through the turbine bypass valves to the condenser, and the radioactivity is confined. If the bypass valves cannot be used, the steam must be discharged to the atmosphere. After this initial reduction in pressure, which takes about 1/2 hour, the affected steam generator can be isolated and cooling of the reactor and steam systems can be completed by use of the other steam generators and cooling systems. Potential radiation doses to the public are kept small in this incident, as in other steam release incidents, by limiting the amount of radioactive iodine in the reactor coolant.

If an assembly of fuel rods were dropped during refueling, the cladding of some of the fuel rods might be damaged enough to release fission products from the gas space. The refueling of a PWR is done inside the containment and the fuel is stored in a pool in an adjacent building. The containment would confine any radioactivity released there and the ventilation system of the fuel storage building is provided with filters and absorbers to reduce the release of iodine to the atmosphere. The BWR is open to the reactor building during refueling and the fuel is stored in the reactor building. Protection is provided by the standby gas treatment system in the reactor building.

Radioactive liquids are processed and stored in tanks in the reactor building or in well-ventilated auxiliary buildings. The buildings are designed so that liquid leakage from the processing equipment and storage tanks drains to sumps from which it can be pumped to other tanks; alternatively the tanks are in pits designed to hold any leakage. Any gaseous leakage is discharged from the plant through the ventilation system. Potential doses to the public are kept small by limiting the amount of radioactivity in the gas in any tank.

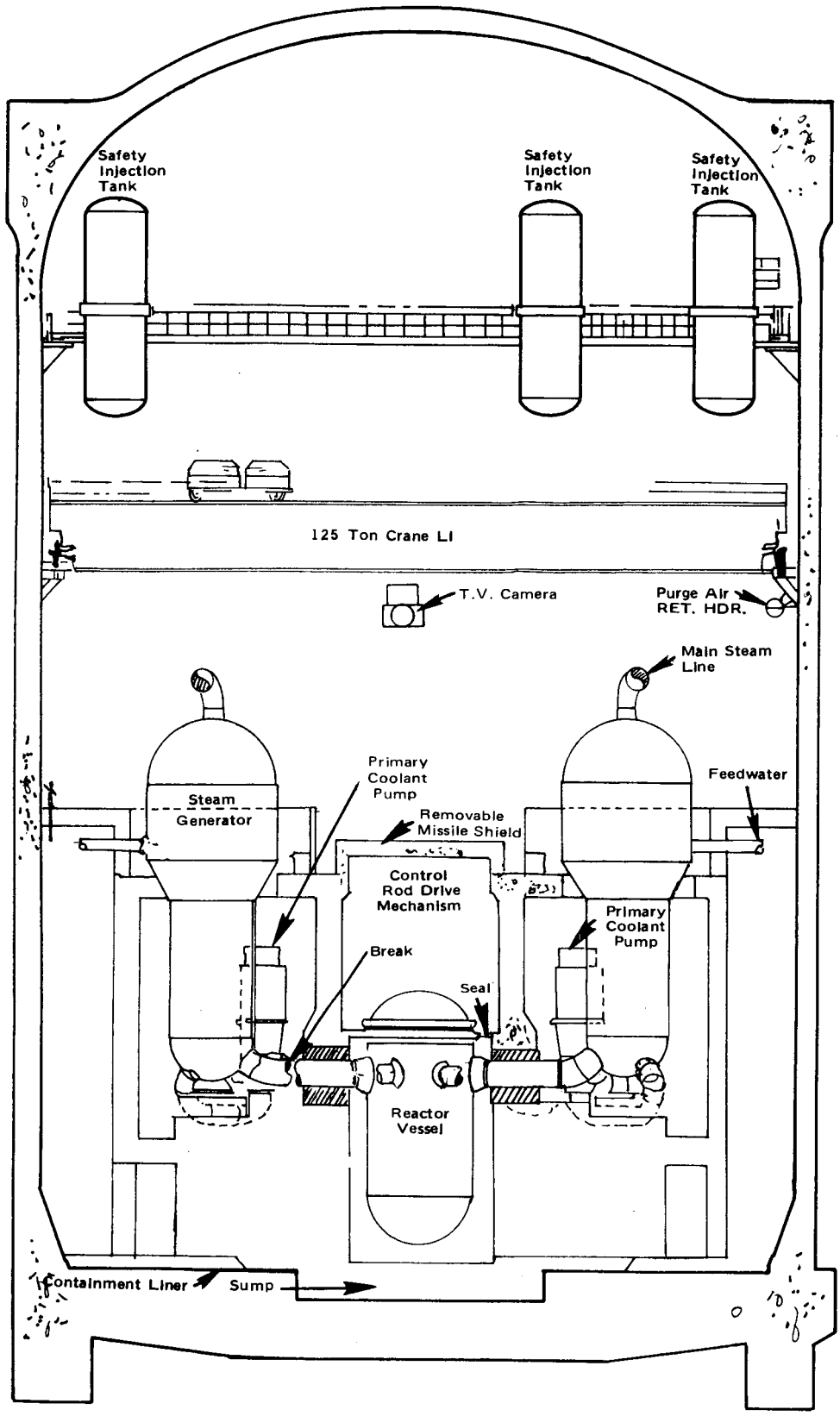


FIGURE IX 6-1 Typical PWR Containment

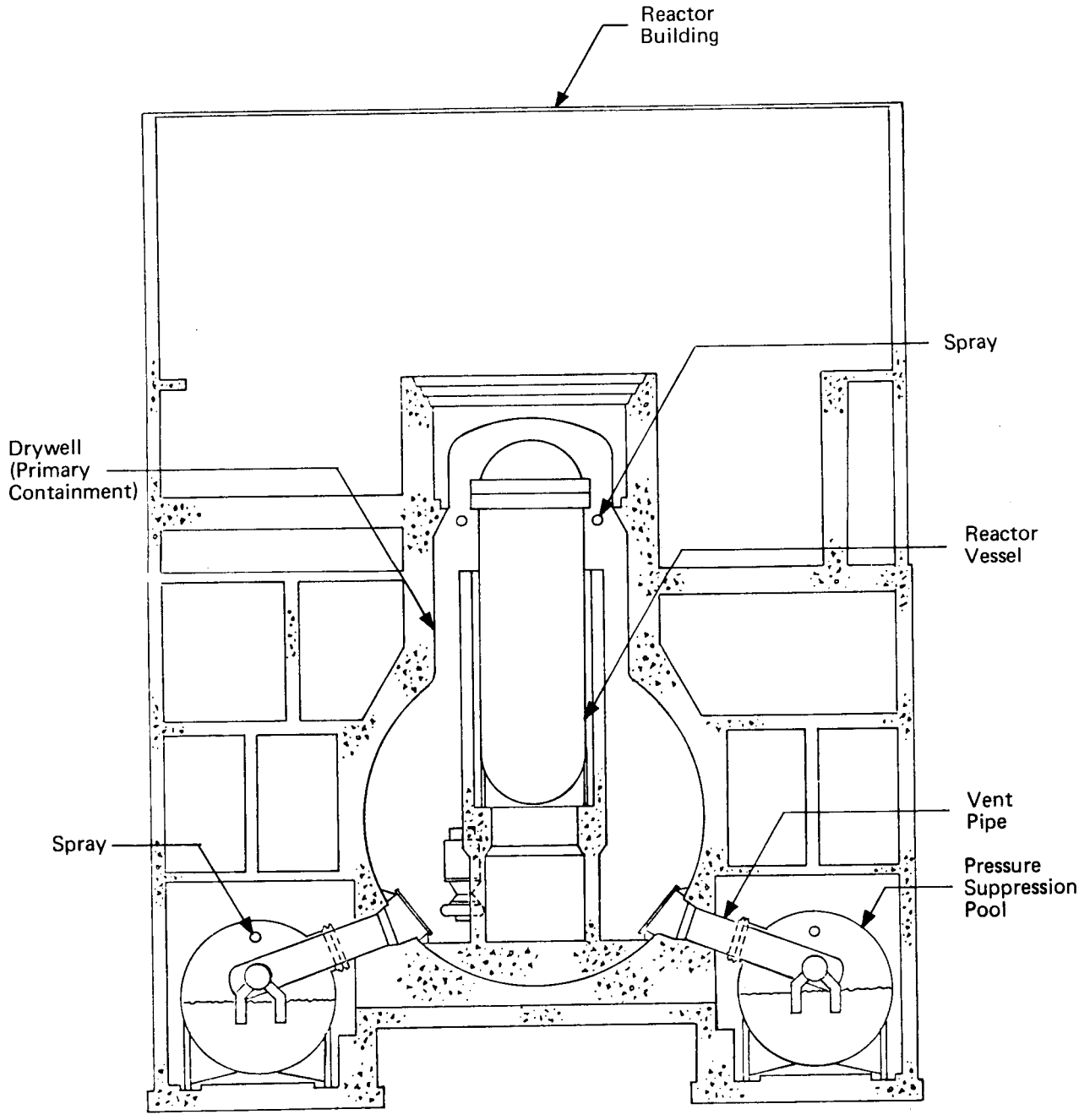


FIGURE IX 6-2 Typical BWR Containment

Section 7
Measures to Ensure Performance of Safety Functions

Having provided special features in the design of the plant for cooling the fuel rods and containing the radioactivity, there must be assurance that the equipment and systems will function when called upon. High quality of design, construction, and operation and redundancy and testability of equipment and systems are important factors in providing this assurance.

7.1 QUALITY ASSURANCE

The dependence on high quality has been mentioned several times in previous sections. Use of appropriate standards and criteria helps to ensure that the plants are designed carefully and conservatively. The minimum requirements for the principal design criteria are specified by the AEC in Appendix A of 10 CFR Part 50[1] of its regulations.

Criteria for quality assurance programs for the design, construction, and operation of each nuclear facility are specified in Appendix B of 10 CFR Part 50. AEC Regulatory Guides describe acceptable methods for implementing specific parts of the regulations.

The technical societies, industry, and the AEC and its laboratories have been working for several years to develop appropriate codes and standards for nuclear power plants. Results of their efforts are embodied in the ASME[2] Boiler and Pressure Vessel Code Section III, "Nuclear Power Plant Components," ANSI[3] B31.7 "Nuclear Piping," IEEE[4] Standard 279 "Criteria for Protection Systems for Nuclear Power Generating Stations," and in many other codes and standards that govern the design, construction, and operation of nuclear facilities. As part of the design, specifications are prepared to ensure that appropriate materials and procedures will be used in constructing the plant. The design criteria, particularly of equipment and systems important to safety, are reviewed and judged to be adequate by the AEC regulatory staff and the Advisory Committee on Reactor Safeguards before a construction permit or an operating license is authorized for a plant.

7.2 PROTECTION AGAINST EFFECTS OF SEVERE NATURAL PHENOMENA

Careful consideration of the effects of severe natural phenomena on the safety of the plant is important in providing a conservative design. Studies are made of local and regional geology, hydrology, meterology, and seismology and of historical records. On the basis of these studies the plant structures and equipment of importance to safety are designed to withstand the effects of earthquakes, tornados, hurricanes, floods, tsunamis, and seiches without loss of capability to perform their safety functions.

Generally this means that the structures must be capable of withstanding tornadic winds having a tangential velocity of 300 mph and a translational velocity of 60 mph. Protection must be provided against missiles, such as heavy planks traveling at high velocity and automobiles traveling at low velocity, that might be propelled by such winds. Depending on the site, the structures and equipment must also be capable of withstanding the effects of the winds of hurricane force.

The plant must be built on ground sufficiently high so that equipment and structures would not be reached by the waters of a flood of the greatest magnitude that can reasonably be projected for the site or barriers against flooding must be incorporated in the design. Wave action generated by hurricane or storm winds at the time of a maximum flood and the effects of seiches and tsunamis, where appropriate, are important factors in establishing the maximum water level and the protection that must be provided.

---

[1] Title 10 - Atomic Energy - of the Code of Federal Regulations, Part 50 Licensing of Production and Utilization Facilities.

[2] American Society of Mechanical Engineers.

[3] American National Standards Institute.

[4] Institute of Electrical & Electronics Engineers.

Because earthquakes occur quickly and without warning and can develop forces large enough to destroy piping systems and structures, much attention is given to designing nuclear power plants to withstand the shaking caused by earthquakes. Earthquakes of two magnitudes are considered: the Safe Shutdown Earthquake and the Operating Basis Earthquake. The Safe Shutdown Earthquake is the most severe earthquake that could reasonably be conceived to occur at the plant site considering the regional and local geology and seismology and the characteristics of the local subsurface material. Some damage would occur, but certain parts of the plant must be designed to remain functional when subjected to the vibratory ground motion produced by such a severe earthquake. They are the structures, systems, and components necessary to ensure

a. The integrity of the reactor coolant piping and vessels,

b. The capability to shut down the reactor and maintain it in a safe shutdown condition, and

c. The capability to prevent or mitigate the consequences of accidents that might result in appreciable radiation exposures to the public.

The Operating Basis Earthquake is one that could reasonably be expected to affect the site during the operating life of the plant. The vibratory motion from such an earthquake might cause the plant to shut down, but the reactor plant must be designed to remain in a condition such that operation can be continued safely.

7.3 RELIABLE POWER SUPPLY

The safety of a nuclear power plant depends on the availability of direct current electricity for operating the instrumentation and control systems and alternating current for operating pumps in some of the safety systems. Two separate battery and distribution systems are installed to provide a reliable source of direct current. Operation of either provides sufficient capacity for essential loads.

Several sources are provided to ensure a supply of alternating current, and details of accomplishing this may differ between plants. Each plant is connected to a regional power grid through at least two separate lines. On shutdown of the plant turbine generator, power would normally be supplied from the grid to continue the operation of essential equipment. However, loss of off-site power can occur, so emergency supplies are provided on-site. Usually the on-site source is two or more diesel generator sets, but at some plants gas-turbine-driven generators or nearby hydrogenerators provide diverse sources of emergency power. At least two systems are installed for distributing the alternating current electricity within the plant. Functioning of one distribution system and part of the emergency generators provides sufficient power for operation of essential equipment. The on-site power sources and distribution systems are designed to safety standards that make them capable of delivering power during floods, storms, earthquakes and accidents.

7.4 REDUNDANCY IN SAFETY SYSTEMS

A basic assumption in the plant design is that some of the equipment in the safety systems will not function or will operate at reduced capacity in an emergency; so extra, or redundant, systems are incorporated. Measures taken in the design of the electrical power supplies is one example. The designs of engineered safety features for the containments and the emergency core cooling systems show other examples.

In some PWR containments sprays alone are depended on to cool the containment and remove fission products from the atmosphere after an accident. Two spray systems are installed, each with more than enough capacity to handle the total load. Each spray system has one or more spray headers in the containment dome and its own pumps, valves, and piping to supply borated water to the sprays. The two spray systems may be interconnected to increase the number of flow paths and pumps available to each system. Two valves in parallel may be installed at critical locations in the piping so that failure of one valve to open will not block the flow. In other PWR containments only one spray system is used, and the air circulation system that cools the containment in normal operation is equipped with charcoal filters to absorb fission products and designed to function in a loss-of-coolant accident environment. This combination has the redundance of two spray systems and greater diversity, thus reducing the probability of a common mode failure causing the simultaneous loss of both cooling systems.

Redundancy of cooling for the fuel rods in the reactor core in an emergency is provided in several ways. In a typical

BWR, the High Pressure Coolant Injection System goes into operation on indication of low level in the reactor vessel or high drywell pressure. Only one pump and piping system is provided, but the pump is driven by a turbine that operates on steam produced by the residual heat in the reactor and requires only direct current power to function. Redundancy is supplied by the Automatic Depressurization System, which lowers the pressure in the reactor by discharging steam to the suppression pool if the High Pressure Coolant Injection System cannot maintain the level. Five relief valves are used and four valves give ample capacity. After the pressure is reduced, the Core Spray System and the Low Pressure Coolant Injection System can each provide more than the required capacity of water delivery and they go into operation simultaneously. The Core Spray System consists of two separate pumping systems, each of which has the required pumping capacity. Each system has 2-50% capacity pumps, and its own piping, valves, instrumentation, and spray header in the reactor vessel. The Low Pressure Coolant Injection System has two separate pumping systems, each discharging into a recirculation loop of the reactor coolant system. Each system has two pumps, and operation of three of the four pumps will provide the required capacity.

The PWR's do not have an Automatic Depressurization System so a typical reactor will contain two separate high pressure injection systems with sufficient pumps so that partial operation of the systems' pumps delivers the flow required for small break loss-of-coolant accidents. The accumulators require only the decrease in reactor coolant system pressure that accompanies a larger break to bring them into operation. Since the location of the break could prevent the contents of one accumulator from reaching the reactor vessel, they are designed so that one of two, two of three, or three of four installed units will have the required capacity. Redundant low pressure pumps, each having the full design capacity, are provided for injecting and recirculating cooling water after the pressure has fallen. They may also function to provide coolant delivery to the containment spray system.

Any of several relevant parameters being out of limits may automatically initiate operation of safety system, e.g., low liquid level in the reactor vessel or high pressure in the drywell in the BWR starts the High Pressure Coolant Injection System. The reactor operator can start any of the systems manually. At least, three sensing circuits are provided to monitor each important parameter. Out-of-limits indication by two of three sensors initiates safety action. This permits a circuit to be tested without interrupting the reactor operation, but the protection system is designed so that a faulted circuit or one under test gives one of the two signals required to start a safety system.

7.5 TESTABILITY OF SAFETY SYSTEMS

As a final measure, the safety systems and their instrumentation and controls must be testable. Some tests, such as a high pressure test of the containment, need be conducted only a few times during the life of the plant. Overall tests of most of the engineered safety features are conducted during the refueling interval which occurs annually in most plants, but some systems are tested semiannually. The operability of many of the components of the safety systems, such as pumps and valves, is tested at least monthly and some of the instrumentation is checked daily. The tests are designed to show, as near as practical, that the safety features would be brought into action and would function properly if a situation required their use.

Section 8
Conclusion

Nuclear Power plants are equipped with many special safety features to prevent excessive amounts of radioactive material from being released in normal operation and in abnormal situations. If these features perform as the designers expect, few, if any, of the fuel rods would be damaged and little radioactivity would be released during reactor transients or accidents. The risk to the public would be very small.

However, in assessing the potential hazard it must be assumed that only onsite emergency power will be available, that it will be delayed in starting, and that the safety features will function at reduced capacity in an accident. Although the designers must show that the fuel rods will not melt under these circumstances, the performance of the containment features in the design basis loss-of-coolant accident is evaluated on the basis of a release of fission products from the fuel that could be produced only by melting. In order for the measures taken in the design of the plant to be considered satisfactory, the designers must show that the probable radiation doses to the most heavily exposed members of the public would be well within AEC guidelines.

For incidents that might occur occasionally in the lifetime of a plant, the potential doses must be far below levels that are considered to be harmful. For serious accidents, which have a considerably lower probability of occurrence, the guideline doses are 25 rem to the whole body and 300 rem to the adult thyroid apply. Calculations of these doses are based on conservative estimates of fission product release from the fuel and removal of airborne fission products by natural phenomena and engineered safety features so that in reality the average doses received by a member of the general public would be far below the potential dose to the most exposed individuals located nearer the plant site boundary.

WASH–1400
(NUREG 75/014)

DESIGN ADEQUACY

APPENDIX X

to

REACTOR SAFETY STUDY

U.S. NUCLEAR REGULATORY COMMISSION

OCTOBER 1975

Appendix X

Table of Contents

Section		Page No.
1.	INTRODUCTION	X-1
2.	RESULTS	X-3
3.	SUMMARY	X-11
APPENDIX A	DESIGN ADEQUACY EVALUATION OF SELECTED SAFETY RELATED EQUIPMENT AND STRUCTURES IN NUCLEAR POWER GENERATING PLANTS	X-13

List of Tables

Table		Page No.
X 2-1	PWR Component Review - Seismic Design Adequacy Summary	X-5
X 2-2	PWR Component Review - Environmental Qualification Summary	X-6
X 2-3	BWR Component Review - Seismic Design Adequacy Summary	X-7
X 2-4	BWR Component Review - Environment Qualification Summary	X-8
X 2-5	Summary of Bases for Reduced Safety Margin Determination	X-9
X 2-6	Summary of Items for Which Design Adequacy Could Not be Assessed	X-10

Section 1

Introduction

The quantitative assessments of failure probabilities performed in this study are based on component failure rate data obtained from various sources, as discussed in Appendix III. However, this data base generally does not include information pertinent to some of the specific conditions under which certain nuclear components important to safety are required to operate. These conditions include loadings due to external phenomena such as earthquakes and tornadoes, and the adverse environmental conditions that certain equipment located inside the reactor containment buildings may be subjected to following potential loss of coolant or transient-caused accidents (e.g., coincident high temperature, high pressure, high humidity and high radiation levels). Since these phenomena are not included in the generic data base and could potentially lead to common mode failures that could affect the probability of occurrence of various accidents, assessments were made of the ability of specific components and structures to perform as designed when subjected to these phenomena. This design adequacy assessment was done to determine whether: (1) these phenomena represent a common mode failure potential; and (2) if dependencies do exist, they are factored into the probability predictions.

In addition to the above, the generic data base did not include component designs built under the quality assurance requirements presently applicable to nuclear power plants. As indicated in Appendix III the limited information currently available on nuclear component failure rates seems to indicate little difference between nuclear and non-nuclear component failure rates. Thus, this study has found little basis for using failure rates for nuclear components that are lower than those for non-nuclear components. The exception to this rule is that of the probability of gross reactor vessel failure. As discussed in Appendix V, the data on the likelihood of failure of conventional pressure vessels has been reduced by a factor of 10 for nuclear pressure vessels due to the high standards and attention given in the design, fabrication, inspection and testing of nuclear vessels.

The design adequacy assessment was performed for the Reactor Safety Study by the Franklin Institute Research Laboratories (FIRL). The general approach used was to take a sample of the components, systems and structures that are engineered safety features or are closely associated with them and to check the adequacy of the implementation of safety design and specialized environmental testing requirements. Some of these samples were checked for seismic design adequacy and others to see if they have been properly designed and qualified for operation in the unusual post-accident environments. In addition, the structures housing the diesel generators were examined with regard to tornado design.

Section 2

Results

Tables X 2-1, X 2-2, X 2-3 and X 2-4 summarize the results of the evaluations. The detailed report of the FIRL investigation is attached as Appendix A.

As shown in Table X 2-1, 30 PWR items were examined with regard to seismic design. Of these, 25 were found to be adequate (83%). Design adequacy was not demonstrated for five items (17%) (reactor coolant pump nozzles, low head safety injection system instrumentation, recirculation spray pump outside containment, the diesel generator day tank, and the AC and DC switchgear), because sufficient information was not available to permit an assessment of adequacy to be made. For three items (the containment crane, the low head safety injection pumps, and the reactor protection system), it was found that the design was adequate in that failure is not expected under seismic excitation. However, the margin to failure was found to be less than that normally expected considering applicable code and qualification requirements because either: (1) errors were found in assumptions used in calculating stresses; or (2) seismic qualification tests were not sufficiently comprehensive or were not performed.

The adequacy of the tornado and tornado missile design was evaluated for the structure housing the diesel generators, the doors to the structure, and fuel tank soil cover. It was found that the structural design and the soil cover were adequate. However, in the event of impact of a tornado missile on the door of the structure, it was found that while the door should survive the impact, the outward rebound of the door may fail the door pins and cause the door to open. This potentially could expose a diesel-generator to adverse environmental conditions (e.g., rain, small missiles, hail, etc.). The probability of diesel failure under these conditions has not been assessed, but it should be considerably less than unity. Furthermore, the loss of a single diesel does not create an immediate safety problem since: (1) the remaining diesel is available should off-site power be interrupted by a tornado; and (2) the steam-driven portions of the auxiliary feedwater system would also be available to remove decay heat even if all AC power is lost.

Table X 2-2 indicates that nine PWR items were examined with regard to environmental qualification. All were found to be adequate although five items (reactor coolant piping snubbers, low head safety injection system snubbers, the low head safety injection ssystem pumps, the containment recirculating spray pump located outside containment, and the reactor protection system) were tested under conditions which were not as comprehensive as tests performed to present standards.

BWR components were also evaluated. Thirty-two BWR items were evaluated with regard to seismic design as shown in Table X 2-3. Of these, 28 (88%) were found to be acceptable. For two of these items (6% of the total evaluated) (the recirculation lines and the reactor protection system), it was found that although the design was adequate, the safety margin is less than normally expected. Adequacy could not be assessed for four items (13%) (the missile barriers inside containment, reactor pressure relief valves, core spray system instrumentation, and the 480-Volt load centers) because sufficient information was not available to permit an assessment to be made.

The BWR diesel-generator housing was also analyzed with regard to tornado and tornado missile design. The design of the structure was found to be adequate. Insufficient information was available to permit an assessment of the adequacy of the door to withstand the rebound following missile impact or the impact of a missile on the corrugated metal barrier attachments. With regard to environmental qualification, as shown in Table X 2-4, eight items were examined. Six (75%) were found to be acceptable. Of these, the reactor coolant system snubbers were found to be acceptable with reduced safety margin because testing had not been performed. Insufficient information was available on the remaining two items (25%) (reactor pressure relief valves, and the electrical cables, terminations and connectors) to permit an assessment of their adequacy.

For both plants, 62 items were examined with regard to seismic design. Thirty-six (58%) were found to be acceptable by

satisfying code and qualification requirements, 12 (19%) were found acceptable based on engineering judgment, and five (8%) were found to be acceptable with reduced margin. Thus, 53 items (85% of those analyzed for seismic design) were found to be acceptable. Design adequacy was not demonstrated for 9 items (15% of the total examined) due to lack of sufficient information.

With regard to tornado design, the diesel generator housings were studied on both plants. Both structures were found to be adequate. The PWR building exterior door was found to be likely to fail when rebounding after impact of a tornado missile. Insufficient information was available to assess the adequacy of the BWR door in this regard, or of the corrugated metal barrier attachments for the BWR diesel generator building.

Seventeen items were evaluated concerning environmental qualification on both plants. Six (35%) were found to meet qualification requirements, three (18%) were found acceptable on the basis of engineering judgement, and four (23%) were found to be adequate with reduced margin mainly because the tests were not sufficiently comprehensive. Thus, 13 (76% of the total evaluated) were deemed to be acceptable. Design adequacy was not demonstrated for four items (24% of the total) because of lack of sufficient information to permit an assessment to be made.

Tables X 2-5 and X 2-6 indicate the bases for determining adequacy with reduced margin and insufficient information to assess adequacy, respectively.

TABLE X 2-1 PWR COMPONENT REVIEW - SEISMIC[a] DESIGN ADEQUACY SUMMARY

Subsection in Text	Component Description	Review Data Basis: Visual Observation	Review Data Basis: Design Calculations	Review Data Basis: Test Report	Assessment of Design Adequacy: Adequate (Failure Not Expected): Design Criteria Satisfied[b]: Analysis and/or Test	Assessment of Design Adequacy: Adequate (Failure Not Expected): Design Criteria Satisfied[b]: Engineering Judgment	Assessment of Design Adequacy: Adequate (Failure Not Expected): Design Criteria Not Completely Satisfied[c]	Assessment of Design Adequacy: Not Demonstrated (Failure Possible): Insufficient Information to Assess Adequacy	Assessment of Design Adequacy: Not Demonstrated (Failure Possible): Information Reviewed Indicates that Failure is Likely	Notes
A6.3.1	Reactor Building									
A6.3.1.1	Soil-Structure Interaction Model		✓		✓					
A6.3.1.2	Containment Internal Structure		✓		✓					(d)
A6.3.1.4	Crane		✓				✓			
A6.3.2	Reactor Coolant System (RCS)									
A6.3.2.1	Reactor Coolant System Loop		✓		✓					
A6.3.2.2	Steam Generator and Pump Supports		✓		✓					
A6.3.2.3	Reactor Coolant Pump Nozzles		✓					✓		(e)
A6.3.2.4	Pipe Whip Restraints:									
	Main Steam Line		✓		✓					
	Feedwater Line		✓		✓					(d)
A6.3.2.5	Snubbers					✓				(f)
A6.3.3	Low Head Safety Injection System (LHSIS)									
A6.3.3.1	Piping	✓	✓		✓					(d)
A6.3.3.2	Pumps and Drives	✓	✓				✓			
A6.3.3.3	Valves					✓				
A6.3.3.4	Motor Operators	✓		✓	✓					
A6.3.3.5	Snubbers and Hangers					✓				(f)
A6.3.3.6	Instrumentation			✓				✓		
A6.3.4	High Head Safety Injection Systems (HHSIS)									
A6.3.4.1	Accumulator Tank Nozzle		✓		✓					(d)
A6.3.4.2	Accumulator Piping Connection to RCS				✓					
A6.3.4.3	Charging Pumps and Drives	✓	✓		✓					
A6.3.5	Containment Recirculation Spray System									
A6.3.5.1	Pump and Motor Located Outside Containment:									
	Pump	✓	✓					✓		
	Motor	✓	✓		✓					
A6.3.5.2	Motor Drives Inside Containment	✓		✓	✓					
A6.3.6	On-Site Electric Power Systems									
A6.3.6.1	Diesel Generator Housing:[a]									
	Walls and Roof	✓	✓			✓				
	Door	✓	✓						✓	
	Soil Cover for Fuel Tanks	✓				✓				
A6.3.6.2	Diesel Generators	✓	✓	✓	✓					
A6.3.6.3	Day Tanks	✓						✓		
A6.3.6.4	Air Bottle Supports	✓				✓				
A6.3.6.5	Batteries and Battery Supports	✓		✓	✓					
A6.3.7	Electric Power Distribution Systems									
A6.3.7.2	Electrical Containment Penetrations and Connectors	✓			✓					
A6.3.7.3	Cable Trays	✓				✓				
A6.3.7.4	AC and DC Switchgear				✓			✓		
A6.3.8	Reactor and Engineered Safeguards Protection Systems Sensors and Logic Cabinets	✓		✓			✓			
A6.3.9	Intake Canal	✓				✓				

(a) Diesel Generator Building was evaluated only for tornado resistance.

(b) Design Criteria as stated in FSAR; or current criteria, if original criteria were not explicit or found to have insufficient margin.

(c) More sophisticated analysis methods may in some cases show that the design criteria have in fact been satisfied; in all cases however, loss of function is not expected.

(d) Deficiencies in original analysis have been either revised or investigated further. Revised results have been evaluated and design is found to be adequate.

(e) Bijlaard formulae not applicable.

(f) Periodic seal replacement in the snubbers is recommended.

TABLE X 2-2 PWR COMPONENT REVIEW - ENVIRONMENTAL QUALIFICATION SUMMARY

Subsection in Text	Component Description	Review Data Basis			Assessment of Design Adequacy					
					Adequate (Failure Not Expected)			Not Demonstrated (Failure Possible)		
					Design Criteria Satisfied[a]					
		Visual Observation	Design Calculations	Test Report	Analysis and/or Test	Engineering Judgment	Design Criteria Not Completely Satisfied[b]	Insufficient Information to Assess Adequacy	Information Reviewed Indicates that Failure is Likely	Notes
A6.3.1	Reactor Building									
A6.3.1.3	Paint Coatings within Containment			✓	✓					
A6.3.2	Reactor Coolant System (RCS)									
A6.3.2.5	Snubbers			✓			✓			(c)
A6.3.3	Low Head Safety Injection System (LHSIS)									(d)
A6.3.3.2	Pumps and Drives	✓		✓			✓			
A6.3.3.5	Snubbers			✓			✓			(c)
A6.3.4	High Head Safety Injection Systems (HHSIS)									(d)
A6.3.5	Containment Recirculation Spray System									
A6.3.5.1	Pump Located Outside Containment	✓		✓			✓			
A6.3.5.2	Motor Drives Inside Containment	✓		✓	✓					
A6.3.6	On-Site Electric Power Systems									(d)
A6.3.7	Electric Power Distribution System									
A6.3.7.1	Electrical Cables and Terminations	✓		✓	✓					
A6.3.7.2	Penetrations and Connectors	✓	✓		✓					
A6.3.8	Reactor Protection System	✓		✓			✓			

(a) Design Criteria as stated in FSAR; or current criteria, if original criteria were not explicit or found to have insufficient margin.

(b) More sophisticated analysis methods may in some cases show that the design criteria have in fact been satisfied; in all cases however, loss of function is not expected.

(c) Periodic seal replacement in the snubbers is recommended.

(d) Active components of this system that are outside of containment and not subject to LOCA environment have not been included.

TABLE X 2-3 BWR COMPONENT REVIEW - SEISMIC[a] DESIGN ADEQUACY SUMMARY

Subsection in Text	Component Description	Review Data Basis: Visual Observation	Review Data Basis: Design Calculations	Review Data Basis: Test Report	Assessment of Design Adequacy: Adequate (Failure Not Expected): Design Criteria Satisfied[b]: Analysis and/or Test	Assessment of Design Adequacy: Adequate (Failure Not Expected): Design Criteria Satisfied[b]: Engineering Judgment	Assessment of Design Adequacy: Adequate (Failure Not Expected): Design Criteria Not Completely Satisfied[c]	Assessment of Design Adequacy: Not Demonstrated (Failure Possible): Insufficient Information to Assess Adequacy	Assessment of Design Adequacy: Not Demonstrated (Failure Possible): Information Reviewed Indicates that Failure is Likely	Notes
A6.4.1	Containment Structures									
A6.4.1.1	Primary Containment Structure	✓	✓		✓					
A6.4.1.2	Reactor Building (Secondary Containment)	✓	✓		✓					
A6.4.1.3	Containment Piping Penetrations	✓	✓		✓					
A6.4.1.4	Suppression-Chamber-to-Drywell Vacuum Breaker Valves	✓	✓			✓				
A6.4.1.5	Missile Barriers Inside Containment	✓	✓					✓		
A6.4.2	Reactor Coolant System									
A6.4.2.1	Reactor Pressure Vessel and Internals		✓		✓					
A6.4.2.2	Reactor Pressure Vessel Nozzles		✓		✓					
A6.4.2.3	Reactor Pressure Vessel Skirt		✓		✓					
A6.4.2.4	Recirculation Lines	✓	✓				✓			
A6.4.2.5	Main Steam Lines		✓		✓					
A6.4.2.6	Main Steam Line Isolation Valves	✓	✓	✓	✓					
A6.4.2.7	Pipe Whip Restraints for Recirculation Lines	✓	✓		✓					
A6.4.2.8	Reactor Pressure Relief Valves	✓		✓				✓		
A6.4.3	Core Spray System									
A6.4.3.1	Piping	✓	✓		✓					
A6.4.3.2	Hangers and Snubbers:									
	Hangers					✓				
	Snubbers					✓				(d)
A6.4.3.3	Pumps and Drives	✓	✓		✓					
A6.4.3.4	Valves	✓		✓		✓				
A6.4.3.5	Valve Motor Operators	✓		✓			✓			
A6.4.3.6	Instrumentation	✓						✓		
A6.4.4	HPCIS Turbine	✓	✓		✓					
A6.4.5	RHR Pumps and Drives	✓	✓	✓	✓					
A6.4.6	On-Site Electric Power Systems									
A6.4.6.1	Diesel Generator Buildings:[a]									
	Structure and Door	✓	✓		✓					
	Door Hinges							✓		
	Corrugated Barrier Attachments							✓		
A6.4.6.2	Diesel Generators	✓	✓		✓					
A6.4.6.3	Batteries and Battery Racks:									
	Batteries	✓				✓				
	Battery Racks	✓	✓		✓					
A6.4.7	Electric Power Distribution Systems									
A6.4.7.2	Electrical Containment Penetrations	✓				✓				
A6.4.7.3	4 kV Switchgear	✓	✓		✓					
A6.4.7.4	480 V Load Centers	✓						✓		
A6.4.7.5	480 V Motor Control Centers	✓		✓	✓					
A6.4.7.6	DC Distribution Panels and Fuse Boxes	✓		✓	✓					
A6.4.7.7	Cable Trays	✓	✓		✓					
A6.4.8	Reactor Protection System	✓		✓			✓			

(a) Diesel Generator Building was evaluated for both seismic and tornado loads.

(b) Design Criteria as stated in FSAR; or current criteria, if original criteria were not explicit or found to have insufficient margin.

(c) More sophisticated analysis methods may in some cases show that the design criteria have in fact been satisfied; in all cases however, loss of function is not expected.

(d) Periodic seal replacement in the snubbers is recommended.

TABLE X 2-4 BWR COMPONENT REVIEW - ENVIRONMENT QUALIFICATION SUMMARY

Subsection in Text	Component Description	Review Data Basis: Visual Observation	Review Data Basis: Design Calculations	Review Data Basis: Test Report	Assessment of Design Adequacy: Adequate (Failure Not Expected): Design Criteria Satisfied[a]: Analysis and/or Text	Assessment of Design Adequacy: Adequate (Failure Not Expected): Design Criteria Satisfied[a]: Engineering Judgment	Assessment of Design Adequacy: Adequate (Failure Not Expected): Design Criteria Not Completely Satisfied[b]	Assessment of Design Adequacy: Not Demonstrated (Failure Possible): Insufficient Information to Assess Adequacy	Assessment of Design Adequacy: Not Demonstrated (Failure Possible): Information Reviewed Indicates that Failure is Likely	Notes
A6.4.1	Containment									
A6.4.1.4	Suppression-Chamber-to-Drywell Vacuum Breaker Valves	✓				✓				
A6.4.1.6	Paint Coatings Within Containment	✓		✓	✓					
A6.4.2	Reactor Coolant System									
A6.4.2.6	Main Steam Line Isolation Valves	✓	✓	✓	✓					
A6.4.2.8	Reactor Pressure Relief Valves	✓						✓		
A6.4.3	Core Spray System									
A6.4.3.2	Snubbers	✓		✓			✓			
A6.4.5	RHR Pumps and Drives	✓		✓		✓				
A6.4.7	Electric Power Distribution Systems									
A6.4.7.1	Electrical Cables Terminations and Connectors	✓		✓				✓		
A6.4.7.2	Electrical Containment Penetrations	✓				✓				

(a) Design Criteria as stated in FSAR; or current criteria, if original criteria were not explicit or found to have insufficient margin.

(b) More sophisticated analysis methods may in some cases show that the design criteria have in fact been satisfied; in all cases however, loss of function is not expected.

TABLE X 2-5 SUMMARY OF BASES FOR REDUCED SAFETY MARGIN DETERMINATION

	Component	Basis
A.	PWR Seismic	
1.	Containment Crane	The charging floor response spectra was used. Use of response spectra at the crane elevation results in calculated stresses in the end ties in excess of the yield strength.
2.	Low Head Safety Injection Pump	No seismic qualification test performed.
3.	Reactor Protection System	Inadequate seismic qualification testing performed.
B.	PWR Environmental	
1.	Reactor Coolant System Snubbers	Inadequate environmental qualification testing performed.
2.	Low Head Safety Injection System Snubbers	Inadequate environmental qualification testing performed.
3.	Reactor Protection System	Inadequate environmental qualification testing performed.
4.	Low Head Safety Injection System Pumps	Inadequate environmental qualification testing performed.
5.	Containment Recirculation Spray Pump	Inadequate environmental qualification testing performed.
C.	BWR Seismic	
1.	Recirculation Lines	Analysis performed assumed a constant spectral acceleration for the vertical component of the earthquakes considered. Use of the vertical response spectra indicates stresses will exceed code allowable but yielding will not occur.
2.	Reactor Protection System	Inadequate seismic qualification testing performed.
D.	BWR Environmental	
1.	Reactor Coolant System Snubbers	There is no evidence that environmental qualification tests were performed.

TABLE X 2-6 SUMMARY OF ITEMS FOR WHICH DESIGN ADEQUACY COULD NOT BE ASSESSED

Component	Basis
A. PWR Seismic	
1. Reactor Coolant Pump Nozzles	Improper Use of Bijlaard Formulae. Revised calculations have not been performed.
2. Low Head Safety Injection System Instrumentation	No evidence of seismic qualification tests.
3. Containment recirculation spray pumps and drive.	No evidence of pump seismic qualification tests.
4. Diesel generator day tank.	No evidence of seismic design having been performed.
5. AC and DC Switchgear	No evidence of seismic qualification tests.
B. BWR Seismic	
1. Missle barriers inside containment.	Improper penetration formulae used.
2. Reactor Pressure Relief Valves	No evidence of seismic qualification tests.
3. Core Spray System Instrumentation	No evidence of seismic qualification tests.
4. 480V load Centers	No evidence of seismic qualification tests.
C. BWR Environmental	
1. Reactor Pressure Relief Valves	No evidence of environmental qualification tests.
2. Electrical Cables, Termination and Connectors	Testing performed not sufficiently comprehensive.

Section 3

Summary

The majority of the items examined were found to be acceptable (seismic design - 85%, environmental qualification - 76%, tornado design - 50%). Nine percent of the seismic items considered acceptable and 31% of the environmental qualification items considered acceptable have a margin to failure somewhat smaller than that which could be expected considering applicable code and qualification requirements. The only item (PWR diesel generator building doors) for which failure was considered likely under design loadings has a negligible impact on the risk assessments performed in this study. In addition, there were items for which design adequacy could not be assessed because sufficient information was not available (15% of those items considered for seismic evaluation, and 24% of those considered for environmental qualification). These inadequacies occurred because either: (1) improper assumptions were made in design calculations or the calculations were not performed; or (2) seismic or environmental qualification tests apparently were not performed. The increased emphasis on qualification testing and quality assurance programs which has developed since the two specific plants under study were designed may have improved the situation.

APPENDIX A

DESIGN ADEQUACY EVALUATION OF SELECTED SAFETY RELATED EQUIPMENT AND STRUCTURES IN NUCLEAR POWER GENERATING PLANTS

Appendix A

Table of Contents

Section			Page No.
A1.	INTRODUCTION		X-23
	A1.1	General Background	X-23
	A1.2	Objectives of the Design-Adequacy Study	X-23
	A1.3	Implementation of the Objectives	X-23
A2.	DESIGN BASIS EVENTS		X-24
	A2.1	Earthquakes	X-24
		A2.1.1 Seismicity of PWR and BWR Plant Environs	X-24
		A2.1.1.1 PWR Plant	X-24
		A2.1.1.2 BWR Plant	X-25
		A2.1.2 Response of Structures to Earthquake Ground Motion	X-25
	A2.2	Tornado Considerations	X-26
	A2.3	Accident Considerations	X-27
A3.	SYSTEMS AND COMPONENTS EXAMINED		X-27
	A3.1	PWR Item Selection Basis	X-28
		A3.1.1 Reactor Building	X-28
		A3.1.2 Reactor Coolant System	X-28
		A3.1.3 Low Head Safety Injection System (LHSIS)	X-28
		A3.1.4 High Head Safety Injection Systems (HHSIS)	X-28
		A3.1.5 Containment Recirculation Spray System	X-29
		A3.1.6 On-Site Electric Power Systems	X-29
		A3.1.7 Electric Power Distribution Systems	X-29
		A3.1.8 Reactor and Engineered Safeguards Protection Systems Sensors and Logic Cabinets	X-29
		A3.1.9 Intake Canal	X-29
	A3.2	BWR Item Selection Basis	X-29
		A3.2.1 Containment Structures	X-29
		A3.2.2 Reactor Coolant System	X-29
		A3.2.3 Core Spray System	X-29
		A3.2.4 High Pressure Coolant Injection System (HPCIS) Turbine	X-29
		A3.2.5 Residual Heat Removal (RHR) Pumps and Drives	X-29
		A3.2.6 On-Site Electric Power Systems	X-30
		A3.2.7 Electric Power Distribution Systems	X-30
		A3.2.8 Reactor Protection System	X-30
A4.	DESIGN CRITERIA AND PRACTICES		X-30
A5.	METHOD OF EVALUATION		X-31
	A5.1	Information Acquisition	X-31
		A5.1.1 Final Safety Analysis Report Review	X-31
		A5.1.2 Site Visits	X-32
		A5.1.3 Visits to Architect/Engineers, Utilities, and Suppliers	X-32
		A5.1.4 Review Data Sheets	X-32
		A5.1.5 Other Documents Reviewed	X-32

Table of Contents (Continued)

Section		Page No.
A5.2	Evaluation of Information	X-32
A5.2.1	Codes and Standards	X-32
A5.2.2	Appropriateness of Mathematical Models	X-32
A5.2.3	Adequacy of Load Definitions	X-33
A5.2.4	Adequacy of Boundary Conditions	X-33
A5.2.5	Adequacy of Computer Code Numerical Techniques	X-33
A5.2.6	Effect of Variation on Material Properties	X-33
A5.2.7	Adequacy of Qualification Test Programs	X-33
A6.	EVALUATION OF COMPONENTS	X-34
A6.1	Seismic Effects	X-34
A6.1.1	PWR Plant	X-34
A6.1.1.1	Seismic Loads	X-34
A6.1.1.2	Damping	X-36
A6.1.2	BWR Plant	X-36
A6.1.2.1	Seismic Loads	X-36
A6.1.2.2	Damping	X-37
A6.2	Tornado Effects	X-37
A6.2.1	PWR Plant	X-37
A6.2.2	BWR Plant	X-38
A6.3	Design Adequacy of PWR Plant Components	X-38
A6.3.1	Reactor Building	X-38
A6.3.1.1	Soil-Structure Interaction Model	X-38
A6.3.1.2	Containment Internal Structure	X-39
A6.3.1.3	Paint Coatings Within Containment	X-40
A6.3.1.4	Crane	X-41
A6.3.2	Reactor Coolant System (RCS)	X-42
A6.3.2.1	Reactor Coolant System Loops	X-42
A6.3.2.2	Steam-Generator and Pump Supports	X-44
A6.3.2.3	Reactor Coolant Pump Nozzles	X-45
A6.3.2.4	Pipe-Whip Restraints	X-46
A6.3.2.5	Snubbers	X-47
A6.3.3	Low Head Safety Injection System (LHSIS)	X-47
A6.3.3.1	Piping	X-47
A6.3.3.2	Pumps and Drives	X-49
A6.3.3.3	Valves	X-50
A6.3.3.4	Valve Motor Operators	X-50
A6.3.3.5	Snubbers and Hangers	X-51
A6.3.3.6	Instrumentation	X-51
A6.3.3.7	Commentary and Conclusion	X-52
A6.3.4	High Head Safety Injection Systems (HHSIS)	X-52
A6.3.4.1	Accumulator Tank Nozzle	X-52
A6.3.4.2	Accumulator Piping Connection to RCS	X-53
A6.3.4.3	Charging Pumps and Drives	X-53
A6.3.4.4	Commentary and Conclusion	X-53

Table of Contents (Continued)

Section			Page No.
	A6.3.5	Containment Recirculation Spray System (CRSS).....	X-53
		A6.3.5.1 Pump and Motor Located Outside Containment.....	X-54
		A6.3.5.2 Motor Drives.....	X-54
	A6.3.6	On-Site Electric Power Systems.....	X-55
		A6.3.6.1 Diesel Generator Building.....	X-55
		A6.3.6.2 Diesel Generators.....	X-57
		A6.3.6.3 Day Tanks.....	X-58
		A6.3.6.4 Air Bottle Support.....	X-58
		A6.3.6.5 Batteries and Battery Support.....	X-58
	A6.3.7	Electric Power Distribution Systems.....	X-59
		A6.3.7.1 Electrical Cables and Terminations.....	X-59
		A6.3.7.2 Electrical Containment Penetrations and Connectors.....	X-59
		A6.3.7.3 Cable Trays.....	X-60
		A6.3.7.4 A-C and D-C Switchgear.....	X-61
	A6.3.8	Reactor and Engineered Safeguards Protection Systems Sensors and Logic Cabinets.....	X-61
		A6.3.8.1 Environmental Qualification.....	X-61
		A6.3.8.2 Seismic Qualification.....	X-61
		A6.3.8.3 Commentary.....	X-62
		A6.3.8.4 Conclusion.....	X-62
	A6.3.9	Intake Canal.....	X-62
A6.4		Design Adequacy of BWR Plant Components.....	X-63
	A6.4.1	Containment Structure.....	X-63
		A6.4.1.1 Primary Containment Structure.....	X-63
		A6.4.1.2 Reactor Building (Secondary Containment).....	X-63
		A6.4.1.3 Containment Piping Penetrations.....	X-64
		A6.4.1.4 Suppression-Chamber-to-Drywell Vacuum Breaker Valves.....	X-65
		A6.4.1.5 Missile Barriers Inside Containment.....	X-66
		A6.4.1.6 Paint Coatings Within Containment.....	X-67
	A6.4.2	Reactor Coolant System.....	X-68
		A6.4.2.1 Reactor Pressure Vessel and Internals.....	X-68
		A6.4.2.2 Reactor Pressure Vessel Nozzles.....	X-69
		A6.4.2.3 Reactor Pressure Vessel Skirt.....	X-69
		A6.4.2.4 Recirculation Lines.....	X-70
		A6.4.2.5 Main Steam Lines.....	X-71
		A6.4.2.6 Main Steam Line Isolation Valves.....	X-71
		A6.4.2.7 Pipe Whip Restraint for Recirculation Lines.....	X-74
		A6.4.2.8 Reactor Pressure Relief Valves.....	X-74
	A6.4.3	Core Spray System.....	X-75
		A6.4.3.1 Piping.....	X-75
		A6.4.3.2 Hangers and Snubbers.....	X-75

Table of Contents (Continued)

Section			Page No.
	A6.4.3.3	Pumps and Drives	X-76
	A6.4.3.4	Valves	X-77
	A6.4.3.5	Valve Motor Operators	X-77
	A6.4.3.6	Instrumentation	X-78
A6.4.4		HPCIS Turbine	X-78
	A6.4.4.1	Commentary	X-79
	A6.4.4.2	Conclusion	X-79
A6.4.5		RHR Pumps and Drives	X-79
	A6.4.5.1	Seismic Qualification	X-79
	A6.4.5.2	Environmental Qualification	X-80
	A6.4.5.3	Commentary	X-80
	A6.4.5.4	Conclusion	X-81
A6.4.6		On-Site Electric Power Systems	X-81
	A6.4.6.1	Diesel Generator Building	X-82
	A6.4.6.2	Diesel Generators	X-84
	A6.4.6.3	Batteries and Battery Racks	X-85
A6.4.7		Electric Power Distribution Systems	X-86
	A6.4.7.1	Electric Cables, Terminations, and Connectors	X-86
	A6.4.7.2	Electrical Containment Penetrations	X-87
	A6.4.7.3	4-kV Switchgear	X-87
	A6.4.7.4	480-V Load Centers	X-88
	A6.4.7.5	480-V Motor Control Centers	X-88
	A6.4.7.6	D-C Distribution Panels and Fuse Boxes	X-89
	A6.4.7.7	Cable Trays	X-89
A6.4.8		Reactor Protection System	X-90
	A6.4.8.1	Commentary	X-90
	A6.4.8.2	Conclusion	X-91
REFERENCES			X-91

List of Tables

Table		Page No.
X A-1	Design Basis Environments - PWR Plant	X-95
X A-2	Design Basis Environments - BWR Plant	X-96
X A-3	PWR Components	X-97
X A-4	BWR Components	X-98
X A-5	PWR Component Review - Seismic Design Adequacy Summary	X-99
X A-6	PWR Component Review - Environmental Qualification Summary	X-100
X A-7	BWR Component Review - Seismic Design Adequacy Summary	X-101
X A-8	BWR Component Reviw - Environment Qualification Summary	X-102
X A-9	Comparison of Damping Values Used in PWR Plant With Those Currently Required	X-103
X A-10	Comparison of Damping Values Used in BWR Plant With Those Currently Required	X-104
X A-11	Comparison of Missile Characteristics	X-104
X A-12	Comparison of Computed Frequencies	X-105
X A-13	Estimate of Modal Damping	X-105
X A-14	Summary of Moments and Stresses in Crane (Trolley at Center Line)	X-106
X A-15	Critical Stress Summary (psi)	X-107
X A-16	Possible f_e/f_s Values	X-107
X A-17	Steam Generator Supports - Maximum Member Loads - Pipe Rupture Plus Seismic	X-107
X A-18	Reactor Coolant Pump Supports - Maximum Member Loads - Pipe Rupture Plus Seismic	X-108
X A-19	Summary of Critical Stresses (psi) in LHSIS	X-109
X A-20	Summary of Accumulator Tank Nozzle Pipe Loads	X-109
X A-21	Load Condition and Stress Limits - Code Case No. 1607	X-110
X A-22	Accumulator Piping Connection Nozzle Loads	X-111
X A-23	Reactor Building Natural Frequencies	X-111
X A-24	Computed Stress Intensities in BWR Vessel Nozzles	X-112
X A-25	Reactor Pressure Vessel Elastic Analysis	X-112
X A-26	Natural Periods and Spectral Acceleration	X-113
X A-27	Critical Stresses (psi)	X-113

List of Tables (Continued)

Table		Page No.
X A-28	Periods of Vibration and Spectral Accelerations for Main Steam Line	X-114
X A-29	Critical Stresses (psi) for Main Steam Line	X-114
X A-30	Summary of Loads on Pipe Whip Constraints	X-114
X A-31	Critical Stresses (psi)	X-115
X A-32	Results of Dynamic Analysis of Battery Racks	X-115
X A-33	Hanger Attachment Types	X-115

List of Figures

Figure		Page No.
X A-1	Design Adequacy Review Data Sheet	X-116
X A-2	Supplementary Review Data Sheet	X-117
X A-3	Example of a Multi-Element Structure Connected to Rigid Structures at Both Ends	X-118
X A-4	Ground Response Spectra (OBE) - PWR	X-118
X A-5	Ground Response Spectra (DBE) - PWR	X-119
X A-6	Response Spectra (DE) - BWR	X-119
X A-7	Response Spectra (MCE) - BWR	X-120
X A-8	Cross Section Through Reactor Building	X-121
X A-9	Soil-Structure Interaction Model	X-122
X A-10	Containment Internal Structure - Cross Section of Lower Portion	X-122
X A-11	Reactor Coolant System - Seismic Analysis Model Used by Supplier	X-123
X A-12	Horizontal OBE Floor Response Spectrum Used for Reactor Building	X-123
X A-13	A/E Mathematical Model for Dynamic Analysis of Primary Coolant Loop	X-124
X A-14	Typical Reactor Coolant Pump	X-125
X A-15	Pipe-Whip Restraint - Main Steam Line (not to scale)	X-126
X A-16	Accumulator Tank Nozzle	X-126

List of Figures (Continued)

Figure		Page No.
X A-17	Horizontal DBE Floor Response Spectrum Used for Diesel Generator Building	X-127
X A-18	Vertical DBE Floor Response Spectrum Used for Diesel Generator Building	X-127
X A-19	Day Tank	X-128
X A-20	Air Bottle Support (Not to Scale)	X-128
X A-21	Elevation View Through BWR Plant	X-129
X A-22	Reactor Building Mathematical Model	X-130
X A-23	Response Spectra Comparison, Design Earthquake, 5% g, 2% Damping	X-131
X A-24	Vacuum Breaker Valve	X-131
X A-25	Missile Barriers Inside Drywell	X-132
X A-26	Safety Valve	X-132
X A-27	Recirculation Line	X-133
X A-28	Main Steam Isolation Valve	X-133
X A-29	Pressure Relief Valve	X-134
X A-30	A/E Mathematical Model for Dynamic Analysis of Core Spray Piping	X-134
X A-31	Core Spray Pump and Drive - Lower Portion Showing Pump Mounting	X-135
X A-32	Core Spray Pump and Drive - Upper Portion Showing Motor and Coupling to Pump	X-135
X A-33	Typical Valve Motor Operator Installation	X-136
X A-34	HPCIS Pump and Interstage Piping	X-136
X A-35	HPCIS Turbine Drive	X-137
X A-36	Watertight Entryway to RHR Pump Room	X-137
X A-37	RHR Pump and Drive	X-138
X A-38	RHR Pump and Motor	X-138
X A-39	Selected Displacement Records from RHR Pump Vibration Tests Showing Cyclic Displacement Peaks	X-139
X A-40	Diesel Generator Building - Side Facing River	X-139
X A-41	Diesel Generator Building - Opposite Side	X-140
X A-42	Lumped Mass Model for Diesel Generator Building Seismic Analysis	X-140
X A-43	Diesel Generator Unit - View from Generator End	X-141
X A-44	View of Diesel Generator Unit Showing Turbo-Charger	X-141

List of Figures (Continued)

Figure		Page No.
X A-45	Diesel Generator Dynamic Model	X-142
X A-46	Batteries and Battery Racks - 125/250-V System	X-142
X A-47	Batteries and Battery Racks - 24-V System	X-143
X A-48	Lumped-Mass Model for Seismic Analysis of 58-Cell FTC-21 Battery Rack. (Typical of Model Scheme for All Battery Racks)	X-143
X A-49	Electric Power and Control Cables Installed in Cable Trays	X-144
X A-50	4-kV Switchgear Unit	X-144
X A-51	4-kV Switchgear Racks	X-145
X A-52	480-V Load Center	X-145
X A-53	480-V Motor Control Centers	X-145
X A-54	D-C Distribution Panels	X-145
X A-55	RPS Instrumentation Racks (Front View)	X-146
X A-56	RPS Instrumentation Racks (Rear View)	X-146
X A-57	Reactor Protection System Logic Cabinet	X-146
X A-58	Control Room Panels for Reactor Safety Systems	X-146

Appendix A
Design Adequacy Evaluation of Selected Safety Related Equipment and Structures in Nuclear Power Generating Plants

A.1 INTRODUCTION

A1.1 GENERAL BACKGROUND

This attachment to Appendix X of the Reactor Safety Study assesses the adequacy of the design of a sample of safety-related nuclear equipment and structures from the viewpoint of resistance to common-mode failures. An earthquake, for example, has the potential for causing a common failure in the piping of both the reactor coolant and the emergency core cooling systems, if these systems are not properly designed. Similarly, a tornado has the potential for causing a common failure of both off-site and emergency on-site power due to wind damage to off-site transmission lines and missile penetration of the diesel generator building if the building is inadequately designed. These are examples of system failures that can result from a single cause. Failure of one system as the result of the failure of another system due to inadequate design would also be classified as a common-mode failure. A break in a recirculation line, for example, could result in a whipping pipe, which could, in turn, cause the failure of engineered safety features, such as the containment barrier or emergency core cooling systems, if pipewhip restraints are inadequately designed.

The Atomic Energy Commission, through its rules and regulations[1] and guides[2], establishes safety design requirements for nuclear power plants to avoid these failures. The objective of the design-adequacy study was to determine whether the AEC requirements have been properly implemented in the samples studied.

Two nuclear power plants of recent design, licensed and presently in operation, were selected for study. One plant is a boiling-water reactor (BWR); the other is a pressurized-water reactor (PWR).

The design-adequacy study was performed by the Mechanical and Nuclear Engineering Department of the Franklin Institute Research Laboratories (FIRL) with support from the Atomic Energy Commission and cooperation from the owners of the two nuclear plants that were studied as well as the architect/engineers (A/E) and nuclear steam supply system (NSSS) suppliers. The A/E, in particular, not only cooperated with the study but spent a considerable amount of time with the FIRL review team.

A1.2 OBJECTIVES OF THE DESIGN-ADEQUACY STUDY

The principal objective of the FIRL study was to assess the design adequacy of a sample of nuclear power plant components and systems, with detailed consideration given to the following design basis events that have the potential for causing common-mode failures:

- Earthquake
- Tornado
- Loss-of-coolant accident (LOCA)

A1.3 IMPLEMENTATION OF THE OBJECTIVES

First, we examined design basis events in general and in particular as they pertain to PWR and BWR plants (section A2 contains a discussion of these events).

---

[1] The AEC Rules and Regulations are published in the Code of Federal Regulations, Title 10, Chapter I (10 CFR) and have the force of law.

[2] Regulatory Guides are aimed at providing acceptable methods for implementing specific parts of the AEC regulations but are not mandatory.

Next, we selected the systems and components to be examined. Lists of these systems and components and the bases for their selection are presented in section A3.

Finally, we evaluated the methods and the results of the analyses and tests used in qualifying the equipment and compared this information with the design criteria in effect at the time the plants were licensed. To provide a realistic assessment of design adequacy, we also evaluated the equipment in accordance with current criteria, which incorporate the latest knowledge. These criteria, as reflected in pertinent codes, standards, regulations, and state-of-the-art knowledge, are briefly discussed in section A4, as are qualification methods anticipated for the future.

In section A5 we describe the procedure we used to acquire and evaluate the design calculations and the tests that were used to qualify the equipment.

The results of our evaluation, with detailed discussions on specific components, are presented in section A6. Tables X A-5 and X A-6 provide a summary of the components reviewed and an assessment of their design adequacy for the PWR and BWR plants, respectively.

A2. DESIGN BASIS EVENTS

Appendix A of Title 10 of the Code of Federal Regulations, Part 50, contains 55 principal design criteria for light water nuclear reactor plants. Of these the following two describe design basis events that must be considered in an assessment of the design adequacy of a nuclear power plant:

a. "Criterion 2 - Design bases for protection against natural phenomena. Structures, systems, and components important to safety shall be designed to withstand the effects of natural phenomena such as earthquakes, tornadoes, hurricanes, floods, tsunamis, and seiches without loss of capability to perform their safety functions. The design bases for these structures, systems, and components shall reflect: (1) Appropriate consideration of the most severe of the natural phenomena that have been historically reported for the site and surrounding area, with sufficient margin for the limited accuracy, quantity, and period of time in which the historical data have been accumulated, (2) Appropriate combinations of the effects of normal and accident conditions with the effects of the natural phenomena and (3) The importance of the safety function to be performed."

b. "Criterion 4 - Environmental and missile design bases. Structures, systems, and components important to safety shall be designed to accommodate the effects of and to be compatible with the environmental conditions associated with normal operation, maintenance, testing, and postulated accidents including loss-of-coolant accidents. These structures, systems, and components shall be appropriately protected against dynamic effects, including the effects of missiles, pipe whipping, and discharging fluids, that may result from equipment failures and from events and conditions outside the nuclear power unit."

Criterion 2 describes natural phenomena that originate outside the plant; Criterion 4 describes events that originate largely inside the plant. Our assessment of the design adequancy of BWR and PWR plants has concentrated on earthquakes, tornadoes, and accident conditions associated with equipment failure. The essential features of these phenomena will be outlined to promote an understanding of their characteristics.

A2.1 EARTHQUAKES

A2.1.1 SEISMICITY OF PWR AND BWR PLANT ENVIRONS

A2.1.1.1 PWR Plant.

The PWR site, located in the Atlantic Coastal Plain Province, is bounded on the east by the Atlantic Ocean and on the west by the fall line and the Piedmont Province. The crystalline basement rock crops out near the fall zone about 50 miles west of the site. The basement surface slopes gently to the southeast and is overlain by Cretaceous and Tertiary sediments, which are about 50 miles west of the site. A postulated fault trending northwest-southeast in the basement rock beneath the James River has been discounted.

Eight earthquakes with epicentral intensities of V through VII on the modified Mercalli scale have been reported within 100 miles of the site since the late 18th century. The closest major earthquakes (estimated to have been about 7

on the Richter magnitude scale, with damage to buildings and bridges) have occurred at Charleston, S.C., with epicenters about 350 miles southwest of the site.

On the basis of the seismic history and the geological structure of the area, it is estimated that the site could experience an earthquake with horizontal ground acceleration equal to 0.07g and a maximum credible earthquake (MCE) equal to 0.15g in the horizontal direction. The vertical component of the earthquake has been estimated to be two-thirds of these values.

A2.1.1.2 BWR Plant.

The BWR site, located within the Piedmont upland section of the Piedmont Province of the Appalachian Province, is underlain by metamorphosed sedimentary and crystalline rocks of the Paleozoic and Precambrian eras. The fall zone, which represents the physiographic boundary between the Piedmont Province and the Atlantic Coastal Plain Province, is located about 20 miles southeast of the site at its closest approach.

Two major Paleozoic and older fault systems are prevalent in the region as are faults of the Triassic period. These faults do not involve younger Mesozoic or Cenozoic strata and are completely healed. There is a Paleozoic fault associated with a syncline that passes about 1 mile south of the BWR site, but this fault has been inactive for 140 to 200 million years.

The BWR plant is built on bedrock overlain by 10 ft of sediment consisting primarily of fine sand and silt with occasional clayey zones.

On the basis of records dating back to the early 18th century, it is estimated that the BWR region has not experienced an earthquake of intensity greater than VII. Two earthquakes estimated to be of intensity VII have been recorded: one occurred in October 1871, 40 miles from the site, and the other occurred in February 1954, 100 miles from the site.

On the basis of the seismic history and geological structure of the area, it is estimated that the site could experience an earthquake with horizontal ground acceleration equal to 0.05g and an MCE with horizontal ground acceleration equal to 0.12g. The vertical component has been estimated to be two-thirds of these values.

A2.1.2 RESPONSE OF STRUCTURES TO EARTHQUAKE GROUND MOTION

Nuclear reactors are housed in massive concrete structures with fundamental frequencies (lowest natural frequency) that generally fall within the peak acceleration response range of earthquakes, i.e., 2.5 to 9 cycles per second (cps).

The response of a building to an earthquake will depend on the dynamic characteristics of the building (stiffness, mass, and damping) as well as on its foundation and on the earthquake itself. If a building is founded on rock (as is the BWR), then the free-field seismic ground motion will be transmitted directly to the base of the building. If, however, the building is founded on soil (as is the PWR), then there will be dynamic interaction between the building and the soil. In this case, a single mathematical model representing both the building and the soil will be required to determine the dynamic response.

The response of structures is usually obtained by a method of analysis in which the mass of the structure is concentrated at discrete locations and stiffness properties are computed on the assumption that the structure will behave like a beam that deflects owing to both shear and bending loads. Since nuclear structures have relatively small aspect ratios (height/width), shear deflection predominates.

The dynamic response of the structure may be obtained by modal analysis methods[1] that use either a real or an artificial time history earthquake record or a response spectrum curve for determining the response.

A single point on a response spectrum curve for a given percent of critical damping η is obtained by determining the time history response of an oscillator with damping η and a given natural frequency to base motion defined by the accelerogram. The maximum response of this oscillator then determines the ordinate of the response spectrum, and the natural period of vibration of the oscillator is the abscissa. The process is then repeated for other assumed periods. The resulting response spectrum curve is quite jagged, and the

[1]See Ref. 1 for a discussion of modal analysis methods and techniques.

process may be repeated for several earthquake records to obtain an average.

The Housner curve is a smoothed average response curve that is in common use.

The dynamic stresses in the structure may be obtained from acceleration response spectra by first determining the natural frequencies and corresponding mode shapes of the structure as well as modal participation factors. The modal acceleration is then equal to the mode shape times the modal participation factor times the acceleration value taken from the acceleration response spectrum curve (for the assumed modal damping), which corresponds to the mode shape frequency. Modal stresses may then be obtained by applying the inertial forces (corresponding to the modal accelerations) to the structure. The total response should be computed by combining these stresses in accordance with the square root of the sum of the squares of the modal stresses except for modes with closely spaced frequencies, as will be explained subsequently. The displacements can be similarly determined.

The response spectrum approach is a convenient method of obtaining displacements, forces, and stresses in the structure; however, since we are dealing only with maximum values in each mode, we do not know the phase relationship between the modal responses. It is customary, therefore, to determine the total response by taking the square root of the sum of the squares (SRSS) of the modal stresses. The response of modes with closely spaced frequencies may, however, be nearly in phase. Recent practice has been to combine the direct sum of the absolute value of these modal responses with the remaining modes in accordance with the SRSS.

The response spectrum method gives total displacement at a given point in the structure, which is neither time- nor frequency-dependent; so it does not allow an analysis of the dynamic response of equipment that is mounted at the various floor levels in the structure. For this purpose, a floor response spectrum curve must be generated by starting with a time history input to the base of the structure and then determining the time history response at the floor of interest. The floor response spectrum may then be generated from the floor time history response. An artificial time history record at the base of the structure must first be generated since it must be compatible with the averaged design ground response spectrum curve. This is usually done by starting with a real time history record, such as the Taft earthquake record, which has been normalized to the defined maximum ground acceleration for the operating basis earthquake (OBE) or design basis earthquake (DBE), and then modifying it so that its corresponding response spectrum curve approximates and envelops the design ground response spectrum.

At the time the PWR and BWR plants were licensed, it was generally assumed that only one horizontal component of the earthquake (e.g., X or Z) would act simultaneously with the vertical component. Assume for the moment that the stress at a given point in the structure due to the X, Y, or Z earthquake components is "σ." Some analysts would assume that the X and Y earthquakes would be in phase; so the total response would be 2σ. Other analysts would assume that the components would be out of phase; so the total response would be given by $\sqrt{2}\,\sigma \approx 1.4\sigma$. Recent evidence indicates that all three components of the earthquake act simultaneously but out of phase; thus the total response in the assumed example would be $\sqrt{3}\,\sigma \approx 1.7\sigma$. Thus, in this example, the analysts who had assumed the X and Z components to act simultaneously but in phase would give results that would be acceptable for the three simultaneous earthquake components which are out of phase. Likewise in more realistic examples, this would be generally, but not universally true. However, the analysts who had previously assumed two components out of phase would have to reexamine their results.

A2.2 TORNADO CONSIDERATIONS

A tornado can develop the greatest concentration of natural atmospheric power on earth. It is the most violent of all storms. Although a tornado covers a very restricted area and is of short duration, it can cause devastating destruction of homes and other common structures and place human life in great jeopardy from blast and flying debris.

Nuclear reactor structures housing safety equipment should be resistant to the following tornado effects:

a. External wind forces.

b. Differential pressure between the inside and outside of fully enclosed buildings.

c. Impact from flying missiles.

Specific definitions of tornado effects are given in sections A6.2.1 and A6.2.2 for the PWR and BWR plants, respectively.

A2.3 ACCIDENT CONSIDERATIONS

Although extensive measures are taken during the design and operation of nuclear power plants to prevent accidents from occurring, the AEC requires that the designer postulate severe accidents, using unrealistically severe assumptions. The effects of the various types of hypothetical accidents are investigated, considering a variety of plant conditions, to determine situations that could result in the off-site release of radioactive material. The following types of accidents are generally considered:

a. Rupture of any single pipe up to and including complete severance of the largest pipe in the reactor coolant system.

b. Rapid power increase beyond design limits caused by reactor control-system failure.

c. Rupture of fuel rod cladding in a fuel assembly or spent-fuel transport cask that is dropped during refueling operations.

d. Rupture of a gaseous-radioactive-waste storage tank.

Each of these types of accidents has the potential for releasing radioactive material to the environment. An analysis of each type of accident is performed to determine whether there is assurance that adequate safety features have been engineered into the plant -- in the form of passive barriers or active systems -- to limit the release of radioactive materials and to show that the maximum radiation dose to an individual at the plant's site boundary and beyond would not exceed the allowable dose even when highly pessimistic assumptions are used.

Accidents with the largest potential for off-site radiation exposures for a given set of assumptions are designated design basis accidents and are analyzed in detail.

Structures, engineered safeguards systems, and the components thereof must be designed to perform adequately under all service conditions including normal operation, maintenance, and testing and under the conditions of postulated design basis accidents. They must also be appropriately protected against flooding and dynamic effects (including the effects of accident-produced missiles, pipe whipping, and discharging fluids) which can result from equipment or piping failures.

Additional conservatism is incorporated into the accident analyses by assuming that an additional, unrelated, unspecified fault in some active component or piece of equipment in the engineered safeguards systems also occurs. This fault is assumed to result in the malfunction of a device that is intended to mitigate the consequences of the accident. The assumed result of such an unspecified fault is restricted to such relatively common events as an electrical failure, instrument error, motor stall, breaker freeze-in, or valve malfunction. Highly improbable failures, such as additional pipe breaks, are not assumed to occur coincident with the assumed accident. The additional failure(s) to be considered are in addition to all possible failures (common-mode or otherwise) caused by the accident itself. For the most severe type of design basis accident, a LOCA, this means that the worst possible single failure must be assumed to occur in one of the systems designed to prevent a LOCA from leading to extreme overheating of the fuel rods (and thereby melting or otherwise releasing large quantities of radioactive materials).

The accident-produced environmental conditions postulated for the BWR and PWR plants are summarized in Tables X A-1 and X A-2, respectively. The numerical values under headings I and II are the design bases for the equipment. Note that the LOCA conditions under heading II are established under the assumption that the worst possible single failure in the engineered safeguard systems has occurred coincident with the accident. The tabulated information has been developed from a number of sources, including the IEEE standard on equipment qualification (Ref. 2) and reports of qualification tests conducted on individual components.

A3. SYSTEMS AND COMPONENTS EXAMINED

The components and systems sampled in this review were selected on the basis of a combination of factors:

a. Safety function.

b. Portions of structures which are known to be vulnerable to high stresses.

c. Component types that have experienced malfunction during normal operation and/or testing in existing nuclear power plants.

d. Potential for common-mode failure.

Some major components, such as the reactor pressure vessel, were deliberately excluded from our review[1] because they require a formal stress report and are subjected to a careful review by the AEC and other organizations, which provides an added measure of assurance as to their adequacy.

Some items, such as the reactor building, were reviewed primarily from the viewpoint of adequate dynamic mathematical modeling to ensure that computed floor response spectra curves used for analyzing equipment were correct.

Our sampling process was biased toward points of potential weakness.

Thirty-one PWR equipment groups (Table X A-3) and thirty-three BWR equipment groups (Table X A-4) were examined by the review team. In the tables each group has been assigned a number that corresponds to the subsection in section A6 where the group is described and evaluated. For each plant type, a complete system was selected for review plus certain components or structures in other systems. The components were selected for examination because they may all be subject to seismic loads and thus have the potential for common-mode failure. In addition, these components either perform a safety-related function or their failure could prevent the safe shutdown of the reactor or cause a breach in containment, as described in sections A3.1 and A3.2.

A3.1 PWR ITEM SELECTION BASIS

The groups shown in Table X A-3 form nine systems whose safety-related functions are described briefly as follows:

A3.1.1 REACTOR BUILDING

The containment structure is the ultimate barrier between any postulated large release of radioactivity and the plant environs. Soil-structure interaction must be considered because the PWR is founded on 1300 ft of soil, which affects the response of structures and equipment to seismic events. The internal structure (also referred to as the crane wall) supports the nuclear steam supply system, the crane, and portions of safety-related equipment, such as the emergency core injection piping. The containment paint coating has the potential for peeling under the severe environment caused by a LOCA and thereby impairing the effectiveness of some of the emergency core cooling and containment cooling systems. Catastrophic failure of the crane or its support could cause a break in the containment spray headers, which are directly below the crane.

A3.1.2 REACTOR COOLANT SYSTEM

Items in this group are necessary to maintain the integrity of the reactor coolant pressure boundary, except the pipe-whip restraints whose failure could cause a breach in the containment. Components or portions thereof were selected on the basis of the criteria discussed previously.

A3.1.3 LOW HEAD SAFETY INJECTION SYSTEM (LHSIS)

This system injects borated water into the cold legs of the reactor cooling system loops as a supplement to the accumulator discharge of borated water in the event of a large LOCA. It also injects water (which collects in the containment sump) during the recirculation phase. The system is necessary to provide for the safe shutdown of the reactor in the event of a LOCA. The snubbers provide seismic restraints on pipe motion and the hangers support the piping weight. Both snubbers and hangers should be designed to limit excessive stress in the piping. Instrumentation controls the LHSIS operation. For this group, all items in the system were considered in our review.

A3.1.4 HIGH HEAD SAFETY INJECTION SYSTEMS (HHSIS)

These systems inject borated water into the cold legs of the reactor in the event of a LOCA. The accumulator discharges borated water when there is a large break in the reactor coolant system (RCS). The nozzle of the accumulator and the connection to the RCS piping

---

[1] The BWR reactor was considered only from the viewpoint of imposing seismic displacements on connecting piping.

were examined because these are critical regions.

A3.1.5 CONTAINMENT RECIRCULATION SPRAY SYSTEM

This system is necessary to depressurize the containment in the event of a LOCA. The key components -- the pumps and their drives -- were considered in our review.

A3.1.6 ON-SITE ELECTRIC POWER SYSTEMS

Emergency on-site power is provided by the diesel generator. The system is necessary to power engineered safeguards systems in the event of loss of off-site power. The day tank provides the initial source of diesel fuel for the system. The air bottle stores compressed air used in starting the diesel engine. The batteries provide emergency power for control systems necessary for the safe shutdown of the reactor.

A3.1.7 ELECTRIC POWER DISTRIBUTION SYSTEMS

These systems distribute power to the pump motors, motor-operated valves, and control-rod drives which are necessary for safe shutdown.

A3.1.8 REACTOR AND ENGINEERED SAFEGUARDS PROTECTION SYSTEMS SENSORS AND LOGIC CABINETS

The protection systems sense reactor water level, reactor pressure, and containment pressure. Through their logic systems, they interpret conditions that call for immediate shutdown, initiate this action, and activate containment isolation and reactor core safety injection systems.

A3.1.9 INTAKE CANAL

The intake canal carries water pumped from the river, which is the only source of cooling for the entire plant.

A3.2 BWR ITEM SELECTION BASIS

The components shown in Table X A-4 fall into eight groups whose safety-related functions are described briefly as follows:

A3.2.1 CONTAINMENT STRUCTURES

The drywell and suppression chamber provide the containment pressure boundary and passive suppression of pressure increase in the event of a LOCA. This structure is housed in the reactor building, which functions as a secondary containment barrier against the release of radioactivity off-site should there be an accident. Containment piping penetrations are intended to provide for the safe transfer of material through the containment boundary so that a pipe break will not cause a breach in containment integrity. The missile barriers provide shielding inside the drywell against a whipping pipe. As in the PWR case, excessive peeling of paint inside the containment could impair the proper functioning of the emergency core cooling systems.

A3.2.2 REACTOR COOLANT SYSTEM

Items in this group maintain the integrity of the reactor coolant pressure boundary as well as that of the radioactive steam produced by the BWR. Pipe lines and nozzle connections to the reactor must be capable of resisting seismic loads. The main steam isolation valves must prevent the large release of radioactive steam from within the containment. The pipe-whip restraints are intended to prevent a break in the recirculation line from causing a secondary failure in containment or engineered features. The reactor pressure relief valves are intended to prevent excessive pressure within the nuclear steam supply system.

A3.2.3 CORE SPRAY SYSTEM

This system provides emergency core cooling in the event of a large LOCA after the pressure in the reactor is reduced. All items in this group must be capable of resisting seismic events (which have the potential for causing a LOCA) and must be capable of continued operation in the environment following a LOCA. For this system, all items were analyzed.

A3.2.4 HIGH PRESSURE COOLANT INJECTION SYSTEM (HPCIS) TURBINE

The HPCIS provides initial injection of emergency core cooling in the event of a LOCA.

A3.2.5 RESIDUAL HEAT REMOVAL (RHR) PUMPS AND DRIVES

The system limits the temperature inside the containment after a LOCA by circu-

lating water from the suppression pool and cooling it via RHR heat exchangers.

A3.2.6 ON-SITE ELECTRIC POWER SYSTEMS

Emergency on-site power is provided by the diesel generator. The system is necessary to power engineered safeguards systems in the event of loss of off-site power. The day tank provides the initial source of diesel fuel for the system. The air bottle stores compressed air used in starting the diesel engine. Batteries provide emergency power for control systems necessary for the safe shutdown of the reactor.

A3.2.7 ELECTRIC POWER DISTRIBUTION SYSTEMS

These systems distribute power to the pump motors, motor-operated valves, and control-rod drives which are necessary for safe shutdown.

A3.2.8 REACTOR PROTECTION SYSTEM

The reactor protection system senses reactor water level, reactor pressure, and containment pressure. Through its logic system, it interprets conditions that call for immediate shutdown, initiates this action, and activates containment isolation and reactor core safety injection systems.

A4. DESIGN CRITERIA AND PRACTICES

Codes and standards for the design, construction, and operation of nuclear power plants, like codes and standards for conventional power plants and other processing plants, are under continual review and revision. The codes and standards in existence at the time the two plants used in this study were approved have undergone considerable revision in the 6 to 8 years since initial review. For this reason, the plants studied fail to meet all the codes and standards that are invoked for plants currently being licensed. On the other hand, the PWR and BWR plants were designed and constructed to somewhat more rigid requirements than were the previously designed fossil and nuclear plants that provide the data base for the component failure rates used in the RSS. It is clear, therefore, that, in principle, the reliability of the PWR and BWR plants should be at least as good as the reliability of those plants from which data have been derived. By the same token, future plants, including those now under construction, must meet more stringent design, construction, and operational codes and standards than do the plants used in this study. Thus, the reliability values used in the RSS are probably somewhat conservative, and, although the plants used in the study may not meet all the requirements of present codes and standards, their design criteria requirements are at least as good as those of the facilities that have provided basic failure rate data.

Our study centers primarily on safety components (i.e., those necessary for safe operation and safe shutdown) and the ability of the engineered safeguard systems to function as required.

Each applicant for a nuclear power plant construction permit or operating license is required to provide assurance that all safety-related equipment will perform adequately under all its service conditions, including normal operation, maintenance, and testing (both of the component itself and of other parts of the plant which may subject the component to unusual service conditions), and design basis events, such as earthquakes and accidents.

Section III, "Design Control," of Appendix B, "Quality Assurance Criteria for Nuclear Power Plants and Fuel Reprocessing Plants," to 10 CFR Part 50, "Licensing of Production and Utilization Facilities," requires that a test program used to verify the adequacy of a specific design feature include suitable qualification testing of a prototype unit under the most adverse design conditions. The overall quality assurance program for nuclear power plant equipment includes, but is not limited to, design, qualification, production quality control, shipping and storage, installation, maintenance, and periodic testing. The FIRL design adequacy study included a review and evaluation of the qualification portion of the overall quality assurance program.

The primary role of qualification is to ensure that, for each item of safety-related equipment, the design and manufacturing processes are such that there is a high degree of confidence in the reliability of installed equipment. The other steps in the quality assurance program require strict control to ensure that the equipment installed in the plant is the same type as that which was qualified and that the production items are suitably applied, installed, maintained, and periodically tested.

Essentially, a component is assumed to be functional only if it meets estab-

lished codes and regulations as evidenced by the SAR and by specific supporting documentation of design adequacy which is kept on file. It is recognized that the evidence presented to establish design adequacy can take many forms.

Equipment qualification requirements and methods are embodied in criteria, standards and guides (Refs. 1 through 8) prepared by committees of the Institute of Electrical and Electronics Engineers (IEEE), American Society of Chemical Engineers (AIChE), and other professional societies. These documents are then forwarded to the American National Standards Institute (ANSI), which either endorses (adopts) them or returns them for revision. The AEC then either accepts this document as its requirement, or issues a Regulatory Guide containing detailed requirements, sometimes supplementing those in the industry guides. It should be noted that AEC personnel hold membership on most of the professional society committees which prepare industry standards documents. In this way the AEC viewpoint usually becomes incorporated into the documents. Meetings of the committees are extremely valuable because they provide a relatively informal setting in which industry and government representatives can explore each other's point of view and basis for desiring that certain features be incorporated into the documents. Misunderstandings can be eliminated, or at least minimized, and a technically strong document developed.

Qualification requirements are constantly changing, becoming more stringent as industry, the AEC, and the professional societies concerned with the preparation of test standards gain knowledge about the procedures needed to ensure the reliability of safety-related equipment. When the BWR and PWR plants considered in this study were designed and the equipment was purchased, qualification requirements were very general. This situation placed a great burden on the design engineers who had to interpret the generalities in terms of specific procedures for each type of equipment. For example, seismic qualification of components was not required initially, and even after seismic qualification became a requirement, it took a long time for the AEC and the industry to translate the general requirements into specific requirements. This process is still under way. Part of the problem has been that the equipment necessary to conduct many of the tests is not available and, because the tests are highly specialized and the test requirements have been changing constantly, test facilities have only slowly come into existence. The greatest part of the problem, however, is that in other fields standards have been developed after practices have become accepted in the industry. In the nuclear industry, the preparation of standards is required before diverse practices are established, and thus aspects of the standards must deal with matters which have not been studied and for which the state of technical knowledge may be rather limited.

The need for a more intensive effort in developing standards for the nuclear industry has been recognized, and the level of activity has increased dramatically in the past two years.

Type testing of actual equipment using simulated service conditions is usually the preferred method of qualifying equipment. However, a type test alone satisfies qualification only if the equipment to be tested is properly aged, subjected to all important environmental influences, and operated under post-event conditions to provide assurance that all such equipment will be able to perform its intended function for at least the required operating time. Partial type tests may be augmented by tests of components when size, applications, time, or other test limitations preclude the use of a full type test on the complete equipment package.

A5. METHOD OF EVALUATION

The following sections describe the procedures by which the review team acquired and evaluated the information used to assess the design adequacy of the systems and components noted in section A3.

A5.1 INFORMATION ACQUISITION

A5.1.1 FINAL SAFETY ANALYSIS REPORT REVIEW

Background material and preliminary information were acquired by reviewing the final safety analysis reports (FSAR) which describe the physical aspects of the PWR and BWR sites, including their geology and seismology, design bases, functional aspects, operational requirements, design evaluation, and test and inspection requirements for the plants and their various systems.

The FSAR is a large document consisting typically of 15 sections, technical specifications, supplements describing

questions by the AEC and answers by the owner, appendices, and supplementary reports.

A5.1.2 SITE VISITS

The review team visited the PWR and BWR sites and toured the plants, with the exception of high radiation areas. The PWR was in operation at the time of the visit, and the BWR was preparing for initial start-up. The PWR safety-related piping, motors, pumps, cable trays, tanks, diesel generator, controls, battery rooms, logic cabinets, and intake canal were inspected. The tours were conducted by plant operating personnel. Special attention was given to the installation, support, and attachment of equipment.

A5.1.3 VISITS TO ARCHITECT/ENGINEERS, UTILITIES, AND SUPPLIERS

The FSAR primarily describe the design bases and functional requirements for the plant systems and components; they do not present the design calculations and test procedures in sufficient detail for an assessment of design adequacy.

The detailed calculations and test reports are retained by the A/E and by the various equipment suppliers. In many cases this information is considered proprietary; so the A/E and the NSSS suppliers would not permit removal of this information from their premises. However, because these firms wanted to cooperate with the RSS, they permitted the review team to examine the material on the premises. The cognizant engineer (if available) responded to our questions, and we were able to make notes and copies of pertinent data.

We also visited the utility that owns the BWR.

A5.1.4 REVIEW DATA SHEETS

The review team used review data sheets and supplementary review data sheets (Figs. X A-1 and X A-2) during the meetings with the A/E and suppliers. We used these sheets as guides in carrying out the review and also as a means of recording pertinent information. The information on these sheets was then evaluated as described in section A5.2. The design adequacy assessment is reported in section A6.

A5.1.5 OTHER DOCUMENTS REVIEWED

In addition to the FSAR, design calculations, and test reports, we reviewed the safety evaluation reports prepared by the AEC for each plant, design specifications, and pertinent portions of governing codes and standards, such as the B31.1 USA Standard Code for Pressure Piping. We also reviewed pertinent AEC regulatory guides, which supplement the codes and standards with the latest methods and techniques acceptable to the AEC. These are referenced in appropriate sections of this report.

A5.2 EVALUATION OF INFORMATION

We evaluated the information acquired with the objective of drawing conclusions about design adequacy, as detailed in section A1.2. Evaluations were based on the considerations described in this section.

Time did not permit extensive spot-check independent analysis. We did, however, perform an independent analysis of the BWR core spray piping (section A6.4.3.1) to compare the results of evaluating the piping in accordance with the currently required NB-3600 of the ASME Code, Section III, with the results obtained using USAS B31.1, which governed the design at the time of construction.

In addition, if our review uncovered calculations or assumptions that seemed unreasonable, we made very conservative simplifying assumptions to estimate an upper bound on stresses. If the results were within the allowables, the design was considered adequate. If, however, the resulting stress values exceeded the allowables, we informed the A/E or NSSS supplier that the original calculations would have to be revised.

A5.2.1 CODES AND STANDARDS

Pertinent portions of the codes and standards cited in the FSAR as governing the design were reviewed to verify that computed stress levels were within allowable values. An assessment was also made to determine whether the equipment would meet current requirements.

A5.2.2 APPROPRIATENESS OF MATHEMATICAL MODELS

Perhaps the most important step in the analysis process is the development of the mathematical model as an idealization of the real system. When the engineer creates a mathematical representation of a real system, he makes a judgment about what kind of phenomena are significant and therefore should be included in the model and what phenomena are insignificant and therefore should be excluded. The review team checked

the appropriateness of the models used in the calculations.

The most common modeling error we encountered during the course of this review was the implicit assumption of a shear connection between multi-element structures having a common connection to a fairly rigid structure at either end, such as the yoke that separates the valve operator from the valve (Fig. X A-3). The analyst assumes that the multi-element structure acts as a single-element cantilevered beam of length L with a cross-sectional moment of inertia described by:

$$2\left(\frac{A}{2}\bar{x}^2 + I_{zz}\right).$$

This incorrect modeling may give rise to computed stiffnesses and associated frequencies which are far in excess of their correct value and which could lead to unconservatively low seismic loads. Dynamic interaction between the structure and heavy equipment, such as the NSS System, should also be considered in modeling. Guidelines for using decoupled models rather than a single, more complex model are given in Ref. 1.

A5.2.3 ADEQUACY OF LOAD DEFINITIONS

Our review included an evaluation of the seismic loads used in the analysis and/or testing of equipment and a comparison of these loads with the expected seismic loads. Since the seismic loads are obtained from the frequency-dependent response spectra curves, an error in the computation of natural frequencies may lead to an error in seismic loads.

Seismic loads are sometimes developed by one group or company and used by another group or company for analysis and evaluation of equipment. This presents potential interface problems that could lead to significant errors. During our evaluation, we looked for these situations.

A5.2.4 ADEQUACY OF BOUNDARY CONDITIONS

Boundary conditions implicit in the analysis of any system that is assumed separated from its surroundings for purposes of study were evaluated to see if the assumed boundary conditions were reasonable. For example, hydraulic snubbers provide a "spring" (albeit generally stiff) support but are often assumed to provide a rigid constraint on pipe displacement. We considered the effect of this departure from the real condition.

A5.2.5 ADEQUACY OF COMPUTER CODE NUMERICAL TECHNIQUES

We did not make an extensive check on computer codes since verification of computer codes with experimental results, or by obtaining the same result for a given problem with two independent codes, is generally required before AEC acceptance.

A5.2.6 EFFECT OF VARIATION ON MATERIAL PROPERTIES

Only the variation in shear modulus for the soil used in the soil-structure interaction model (see section A6.3.1.1) was considered in our evaluation. Variation in Young's modulus for concrete is generally accounted for in the peak broadening of the floor response spectra curves.

The modulus of elasticity for various steels for nuclear applications is given in Table I-6.0 of the ASME Code, Section III. There is negligible variation of Young's modulus, E, for steel of a given composition; there is a slight decrease with increasing temperature, however. The value of E for austenitic stainless steel, for example, decreases from 28.3 x 10^6 psi at 70°F to 27.1 x 10^6 psi at 300°F. This represents a decrease of 4% and would give rise to a decrease in natural frequency of 2%, a change which is not considered significant.

A5.2.7 ADEQUACY OF QUALIFICATION TEST PROGRAMS

The procedure for evaluating the adequacy of equipment that had been qualified, wholly or partially, by test included the following salient features. First, we made an effort to establish the safety-related function of the equipment and the conditions under which it is expected to function. Then we evaluated the available reports containing information on qualification tests with reference to applicable AEC regulatory guides and industry standards (principally IEEE and ANSI equipment qualification guides). This included an evaluation of the applicability of, and the adequacy of proof for, satisfactory performance under the following conditions:

a. Degradation occurring during the installed life under normal conditions, including thermal aging, radiation aging, and normal wear aging.

b. Seismic disturbance.

c. Loss-of-coolant accident (LOCA), including exposure to nuclear radiation, steam, and sprays of demineralized water and chemical solutions.

Although we were able to note whether aging had been simulated, we were generally unable to evaluate the adequacy of the simulation. Not only is the theory of accelerated thermal aging to simulate exposures of up to 40 years not well established but data on the bases for the selection of the temperature and the duration of thermal aging exposures for particular equipments were not available to us. Since the radiation exposures required to simulate normal and accident conditions have been established, the adequacy of radiation resistance was relatively easy to evaluate. The evaluation of seismic qualification involved a comparison of the acceleration levels and frequency response spectrum anticipated at the equipment location with those used in the tests and, in some cases, independent qualitative analysis of the vulnerability of equipment to seismic disturbances. Evaluation of equipment performance under LOCA conditions included a comparison of the predicted in-plant environmental exposure profiles with the exposure profiles used in the test program.

A6. EVALUATION OF COMPONENTS

This section summarizes the results of the review of PWR and BWR plant components.

Section A6.1 describes the overall seismic effects, with particular emphasis on the definition of seismic loads for PWR and BWR plants.

Section A6.2 describes the tornado effects on the diesel generator buildings which house the source of emergency power.

Sections A6.3 and A6.4 present the results of the component reviews for the PWR and BWR plants, respectively, together with commentary and conclusions.

Tables X A-5 and X A-6 (PWR) and Tables X A-7 and X A-8 (BWR) provide a summary of the components reviewed and an assessment of their design adequacy. Tables X A-5 and X A-7 give the results for components that were reviewed from the viewpoint of seismic design adequacy. An assessment of the tornado resistance of the diesel generator building is also included in Tables XA-5 and X A-7. Tables X A-6 and X A-8 give the results for components that were reviewed from the viewpoint of resistance to normal and LOCA environments.

The tables indicate whether the design of a component is such that failure is not expected and the component is therefore judged "adequate" or whether failure is possible so that adequacy is "not demonstratated." The assessment of design adequacy is indicated by a check mark in one of five columns as follows:

Failure Not Expected (Design is considered adequate)

1. Design criteria, as explicitly stated in FSAR (or in accordance with current criteria and practice if not explicitly stated in the FSAR), have been satisfied by analysis and/or test.

2. Design criteria have been satisfied on the basis of engineering judgment.

3. Although the design criteria have not been completely satisfied, loss of function is not expected. In some cases more sophisticated analysis methods may show that the design criteria have been satisfied.

Failure Is Possible (Design adequacy has not been demonstrated)

4. There is insufficient information to assess adequacy.

5. The information reviewed indicates that failure is likely.

The tables generally summarize our evaluation of design adequacy in accordance with the criteria stated in the FSAR. We made exceptions only when current knowledge indicated that the original criteria were in error (for example, the original design temperature for the BWR of 286°F was superseded by a higher design temperature of 340°F) or when explicit criteria were not stated in FSAR.

Current criteria and practice are discussed and compared with the original criteria in the "commentary" portions of the text.

A6.1 SEISMIC EFFECTS

A6.1.1 PWR PLANT

A6.1.1.1 Seismic Loads.

The site of the PWR is founded on 1300 ft of soil above bedrock. On the basis

of tectonic considerations and the seismic history of the area within a 350-mile radius of the site, the maximum acceleration at bedrock is expected to be no higher than 0.07g. With soil damping equal to 10% of the critical value, soil-surface acceleration is calculated to be 0.14g. This figure does not include soil-structure interaction.

The following seismic loads are considered for this plant:

a. Operating basis earthquake (OBE)

0.07g horizontal
2/3 (0.07)g vertical

b. Design basis earthquake (DBE)

0.15g horizontal
2/3 (0.15)g vertical

The adequacy of Class I structures is evaluated on the basis of the ground response spectra shown on Fig. X A-4 (OBE) and Fig. X A-5 (DBE). These curves are taken directly from the FSAR for the BWR plant and (although somewhat atypical in appearance) were derived from Housner's average response spectra normalized to the maximum expected ground acceleration for this plant.

The adequacy of Class I components is evaluated on the basis of floor spectra calculated from Taft's earthquake time history record normalized to the ground acceleration levels of this site. Initial analysis of components was based on ground acceleration spectra. Later this was modified to include amplification due to structural response.

A6.1.1.1.1 Commentary. The maximum ground acceleration experienced within a 100-mile radius of the site since the 18th century is estimated at 0.05g on the basis of the estimated seismicity of the region. The tectonics of the region appear to have been carefully considered. The ground accelerations of 0.07g for the OBE and 0.15g for the DBE therefore appear to be reasonable values for the purpose of design. The design ground response spectra currently required by the AEC (Ref. 1) generally give higher responses than those derived from the average Housner spectra. The damping values currently required by the AEC (Ref. 2) are generally higher than those acceptable at the time the plant was designed. For example, 5% damping for both the DBE and OBE was used for the reinforced-concrete containment structure. As shown in Table X A-9, this value is lower than the currently acceptable value of 7% for the DBE but is higher than the current 4% for the OBE. The 5% response spectra curve used in the design of the BWR (curve 5) for the OBE may be compared with the ground response spectra curve currently required (curve 4) in Fig. X A-4. Note that the current design curve gives a maximum acceleration of 0.22g at 2.5 cps compared to the PWR design value of 0.11g between 2 and 4 cps.

Figure X A-5 shows a comparison between the response spectra used in the design of the PWR for the DBE (curve 5) and that currently required (curve 7). The current design curve gives a maximum acceleration of 0.4g at 2.5 cps as compared to the PWR value of 0.22g between 2 and 4 cps.

It is not surprising that the current design response spectra given in Regulatory Guide 1.60 are higher than those used in the design of the PWR. The PWR curves were based on the Housner spectra, which represent average values, whereas the current design response spectra represent 1 positive standard deviation from the average values.

It should be emphasized here that Regulatory Guide 1.60 indicates that the design response spectra curves may not be applicable for sites that "have physical characteristics that could significantly affect the spectral combination of input motion." For such sites the design response spectra should be developed individually according to the site characteristics. Because the PWR is on 1300 ft of soil over bedrock, individual spectra would be more appropriate.

The vertical component of the earthquake for the PWR design is two-thirds of the horizontal component; the current design requirement (as indicated in Regulatory Guide 1.60) is as follows:

Frequency (cps)	Horizontal / Vertical
<0.25	2/3
0.25 to 3.5	2/3 to 1
>3.5	1

The first two frequencies for the seismic analysis model of the PWR reactor building were computed to be 2.34 and 5.10 cps, which fall on either side of 3.5 cps, implying that the required seismic response spectra in the vertical direction are approximately the same as in the horizontal direction.

The seismic loads used in the design of the PWR were in accordance with accepted practice at the time the plant was built; however, the Class I structures would be subject to seismic loads higher by a factor of approximately 2 if current design spectra and damping values were imposed. On the other hand, specially developed spectra that account for the 1300 ft of soil over bedrock may show the factor to be less than 2.

Floor response spectra at the charging level of the reactor building were developed on the basis of the Taft earthquake time history record. A damping value of 0.5% critical was used to generate these curves. Table X A-9 shows that currently acceptable damping values are 2% critical or higher. It is estimated that the higher damping values would lead to a seismic load reduction of 30%. However, since the seismic loads on structures may increase by a factor of 2, the net result may be an increase of 40% in the seismic loads on equipment.

A6.1.1.1.2 Conclusion. We conclude that:

a. The seismic loads used in the design of the PWR were in accordance with accepted practice at the time the plant was built.

b. The use of current design response spectra curves and current damping values could lead to:

   1. An increase in seismic loads on PWR structures by a factor of up to 2.

   2. An increase in seismic loads on PWR equipment of up to 40%. (Note that we do not consider the effect of these higher loads.)

c. A specially prepared site spectra accounting for local soil characteristics may show that the increases are not as large as indicated in item b.

A6.1.1.2 Damping.

Table X A-9 shows the damping values used in determining the dynamic response of the PWR and the values currently required by the AEC as described in Ref. 2.

A6.1.2 BWR PLANT

A6.1.2.1 Seismic Loads.

Two Earthquakes with maximum ground acceleration have been considered as follows:

a. Design earthquake (DE)[1]

   0.05g horizontal
   2/3 (0.05)g vertical

b. Maximum credible earthquake (MCE)[2]

   0.12g horizontal
   2/3 (0.12)g vertical

Class I structures have been analyzed on the basis of the ground response spectra shown in Fig. X A-6 (DE) and Fig. X A-7 (MCE). These curves are based on Housner's average response spectra normalized to the maximum expected ground acceleration.

Class I BWR structures (reinforced concrete) have been assigned 2% critical damping for the DE and 5% critical for the MCE; currently acceptable values are 4% and 7% (Table X A-10).

Figure X A-6 shows the current Regulatory Guide 1.60 design response spectra for 4% critical damping (curve 4) as compared to the 2% (curve 2) used in the design of the BWR structures for the DE. These curves show a current peak acceleration of 0.18g at 2.5 cps as compared to a peak value of 0.15g at 3.5 cps for the DE. Similarly, Fig. X A-7 shows a current peak acceleration of 0.27g at 2.5 cps as compared to 0.23 g at 2.5 cps for the MCE.

Note that the vertical stiffness of the Class I structure was high; thus a maximum vertical ground acceleration of two-thirds of the horizontal ground acceleration was used in the design. Regulatory Guide 1.60 indicates that for frequencies greater than 3.5 cps the

---

[1]The DE for the BWR is the same as the OBE for the PWR, i.e., an earthquake for which safety-related equipment should remain operational during and after the event.

[2]The MCE for the BWR is the same as the DBE for the PWR, i.e., an earthquake for which safety-related equipment should remain operational so that a safe and orderly shutdown of the plant can be achieved and maintained.

vertical acceleration is equal to the horizontal acceleration.

Equipment was designed using floor response spectra generated on the basis of a Taft earthquake time history record modified so that its associated response spectra are equal to or greater than the site ground response spectra.

Table X A-10 shows that currently acceptable damping values are generally 2% critical or higher as compared to the 0.5% used in the BWR for equipment such as piping. This difference could lead to a seismic load reduction of 30% on equipment, which, when factored with the increased seismic loads on structures, leads to a slight net reduction in seismic loads on equipment.

A6.1.2.1.1 Commentary.

a. The DE and MCE maximum ground accelerations appear to be reasonable and appropriate in view of the seismological characteristics of the area as described in section A2.1.2.

b. Since Class I structures are built directly on bedrock (which was overlain by only 10 ft of soil), there is no need to consider the problems and uncertainties associated with soil-structure interaction (see section A6.3.1.1). Thus, the basic seismic input load characteristics can be viewed with a high level of confidence.

c. The design response spectra curves currently required by the AEC (Ref. 1) could lead to an increase in seismic loads of up to 20% for the DE and 17% for the MCE in the horizontal direction and an increase of 50% in the vertical direction for Class I structures.

A6.1.2.1.2 Conclusion. We conclude that:

a. The seismic loads used in the design of the BWR were in accordance with accepted practice at the time the plant was built.

b. Class I structures could be subject to seismic loads up to 20% in excess of those used for the horizontal earthquake and 50% higher for the vertical earthquake if current design response spectra were imposed. Our review considered the design adequacy of buildings only from the viewpoint of mathematical modeling to obtain seismic inputs for equipment. The effect of higher seismic stresses on structures due to these higher loads has not been evaluated therefore.

c. Seismic loads on equipment could be slightly reduced if current response spectra and damping values were used.

A6.1.2.2 Damping.

Table X A-10 shows the damping values used in determining the dynamic response of the BWR and the values currently required by the AEC as described in Reference 2.

The damping values used in analyzing for the DE are all less than or equal to currently accepted values. Similarly, the values used for the MCE are less than the currently accepted values, with the exception of those for steel-frame structures and bolted and riveted assemblies, which are somewhat higher than the current values.

A6.2 TORNADO EFFECTS

A6.2.1 PWR PLANT

The tornado design criteria governing the diesel generator building are given in Reference 3 and summarized as follows:

a. External wind forces resulting from a tornado having a rotational velocity of 300 mph and a translational velocity of 60 mph for a combined maximum velocity of 360 mph. The diameter of the eye of the tornado is 1000 ft, and the maximum winds extend a radius of 200 ft.

b. Atmospheric pressure drop of 3 psi in 3 sec. Venting can be used to relieve or reduce this pressure drop.

c. Missiles equivalent to a 40-ft-long by 12-in.-diameter 50 lb/ft^3 utility pole with a velocity of 150 mph and impacting on horizontal or vertical building surfaces and a 1-ton auto with a velocity of 150 mph.

In addition, the criteria incorporate a procedure for calculating the wind forces, as set forth in ASCE Paper No. 3269, Transactions, 1961, and state that wind forces and the effects of missiles shall be considered simultaneously. The following allowable stresses are also established:

a. Rolled steel plates and shapes - 90% of minimum specified yield stress.

b. Steel-reinforcing bars - the minimum yield stress multiplied by the capacity reduction factors as specified in Section 1504 of ACI 318-63.

c. Concrete - 75% of the ultimate strength.

Commentary

The criteria for tornado winds and missiles are similar to those considered today and are considered adequate. The allowable stress limits for the steel reinforcing bars appear to have no conservative margin.

Section A6.3.6.1 presents a detailed discussion of the structural resistance of the diesel generator building to tornado loads.

A6.2.2 BWR PLANT

The diesel generator building is required to meet the design limits under the following loading conditions:

a. External wind forces resulting from a tornado having a horizontal peripheral tangential velocity of 300 mph, which includes the tangential and translational components.

b. Differential pressure of 3 psi between the inside and outside of fully enclosed areas. Blowout panels are to be included where necessary in the design of the structure to limit pressure differentials.

c. Missiles equivalent to a 4-in.-thick by 12-in.-wide by 12-ft-long wood plank traveling end-on at 300 mph, or a 4000-lb passenger auto, with a contact area of 20 ft^2, flying through the air at 50 mph not more than 25 ft above ground.

d. A torsional moment resulting from applying the wind specified in item a, above, acting on one-half the length of the building.

Commentary

General practice at present is to consider a tornado with a combined horizontal peripheral tangential velocity of 360 mph.

More recent plant design criteria consider a greater variety of more severe missiles. A comparison of the missiles used in the BWR design with those used in more recent plants is given in Table X A-11.

A comparison of the characteristics listed in Table X A-11 shows that the currently considered auto missile with a velocity of 147 ft/sec (100 mph) has about twice the momentum of the auto specified for the BWR under review. The sliding panel under current design requirements has a kinetic energy per unit impact area (a measure of penetration capability) more than four times as great as the wood plank considered in the BWR design.

Section A6.4.6.1 presents a detailed discussion of the structural resistance of the diesel generator building to tornado loads.

A6.3 DESIGN ADEQUACY OF PWR PLANT COMPONENTS

A6.3.1 REACTOR BUILDING

The reactor building in this plant is a reinforced-concrete containment structure. As shown in Fig. X A-8, the structure is basically a cylinder with a hemispherical dome and a flat base. The internal height is 185 ft and the ID is 126 ft. The base mat is 10 ft thick, and the cylindrical walls are approximately 5 ft thick. During normal plant operation the containment is maintained at a subatmospheric pressure of 9.0 to 11.0 psia.

A6.3.1.1 Soil-Structure Interaction Model.

The seismic response of the PWR reactor building structure to the horizontal component of the earthquake was originally obtained on the basis of a 4-degree-of-freedom mass-spring model as shown in Fig. X A-9. Here k_1 and k_4 represent the static horizontal and rocking soil stiffnesses, respectively. A subsequent analysis was performed using a 14-degree-of-freedom model. In this model the external and internal structures are represented by 7 and 5 masses, respectively, as compared to 1 mass each in the 4-degree-of-freedom model. For both models each mass is assumed to have a horizontal translational degree of freedom. In addition, the structure is assumed to be capable of rotating as a rigid body in a single rocking mode.

An independent check was made to determine if significant rocking modes other than those permitted by the A/E model could exist. In particular, it was noted that the internal structure from the base mat to a height of 25 ft above the base mat consists of a blocked-out

structure (columns uniformly distributed on the outside diameter of the structure). A rough calculation indicates that the rotational stiffness of the internal structure supported on the blocked-out section is 7.7×10^9 ft-kip/rad as compared to 2.7×10^9 ft-kip/rad rotational stiffness of the soil. The total rotatory inertia participating in the rigid-body rocking mode is estimated at 20×10^6 kip-sec^2-ft, while the rotatory inertia associated with the internal structure is only 0.8×10^6 kip-sec^2-ft. It follows then that the frequency associated with the rocking of the internal structure is considerably higher than that of the overall rigid-body rocking mode. This implies that the dynamic response of the internal structure rocking mode is of no significance compared to the overall rigid-body rocking mode.

The frequencies computed using the 4-degree-of-freedom model are compared with those computed using the 14-degree-of-freedom model in Table X A-12.

The results shown in the table are based on a soil shear modulus of G = 18,000 psi (2592 ksf). The A/E estimates that this value may in fact vary as much as +15% or -30%. The sensitivity to this variation in soil property was considered by the A/E in the 14-degree-of-freedom model but not in the 4-degree-of-freedom model.

The 4-degree-of-freedom model was used to compute the seismic stresses in the reactor building on the basis of the ground response spectra, whereas the 14-degree-of-freedom model with a time history record was used to determine the floor response spectra at the charging floor elevation.

The A/E investigated the possibility of soil liquefaction (loss of shear resistance) under seismic vibratory loads and concluded that there is an adequate margin of safety against liquefaction for a hypothetical ground acceleration of up to 0.25g.

The response of the system was determined from the ground response spectra curves corresponding to 5% of critical damping for the OBE and 10% of critical damping for the DBE. The A/E performed calculations to estimate strain energy dissipated in each mode and came up with average values of percent critical damping for each mode as shown in Table X A-13.

A6.3.1.1.1 Commentary. The soil-stiffness calculation is based on elastic half-space loaded with a rigid disk (representing the base mat), with formulae taken from Reference 4. The analysis, however, did not consider the effective mass of the soil, which is estimated to be approximately 25% of the base mat mass or less than 10% of the total mass of the reactor building and hence of minor significance.

Since the motion of the structure is dominated by the first three modes, Table X A-13 indicates that the 5% and 10% damping values used to determine the dynamic response are reasonable.

The model does not account for embedment of the containment structure in the soil nor does it account for the differing shear moduli of the various soil layers. Re-examination of the soil-structure interaction problem using finite element techniques could account for these effects.

A6.3.1.1.2 Conclusion. We conclude that the soil-structure interaction model gives reasonably conservative seismic loads on the structure.

A6.3.1.2 Containment Internal Structure.

The containment internal structure consists of a reactor support pedestal (13 1/2 ft radius, 4 1/2 ft thick) and 25-ft-tall columns arranged around a 103-ft-diameter circle (see Fig. X A-8). The cross sections of these columns are approximately 8 ft in the circumferential direction and 2 ft in the radial direction. The lower portion of the reactor support pedestal (approximately 14 ft above the base mat) has a part cut out of its cross section (Fig. X A-10).

The internal structure was reviewed only from the viewpoint of mathematical modeling to obtain seismic inputs to equipment such as the reactor coolant system loop. The structure itself was not evaluated from the viewpoint of seismic resistance.

A6.3.1.2.1 Commentary. Review of the design calculations indicated that the mathematical modeling of the lower portion of the internal structure (the first 25 ft above the base mat) does not properly account for the considerable reduction in the lateral stiffness due to the blocked-out structure. The A/E replaced the individual circumferential column cross sections by an "equivalent" annular ring with a reduced thickness. The cross-sectional moment of inertia of this ring, together with that of the core, was computed, and the sum of these

values, together with the sum of the cross-sectional shear areas, was assigned to the beam properties of the structure between the base mat and the mass 1 of the 14-degree-of-freedom model.

Independent calculations indicate that a stiffness value equal to 2,812,000 kip/ft would result for the lower portion of the internal structure with the dimensions indicated for the equivalent solved cylinder representing the blocked-out internal structure.

This stiffness value, however, is unrealistic in that the A/E's mathematical modeling implies that all the columns have some shear connection throughout their 25 ft length when, in fact, they are connected only at the top (via floor slabs) and at the base mat. The appropriate method of computing the lateral stiffness of the lower portion of the internal structure is by summation of the lateral stiffness of the individual columns, under proper consideration of individual column orientations, and of the core. Such an independent calculation results in a lateral stiffness of 1,262,041 kip/ft for the reactor support and 185,000 kip/ft for the peripheral columns or a total of 1,447,016 kip/ft.

In accordance with the above, the actual stiffness of the internal structure is about 51% of that used by the A/E. In addition, since the lateral stiffness of the lower portion of the internal structure is only a fraction of that of the upper 96 ft, more of the internal structure mass will participate in the first flexural mode (the third mode of the soil-structure interaction model) than is accounted for in the A/E's model. It is estimated that twice as much of the internal structure mass will participate in the flexural mode than is calculated by the A/E. This means that both the modal participation factor (which is a measure of the participation of a particular mode to the total forcing function) and the modal effective mass (which is a measure of the modal reaction at the base of the structure) will be greater for the flexural mode than is implied by the A/E model.

As a result of our investigation, the A/E revised his calculations using the correct stiffness properties and recomputed frequencies, mode shapes, modal participation factors, and seismic response. A comparison of the original calculations with the revised calculations shows very small differences of less than 10%. The reason for this small difference, in spite of a difference of almost 100% in an element stiffness value, can be explained by referring to Fig. X A-9. Note that the internal structure (m_3) mass is 310 kip-sec^2/ft as compared to a total mass of 3185 kip-sec^2/ft, that is, less than 10%. Apparently the system dynamics are dominated by the rigid-body motion associated with the first two modes as revealed by the modal participation factors shown in the following table.

Mode	Modal Participation Factor
1	1.563
2	-0.708
3	0.140
4	-0.012

A6.3.1.2.2 Conclusion. In spite of the differences noted in the commentary, the significance of the error in computing the stiffness properties of the internal structure is negligible since the seismic response is dominated by the rigid-body modes (rocking and translation) of the system. We conclude, therefore, that the seismic input to equipment resulting from the seismic analysis of the internal structure is adequate.

A6.3.1.3 Paint Coatings Within Containment.

The internal surface of the containment liner, internal concrete structure, and metallic components are coated with special paint coatings. Aside from aesthetic purposes, coatings are used to prevent corrosion of metal surfaces and to seal the concrete. The coatings must be able to withstand normal and accident environments without becoming separated from the walls in any way, such as by ruptured blisters, flaking, and cracking. Excessive delamination of coating films could cause the strainers in the containment spray and safety injection systems to clog and would interfere with their proper operation.

Two specimens of each of the coating systems were subjected to a qualification test involving simultaneous exposure to gamma radiation, steam, and chemical spray for a period of 7 days. The exposure to simulated LOCA conditions began with a rapid injection of steam, followed by a 40-min dwell at 280°F and a 20-min drop to 140°F, where the temperature was held for the remainder of the test. The coating specimens were sprayed with three different chemical solutions during the test. The total gamma-radiation dose

received by the coatings during the test was 100 megarads.

The specimens at the conclusion of the test showed no significant degradation of any type.

A6.3.1.3.1 Commentary. Comparison of the qualification test conditions with those postulated under maximum LOCA conditions shows that during the first hour, the test temperature profile exceeds the calculated containment temperature profile by a substantial margin, the smallest difference being about 10°F at the peak containment temperature. The margin between the two temperatures decreased during the second hour of the test; thereafter, the test temperature was the same as the calculated design basis accident (DBA) temperature. The gamma-radiation exposure and chemical sprays used in the test were essentially the same as those expected in the plant.

Based on present qualification philosophy and ignoring, for the moment, considerations regarding the number of specimens tested, the coatings may be regarded as being qualified for somewhat less than a week following a LOCA event. The utility has reported that this is an adequate period for the coatings to retain their integrity. A few days after a LOCA event, cooling requirements are not critical, and any degradation of cooling system performance caused by coating failure would not have serious consequences.

There remains the question of whether two specimens constitute an adequate sample of each coating system. Analysis of this subject has shown that tests must be made of a relatively large number of specimens (about 50) with no coating failures to yield modest confidence (about 90% confidence level) in the adequacy of the coating system. In addition, experience has shown that it is difficult to establish that the coatings on test samples are fully equivalent to the coating actually applied because the application techniques and local climatic conditions have a strong influence on the ability of the coating to adhere properly under LOCA conditions. In this respect the qualification test is somewhat deficient when judged in terms of the evolving qualification philosophy.[1] At the time the plant was constructed, however, the qualification requirements were relatively rudimentary; thus the results obtained were regarded as being adequate to demonstrate satisfactory performance. It should also be stated that the qualification test was more realistic than many that are conducted in that nuclear radiation, steam, and chemical spray were applied simultaneously. Most tests that have been conducted have involved sequential exposures to these environmental conditions.

A6.3.1.3.2 Conclusion. The qualification test established that there is a reasonably good probability that the coating systems will not experience large-scale failure (flaking and/or delamination) should a LOCA occur.

A6.3.1.4 Crane.

The crane is at elevation 99 ft 1 1/2 in. directly over the containment spray headers. A dynamic analysis of the crane was performed by the A/E. The fundamental frequencies of the crane with the hoist trolley at mid-span with no hoisted load on the hook were found to be 4.2 cps in the vertical direction and 2.27 cps in the horizontal direction. The A/E determined the seismic accelerations from the 5% equipment damping response spectra curves at the charging floor elevation to be as follows:

Earthquake	Acceleration (g)
Vertical-OBE	0.19
Vertical-DBE	0.30
Horizontal-OBE	0.62
Horizontal-DBE	0.84

The A/E stresses computed on the basis of the above accelerations are shown in Table X A-14. Note that the maximum stress was found to be 24.12 ksi; it occurs in the end ties (which connect the two girders that span the crane wall) and is due to the horizontal DBE. This stress value is compared to 90% of the yield strength = 32.4 ksi.

A6.3.1.4.1 Commentary. The seismic evaluation of the crane, under the assumption that there is no lifted load on the hook, is reasonable since this would be the normal condition when the reactor is in operation.

The acceleration values considered by the A/E were based on the response spec-

[1] At this time, a formal, accepted standard is not in existence, and there is no explicit requirement regarding sample size.

trum at the charging floor elevation, assuming equipment damping of 5% of critical. This high damping value is not in agreement with the values given in the FSAR. Table X A-9, which summarizes the FSAR values, shows a 2% damping value for mechanical equipment for both the OBE and the DBE. The currently accepted values, as given in Regulatory Guide 1.61, allow 2% for the OBE and 3% for the DBE. In our judgment, if these damping values are used, the higher design ground response spectra given in Regulatory Guide 1.48 should be used. If we adhere to the 2% values given in the FSAR for the PWR, then the peak accelerations in the horizontal direction would be 1.425g for the DBE and 1.05g for the OBE, which occur over the frequency bandwidth of 1 to 8 cps, encompassing the 2.27 cps natural frequency of the crane in the horizontal direction.

In addition, the response spectrum at the charging floor (elevation 47 ft 4 in.) would not reflect the higher accelerations at the crane elevation because of the rocking mode of the containment structure. An estimate of the relative values of acceleration at the two elevations may be obtained by comparing the product of the modal participation factor times the mode shape coefficient for each elevation. Examination of the A/E's computer output for the seismic analysis of the containment structure reveals that this product for the rocking mode is 1.274 for the crane elevation as compared to 0.9033 for the charging floor elevation.

In light of the above it is estimated that the maximum computed stress in the end ties for the horizontal DBE would be:

$$\frac{1.425}{0.84} \times \frac{1.274}{0.9033} \times 24.1 = 57.7 \text{ ksi}$$

Similarly for the OBE, the maximum computed stress would be:

$$\frac{1.05}{0.62} \times \frac{1.274}{0.9033} \times 17.81 = 42.5 \text{ ksi}$$

It is apparent that the OBE will induce some plastic flow and that the DBE will induce plastic flow. The plate is approximately 3 ft deep and 3/8 in. thick; thus buckling on one side under these loads is likely, thereby further increasing plastic flow on the tension side.

A6.3.1.4.2 Conclusion. Although the estimated stress levels exceed the 90% yield strength criterion established by the FSAR, it is our judgment that there is sufficient reserve strength (the ultimate tensile strength is estimated to be twice the yield strength) to prevent catastrophic failure.

It is our judgment that catastrophic failure of the crane, which in turn could damage the recirculation spray headers (Fig. X A-8), is not expected.

A6.3.2 REACTOR COOLANT SYSTEM (RCS)

The reactor coolant system consists of the reactor pressure vessel (containing the fuel), the pressurizer, three essentially identical coolant loops, a pressurizer relief tank, connecting piping, and instrumentation. Each reactor coolant loop contains a steam generator, a reactor coolant pump, two loop isolation valves, and interconnecting piping.

The reactor coolant piping, steam generators, and reactor coolant pumps are provided with snubbers, which accommodate the thermal expansion from the fixed or anchored reactor vessel with no resistance, but which do resist earthquake and pipe-whip forces. Steam-generator restraints are provided near the bottom of each steam generator to resist lateral and vertical loads resulting from seismic and pipe-rupture forces. Additional restraints are provided at a higher elevation to resist lateral loads resulting from seismic and pipe-rupture forces.

Portions of the system are discussed in section A6.3.2.1 through A6.3.2.5.

A6.3.2.1 Reactor Coolant System Loops.

The mathematical model for one of the reactor coolant systems loops, as developed by the supplier, is shown in Fig. X A-11. Joint 33 represents the support point for the pump. Joints 14 and 18 represent support points for the steam generator. The loop is estimated to weigh 1340 kip.

The mathematical modeling is characterized by the following features:

a. Local flexibility of the nozzle-shell juncture is not accounted for.

b. The actual pump and steam generator support members are not represented in the model; instead, their stiffness characteristics are determined in a separate calculation and assigned to the support points.

c. The main steam lines and feedwater lines are not represented in the model.

d. Dynamic interaction between the loop and the reactor building internal structure (which is estimated to weigh 27,000 kip) is not considered.

The supplier has determined that the fundamental frequency of the loop is 5.12 cps and that the pump motion dominates the fundamental mode. The next two modes in which steam-generator motion predominates have frequencies of 6.57 cps and 7.08 cps.

The OBE floor response spectrum used in determining the seismic response of the loop is shown in Fig. X A-12. Note that the peak acceleration value 1.68g occurs between natural periods of 0.125 sec and 0.9 sec corresponding to frequencies of 8 and 1.1 cps.

Critical stresses were computed for the 40° elbow in the upper crossover leg near the steam generator outlet nozzle as shown in Table X A-15.

A6.3.2.1.1 Commentary. The A/E computed a fundamental frequency of 8.32 cps, as noted in section A6.3.2.2. As noted in the commentary, this higher value is probably correct. If the fundamental frequency is indeed higher than 8 cps, then Fig. X A-12 indicates that the spectral acceleration values for the OBE would be between 0.14g and 0.21g, which is 1/8 the peak value of 1.68g. The actual seismic loads may be significantly less than indicated in the analysis performed by the supplier.

The fundamental frequency of 5.12 cps computed by the supplier for the loop is 97% of the computed third-mode frequency (5.3 cps) of the containment, which is dominated by flexure of the reactor building internal structure. Since the loop is braced to the internal structure via steam generator and pump supports, there could be significant dynamic interaction between the structure and the loop.

RDT Standard F9-2T (tentative), p. 20, (Ref. 5) indicates that a single model which couples both the equipment (the loop in our case) and the support (the internal structure in our case) should be used if:

$$0.5 \leq f_e/f_s \leq 2.0$$

unless;

$$M_e/M_s < 0.0001$$

where:

f_e = natural frequency of supported system (the loop)

f_s = natural frequency of support (internal structure)

M_e = total mass of supported system

M_s = total mass of support

In this case M_e/M_s = [3(1340)]/27,000 = 0.15 since there are three loops.

The possible values for f_e/f_s for each of 2 configurations are given in Table X A-16.

Note that both configurations indicate the need for a coupled model. The supplier has indicated that in the design of recent reactor plants a coupled model was used and this has resulted in a decrease in seismic stresses in the loop by 30%; so, in this special configuration, inclusion of coupling appears to have value only for obtaining a more accurate assessment of stress in the internal structure.

A6.3.2.1.2 Conclusion. It appears that the computed stiffness matrix for the reactor coolant pump support does not reflect the as-built condition; so the computed seismic stresses shown in Table X A-15 are probably higher than they would be for the defined DBE and OBE floor response spectra.

Dynamic coupling between the loop and the internal structure may provide additional lowering of seismic stresses in the loop. We did not evaluate the seismic resistance of the internal structure; thus we cannot judge the significance of the effect that inclusion of coupling would have on seismic stress in the internal structure.

We conclude that the seismic resistance of the reactor coolant system appears to be adequate.

A6.3.2.2 Steam-Generator and Pump Supports.

Each primary loop is composed of a steam generator, a primary coolant pump, and piping that connects these units to each other and to the reactor vessel. In this particular plant the A/E, not the supplier, is responsible for the design of the component support. Both the A/E and the supplier have performed independent dynamic seismic analyses of the primary loop. The A/E states in Ref. 6 that the steam generator and reactor coolant pump were modeled as rigid members. Figure X A-13 shows the mathematical modeling used by the A/E. The supplier accounts for the flexibility in these members. The A/E provided the supplier with the design details for the support of the pump and steam generator to be included in the mathematical dynamic model of the loop.

The design of the support structure for the steam generator and the primary coolant pump is governed by loads resulting from postulated circumferential and longitudinal pipe breaks. These loads are far in excess of the computed seismic loads. Support loads due to 10 postulated pipe ruptures were determined on the basis of a time history dynamic analysis using the first 30 modes of the mathematical model shown in Fig. X A-13 under the following assumptions:

a. 0% critical damping.

b. 0.015-sec rise time to reach maximum jet force at pipe break.

c. Longitudinal break assumed to occur over two pipe diameters.

d. Section of longitudinal break assumed to maintain full axial load capabilities but cross-sectional moment of inertia reduced to 10% of that of unbroken pipe.

Table X A-17 summarizes the computed steam-generator support member loads resulting from seismic and pipe-rupture events. Table X A-18 summarizes the computed loads in the members supporting the primary coolant pump. The original support design of the pump had no horizontal snubbers.

Member loads were evaluated in accordance with the following criteria:

Load[(a)]	Allowable[(a)]
W	AISC code allowable
W + DBE	1.33 x (AISC code allowable)
	Tension - F_y
	Shear - 0.7 F_y
W + DBE + R	Bending - F_y
	Compression - 1.6 F_a

(a) W - normal operating conditions;
DBE - design basis earthquake;
R - pipe rupture;
F_y - specified yield point; and
F_a - allowable compressive stress.

The A/E computed a fundamental frequency of 8.32 cps for the loop; the supplier computed 5.12 cps. The supplier also determined second- and third-mode frequencies of 6.57 cps and 7.08 cps, respectively. The fundamental frequency mode is dominated by pump motion, whereas the second and third modes are dominated by the steam generator.

A6.3.2.2.1 Commentary. The 8.32-cps fundamental frequency computed by the A/E gives a horizontal seismic spectral acceleration of 0.21g; the 5.12-cps fundamental frequency computed by the supplier gives 1.68g. This could lead to an increase in seismic loads in the support members by a factor of 8. We believe, however, that the A/E's computations reflect the addition of the horizontal snubbers for the pump, indicating that the higher frequency value represents the lower bound for the actual structure, so that 0.21g acceleration is applicable.

In addition, the assumption of 0% critical damping in determining the dynamic response from pipe-rupture loads is extremely conservative; Regulatory Guide 1.61 permits 3%. In our judgment any support member increase in seismic loads due to a lowered fundamental frequency would be more than offset by a decreased dynamic response to pipe rupture loads with 3% critical damping.

A6.3.2.2.2 Conclusion. The support design for the pump and generator should be capable of withstanding loads induced by combined seismic and pipe rupture events. The design appears to be adequate.

A6.3.2.3 Reactor Coolant Pump Nozzles.

Each of the three reactor coolant loops contains a vertically mounted coolant pump and drive motor assembly (Fig. X A-14). The overall height of the unit is 25 ft 3 in.

This single-stage centrifugal pump is designed to deliver 88,500 gpm against a 280-ft head. It is driven by a 6000-hp, single-speed, air-cooled induction motor mounted directly above it.

Coolant returning to the reactor from the steam generator is drawn up through the 31-in.-ID suction nozzle into the impeller and discharged through the 27.5-in.-ID nozzle in the side of the pump casing.

As a part of the primary coolant loop, the pump casing and nozzles are classified as Class I seismic components. Table 4.1.6-1 of the FSAR (Ref. 3) indicates that although no specific code provision for pumps was in effect at the time the pump was designed, the reactor coolant pump casing was designed per Article 4 of Section III of the ASME Boiler and Pressure Vessel Code (i.e., to the same rules used for the reactor vessel design).

The analysis of the PWR reactor coolant pump nozzles is contained in a generic report prepared by the major equipment supplier (Ref. 7).

In general, this major equipment supplier seeks to qualify standard components of the steam supply system on the basis of a master one-time analysis applicable to all reactor plants in which the system is installed.

To accomplish this objective, the supplier performs the master analysis for a set of thermal and mechanical loadings chosen to represent a conservative envelope of the most severe loading cases expected in any specific application. The loading cases used in the master analysis are referred to as the umbrella loads. In the master analysis this component is shown to meet the requirements of the applicable structural code under the umbrella loads. If the actual loadings in a given plant installation are subsequently shown (either by loading limitations established in the specifications or by analysis) to be less severe than the umbrella loads, then the structural adequacy of the component is considered to have been demonstrated for the specific application.

Stresses arising from a variety of loading sources are required for structural evaluation of the nozzles. In the analysis of the 93A casing nozzles (Ref. 7), the following procedures are used to obtain these stresses or to qualify components:

a. Determine stresses in the nozzle walls from pipe reactions using beam type formulae. These equations are incorporated in computer program NUMBRA used for this analysis.

b. In the pump casing wall at the junction with the nozzles, determine stresses from pipe reactions using the formulae of Welding Research Bulletin 107 (Ref. 8). These Bijlaard equations are also incorporated in computer program NUMBRA.

c. Determine thermal stresses (for normal and upset conditions only) in the nozzle wall due to radial temperature gradients, using simple cylindrical models of corresponding diameter and wall thickness.

d. Qualify the discharge nozzle for the faulted condition with a special finite element model in conjunction with a limit analysis using computer program ANSYS. The model used is a full 360° model with a refined grid of triangular flat-plate elements with plastic properties. In this analysis the boundary at the junction with the pump casing was taken as fixed.

e. Qualify the casing and nozzles for fatigue by invoking the exemption provisions of paragraph NB-3222.4d, Section III, ASME Code.

A6.3.2.3.1 Commentary. When the method of a master analysis using umbrella loads is used to qualify a component for a specific application, it should be demonstrated that actual loads do in fact fall within the limits of the umbrella. The equipment supplier had, at our request, prepared such a comparison for the working session. However, this comparison was confined solely to the pipe reactions at the nozzles due to seismic loads. Although this limited comparison showed actual loads to be below the corresponding umbrella loads, it did not include other simultaneous loadings required by the code to be combined with those of seismic origin. The equipment supplier recently indicated that other loads have been combined with the seismic loads and that the umbrella loads have not been exceeded.

For the discharge nozzle, the stresses in the pump casing wall at the junction with the nozzle are assessed using Bijlaard's method of analysis. This approach is of doubtful value in this application since the conditions for valid application of Bijlaard's method are not present.

Bijlaard's analysis may be used to determine the stresses in a shell at its junction with a smaller cylinder (nozzle), provided the shell is either spherical or cylindrical, the intersecting cylinder is normal to the surface, and its diameter is less than one-third the diameter of the shell. In addition, since the analysis is based upon the deformation characteristics of the shell, the shell is presumed to be thin and uniform.

In this application, the following conditions invalidate the approach:

a. The nozzle diameter exceeds one-third the diameter of the pump casing.

b. The casing wall certainly cannot be considered uniform in the vicinity of the discharge nozzle. Along its upper periphery, this nozzle abuts a thick flange.

c. The required condition of uniformity for the shell is also violated in both cases by the mutual proximity of the two nozzles; interaction stresses may also occur in the region between the nozzles.

The pump casing was not specifically modeled so that the general stress distribution in the pump casing wall under faulted conditions was not established. For the discharge nozzle to qualify, a limit analysis using finite elements with plastic properties was required. This suggests that stresses in the pump casing for the faulted condition may be quite high and that a corresponding finite element analysis of this region is needed.

A6.3.2.3.2 Conclusion. There is insufficient information to assess design adequacy. In our judgment a finite element analysis is needed before design adequacy can be established.

A6.3.2.4 Pipe-Whip Restraints.

Both the main steam line and the feedwater lines that connect to the top and side of the steam generator, respectively, are provided with pipe-whip restraints designed to prevent a ruptured pipe from damaging the containment structure. Restraints for the main steam line, for example, are installed on 5-ft centers, which is equal to the radial distance between the pipe line and the inside of the containment wall.

Figure X A-15 shows the restraint design concept for the main steam line. Note that the 6-in. space between the outside of the pipe and the inside of the restraint should allow unrestrained motion of the pipe under thermal and seismic loads. The pipe comes in contact with the restraint only if a pipe break causes jet forces that induce very large pipe movements.

The restraints for the main steam line have been designed to resist a pipe-rupture load equal to:

$$P = 1.25\ p\ A$$

where

p = the design pressure, and

A = the flow area.

The restraints have been designed to develop a plastic hinge when the thrust load P is applied at the point of contact between the pipe OD and the inside of the restraint.

The same procedure (including the use of the formulae for calculating P) was applied in designing the restraints for the feedwater line. Material for the feedwater line pipe-whip restraint is AlSl 1144 bar stock with a minimum yield strength of 53,000 psi.

A6.3.2.4.1 Commentary. Analyses were performed to establish the thrust coefficient appropriate to the PWR plant feedwater line. When the steam generator water level drops below the feed ring, high pressure steam will enter the feedline and accelerate an ever diminishing water mass down the pipe to the break.

Analysis of a break near the check valve of a 170 ft feedline shows that with conservative mathematical approximations, an impulse with peak force 1.35 pA will occur. The analysis is based on the water in the steam generator being subcooled by the amount corresponding to normal operation. It is anticipated that a more refined calculation would reduce the coefficient below 1.25 for this case. The refined calculation should also be carried out for the

minimum amount of subcooling that may occur in the steam generator.

A6.3.2.4.2 Conclusion. The pipe-whip restraint design for the main steam line appears to satisfy the design criteria. Present analysis for the thrust coefficient in the feedwater line predicts a thrust coefficient of 1.35 existing for a very short time. However, the analysis has some conservatism. In our opinion the integrity of pipe-whip restraints for the feedwater line (based on a design thrust of 1.25 pA) is unlikely to be compromised; therefore, these restraints also may be judged as satisfying the design criteria.

A6.3.2.5 Snubbers.

The hydraulic snubbers are designed to offer no resistance to slowly varying pipe displacements which, for example, accompany thermal transients but "lock" under the rapid pipe motions induced by dynamic loads such as earthquakes.

The snubbers contain a hydraulic fluid and a movable piston; hence seals must be provided to prevent the loss of fluid around the shaft and at certain other locations. At the time the snubbers for the PWR plant were being designed, polyurethane was recommended by the seal industry on the basis of limited laboratory testing. Additional testing since that time, plus the fact that the seals in a large number of snubbers built by a manufacturer different from the one who built those for the PWR plant have failed after installation in nuclear generating plants, has resulted in the industry being more keenly aware of the effects of the hydraulic fluid, ambient temperature and nuclear radiation on the seal materials. We have been provided with a copy of the report of tests performed by the supplier of the seal material used in the snubbers at the PWR plant, and a copy of the specification sheet for the hydraulic fluid (Ref. 9).

A6.3.2.5.1 Commentary. Opinion is divided about whether polyurethane, ethylene propylene, or some other material is best, but, from a review of the available information, it appears that there are formulations of either compound that are adequate for at least the period of time between refueling outages. A formal qualification program to demonstrate the ability of snubbers to maintain proper sealing of the hydraulic fluid under the operating environment (including severe seismic disturbance following temperature and radiation aging, and a LOCA environment) should be conducted.

A6.3.2.5.2 Conclusion. Our evaluation of the information available regarding the hydraulic snubbers installed at the plant leads to the conclusion that they are probably adequate for the period of time between refueling outages.

A6.3.3 LOW HEAD SAFETY INJECTION SYSTEM (LHSIS)

The LHSIS consists of two pumps, which, in the event of a large-break LOCA, initially draw borated water from the refueling water storage tank and inject it into the RCS hot legs. After the initial injection phase, system valves are realigned, and these pumps recirculate to the RCS the spilled reactor coolant and injected borated water.

The low head safety injection pumps are located in the safeguards area alongside the containment building; their pump impellers are actually located within an extension of the containment boundary. The pump casing is connected by a horizontal length of piping to the containment sump.

The vertical centrifugal pumps have a design discharge pressure of 300 psig and a design flow rate of 3000 gpm each. An unusual feature of these pumps is the relatively long shaft necessary to connect the impeller, at elevation -32 ft, to the motor, at elevation +12 ft.

A6.3.3.1 Piping.

The LHSIS piping system, consisting of 10-in. and 12-in. Schedule 140 piping, is extensive with lines running inside, outside, and around the containment structure; it also extends in elevation (in some sections) between the accumulator tank supported at the base mat at elevation -27 ft. 7 in. to a maximum elevation of 24 ft. 6 in. and finally connects to the reactor vessel primary piping at elevation 14 ft.

The A/E determined seismic stresses for sections of the piping between anchor points in accordance with the following procedure:

a. Masses are lumped at short intervals along the pipe line, and each mass is assigned 3 translational degrees of freedom.

b. Frequencies, mode shapes, and participation factors are computed for each mode.

c. Spectral acceleration values are selected for each mode for earth-

quakes occurring in each of the principal directions.

d. If the anchor points are at two different elevations, then the maximum response spectrum for the most severe point is used.

e. Modal forces on the basis of items a through d are then computed.

f. Seismic stresses at various locations in the piping are computed by selecting the highest modal force for each principal direction at each mass point and combining it with the square root of the sum of the squares of the remaining modal forces. The resulting force values for each principal direction are then applied to the mass points as an equivalent static load on the structure, and seismic stress values are computed.

g. Stresses due to seismically induced differential anchor motion are computed by applying the root mean square of the seismic displacements at the anchor position in opposite directions.

h. Seismic stresses generated in items f and g are combined with longitudinal pressure and dead weight stresses and evaluated in accordance with the following criteria:

$$S_{LP} + S_{DL} + S_{OBE} \leq 1.2\ S_h$$

$$S_{LP} + S_{DL} + S_{DBE} \leq 1.8\ S_h$$

where

S_{LP} = longitudinal pressure stress

S_{DL} = dead weight stress

S_{OBE} = operational basis earthquake stress

S_{DBE} = design basis earthquake stress

(Primary Stresses)

S_h = allowable stress at operating temperature

i. In addition, non-seismic stresses are evaluated in accordance with the following criteria:

$$S_{LP} + S_{DL} \leq S_h$$

$$S_{TH} \leq 1.25\ S_c + 0.25\ S_h$$

where

S_{TH} = secondary stress due to thermal expansion

S_c = allowable stress at ambient temperature

A summary of computed stresses and margins of safety is presented in Table X A-19.

During construction of the PWR certain sections of the LHSIS cold bent stainless steel piping (together with portions of other piping systems) became sensitized; that is, their corrosion resistance was lowered owing to chromium carbide precipitation at the grain boundaries.

A test program was conducted to determine the environmental effects that produce chloride stress corrosion of sensitized steel. It was concluded that:

a. Chloride stress corrosion can occur in acid solutions.

b. Chloride stress corrosion is strongly inhibited in an alkaline solution with a pH of 8.0 or higher.

c. Chloride stress corrosion is inhibited by boric acid at a concentration of 2500 ppm.

The AEC set forth criteria to be followed regarding the use of sensitized stainless steel piping in the PWR. The A/E reviewed the affected systems including portions of the LHSIS (Ref. 10). This report shows compliance with the criteria.

A6.3.3.1.1 Commentary. The method of combining modal inertial forces in the principal directions to determine seismic stresses is not correct. The correct method requires that stresses be computed for each set of modal forces and that the modal stresses then be combined. Nevertheless, in our judgment the A/E's method leads to conservative results because:

a. The method of combining the maximum modal force with the square root of the sum of the squares is conservative.

b. Use of maximum response spectra for pipe sections connecting to different elevations is a conservative approach.

c. The method of applying the seismic input simultaneously in all three principal directions in effect means that the earthquake components act simultaneously and in phase, which is conservative.

In connection with item c, at the time the PWR was built, the AEC generally accepted seismic inputs in only one horizontal direction and one vertical direction, which, for example, could lead to a stress value of 1.4S or 2.0S depending on whether the A/E assumed that the earthquake components were out of phase or in phase. On the basis of further evaluation of earthquake records, the AEC is now requiring that all three components of the earthquake be considered to act simultaneously but out of phase; this could lead to a stress value of 1.7S. The approach used in the analysis of the LHSIS piping could lead, in effect, to a stress value of 3.0S and is therefore considered to be conservative.

The evaluation considered primary stresses and thermal expansion stresses as required by the B31.1 piping code. Current practice would require analysis and evaluation in accordance with the Nuclear Code (NB 3600 of ASME Code Section III), which considers evaluation of secondary stresses due to thermal gradients and cyclic loads. Since the LHSIS piping is not subject to significant thermal gradients and less than 4,000 cycles of operation, secondary stresses and cyclic loading conditions are judged acceptable.

The sensitization of portions of the piping appears to have been properly handled and should present no compromise to design adequacy provided the surveillance program outlined in Ref. 10 is maintained.

A6.3.3.1.2 Conclusion. The design of the LHSIS piping appears to be adequate.

A6.3.3.2 Pumps and Drives.

The motor drive is mounted at elevation 12 ft. 0 in.; the pump end is approximately 50 ft. below that level. The shaft that drives the pump is laterally braced inside a pipe, which in turn is encased in concrete at elevation -27 ft. 6 in. and laterally braced by a 2 3/8-in.-thick plate at elevation 12 ft. 0 in.

The supplier performed calculations which indicate that the fundamental frequency is 3.55 cps. Seismic loads were taken as 3.0g. The analysis indicated that the shaft casing would deflect 1.15 in. at the pump. A maximum stress of 9519 psi was computed for the inner casing at the lower seismic support.

The LHSIS pump supplier prepared static g-load (3.0 g) calculations to investigate the ability of LHSIS pump to operate during and after MCE deflections of 1.15 inches. These calculations included:

a. Examination of pump shaft deflections and stator-rotor clearances under conditions of maximum deflection due to lateral seismic acceleration.

b. Computation of pump shaft bearing loads due to lateral seismic acceleration.

c. Computation of simultaneous additional bearing loads due to gyroscopic torque during seismic vibration.

The LHSIS pump supplier's computations show:

a. Stator-rotor clearance is not functionally impaired.

b. The maximum bearing loads to be expected are small compared to the rated load capacity of the bearings.

The pump internals (gaskets, seals, etc.) can be exposed to high levels of nuclear radiation during the recirculation phase following a LOCA, and the A/E states that these items can withstand this environment. Documentation made available to substantiate this assertion are Refs. 11, 12, and 13.

We understand that the motor drives are identical to those used on the containment recirculation spray pumps, for which a qualification program was conducted (see section A6.3.5.2).

A6.3.3.2.1 Commentary. The analysis indicates that stresses in the pump are within acceptable limits. In our judgment the analysis provided to verify the ability of the pump to operate under deflections as large as 1.15 inches provides reasonable engineering assurance that operability will not be impaired by deflections of this magnitude.

However, these computations were static not dynamic analyses and are not the equivalent of a seismic vibration test

under conditions that simulate pump support, as installed. Because of its unconventional support seismic testing may be particularly significant for this unit. However, there is no evidence of seismic qualification tests.

A6.3.3.2.2 Conclusion. The ability of the pump to function after pump casing deflections of 1.15 has been demonstrated by static analyses. Actual seismic tests have not been made; consequently, design adequacy has not been rigorously demonstrated. However, results of the analysis undertaken enhance the probability that the pump would qualify if seismic testing were performed. Therefore in our judgment, for purposes of this study only, the pump and drive design may be considered adequate, although design criteria are not completely satisfied.

A6.3.3.3 Valves.

The valves on the suction side of the LHSIS are 12-in. motor-operated gate valves with body rated at 150 lb/ANSI-B16.5. The disk is guided during closing and opening.

The drawings (Ref. 14) show that the design of the valves is compact; their natural frequency is estimated to be greater than 10 cps.

Some of the valves have an extended 1 1/2-in.-diameter stem, approximately 40 ft between the disk and the motor operator. The stem is protected by a 2 1/2-in. pipe sleeve.

A6.3.3.3.1 Commentary. In the absence of a formal qualification program we could not make a rigorous assessment of the design adequacy of the valves. On the basis of our experience in performing stress analyses of similar valves, we conclude that there is a good probability that the valves will function properly under an accident situation.

We examined extended stem details. There is a 0.11-in. radial gap between the OD of the coupling that connects the stem sections (approximatey 7 ft. long) and the ID of the 2 1/2-in. pipe sleeve. Assuming that the stem ends at the valve and the motor operator are fixed, we estimate that a side load of 0.1 lb/ft would close the gap at mid-height and the associated end moments would be 13.33 ft-lb. In our judgment this end moment can readily be reacted by the valve bonnet.

A6.3.3.3.2 Conclusion. We conclude that the design of the valve is adequate.

A6.3.3.4 Valve Motor Operators.

All active valves in the LHSIS are located outside the containment structure; hence the motor operators for these valves cannot be exposed to the high radiation level, high-pressure steam, and chemical-spray environment that characterizes the LOCA conditions within the containment. The VMO were nevertheless subjected to a rigorous qualification testing program, which consisted of aging, nuclear radiation, simulated seismic conditions, and simulated LOCA exposures. The simulated seismic test (Ref. 15) consisted of two parts: (1) a resonance scan between 5 and 35 cps (acceleration level not stated) and (2) five 2-min vibration exposures at 3g acceleration, 35 cps, with a 1-min pause (no vibration) between individual exposures. No resonances were "observed" during part 1.

Tests to demonstrate the ability of VMO to function after exposure to high temperatures, pressure, and radiation were conducted in two groups (Ref.15). In the first group, a VMO was aged in an oven and then exposed for 9 hr to both high temperature and high pressures (300°F/90 psig peak); these conditions exceed the peak environmental conditions within the containment. The VMO was cycled every 30-min throughout the exposure under simulated valve operating loads. In the second group, the motor from the valve operators was exposed to more than 150 megarads of gamma radiation in approximately 1 month. This exposure is more than the VMO would experience after 1 year following a LOCA if it were installed within the containment.

A6.3.3.4.1 Commentary. From the information provided to us about the seismic test program, it appears that the program was typical of those being conducted a few years ago. Certain aspects of the test do not meet current seismic test requirements: the lowest frequency is rather high; the method of determining resonances is not stated (there is a large number of individual pieces in the unit, inside the case, and it is doubtful that resonances of these would be detected by sensors on the outside of the case); and a bi-axial excitation was not used. Nevertheless, from the test conducted and from our experience in seismic qualification, we would expect that the unit would perform

adequately following a severe earthquake at the PWR plant.

The other aspects of the test program, as reported in Ref. 15, demonstrate that the VMO design is rugged and can be reasonably expected to function properly in the plant. This conclusion is reinforced by the fact that the VMO are located separate from any high energy piping systems.

A6.3.3.4.2 Conclusion. We judge the design of the VMO in the LHSIS to be adequate for the service conditions to which they may be subjected.

A6.3.3.5 Snubbers and Hangers.

The LHSIS piping is provided at various points with the following types of supports:

a. Hydraulic Snubbers. These units are designed to offer no resistance to slowly varying pipe displacements that, for example, accompany thermal transients, but they "lock" under the rapid pipe motions induced by dynamic loads, such as earthquakes.

b. Hangers. Spring hangers support the pipe weight only, and offer negligible resistance to pipe displacements. Rod hangers also support the pipe weight but offer resistance to downward pipe motion (since the rod is in tension) and negligible resistance to pipe motion in other directions (since the rod readily buckles).

c. Restraints. These units are designed to restrain pipe motion at a particular point in one or two directions.

d. Anchors. These units are designed to restrain pipe displacements at a particular point in all directions.

The piping drawings tabulate the calculated displacements at each support as well as the calculated forces that the support should be capable of resisting for the various load conditions. This information is used by the supplier to design the support. Support design calculations were not reviewed.

The design features of the hydraulic snubbers and the environmental test results described in section A6.3.2.5 are applicable to the LHSIS snubbers.

A6.3.3.5.1 Commentary. Hangers have been used extensively in industry for many years. In addition, since they do not resist seismic loads, we need not investigate their design adequacy. Restraints and anchors have also been used extensively, and their design is such that they present no special maintenance problems. Since anchors and restraints resist thermal loads during normal plant operation, routine inspection would show any weaknesses to resist seismic loads. The hydraulic snubbers, however, only resist dynamic loads and are not "exercised" by thermal loads during normal plant operation. As indicated in section A6.3.2.5 opinion is divided as to whether polyurethane, ethylene propylene, or some other material is best, but, from a review of the available information, it appears that there are formulations of either compound that are adequate for at least the period of time between refueling outages. A formal qualification program to demonstrate the ability of snubbers to maintain proper sealing of the hydraulic fluid under the operating and accident environments (including severe seismic disturbance following temperature and radiation aging, and a LOCA environment) should be conducted.

A6.3.3.5.2 Conclusion. We judge anchors, restraints, and hangers to be adequate on the basis of experience and normal plant operation. As indicated in section A6.3.2.5, in our judgment, the hydraulic snubbers are probably adequate for the period of time between refueling outages.

A6.3.3.6 Instrumentation.

The instrumentation and logic circuits which determine that a LOCA event has occurred and which then initiate functioning of the LHSIS are part of the plant protection system. None of the instrumentation within the LHSIS appears to be vital to the successful operation of the system during the injection phase, but rather it serves to inform the operator (via indicating lights and gauges in the control room) that the system is performing properly.

Two highly important instrumentation items are the level sensors and the level alarms on the Refueling Water Storage Tank (RWST); these are essential to inform the operator when to change the valve alignment to change from the injection phase to the recirculation phase. Because the operator can obtain comparable information from other sources (i.e., the clock, which advises the duration of the injection phase and hence approximately how much water could have been withdrawn from the RWST, and the containment sump level indicators,

which advise whether there is sufficient water there to supply the LHSIS), failure of the RWST level instrumentation does not automatically lead to a failure of the LHSIS. It must be recognized, however, that failure of this level instrumentation could result in maloperation of the system unless the operator is alert to the situation and takes the proper action based upon the secondary instrumentation cited above.

The RWST level instrumentation sensors are located outside the plant and hence cannot be exposed to LOCA conditions. The control room instruments are within the plant, but are in an area protected from adverse environmental conditions. Both portions of the instrumentation system are potentially vulnerable to damage as a result of a severe seismic disturbance, however. Because the PWR plant was constructed before a formal qualification program became an explicit AEC licensing requirement, we have not been able to obtain documentation of such qualification in order to make an evaluation of design adequacy.

A6.3.3.7 Commentary and Conclusion.

Because of the absence of evidence that the RWST level instrumentation sensors and control room instruments will function properly following a severe seismic event, we cannot make a determination of design adequacy.

A6.3.4 HIGH HEAD SAFETY INJECTION SYSTEMS (HHSIS)

There are two independent HHSIS at this plant: (1) the three 150-gpm charging pumps (which are normally used to provide makeup flow to the RCS) and associated valves and piping to enable these pumps to be used to inject borated water from the boron injection tank and the refueling water storage tank into the RCS loop piping and (2) three accumulators and associated valves and piping which can supply their contained borated water into the RCS loop piping cold legs.

The safety injection charging pumps are located in the auxiliary building, and the accumulators are mounted on the floor of the containment. The accumulators are passive safety elements, prepressurized with nitrogen. Coolant flows from these storage tanks as soon as RCS pressure falls below accumulator pressure (650 psig). Our review focused on (1) the main piping nozzles of the accumulators, (2) the piping connections to the RCS, and (3) the charging pumps.

A6.3.4.1 Accumulator Tank Nozzle

Figure X A-16 shows the details of the accumulator piping nozzle connection to the hemispherical head of the accumulator tank. The ratio of nozzle to shell is 8.25/69 = 0.12. The DBE pipe loads on the nozzle were determined by the A/E's piping flexibility analysis (see Table X A-20).

The FSAR indicates that the tank is classified as Class C (ASME Code Section III), which requires that pipe connections to the vessel shall "not overstress the vessel wall" without setting specific limits; however, stresses in the nozzle region of the tank hemispherical head would currently be evaluated in accordance with ASME Code Case No. 1607, "(Special Ruling) Stress Criteria for Section III, Class 2 and 3 Vessels Subject to Upset, Emergency and Faulted Operating Conditions" - Approved by Council November 5, 1973. Load condition and stress limits for this code case are given in Table X A-21.

The stresses in the vessel wall due to DBE pipe loads for System No. 2 were determined on the basis of a Bijlaard analysis. These stresses were combined with the membrane stresses due to internal pressure and are compared with the stress limits for a faulted condition as follows:

Stress (psi)	Stress Limit (psi)
Membrane = 19,150	2.0 S = 34,580
Membrane + bending = 32,450	2.4 S = 41,496

A6.3.4.1.1 Commentary. In the event of a large LOCA, the accumulator tank provides an initial high flow rate of injection water to the cold legs of the reactor via a check valve. This is supplemented later by water from the injection pumps. Since the accumulator tank is not called upon to provide its function during any normal reactor operation, Safety Guide 26 (Ref. 18) would currently require it to be designed, constructed, and stamped in accordance with the rules of Subsection B. This option, for example, would require more stringent weld inspection procedures than required for Class C vessels.

We note that the stresses in the vessel wall due to pipe loads on the nozzle have been computed for System No. 2. Table X A-20 shows that the DBE pipe loads for System No. 3 are significantly higher.

The supplier of the accumulator tank performed an additional analysis for System No. 3 (after we indicated that higher pipe loads should be used for this system) with the following result:

Membrane Stress	Pressure (psi)
Due to radial load	880
Due to moment load	9,530
Subtotal	10,410
Due to internal pressure	16,780
Total	27,190

In the analysis for the System 3 nozzle all bending at the nozzle is classified as secondary bending (as permitted by Table NB-3217-1 of Section III of the ASME Code), thus 27,190 psi is also the $P_M + P_B$ stress for this nozzle.

This classification for bending stress was not invoked in the analysis of the System No. 2 nozzle; instead, as conservatism, all bending at the shell-nozzle junction was there taken as primary. It results between nozzles are to be compared on a consistent basis this conservatism may be removed; then $P_L + P_B$ for System No. 2 becomes 19,150 psi.

Additional information, data and results for the accumulator head at the nozzle junction was furnished us in Ref. 19 and was carefully reviewed.

A6.3.4.1.2 Conclusion. Based on clarification and data provided by Ref. 19 it is our judgment that the analysis now meets the requirements of the ASME Code, Section III (including code case 1607) for Class 3 vessels.

A6.3.4.2 Accumulator Piping Connection to RCS.

The 12-in. accumulator piping connects to the 27 1/2-in. piping cold leg of the reactor via a nozzle. Pipe loads on the nozzle were determined by the A/E. System No. 2 was found to be the most severely loaded and therefore was analyzed. The NSSS vendor performed an analysis to determine and evaluate stress at the nozzle juncture by two methods as follows:

a. Using the rules set forth in paragraph 119.6.4 of the B31.1 Code, but with the stress indices from the Nuclear Piping Code (B31.7).

b. Using the Bijlaard method as outlined in the Welding Research Council Bulletin No. 107 to determine stresses resulting from pipe loads combined with the B31.1 Code to determine stresses due to internal pressure and loop loadings.

The resulting stresses were then compared with the allowables in accordance with B31.1. The results are given in Table X A-22.

A6.3.4.2.1 Commentary. The two methods give results that are in reasonable agreement for the earthquake and pressure loads, although thermal-expansion stress results do not agree as well. The supplier asserts that the stresses due to the seismic response of the NSSS loop are included in the results.

A6.3.4.2.2 Conclusion. We conclude that the nozzle connection of the accumulator piping to the reactor cold leg satisfies the design criteria and is adequate.

A6.3.4.3 Charging Pumps and Drives.

All three of the charging pump and drive units are installed in the safeguard area outside containment.

The charging pumps and drives are compact and are connected via horizontal shafts. The supplier has computed the fundamental frequency to 55 cps and has determined that the maximum seismic stress is 1229 psi.

A6.3.4.4 Commentary and Conclusion.

The charging pumps and drives are outside containment; LOCA environments need not be considered therefore.

The seismic analysis results appear to be reasonable and we conclude that the units satisfy design criteria and are adequate.

A6.3.5 CONTAINMENT RECIRCULATION SPRAY SYSTEM (CRSS)

This system recirculates water from the containment sumps through heat exchangers to spray headers mounted high within the containment. The water thus circulated removes heat from the containment, aids in lowering the temperature and pressure within the containment, and

maintains the containment at sub-atmospheric conditions once it is depressurized. There are four pumps and associated drives in the CRSS; two are located outside the containment and two within it. All four pumps take suction from the containment sump. The CRSS pumps are electric-motor driven from either normal or emergency power sources, and are the vertical centrifugal type with a 3500-gpm flow rating.

The pressure head rating for the inside-containment pumps is 230 ft; that for the outside-containment pumps is 249 ft. The former have a throttle bushing seal, and the latter have a tandem mechanical seal. The inside-containment units are relatively short and have their motor drive closely coupled. The outside-containment units are mounted in a manner very similar to that of the LHSIS pumps, the pump being located approximately 45 ft below the drive and connected by a long shaft.

A6.3.5.1 Pump and Motor Located Outside Containment.

The installation of the CRSS pump and motor is similar to that of the LHSIS as described in section A6.3.3.2. The CRSS motor weighs 2000 lb, the pump 3107 lb, and the interconnecting piping 3893 lb.

The A/E performed a dynamic analysis which indicates that the installation has a natural frequency of 1.9 cps in the horizontal direction and 63 cps in the vertical direction.

The pump manufacturer was given the following seismic load requirements:

a. Must be able to operate during and after experiencing

   1. 0.17g horizontal and
   2. 0.11g vertical.

b. Must be able to function with no loss of structural integrity after experiencing

   1. 0.34g horizontal
   2. 0.22g vertical

The A/E's evaluation of the installation was based on the frequency computations and corresponding acceleration response spectra values:

a. 1.68g horizontal, 0.19g vertical } OBE

b. 2.48g horizontal, 0.3g vertical } DBE

The A/E's analysis indicates that the installation is adequate for the above loads. However, no evidence was presented to indicate whether or not the pump manufacturer qualified the pump operation for the higher seismic loads.

The motor manufacturer performed a static analysis for the motor and its installation assuming that the maximum horizontal g load would be 1.45g and obtained maximum stresses of 12,170 psi in the motor mounting bolts; the allowable stress is 13,850 psi. A comprehensive qualification test of the motor was conducted and is discussed in the next subsection.

A6.3.5.1.1 Commentary. The motor mounting bolts would be stressed to 17,848 psi under the higher seismic load of 2.48g, which would exceed the allowable. In our judgment, however, the motor would vibrate in the higher modes of the installation so that its participation in the lower mode would be small.

It is not clear, however, whether or not the pump would be capable of continued functioning under the higher seismic loads.

The basis (Refs. 11,12 and 13) for establishing the radiation resistance of the pump internals leaves some questions unanswered, but it shows that the pump internals probably have adequate radiation resistance.

A6.3.5.1.2 Conclusion. The seismic design of the motor and motor mounting appear to be adequate.

There is insufficient information to judge the ability of the pump to continue functioning after exposure to seismic environments. Design adequacy of the pump has not been demonstrated.

A6.3.5.2 Motor Drives.

All four motors are rated at 300 hp, 460 V, 3-phase, 60 cps. They are fully enclosed, sealed motors with encapsulated insulation. The inside containment units are located at approximately elevation -20 ft; the outside containment units are at elevation +16 ft.

A topical report (Ref. 20) describes a comprehensive qualification test program consisting of four parts conducted on the same motor in the following sequence(1) thermal aging, (2) seismic test, (3) nuclear-radiation exposure, and (4) steam/chemical-spray exposure. It should be noted that only the inside-

containment units are subject to steam/chemical-spray and high-level nuclear-radiation exposures.

Thermal aging consisted of exposing the stator to an average temperature of 203°C for 155 hr. The report states that the aging exposure is based on IEEE 275 and IEEE 384, Sec. 4.3.1, but supporting data are not presented. The aging exposure is reported to be equivalent to 18,000 hr at 130°C, the maximum operating temperature under "normal" (non-accident) conditions, which is equivalent to 450 hr per year for 40 years. (In the plant, the motors are not expected to be operated more than 15 hr per year.)

The motor was exposed to 2×10^8 rads of gamma radiation at a maximum rate of 0.5 megarad per hour. This dose is the integrated dose that the motor could be expected to receive during 40 years of normal life plus the exposure for a year following a LOCA.

The seismic qualification test consisted of vibrating the motor sequentially along three mutually perpendicular axes (one vertical and two horizontal) at an input acceleration amplitude of 0.4g within the frequency range 4 to 70 cps. Because the motors in the plant are located below grade, an analysis performed by the A/E shows that qualification can be demonstrated by vibration at an acceleration amplitude of twice the maximum ground acceleration level, which is 0.15g.

The steam/chemical-spray exposure included five cyclic transient exposures to 45 psig/270°F, with dwells of 30 min at these conditions, followed by 7 days at 0 psig/150°F. Except for brief interruptions for electrical measurements and to check the ability of the motor to restart, the motor was operated at full load during the high temperature portion of each of the five cycles and throughout the seven-day exposure at 150°F. The A/E's qualification test specification states that the motor is required to start and operate at rated load for 30 min during each transient and to be operable for a minimum of 24 hr at 150°F $\pm$ 5°F and 14.7 to 10.0 psia.

A6.3.5.2.1 Commentary. The gamma-radiation dose used in the qualification test was more than adequate; and, since it preceded the seismic test and the steam/chemical-spray exposure, the test was conducted in a conservative manner.

During the steam/chemical-spray exposure test, the winding temperature never exceeded the rating, 180°C (356°F), of the Class H insulation used in the motor. While present qualification requirements call for testing at a temperature exceeding the expected service temperature by a margin of 15°F, the fact that five transients were conducted would appear to provide a margin that tends to compensate for the lack of a temperature margin.

A6.3.5.2.2 Conclusion. The qualification test program clearly demonstrates that the motor satisfies the design criteria and thus is adequate.

A6.3.6 ON-SITE ELECTRIC POWER SYSTEMS

The electrical power systems at the PWR plant are designed to provide a diversity of dependable power sources which are physically isolated so that any failure affecting one source of supply will not propagate to other sources.

The plant is connected to six separate off-site substations with 230-kV transmission lines and to two substations with 500-kV transmission lines. In the event of total loss of power from off-site sources, auxiliary power is supplied from diesel generators located within the plant. Station batteries are provided as a reliable source of control power for specific engineered safeguards and for other functions required when a-c power is not available.

A6.3.6.1 Diesel Generator Building.

The diesel generators are housed in cubicles that are part of the service building. These cubicles are protected from tornado effects as described in section A6.2.1. A discussion of and an evaluation of the housing's resistance to tornado effects follows:

A6.3.6.1.1 Resistance to Missile Penetration. Three types of barriers are used to protect the diesel generator system:

a. Monolithic concrete walls - 2 ft thick, reinforced in both faces with No. 11 deformed steel bars on 10-in. centers.

b. Precast reinforced concrete - 2-ft by 2-ft by 12.5-ft beams used to build up "doors."

c. Six feet of compacted soil.

No penetration calculations were made available for review. According to the A/E, tests on the 2-ft-thick concrete section are currently under way.

A6.3.6.1.1.1 Concrete Walls. On the basis of experience with other structures and different missiles, we concluded that neither of the two missiles will penetrate the concrete wall. (Calculations indicate a penetration of only 1 in. for the utility pole.) Penetration calculations for the auto missile are not considered necessary since the impact area is so large.

A6.3.6.1.1.2 Precast Beams Used for "Door." Same comments as for concrete walls.

A6.3.6.1.1.3 Compacted Soil. On the basis of the work of Kornhauser, a penetration of about 20 ft of sand would be expected for the utility pole. The penetration in the compacted soil over the fuel storage tanks could be the same or less depending on the colloidal content of the particular material and the degree of compaction achieved. Under the stated criteria it appears that missile contact with the fuel tanks could occur. Details of the fuel line layout and manifold were not made available; therefore, we could not make a final estimate of the damage potential. However, it should be noted that 6 ft of compacted soil is a significant cover, and most missiles would therefore probably not be able to do any damage.

A6.3.6.1.2 Overall Response Calculations. No overall response calculations had been made by the A/E.

A6.3.6.1.2.1 Monolithic Concrete Walls and Roof. No independent overall response calculations were made owing to time limitations. However, the similarity of this structure to others for which calculations have been made (but with different missiles) leads us to believe that the structure is adequate.

A6.3.6.1.2.2 Precast Reinforced Concrete Beams. Unlike the walls discussed above, the beams appear to have less potential for withstanding the effect of the utility pole impact because this type of beam cannot distribute the impact load to a wider portion of the structure (as occurs in a slab) until the load reaches the door jamb. In addition, only a single 1-in.-diameter bolt at each end of the beam is available to resist rebound forces after impact. However, for the missiles specified the door beams are considered adequate.

A6.3.6.1.3 Wind Loads. In spite of the design criterion of a 360-mph peak wind velocity, a velocity of 300 mph was used to produce a dynamic pressure of 230 psf. The wall openings were computed at 23.6% of the building envelope area, which led to the conclusion that the 3-psi differential pressure in 3 sec would not lead to any significant loading. The dynamic pressure of 230 psf was modified by the pressure coefficients as recommended in ASCE Paper No. 3269, i.e., 0.9 on the windward side and -0.4 on the leeward side, before being applied to the walls. For the roof load a factor of -1.4 was used. This results in a 300-psf uplift force, which, however, is completely neutralized by the dead weight of the roof.

We did not examine wind loads on the door structure, but the reviewer believes this load would not be critical.

One important point noted is that a steel brace from the turbine building is anchored on the top of one of the internal dividing walls of the emergency generator building. The brace introduces a load, which has horizontal as well as vertical components, at this point of the diesel generator building. Calculations based on the design wind loading for the turbine building, which is lower than the tornado loading, were made for the braced load. This was justified on the basis that blowout panels, etc., will partially relieve the wind loading on the turbine building. Older calculations based on a different preliminary design (braces of a different design) were made using the ultimate load-carrying capability of the brace as the load applied to the diesel generator building. New calculations made by the A/E at our request indicate that the new anchor design can take the ultimate load-carrying capacity of the brace with some plastic straining but no rupture.

No calculations were made to combine wind loads with missile loads.

A6.3.6.1.4 Commentary. Only wind loads were considered in any depth in the design calculations reviewed, and these were based on 300-mph winds rather than the 360-mph winds called for in the specifications. However, the reviewer's opinion is that wind loads will not be critical for this design. The following items, while not considered critical, are of some concern:

a. Capability of the compacted soil cover to protect the fuel tank against damage by a utility pole missile.
b. The effects of fuel spillage and ignition in the event of an auto impact.

c. Analysis of the overall impact and wind-load response of the removable concrete beam doors with an evaluation of the rebound forces for the door. (The A/E indicates the rebound force will fail the door pins.)

Note: The A/E made additional calculations which indicate that the door pins would fail owing to the rebound force after missile impact. The A/E did not consider this to be a problem, however, since the chances of an additional missile entering the diesel generator area would be very small. The A/E further points out that there are obstructions in front of the door that would prevent the direct impact of missiles; however, a 45° impact is possible. In our judgment, if the door rebound forces due to missile impact were to fail the pins and expose the diesel generator to the driving rain and hail often associated with a tornado, this could cause an interruption of emergency power.

A6.3.6.1.5 Conclusion. We conclude the following:

a. The walls and roof satisfy the design criteria and are adequate on the basis of experience and judgment.

b. The doors may fail to perform their function; failure of the door pins in particular is likely. Adequacy has not been demonstrated.

c. The soil cover for the fuel tanks is adequate in our judgment.

A6.3.6.2 Diesel Generators

Each diesel generator weighs 54 tons, is anchored to its base by ten 1 1/2-in.-diameter bolts, and is subject to DBE horizontal and vertical spectral accelerations, as shown in Figs. X A-17 and X A-18. Note that the peak horizontal acceleration equal to 2.475g occurs between 1.33 and 6.67 cps, with accelerations of between 0.3 and 0.225g for frequencies greater than 6.67 cps. The vertical peak of 3.6g occurs between 1.25 and 3.33 cps and then drops to 0.3g for frequencies greater than 3.33 cps.

The A/E performed calculations to check the adequacy of the anchor bolts and found that they would not be strong enough to resist the peak accelerations but would be strong enough to resist a transverse horizontal acceleration of 0.3g, conservatively neglecting the 0.7g net restoring force in the vertical direction. The A/E computed a tensile stress of 3080 psi and a shear stress of 2310 psi in the bolt, whose yield strength is 36,000 psi. The A/E justified the use of the lower accelerations on the assumption that the fundamental frequency of the diesel generator is greater than 6.67 cps.

The supplier of the diesel generator provided test results which indicate that the units frequently experience longitudinal (horizontal) accelerations of 1g and vertical accelerations of between 0.25 and 0.5g during locomotive operation with "no detrimental results on the operation of this equipment." When the locomotive is coupled with the rail cars, the equipment experiences longitudinal accelerations of 4g and higher.

A6.3.6.2.1 Commentary. The assumption that the fundamental frequency of the diesel generator is greater than 6.67 cps is reasonable. Section A6.4.6.2, for example, indicates that the computed fundamental frequency for the BWR diesel generator is 9.63 cps, which is dominated by the motion of the turbochargers.

The A/E's analysis of the anchor bolts assumes that they equally resist the shear load, a situation that could occur only if all bolts are fitted. In all likelihood, however, the shear load = 0.3 x 108,000 = 32,400 lb would be resisted by friction between the unit and its base.

It is estimated that without any preload in the bolts, there would be an available friction force equal to 0.7 x 108,000 x 0.3 = 22,680 lb., assuming a coefficient of friction of 0.3. The additional required shear resistance would be provided by the bolt preload force.

The information supplied by the diesel generator vendor is convincing evidence that the unit can continue to operate after experiencing 0.3g in the horizontal longitudinal direction together with 0.3g in the vertical direction. Although no mention is made of transverse g-load measurements, the rocking loads in normal diesel engine service could give rise to non-trivial transverse g loads. It is our judgment that on the basis of in-service experience the diesel generator should be able to withstand a transverse acceleration of 0.3g.

A6.3.6.2.2 Conclusion. We conclude that the diesel generator is adequate

and capable of withstanding the DBE seismic loads without loss of function.

A6.3.6.3 Day Tanks.

Fuel for each diesel generator comes from the day tank, which is housed in the diesel generator cubicle. Each day tank, in turn, is supplied with fuel from the storage tanks, which are buried in the ground outside the building. The day tank is supported in a horizontal position by four unbraced posts (approximately 3 in. in diameter) as shown schematically in Fig. X A-19.

No seismic analysis was available for our review. However, visual inspection of the as-built unit during a site visit to the PWR plant revealed that one of the support posts was noticeably out of plumb.

A6.3.6.3.1 Commentary. The seismic resistance of the day tank to lateral loads with unbraced posts must be derived from post bending stiffness. This stiffness, however, is normally lower than that obtained from supports with braces acting as truss members.

A6.3.6.3.2 Conclusion. A seismic analysis should be performed to demonstrate the ability of the day tank supports[1] to resist seismic loads. Design adequacy has not been demonstrated.

A6.3.6.4 Air Bottle Support.

The air bottles provide compressed air for starting the diesel generator. The bottles are supported in the vertical position by a back frame (Fig. X A-20). Each bottle is clamped to the back frame by an upper and a lower strap so that the vertical inertia force on the bottle is resisted by friction induced by the clamping action of the strap.

No seismic analysis of the air bottle support was made available for our review. However, the installation was visually inspected during a site visit to the PWR plant.

A6.3.6.4.1 Commentary. The ability of the air bottle support to resist vertical seismic loads depends on proper installation to ensure that the straps provide sufficient clamping action. There is obviously sufficient clamping to support the weight (1g) of the bottles. On the basis of inspection, the fundamental frequency is greater than 3.33 cps; so the maximum expected seismic g load in the vertical direction would be 0.3g (see Fig. X A-18), which represents a 30% increase over the dead weight.

A6.3.6.4.2 Conclusion. In our judgment, the design of the air bottle support is adequate. This conclusion assumes proper installation with sufficient clamping action of the straps.

A6.3.6.5 Batteries and Battery Support.

Station batteries are provided as a reliable source of control power for specific engineered safeguards and for other functions required when a-c power is not available (e.g., to operate circuit breaker controls, turbine shutdown oil pumps, instrumentation, emergency lighting, and plant protection circuits). Two separate 125-V d-c systems are installed, with an additional system to supply essential services at the remote circulating-water intake structure. The batteries for each system are located in separate ventilated battery rooms. Each 125-V battery consists of 60 individual sealed cells with sealed covers. Each battery is served by a separate charger connected to "float charge" the battery. The chargers are capable of carrying the normal d-c system load and at the same time supplying sufficient current to keep the batteries in a fully charged condition. The chargers are supplied from separate 480-V a-c motor control centers, each connected to an independent emergency a-c bus.

The batteries were subjected to a seismic qualification test as follows:

Test No. 1
(front to back)

1.6g @ 11.5 cps horizontal
0.7g @ 19.3 cps vertical
} Simultaneous

Test No. 2
(side to side)

0.4g @ 28.7 cps horizontal
0.7g @ 19.3 cps vertical
} Simultaneous

After completion of each test the batteries were inspected; there was no visible damage. In addition, a discharge test subsequent to testing proved that 100% capacity of the cell was still available.

[1] It is our understanding that the day tank support is being provided with bracing as a result of the review.

For this plant the batteries are supported directly on massive, poured in place, concrete blocks. Batteries are tied to the concrete block to prevent sliding or overturning should a seismic event occur.

Commentary and Conclusion

Visual inspection shows the battery support to be capable of resisting seismic loads. The testing of the batteries demonstrates the adequacy of the batteries. We conclude that the batteries and supports satisfy the design criteria and are adequate for seismic loads.

A6.3.7 ELECTRIC POWER DISTRIBUTION SYSTEMS

The electric power distribution systems consist of transformers, switchgear and motor control centers, emergency buses, containment penetrations, and associated electric power and control cables and their supporting cable trays.

A6.3.7.1 Electrical Cables and Terminations.

Because safety-related electric power and control cables are installed in virtually every area of the plant, both within and outside the primary containment, they will be required to function under severe environmental conditions should an accident occur in the plant. Their ability to withstand such conditions was established by subjecting samples of the cables and cable splices used in the plant to a qualification testing program (Ref. 21). In general, these programs consisted in thermal and nuclear radiation aging and steam/chemical-spray exposure. The steam/chemical test of electrical cables involved a temperature in excess of 300°F for a duration of approximately 3 weeks. The scope of the tests, the test parameters, and the procedures followed were typical of those used at the time the test programs were conducted. Fire-retardant construction was used in the cables to reduce the fire hazard.

A6.3.7.1.1 Commentary. Because qualification requirements have become more definitive during the 4 years since the qualification tests were performed, most of the tests would probably not be considered adequate by a strict interpretation of today's qualification standards (Ref. 22). For example, not all the cables were energized during the full period of the test, and the test duration did not exceed the post-LOCA period during which some of the cables should be functional. The fact that the cables did perform adequately for 3 weeks confirms that their design is adequate for the most crucial period following a LOCA. A cable failure at a later time, should one occur, may cause a relatively minor operational problem but is not expected to result in a safety problem.

Because the cables are not structural members and are presumably properly supported by cable trays, seismic qualification is not explicitly required. In principle, there is concern that cable insulation may become embrittled as a result of aging (exposures to temperature and nuclear radiation during their installed life) and that the insulation may therefore be subject to failure by cracking during a severe seismic event. The current qualification philosophy is to cover this possibility by requiring a bend test (wrapping the cable specimens being tested around a mandrel) after the simulated LOCA exposure. The qualification test that was performed evidently did not include this aspect of the design requirements. This omission is not regarded as serious, however, because the nuclear-radiation dose levels in the plant are not high enough to produce embrittlement of the insulating materials used in cables installed in safety-related systems.

A6.3.7.1.2 Conclusion. Although certain aspects of the qualification test program were not as comprehensive as current requirements, we nevertheless believe that the program meets the original design criteria and does provide reasonable assurance that the electrical cables and terminations will perform adequately during and following design basis events at the plant. This conclusion is tempered by the reservation that, because the state of knowledge with regard to long-term thermal, humidity, and nuclear-radiation aging effects is somewhate limited, periodic surveillance testing of the installed cables should be conducted.

A6.3.7.2 Electrical Containment Penetrations and Connectors.

The electrical containment penetrations are components that provide pressure-withstanding, leak-tight, electrically insulated paths through the wall of the primary containment structure for transmitting electrical signals and electric power to motors and solenoids. Generally speaking, current specifications require that penetration assemblies employ two seals in series to permit monitoring and testing in situ. Both seals must fail to permit leakage from containment.

The design and qualifications of the electrical mating connectors are based upon the requirements of military specification number MIL-C-5015. Connector design is such that silastic components are provided in the connector to feed through the interface. The A/E believes that this specification is equivalent to specifications for nuclear power plant application, and that this type of interface has been proven adequate to meet environmental requirement. Additional capability to withstand elevated temperatures is provided in the silicone material used for the sealing members.

Tests conducted by the manufacturer consisted of the following (Ref. 3):

> "Connectors installed in the flanges normally operate at ambient conditions of 105°F and 9.75 psia and were tested for leak rate and tagged for integrity before shipment to the job. A test facility was set up by the manufacturer suitable for 50 psig with provisions for thermocycling from 32°F to 300°F. A thermocycle run of at least three cycles was made on one of each type flange. A time interval of 30 minutes was allowed between the thermocycles. The leak rate test after thermocycling was made at 50 psig and 300°F. Each completed flange had a leak rate of less than 1×10^{-6} cc/sec per assembled flange. All flanges were leak tested at 50 psig and 300°F. Helium gas was used in the test facility."

Reference 3 also reports that for the triaxial cable penetrations a more detailed procedure for the thermocycle test was followed in shop test, as follows:

> "The type sample consisted of a containment side flange disk with hermetic assemblies welded in place. A thermocouple was installed to monitor disk temperature. The disk was stabilized at 32°F and then placed in an oven heated previously to 280°F. On entrance of the disk, the oven temperature was reduced, straight line, to 150°F over a 60 minute period. The disk was removed and cooled to 100°F, while the oven was reheated to 280°F. The disk was then returned to the oven and the oven temperature reduced to 150°F as before. The highest metal temperature reached during this cycle was recorded and a 50 psig helium leak test was conducted at this metal temperature for all disks of this type."

Each penetration assembly, without external cable mating connectors, has been tested in the factory to demonstrate insulation resistance of at least 1000 megohms at 1000 V d-c. In addition, each penetration has passed a high-potential test. After installation, each penetration with external cables connected was tested at 1000 V d-c for 5 min.

We understand that an environmental test which would simulate pressure, temperature, moisture, and radiation associated with a LOCA was scheduled, but the results have not been made available to us.

Both an analysis and a test were performed to qualify the electrical containment penetrations for seismic environments. The fundamental frequency was found to be 3094 cps. Maximum computed seismic stress was found to be 56 psi in the mounting bolt. A shake test was performed over a frequency range up to 10 cps. The acceleration was 5g at 10 cps. No visible damage and no loss of electrical function was observed after the test.

Conclusion

From our review of the qualification program for the electrical containment penetrations and connectors, we conclude that their design is adequate, assuming that the results of the LOCA environment test are positive.

A6.3.7.3 Cable Trays.

The cable trays, which provide support for electrical cables, are covered by corrugated sheets and consist of two side rails connected by rungs, the centers of which are typically spaced 9 in. apart. The trays are supported from above approximately every 8 ft. No seismic analyses of the trays were provided for our review. The trays were, however, visually inspected during a site visit to the PWR plant. The trays appeared to be well constructed and supported. Natural frequencies are estimated to be above the peak spectral acceleration range.

Commentary and Conclusion

From our inspection of the trays, we conclude that their design is adequate.

A6.3.7.4 A-C and D-C Switchgear.

No seismic or environmental qualification information has been made available for review and evaluation. We cannot therefore make an assessment of design adequacy of those components.

A6.3.8 REACTOR AND ENGINEERED SAFEGUARDS PROTECTION SYSTEMS SENSORS AND LOGIC CABINETS

The reactor protection system monitors nuclear, thermal, and hydraulic parameter associated with the reactor core, determines whether conditions are such that the reactor should be shut down immediately, and, if so, initiates a shutdown. The engineered safeguards instrumentation monitors parameters to detect failures in the reactor coolant system and to initiate containment isolation and engineered safeguards equipment operation.

The only portions of the plant protection systems that were considered in the design adequacy review were:

a. Pressure and differential pressure transmitters.

b. Nuclear instrumentation system cabinets.

c. Radiation monitoring system cabinets.

d. Signal conditioning equipment (modules and racks) for monitoring pressurizer level and pressure; containment pressure; reactor coolant flow, pressure, and temperature; and steam-generator water level and feedwater pressure.

e. Safeguards actuation logic racks.

Instrument piping is connected to the plant components and routed to instrumentation racks. The instruments that monitor reactor, reactor coolant system, and steam-generator process parameters are located within the containment structure; the others are located external to the containment. These racks contain the pressure transmitters and differential pressure transmitters which transform hydraulic pressure signal inputs into electrical signals. The electrical signals are conveyed by electrical control cables to instruments and to cabinets containing signal conditioning equipment and components that provide the 2-out-of-4 logic functions. Other electrical cables then carry the processed signals, which initiate reactor shutdown, containing isolation, and ECCS initiation, to the control rod drive system and to the various motor control centers that initiate valve movements and motor start ups. Additional signals are generated in the various systems and carried by electrical cables to the control room, where gauges and lights are displayed to provide to the plant operator such information as motor current, system flow and pump discharge pressure, and valve positions. The control room also contains switches to permit the manual operation of motors and valves should their automatic functioning fail to occur.

A6.3.8.1 Environmental Qualification.

As noted above, some of the pressure and differential pressure transmitters are located within the containment and therefore can be subjected to extreme environmental conditions should a LOCA occur. Environmental qualfication tests have been conducted on these components (Ref. 15).

A6.3.8.2 Seismic Qualification.

Evaluation of the seismic qualification of the PWR protection system was based primarily on a review of References 23 through 25. The rationale of the test procedure is presented in References 26 and 27. The seismic tests of electrical and control equipment described in these reports cover essentially three series of tests, one for low and two for high seismic disturbances. The more severe set of test criteria (high seismic) were developed to simulate the effect of disturbances at the base of equipment located on floors of plants with a DBE having horizontal ground accelerations in the range of 0.2 to 0.4g and higher. Since it was found that mechanical deformations (e.g., slippage at bolted joints) caused the equipment resonant frequencies at high input accelerations to be different from those observed during resonance scans at low input levels, the tests were conducted for the most part at discrete frequencies separated by intervals that were intended to be small enough so that any equipment resonance in the range between 1 and 35 Hz would be accounted for. Tests were conducted sequentially along three orthogonal axes, two horizontal and one vertical. The amplitude of the horizontal, sine-beat input motion at the base of the equipment tested was a function of frequency, having a plateau of 1.5g between 5 and 10 Hz and dropping to 0.5g at 1 Hz and 25 Hz; the amplitude of vertical input motion was two-thirds of the horizontal input motion.

The control board was designed to withstand earthquake conditions. An analysis was performed to verify the adequacy of the seismic design, and this was complemented by tests performed on sections of the main control board with some safety related instruments in position.

A6.3.8.3 Commentary.

A6.3.8.3.1 Environmental Qualification. A review of the information presented in Ref. 15 discloses that two pressure transmitters and one differential pressure transmitter were subjected to simulated LOCA environments that were more severe than the worst environment expected within the plant under LOCA conditions. The durations of the exposures were 2 to 3 hr, which is very much longer than the time (a few minutes) the sensors that detect abnormal conditions and initiate plant shutdown, etc., must function. On the other hand, it is highly desirable that instrumentation be available to monitor the conditions within the plant for a long period (several weeks) following a LOCA.

Although the equipment samples that were subjected to the environmental qualification tests were not first subjected to an aging exposure, which is a current requirement, there are several obviating factors. According to the manufacturer, the pressure transmitters are parts of repairable systems which are required to be tested at one-month intervals during operation with the reactor at power. Any degradation of performance resulting from normal aging would be detected during such tests, and the component would be replaced. Also, to the extent that the duration of the simulated LOCA environment exceeded the minimum required for qualification, it may be regarded as partly compensating for the lack of prior aging. We have not seen any qualification information that would permit an evaluation of the capability of these components to function properly under the following conditions:

a. Envelopment in a steam cloud following a severe seismic event.

b. Heavy wetting by water spray following a severe seismic event.

A6.3.8.3.2 Seismic Qualification. The seismic qualification tests were conducted in accordance with procedures that were considered acceptable at the time the tests were conducted. However, the information available was not adequate to permit a determination of the adequacy of the tests with respect to current seismic qualification requirements. In particular, it presently must be demonstrated that multi-frequency testing, involving simultaneous vibration in horizontal and vertical directions, is not essential for the specific equipment tested. The blanket comparison of earlier test procedures with new requirements in Reference 27 does not accomplish this.

Other reservations regarding seismic qualification include the following: The information available did not permit us to determine that the equipment tested was the same as, or adequately similar to, the equipment that was installed in the plants. Also, in those cases where equipment failed during a test and a modification was made, the test was usually continued from the point of failure. Presumably, it was assumed that the "improved" equipment would not fail during a repetition of that part of the test that had been completed before any change was made; while this is probably usually true, there may be cases in which the change might cause an unforeseen degradation of performance under conditions not retested. Furthermore, in those cases where a component failure was judged to be an "isolated incident," and therefore not an indication that the test unit had failed, the rationale was questionable.

A6.3.8.4 Conclusion.

The results of the extensive qualification tests conducted on the protection systems sensor and logic cabinets leads us to conclude that they would probably function satisfactorily. However, because of the reservations expressed in the commentary, the design criteria have not been completely satisfied.

A6.3.9 INTAKE CANAL

The intake canal, which channels water from the reservoir to the plant, is higher in elevation than the discharge canal; so it provides a passive pressure head that ensures a flow of cooling water to safety systems.

The intake canal is lined with concrete and is supported by earth below and around the entire canal. No seismic analysis was provided for review, but the entire canal was visually inspected from the pump house where water from the reservoir is pumped into the intake canal to the screens at the plant.

Commentary and Conclusion

Our visual inspection of the intake canal indicates that there is no danger

of the canal losing its inventory as a result of the liner cracking during a seismic event, since the surrounding earth will prevent rapid loss of water. We conclude that the seismic design adequacy of the intake canal is adequate.

A6.4 DESIGN ADEQUACY OF BWR PLANT COMPONENTS

A6.4.1 CONTAINMENT STRUCTURE

The containment system at the BWR plant consists of a multi-barrier design with:

a. A primary barrier consisting of the steel primary containment with its pressure-suppression feature.

b. A secondary barrier consisting of the reactor building with a system to limit the ground level release of airborne radioactive material from the secondary containment.

Figure X A-21 shows a cross section of the containment structure. The containment structure was reviewed only from the viewpoint of mathematical modeling and the method of obtaining seismic inputs to equipment that is mounted on the containment structure.

A6.4.1.1 Primary Containment Structure.

The primary containment is an enclosure for the reactor vessel, the reactor coolant recirculation system, and other branch connections of the reactor coolant system. Structurally, the containment consists of a drywell and a pressure-suppression chamber connected by eight large vent pipes. The drywell is a steel pressure vessel in the shape of a light bulb, and the pressure-suppression chamber is a torus-shaped steel pressure vessel located below and encircling the drywell (see Fig. X A-21). The suppression chamber is half-filled with water.

The A/E indicated that preliminary studies showed that the drywell does not dynamically interact with the system; thus its mass was lumped with the reactor building in the mathematical model.

A seismic analysis of the pressure suppression chamber (torus) was performed by the A/E under the assumption that the torus is fully flooded with water. The water was assumed to behave like a frozen mass. The fundamental frequency under these assumptions was found to be 4.75 cps. The A/E found that the maximum displacement of the torus under the assumed conditions was 0.064 in.

The torus was originally installed with baffle plates, but these were removed after installation.

A6.4.1.1.1 Commentary. The assumption of a fully flooded torus appears conservative from the viewpoint of loads on the seismic restraints. The flooded condition is not considered to be a realistic one. Normally, the torus is half-filled with water.

Sloshing modes could be excited by seismic events since the baffles in the torus have been removed. The A/E has recently supplied us with information which indicates that the natural frequency of the suppression chamber pool is on the order of 0.1 cps. The ground response spectrum curve (5% damping) for the BWR maximum credible earthquake (Fig. X A-7) shows a horizontal displacement of 4 in. at 0.1 cps, which is not considered to be significant.

A6.4.1.1.2 Conclusion. From our review of the information we have received from the A/E, we conclude that the modeling of the primary containment structure for providing seismic inputs to components mounted on the primary containment structure is adequate.

A6.4.1.2 Reactor Building (Secondary Containment).

The building is a cast-in-place reinforced concrete structure from its foundation floor at elevation 91 ft 6 in. to its refueling floor at elevation 234 ft. Above this floor, the building superstructure consists of metal siding and decking supported on a structural steel framework. The building is designed to be nominally 150 ft by 150 ft below elevation 135 ft and is 150 ft by 120 ft above this level. The foundation of the building consists of a monolithic concrete mat supported on sound rock. The mat also supports the primary containment and its internal components, including the reactor vessel pedestal. The exterior and some interior walls of the building above the foundation are cast-in-place concrete. Other interior walls are normal-weight concrete block walls. The floor slabs of the buildings are of composite construction with cast-in-place concrete over structural steel beams and metal deck. The thicknesses of walls and slabs were governed by structural or nuclear-radiation shielding requirements.

Each steel-framed superstructure is cross-braced to withstand wind and earthquake forces and supports metal

siding and metal deck for the roof. The roof consists of built-up roofing over the metal deck. The frame also supports a runway for the 125-ton traveling bridge crane.

The configuration of the reactor building and adjacent buildings is shown in Fig. X A-21.

The mathematical model used for determining the seismic loads on the reactor building, together with the interaction with the reactor vessel and sacrificial shield, is shown in Fig. X A-22. The first three natural frequencies in the horizontal directions were computed as shown in Table X A-23.

Modal inertia forces were found from the ground response spectra curves shown in Fig. X A-6 (2% critical damping design earthquake) and Fig. X A-7 (5% critical damping MCE). The associated modal shears, moments, and deflections in each of the building structural elements were then computed. Next, the modal loads in the building structural elements were combined on an absolute sum basis.

No dynamic amplification of the vertical ground motion was assumed to occur in the building because of its stiffness in the vertical direction and because the building is founded directly on rock.

Floor response spectra curves were generated by imposing a modified time history Taft earthquake at the base of the structure. The time history response at various elevations was then used to construct floor response spectra for designing equipment. Figure X A-23 shows a comparison between the response spectrum for 2% critical damping, which corresponds to the modified Taft earthquake, and the design ground response spectrum for the DE. Note that the design spectrum peaks at 3.8 cps, whereas the Taft spectrum peaks at 2.8 cps. Also note that the Taft spectrum exceeds the design spectrum at all frequencies above 0.6 cps.

A6.4.1.2.1 Commentary. The mathematical model appears to be a reasonable representation of the actual structure. The method of combining modal forces in the structural elements is conservative.

Figure X A-23 shows that the modified Taft earthquake used in generating the floor response spectra is conservative.

A6.4.1.2.2 Conclusion. The method of determining the seismic response of the reactor building is more than adequate, and the generated floor response spectra for designing equipment may be used with confidence.

A6.4.1.3 Containment Piping Penetrations.

Two general types of pipe penetrations are provided: (1) those which must accommodate thermal movement and (2) those which experience relatively little thermal stress.

The piping penetrations that accommodate thermal movement are the high-temperature lines, such as the steam lines, feedwater lines, and other reactor auxiliary system lines. The drywell nozzle passes through the concrete shield and is attached to a bellows expansion joint which, in turn, is attached to the penetration adapter to form a containment pressure boundary. The process line which passes through the penetration, is attached to the penetration adapter and is free to move axially. A guard pipe immediately surrounds the process line and is designed to protect the bellows and containment boundary should the process pipe fail within the penetration. Thermal insulation is installed in the annular space between the guard pipe and the process pipe.

The bellows assembly accommodates the thermal expansion of the process pipe and drywell. The hot process pipe is anchored at the penetration adapter external to the drywell and guided at the other end of the penetration to allow thermal movement of the pipe parallel to the penetration. Two isolation valves are provided, one outside the drywell and the other inside the drywell. These valves are located as close to the drywell penetration as practical.

The bellows expansion joints are of two-ply construction and permit leak testing of these penetrations at pressures up to the primary containment design pressure. The expansion joint assembly is designed, constructed, and tested in accordance with the previously specified requirements for the primary containment and code case interpretations, including Code Cases 1177-5 and 1330-1. The bellows are fabricated from stainless steel. Non-destructive tests of the assemblies include radiography and liquid penetrant tests of welds and pneumatic pressure tests of bellows.

Penetration adapters are one-piece forgings with integral flues made of the same material as the process pipe. The adapters are designed, fabricated, and tested in accordance with the previously

specified requirements for the primary containment.

The design of the penetrations takes into account the simultaneous stresses associated with normal thermal expansion, live and dead loads, seismic loads, and loads associated with a LOCA within the drywell. For all these conditions, including combinations of these loads, the resultant stresses in the pipe and penetration components do not exceed the code allowable design limits.

The design also takes into account the jet force loading resulting from the failure of the steam piping in addition to the other loadings given. The resultant stresses in the pipe and penetration for this condition do not exceed 90% of the yield stresses of the material.

Cold piping and ventilation ducts are welded directly to the drywell penetrations. Bellows and guard pipes are not necessary since the thermal stresses are small and are accounted for in the design of the weld joints.

The A/E performed design calculations to determine stresses in the framework that anchors the adapters to the reactor building structure. The final design of the framework was then analyzed with computer techniques.

Commentary and Conclusion

The calculations appear to be adequate. There is an inherent check between hand calculations and the computer results. We conclude that the piping penetrations satisfy design criteria and are adequate.

A6.4.1.4 Suppression-Chamber-to-Drywell Vacuum Breaker Valves.

Twelve self-actuating valves connect the drywell to the suppression chamber to prevent excessive negative pressure in the drywell. These valves are located within the suppression chamber at an approximate elevation of 116 ft on the eight large-diameter vent lines (four of these have two valves each, and the remaining four have one each). These valves are exercised by auxiliary air actuators operable at local control stations external to the containment. Figure X A-24 is a photograph of a valve similar to those installed within the suppression chamber.

It is important that the drywell-to-suppression-chamber vacuum breaker valves remain in a fully closed position until they are called upon to open to prevent the pressure in the suppression chamber from exceeding that in the drywell. If the valves were not closed, a path would exist for steam resulting from a small leak in the primary system (which does not entail a significant pressure build-up to help ensure that the valve is held closed) to pass directly into the vapor space in the suppression chamber.

At the time of the review, the vacuum breaker design for the prototype BWR plant was under active review and modification. The tentative new design existed on the A/E's drawing (Ref. 28) as marked up for proposed revisions.

The original design is identical to that of the breakers for an earlier BWR plant. Modifications have been effected in the electrical circuitry that provides valve-position signals in the control room and also in the auxiliary valve operator. Possible modification to the valve plate was also under consideration, but no change in the valve body design is contemplated.

The original specification for the valve was contained in the A/E's purchase specification (Ref. 29) which did not impose seismic requirements on the valve design. It has since been supplemented with the A/E's general seismic specification (Ref. 30) which requires a dynamic seismic analysis for all Class I components.

The only analysis that the A/E had on hand was that initially provided for the BWR plant, primarily concerning bolt stresses. The A/E has marked up this document with comments on omissions and suggested procedures. The A/E has requested that a more comprehensive analysis be furnished by the vendor and that the analysis be updated to reflect the supplementary seismic specification.

A6.4.1.4.1 Commentary. The seismic analysis of the design has not been provided; however, it is felt unlikely that the valve body (a short, large-diameter hollow cylinder) would be found to be highly stressed by seismic loadings.

Moreover, the A/E states that the new design (which has been installed) will avoid a feature of the original design that might cause impairment of the valve function. The original design employs a microswitch recessed into the rim of the valve seat to initiate a signal indicating that the valve is in the closed position. The operating button is

depressed by the valve rim when the valve is seated (like a door latch). However, a 9-lb force is needed to depress the switch. As a consequence, the valve plate must close with sufficient momentum to cam the switch. It was observed that in the event of an earthquake the valve plate might be jiggled slightly open. The switch might then act as a detent to prevent full closure, defeating one of the principal purposes of the valve.

No environmental qualification tests have been performed. Although such a test would be desirable to provide assurance that the position switches function properly, the absence of such materials as electrical insulation in the portions of the valve which are essential to its vital functions leads us to believe that it will function adequately in the event of either a small-leak or large-leak LOCA.

A6.4.1.4.2 Conclusion. There is no apparent reason to believe that these valves will fail to function under postulated seismic loads. The design criteria appear to be satisfied on the basis of engineering judgment.

A6.4.1.5 Missile Barriers Inside Containment.

The recirculation line is provided with pipe-whip constraints but the main steam and feedwater lines are not. The A/E made a thorough examination of the main steam and feedwater line configurations, postulating instantaneous circumferential pipe breaks at butt welds and selecting regions on the inside surface of the drywell that would be vulnerable to impact by the broken pipe whipping about a plastic hinge. These vulnerable regions of the drywell (which are quite extensive) have been provided with reinforcing shielding missile barrier plates, as described on pages Q.4.9.2-1 through Q.4.9.2-5 of the FSAR (Ref. 31). Figure X A-25, taken from Ref. 31, shows the location and "thickness" of the reinforcing plates.

The A/E's calculations indicate that the impact energy, E_I, to be absorbed by the barrier is derived from the relationship:

$$E_I = E_T - E_H$$

where E_T is equal to the thrust load (1.2 x operating pressure x break area for the main steam line) times the arc length of travel and E_H is the energy dissipated in forming the plastic hinge. E_I is then compared with U, the energy required to penetrate a plate, using an empirical formula derived by Stanford Research Institute (SRI):

$$U = D_m \sigma_u \, (0.344T^2 + 0.00806WT)$$

where:

D_m = width parameter of penetrating missile

W = height parameter of penetrating missile

σ_u = ultimate strength of target material

T = thickness of target material.

One part of the calculation indicates that a 3 1/2 in. plate thickness would not be sufficient to withstand an impact energy of 11.71×10^6 ft-lb but that the additional thickness of the drywell plate (3/4 in. thick) would provide sufficient protection. The installation drawings indicate that the final design consists of two plates, each 1 5/8 in. thick, which, along with the drywell 3/4-in.-thick plate, gives a total of 4 in. The A/E's calculations state that the empirical SRI formula for U may be modified for multiple thickness barriers by replacing T with ΣT_i.

A6.4.1.5.1 Commentary. The assumption that T can be replaced by ΣT_i in the SRI formula is incorrect since the relationship has a square term in T as well as a linear term. The energy required to penetrate multiple-plate barriers should be calculated on the basis of ΣU_i, where U_i is the energy required to penetrate each plate of thickness T_i. A rough calculation using the above application of the formula indicates that the multiple barriers could provide penetration resistance to roughly 8.8×10^6 ft-lb impact energy as opposed to the required 11.71×10^6 ft-lb, implying a negative margin of 33%.

Note: The A/E has at our request reviewed the original design and now finds that the pipe will impact the missile barriers at an angle of 41°; this reduces the impact velocity by approximately 25%. The A/E's revised calculations predict a 17% margin of safety. A reduction of impact velocity by 25% reduces the impact energy by 44%; however, the effective penetration area may also be very significantly reduced, and the impact energy per unit area may

actually increase if the missile strikes at an angle.

Additional analysis or penetration test data for multiple plates is required before the design adequacy can be assessed. More refined calculations, which would account for the effective increase in penetration area as each successive plate is penetrated, may show that the design is adequate. Some additional margin may be obtained in the computation of the energy dissipated at the plastic hinge if strain hardening is considered.

A6.4.1.5.2 Conclusion. In our judgment there is insufficient information to assess the adequacy of the missile barriers. Design adequacy has not been demonstrated.

A6.4.1.6 Paint Coatings Within Containment.

The internal surface of the containment liner, internal concrete structures, and metallic components are coated with special paint coatings. Aside from aesthetic purposes, coatings are used to prevent corrosion of metal surfaces and to seal the concrete. The coatings must be able to withstand normal and accident environments without becoming separated from the walls in any way, such as by ruptured blisters, flaking, and cracking. Excessive delamination of coating films could cause the clogging of strainers on the suction lines of the core spray and safety injection systems and interfere with their proper operation.

The coating system was applied in two stages. In the first stage an inorganic zinc prime coat was applied on the individual shop-fabricated assemblages by the steel fabricator. The finish phenolic coating was applied after the containment had been assembled and after damaged (e.g., scratched) areas and regions affected by welding had been touched up.

In March 1971, during a routine inspection of the torus (suppression chamber) portion of the containment, failure of the finish coating was found in the below-the-waterline regions (loss of adhesion over a significant area) and localized failures were found in the upper air-filled region. The following repair program was carried out in 1972:

a. Below waterline: Sand blast to white metal and apply one coat of inorganic zinc.

b. Waterline level: Sand blast to white metal in 2-ft band and apply one coat of inorganic zinc and one top coat of a phenolic coating.

c. Vapor zone (above waterline): Repair defective areas only.

The top coating in the vapor zone was retained because the condition of the coating was essentially good. Coating adhesion tests performed during the recoating investigation substantiated this decision.

During preoperational testing of the plant systems in May 1973, the torus was subjected to a relatively severe dynamic steam test (demineralized water heated to 180°F, held at this temperature for approximately 48 hours, followed by a fast cooldown). Following this test, blister formation was observed in the vapor zone. The total area of phenolic coating failure was estimated to cover less than 1% of the surface area. The inorganic zinc base coat in failure areas was reported by the utility to be in excellent condition. In general, the blistering or delamination occurred in the areas where a two-coat phenolic system existed because of unavoidable overlapping during the repair work. This determination was made by measuring the thickness of paint chips and by visual examination of exposed areas where the phenolic finish coating still existed. The examination also showed that the bonding between inorganic zinc and the metal surface was still intact.

In June 1973, those portions of the phenolic finish coat which exhibited poor adherence were removed. A testing program to determine the integrity of the remaining phenolic top coat was then initiated. This program included steam dynamic tests simulating the conditions experienced during the preoperational test. The utility reported that the results of inspections made after the conclusion of these tests clearly indicated that the inorganic zinc primer was performing its corrosion resistance function and that the vast majority of the remaining phenolic finish coat was firmly adhered and was satisfactory from a performance standpoint.

In view of the foregoing, the torus coating was then repaired a second time:

a. Below waterline: Sand blast to white metal and apply one coat of inorganic zinc.

b. Vapor zone: Repair defective areas in present inorganic zinc coating.

This procedure provided an inorganic zinc coating on the entire internal surfaces of the torus.

A6.4.1.6.1 Commentary. No documentation pertaining to a qualification program was provided to the reviewers, but we were informed that the manufacturer of the coating materials and the A/E had both conducted extensive testing programs which established that the coating system can be expected to perform adequately should a LOCA occur. Within the limits of our familiarity with the tests, this seems to be a valid conclusion. As is noted in section A6.3.1.3, however, it is extremely difficult to devise a qualification test for paint coatings which has a significant statistical basis and is not challengeable on the ground that the samples tested are not accurately representative of the coating actually applied in the field.

The utility has also presented an analysis which demonstrates that there probably will not be a safety problem even if the phenolic top coat should fail during a LOCA. The point is made that this material is thermosetting and has a melting point of about 1100°F. Should it come loose in an accident, the material will harden, become more brittle, and will not react with the deionized water. Also, since the phenolic is heavier than water, it will settle to the bottom of the torus. Plugging of strainers is not likely because of the configuration of the torus (segmented by structural ring girders) and because the core spray and HPCI strainers are connected to 16-in. pipe, the residual heat removal strainer is connected to 24-in. pipe, and the strainers are truncated cones with areas of 4.7 and 7 ft^2, respectively. The latter are mounted 1 ft above the torus invert and have 1/8-in. holes. Further, the strainer flow area is conservatively designed with twice the area required to pass the design flow at design pressure drop.

A6.4.1.6.2 Conclusion. The qualification programs conducted by the paint manufacturer and for the A/E, in conjunction with the testing performed on the actual coatings in the plant, provide reasonable assurance that the coating systems will not experience large-scale failure (flaking and/or delamination) should a LOCA occur. In addition, the construction features of the plant safety systems are such that, even if the containment coating should experience a large-scale failure, it is extremely unlikely that the performance of these systems will be significantly degraded.

The paint coatings within the containment satisfy the design criteria and are adequate.

A6.4.2 REACTOR COOLANT SYSTEM

The principal components of the reactor coolant system considered in this study included the reactor vessel and internals, the reactor vessel support, the two recirculation lines, the main steam lines and isolation valves, and the pressure relief system. The reactor vessel is supported by a cylindrical skirt that rests on a ring girder atop a concrete and steel support pedestal. The pedestal is an integral part of the building foundation (see Fig. X A-21).

The reactor pressure relief system consists of 11 relief and 2 safety valves mounted on the main steam lines within the drywell. The safety valves (Fig. X A-26) are spring-loaded valves set at 1230 psig. Each relief valve is self-actuating at set points ranging between 1080 and 1100 psig. The relief valves can also be actuated by remote control.

A6.4.2.1 Reactor Pressure Vessel and Internals.

Design calculations prepared by the reactor vendor on this unit were reviewed primarily from the viewpoint of dynamic mathematical modeling. These calculations provide an independent check on the A/E's model shown in Fig. X A-22.

The reactor building frequencies determined by the A/E and those found by the reactor vendor are as follows:

Reactor Building Mode	Direction	Natural Frequency (cps) A/E	Natural Frequency (cps) RCS Supplier
1	N-S	5.05	5.05
2	N-S	6.13	6.21
1	E-W	3.64	3.63
2	E-W	5.49	5.56

The maximum shear and moment at the reactor pressure vessel skirt base due to the seismic response of the system was found to be 205 kips and 6320 kip-feet, respectively; the allowables were 2396 kips and 96,276 kip-feet.

A6.4.2.1.1 Commentary. There appears to be excellent agreement between the buildings natural frequencies computed by the A/E and the RCS supplier, and this provides a high level of confidence in these values.

A6.4.2.1.2 Conclusion. The mathematical modeling for determining the seismic response of the vessel and internals is adequate.

A6.4.2.2 Reactor Pressure Vessel Nozzles.

The analyses of the structural integrity of a number of the nozzles at penetrations into the BWR vessel were reviewed. These include:

a. Main Steam Outlet Nozzle, No. 14.

b. Recirculation Line Inlet Nozzle, No. 7.

c. Recirculation Line Outlet Nozzle, No. 8.

d. Feedwater Nozzle, No. 10.

e. Core Spray Nozzle, No. 11.

f. 2-in. Instrumentation Nozzle, No. 12.

g. Control Rod Drive Hydraulic System Return Nozzle, No. 13.

h. Jet Pump Instrumentation Nozzle, No. 19.

i. 2-in. Drain Nozzle, No. 22.

j. Vent Nozzle, No. 204.

k. Head Spray Nozzle, No. 206.

The analyses for these nozzles were prepared by the reactor vessel manufacturer to the reactor vendor's specifications and are outlined in References 32 and 33.

The same analytical technique was used in evaluating all these nozzles. A Bijlaard analysis, computerized for cylinder-to-cylinder junctions, was used to obtain stresses in the vessel wall. Corresponding stresses for the nozzles were computed from beam-type formulae. The membrane stresses due to internal pressure are also considered. In addition, the provisions of article NB-3222.4(d) (Components Not Requiring Analysis for Cyclic Operation) of Section III of the ASME Code were invoked to qualify most of the nozzles in fatigue.

Table X A-24 presents the stress intensities reported for the nozzles. Nozzles that qualified in fatigue under Article NB-3222.4(d) are indicated.

A6.4.2.2.1 Commentary. There is no evidence in the documents offered for our review that the discontinuity stresses in the nozzles due to pressure loadings are accounted for in this analysis.

Moreover, none of the documents submitted for out review contained a thermal analysis. However, without an analytical demonstration or stress analysis, Reference 33 states that "...these nozzles are not subjected to severe thermal transient conditions, therefore primary and secondary stresses will not be critical." We believe, however, that an analytical demonstration of this point for at least one of the nozzles, preferably the 24-in. outlet nozzle, should be in the documentary record.

A6.4.2.2.2 Conclusion. Although these analyses do not entirely conform to analytical standards and procedures in effect today, we believe that in view of the adequate margins exhibited under the loadings considered, the structural integrity of these nozzles can be considered adequate.

A6.4.2.3 Reactor Pressure Vessel Skirt.

The analysis of the reactor vessel support skirt was performed by the vessel manufacturer (Ref. 34) using a finite element model of the skirt vessel junction and computerized techniques of structural and thermal analysis. Both thermal transient and mechanical loading conditions were considered, including the effects of the maximum seismic event and jet loads.

An elastic analysis was performed first with the results given in Table X A-25. As can be seen the allowable stress intensity range computed on an elastic basis exceeds the code allowable. The critical location was found to occur at the end of the filleted section nearest the skirt.

A simplified elastic-plastic analysis was therefore performed. The method used was subsequently incorporated into Section III of the ASME Code under para-

graph NB-3228.3. Although the current code requires demonstration that some collateral conditions be satisfied, these were not mandatory at the time the analysis was made. The analysis for the vessel skirt demonstrated that the elastic-plastic usage factor was 0.55 < 1.0 and concluded therefore, that the skirt was acceptable.

COMMENTARY AND CONCLUSION.

The analysis is judged to be in conformance with all code requirements in effect at the time it was made. In our opinion the structural adequacy of the vessel support skirt has been demonstrated.

A6.4.2.4 Recirculation Lines.

The recirculation lines extend between elevations 122 ft 4 in. and 163 ft 4 in. (Fig. X A-27) and are attached to the reactor pressure vessel at the upper elevation.

Each recirculation line was modeled by the supplier as a 27 lumped mass system subject to floor response spectra (135-ft elevation, 0.5% critical damping generated by the A/E) for the horizontal components (X and Z) of the earthquake and to a constant spectral acceleration of 0.033g for the vertical (Y) component of the DE and 0.08g for the vertical component of the MCE.

The following load cases were considered:

a. X + Y.

b. Z + Y.

c. Differential anchor motion = 0.022 in. in the X-direction.

d. Differential anchor motion = 0.022 in. in the Y-direction.

Stresses due to load case a were then linearly combined with the stresses due to load case c; stresses for load cases b and d were similarly combined.

Natural periods and the spectral acceleration values for the horizontal components of the earthquake used in generating modal inertia forces are shown in Table X A-26.

Critical stresses computed by the supplier, based on the assumptions and techniques described above, are summarized in Table X A-27.

A6.4.2.4.1 Commentary.

A6.4.2.4.1.1 Dynamic Response to Vertical Inputs. By taking a constant spectral acceleration of 0.33g and 0.08g for the vertical component of the DE and MCE, the supplier has not considered the dynamic response of the system to vertical inputs. Since the reactor building structure is extremely stiff in the vertical direction, it seems reasonable to assume that the building will transmit the ground motion directly (with no amplification). One can therefore take the vertical ground response spectra for 0.5% critical damping as the input for the vertical direction.

Taking two-thirds of the maximum g values for 0.5% critical damping (Figs. X A-6 and X A-7), one finds the vertical spectral accelerations and their associated frequencies to be:

a. DE - 0.18g (69.6 in./sec^2) @ 5 cps

b. MCE - 0.44 g (169.9 in./sec^2) @ 5 cps

These spectral acceleration values are considerably in excess of the 0.033g and 0.08g values used in the analysis performed by the supplier. Should the lowest vertical mode frequency of the recirculation line fall in the range of 5 cps, there would be a significant increase in the seismic stresses computed by the supplier.

If, for example, we consider the 12-in. elbow and assume that the vertical seismic stress contribution is two-thirds the seismic stresses shown in the critical stress summary (Table X A-27), the revised total stress for the P + W + MCE load combination would be 21,000 + 2/3 (13,180) = 29,787 psi, which is in excess of the 25,969 psi allowable.

A6.4.2.4.1.2 Closely Spaced Frequencies. We note from Table X A-26 that there are four sets of modes whose frequencies are closely spaced, i.e., the deviation from their mean value is on the order of 1%. It could be that the mode shapes for these closely spaced frequencies are not in the same direction, in which case there would be no problem; however, if they are along the same axis, the associated modal stress values should be combined on an absolute sum basis rather than by the square root of the sum of the squares.

A6.4.2.4.2 Conclusion. Additional analysis taking into consideration appropriate spectral accelerations for vertical earthquakes is required for a

final evaluation of the adequacy of the recirculation lines.

The reactor vendor has provided the results of a stress analysis of a main steam line (for a power plant of more recent design) which does take into account the dynamic amplification of the vertical component of the earthquake. The results show that stresses are within allowables. We have reviewed the analysis and note the following differences between the design which is the subject of this study and design analyzed:

a. The recirculation pump has four shock suppressors on the analyzed design compared to two on the study design.

b. There are a total of ten shock suppressors on each loop of the analyzed design compared to a total of four on the study design.

c. The analyzed design has one vertical and one near vertical shock suppressor compared to none for the study design.

It is apparent that the analyzed design has significantly more seismic restraints than the design we are studying; therefore the seismic analysis results of the other design are not applicable.

We conclude that the recirculation line from the viewpoint of seismic resistance does not completely satisfy the design criteria. Nevertheless, estimated stress levels indicate that failure is not expected and the design is considered adequate.

A6.4.2.5 Main Steam Lines.

The main steam lines extend between elevations 138 ft 2 in. and 203 ft 1 1/2 in. The piping system was seismically qualified by the supplier on the basis of an analysis performed for a similar plant at another site. Only the horizontal response spectra were used here, with the vertical response computed on the basis of constant 0.033g and 0.08g spectral accelerations in the same way as it was applied to the recirculation lines (see section A6.4.2.4). A summary of the natural periods and spectral acceleration values used in the analysis for the first nine modes is shown in Table X A-28.

The spectral acceleration values used by the analyst were exactly as found on the floor response spectrum curve without peak broadening. For example, the computed period for mode 2 is 0.187 sec, for which the analyst picked the exact spectral acceleration value of 1.81g. The same curve indicates, however, that for a natural period of 0.19 sec, (an increase of 1.6%), the spectral acceleration value would be 3.0g, i.e., an increase of 66% over the actual value used. Critical stresses are summarized in Table X A-29.

A6.4.2.5.1 Commentary. General comments regarding the dynamic response due to the vertical component of the earthquake are identical to those given in section A6.4.2.4. In addition, since it is not unreasonable to expect that the actual second-mode frequency could be higher than the computed value by 1.6%, it would be more appropriate to use the 3.0g value rather than 1.81g.

A6.4.2.5.2 Conclusion. The reactor vendor has provided the results of an analysis of a more recent design which accounts for the dynamic amplification of the vertical component of the earthquake and shows that streses are within the allowable. A comparison between the more recent design and the design which is the subject of this study shows that the degree of seismic restraint is similar.

On the basis of this additional evidence, we conclude that the design of the main steam line is adequate.

A6.4.2.6 Main Steam Line Isolation Valves.

Because they represent a potential large-diameter path for the escape of radioactivity to the environment should a steam line break outside the containment structure, the main steam lines are given special isolation consideration. Two 26-in. automatic isolation valves, each powered by both air pressure and spring force, are provided in each of the four main steam lines (see Fig. X A-28). One valve is located outside the primary containment and the other inside, approximately at elevation 135 ft. Each valve is provided with a hydraulic damper to prevent excessively fast closing rates that might damage the valve or piping system.

The valves have a Y-pattern body and a cylindrical main plug that moves on a center line 45° from vertical. The air cylinder operator is supported from the valve body by four rods that also serve as guide shafts for springs which provide a closure mechanism with sufficient

stored energy to seat the valve should the air supply be lost.

Normal closure is powered by a solenoid-triggered air cylinder that drives a central stem connected to the main plug. A spring and dashpot are incorporated into the stem to help control closure rates.

The analytical document prepared for the seismic analysis of the BWR MSIV (from which data used in the FSAR were taken) was originally presented for our review (Ref. 35). It contains errors as noted in our commentary.

During our initial examination of this document, we questioned some of its assumptions and methods. Consequently we were shown Reference 36, an analysis prepared for the seismic qualification of a MSIV for another plant. The valve is of the same nominal size, is supplied by the same manufacturer, but differs in some dimensions. However, the dimensional differences are not sufficient to invalidate the applicability of the calculations to the BWR valve; we therefore also reviewed this second analysis.

These calculations were prepared to the BWR NSSS supplier's specification that seismic coefficients of 0.6g vertical and 1.5g horizontal be applied as constant shock acceleration spectra from 0.25 to 33 cps.

The valve operator weighs about 3/4 ton and is supported from the valve body on four 3-in.-diameter rods about 4 ft long. During an earthquake the operator mass will be set into vibratory motion. Items of concern are the consequent stresses in the rods and the ability of the valve to remain functional throughout the seismic event.

Consequently, a 39-node 21-mass dynamic model of the actuator, the support rods, and their appurtenances was prepared. Using the STARDYNE computer program, mode shapes and corresponding frequencies were computed. The natural frequency was found to be 13.3 cps and is the only mode within the range of interest (0.25 to 33 cps). Because of the symmetry of the support rod arrangement, the structure is equally stiff in all transverse directions. It will respond to horizontal accelerations in the plane of the excitation and exhibit the same natural frequency in all directions.

The maximum stress was found to be 20,130 psi; the allowable value is 48,000 psi.

Experimental and analytical evidence bearing on the ability of the main steam isolation valve to function under a wide variety of accident flow conditions is contained in the NSSS supplier's topical report (Ref. 37). This report describes an extensive test demonstration program in which a commercial main steam isolation valve was installed in a full-scale flow test facility and operated under high flow conditions closely simulating those anticipated during a plant accident. Forty tests encompassing both single-phase and two-phase flow were conducted, a number of these being at the highest flow rates postulated for a design basis accident. These tests included:

Test Type	Flow Range (lb/sec)
Steam	50 to 1080
Water	240 to 3490
Two Phase (various qualities, 0.17 to 0.45)	1530 to 3860
Surge (quality 0.1 to 0.33)	520 to 2970

The report concludes that the MSIV will close under reactor accident flow conditions as evidenced by their closure during experimentally simulated reactor accident flow conditions.

In another test reported in an appendix to Reference 36, a valve similar to that installed in the BWR plant was loaded perpendicular to the valve stem center line by a dead weight applied through a pulley. The valve was then operated under the side thrust load. The loading produced transverse deflections equal to those expected under dead weight plus 1.5g seismic acceleration.

Closing time was insignificantly different from that when the valve was not loaded.

A6.4.2.6.1 Commentary.

A6.4.2.6.1.1 Seismic Analysis of Reference 35. The author, although properly identifying the fundamental character of the analytical problem as that of a frame, nevertheless subsequently treats the multi-rod structure as a single cantilever beam. This implies a shear connection between the rods and results in

a misevaluation of the stiffness of the operator structure. The computed stiffness is too high by approximately 25 times and results in an estimate of the natural frequency of 74.1 cps, which is about 5 times too high. Stress estimates are about 25% of those which the structure may actually experience during an earthquake.

This computation bears the major equipment supplier's stamp attesting to the fact that the document was approved and no further action was required.

A6.4.2.6.1.2 Seismic Analysis of Reference 36. Although the computation sheets in this report are signed off as checked by a member of the consulting firm that prepared them:

a. The weight of the modal masses does not total to the weight of the structural components (due to an error in weight allocation on page 17 of Reference 36.

b. A spot check indicates that the structure is not in equilibrium, even for simple dead weight loading. The reactions reported on page 14 for dead weight (θ = 0°) do not balance the applied loads (i.e., the set of weight loads actually used in the model). Neither the forces along the rod axis nor the overturning moment is equilibrated by the reported reactions at the base of the structure. We suspect an input error.

The error in assigning masses to nodes has only a small effect on results. Much more disturbing is the fact that the structure does not appear to be in equilibrium under its own weight (or more precisely, under the weight loads it was taken to have). Failure to satisfy this kind of a check often signals significant errors.

However, we believe that in this analysis the error falls to the conservative side. It appears to lower the natural frequency (which we estimate to be about 15 cps) and to overstate stresses.

Moreover, there are subsequent conservatisms deliberately introduced into the analysis:

a. Stress resultants are computed by summing absolute values of seismic and dead weight stresses without regard to sign.

b. The analysis considers the possibility that the valve might be installed with the actuator axis tilted 40° out of plane (i.e., rotated 40° off the vertical, about the pipe axis). This condition produces significantly higher stresses than would upright installation. In the summary, this worst-case stress is reported. Since one expects vertical installation to be the usual practice, the reported maximum stress is conservative for the majority of actual installations.

The functional flow tests were conducted using a 20-in. valve supplied by a manufacturer different from the one who supplied the MSIV for the BWR plant. The A/E contends that in light of the similarity of design among valves of this type supplied by various manufacturers for this application the results have general relevance for all such valves. The report implies that the effects of such differences as may exist between designs can be analytically accounted for and are not sufficient to alter the main results. This contention does not seem unreasonable.

Although these tests were conducted with some flow rates in excess of those predicted for major accidents, the predicted fluid pressures could not be fully duplicated. This limitation on the test was imposed by the engineers of the (conventional) steam generating plant furnishing the steam and water used as the test fluid. They feared structural damage to plant equipment from such pressures. Since MSIV have been tripped many times under normal flow conditions at full reactor pressure, we do not feel that the inability to duplicate pressures invalidates the conclusions reached in Reference 37.

A6.4.2.6.1.3 Environmental Qualification. Evidently, a formal qualification program has not been conducted to demonstrate by test that the electropneumatic control assembly on the MSIV will be functional when exposed to the ambient environmental conditions within the primary containment following a LOCA. Discussions with the NSSS supplier's representatives disclosed the following information pertinent to environmental qualification of the two components of this assembly which are subject to degradation:

a. Solenoid Actuators: Qualification is not needed because the design is fail-safe. The electrical signal is needed to hold the valve open; its removal for any reason will result in valve closure unless movement of the pneumatic control valve control-

led by the solenoid is impeded (i.e., by excessive binding of the seals).

b. Seals on Pneumatic Valves: Analysis shows that these will not degrade appreciably during 5 years of normal plant service (aging due to exposure to the temperature, humidity, and radiation environments). The seals will be replaced every 2 years in the preventive maintenance program.

These discussions also disclosed that a seismic qualification of the assembly was not conducted because of the fail-safe design and lack of a mechanism whereby an earthquake could cause a hang-up in the proper operation of the pneumatic valves.

The previous discussion gives reasonable assurance of the adequacy of the electromagnetic control assembly. A formal qualification program would, however, provide additional assurance.

A6.4.2.6.2 Conclusion. The ability of the main steam isolation valve to close under the maximum flow rates expected from a major plant accident has been demonstrated in full-scale tests. Seismic resistance has also been demonstrated. The design is adequate.

A6.4.2.7 Pipe Whip Restraint for Recirculation Lines.

The pipe whip restraints for the recirculation line are designed to constrain the piping only in the event of very large pipe movement due to a large break. This is accomplished by having a large radial clearance between the OD of the pipe and the ID of the restraint. The restraints are anchored to the structural framing surrounding the reactor vessel. Maximum spacing of the restraints is determined by assuming a pipe break and finding the moment arm that will just develop a plastic hinge in the pipe at the restraint. The thrust load is taken as the system pressure times the pipe flow area. The restraints are designed to have a maximum stress of 90% of the yield strength. They have been designed to withstand the following load cases:

a. Case I: Load is along the restraint symmetry line; it has only one component, T.

b. Case II: Load is transverse to the constraint symmetry line; it has a transverse component, S, and gives rise to a moment on the anchor bolts, M.

c. Case III: Load is at 45° to the constraint; it has components T and S and gives rise to a moment, M, at the anchor bolts.

A summary of the actual and allowable loads for the three cases is given in Table X A-30.

A6.4.2.7.1 Commentary. Although the recirculation line carries water, the design pressure and temperature are 1250 psig and 575°F, respectively; so, if there is a pipe break, the water will flash into steam. A thrust coefficient of 12.5 is therefore appropriate. Since the operating pressure is actually 1000 psig, use of a pressure of 1250 psig does, in effect, give the thrust coefficient. The calculations appear to be reasonable, and the results show that actual expected loads are within the allowables.

A6.4.2.7.2 Conclusion. The pipe whip restraints for the recirculation line satisfy the design criteria and are adequate.

A6.4.2.8 Reactor Pressure Relief Valves.

The 11 pressure relief valves are mounted on the main steam line headers within the drywell portion of the containment at elevation 160 ft. Each relief valve (Fig. X A-29) is self-actuating at the present relief pressure (set-point ranges between 1080 and 1100 psig for the various valves) but may also be actuated by a solenoid-operated air valve to permit remote manual or automatic opening at lower pressures. Each valve consists of a main valve disk and piston, operated by a second-stage disk and piston displaced by either a pressure sensing pilot or a pneumatically operated mechanical push rod.

The automatic depressurization system (ADS), a subsystem of the steam supply pressure relief system, serves as a backup to the high pressure coolant injection system (HPCIS) under small-leak LOCA conditions. Five of the relief valves are connected to provide for automatic depressurization of the reactor in this type of accident. These valves are equipped with accumulators and check valves arranged to ensure that the valves can be opened and held open even if the air supply should fail. The accumulators are sized for a minimum of five valve operations. The relief valves also can be operated by remote controls from the main control room.

A6.4.2.8.1 Commentary. Discussions with representatives of the reactor vendor (who was responsible for supplying the valves) disclosed that no formal qualification program has been conducted. Because these valves must function properly at the time of peak temperature conditions following a small-break LOCA, because they contain some nonmetallic materials (e.g., seals and electrical insulation) which are known to be adversely affected by thermal and radiation aging and by LOCA conditions, and because the valves are subjected to high internal and ambient temperatures during their installed life, we strongly believe that a proper, comprehensive qualification program (i.e., one including aging simulation, seismic testing, and LOCA exposure) should be conducted.

We note that Reference 31 states, "A solenoid control valve, identical to those associated with the [BWR plant] safety/relief valve was tested for 10 hours at temperature in excess of 300°F and a pressure of 62 psig. Results of this test show that the solenoid valve performed satisfactorily and there was no indication that temperature limits were approached." Since an ambient temperature of 340°F can reasonably be expected to occur at the time when these valves are required to operate, this statement is inconclusive. It is particularly important that the electric solenoid valves that provide for both ADS and manual actuation be fully qualified.

A6.4.2.8.2 Conclusion. We cannot conclude that the design of this component is adequate on the basis of available information. Design adequacy has not been demonstrated.

A6.4.3 CORE SPRAY SYSTEM

The core spray system consists of two independent, identical loops, each of which is capable of preventing excessive fuel cladding temperatures by cooling the fuel in the core should a LOCA occur. Each loop has two 50% capacity centrifugal pumps driven by electric motors, a spray sparger in the reactor vessel above the core, piping and valves to carry water from the suppression pool to the sparger, and associated controls and instrumentation.

The subsequent sections present detailed descriptions and design adequacy assessments of the following components of the core spray system: piping, piping hangers and snubbers, pumps and drives and pump and drive mounting, valves, valve motor operators, and instrumentation.

A6.4.3.1 Piping.

An isometric drawing of a portion of the core spray piping inside the containment is shown in Fig. X A-30. The piping is anchored to the drywell shield wall at elevation 143 ft 6 in. and connects to the reactor vessel nozzle at elevation 188 ft 7 1/2 in.

The fundamental frequency was computed to be 7.5 cps. Seismic loads were based on an average of the response spectra for the upper and lower anchor points assuming 0.5% critical damping values.

Table X A-31 summarizes the critical stresses. Modal stresses were combined by the square root of the sum of the squares method. The highest of the horizontal responses was added to the vertical response. The piping was evaluated in accordance with the B31.1 Piping Code.

A6.4.3.1.1 Commentary. An independent computer analysis was made, and the results were evaluated in accordance with the rules of B31.1 as well as the rules of the current NB-3600 portion of the ASME Code, Section III.

The independent analysis results show good agreement with the A/E result.

Discussion with the A/E indicates that the jump discontinuity in the temperature from 150 to 575°F shown on the isometric drawing (Fig. X A-30) is not realistic since the piping is exposed to the ambient temperature. It is expected that the actual thermal gradient along the pipe length is a gradual one.

Evaluation of computed stresses in accordance with the current code requirements showed the stress levels to be within the allowables if we neglect the unrealistic gross thermal discontinuity shown on the isometric drawing.

A6.4.3.1.2 Conclusion. The core spray piping inside the containment satisfies the design criteria and is adequate.

A6.4.3.2 Hangers and Snubbers.

As with other seismic Class I piping systems, the core spray system piping is supported by both conventional piping hangers and special shock absorbers termed snubbers. The locations of these components are shown in Fig. X A-30. The hangers are designed to avoid placing twisting forces on the piping system and to provide a constant supporting force even when the piping moves as a

result of thermal expansion as the temperature of the contained fluid changes.

A6.4.3.2.1 Commentary. No separate documentation pertaining to hanger design is available. The hangers are rugged devices, do not contain components that can be degraded as a result of the nuclear radiation and temperature conditions present in the plant or which may occur in an an accident, and have been extensively used in both fossil and nuclear power plants for many years.

The snubbers contain a hydraulic fluid and a movable piston. Seals must be provided to prevent the loss of fluid around the shaft. The seals used in snubbers installed in several power plants have deteriorated within a period of only several months, resulting in a loss of fluid and consequent loss of effectiveness. However, the snubbers installed in the BWR plant were produced by a manufacturer other than the one that produced the malfunctioning snubbers. The hydraulic fluid and the seals used in the snubbers that were installed in the plant were reported to be radiation-resistant materials.

No reports on qualification programs conducted for the snubbers used in the BWR plant were made available to the reviewers. It is our understanding, however, that the snubbers at the BWR plant have been modified to use the best materials now available (similar to the modifications made at the PWR plant).

A6.4.3.2.2 Conclusion. On the basis of engineering judgment, we consider the design of the hangers and snubbers to be adequate. In view of the fact that seal failure and loss of snubber fluid have occurred in other installations and that a proper qualification program has not been conducted, it is essential that a periodic surveillance of the snubbers be made, and that the seals and other materials that are susceptible degradation as a result of exposure to temperature, humidity, radiation, etc., be replaced before properties are seriously altered.

There is insufficient information to assess adequacy of the seal design of the snubbers. Resistance to seismic loads may be negated due to loss of hydraulic fluid.

A6.4.3.3 Pumps and Drives.

There are four core spray (CS) pumps and motor units located in four separate flood-protected rooms, two in the southeast corner and two in the northeast corner of the reactor building. The watertight entryway is identical to that shown in Fig. X A-36 for the residual heat removal (RHR) pump rooms.

Each pump and motor is vertically mounted, and the motor is supported on a bracket that bolts to the pump casing (Fig. X A-31). The pump itself is bolted to a foundation pad on the floor (Fig. X A-32). Pump mountings are oriented in three different directions: two of the pumps are parallel and the other two are oriented at 45° to the first pair and 90° to each other. Each pump can deliver water to the reactor core at a rate of 3125 gpm when a 105-psi pressure difference exists between the reactor vessel and primary containment. Each CS motor is rated at 600 hp and operates at 482 kW.

The weights and heights of the center of gravity for the core spray pumps and motors are:

Unit	Weight (lb)	Height of CG Above Mounting Pad (ft)
Motor	5200	6.51
Mounting Bracket	5300	3.94
Pump	3000	1.92

The A/E's original seismic calculations for the anchor positioned the entire horizontal inertia force of the motor and pump at the pump CG, thus reducing the overturning moment due to the higher position of the motor CG. This was pointed out to the A/E during the course of the review. The A/E then computed the fundamental frequency of the pump-motor, which permitted the use of lower acceleration values from the floor response spectra curves. The revised results showed a small positive margin. Nevertheless, the A/E has strengthened the anchor installation to provide additional margin.

There are no piping systems in the CS pump rooms other than those associated with the respective pumps.

The A/E has performed an analysis which shows that the pump seals will not be significantly degraded by exposure to nuclear radiation emanating from the radioactive water pumped under accident conditions.

A6.4.3.3.1 Commentary. A formal qualification program for the pumps and drives has not been conducted. However, the reactor vendor has functionally

tested a similar motor in a saturated steam environment at atmospheric pressure (Ref. 38).

From the viewpoint of seismic protection, the pumps are strategically located and oriented as follows:

a. They are at or near ground level, where amplification of the ground response spectrum is minimal.

b. They are located in separate rooms in different areas of the building.

c. Their mountings are oriented in three different directions.

Thus, for a seismic event, only two pumps (at most) are likely to experience the same excitations and consequently exhibit similar responses.

A static analysis (using 0.6g horizontal and 0.07g vertical) was performed. The maximum g load from the floor response spectra is 0.3g horizontal for the DE and 0.72g horizontal for the MCE. Independent calculations performed by the A/E show that the fundamental frequency of the unit is 12 cps. The spectral acceleration value for this frequency is 0.14g for the DE and 0.336g for the MCE. The 0.6g value used in the analysis is therefore conservative.

The most critical stress was found to occur in the driver stand bolting (16,500 psi computed, compared to the stated allowable stress of 20,000 psi). Margins above allowable stresses are substantially larger for all other sections examined.

As discussed in section A6.4.5, a pseudo seismic qualification test of the RHR pump has been conducted in which a pump, motor and coupling were set up and run in a test loop. The RHR and CS pumps are made by the same manufacturer. The RHR pump is about twice the size of the CS pump; so its natural frequency would be lower. Since the pumps are similarly mounted, it is reasonable to expect that the CS pump would successfully pass a qualification test under a maximum load of 0.34g. An actual test of the CS pump would offer more assurance, however.

A6.4.3.3.2 Conclusion. We believe that (1) the seismic computations justify the assumption that the structural support of the core spray pumps and motors is capable of meeting the seismic requirements of the specifications, (2) on the basis of physical isolation considerations and the test conducted on a similar motor, there is no reason to expect that the functioning of the pumps and drives will be impaired as a result of a pipe break, and (3) it is reasonable to expect that the pump and motor will function adequately following a safe shutdown earthquake, based upon the performance demonstrated in the vibration test of the RHR pump. The units satisfy the design criteria and are adequate.

A6.4.3.4 Valves.

Several valves are associated with the core spray system. Specifications for several of the valves were reviewed, and the procedures that were followed in the design of the valves were discussed with the A/E. We were informed that a qualification program for the various valves was under way but that no data were yet available.

A6.4.3.4.1 Commentary. The specifications do not require that the ability of the valves to function properly under seismic events be demonstrated but rather that they not fail as pressure containing members. Some relatively minor inconsistencies among the specifications were also noted (e.g., the requirement to withstand aging and nuclear-radiation exposures under LOCA and post-LOCA conditions).

A6.4.3.4.2 Conclusion. In the absence of a formal qualification program, we cannot make a rigorous assessment of the design adequacy of the valves. On the basis of the reviewer's experience in performing stress analyses of similar valves, we can conclude that there is a good probability that the valves can be expected to function properly under an accident situation. In our judgment the valves satisfy the seismic criteria.

A6.4.3.5 Valve Motor Operators.

Figure X A-33 shows the valve motor operators (VMO) appended to and supported by the valves they control. A large number of VMO, of varying size but similar in design, are used in the plant. The VMO units used inside the primary containment have Class H insulation; the units installed outside have Class F insulation. None of the VMO in the CSS are installed within the primary containment.

A6.4.3.5.1 Commentary. The VMO installed in the BWR plant were subjected to a rigorous qualification testing program that consisted of aging, nuclear radiation, simulated seismic conditions, and simulated LOCA exposures in the simulated seismic test (Refs. 39 and 40). An

aged operator was mounted on a vibration table and subjected to vibration of 20 cps at 1g for 2 min on and 1 min off, repeated five times along both the vertical and horizontal axes of the actuator. This test does provide considerable reassurance that the VMO will function adequately even though the test does not conform to the current requirements.

A6.4.3.5.2 Conclusion. We believe that the qualificaton testing program that was performed, although not fully equivalent to the current requirements, does nevertheless demonstrate design adequacy.

A6.4.3.6 Instrumentation.

The instrumentation and controls which sense that a LOCA event has occurred and which initiate functioning of the core spray system are part of the reactor protection system. The CSS instrumentation includes pressure switches on the discharge line from each set of core spray pumps to indicate the successful start-up of the respective pumps, the flow-measuring instrumentation in each of the pump discharge lines, the motor current, and the valve-position-indicating switches (included as part of the valve operators). Flow rates, motor currents, and valve positions are displayed in the control room.

A6.4.3.6.1 Commentary. Specific information relating to the qualification of these instruments is not available; hence we cannot assess design adequacy. However, the failure of the instrumentation cannot completely negate the functioning on the system. The discharge flow rate would be lowered if the pump discharge pressure signal were not present to cause the bypass valves to be closed and thereby enable all the flow to be directed to the core.

A6.4.3.6.2 Conclusion. Either the core spray instrumentation should be qualified or the effect of reduced delivery to the reactor in the event of a LOCA should be evaluated. There is insufficient information to assess adequacy of the CS instrumentation.

A6.4.4 HPCIS TURBINE

The high pressure coolant injection system (HPCIS) consists of a steam turbine driving a constant-flow pump, system piping, valves, controls, and instrumentation. The pump has a design flow rate of 5000 gpm at 1120 to 150 psid (pounds per square inch differential between reactor vessel and primary containment). The HPCIS is capable of reaching the design flow rate within 25 sec from receipt of an appropriate signal from the automatic controls.

The HPCIS is installed in the reactor building at elevation 88 ft. Suction is from the condensate storage tank and the suppression pool. Injection water is supplied to the reactor feedwater piping at a T-connection. Steam supply for the turbine is piped from a main steam header within the primary containment. This piping is provided with an isolation valve on each side of the drywell wall. Exhaust steam from the HPCIS turbine is discharged to the suppression pool. Remote controls for valve and turbine operation are provided in the main control room.

As is shown in Fig. X A-34, the HPCI pump and turbine are mounted on a massive concrete foundation block, which in turn is an integral part of the reactor building foundation. A speed reducer is provided between the two stages of the pump (booster pump and main pump). The large pipe in the foreground of the photograph connects the pump stages. Figure X A-35 shows the turbine end of the unit.

The turbine has two devices for controlling power: (1) a speed governor, which limits turbine speed to its maximum operating level, and (2) a control governor, which is positioned by a demand signal from a flow controller, to maintain constant flow over the pressure range of HPCIS operation.

A consulting organization performed seismic calculations (Ref. 41) for the turbine.

The shafts for the turbine and pump are horizontal and are connected via a flexible coupling. Equivalent static loadings of 1.5g horizontal and 0.48g vertical were applied.

Seismic stresses were found in the turbine casing, shaft, hold-down bolts and connections, pedestals, base plate, and tie-down to the foundation.

The analysis determines stresses and displacements in 10 critical areas including bolting, turbine shaft, pedestals, the stop valve assembly and the base plate connection.

The analysis of the yoke that connects the cylinder to the stop valve makes the implicit assumption that there is a shear connection between the two legs of the yoke.

A6.4.4.1 Commentary.

The implicit assumption that there is a shear connection between the two legs of the yoke is incorrect. We estimate that the correct stresses in the yoke would be approximately 20,000 psi rather than the 13,100 psi computed by the vendor. This value is still within the limit of 33,000 psi.

Other than the above error the analysis is thorough and adequate.

A6.4.4.2 Conclusion.

We conclude that the HPCIS turbine is capable of resisting seismic environments. Design criteria are satisfied. Seismic design adequacy has been established.

A6.4.5 RHR PUMPS AND DRIVES

The plant has four identical residual heat removal pumps. These are the main pumps for the residual heat removal (RHR) system. This system can be assigned several functions:

a. Removal of residual core heating during and after plant shutdown (the system's normal operating function).

b. Re-flooding of the core after an accident in which watering the core is temporarily lost. The RHR system is one of three pumping systems which can be assigned this function and is activated when reactor pressure is reduced and rapid delivery of a large volume of water is required.

c. Post-accident containment cooling. Heat is removed from inside the containment by continual cooling of suppression pool water by circulation through the RHR heat exchangers.

d. Reduction of primary containment pressure. After an accident the RHR system can be used to spray water into the primary containment (condensing steam and thereby reducing pressure) simultaneously with the function described in item c.

Each pump is housed in a separate flood-protected room of the reactor building. Figure X A-36 shows the watertight entryway to one of the rooms. One pair of rooms is located in the northwest corner of the building, the other in the southwest corner. In each room the pumps are mounted on the floor at elevation 91 ft 6 in. (see Fig. X A-37).

In addition to the dispersion of pump locations, the orientations of the pump mountings and connected piping are also disparate. Two of the pump discharge connections are parallel, and each of the remaining pair of pumps is oriented at 45° to the first pair and at 90° to each other.

A6.4.5.1 Seismic Qualification.

Each pump and its motor drive are vertically mounted as a unit, and the motor is supported on a stand that bolts to the pump casing. The casing, in turn, is mounted on a footing that bolts to a foundation pad. The piping also provides a measure of lateral restraint to the pump casing. The configuration is shown in Fig. X·A-38.

The weights and heights of the center of gravity for this equipment are tabulated below:

Unit	Weight (lb)	Height of CG Above Mounting Pad (ft)
Motor	14,000	9.8
Mounting Bracket	2,200	3.67
Pump	5,600	1.5

The structural adequacy of the pump and motor mountings was assessed with a static g-load analysis using 0.6g for horizontal and 0.07g for vertical loading.

This original seismic analysis is part of the supplier's design computations (Ref. 42). These computations cover only the sizing of structural members supporting the RHR pump and motor masses.

The effects of the seismic static g loads were examined at five critical cross sections:

a. The motor mounting bolts.

b. The cross section of the driver stand at bottom of the cutouts.

c. The driver stand mounting bolts.

d. The base plate welds.

e. The foundation bolts.

The results of these computations show that design stresses are well below the allowable stresses.

A vibration test of the RHR pump has also been conducted; results are reported in Reference 43. In this test a pump, motor, and coupling were set up and run in a test loop. Vibrations were produced by suppressing the net positive suction head of the pump, i.e., by introducing cavitation at the intake.

Horizontal accelerations and displacements along two perpendicular axes were recorded for stations at three different elevations on the pump and motor assembly.

The maximum horizontal acceleration occured at the top of the motor and was approximately 3.5g.

Twenty tests, lasting at least 30 sec each, were run for a number of net positive suction head (NPSH) conditions while the pump was operating in the loop. The pump operated successfully under these vibratory conditions.

A comparative inspection of bearing seal, wear ring, and shaft runout was made before and after the set of test runs. No visible damage occurred.

The report concludes in para. A6.4.5.3.3 that the natural period of vibration of the pump is about 0.033 sec.

In addition, Ref. 43 includes a section in which further static g-design computations of the type described in Ref. 42 are reported. These computations generally confirm the results of the previous analysis, and the report concludes that the structure is adequate under horizontal g loadings of at least 1.5g.

A6.4.5.2 Environmental Qualification.

A formal qualification program for the pumps and drives has not been conducted. However, the reactor vendor has functionally tested a similar motor while it was subjected to a saturated steam environment at atmospheric pressure (Ref. 38). In addition, as in the case of the core spray pumps, the A/E performed an analysis which shows that for 6 months following a LOCA the pump seals will not be significantly degraded by exposure to nuclear radiation emanating from the pumping of radioactive water. A formal qualification program has not been conducted, however.

A6.4.5.3 Commentary.

A6.4.5.3.1 Location, Arrangement, and Housing. The physical arrangement of these pumps and the manner in which they are housed have important implications for the seismic and environmental integrity of the units.

From the viewpoint of seismic protection, the pumps are strategically located and oriented as follows:

a. They are at or near ground level, where building amplification of the ground response spectrum is nonexistent or minimal.

b. They are located in separate rooms in different areas of the building.

c. Their mountings are oriented in three different directions.

Thus, for a seismic event, only two pumps (at most) are likely to experience the same excitations and consequently exhibit similar responses.

From the viewpoint of the ability of the pumps to perform under accident conditions, the manner in which the pumps are housed adds a substantial measure of assurance that they will operate despite adverse environmental conditions in the plant.

The individual pump compartments contain no other piping than those required for RHR pump operation (i.e., pump loop piping, RHR heat exchanger piping, service water lines for pump cooling, and the room cooling system). The pump room hatchway doors (which protect the pump from floods) also isolate the pump from spray or steam that could result from rupture of other pipe systems outside the pump room.

A6.4.5.3.2 Seismic Analysis. The seismic design computations of Ref. 42 present credible evidence that the main structural members supporting the RHR pump and motor have been designed to code requirements for the specified earthquake loadings based on the following considerations:

a. The static g loading of 0.6g horizontal and 0.07g vertical is adequate when compared to the peak floor response levels of 0.5g and 0.07g vertical.

b. The computations employ standard strength-of-material formulas. Although these are first-order design approximations involving simplifications and although they may not account for all stresses in the structure, they do reflect the major effects of the design loads. Moreover, the designer preserved sub-

stantial margins over and above the allowable stresses at every section be examined.

c. The formulas used are appropriate to the situations considered. For example, when the stresses in the motor mount at sections with cutouts was examined, a formula was selected which takes into account the reduction in the moment-carrying capacity of such sections due to the lack of shear connection.

d. For the structural members supporting the pump and motor (the main thrust of this computation), the results are conservative since they take no credit for the additional restraint provided by the piping.

e. The computations show evidence of having been numerically checked and (although some numerical disparities are indicated) were found to have no numerical errors of engineering significance.

A6.4.5.3.3 Seismic Tests. The natural period of the pump and motor is reported in Reference 43 to be about 0.033 sec; that is, the natural frequency is 30 cps. In our judgment, what we observed was that the shaft speed was: 30 rev/sec x 60 sec/min = 1800 rpm; rather than the natural frequency.

Considering the method of excitation - inducing cavitation by starving the suction head - one should not be surprised to find the shaft frequency strongly represented in the data since cavitations (although a complex process) can be expected to provide a form of unbalanced rotor.

Moreover, if it were thought that the reported frequency was actually the natural frequency of this structure, a serious design deficiency should have been declared, since the structure could then be excited by the motor's rotation.

Nevertheless, the test record may supply an indication of the structural response. Figure X A-39 shows two of the test records. These are traces of the horizontal displacement vs. time recorded at the top of the motor. The traces exhibit detectable repetitive scallops at 6 to 7 cps which may have been produced by the structure's response. This evidence is too meager to support a substantive conclusion. However, the frequency of 6 to 7 cps is close to the natural frequency we predict for this structure on the basis of a simple 1 degree-of-freedom independent calculation.

It is evident that the excitation method used in these tests fails to model earthquake-induced vibrations. However, this unit did experience repeated severe vibrations over time periods at least as long as those an earthquake would produce and also experienced g loadings (at least at the motor mass, which is both the largest system mass and the one farthest from the supports) significantly larger than those expected from the design earthquake. On this basis, one can reasonably infer structural seismic adequacy.

A6.4.5.3.4 Environmental Qualification. The residual heat removal system stands out among the engineered safeguards features as one whose postaccident function calls for heavy-duty operation over a prolonged period. Therefore, the environmental qualification of this system is particularly significant and should be reported in a unified document.

Nevertheless, it does appear, on the basis of physical isolation considerations, tests conducted on a similar pump drive, and analysis of possible radiation degradation of the pump seals, that there is no reason to expect that the functioning of the pump or motor will be impaired as a result of pipe breaks in other systems or ambient temperatures, steam environments, or radiation exposure following a LOCA.

A6.4.5.4 Conclusion.

Seismic adequacy of the RHR pump and drive has been demonstrated by static analysis and may be inferred from the vibration test.

A6.4.6 ON-SITE ELECTRIC POWER SYSTEMS

The electrical power systems at the plant are designed to provide a diversity of dependable power sources which are physically isolated so that any failure affecting one source of supply will not propagate to other sources.

The plant receives power from two separate off-site sources. In the event of a total loss of power from off-site sources, auxiliary power is supplied from diesel generators located on the site. Each power source, up to the point of its connection to a 4-kV emergency auxiliary power bus, is capable of complete and rapid electrical isolation from any other source. Loads important to plant safety are split and

diversified between auxiliary bus sections, and means are provided for rapid isolation of system faults. Station batteries are provided as a reliable source of control power for specific engineered safeguards and for other functions required when a-c power is not available. The diesel generators are housed in a separate building, and the batteries are housed within the complex of main plant buildings.

A6.4.6.1 Diesel Generator Building.

The diesel generators are housed in a reinforced-concrete seismic Class I structure with the floor at elevation 127 ft. Each of the diesel generator units is located in an individual room. The building is watertight to the design flood level of elevation 135 ft, and is also intended to provide protection against other natural phenomena, such as tornados, lightning, rain, ice, and snow. The building, which measures approximately 62 ft deep, 134 ft wide, and 33 ft high, is located approximately 80 ft south of the turbine building. Figures X A-40 and X A-41 show two sides of the building. The large-equipment accesses are provided with missile-protected doors; the air intakes on the second floor are also designed to prevent the entry of tornado-generated missiles.

The diesel generator building is supported by concrete shear walls and H-beam piles which are carried down to rock. The elevation of the rock is well below the floor slab and varies as the general terrain falls off toward the river. Consequently, the depth to which the shear walls extend below the floor slab differs significantly at either end of the building. The floor slab is intermediately supported on sets of H-beam piles embedded in the rock.

A6.4.6.1.1 Seismic Resistance. Seismic design was carried out in accordance with the rules of the ACI code and is contained in the design report of Ref. 44. A dynamic analysis was performed to determine the building response to seismic excitation. The model for this analysis is shown in Fig. X A-42.

The model departs slightly from the conventional equivalent beam model used by the A/E to represent other building structures. The slab is represented as a rigid beam supported at either end by massless springs assigned lateral shear stiffnesses based upon the shear area of the individual walls at either end of the building. This representation was used to take into account the unequal heights of the shear walls under the slab. In the model the floor slab is assigned near-rigid stiffness sectional properties.

With these assumptions the lowest fundamental frequency was found to be 6.9 cps (north-south direction) and 10.5 cps (east-west direction).

Assuming 2% damping for the design earthquake (DE) and 5% damping for the maximum credible earthquake (MCE) and using the site response spectra, the maximum deflections of the building were determined. These were found to occur at the roof and were:

a. 0.00262 ft = 0.031 in. (N-S, DE)
b. 0.00453 ft = 0.054 in. (N-S, MCE)

The most critically loaded members were found to be rebars at the bottom of the south wall. Computed stresses and their corresponding allowable values are tabulated below:

Type	Rebar Seismic Stress	Allowable
DE	13,500 psi	20,000 psi
MCE	24,200 psi	36,000 psi

The A/E stated that these results were confirmed by another independent analysis.

This model was also used to generate floor response spectra. For this purpose the time-history input (modified Taft 1952 record) used for the reactor building was employed.

A6.4.6.1.2 Commentary. The assumptions, modeling methods, and computational procedures used for this analysis are judged to be appropriate to show code compliance for this structure.

It is concluded that the diesel generator building is designed with adequate margin for seismic loads.

A6.4.6.1.3 Tornado Resistance. The diesel generator building was subject to tornado loads as described in section A6.2.2.

A6.4.6.1.3.1 Penetration Calculations. Four types of barriers are used to protect the generator system:

a. Monolithic concrete walls: 2-ft thick, reinforced in both faces with 0.44 in.^{2}/ft steel rods.

b. Steel doors: 2.5-in. thick.

c. Double-thickness corrugated metal barriers with a single flat sheet between, i.e., three layers of 12-gauge high-strength steel.

d. 3.5 ft of compacted soil.

Kinetic energy per unit area of impact of the 4-in. by 12-in. by 12-ft plank is greater than that of the auto; hence, through the barriers provided, it governs the design against missile penetration.

Concrete walls were originally sized to protect against turbine missiles. At a later time the turbine missile was ruled out because the orientation of the generator building made the probability of such a missile striking the building unlikely. The initially calculated 2-ft thickness of the walls was, however, maintained. Calculations using the Petry formula indicate that a thickness of 1 ft is required to prevent scabbing by the plank.

Calculations of the penetration resistance of steel doors, using the Stanford formula, showed that the required minimum thickness is 1-3/16 in.

The resistance of corrugated metal barriers to penetration was demonstrated by tests carried out by the vendor in conjunction with a testing laboratory.

Penetration of the cover of compacted soil over the fuel tank was not considered. However, since a manifold system connecting all tanks is provided, penetration here would not represent a safety problem.

An approximate calculation made by the reviewer indicates that the plank would penetrate about 8 ft of sand.

A6.4.6.1.3.2 Overall Response Caculations. The type of failure associated with overall response may occur away from the immediate impact area and give rise to collapse of the missile barrier in much the same manner as would be produced by an excessively large load of any other origin.

The areas considered for penetration, except for the soil cover, are again examined for the overall response.

A6.4.6.1.3.2.1 Concrete Walls. An approximate analysis based on an estimate of the energy to be absorbed by the structures was performed. The procedure, as used, appears to be generally conservative and the adequacy of the concrete was demonstrated.

A6.4.6.1.3.2.2 Steel doors. An overall response analysis was performed by a vendor and checked by the A/E. The approach used was that of the energy balance. Part of the missile kinetic energy was assumed to be absorbed by the door, the remaining energy being dissipated by plastic deformation of the missile. The energy-absorbing capacity of the door was computed by the limit load method. This method gives an upper bound (conservative) estimate for the energy absorbed by the door. The method also neglects the momentum of the plate, which is a conservative assumption, and thus the net result appears conservative. The analysis indicated that the doors must absorb 50% of the impact energy.

Only the plank missile was considered. However, since the kinetic energies of the plank and auto are about the same, the only question is related to the assumption of a 50% reduction in the kinetic energy of the missile due to the plastic behavior of the missile during the impact. An examination of this question indicates that about 95% of the kinetic energy of the plank missile and about 50% of the kinetic energy of the car missile are dissipated through the plastic behavior of the missile at the impact. Therefore, it appears that the analysis made was reasonable for the auto and conservative for the plank missile.

No calculations were made to demonstrate the ability of the steel door fastenings (hinges, lugs, etc.) to withstand the door rebound force after the initial impact.

A6.4.6.1.3.2.3 Corrugated Metal Barriers. No overall structural response calculations were made. It is not clear from the vendor's test report how the panel was supported during the penetration test. While of little consequence for the penetration resistance, the method of support is important with regard to overall behavior. For example, the two braces supporting the top of the panel are secured to the floor with only four 3/4-in.-diameter bolts each. An approximate calculation indicates that a strike by the plank missile near the top of the barrier would most likely shear these bolts.

A6.4.6.1.3.3 Wind Loads. The wind loads on concrete walls were dismissed by comparison with seismic loads. This comparison was based on the differential

pressure induced by 300-mph winds and not on the 3-psi differential specified in the criteria. This, in turn, was based on the assumption that adequate venting is provided to prevent realization of the full 3-psi differential in the emergency generator building.

No calculations were made for the steel doors. An approximate analysis indicates that these doors would have to be subjected to a pressure well in excess of the full 3-psi differential specified before collapse would occur. However, this load acts outward so that full differential pressure load would be reacted by the hinges, lugs, etc., for which an analysis has not been done.

The criteria regarding the torsional moment (see item 4 in section A6.2.2) were of no consequence for a building as small and as compact as the diesel generator building.

A6.4.6.1.4 Conclusion. We conclude that design criteria for seismic resistance of the diesel generator structure have been satisfied.

Considering the governing criteria, this review indicates that the emergency diesel generator building structure and door adequately resist tornado effects.

There is insufficient information to assess the tornado resistance of the following items:

a. Corrugated metal barrier attachments.

b. Steel door supports, i.e., their adequacy to resist the differential pressure and the elastic rebound forces caused by missiles.

A6.4.6.2 Diesel Generators.

Four diesel generator units are provided, each consisting of a diesel engine, a generator (3250 kW at continuous operation), and the associated auxiliaries mounted on a common base. Figure X A-43 shows the diesel generator from the generator end, and Fig. X A-44 shows the turbo-charger.

The seismic analysis for the diesel generators was performed by the vendor. Although the analysis (Ref. 45) was performed for units to be installed at another nuclear power plant and does not form an official part of the documentation of the BWR plant, it has been reviewed by the A/E and approved as suitable (with minor modification) to demonstrate the seismic integrity of the diesel generators at the BWR plant.

Figure X A-45 shows the model used for the dynamic analysis. The unit, including two turbo-chargers, weighs about 40 tons; the mass is distributed to five lumped-mass points.

Two of the masses represent the engine and are placed symmetrically about the engine center of gravity to simulate the rotational inertia of the engine. The engine block, in which the masses are imbedded, was assumed effectively rigid. The generator rotor and stator are considered separate masses and are joined by a spring simulating the bending stiffness of the rotor shaft. The effective stiffness of the stator support beams is also represented. The turbo-chargers (which are mounted on a bracket bolted to the front of the engine) comprise a fifth mass with the stiffness of their support bracket modeled by the spring between the turbo-chargers and the engine block. In addition, a flexibility matrix was developed to represent the effects of the skid that supports the diesel generators.

This model is used to determine the response of the unit to transverse horizontal excitations. Under vertical accelerations, the generator stator can be excited in a rocking motion, fore and aft. The model for vertical excitation is, therefore, slightly modified to detect and display such motions.

With this model, modal frequencies were found by computer to be:

	Natural Frequencies (cps)	
Mode	Horizontal Transverse	Vertical
1	9.63	20.21
2	13.52	45.44
3	38.60	---

Examination of the displacement amplitudes shows that the turbo-charger units are the only masses exhibiting significant response to the lowest natural frequency (9.63 cps). Stresses in the turbo-charger supporting bracket and its bolts were therefore computed. In this computation, modal forces were combined on an absolute basis (conservative practice), and vertical and horizontal reactions were assumed to occur simultaneously.

The bracket is retained by eight bolts. Although these are only 5/8-in. bolts

(about minimum engineering practice for heavy equipment), the most severely stressed bolt is under 19,400 psi tension vs. a proof load equivalent to 52,000 psi. The most critical section of the bracket was also examined and found to have a maximum principal stress of 19,400 psi vs. a material yield strength of 33,000 psi.

Stator-rotor clearances under seismic excitations were also checked and found adequate.

A6.4.6.2.1 Commentary. The modeling appears to have been carefully considered, the computations are clearly presented, and the analysis is judged to be of high quality.

For the BWR installation, the diesel generator building floor response spectum (elevation 125-ft, 0-in.) indicates that a slightly greater acceleration is appropriate for the safe shutdown earthquake than was used in the analysis reviewed - 0162g at the BWR site vs. 0.525g used in the analysis. However, considering the conservatism in the analytical procedures and the margin of safety shown in the calculations, the analysis is regarded as satisfactory evidence that the design also complies with the structural requirements for the BWR application.

A6.4.6.2.2 Conclusion. We judge the seismic design adequacy of the diesel generator units to have been well demonstrated.

A6.4.6.3 Batteries and Battery Racks.

Station batteries are provided as a reliable source of control power for specific engineered safeguards and for other functions required when a-c power is not available.

The battery racks were furnished by the battery vendor. Racks come in 6-, 12-, and 17-ft lengths. General construction is in the form of a two-step two-level frame as shown in Figs. X A-46 and X A-47. Batteries at each of the two levels rest on a pair of longitudinal bottom rails attached to the frame. Diagonal cross-brancing of the frame is provided in the longitudinal direction by use of cross ties between every other pair of rear uprights (i.e., the general scheme is to cross-brace one bay, leave the next unbraced, cross-brace the third, and so on). No other bracing is used. Appended to the frame are side rails used to fence-in the batteries so they will not slide. These rails are supported by L-shaped brackets that bolt to the bottom rails on which the batteries rest.

The general configurations for these racks are shown on vendor drawings in Ref. 46 (12- and 17-ft racks) and Ref. 47.

The battery vendor also supplied a seismic analysis for the battery racks to the A/E's specification (Ref. 48). This specification (written before the appropriate floor response spectra were available) required that the battery rack design satisfy both of the following seismic conditions:

a. 0.1g horizontal and 0.033g vertical accelerations with the resulting stressed combined with other applicable stresses not to exceed normal design stresses.

b. 0.24g horizontal and 0.08g vertical accelerations with the resulting stresses combined with other applicable stresses not to exceed 90% of the yield point of the materials.

Subsequent to the original purchase order for the batteries and their racks, the A/E introduced a general specification governing the seismic design of all Class I equipment, instrumentation, and components. This document (Ref. 30) requires that Class I components be dynamically modeled as a multi-degree-of-freedom lumped-mass system and that their natural frequencies and mode shapes be determined.

Furthermore, if any of the natural frequencies so calculated are such that they fall within the range in which amplification of the floor accelerations are predicted by the floor response spectra, a dynamic analysis must be performed. If the lowest natural frequency exceeds the range for which amplification of the floor acceleration is predicted, a static analysis may be made.

Consequently, the seismic analysis of the battery racks was reexamined using dynamic methods of analysis, as required by this specification. The analysis was carried out by the A/E and is shown in the A/E's design report.

A six-bar two-mass model, as shown in Fig. X A-48, was used for this analysis. The model represents an end-on view of the frame and emplaced batteries and was selected because the lowest natural frequencies for the structure are expected to develop when seismic excitation

occurs in a direction parallel to the depth of the structure. The modeling assumes that the batteries can be considered rigidly attached to the frame.

The response of the battery racks to vertical seismic excitation was also examined. This analysis employed the same dynamic models as the horizontal analysis except that battery masses at each level were distributed to the nodes at the end of vertical bars, i.e., were assigned to nodes 1, 3, 4 and 6.

The computations for the dynamic analysis found in Ref. 32 were originally carried out by hand. The A/E stated that this analysis was subsequently checked by running the problem on the computer.

Major results of the dynamic analysis for the battery racks are shown in Table X A-32.

As can be seen from the table, results of the dynamic analysis show that the computed maximum accelerations exceed the equivalent g loads originally specified for battery rack design.

To check design adequacy, the A/E reviewed the vendor's stress report and applied correction factors to the originally computed stresses. These factors were taken as the ratio of the accelerations for the MCE, as shown in Table X A-32, to those originally specified.

The A/E stated that the stresses so determined fall within allowable limits.

A6.4.6.3.1 Commentary. The A/E's procedure for determining the dynamic loading of the battery racks appears to be proper. The agreement between independent hand computations and computer results lends credence to the results obtained.

The stress correction scheme includes a conservatism, since the ratio used for the correction factor to be applied to MCE stresses does not take credit for additional damping customarily allowed in the case of the MCE. (That is, the stress ratios are based on 2% damping, whereas credit could have been taken for 5% damping. Substantial reductions in stress levels would then be expected if the higher damping ratio had been assumed.)

No qualification program was conducted for the batteries, and therefore a rigorous assessment of their adequacy to withstand a severe seismic disturbance cannot be made. Based on the successful use of batteries of similar design in automotive, truck, and submarine applications, where they are subjected to severe shocks and vibrations for long periods of time, it can be expected that they will probably perform satisfactorily following an earthquake. Without the results of a formal qualification program, however, we cannot make a more definitive statement.

A6.4.6.3.2 Conclusion. We consider the batteries adequate on the basis of engineering judgment. The battery racks satisfy the design criteria on the basis of the analysis.

A6.4.7 ELECTRIC POWER DISTRIBUTION SYSTEMS

The electric power distribution systems consist of transformers switchgear and motor control centers, emergency buses, containment penetrations, and associated electric power and control cables and their supporting cable trays. For this plant all 13- and 4-kV cables are installed in conduits. Cables of 440-V power circuits and 125-V control circuits are installed in conduits and metal trays (see Fig. X A-49).

A6.4.7.1 Electric Cables, Terminations, and Connectors.

Because the electrical cables are installed both within and outside the primary containment, they will be required to function under severe environmental conditions should an accident occur in the plant. The same type of cable was used in both locations to eliminate the possibility that cables designed to withstand only the less severe conditions outside the containment might be inadvertently installed within the containment.

A6.4.7.1.1 Commentary. A qualification test program for the 480-V electrical cables was conducted in March 1970 (Refs. 49 and 50). Since that time, the qualification test requirements have been made considerably more severe. The cables tested were exposed to 200 megarads of gamma radiation and were given a 7-1/2-day steam/chemical exposure (including 12 hr at 298°F and 7 days at 160°F). Today, in recognition of the fact that it is possible that temperatures within the containment could reach 340°F under the small-break LOCA, the temperature profile suggested for the steam/chemical exposure includes dwells

of several hours at 340°F and a total exposure of 30 days, with the temperature never going below 200°F. The exposure to LOCA conditions must be preceded by an aging exposure to induce whatever degradation may occur during the installed life of the cables prior to the postulated accident. Similarly, the IPCEA horizontal flame test specified for these cables has been replaced by a more severe vertical flame test. Although the electrical performance of the cables was satisfactory, it is not possible to predict whether they would qualify under the current requirements.

Documentation of a qualification program for the 5-kV cables was not available to the reviewers; however, this omission is not regarded as serious because (1) the cables within the primary containment do not serve safety-related functions and (2) the safety-related cables outside the containment are installed within rigid metal conduits.

Because the cables are not structural members and are supported by cable trays, seismic qualification is not explicitly required. In electrical systems critical to safety, redundant cables are provided. Cable redundancy substantially reduces the probability of system inoperability due to cable failure. In principle, there is concern that cable insulation may become embrittled as a result of aging (exposures to temperature and nuclear radiation during their installed life) and that the insulation may therefore be subject to failure by cracking during a severe seismic event. The current qualification philosophy is to cover this possibility by requiring a bend test (wrapping the cable specimens being tested around a mandrel) after the aging exposure and before the LOCA exposure. The qualification test that was performed included a total nuclear radiation exposure in excess of the total exposure to which the cables would be subjected in the plant, considering both normal operating and accident conditions. There is no evidence that either thermal aging or a bend test was performed, however.

No qualification program was conducted for terminations and connectors; therefore, an evaluation of design adequacy cannot be made.

A6.4.7.1.2 Conclusion. The information available is insufficient for us to conclude that the cables, connectors, and terminations will perform properly under all conceivable accident conditions. There is reasonable assurance, however, that the electric cables will perform adequately for at least the first few weeks following a "large break" LOCA.

A6.4.7.2 Electrical Containment Penetrations.

The electrical containment penetrations are components that provide pressure-withstanding, leak-tight, electrically insulated paths through the wall of the primary containment structure for the purpose of transmitting electrical signals and electric power to motors and solenoids. The penetrations are provided with both inner and outer insulating seals made of an epoxy material. No qualification program was conducted for these components, although the A/E did perform a brief analysis which indicated that, although the strength of the inner seal may become marginal as a result of the cumulative effects of nuclear irradiation several months after a major LOCA, the outer seal would maintain its integrity.

A6.4.7.2.1 Commentary. Although no seismic or thermal testing or analysis was performed, our experience indicates that this should present no problems. Other penetration units have been tested extensively without mechanical or electrical failures occurring.

A6.4.7.2.2 Conclusion. We conclude on the basis of engineering judgment that the penetrations are adequate for expected seismic, normal and LOCA environments.

A6.4.7.3 4-kV Switchgear.

The 4-kV switchgear units control the connection of electric power sources (either of the two off-site supplies or, should these be unavailable, the diesel generator) to the four 4-kV emergency switchgear buses. These units also supply power to safety-related motors larger than 200 hp. One of the switchgear units is shown in Fig. X A-50. A row of switchgear cabinets is shown in Fig. X A-51. This equipment is segregated from non-safety-related electrical equipment in a separate room located at elevation 135 ft near the center of the plant buildings.

Because the switchgear cabinets are located in a shielded room that is isolated from nonelectrical equipment, this equipment is not expected to be subjected to the nuclear radiation, steam, or temperature environments that could result in the event of a high-

energy pipe break outside the primary containment. Any steam that may seep into the room around the door was expected to be removed by the room ventilation system. Therefore, the only significant design basis event for this equipment was the safe shutdown earthquake.

For newer plants AEC Regulatory Guide 1.70 (Rev. 1, Oct 1972) in section 3.11.4 entitled "Loss of Ventilation" requires that the base should be provided which assures that loss of air conditioning and/or ventilation system will not adversely affect the operability of safety related control and electrical equipment located in the control room and other areas.

A seismic analysis of the 4-kV switchgear was performed by the vendor and reported in Ref. 51. We note that the information contained in Ref. 51 reports the results of analysis and test and the inspection result of a switchgear like the one installed in the BWR which had been exposed to an actual earthquake environment. Maximum calculated stresses are 9379 psi in the jacking screw, compared to an AISC allowable of 20,000 psi. A fundamental frequency of 19 cps was computed, compared to 20 cps determined by test. Functional adequacy was verified by test. The inspection of switchgear that had experienced an actual earthquake revealed no deficiencies.

A6.4.7.3.1 Commentary. The data described above offer convincing evidence that the switchgear will resist seismic environments.

A6.4.7.3.2 Conclusion. The design of the switchgear is adequate for the expected seismic conditions.

A6.4.7.4 480-V Load Centers.

The 500-kVA 480-V emergency auxiliary load centers consist of a combination of a transformer, which reduces the voltage from 4-kV to 480-V, and a group of 480-kV switchgear units. One of the two load centers is shown in Fig. X A-52. Each load center is located at a partial enclosure in the reactor building at elevation 165 ft.

A6.4.7.4.1 Commentary. Although we understand type qualification data is now generally available for such equipment from manufacturers, no qualification data has been submitted for our review and apparently does not exist in the documentary record of this particular plant.

A6.4.7.4.2 Conclusion. We cannot make an assessment of design adequacy.

A6.4.7.5 480-V Motor Control Centers.

A typical rack containing several 480-V motor control centers (MCC) is illustrated in Fig. X A-53. Each MCC controls a component, such as a valve motor operator. This equipment is situated at several locations throughout the plant in the vicinity of the motor being controlled. A seismic test program of a 480-V motor control center is reported in Ref. 52.

A6.4.7.5.1 Commentary. In the seismic test program, a steel frame structure with angle braces was used to simulate "attachment of the cabinet top to a building wall or a rigid floor-mounted structure, and was used as top bracing in all three axes." This limits the validity of the test results to applications where the cabinet is similarly supported at the top, such as at the BWR plant.

The frequency range of the tests was 2 to 35 cps. While it is generally desirable to extend the range down to 1 cps, for this plant application the 2-cps lower limit is probably adequate because lower frequencies are highly attenuated by the building structure.

Functional performance was evaluated by "monitor circuits that detected interruptions of 1 millisecond or longer in the open and closed circuits." The adequacy of this evaluation procedure is not documented. Therefore, lacking other information, we must comment that the maximum acceleration levels for satisfactory operation listed in the report are applicable only if interruptions of less than 1 msec are acceptable.

A 2-pole switch that intermittently failed to make contact in the closed position was replaced with a new switch, which functioned correctly. This practice is highly questionable. In the absence of any justification for the replacement, it must be concluded that a switch of the same type could fail if subjected to a seismic disturbance.

The report states that "snap-on terminal strips were modified ... to keep them from falling off during seismic evaluation" and that a "plastic insulation covering the buss bars ... was replaced ... with a stronger insulation material ...." The test results are therefore applicable only to motor control centers with equivalent modifications.

During front-to-back vibration, the cabinet doors swung open. The door latches were adjusted in an unsuccessful effort to prevent this. It must be assumed that the doors could swing open during a seismic disturbance. Although not a likely occurrence, it is possible that the impacts of the doors against adjacent cabinets might cause a malfunction.

Interpretation of the test results was complicated by resonances that occurred in the test apparatus within the frequency range of the test. For example, this made it impractical to determine the damping characteristics of the cabinet in the front-to-back axis.

A6.4.7.5.2 Conclusion. On the basis of the information in the report reviewed, and assuming that the deficiencies identified in the test program were corrected in the units installed in the plant, the seismic design of the 480-V MCC is judged to be adequate for their intended application in this plant.

A6.4.7.6 D-C Distribution Panels and Fuse Boxes.

The d-c distribution panels (Fig. X A-54) and fuse boxes are located outside the primary containment in a separate room and hence are not subject to deleterious nuclear-radiation, steam, or temperature environments. The small quantity of steam which may seep into the room was expected to be removed by the room ventilation system. Therefore, the only significant design basis event for this equipment item was the safe shutdown earthquake. For newer plants AEC Regulatory Guide 1.70 (Rev. 1, Oct. 1972), Section 3.11.4 would, in addition, require a demonstration that loss of ventilation would not adversely affect the operability of this equipment. The manufacturer of the equipment conducted a qualification testing program and reported the results in Ref. 53.

The switchboard and components were tested on a machine that permitted simultaneous (in-phase) vibration in the horizontal and vertical directions. The equipment was vibrated in two perpendicular vertical planes. The test program included resonance searches, followed by continuous sine, sine-beat, and random vibration.

No malfunctions were observed except on two relays. The report implies that the relays are not necessarily to be considered unqualified to withstand seismic disturbances because of the severity of the test, provided certain precautions and protective measures are taken. The relays that malfunctioned during the vibration test reported in Ref. 53 were removed from the panelboard and placed in their own enclosure and are not included in the seismic qualification.

A6.4.7.6.1 Commentary. From the referenced qualification test reports and from conversations with their principal author, we know that the supplier regards the individual components (relays, switches) of the control boards to be essentially single-degree-of-freedom systems for which single-frequency testing is adequate. The components do appear to be single-degree-of-freedom devices, based on physical inspection. Therefore, the tests conducted on these components satisfy the current regulatory requirements in this regard. However, the assemblies were not rotated 180° for a repeat of the test in a given plant as currently required. Although it is possible that the omission of such repeat tests can be justified analytically for the assemblies tested, no such analysis was offered because the tests were conducted prior to the establishment of the current AEC regulatory position.

A6.4.7.6.2 Conclusion. The d-c distribution panels and fuse boxes satisfy the design criteria and are considered adequate.

A6.4.7.7 Cable Trays.

The cable trays for the BWR were designed to act like a low frequency pendulum so that they would be subject to seismic spectral accelerations which are low.

The cable tray hanger attachment to the overhead structure is either a swivel type of fixed, depending on the length of the support and the number of trays that are hung from the support, as shown in Table X A-33.

A6.4.7.7.1 Commentary. The design approach described above seems to be a reasonable method of minimizing the seismic loads. Very low frequency structures, however, are subject to large seismically induced displacements. Sufficient cable slack is normally provided to allow for tray movement without cable damage. A large swing of the cable trays might possibly cause impact with adjacent structures. Adequacy of cable slack and the possibility of impact could be easily checked by visual inspection and by simply pushing the trays laterally in critical areas and observing the results: such checks were

made by the FIRL review team at the site.

A6.4.7.7.2 Conclusion. The cable tray design appears to be adequate for seismic loads.

A6.4.8 REACTOR PROTECTION SYSTEM

The function of the reactor protection system (RPS) is to (1) accurately and reliably determine whether conditions in the plant are such that the reactor should be immediately shut down, the containment isolated, and the emergency core cooling system (ECCS) activated and (2) if so, to initiate these actions (the ECCS is to be initiated within 0.050 sec). The RPS can also be manually initiated by means of scram pushbuttons in the control room.

The only portions of the RPS that were considered in the design adequacy review were:

a. Pressure transmitters.

b. Pressure switches.

c. Monitoring racks.

d. Electrical cables.[1]

e. Logic cabinets containing relays.

f. Control room instrumentation and controls.

Instrumentation piping is connected to the reactor vessel and is routed through a special penetration in the drywell wall and isolation valves to instrumentation racks (see Figs. X A-55 and X A-56) located at elevation 165 ft in the reactor building. These racks contain the pressure transmitters that transform hydraulic pressure signal inputs into electrical signals proportional to reactor pressure and reactor water level and pressure switches that initiate an electrical signal when certain preselected conditions are reached. Other pipe lines, transmitters, and switches similarly provide information concerning pressure within the drywell. Four lines and transmitters are provided for each physical parameter. Adjacent panels containing circuits of redundant systems having less than 3-ft separation have steel barriers installed between panels (Fig. X A-55).

The electrical signals are conveyed by electrical control cables to instruments and to cabinets containing relays (similar to those in Fig. X A-57) which provide the logic functions. These components are located in the control room at elevation 165 ft. Other electrical cables carry the signals that initiate reactor shutdown, containment isolation, and ECCS functioning to the control rod drive system and to the various motor control centers that activate valve closures and motor start-ups. A portion of the control room panels pertaining to the reactor safety functions is shown in Fig. X A-58. These panels contain instruments that provide such data as motor current, system flow, and pump discharge pressure to the operator, lights which inform him of valve positions, and control switches to permit the manual operation of motors and valves.

A6.4.8.1 Commentary.

The RPS components considered in the review are located outside of the primary containment, and hence are not exposed to severe environmental conditions in the event of a LOCA. The pressure transmitters and switches installed in various plants have had a tendency to experience set-point drift under normal plant conditions. We have not seen any qualification information that would permit an evaluation of the stability of these components with regard to set-point drift under the normal plant operating conditions, and the consequences of such drift as may occur.

The seismic qualification was reviewed primarily on the basis of information in a report (Ref. 53) that summarized qualification for instrument racks and panels and various electronic devices. The testing was conducted in accordance with the requirements of IEEE 344-1971 (Ref. 54), except that there is no indication that the units were pre-aged before being subjected to the simulated seismic exposure. The latter involved a resonance scan at 0.2g followed by continuous sinusoidal vibration at resonant frequencies to determine malfunction limits, the procedure being repeated along three orthogonal axes. Because of test facility limitations, the testing did not cover frequencies below 5 cps. Although conditions below 5 cps were analyzed, it is difficult to demonstrate seismic qualification of complex devices by analysis; and, in the absence of the detailed calculations, a definitive evaluation is not possible.

[1]Covered in section A6.4.7.1.

Present seismic qualification requirements emphasize multi-axis testing and the use of random vibration. Past, or future, qualification testing should be reviewed particularly with respect to multi-axis effects.

A6.4.8.2 Conclusion.

Qualification of this equipment for seismic exposures in the low frequency range could not be evaluated completely with the information available. The qualification programs that were conducted to demonstrate that the equipment does function satisfactorily when exposed to severe conditions which can be considered as segments in the type of more comprehensive qualification program that is presently regarded as necessary to conclusively demonstrate design adequacy.

Although the design criteria are not completely satisfied, the testing that was performed indicates that failure is not expected. The RPS components examined are adequate.

Section A2

References

1. Hurty and Rubenstein, Dynamics of Structures, Prentice-Hall, Englewood Cliffs, N.J., 1964.

2. IEEE Standard 323-1974, "IEEE Standard for Qualifying Class IE Equipment for Nuclear Power Generating Stations."

Section A4

References

1. IEEE Standard 323-1974, "IEEE Standard for Qualifying Class IE Equipment for Nuclear Power Generating Stations."

2. IEEE Standard 279-1971, "Criteria for Protection Systems for Nuclear Power Generating Stations."

3. IEEE Standard 308, "Criteria for Class IE Electric Systems for Nuclear Power Generating Stations."

4. ANSI N45-3.4 and IEEE 336-1971, "Installation, Inspection, and Testing Requirements for Instrumentation and Electric Equipment During the Construction of Nuclear Power Plants."

5. IEEE Standard 344-1971, "Guide for Seismic Qualification of Class I Electrical Equipment for Nuclear Power Generating Stations,"

6. IEEE Standard 334/1971, "Guide for Type Tests of Continuous Duty Class I Motors Installed Within the Containment of Nuclear Power Generating Stations."

7. IEEE Standard 382-1972 (ANSI N41.6), "IEEE Trial-Use Guide for Type Test of Class IE Electric Valve Operators for Nuclear Power Generating Stations."

8. IEEE Standard 383-1974 (Draft), "IEEE Trial-Use Guide for Type Test of Class IE Electric Cables, Field Splices and Connections for Nuclear Power Generating Stations."

Section A5

References

1. RDT Standard F9-2T, "Seismic Requirements for Design of Nuclear Power Plants and Test Facilities," Oak Ridge National Laboratory, January 1974.

Section A6

References

1. U.S.A.E.C. Regulatory Guide 1.60, "Design Response Spectra for Seismic Design of Nuclear Power Plants."

2. U.S.A.E.C. Regulatory Guide 1.61, "Damping Values for Seismic Design of Nuclear Power Plants," Oct. 1973.

3. Final Safety Analysis Report for Surry Power Station Units 1 and 2, 1970.

4. Vibration in Civil Engineering - Proceedings of Symposium Organized by the British National Section of the International Association for Earthquake Engineering - Section V: "The Dynamic Behaviour of Foundations," by Robert V. Whitman, Butterworths, London W.C.-2, England, 1965.

5. RDT Standard F9-2T, "Seismic Requirements for Design of Nuclear Power Plants and Test Facilities," Oak Ridge National Laboratory, January 1974.

6. Virginia Electric and Power Co., "Seismic Design Review and Piping - Surry Power Station," June 30, 1971, Rev. Sept. 15, 1971.

7. Westinghouse Electric Engineering Memorandum 4528, "Analysis of the 93A Casing Nozzles Using Umbrella Loads," January 7, 1974.

8. Welding Research Council Bulletin 107, "Local Stresses in Spherical and Cylyndrical Shells Due to External Loadings," August 1965, Rev. July 1970.

9. Letter from ITT-Grinnel Corp. to FIRL dated 4/19/74 with enclosure (Parker Seal Co. Report No. K10, 151-466, dated Nov. 30, 1973).

10. Stone and Webster Engineering Corporation, Supplement B to Report No. SW-MER-1A, "Sensitized Stainless Steel in Pressurized Water Reactor Applications, Surry Power Station," prepared for Virginia Electric and Power Co., November 30, 1971.

11. C. G. Collins, et al., "Estimated Radiation Stability of Aircraft Components," APEX 357, General Electric (no date available).

12. Crane Packing Company Bulletin No. 3472.

13. Crane Packing Company Bulletin No. 100.1.

14. ALOYCO Drawing No. E-45467, April 19, 1968.

15. Topical Report, "Environmental Testing of Engineered Safety Features Related Equipment," WCAP-7744, Volume I.

16. Stone and Webster Engineering Corporation, Piping Flexibility Analysis Summary Sheets 1 through 4, Drawings numbered 11448-MSK-122 D1/5, D2, D3/6, D4/1.

17. Stone and Webster Engineering Corporation, Piping Flexibility Analysis Summary Sheets 1 through 4, Drawings numbered 11448-MSK-122 A1/5, A2/2, A3/5, A4/1.

18. U.S.A.E.C. Safety Guide 26, March 23, 1972.

19. Westinghouse Electric Corporation Letter with Attachments to Franklin Institute Research Laboratories, dated May 23, 1975 (Paddleford to Sailwell).

20. M.W. Sheets, "Topical Report on GE Vertical Induction Motors Inside Containment Recirculation Spray Pump Motors - Surry Power Station," General Electric, June 12, 1973.

21. Topical Report, "Environmental Testing of Engineered Safety Features Related Equipment," WCAP-7744, Volume II.

22. IEEE Std. 383-1974, "IEEE Standard for Type Test of Class IE Electric Cables, Field Splices, and Connections for Nuclear Power Generating Station."

23. Topical Report, "Seismic Testing of Electrical and Control Equipment," WCAP-7817 and Supplements 1 through 3, December 1971.

24. L. M. Potochnik, "Seismic Testing of Electrical and Control Equipment (High Seismic Plants)," WCAP-7821 and Supplements 1 through 4, Westinghouse Electric Corporation, October 1971.

25. L. M. Potochnik, "Seismic Testing of Electrical and Control Equipment (PG&E Plants)," Westinghouse Electric Corporation, May 1973.

26. A. Morrone, "Seismic Vibration Testing with Sine Beats," WCAP-7558, Westinghouse Electric Corporation, October 1971.

27. E. G. Fischer and S. J. Jarecki, "Qualification of Westinghouse Seismic Testing Procedure for Electrical Eqiupment Tested Prior to May 1974." Westinghouse Electric Corporation, August 1974.

28. Bechtel Drawing LF-240-121.

29. Bechtel Specification 6280-M-120.

30. Bechtel Specification 6280-G-14 (Rev. 1), "General Project Class I Sesimic Requirements for Equipment, Instrumentation, Systems and Components for Peach Bottom Atomic Power Station Units 2 and 3 for the Philadelphia Electric Company," May 1973.

31. Final Safety Analysis Report for Peach Bottom Power Station Units 2 and 3, 1971.

32. Chicago Bridge and Iron Co., Report No. 6, "Stress Analysis of Miscellaneous Nozzles, Peach Bottom II," Prepared for General Electric Co., Nuclear Energy Division.

33. Chicago Bridge and Iron Company, Report No. 7, "Piping Reactions for Peach Bottom II," Prepared for General Electric Co., Nuclear Energy Division.

34. Chicago Bridge and Iron Co., Report No. 8, "Stress Analysis of Support Skirt for General Electric Co., Nuclear Energy Division, Peach Bottom II."

35. General Electric Company, "Sesimic Analysis for Atwood and Morrill 26 'Size y' Type Main Isolation Valve, Ref. Dwg. 20851-H," Document No. 2258-44-1, March 26, 1970.

36. General Electric Company, "Seismic Analysis for Atwood and Morrill 26 'Y' Type MSIV, Ref. Dwg. 21150-H," Document No. 296418-2, October 11, 1973.

37. General Electric Company, "Design and Performance of G.E.-BWR-MSIV," Report No. APED-5750, by Rockwell and Zylstra, March 1969.

38. P. J. Thiemann, "Environmental Qualification Test of Vertical Induction Motor for ECCS Service in Nuclear Power Plants," NEDM-10672, 72NED93, General Electric Company, San Jose, California, August 1972.

39. Philadelphia Gear Corp., "Test of Limitorque Valve Operator to Meet General Requirements of an Electric Valve Actuator in Nuclear Reactor Containment Environment," Jan. 2, 1969.

40. Addendum #1 dated April 29, 1969 to preceding report.

41. Keith, Feibusch Associates, Engineers, "Seismic Capability of HPCl Turbines (CS and CCS)," Document No. 2763-43-1, prepared for General Electric Company, April 30, 1970.

42. General Electric Company, "Design Calculations for RHR Pump," Document 21A5790A5 (Rev. 5), 1969.

43. Keith, Feibusch Associates, Engineers, "Seismic Capability of the Residual Heat Removal Pump," prepared for General Electric Company, San Jose, California, July 31, 1970.

44. Bechtel Report on Diesel Generator Building Structure, April 11, 1971.

45. Development Engineering Department, Fairbanks Morse Power Systems Division, "A Seismic Analysis for the Diesel Generators to be Installed at Baltimore Gas & Electric's Calvert Cliffs Nuclear Power Station," March 1971.

46. Exide Drawing No. PH27004/08, Rev. 0, 2/27/70.

47. Exide Drawing No. PH27006, Rev. 0, 2/27/70.

48. Bechtel Specification 6280-E-13, "Specification for Batteries, Battery Racks and Chargers for the Peach Bottom Atomic Power Station Units 2 and 3 for the Philadelphia Electric Company," July 1969.

49. L. E. Witcher and W. H. Steigelmann, "Test of Electrical Cables Under Simulated Post-Accident Reactor Containment Service," Addendum to FIRL Final Report F-C2750, Franklin Institute Research Laboratories, June 1970.

50. J. G. Stone and L. S. Chapman, Supplement to Ref. 48, Technical Report No. NP-03, Cerro Wire & Cable Co., July 1970.

51. General Electric Requisition 320-67245, "Seismic Analysis of 5kV M26 Switchgear," Millstone Point Nuclear Unit 2, March 1972.

52. D. W. Caba and R. H. Prause, "Seismic Evaluation of an Old Style Unitrol Motor Control Center with G. E. Components and Top Support," Battelle Columbus Laboratories, Dec. 22, 1972.

53. L. D. Test, "Seismic Qualification of Class 1 Electric Equipment," General Electric Licensing Topical Report NEDO-10678, Nov. 1972.

54. IEEE Standard 344-1971, "Guide for Seismic Qualification of Class I Electrical Equipment for Nuclear Power Generating Stations."

TABLE X A-1 DESIGN BASIS ENVIRONMENTS - PWR PLANT

Condition and Location	Temp. (°F)	Press. (psig)	Rel. Hum. (%)	Rad. Dose Rate (rad/hr)	Intergrated[a] Rad. Dose (rad)	Duration
I. Normal (No Accident):						
A. Inside Containment	80-105	-4	40-100	55	20×10^6	40 yr
B. Outside Containment[b]	60-120	∿0	40-90	0.001-0.015	2	40 yr
II. LOCA (Safety-related systems functioning except for worst single failure):						
A. Inside Containment[c]	Incr. to 280	Incr. to 45	100	7.2×10^6	--	10 sec
	280	45	100	6.2×10^6	3.3×10^6	Next 30 min
	Decr. to 150	Decr. to -1	100	5.8×10^6	6.3×10^6	Next 30 min
	150	-1 to -2	Decr. to 50	Decr. to 0.1 1.4×10^5	1.5×10^8	Next 100 days[d]
B. Outside Containment (Localized)[b]	Incr. to 212	0	100	0.001-0.3	--	30 sec
	212	0	100	0.001-0.3	0.006-0.02	Next 6 hr
	150	0	Decr. to 50	0.001-0.2	2-50	Next 100 days[d]

(a) Based upon extremely conservative assumptions; actual expected dose rates and doses about 100 times smaller.

(b) Conditions may be higher in closed cubicles and adjacent to piping and equipment containing radioactive materials.

(c) Plus a continuous spray vertically downward with a recirculating aqueous solution containing 3,000 ppm boron adjusted to a pH of 8.0 with sodium hydroxide, at a rate of 0.15 (gal/min)/(ft^2 in a horizontal plane) for a period of 7 days. Effectiveness of spray in decreasing radiation dose rate (approximately a factor of 2 reduction) is not included.

(d) Assumes that accident conditions have essentially disappeared after 100 days.

TABLE X A-2 DESIGN BASIS ENVIRONMENTS - BWR PLANT

Condition and Location	Temp. (°F)	Press. (psig)	Rel. Hum. (%)	Rad. Dose Rate (rad/hr)	Integrated[a] Rad. Dose (rad)	Duration
I. Normal (No Accident):						
A. Inside Primary Containment	135-150	∿0	40-100	25	7×10^6	40 yr
B. Outside Primary Containment[b]	60-120	∿0	40-90	0.001-0.015	250-3000	40 yr
II. LOCA (Safety-related systems functioning except for worst single failure):						
A. Inside Drywell[c]	Incr. to 280	Incr. to 62	100	3.3×10^6	9000	10 sec
	Incr. to 340[d]	62[d]	100	3.3×10^6	0.3×10^6	Next 5 min
	340[d]	35[d]	100	2.3×10^6	7.5×10^6	Next 3 hr
	320[d]	35[d]	100	1.1×10^6	12×10^6	Next 3 hr
	250[d]	25[d]	100	0.3×10^6	18×10^6	Next 18 hr
	200[d]	20[d]	100	8×10^4	25×10^6	Next 3 days
	Decr. to 110	Decr. to 0	Decr. to 50	Decr. to 200	32×10^6	Next 96 days[e]
B. Inside Supression Chamber	Incr. to 150	Incr. to 25	100	0.12×10^6	--	30 sec
	150	25	100	1.0×10^6	4×10^5	Next 20 min
	Incr. to 200	Decr. to 15	100	0.3×10^6	3×10^6	Next 10 hr
	200	Decr. to ∿0	Decr. to 50	Decr. to 2000	100×10^6	Next 100 days
C. Outside Primary Containment[b]	Incr. to 212	∿0	100	0.001-0.03	--	30 sec
	212	∿0	100	0.001-0.03	0.006-0.2	Next 6 hr
	150	∿0	Decr. to 50	0.001-0.02	2-50	Next 100 days[e]

(a) Based upon extremely conservative assumptions; actual expected dose rates and doses about 100 times smaller.

(b) Conditions may be higher in closed cubicles and adjacent to piping and equipment containing radioactive material.

(c) Plus a continuous spray vertically downward with demineralized water at a rate of 0.15 (gal/min)/(ft^2 in a horizontal plane) for a period of 24 hr.

(d) These temperatures and pressure conditions would not occur simultaneously.

(e) Assumes that accident conditions have essentially disappeared after 100 days.

TABLE X A-3 PWR COMPONENTS

A 6.3.1	Reactor Building
A 6.3.1.1	Soil-Structure Interaction Model
A 6.3.1.2	Containment Internal Structure
A 6.3.1.3	Paint Coatings Within Containment
A 6.3.1.4	Crane
A 6.3.2	Reactor Coolant System (RCS)
A 6.3.2.1	Reactor Coolant System Loops
A 6.3.2.2	Steam Generator and Pump Supports
A 6.3.2.3	Reactor Coolant Pump Nozzles
A 6.3.2.4	Pipe-Whip Restraints
A 6.3.2.5	Snubbers
A 6.3.3	Low Head Safety Injection System (LHSIS)
A 6.3.3.1	Piping
A 6.3.3.2	Pumps and Drives
A 6.3.3.3	Valves
A 6.3.3.4	Valve Motor Operators
A 6.3.3.5	Snubbers and Hangers
A 6.3.3.6	Instrumentation
A 6.3.4	High Head Safety Injection System (HHSIS)
A 6.3.4.1	Accumulator Tank Nozzle
A 6.3.4.2	Accumulator Piping Connection to RCS
A 6.3.4.3	Charging Pumps and Drives
A 6.3.5	Containment Recirculation Spray System
A 6.3.5.1	Pump and Motor Located Outside Containment
A 6.3.5.2	Motor Drives Inside Containment
A 6.3.6	On-Site Electric Power System
A 6.3.6.1	Diesel Generator Housing
A 6.3.6.2	Diesel Generators
A 6.3.6.3	Day Tanks
A 6.3.6.4	Air Bottle Supports
A 6.3.6.5	Batteries and Battery Supports
A 6.3.7	Electric Power Distribution Systems
A 6.3.7.1	Electrical Cables and Terminations
A 6.3.7.2	Electrical Containment Penetrations and Connectors
A 6.3.7.3	Cable Trays
A 6.3.7.4	AC and DC Switchgear
A 6.3.8	Reactor and Engineered Safeguards Protection Systems Sensors and Logic Cabinets
A 6.3.9	Intake Canal

TABLE X A-4 BWR COMPONENTS

A 6.4.1	Containment Structures
A 6.4.1.1	Primary Containment Structure
A 6.4.1.2	Reactor Building (Secondary Containment)
A 6.4.1.3	Containment Piping Penetrations
A 6.4.1.4	Suppression-Chamber-to-Drywell Vacuum Breaker Valves
A 6.4.1.5	Missile Barriers Inside Containment
A 6.4.1.6	Paint Coatings Within Containment
A 6.4.2	Reactor Coolant System
A 6.4.2.1	Reactor Pressure Vessel and Internals
A 6.4.2.2	Reactor Pressure Vessel Nozzles
A 6.4.2.3	Reactor Pressure Vessel Support Skirt
A 6.4.2.4	Recirculation Lines
A 6.4.2.5	Main Steam Lines
A 6.4.2.6	Main Steam Line Isolation Valves
A 6.4.2.7	Pipe-Whip Restraints for Recirculation Lines
A 6.4.2.8	Reactor Pressure Relief Valves
A 6.4.3	Core Spray System
A 6.4.3.1	Piping
A 6.4.3.2	Hangers and Snubbers
A 6.4.3.3	Pumps and Drives
A 6.4.3.4	Valves
A 6.4.3.5	Valve Motor Operators
A 6.4.3.6	Instrumentation
A 6.4.4	High Pressure Coolant Injection System (HPCIS) Turbine
A 6.4.5	Residual Heat Removal (RHR) Pumps and Drives
A 6.4.6	On-Site Electric Power Systems
A 6.4.6.1	Diesel Generator Building
A 6.4.6.2	Diesel Generators
A 6.4.6.3	Batteries and Battery Racks
A 6.4.7	Electric Power Distribution Systems
A 6.4.7.1	Electrical Cables, Terminations, and Connectors
A 6.4.7.2	Electrical Containment Penetrations
A 6.4.7.3	4-kV Switchgear
A 6.4.7.4	480-V Load Centers
A 6.4.7.5	480-V Motor Control Centers
A 6.4.7.6	DC Distribution Panels and Fuse Boxes
A 6.4.7.7	Cable Trays
A 6.4.8	Reactor Protection System

TABLE X A-5 PWR COMPONENT REVIEW - SEISMIC[a] DESIGN ADEQUACY SUMMARY

Subsection in Text	Component Description	Review Data Basis: Visual Observation	Review Data Basis: Design Calculations	Review Data Basis: Test Report	Assessment of Design Adequacy: Adequate (Failure Not Expected): Design Criteria Satisfied[b]: Analysis and/or Test	Assessment of Design Adequacy: Adequate (Failure Not Expected): Design Criteria Satisfied[b]: Engineering Judgment	Assessment of Design Adequacy: Adequate (Failure Not Expected): Design Criteria Not Completely Satisfied[c]	Assessment of Design Adequacy: Not Demonstrated (Failure Possible): Insufficient Information to Assess Adequacy	Assessment of Design Adequacy: Not Demonstrated (Failure Possible): Information Reviewed Indicates that Failure is Likely	Notes
A6.3.1	Reactor Building									
A6.3.1.1	Soil-Structure Interaction Model		✓		✓					
A6.3.1.2	Containment Internal Structure		✓		✓					(d)
A6.3.1.4	Crane		✓				✓			
A6.3.2	Reactor Coolant System (RCS)									
A6.3.2.1	Reactor Coolant System Loop		✓		✓					
A6.3.2.2	Steam Generator and Pump Supports		✓		✓					
A6.3.2.3	Reactor Coolant Pump Nozzles		✓					✓		(e)
A6.3.2.4	Pipe Whip Restraints:									
	Main Steam Line		✓		✓					
	Feedwater Line		✓		✓					(d)
A6.3.2.5	Snubbers					✓				(f)
A6.3.3	Low Head Safety Injection System (LHSIS)									
A6.3.3.1	Piping	✓	✓		✓					(d)
A6.3.3.2	Pumps and Drives	✓	✓				✓			
A6.3.3.3	Valves					✓				
A6.3.3.4	Motor Operators	✓		✓	✓					
A6.3.3.5	Snubbers and Hangers					✓				(f)
A6.3.3.6	Instrumentation			✓				✓		
A6.3.4	High Head Safety Injection Systems (HHSIS)									
A6.3.4.1	Accumulator Tank Nozzle		✓		✓					(d)
A6.3.4.2	Accumulator Piping Connection to RCS				✓					
A6.3.4.3	Charging Pumps and Drives	✓	✓		✓					
A6.3.5	Containment Recirculation Spray System									
A6.3.5.1	Pump and Motor Located Outside Containment:									
	Pump	✓	✓					✓		
	Motor	✓	✓		✓					
A6.3.5.2	Motor Drives Inside Containment	✓		✓	✓					
A6.3.6	On-Site Electric Power Systems									
A6.3.6.1	Diesel Generator Housing:[a]									
	Walls and Roof	✓	✓			✓				
	Door	✓	✓						✓	
	Soil Cover for Fuel Tanks	✓				✓				
A6.3.6.2	Diesel Generators	✓	✓	✓	✓					
A6.3.6.3	Day Tanks	✓						✓		
A6.3.6.4	Air Bottle Supports	✓				✓				
A6.3.6.5	Batteries and Battery Supports	✓		✓	✓					
A6.3.7	Electric Power Distribution Systems									
A6.3.7.2	Electrical Containment Penetrations and Connectors	✓			✓					
A6.3.7.3	Cable Trays	✓				✓				
A6.3.7.4	AC and DC Switchgear				✓			✓		
A6.3.8	Reactor and Engineered Safeguards Protection Systems Sensors and Logic Cabinets	✓		✓			✓			
A6.3.9	Intake Canal	✓				✓				

TABLE X A-5 FOOTNOTES

(a) Diesel Generator Building was evaluated only for tornado resistance.

(b) Design Criteria as stated in FSAR; or current criteria, if original criteria were not explicit or found to have insufficient margin.

(c) More sophisticated analysis methods may in some cases show that the design criteria have in fact been satisfied; in all cases however, loss of function is not expected.

(d) Deficiencies in original analysis have been either revised or investigated further. Revised results have been evaluated and design is found to be adequate.

(e) Bijlaard formulae not applicable.

(f) Periodic seal replacement in the snubbers is recommended.

TABLE X A-6 PWR COMPONENT REVIEW - ENVIRONMENTAL QUALIFICATION SUMMARY

Subsection in Text	Component Description	Review Data Basis			Assessment of Design Adequacy				
					Adequate (Failure Not Expected)			Not Demonstrated (Failure Possible)	
					Design Criteria Satisfied[a]				
		Visual Observation	Design Calculations	Test Report	Analysis and/or Test	Engineering Judgment	Design Criteria Not Completely Satisfied[b]	Insufficient Information to Assess Adequacy	Information Reviewed Indicates that Failure is Likely	Notes
A6.3.1	Reactor Building									
A6.3.1.3	Paint Coatings within Containment			✓	✓					
A6.3.2	Reactor Coolant System (RCS)									
A6.3.2.5	Snubbers			✓			✓			(c)
A6.3.3	Low Head Safety Injection System (LHSIS)									(d)
A6.3.3.2	Pumps and Drives	✓		✓			✓			
A6.3.3.5	Snubbers			✓			✓			(c)
A6.3.4	High Head Safety Injection Systems (HHSIS)									(d)
A6.3.5	Containment Recirculation Spray System									
A6.3.5.1	Pump Located Outside Containment	✓		✓			✓			
A6.3.5.2	Motor Drives Inside Containment	✓		✓	✓					
A6.3.6	On-Site Electric Power Systems									(d)
A6.3.7	*Electric Power Distribution System*									
A6.3.7.1	Electrical Cables and Terminations	✓		✓	✓					
A6.3.7.2	Penetrations and Connectors	✓	✓		✓					
A6.3.9	Reactor Protection System	✓		✓			✓			

(a) Design Criteria as stated in FSAR; or current criteria, if original criteria were not explicit or found to have insufficient margin.

(b) More sophisticated analysis methods may in some cases show that the design criteria have in fact been satisfied; in all cases however, loss of function is not expected.

(c) Periodic seal replacement in the snubbers is recommended.

(d) Active components of this system that are outside of containment and not subject to LOCA environment have not been included.

TABLE X A-7 BWR COMPONENT REVIEW - SEISMIC[a] DESIGN ADEQUACY SUMMARY

Subsection in Text	Component Description	Review Data Basis: Visual Observation	Review Data Basis: Design Calculations	Review Data Basis: Test Report	Assessment of Design Adequacy: Adequate (Failure Not Expected): Design Criteria Satisfied[b]: Analysis and/or Test	Assessment of Design Adequacy: Adequate (Failure Not Expected): Design Criteria Satisfied[b]: Engineering Judgment	Assessment of Design Adequacy: Adequate (Failure Not Expected): Design Criteria Not Completely Satisfied[c]	Assessment of Design Adequacy: Not Demonstrated (Failure Possible): Insufficient Information to Assess Adequacy	Assessment of Design Adequacy: Not Demonstrated (Failure Possible): Information Reviewed Indicates that Failure Is Likely	Notes
A6.4.1	Containment Structures									
A6.4.1.1	Primary Containment Structure	✓	✓		✓					
A6.4.1.2	Reactor Building (Secondary Containment)	✓	✓		✓					
A6.4.1.3	Containment Piping Penetrations	✓	✓		✓					
A6.4.1.4	Suppression-Chamber-to-Drywell Vacuum Breaker Valves	✓	✓			✓				
A6.4.1.5	Missile Barriers Inside Containment	✓	✓					✓		
A6.4.2	Reactor Coolant System									
A6.4.2.1	Reactor Pressure Vessel and Internals		✓		✓					
A6.4.2.2	Reactor Pressure Vessel Nozzles		✓		✓					
A6.4.2.3	Reactor Pressure Vessel Skirt		✓		✓					
A6.4.2.4	Recirculation Lines	✓	✓				✓			
A6.4.2.5	Main Steam Lines		✓		✓					
A6.4.2.6	Main Steam Line Isolation Valves	✓	✓	✓	✓					
A6.4.2.7	Pipe Whip Restraints for Recirculation Lines	✓	✓		✓					
A6.4.2.8	Reactor Pressure Relief Valves	✓		✓				✓		
A6.4.3	Core Spray System									
A6.4.3.1	Piping	✓	✓		✓					
A6.4.3.2	Hangers and Snubbers:									
	Hangers					✓				
	Snubbers					✓				(d)
A6.4.3.3	Pumps and Drives	✓	✓		✓					
A6.4.3.4	Valves	✓		✓		✓				
A6.4.3.5	Valve Motor Operators	✓		✓			✓			
A6.4.3.6	Instrumentation	✓						✓		
A6.4.4	HPCIS Turbine	✓	✓		✓					
A6.4.5	RHR Pumps and Drives	✓	✓	✓	✓					
A6.4.6	On-Site Electric Power Systems									
A6.4.6.1	Diesel Generator Buildings:[a]									
	Structure and Door	✓	✓		✓					
	Door Hinges							✓		
	Corrugated Barrier Attachments							✓		
A6.4.6.2	Diesel Generators	✓	✓		✓					
A6.4.6.3	Batteries and Battery Racks:									
	Batteries	✓				✓				
	Battery Racks	✓	✓		✓					
A6.4.7	Electric Power Distribution Systems									
A6.4.7.2	Electrical Containment Penetrations	✓				✓				
A6.4.7.3	4 kV Switchgear	✓	✓		✓					
A6.4.7.4	480 V Load Centers	✓						✓		
A6.4.7.5	480 V Motor Control Centers	✓		✓	✓					
A6.4.7.6	DC Distribution Panels and Fuse Boxes	✓		✓	✓					
A6.4.7.7	Cable Trays	✓	✓		✓					
A6.4.8	Reactor Protection System	✓		✓			✓			

(a) Diesel Generator Building was evaluated for both seismic and tornado loads.

(b) Design Criteria as stated in FSAR; or current criteria, if original criteria were not explicit or found to have insufficient margin.

(c) More sophisticated analysis methods may in some cases show that the design criteria have in fact been satisfied; in all cases however, loss of function is not expected.

(d) Periodic seal replacement in the snubbers is recommended.

TABLE X A-8 BWR COMPONENT REVIEW - ENVIRONMENT QUALIFICATION SUMMARY

Subsection in Text	Component Description	Review Data Basis			Assessment of Design Adequacy					
					Adequate (Failure Not Expected)			Not Demonstrated (Failure Possible)		
					Design Criteria Satisfied[a]					
		Visual Observation	Design Calculations	Test Report	Analysis and/or Text	Engineering Judgment	Design Criteria Not Completely Satisfied[b]	Insufficient Information to Assess Adequacy	Information Reviewed Indicates that Failure is Likely	Notes
A6.4.1	Containment									
A6.4.1.4	Suppression-Chamber-to-Drywell Vacuum Breaker Valves	✓				✓				
A6.4.1.6	Paint Coatings Within Containment	✓		✓	✓					
A6.4.2	Reactor Coolant System									
A6.4.2.6	Main Steam Line Isolation Valves	✓	✓	✓	✓					
A6.4.2.8	Reactor Pressure Relief Valves	✓						✓		
A6.4.3	Core Spray System									
A6.4.3.2	Snubbers	✓		✓			✓			
A6.4.5	RHR Pumps and Drives	✓		✓		✓				
A6.4.7	Electric Power Distribution Systems									
A6.4.7.1	Electrical Cables Terminations and Connectors	✓		✓				✓		
A6.4.7.2	Electrical Containment Penetrations	✓				✓				

(a) Design Criteria as stated in FSAR; or current criteria, if original criteria were not explicit or found to have insufficient margin.

(b) More sophisticated analysis methods may in some cases show that the design criteria have in fact been satisfied; in all cases however, loss of function is not expected.

TABLE X A-9 COMPARISON OF DAMPING VALUES USED IN PWR PLANT WITH THOSE CURRENTLY REQUIRED

Structure or Component	Damping Values (% Critical) OBE PWR	OBE Current	DBE PWR	DBE Current
Reactor-Vessel Internals				
Welded Components and Assemblies	1.0	2.0	1.0	3.0
Bolted Components and Assemblies	2.0	2.0	2.0	3.0
Reinforced Concrete	5.0	4.0	5.0	7.0
Steel-Frame Structures				
Welded	1.0	2.0	1.0	4.0
Bolted	2.5	4.0	2.5	7.0
Mechanical Equipment	2.0	2.0	2.0	3.0
Piping				
>12.0 in. dia.	0.5	2.0	0.5	3.0
<12.0 in. dia.	0.5	1.0	0.5	2.0

TABLE X A-10 COMPARISON OF DAMPING VALUES USED IN BWR PLANT WITH THOSE CURRENTLY REQUIRED

Structure or Component	Damping Values (% Critical)			
	DE		MCE	
	BWR	Current	BWR	Current
Reinforced-Concrete Structures	2.0	4.0	5.0	7.0
Steel-Frame Structures	2.0	2.0	5.0	4.0
Welded-Steel Assemblies[(a)]	1.0	2.0	2.0	3.0
Bolted and Riveted Assemblies[(a)]	2.0	2.0	5.0	3.0
Piping				
>12.0 in. dia.	0.5	2.0	0.5	3.0
<12.0 in. dia.	0.5	1.0	0.5	2.0

(a) "Assemblies" refers to equipment components or their assemblies internal to (or supported on) "Structures."

TABLE X A-11 COMPARISON OF MISSILE CHARACTERISTICS

Missile	Wt. (lb)	Vel. (ft/sec)	Impact (area-ft^2)	Momentum (lb-sec)	Kinetic Energy Impact Area (lb/ft)
Missiles for BWR Design Under Review:					
Wood Plank (4 in. x 12 in. x 12 ft)	108	440	0.333	1476	9.75×10^5
Auto	4000	73	20.0	9110	1.66×10^4
Missiles Recent Plants:					
Utility Pole	1200	293	1.0	10900	1.60×10^6
Auto	4000	147	30.0	18300	4.47×10^4
Sliding Panel	400	528	0.4	6560	4.32×10^6

TABLE X A-12 COMPARISON OF COMPUTED FREQUENCIES

Mode	Frequency (cps)	
	4-Degree-of-Freedom Model	14-Degree-of-Freedom Model
1	1.49	1.52
2	2.87	3.65
3	4.68	5.307
4	6.03	10.0

TABLE X A-13 ESTIMATE OF MODAL DAMPING

Mode	Type	% Critical Damping
1	Rocking	10.4
2	Translation	36.8
3	Flexure	2.5
4	Translation	3.8

TABLE X A-14 SUMMARY OF MOMENTS AND STRESSES IN CRANE (TROLLEY AT CENTER LINE)

Loading	Section	Moment		Section Modulus		Stress		Max. Total Stress (ksi)	Allow Stress (ksi)
		Vert. (kip-ft)	Horiz. (kip-ft)	Vert. (in^3)	Horiz. (in^3)	Vert. (ksi)	Horiz. (ksi)		
Main Girder									0.49 σ_y = 17.6
Dead Load		1781	--	S_c = 8433		5.07			
Live Load		1550	--	S_T = 7612	2231	5.62	--	5.62	< 17.6
Impact @ 15%		233	--						
		3564							
Dead Load		1781	--	S_c = 8433		6.30			0.9 σ_y = 32.4
Live Load		1550	--	S_T = 7612	2231	9.70	9.05	16.03	< 32.4
DBE		999	1529						
10% DBE		99	153						
		4429	1682						
Dead Load		1781	--	S_c = 8433		5.73			0.9 σ_y
Live Load		1550	--	S_T = 7612	2231	6.35	6.68	13.03	< 32.4
OBE		633	1128						
10% OBE		63	113						
		4027	1241						
End Tie									
Dead Load		--	--	S_c = 1065.0		--			0.9 σ_y
Live Load	E∿E	--	--	S_T = 670.6	553.7	--	24.12	24.12	< 32.4
DBE		--	1012						
10% DBE		--	101						
			1113						
Dead Load		--	--	S_c = 588.6		--			0.9 σ_y
Live Load	F∿F	--	--	S_T = 510.7	548.5	--	10.72	10.72	< 32.4
DBE		--	445						
10% DBE		--	45						
			490						
Dead Load		--	--	S_c = 1065.0		--			0.9 σ_y
Live Load	E∿E	--	--	S_T = 670.6	553.7	--	17.81	17.81	< 32.4
OBE		--	747						
10% OBE		--	75						
			822						
Dead Load		--	--	S_c = 588.6		--			0.9 σ_y
Live Load	F∿F	--	--	S_T = 510.7	548.5	--	7.92	7.92	< 32.4
OBE		--	329						
10% OBE		--	33						
			362						

TABLE X A-15 CRITICAL STRESS SUMMARY (psi)

Load[(a)]	Seismic Stress	Total Stress	Allowable Stress	Margin Safety
P + W + OBE	10,090	16,343	18,750[(b)]	0.15
P + W + DBE	14,863	21,116	28,125[(c)]	0.33

(a) P = Pressure, W = Dead Weight

(b) 1.2 S_h.

(c) 1.8 S_h.

TABLE X A-16 POSSIBLE f_e/f_s VALUES

Configuration	f_e[(a)]	f_s[(a)]	f_e/f_s
1	5.12	5.3	0.97
2	8.31	5.3	1.57

(a) cps

TABLE X A-17 STEAM GENERATOR SUPPORTS - MAXIMUM MEMBER LOADS - PIPE RUPTURE PLUS SEISMIC

Member No.	Pipe Rupture - Maximum Loads (kip)	Seismic - Maximum Loads (kip)	Rupture and Seismic - Maximum Loads (kip)
21-47	1609.6	-98.5	-1708.1
22-48	242.7	+48.0	290.7
23-49	-242.7	-48.0	-290.7
24-50	-1603.1	-98.5	-1701.6
25-51	412.0	46.0	458.0
27-52	-412.0	-46.0	-458.0
31-57	549.7	115.2	664.9
16-58	-635.4	-116.0	-751.4
33-59	613.3	115.4	728.7
32-56	1526.0	25.6	1551.6
30-55	1555.9	25.5	1581.4
30-54	2183.3	64.6	2247.9
29-53	-1444.0	-30.7	-1474.7

TABLE X A-18 REACTOR COOLANT PUMP SUPPORTS - MAXIMUM MEMBER LOADS - PIPE RUPTURE PLUS SEISMIC

Member No.	Pipe Rupture - Maximum Loads (kip)	Seismic - Maximum Loads (kip)	Rupture and Seismic - Maximum Loads (kip)
11-40	493.9	22.0	515.9
11-60	-114.9	-12.3	-127.2
12-60	-696.8	-20.7	-717.5
13-41	743.3	10.3	733.6
13-44	-680.2	-17.3	-697.5
14-42	538.9	20.7	559.6
14-43	577.0	13.9	590.9
14-44	-117.2	-11.5	-128.7
40-42	-212.7	-3.4	-216.1
40-60	-210.2	-3.6	-213.8
40-64	-29.7	-5.5	-35.2
40-65	1243.6	21.9	1265.5
42-44	-212.8	-3.4	-216.2
42-64	1257.7	20.2	1277.9
44-60	134.3	1.9	136.2
44-64	313.6	1.9	315.5
44-67	-963.1	-11.4	-974.5
60-65	348.6	2.1	350.7
60-67	-18.6	-2.4	-21.0
60-69	-1041.0	-14.4	-1055.4

TABLE X A-19 SUMMARY OF CRITICAL STRESSES (psi) IN LHSIS

Load Combination	Seismic Stress	Total Stress	Allowable Stress	Margin Safety	Piping Section
P + W + OBE	9,389	14,698	16,860	0.23	Accumulator Piping
P + W + DBE	13,944	19,247	25,290	0.43	Accumulator Piping
P + W + OBE	7,191	14,941	19,320	0.61	LHSI - Pump to Cold Leg - Loop 1
P + W + DBE	10,707	18,451	28,980	0.98	LHSI - Pump to Cold Leg - Loop 1
P + W + OBE	8,641	16,368	19,320	0.34	LHSI - Pump to Cold Leg - Loop 2
P + W + DBE	12,834	20,552	28,980	0.65	LHSI - Pump to Cold Leg - Loop 2
P + W + OBE	8,447	15,968	19,320	0.39	LHSI - Pump to Cold Leg - Loop 3
P + W + DBE	12,445	19,988	28,980	0.72	LHSI - Pump to Cold Leg - Loop 3

TABLE X A-20 SUMMARY OF ACCUMULATOR TANK NOZZLE PIPE LOADS

Pipe Load[a]	System No. 2[b]		System No. 3[c]	
	DBE	Thermal	DBE	Thermal
F_x	1,767 lb	1,615 lb	26,647 lb	252 lb
F_y	5,670 lb	165 lb	4,442 lb	2,153 lb
F_z	9,903 lb	1,214 lb	4,046 lb	3,921 lb
M_x	14,337 ft-lb	9,924 ft-lb	13,223 ft-lb	11,759 ft-lb
M_y	26,302 ft-lb	22,307 ft-lb	35,226 ft-lb	50,043 ft-lb
M_z	42,119 ft-lb	14,932 ft-lb	160,654 ft-lb	30,775 ft-lb

(a) x, y, z refer to global coordinates for piping analysis; F is force, and M is moment.

(b) Ref. 16.

(c) Ref. 17.

TABLE X A-21 LOAD CONDITION AND STRESS LIMITS - CODE CASE NO. 1607

Load Condition	Stress Limits
Upset	$\sigma_m \leq 1.1\ S$
	$(\sigma_m \text{ or } \sigma_L) + \sigma_b \leq 1.65\ S$
Emergency	$\sigma_m \leq 1.5\ S$
	$(\sigma_m \text{ or } \sigma_L) + \sigma_b \leq 1.8\ S$
Faulted	$\sigma_m \leq 2.0\ S$
	$(\sigma_m \text{ or } \sigma_L) + \sigma_b \leq 2.4\ S$

(a) σ_m = general membrane stress (no discontinuity effects) produced only be mechanical loads.

σ_L = local membrane stress (including discontinuity effects) due to mechanical loads only.

σ_b = bending stress due to mechanical loads only.

S = allowable stress value given in Tables I-7.1, I-7.2, I-7.3 of Appendix I of current ASME Code Section III.

TABLE X A-22 ACCUMULATOR PIPING CONNECTION NOZZLE LOADS

Method	Load	Maximum Stress (psi)	Code Allowable Stress (psi)
1. B31.1 only	Thermal expansion	13,050	25,790
	OBE + pressure	12,670	18,800 ($1.2S_h$)
	DBE + pressure	16,380	28,200 ($1.8S_h$)
2. Bijlaard and B31.1	Thermal	7,530	25,790
	OBE + pressure	12,730	18,800 ($1.2S_h$)
	DBE + pressure	15,790	28,200 ($1.8S_h$)

TABLE X A-23 REACTOR BUILDING NATURAL FREQUENCIES

Mode	North-South (cps)	East-West (cps)
1	5.05	3.64
2	6.13	5.49
3	8.15	8.08

TABLE X A-24 COMPUTED STRESS INTENSITIES IN BWR VESSEL NOZZLES

Nozzle Description	Mark No.	Primary Membrane Plus Pressure Stress Max. Stress Intensity (ksi)	Allowable Stress 1.5 S_m (ksi)	Secondary Plus Primary Stress Max. Stress Intensity (ksi)	Allowable Stress 3.0 S_m (ksi)
Recirculation outlet	8	27.09	40.0	30.20	80.0
Recirculation inlet	7	26.33	40.0	27.77	80.0
Steam outlet(a)	14	26.79	40.0	27.01	80.0
Feedwater	10	26.41	40.0	27.39	80.0
Core spray	11	26.33	40.0	27.35	80.0
Jet pump instrumentation(a)	19	26.29	40.0	26.46	80.0
CRD hydraulic system return	13	26.29	40.0	26.43	80.0
Head spray(a)	206	19.88	40.0	23.22	80.0
Vent(a)	204	19.65	40.0	20.36	80.0
Drain(a)	22	9.85	40.0	10.00	80.0
2 in. instrumentation	12	τ_{avg} = 3.624	τ Allowable = 12		

(a) Nozzles qualified in fatigue under Article NB-3222.4(d), Section III, ASME Code.

TABLE X A-25 REACTOR PRESSURE VESSEL ELASTIC ANALYSIS

Stress Intensity Category	Critical Loading	Maximum Computed Stress Intensity (ksi)	Code Allowable Value (ksi)
Primary Membrane	SSE + Dead Load	15.1	S_m = 26.7
	SSE + Jet Load + Dead Load	28.5	1.5 S_m = 40.1
Primary Plus Secondary Stress Intensity Range		111.0	$3S_m$ = 80.0

TABLE X A-26 NATURAL PERIODS AND SPECTRAL ACCELERATIONS

Mode	Period (sec)		Spectral Acceleration (in./sec^2)
1	0.3355		112.05
2	0.3039	(a)	115.69
3	0.2967		116.47
4	0.2832		117.92
5	0.2653		119.84
6	0.2243		142.40
7	0.2117	(a)	177.83
8	0.2107		180.53
9	0.1889	(a)	241.65
10	0.1810		270.87
11	0.1685		321.15
12	0.1454		358.98
13	0.1400	(a)	358.98
14	0.1378		356.71
15	0.1288		268.35
16	0.1271		252.36
17	0.1165		169.48
18	0.1047		84.74
19	0.0996		82.13
20	0.0930		78.73
21	0.0898		77.08

(a) Note: Closely spaced periods.

TABLE X A-27 CRITICAL STRESSES (psi)

Loads Considered[a]	Seismic Stress	Total Stress	Allowable Stress	Margin Safety	Location
P + W + DE	5,910	14,409	17,312[b]	0.20	#44-12 in. Elbow
P + W + MCE	13,180	21,000	25,969[c]	0.24	Near Reactor
P + W + DE	2,341	7,803	17,312	1.22	#48-Branch above
P + W + MCE	4,682	10,144	25,969	1.56	Gate Valve

(a) P, pressure; W, weight; DE, design earthquake; and W, weight
(b) 1.2 S_h.
(c) 1.8 S_h.

TABLE X A-28 PERIODS OF VIBRATION AND SPECTRAL ACCELERATIONS FOR MAIN STREAM LINE

Mode No.	Period (sec)	Spectral Acceleration (g)
1	0.338	0.47
2	0.187	1.81
3	0.158	1.83
4	0.106	0.3
5	0.101	0.3
6	0.099	0.3
7	0.058	0.65
8	0.054	0.48
9	0.053	0.42

TABLE X A-29 CRITICAL STRESSES (psi) FOR MAIN STEAM LINE

Loads Considered	Seismic Stress	Total Stress	Allowable Stress	Margin Safety	Location
P + W + DE	7,492	15,938	21,000	0.32	HPCI Tee (pt #118)
P + W + DE + T[(a)]	4,643	45,285	52,550	0.16	@ 26 in. Tee (pt #79)
P + W + MCE	14,984	23,147	31,500	0.36	HPCI Tee (pt #118)

(a) T, thermal expansion.

TABLE X A-30 SUMMARY OF LOADS ON PIPE WHIP CONSTRAINTS

	Case I		Case II				Case III					
	T (kip)		S (kip)		M (in.-kip)		T (kip)		S (kip)		M (in.-kip)	
	Act. Load	Allow. Load	Act. Load	Allow. Load	Act. Load	Allow. Load	Act. Load	Allow. Load	Act. Load	Allow. Load	Act. Load	Allow. Load
12 in. ϕ	127	169	127	155	1650	2020	90	122	90	122	1170	1580
22 in. ϕ	394	525	394	437	670	7420	279	324	279	324	4740	5500
28 in. ϕ	637	860	637	662	10800	14600	450	510	450	510	9900	11200

TABLE X A-31 CRITICAL STRESSES (psi)

Earthquake	Total	Seismic	Allowable	Margin
DE	14,538	6,232	17,375	0.2
MCE	23,263	14,957	27,800	0.2

TABLE X A-32 RESULTS OF DYNAMIC ANALYSIS OF BATTERY RACKS

Type of Rack	Fundamental Frequency (cps)	Acceleration (g)	
		Design Earthquake (from Floor Response Spectrum) (2% Damping)	Maximum Credible Earthquake (Taken 2.4 Times Design Earthquake)
Horizontal Excitation			
12- and 17-ft racks	9.2 (hand computation) 8.0 (computer check)	0.18	0.43
6-ft racks	16.5	0.12	0.288
Vertical Excitation			
12- and 17-ft racks	8.0	0.16	0.38
6-ft racks	13.9	0.17	0.41

TABLE X A-33 HANGER ATTACHMENT TYPES

Hanger Length (ft)	No. of Trays	Types of Hanger Attachment
3 to 16	1	swivel
3 to 9	2 to 4	swivel
16 and up	1	fixed
9 and up	2 to 4	fixed

Plant {PWR / BWR}

SAFETY STUDY DESIGN ADEQUACY
REVIEW DATA SHEET

FIRL Reviewer _____

1 - Component Description: _____

_____

2 - Drawing References: _____

_____

3 - Installed Elevation: _____ 4 - Location: _____

5 - Design Criteria: _____

_____

6 - Data Basis Description: _____

_____

7 - Estimated Weight: _____ 8 - Fundamental Frequency: _____

9 - Mathematical Model: _____

_____

_____

10 - Method of Analysis: _____

_____

11 - Seismic Load Definition: _____

_____

12 - Maximum Stresses: (Location _____)

	Total Stress	Seismic Stress	Allowable	Margin
OBE				
DBE				

13 - Maximum Deflection: _____ Location: _____

14 - Comments: _____

_____

_____

_____

_____

FIGURE X A-1 Design Adequacy Review Data Sheet

Plant {PWR / BWR}

SAFETY STUDY DESIGN ADEQUACY
SUPPLEMENTARY REVIEW DATA SHEET

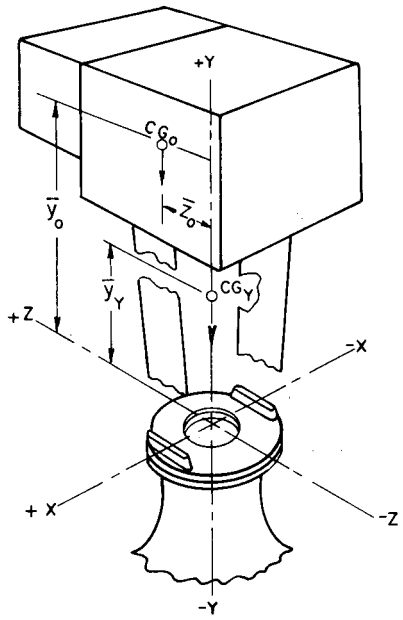
FIRL Reviewer _____

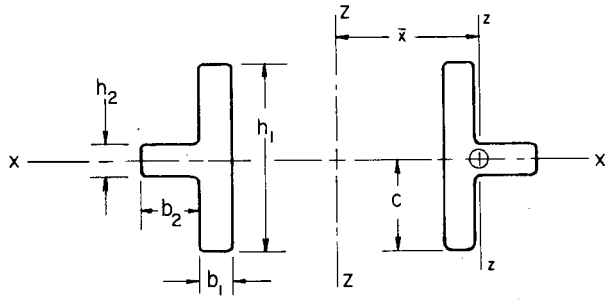
1 - Component Description: _____

_____

Reviewed Item	Supplementary Data

FIGURE X A-2 Supplementary Review Data Sheet





YOKE WEB DIMENSIONS AT WEAKEST CROSS SECTION

b_1 = 0.50 IN.

h_1 = 4.50 IN.

b_2 = 2.00 IN.

h_2 = 0.50 IN.

I_x = 7.64 IN.^{4} (MOMENT OF INERTIA)

A = 6.50 IN.^{2} (AREA)

C = 2.25 IN. (DIMENSION TO OUTER FIBER)

FIGURE X A-3 Example of a Multi-Element Structure Connected to Rigid Structures at Both Ends

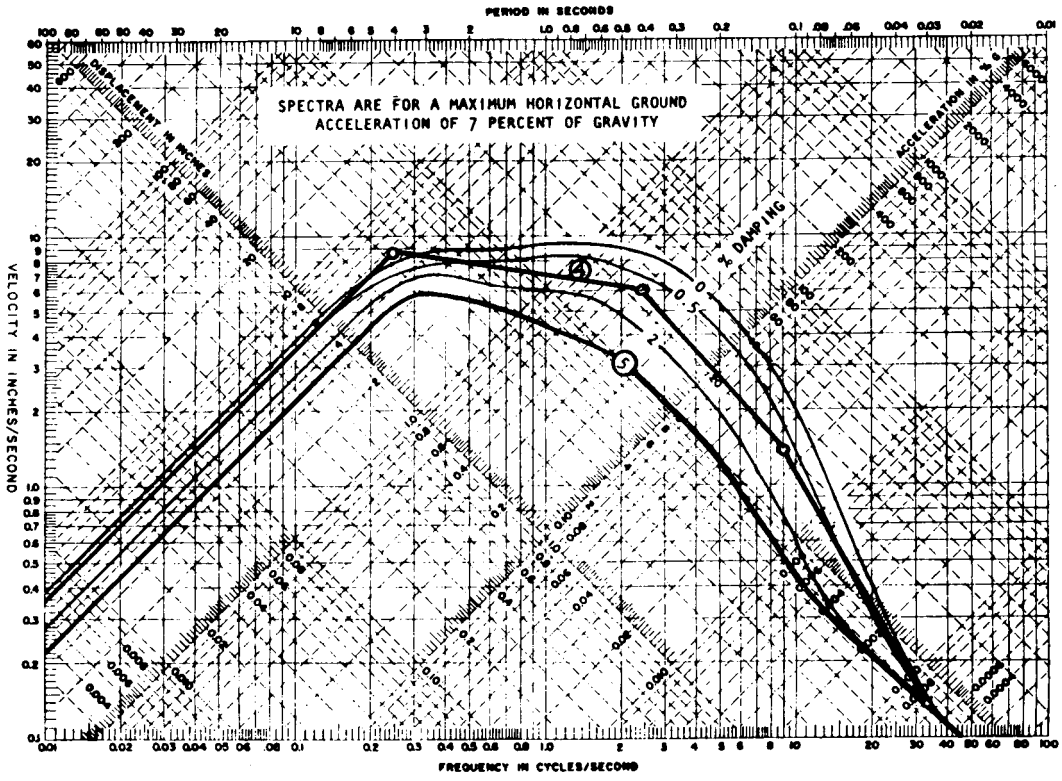


FIGURE X A-4 Ground Response Spectra (OBE) - PWR

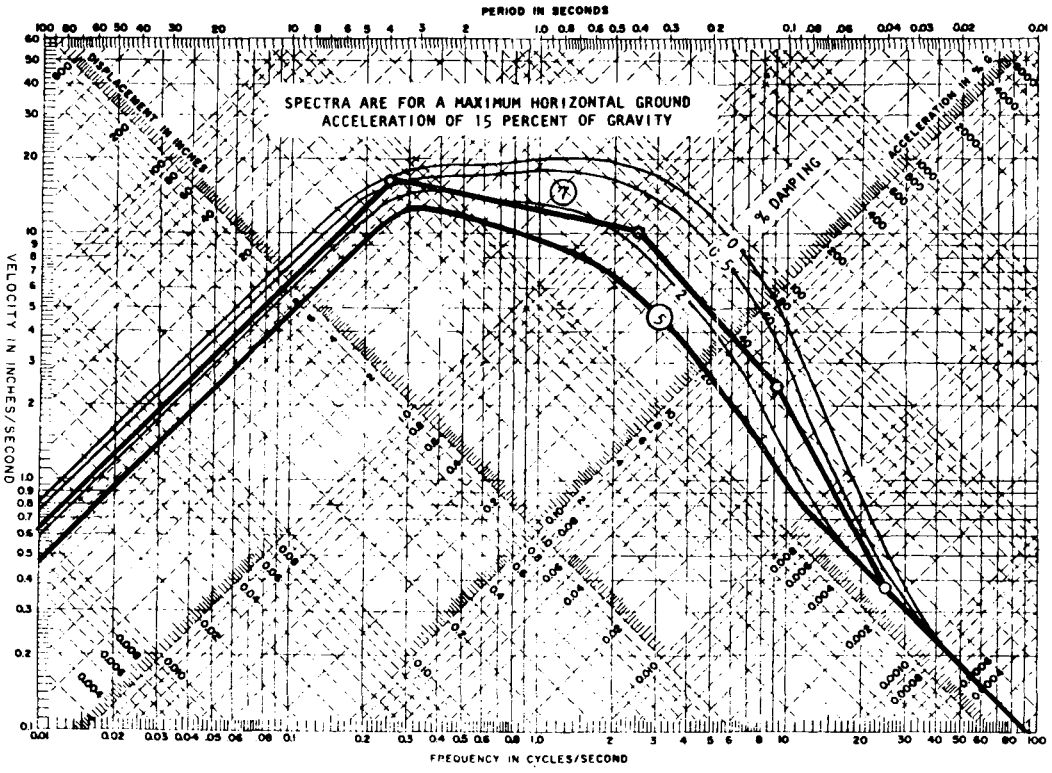


FIGURE X A-5 Ground Response Spectra (DBE) - PWR

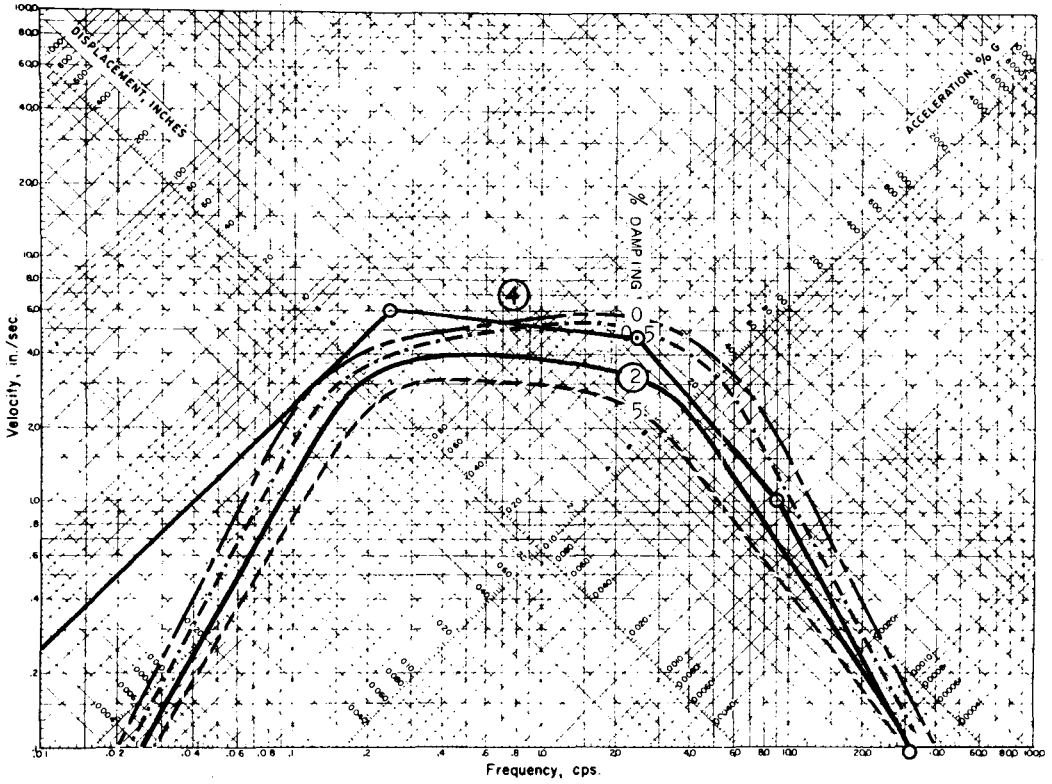


FIGURE X A-6 Response Spectra (DE) - BWR

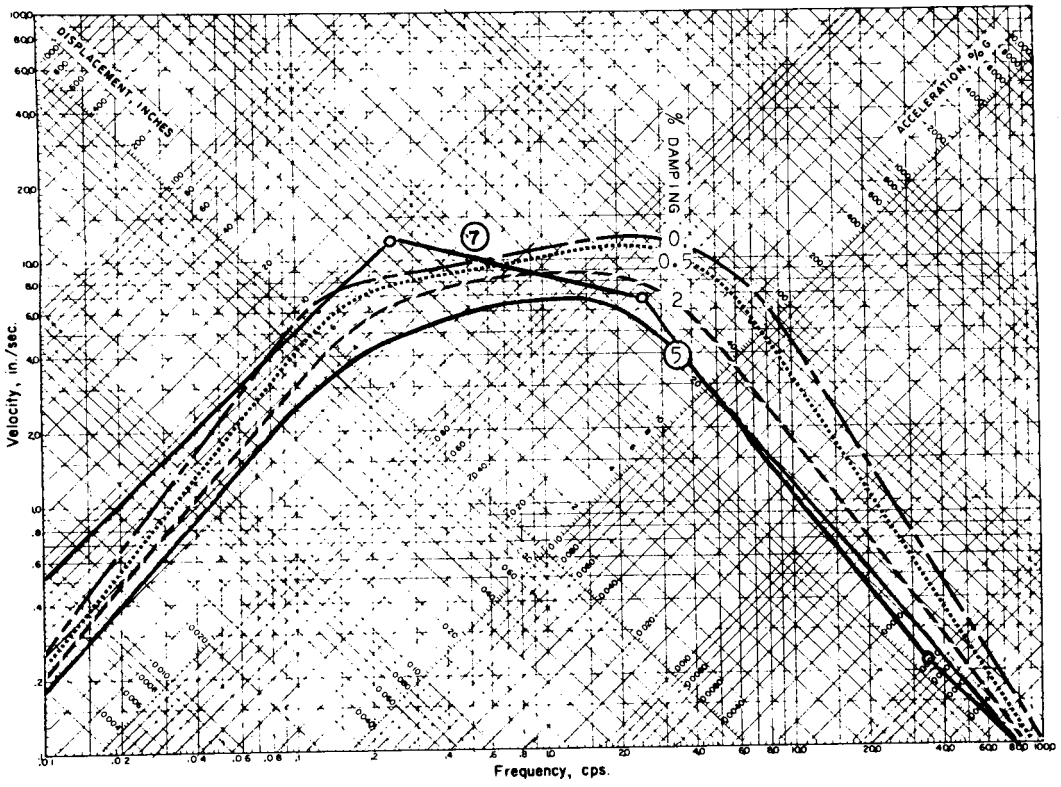


FIGURE X A-7 Response Spectra (MCE) - BWR

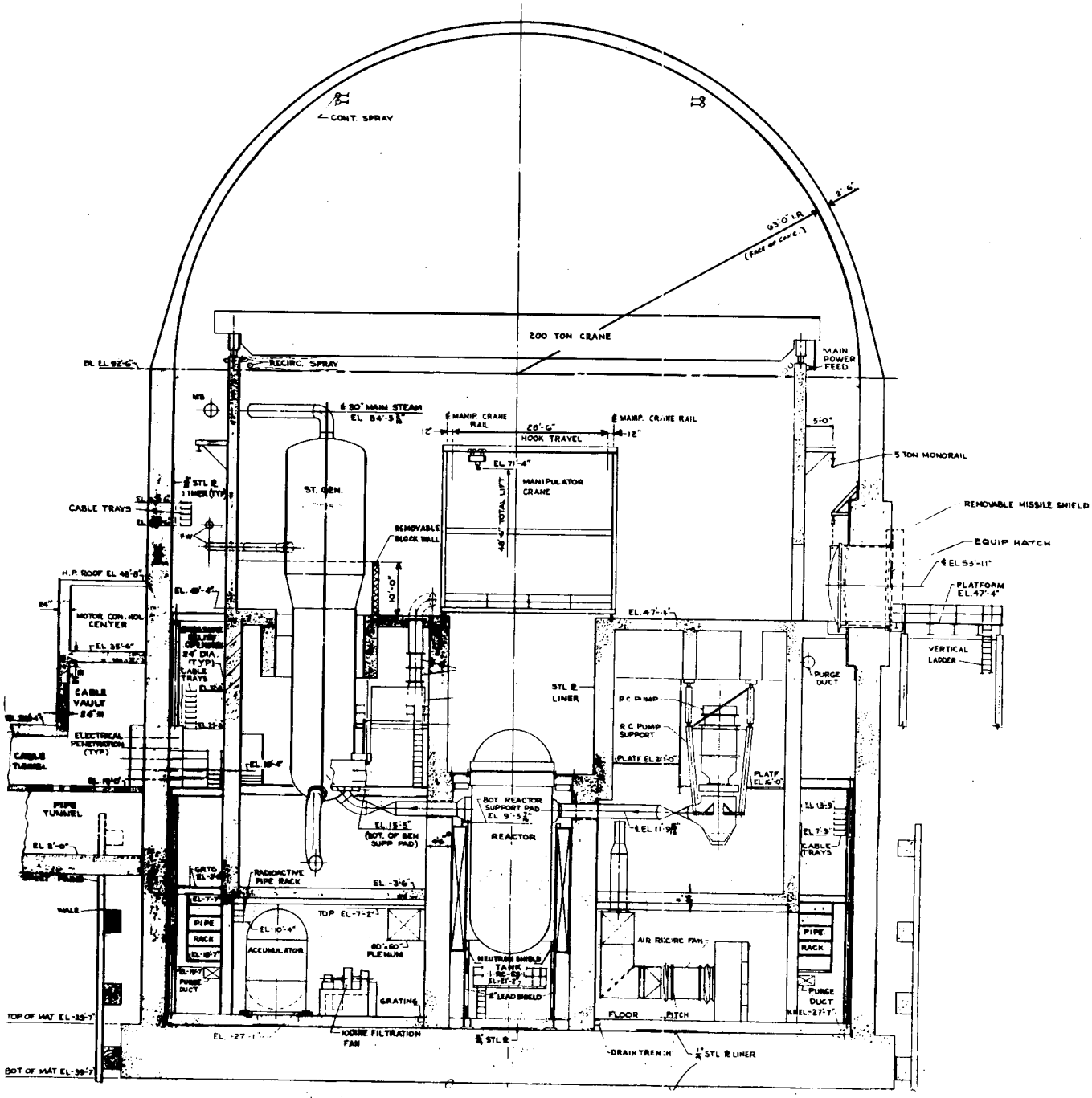
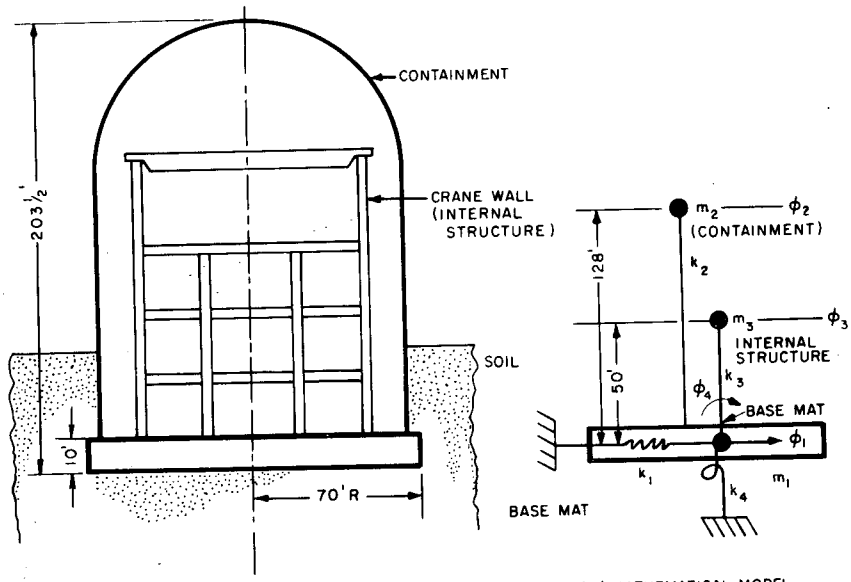


FIGURE X A-8 Cross Section Through Reactor Building



MASS PROPERTIES

m_1 = 2400 kip-sec^2/ft
m_2 = 475
m_3 = 310
J_o = 20 x 10^6 kip-sec^2-ft

STIFFNESS PROPERTIES

k_1 = 5 GR = 10^6 kip/ft
k_4 = 3 GR^3 = 2.7 x 10^9 ft-kip/rad
k_3 = 0.3 x 10^6 kip/ft
k_2 = 0.31 x 10_6 kip/ft

FIGURE X A-9 Soil-Structure Interaction Model

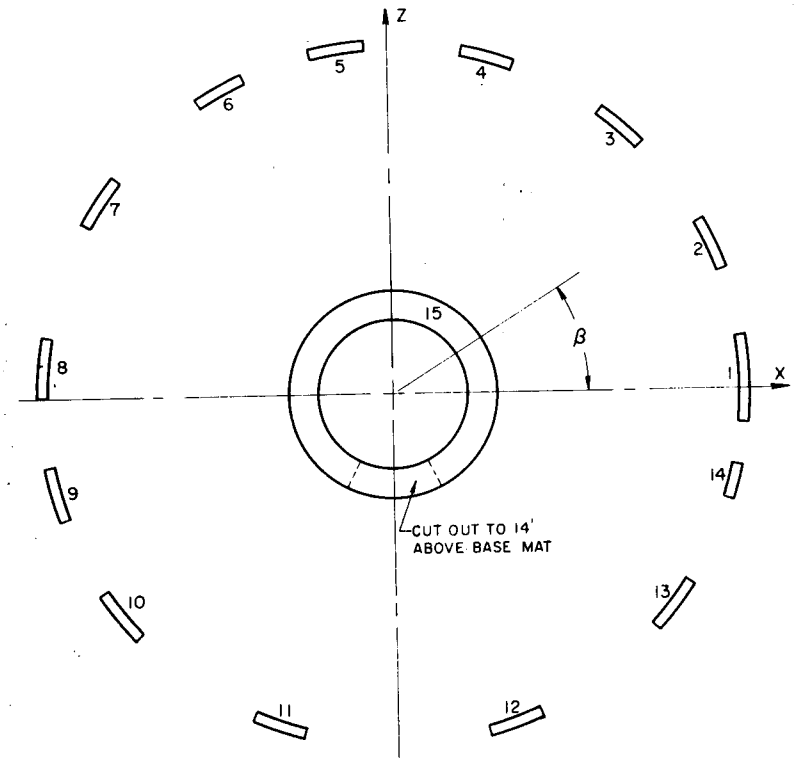


FIGURE X A-10 Containment Internal Structure - Cross Section of Lower Portion

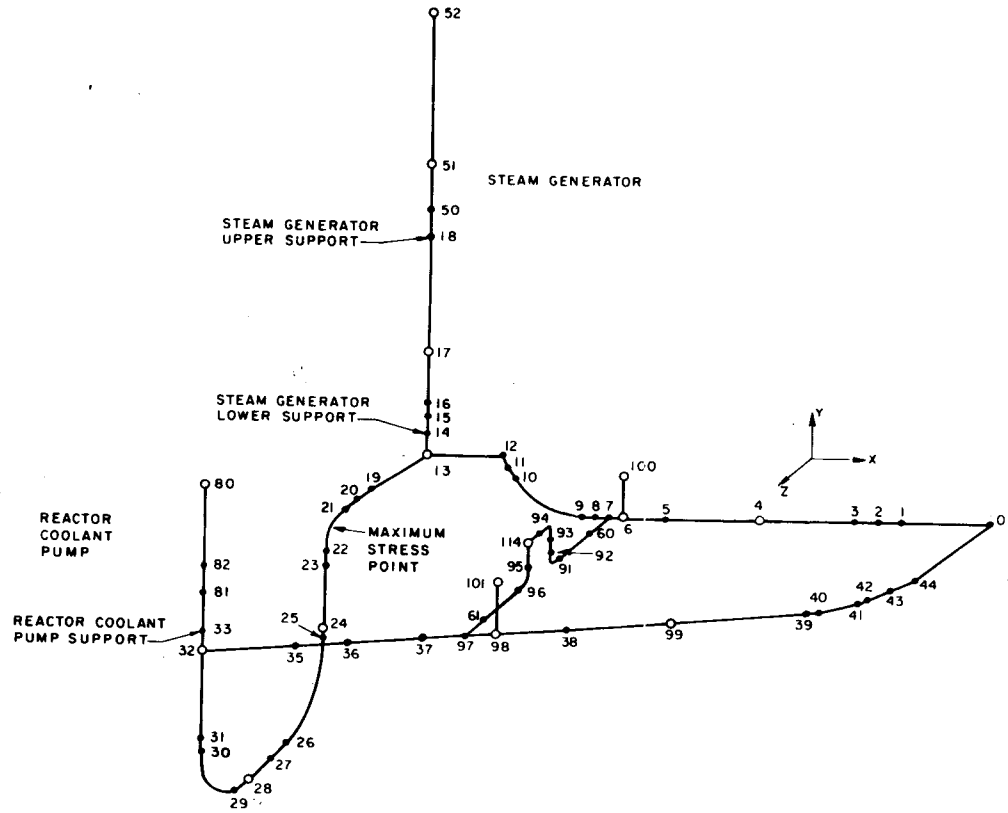


FIGURE X A-11 Reactor Coolant System - Seismic Analysis Model Used by Supplier

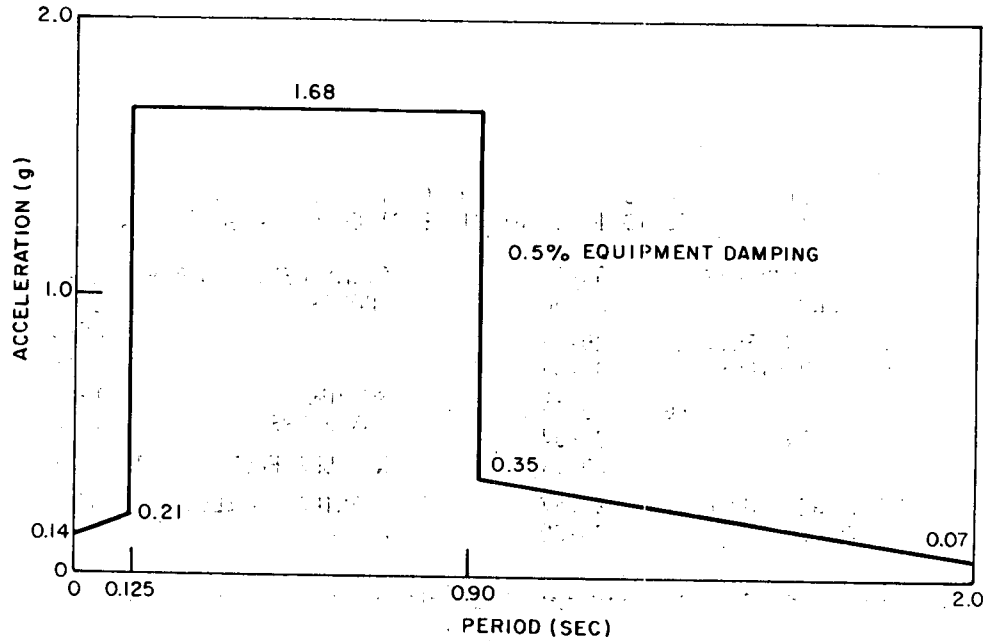
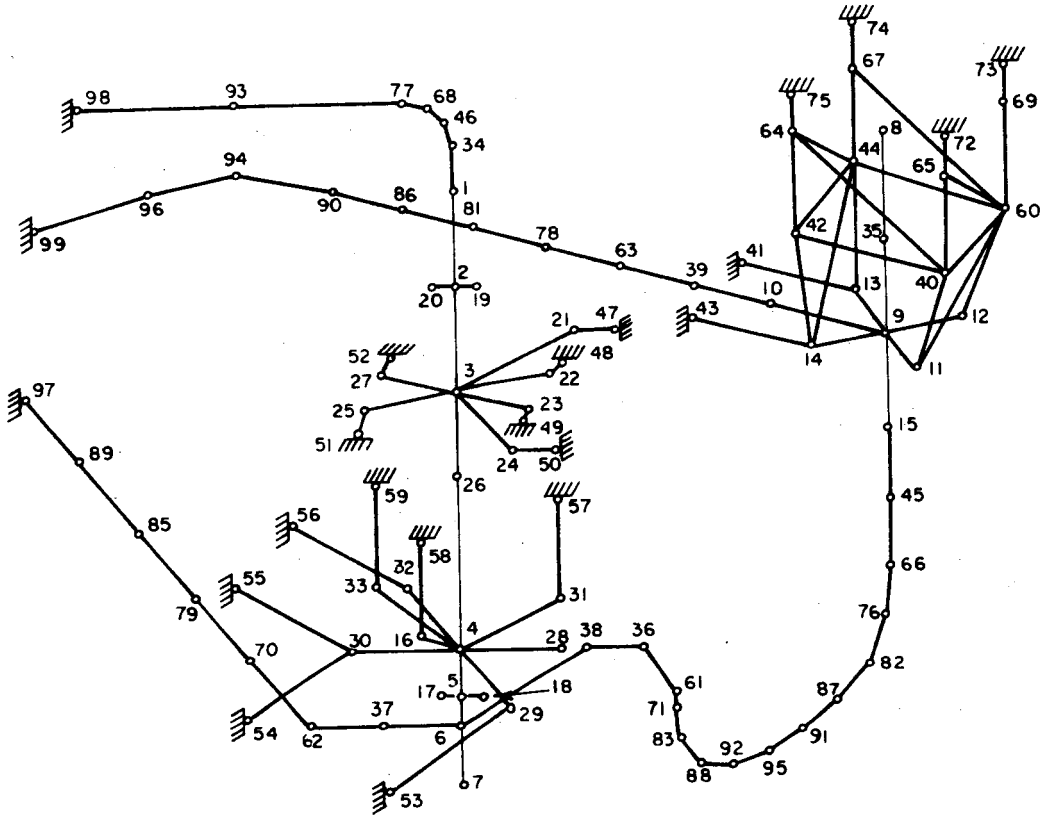


FIGURE X A-12 Horizontal OBE Floor Response Spectrum Used for Reactor Building



LEGEND

STEAM GEN. CENTER LINE	1-2-3-26-4-5-6-7
RC PUMP CENTER LINE	8-35-9-15
HOT LINE	97-89-85-79-70-62-37
PUMP SUCTION LINE	38-36-61-71-83-88-92-95-91-87 82-76-66-45-15
COLD LINE	39-63-78-81-86-90-94-96-99
MAIN STEAM LINE	1-34-46-68-77-93-98

FORCING FUNCTIONS

1	2	3	4	5	6	7	8	9	10	11	12	13	14	15	16
70	37	17	20	19	18	38	61	71	95	91	66	45	39	90	98

LOWER STEAM GEN. SNUBBERS	30-55 32-56
STEAM GEN. SWIVEL END COUPLINGS	29-53 30-54
STEAM GEN. HANGING SUPPORTS	16-58 31-57 33-59
STEAM GEN. UPPER SNUBBERS	21-47 24-50
STEAM GEN. SNUBBER BOLTS	22-48 23-49 25-81 27-52
RC PUMP SNUBBERS	13-41 14-43
RC PUMP FEET	11,12,13,14
REACTOR NOZZLES	97,99

FIGURE X A-13 A/E Mathematical Model for Dynamic Analysis of Primary Coolant Loop

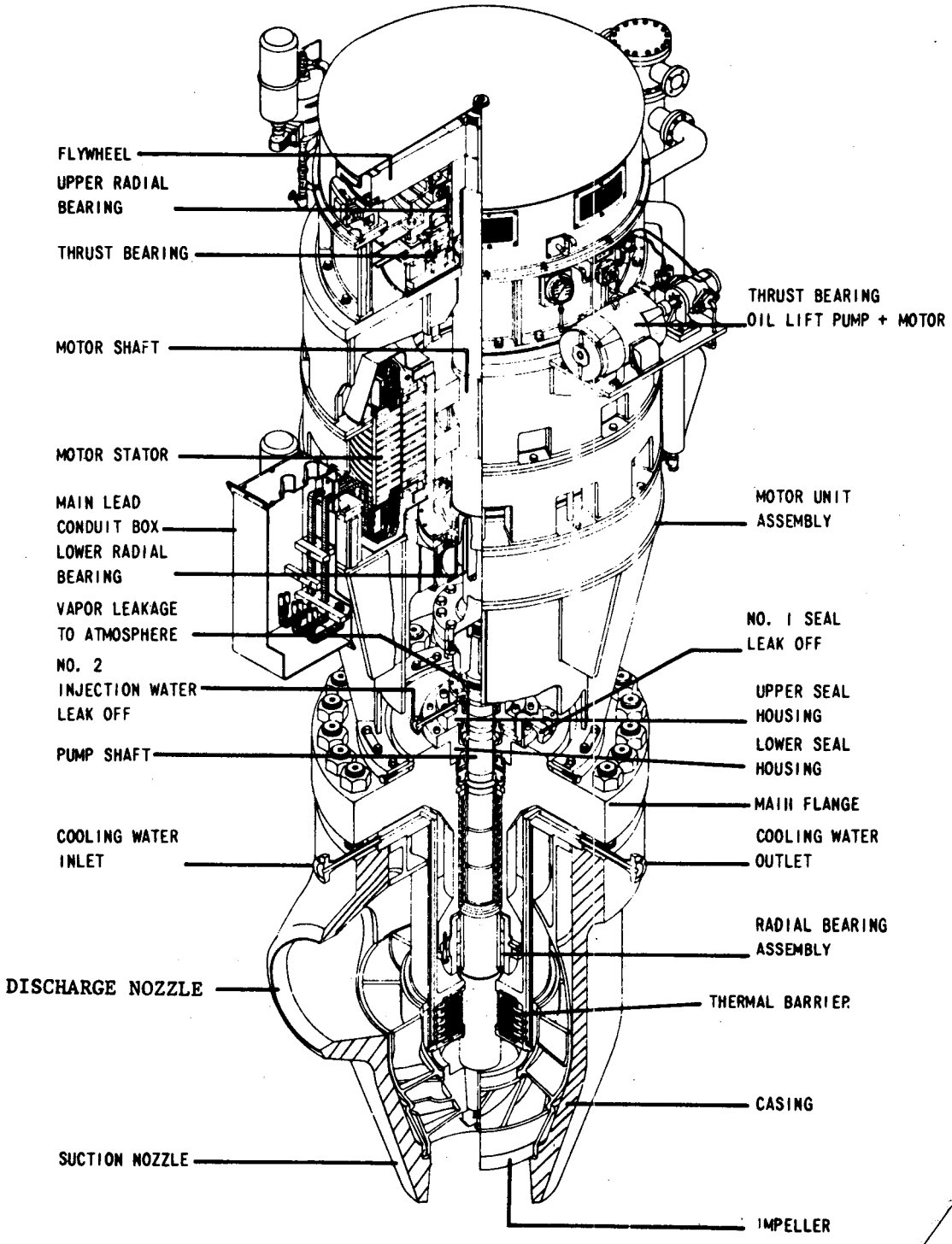


FIGURE X A-14 Typical Reactor Coolant Pump

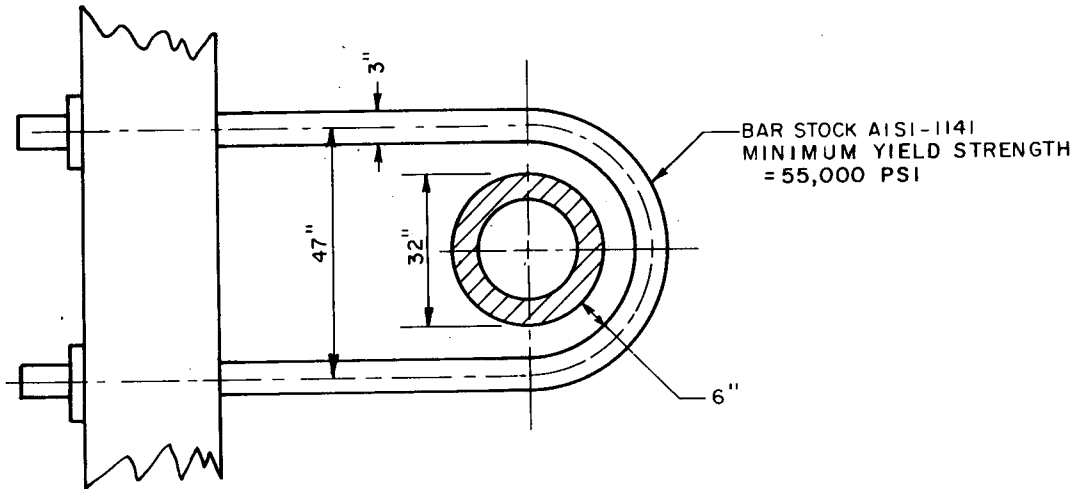


FIGURE X A-15 Pipe-Whip Restraint - Main Steam Line (not to scale)

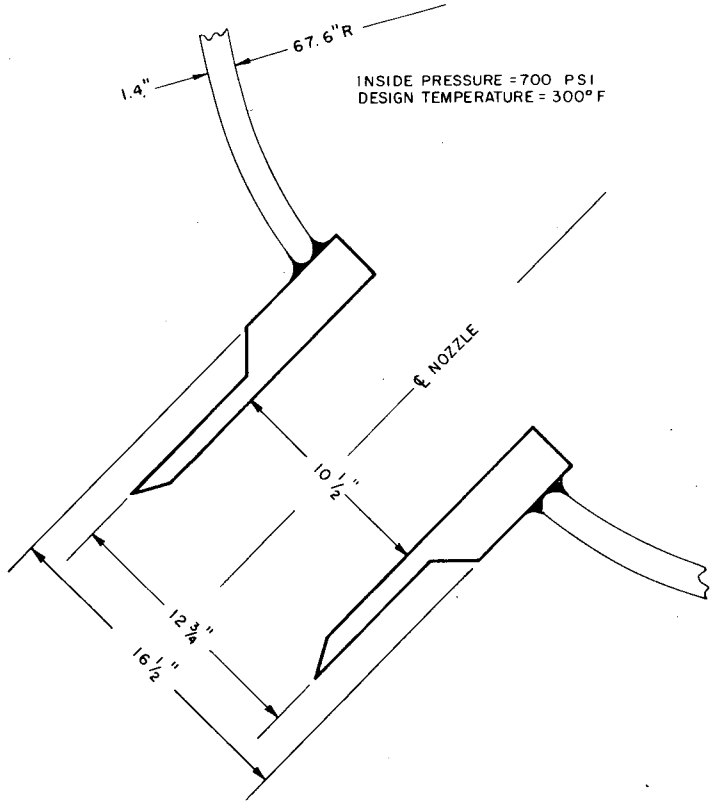


FIGURE X A-16 Accumulator Tank Nozzle

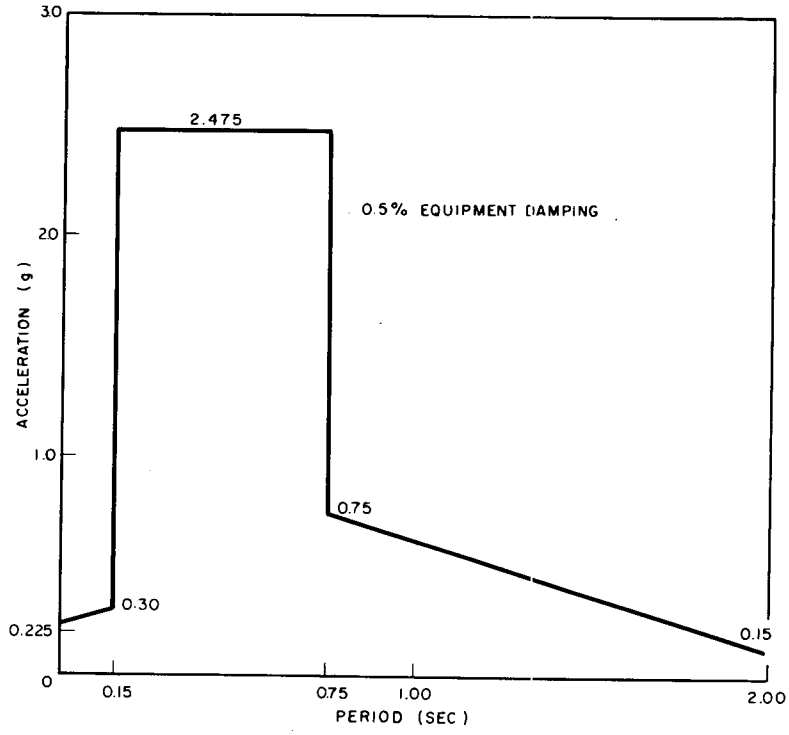


FIGURE X A-17 Horizontal DBE Floor Response Spectrum Used for Diesel Generator Building

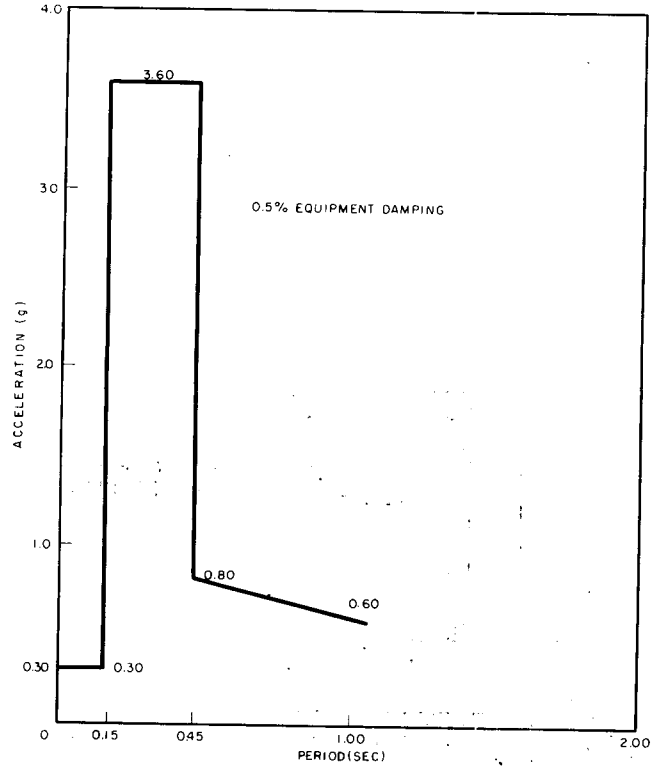


FIGURE X A-18 Vertical DBE Floor Response Spectrum Used for Diesel Generator Building

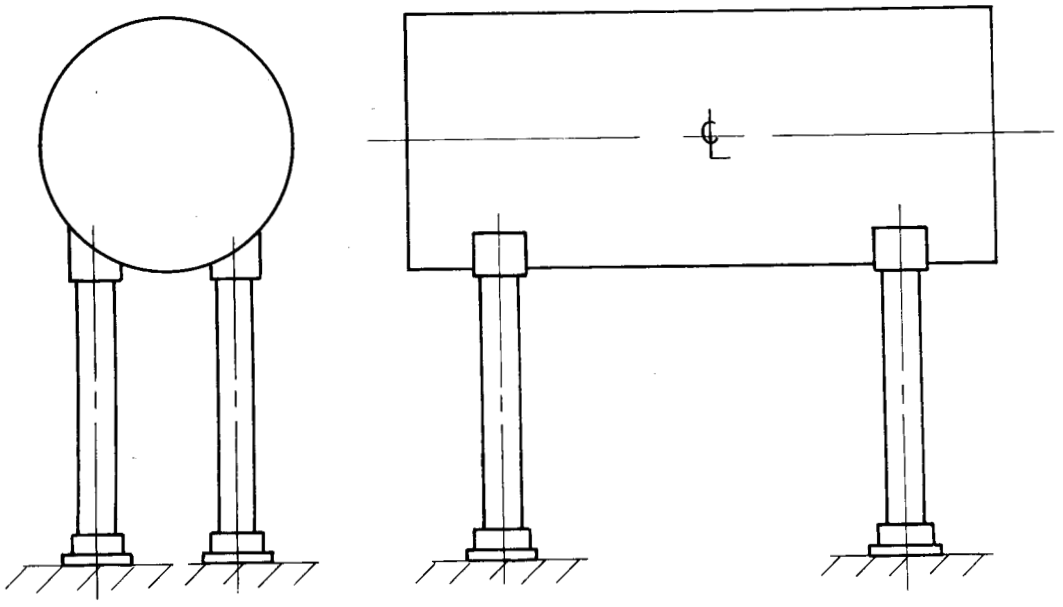


FIGURE X A-19 Day Tank

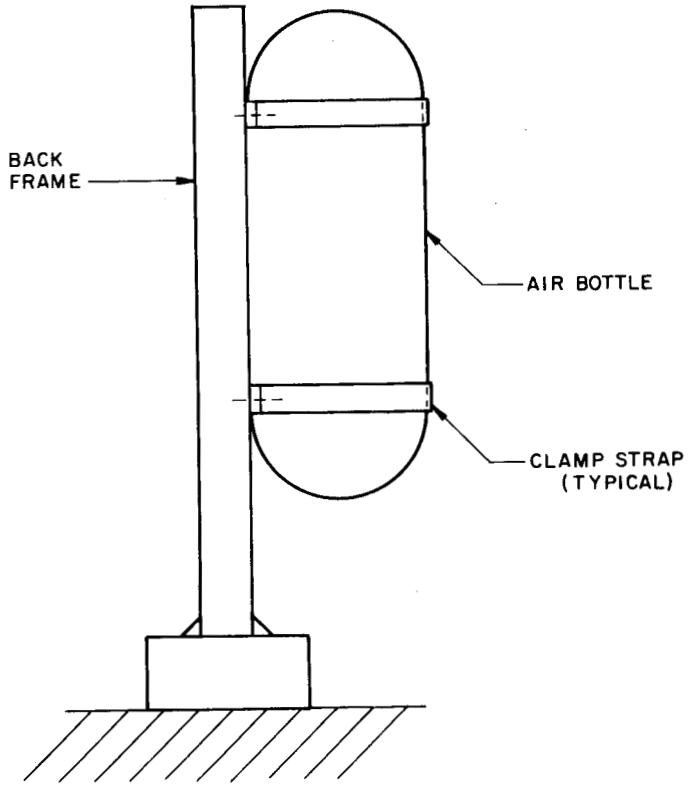


FIGURE X A-20 Air Bottle Support (Not to Scale)

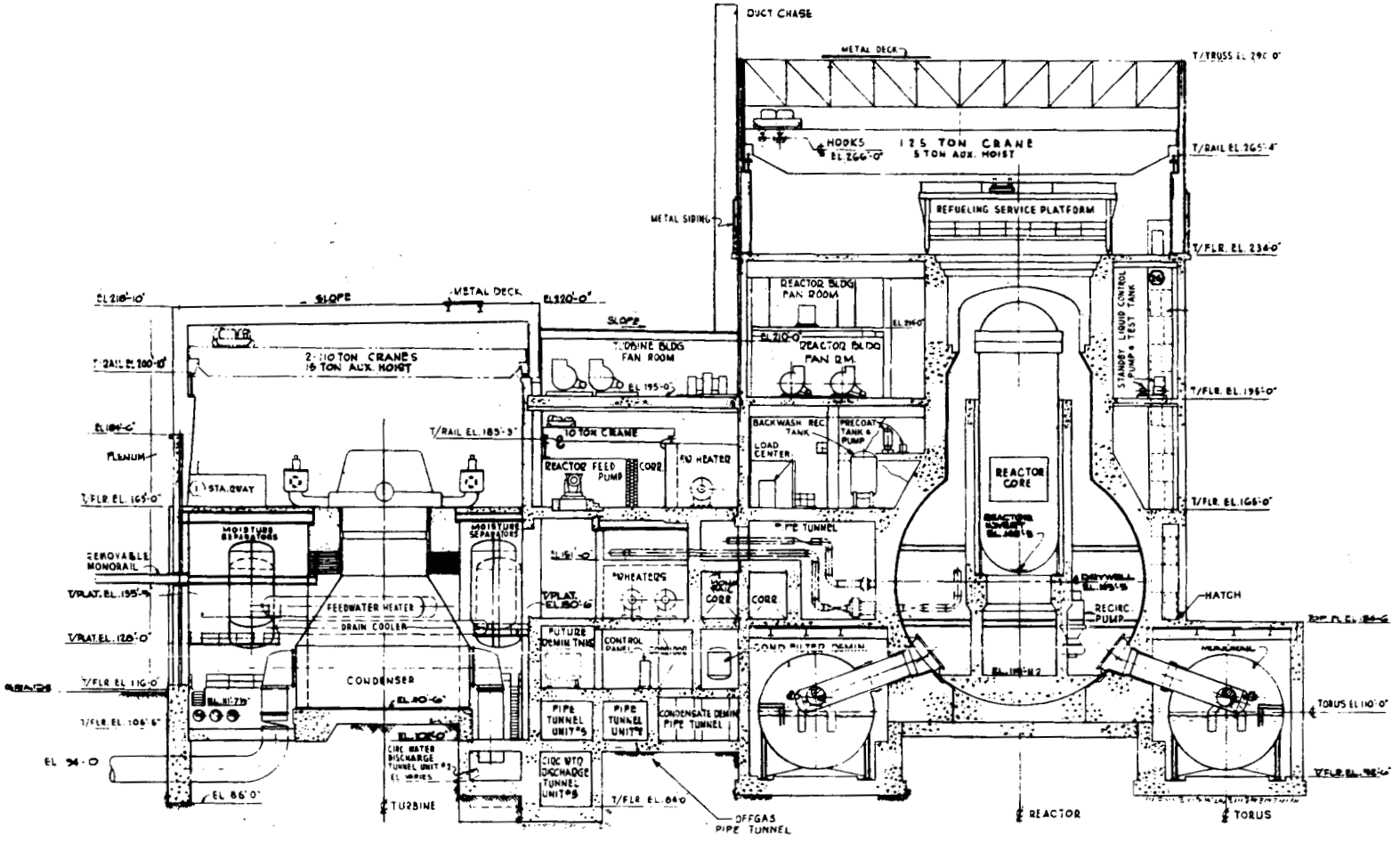


FIGURE X A-21 Elevation View Through BWR Plant

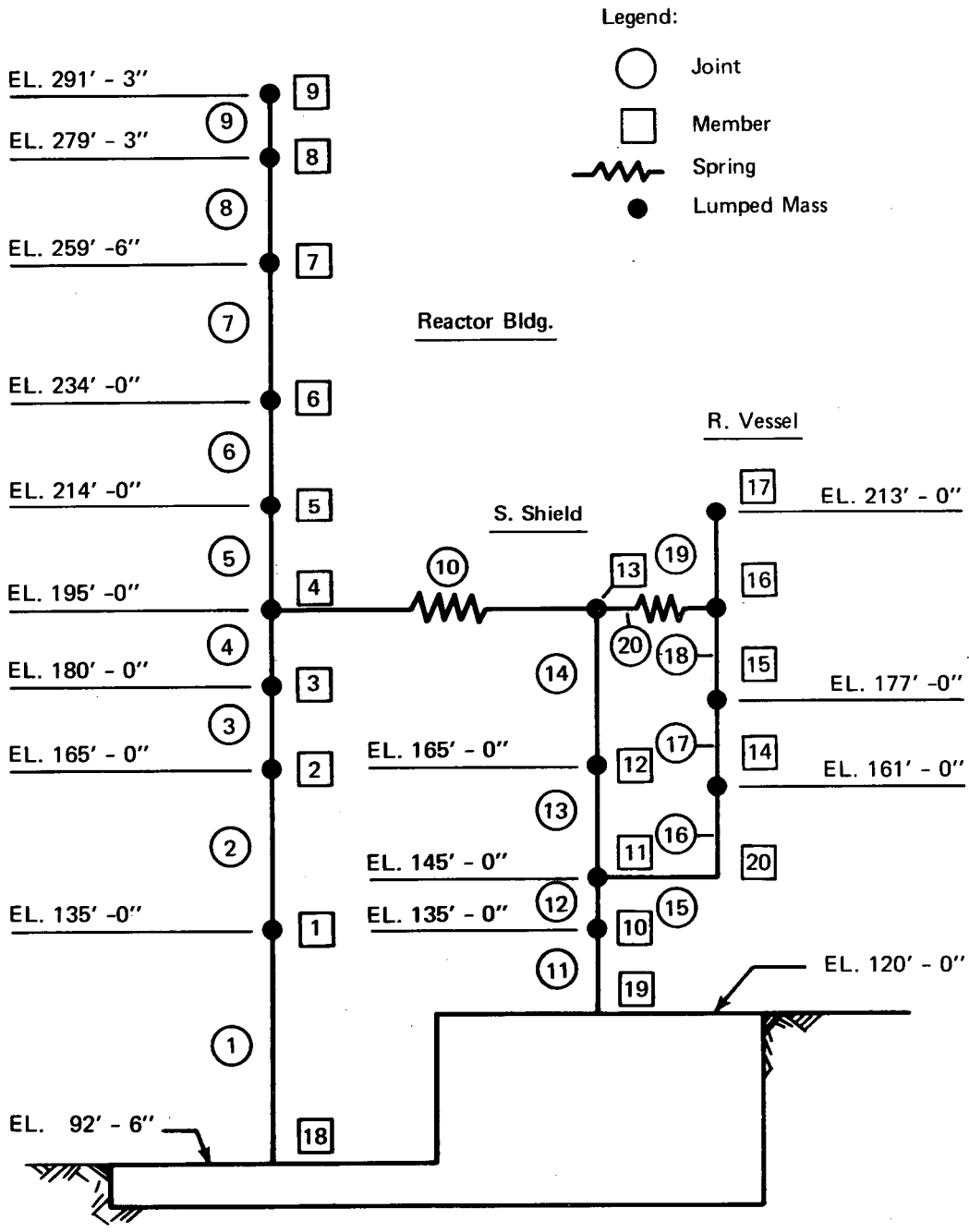


FIGURE X A-22 Reactor Building Mathematical Model

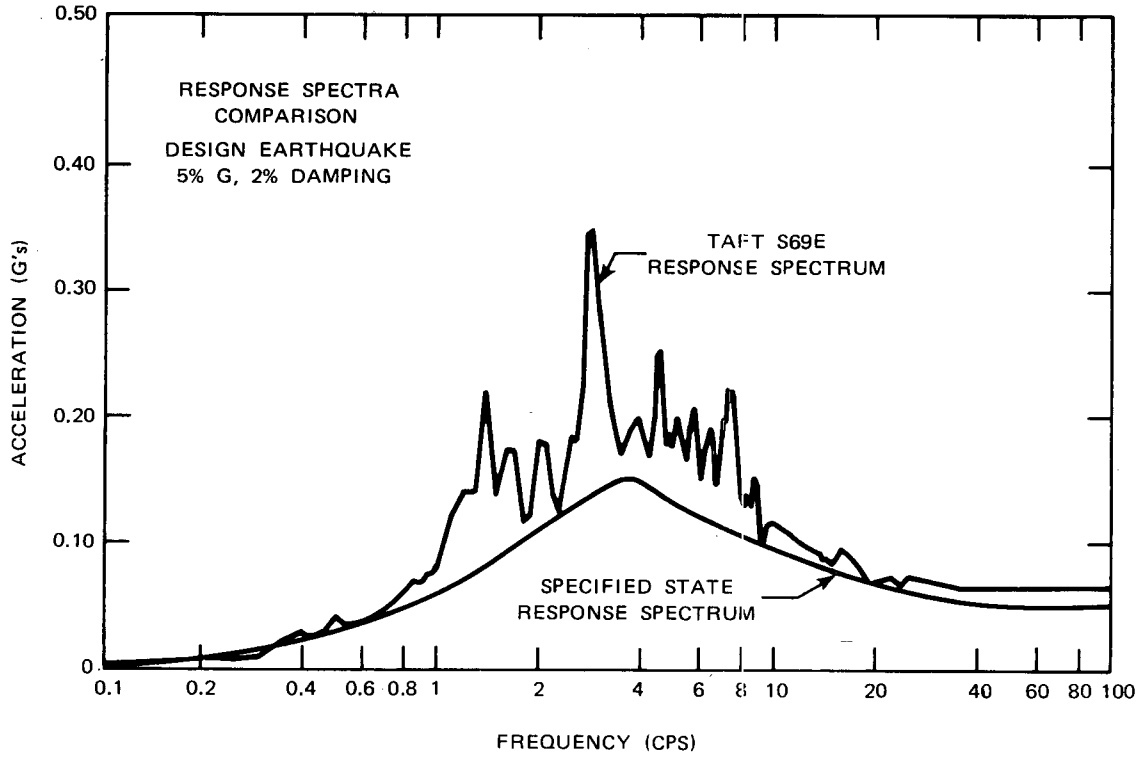


FIGURE X A-23 Response Spectra Comparison, Design Earthquake, 5% g, 2% Damping

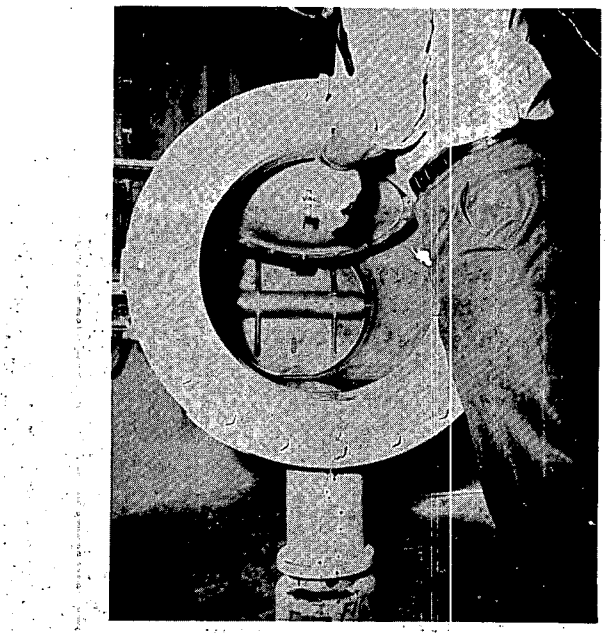
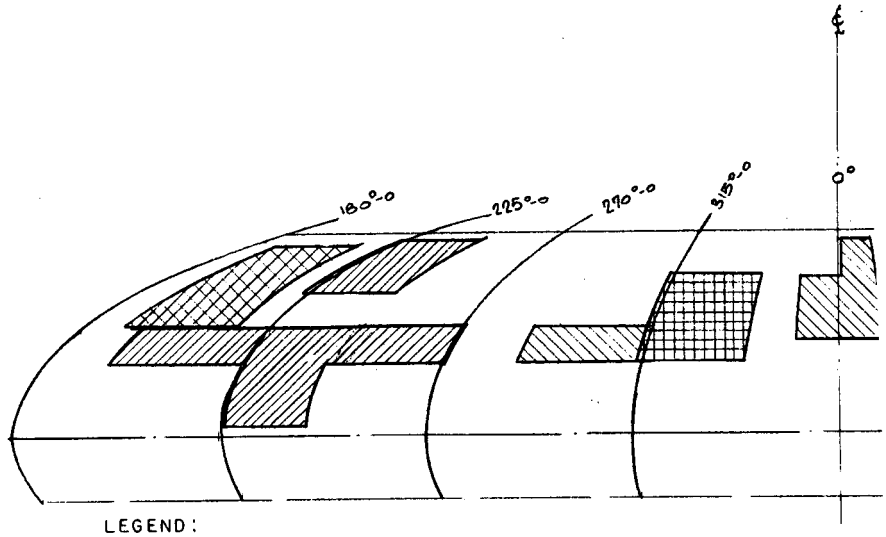


FIGURE X A-24 Vacuum Breaker Valve



LEGEND:

3 1/4" THICK PLATE

1 1/2" THICK PLATE

2 1/2" THICK PLATE

1 1/4" THICK PLATE

Shell Stretchout - Inside View of Reinforcing Plates. Scale 1/16" - 1'-0"

FIGURE X A-25 Missile Barriers Inside Drywell

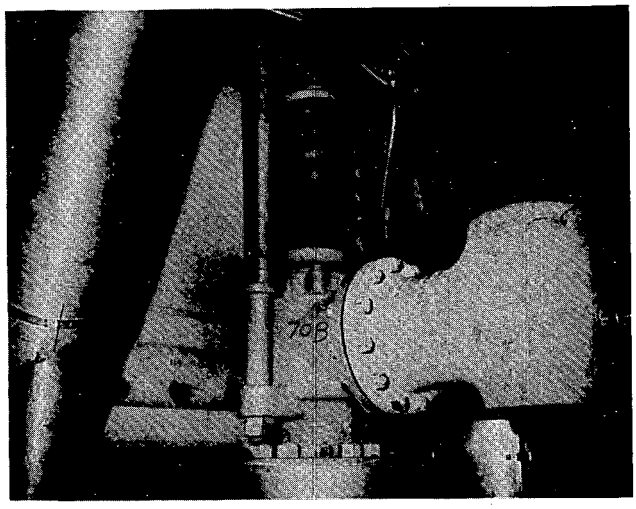


FIGURE X A-26 Safety Valve

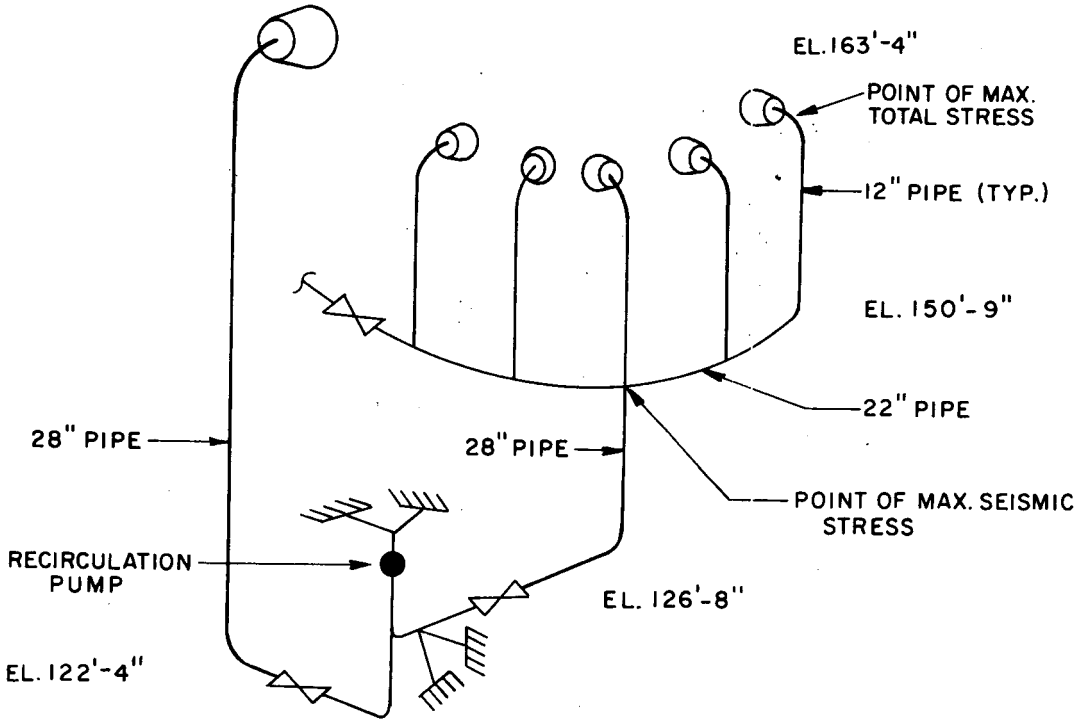


FIGURE X A-27 Recirculation Line

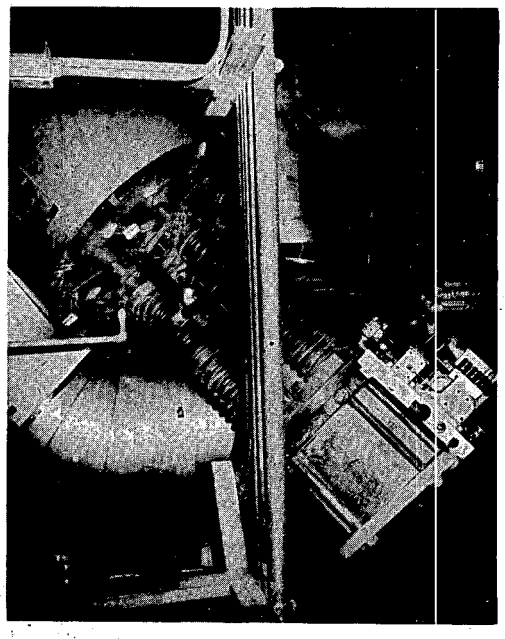


FIGURE X A-28 Main Steam Isolation Valve

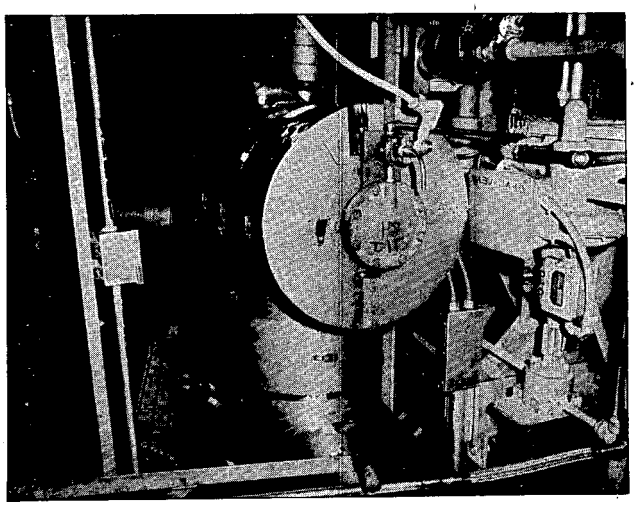


FIGURE X A-29 Pressure Relief Valve

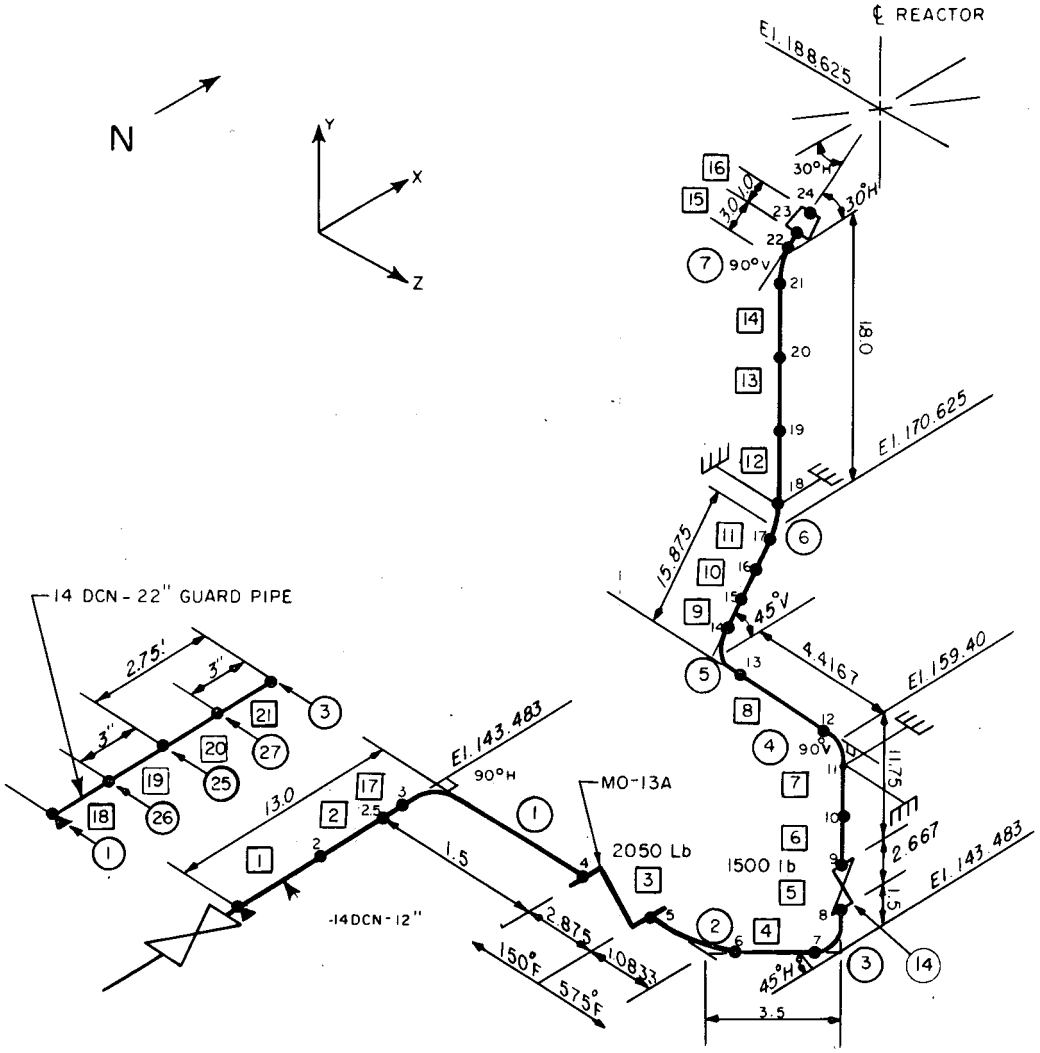


FIGURE X A-30 A/E Mathematical Model for Dynamic Analysis of Core Spray Piping

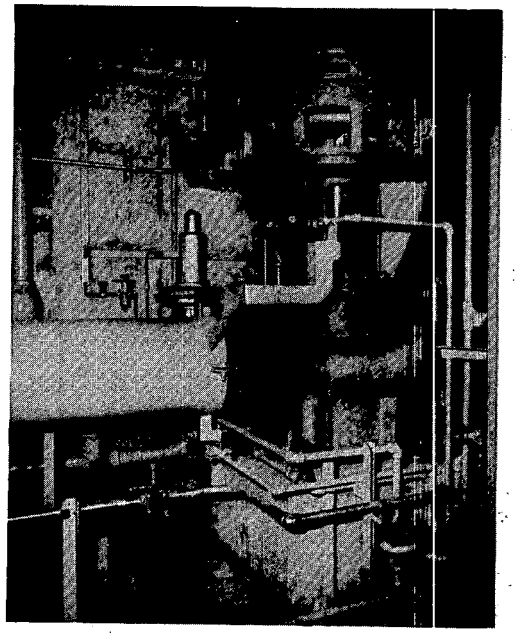


FIGURE X A-31 Core Spray Pump and Drive - Lower Portion Showing Pump Mounting

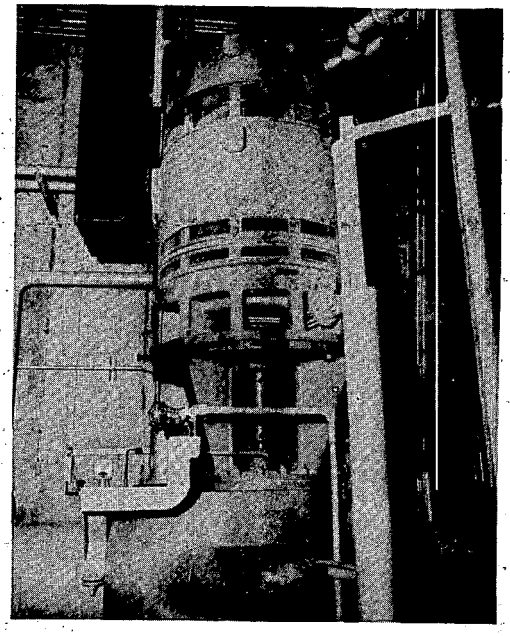


FIGURE X A-32 Core Spray Pump and Drive - Upper Portion Showing Motor and Coupling to Pump

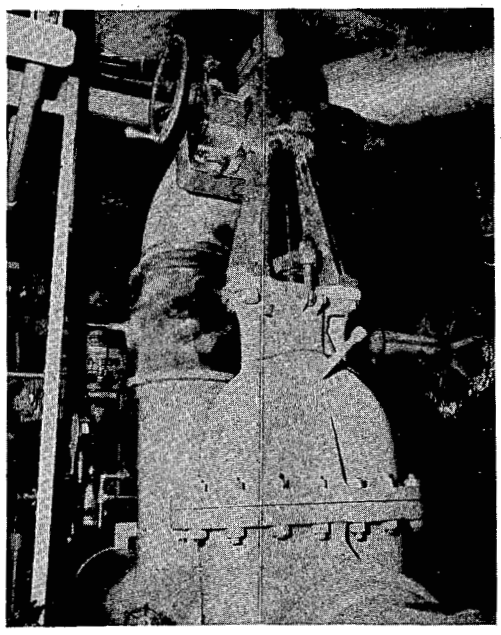


FIGURE X A-33 Typical Valve Motor Operator Installation

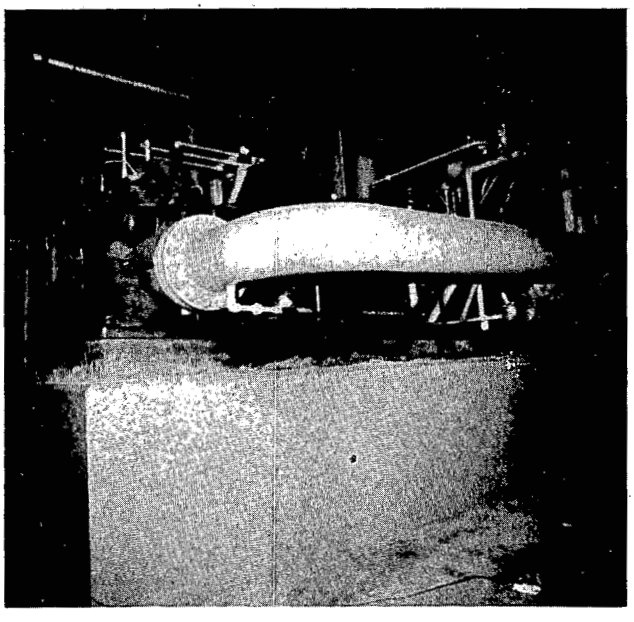


FIGURE X A-34 HPCIS Pump and Inter-stage Piping

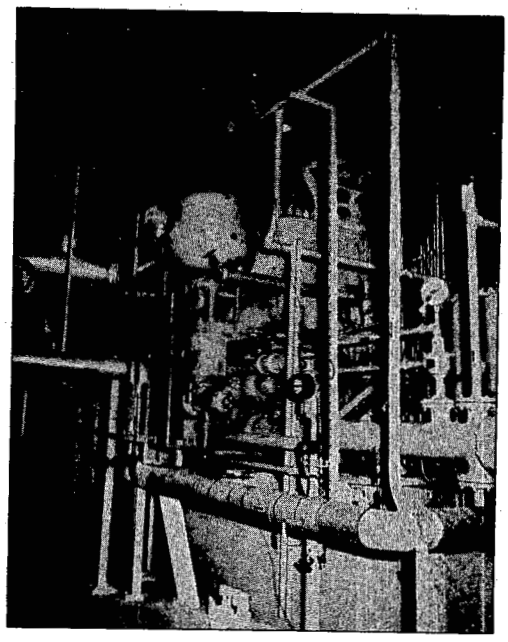


FIGURE X A-35 HPCIS Turbine Drive

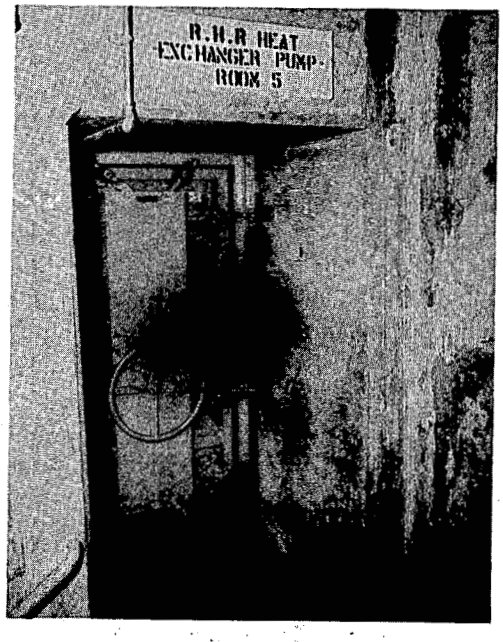


FIGURE X A-36 Watertight Entryway to RHR Pump Room

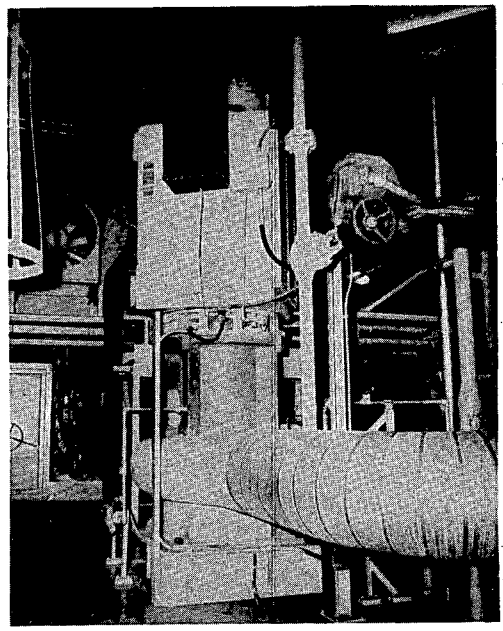


FIGURE X A-37 RHR Pump and Drive

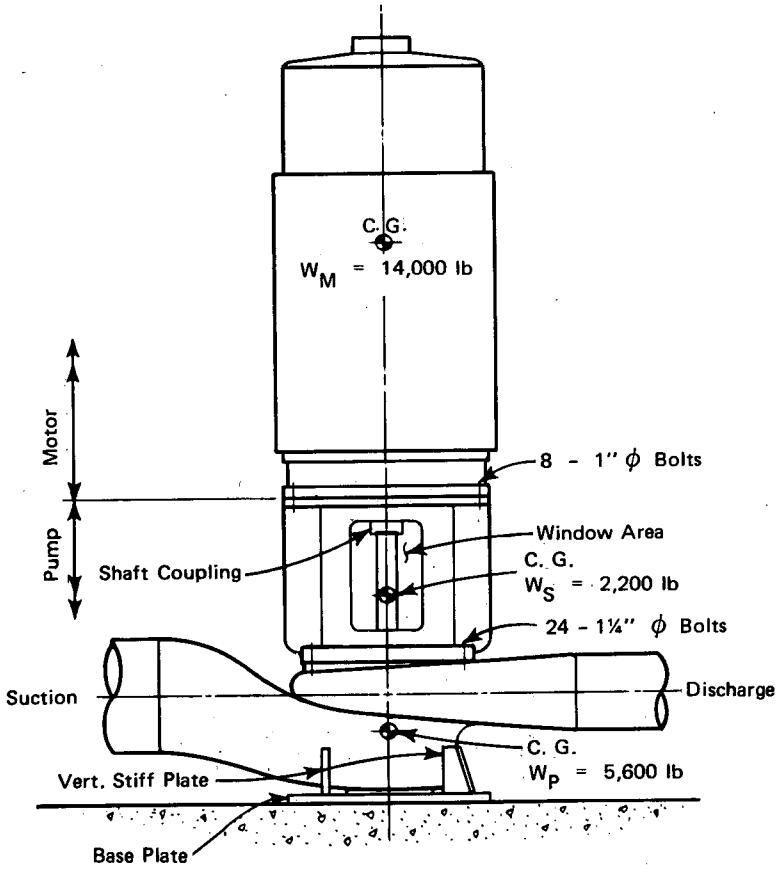


FIGURE X A-38 RHR Pump and Motor

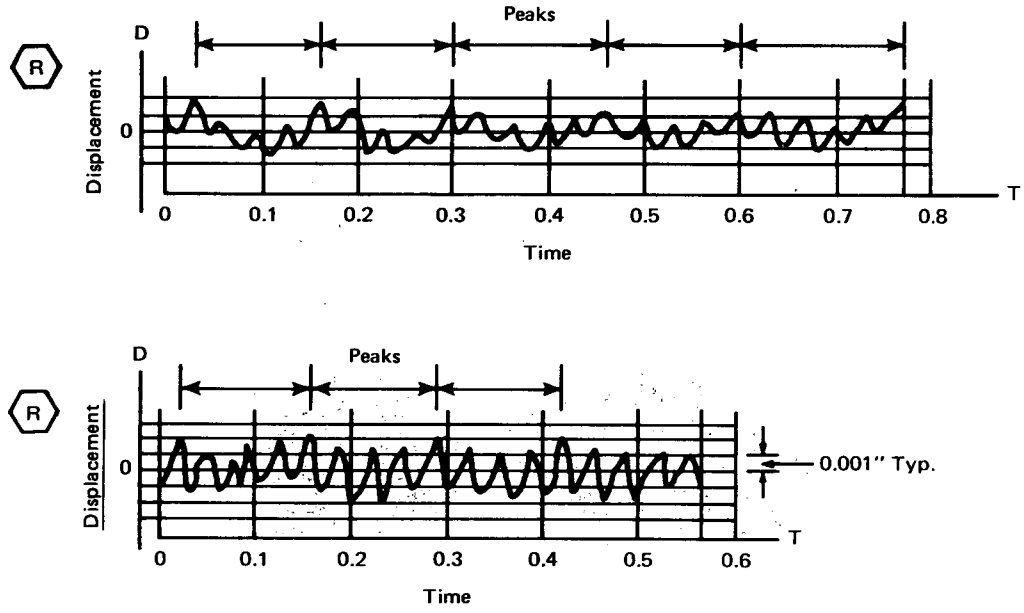


FIGURE X A-39 Selected Displacement Records from RHR Pump Vibration Tests Showing Cyclic Displacement Peaks



FIGURE X A-40 Diesel Generator Building - Side Facing River

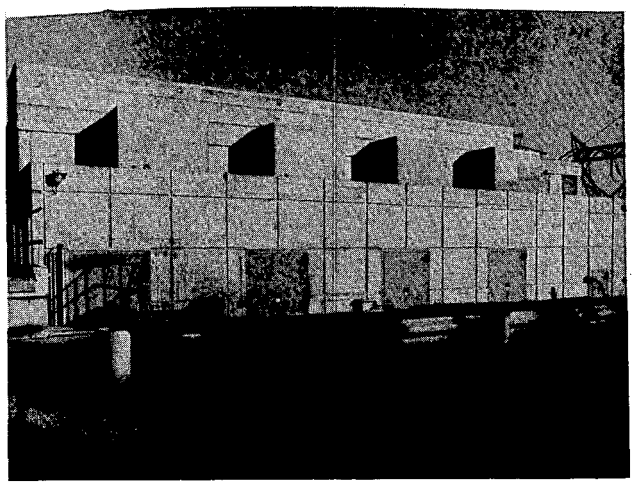


FIGURE X A-41 Diesel Generator Building - Opposite Side

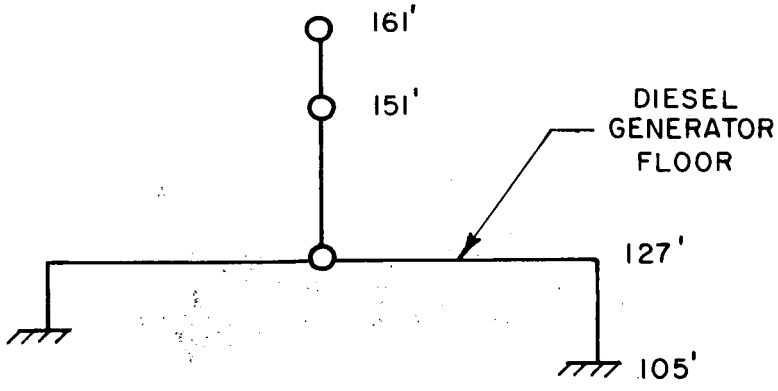


FIGURE X A-42 Lumped Mass Model for Diesel Generator Building Seismic Analysis

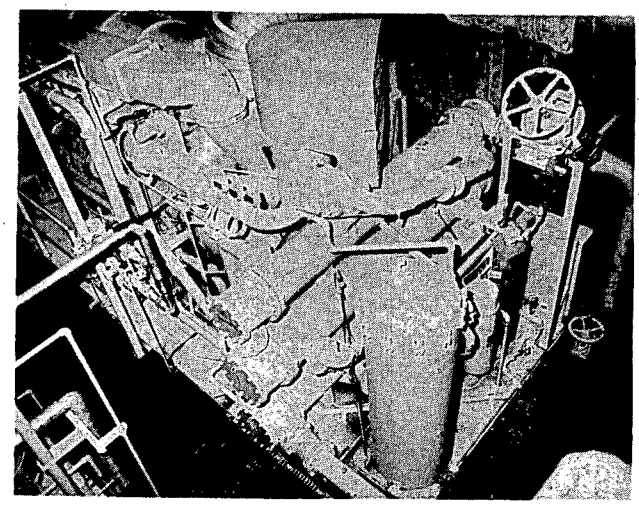


FIGURE X A-43 Diesel Generator Unit - View from Generator End

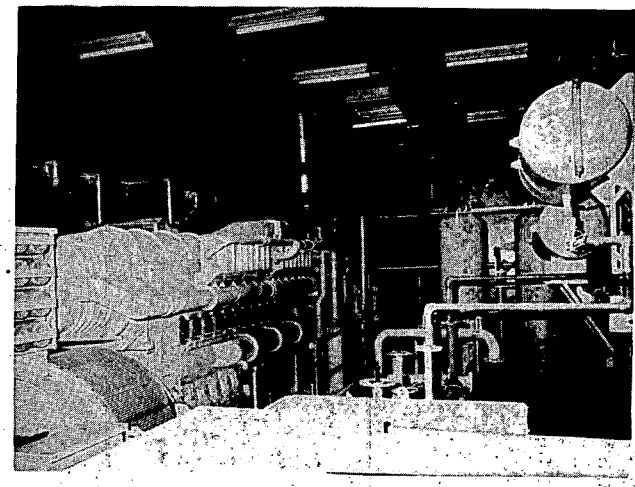


FIGURE X A-44 View of Diesel Generator Unit Showing Turbo-Charger

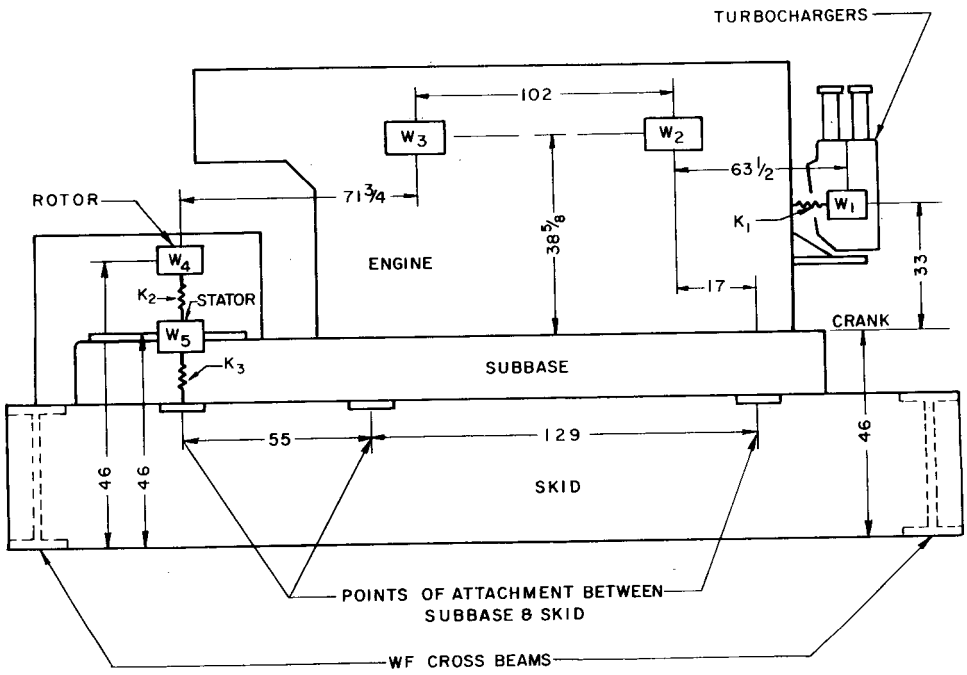


FIGURE X A-45 Diesel Generator Dynamic Model

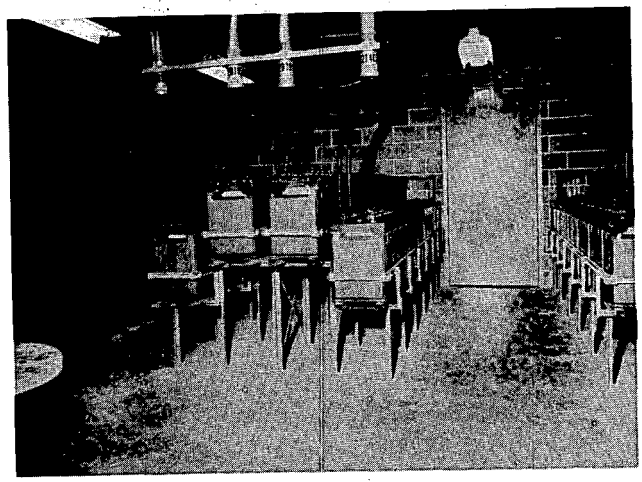


FIGURE X A-46 Batteries and Battery Racks - 125/250-V System

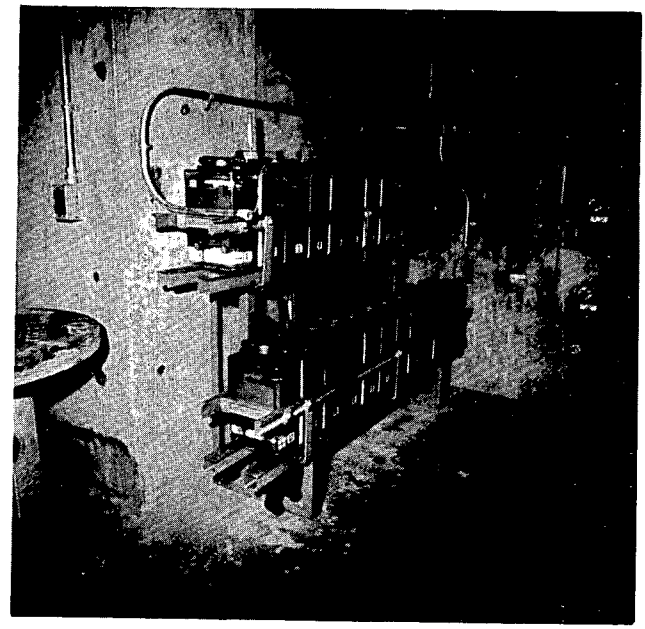


FIGURE X A-47 Batteries and Battery Racks - 24-V System

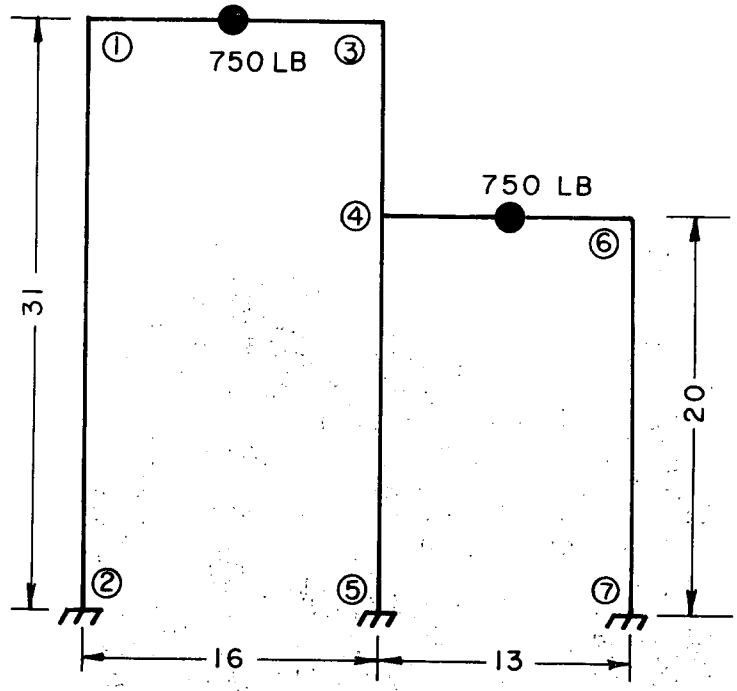


FIGURE X A-48 Lumped-Mass Model for Seismic Analysis of 58-Cell FTC-21 Battery Rack. (Typical of Model Scheme for All Battery Racks.)

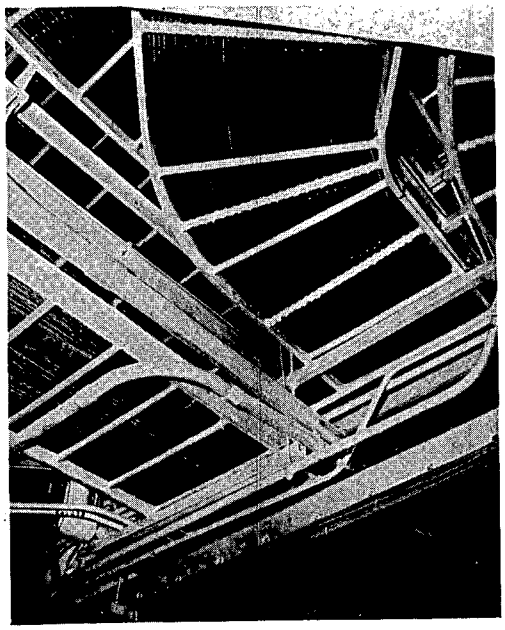


FIGURE X A-49 Electric Power and Control Cables Installed in Cable Trays

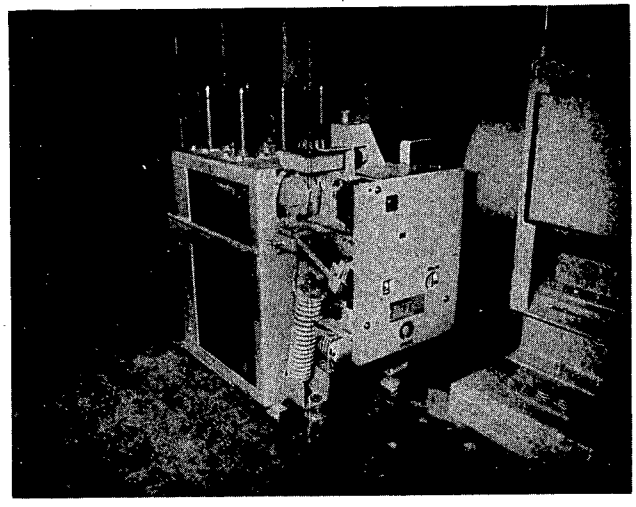


FIGURE X A-50 4-kV Switchgear Unit

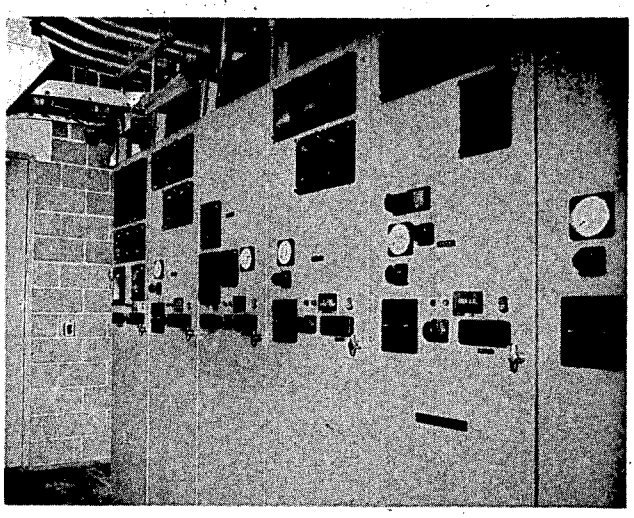


FIGURE X A-51 4-kV Switchgear Racks

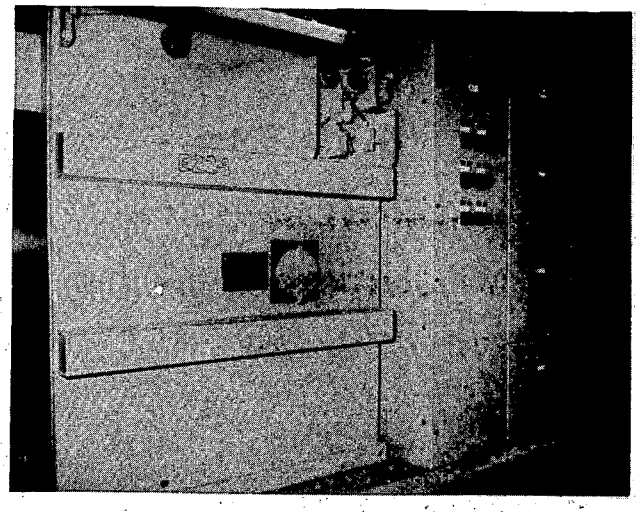


FIGURE X A-52 480-V Load Center

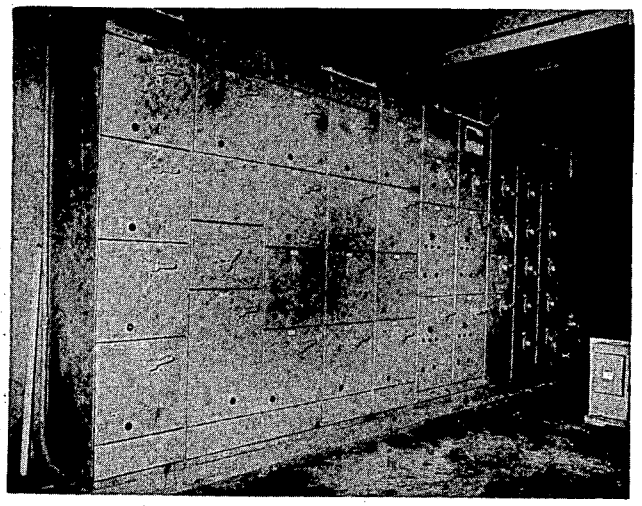


FIGURE X A-53 480-V Motor Control Centers

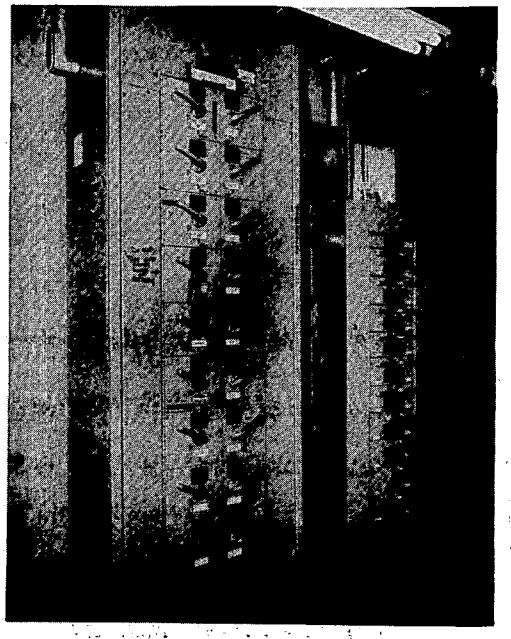


FIGURE X A-54 D-C Distribution Panels

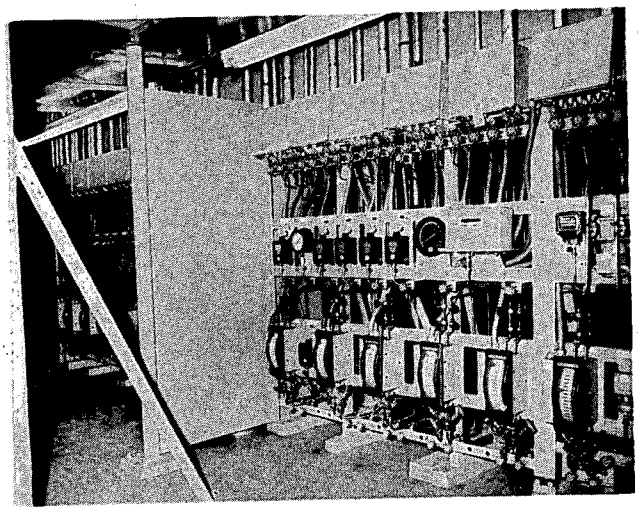


FIGURE X A-55 RPS Instrumentation Racks (Front View)

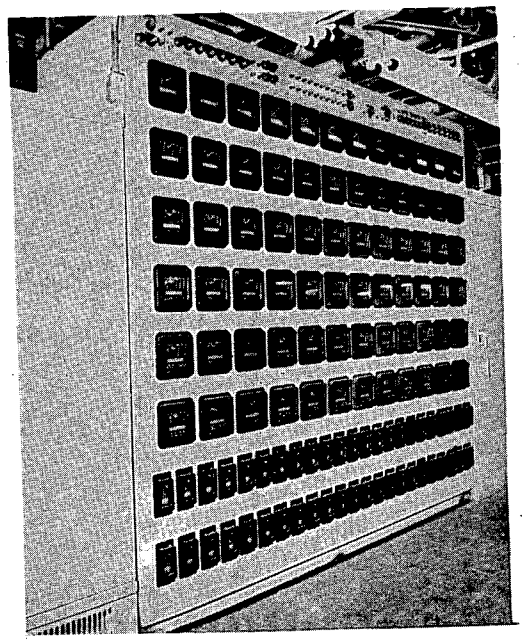


FIGURE X A-57 Reactor Protection System Logic Cabinet

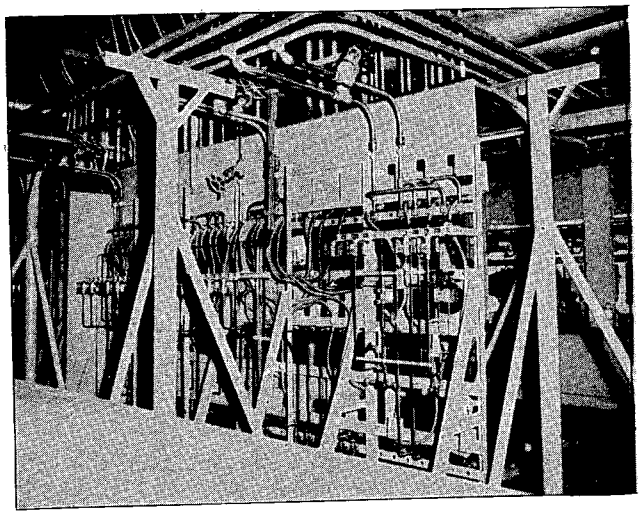


FIGURE X A-56 RPS Instrumentation Racks (Rear View)

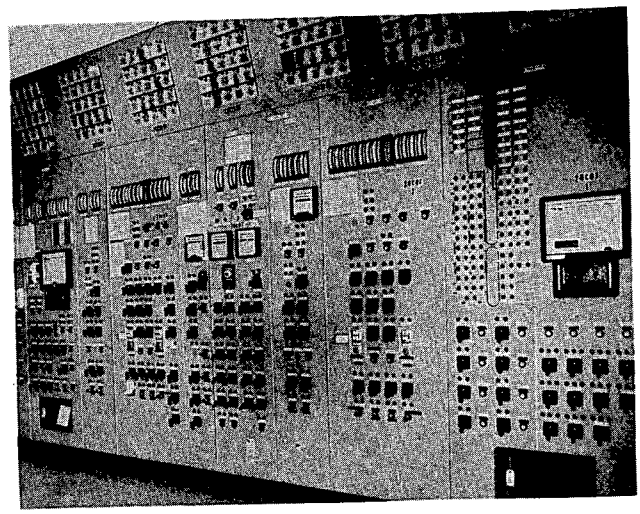


FIGURE X A-58 Control Room Panels for Reactor Safety Systems